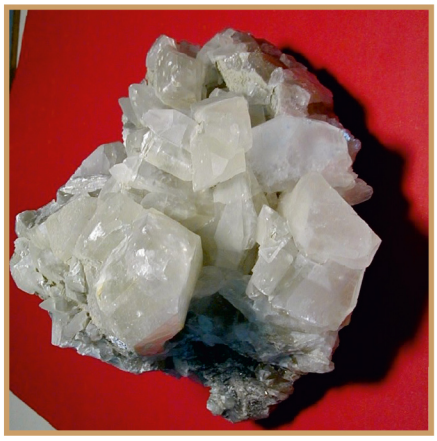
ESKİŞEHİR OSMANGAZİ ÜNİVERSİTESİ



Proceedings of the 18th International Mineral Processing Symposium

Yazarlar
Prof.Dr. Volkan BOZKURT
Prof.Dr. Halil İPEK
Doç.Dr. Serkan GÖKÇEN
Dr.Öğr.Üyesi Kemal BİLİR





ESKİŞEHİR OSMANGAZİ ÜNİVERSİTESİ
1970

XVIII. INTERNATIONAL MINERAL PROCESSING SYMPOSIUM
ESKİŞEHİR - TÜRKİYE
2024

Proceedings of the 18th International Mineral Processing Symposium

October 16 - 18, 2024

Anemon Grand Eskişehir Hotel, Türkiye

Editors

Prof. Dr. M. M. Volkan Bozkurt
Prof. Dr. Halil İpek
Assoc. Prof. Dr. Hasan Serkan Gökçen
Assist. Prof. Dr. Kemal Bilir





ESKİŞEHİR OSMANGAZİ UNIVERSITY
1970
+90 222 239 37 50 / 3414
maden@tm.ogu.edu.tr

Yurt Madenciliğini Geliştirme Vakfı

ARBER
arber@arber.com.tr
+90 312 441 07 00
www.arber.com.tr

Eskişehir Osmangazi Üniversitesi Yayınları No: 403

Sahibi : Prof. Dr. Kâmil ÇOLAK (Rektör)
Yayın Yönetmeni : Prof. Dr. Emine GÜMÜŞSOY (Rektör Yardımcısı) :
Yayın Komisyonu Prof. Dr. Emine GÜMÜŞSOY (Rektör Yardımcısı)
Prof. Dr. Mahmut KEBAPÇI
Prof. Dr. Haldun KURAMA

İdari Sorumlu : Mustafa ARSLAN
İ.M.İ.D. Başkanı
Basımevi Sorumlusu : Yüksel ASLAN
ESOGÜ Basımevi Şube Müdürü

Bu kitabın basım, yayım ve satış hakları Eskişehir Osmangazi Üniversitesi'ne aittir. Bütün hakları saklıdır.

Kitabın tümü ya da bölümü/bölümleri Eskişehir Osmangazi Üniversitesi'nin yazılı izni olmadan elektronik, optik, mekanik ya da diğer yollarla basılamaz, çoğaltılamaz ve dağıtılamaz. Copyright 2024 by Eskişehir Osmangazi University. All rights reserved.

No part of this book may be printed, reproduced or distributed by any electronically, optical, mechanical or other means without the written permission of Eskişehir Osmangazi University.

Kapak Tasarım
Prof. Dr. Şirin ŞENGEL

Dizgi
Prof. Dr. M. M. Volkan Bozkurt,
Prof. Dr. Halil İpek,
Assoc. Prof. Dr. H. SerkanGökçen,
Assist Prof. Dr. Kemal Bilir

ISBN NO
978-605-9975-87-2

1. Baskı

Baskı Tesisleri
ESOGÜ Basımevi

T.C. Kültür ve Turizm Bakanlığı Matbaa Sertifika No.: 64281

ESKİŞEHİR 2024

Publisher	: Department of Mining Engineering, Eskişehir Osmangazi University
ISBN	: 978-605-9975-87-2
Edited by	: Prof. Dr. M. M. Volkan Bozkurt, Prof. Dr. Halil İpek, Assoc. Prof. Dr. H. Serkan Gökçen, Assist Prof. Dr. Kemal Bilir
Cover Design	: ARBER
e-Book Layout	: Assoc. Prof. Dr. Hasan Serkan Gökçen, Assist Prof. Dr. Kemal Bilir
Composition	: Assoc. Prof. Dr. Hasan Serkan Gökçen, Assist Prof. Dr. Kemal Bilir

COMMITTEES

Co-Chair

Prof. Dr. Halil İpek	Eskişehir Osmangazi University
Prof. Dr. M. M. Volkan Bozkurt	Eskişehir Osmangazi University

Secretary

Assist Prof. Dr. Kemal Bilir	Eskişehir Osmangazi University
Assoc. Prof. Dr. H. Serkan Gökçen	Eskişehir Osmangazi University

Executive Committee

M. Ali Türkoğlu,	President of YMGV
Prof. Dr. Volkan Bozkurt	Eskişehir Osmangazi University
Prof. Dr. Feridun Boylu	Istanbul Technical University
Prof. Dr. Halil İpek	Eskişehir Osmangazi University
Prof. Dr. Naci Emre Altun	Middle East Technical University
Dr. Selahaddin Anaç	Minertolia
Prof. Dr. Vedat Arslan	Dokuz Eylül University
Prof. Dr. Ali İhsan Arol	Eti Bakır A.Ş.
Prof. Dr. A. Hakan Benzer	Hacettepe University
Prof. Dr. Gülay Bulut	Istanbul Technical University
Prof. Dr. Murat Olgaç Kangal	Istanbul Technical University
Sabri Karahan	Dama Engineering
Prof. Dr. Abdullah Obut	Hacettepe University
Prof. Dr. Mehmet Tanrıverdi	Dokuz Eylül University

Honorary Members

Prof. Dr. Suna Atak	Istanbul Technical University
Prof. Dr. Ümit Atalay	Middle East Technical University
Prof. Dr. Neşet Acarkan	Istanbul Technical University
Prof. Dr. İrfan Bayraktar	Tüfekçioğlu Kauçuk Ve Makine
Prof. Dr. Mehmet Canbazoğlu	Cumhuriyet University
Prof. Dr. Halim Demirel	Hacettepe University
Prof. Dr. Levent Ergün	Hacettepe University
Prof. Dr. Özcan Y. Gülsoy	Hacettepe University
Prof. Dr. Üner İpekoğlu	Dokuz Eylül University
Prof. Dr. Mevlüt Kemal	Dokuz Eylül University
Prof. Dr. Gülhan Özbayoğlu	Middle East Technical University
Dr. Avni Yazan	Çayeli Bakır İşletmeleri Inc

Local Committee (Eskişehir Osmangazi University)

Prof. Dr. Muammer Kaya	Eskişehir Osmangazi University
Prof. Dr. Sabiha Koca	Eskişehir Osmangazi University
Prof. Dr. M. M. Volkan Bozkurt	Eskişehir Osmangazi University
Prof. Dr. Haldun Kurama	Eskişehir Osmangazi University
Prof. Dr. Halil İpek	Eskişehir Osmangazi University
Prof. Dr. Adem Taşdemir	Eskişehir Osmangazi University
Assoc. Prof. Dr. Tuba Taşdemir	Eskişehir Osmangazi University
Assoc. Prof. Dr. Derya Öz Aksoy	Eskişehir Osmangazi University
Assoc. Prof. Dr. Yakup Umucu	Eskişehir Osmangazi University
Assoc. Prof. Dr. Hasan Serkan Gökçen	Eskişehir Osmangazi University
Assist. Prof. Dr. Kemal Bilir	Eskişehir Osmangazi University
Assist. Prof. Dr. Y. Hakan Gürsoy	Eskişehir Osmangazi University
Research Asst. Dr. Işıl Tokcan	Eskişehir Osmangazi University
Research Asst. Dr. Semih Oluklulu	Eskişehir Osmangazi University

Scientific Committee

Prof. Dr. Zhenghe Xu	Southern University of Science and Technology
Prof. Dr. Pshem Kowalczuk	Norwegian University of Science and Technology
Asst. Prof. Kemal Bilir	Eskişehir Osmangazi University
Assoc. Prof. Hasan Serkan Gökçen	Eskişehir Osmangazi University

Special Thanks to Our Sponsors

Main Sponsor

GÜBRETAŞ MADEN YATIRIMLARI A.Ş.

Gold Sponsor

ETİ BAKIR

Silver Sponsors

ÖKSÜT MADENCİLİK

ALAGRUP "Enerjimiz Enerjiniz"

Bronze Sponsors

TÜMAD MADENCİLİK SANAYİ VE TİCARET A.Ş.

ERSEL AKER MAKİNE SAN. VE TİC. A.Ş.

Kale

Asos process engineering

Dimin

TÜPRAG

LABRİS

MPES

YPT YILMAZ PROJE TEKNOLOJİLERİ DIŞ TİCARET A.Ş.

LİDYA MINES EARTH TO PEOPLE

albacore

MUTAŞ

ARGETEST

SKYMinerals

terralab

Name Badge Sponsor

Mining technology for a sustainable future WEIR

Bag Sponsorship

KIRLIOĞLU

Pen and Notepad Sponsor

Ant Group

Coffee Break Sponsors

SELKA PREFABRİK

Other Sponsors

PRES-SAN

KUTAHYA PORSELEN

kromder Krom Üreticileri Derneği

ONURMAKSAN

AMD 2006

TABLE OF CONTENTS

TABLE OF CONTENTS v

PREFACE xi

INVITED SPEAKERS

Optimisation of Compressive Crushing

Magnus Evertsson

Understanding Classification and its Complexities in Different Circuit Applications

Aubrey Mainza

Eco-efficient Comminution Technologies

Hakan Benzer

Enhancing Flotation Separation of Fine Particles Using Switchable Collectors

Zhenghe Xu

Anatomy of Lithium-Ion Batteries (LIBs) and their Recycling Technologies

Muammer Kaya

CHARACTERIZATION AND MINERALOGY

Geometallurgical approach for arsenic challenges solution in Cu – Mo porphyry ores (Case study: Sungun mine)

Ataallah Bahrami, Reza Hassanpour Kashani, MirSaleh Mirmohammadi, Fatemeh Kazemi, Ahmad Fathzadeh, Yousef Ghorbani 1

Characterization and Evaluation of Glycine and Cyanide Leaching Application on Artisanal Gold Mining Tailings

Abdulbagi Hassan Abdallah Mohamed[a], Abdou Azizi YOUPOUNGAM[a], Taha BOYRAZ[a], İbrahim ALP[a] 11

A Review on Shape Characterization of the Gold and Copper Metallic Particles Recovered from the Flotation of Various E-wastes

Fırat Burat, Beyzanur Keleş, Nazlım İlkyaz Dinç, Halide Nur Dursun, Ugur Ulusoy,..... 21

Minor Cu-Au-Co-Bi-Te Mineralization at The Jalal-Abad Iron Ore Deposit, Northwestern Zarand, Iran

Behrouz Karimi Shahraki, Behzad Mehrabi , Ziaeddin Pourkarimi 33

Effects of Low-Grade Refractory Gold Mineralogy on Flotation Properties

Sena Naz GÖKDEMİR, İlkay Bengü CAN, Ahad HARZANAK..... 41

Effect of Rheology on Mineral Processing Operations

Işıl Tokcan 55

CRUSHING/GRINDING

HPGR influences on downstream ball mill according Bond tests and energy calculations

F Heinicke, H Lieberwirth and M Pfeifer..... 65

Investigating the Influence of Grinding Aids on Flow Characteristics and Grinding Performance in a Dry Stirred Mill

Hasan Serkan GOKCEN, Serkan CAYIRLI, Nuri YUCE, Obaidullah ELCHI 75

Determination of Ball Trajectory in Tumbling Mill Considering Mill Liner Dimensions

Yusuf Enes Pural, Feridun Boylu, ... 83

The Effect of Kinetics Model Parameters in Coarse and Fine Particle Size on The Prediction of Simulation Program (MODSIM©)

Yakup UMUCU , Vedat DENİZ, Y. Hakan GÜRSOY 91

Ball Mill Optimization in The Cement Grinding Plant

Yakup UMUCU , Nazmi ÜNAL, Ali FIRAT, Vedat DENİZ, Y. Hakan GÜRSOY, Hüseyin SENDİR 103

Comparative Analysis of Rod Mills and Ball Mills: Assessing Impact on Talc Ore Beneficiation Efficiency

Alaa ABBADI, Ádám Rácz, Christoph Luckeneder, and Ljudmilla Bokányi, Author3 111

SCREENING & CLASSIFICATION

Effect of Deviation in The Unbalance Excitation on The Performance of an Inclined Screen

Zehra Bayın, Engin Can Çelik, Vilaiat Alekperov, Ekrem Savaş, Tuncay Karaçay 127

PHYSICAL ENRICHMENT

The Beneficiation Studies of Barite-Florite from Eskisehir-Beylikova Ore by Gravity Separation Methods

Akar H., Gunaydın, N. , Cugu S., Sahin, Y., Savran C., Gurkan, O.M., Basturkcu, E., Yuce, A.E. 135

Investigation of Operational Parameters for High Capacity – High Intensity Prototype Magnetic Separator (D:300 mm) to Produce A-Grade Egyptian Sand

B. E. Uğurlar, B. İbis, Ç. Ulusoy, H. Baştürkcü 141

Pre-concentrate Production from Oolitic Iron Ore by Physical and Chemical Separation Methods.

Nassima Chebel, Djamel Nettour, Mohamed Chettibi 149

Investigating the Use of Chromite Beneficiation Plant Data in Simulation Studies

Betül AYDOĞMUŞ, Yakup UMUCU , Halil İPEK 157

Enrichment of Waste Printed Circuit Boards using a Zig-Zag Air Separator

Ersin Yener Yazici , Elif Yilmaz , Yunus Emre Cavdar , Oktay Celep , Haci Deveci 165

FLOTATION & SURFACE CHEMISTRY

The effect of grinding type on roughness and coagulation of magnesite particles

Halim Recep Kayabaşı, Arman Ehsani, Burçin Kaymakoğlu, Tuğba Deniz Tombal Kara, Onur Güven 175

Beneficiation Performance of Heterogenous Ore Grades from a REE-Carbonatite Deposit

Ezgi Akyildiz , Stefanie Lode, Camilo M. Silva, Kornel Tobiczyk, Pshem Kowalczuk 183

Flotation Research on Magnesite Tailings

F.Göktepe, B. Aydın, G.Bulut 193

Investigation of the collector effect on the chalcopyrite flotation

Adnan Ceylan , Gülay Bulut 201

Enrichment of Lead-Zinc Sulfide Ore of Bolkar-Tepeköy Deposit by Flotation
Oğuzhan Mert Gürkan, Buse Yılmaz, Ş. Beste Aydın, Alim Gül 209
Investigation of the production of high carbon concentrate from Kütahya-Oysu graphite ores by flotation method
Gülşah Güven, Hasret Demir, İbrahim Eren Püsür, Uğur Ulusoy, Fırat Burat 215
Enrichment of Yozgat Potassium Feldspar by Different Methods
Tülay Türk, Yunus Emre Çavdar, Murat Olgaç Kangal 225
Comparison of Amine Type and Xanthate Type Collectors in Pyrite Flotation
İbrahim GÖKTAŞ, Begüm ÖZDUR, Ahmet YAKAR, Gizem DEMİRDAĞ ÖZEL 235
Optimization of Stibnite Flotation Conditions In The Presence of Activator And Dispersant
Seyed Ramin Banihashemi, Mehdi Rahimi, Gholamreza Parvareh, Ziaeddin Pourkarimi 243
The Effect of Different Storage Times of Drilling Cores on Flotation Performance
Seda Özçelik , Cankut Çendik, Özlem Bıçak 253
Effects of Various Salts on Foam Stability of Surfactants
Yunus Emre Çavdar, Orhan Özdemir 261
Effect of sodium silicate, sodium tripolyphosphate, and sodium hexametaphosphate dispersants on particle size distribution of the halloysite, kaolinite, and quartz minerals in the dispersion process
Emrah Durgut, Yunus Emre Çavdar, Mustafa Çınar, Osman Yavuz, Orhan Ozdemir 269
Investigation of the Effectiveness of Oleate in Fine-Sized Magnesite Flotation
S. Koca, D.O. Aksoy, H. Koca 277

HYDROMETALLURGY AND BIOLOGICAL PROCESSES

Characterization and Leaching Behavior of Mixed Oxide-Sulfide Zinc Ore from Hakkari-Türkiye
İlhan Ehsani, Arman Ehsani, Fatih Çavuşlu, Sadiye Kantarcı 283
Investigation of arsenic removal from copper concentrates by alkaline sulphur leaching
Taha Boyraz, Tuğba Türk, İbrahim Alp 291
Improvement in the Performance of Solvent Extraction Operation Using Solutions Spray System
Muhammad Zubair Rahim, Ali Ihsan Arol 299
Acidic Dissolution of Metals from Waste Printed Circuit Boards
Şule Ilgın, Nazlım İlkyaz Dinç, Fırat Burat, Arslan 309
Leaching Behaviour of Base and Precious Metals During Cyanide Leaching of a Pyrite Concentrate
Oktay Celep, Ersin Yener Yazici,Hacı Deveci, Murat Mercimek, Alper Gönen, CumhurDemirel, Melih Cingöz, Hüseyin Kömürcü, Serkan Çakmak 317
Cu Zn and Co Recovery from Pyrite Calcine at Atmospheric and Pressure Sulfuric acid leaching: Investigation of Reactions
Mehmet Canbazoğlu, Arzu Yılmaztürk, Fatih Özel, Sezer Kabaoğlu, Gizem Demirdağ Özel 327
Optimization of Alkaline Pre-Treatment in Zarshuran Gold Mine for Enhancing Gold Recovery
Seyed Hossein Hashemi, Ziaeddin Pourkarimi, Faraz Soltani, Qolamreza Parvareh, Mehdi Rahimi 335

Effect of refractory ore character on silver recovery by acidified sodium chloride-hypochlorite leaching

Ömer Canıeren, Cengiz Karagüzel 343

Optimization of nickel and cadmium leaching process from spent batteries

Mohsen Mirzaei, Mohammad Ali Moradzadeh, Ziaeddin Pourkarimi, Mehdi Rahimi, Seyed Javad Mousavi 349

Zinc Recovery From Flue Dust of Blast Furnace and Arc Furnace Plants in Iron and Steel Industry

Onur ATAŞ, Mehmet BİLEN, ... 359

Valuable Metals dissolution from Flash Furnace Electrostatic Precipitators (ESP) Dust by atmospherically Sulfuric acid leaching

Mehmet Canbazoğlu, Arzu Yılmaztürk, Gizem Demirdağ Özel 372

Pipeline Leaching of Poor Ferrous Zinc Tailings following Microwave Tube Radiation - Cu and Zinc Recovery

Yıldırım İ. TOSUN, ... 379

Ivrindi Gold And Silver Mine Permeability Testwork

Melis N. ERDEM 388

COAL PREPARATION

Fuzzy Logic Estimation of Coal Recovery by Knelson concentrator

Sevgi Karaca , Ali Uçar , Oktay Şahbaz 391

Utilization of TTK Armutçuk Region Coal in Sectors Other Than General Consumption

Faik ALP, Serdar YILMAZ, İhsan TOROĞLU, Mehmet BİLEN

PLANT DESIGN, MODELING, AND SIMULATION

Performance of Sequential Gas Scrubber Systems at High Sulfur Dioxide (SO_2) Concentration

Furkan Enes ÖZEL, Arzu Sinem SATILMIŞ, ... 409

Detailed Mass Balance Development of a Heap Leaching Operation Using Modelling and Simulation

Manuel Gonzalez, Tuğcan Tuzcu, Marie-Veronique Durance, Stephane Brochot 415

Investigation of the rheological behavior of acid-leached sepiolite

Kemal Bilir, and Utku Çağlar 423

INDUSTRIAL RAW MATERIALS

Enhanced Hydrophobic Sensing Using Hydrophobized Halloysite Biocomposite Fillers: Ball Milling vs. Surfactant

Mervenur Kirazoğlu, Birgül Benli..... 433

Investigation of Aluminum Concentrate Production Potentials from Bauxite Ore with High Iron Content

Zeynep ÜÇERLER-ÇAMUR, Tülay TÜRK, Yusuf Enes PURAL, Mahmut Emre Çoban, Murat Olgaç KANGAL..... 443

An Investigation into the Prevention of Black Core Formation in Ceramic Bodies

M. Uğur Taşkıran, Kağan Kayacı, A. Ali Sirkeci, Hatice Turgut, Barış Darcan 453

Development Of Alternative Wall Tile Compositions By Using Different Industrial Wastes

M.Uğur Taşkıran, Kağan Kayacı, Enrique Sanchez Vilches, Vicente Sanz Solana 459

GOLD AND SILVER ENRICHMENT

Comparison of Gravity and Flotation Methods for Gold Recovery from Pyrite Ores

Ceyda Şavran, Tülay Türk, Alim Gül, M.Olgaç Kangal 467

Research and Application of Enrichment Methods for Gold in Refractory Form Found in Pyrite and Arsenopyrite Minerals

Alperen KÖLE, Ahmet YAKAR, Kutay AYDINBURUN, Hande Burçin HARMANCI, Begüm ÖZDUR, Mustafa ÖZTÜRK, İbrahim GÖKTAŞ

Production Of Porphyry Copper Ore Containing Gold And Silver By The Sart Process Method

Gökçe Çıkın, Sercan Sevgül, Serhat Biçer, Ruveyda Nur Aytop 485

Gold Recovery With Cyanide Leaching: Tank Leaching Application

Mert Kuzu, Ali Uluturk 493

Zenit Mining, Kızıltepe Gold Plant Cyanide Destruction Circuit

Yıldız GÖKTAŞ, Nursun ŞİRVANCI 501

Heap Leaching Stability and Monitoring in İvrindi Gold and Silver Mine

Burak KAYACIK, Ali B. AKTAS, Alper ARUER, Yahya K. UZUNER, Serhat OZDOGAN 509

Safe Use of Cyanide in Gold Production: International Cyanide Management Code

Bilge KÜÇÜKAYTAN 515

Sogut Gold Mine: Gravity + CIL Processing Plant Overview

Fehmi Can Süter 523

RARE EARTH ELEMENTS (REE) AND STRATEGIC MINERALS

Optimization of Rare Earth Element Recovery from Kızıldağ (Karaman-Türkiye) Shale Ore Using Response Surface Methodology

Turan Uysal, Ceren Erüst Ünal, Muhammed Esat Akça, Hikmet Sis, Murat Erdemoğlu 525

Green Chemistry Approaches in Mineral Processing with Deep Eutectic Solvents: A case of NdFeB magnets

Birgül Benli, Mert Sarıkaya 533

NEW PROCESSES AND TECHNOLOGIES

The Use of a Reflux Classifier for Chromite Ores: Assessment of Different Circuit Alternatives at Pilot Scale

Özgür ÖZCAN 541

DEWATERING AND WATER MANAGEMENT

Scale, Deposit and Corrosion Control in Mineral Processing Growing Challenges and Emerging Solutions

Brian Danyliw 551

Removal of Anions (SO42- , S2O32- and SCN-) from Gold Mining Process Water by Membrane Capacitive Deionization Process

Yasemin Ozturk 559

RECYCLING AND WASTE MANAGEMENT

Recovery of metals from coal power plant fly ashes via hydrometallurgical route

K. Tahsin Perek, Esra Baştürkcü, Mustafa Özer, Y. Enes Pural, Fatma Arslan 567

Effective Removal of Boron and Arsenic from Industrial Wastewater Using Coagulation and Electrocoagulation Methods

Buğra ÖZDEMİR, Tolga GÜLSEVER 575

Techno-Economic and Environmental Assessments for Hydrometallurgical Treatment of Waste Lithium-Ion Batteries (LIBs): The ELiMINATE Project

E. Y. Yazici, H. Deveci, O. Celep, F. Ahlatci, E. Esen, C. Dorfling, R.F. van Schalkwyk, G. Akdogan, L. Louw, R. F. Maritz, M. W. J. Kuhn, D. T. Vooght, E. Emilsson, A. Wu, N. Elginoz, J. Ots, A. N. Ozturk, M. Petranikova, E. Cuhadar, C. Eyupoglu, E. Eken Torunoglu 581

The Recovery of Graphite from Black Mass using Centrifugal and Magnetic Separation

Halide Nur Dursun, Argun Çiper, Doğukan Akardaş, Emircan Uysal, Beril Tanç Kaya, Fırat Burat 591

The Recycling of End-of-Life Crystalline Silicon Solar Panels

Nazlım İlkyaz Dinç, Tülin Ulucan, Fırat Burat 601

Efficient Photocatalytic Degradation of Textile Dye Contaminants Using Novel Materials: Thermally Exfoliated Boron Doped Graphitic Carbon Nitride

Haldun Kurama , Halit Levent Hoşgün, Ayşe Gül Türe 611

Physico-Chemical Bases of Selective Extraction of Metals from Dust Concentrate of Blast Furnaces by Organic Acids. I. General conception

Vitaly Prokopenko, Volodymyr Chernenko, Olena Tsyganovich, Igor Volobaiev 615

Microwave Tube Radiated CIP Process Using Active Carbon of Popped Corn/Rice /Cotton in Leaching of Poor Ferrous Zinc Tailings

Yıldırım İ. TOSUN, ... 633

CARBON FOOTPRINT REDUCTION

Acid Mine Drainage (AMD): Revisiting and Recent Insights

Hikmet Sis, Osman Dolmaz 641

GENERAL SUBJECTS

Umrek And Mineral Processing

Halim Demirkan , Ahmet İbuk 642

Judicial Approach to the Planning and Environmental Impacts of the Ore Preparation and Enrichment Facilities: The Case of Türkiye

Kerem Canbazoğlu 652

Evaluation of a Complex Polymetallic Sulphide Ore

H.M. Toprak, H. Baştürkcü 666

Dizin 674

PREFACE

The International Mineral Processing Symposium (IMPS) series has been organized biennially since 1986, rotated among five distinguished Turkish universities: Dokuz Eylül University, Istanbul Technical University, Middle East Technical University, Hacettepe University, and Eskişehir Osmangazi University. With a history spanning more than 35 years and international recognition, the IMPS continues to serve as a platform where both domestic and international scientists and professionals in the mineral processing sector share current information, developments, and thoughts on the future of the industry. Undoubtedly, one of the main factors contributing to the symposium's longstanding success has been the support provided by both public and private sectors. We anticipate that this tradition of support will continue and grow in the same manner.

This proceeding is a compilation of 78 papers from 14 different countries presented in oral and poster sessions at the symposium. Topics included: Characterization and Mineralogy; Crushing and Grinding; Screening and Classification; Physical Separations; Flotation and Surface Chemistry; Hydrometallurgy and Bioprocessing; Concentration of Fine and Ultrafine Particles; Coal Preparation; Pelletizing, Agglomeration, and Sintering; Plant Design, Modelling, and Simulation; Industrial Minerals; Boron Minerals and Trona; Gold and Silver Processing; Rare Earth Elements (REE) and Strategic Minerals; New Processes and Technologies; Dewatering and Water Management; Recycling and Waste Processing; and Carbon Footprint Reduction.

In addition to the contributed elements of the program, we are honored to have five prominent plenary lecturers covering important topics titled:

"Optimization of Compressive Crushing"

"Understanding Classification and its Complexities in Different Applications"

"Eco-efficient Comminution Technologies"

"Enhancing Flotation Separation of Fine Particles Using Switchable Collectors"

"Anatomy of Lithium-Ion Batteries (LIBs) and their Recycling Technologies"

We would like to take this opportunity to thank the reviewers and chairpersons for their help, the authors for their contributions, and the sponsors for their generous support. We also extend our gratitude to the organizing committees. The Turkish Ministry of Energy and Natural Resources, Eti Mine Works General Management, Eskişehir Osmangazi University Chancellorship, and the Faculty of Engineering and Architecture Dean's Office are gratefully acknowledged for their support. We would also like to thank The Turkish Mining Development Foundation and ARBER Professional Tourism and Congress Services.

M. M. Volkan BOZKURT, Halil İPEK, Kemal BİLİR & H. Serkan GÖKÇEN

Geometallurgical approach for arsenic challenges solution in Cu – Mo porphyry ores (Case study: Sungun mine)

Ataallah Bahrami [1]*, Reza Hassanpour Kashani [1], MirSaleh Mirmohammadi [2], Fatemeh Kazemi [3], Ahmad Fathzadeh [4], Yousef Ghorbani [5]

[1] Department of Mining Engineering, Faculty of Engineering – Urmia University, Urmia - Iran. P.O. Box 57561/51818.

[2] School of Mining Engineering, University of Tehran, Tehran – Iran.

[3] Ph.D. student of mineral processing, Faculty of Engineering – University of Kashan, Kashan - Iran.

[4] Complex of Copper Processing – Sungun, East Azerbaijan Province, Headquarters Rd, Tabriz – Iran.

[5] School of Natural Sciences, University of Lincoln, Lincoln – UK.

*Corresponding author: A.bahrami@urmia.ac.ir (Ataallah Bahrami)

Abstract:

This study in the form of two paper part I and part II, aimed to investigate possible controlling factors on the amount of arsenic in copper concentrate by applying a systematic geometallurgical approach. The Sungun Cu-Mo mine and its processing plant – located in northwestern of Iran – were considered as a case study. In this paper, by point analysis of drill cores, the changes of As in different zones of Cu-Mo porphyry deposit were investigated. Examination of changes in As in the mine indicates to be in the range of 0.5-5300 ppm, which increases with increasing depth of mine. Based on mineralogical studies, As is formed in the sulfosalt group minerals including tenantite and enargite. Due to the use of flotation method for copper sulfide minerals and similar flotation properties of arsenic-bearing minerals with copper sulfides, these minerals are recovered to copper concentrate. Increasing arsenic from 0.2% in copper concentrate leads to economic and environmental challenges in downstream processes such as smelting. A very effective solution for reduction the As in concentrate is the utilization of block extraction and simultaneous attention to the grade of copper and arsenic in the order of block extraction and their blending. In general, developing a mining program with a view to controlling the amount of arsenic in the amount of less than 70 ppm at the inlet load to the plant, along with adjusting the copper limit to 0.6%, can be an effective way to reduce the amount of arsenic in copper concentrate.

Keywords: *Cu-Mo porphyry ores, Arsenic, Mining, Geometallurgy, Environment.*

1. Introduction

One of the most important tasks of experts in the major of mines and mineral processing is the monitoring of environmental pollution caused by mining activities in the form of geo-environmental programs. The presence of heavy metals from mining-industrial activities, which often enter the environment with concentrate and tailings, or in the form of dust (fine particles from the accumulation of tailings) and dust (exhaust from the smelters), is a great danger for the environment [1, 2]. Arsenic is one of the most important and toxic inorganic pollutants; it is mainly produced as a by-product of extraction, processing, and smelting of base metals, especially copper-molybdenum ores (porphyry deposits), lead, cobalt, and nickel. In general, about 60% of arsenic in the environment comes from anthropogenic cycles, and the rest is nature-related [1, 3]. Arsenic and all its compounds are very toxic. The most toxic arsenic compound is arsenic gas (AsH_3); Breathing this gas at the rate of 0.01 (mg/m^3) in less than 5 seconds leads to human death.

In sulfide copper reserves, which are classified into three categories: arsenic-free reserves, low arsenic content reserves, and high arsenic content reserves; the occurrence of arsenic minerals (in low arsenic content reserves and high arsenic content reserves) is associated with hydrogen metasomatism, and is not associated with geotechnical changes in porphyry copper deposits [3, 4, 5]. During the formation process of these reserves, the evolution of liquids leads to a decrease in the amount of K^+, Na^+, Cu^+ ions

vis-à-vis H^+ ions and consequently the deposition of arsenic sulfosalts. Arsenic is found in porphyry-type copper sulfide deposits, in combination with elements such as copper, iron, etc., in the form of tennantite ($(Cu, Fe)_{12}As_4S_{13}$), arsenopyrite (FeAsS) minerals, to a lesser extent enargite (Cu_3AsS_4), and arsenic pyrite. In rare and complex cases, even small amounts of arsenic have been reported in the chalcopyrite mineral structure [4, 6-9]. For example, in the El Indio gold and copper deposit, Chile, enargite, and tennantite are the major minerals, and chalcopyrite, arsenopyrite, and tetrahedrite are the minor minerals in the deposit [10]. Arsenic is also present in copper mineralization of the Chelopech mine, Bulgaria, mainly in the form of copper-arsenic sulfosalts [7]. Therefore, the occurrence, dispersion, and distribution of arsenic will be different in different zones of a deposit. Accurate knowledge of grade variability, mineralogy, and processing properties of arsenic and copper ores in a copper sulfide deposit will make subsequent mining and processing decisions less risky.

The arsenic in copper ores can cause problems during extraction, processing, pyrometallurgy, and even in copper products. In addition, with the arsenic increase in the form of arsenite (AsO_3^{3-}) or arsenate (AsO_4^{3-}) in the tailings of sulfide ores and related processing plants, the acid mine drainage (AMD) generation issue arises [2, 11]. In suitable chemical dynamics and conditions (at the specific pH, Eh ranges) within the tailings deposition environment, arsenic-bearing species convert to each other and accumulate on the surface of other metal oxides and existing clay minerals. In the pH range of ordinary water, arsenite, which is more toxic than other arsenic compounds, will be more mobile and reactive. These problems lead to the dissolution of arsenic in water, and consequently the pollution of surface and groundwater as well as soil [12]. On the other hand, in the process of copper concentrate smelting, arsenic evaporates faster than other elements (temperature of 613 ˚C) and enters the environment through the chimneys of smelting furnaces. Arsenic-bearing gases (including AsO_3) will react rapidly during the condensation process in the environment with other elements (such as sulfur) due to their weight and will permeate the surrounding soil [7, 12-14]. According to measurements taken [15] to determine the amount of arsenic in the soils around copper smelters, the arsenic concentration of up to 40 mg/kg has been reported, while the amount of arsenic in non-contaminated soils is lower (5 mg/kg). The presence of arsenic with copper will cause problems in its applications. For example, arsenic will have adverse effects on its electrical properties due to the formation of compounds along the grain boundary after copper stabilization [8, 16]. Arsenic is a p-type metalloid and its four valance electrons are involved in bonding. As a result, arsenic is a non-conductive metalloid, and the lack of conductivity of arsenic is due to the lack of free electrons in its structure. Therefore, the presence of As atoms with Cu in equipment made of copper will affect its electrical properties. So, from a geo-environmentally standpoint, there are strict rules worldwide regarding the permissible level of arsenic in sulfide copper concentrate for entry into smelters. Smelters are only allowed to melt copper concentrates with less than 0.5% arsenic content, and if they receive more than 0.2% arsenic, they will be fined. According to commercial market rules, an increase of 0.2% arsenic in copper concentrate results in a fine of 2.5 $ per tonne for each 0.1% arsenic [17, 18].

The use of geometallurgical applications can be an effective solution to solve the arsenic challenge in copper concentrates. Although geometallurgy is not a new science, it has newly caught the attention of mineral processing industry. Geometallurgy combines geological information, mineral processing, and downstream processes, and provides a quantitative and comprehensive 3D model based on ore modifications for effective use in production planning and downstream process management. In fact, geometallurgy should be considered as a powerful tool for efficient utilization of resources and proper risk management, e.g. adaptation of the process to variations of ore, "what-if" analysis of alternative production strategies, forecasting of financial results, and assessment of environmental impact. In the present study, a geometallurgical approach were applied to address the challenge of arsenic in copper ore processing products and introduce a method for arsenic removal from copper concentrate in the Cu-Mo flotation circuit. The Sungun copper-molybdenum processing complex (located in northwestern Iran) was selected as a case study. In the part I of this study, the distribution of arsenic in different zones of the mine has been determined by examining the data and analysis of the selected core samples. Then, in the paper II by implementing a mineralogical approach, comprehensive information about the texture and structure of copper minerals and their relationship with arsenic-bearing minerals, have been obtained. On the other hand, the operating conditions of the existing circuit are examined, and then by

combining them with the mineralogical information of the process, the circuit is optimized to solve the challenge of the presence of arsenic in copper concentrate.

2. Sungun Cu-Mo deposit (case study)

Sungun copper-molybdenum deposit located in northwestern of Iran is of porphyry-monzonite type. Three different types of hydrothermal alteration and sulphide mineralization are recognized in Sungun (1) hypogene, (2) contact metasomatic (skarn), and (3) supergene. The first two types occurred almost simultaneously shortly after replacing porphyry stokes. The third type occurred after stokes is appeared on the ground (Fig. 1). Sungun deposit contains sulfide minerals and sulfosalts, including chalcopyrite, bornite, chalcocite, covellite, pyrite, molybdenite, sphalerite, marcasite, pyrrhotite, tennantite, enargite, galena, and digenite [2]. Chemical factors such as pH, Eh, and mineralogy of host rocks are the most important indicators of the formation of sulfide mineral complexes in the supergene and hypogenic zones of Sungun deposit [2, 19, 20].

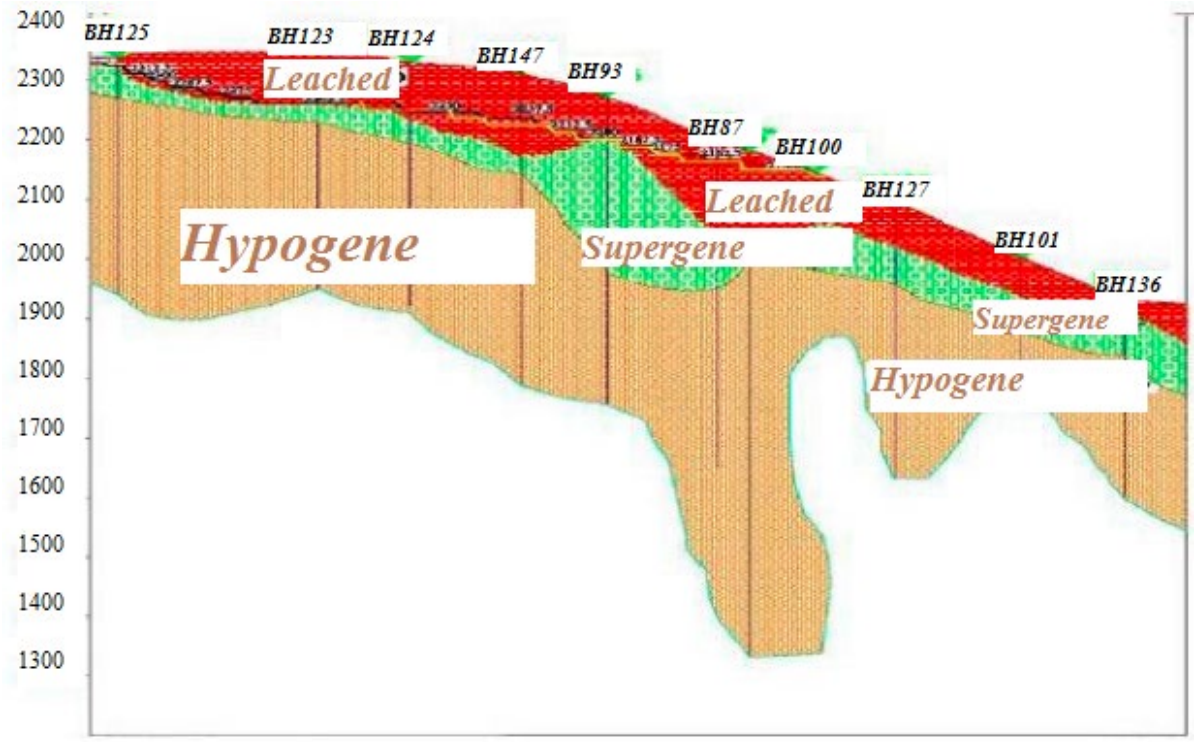


Fig. 1. Status of leached, hypogene and supergen zones in Sungun copper deposit in a vertical section [21]

The main mineralization of the Sungun deposit consists of copper and molybdenum sulfide minerals. According to the latest pit designs, the usable reserves in Sungun deposit are 522 million tons with a grade of 0.59% copper. In total, the total definite, probable and possible reserves in the Sungun deposit are about 1.9 billion tons of copper ore with a grade of 0.6%. It should be noted that in this mine, in addition to copper, molybdenum, other valuable elements including gold and silver are formed as associated metals. The presence of arsenic-bearing minerals or sulfosalt minerals containing arsenic including enargite – lawsonite and tennantite – tetrahedrite groups in Sungun porphyry deposit, is of great importance from the flotation of this ore and recovery of arsenic minerals to copper concentrate, standpoint. Therefore, understanding the behavior and distribution of arsenic in the Sungun mineral deposit and its changes in the extracted ore (processing plant feed) is an important and practical issue.

3. Distribution of arsenic in Sungun Cu-Mo deposit

To identify and exploration in the Sungun deposit, 186 exploratory boreholes with an approximate length of 60,000 meters have been drilled. On the cores obtained from these boreholes, about 27390 analysis have been performed to determine the amount of elements of copper (sulfide-oxide), iron, gold, silver, arsenic, lead and so on. Table 1 provides some information on the grade analysis of Sungun deposit exploration boreholes.

Table 1. Data from a number of exploratory boreholes at the Sungun copper mine

Sample No.	Depth (m)		Grade				
	From	To	As (ppm)	Cu (T) %	Cu (Ox.) %	Fe %	Mo (ppm)
NBH-03007	14	16	5300.9	0.0112	0.0024	25.70	73.7
NBH-05027	46	48	2326.2	0.9355	0.0411	6.12	30.0
NBH-52034	62	64	2166.9	1.1326	0.0275	5.16	67.8
NBH-07051	94	96	3402.0	1.2570	-	10.78	5.9
NBH-07053	98	100	1762.5	1.2056	0.0330	3.01	22.8
NBH-07055	102	104	1898.7	0.8878	0.0334	3.20	16.9
NBH-25070	126	128	1551.7	0.6477	0.0086	2.32	17.2
NBH-02107	190	192	1404.1	0.6515	0.0175	3.76	93.0
NBH-29123	220	222	1903.2	1.5084	0.0019	2.79	72.8

To investigate arsenic changes in the Sungun deposit, a block model of this deposit prepared by Macromine software (Fig. 2). Then, using the kiriging method, a variogram of arsenic grade changes (and other harmful elements in this reserve such as lead, zinc, etc.) is formed (Fig. 3). Based on the variogram drawn (Fig. 3) and the models fitted on it, the dispersion of arsenic is spherical. From arsenic variogram, arsenic grade kiriging method has been estimated for empty block model blocks. Finally, the block model of Sungun deposit is presented based on the above. Fig. 4 shows an image of a 3D modeled pit for the Sungun copper deposit in the Micromine software. This pit is modeled based on the concentration of harmful elements including arsenic in the mine area. In Fig. 4, the color change from blue to yellow and red indicates an increase in the concentration of harmful elements in that range. Depending on the shape, at the level of X in the range of 5200 to 5400, Y in the range of 8400 to 8600, and Z at the depth of 1850 to 2050, harmful elements, especially arsenic, have higher concentrations. In some parts of this range, the concentration of arsenic has reached about 0.1%. According to fig. 4, the arsenic concentration will increase with increasing mining depth and extraction of deeper nest pit.

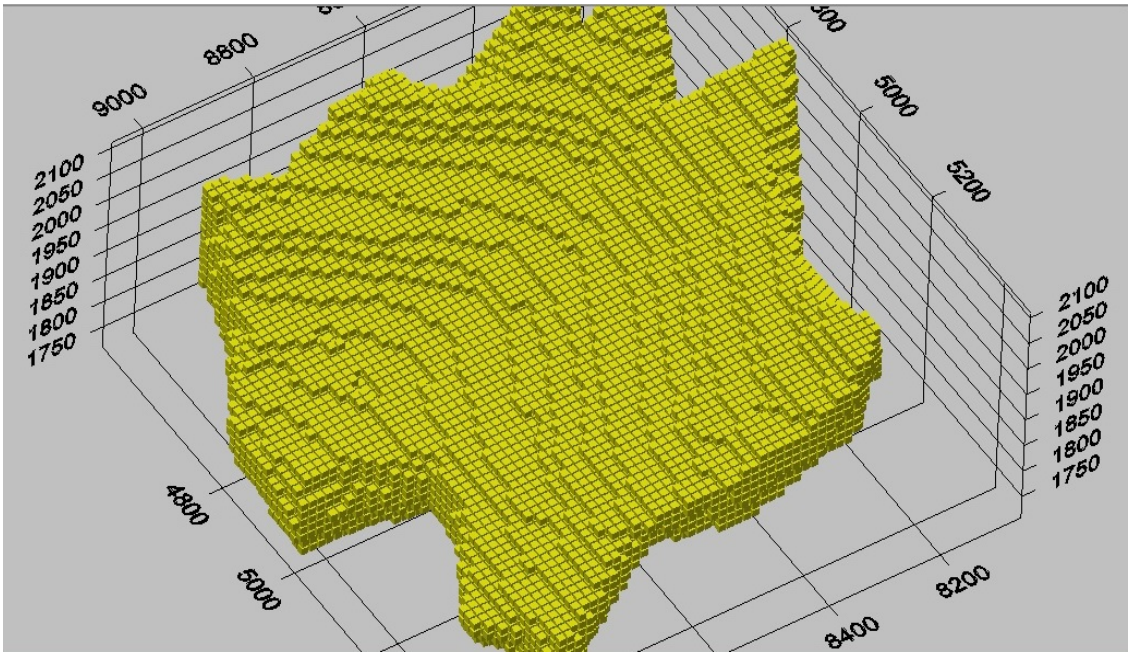


Fig. 2. Sungun deposit block model - Macromine software

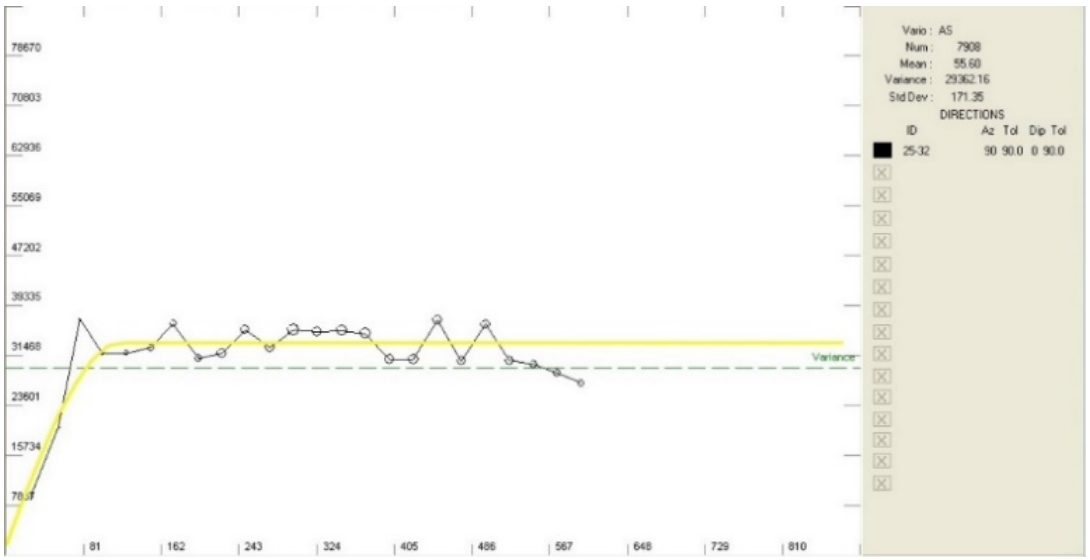


Fig. 3. Arsenic variogram in the Sungun deposit

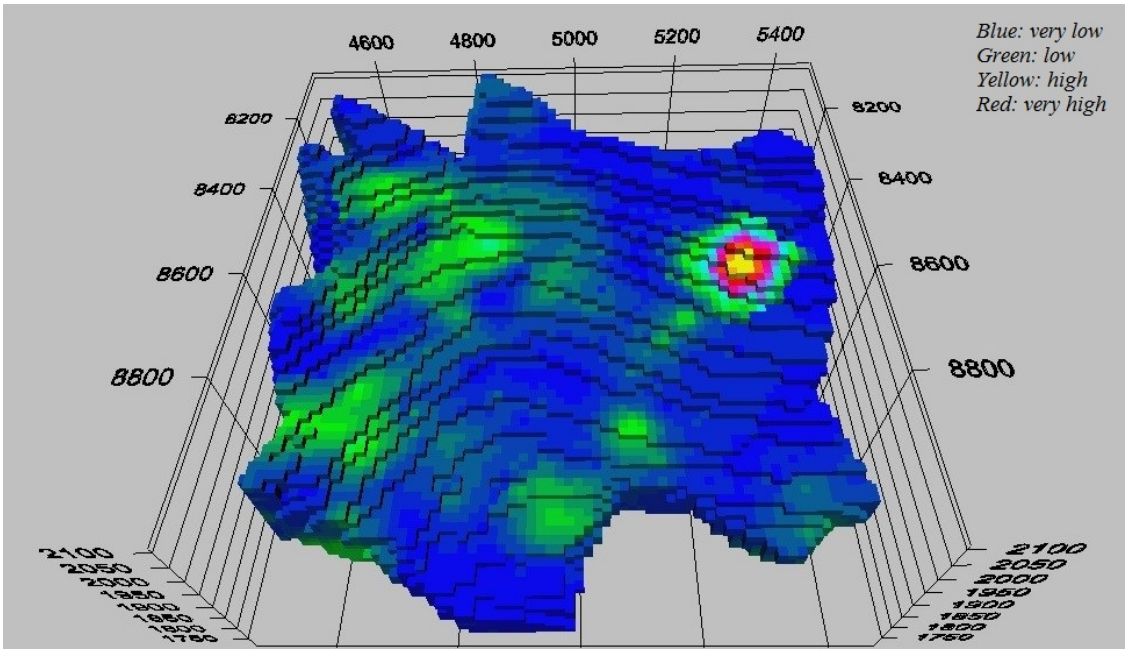


Fig. 4. Pit designed for Sungun copper deposit - green, colors indicate the concentration of harmful elements including arsenic (Micromine software)

The copper grade in the feed entering the plant is 0.6% and the exploitation cut-off grade in the Sungun copper mine is 0.2%. Examination of the amount of copper element in several existing cores samples from Sungun copper deposit (including 186 exploratory boreholes with an approximate length of 60,000 meters, about 27,390 point analysis of boreholes) indicates that about 15,430 points from this deposit have a copper grade more than 0.2%. Therefore, the volume containing the mentioned points after mixing (to obtain an input load with a copper grade of 0.6%), enters the Sungun copper processing plant as input load. Examination of points with a copper grade of more than 0.2% in the mentioned deposit has shown that in about 1180 points, the arsenic grade is more than 70 ppm. Considering the recovery values of copper and arsenic in the final concentrate of the plant, if the grade of arsenic in the input load to the plant is equal to or more than 70 ppm, its grade in copper concentrate will be more than the permissible level, i.e. 0.2%. On the other hand, extraction blocks with a copper grade of less than 0.2% copper will be transferred to the tailings dam; the arsenic content in which varies from 0.5-70 ppm and even more than 70 ppm. Due to the climatic conditions of the region (precipitation and wind), topography, ground and surface water conditions, the arsenic in the tailings depots will be prone to the generation of acidic drains and environmental problems.

4. Production planning of Sungun copper mine with a view to controlling the amount of arsenic

In the discussion of open pit mining planning, the phasing process takes place within the final area of the mine. The first phase of the mine is the part of the deposit, that grade of valuable element is the maximum amount and makes its extraction the most possible profit for the mine. As moved from phase one to the bottom phases, the net peresnt value from extraction per unit weight of ore decreases; So that the last phase of the mine, which will be according to its final range, will have the lowest profit. The above is related to economic phasing based on the present net value, which is also the basis for planning the production of the Sungun copper mine. An effective solution to solve the arsenic problem in Sungun concentrate is to desigen mining production planning based on geometallurgical models. In this way, the extraction of blocks and the order of nest pits in Sungun mine should be done based on the grade of copper and arsenic elements. The production planning of Sungun copper mine was carried out in eight phases with the view of ranking the blocks that play the most important role in arsenic extraction. Fig. 5 shows the phasing images used to extract the Sungun copper mine. In the design, the first phase contains the highest amount of arsenic and the eighth phase has the lowest arsenic hazards compared to other areas.

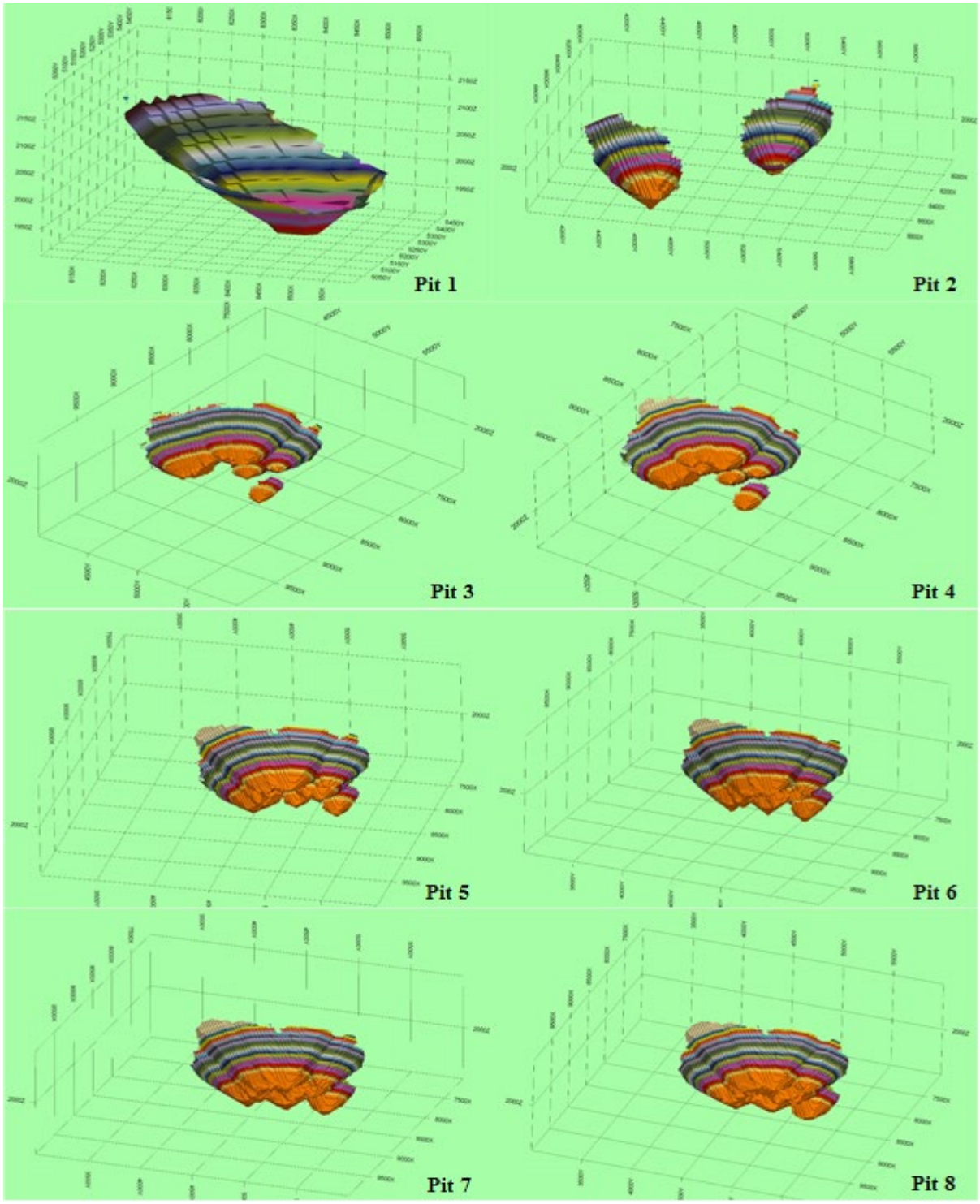


Fig. 5. 3D images of pits designed based on the geometallurgical program - production planning of Sungun copper mine (Blue: very low As, Green: low As, Yellow: very high As)

5. Conclusion

Examination of exploratory data from drilled boreholes for the Sungun copper deposit indicates that about 7.5% of the Sungun deposit contains arsenic more than 70 ppm. The entry of this feed into the Sungun processing plant, and the flotation process on it, will cause the concentration of arsenic with a grade of more than 0.25% in copper concentrate. This amount of arsenic in copper concentrate is more than the permissible standard. Modeling of Sungun pit based on the concentration of heavy elements and pollutants in it indicates the concentration of pollutants, including arsenic in a certain area of the

deposit, which increases with increasing depth, i.e. with increasing depth of mining in Sungun pit, the problem of arsenic in copper concentrate will become more serious and problematic. Therefore, a very effective solution to solve the problem of the arsenic presence in copper concentrate is the utilization of block extraction and simultaneous attention to the grade of copper and arsenic in the order of block extraction and their blending, i.e. development of mining production plan from a geometallurgical perspective can lead to a solution for the existing problem.

References

[1] Shayestehfar, M.R., Shafiee, N., Shirani, H., Rezaei, A. and Kargar Dianati, M.R. (2012). Distribution of As and Se elements in the soil of the Sarcheshmeh Copper mine area, Kerman. Journal of water and soil, 26(3): 533-534.

[2] Bahrami, A., Ghorbani, Y., Sharif, J.A., Kazemi, F., Abdollahi, M., Salahshur, A. and Danesh, A. (2021). A geometallurgical study of flotation performance in supergene and hypogene zones of Sungun copper deposit. Mineral Processing and Extractive Metallurgy, 130(2): 126-135.

[3] Tayebi-Khorami, M., Manlapig, E., Forbes, E., Bradshaw, D. and Edraki, M. (2017). Selective flotation of enargite from copper sulphides in Tampakan deposit. Minerals Engineering, 112, pp.1-10.

[4] Drahota, P. and Filippi, M. (2009). Secondary arsenic minerals in the environment: a review. Environment international, 35(8): 1243-1255.

[5] Lu, J., Tong, Z., Yuan, Z. and Li, L. (2019). Investigation on flotation separation of chalcopyrite from arsenopyrite with a novel collector: N-Butoxycarbonyl-O-Isobutyl Thiocarbamate. Minerals Engineering, 137: 118-123.

[6] Leybourne, M.I. and Cameron, E.M. (2008). Source, transport, and fate of rhenium, selenium, molybdenum, arsenic, and copper in groundwater associated with porphyry–Cu deposits, Atacama Desert, Chile. Chemical Geology, 247(1-2): 208-228.

[7] Long, G., Peng, Y. and Bradshaw, D. (2012). A review of copper–arsenic mineral removal from copper concentrates. Minerals Engineering, 36: 179-186.

[8] Plackowski, C., Nguyen, A.V. and Bruckard, W.J. (2012). A critical review of surface properties and selective flotation of enargite in sulphide systems. Minerals Engineering, 30: 1-11.

[9] HoungAloune, S., Hiroyoshi, N. and Ito, M. (2015). Stability of As (V)-sorbed schwertmannite under porphyry copper mine conditions. Minerals Engineering, 74: 51-59.

[10] Oyarzun, R., Lillo, J., Higueras, P., Oyarzún, J. and Maturana, H. (2004). Strong arsenic enrichment in sediments from the Elqui watershed, Northern Chile: industrial (gold mining at El Indio–Tambo district) vs. geologic processes. Journal of Geochemical Exploration, 84(2): 53-64.

[11] Bahrami, A., Kazemi, F., Alighardashi, A., Ghorbani, Y., Abdollahi, M. and Parvizian, A. (2020). Isolation and removal of cyanide from tailing dams in gold processing plant using natural bitumen. Journal of environmental management, 262: 110286.

[12] Cheng, H., Hu, Y., Luo, J., Xu, B. and Zhao, J. (2009). Geochemical processes controlling fate and transport of arsenic in acid mine drainage (AMD) and natural systems. Journal of hazardous materials, 165(1-3): 13-26.

[13] Bruckard, W.J., Davey, K.J., Jorgensen, F.R.A., Wright, S., Brew, D.R.M., Haque, N. and Vance, E.R. (2010). Development and evaluation of an early removal process for the beneficiation of arsenic-bearing copper ores. Minerals Engineering, 23(15): 1167-1173.

[14] Lane, D.J., Cook, N.J., Grano, S.R. and Ehrig, K. (2016). Selective leaching of penalty elements from copper concentrates: A review. Minerals Engineering, 98: 110-121.

[15] Mohamadi, S. (2019). Spatial distribution analysis of Copper, Zinc and Arsenic heavy metals in the soil of surrounding areas of Khatoon-abad copper smelter industry. Applied Soil Research, 6(4): 84-96.

[16] Cordova, R., Gomez, H., Schrebler, R., Real, S.G. and Vilche, J.R. (1996). An electrochemical study of enargite in aqueous solutions by transient techniques. Woods, R., FM Doyle and P. Richardson. Electrochemistry in Mineral and Metal Processing IV. Pennington: The Electrochemical Society Proceedings Series, 356.

[17] Fountain, C. (2013). The whys and wherefores of penalty elements in copper concentrates. Australasian Institute of Mining and Metallurgy. 5: 502–518.

[18] Hassanpour Kashani, R. (2021). Investigation of arsenic removal in the final concentrate of Sungun copper concentrators. MSc thesis in minerals processing, Urmia University.

[19] Abdollahi, M., Bahrami, A., Mirmohammadi, M.S., Kazemi, F., Danesh, A. and Ghorbani, Y. (2020). A process mineralogy approach to optimize molybdenite flotation in copper–molybdenum processing plants. Minerals Engineering, 157: 106557.

[20] Bahrami, A., Abdollahi, M., Mirmohammadi, M., Kazemi, F., Danesh, A. and Shokrzadeh, M. (2020). A process mineralogy approach to study the efficiency of milling of molybdenite circuit processing. Scientific Reports, 10(1): 21211.

[21] Bagheryan, A. (2006). Copper concentration process in the Sungun copper complex. National Iranian Copper Co.

Characterization and Evaluation of Glycine and Cyanide Leaching Application on Artisanal Gold Mining Tailings

Abdulbagi Hassan Abdallah Mohamed [1, 2, 4*], Abdou Azizi YOUPOUNGAM [3, 4], Taha BOYRAZ [1, 4], İbrahim ALP [1, 4]

[1] Karadeniz Technical University

[2] Hacettepe University

[3] University of Ngaounderé

[4] Ergold Innovation Eng. Srv. Ltd. Co., Teknokent No: 19/B

No:3301, 61080 Trabzon, Turkey

* Corresponding author: abdulbagiha94@gmail.com (Abdulbagi H. A. Mohamed)

Abstract:

In artisanal gold mining industry, due to the use of the inefficient amalgamation process, high grade gold and an alarming amount of mercury-containing tailings are released to the environment. Despite its distractive environmental effects, these tailings can be a potentially profitable source of gold. The current study focuses on artisanal gold mining (ASGM) tailing sourced from Cameroon. The sample was characterized physically, chemically, and mineralogically, as well as hydrometallurgically by applying traditional cyanidation and innovative glycine leaching. To identify the mineralogical and chemical composition of the sample, X-ray diffraction (XRD), X-ray Fluorescence (XRF) and scanning electron microscopy coupled with energy-dispersive X-ray spectroscopy (SEM-EDS) were used. Fire Assay and acidic digestion coupled with Inductively Coupled Plasma Mass Spectrometry (ICP-MS) were used to measure the grades of gold and other elements respectively. Mineralogical analysis indicated that the sample predominantly consists of quartz and some low aluminium and iron minerals grades. The main constituents were SiO_2, Al_2O_3, and Fe_2O_3. The gold and mercury grades of the sample were 14 ppm and 8 ppm, respectively. The median particle size of the sample (d_{50}) was 360µm. The results of leaching experiments revealed that by applying cyanide leaching, 87% of gold recovery was reached while the recovery rate of glycine leaching remained around 45%. On the other hand, both lixiviants did not achieve a satisfying mercury recovery which remained around 30 %.

Keywords: *ASGM Tailings, Characterization, Gold leaching, Mercury removal, Glycine leaching*

1. Introduction

Artisanal gold mining industry (ASGM) presents an important source of income in the developing countries where the alternative livelihood sources are limited (Hinton, et al. 2003); (Fisher 2007); (Tschakert 2009). Despite numerous attempts to give ASGM a precise definition, it seems to vary depending on the region. In some cases, it is considered an illegal mining practice carried out by individuals, families, and cooperative groups using rudimentary tools. In other situations, it is recognized as a fully manual, very small-scale illegal mining activity (Hentschel, et al. 2002). In this industry, mercury is used to extract gold and silver from the ground ores through amalgamation. The amalgam is then exposed to a source of heat to evaporate mercury and produce a billion consists of gold, silver and other metals (Adams 2016). But in some cases, mercury is removed by washing with hot nitric acid (Branch 1994).

ASGM industry is notorious for its adverse effect on the environment due to the utilization of mercury (Stoffersen, et al. 2019). Previous studies made before 2006 have estimated that ASGM releases around 1000 tons of mercury annually (Veiga, et al. 2006). According to recent estimations, ASGM stands as the world's largest air and water pollutant with mercury, accounting for approximately 37% (2058 tons) of

the total mercury emissions annually (Marshall, et al. 2020). However, the actual figures surpass these estimations. It was stated that to recover 1 gram of gold, 20 grams of mercury are required. Where 95% of it ends up in the tailings, while the remaining portion is released into the atmosphere (Ilyas & Lee 2018) this huge amount of mercury released annually serves as a strong indicator that millions of tons of ASGM tailings are generated every year creating a real threat to the environment Youpoungam, et al. (2024).

Despite the aforementioned disadvantages, ASGM has emerged as a significant economic contributor at both the individual and global levels (Marshall, et al. 2020). Some reports dated to 1998 estimated that the number of countries engaging in the industries was more than 55, which suggests that about 100 million citizens depend on this industry to secure their livening (Veiga, et al. 2006). Recent reports showed that the ASGM sector expanded to reach more than 70 countries and it accounts for approximately 20% of the world's total gold production, equivalent to 400 tons of gold per year (Marshall, et al. 2020).

ASGM is remarked with low gold recovery (Youpoungam, et al. 2024); during the amalgamation process there are many factors such as the degree of liberation of gold, gold grains size, pH of the pulp, mineralogy of the ore -especially sulphide minerals-, Need to be considered (Marsden and House 2006). Depending on these factors, in the best conditions, only about 60% of Au can be recovered while the remaining gold reports to the tailing which makes the ASGM tailing an attractively rich secondary source of gold that draws the attention of small and large mining scale companies (Bansah, et al. 2018). The economic potential of the tailings on the other hand has tempted many researchers to study them in order to propose a possible solution to assess and mitigate their environmental damage in addition to extracting the precious metals using either well-known methods such as cyanidation or newly invented technologies such as glycine leaching.

For more than a century, cyanide leaching has been the dominant process for extracting gold from primary and secondary sources due to its simplicity and cost-effectiveness. Mining operations worldwide utilize over 18% of the total global cyanide production, employing highly water-soluble forms of KCN and NaCN (Birich, et al. 2019). The mechanism behind gold dissolution in cyanide involves an electrochemical process, where sodium cyanide solutions with low concentrations (100-500 ppm) are used for gold recovery (Syed 2012). Recently, there has been a growing trend among major mining operators to invest in ASGM by purchasing them and extracting gold through conventional cyanide leaching. However, this practice poses a significant environmental threat as it results in the production of highly toxic cyanide-mercury compounds (Kozin and Hansen 2013), which can incredibly contaminate inland water through methylation and runoff (Ilyas and Lee 2018). Additionally, the well-known disadvantages of the cyanidation process have driven the industry to explore alternative methods that can provide safe and ecological gold recovery methods (Hilson and Monhemius 2006).

Recently, the glycine process was proposed as an alternative to cyanidation. The newly arising alternative does not only resolve the environmental shortcomings but also competes with cyanide in terms of cost and technical efficiency (Oraby, Eksteen et al. 2020) . Using this novel method, Youpoungam et al., (2023). conducted a study to address the environmental concerns associated with the use of cyanide in processing mercury-bearing ASGM tailings. The results of both gold leaching and mercury removal were very promising and can pave the way for more sustainable exploitation of ASGM tailings and eventually provide a dignified livelihood in the diverse geographies where the industry is practised.

The industry is mainly practised in Africa, South America and some parts of Asia (Hilson and Maconachie 2017). This study is dedicated to study an ASGM tailings sourced from Kombo Laka region in Cameroon, which is located approximately 490 km northeast of the capital Yaoundé and 51 km west of the Meiganga district. The area is geologically distinguished by the occurrence of many rock types present in the area such as volcano-sedimentary, metamorphic and other consolidated clays. However, Quartzites are the most common in the region (Ngouo, et al. 2021). According to Danga, et al. (2023) region's mineralogical composition mainly consists of quartz, kaolinite and muscovite, in addition to low concentrations of hematite, limonite, gibbsite, orthoclase, albite and calcite.

Generally, there are scarce studies on ASGM tailings Youpoungam, et al. (2024). However, some studies were conducted over samples from this area to serve a diversity of purposes, some were done to assess the pollution threats to the soil (Léopold, et al. 2016). Danga, et al. (2023) performed a study to measure the concentrations of the potentially toxic elements (PTEs) in the region while very few others were done to characterize the ASGM tailings. In this study the particle size distribution, mineralogical and the chemical composition of the sample will be studied. In addition, the applicability of gold leaching and mercury removal with the traditional cyanide leaching process as well as the novel and ecofriendly glycine leaching will be tested, which will open the avenue to the potential of gold recovery and save mercury removal.

2. Material and Methods

2.1. Material

A sample of about 13.5 kg was sourced from the Kombo Laka artisanal mining area in east Cameroon where ASGM activities are widely spread. In order to obtain two equally representative samples, the original sample was riffled into two samples. One of them was stored as a reference sample in a zipped plastic bag, while the other for the sake of conducting the planned experiments, was divided into sub-samples of about 870 grams using a rotary sample divider (Fritsch 27).

2.2. Sample Characterization

The particle size distribution of the sample was performed using vibratory wet sieving between 1400 to 38µm at The Department of Mining Engineering – Karadeniz Technical University. To determine the chemical composition of the sample, fire assay and inductively coupled plasma mass spectrometry analysis (ICP-MS) were used to determine the gold grade, while the other metals and elements concentrations were determined using acidic digestion and ICP-MS analysis. Followed by the conduction of X-ray fluorescence (XRF) to determine the major oxides in the sample, these tests were conducted at AR-Ge Test Laboratories - Türkiye. The mineralogical composition of the sample was determined with X-ray diffraction (XRD), and scanning electron microscopy (SEM) coupled with energy-dispersive X-ray spectroscopy (EDS) at The Central Laboratories of Karadeniz Technical University.

2.3. Characteristic Leaching

To evaluate the recovery of gold and removal of mercury hydrometallurgical, a conventional cyanide leaching was performed over the sample. The experiments' conditions were pH 10.5, cyanide concentration 1.5 g/l and leaching time of 24 hours. Parallelly, at the same experiment conditions but for less leaching time of 10 hours, another leaching experiment using 3 g/l of each glycine was also implemented. All the experiments were conducted at room temperature, agitation speed of 600 rpm and a liquid/solid ratio of 3. To measure gold concentration, leaching samples were analysed using (Perkin Elmer AAS AAnalst 400) Atomic Absorption Spectrometer, while the concentration of mercury was determined using (Perkin Elmer AAS AAnalyst 400) Atomic Absorption Spectrometer coupled with (Perkin Elmer/FIAS100) Flow Injection - Atomic Spectroscopy technique.

2.4. Reagents

For cyanide leaching, sodium cyanide (≥ 95 %), for glycine leaching analytical grade glycine were used. All these reagents are sourced from Merck. To adjust the pH of the solution and maintain it above 10.5 to create an alkali environment for the leaching process and prevent any formation of HCN in the case of cyanide leaching, 2 M of each sodium hydroxide (99%) and hydrochloric acid (37%) sourced from Isolab were used.

3. Results and discussions

3.1. Sieve Analysis

Particle size distribution is very crucial in the mining industry; it plays a substantial role in the behaviours of particles during the size reduction operations, concentration and dewatering processes (Fuerstenau and Han 2003). The result of particle size distribution of the tailings is presented in Fig. 1. The graph clearly indicates that the sample is relatively coarse, with a median particle size (d_{50}) of approximately 360 µm and d_{80} of 700 µm. This observation strongly implies that the gold present in the tailings is not sufficiently liberated due to the usage of primitive grinding machines in the ASGM sites. This observation is in agreement with what was reported by de Andrade Lima, et al. (2008); Saim, et al. (2021). However, the liberation process is more important if gold is to be recovered through leaching process, according to Veiga and Gunson (2020), the importance of the liberation becomes minimal when applying the gravity separation to separate quartz particles that contain about at least 15% gold, which gives it a specific gravity of 5.15 and therefore eases their separation.

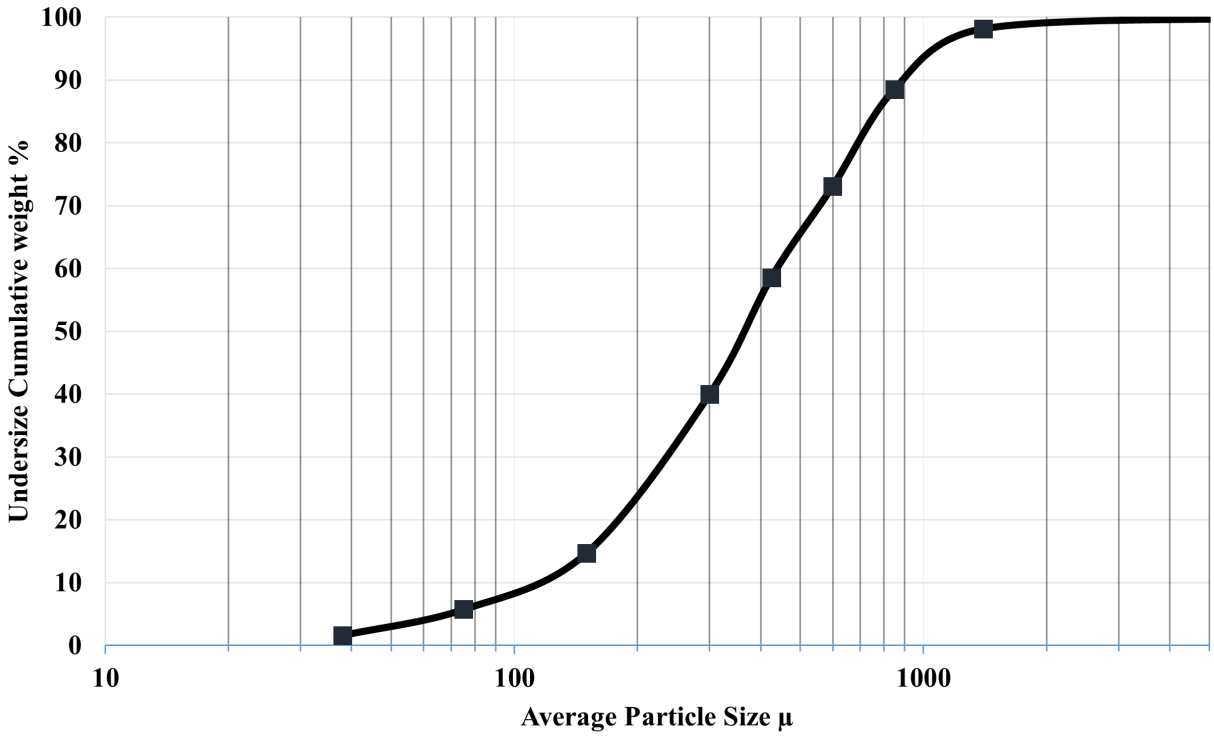


Fig. 1. Particle size distribution of the sample

3.2. Chemical Analysis

The results of the chemical analysis are represented in Table. 1. The sample's content of gold was found to be 14.5 ppm while the grades of silver, copper, and mercury were, 4.07, 275, and 8.2 ppm, respectively. The high grade of gold can be justified by the tailings' coarse particle size that led to insufficient liberation of gold and therefore poor recovery of the metal by the amalgamation process. Bansah, et al. (2018), reported the ASGM tailings are famous for their high mercury content. Accordingly, the low content of mercury in the sample can also be because of the large grains size of the sample which creates channels through which mercury leaks out. Either due to its high density or the washing out with rainwater. However, the sample's mercury content is still alarmingly higher than the globally allowed quantities.

Table 1. Concentrations of some important elements in the sample

Element	Au	Ag	As	Hg	Cu	Co	Bi	Ba	La	Mn
ppm	14.45	4.07	4.8	8.2	274.9	45.9	243.1	168.	9.9	724.4
Element	Mo	Ni	Pb	Sb	Sn	Sr	V	W	Zn	Zr
ppm	16.7	16.89	51.9	129.8	<5	4.1	56.6	<5	31	5.4
Element	Al	Ca	Fe	K	Mg	Na	P	S		
%	0.61	0.02	3.12	0.29	0.03	0.01	0.02	0.07		

The results of XRF revealed that the main component of the sample was found to be SiO_2 78%, accompanied by 9.65% and 5.8% of Al_2O_3 and Fe_2O_3, respectively as it is revealed in Table. 2. These results align with the results presented by Ayiwouo, et al. (2020), who related the abundance of these three oxides to the mineralogical domination of smectite in the area.

Table 2. Sample's major oxides composition%

Compound	SiO2	Al2O3	Fe2O3	K2O	MgO	TiO2	SO3	P2O5	CaO2	LOI
Grade%	78.07	9.65	5.79	3.38	0.54	0.21	0.17	0.06	0.04	1.94

3.3. Mineralogical Analysis

Mineralogically, as it is depicted in Fig. 2., the results of XRD showed a drastic domination of quartz. Kantarcı, et al. (2024); Youpoungam, et al. (2024) repeated almost the same composition of a sample sourced from Sudan. In addition to quartz, the analysis revealed the presence of various iron minerals such as goethite, ilmenite and magnetite, furthermore, the presence of rutile was also identified. For further characterization of the sample, SEM-EDS results were also presented.

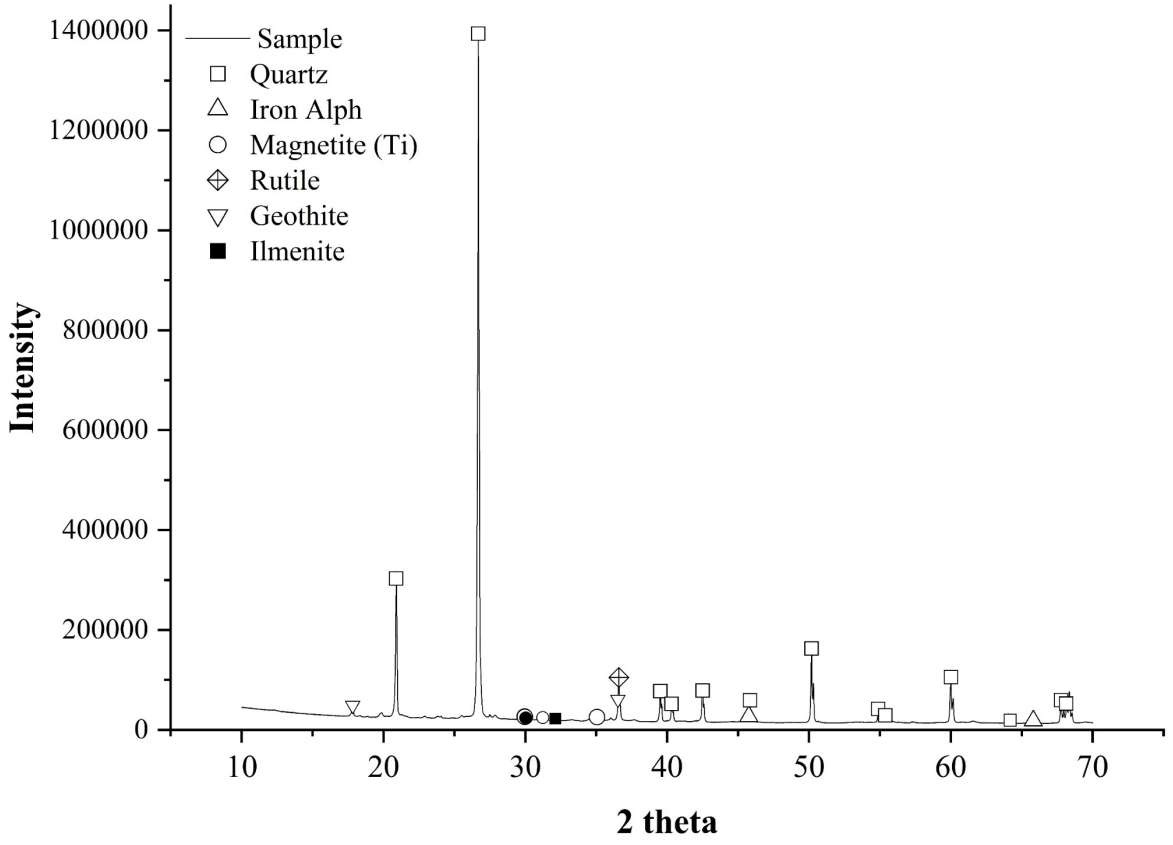


Fig. 2. XRD analysis of the sample

The SEM images and EDS spectra are shown in Fig. 3. It can be noticed from the EDS spectrum (a) of spot 1 that gold was found together with some aluminium and iron minerals which indicates that gold was not fully liberated, the percentage of gold in the very spot was found to be more than 93%. The composition of the spectrum (b) was another validation of the domination of quartz in the sample, it also indicated the occurrence of some clay minerals. Similarly, spectrum (c) showed the composition of spot 2. where the existence of mercury in addition to some iron and copper was determined. The existence of sulphur at this spot not only indicated the presence of some iron and copper sulphide minerals but might also designated that the sample contained some cinnabar which explains the low recovery of mercury during leaching experiments.

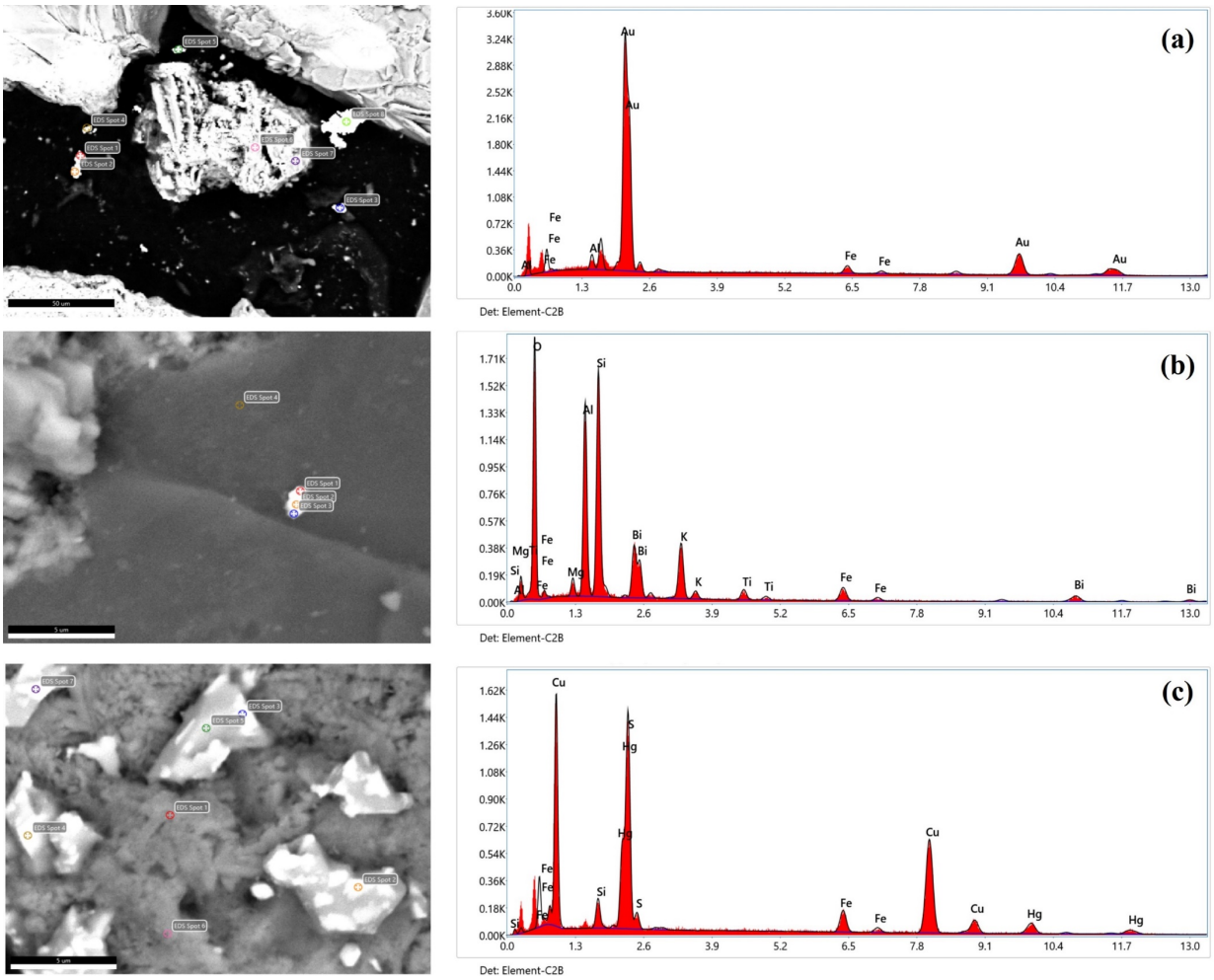


Fig. 3. SEM Imaging, and EDS spectra of the sample

3.4. Leaching Results

In their experiment on an ASGM tailing with almost similar mineralogy to the currently used sample Alkloos and Aydoğan (2024), obtained gold recovery of 87.5% at experimental conditions of stirring speed of 400 rpm, a temperature of 25 °C, a liquid/solid of 1.5, a pH of around 10.5 and a cyanide concentration of 500 ppm. Regarding mercury leaching Pramudya (2015) reported that extraction rates of mercury alongside gold can vary between 10 – 40% depending on many factors, however, de Andrade Lima, et al. (2008) claimed the achievement of gold and mercury recovery of 89% and 100%, respectively. In this study as it is depicted in Fig. 4. (a), cyanide gold leaching rate reached 87% within a time frame of 24 hours while only 28% of mercury was recovered.

In a study conducted by Youpoungam A. A., (2023), under leaching conditions of pH range of 10-11, temperature of 20-25°C, and glycine concentration of 2 g/l, more than 90% of the gold and mercury were recovered from a fine grinding ASGM tailings within 8 hours. On the light of these findings the

leaching kinetics of gold and mercury were tested for period of 10 hours as in Fig.4 (b). unexpectedly, the recoveries were very low wherein only 45.6% of gold was recovered. On the other hand, the recovery of mercury reached its maximum rate of 33% in the 4th hour before starting to fluctuate between 20 – 30%.

Overall, the low gold kinetics during both cyanide and glycine leaching can be ascribed to the coarse particles of the sample which require a long time for cyanide to defuse to locked-in gold particles and a longer time for glycine to reach unliberated particles owing to its larger molecular diameter which hinders its diffusion as compared to cyanide, also the based on the literature, glycine leaching in this study was not given sufficient time as compared to cyanide leaching. in the same context, the insufficient mercury recovery may be due to fierce the competition between mercury and sliver during the leaching process.

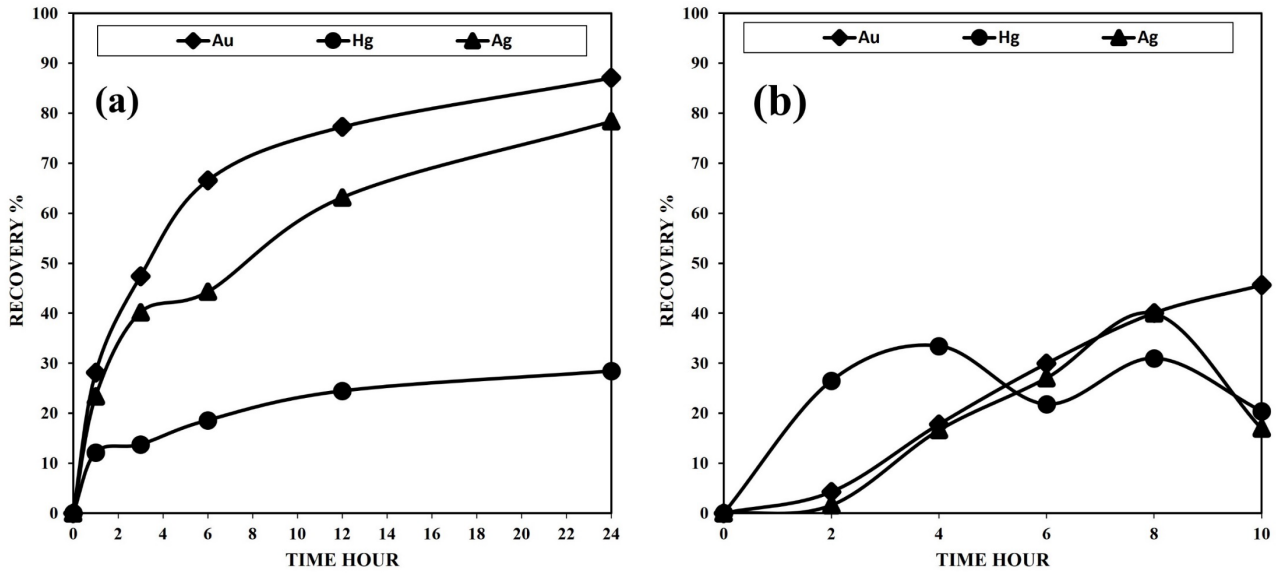


Fig. 4. Results of cyanide leaching (a), pH 10.5, NaCN 1.5 g/l, time 24 hours, L/S 3 and agitation speed 600 rpm, and glycine leaching (b), pH 10.5, glycine 3 g/l, time of 10 hours, L/S 3 and agitation speed 600 rpm.

4. Conclusion

This study mainly aimed to characterize and assess the possibility of applying cyanide and glycine leaching to economically and ecofriendly exploit the tailings. The results of sample characterization revealed that the sample primarily consisted of quartz, along with aluminium and titanium as well as various iron minerals. Chemical analysis results indicate the sample contains a considerably high grade of gold with 14.45 ppm. Mercury content of the sample was assessed to be 8 ppm weaving a quite serious threat to the ecological system.

The results of cyanide leaching test, despite its low kinetics, yielded a good gold recovery of 87%. Unlike glycine leaching which reached only 45%, which was justified by the large particle size of the sample (d_{80} = 700 µm) that impeded the diffusion of glycine solution to the locked-in gold particles in addition to the insufficient leaching time. Overall, mercury leaching rates were very low which can be attributed either to the serious competition imposed by other metals or the occurrence of some mercury as stubbornly insoluble cinnabar.

The authors believe that if the sample is sufficiently ground and the leaching time extended, the gold and mercury leaching rate of glycine can tremendously be enhanced whereas a saver gold recovery and mercury removal can be sought. Additionally, the authors think that more characterization is required to identify the nature of mercury in the sample, according to which suitable removal and mitigation procedures can be made in case glycine leaching does not achieve the expected results.

Acknowledgement

The authors hereby, acknowledge the support of The Scientific and Technological Research Council of Turkey - Directorate of Scientist Support Programs (TÜBİTAK - BİDEP) for financing this research through project NO: (122M489).

References

Adams, M. (2016). Gold ore processing: Project development and operations. Elsevier.

Alkloos, B., & Aydoğan, S. (2024). Cyanidation of tailings in artisanal small-scale gold mining at Arbaat Region in Red Sea State, Sudan. Scientific Mining Journal, 62(4), 191-196.

Ayiwouo, M. N., Ngueyep, L. L. M., Mache, J. R., Kingni, S. T., & Ngounouno, I. (2020). Waters of the Djouzami gold mining site (Adamawa, Cameroon): Physicochemical characterization and treatment test by Bana smectite (West, Cameroon). Case Studies in Chemical and Environmental Engineering, 2, 100016.

Bansah, K., Dumakor-Dupey, N., Stemn, E., & Galecki, G. (2018). Mutualism, commensalism or parasitism? Perspectives on tailings trade between large-scale and artisanal and small-scale gold mining in Ghana. Resources Policy, 57, 246-254.

Birich, A., Stopic, S., & Friedrich, B. (2019). Kinetic investigation and dissolution behavior of cyanide alternative gold leaching reagents. Scientific Reports, 9(1), 7191.

Branch, S. W. (1994). Technical Resource Document, Extraction and beneficiation of ores and minerals. (Vol. 4): U.S. Environmental Protection Agency Office of Solid Waste.

Danala Danga, S., Ekengele Nga, L., Makhubela, T., Ibrahim, B., Bitom, D., & Kramers, J. (2024). Assessing soil contamination by potentially toxic elements in artisanal and small-scale gold mining sites of the Adamawa Region, Cameroon. Geochemistry: Exploration, Environment, Analysis. https://doi.org/10.1144/geochem2023-2055

Danga, S. D., Nga, L. E., Makhubela, T. V., & Bitom, D. L. (2023). An assessment of soil pollution from artisanal gold mining in Wantia Area (Meiganga, Cameroon). Copernicus Meetings.

de Andrade Lima, L., Bernardez, L., & Barbosa, L. A. D. (2008). Characterization and treatment of artisanal gold mine tailings. Journal of Hazardous Materials, 150(3), 747-753.

Fisher, E. (2007). Occupying the margins: Labour integration and social exclusion in artisanal mining in Tanzania. Development and Change, 38(4), 735-760.

Fuerstenau, M. C., & Han, K. N. (2003). Principles of mineral processing. SME.

Hentschel, T., Hruschka, F., & Priester, M. (2002). Global report on artisanal and small-scale mining. Report commissioned by the Mining, Minerals and Sustainable Development of the International Institute for Environment and Development. http://www.iied.org/mmsd/mmsd_pdfs/asm_global_report_draft_jan02.pdf

Hilson, G., & Maconachie, R. (2017). Formalising artisanal and small-scale mining: Insights, contestations and clarifications. Area, 49(4), 443-451.

Hilson, G., & Monhemius, A. J. (2006). Alternatives to cyanide in the gold mining industry: What prospects for the future. Journal of Cleaner Production, 14(3-4).

Hinton, J., Veiga, M. M., & Beinhoff, C. (2003). Women and artisanal mining: Gender roles and the road ahead. In The socio-economic impacts of artisanal and small-scale mining in developing countries (Vol. 2, pp. 161-203).

Ilyas, S., & Lee, J.-C. (2018). Gold metallurgy and the environment. CRC Press.

Kantarcı, S., Alp, İ., & Youpoungam, A. A. (2024). Potassium Amyl Xanthate (PAX) as an alternative organic reactive for mercury removal from cyanidation process of amalgamation tailing. Environmental Geochemistry and Health, 46(1), 28.

Kozin, L. F., & Hansen, S. C. (2013). Mercury handbook: Chemistry, applications and environmental impact. Royal Society of Chemistry.

Léopold, E. N., Sabine, D. D., & Jung, M. C. (2016). Physical and metals impact of traditional gold mining on soils in Kombo-Laka area (Meiganga, Cameroon). International Journal of Geosciences, 7(09), 1102.

Marsden, J., & House, I. (2006). The chemistry of gold extraction. SME.

Marshall, B. G., Camacho, A. A., Jimenez, G., & Veiga, M. M. (2020). Mercury challenges in Mexico: Regulatory, trade and environmental impacts. Atmosphere, 12(1), 57.

Ngouo, K. S., Rose, Y. F., & Séverin, K. D. (2021). Prospecting of gold mineralization indices in the eastern of Meiganga (Adamawa Region, Cameroon). Open Access Library Journal, 8(7), 1-21.

Oraby, E., Eksteen, J., & O'Connor, G. (2020). Gold leaching from oxide ores in alkaline glycine solutions in the presence of permanganate. Hydrometallurgy, 198, 105527.

Pramudya, I. (2015). Investigation of mercury reduction in gold stripping process at elevated temperature (Doctoral dissertation). University of Nevada, Reno.

Saim, A. K., Cobbinah, I. J., Gbedemah, G. M. K., Nurudeen, Z. K., & Amankwah, R. K. (2021). Characterisation of small-scale gold mining tailings in the Western Region of Ghana. Ghana Mining Journal, 21(2), 27-32.

Stoffersen, B., Køster-Rasmussen, R., Cardeño, J. I. C., Appel, P. W., Smidth, M., Na-Oy, L. D., Lardizabal, D. L., & Onos, R. W. (2019). Comparison of gold yield with traditional amalgamation and direct smelting in artisanal small-scale gold mining in Uganda. Journal of Health and Pollution, 9(24).

Syed, S. (2012). Recovery of gold from secondary sources—A review. Hydrometallurgy, 115, 30-51.

Tschakert, P. (2009). Recognizing and nurturing artisanal mining as a viable livelihood. Resources Policy, 34(1-2), 24-31.

Veiga, M. M., & Gunson, A. J. (2020). Gravity concentration in artisanal gold mining. Minerals, 10(11), 1026.

Veiga, M. M., Maxson, P. A., & Hylander, L. D. (2006). Origin and consumption of mercury in small-scale gold mining. Journal of Cleaner Production, 14(3-4), 436-447.

Youpoungam, A. A. (2023) Investigation of Mercury Removal and Gold Recovery Methods from Amalgaming Wastes. K. T. U., The Graduate School of Natural and Applied Sciences, PhD Thesis, Trabzon.

Youpoungam, A.A., Kantarcı, S. & Alp, İ. Characterization and Reprocessing of Artisanal and Small-Scale Gold Mine Tailings. Mining, Metallurgy & Exploration (2024). https://doi.org/10.1007/s4246

A Review on Shape Characterization of the Gold and Copper Metallic Particles Recovered from the Flotation of Various E-wastes

Fırat Burat [1], Beyzanur Keleş [1], Nazlım İlkyaz Dinç [1], Halide Nur Dursun [1], Ugur Ulusoy [2]*,

[1] Istanbul Technical University, Mineral Processing Engineering Department, Maslak Istanbul, 34469, Türkiye,

[2] Sivas Cumhuriyet University, Chemical Engineering Department, Sivas 58140, Türkiye

*Corresponding author: uulusoy@cumhuriyet.edu.tr (Ugur Ulusoy)

Abstract:

The recovery of copper and gold metals from waste electrical and electronic equipment (WEEE) materials, which accumulate rapidly as a result of the renewal of technology in the world day by day, is not only necessary but also mandatory due to the principle of circular economy and ecological concerns. Although it is known that particle shape plays an active role in ore flotation, the effect of particle shape in the flotation process used in the recycling process of e-waste materials has not yet been fully examined. Moreover, the inherent difficulties encountered in floating coarse grains in conventional flotation of these metallic ores are well known. Thus, in this work, a novel flotation approach was used to recycle various e-wastes, including waste printed circuit boards (WPCBs), waste electrical wires (WEWs), and waste RAM boards (WRAMs), in an easier, and environmentally friendly manner. It aims to pre-concentrate valuable (Cu, Au) metallic particles by selective and coarse-grained flotation after removing the plastic. In this pursuit, the shapes of particles from each flotation product were quantified in terms of shape descriptors such as elongation and roundness to investigate the effect of shape on the flotation recovery. It was found that coarse flat metallic particles were successfully recovered by two-stage selective flotation with high grade and recovery by taking advantage of the fact that these metals flatten during the comminution process and become particles with a large surface area due to their softness and ductility properties.

Keywords: *Particle shape, recycling, flotation, gold, copper*

1. Introduction

In the global decarbonization transition toward the accomplishment of sustainable, effective, and net-zero operations by 2050, metals such as copper and gold are vital materials for the emerging technologies batteries, fuel cells, motors, wind, PV, robotics, drones, 3D printing, and ICT (European Commission, 2020).

On the other hand, e-waste production, which is rising at a concerning rate of roughly 2.5 Mt per year (Forti et al., 2020) is expected to reach 74.7 Mt in 2030 (Nithya et al., 2021). In this regard, enormous quantities of various waste electrical and electronic equipment (WEEE) resources such as waste printed circuit boards (WPCBs), waste electrical wires (WEWs), and waste RAM boards (WRAMs) are annually accumulated in the world.

Today, the focus is on how to reduce environmental impact while simultaneously providing maximum production through improved accuracy in mining and processing, as traditional mining methods involve energy-intensive processes producing a lot of waste and emitting greenhouse gases (GHG). Because recycling is a more practical and economical method of obtaining and using these metals as it requires less energy than metal production, it is a core part of the overall copper and gold value chain. For instance, printed circuit boards and mobile phones contained 200 to 350 grams of gold per metric ton (Grehl and Sehrt, 2012). In addition, it is important to note that the purity of copper and gold metals recovered from e-waste materials is higher than ore concentrates. Moreover, the recycling of metals from WEEE has significant benefits for the environment, the economy, and society (Charles et al., 2017;

Bunting et al., 2006; WCED, 1987). Environmentally speaking, one 32 MB RAM module requires 32 L of water, 1.6 kg of fossil fuels, 700 g of gases, and 72 g of extra chemicals (Goosey, 2009).

Recently, flotation has become increasingly used in the separation of e-waste materials. When secondary electronic resources such as WEWs, WPCBs, and WRAMs are recycled to recover metals they first go into size reduction, metal particles with plastics are made up of solid particles that can be classified according to several factors, such as particle size and shape. Since particle shape is a variable that has a big impact on how the particulate systems behave and how products are processed and performed, it is essential to measure this metric as a result. Thus, particle shape can be changed based on the intended performance, enhancing the quality and functionality of the end product. However, it turns out to be rather challenging to estimate particle shape precisely in practice since there is currently no accepted method for measuring particle shape.

When recovering metals became challenging, the metal mining industry recognized the significance and implemented the flotation method. Thus, coarse particle flotation has been considered one of the most promising methods (Patel, 2021). It has been reported that coarse particle flotation implies floating feed particles above the typical range of conventional flotation (>150 μm) (Kohmuench et al. 2018). The use of coarse particle flotation presents the chance to decrease comminution-related energy costs, boost throughput by reducing the amount of time spent in the comminution circuit and prevent the release of gangue phases that might be harmful to subsequent processes (Asamoah et al., 2018; Dankwah et al., 2022). Therefore, it has drawn interest from both the mining industry and flotation research in recent years. Previous works propose that the flotation of free or liberated gold is greatly influenced by physical constraints, such as the size and shape of the particles, as well as froth stability and bubble loading (Dunne, 2005; Teague et al., 1999). Since particle shape is a factor that significantly affects the attachment of hydrophobic particles to the air bubble in the flotation process (Ulusoy, 2023), it is critical to measure this parameter in this approach. For example, particle shape, surface coatings, liberation, and composites are physical factors that can affect native gold's flotation (Allan and Woodcock, 2001). The comminuted WEEE's flotation behavior in the system will differ because it contains composite materials of various sorts, as well as various particle sizes and shapes to liberate gold and copper. In addition, coarse flotation of copper and gold metal particles is more advantageous regarding efficiency, energy consumption, and environmental concerns than fine flotation methods. Moreover, there is a paucity of research focused on the correlation between particle shape and the flotation of e-waste materials. To the best of the authors' knowledge, this study is one of its kind, i.e., the production of coarse WEEE particles (e.g., 1-5 mm) eliminates the fine grinding steps. With this motivation in mind, applying a coarse and selective flotation approach is introduced as the promising parameter in this review to explore the effect of particle shape on the recovery of copper and gold metallic particles in secondary metallic resources like WEEE for less environmental impact and more economic benefits.

2. Materials and Methods

2.1. Material Preparation

In this review, various WEEE material samples such as WPCBs and WEWs from Turkish recycling companies working in Kocaeli, and Ankara of Turkiye were used (Burat et al., 2023; Keleş et al., 2024). The schematic flowsheet for flotation studies of various WEEE materials such as WPCBs and WEWs (Burat et al., 2023) and WRAMs (Keleş et al., 2024) are given in Fig. 1.

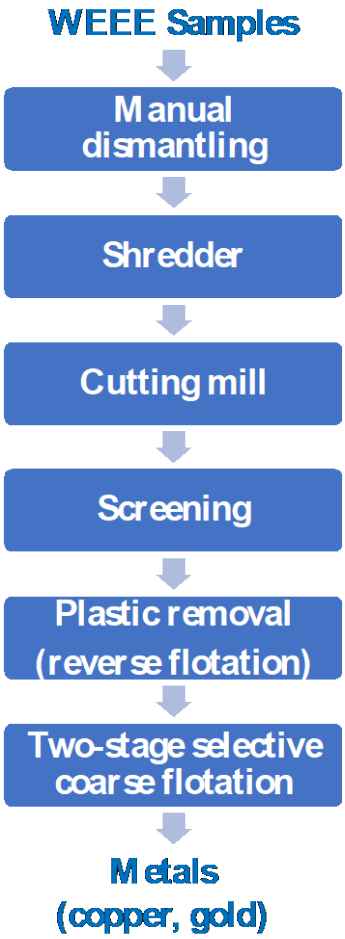


Fig. 1. Flowsheet of the flotation of WEEE materials

Before flotation tests, WEEE materials were manually disassembled to remove the detrimental impact of contaminants in chemical enrichment processes that will be used in the advanced stage. Following dismantling and manual sorting, size reduction of WEEE samples was first conducted by using a shredder (Netplasmak Co.) and a cutting mill (RAM200 Rantek Co.) in the Pilot Plant of the Mineral Processing Engineering Department in ITU to liberate metals from plastics, and fibers in this composite material. After sieve analysis, samples that had undergone various size reduction processes were divided into various size fractions for the flotation tests, i.e., −1, −0.5, −0.212, and −0.106 mm sized samples for WPCBs and WEWs, and −4, −2, −1, and −0.5 sized samples for WRAMs.

2.2. Flotation Experiments

With the presence of a collector and frother and making use of the variations in surface properties between plastic and metal particles, multi-stage flotation tests were conducted by using a self-aerated 1.5 L Denver-type cell.

Since plastic particles due to their natural hydrophobic properties were floated without a collector or frother, and then in the first stage, large plastic particles were floated using 300 g/t MIBC for WPCBs and WRAMs. In the second stage of flotation, copper particles were concentrated with 900 g/t KAX.

For the case of WRAMs flotation tests, after the plastic removal by the first stage, copper particles begin to float in the second stage of metal flotation, and gold particles start to float in the third stage (after 600 g/t of KAX addition) of metal flotation.

The flotation experiments for the plastics and metallic particles recovered from various WEEE materials used were given in Table 1 based on the following conditions.

The following equation (1) was used to determine the recovery rate:

$$R\ (\%) = \frac{Cxc}{Fxf} x100 \quad (1)$$

where F and C are the feed and concentrate quantities, respectively. In addition, f and c are the metal content of the feed and concentrate products, respectively.

Table 1. Flotation test conditions of various WEEE materials used in this work (modified from Burat et al., 2023; Keleş et al., 2024).

Material	Type of Flotation	Parameters	Values
WPCBs-WEWs	Plastic flotation	Particle size, mm	−1
		Stirring speed, rpm	1100
		pH	8.1 for WPCBs 7.6 for WEWs
		MIBC, g/t	100+100+100
		Conditioning time, min.	3+3+3
		Flotation time, min.	3+3+3
		Air flow rate, L/min	3
	Metal flotation	Particle size, mm	−1
		Stirring speed, rpm	1200
		pH	8.1 for WPCBs 7.6 for WEWs
		KAX, g/t	900
		MIBC, g/t	300
		Conditioning time, min.	3+3+3
		Flotation time, min.	3+3+3
		Air flow rate, L/min	4
WRAMs	Plastic flotation	Particle size, mm	−4, −2, −1, and −0.5
		Stirring speed, rpm	1100
		pH	7.8
		MIBC, g/t	100+100+100
		Conditioning time, min.	3+3+3
		Flotation time, min.	3+3+3
	Metal flotation	Particle size, mm	−4, −2, −1, and −0.5
		Stirring speed, rpm	1200
		pH	7.8
		KAX, g/t	300+300+300
		MIBC, g/t	50+50+50
		Conditioning time, min.	3+3+3
		Flotation time, min.	3+3+3

2.3. Particle Shape Characterization

Owing to the natural hydrophobic properties, the plastics were removed by reverse flotation firstly for the investigation of the behavior of the shape of the copper and gold particles in flotation. Then, the shape characterization tests of the copper and gold particles in the concentrate and tailing products were implemented. Shape characterization studies of representative samples of products obtained after flotation of WEWs, WPCBs, and WRAMs were carried out using an optical microscope. Microscopical images provide insight into the characterization of the shape of the precious and other particles in the various flotation products as well as liberated particles, in addition to helping to see the color differences of particles in the samples (Ulusoy and Atagun, 2023). Material was obtained from each size fraction and put in an observation glass to be looked at under an optical microscope (Leica, Germany). Then, analog signals from the collected images were transmitted through a camera to digital media. The particle shape of each sample was characterized by recording microscope images of representative samples of flotation products as digital images with a camera and performing a 2D manual measurement of the axis of each particle projection on these images. The major (length; L) and minor (width; W) axes of the metallic particles were measured after importing the images in the COREL DRAW 10 program, as shown in Fig. 2. It was used as input in the Microsoft Excel to calculate the shape parameters based on the data obtained, assuming that the projection of the particle had an elliptical form (Forssberg and Zhai, 1985).

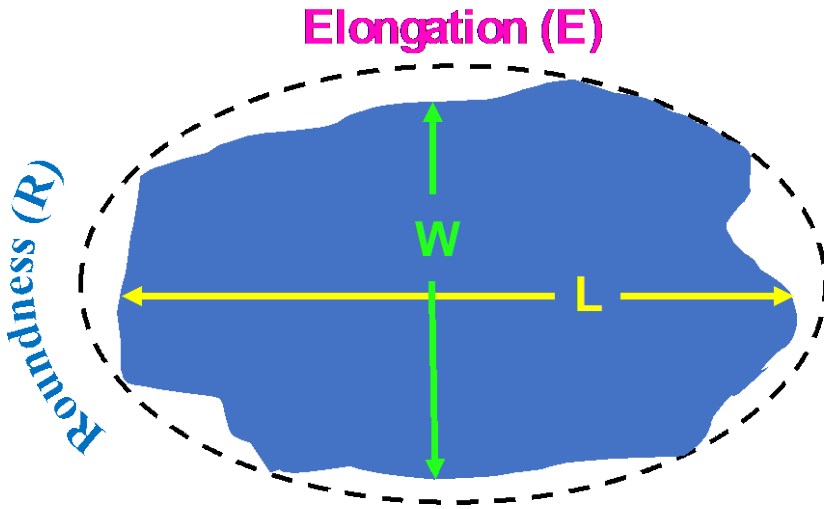


Fig. 2. The elliptical approach used for the shape characterization by the measurement of the major and minor axis for the particle projection

Each particle underwent five measurements along its major (L) and minor (W) axes, and the arithmetic mean of those measurements was determined. The mean length (L) and width (W) of those particles were then calculated using the image's scale. Approximately all particles for every image were subjected to the same method for each product. As a consequence, the area (A) and perimeter (P) of the particle projection were calculated (Equations (2) and (3)), using the measured mean length and breadth as input (Beyer, 1978).

$$\text{Area (A)} = \frac{\pi LW}{4} \tag{2}$$

$$\text{Perimeter (P)} = \frac{\pi}{2}\,\frac{3(L+W)-\sqrt{(LW)}}{2} \tag{3}$$

The parameters Elongation (E) and roundness (R) (equations (4) and (5)), the two most commonly used shape factors in the literature for particle shape characterization, were calculated from the average L and W values for each sample (Heywood, 1947; Hausner, 1966; Hagerman et al., 1980). It should be noted that irregular particles have roundness values ranging from 0 to 1, while a perfectly round grain has a maximum roundness value of 1.0. On the other hand, it should be known that elongation

corresponds to a minimum value of 1 for a perfectly round ideal grain, and this ratio becomes larger than 1 as the grain becomes irregular (Ulusoy, 1996; Ulusoy, 2003).

$$\text{Elongation (E)} = \frac{L}{W} \quad (4)$$

$$\text{Roundness (R)} = \frac{4\pi A}{p^2} \quad (5)$$

3. Results

3.1. Waste Printed Circuit Boards (WPCBs)

Since it is well known that WEEE materials are significantly heterogeneous and complex in terms of the type, size, and shape of components and materials (Cui and Forssberg, 2003), the role of particle shape on the recovery of copper and gold metals from WEEE was investigated. Fig. 3 shows that coarse platy copper particles were found in the concentrate compared to the sink products that contain round alloy particles along with locked copper particles.

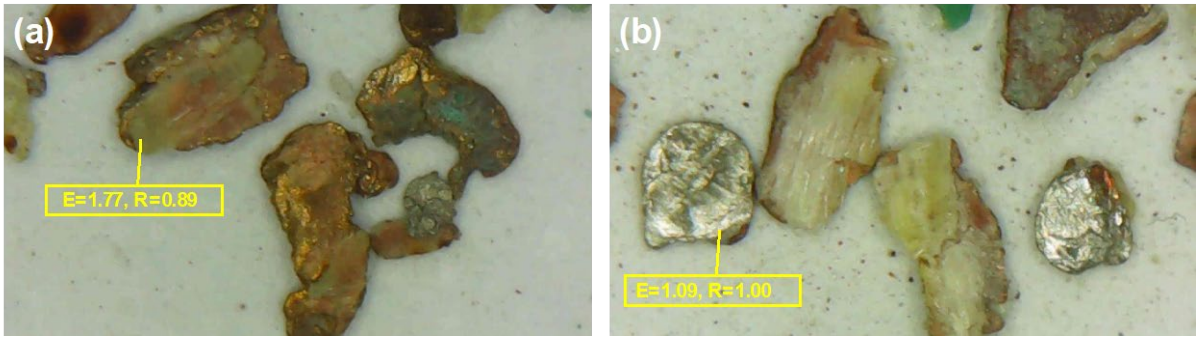


Fig. 3. Comparison of particle shape between flotation products of WPCB (a) float 2 product (copper) and (b) sink product.

3.2. Waste Electric Wires (WEWs)

The surface characteristics of the particles have a direct impact on the flotation process in addition to the effects of particle size and shape. The results of particle shape characterization tests for the WEWs are given in Fig. 4. As clearly seen in Fig. 4 the concentrate product (float 3) has coarse and flat copper particles while mostly coarse and pressed-shaped aluminum particles, hydrophilic ceramic particles, and extremely thick copper wires were found in the sink product. Additionally, the sink product has a high Sn content. This is due to the fact that copper particles with tin-coated surfaces do not float and stay in the sink product.

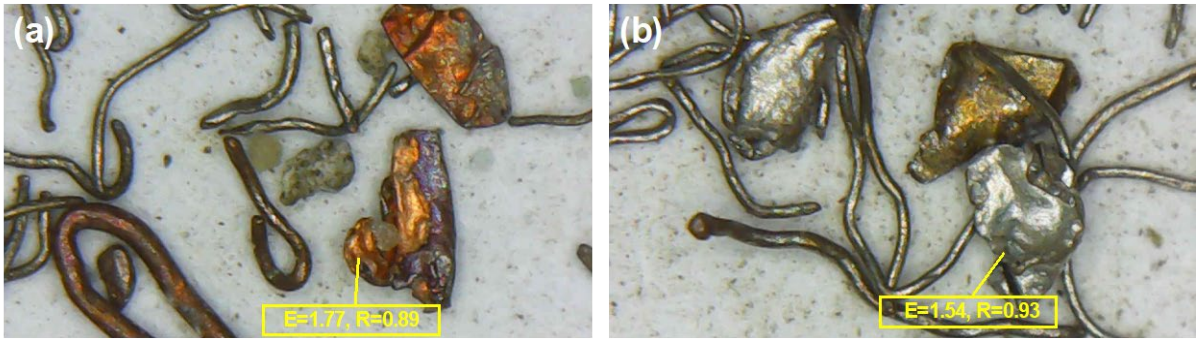


Fig. 4. Comparison of particle shape between flotation products of WEW (a) float 2 (copper) and (b) sink product.

3.3. Waste RAM Cards (WRAMs)

The results of particle shape characterization tests for the WRAMs are given in Fig. 5. As seen from Fig. 5 a, d, g, and j, copper particles measured for shape characterization of each size fraction such as −4, −2, −1, and −0.5 mm, represent coarse flaky, and elongated particles recovered from WRAMs samples by flotation, i.e., the E values vary between 2.50 and 1.77 on the other hand R values were changed from 0.73 to 0.93. Because RAMs usually contain small but significant amounts of gold-plated needles and a thin layer of gold on their surface, coarse elongated and platy gold particles recovered from WRAM samples by flotation as seen from Fig. 5 b, e, h, and k for the size fraction such as −4, −2, −1, and −0.5 mm. Moreover, it has been observed that gold particles have rounded surfaces as the particle size is reduced. As clearly seen in Fig. 5 c, f, i, and l, the sink product has still unlocked coarse particles, which cause insufficient metal and non-metal particle separation. Because it is clear that the solder mask and fiberglass remain bound to the crushed board components. It should be noted that the shape parameters like E and R were calculated based on 2D elliptical assumption and the third dimension (thickness) was not considered. Therefore, the greater particle size and surface area are of importance for the floatability as well as E and R parameters. A higher surface expression shown by coarse free particles compared to fine particles is also important for their floatability, as they provide more sites for bubble attachment (Kohmuench, 2018).

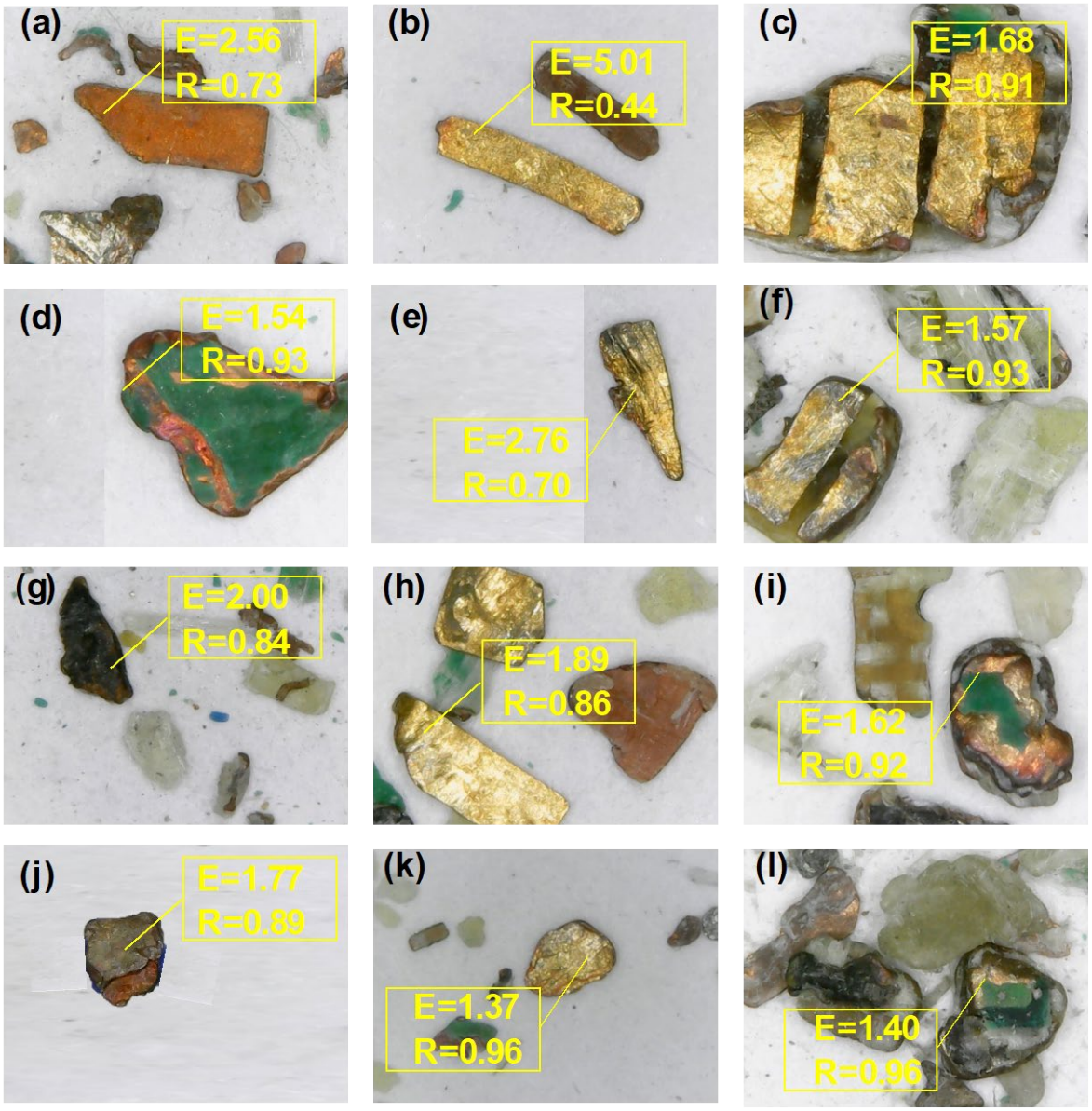


Fig. 5. Comparison of particle shape between flotation products of WRAMs (a) −4 mm float 1 (copper) and (b) −4 mm float 3 (gold) and (c) −4mm sink product (d) −2 mm float 1 (copper) and (e) −2mm float 3 (gold) and (f) −2 mm sink product (g) −1mm float 1 (copper) and (h) −1 mm (gold) and (i) −1 mm sink product (j) −0.5 mm float 1 (copper) and (k) −0 5 mm float 3 (gold) and (l) −0.5 mm sink product (Burat et al., 2023; Keleş et al., 2024).

4. Discussion

In gold ore flotation, it is known that if gold particles are larger than 200 µm, it becomes difficult to transport them to the concentrate with air bubbles due to the weight of the particles (Teague et al., 1999; Malhotra and Harris, 1999). Besides, gold flattens and becomes particles with a large surface area during grinding processes prior to flotation because gold metal has an important property of softness. In other words, thanks to the ductile properties of WEEE material, it is inevitable to obtain different metallic particles in different shapes during crushing and grinding. This makes it difficult for the gold particles to be carried by air bubbles and increases the amount of collectors that must be used (Adams, 2016; Dunne, 2005). Moreover, the softness of gold is also an issue because it can prevent different mineral particles from adhering to the gold surface during the grinding processes (Taggart and Behre, 1945). Traditional flotation machines, which are used to recover precious metals such as gold and copper from their ores by flotation, are mostly designed for particles smaller than 150 µm. However, in this study, it was possible to obtain these metals as separate concentrates thanks to the flat, large (approximately 1 to

4 mm) particles that they transformed into by size reduction. In other words, valuable metallic particles such as copper and gold can be recovered as free coarse particles in the concentrate due to their affinity to attach air bubbles with their platy shapes by the size reduction equipment. Overall results are in good agreement with the previous studies, i.e., it is well known that native gold frequently becomes flattened during grinding (Hallbauer and Joughin, 1973; Pevzner et al., 1966). Tourtelot and Riley (1973) observed irregular flattish lumps of native gold in coarser sizes, which are or may be significant in regard to their flotation. Native gold flakes mined from a placer deposit in Mexico, according to Aksoy and Yarar (1989), exhibited natural hydrophobicity. It has also been previously reported that its flaky shape, porosity, and hydrophobic surface properties often cause gold to float (Wang and Poling, 1983; Mitchell et al., 1997). It has been reported by another study that flat particles definitely affect the recovery of gold by flotation, as they offer a larger surface area against the action of collectors and air bubbles and settle more slowly in a fluid compared to cubic particles of equal mass (Allan and Woodcock, 2001). Tatariants et al. (2018) successfully recovered flaky gold particles from full-size WRAMs after the separation of all metallic and non-metallic components of RAM by using organic solvent and ultrasonication treatment in a developed reactor. It is also worth noting that the results are in good agreement with the findings of the article by Ma et al. (2023), who concluded that the fact that the floated particles have more edges and vertex increases the efficiency of their adhesion to air bubbles and enlarges the three-phase contact line. In other words, the edge makes it easier for the water film between the bubble and the particle to drain, thin, and rupture, which raises the attachment efficiency.

5. Conclusions

This work provides a straightforward, efficient, and practical solution for secondary resource utilization by recovering gold and copper metallic particles by using a coarse particle selective flotation approach after plastics removal.

Since particles with different sizes and shapes are created by the size reduction in the recycling of WEEEs, the separation of particles with different particle shapes and sizes in pre-concentration processes was turned into an advantage. In other words, it is obvious that the large-sized metallic concentrate obtained will directly contribute to process improvement and environmental problems in subsequent metallurgical processes.

After the plastics were successfully removed by reverse flotation due to their hydrophobic structure in the first stage of the flotation, coarse copper particles were recovered in the second stage and gold particles were recovered with high efficiency by selective flotation in the third stage.

Moreover, when the shapes of the particles in various flotation products were quantified by shape characterization tests in terms of elongation and roundness parameters, it was found that the copper and gold particles in WPBCs, WEWs, and WRAMs were released in large sizes and were flat-shaped and floated by easily attach to air bubbles with the help of the collector.

Therefore, the approach used in this study will shed light on designing an economical and environmentally friendly process by producing a pre-concentrate with high metal content through selective coarse particle flotation processes to be applied before metallurgical processes. Separation of coarse metal particles is more advantageous than the separation of fine particles by traditional flotation, as it is more efficient, consumes less energy, and is more environmentally friendly making it a particularly ideal technology to accomplish sustainable development goals (SDG 3, 6, 8, 11, 12, and 14) for WEEE. Therefore, the recovery of coarse copper and gold metallic particles by the flotation approach developed in this work will help to contribute to the regenerative economy to restore and replenish resources and ecosystems as well as emphasizing long-term thinking and promoting circular systems, and innovative solutions that benefit both people and planet.

Finally, with this approach, the production of copper and gold metals from primary sources can also be reduced. Thus, it is hoped that the approach used in this study will pave the way for future research in the recovery of metals from e-waste materials.

Funding

This research received no external funding.

References

Adams, M.D. (2016). *Gold Ore Processing – Project Development and Operations*. second ed.: Elsevier Science, Amsterdam.

Aksoy, B.S., & Yarar, B., (1989). *Natural hydrophobicity of native gold fales and their flotation under different conditions*. Proceedings of Complex Ores, New York (pp.19–27): Halifax, Pergamon Press.

Allan, G.C., & Woodcock, J.T. (2001). Review of flotation of native gold and electrum. *Minerals Eng*. 14, 9, 931–962. doi: 10.1016/S0892-6875(01)00103-0.

Asamoah, R.K., Skinner, W., & Addai-Mensah, J. (2018). Alkaline cyanide leaching of refractory gold flotation concentrates and bio-oxidised products: The effect of process variables. *Hydrometallurgy*, 179, 018, 79–93, doi: 10.1016/j.hydromet.2018.05.010.

Beyer, W.H. (1978). *Handbook of Mathematical Sciences*, 6th ed. (pp. 7–30): CRC Press.

Bunting, G., Huxtable, L., & Clement, M., (2006). *Strategic solutions for resource efficiency*. The 13th International Conference of the Greening of Industry Network – Integration and Communication: A Clear Route to Sustainability? Cardiff, Wales, UK.

Burat, F., Dinç, N.İ., Dursun, H.N., & Ulusoy, U. (2023). The Role of Particle Size and Shape on the Recovery of Copper from Different Electrical and Electronic Equipment Waste. *Minerals* 13 (7) 847. doi: 10.3390/min13070847.

Charles, R.G., Douglas, P., Hallin, I. L., Matthews, I., & Liversage, G. (2017). An investigation of trends in precious metal and copper content of RAM modules in WEEE: Implications for long term recycling potential. *Waste Management,* 60, 505-520. doi: 10.1016/j.wasman.2016.11.018.

Cui, J., & Forssberg, E. (2003). Mechanical recycling of waste electric and electronic equipment: A review. *The Journal of Hazardous Materials*, 243–263. doi: 10.1016/S0304-3894(03)00061-X.

Dankwah, J.B. Asamoah, R.K. Zanin, M., & Skinner, W. (2022). Dense liquid flotation: Can coarse particle flotation performance be enhanced by controlling fluid density?. *Minerals Eng*ineering, 180, 107513. doi: 10.1016/j.mineng.2022.107513.

Dunne, R. (2005). *Flotation of gold and gold-bearing ores*, Developments in Mineral Processing, 15, 309–344. doi: 10.1016/S0167-4528(05)15014-5

European Commission, (2020). Critical materials for strategic technologies and sectors in the EU – a foresight study, https://rmis.jrc.ec.europa.eu/uploads/CRMs_for_Strategic_Technologies_and_Sectors_in_the_EU_2020.pdf

Forssberg, E., & Zhai, H. (1985). Shape and surface properties of particles liberated by autogenous grinding. *Scandinavian journal of metallurgy,* 14, 1, 25–32.

Forti, V., Baldé, C. P., Kuehr, R., & Bel, G. (2020). *The Global E-waste Monitor Quantities, flows and the circular economy potential.* https:// www. itu. int/ en/ ITU-D/ Environment/ Documents/ Toolbox/ GEM_ 2020_def. pdf (accessed on 30 April 2023).

Goosey, M. (2009). Introduction and overview. *Electronic Waste Management – Design, Analysis and Application*, (pp. 4–39): Cambridge University Press.

Grehl, M. & Sehrt, U., (Eds.) (2012). *Precious Materials Handbook*, first ed. Umicore AG & Co KG, Hanau-Wolfgang, Germany.

Ma, G., Bu, X., Ulusoy, U. & Xie, G. (2023). Effect of particle shape on bubble-particle attachment behavior: roles of surfaces, edges and vertexes. *Journal of Cleaner Production* 429, 139606. doi: 10.1016/j.jclepro.2023.139606

Hagerman, T.H., Black, K., Lilliesköld. 1980. Shape and surface of mineral grains tested for mortar and concrete purposes through image analysis. *Swedish Council for Building Research*: Stockholm, Swedish, Volume 26, pp. 63–72.

Hallbauer, D.K., & Joughin, N.C. (1973). The size distribution and morphology of gold particles in Witwatersrand reefs and their crushed products. *Journal of the Southern African Institute of Mining and Metallurgy,* 73, 395–405.

Hausner, H.H. (1966). Characterization of the powder particle shape. *Planseeberichte für Pulvermetallurgie,* 14 (2), 75–84.

Heywood, H. (1947). The scope of particle size analysis and standardization. *The Institution of Chemical Engineers, Symposium on Particle Size Analysis*, February 4, 1947. Supplement to Transactions, Institution of Chemical Engineers, London, Vol. 25, pp. 14-24.

Keleş, B., Dinç, N., Dursun, H., Burat F., & Ulusoy, U. (2024). The effect of particle geometry (size & shape) on the recovery of gold and copper metallic particles from end-of-life random access memory cards by flotation. *Waste Management*, 179, 66-76. doi: 10.1016/j.wasman.2024.03.008.

Kohmuench, J., Mankosa, M., Thanasekaran, H., & Hobert, A. (2018). Improving coarse particle flotation using the HydroFloat™ (raising the trunk of the elephant curve). *Minerals Eng*. 121, 137–145. doi: 10.1016/j.mineng.2018.03.004.

Malhotra, D., & Harris, L. (1999). *Review of plant practices of flotation of gold and silver ores, Advances in flotation technologies,* Southfield, MI, USA, (p. 167–181): SME.

Mitchell, C.J., Evans, E.J., & Styles, M.T. (1997). *A Review of Gold Particle-size and Recovery Methods, British Geological Survey Technical report* WC/97/14, February, Overseas Geology Series, https://nora.nerc.ac.uk/id/eprint/9014.

Nithya, R., Sivasankari, C., & Thirunavukkarasu, A. (2021). Electronic waste generation, regulation and metal recovery: A review. *Environmental Chemistry Letters,* 19, 1347–1368. doi: 10.1007/s10311-020-01111-9.

Patel, H.A. (2021). Coarse Particle Flotation of Coarse Gold and Gold-bearing Ore by Fluidized-bed-flotation, *MSc. Thesis*: University of Nevada.

Pevzner, M.L., Shcherbakov, V.I., & Kosova, L.Ya, (1966). Behavior of gold during grinding (in Russian). *Tsvetne Metally*, 1966, 39(5) 11-12.

Taggart, A.F., & Behre, H.A. (1945). *Handbook of mineral dressing, ores and industrial minerals*: John Wiley & Sons.

Tatariants, M., Yousef, S., Denafas, G., Tichonovas, M., & Bendikiene, R. (2018). Recovery of gold, other metallic and non-metallic components of full-size waste random access memory. *The Journal of Cleaner Production,* 172, 2811–2823. doi: 10.1016/j.jclepro.2017.11.132.

Teague, A.J., Van Deventer, J.S.J., & Swaminathan, C. (1999). A conceptual model for gold flotation. *Minerals Engineering*, 12(9), 1001–1019. doi: 10.1016/S0892-6875(99)00087-4.

Tourtelot, H.A., & Riley, L.B. (1973). *Size and Shape of Gold and Platinum Grains. Ores in Sediments*. International Union of Geological Sciences, (vol 3): Springer.

Ulusoy, U. (1996). *M.Sc. Thesis* (Unpublished), METU, Ankara, Turkey.

Ulusoy, U. (2003). *Ph.D. Thesis* (Unpublished), Cumhuriyet University, Sivas, Turkey.

Ulusoy, U. (2023). A review of particle shape effects on material properties for various engineering applications: From macro to nanoscale. *Minerals*, 13, 91. doi: 10.3390/min13010091.

Ulusoy, U., & Atagun, O.N. (2023). Particle shape characterization of shaking table streams in a Turkish chromite concentration plant by using dynamic imaging and microscopical techniques. *Particulate Science and Technology*, 41, 141–150. doi: 10.1080/02726351.2022.2046666.

Wang, W., & Poling, G.W. (1983). Methods for recovering fine placer gold, *CIM Bulletin*, 76, 860, 47–56.

WCED, (1987). *Report of the World Commission on Environment and Development: Our Common Future.* Oxford University Press, Oxford, http://un-documents.net/ocf-02.htm (accessed 23 September 2023).

Yoon, R-H., Mao, L.Q.J. (1996). Application of Extended DLVO Theory, IV: Derivation of Flotation Rate Equation from First Principles. *Journal of Colloid and Interface Science*, 181 (2) 613–626. doi: 10.1006/jcis.1996.0419.

Minor Cu-Au-Co-Bi-Te Mineralization at The Jalal-Abad Iron Ore Deposit, Northwestern Zarand, Iran

Behrouz Karimi Shahraki [1]*, Behzad Mehrabi [2], Ziaeddin Pourkarimi [1]

[1] Iran Mineral Processing Research Center (IMPRC)

[2] Kharazmi University, Faculty of Earth Sciences, Geochemistry department

*Corresponding author: e-mail (Behrouzkarimi1389@gmail.com)

Abstract:

Jalal-Abad Iron Ore Deposit hosted by the Early Cambrian volcanic and sedimentary units (CVSU). The main ore mineral is magnetite, without surface exposure, and has been oxidized to hematite and goethite at shallow level and along fractures. The large volumes of hydrothermal alteration surround the orebodies and mainly localized along shear zones. The alteration assemblages include sodic-calcic (albite, actinolite), potassic, sericite, chlorite, quartz, and carbonate. Copper mineralization is dominated by supergene minerals (malachite, atacamite and azurite) which replace former sulphide mineralization, and chalcopyrite is only observed at deeper levels which is associated with magnetite. Cu mineralization occured as disseminated form in magnetite or as a veins and is normally replaced by covellite along the fractures and crystals rim. Gold is mainly associated with copper sulphides and gold-bearing chalcopyrite veins generally crosscut the pyritic ore. Native gold detected as less than 50 µm grain size in pyrite and chalcopyrite. EPMA analyses indicate that arsenopyrite, cobaltite [(Co,Fe)AsS] and bismuthinite (Bi_2S_3) occur as open space and fracture filling texture and bismuthinite is accompanied by a small amount of tsumoite (BiTe). The Jalal-Abad deposit exhibits many features which have also been described from major IOCG deposits.

Keywords: *Jalal-Abad, Iron Oxide, IOCG, Cu Mineralization, Gold*

1. Introduction

The Jalal-Abad iron ore deposit is located 38 km northwest of Zarand town in Kerman province in the Poshtebadam-Bafq-Zarand mining district, Iran (Fig. 1). It contains 200Mt of iron ore with an average grade of 45% Fe, 1.18% S and 0.08% P (Technoexport 1976). Iron ore deposit is hosted by the Early Cambrian Rizu Series (CVSU), composed mainly of sedimentary, volcanic, and volcaniclastic rocks which are dominated by dolomite, sandstone, shale, siltstone, tuff, ignimbrite, and rhyodacite. The Poshtebadam-Bafq-Zarand district is located in the central and southern sections of the Kashmar-Kerman Zone (KKZ) and comprises more than 34 iron ore anomalies and deposits which host over 2 Gt of iron oxide ore (NISCO 1980; Torab and Lehmann 2007; Stosch et al. 2011; Bonyadi et al. 2011). The Jalal-Abad iron deposit is located in the southeastern part of KKZ (Fig. 1). Zircon U–Pb dating of rhyodacite in the CVSU unit assign a minimum age of 528±0.8Ma (Ramezani and Tucker 2003). Iron oxide deposits in the Poshtebadam-Bafq-Zarand district considered as the major iron metallogenic province in central Iran. These deposits display many similarities in respect of ore mineralogy and hydrothermal alteration (Stosch et al. 2011; Bonyadi et al. 2011; Mehrabi et al. 2019). These known deposits contain significant amounts of apatite, with negligible Cu mineralization and unreported Au mineralization which classified them as iron oxide-apatite (IOA) deposits (Bonyadi et al. 2011). The igneous activity in the Jalal-Abad includes felsic volcanic rocks, small mafic intrusive bodies and diorite and gabbro dykes (Mehrabi et al. 2019). Locally diorite and gabbro at the Jalal-Abad depositexhibit which have been altered to chlorite and sericite. The Geological and geochemical evidenses indicate that hydrothermal activity during the Early Cambrian at the Jalal-Abad deposit caused the iron ore mineralization as well as high temperature dolomitization (Mehrabi et al. 2019; Mehrabi et al. 2014). In this study we present the detailed mineralogy mainly aimed at investigation on Cu-Au-Co-Bi-Te Mineralization in the Jalal-Abad deposit.

2. Material and methods

Thin sections, polished thin sections and polished blocks were prepared for petrographic studies and were examined using a Zeiss Axioscope optical microscope at the Iranian Mineral Processing Research Center (IMPRC). X-ray diffraction analyses were performed on a Philips Xpert-pro model using Co Kα1 (1.789010Å) radiation, monochromator on secondary optics, 40kV power and 35mA current at IMPRC. Mineral analyses were obtained by a CAMECA SX100 Electron Microprobe (EPMA) at IMPRC.

2.1. Material

2.1.1. Mineralization

Iron mineralization at the Jalal-Abad deposit has occurred in the surface and mostly in deep parts. In the deep parts, iron mineralization is mainly associated with hydrothermal alteration minerals. Researches have been carried out in deep sections on drilled boreholes core. Magnetite is the most important mineral in depth and is associated with actinolite, chlorite, sericite, quartz, dolomite, calcite and talc (Fig.2a and 2b) and formed as massive, space filling, and vein forms (Mehrabi et al. 2019; Mehrabi et al. 2014). In the north-western and central part of the study area, small outcrops of massive iron ores are in contact with dolomite (Fig.1). In the Jalal-Abad deposit, iron oxide ore has very limited outcrop, and information on its extent is mostly obtained from geophysics and drilling. Mineralization has occurred in siltstone, tuff, acidic volcanic and dolomite rocks, and the original nature of these rocks has been completely changed and altered minerals have replaced them. Electron microscopic studies showed that apatite is present in the Jalal-Abad deposit in a very small size and in small amounts. Due to hydrothermal fluids water rock interaction, dolomite has recrystallized and in addition, tremolite-actinolite and talc have been formed (Mehrabi et al. 2014). Chlorite, talc, calcite, dolomite, actinolite and quartz are the most important gangue minerals in the Jalal-Abad deposit, which fill the space between magnetite crystals. Oxidation of magnetite to hematite (martitization) is not observed in the deep levels of the deposit and mainly occurred in the surface and shallow levels (Fig.2b and Fig.3a). The oxidation of magnetite to hematite is so intense in some cases that all magnetite changes to hematite and only remnants of magnetite can be seen in hematite (Fig.3a). Pyrite is widely formed in the Jalal-Abad deposit and is considered as the most important sulfide minerals in the deposit. Pyrite formed as large and small euhedral crystals but usually is less than 1 cm diameter, and also as veins (Fig. 2C and 2d). Pyrite is formed in different stages of mineralization, including the initial stages and also in the copper sulfide mineralization stage. Close to the fault and the sheared zones, pyrite is more abundant and has changed to goethite.

Copper mineralization in Jalal-Abad deposit is in form of sulfide and oxide mainly in the surface levels, and volumetrically is mainly oxide type. It seems that faults and fractures act as the copper-bearing hydrothermal fluid channel conduits and always there are traces of copper mineralization at their surface plane (Fig.2e). In order to identify copper oxide minerals, the samples were examined by XRD and the results showed that the minerals are malachite [$Cu_2(CO_3)(OH)_2$], azurite [$Cu_3(CO_3)_2(OH)_2$] and atacamite. [$Cu_2Cl(OH)_3$] (Fig.2f). Chalcopyrite is the most important copper sulphide mineral in the Jalal-Abad deposit, which is found in the form of space filling, disseminated, veins and veinlets in shear zones and fractures (Fig.3b). Chalcopyrite is associated with pyrite and fills the holes and fractures of pyrite. Copper sulphide mineralization is mainly observed in massive magnetite ore and in the deep parts of the deposit, and its abundance decreases towards the surface levels. In magnetite ore, chalcopyrite fills the fractures and intergrains boundary of magnetite (Fig.3b). Chalcopyrite is hypogene mineral and copper-bearing supergene zone is not developed in the Jalal-Abad deposit, and only locally covelite and chalcocite were identified. Bornite is another hypogene mineral containing copper, which is found in small amounts in some samples, which is formed in association with chalcopyrite. Chalcopyrite is the only economically important hypogene copper mineral in most IOCG deposits rich in magnetite and hematite (Williams et al., 2005). Along faults and fractures wide hydrothermal fluid rock interaction occurred, and meteoric fluids in the region caused development of widespread copper oxide zone. Malachite and azurite are secondary minerals that formed by the alteration of primary copper minerals (chalcopyrite, bornite, etc.).

Optical microscopy and EPMA studies showed that gold mineralization is mainly associated with chalcopyrite. Fine gold inclusions smaller than 50 microns are present inside the chalcopyrite veinlets. Copper-gold association is usually common in IOCG deposits. There are also inclusions of gold in chalcopyrite, pyrite, magnetite and dolomite (Fig.3c and 3d). EPMA analysis of chalcopyrite showed that invisible gold is present in chalcopyrite in some samples, with 150 to 600 ppm content and As content varies from 0.02 to 0.22% (Table 1). The pyrites that were formed at the same time with chalcopyrite contain native gold inclusions. The average Au content in gold particles is 93.12%, Ag varies from 4.24 to 6.78%, and Cu content is less than 0.41% (Table2). Bismutinite, cobaltite, arsenopyrite and cassiterite formed in a small amount as holes and fractures filling (Fig.4d). Based on EPMA analyses Bi content in Bismutinite varies between 79.00 and 80.36 %, and S varies between 18.03 and 19.86% (Table3). In arsenopyrite, Co partially substitutes Fe, sometime close to cobaltite composition (Table4). Amount of Co in cobaltite varies from 33.23 to 33.57% and Fe varies between 2.48 and 3.00 %(Table4). Tsumoite (BiTe) usually form as inclusions with of less than 20 µm size in chalcopyrite, magnetite and quartz (Fig.3f). EPMA data of tsumoite (BiTe) show Bi content of 58.318% to 56.196% and Te contents of 30.511% to 33.954% (Table 5).

Bismutinite, cobaltite, and arsenopyrite coexist with each other, and it was not possible to separate them accurately by backscattered electron images. The presence of cobaltite indicates formation under high temperature conditions which associated with arsenopyrite in the deposit. Arsenopyrite and cobaltite identification were carried out by using the EPMA, using changes in the profile analysis of Fe, As and Co (Fig.4). In the X-ray elemental maps prepared by EPMA mapping software, these two minerals are clearly separated (Fig.4a). The EPMA line (profile) analysis shows that the Co content in cobaltite is high, while in arsenopyrite, Fe content has increased whilst As values did not change in the both minerals (Fig.4b).

3. Discussion:

Mineral species of bismuth with tellurium, selenium and sulfur occur in a wide range of magmatic, hydrothermal or metamorphogenic gold, copper–gold and polymetallic ore deposits (Cook et al. 2007). Au, Te, Bi and Co mineralization related to hydrothermal- metasomatic processes in the KKZ region. Our study indicate that gold is not only in a native form and also occurred as invisible state in sulfides including chalcopyrite and pyrite. Significant amounts of Au, Bi, Co, and Te were present in the hydrothermal fluids that may was dissolved from early mineralization stage. Based on the existing geological and petrographic data, we believe that the Au, Bi, Co and Te occur in the mineral assemblages were scavenged from the various earlier generations of magnetite and pyrite by the hydrothermal fluids contemporaneously. The paragenesis includes cobaltite (± arsenopyrite), bismuthinite, pyrrhotite and or pyrite, chalcopyrite, carbonates, talc, chlorite and native gold, similar to a low-sulfidation environment (Nimis etal. 2014). Compositional variations are mainly due to variations in the Co/Fe ratio of arsenopyrite, or the Co/Fe or the Ni/ (Fe + Co) ratios of the coexisting cobaltite (Nimis etal. 2014). The As/S molar ratios in the cobaltite are varies from 2.16 to 2.27. Formation of cobaltite probably is related to circulation of (Co-As-Bi)-rich fluids during the sulfidation stage. EPMA analyses of gold grains (Table 2) showed the highest fineness between 932 and 957 FN, [FN = 1000 *Au/ (Au + Ag)], which indicates the presence of both electrum and native gold in Jala Abad. The association of Fe–Cu-sulfides with gold suggests that it may was initially deposited as solid solution in these sulfides. Experiments in the Cu–Fe–S–Au system shows that Cu–Fe-sulfides can incorporate a large amount of gold in solid solution form (Simon et al., 2000, Cepedal et al., 2006). The temperatures of Cu–Fe-sulfide formation obtained for the Jalal-Abad deposit, is less than 500 °C (Mehrabi et al., 2019), indicate that a part of the gold could have initially been in solid solution form within chalcopyrite and bornite, and later was exsolved which is supported by the occurrence of small gold grains in chalcopyrite.

3.1. Figures

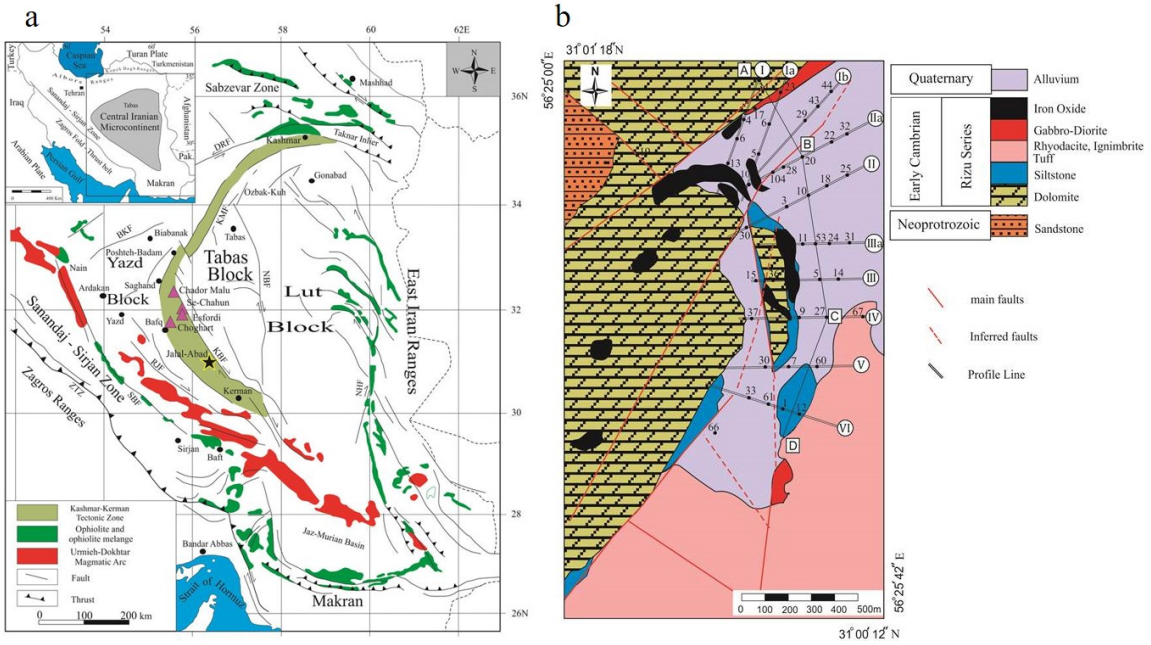


Fig. 1. a) Structural map and location of iron ore deposit in Central Iran (Ramezani and Tucker 2003, Torab and Lehmann 2007), b) Geological map of the Jalal-Abad deposit.

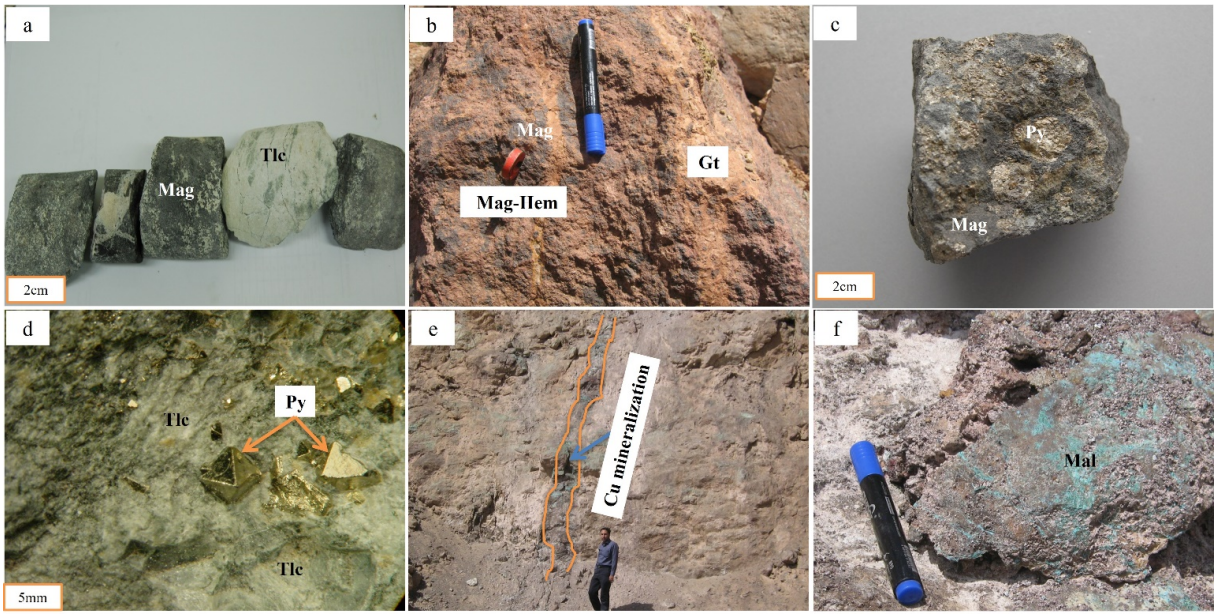


Fig. 2. Photographs of samples from selected mineralization in the Jalal-Abad deposit. a) collected samples from boreholes include magnetite (Mag), hematite(hem) and talc (Tlc). b) extreme martitization of magnetite in oxide ore and hematite replacement by goethite (Gt), c and d) subhedral and euhedral pyrite (Py) associated with magnetite and talc, e) Cu mineralization along fault and fractures, f) malachite (Mal) mineralization.

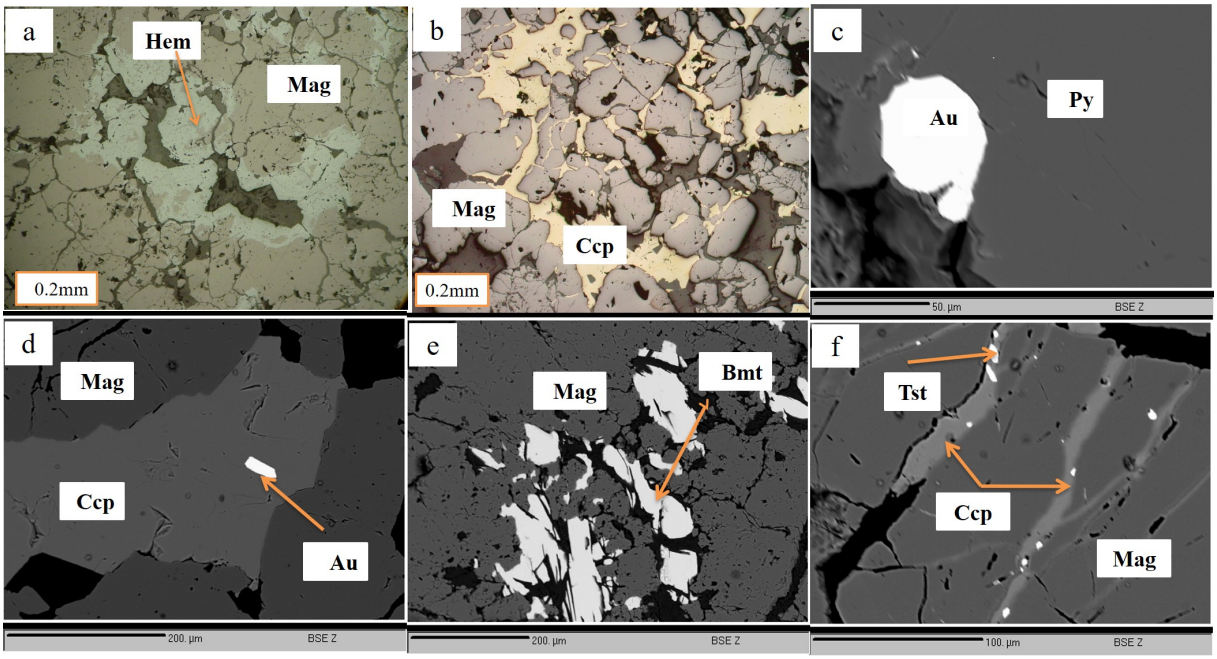


Fig. 3. Photomicrographs and back-scattered electron (BSE) images of the ore minerals in the Jalal-Abad deposit. a) replacement of magnetite (Mag) by hematite (Hem) by martitization process, b) chalcopyrite (Ccp) filled the space between magnetite crystals, c and d) gold grains (Au) within pyrite (Py) and chalcopyrite, e) bismuthinite filled spaces and fractures in magnetite. f) tsumoite (Tst) within chalcopyrite fractures.

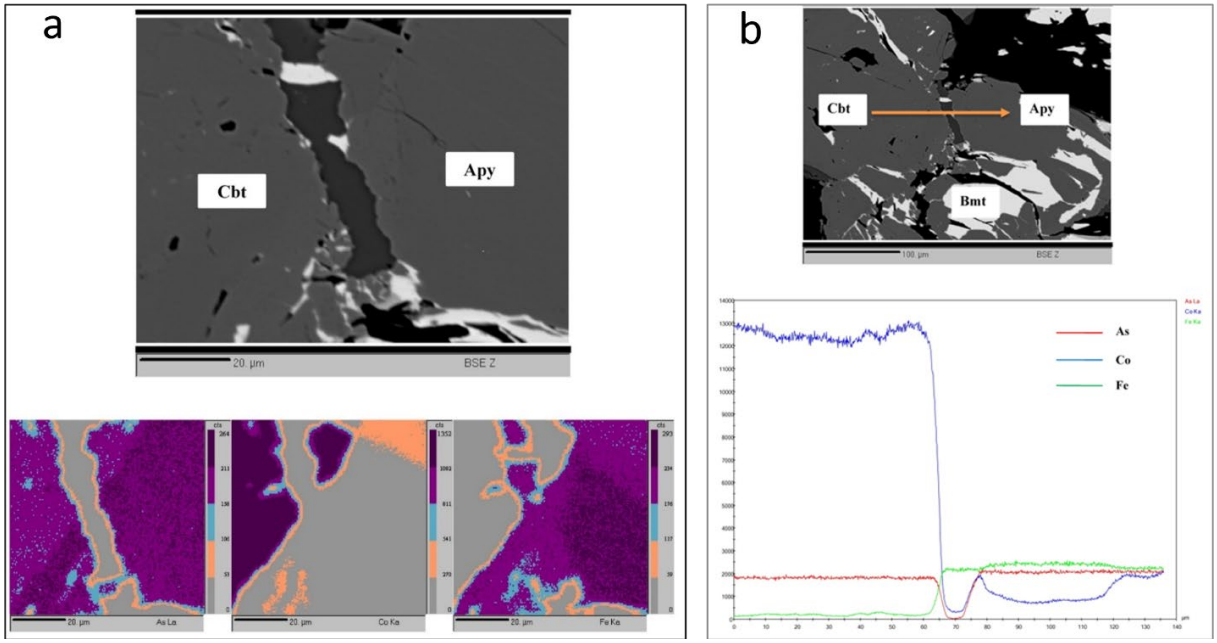


Fig. 4. Intergrowth between arsenopyrite and cobaltite a) BSE image and X-ray mappings showing the distribution of As, Fe, Co in arsenopyrite and cobaltite by EPMA. b) Back-scattered electron (BSE) images of bismuthinite, arsenopyrite and cobaltite, EPMA line profile show the contents of As, Co and Fe across the arsenopyrite and cobaltite which is similar to the X-ray mappings data.

3.2. Tables

Table 1. Representative Results of Electron Microscope Analyses (EPMA) of chalcopyrite

	1	2	3	4	5	6	7	8	9	10
S	35.054	35.481	35.050	35.372	34.864	35.230	35.045	34.483	35.073	**35.370**
Fe	30.564	30.294	30.515	30.966	30.467	29.879	31.242	30.966	30.612	**30.823**
Ni	0.000	0.000	0.000	0.000	0.000	0.012	0.000	0.000	0.005	**0.011**
Cu	34.246	34.331	34.309	33.972	34.093	34.452	34.639	34.011	34.887	**34.481**
Zn	0.000	0.021	0.012	0.000	0.000	0.057	0.000	0.017	0.000	**0.000**
As	0.224	0.031	0.082	0.091	0.114	0.120	0.054	0.068	0.099	**0.065**
Sn	0.040	0.000	0.016	0.000	0.005	0.000	0.024	0.000	0.028	**0.000**
Te	0.000	0.001	0.001	0.039	0.000	0.037	0.012	0.008	0.000	**0.000**
Bi	0.096	0.034	0.000	0.000	0.000	0.193	0.000	0.000	0.052	**0.011**
Ag	0.019	0.000	0.080	0.018	0.019	0.000	0.000	0.000	0.000	**0.071**
Au	0.000	0.060	0.000	0.000	0.042	0.000	0.000	0.000	0.017	**0.029**
Total	**100.244**	**100.254**	**100.065**	**100.459**	**99.605**	**99.981**	**101.016**	**99.567**	**100.772**	**100.861**

Table 2. EPMA Analyses of gold

	Au	Cu	Fe	Bi	Te	Ag	As	S	Total
1	93.795	0.083	0.164	0.000	0.000	6.680	0.000	0.114	**100.836**
2	92.830	0.040	0.244	0.000	0.000	6.739	0.045	0.051	**99.950**
3	93.508	0.418	0.304	0.000	0.000	4.243	0.000	0.049	**98.523**
4	**93.476**	**0.064**	**0.270**	**0.000**	**0.000**	**6.781**	**0.048**	**0.101**	**100.740**

Table 3. EPMA Analyses of bismttinite

	1	2	3	4	5	6	7	8	9	10
S	18.17	18.03	18.36	19.04	19.73	19.86	19.48	19.60	19.69	19.75
Co	0.62	0.41	0.43	0.67	0.00	0.02	0.00	0.03	0.00	0.01
Ni	0.02	0.01	0.02	0.00	0.00	0.00	0.00	0.00	0.00	0.00
Cu	0.01	0.05	0.00	0.08	2.51	0.01	0.08	0.03	0.01	0.03
As	0.00	0.01	0.03	0.03	0.03	0.00	0.04	0.01	0.00	0.03
Sb	0.32	0.33	0.39	0.40	0.00	0.00	0.00	0.00	0.00	0.00
Bi	80.01	80.36	80.11	78.53	78.62	78.92	80.01	79.00	79.61	79.51
Fe	1.15	0.71	0.73	1.17	0.04	0.11	0.00	0.30	0.05	0.06
Ag	0.00	0.00	0.00	0.00	0.00	0.11	0.01	0.00	0.00	0.03
Total	100.30	99.91	100.07	99.92	100.93	99.03	99.62	98.97	99.36	99.42

Table 4. EPMA Analyses of cobaltite (Cbt) and arsenopyrite (Apy)

	1(Cbt)	2(Cbt)	3(Cbt)	4(Cbt)	5(Cbt)	6(Cbt)	1(Apy)	2(Apy)	3(Apy)	4(Apy)	5(Apy)
S	19.316	19.525	19.303	19.354	20.065	19.371	17.292	18.235	17.484	17.292	**17.787**
Fe	2.395	2.519	2.541	2.478	2.614	3.003	31.897	32.827	32.757	31.153	**32.998**
Co	33.575	33.549	34.214	34.233	33.645	33.461	3.367	1.815	2.754	3.841	**2.169**
Ni	0.003	0.741	0.210	0.026	0.008	0.013	0.015	0.011	0.011	0.000	**0.000**
Cu	0.018	0.008	0.054	0.076	0.008	0.018	0.019	0.000	0.027	0.000	**0.009**
As	43.788	43.452	43.502	43.717	43.308	43.408	47.732	46.236	46.929	47.116	**46.655**
Ag	0.063	0.016	0.000	0.000	0.024	0.034	0.000	0.000	0.000	0.004	**0.072**
Au	0.000	0.000	0.000	0.006	0.001	0.000	0.000	0.000	0.035	0.002	**0.000**
Zn	0.026	0.004	0.021	0.000	0.047	0.038	0.000	0.000	0.000	0.067	**0.000**
Total	**99.184**	**99.817**	**99.862**	**99.891**	**99.730**	**99.360**	**100.376**	**99.328**	**100.028**	**99.520**	**99.770**

Table .5 Representative Results of EPMA Analyses of tsumoite

	1	2	3	4	5
S	4.666	4.011	4.481	4.820	**4.209**
Fe	1.068	0.961	1.045	1.596	**1.394**
Ni	0.000	0.008	0.004	0.013	**0.000**
Cu	0.988	0.000	0.581	3.248	**0.030**
Pb	0.000	0.000	0.000	0.000	**0.000**
Bi	58.251	58.318	57.679	56.196	**57.718**
Ag	0.035	0.013	0.016	0.000	**0.017**
Te	32.829	32.351	31.898	30.511	**33.954**
Total	**97.836**	**95.662**	**95.706**	**96.385**	**97.323**

4. Conclusions

In addition to iron oxide, economical Cu mineralization occurs in the Jalal-Abad deposit with traces of Au, Bi, Co, As, Te, Sn and Ba and insignificant apatite. The Cu sulfides mostly formed under brittle conditions as disseminations and veinlets. Iron metallogenic province of central Iran consist variety of iron oxide–apatite (IOA) deposits to iron oxide-Cu-Au deposit which in the Jalal-Abad deposit amount of sulphide minerals and quartz are increased and apatite decreased. The evidences show the Jalal-Abad deposit is similar to the IOCG deposits. The paragenetic sequence at the Jalal-Abad deposit can be subdivided into three hydrothermal stages: an early iron oxide stage, Cu sulfide and Au stage, and a late hydrothermal stage. Magnetite is the dominant ore mineral and is mainly associated with talc, chlorite, actinolite, dolomite and euhedral pyrite. Mineralization at the Jalal-Abad deposit occurs as massive, vein–veinlet, networks, breccia, open space filling and dissemination textures. Gold in the deposit is mainly associated with chalcopyrite veins also occurs as small inclusions (normally <50μm) within chalcopyrite, pyrite and magnetite. The results of current study show that rare-metal (Bi, Te, Co, Au) mineralization also occurred in the Jalal Abad deposit, genetically related to the hydrothermal process (Cu sulfide and Au stage). Visible gold grains were precipitated in chalcopyrite and also Bi-S, Bi-Te and Co minerals were crystallized in later stage. Copper oxide mineralization and formation of malachite, azurite and atacamite has occurred in the Jalal-Abad deposit in weathering stage.

Acknowledgments

We would like to acknowledge the IMIDRO (Iranian Mines and Mining Industries Development and Renovation Organization) and IMPRC (Iranian Mineral Processing Research Center) for their financial supports.

References

Alavi, M.(1991). Tectonic map of the Middle East, 1/5000000. Geol. Surv. Iran

Bonyadi, Z., Davidson, G., Mehrabi, B., Meffre, S., & Ghazban, F. (2011). Significance of apatite REE depletion and monazite inclusions in the brecciated Se–Chahun iron oxide–apatite deposit, Bafq district, Iran: Insights from Paragenesis and geochemistry. Chemical Geology, 281(3-4),253-269. DOI: 10.1016/j.chemgeo.2010.12.013

Cepedal, A., Fuertes-Fuente, M., Martı´n-Izard, A., Gonza´lez-Nistal, S., & Rodrı´guez-Pevida, L.(2006). Tellurides, selenides and Bi-mineral assemblages from the Rı´o Narcea Gold Belt, Asturias, Spain: genetic implications in Cu–Au and Au skarns. Mineralogy and Petrology, 87, 277–304. DOI 10.1007/s00710-006-0127-7

Cook, NJ., Ciobanu, Cl., Wagner, T., & Stanley, CJ.(2007). Minerals of the system Bi-Te-Se-S related to the tetradymite archetype: Review of classification and compositional variation. The Canadian Mineralogist 45, 665-708. DOI: 10.2113/gscanmin.45.4.665

Mehrabia,B., Karimishahrakia, B., Bazargani Guilani, K., &Masoudi ,.F.(2014). Early Cambrian high-temperature dolomite of the Rizu Series in the Jalal-Abad iron ore deposit, Central Iran. Arabian Journal of Geosciences 8(9), 7163–7176, DOI: 10.1007/s12517-014-1684-4

Mehrabia,B., Karimishahrakia, B., Banksb ,B., & Boycec ,A., Yardley,B.(2019). Hydrothermal iron oxide-Cu-Au (IOCG) mineralization at the Jalal-Abad deposit, northwestern Zarand, Iran. Ore Geology Reviews(106), 300-317. DOI: 10.1016/j.oregeorev.2019.01.019.

Nimis, P., Dalla Costa, L., & Guastoni,A.(2014). Cobaltite-rich mineralization in the iron skarn deposit of Traversella (Western Alps, Italy). Mineralogical Magazine, 78(1), 25-41. DOI: 10.1180/minmag.2014.078.1.02

NISCO. (1980). Result of search and valuation works at magnetic anomalies of the Bafq iron ore region during 1976-1979, Unpubl Rept, National Iranian Steel Corporation

Ramezani, J., &Tucker, RD. (2003). The Saghand region, central Iran: U –Pb geochronology,petrogenesis and implications for Gondwana tectonics. American Journal of Science, 303(7), 622-665, DOI: 10.2475/ajs.303.7.622

Simon, G., Kesler, SE., Essene, EJ., & Chryssoulis, SL. (2000). Gold in porphyry copper deposits: experimental determination of the distribution of gold in the Cu–Fe–S system at 400 °C to 700 °C. Econ Geol ,95, 259–270. DOI: 10.2113/gsecongeo.95.2.259

Stosch, HG.,Romer, RL., & Daliran, F. (2011). Uranium–lead ages of apatite from iron oxide ores of the Bafq District, East-Central Iran. Mineralium Deposita, 46(1), 9-21. DOI: 10.1007/s00126-010-0309-4

Technoexport .(1976). Internal Report, National Iranian Steel Corporation

Torab, FM., & Lehmann, B. (2007). Magnetite–apatite deposits of the Bafq district, Central Iran: apatite geochemistry and monazite geo-chronology. Mineral Mag 71, 347–363, doi .org/10.1180/minmag. 2007.071.3.347

Williams, PJ., Barton, MD., Johnson, DA., Fontbote, L., DeHaller, A., Mark, G., Oliver, NHS., & Marschik, R. (2005). Iron oxide copper-gold deposits: geology, space-time distribution and possible modes of origin. Econ Geol (100th anniversary volume), 100(4),371–405, doi.org/10.5382/AV100.13

Effects of Low-Grade Refractory Gold Mineralogy on Flotation Properties

Sena Naz GÖKDEMİR [1]*, İlkay Bengü CAN [2], Ahad HARZANAK [1]

[1]Demir Export A.Ş. 1

[2]Hacettepe University 2

*Corresponding author: senag@demirexport.com (Sena Naz GÖKDEMİR)

Abstract:

Gold can be found in native and free form in nature, but it can also be associated with other minerals or in the form of inclusions. These different forms of occurrence lead to the need for different beneficiation methods. To decide on the right enrichment method, mineralogical information describing the formation of gold, which minerals it is associated with, and the degree of liberation is needed. Gold ores are simply classified into three main groups such as free milling, complex, and refractory gold ores.

Gold that is easily liberated by traditional milling methods when it is associated to another mineral is called "free milling gold ores" (Zhou et al., 2004). Ores containing minerals that cause reagent consumption or losses of valuable minerals during the enrichment process are called "complex gold ores" (Vaughan, 2004). The definition of refractory gold includes situations where the ore formations exhibit a resistance to conventional cyanide leaching even fine grinding is applied (Fernandez et al., 2000). Refractory gold refers to ore formations that exhibit a low response to standard cyanide leaching (<80%) (La Brooy et al., 1994) such as:

Keywords: *Gold, Refractory, Mineralogy, Flotation, Recovery/Grade*

1. Introduction

G Gold can be found in native and free form in nature, but it can also be associated with other minerals or in the form of inclusions. These different forms of occurrence lead to the need for different beneficiation methods. To decide on the right enrichment method, mineralogical information describing the formation of gold, which minerals it is associated with, and the degree of liberation is needed. Gold ores are simply classified into three main groups such as free milling, complex, and refractory gold ores.

Gold that is easily liberated by traditional milling methods when it is associated to another mineral is called "free milling gold ores" (Zhou et al., 2004). Ores containing minerals that cause reagent consumption or losses of valuable minerals during the enrichment process are called "complex gold ores" (Vaughan, 2004). The definition of refractory gold includes situations where the ore formations exhibit a resistance to conventional cyanide leaching even fine grinding is applied (Fernandez et al., 2000). Refractory gold refers to ore formations that exhibit a low response to standard cyanide leaching (<80%) (La Brooy et al., 1994) such as:

- The The presence of ions that consume the oxygen necessary for dissolution to occur in cyanide leaching (Komnitsas and Pooley, 1989),
- The presence of compounds that are difficult to dissolve in cyanide solution, resulting in low gold recovery (Fernandez et al., 2000),
- Gold is present as submicroscopic (solid solution, encapsulated in silica or colloidal) inclusions in the structure of other minerals and hence cannot reach the cyanide solution (La Brooy et al., 1994; Komnitsas and Pooley, 1989; Chen et al., 2002; Zaghloul, 2020),
- The presence of some sulfide minerals that form cyanicides and cause cyanide consumption (Komnitsas and Pooley, 1989),

- The presence of carbonaceous minerals leads to preg-robbing (Afenya, 1991).
- The presence of clay absorbing gold cyanides (Jha, 1987; Berezowsky and Weir, 1989).

According to these definitions in the literature, refractoriness exists when one or more of these conditions are present in an ore. In cases where fine gold grains are found as inclusions in the crystal structure of other sulfide or oxide minerals, the first solution is fine grinding. High recoveries can only be achieved by fine grinding if the gold occurs as physically inclusions. However, if the gold grains are inclusions in submicroscopic shapes, refractoriness cannot be eliminated by fine grinding. Some pre-treatments like physical, chemical, biological, and thermal may be required for such gold ores (Spickelmier, 1993).

Gravity concentration, flotation, and conventional cyanide leaching are the well-known main methods for gold enrichment. Flotation is particularly preferred in refractory gold deposits where gold is associated with sulfide minerals or in areas where cyanide cannot be used due to its adverse effects. As a pre-enrichment product, the flotation concentrate is then subjected to other pre-treatment such as roasting, bacterial leaching or pressure oxidation to make it suitable for cyanide leaching. Applying these expensive pre-treatments to only the flotation concentrate products rather than the whole ore has a positive impact on operating costs (Bulatovic and Wyslouzil, 2000). In addition, flotation prior to cyanide leaching helps to remove other minerals that may cause cyanide consumption from the system, providing both capacity relief and reducing reagent consumption (Adams, 2005). The floatability of gold minerals and/or other gold-bearing minerals depends on many parameters such as the free gold grain size and shape (Teague et al., 1999a; Bulatovic, 1997), Ag content of the native gold, the composition of the gold-bearing mineral (O'Conner and Dunne, 1991), the type and dosage of reagents used, the loading capacity of air bubbles, the Eh and pH of the pulp (Zaghloul, 2020). Free gold generally floats at natural pHs with a small amount of collector and dixanthogen form (Dunne, 2005; Miller et al., 1986). Some studies have shown that the potential values at which gold begins to float are close to the dixanthogen formation potential (Woods et al., 1994). As the chain length of thiol collectors increases, the contact angle of the mineral with the froth increases, thus increasing the hydrophobicity of the mineral surface. Therefore, long chain xanthates are preferred for free gold flotation (Dunne, 2005). At the same time, long chain collectors form dixanthogen at low potentials (Gardner and Woods, 1974). In most flotation plants, instead of using a single type of collector, the synergistic effect of the collectors is now utilized, and thus better results are obtained in terms of grade and recovery (Bradshaw and O'Connor, 1994). For example, dithiophosphates are used as secondary collectors together with xanthates to increase flotation efficiency, especially they are highly selective for sulfide minerals (Dunne, 2005; Nagaraj, 1997; Allan and Woodcock, 2001). Mercaptobenzothiazoles are very important thiol-type collectors for flotation of gold and gold-bearing minerals (Finkelstein and Poling, 1977) and are preferred for flotation of gold and gold-bearing pyrite in acidic mediums (O'Connor and Dunne, 1991). These types of collectors have a fine crystal structure, so they are insoluble in water. However, they can be easily dissolved with alkaline solutions (Bulatovic, 2007).

The presence of gold in free or refractory form, in association with sulfide minerals such as pyrite, pyrrhotite and arsenopyrite differs in terms of many parameters such as copper sulfate ($CuSO_4$) addition, pre-aeration, galvanic interaction, synergistic effects of collectors applied in flotation. For example, it is reported that gold recovery showed variability in flotation tests using sodium isobutyl xanthate (SIPX) collector at different pH and $CuSO_4$ dosages of sulfide refractory gold ore from a gold mine in Ghana, West Africa (Owusu et al., 2020). It was observed that flotation kinetics were faster in acidic media without copper activation, but adsorption was reported to decrease in alkaline media (pH10-10.5) due to competition between OH- and SIPX. Oxidation products (arsenic oxides and ferric hydroxide) are hydrophilic in nature and act as a barrier for collector interaction with sulfide minerals present in the ore (Valsivieso, 2006). The effect of copper activation on pH and SIPX adsorption was investigated, and it was concluded that the maximum adsorption occurred in the natural pH range of 8-8.5. In a study of Teague et al. (1999a), Stawell Central ore containing both free and refractory gold, it was reported that the flotation behavior of these two types of gold occurrences is different. It has been stated that the recovery of free gold is mostly affected by particle size and shape, froth stability, water recovery to froth etc. It was even claimed that there is an inverse relationship between the recovery of refractory and free gold by true flotation and that free gold is recovered mostly by entrainment. The

addition of $CuSO_4$ before or after the collector addition was also reported to change the Au recovery. While Au recovery was higher when the addition of collector was made prior to $CuSO_4$ activation, it was observed that the recovery decreased considerably when the addition was made after activation. The reason for this is that the strong hydrophobic Cu-X compounds formed by $CuSO_4$ activation, and the sulfide minerals adhere to the air bubbles in large amounts, reducing the chance of free gold adhesion and reducing the recovery by entrainment.

In this study, the mineralogical characterization and metallurgical deportment of different zones of a refractory gold deposit located between the North Anatolian and East Anatolian fault lines, were carried out. The results of this preliminary work will be the basis for establishing a process route for such an ore type. With the characterization studies, it was aimed to determine the appropriate beneficiation method by determining the gold formation and its association. In the next stage, the potential of different zones to be enriched together with a single method was examined.

2. Material and methods

2.1. Material

To determine the overall characterization of the deposit, representative core samples were taken from different locations and their modal mineralogical compositions/associations were determined at Amtel laboratories (Canada) using QemSCAN (Quantitative Evaluation of Minerals by Scanning Electron Microscopy). As a result of this preliminary study, which examined the gold deportment in detail, the ore deposit was classified into three main types named oxide, transition, and sulfide in terms of structural characteristics. After the identification of the zones, new samples were taken from different meters of selected drill logs representing each zone and they were prepared for detailed mineralogical characterization, chemical analyses, and metallurgical testing. Within the scope of chemical analysis, all base metals were determined by ICP (Inductively Coupled Plasma Emission Spectrometry) method while for gold values, fire assay method was used. The surface oxidation of the samples representing the zones was determined by EDTA (ethylene diamine tetra acetic acid) method, the solid and liquid phases after EDTA test were analyzed by Atomic Absorption Spectrometry (AAS). Detailed mineralogical characterization analysis was performed by preparing -106+53 µm and -53+20 µm grain size fractions of representative samples of each zone to be used in enrichment tests. Modal mineralogy, XRD (X-ray Diffraction), SEM (Scanning Electron Microscope), and EDS (Energy Dispersive Spectrometry) were performed by MLA (Mineral Liberation Analyzer) method, using FEI MLA 650.

In the first phase of the studies, bottle-roll tests were conducted to prove the refractoriness of the deposit, which was defined as refractory according to mineralogical tests, and to examine the susceptibility of the ore deposit to conventional cyanide leaching. Forty-eight drill core samples representing the sulfide, transition and oxide zones were crushed and sieved using jaw and roller crushers with a particle size of p_{80}: 1.7 mm and prepared as 500 g for bottle-roll tests. The samples were then placed in 2.5-liter amber glass bottles and rotated for 120 hours under atmospheric conditions with sodium cyanide (NaCN) at a concentration of 1g/L and 750 mL of distilled water. Oxygen was supplied by atmospheric air throughout the test and no external air was added (Fig. 1). The pulp pH (pH > 10.5 - 11.0) and the amount of dissolved oxygen in solution (> 4 mg/L), which affect the leaching kinetics and the interaction with cyanide, were measured periodically throughout the test and the values were always kept within ideal limits.



Fig. 1. Bottle-roll test set-up

The flotation method was preferred for enrichment purposes based on the information that gold is generally found together with pyrite minerals in sulfide and transition zones. Prior to the flotation tests, the grinding was carried out in a rod mill using 1 kg of ore at a solid density of 60% (w/w). In the flotation tests, a 2.5L Denver type flotation machine was used with a rotation speed of 1500 rpm, 3.5 L/min air rate and the solids density of approximately 30% (w/w). In the grinding stage, 2 kg/t sodium silicate (Na_2SiO_3) was used as dispersant and MIBC (methyl isobutyl carbinol) was preferred as frother. Prior to the flotation tests, preliminary tests were conducted using a strong collector, potassium amyl xanthate (PAX), based on the information that gold was associated with pyrite. In these tests, the effect of pH was also analyzed. Considering the liberation data, grinding calibration was performed for each sample of the zones and the samples were ground down to p_{80}: 50 µm, p_{80}: 42 µm and p_{80}: 43 µm for the sulfide, transition, and the oxide zones, respectively. The collectors used for the flotation tests were selected from those commonly used for iron sulfide, FeOx and Au (Aravjo, 2005; Bulatovic, 2007). For anionic collectors, petroleum-based sulfonates were preferred (Day, 2002 and Nakhaei, 2018). The following collector types were scanned for the zones:

- PAX (potassium amyl xanthate)
- Aero 407 promoter (mercaptobenzothiazole and dithiophosphate formulation)
- XD-702 promoter (formulated dithiocarbamate)
- Aero 8045 (Dithiophosphate formulation)
- Aero Maxgold 900 (modified dithiocarbamate)
- Aerofloat MX-505 (dithiophosphate)
- Aero 825 (petroleum sulfonate)

In the next stage, some collectors were used together to improve Au recovery, and their synergistic effects were explored. After determining the most appropriate collectors, the zones were blended according to their reserve ratios and flotation tests were carried out. Blend1 was prepared by mixing the sulfide and transition zone while Blend2 was the blend of all three zones.

3. Results and discussion

3.1. Ore Characterization

The drill core samples selected for general characterization of the ore deposit were classified according to their mineral content as sulfide (KT2, KT3 and KT6), transition (KT1, KT4 and KT7) and oxide (KT5 and KT8) ores. According to the modal mineralogy data given in Table 1, quartz and K-feldspar are the major gangue minerals in all three zones. While pyrite is the dominant sulfide mineral in the sulfide zone samples, goethite mineral is prominent in the oxide zone. The fact that the amounts of both pyrite

and goethite are close in the transition zone samples shows that mineralogical analysis and oxidation classification do not contradict.

Table 1. The modal mineralogy of the samples representing the ore deposit

Mineral	Codes of drill-core samples							
	KT-1	KT-2	KT-3	KT-4	KT-5	KT-6	KT-7	KT-8
Quartz	35.0	39.4	42.0	62.0	36.0	38.3	30.6	34.0
K-Feldspar	30.8	29.7	18.4	5.5	26.4	30.3	25.0	19.7
Na-Feldspar	3.9	1.7	0.9	0.4	1.5	1.3	9.8	3.4
Illite	13.2	11.5	14.4	10.9	14.7	10.9	17.9	19.9
Biotite	2.7	1.2	1.0	2.1	2.9	1.0	2.2	4.4
Kaolinite	7.6	3.7	9.3	4.9	13.8	12.4	7.7	8.0
Clorite	0.0	0.0	0.0	0.0	0.0	0.0	1.2	3.5
Rutile	0.2	0.2	0.2	0.1	0.2	0.1	0.2	0.2
Barite	0.2	0.1	0.1	0.2	0.2	0.1	0.1	0.2
Goethite	3.1	1.2	0.0	4.5	3.5	0.1	3.2	5.6
Pyrite	2.7	11.0	12.8	9.1	0.3	2.0	1.0	0.0
Arsenopyrite	0.6	0.0	0.0	0.0	0.1	0.1	0.2	0.0
Galena	0.0	0.2	0.1	0.1	0.0	0.0	0.0	0.0
Sphalerite	0.0	0.1	0.1	0.1	0.0	0.0	0.0	0.0
Augite	0.0	0.0	0.0	0.0	0.0	3.4	0.9	0.0
Total	**100**	**100**	**100**	**100**	**100**	**100**	**100**	**100**

The gold has been observed as visible gold particles are both free and associated with sulfides and iron oxides (Fig. 2). Also, submicroscopic gold, on the other hand, was found as solid solution with pyrite and arsenopyrite, and in colloidal micro-inclusions within FeOx.

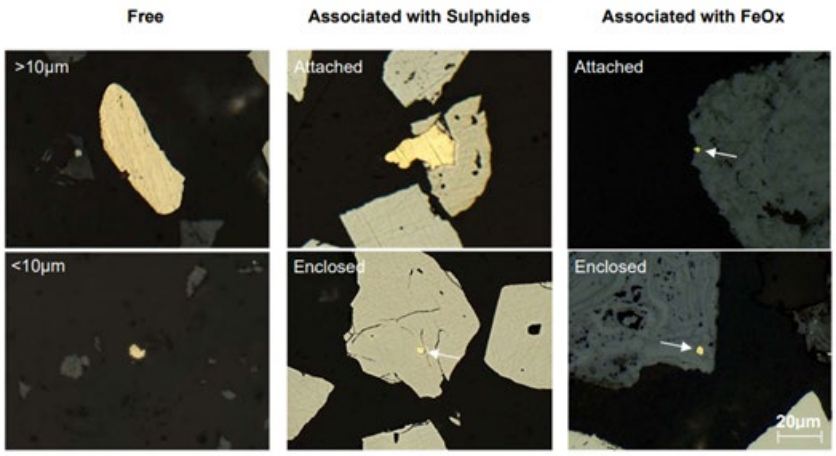


Fig. 2. The liberation of native gold and its association with other minerals

After classification, the head assays of all three zones were determined (Table 2). In general, the Au content of all zones was quite low, however the Au grade of the sulfide zone was slightly higher than the other zones and the Au grades of the transition and oxide zones were quite close to each other.

Table 2. Chemical analyses for all zones

Zone	Au (ppm)	Ag (ppm)	As (ppm)	Cu (ppm)	Pb (ppm)	Zn (ppm)	Sb (ppm)	Ni (ppm)	Fe (%)	S (%)
Sulfide	1.13	10.4	2894	235	1430	911	343	24	5.73	5.77
Transition	0.71	3.5	2329	61	202	91	49	12	3.71	1.79
Oxide	0.76	1.7	3584	66	347	208	1534	15	4.94	0.22

As a result of the EDTA test, the Es_Fe value in the sulfide zone was calculated as 0.80 mg/g, 0.84 mg/g in the transition zone and 0.60 mg/g in the oxide zone. These values are an indication that Fe minerals are not exposed to surface oxidation.

According to modal mineralogy (Table 3), quartz, feldspar and pyrite minerals account for approximately 87% of whole sulfide zone both in coarse and fine fractions. Quartz, feldspar, Fe-oxides, muscovite, and pyrite are the major minerals in the transition zone. In the oxide zone, quartz, feldspar, and Fe-oxides are dominant.

According to the results of chemical analyses, the native gold content in the zones is 1 ppm or less. The number of gold grains detected in the MLA analysis is given in Table 4. The trace amounts of these gold grains indicate the refractoriness of these samples.

Table 3. The modal mineralogy of the zones

	Distribution (%)					
	Sulfide Zone		Transition Zone		Oxide Zone	
	-106+53 µm	-53+20 µm	-106+53 µm	-53+20 µm	-106+53 µm	-53+20 µm
Quartz	43.15	36.33	51.25	47.64	48.80	46.56
K-feldspar	25.56	23.41	21.71	24.79	29.75	32.41
Albite	2.33	2.67	2.24	0.00	1.53	1.46
Pyrite	19.26	27.54	7.26	9.67	0.55	1.25
Arsenopyrite	0.42	0.99	0.68	1.12	0.02	0.07
Kaolinite	0.59	0.56	1.28	1.28	1.43	1.1
Fe-oxide	0.37	0.65	5.67	4.03	10.35	10.57
Muscovite	5.88	4.69	6.84	5.40	3.74	3.02
Biotite	0.19	0.34	1.85	2.18	1.01	0.92
Rutile	0.07	0.13	0.06	0.13	0.14	0.25
Barite	0.03	0.18	0.20	0.21	0.14	0.22
Dolomite	1.20	1.24	0.01	0.01	0.03	0.01
Plagioclase	0.00	0.00	0.55	2.84	0.12	0.00
Sb_Fe Oxide	0.00	0.00	0.00	0.00	0.90	1.46
Apatite	0.09	0.16	0.11	0.25	0.01	0.01
Jarosite	0.00	0.00	0.06	0.00	0.22	0.26
Sphalerite	0.20	0.25	0.00	0.00	0.00	0.00
Chlorite	0.00	0.00	0.00	0.18	0.84	0.01
Others	0.66	0.86	0.23	0.27	0.42	0.42
Total	**100.00**	**100.00**	**100.00**	**100.00**	**100.00**	**100.00**

Table 4. Number of Au grains detected in all zones

Zones	Size (µm)	# of Au grains
Transition	-106+53	3
	-53+20	1
Oxide	-106+53	0
	-53+20	0
Sulfide	-106+53	0
	-53+20	2

According to the resource estimation report, the ore deposit consists of 83% sulfide zone, 10% oxide zone and 7% transition zone. Mineralogical characterization studies revealed that gold grains were 100% of association with pyrite particularly in sulfide and transition zones. A typical BSE (back scattered electron) image and MLA mapping for transition zone are depicted in Fig. 3.

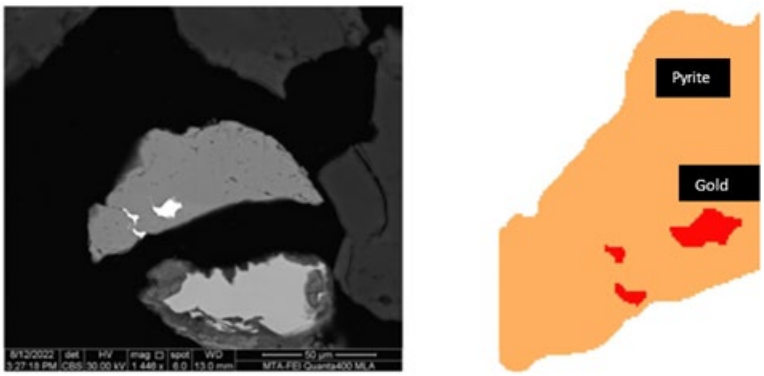


Fig. 3. The association of pyrite with gold in the transition zone

As pyrite was accepted as the target mineral, its liberation status was examined in detail. According to the liberation analysis, pyrite has over 77% liberation in the -106+53 µm fraction in all zones. In the finer fraction of -53+20 µm, this value exceeds 91%. Even in the fine size fraction of the sulfide (Fig. 4a) and transition zones (Fig. 4b), 100% of the gold observed is in the form of binary particle.

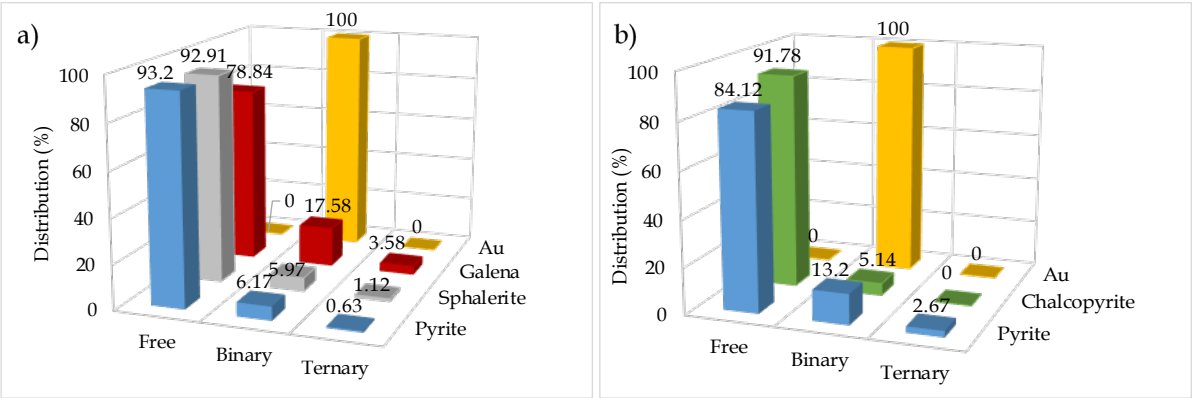


Fig. 4. The liberation of sulfide minerals and gold in -53+20µm fraction of sulfide zone (a) and -106+53µm fraction in transition zone (b)

Although gold was detected by chemical analysis in the oxide zone, no gold grains were found in MLA analysis. However, in the preliminary analyses carried out to characterize the deposit, it was reported that gold existed in the oxide zone in submicroscopic form and generally with Fe-Oxides (Fig. 2).

Accordingly, Fe-Oxides identified in the MLA analysis were considered to probably contain gold and their locking status was also examined. It was determined that Fe-Oxides showed less liberation compared to pyrite (62% liberation in coarse size and only 70% in fine size) and exhibited a more complex mineralogy in the form of both binary and multiple locked grains with minerals such as quartz, Sb-oxide, K-feldspar.

When the liberation status of the gold grains, which could be counted in few numbers in the MLA analysis, was examined, it was deduced that gold was locked only with pyrite mineral in both the sulfide and transition zone and only in the liberation class of 0%<x<15% of the particle area. In this sense, it is concluded that pyrite particularly can be recovered by sulfide mineral flotation and maximizing pyrite recovery would be important in terms of gold recovery.

3.2. 3Enrichment Tests

3.2.1. Bottle-roll Tests

The bottle-roll test, which was applied to 48 drill core samples representing the ore deposit, aimed to determine the refractoriness of the gold content in the zones. The samples were taken from different depths and locations of the deposit (Table 5). After approximately three months of bottle-roll tests, it was determined that the leaching efficiency of the three zones varied considerably, and this variability was not correlated with depth. According to the results of the bottle-roll test of the samples taken from different depths and locations of the oxide zone, Au leach recovery and grade ranged between 9-79.6% and 0.24-0.87 ppm, respectively. For the transition zone, Au leach recovery was 10.6-74% and Au grade was 0.04-1.11 ppm, while in the sulfide zone these values ranged between 8.6-72.6% and 0.19-1.30 ppm, respectively. It is known from mineralogical analysis that there were no carbonaceous structures in the ore that would cause cyanicides or 'preg-robbing'. Therefore, considering the low cyanide consumption and low/medium gold dissolution recoveries of the samples, this ore deposit was categorized as "refractory".

Table 5. Results of bottle-roll tests

Zone	Drill cores (meter)	# of samples	Average Au grade (ppm)	Average Au leach recovery (%)
Oxide	1.90-69.50	9	0.60	9.00-79.6
Transition	44.20-137.80	7	0.67	10.60-74.00
Sulfide	55.60-288.50	32	1.06	8.60-72.60

3.2.2. Flotation Tests

To determine the optimum flotation condition, preliminary tests were performed to analyze the effect of pH. Flotation was conducted at both acidic (pH: 6) and neutral (pH: 8.5-9) pH values to examine its effect, particularly on gold recovery (Table 6). It has been reported that xanthates are more unstable at acidic pH (Day, 2002) and neutral values such as 8-8.5 give more favorable results especially in terms of gold recovery rather than acidic and alkaline pH (Owusu et al., 2020; Goktepe, 2002). Similar result was obtained in this study that pH 8.5-9 range gave the most proper results (Table 6).

Table 6. Effects of pH

Condition	Au recovery, %
Acidic pH	36.6
Neutral pH	97.0

Sulfide Zone

As a result of preliminary tests on collector dosage and staged addition, it was determined that better results in terms of gold recovery could be obtained by adding the collector gradually at a total dosage of 250 g/t for the sulfide zone. In addition to PAX, a strong collector known to give efficient results in gold and pyrite flotation, kinetic tests were carried out with five different collectors (Aravjo, 2005; Bulatovic, 2007). Fig. 5a shows that the highest Au recovery (98.6%) was achieved with MX-505, while the lowest Au recovery (60%) was observed with XD-702 collector. It was noted that the flotation behavior of PAX, Aero 8045, and Aero 407 was similar, particularly in the initial minutes. However, in the cumulative concentrate, Aero 8045 and Aero 407 were more selective than other types of collectors. The higher Au recovery obtained with the other collectors was achieved with lower mass pull and pyrite recovery values with the Aero 8045 and Aero 407 collectors, indicating that these collectors were more selective (Fig. 5b).

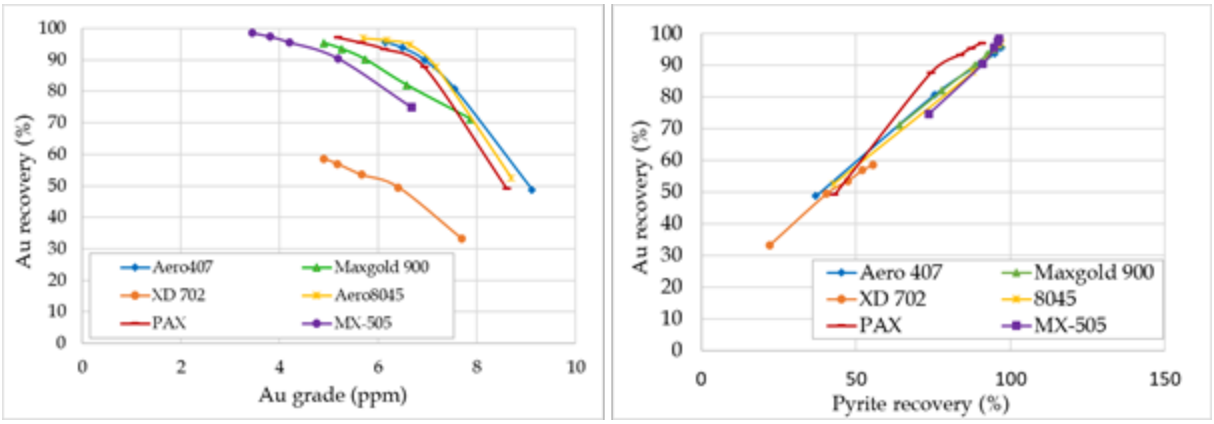


Fig. 5. Au recovery & grade (a) and pyrite recovery (b) relationship with different collectors for the sulfide zone

Following the tests using single collectors, the next step was to investigate whether the use of collectors in combination had a potential synergistic effect on Au recovery. In preference of the collectors, attention was given to the first collector with low cost and strong characteristics, while the second one was chosen for its selectivity. Hence, in the collector mixtures, Aero 407 and Maxgold 900 collectors were added to PAX for further testing in 1:1 ratio. The results showed that the PAX+Aero 407 mixture had Au recovery of 94%, while PAX+Maxgold 900 mixture had Au recovery of 88.4% (Fig. 6a). Moreover, when the synergistic effect of the collectors was compared with the tests where Aero 407 and PAX were used separately, it was determined that the highest Au grade was obtained in the case of the combination of these collectors. The comparison of pyrite and Au recoveries for the collector mixtures is given in Fig. 6b. It is stated that the combination more favorable to pyrite was PAX+Aero 407.

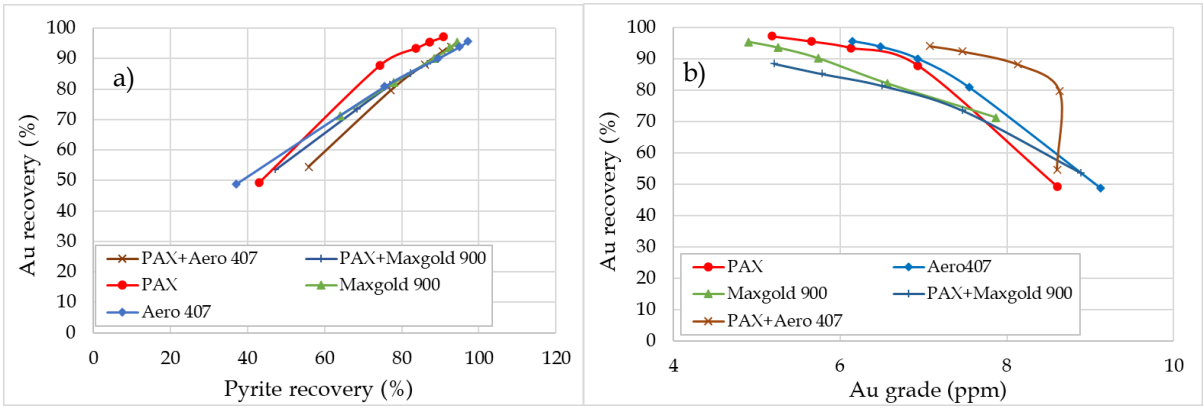


Fig. 6. Au recovery & grade (a) and pyrite recovery (b) relationship with combination of collectors for the sulfide zone

Transition Zone

Based on the results of mineralogical and chemical analysis, the transition zone has less Au content and less liberation of Au-containing pyrite and more locked grains compared to the sulfide zone. According to these data and due to the submicroscopic form of gold, the grain size of the sample was ground finer with a p_{80} value of approximately ~42 µm. As a result of this test, where PAX was staged added in 250 g/t dosage, the Au recovery in the cumulative concentrate was recorded as 77.4% despite finer grinding. Whether the lower values obtained in recovery and grade despite a finer grain size were related to the collector dosage was tested with a second test condition and the PAX dosage gradually increased to 300 g/t. It was observed that increasing the PAX dosage increased the flotation kinetics from the first minutes of flotation and increased the Au recovery to 86.1%. With the increase in PAX dosage, Au grade increased from 3.3 ppm to 5.2 ppm in the cumulative concentrate. Therefore, it was deemed appropriate to use 300 g/t of collector for further testing of the transition zone which contains less pyrite than the sulfide zone.

Kinetic tests for the transition zone were conducted with PAX, Aero 8045, and Aero 407 collectors, which had highest recovery results for the sulfide zone. When the test results were analyzed in terms of recovery, Au recovery was 86.1%, 86.7% and 75.3% for PAX, Aero 8045, and Aero 407 respectively. It was observed that PAX and Aero 8045 collectors gave similar results (Fig. 7a). Fig. 7b shows the Au recovery versus pyrite recovery relationship for these three collectors. Although Aero 8045 and PAX have very similar recovery values during flotation time, it is observed that Aero 8045 collected Au-bearing pyrite particles into the concentrate better than PAX.

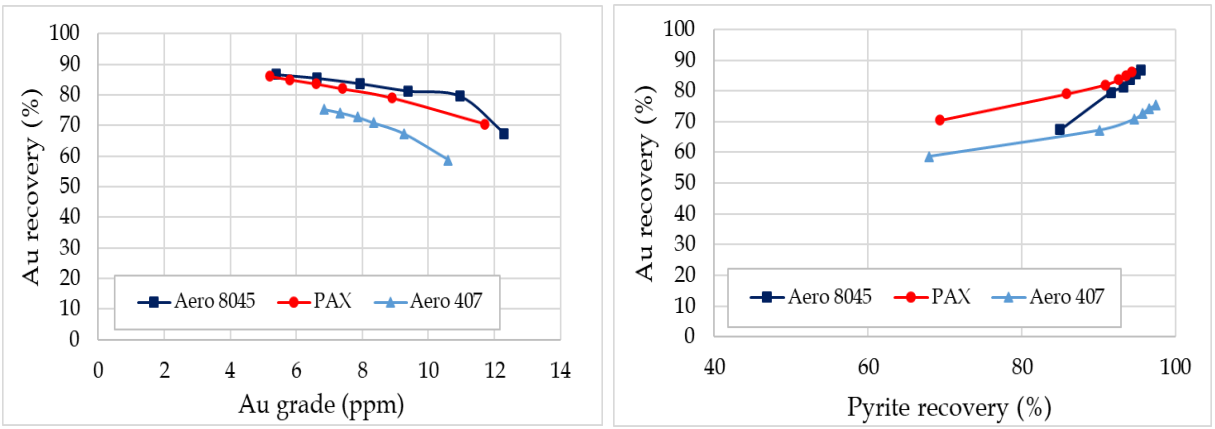


Fig. 7. Au recovery & grade (a) and pyrite recovery (b) relationship with different collectors for the transition zone

Since the most favorable results were obtained with the PAX+Aero 407 combination in the collector mixtures tested for the sulfide zone, flotation tests were carried out with the same approach for the transition zone sample. Au recovery and grade were noted as 80.7% and 10.4 ppm respectively with combined use of PAX+Aero 407 in a ratio of 1:1. In terms of Au grade, concentrate was obtained at a better grade in the mix than when these two collectors were used separately. It was observed that the selectivity effect of Aero 407 reflected very well on the grade but did not provide the desired efficiency on the recovery (Fig. 8).

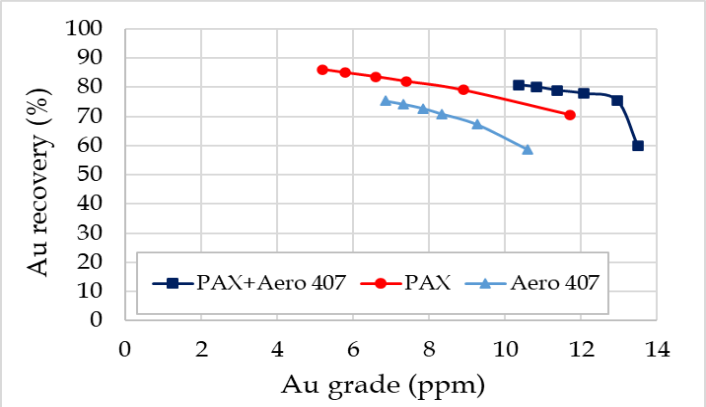


Fig. 8. Au recovery & grade relationship for the collector mixture in the transition zone

Oxide Zone

Mineralogical and chemical analyses indicated that S and Au contents were low in the oxide zone and sulfide minerals existed in trace amounts. In the mineralogical evaluation carried out for the characterization of the deposit, it was determined that Au grains, which were detected slightly, were mostly associated with FeOx minerals. However, to get an idea of how the oxide zone would response to sulfide mineral flotation if it were to be blended with the sulfide and transition zones, a trial test was carried out and 250 g/t PAX was staged added, resulting in a cumulative concentrate Au recovery and grade of 33.7% and 1.6 ppm, respectively. In the next stage, based on the data that gold is associated with FeOx minerals, the aim was to float these minerals. A-825, a petroleum-based sulfonate type collector commonly used in FeOx mineral flotation, was tested as in 500 g/t dosage and at pH 5-5.5. As a result of several repeated flotation tests, no successful results were obtained in terms of Au recovery and grade, the best results obtained were 27% and 0.9 ppm, respectively. However, the higher recovery and grade obtained with PAX suggests that gold may not only be present with FeOx minerals. It may be recommended to further characterize the submicroscopic gold in this zone by Electron Microprobe Analysis or Laser Ablation ICP-MS methods (Chingwaru et.al., 2024).

Blend Possibility of the Zones

After conducting flotation tests for each zone separately, the behavior of processing these three zones together was also investigated. In this regard, two different blends were prepared from the zones defined as sulfide, transition, and oxide zones by mixing them in the proportions of the reserve amount specified in the resource estimation report of the ore deposit. As sulfide and transition zones were much similar to each other in terms of mineralogically and chemically, the sample Blend1 was prepared by mixing 92.2% from the sulfide zone and 7.78% from the transition zone. Blend2 was prepared by adding 10% material from the oxide zone to investigate the possibility of blending this zone into Blend1 over time at the plant. As PAX-Aero 407 collector mixture showed positive results in previous tests particularly in terms of selectivity and recovery, it was tested at a ratio of 1:1 for both Blends. It is clearly seen in Fig. 9 that the blending of sulfide and transition zones, which have similar properties, will not pose a problem in terms of Au recovery and grade. However, with the addition of the oxide zone to this mixture, the ore behavior deteriorates, especially in favor of grade. It should be considered that oxide zone should not be processed together with the other zones unless further detail characterization studies in terms of Au content and its mineral association are performed.

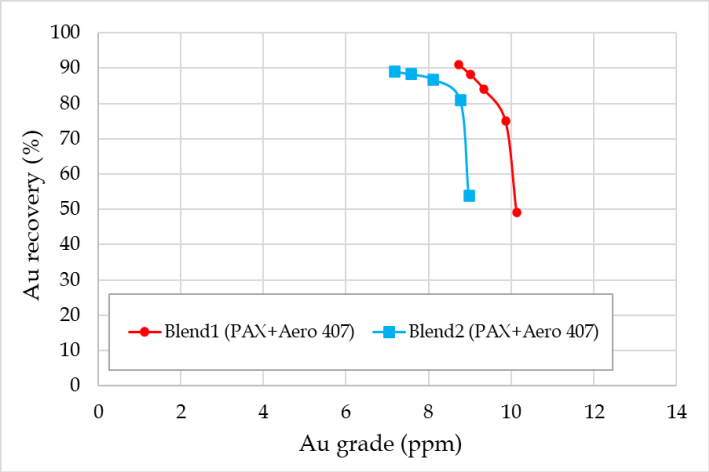


Fig. 9. Au recovery & grade relationship for the blend samples

4. Conclusions

This study has demonstrated that mineralogical characterization is a useful tool in evaluating the effects of gold ore refractoriness on rougher stage of flotation. Accordingly, the following findings are deduced:

- The The ore deposit was divided into three different zones as sulfide, transition, and oxide according to the containing mineral classes/quantities, and Au contents were measured as 1.13 ppm, 0.71 ppm and 0.76 ppm, respectively.
- The main sulfide and Au-bearing mineral in the sulfide and transition zone was determined to be pyrite and the grain size of native gold was generally <10 µm from MLA BSE images. In the oxide zone, gold was reported to be submicroscopic in size and associated with FeOx minerals in the preliminary characterization study, but no gold-containing grains were detected in MLA analysis.
- The average Au recovery values of the sulfide, transition and oxide zones obtained from bottle-roll tests were calculated as 38.3%, 56.5% and 39.6%, respectively. The low gold Au recovery of all zones indicated that the ore deposit can be classified as refractory.
- It was observed that the flotation behavior of PAX, Aero 8045 and Aero 407 in the sulfide zone was similar, especially in the first minutes of flotation, but as for the cumulative concentrate PAX and Aero 8045 reached 97% efficiency. The potential synergistic effects of using these collectors together on gold recovery was also investigated. PAX+Aero 407 collector mixture resulted in 94% Au recovery in cumulative and provided a more selective concentrate compared to other collector mixtures.
- As for the transition zone, PAX and Aero 8045 collectors gave similar results. However, the combination of PAX and Aero 407 collectors failed while the selectivity effect of Aero 407 was evident in the grade, Au recovery remained at 80%.
- Unfortunately, flotation with A-825 sulfonate type collector based on the data that gold associated with FeOx minerals at submicroscopic size was not successful. It is concluded that the flotation conditions should be optimized after determining the occurrence of gold in this zone with a more detailed mineralogical characterization study.
- The blending possibility of these three zones was also evaluated. Blend1 was prepared by mixing the sulfide and transition zones, which have similar chemical and mineralogical properties, while Blend2 was the mix of all three zones. As PAX+Aero 407 collector mixture showed positive results in previous tests particularly in terms of selectivity and recovery, it was tested at a ratio of 1:1 for both Blends.
- The results showed that, especially sulfide and transition zones could be processed together, bulk flotation method can be applied, and high recovery of concentrate can be achieved with

Aero 8045 collector alone or with PAX + Aero 407 collector mixtures. However, the presence of gold in the ore deposit in a submicroscopic form and at a very low grade confirms the refractoriness of the ore deposit. Implementing a regrinding stage prior to obtaining the final concentrate can be considered. According to the data of this study, it is concluded that the oxide zone should not be blended with the other two zones. It is concluded that this zone should be examined in more detail in terms of both gravity and flotation methods. For the leaching method to be successful, it may be recommended to apply leaching after grinding to a finer particle size to reduce the interlocking of gold within other minerals to facilitate solvent penetration. However, in this case, the grinding cost should also be taken into consideration. To optimize all these methods, EMPA or Laser Ablation mineralogical analyses, which can provide more detailed data on this zone, will definitely provide more useful information.

Acknowledgments

The authors would like to express their sincere thanks to Demir Export A.Ş. for providing the ore samples and for helping with the analyses. This publication is a part of MSc thesis of Sena Naz Gökdemir submitted to the Graduate School of Science and Engineering, Hacettepe University.

References

ADAMS, M.D., 2005, *Advances in Gold Ore Processing*, Elsevier.

AFENYA, P.M., 1991, *Treatment of Carbonaceous Refractory Gold Ores*, Miner. Eng., 4(7-11), 1043-1055.

ALLAN, G.C., WOODCOCK, J.T., 2001, *A review of the flotation of native gold and electrum*, Miner. Eng., 14(9), 931–962.

ALLISON, S.A., DUNNE, R.C., De WAAL, S.A., 1982, *The flotation of gold and pyrite from South African gold-mine residues*, In: 14th International Mineral Processing Congress, Toronto, Canada, paper II-9.18.

ARAVJO, A.C., VIANA, P.R.M., PERES, A.E.C., 2005, *Reagent in iron ores flotation*, Miner. Eng., 18(2), 219-224.

BEREZOWSKY, M.G.S., WEIR, D.R., 1989, *Factors affecting the selection of pressure oxidation for the pretreatment of refractory gold ores*, Paper Presented at the E&MJ International Gold Expo and Conference, Reno, NV, Sept. 7-9.

BULATIVIC, S.M., 1997, *Flotation behavior of gold during processing of porphyry copper-gold ores and refractory gold bearing sulfides*, Miner. Eng. 10(9), 895-908.

BULATOVIC, S., WYSLOUZIL, D.M., 2000, *Gold Recovery: Flotation, Lakefield Research*, Ontario.

BULATOVIC, S.M., 2007, *Handbook of flotation reagents*, Vol. 1, Elsevier.

BRADSHAW, D.J., O'CONNOR, C.T., 1994, *The flotation of pyrite using mixture of dithiocarbamates and other thiol collectors*, Miner. Eng., 7(5-6), 681-690.

CHEN, T.T., CABRI, L.J., DUTRIZAC, J.E., 2002, *Characterizing gold in refractory sulfide gold ores and residues*, JOM, 54(12), 20–22.

CHINGWARU, S.J., TADIE, M., VON DER HEYDEN, B., 2024, *Characterizing low-grade refractory gold ores using automated mineralogy coupled with LA ICP-MS*, Miner. Eng., 210.

DAY, A., 2002, *Cytec Mining Chemicals Handbook*, Revised Edition.

DUNNE, R., 2005, *Flotation of gold and gold-bearing ores, Developments in Mineral Processing*, Vol. 15, Elsevier, Chapter 14.

FERNANDEZ, R.R. SOHN, H.Y., LEVIER, K.M., 2000, *Process for Treating Refractory Gold Ores by Roasting Under Oxidizing Conditions*, Miner. Metall. Process., 17(1), 1-6.

FINKELSTEIN, N.P., POLING, G.W., 1977, *The role of dithiolates in the flotation of sulfide minerals*.

GARDNER, J.R., WOODS, R., 1974, *An electrochemical investigation of contact angle and of flotation in the presence of alkyl xanthates, I, platinum and gold surfaces*, Aus. J. Chem. 27, 2139-2148.

GOKTEPE, F., 2002, *Effect of pH on pulp potential and sulfide mineral flotation*, Turk. J. Eng. Environ. Sci., 6, 309 – 318.

JHA, M.C., 1987, R*efractoriness of certain gold ores to cyanidation - Probable causes and possible solutions*, Miner. Process. Extr. Metall. Rev., Vol. 2, 331-352.

KOMNITSAS, C., and POOLEY, F.D., 1989, *Mineralogical Characteristics and Treatment of Refractory Gold Ores*, Miner. Eng., 2(4), 449-457.

La BROOY, S.R., LINGE, H.G., WALKER, G.S., 1994, *Review of gold extraction from ores*, Miner. Eng., 7(10), 1213-1241.

MILLER, J.D., MISRA, M., GOPALAKRISHNAN, S., 1986, *Gold flotation from Colorado river sand with air sparged hydrocyclone*, Miner. Metall. Process, 3, 145-148.

NAGARAJ, D.R., 1997, *Developments of new flotation chemicals*, Trans. Indian Inst. Met., 50(5), 355–363.

NAKHAEI, F., IRANNAJAD M., 2018, *Reagents types in flotation of iron oxide minerals: A review*, Miner. Process. Extr. Metall. Rev., 39(2), 89-124.

O'CONNOR, C.T., DUNNE, R.C., 1991, *The practice of pyrite flotation in South Africa and Australia*, Miner. Eng., 4(7-11), 1057-1069.

OWUSU, C., AGORHOM, E.A., FOSU, S., BUDU-ARTHUR, E., 2020, *Adsorption Studies of Sulphidic refractory gold ore*, Powder Technology, 310-316.

SPICKELMIER, K., 1993, *Round Mountain Halves Its Cutoff Grade*, Miner Eng. (194) 41-48.

TEAGUE, A.J., VANDEVENTER, J.S.J., SWAMINATHAN, C., 1999a, *A conceptual model for gold flotation*, Int. J. Miner. Process., 1001-1019.

VALSIVIESO, A.L., 2006, *Flotation and depression control of arsenopyrite through pH and pulp redox potential using xanthate as the collector*, Int. J. Miner. Process., 81(1), 27-34.

VAUGHAN, J. P., 2004, *The process mineralogy of gold: The classification of ore types*, JOM, Metals and Materials Society, 56, (7), 46-48.

WOODS, R., BASILIO, C.I., KIM, D.S., YOON, R.H., 1994, *Chemisorption of ethyl xanthate on silver-gold alloys*, Coll. Surf. A: Physicochem. Eng. Aspects 83, 1-7.

ZAGHLOUL, K., 2020, *Mineralogical investigation of gold ores*, Egyptian Mineral Resources Authority.

ZHOU, J., Jago, B., MARTIN, C., 2004, *Establishing the process mineralogy of gold ores*, SGS Minerals, Technical Bulletin.

Effect of Rheology on Mineral Processing Operations

Işıl Tokcan

Eskişehir Osmangazi University, Mineral Processing Department

Corresponding author: ikilickaplan@ogu.edu.tr

Abstract:

Companies in the mining industry are being compelled to mine rheologically complicated ore bodies due to the ongoing depletion of high-grade mineral reserves. This has created further challenges in mineral processing, as these ores are more complex and often need to be ground to finer particle sizes, resulting in significant alterations to the rheology of the mineral slurry. The whole effect of inter-particle interactions, including the aggregation and dispersion states of the particles in the slurry, which are more significant under the fine-particle effect, has long been recognized as slurry rheology. Complex flow behaviors in slurries can impact the majority of unit activities, including grinding, classification and flotation.

***Keywords**: mineral processing, rheology, viscosity*

1. Introduction

The supply of easily processed ores is diminishing, and mining operations are increasingly required to handle low-grade, complex ores (Schubert, 2008; Zbik, 2010; Ndlovu et al., 2011; Otsuki et al., 2014; Rosenkranz and Lamberg, 2014). Since these ores frequently need to be processed to a finer particle size and occasionally have a high clay or fibrous minerals like serpentine content, which causes major changes in the rheology of the mineral slurry, this has added to the difficulties associated with mineral processing (Schubert, 2008; Xu et al., 2012; Farrokhpay, 2012; Patra et al., 2012; Ndlovu et al. 2013; Bobicki et al., 2014; Rosenkranz and Lamberg, 2014; Cruz and Peng, 2016).

Understanding the rheology in mineral processing operations and associating rheology with these operations can help us to identify process limitations and offer more insightful input to enhance process performance. In this review paper, the effects of rheology on grinding, classification and flotation processes are given with rheology fundamentals.

2. Rheology Fundamentals

The science of analyzing fluid materials' flow and deformation behaviors is known as rheology. Rheology makes it possible to correlate the structure of the studied material with the seen mechanical behavior. Rheological measurements are frequently used to analyze particle-particle interactions because the rheological behavior of dispersed systems reflects the properties of both the suspended solid particles and the liquid medium in which the solid particles are dispersed. Therefore, it can serve as an effective parameter for process control.

Plotting the shear stress (τ) versus the shear rate (γ) acquired from a rheometer yields a "flow curve" or "rheogram" that frequently illustrates the rheological behavior of a material. There are several typical shear stress–shear rate relationships, which can be seen in Figure 1. Suspensions can generally behave in two ways: Newtonian or non-Newtonian. The second category includes behaviors such as dilatant, plastic, pseudo-plastic, and Bingham (Mewis and Wagner, 2012). The measure of a fluid's internal friction is called viscosity (η). When shear stress is plotted against shear rate for Newtonian fluids, the result is a straight line with a zero intercept; the slope of the line indicates η. Shear stress in non-Newtonian systems is no longer directly proportional to shear rate; in such cases, the viscosity is referred to as "apparent viscosity (η_a)".

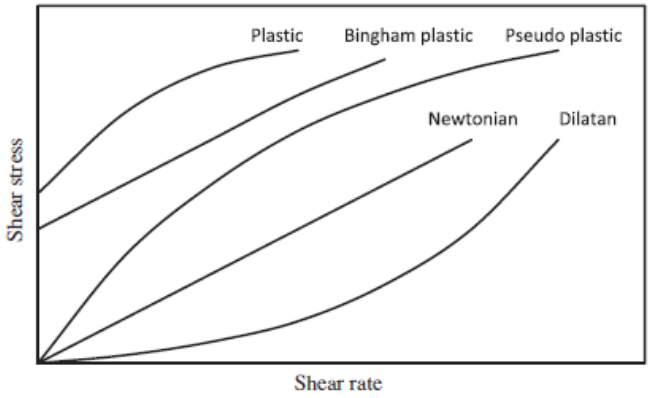


Fig. 1. Schematic diagram of different rheological systems

Another significant term frequently employed in mineral processing is yield stress. Yield stress, a critical rheological parameter, is the minimum shear stress required to initiate fluid motion. This property indicates a structured network of interparticle interactions that must be overcome to commence flow. It is predominantly observed in highly concentrated suspensions composed of fine, aggregated particulate matter. The presence of yield stress signifies a transition from solid-like behavior to fluid-like behavior, marking a crucial point in the material's rheological profile.

The literature presents various methodologies for yield stress quantification, employing various rheometer configurations (cone and plate, parallel plates and bob and cup), and measurement protocols. These techniques typically involve the application of either constant shear rates or controlled stress modes, allowing for comprehensive characterization of the material's rheological profile. A direct measurement methodology, vane technique, was employed to quantify the yield stress of concentrated fine particulate suspensions. This approach utilized a constant low shear rate mode, allowing for precise determination of the yield stress (Nguyen and Boger, 1985). The vane method, known for minimizing sample disturbance and wall slip effects, provides a robust means of characterizing the rheological behavior of complex, structured fluids. Despite the theoretical benefits, conducting measurements at meager shear rates often proves challenging in practice. Therefore, specific analytical rheological models determine yield stress by extrapolating shear stress-shear rate data corresponding to a zero shear rate. The flow behavior of the suspensions can frequently be described using the Bingham and Casson models.

The rheological properties of mineral slurries significantly impact their fluidity and flow characteristics. These attributes directly influence the efficacy of various energy and mass transfer-based unit operations in mineral processing facilities. Such operations encompass grinding, mixing, pumping, screening, and diverse solid-liquid separation processes, including settling, thickening, screening, and cycloning. The rheological behavior of these suspensions thus plays a critical role in determining the overall performance of mineral processing plants (Beazley and Kyle, 1989; Menne, 1991; Healy et al., 1994; Mezei et al., 1999).

2.1. Rheology Effects on Grinding

Comminution processes have been widely implemented across diverse industrial sectors, including ceramics, mineral processing, pharmaceuticals, cosmetics, and food manufacturing (Choi et al., 2001; Kotake et al., 2002; Fuerstenau and Abouzeid, 2002; He et al., 2004; Ipek et al., 2005; Vital et al., 2008). Using a liquid medium in tumbling mill comminution processes is predominantly favored due to its enhanced process efficiency (Yekeler et al., 2001; Tangsathitkulchai, 2002, 2003). The approach of wet comminution presents an opportunity for accurate adjustment of different process parameters like suspension viscosity and rheological behavior, making it easier to produce materials with precisely customized qualities.

Extensive research has been conducted to elucidate the relationship between particle grinding and slurry rheology. Klimpel (1982, 1983, 1984) conducted comprehensive laboratory and industrial-scale investigations for two decades focusing on the rheological impacts on grinding processes. His findings revealed a significant correlation between increasing solid content and the evolution of rheological properties, progressing from dilatant to pseudoplastic, and ultimately to yield pseudoplastic behavior. The critical solid content at which these rheological transitions occurred was found to be contingent upon various slurry characteristics, including the particle size distribution, the material's specific breakage properties, and the prevailing chemical environment. This research elucidated the complex interaction between solid concentration and other physicochemical parameters in determining the rheological regime of grinding slurries. Additional studies were performed by Hockings et al. (1965), Clarke and Kitchener (1968), Tucker (1982), Fuerstenau et al. (1990), Gao and Forssberg (1993), and Shi and Napier-Munn (2002) demonstrated the impact of slurry rheology on industrial grinding processes.

At lower solid concentrations, dispersions typically show Newtonian rheological characteristics (Krieger, 1972). Conversely, as the solid content increases, there is a dramatic change in the slurry viscosity and a transition to non-Newtonian behavior is frequently observed. This non-Newtonian rheological response is intrinsically linked to particle size distribution, becoming particularly pronounced in highly concentrated suspensions composed of fine particulate matter. At a constant volume fraction, a reduction in particle size correlates with an increase in the number of particles in suspension, leading to enhanced particle-particle interactions and consequently, elevated viscosity (Malvern, 2009). These interparticle interactions are characterized as weak forces, their impact on viscosity is more pronounced in the lower shear rate regime. Conversely, an increase in particle size results in a decrease in viscosity, which is attributed to diminished particle interactions (Malvern, 2009). Suspensions predominantly consisting of coarse particles exhibit markedly different behavior; the apparent viscosity demonstrates only marginal increases with increasing solid content. Consequently, these coarse particle systems may retain Newtonian fluid characteristics up to comparatively high solid concentrations.

Grinding aids diminish the viscosity of mineral slurries in grinding mills. This enables effective comminution at higher solids content, facilitating increased throughput or the utilization of fewer mills. (Pearse, 2005). The addition of polymeric and inorganic dispersants decreased yield stress, leading to reduced energy consumption and a finer, narrower product size distribution. This ability to influence particle size distribution through rheology control has potentially significant implications for downstream processes including flotation, leaching, and dewatering (Yue and Klein, 2004).

The rheological properties of slurries exert a significant influence on both the grinding dynamics and the mass transfer mechanisms within grinding mills. Therefore, slurry rheology plays a crucial role in determining the overall energy efficiency of the milling process. The literature presents divergent conclusions regarding the impact of rheology on grinding processes. This discrepancy may be attributed, in part, to the intricate and interrelated nature of rheological effects on particle comminution, mass transfer phenomena, and energy efficiency within grinding mills. Such interactions are far more noticeable in closed industrial grinding circuits, and these effects might even cancel each other out in certain situations. Consequently, selecting an appropriate performance criterion becomes important when investigating the rheological influence on industrial grinding operations.

2.2. Rheology Effects on Hydrocyclone

In industrial comminution processes, mills are predominantly operated in closed circuits incorporating classifiers. These classifiers' efficiency significantly influences mill operation through modulation of the recirculating load, thereby impacting throughput, fines content in mill feed, and slurry density. Consequently, the classifier can be conceptualized as a rheological control mechanism for the grinding mill (Shi and Napier-Munn, 2002).

The prevailing design and operational protocols for hydrocyclones are primarily optimized for dilute slurries (Bradley, 1965; Lynch, 1977; Svarovsky, 1984). However, in the context of mineral processing plants, slurries with high solids concentrations coupled with broad particle size distributions exhibit

yield pseudoplastic rheological characteristics (Horsley and Allen, 1987). The solids content effects on the apparent slurry viscosity for different particle size distributions are shown in Figure 2.

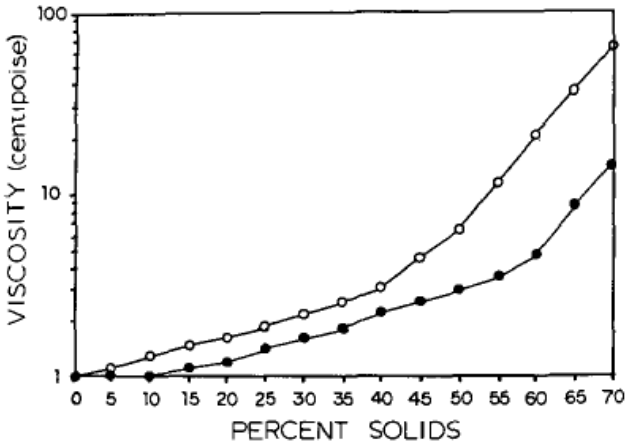


Fig. 2. Apparent slurry viscosity changes with increasing solids content for two particle size distributions samples of iron-ore (•: cyclone feed, 80% - 200 mesh; o: cyclone overflow, 80% -325 mesh) (Kawatra and Eisele, 1988).

Slurries with less than 70% solid content by mass typically behave as Newtonian fluids or display Newtonian-like properties, as noted by Kawatra et al. (1996). However, some slurries may exhibit non-Newtonian characteristics even at concentrations below this threshold (Shi and Napier-Munn, 1996). When processing non-Newtonian slurries in a hydrocyclone, the slurry's viscosity and flow behavior change with shear rate, making this factor crucial. As the slurry enters the cyclone body through the feed inlet, it undergoes increasing shear rates. This shear rate peaks at the point where the tangential velocity is highest. Because of their smaller radius, smaller cyclones have higher tangential velocities and, consequently, higher shear rates. According to Castro (1990), a slurry that displays pseudoplastic behavior (thixotropy) would typically exhibit a drop in viscosity once it achieves a shear rate that is higher than what it experienced before entering the cyclone. These greater shear rates would enhance the viscosity of a slurry with dilatant properties (rheopexy) (Van Wazer et al., 1963). It is noted that the shear forces within cyclones can disrupt clay agglomerates, providing an advantage in processing thixotropic and Bingham plastic slurries (Svarovsky, 2001; Marthinussen, 2011). Conversely, these shear forces prevent the use of flocculation to enhance separation, unlike in gravity thickeners.

While shear rate is a key factor, it is not the only one that affects the flow behavior of slurry in a hydrocyclone. At volume concentrations greater than 30%, hindered settling becomes significant, resulting in increased viscosity due to enhanced particle interactions (Cheng, 1980). As the concentration increases towards the apex of the hydrocyclone, the velocities (and shear rates) decrease, thereby influencing the rheological properties. A Newtonian slurry entering a hydrocyclone typically does not experience major changes in its flow characteristics, and its viscosity tends to remain relatively stable throughout the process (Kelsall, 1953; Bradley, 1965).

The presence of fibrous and swelling clay minerals in slurries complicates rheology, necessitating additional measurements for accurately quantifying their effects on hydrocyclone efficiency. Fibrous asbestos can produce atypical overall partition curves (Wills and Finch, 2016) while swelling clays restrict hydrocyclone performance (Özgen et al., 2010; Boylu et al., 2010). Comprehending rheology's impact in hydrocyclones is challenging due to the highly complex nature of the flow behavior (Narasimha et al., 2014). Centrifugal separation of highly viscous fluids is necessitating pretreatment processes to reduce viscosity. These include heating, using rheology modifiers, and injecting gas or lower-viscosity fluids. However, these methods may not always sufficiently improve separation performance. Furthermore, implementing such pretreatments can lead to alterations in the final product and increased operational costs (Jing et al., 2021).

2.3. Rheology Effects on Flotation

Froth flotation is the most common method for the beneficiation of complex, low-grade, and finely disseminated ores. It can be presumed that rheological characteristics have no effect on flotation efficiency since flotation pulps contain a substantially lower concentration of particles than wet grinding. Particle size, size distribution, particle shape, solids content, pulp chemistry, and particle surface characteristics are some of the slurry parameters that significantly affect slurry rheology. The rheological properties of mineral slurries significantly impact processing performance. Consequently, even minor alterations in slurry characteristics can substantially affect processes like flotation.

Since yield stress is a key indicator of suspension behavior, it enables the examination of aggregation and dispersion phenomena arising from interparticle interactions in colloidal systems. Figure 3 shows the relationship between yield stress and solids volume fraction as a function of pH. However, due to the direct correlation between yield stress and bond strength, the circumstances in which it manifests can impact gas dispersion, bubble-particle attachment, and separation. This direct link also indicates the number of particle bonds that had to be broken for improved grade and recovery (Cruz et al., 2019).

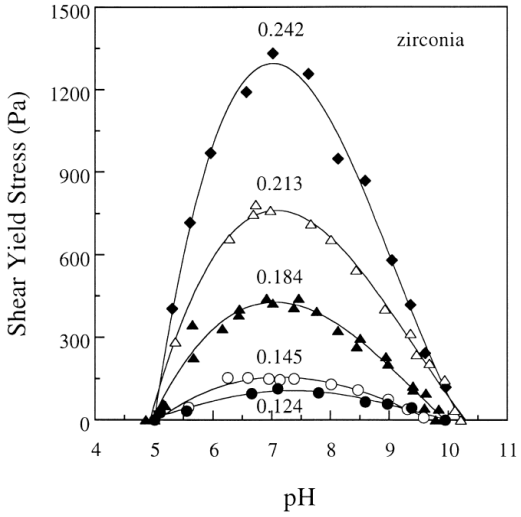


Fig. 3. Concentrated zirconia suspensions' yield stress values in relation to pH and solids volume fraction (Johnson et al., 2000)

The maximum packing fraction and, consequently, the concentration/viscosity relationship are significantly influenced by particle shape. The packing density of particles is also impacted by their irregular shapes. Barnes et al. (1989) investigated how irregularly shaped particles affect viscosity and showed that rod-shaped particles had a bigger impact on suspension viscosity than disc-shaped particles. The effects of fiber particle concentration on viscosity are significantly more noticeable (Horie and Pinder, 1979). It is evident that the shape of the mineral has a significant impact on the rheological behavior of flotation pulps, and phyllosilicate minerals, especially swelling clays and serpentine minerals, can produce higher viscosities than non-phyllosilicate minerals like quartz (Ndlovu et al., 2014). The effect of particle shape on the rheology is shown in Figure 4.

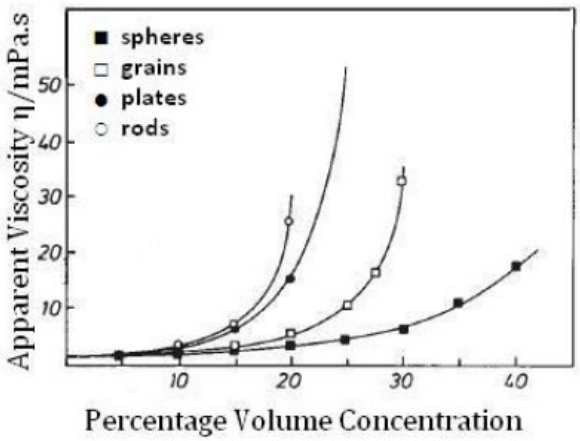


Fig. 4. The influence of particle morphology on apparent viscosity across different volume concentrations (at a shear rate of 300 s^{1-}) (Clarke, 1967).

The flotation medium's viscosity may also impact the flotation recovery. A higher pulp viscosity usually corresponds to a lower recovery of valuable minerals (Ogawa et al., 1997; Genc et al., 2012; Genovese, 2012). Increased viscosity of the suspending medium has been observed to enhance the durability of complexes formed between bubbles and particles (Xu et al., 2011). Moreover, the amount of solids in the pulp strongly influences recovery through entrainment. Higher concentrations of solids, more viscous pulps, reduce turbulence in the cell, leading to bubble coalescence (Rubinstein, 1995).

Rheology's role in mineral flotation is recognized as significant, yet how it affects flotation performance through pulp or froth phases remains unclear. This gap in understanding may stem from difficulties in accurately measuring the rheological properties of mineral slurries, as solid particles often settle during measurement.

3. Conclusions

In this review article, some of the effects of rheology on unit mineral processing operations are given. Due to the global depletion of high-grade ores (both metallic and nonmetallic), low-grade and complex ores such as clayey and fibrous ores are being processed in large quantities, often resulting in rheological challenges and complications in the processes. The transportation of mineral slurry, ore grinding, and mineral separation processes like flotation have all seen a significant impact on the rheological behavior of mineral particles in the mineral processing industries.

Several physical, chemical, and mechanical parameters that affect the mineral processing performance of particles have been discussed by researchers over the years. However, there is still a gap between rheology and mineral processing operations due to the complexity of rheological conditions and measurements through the operations. Developing a reliable method to measure these slurries' rheology continues to be a research challenge for future studies.

References

Barnes, H.A, Hutton, J.F. & Walters, K. (1989). An introduction to rheology, Elsevier Scientific Publishing Company.

Beazley, J.L. & Kyle, J.H., 1989. The pulp rheology of some Australian gold ores. In: Bhappu, R.P., Harden, R.J. (Eds.), World Gold’89 Conference. Reno, Nevada, Proceedings SME. November 5–8, 1989, 282–287.

Bobicki, E.R., Liu, Q. & Xu, Z. (2014). Effect of microwave pre-treatment on ultramafic nickel ore slurry rheology, *Miner. Eng*., 61, 97–104.

Boylu, F., Çinku, K., Esenli, F.& Çelik, M. S. (2010). *Int. J. Miner. Process*., 4, 196.

Bradley, D. (1965). The hydrocyclone. Pergamon, London

Burdukova, E., Becker, M., Ndlovu, B., Mokgethi, B. & Deglon, D. (2008). Relationship between slurry rheology and its mineralogical content, *24th International Minerals Processing Congress, CAE, CMA, CNI-A, CISA, CNCA, and CBMIA*, Beijing, 24–28 September 2008.

Clarke, B. (1967). Rheology of coarse settling suspensions. *Trans. Inst. Chem. Engrs*. 45, 251–256.

Clarke, B. & Kitchener, J.A., 1968. The influence of pulp viscosity on fine grinding in a ball mill. Br. Chem. Eng. 13, 991–995.

Cruz, N. & Peng, Y. (2016). Rheology measurements for flotation slurries with high clay contents-a critical review, *Miner. Eng*., 98, 137–150. [

Cruz, N., Forster, J. &. Bobicki, E. R (2019). Slurry rheology in mineral processing unit operations: a critical review, *The Canadian Journal of Chemical Engineering*, 97, (7), 2102–2120,.

Farrokhpay, S. (2012). The importance of rheology in mineral flotation: a review, *Miner. Eng*., 36–38, 272–278.

Fuerstenau, D.W., Kapur, P.C. & Velamakanni, B.V. (1990). A multi-torque model for the effects of dispersants and slurry viscosity on ball milling, *Int. J. Miner. Process*., 28, 81–98.

Fuerstenau, D.W. & Abouzeid, A.-Z.M. (2002). The energy efficiency of ball milling in comminution, *Int. J. Miner. Process*., 67: 161–185.

Gao, M.W. & Forssberg, E. (1993). The influence of slurry rheology on ultra-fine grinding in a stirred ball mill, *Proceedings XVIII Int. Min. Process. Cong*., Sydney. The Australasian Institute of Mining and Metallurgy (AusIMM), Melbourne, 237– 244.

Genc, A.M., Kilickaplan, I. & Laskowski, J.S. (2012). Effect of Pulp Rheology on Flotation of Nickel Sulphide Ore with Fibrous Gangue Particles, *Can. Metall. Q*., 51, 368–375.

Genovese, D.B. (2012). Shear rheology of hard-sphere, dispersed, and aggregated suspensions, and filler-matrix composites *Adv. Colloid Interface Sci.* , 171–172, 1–16.

He, M., Wang, Y. & Forssberg, E. (2004). Slurry rheology in wet ultrafine grinding of industrial minerals: a review, *Powder Technol*., 147: 94–112.

Healy, T.W., Boger, D.V., White, L.R., Leong, Y.K. & Scales, P.J., 1994. Thickening and clarification; how much do we really know about dewatering. In: 6th Aus. IMM Extractive Metallurgy Conference, 3–6 July. Brisbane, Australia.

Horie, M. & Pinder, K.L., 1979. Time-dependent shear flow of artificial slurries in coaxial cylinder viscometer with a wide gap, *The Canadian Journal of Chemical Engineering*, 57, 125-134.

Horsley, R.R. & Allen, D.W. (1987). The effect of yield stress on hydrocyclone performance in the mining industry. *3nd Int. Conf. on Hydrocyclones*, 30 Sept - 2 Oct., Oxford, England, 269-275.

Ipek, H., Ucbas, Y., Yekeler, M. & Hoşten, C. (2005). Dry grinding kinetics of binary mixtures of ceramic raw materials by Bond milling, *Ceram Int*, 31: 1065–1071.

Jing, J., Zhang, S., Qin, M., Luo, J., Shan, Y., Cheng, Y. & Tan, J. (2021). Numerical simulation study of offshore heavy oil desanding by hydrocyclones, *Separ. Purif. Technol*., 258, 118051

Johnson, S.B, Scales, P.J, Franks, G.V, Boger, D.V. & Healy, T.W. (2000). surface chemistry- rheology relationships in concentrated mineral suspensions, *Int. Journal of Minerals Processing*, 58, 267-304.

Kawatra, S. K. & Eisele, T. C. (1988). Rheological effects in grinding circuits, International Journal of Mineral Processing, 22(1-4): 251-259.

Kawatra, S.K., Bakshi, A.K. & Miller, T.E. (1996). Rheological characterization of mineral suspensions using a vibrating sphere and a rotational viscometer, *Int. J. Miner. Process*., 44–45, 155–165

Kelsall, D. F. (1953). A further study of the hydraulic cyclone, *Chemical Engineering Science,* 2: 254-273.

Klimpel, R.R. (1982). Slurry rheology influence on the performance of mineral/coal grinding circuit. Part 1, *Miner. Eng*., 34 (12), 1665–1668.

Klimpel, R.R. (1983). Slurry Rheology Influence on the Performance of Mineral/Coal Grinding Circuits-Part 2, *Mining Engineering*, 21-26.

Klimpel, R.R. (1984). Use of chemical reagents in flotation, *Chem. Eng*. 91 (18), 75_79.

Kotake, N., Suzuki, K., Asahi, S. & Kanda, Y. (2002). Experimental study on the grinding rate constant of solid materials in a ball mill, *Powder Technol*., 122: 101–108.

Lynch, A. J. (1977). *Mineral crushing and grinding circuits: Their simulation, optimization and control.* Elsevier, Oxford.

Marthinussen, S.-A. (2011). *The effect of fluid viscosity on hydrocyclone performance - Design and commissioning of an experimental rig and results*, MA thesis, University of Bergen, Bergen, 96.

Menne, D.M. (1991). Gold Cyanidation, *Electromagnetic Books*, Mt. Claremont, W.A.

Mewis, J. & Wagner, N. J. (2012). *Colloidal Suspension Rheology*, Cambridge University Press, New York, NY, USA.

Mezei, A., Ferron, C.J. & Ashbury, M. (1999). Practical aspects of rheological studies for the mineral and process slurries. *Engineering Foundation Conferences, ''Rheology in the Mineral and Energy Industries II''*, March 14–19, Hawaii.

Muster, T. H. & Prestidge, C. A., (1995). Rheological investigations of sulphide mineral slurries, *Minerals Engineering*, 8 (12), 1541–1555,.

Napier-Munn, T. J., Morrell, S., Morrison, R. D. & Kojovic, T. (1996). Mineral comminution circuits: their operation and optimisation, *JKMRC Monograph series*, Vol.2.

Narasimha, M., Mainza, A. N., Holtham, P. N., Powell, M. S. & Brennan, M. S. (2014). Int. J. Miner. Process. , 133, 1.

Ndlovu, B., Becker, M., Forbes, E., Deglon, D. & Franzidis, P. (2011). The influence of phyllosilicate mineralogy on the rheology of mineral slurries, *Minerals Engineering*, 24 (12), 1314–1322.

Ndlovu, B., Farrokhpay, S. & Bradshaw, D. (2013). *Int. J. Miner. Process*., 125, 149.

Ndlovu, B., Forbes, E., Farrokhpay, S., Becker, M., Bradshaw, D. & Deglon, D. (2014). A preliminary rheological classification of phyllosilicate group minerals, *Minerals Engineering*, vol. 55, pp. 190–200.

Nguyen, Q.D. & Boger, D.V. (1985). Direct yield stress measurement with the vane method. *J. Rheol*. 29 (3), 335–347.

Ogawa, A., Yamada, H., Matsuda, S., Okajima, K.& Doi, M. (1997). Viscosity equation for concentrated suspensions of charged colloidal particles, *J. Rheol*., 41, 769–785

Otsuki, A., Chen, Y. & Zhao, Y. (2014). Characterisation and beneficiation of complex ores for sustainable use of mineral resources: Refractory gold ore beneficiation as an example, *International Journal of the Society of Materials Engineering for Resources*, 20, 126.

Özgen, S. & Yildiz, A. (2010). Clay. *Clay Miner*. 58, 431.

Patra, P., Bhambhani, T., Nagaraj, D. R. & Somasundaran, P. (2012). Impact of pulp rheological behavior on selective separation of Ni minerals from fibrous serpentine ores, *Colloids and Surfaces A: Physicochemical and Engineering Aspects*, 411, 24–26.

Pearse, M.J. (2005). An overview of the use of chemical reagents in mineral processing, *Miner. Eng*. 18, 139–149.

Rosenkranz, J. & Lamberg, P. (2014). Sustainable processing of mineral resources, *International Journal of the Society of Materials Engineering for Resources,* 20, 17-22.

Schubert, H. (2008). On the optimization of hydrodynamics in fine particle flotation. *Miner. Eng*. 21, 930–936.

Shi, F. N. & Napier-Munn, T. J. (1996a). Measuring the rheology of slurries using an on-line viscometer. *Int. J. Miner. Process*. 47, 153-176.

Shi, F.N. & Napier-Munn, T.J. (2002). Effects of slurry rheology on industrial grinding performance, *Int. J. Miner. Process.*, 65, 125–140.

Svarovsky, L. (1984). *Hydrocyclones.* Holt, Rinehart and Winston, London.

Tangsathitkulchai, C., (2003). The effect of slurry rheology on fine grinding in a laboratory ball mill, *Int J Miner Process,* 69: 29–47.

Tangsathitkulchai, C. (2002). Acceleration of particle breakage rates in wet batch ball milling, *Powder Technol*, 124: 67–75.

Tucker, P. (1982). The role of viscosity in the wet-grinding of ores, with special reference to grinding aids, *Warren Spring Laboratory Report*, LR 421 (MP).

Van Wazer, J. R., Lyons, J. W., Kim, K. Y. & Colwell, R. E. (1963). Viscosity and flow measurement - A laboratory handbook of rheology, Interscience Publishers

Wills, B. A. & Finch, J. A. (2016). Classification, Will's Mineral Processing Technology - An Introduction to the Practical Aspects of Ore Treatment and Mineral Recovery, Butterworth- Heinemann, Oxford, 199–221.

Xu, D., Ametov, I., Grano, S.R., 2011. Detachment of coarse particles from oscillating bubbles – The effect of particle contact angle, shape and medium viscosity. *Int. J. Miner. Process*. 101 (1–4), 50–57.

Xu, M., Dai, Z., Dong J., Ford, F., Lee & A. W. (2012). *CIM Journal,* 3, 1.

Yekeler, M., Ozkan, A. & Austin, L.G. (2001). Kinetics of fine wet grinding in a laboratory ball mill. *Powder Technol*, 114: 224–228.

Yue, J. & Klein, B. (2004). Influence of rheology on the performance of horizontal stirred mills, *Minerals Engineering*, 17 (11-12), 1169-1177.

Zbik, M., Raftery, N.A., Smart, R.S.C. & Frost, R.L. (2010). Kaolinite platelet orientation for XRD and AFM applications, *Applied Clay Science,* 50, 299–304.

HPGR influences on downstream ball mill according Bond tests and energy calculations

F Heinicke [1]*, H Lieberwirth [2] and M Pfeifer [1]

[1] Köppern Aufbereitungstechnik, Freiberg, 09599

[2] Institute for Mineral Processing Machines and Recycling Systems Technology, Technical University Bergakademie Freiberg, 09599

*Corresponding author F.Heinicke@koeppern.com (F Heinicke)

Abstract:

HPGRs (high pressure grinding rolls) have been developed within the last decades for energy efficient processing of a wide variety of ores. Special interest has been raised by projects increasing the capacities of processing plants by installing HPGRs prior to ball mills. Bond ball mill tests have been used for decades as a base for ball mill dimensioning in mineral circuits. For final CAPEX-OPEX considerations of the processing circuit, one key question is about the level of grinding energy split between HPGR and downstream grinding stages. This is especially interesting if the downstream process comprises multiple grinding stages combined with separation steps.

The paper presents investigations on grinding energy consumption, size distribution and microfracturing of HPGR products, which affect the efficiency of the whole comminution and sorting process.

Keywords: *HPGR*

1. Introduction

The comminution process of High Pressure Grinding Rolls (HPGR) was discovered in the 1980s by the research work of the German Professor Schönert. Its main advantage is the high energy efficiency in comparison to ball mill grinding which has been the benchmark process in the cement industry by then (Schönert, 1988). Since then, a worldwide trend towards HPGR application has been established (Klymowsky *et al*, 2002), first in the cement industry but soon after also in ore processing.

Nevertheless, it has to be noted that the technology has its roots much earlier. Köppern, as one supplier of HPGR, has been working for more than 120 years on roller presses, starting with the formation of coal briquettes between two rollers. Subsequently, other fields of application, eg for fertilizer compaction, emerged (Schönert, 1966).

Even based on this history, it was a large step to transfer this process principle to minerals applications due to the much higher wear caused by the higher abrasivity of those materials. The first applications started in iron ore concentrate grinding. Meanwhile, with the optimisation of the roller surfaces using studs (Morley, 1995), the service life of the rollers substantially increased and the technology has been well established for ores and hard rock applications.

Figure 1 refers to a common installation of a HPGR for iron ore. Other set-ups with primary ball mills in circuit with cyclones which are prevalent in non-ferrous industries shall not be addresses in this paper. The material is pre-crushed to a feed size of 25 mm and then processed by HPGR within a pregrinding application in front of a primary ball mill (Morely, 1995). The HPGR is designed to work in open circuit in this case, with the transfer size to the ball mill being in the range of 80 per cent passing 7 mm. The primary ball mill is operated in a closed circuit with a screw classifier, followed by a magnetic separation stage. Tailings of this stage are reground in a ball mill hydrocyclone circuit for further processing.

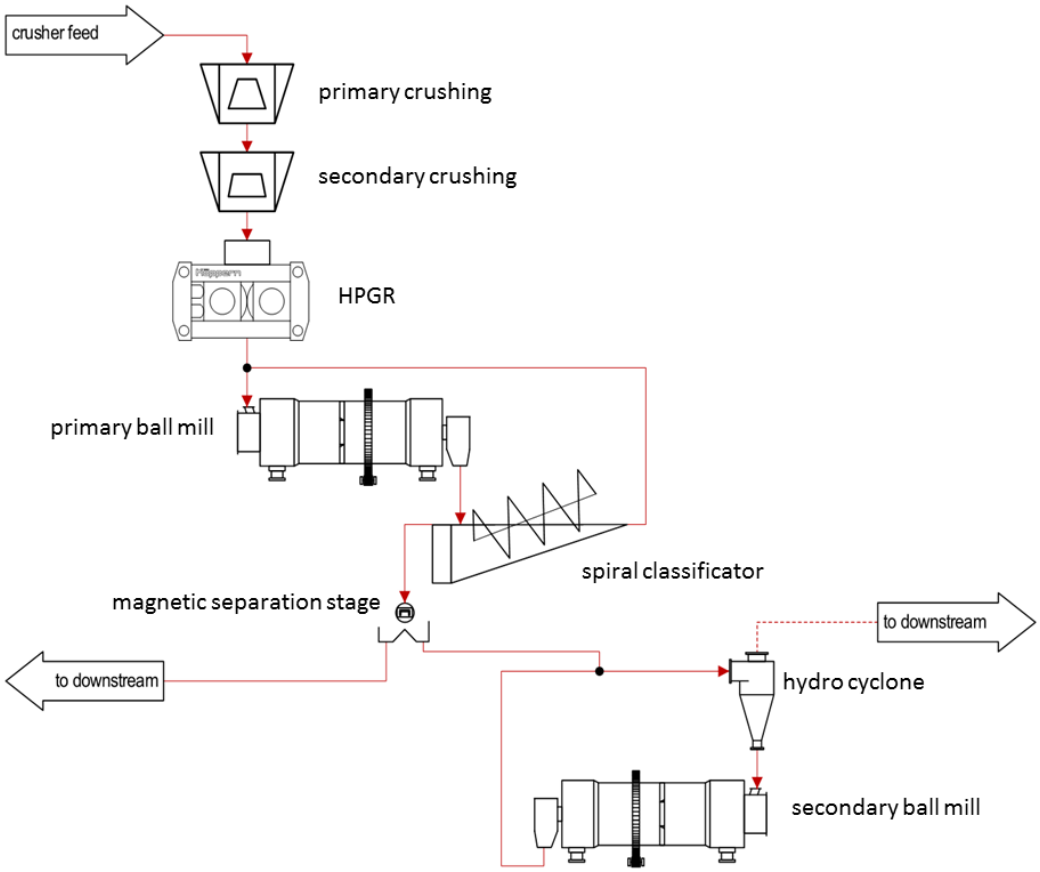


FIG 1. Typical Flow sheet of HPGR processing in front of ball mill.

To achieve the best grinding efficiency, HPGR are available in a wide size range. Figure 2 shows a state-of-the art Köppern type HPGR. The key questions for sizing of such a machine are:

1. What throughput is to be processed by the machine?
2. What is the desired transfer size to the downstream process?
3. Which energy input shall be achieved?
4. How does the downstream flow sheet look like?
5. Which downstream effects shall be fostered, especially with regard to the subsequent ball mill grinding stage?

All those questions need to be answered in the process design phase, prior to selecting and sizing the key equipment.



FIG 2. Typical example of a state-of-the-art HPGR.

2. SIZING KEY EQUIPMENT

The performance of HPGR primarily depends on the ore and its characteristics (Morley, 2006). Grinding tests are still indispensable to determine those characteristics and to predict the operational behaviour of the machine comminuting a certain material. The most important parameters are the specific throughput and specific energy consumption which allows selection of the appropriate HPGR for the required material and process parameters (Heinicke, 2016a and Gruendken, 2008). The specific energy consumption is a mass rate normalised value to describe the amount of energy transferred to the material in one single grinding pass.

$$W_{Sp,HPGR} = \frac{(P_{t,HPGR} - P_{i,HPGR})}{\dot{M}_{HPGR}} \quad (1)$$

where:

$W_{Sp,HPGR}$ mass specific energy consumption of HPGR

P_t total power draw under load

P_i idle power draw

$\dot{M}_{HPGR}$ total HPGR throughput equals fresh feed rate in open circuit operation

The Bond ball mill test (Bond, 1952) is a proven method to predict the performance of a ball mill. The power draw can be calculated respectively, using the following formula:

$$W_{Sp,BM} = W_i * k * \left(\frac{10}{\sqrt{P_{80}}} - \frac{10}{\sqrt{F_{80}}}\right) \quad (2)$$

where:

$W_{Sp,BM}$ power draw of ball mill

W_i Bond work index as material specific parameter

k product of correction factors according to Bond

P_{80} 80 percent product size passing of ball mill

F_{80} 80 percent feed size passing of ball mill

If the formula is analysed in an analytical way there are three influences to reduce the energy consumption which have different level of effect:

HPGR influences on downstream ball mill according Bond tests and energy calculations

- reduce F_{80} at low impact
- reduce P_{80} at medium impact
- reduce work index at highest impact.

Figure 3 shows those effects on the throughput of a ball mill (varied parameters as per Table1):

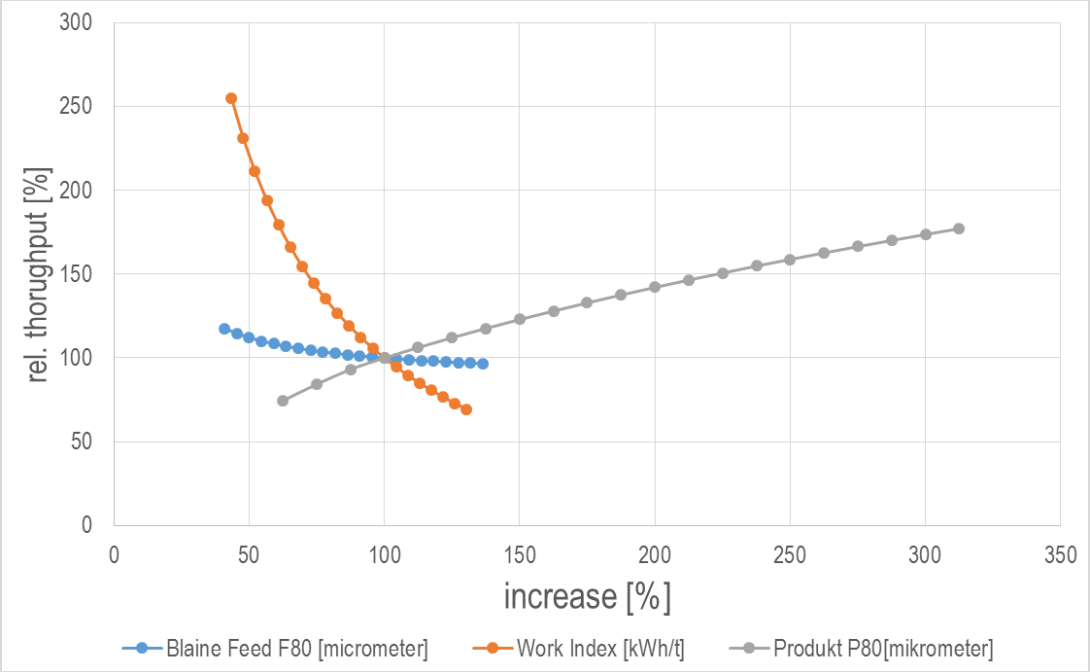


FIG 3. Effect on throughput of Bond parameters.

Table1. Input parameters for Bond variation graph of a brownfield plant (see also Povey, 2017).

Feed rate	466 t/h
Feed size F_{80}	11 mm
Product size P_{80}	0.181 mm
Mill power effective	3575 kW
Estimated Bond Wi	11.5 kWh/t

The total grinding energy according to the flow sheet shown in Figure 1 can be calculated as follows:

$$P_{TOTAL} = P_{HPGR} + P_{BM,1} + P_{BM,2} \quad (3)$$

where:

P_{Total} total grinding power consumption

P_{HPGR} power consumption of HPGR

$P_{BM,1/2}$ power consumption of primary (1) and secondary (2) ball mill

The combination of (1) and (3) results in (4):

$$P_{TOTAL} = W_{Sp,HPGR} * \dot{M}_{HPGR} + W_{Sp,BM,1} * \dot{M}_{BM,1} + W_{Sp,BM,2} * \dot{M}_{BM,2} \quad (4)$$

where:

$\dot{M}_{BM,1/2}$ total primary (1) and secondary (2) ball mill throughput

$W_{Sp,BM,1/2}$ primary (1) and secondary (2) ball mill work index

If a mass split of 50 percent is assumed in the magnetic separation stage, the masses are related as follows:

$$\dot{M} = \dot{M}_{HPGR} = \dot{M}_{BM,1} = \dot{M}_{BM,2} * 2 \quad (5)$$

where:

$\dot{M}$ fresh feed rate

Thus, the combination of (2), (4) and (5) results in (6):

$$P_{TOTAL} = \dot{M} \left\{ \begin{array}{c} (P_{t,HPGR} - P_{i,HPGR}) + W_{i,1} * k * \left(\frac{10}{\sqrt{P_{80,\mathrm{BM1}}}} - \frac{10}{\sqrt{P_{80,\mathrm{HPGR}}}} \right) \\ + W_{i,2} * k * \left(\frac{10}{\sqrt{P_{80,\mathrm{BM2}}}} - \frac{10}{\sqrt{P_{80,\mathrm{BM1}}}} \right) * 0{,}5 \end{array} \right\} \quad (6)$$

where:

$W_{i,1/2}$ Bond ball mill work index as material specific parameter of primary (1) and secondary (2) ball mill

k product of correction factors

In a given brownfield application, the installed power of the ball mills is fixed which means that the product of specific energy and maximum attainable throughput has to be the same for each mill at all times. Also, the transfer size to the downstream process after second ball mill is defined by the material characteristics and respective specifications of the downstream process such as liberation size and throughput. The product size of the HPGR, however, can be adjusted by increasing the hydraulic piston pressure in the machine. Thus, also the feed size to the primary ball mill can be controlled. An increase of the hydraulic pressure in the HPGR leads to an increased power draw of the HPGR roll drives as well (see Figure 4).

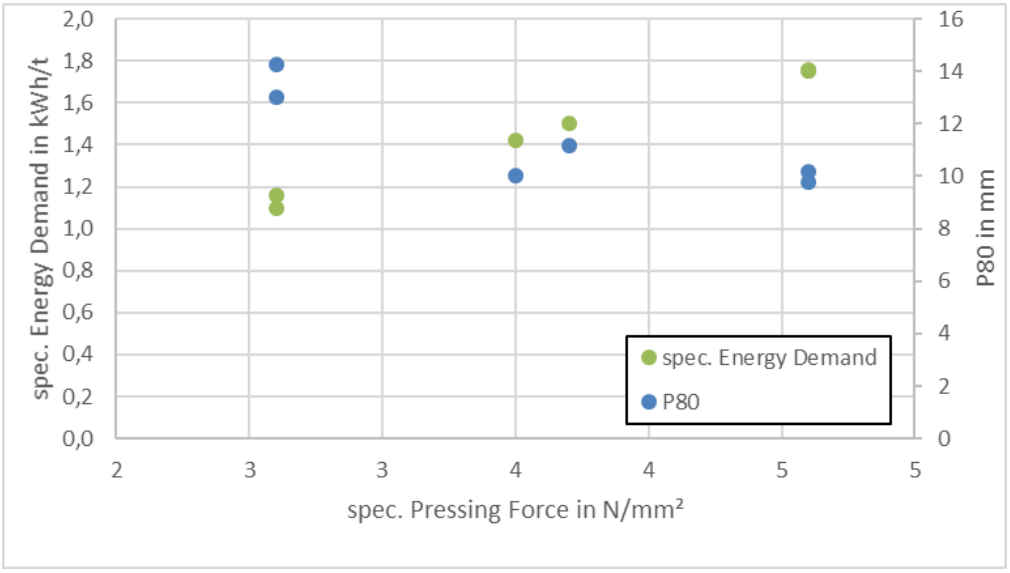


FIG 4. Correlation of specific hydraulic pressure and specific energy demand from a test series with iron ore.

Moreover, the high pressure grinding regime leads to micro-fractures within the product as shown in Figure 5. Those micro-fractures reduce the strength of the ore fed to subsequent comminution machines. In the presented flow chart, they reduce the Bond ball mill work index of the material transferred from the HPGR to the primary ball mill. Thus, the throughput or the size reduction degree of the primary ball mill can be increased to fully exploit the installed power of the ball mill. It became clear that there

is an optimisation potential between energy efficient grinding in the HPGR and downstream ball mill grinding.

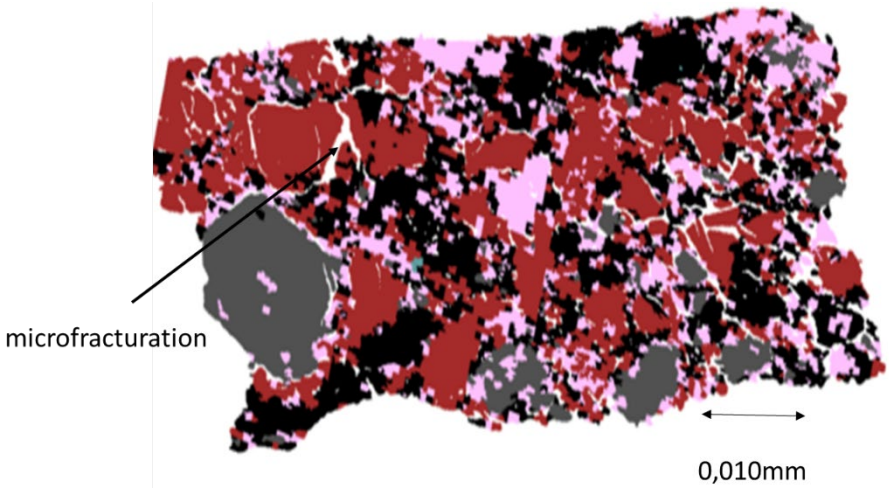


FIG 5. Example of a micro-fractured particle of a HPGR.

Such an optimisation has to include the whole downstream process. An simple increase of the throughput in the primary ball mill would mean that the second ball mill would receive a higher feed rate as well. It can be assumed that the mircro-fracturing initiated by the HPGR will be exploited in the primary ball mill. Therefore, the secondary ball mill has to be designed considering a higher Bond ball mill work index than the primary one. The best way to avoid a potential overload of the secondary ball mill is to reduce the transfer size from primary ball mill. This affects the sorting behaviour and impacts the optimum process as well. The micro-fracturation of the particle is known to increase the liberation degree and therefore can influence the magnetic separation (Michaelis, 1995). Again the design of mass flows is influenced and need to be optimised. For this optimisation, it is essential to understand of the differences between ball mill grinding and HPGR grinding in view to the downstream energy efficiency effects.

3. INFLUENCES ON BOND WORK INDEX USING HPGR

To assess the energy efficiency effect of HPGR, various Bond ball mill test series were performed (see also Brüggemann, 2019), all of them following the stipulations of Bond. The feed material for the Bond tests was a medium grained granodiorite from Kindisch (Germany) with a compression strength of σ_D = 176 MPa, produced by a hammer mill with grate (HAZEMAG Unirotor 490/380), a single toggle jaw crusher (Retsch BB 250 XL) and an HPGR (Köppern HPGR 60/10–230 and HPGR 22/3), see Figure 6. In those three machines, the material is stressed in different ways, merely by compression in the jaw crusher and the HPGR or by blow and shear in the hammer mill.

Despite the upper limit of the feed size of the material for the tests was always the same (-3150 µm), the particle size distributions PSD vary significantly. The first mayor difference is the slope of the particle size distribution curve (see Figure 7). While the particle size curves distribution curves of the jaw crusher and hammer mill product in the respective size range show only minor differences, the slope of the HPGR product size distribution is shallower, which is a common observation for HPGR grinding (Heinicke, 2012).

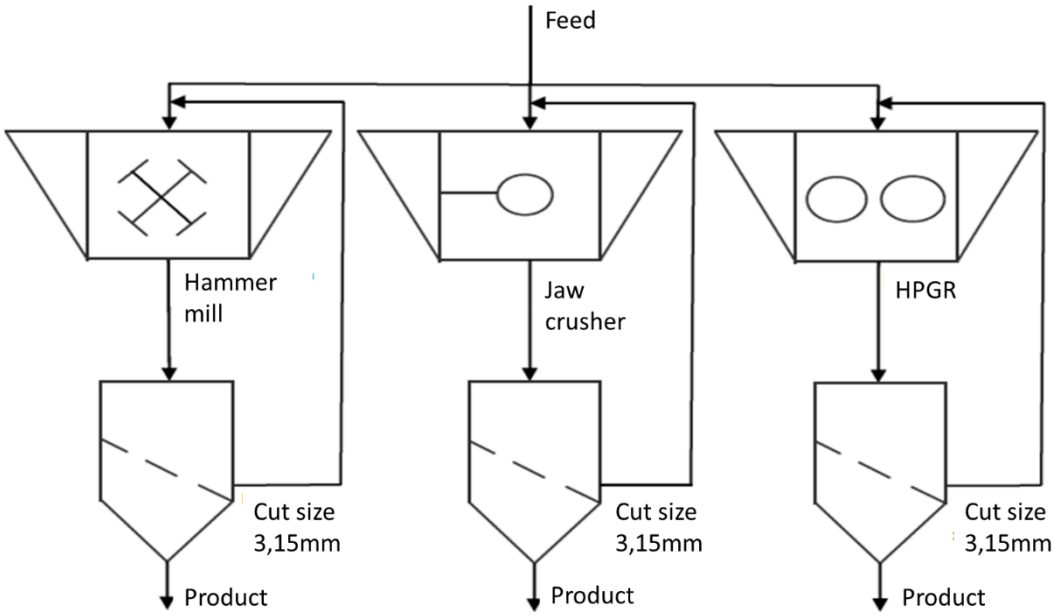


FIG 6. Test work set-up for preparation of sample.

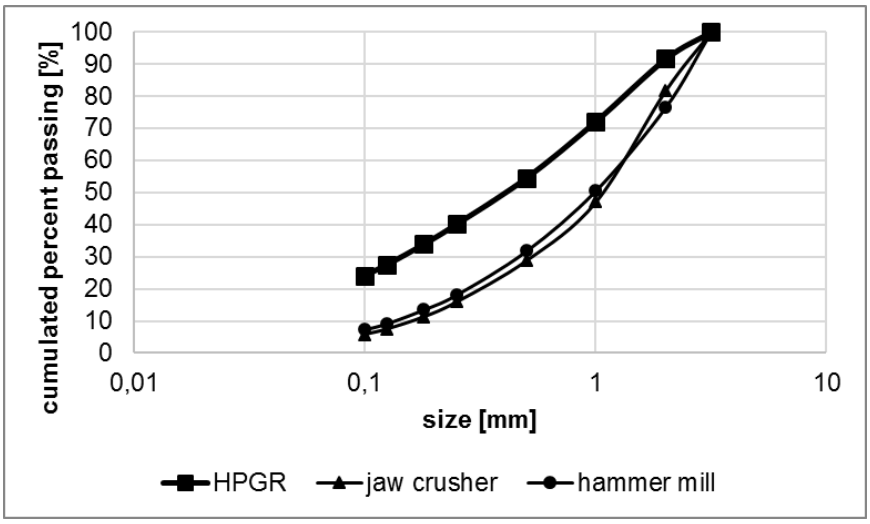


FIG 7 – Particle sizes for different preparations.

It has been well established, that among others the preparation of the feed material influences the results of the Bond test (Gonzáles, 2021; Weier and Chenje, 2018; Vizcarra and Wong, 2019) but the experimental error is usually small (Ballantyne and Giblett, 2019). The small experimental error was also confirmed in our own tests with the scatter of three repeated tests being around 0.4 per cent (±0.07 kWh/t of a medium 18.08 kWh/t). Therefore, the Bond test is used also in this paper to assess the influence of micro-fractures generated by HPGR onto the grindability. Initially the W_i values were assessed for the PSD of the materials as obtained by just screening at a cut size of 3150 µm, see Figure 7. The resulting values of the Bond test are given in Table 2. They showed a reduction of the Bond work index of up to 8 per cent for the material ground by the HPGR.

TABLE 2. Overview of Bond work index for different feed preparations.

Preparation aggregate	W_i [kWh/t]
Hammer mill	17.89
Jaw crusher	18.09
HPGR	16.79

This reduction included potential effects of micro-fractures caused by HPGR as well the difference of the three feed materials. To reduce the influence of the differing PSD distributions, the product materials of jaw crusher and hammer mill were screened and classified into eight size fractions between 0 and 3150 µm. For comparison, the same procedure was also conducted for the original fresh secondary crushed material from the quarry (fraction -3150 µm directly separated from original feed size -32 000 µm without further comminution). Afterwards, the mass per each fraction was adjusted to the shear of the respective fraction in the HPGR product. The modified fractions of each feed material were combined again and thoroughly blended and homogenised, finally well matching the particle size distribution of the HPGR product.

With the three modified feed materials, the Bond tests were repeated. The results are presented in Table 3. The reduction of the Bond work index increased even further to 15 per cent which indicates a remarkable effect for the power draw of a ball mill installed after the HPGR.

TABLE 3. Overview of Bond index for different feed preparations at same feed PSD.

Preparation aggregate	W_i [kWh/t]
Hammer mill screened to match HPGR	19.34
Jaw crusher screened to match HPGR	18.34
Fresh feed screened to match HPGR	18.32
HPGR	16.79

A further effect of an HPGR installation prior to ball milling in ore processing can be seen in the high comminution selectivity, as shown in Figure 8 (Kühnel, 2021). During size reduction in the sample preparation for the Bond tests deploying different machine types, the coarser particles report to the finer classes depending on their mineral content and the type of stressing introduced by the comminution machines. While selectivity in comminution is generally limited with machines such as jaw or cone crushers, machines deploying the confined bed comminution principle such as HPGRs may support such selectivity as shown in Figure 8. Here, the fine fractions (-1 mm) exhibit a remarkable reduced quartz content while the iron is enriched.

A sample collected from such material for the Bond test by just classifying the -3150 µm fraction would simply reflect the increased content of the softer iron containing minerals. Assessing such a sample in a Bond test may again result in overdesigning mills for a production process which do not account for the special comminution characteristics with an HPGR. This effect has not been quantified so far as the preparation method of material for the Bond tests is not further specified and typically does not reproduce the real production conditions appropriately for HPGR.

Those effects have to be carefully analysed for HPGR test work design. Typical vendors of HPGR have this ability and knowledge and will consult the individual clients accordingly for the individual ore type of the project (Heinicke, 2016b).

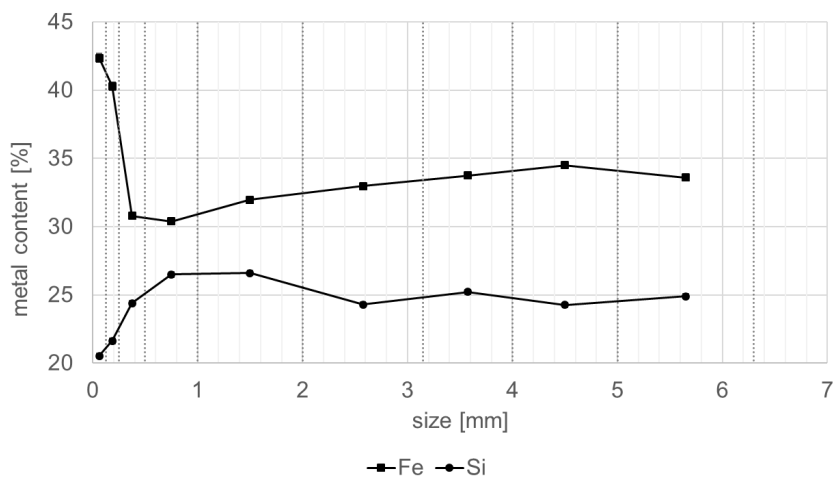


FIG 8. Selective comminution effects in feed material processed by HPGR for an ore with high quartz and low iron contents.

4. CONCLUSIONS

The grinding with HPGR showed remarkable effects on the downstream energy efficiency in ore processing. To quantify those effects, common test routines according Bond may be oversate the actual specific energy consumption as they are influenced by size distribution, particle weakening and selective grinding effects of HPGR. A careful planning of HPGR test series has to be done to balance the effect to downstream processes correctly. As the ores will differ from project to project this procedure shall be addressed by client and vender for each individual project.

ACKNOWLEDGEMENTS

This work was funded by Köppern within a research cooperation with Technical University of Freiberg. The authors would like to thank Köppern for the right to publish this paper and Jonas Brüggemann for the excellent test work performed within his thesis.

REFERENCES

Ballantyne, G and Giblett, A, 2019. Benchmarking comminution circuit performance for sustained improvement. SAG Conference, Vancouver.

Bond, F C, 1952. The third theory of comminution. *Mining Engineering*, p. 484–494.

Brüggemann, J, 2019. Diskretisierung des Bondtest für GBWM Anwendungen. Masterarbeit. Technische Universität Bergakademie Freiberg.

Gonzáles, G G, Coello-Velazquez, A l, Fernandez, B, Menendez-Aguado, J, 2021. Multivariate Analysis of the Ball Mill Bond's Standard Test on 2 Tantalum Ore. *Metals*, 11, 1606.

Gruendken, A, Matthies, E, vanderMeer, F D, 2008. Flowsheet considerations for optimal use of high pressure grinding rolls. *Proceedings of Comminution 08*, pp 1–37.

Heinicke, F, 2012. Beitrag zur Modellierung der Zerkleinerung in Gutbettwalzenmühlen. Dissertation. Rheinisch-Westfälische Technische Hochschule Aachen.

Heinicke, F, Guenter, H, Kamptner, A, 2016a. How to avoid errors in HPGR product characterization. *Proceedings of Procemin*, in Santiago de Chile, pp 1–11.

Heinicke, F, Lieberwirth, H, Guenter, H, 2016b. Modelling of HPGR Edge recycling data with progressive grinding data. *Proceedings of Comminution*, pp 1–11.

Klymowsky, R, Patzelt, N, Knecht, J, Burchardt, E, 2002. Selection and sizing of High Pressure Grinding Rolls. *SME Handbook*, pp 1–40.

Kühnel, R, 2021. Untersuchungen zur trockenen Aufbereitung von Magnetiterzen unter besonderer Berücksichtigung des Trennverhaltens im Luftstrom. Dissertation. Technische Universität Bergakademie Freiberg.

Michaelis, H, 1995. Real and potential metallurgical benefits of HPGR in Hard Rock Ore Processing. *Randol Conference*, pp. 1–9.

Morley, C, 1995. The case for High Pressure Grinding Rolls. *Randol Conference*, pp. 1–16.

Morley, C, 2006. Flowsheets for HPGR. *SAG Conference*, pp. IV172-IV189.

Povey, B C, Nol, Lifanov, D, 2017. The introduction of HPGRs to the SGOK magnetite plant in Russia. *Proceedings of Metplant*, pp 1–19 (The Australasian Institute of Mining and Metallurgy: Melbourne).

Schönert, K, 1966. Einzelkorn-Druckzerkleinerung und Zerkleinerungskinetik. Untersuchungen an Kalkstein-, Quarz-, und Zementklinkerkörnern des Größenbereiches 0,1–0,3 mm. Dissertation. TH Karlsruhe.

Schönert, K, 1988. A first survey of grinding with high-compression roller mills. *International Journal of Mineral Processing* 22, pp 401–412.

Vizcarra, T, Wong, B, 2019. Testwork variabililty – implications for grinding circuit design. *SAG Conference*, Vancouver.

Weier, M L, Chenje, T, 2018. Accuracy of the Bond ball mill test and its implications. *14th International Mineral Processing Conference & 5th International Seminar on GeoMetallurgy*. Santiago, Chile, Procemin-Geomet.

Investigating the Influence of Grinding Aids on Flow Characteristics and Grinding Performance in a Dry Stirred Mill

Hasan Serkan GOKCEN [1]*, Serkan CAYIRLI [2], Nuri YUCE [2], Obaidullah ELCHI [2]

[1]Eskişehir Osmangazi University

[2]Niğde Ömer Halisdemir University

*Corresponding author: sgokcen@ogu.edu.tr (Hasan Serkan GOKCEN)

Abstract:

Ensuring the energy-efficient manufacturing of fine materials is important due to the growing demand for fine-sized minerals. In addition, the rising importance of water daily brings dry processes to the fore. In recent years, there has been a great interest in the research and development of dry-operating stirred ball mills with high energy density as well as high production capacities in fine-grinding processes. The issue encountered in dry grinding processes and needs to be investigated significantly is the material's flow characteristics during grinding. Therefore, this study focuses on investigating the product flow behavior related to grinding performance in a dry-operating stirred mill. In this context, the effects of different grinding aids on grinding performance were examined in terms of flowability, mill power, and product fineness.

Keywords: *Powder flow characteristics, Grinding aids, Dry stirred mill*

1. Introduction

In mineral processing operations, size reduction processes include energy-intensive processes. Developing technologies and increasing fine particle requirements contribute to these processes. In grinding processes, the most well-known grinding type, traditionally and even standardized, is ball mills. Due to mineral properties and compression problems, operating ball mills for fine and ultra fine grinding and even submicron grinding becomes difficult. In addition, due to commercial processes, taxes, emission reduction requirements and efforts, and the importance of water, there is a need to optimize energy consumption. Therefore, the adaptation of alternative high-energy mills to dry grinding circuits has been among the studies carried out in recent years. The most prominent of these mills is stirred ball mills. Many parameters of these mills, such as shaft speed, ball type/density/size, ball filling, design parameters, etc. have been studied by researchers for dry grinding processes, and a certain amount of knowledge has been achieved. However, due to the difficulty of controlling the fine grinding process in dry stirred ball mills, adjustment of the mill flow regime emerges as an important optimization parameter. For this reason, the system-improving effect of a process parameter such as grinding aid comes to the forefront in addition to other parameters. Studies conducted in this context have investigated and discussed the effectiveness of grinding aids in the context of energy efficiency, target particle size, different analysis methods, and grinding equipment performance (Altun et al., 2015; Chipakwe et al., 2020; Gokcen et al., 2015; Prziwara, Breitung-Faes, et al., 2018; Prziwara, Hamilton, et al., 2018; Toraman et al., 2016). Studies examining the effects of grinding aids on powder flowability, energy consumption, and grinding efficiency in dry stirred ball mills are limited. Within the scope of this study, the relationships between the use of different grinding aids and mill power, powder flowability, and particle size in the dry grinding of calcite ore in a laboratory-scale stirred ball mill were investigated.

2. Material and methods

2.1. Material

The calcite sample provided by Mikron'S Inc. was used in the dry grinding tests (2.71 g/cm ^{3}). The particle size analysis of the sample was performed with the Malvern Mastersizer 2000 model, and the particle size characteristic values were measured as d_{90}: 205.96 µm, d_{50} 83.77 µm (Figure 1). In addition, as a result of the chemical analysis (X-Ray Fluorescence Spectroscopy-Panalytic Zetium) of the sample shown in Table 1, it was determined that it contained 98.838% $CaCO_3$.

In dry grinding tests, triethanolamine (TEA) (Merck, ≥ 99%, 1.11 g/cm ^{3}) and triisopropanolamine (TIPA) (Acros Organics, 98%, 1.02 g/cm ^{3}) were preferred as pure grinding aids. Since triisopropanolamine is in solid form and attracts a lot of moisture, it was used after being converted to liquid form in an oven at ~55°C.

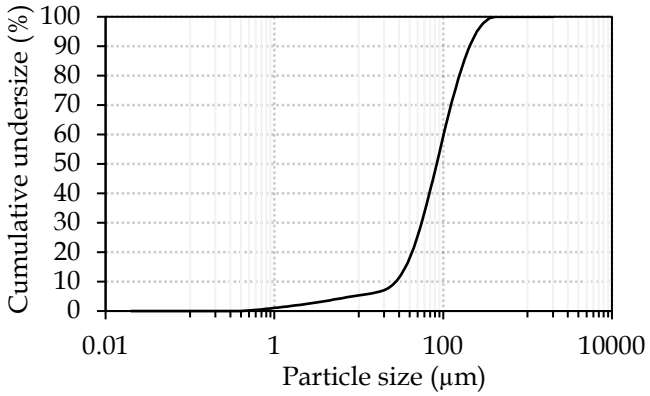


Fig. 1. The size distribution of the feed material

Table 1. The feed material chemical analysis.

	$CaCO_3$	Na_2O	MgO	Al_2O_3	SiO_2	P_2O_5	SO_3	Fe_2O_3	SrO
%	98.838	0.026	0.472	0.181	0.245	0.027	0.036	0.119	0.055

2.2. Method

Dry grinding tests were carried out in a laboratory type vertical stirred ball mill (Fig. 2.). As described in previous studies (Cayirli, Gokcen, Yuce, et al., 2023; Çayırlı et al., 2021), sample loading, experiment continuation, and emptying operations in grinding experiments were carried out intermittently and under a certain procedure. Experimental conditions are summarized in Table 1.



Fig. 2. The laboratory type vertical stirred ball mill

Table 1. Dry grinding test conditions

Parametre	Değer
Material amount (g)	380
Ball amount (g)	1598 - 2548
Ball size (mm)	3
Ball densty (g/cm ^{3})	3.7 (aluminum)– 5.9 (zirconium)
Speed (m/s)	2, 3.4, 4, 6
Grinding aids type and dosage (g/t)	Triethanolamine, triisopropanolamine – 1000

The particle size analysis of the products obtained as a result of the experiments carried out under feed and different conditions was carried out with a particle size measuring device (Malvern Mastersizer Hydro 2000 MU-Malvern Co., Ltd., UK) operating with the Laser Diffractometer method (wet). At the end of each grinding experiment, the products reduced according to the sample division rules were subjected to analysis. The device measures the size of the placed samples three times by repeating them at certain intervals and gives the average of these three measurements. At the end of the measurements, the averages of the analyses obtained for a test product were noted and used in the evaluation of the results. An Entes brand (ES-32L) energy meter recorded time-dependent wattage changes during experiments.

The flowability analyses of the products obtained as a result of the grinding tests were carried out with the powder flow meter device (Brookfield Powder Flow Tester 230VAC-UK) purchased within the scope of the project (Fig. 3). The sample cell of the device (230 cm ^{3}, 15.2 cm inner diameter) consists of a movable upper disk and a stationary lower chamber. There are 18 compartments in the upper disk to create shear stress in the powder whose fluidity is to be measured. The lower chamber is designed as a perforated plate to prevent the sliding movement of the powder material on the surface. While the lower chamber is stationary, the upper disk applies compressive stress (σ_1) at varying rates with linear movement downwards and at the same time causes shear stress in the powder sample with rotational movement. The basic measurement principle of the powder flow meter is based on the measurement of the shear stress (σ_c) required for the powder material to start flowing or deform after compressive stress is applied (Slettengren et al., 2016). The σ_1/σ_c ratio (ffp) is proportional to the deformation behavior of the tested material (Fitzpatrick et al., 2004; Schulze, 2010). A high value of this ratio (>10) indicates a free-flow material, and a low value (<1) is a non-flowing material (Ermis et al., 2018).

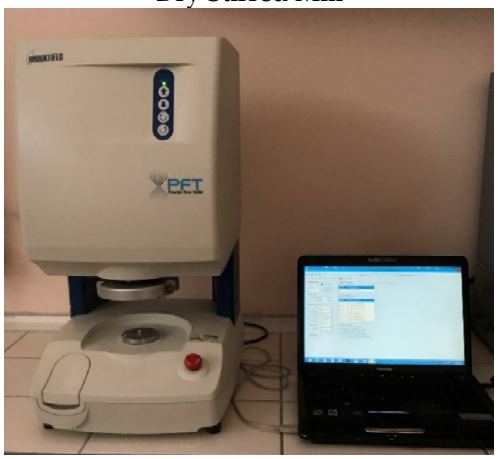


Fig. 3. Powder flow tester

3. Results and discussions

3.1. Impact of stirrer speed and grinding ball material on powder flowability and mill power

In this section, the relationship between mill power, powder flowability, and particle size at different speeds and ball densities without using grinding aids was investigated (Fig. 4). As the ball density increased, the mill power consumption increased. The particle fineness increased (d_{50}) and the powder flowability decreased depending on the size. Inefficient grinding performance was achieved when the stress conditions were low (low ball density and speed) and high (high ball density and speed). It was also observed that the fluidity did not change after a certain size.

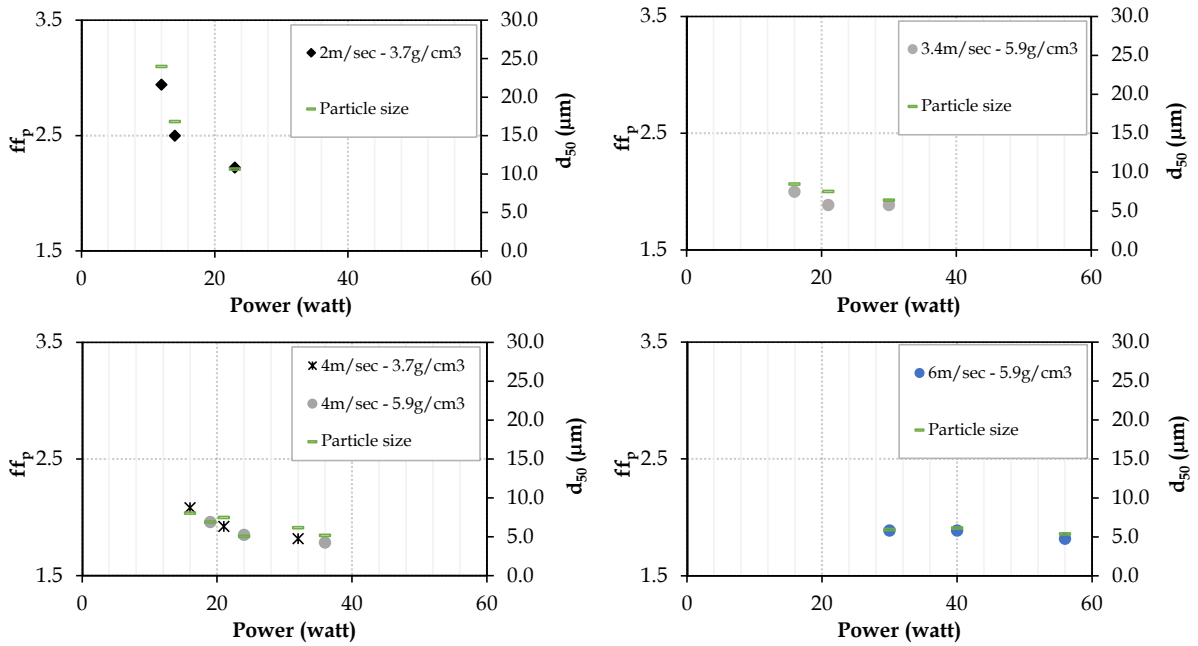


Fig. 4. Impact of the stirrer speed and grinding ball material on the grinding result

Fig. 5. The graph of grain size and mill power of 3 mm ball size at different speeds and densities shows that the power-size and particle size-flowability relationships are parallel. In other words, as the consumed power increases according to the grinding parameter, the size decreases and the fluidity decreases depending on the size.

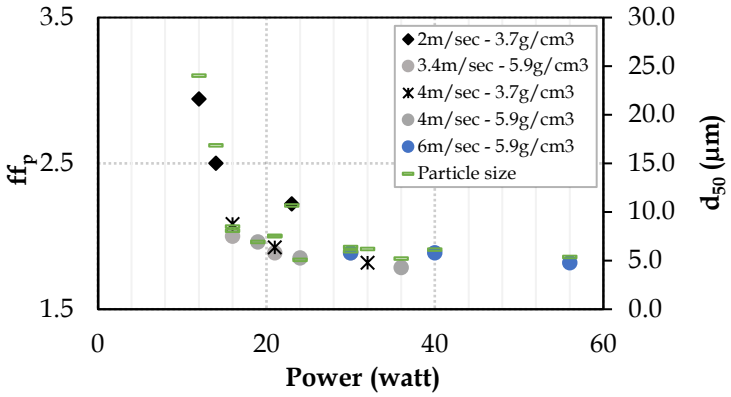


Fig. 5. The comparison of all tested stirrer speed and grinding ball material

3.2. Impact of grinding aids on powder flowability and mill power

Fig. 6 presents a comparison of the tested grinding aid's particle size and powder flowability as a function of power input. When the comparison performed under the same conditions (stirrer speed, ball size and density) is examined, with the usage of 1000 g/t grinding chemical, the size becomes finer, the powder flowability increases and the power consumption decreases. While 8.05 µm product size was obtained with 32-watt power input without using a grinding aid, 4.37 µm product was obtained by using 1000 g/t TIPA with 26-watt power consumption.

Here, an overlapping impact of the powder flowability with power consumption and product size, which may strongly rise at a certain concentration of grinding aids, was shown. In addition, the effect of grinding aids becomes more apparent when comparing all tested experiments (see the flowability and size values in the marked areas).

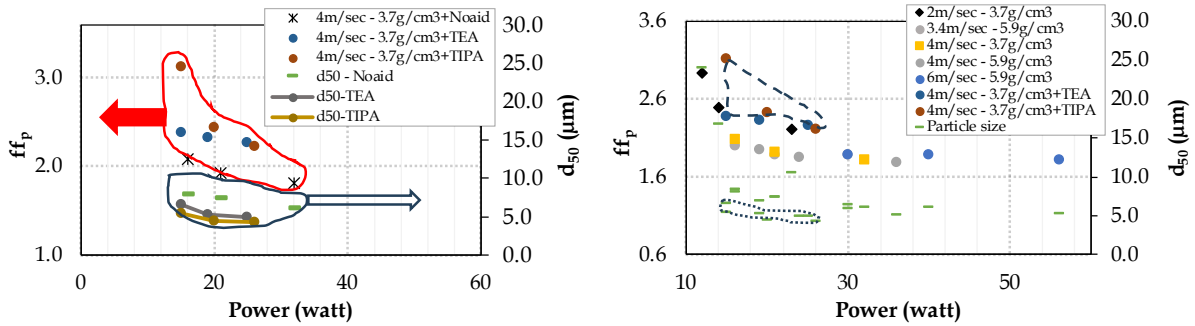


Fig. 6. Impact of testing the grinding aid's particle size and powder flowability as a function of power input (left: certain conditions, right: all variations).

Another property affected by grinding aids is the particle size distribution width of the product. The particle size became narrower with the addition of the grinding aids, which could be indicated by the smaller d_{90}/d_{10} ratio (Fig. 7). The particle size distribution width supports previous observations since TIPA and TEA affect both higher powder flowabilities and lower d_{90}/d_{10} ratios compared to the no aid conditions. Schönert (1996) showed, that the particle size distribution becomes wider when stressing particle bed arrangements with increasing bed heights. Even though this work does not deal with classical particle bed comminution, the material is supposed to be stressed mainly as particle beds. Thereby, a high powder flowability affects a lower mass of stressed particles which reduces the height of the bulk material arrangement at each grinding ball collision (Prziwara, Breitung-Faes, et al., 2018). Consequently, the use of TEA and TIPA allows for reaching narrow size distributions with lower d_{90}/d_{10} ratios. In fact, similar findings were revealed in the aspect ratio calculations in muscovite grinding studies conducted by Cayirli, Gokcen, et al. (2023).

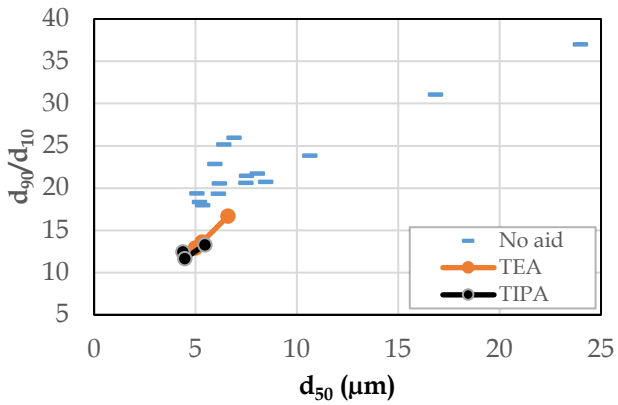


Fig. 7. Impact of grinding aid on d_{90}/d_{10} ratio.

4. Conclusions

This study investigated the influence of grinding aids on flow characteristics and grinding performance in a dry stirred mill, focusing on calcite grinding. The results demonstrate the interplay between operational parameters, mill power, grinding aid usage, and the resulting product characteristics.

Key findings include:

1- Ball density and stirrer speed significantly impact mill power consumption, particle fineness, and powder flowability. An optimal balance of these parameters is crucial for efficient grinding performance.

2- The use of grinding aids (TEA and TIPA) at 1000 g/t concentration led to finer particle sizes, improved powder flowability, and reduced power consumption compared to grinding without aids.

3- Grinding aids demonstrated a notable effect on particle size distribution, resulting in narrower distributions as indicated by lower d_{90}/d_{10} ratios.

4- A relationship was observed between powder flowability, power consumption, and product size, with grinding aids enhancing these relationships. Future studies with a more comprehensive data evaluation will focus on this relationship.

These findings have important implications for industrial mineral processing, particularly in dry grinding operations. The use of appropriate grinding aids can lead to significant improvements in energy efficiency and product quality. However, the selection and dosage of grinding aids should be carefully optimized for specific mineral systems and operational conditions.

In conclusion, this study underscores the potential of grinding aids to enhance the performance of dry stirred mills, offering a promising avenue for improving the efficiency and sustainability of fine grinding processes in the mineral processing industry.

Acknowledgments

This study was supported by TÜBİTAK (Grant No. 119M216). The authors thank Mikron'S Inc. for providing calcite samples.

References

Altun, O., Benzer, H., Toprak, A., & Enderle, U. (2015). Utilization of grinding aids in dry horizontal stirred milling. *Powder Technology*, *286*, 610–615.

Cayirli, S., Gokcen, H. S., Bozkurt, V., & Ucbas, Y. (2023). The effect of liquid grinding aids on the dry fine grinding of muscovite. *Physicochemical Problems of Mineral Processing*, *59*(2). https://doi.org/10.37190/ppmp/165854

Cayirli, S., Gokcen, H. S., Yuce, N., & Elchi, O. (2023). Investigation of the usage of waste materials and By-Products as grinding aids in calcite grinding. *Minerals Engineering*, *202*(July), 108267. https://doi.org/10.1016/j.mineng.2023.108267

Çayırlı, S., Gökçen, H. S., Yüce, N., & Elchi, O. (2021). Pirina yağının öğütme yardımcısı olarak kullanabilirliğinin araştırılması. *J ESOGU EnginArch Fac.*, *29*(2), 189–201.

Chipakwe, V., Semsari, P., Karlkvist, T., Rosenkranz, J., & Chelgani, S. C. (2020). A critical review on the mechanisms of chemical additives used in grinding and their effects on the downstream processes. *Journal of Materials Research and Technology*, *9*(4), 8148–8162. https://doi.org/10.1016/j.jmrt.2020.05.080

Ermis, E., Yasasin, M., Bozkurt, F., & Yilmaz, M. T. (2018). Powder Flow Tester (PFT): a new tool to evaluate wheat flour dough behavior by measuring unconfined failure strength under variable consolidation stresses. *Journal of Food Measurement and Characterization*, *12*(3), 1678–1685. https://doi.org/10.1007/s11694-018-9783-7

Fitzpatrick, J. J., Barringer, S. A., & Iqbal, T. (2004). Flow property measurement of food powders and sensitivity of Jenike's hopper design methodology to the measured values. *Journal of Food Engineering*, *61*(3), 399–405. https://doi.org/10.1016/S0260-8774(03)00147-X

Gokcen, H. S., Cayirli, S., Ucbas, Y., & Kayaci, K. (2015). The effect of grinding aids on dry micro fine grinding of feldspar. *International Journal of Mineral Processing*, *136*, 42–44.

Prziwara, P., Breitung-Faes, S., & Kwade, A. (2018). Impact of grinding aids on dry grinding performance, bulk properties and surface energy. *Advanced Powder Technology*, *29*(2), 416–425. https://doi.org/10.1016/j.apt.2017.11.029

Prziwara, P., Hamilton, L. D., Breitung-Faes, S., & Kwade, A. (2018). Impact of grinding aids and process parameters on dry stirred media milling. *Powder Technology*, *335*, 114–123. https://doi.org/10.1016/j.powtec.2018.05.021

Schönert, K. (1996). The influence of particle bed configurations and confinements on particle breakage. International Journal of Mineral Processing, 44–45(SPEC. ISS.), 1–16. https://doi.org/10.1016/0301-7516(95)00017-8

Schulze, D. (2010). Flow properties of powders and bulk solids (fundamentals). In *Powder Technology* (Vol. 65, Issues 1–3, pp. 321–333).

Slettengren, K., Xanthakis, E., Ahrné, L., & Windhab, E. J. (2016). Flow properties of spices measured with Powder Flow Tester and Ring Shear Tester-XS. *International Journal of Food Properties*, *19*(7), 1475–1482. https://doi.org/10.1080/10942912.2015.1083576

Toraman, O. Y., Çayirli, S., & Uçurum, M. (2016). The grinding-aids effect of moisture , triethanolamine (TEA) and ethylene glycol (EG) on grinding performance and product quality of calcite. *International Journal of Engineering Research & Science*, *2*(12), 121–128.

Determination of Ball Trajectory in Tumbling Mill Considering Mill Liner Dimensions

Yusuf Enes Pural [1]*, Feridun Boylu [1],

[1]Istanbul Technical University, Mineral Processing Engineering Department, Istanbul, Turkey

*Corresponding author: pural@itu.edu.tr (Yusuf E. Pural)

Abstract:

Tumbling mills are critical in mineral processing due to their high energy consumption and impact on downstream processes. Mill liner design significantly influences grinding efficiency by guiding media movement and protecting the mill shell. Effective liner design and ongoing monitoring are essential for maintaining optimal performance throughout the liner's lifespan. This study introduces a Python-based tool that addresses these challenges by combining the Morrell C model for charge shape prediction and Powell's model for media trajectory calculation. The tool provides visual simulations of mill dynamics, serving as a decision support system for both design and operational optimization. By enabling engineers to visualize and adjust operational parameters and lifter configurations, the tool aids in optimizing charge shape and media trajectory. A hypothetical case study demonstrates the tool's application in determining optimal lifter geometries and adapting to liner wear, potentially leading to improved grinding efficiency, extended liner life, and reduced operational costs in mineral processing.

Keywords: *Grinding, Tumbling mill, Mill liner, Media trajectory, Python simulation*

1. Introduction

Comminution is an energy-intensive and inefficient process. However, there is significant potential to reduce energy consumption through appropriate practices (Napier-Munn, 2015). Achieving this requires a thorough understanding of the grinding mechanism and the use of appropriate tools. A key focus must be placed on understanding the mechanics of tumbling mills, predominantly used for fine grinding in mineral processing. The performance and cost-effectiveness of these mills largely depend on two key factors: charge shape and media trajectory. The shape of the charge influences how material is distributed within the mill, which impacts the grinding mechanism. Furthermore, the trajectory of the grinding media determines how effectively energy is transferred to the ore particles. Thus, understanding and controlling both the charge shape and media trajectory is essential for optimizing mill performance.

Optimal grinding occurs when the media strike the charge toe, ensuring maximum energy transfer and effective particle breakage. However, if the media impacts too high on the charge, energy transfer becomes ineffective, leading to poor grinding performance. Conversely, if the media strike the mill liners directly, it can result in excessive wear and potential damage, further reducing efficiency. These conditions are visually represented in Figure 10, which illustrates (a) media impacting too high on the charge, (b) direct impact on the liners, and (c) the optimal scenario where media strikes the charge at the toe. This consideration is particularly important for SAG (Semi-Autogenous Grinding) mills, as size reduction in these mills heavily relies on the impact mechanism.

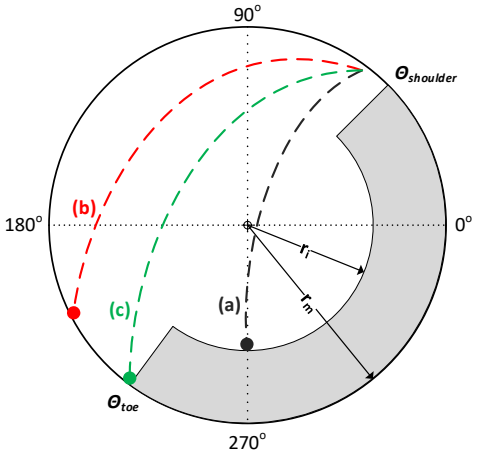


Figure 10. Charge shape and different media trajectory

Liner geometry, along with operating conditions, plays a crucial role in controlling the trajectory of the grinding media and maintaining the optimal charge shape. Well-designed liners guide the media towards effective collision points with the charge, enhancing overall grinding efficiency. However, as liners wear over time, their ability to control media trajectory diminishes. This wear necessitates regular monitoring and timely adjustments to operating conditions such as mill speed and charge volume. Without these adjustments, grinding efficiency declines, leading to increased energy consumption and higher operational costs due to more frequent maintenance and unscheduled downtime (Powell et al., 2006)

Given the significant impact of charge shape and media trajectory on mill performance and operational costs, accurately predicting and monitoring these factors is of paramount importance. Effective prediction and control can lead to enhanced grinding efficiency, extended liner life, and overall improvements in the sustainability and cost-effectiveness of grinding operations.

To address this need, we have developed a visual tool that employs the Morrell C model for charge shape prediction and Powell's model for trajectory calculation. Implemented through Python programming, this tool offers a practical and efficient solution for optimizing mill design and operation. It improves upon the widely-used MillTraj software by additionally computing and visualizing charge shape, offering a more comprehensive analysis (*MillTraj Liner Design Software*, n.d.). It enables engineers to simulate and visualize different operating conditions and lifter configurations, providing valuable insights for decision-making. Through several case studies, we demonstrate how this tool can be applied to real-world scenarios, showcasing its potential to significantly improve tumbling mill performance across various operational parameters.

2. Models and methodology

2.1. Morrell C model for charge shape prediction

Morrell (1993) developed a series of empirical equations to predict the charge shape inside a tumbling mill. The model uses mill speed and filling fraction to determine the toe angle (θ_T), shoulder angle (θ_S), and the inner radius of the charge (r_i). Toe angle is calculated using the Equation $\theta_T = 2.5307 \cdot (1.2796\text{-}J_t) \cdot \left(1\text{-}\exp\left(\text{-}19.42 \cdot (\Phi_c\text{-}\Phi)\right)\right) + \frac{\pi}{2}$ (1 in radians:

$$\theta_T = 2.5307 \cdot (1.2796 - J_t) \cdot \left(1 - \exp\left(-19.42 \cdot (\Phi_c - \Phi)\right)\right) + \frac{\pi}{2} \quad (1)$$

where J_t is the filling fraction, Φ denotes the fraction of the critical speed at which the mill operates,Φ_c indicates the experimentally determined fraction of the theoretical critical speed required to achieve complete centrifuging and can be determined based on the following conditions:

$$\Phi_c = \begin{cases} \Phi, & \Phi > 0.35 \cdot (3.364 - J_t) \\ 0.35 \cdot (3.364 - J_t), & \Phi \leq 0.35 \cdot (3.364 - J_t) \end{cases} \quad (2)$$

The shoulder angle (θ_S) in radians, is then calculated by Equation $\theta_s = \frac{\pi}{2}$-(0.3386-0.1041 · Φ) + (1.54-2.5673 · Φ) · J_t·$\left(\theta_T - \frac{\pi}{2}\right)$ (3:

$$\theta_s = \frac{\pi}{2} - \left((0.3386 - 0.1041 \cdot \Phi) + (1.54 - 2.5673 \cdot \Phi) \cdot J_t\right) \cdot \left(\theta_T - \frac{\pi}{2}\right) \quad (3)$$

Finally, the inner radius of the charge is calculated using the following Equation $r_i = r_m \cdot \left(1 - \frac{2\pi \cdot \beta \cdot J_t}{2\pi \cdot \theta_s - \theta_t}\right)^{0.5}$ (4:

$$r_i = r_m \cdot \left(1 - \frac{2\pi \cdot \beta \cdot J_t}{2\pi \cdot \theta_s - \theta_t}\right)^{0.5} \quad (4)$$

where β represent the active part of the charge expressed as a fraction of the total charge, determined as:

$$\beta = \frac{t_c}{t_c + t_f} \quad (5)$$

here t_c is the mean time spent by the media in contact with the charge, and t_f is the mean time spent in free flight which they can be approximated based on rotational speed and toe and shoulder angles.

2.2. Powell's model for trajectory calculation

Powell's first principal model (Powell, 1991) provides a detailed approach to understand the trajectory of grinding media within a mill. The model uses two key parameters to represent the liner geometry: lifter height and lifter face angle. Additionally, the lifter base width has been incorporated into the software, enabling further calculations and visualizations. These aspects are illustrated in Figure 11.

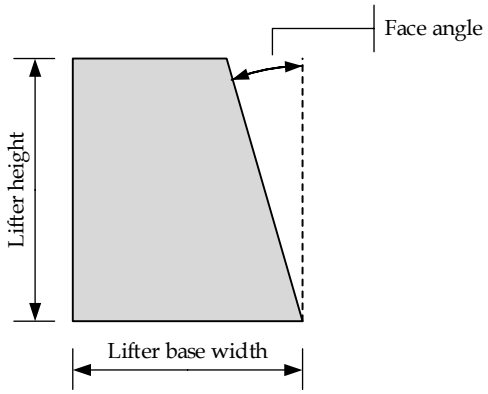


Figure 11. Visualization of lifter height, lifter face angle, and lifter base width parameters.

Calculations begin by determining the point of equilibrium on the lifter bar, where the forces acting on the grinding media balance each other. After the ball passes this equilibrium point, it starts to roll under the influence of static friction between the ball and lifter bar. The model calculates the ball's displacement and velocity over time, considering initial conditions and angular position. When the static friction can no longer sustain the motion, the ball transitions to sliding motion under kinetic friction.

Once sliding begins, the model continues to track the ball's motion until it reaches the tip of the lifter bar. At this stage, the ball starts a free flight phase. The model provides equations to describe the ball's

position and velocity during free flight until it impacts the mill shell. The impact velocity and angle are then calculated based on the final position.

2.3. Python implementation

Python was chosen for its flexibility, provided by its extensive and customizable open-source libraries. Data input for computations is facilitated through an interactive interface using the *IPyWidgets* library, allowing for real-time adjustments. An example of the data input screen is shown in Figure 12.

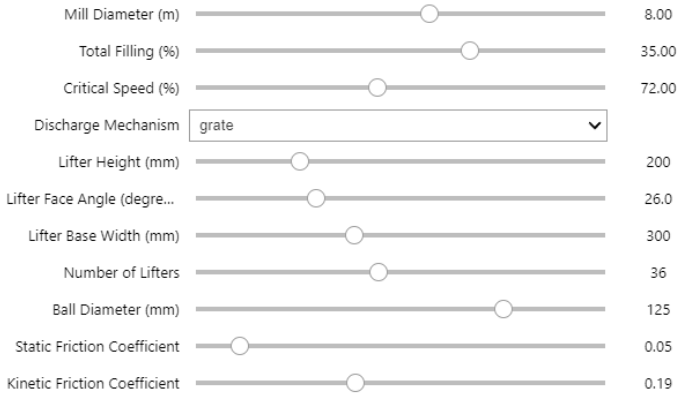


Figure 12. Software interface for model parameters input

Mathematical and array computations are handled using the *Numpy* library, which ensures efficient processing of numerical operations. The *Scipy* library's *optimize* module is utilized to solve the equations of motion.

Results are dynamically displayed using *Matplotlib* library, reflecting changes based on the input data.

3. Results and Discussion: A Hypothetical Case Study

To evaluate the effectiveness of the developed Python-based tool, a hypothetical case study was designed involving a SAG mill equipped with a variable speed drive operating under typical conditions. The mill has an internal diameter of 8 meters and is set to operate at 72% of its critical speed, with a charge filling fraction of 27%. Additionally, there are 35 rows of bolting on the mill shell, based on the formula (4/3) * Diameter (ft). The grinding media consists of steel balls with a maximum size of 120 mm.

For simulation purposes, reasonable estimates for the coefficients of friction are 0 or 0.05 for static friction and 0.19 for kinetic friction. These values provide a practical basis for modeling the interactions between the grinding media and the liner surfaces within the mill.

One of the most important factors is the spacing between the lifter bars and the spacing-to-height (S/H) ratio. If the spacing between the lifter bars is too wide, slippage against the shell plate may occur, leading to excessive wear. Conversely, if the spacing is too short relative to the height of the lifter bar, pockets of material may form between the bars. This can create a relatively smooth lining, resulting in accelerated wear on the tops of the lifter bars (Moller & Brough, 1989). Additionally, the S/H ratio has a significant impact on mill throughput (Yahyaei & Banisi, 2010). The S/H ratio is not fixed but varies depending on the mill's critical speed.

Based on the given mill geometry, an appropriate lifter bar height will first be selected to match the ideal S/H ratio. For the specified critical speed, the ideal S/H ratio is approximately 3.6. Considering that the lifter bar will wear down over time, it is advisable to achieve the ideal S/H ratio when the lifter bar is at approximately half of its lifespan. Using these parameters in the tool the lifter height is determined to be 135 mm. The lifter height should be allowed to decrease to a minimum of 60 mm, based on the 120 mm grinding media size. If the height decreases further, the lifters will no longer be able to effectively lift the balls, resulting in excessive wear due to increased slippage. Given this

minimum height and the accelerated wear rate as the lifter height decreases, it would be appropriate to design the new lifters with an initial height of 200 mm. When the lifter base width is set to 200 mm, the resulting charge shape and media trajectory under these conditions are shown in Figure 13. The default value for the lifter face angle in the software is 15 degrees. As can be seen, at this angle, the media directly impacts the liner, which is an undesirable outcome.

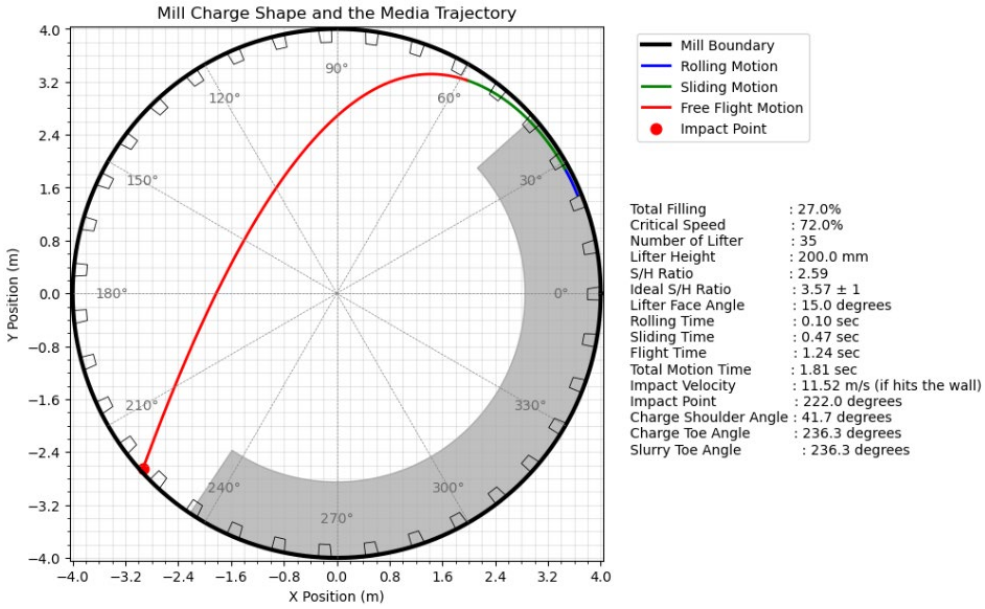


Figure 13. Charge shape and trajectory with 200 mm lifter base width and 15° lifter face angle.

To ensure that the grinding media lands at the charge toe, the lifter face angle was increased to 24 degrees. The trajectory in this scenario is illustrated in **Hata! Başvuru kaynağı bulunamadı.**, where the impact point and the toe point are approximately the same, indicating optimal media behavior.

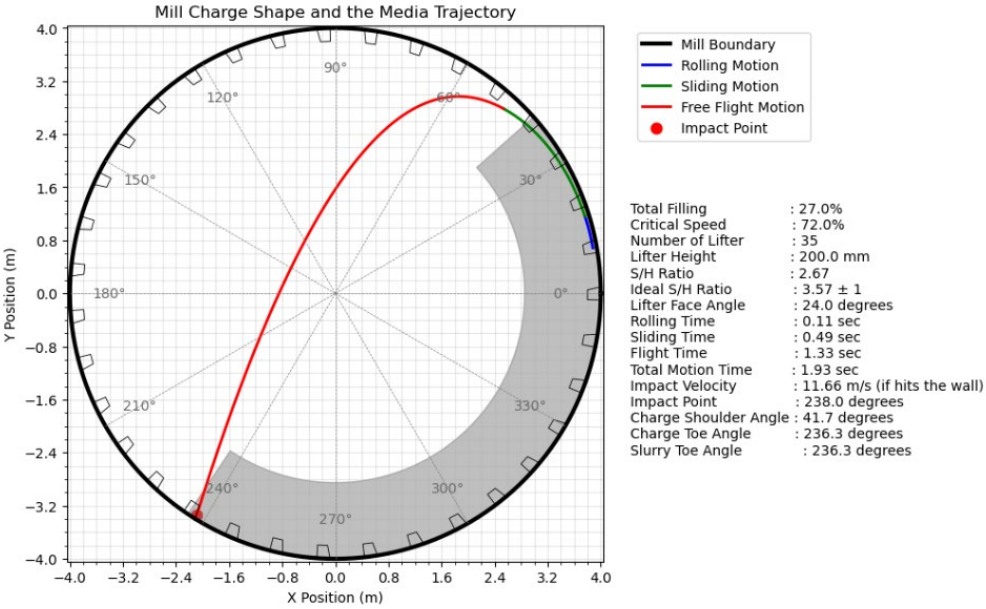


Figure 14. Charge shape and trajectory with 200 mm lifter base width and 24° lifter face angle.

The design phase has highlighted the tool's benefits for optimizing mill performance. Furthermore, it can be employed to adjust operating conditions based on liner wear in a functioning mill, ensuring continued efficiency and effectiveness throughout its lifecycle.

4. Conclusion

This study introduces a Python-based tool that combines the Morrell C and Powell's models to predict charge shape and media trajectory in tumbling mills. The tool effectively simulates lifter configurations and operational conditions, as demonstrated in a hypothetical case study optimizing lifter heights and face angles to achieve the ideal trajectory. It also shows the potential to adapt to liner wear, maintaining efficiency and cost-effectiveness over a mill liner's lifecycle. Future work could expand the tool's capabilities by incorporating rod trajectory alongside ball trajectory and accounting for liner wear.

References

MillTraj Liner Design Software. (n.d.). Retrieved September 30, 2024, from https://www.milltraj.com/milltraj

Moller, T. K., & Brough, R. (1989). Optimizing the performance of a rubber-lined mill. *MINING ENGINEERING*.

Morrell, S. (1993). *The prediction of power draw in wet tumbling mills* [PhD Thesis, The University of Queensland]. https://doi.org/10.14264/252760

Napier-Munn, T. (2015). Is progress in energy-efficient comminution doomed? *Minerals Engineering*, *73*, 1–6. https://doi.org/10.1016/j.mineng.2014.06.009

Powell, M. (1991). The effect of liner design on the motion of the outer grinding elements in a rotary mill. *International Journal of Mineral Processing*, *31*(3–4), 163–193. https://doi.org/10.1016/0301-7516(91)90025-E

Powell, M., Smit, I., Radziszewski, P., Cleary, P., Rattray, B., & Schaeffer, L. (2006). The Selection and Design of Mill Liners. In *Advances in Comminution* (pp. 331–376). SME.

Yahyaei, M., & Banisi, S. (2010). Spreadsheet-based modeling of liner wear impact on charge motion in tumbling mills. *Minerals Engineering*, *23*(15), 1213–1219. https://doi.org/10.1016/j.mineng.2010.08.013

The Effect of Kinetics Model Parameters in Coarse and Fine Particle Size on The Prediction of Simulation Program (MODSIM©)

Yakup UMUCU [1] *, Vedat DENİZ [2], Y. Hakan GÜRSOY [1]

[1]*Eskişehir Osmangazi University, Department of Mining Engineering, Türkiye,*

[2]*Hitit University, Department of Polymer Engineering, Türkiye,*

*Corresponding author: yakup.umucu@ogu.edu.tr (Yakup Umucu)

Abstract:

By using a phenomenological grinding kinetic theory based on the pace of the process as described by the selection function and breakage product distribution known as the breakage function, the predicted grinding performance of a mill can be approximated. This method is now widely accepted and has been thoroughly explored by renowned scholars such as Austin et al. Insufficient studies were conducted in the past on the kinetic model for fine sieve sizes. Since there is no extensive investigation on the fluctuation of model parameters over various sieve size groups, this paper presents one. There are programs for the computer design of mineral processing circuits; these programs include simulation models for the design of ball mills. MODSIM calculates the exact mass balance for every ore dressing facility. MODSIM is capable of simulating integrated flow diagrams that incorporate grinding. The Si and Bi,j (selection and breakage distribution functions) equations were derived using the size distributions at varied grinding times and with model parameters (S_i, a_t, α, γ, β and ϕ_J) for various sieve size groups (coarse and fine). Experimentally derived data were statistically compared to MODSIM simulator data using model parameters.

Keywords: *Grinding, Ball mill, Kinetic model, MODSIM©*

1. Introduction

Numerous industries want fine and ultra-fine grinding. Fillers for paper or plastics, coatings, pigments, ceramics for abrasives and structural reasons, toners for copy machines and printing, and metals and metallic compounds for electronics, medicine, and other uses are a few examples. Bel Fadhel et al. (1999) say that there are no strict rules about both the top size of the ground material and the narrow size distributions.

There are three different forms of grinding: coarse grinding, fine grinding, and mechanical activation. Coarse grinding is performed to decrease particle size, while mechanical activation is employed to alter the structure and enhance the reactivity of the particles (Boldyrev et al., 1996). Fine grinding is a subset of mechanical activation that lies between coarse grinding and mechanical activation. In addition to size reduction, it is known that severe and intense mechanical action on the solid surface during fine grinding causes physical and chemical changes (known as physicochemical effects) in the near-surface region where solids come into contact under mechanical forces as a result of the enormous amount of energy delivered by the grinding mills. Mechanochemical effects are physicochemical effects initiated by mechanical forces in particles (Venkataraman And Narayanan, 1998).

In recent years, researchers have concentrated on evaluating size reduction in tumbling ball mills using the ideas of particular rates of breaking and main daughter fragment distributions. Austin reviewed the merits of this strategy, and several studies have explored the scaling-up of laboratory data to full-scale mills, as described by Austin et al., (1981).

The fundamental assumption of first-order kinetics in tumbling ball mills is beneficial for simulation models, as proved by various assessments of particular rates of fragmentation. As several experimenters have learned, however, exact first-order kinetics is the exception rather than the norm. According to a recent paper, a degree of divergence from the first order is predicted for all particle sizes due to the

variation of particle strength within a size fraction. Austin et al. (1984) say that the model is based on the idea that the rate at which a particle break is related to the load at which it breaks.

This last premise is a priori disputed. However, it was indirectly confirmed by comparing the predicted population of particles left after a certain grinding interval to the actual population of particles remaining, with the average strength rising as grinding continued. The preferred breakage or non-first-order breakage kinetics of large particle sizes in a tumbling ball mill have been explored in terms of a spectrum of grinding medium forces. Several articles (Austin et al., 1984) use these ideas to give a quantitative explanation for the strange large-size breaking in lab mills.

The size interval of the relevant size fraction influences the departure from first-order kinetics. With thinner size fractions, the distribution of failure loads or particle strength has a lower coefficient of variation (standard/average). Depending on the size interval of the size fraction, the parameter values of selection functions and breakage functions influence the degree of departure from first-order kinetics (Austin et al., 1984).

Since the 1970s, models and simulators have been used for plant technical study. Some of these models and simulations were developed expressly for mineral processing, while others were industry-specific. JKSimMet (JKTECH, JKSIMMET, 1989), MODSIM (King, 2001; Yan and Eaton, 1994), and its variants are significant works for mineral processing applications.

MODSIM is a mass balance simulator for any mineral or coal processing facility. In addition, microscopic particle qualities, such as shape and surface characteristics, may have a significant impact on the performance of certain mineral processing units. MODSIM supports all of these particle characteristics. The primary unit operations of ore dressing include size reduction (crushing and grinding), particle classification based on particle size, concentration methods that separate particles based on their mineralogical composition, and solid-liquid separations. MODSIM presents a comprehensive view of the popular models for these activities (King, 2001; Umucu, 2015).

Changes in kinetic model parameters for particles of fine size are the most important topics to examine. Researchers have not proved how model parameters alter when fine particle size decrease. Prior to this, researchers determined the breakage rate and distribution for the -3.35 mm and 0.106 mm coarse size groups. However, few scientists worked on fine particle size groups (such as -0.106+0.045). This research reveals that the grinding efficiency, with a particular rate of fragmentation and cumulative distribution function, is connected to the grinding behavior of coarse and fine particles. Coarse (-1.00+0.106 mm) and fine (-0.106+0.045 mm) sieve size groups were used for the grinding process. The percentage quantities based on product sieve size distribution were computed in MODSIM using model parameters derived from grinding experiment data on breakage rate and time. For the same material, the change in model parameters caused by different particle size distributions has been shown to affect the simulation.

2. Theory

2.1. Kinetic Model

In the examination of the fragmentation materials, it is helpful to assume that the fragmentation of each size fraction is of first-order nature. In other words, the rate of size 1 disappearance due to breakage is proportional to the quantity of size 1 material in the mill's storage bins (Austin and Luckie, 1971).

$$-\frac{d[w_1(t)W]}{dt} \infty w_1(t)W \quad (1)$$

Since the mill hold up, *W*, is constant, this becomes:

$$dw_i = \frac{(t)}{dt} = -S_1 w_1(t) \quad (2)$$

Since S_1 is the proportionality constant, it is referred to as the particular rate of breakage, with units of time $^{-1}$. If S_1 is constant throughout time (Austin and Bhatia, 1972).

$$w_1(t) = w_1(0)\, exp(-S_1 t) \tag{3}$$

that is,

$$log[w_1(t)] = log[w_1(0)] - \frac{S_1 t}{2.3} \tag{4}$$

where $w_1(t)$ is the weight fraction of size 1 mill hold up at time t (Austin and Bagga,1981). The formula suggested by Austin et al. for the relationship between particle size and the specific rate of breakage S_i is:

$$S_i = a_T \left(\frac{X_i}{X_0}\right)^{\alpha} Q \tag{5}$$

where X_i is the upper limit of the size interval indexed by i, X_0 is 1 mm, a_T and a are model parameters that rely on the material's characteristics and grinding conditions. Q_i is a correction factor that is 1 for smaller sizes (normal breakage) and less than 1 (abnormal breakage) for particles that are too big to be properly nipped and shattered by the mill's ball size. In the zone of atypical breakage, each size acts as if it contains a portion of weak material and the remainder of strong material. Using a mean value for S_i in this location, the empirical description of Q_i values is given by

$$Q_i = \frac{1}{1+\left(\frac{X_i}{\mu}\right)^{\Lambda}}, \Lambda \geq 0 \tag{6}$$

where μ is the particle size at which the correction factor is 0.5 and λ a positive number which is an index of how rapidly the rates of breakage fall as size increases that is the higher the value of Λ, the more rapidly the values decrease. The cumulative breakage distribution, $B_{i,j}$, is defined as ''The weight fraction of material broken from size j which falls less than the upper size of size interval "i'' is commonly used to characterize the size distribution resulting from breakage of material from a particular size interval to a smaller size (Austin et al., 1989).

The $B_{i,j}$ values can be calculated using the BII method which is described by.

$$B_{i,j} = \phi_j \left(\frac{X_{i-1}}{X_j}\right)^{\gamma} + (1-\phi_j)\left(\frac{X_{i-1}}{X_j}\right)^{\beta} \tag{7}$$

where δ, φ_φ, γ, and β are model parameters that depend on the properties of the material. If $B_{i,j}$ values are independent of the initial size, i.e. dimensionally normalizable, then δ is zero (Deniz et al., 2011; Deniz, 2012; Deniz, 2013). The parameter ϕ is the intercept at $(X_{i-1}/X_j) = 1$, γ is the slope of the lower section of the $B_{i,j}$ curve and β is the slope of the steeper section of the $B_{i,j}$ curve (Ipek et al., 2005).

3. Materials and Experimental Methods

3.1. Materials

This research used barite from the Isparta region as its feed mineral since barite is an important raw ingredient for industrial paints. The average density of raw material, as determined by a pycnometer, is 4.50 g/cm^3, and the work index (W_i) of this material is 7.03 kWh/t. Using the usual Bond test process, the Bond work index is obtained. In addition, chemical analyses of this substance are provided in Table 1.

Table 1. Chemical composition of material

Oxides	SiO_2	Al_2O_3	Fe_2O_3	CaO	MgO	Na_2O	SO_3	K_2O	$BaSO_4$	LOI
%	0.51	0.02	0.06	0.42	0.13	0.02	40.93	0.02	98.82	21.89

3.2. Grinding tests

The breakage parameters were determined experimentally using the one-size fraction technique (Austin et al., 1984). The two size fractions chosen for tests were, first group; -1180+850, -600+425, -300+212 and -150 + 106 µm and second group; -0.106+0.090, -0.090+0.075, -0.075+0.063, -0.063+0.045 µm where, for example, -300 + 212 µm denotes that 100% of the particles are passing by weight at 300 µm and 100% of particles are remaining at 212 µm. The standard set of grinding conditions used is shown in Table 2 for a laboratory mill with a 6283-cm^3 volume.

Table 2. Ball mill characteristics and test conditions

Mill	Diameter, D (mm)	200
	Length, L (mm)	200
	Volume (cm^3)	6283
	Mill speed Critical, *Nc* (rpm)	102
	Operational speed	77
Media (Balls)	Grinding Diameter, d (mm)	30
	Media (balls) Specific gravity, g/cm^3	7.80
	Quality	Alloy steel
	Assumed porosity (%)	40
	Ball-filling volume fraction, J_b	0.30
Material	Specific gravity, g/cm^3	4.50
	Powder-filling volume fraction, f_c	0.096
	Interstitial filling, *U*	0.80

Calculated from $Nc = 42.3\sqrt{D-d}$ (D, d in metres)

Calculated from $J = \left(\frac{mass\ of\ \ balls / ball\ density}{mill\ voluma} \right) x \frac{1.0}{0.6}$

Calculated from $fc = \left(\frac{mass\ of\ \ powder / formal\ bulk\ density}{mill\ voluma} \right)$

Calculated from $U = \frac{fc}{0.4J}$

The interstitial filling rate of the mill has been identified for the 0,8-1,0 is selected for efficient grinding in industrial applications (Deniz, 2012). In this study, the interstitial filling rate (*U*) was selected as 0,8.

4. Results And Discussion

4.1. Determination of S Parameters

According to the data, breakage typically follows the first order relation, and values of S_i may be calculated from the slope of the straight line of first-order plots. In addition, Figures 1 and 2 illustrate the relationship between S_i and the proportion of coarse (-1180+106 m) and fine (-106+0.045 m) particle size for barite, respectively.

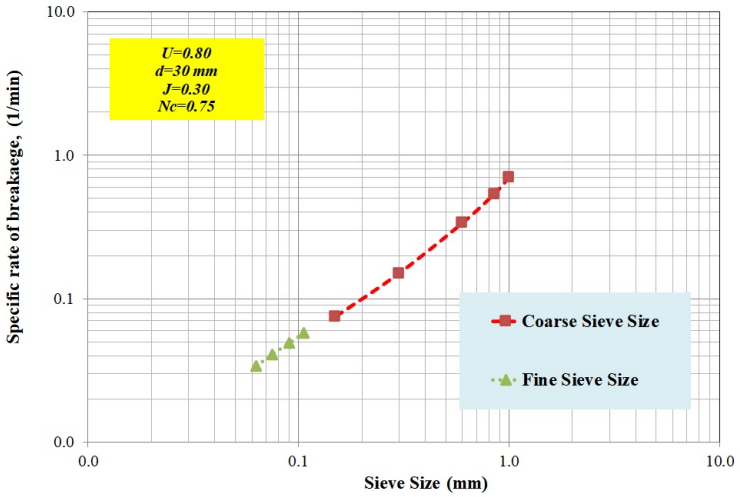


Figure 1. Variation of S_i values of barite with different particle size group in the same grinding condition

Figure 1 also shows variations of the specific rates of breakage, *Si*, values with the particle feed sizes ground in the mill for barite.

4.2. Breakage distribution functions

Using the *BII* method, the values of cumulative breakage distribution functions, $B_{i,j}$, which commonly characterize the size distributions resulting from the breakage of material from a particular size interval to a smaller size, were determined from the size distributions at the shortest grinding times (Deniz, 2003; Umucu et al., 2012). Figure 2 shows the values of $B_{i,j}$ against particle size derived from *BII* calculations for each size fraction.

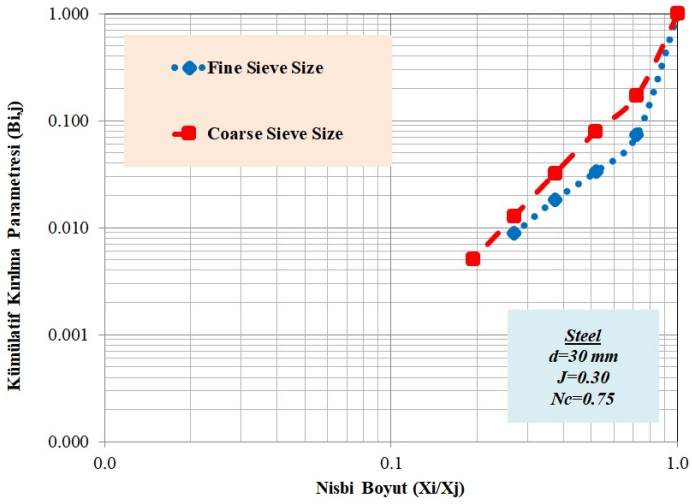


Figure 2. Cumulative breakage distribution functions for different powder filling

The results exhibited a typical normalized behavior in which the progeny distribution was independent of the feed particle size and the parameter was equal to zero. In addition, the model parameters are shown in Table 3.

Table 3. Characteristic breakage parameters of different sieve size groups obtained from the laboratory test

Sieve size (mm)	Sieve size group	U (%)	a_t	α	Φ_j	γ	β	δ
-1.00+0.106	Coarse Sieve Size	0.80	0.68	1.32	0.520	2.83	9.90	0.00
-0.106+0.045	Fine Sieve Size	0.80	0.58	1.03	0.130	2.04	9.50	0.00

Dry grinding of barite samples over size intervals revealed that the various sieve sizes followed the first-order breakage rule with consistent normalized primary breakage distributions. Also, these samples don't depend on the cumulative breakage threshold of the particle size distribution function.

According to the data shown in Table 3, the model parameter values for the various sieve size groups deviate from the literature about coarse and fine sieve sizes. When examining Table 3, it was established that coarse sieve sizes result in quicker grinding. It was discovered that both the breakage rate and the breakage rates of the larger sieve sizes reduced as sieve sizes became finer. This scenario was explained by the existence of macrocracks and pores on fine sieves.

4.3. Prediction of particle distribution with MODSIM© in fine and coarse sieve size for model parameters

MODSIM's framework is entirely modular, enabling the addition of models for unit operations. As a consequence, the models used to simulate the operation of different unit activities may be developed and updated to fit the needs of each application and any operating state. This feature of MODSIM also allows the user to include current research discoveries into the mathematical modeling of mineral processing unit operations. As users add new models, the system's model library continues to expand. Any model is made available to the user (King, 2001). Figure 3 demonstrates how to add mill feed material.

The unit models are fundamental to MODSIM. The model quality of the simulator is only as good as its included models. The simulator cannot produce a believable depiction of the plant's behavior if no model adequately explains the unit's functioning. For accurate work, models must be properly crafted and calibrated against sufficient experimental data (King, 2001).

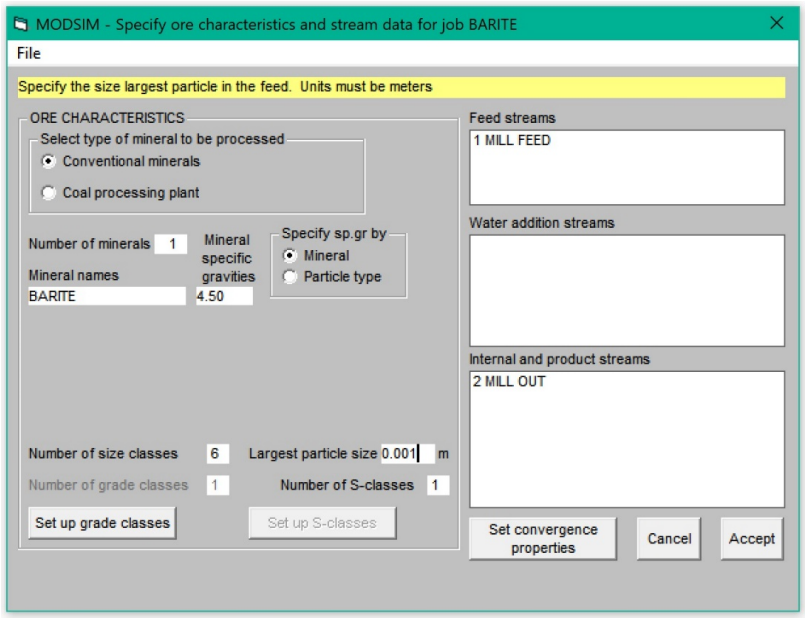


Figure 3. Input format about the mill in the MODSIM

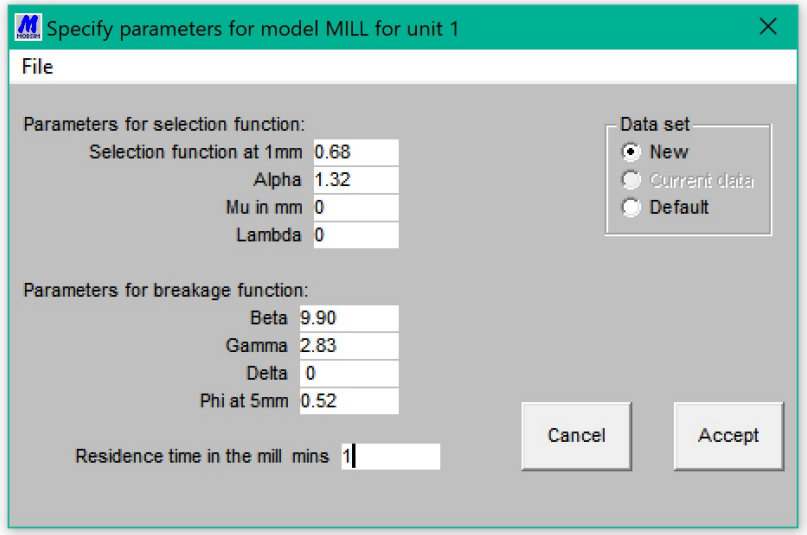


Figure 4. Input format of selection and breakage function model parameter for coarse sieve size group in the MODSIM

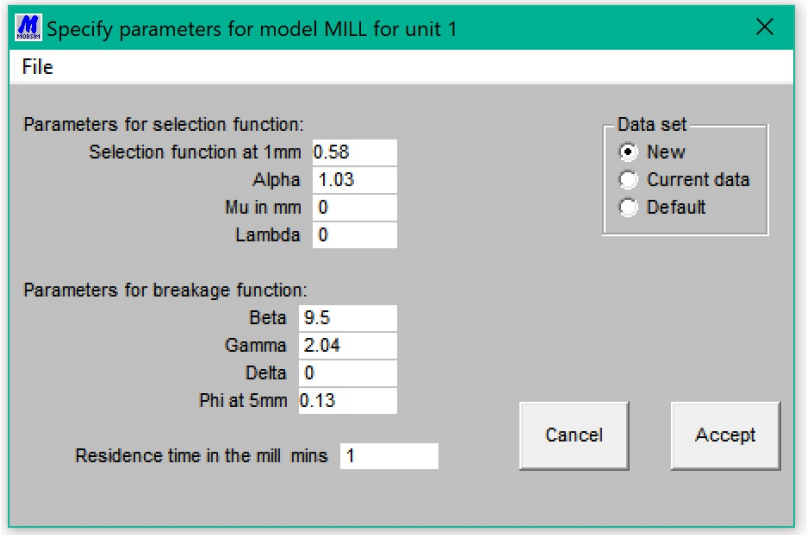


Figure 5. Input format of selection and breakage function model parameter for fine sieve size group in the MODSIM

Depending on the mill's circumstances, the breakage function and cumulative distribution function of the model parameters are shown in Figures 3, 4, and 5. Using the selection and breakage functions, this is the simplest model for a ball mill. It is believed that the mill has a single, properly mixed zone. The selection function is the usual function, with the maximum defining the reduction in breakage rate as size increases.

For experimental tests involving materials processed under identical circumstances, a feed mill for various sieve size groups at 60 seconds yielded the quantity of specified products. Then, the MODSIM simulation tool was used to estimate the parameters of the kinetic model for the same amount of time.

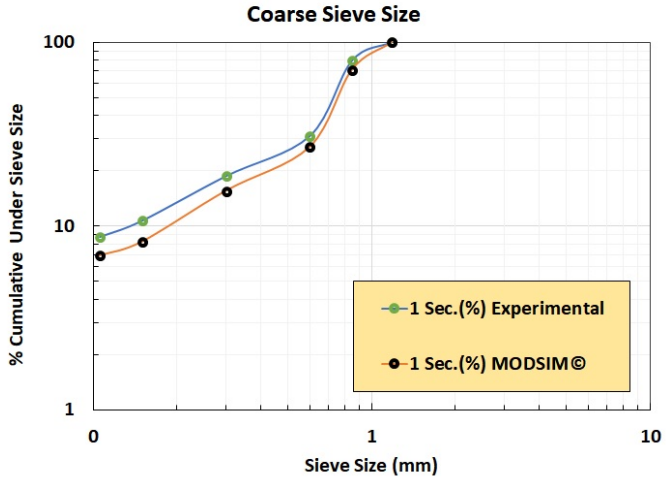


Figure 6. Comparison of MODSIM and experimental product size distributions of barite at coarse sieve size

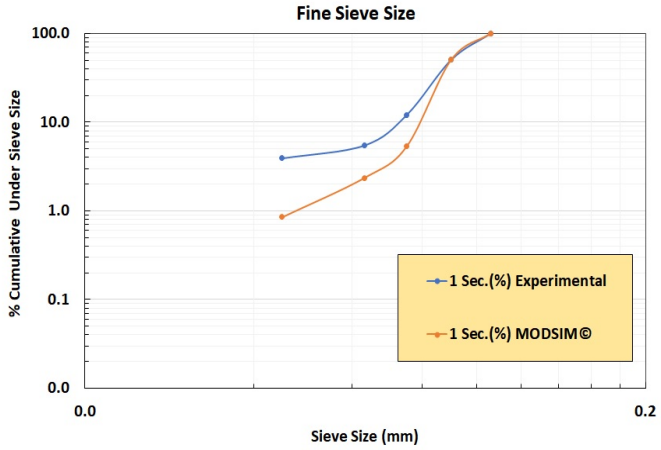


Figure 7. Comparison of MODSIM and experimental product size distributions of barite at fine sieve size

4.4. Comparison of MODSIM© and Experimental of Product Size Distributions

Mean Absolute Error (MAE) and Root Mean Squared Error are two of the most commonly used metrics for estimating the correctness of continuous data (RMSE). It seems that the majority of the publications I see nowadays use RMSE or a form of R-squared.

MAE is a statistic that calculates the average magnitude of mistakes in a collection of predictions without considering their direction. It is the weighted average of the absolute discrepancies between predicted and actual observations across the test sample.

$$MAE = \frac{1}{n}\sum_{i=1}^{n}|y - yi| \quad (8)$$

where y is the measured value, yi is the predicted value, and n is the number of samples.

The root mean square error (RMSE) is a quadratic scoring method that additionally calculates the average size of the error. It's the square root of the average squared difference between the actual and predicted values. The following performance indices were used to measure the MODSIM models. In Equation 9, Root mean square error, RMSE, was given. (Grima and BabusÏka, 2005; Umucu et. al., 2016).

$$RMSE = \sqrt{\frac{1}{n}\sum_{i=1}^{n}(t - ti)^2} \quad (9)$$

Where t is the measured value, t_i is the predicted value, and n is the number of samples.

In terms of RMSE, taking the square root of the average squared errors has some interesting consequences. Because the errors are squared before being averaged, the RMSE gives large errors a lot of weight. As a result, when large errors are particularly undesired, the RMSE should be more effective. In the three tables below, MAE remains constant but RMSE rises as the variance associated with the frequency distribution of error magnitudes rises.

Table 4. The different sieve sizes for barite sample statistical evaluation of data from experimental and MODSIM©

Rating	Coarse Sieve Size	Fine Sieve Size
RMSE	3.99	3.70
MAE	2.81	2.71

Another implication of the RMSE formula that is not often discussed has to do with sample size. Using MAE, we can put a lower and upper bound on RMSE.

1.**[RMSE] ≥ [MAE],** The RMSE value will always be greater than or equal to the MAE value. RMSE=MAE if all of the anomalies are of the same magnitude.

2. **[RMSE] ≤ [MAE * sqrt(n)],** where n represents the number of test samples. When all of the prediction errors derive from a single test sample, the difference between RMSE and MAE is highest. For that one test sample, the squared error equals [MAE ^{2} * n], but for all other samples, it equals 0. RMSE equals [MAE * sqrt(n)] after taking the square root.

Focusing on the upper bound, means that RMSE has a tendency to be increasingly larger than MAE as the test sample size increases. According to all these results, it was determined that the estimation results made in MODSIM were good.

5. Conclusion

In general, it is understood that grinding kinetic parameters may vary depending on the sample. Consequently, it seems that any material's product sieve size distribution and energy must be determined using the grinding kinetic. Therefore, experimental research is not only time-consuming but also labor-intensive and subject to changing circumstances. Creating a model for getting the same results in extremely sensitive real-world trials is crucial and essential for this aim.

The standard value of the Bond work index for barite powder was 7.03 kWh/t. According to these findings, barite powder grinding is simple.

In this study, barite samples were given effective breakage for *the coarse sieve size group*. Furthermore, because it is a suitable value for different sieve size groups for barite sample, grinding is faster for the coarse sieve size group. When the model parameter changes were investigated, different values were obtained for each of the sieve size groups. An a_T 0.68 for the coarse sieve size, and 0.58 for the fine sieve size group was obtained. Different values were obtained for the same sample, which is a situation encountered for the first time in the literature. This situation also appeared in the estimations made with MODSIM.

It is seen that the estimations made for MODSIM are compatible with the experimental results. While making the calculations in MODSIM, it has been revealed that the model parameters and values related to the different sieve sizes defined for the system do not play a large role in the calculation. According to the RMSE and MAE results, the estimation results obtained from MODSIM were good. However, while the results obtained according to the coarse grain sizes were expected to be better, the prediction results obtained for the fine grain size were better. This situation has emerged as one related to the amount of data and calculation methods.

Since the model parameters for each sieve size group in the same sample are different, research needs to be done on different samples.

Nomenclature

J	fraction of mill volume filled by the ball bed
fc	powder-filling volume fraction
U	fraction of the interstices of the ball bed filled by powder
d	ball diameter (mm)
W	total powder mass in the mill
t	grinding time (min)
$w_{1(t)}$	weight fraction of mill hold-up that is of size 1 at time t
i	an integer indexing a √2 screen interval
S_i	specific rate of breakage (min^{-1})
X_i	the upper limits of the size interval indexed by i(mm)
a_T	model parameter
α	model parameter
$b_{i,j}$	breakage distribution function, part of interval j fall into interval i
$B_{i,j}$	cumulative breakage distribution function
$P_{i(0)}$	cumulative weight fraction at time 0 for size interval i
$P_{i(t)}$	cumulative weight fraction at time t for size interval i
γ	model parameter
β	model parameter
Φ_j	model parameter
δ	model parameter

References

Alvarez Grima, M., BabusÏka, R. Fuzzy Model for the Prediction of Unconfined Compressive Strength of Rock Samples International Journal of Rock Mechanics and Mining, 2005.

Austin, L.G. A review introduction to the description of grinding as a rate process. Powder Technology, 5, p.1–7, 1972.

Austin L.G.; Bhatia V.K. Experimental methods for grinding studies in laboratory mills. Powder Tech. 5, 261–266, 1972.

Austin L.G.; Luckie P.T. The estimation of non-normalized breakage distribution parameters from batch grinding tests. Powder Tech. 5, 267–271, 1972.

Austin L.G.; Bagga P. An analysis of fine dry grinding in ball mills, Powder Tech. 28, 83–90, 1981.

Austin, L.G.; Bagga, R.; Çelik, M. Breakage properties of some materials in a laboratory ball mill. Powder Technology, 28, 235–241, 1981.

Austin L.G.; Klimpel R.R.; Luckie P.T. The Process Engineering of Size Reduction. SME-AIME, New York, p. 561, 1984.

Austin, L.G.; Yıldırım, K.; Luckie, P.T.; Cho, H.C. Two Stage Ball Mill Circuit Simulator: PSUSIM. Penn State University, USA, 1989.

Bel Fadhel, H.; Frances, C.; Mamourian, A.; Investigations on ultra-fine grinding of titanium dioxide in a stirred media mill'. Powder Technology, 105, 362–373, 1999.

Boldyrev, V.V.; Pavlov, S.V.; Goldberg, E.L. Interrelation between fine grinding and mechanical activation. International Journal of Mineral Processing 44-45,181-185, 1996.

Deniz, V. A study on the specific rate of breakage of cement materials in a laboratory ball mill. Cement and Concrete Research. 33 (3), 439-445, 2003.

Deniz, V.; Çayırlı, S.; Umucu, Y. Investigation of breakage behavior of different mineralogical and morphological characteristic pumices. Granular Matter. 13 (5), 623-629, 2011.

Deniz, V. A study on the effect of ball diameter on breakage properties of clinker and limestone. Indian Journal of Chemical Technology. 19 (3), 180-184, 2012.

Deniz, V. Effects of mill speed on kinetic breakage parameters of four different particulates pumices. Particulate Science and Technology, 31 (2), 101-108, 2013.

İpek H.; Uçbaş Y.; Yekeler M.; Hoşten Ç. Dry grinding kinetics of binary mixtures of ceramic raw materials by Bond milling. Ceramics International, 31, 1065–1071, 2005.

King R.P. Modeling and Simulation of Mineral Processing System. Department of Metallurgical Engineering University of Utah, USA, 2001.

Umucu Y.; Deniz V.; Bozkurt V. The Evaluation of Grinding Process Using MODSIM©. AGH Journal of Mining and Geoengineering, 36, 2, 505-513, 2012.

Venkataraman and Narayanan. Energetics of collision between grinding media in ball mills and mechanochemical effects. Powder Technology, Volume 96, Issue 3, 15 May 1998, Pages 190-201, 1998.

Ball Mill Optimization in The Cement Grinding Plant

Yakup UMUCU [1] *, Nazmi ÜNAL [2], Ali FIRAT [2], Vedat DENİZ [3], Y. Hakan GÜRSOY [1], Hüseyin SENDİR [4]

[1]*Eskişehir Osmangazi University, Department of Mining Engineering, Türkiye,*

[2]*Tracim Cement Factory, Kırklareli, Türkiye,*

[3]*Hitit University, Department of Polymer Engineering, Türkiye,*

[4]*Eskişehir Osmangazi University, Department of Geological Engineering, Türkiye*

*Corresponding author: yakup.umucu@ogu.edu.tr (Yakup Umucu)

Abstract:

In ball mill applications, ball size distribution is an important parameter. Many literature studies have revealed that the design to be made affects performance. Mill optimization evaluations are an important stage to find weak points. A thorough examination of the characteristic features of the current system and the accuracy of the model approaches used are critical to increasing or optimizing the circuit's performance. Furthermore, at grinding sizes smaller than 45 microns, the efficiency of the mills significantly decreases, leading to an excessive increase in energy consumption, which ultimately renders grinding uneconomical. For this reason, it is very important to make good optimizations. The study examined how to alter the particle size in the current mill. In addition, similar studies were conducted on the same mill with a design change, and a comparison was made. The studies led to the addition of a new ball charge of 220.69 tons to the mill, with a maximum ball size of 25 mm. Despite working fewer sieves below 32 microns than the previous year, the mill's capacity remained unchanged. Examining the classifier efficiency revealed a decrease in product escaping into the mill as the separation particle size increased to 23.68 microns.

Keywords: *Grinding, Ball mill optimization, Separator performance*

1. Introduction

Cement grinding is a crucial step in the manufacturing process of cement. It involves grinding clinker, which is a combination of limestone, clay, and other materials, into a fine powder to create cement. The quality and characteristics of the final product are significantly influenced by the grinding process.

The fineness of the cement affects the rate of hydration, strength development, and overall performance. Finer cement particles hydrate faster, leading to quicker strength gain and better bonding in concrete. A higher surface area increases the rate of chemical reactions, which is crucial for the setting and hardening of cement. Proper grinding enhances the early strength of cement, which is important for construction timelines and structural stability. Consistent and controlled grinding ensures long-term durability and strength of concrete structures. Grinding ensures a uniform particle size distribution, leading to consistent performance in concrete. A controlled grinding process helps maintain quality standards and reduces variations in cement properties (Deniz, 2004, Umucu et. al., 2015).

Efficient grinding processes reduce energy consumption and operational costs. This is particularly important as cement production is energy-intensive. Reducing energy use in grinding contributes to sustainability and lowers the carbon footprint of cement production. Grinding allows for the incorporation of various additives (e.g., fly ash, slag, limestone) which can improve performance, reduce costs, and enhance specific properties of the cement. The ability to blend different materials during grinding helps produce a variety of cement types tailored for specific applications (Mejeoumov, 2007).

Cement grinding is a vital process that affects the quality, efficiency, and sustainability of cement production. By ensuring optimal fineness, surface area, and particle size distribution, the grinding

process directly impacts the performance characteristics of the final product, influencing workability, setting time, strength, and durability. Effective cement grinding processes are essential for producing high-quality cement that meets industry standards and supports the demands of modern construction projects (Genç, 2016; www.mdpi.com).

During the last decade, semi-finish-grinding plants have been used more and more for the energy efficient grinding of high-quality cement. Recent research work has shown that the operational performance of the ball mill, which is situated downstream of the high-pressure grinding roll separator cycle can be improved significantly. The results of extensive investigations carried out on industrial semi-finish grinding plants indicated that the specific power consumption of the ball mill could be decreased by about 20% when lowering the ball charge filling ratio from about 30% to about 20%. However, the throughput is decreased also by about 20% (Schnatz and Knobloch, 2000).

There are many parameters that influence the energy efficiency of the grinding operation in ball mills. Arrangement of the grinding plant (i.e. open or closed circuit), amount of the circulating material, type of the system used for removing the grinding heat are overall process parameters that influence the energy consumption of the mill. The relationship length to diameter, number and length of the grinding compartments, type of lining, type of material transfer and discharge devices, degree, type and size of grinding ball charge and mill speed are important parameters when the design of the mill is considered. On the other hand, grindability, grain size, flow characteristics, influence on the friction between grinding ball and lining, temperature, microstructure, tendency to agglomerate are parameters that should be optimized for the optimal mill operation when the mill feed material is considered (Tiggesbäumker and Müller, 1983).

In this study, a pre-crusher system investment was made in 2015 in order to increase the performance of the facility-scale mill. After the investment, the mill was converted to a single-chamber system by removing the intermediate partition diaphragm due to the decrease in the particle size analysis entering the mill. After the change, the ball charge was updated in 2015, but it was found to be insufficient.

In this context, the facility's first stage of studies presented an analysis of the current grinding system, taking into account mill design factors and separator efficiency. After the mill design was changed, the analyses were repeated. The data obtained in both cases were compared. In the conclusion section, the benefits of the design process were discussed.

2. Materials and Method

In the study, chemical analysis was performed on samples taken from the cement grinding facility belonging to Traçim Cement Industry and Trade Inc. (Figure 1.) located in Vize (Kırklareli) in Table 1, and necessary analyses were performed on the particle in the Malvern grain size analyzer, and the averages of the results were calculated and presented in Table 2.

Ball mill efficiency directly affects the cost of mineral processing. Grinding media play a vital role in enhancing the efficiency of a ball mill through their direct effect on the breakage rate, mill load behavior, power draw, and general energy consumption. These factors have a crucial effect on the energy consumption of tumbling mills and on the general operating costs. Therefore, selecting the most appropriate operating parameters (ball size distribution, mill speed, pulp density and media filling) and ball properties (size, density, shape, microstructure, and hardness) improves the performance of the mill. The grinding media affect the power consumption by ball mill, breakage parameters and the product particle size distribution (PSD). They should thus have the largest possible surface area and be as heavy as possible (www.mdpi.com).

Table 1. Average chemical results of the samples used in the study

Minerals	Amount (%)
SO_3	3.57

F.CaO	1.39
SiO_2	19.73
Al_2O_3	4.85
Fe_2O_3	3.34
CaO	63.98
MgO	1.60
Na_2O	0.64
K_2O	0.92
Cl	-
Cr $^{+6}$ (ppm)	1.40
Loss of Ignition	2.47
Total	100.00

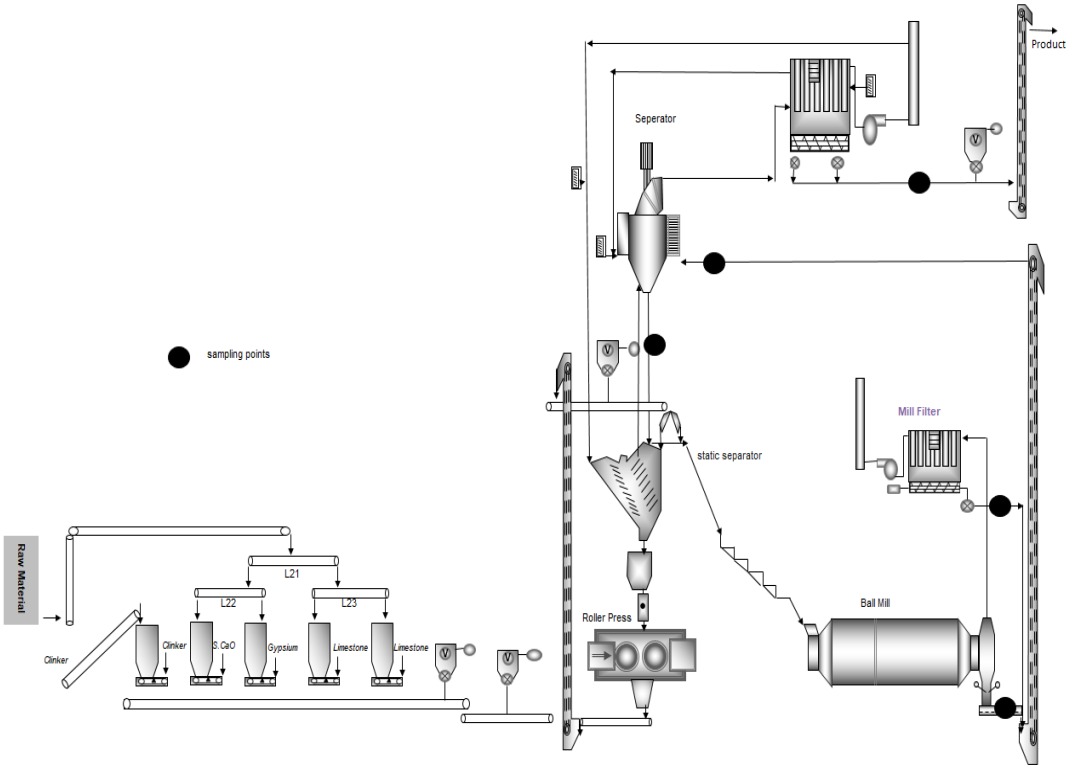


Figure 1. Cement grinding plants of Traçim Cement Industry and Trade Inc.

3. Experiments

A roller press unit was installed in the cement mill unit of the facility in 2015. After this stage, the chamber mill intermediate section was cut and converted into a standard ball mill. The data used in the mill design are given in tables 2, 3 and 4.

Table 2. Mill Information

Ball Mill		Mill Feed	
Diameter (m)	4,25	Fresh Feed (t/h)	145
Length (m)	14,53	Return (t/h)	250

		Sirk. Factor	2,72

Table 3. Mill design parameters

EF1	EF2	EF3	EF4	EF5	EF6	EF7	EF8	∏EF	W_i	P_{80}	F_{80}
1,3	1	0,914	1	1,23	1,04	1,04	1	1,57	16	20	98
Tonnage (Kwh/t)		180	3609					Kwh/t			
			4840					HP			

After adding a roller press to the grinding unit, the largest ball size in the ball distribution was selected as 30 mm. As seen in Table 4, the ball size distribution in grinding was selected as coarse.

Table 4. Ball load distributions

Ball Size	Amount (t/m^3)	
30 mm	35,57	t
25 mm	53,02	t
20 mm	69,10	t
17 mm	76,72	t
Total	236,41	t
Volume	206,02	m^3

Before the mill revision, samples were taken from the mill by making sudden stops. Samples were taken from the grinding circuit for grinding efficiency and separator performance, and their analyses were performed (Figure 1-Figure 2).

For grinding efficiency, sampling operations were carried out by stopping all flows of the circuit and the mill. Since the number of sample points in the mill is important, samples were taken separately from each meter and from three different points of each meter taken to follow the change in grain size reduction. The grain size distribution of the samples was determined with the help of the Malvern-Mastersizer brand particle size measurement device, and the results are given in Figure 1.

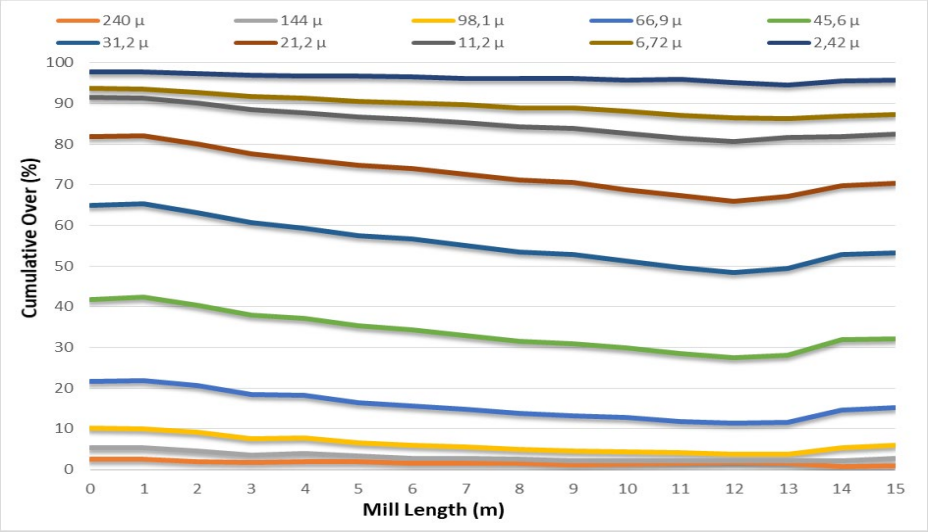


Figure 2. Change in sieve size distribution in the mill before the revision

After achieving the mill balance condition, we took two samples per shift for classification performance analysis. The separator performance demonstrates the impact of the mill design changes. We determined the separation particle size of the separator to be 20.7 microns, while the desired 32-micron sieve oversize amount in the product was 3.4%. As shown in the figure 2, the By-Pass ratio is 19.93%, whereas the Fishhook value is around 10%.

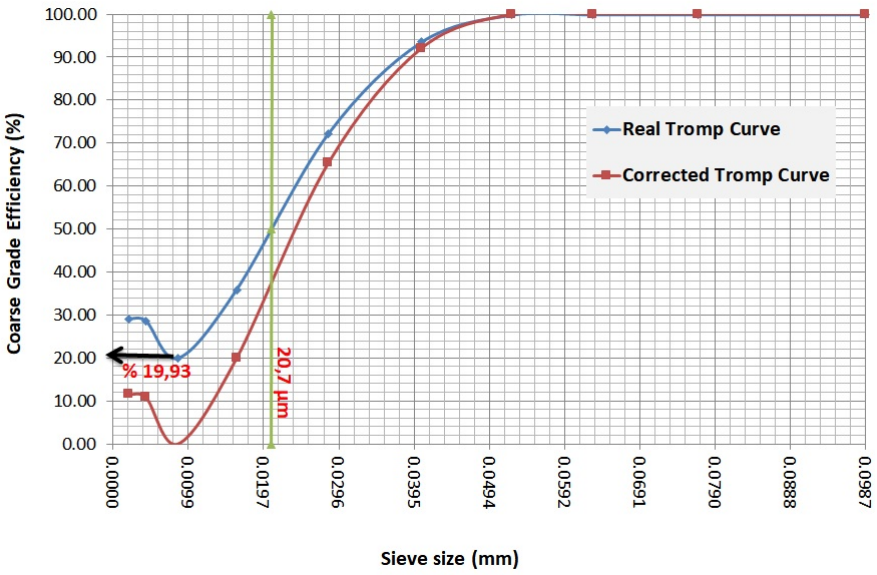


Figure 2. Trump curves before revision

The mill's grinding performance has been examined by taking samples from each meter. As a result of the obtained samples, the grinding medium design values (Table 5, 7) and quantity (Table 6) have been recalculated.

Table 5. Mill Information

Ball Mill		Mill Feed		
Diameter	4,25 m	Fresh Feed	144	t/h
Length	14,53 m	Return	250	t/h
		Sirk. Factor	2,74	

Table 6. New Ball Size Estimation

K	F	W_i	S_g	C_s	D
335	666	16	3,15	75,61	4,2
Ball Size		20,21 mm			

Table 7. New Ball Charge

Ball Size	Amount (t/m^3)	
30 mm	0.00	t
25 mm	62.52	t
20 mm	72.41	t
17 mm	85.76	t
Total	220.69	t

Grain size analysis of samples taken from certain distances within the mill is given in Figure 3.

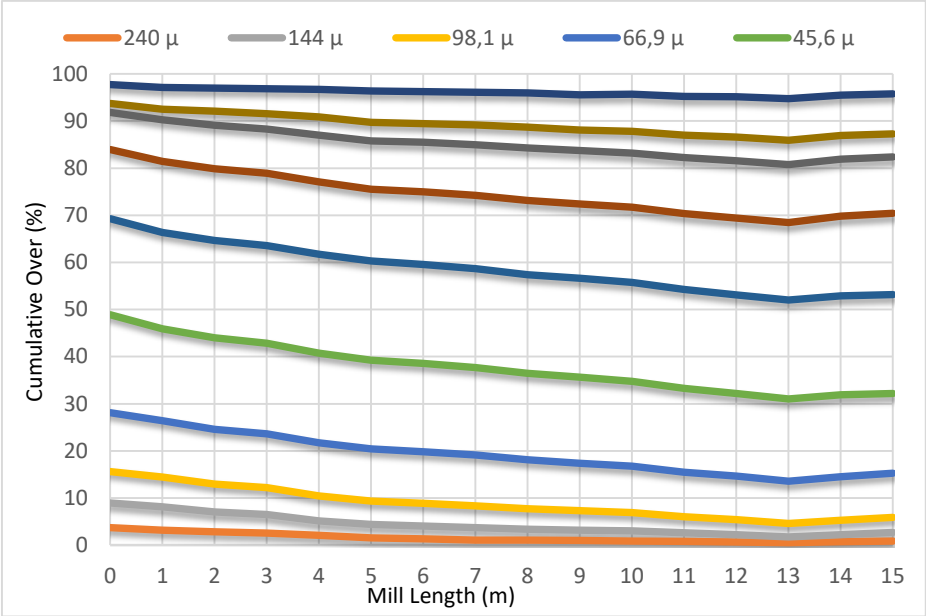


Figure 3. Change in sieve size distribution in the mill after the revision

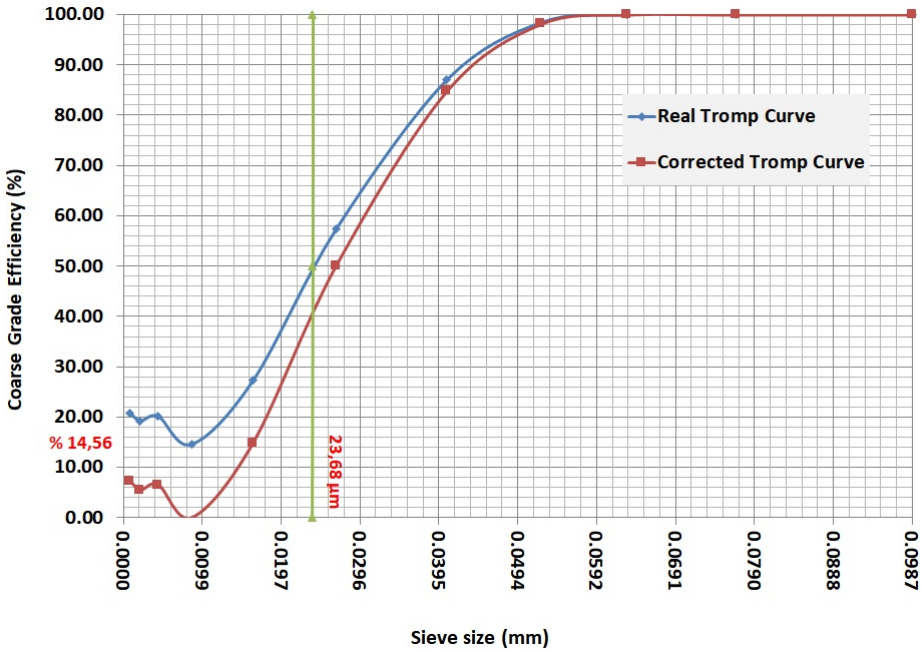


Figure 4. Trump curves after revision

Figure 4 shows a positive change in separator efficiency after the revision. It has been determined that the particle size (d50) of the separation with revision has not changed. As shown in Figure 4, the By-Pass ratio is 14.56%, while the Fishhook value is approximately 8%.

4. Conclusion

Based on the analyses conducted, the maximum material size fed into the mill in the current operating system is 0.67 mm. Under these conditions, it is observed that the 30 mm balls take up unnecessary space in the mill, while the lower fraction balls deform more quickly, increasing the scrap ball ratio.

The calculations show that the mills' optimal operating conditions require a maximum ball size of 20.21 mm. Simultaneously, the fineness curves reveal that the 30 mm ball occupies unnecessary space within

the mill. Calculations have demonstrated that excessive charging has caused the main drive motor to bear an excessive load, ensuring the filling rates of the balls inside the mill align with the literature.

The studies led to the creation of a new ball charge of 220.69 tons for the mill, with a maximum ball size of 25 mm. The balance of the 32 microns sieve has operated at a lower level compared to the previous year, yet there have been no losses in mill capacity. Upon examining the separator's efficiency, we observed a decrease in the amount of product escaping the mill as the separation size increased to 23.68 microns.

This way, the mill has reduced the unnecessary load on the main drive motor. At the same mill capacity, we achieved a savings of 1.72 points in specific energy. (Table 8)

Table 8. Product Data by Years

Years	Product (tons/year)	Working hours (h)	Tonaj (t/h)	Energy (kw/year)	Specific Energy	Size (32µ)	Blaine (g/cm^3)	Limestone (%)
2022	1.785.314	12.230	146	71.566.742	40,09	3,40	4117	3,70
2023	1.970.642	13.610	145	75.606.266	38,37	3,10	4106	4,70

References

Deniz V., 2004. The effect of mill speed on kinetic breakage parameters of clinker and limestone Cement and Concrete Research v: 34, n: 8.

Genç, Ö, 2016. Optimization of an industrial scale open circuit three-compartment cement grinding ball mill with the aid of simulation, International Journal of Mineral Processing v154, pp1–9.

Mejeoumov GG (2007). Improved Cement Quality and Grinding Efficiency by Means of Closed Mill Circuit Modeling.Ph.D. Thesis. Civil Engineering Department, Texas A&M University.

www.mdpi.com

Schnatz, R., Knobloch, O., 2000. Influence of the ball filling factor on the power consumption and throughput of ball mills in combined grinding plants. ZKG Int. 53 (8), 438–447.

Tiggesbäumker, P., Müller, M., 1983. The influence of ballmill speed on the specific energy expenditure and the throughput capacity. Aufbereitungs-Technik. No. 10, pp. 565–574.

Umucu Y., Deniz V., Saraç M, F., Kuzgun E., 2015. The relationship between cement quality and separation cut size, Inzynieria Mineralna-Journal of the Polish Mineral Engineering Society V:16, n: 36(2).

Comparative Analysis of Rod Mills and Ball Mills: Assessing Impact on Talc Ore Beneficiation Efficiency

Alaa ABBADI [1*], Ádám Rácz [1], Christoph Luckeneder [2], and Ljudmilla Bokányi [1], Author3 [1]

[1] aInstitute of Raw Materials Preparation and Environmental Technology, University of Miskolc

[2]Baumit Beteiligungen GmbH, Austria

*Corresponding author: abbadi.alaa.imad@uni-miskolc.hu (Alaa Abbadi)

Abstract:

Grinding is an essential unit operation in mineral beneficiation, significantly influencing subsequent separation processes. This study examined how rod and ball tumbling milling affect talc ore processing through dense media separation (DMS) and froth flotation, focusing on the impact of grinding media on particle size distribution and pyrite removal in DMS. The investigation used zeta potential measurements to analyze talc surface changes and assess flotation performance. A combination of single-stage batch tests and continuous closed-cycle grinding experiments highlighted important differences between the two milling methods. The rod mill displayed superior early stage grinding progression and selectivity for coarse particles, whereas the ball mill produced a higher proportion of fine particles. Closed-cycle rod milling resulted in a greater quantity of coarse particles suitable for DMS, leading to improved recovery of coarse pyrite particles. Zeta potential measurements showed slight differences in hydrophobicity between talc samples, which were neutralized after frother conditioning. The study also assessed the influence of grinding media type on talc recovery during flotation, finding that closed-cycle ball mill grinding optimized the particle size distribution of the flotation feed, yielding the highest talc recovery. Furthermore, pyrite rejection in the flotation circuit was effectively managed with both milling methods, ensuring minimal pyrite contamination in the final talc concentrate. The research concluded that while both rod and ball mills meet the required objectives, ball mills provide higher grinding stage capacity and better talc flotation recoveries.

Keywords: *talc; flotation; ball mill; rod mill*

1. Introduction

Talc is an industrial mineral belonging to the phyllosilicate family and is composed of layered magnesium sheet silicate hydroxides represented by the chemical formula $Mg_3Si_4O_{10}(OH)_2$ (Brezáni et al., 2013). The most common gangue minerals found along with talc are carbonates, magnesite, dolomite, serpentine, chlorite and calcite. The presence of these associated gangue minerals leads to undesirable impurities in talc. Additionally, trace amounts of other minerals, such as magnetite, pyrite, quartz and tremolite, may also occur within talc ores as minor impurities (Ahmed et al., 2007).

Talc possesses advantageous physical and chemical properties, including ease of handling, chemical stability, high adsorptivity, low plasticity, and low thermal and electrical conductivity, making it a valuable component in industries such as paper, paint, rubber, ceramics, refractory materials, polymers, and pharmaceuticals (Ahmed et al., 2011; Bazar et al., 2021). Notably, recent data from the United States Geological Survey (USGS) indicate a substantial increase in global talc production in 2020 and 2021, driven by the rising demand for rubber stoppers in response to the widespread distribution of COVID-19 vaccinations (U.S. Geological Survey, 2023).

The process of talc enrichment in concentrating plants includes several steps, such as crushing, grinding, mechanical separation (magnetic and spiral separation), and flotation (Yehia & Al-Wakeel, 2000). Among these steps, froth flotation is the most important and effective stage in the beneficiation process. Froth flotation is preferred for talc beneficiation because talc is naturally hydrophobic, which is closely related to its three-layer sheet crystal structure (Kursun & Ates, 2010).

Grinding serves as a crucial unit operation that significantly influences downstream processes by reducing ore particle size and liberating valuable minerals from gangue (Kursun & Ulusoy, 2006). The most widely employed technologies for grinding ores are tumbling ball mills (BMs) and rod mills (RMs). BMs allow easy modification of media filling rates to regulate and control the particle size distribution of ground products. Despite being less common, RMs are sometimes preferred in mineral processing plants to generate relatively uniform grinding products and prevent overgrinding. This approach helps improve separation efficiency, especially in plants involving gravity separation processes (C. Li & Gao, 2017).

The choice of grinding method type introduces variations in loading behavior, contact mechanism, product size, grinding kinetics, mill power, overall grinding costs and wear, with grinding media playing a pivotal role (Simba & Moys, 2014). In RMs, grinding occurs through line contact between rods and ore particles, facilitating a series of crushing interactions, while BMs employ random point contacts between balls and ore particles, potentially leading to a broad spectrum of particle sizes (Vizcarra et al., 2011).

Several parameters govern the performance and efficiency of froth flotation processes. Extensive research has established mineral particle size as one of the most critical factors influencing flotation response (Gaudin et al., 1942; Trahar, 1981; Vinnett et al., 2022). Every flotation system has an optimum particle size range for achieving maximum recovery and selectivity. When the feed particles fall within this critical size distribution, the flotation kinetics, grade and recovery are enhanced significantly. However, operating outside the ideal size range lowers the selectivity and recovery drastically (Liu et al., 2022; Wang & Liu, 2021; Yekeler & Sönmez, 1997).

In the context of talc, research shows that the hydrophobicity of talc particles strongly correlates with the particle size or surface-to-edge ratio. Talc delamination during grinding exposes additional surface faces, enhancing hydrophobicity as the size decreases (Leterme et al., 2005). However, excessive grinding below 10 microns causes a decrease in hydrophobicity (increase in hydrophilicity), potentially due to higher edge-to-face ratios for smaller particles, altering contact angles and surface chemistry (Feng & Aldrich, 2004).

The Gemerská Poloma talc processing plant currently utilizes a RM to grind talc ore. This process aims to achieve an optimal particle size distribution for the subsequent froth flotation and spiral separation stages. The narrow size distribution provided by the RM not only aids in removing pyrite in spirals at a coarse size but also minimizes the presence of slime, which can negatively impact flotation performance. However, there are operational challenges associated with RMs. By replacing them with BMs, the plant can enhance its overall economy. This includes reducing liner wear, lowering metal consumption, improving the handling of grinding media, and minimizing downtime (Rácz et al., 2021). Nonetheless, implementing a BM as the grinding stage may lead to a shallower particle size distribution. Additionally, there may be higher fractions of fine and ultrafine particles, which could hinder the performance of the spiral separator and flotation stages, respectively.

This study seeks to fill a knowledge gap concerning the influence of grinding media type, specifically rod milling and ball milling, on an actual talc ore feed and how this in turn affects process efficiency in a talc beneficiation plant. To explore these effects, a series of grinding tests, encompassing both batch and closed-cycle grinding, were conducted. The designed experiments allowed the determination of the changes in the ground talc ore particle size distribution, pyrite removal, surface properties, and flotation performance when the grinding media was changed from RM to BM for the same ore feed. This study provides insights into how the choice of grinding media type affects key outcomes related to process efficiency in talc beneficiation. Additionally, the findings will facilitate informed decisions regarding the implementation of this operational change.

2. Materials and methods

2.1. Ore sample

Representative talc ore samples were obtained from Eurotalc s.r.o. beneficiation plant Gemerská Poloma, Slovakia. Chemical analyses were carried out by the Laboratory of Gemerská Poloma Plant.

LOI was determined using burning of 4 g for 2 h at 1050 °C in a muffles furnace, while for the measuring carbon and sulfur LECO elemental analyser was used. MgO, SiO_2, Al_2O_3, Fe_2O_3, CaO were determined by XRF. A probable and plausible distribution between talc, quartz, magnesite, dolomite, pyrite and chlorite was calculated using the above data. Chemical analysis indicated that the talc grade of the ore was 60.1% by mass (Table 1). Characterization of the physical properties revealed that the moisture content of the ore was 2.10 % on a mass basis. The wet and dry bulk densities were measured as 1.69 g/cm^3 and 1.84 g/cm^3, respectively, while the average particle density was determined to be 2.75 g/cm^3.

Table 1. Chemical composition of the flotation feed (L.O.I. = lost on ignition).

Component	SiO_2	MgO	CaO	Al_2O_3	Fe_2O_3	S	L.O.I	Talc
%	40.61	29.17	3.08	0.32	2.90	0.58	21.34	60.10

2.2. Grinding tests

Two grinding test configurations were tested: closed-circuit and open-circuit single-stage batch tests. A laboratory tumbling mill with an inner diameter of 300 mm and length of 600 mm was fitted with smooth liners and was utilized for both tests. The mill speed was set at 46 rpm, corresponding to 60% of the critical speed, matching the operation of the industrial RM used at the plant under study. The identical ball and rod charge masses were used for comparative grinding performance evaluation. Details on the media charge conditions are presented in Table 2. All the tests involved wet grinding with a solid concentration of 40 wt.%.

Table 2. The media charge conditions used.

Charge type	Size (mm)	Number of balls	Mass (kg)	Surface area (m^2)
Balls	45	18	6.563	0.111
	38	82	18.430	0.371
	35	15	2.326	0.051
	30	85	9.469	0.241
	26	18	1.303	0.038
	24	12	0.671	0.021
	15	235	3.240	0.165
	Total	465	42	1
	Size Diameter * length (mm)	Number of rods	Mass (kg)	Surface area (m^2)
Rods	38.1 * 530	6	28.8	0.39
	44.5 * 530	2	13.2	0.15
	Total	8	42	0.54

Single-stage batch grinding tests were carried out in the same laboratory tumbling mill under open-circuit conditions using both rod and ball milling media. Batch grinding durations of 5, 10, 20 and 30 minutes were evaluated.

Closed-cycle grinding tests were conducted to simulate the continuous industrial grinding and flotation circuit used at the Gemerská Poloma talc processing plant. The standard plant flowsheet was slightly modified for laboratory simulation by replacing the spiral separator stage with a dense media separation (DMS) process to treat the –1000+315 µm fraction from the mill discharge (Fig. 1). A heavy media density using sodium polytungstate as a separation medium with a density of 3 g/cm^3 enabled the separation of pyrite grains (sinks).

After each grinding cycle, the mill discharge was screened at 315 µm to extract the undersized product fraction that was directed to subsequent flotation stages. The –1000+315µm coarse particles from the screening underwent DMS. The floating fraction from this separation was recombined with any +1000 µm oversize particles and returned to the mill feed to continue grinding in the next cycle. Make-up feed was added to replace the mass of removed material in each cycle. The duration of grinding time per cycle was modulated to attain a circulating mass 2.5 times greater than the mass withdrawn. Under these conditions, the experiment simulated a steady-state continuous closed-circuit grinding operation with a circulating load of 250%.

2.3. Particle Size Distribution Analysis

Upon completion of the grinding tests, the products were screened at 315 µm. The +315 µm oversize underwent dry sieving using standard test sieves with √2 progression. The –315 µm undersize fraction was analyzed via laser diffraction using a Horiba LA-950 V2 instrument in wet measurement mode.

2.4. Zeta potential measurements

To prepare samples for zeta potential analysis, 5 g rod or ball mill ground talc was dispersed in 100 mL of tap water in the presence and absence of the used frother. The suspensions were agitated for 10 min using a magnetic stirrer to ensure thorough mixing. The suspensions were subsequently allowed to settle. After settling, 20 mL aliquots of supernatant were extracted using a pipette and subjected to zeta potential quantification utilizing ZetaPALS (Brookhaven Instrument Corporation). Five repeat measurements were performed per test condition. The average zeta potential was documented along with standard deviations consistently under ±1 mV.

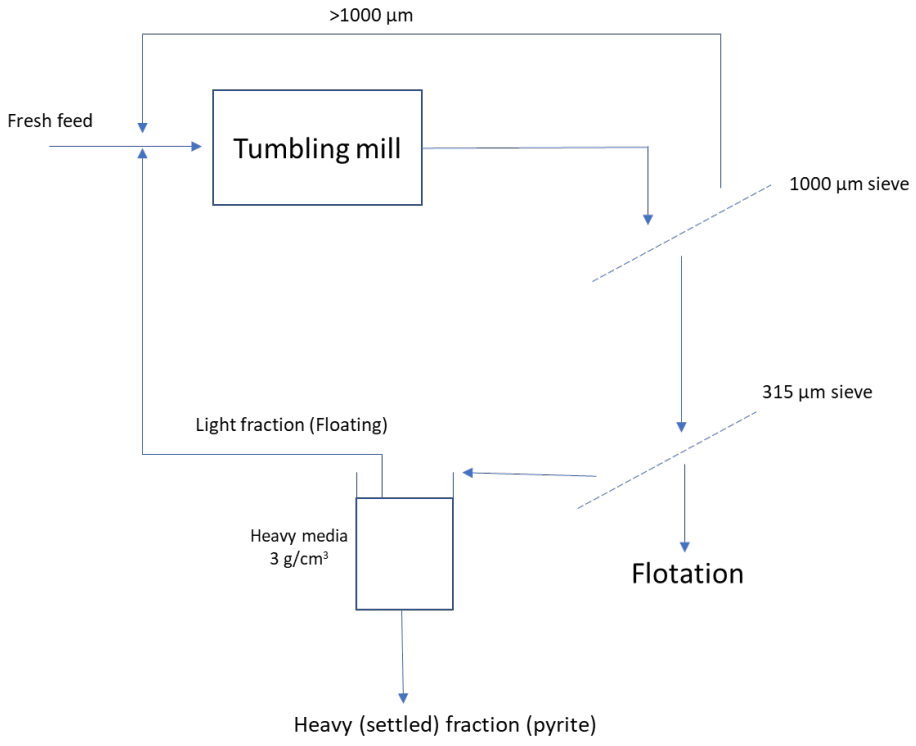


Figure 1. Flowsheet of a laboratory grinding circuit simulating the continuous process design operating at the industrial plant under study.

2.5. Batch-flotation tests

A laboratory self-aerated flotation machine (KHD Humboldt Wedag AG) with a 1 L cell was used for batch flotation tests at an impeller speed of 1900 rpm. The pulps were prepared by adding 310 g of –

315 µm ground ore from ball and RM grinding along with tap water into the flotation cell to reach a volume of 1 L. Conditioning was provided for 2 minutes before introducing 15 g/t of Aerofroth 70 (alcohol- and glycol-based) frother and conditioning for an additional 2 minutes. The flotation test procedure consisted of rougher flotation followed by two cleaner stages (Fig. 2), simulating the industrial flotation circuit at the Gemerská Poloma plant.

3. Results and discussion

3.1. Single-stage batch grinding results

The grinding test was performed according to the conditions described above, and Fig. 3 shows the particle-size distributions at 5, 10, 20, and 30 min of grinding for both types of grinding media. A preliminary examination of the data revealed that while the particle size distribution shifted toward finer sizes as the grinding time increased for both the BM and the RM, the rate of additional grinding decreased after approximately 20 minutes. This is evidenced by the fact that the percentage of material passing through the 500 µm sieve increases rapidly from 5 to 20 minutes for both mills but then plateaus between 20 and 30 minutes. For example, in the BM, the below 500 µm mass percentage increases from 58.23% at 5 minutes to 82.41% at 20 minutes, increasing only slightly to 84.38% after 30 minutes. A similar trend is observed for the RM.

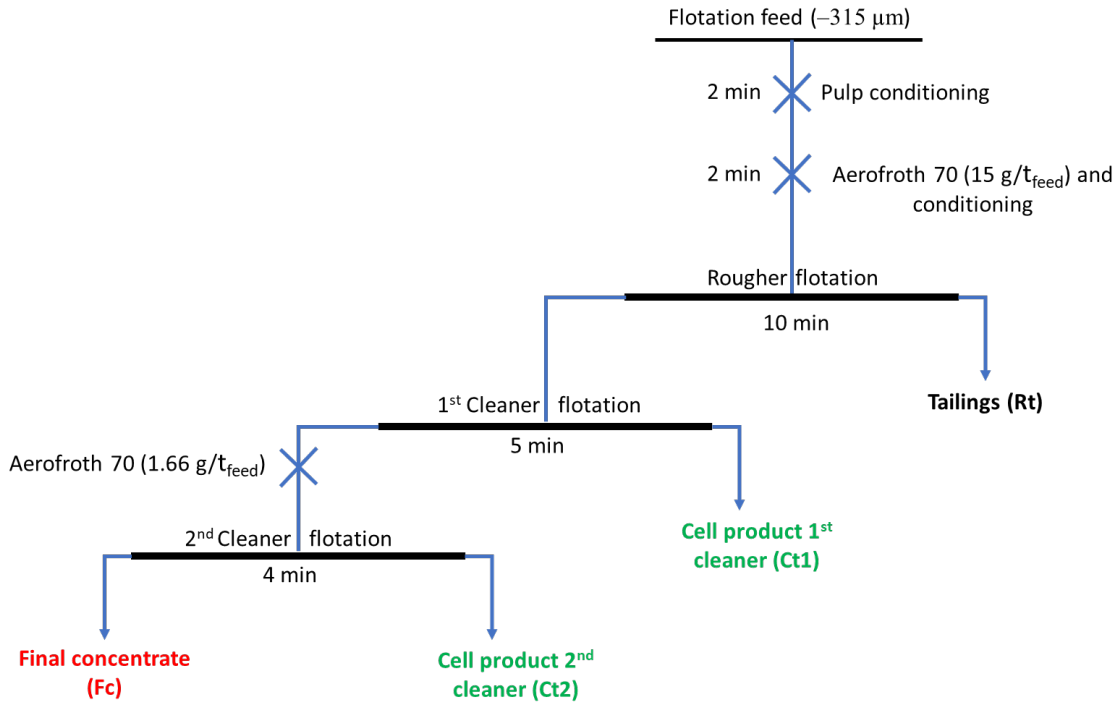


Figure 2. Flowsheet of the flotation experiments.

A comparison of the performances of the two-grinding media revealed distinct differences in grinding behavior. While the BM generates more fine particles below 315 µm at all durations tested, the RM displays superior grinding selectivity toward coarse feed particles in the initial grinding stages. For example, after just 5 minutes, 91.32% of a RM passed through a 4000 µm sieve, whereas only 71.66% of the BMs passed. This preferential breakage of coarse particles by the RM is also consistently observed at the later grinding time points. This enhanced selectivity of the RM toward coarse particle grinding can be attributed to the configuration the rods adopt upon coarse particles.

The coarse particles tend to push the rods apart, organizing them into a wedge or cone-shaped array. This orientation serves to increase the likelihood of rod stress events specifically targeting and acting upon coarse particles first (Runge et al., 2013). Shoji and Austin (Shoji & Austin, 1974) indicated that, compared to BMs, RMs do not break large particles more slowly than expected per se. Rather, the BM

displays slower coarse particle breakage progression than would be anticipated based on subsequent finer grinding behavior.

Fig. 4 shows the characteristic particle sizes X_{80} and X_{50} as a function of grinding time for both the BM and the RM. Aligned with the trends in the cumulative particle size distribution data, the X_{80} and X_{50} metrics highlighted key differences in grinding behavior between the two mills. Specifically, the RM displays faster early-stage grinding progression and superior selectivity toward coarse particle breakage, as evidenced by the rapid and substantial reduction in the X_{80} value within the first 10 minutes. For example, after 5 and 10 minutes, the RM X_{80} decreases from 11330 µm to 1035 µm and then to 800 µm, respectively, whereas that of the BM decreases from 6200 µm to 3645 µm.

Additionally, the BM generates finer particles more effectively, as shown by the significantly lower X_{50} values of 190 µm and 64 µm after 5 and 10 minutes, respectively, relative to those of 320 µm and 141 µm in the RM. However, these differences in selectivity, and fine particle production between the two mills equalize after enough grinding time elapses—in this case, between 20 and 30 minutes. Beyond this point, both mills converge to similar characteristic size values.

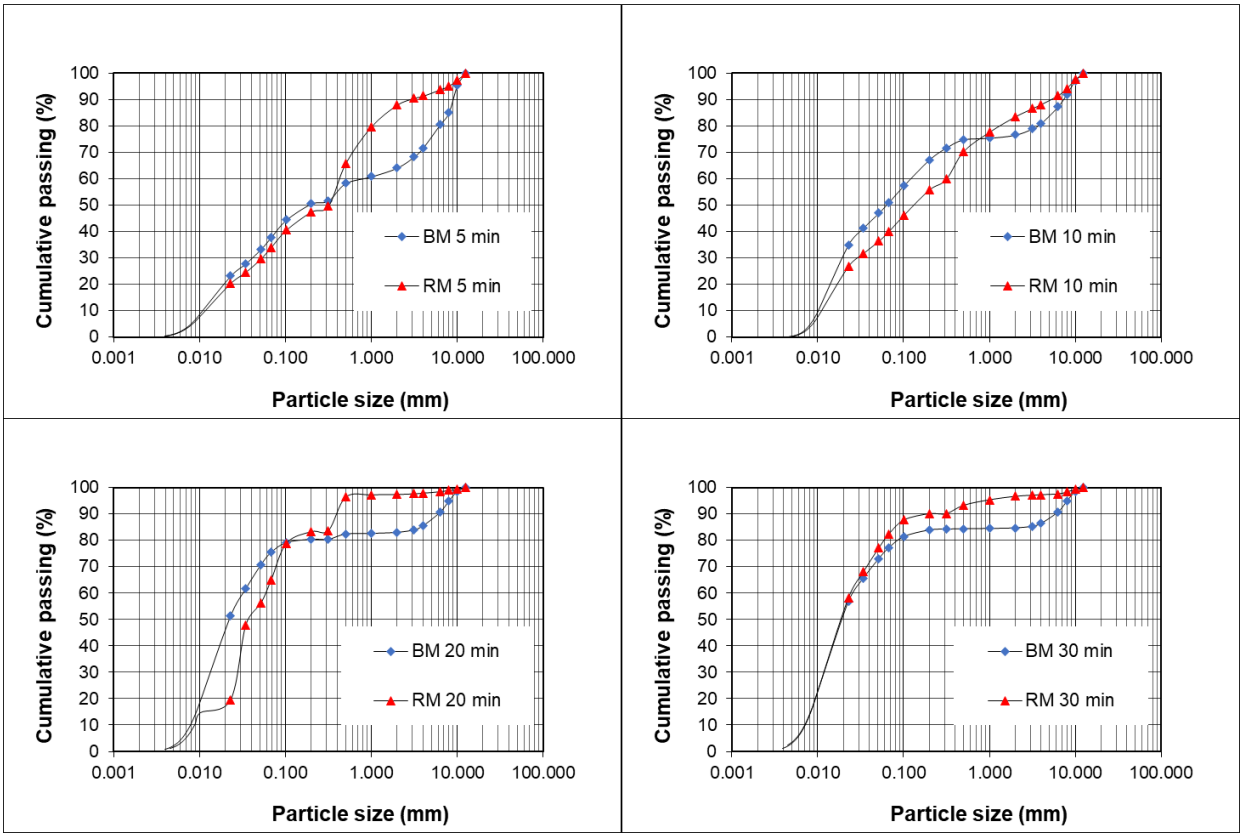


Figure 3. Particle size distributions of the ground product obtained using ball and rod mills at various grinding times.

3.2. Closed-cycle grinding results

Closed-cycle grinding tests were performed using ball-and-rod tumbling mills at equivalent mass loading and with similar feed size distributions. The mass percentages produced in the coarse (–1000+315µm) and fine (–315 µm) fractions at equilibrium (Fig. 5) showcase contrasting ground size distributions.

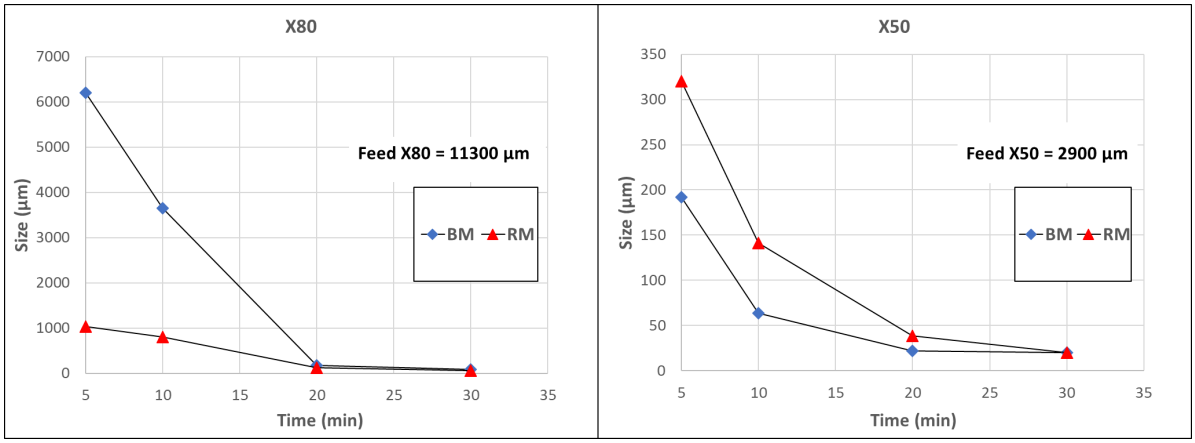


Figure 4. Characteristic particle size (X_{80}, X_{50}) as a function of grinding time using ball and rod tumbling mills.

Both the BM and RM required 6 cycles to reach steady state, suggesting equal grinding time and energy input during the comparative tests. Consequently, the observed differences in product size distributions, as shown in Fig. 5 and Fig. 6, can be attributed to the inherent grinding mechanisms of each media type rather than external factors.

The RM produces approximately 5 times more of the –1000+315µm size fraction than the BM. However, compared with rod milling, ball milling produces approximately 30% more –315 µm fines. This indicates that the BM product is significantly finer overall, with a 90% distribution below 315 µm versus a more even distribution for the RM.

Transitioning from rod milling to ball milling is predicted to substantially decrease the mass flow rate of the –1000+315µm particle size fraction directed to DMS by approximately fivefold. This significant reduction in coarse fraction loading has the potential to detrimentally impact the efficiency of pyrite removal achieved in the density separation stage. On the other hand, the increased –315 µm fines from the BM and subsequent higher cumulative fresh feed mass after achieving steady-state is projected to raise plant capacity approximately 3%.

The size distribution of the –315 µm size fraction from the final run mill content is shown in Fig. 6. Like in batch grinding tests, the BM appears to produce a finer product than the RM. This can be attributed to the greater surface area per unit weight for ball charges than for rod charges (Camalan & Hoşten, 2015).

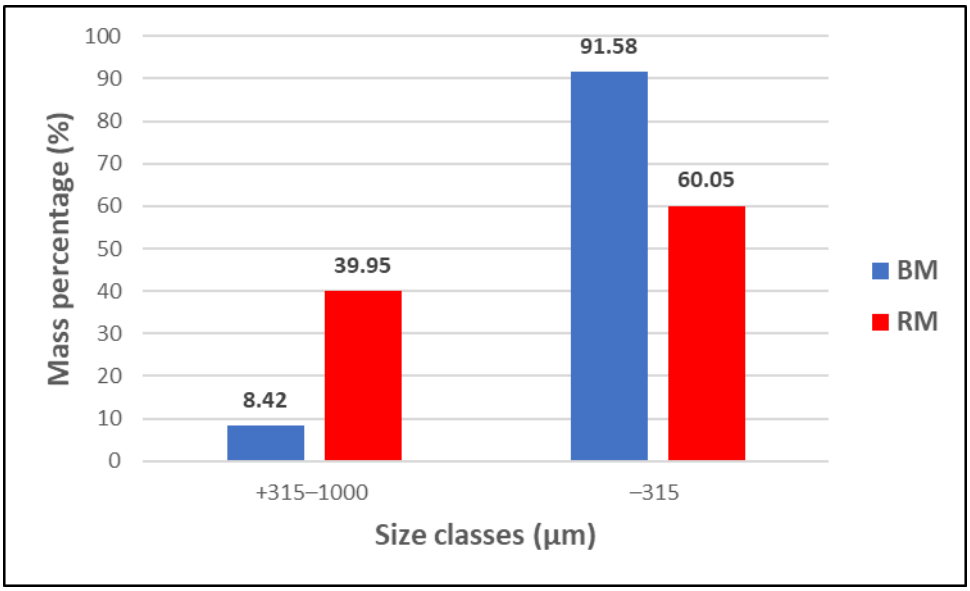


Figure 5. Percentage mass produced for two size fractions after achieving equilibrium in closed-cycle grinding using BM and RM.

In line with this study, the ball charge surface area was twice that of the rod charge surface area, as reported in Table 2. Additionally, the finer product from the ball charge can be attributed to the randomized ball striking action, where fine and coarse particles have equal probabilities of impact (Duroudier, 2017). However, within this fine –315 µm fraction, the BM achieves a narrower size distribution, with 80% passing through between 100 µm and 10 µm. In contrast, the RM produced a wider distribution of particles in this fine fraction, with 80% of the particles passing through a broader range from 200 µm to 10 µm.

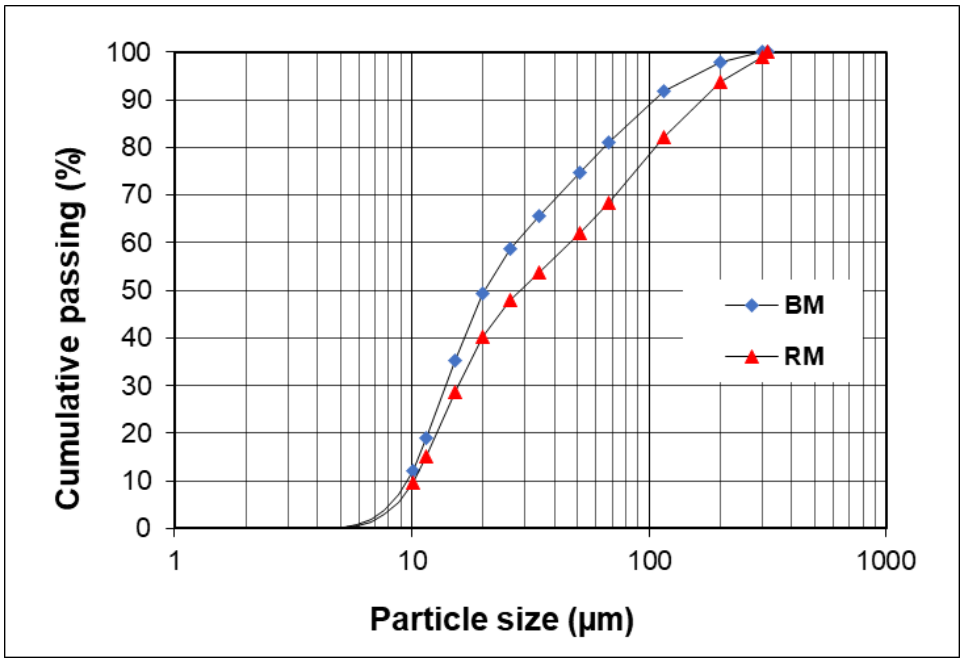


Figure 6. Size distributions of the ground product with a –315 µm fraction obtained using ball and rod mills during closed-cycle grinding.

3.3. Pyrite removal by dense media separation

The –1000+315 µm size fraction produced by the closed cycle grinding stage was subjected to DMS for pyrite removal after each grinding cycle for both types of mills, and the results in terms of the sink yield and pyrite recovery are presented in Fig. 7.

The RM, as established in the previous section, resulted in substantially higher yields of the –1000+315 µm size fraction directed to the DMS stage. The increased loading from the RM enabled higher recoveries of pyrite in the DMS sink product. Pyrite recoveries ranged from 6.4-14.5% for the RM discharge, while the BM achieved lower recoveries of 3.16-8.81% (excluding cycle 4). The very low sink product yield from the BM in cycle 4 (<5 g) was insufficient for chemical analysis of pyrite recovery.

In addition to the higher loading of coarse particles, the RM may also improve the liberation of pyrite particles compared to the BM for the –1000+315 µm size fraction. As discussed in Li et al. (Z. Li et al., 2018), the compressive forces inherent in RM grinding tend to cause separation along grain boundaries, resulting in reduced mineral boundary lengths. In contrast, the impact forces in BMs lead to greater reductions in the mineral surface area. For components with high levels of content, as in the case of this ore, the RM's mechanism of boundary length reduction enables improved liberation. The BM instead decreases the pyrite surface area to a greater extent through impact crushing. As a result, the RM discharge process results in higher yields of liberated, coarse pyrite particles amenable to separation by density. These aspects will be addressed in a future study through detailed liberation analysis.

The combination of increased loading and the potential improved liberation of coarse pyrite particles gave the RM a clear advantage over the BM for pyrite rejection. The BM reduced the particle size and pyrite surface area to a level that hindered both the quantity and liberation characteristics for effective DMS. This will result in more pyrite reporting to the froth flotation stage with the fine –315 µm fraction.

The extent of pyrite contamination and rejection during flotation will be examined in addition to other factors in the following section.

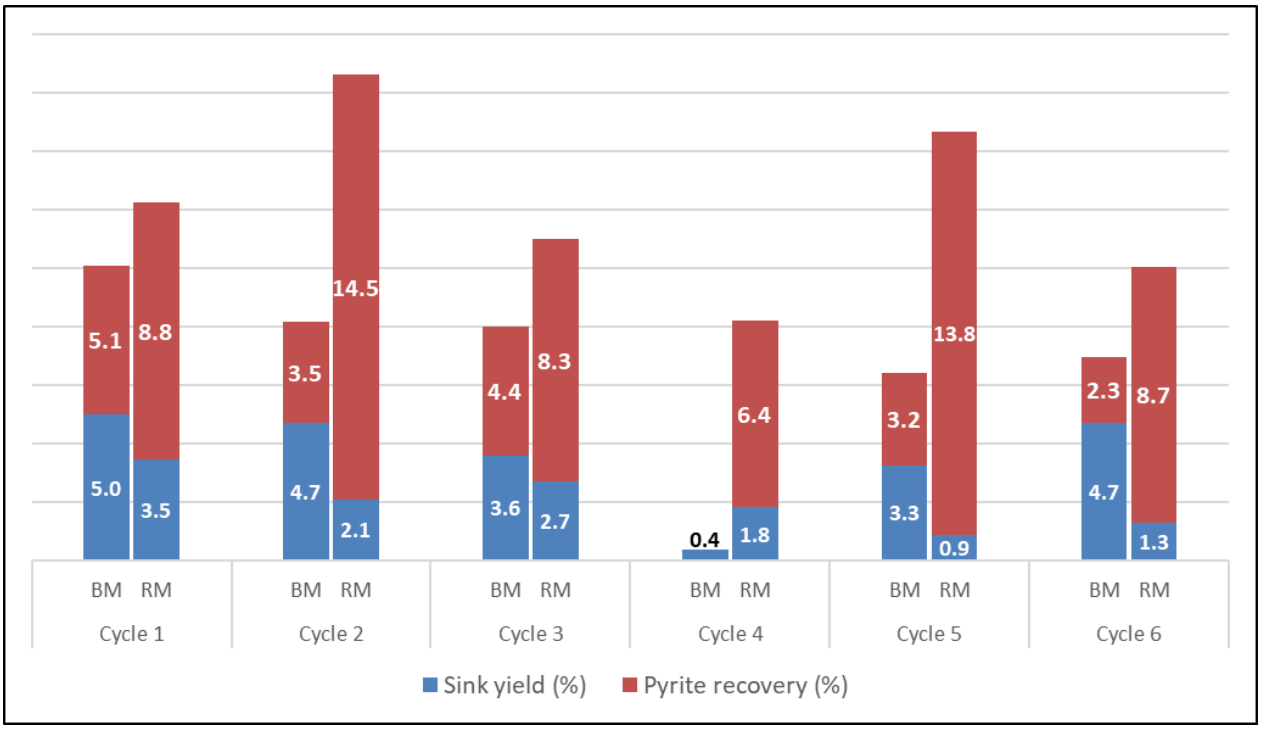


Fig. 7: Yield and pyrite recovery of DMS sinks for rod and BM discharge from grinding cycles.

3.4. Surface properties of talc ground in tumbling BM and RM

Zeta potential measurements were conducted on BM and RM ground talc to gain further insights into how the grinding media type could influence talc surface properties. Zeta potential is used to describe and determine the relationship between the adsorption behavior of reagents and the surface charge of mineral particles (Bulatovic, 2007; Wonyen et al., 2018). For talc specifically, a higher hydrophobic basal plane to hydrophilic edge ratio corresponds to a lower overall zeta potential magnitude (Beattie et al., 2006; Steenberg & Harris, 1985). However, a definitive correlation between talc zeta potential and floatability remains to be established (Yehia & Al-Wakeel, 2000).

While directly relating talc zeta potential and floatability can be complex, comparative analysis can provide valuable insights. Shifts in zeta potential distribution or magnitude between milling types may indicate variations in exposed basal plane versus edge site area. These distinctions likely arise from divergent fracture mechanisms induced by the contrasting stress regimes inherent to each grinding media type. Fig. 8 presents the zeta potential of BM and RM ground talc, measured both with and without alcohol- and glycol-based frothers introduced into the system. This type of frother has shown the capability of adsorbing onto the talc particle surfaces (Kuan & Finch, 2010).

The minor differences in zeta potential between the rod milled and ball milled talc samples (Fig. 8) provide some indications about their relative surface properties. The ball milled talc exhibited a slightly less negative zeta potential value prior to frother addition, which suggests a modestly higher ratio of hydrophobic basal plane area to hydrophilic edge sites. However, upon frother introduction during the conditioning stage, both talc samples exhibited similar shifts of approximately -3 mV. This comparable magnitude change implies that the grinding media type did not substantially impact the adsorption capacity of the frother. Ultimately, the type of milling does not appear to dramatically alter the surface characteristics of the produced talc particles. Thus, observed differences in subsequent flotation behavior would not likely originate from modifications induced uniquely by the choice of rod or ball milling.

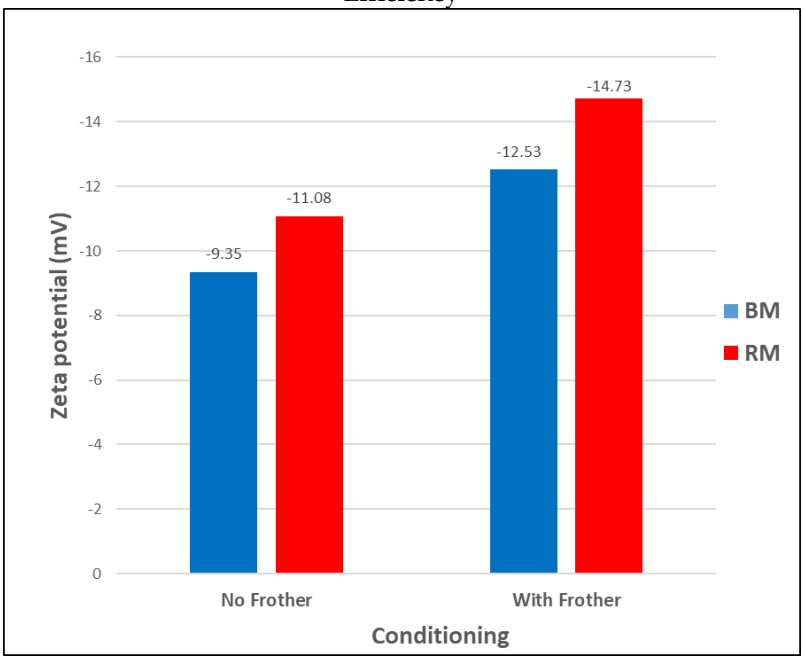


Figure 8. Zeta potential of BM and RM ground talc in the presence and absence of frother.

3.5. Batch-flotation experimental results

To verify the effects of mill charge type on flotation performance, flotation experiments were performed on talc ore samples ground in closed cycle and batch mode after 20 and 30 minutes using ball and rod mills, and the results are shown in Fig. 9. The ground ore samples underwent rougher and cleaner flotation stages. Although, the rougher stage results will be discussed to showcase differences in flotation performance, since at this stage all the differences in the liberation degree and particle size regarding flotation can be clearly revealed. The cleaner stage results will be examined to highlight pyrite contamination levels in the final concentrate.

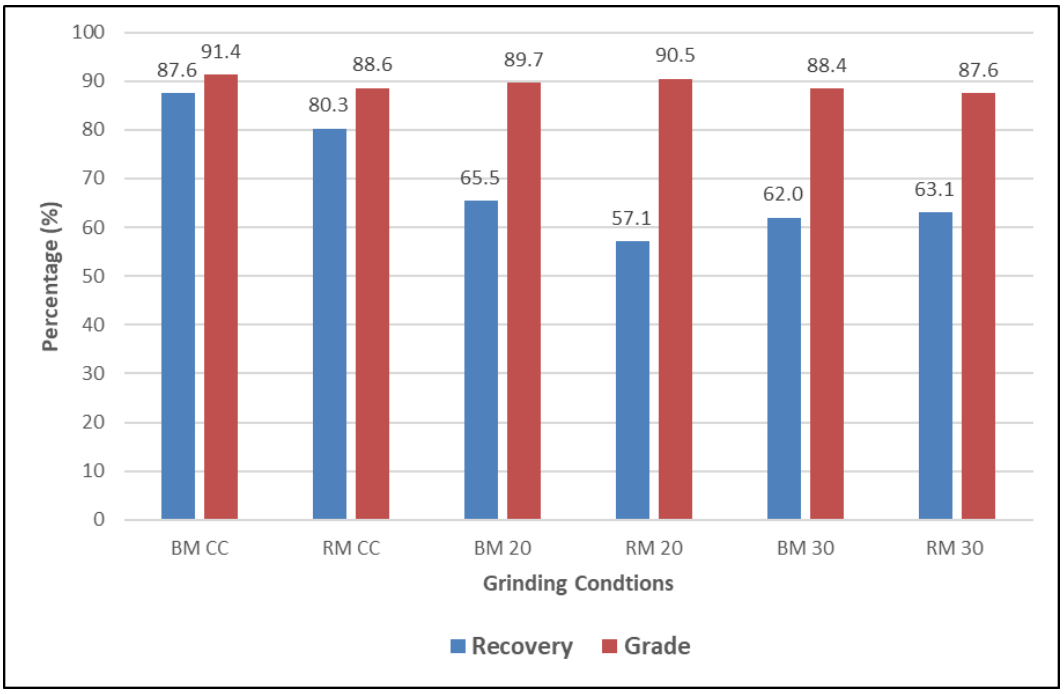


Figure 9. Rougher flotation stage results in relation to grinding conditions used.

Talc recovery at rougher stage flotation varied from 57.1% to 87.6% depending on the grinding conditions used. Importantly, the talc grade in all the cases was high, ranging from 87% to 91%, indicating selectivity in the flotation process and high liberation of the talc particles. Nevertheless, the highest recovery of 87.6% was obtained with closed-cycle BM grinding, while closed-cycle RM grinding gave the second-best recovery of 80.3%. In batch grinding tests, talc recovery decreased with increasing grinding time from 20 to 30 min for both the rods and BMs. Specifically, the BM batch grinding recoveries were 65.5% and 62.0% after 20 and 30 min, respectively. On the other hand, compared with grinding for 20 min, RM batch grinding slightly increased the recovery by 63.1% and 57.1%, respectively.

Previous studies have identified an optimal particle size range of 10-125 µm for maximizing talc recovery and grade during flotation (Boujounoui et al., 2020; Chen et al., 2018; Kursun & Ates, 2010; Yekeler & Sönmez, 1997). Beyond this specified size range, both recovery and flotation kinetics exhibit a decline, which can be attributed to unfavorable hydrodynamic conditions during flotation. This is manifested in inadequate collision frequencies for finer particles and heightened detachment probabilities for coarser particles. Furthermore, the hydrophobic properties of the talc particle surface may also undergo alterations outside of the optimal size range (Schubert, 2008).

To explain the differences in talc recovery observed after rougher flotation under various grinding conditions, the particle size distribution of each flotation feed was examined. As shown in Fig. 10, the particle size distributions were categorized into three size classes: coarse-fine (–315+100 µm), intermediate-fine (–100+10 µm), and ultrafine (–10 µm).

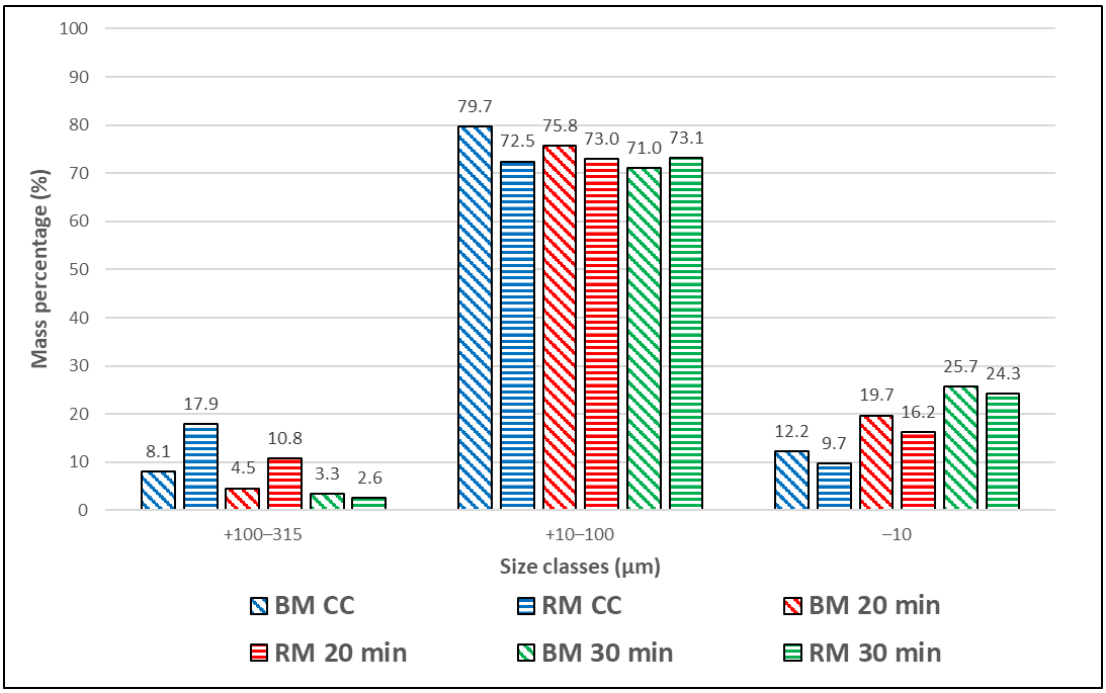


Figure 10. Mass percentages of the three size classes in relation to grinding conditions.

The data in Fig. 10 demonstrate a clear correlation between the mass percentage of particles in each size class, determined by the grinding media type, and the resulting talc recovery. Specifically, closed-cycle BM grinding produced the highest percentage of intermediate-fine size –100+10 µm particles (79.7%), along with minimal amounts of coarse-fine and ultrafine fractions (<20%). This particle size distribution corresponded to a maximum talc recovery of 87.6%. In contrast, closed-cycle RM grinding generated fewer –100+10 µm particles (72.5%) and more than twice the amount of coarse-fine particles, resulting in a lower recovery of 80.3%.

This trend is further evidenced in the batch grinding tests. Increasing the grinding time from 20 min to 30 min decreased the mass percentage of the coarse-fine fraction to less than 4% for both the ball and RMs. However, this process significantly increased the ultrafine talc fraction to approximately 25%. This

particle size distribution was reflected in the flotation performance, where the talc recovery was lower than 65% for both mill types after 30 min of batch conditions.

Incorporating Pearson correlation analysis further quantifies the relationships observed between particle size distribution and talc recovery. Specifically, the results revealed a stronger positive correlation (r = 0.649) between the intermediate-fine size (–100+10μm) and recovery compared to the other size fractions. This suggests that as the percentage of particles in this intermediate size range increases recovery rates tend to show the most substantial corresponding improvement. A moderate positive correlation (r = 0.454) was also observed between the proportion of coarse-fine particles (–315+100 μm) and recovery, indicating that while an increase in coarse particles exhibits a positive relationship with recovery, the effect is less pronounced. Finally, a strong negative correlation (r = -0.722) was found between the percentage of ultrafine particles (–10 μm) and recovery. This implies that as the relative amount of ultrafine fraction rises, recovery decreases dramatically. While these correlations provide valuable insights into the relationship between particle size distribution and recovery, it is acknowledged that both particle shape and liberation characteristics, which can differ based on the grinding media used, may also play significant roles in talc flotation performance. These factors will be examined in detail in future research to provide a more comprehensive understanding of the grinding media effects on talc beneficiation.

As discussed in Section 3.3, closed-cycle BM grinding yields lower loading rates and reduced pyrite recovery in the DMS stage than does closed-cycle RM grinding. This shift to BM grinding increases the pyrite content in the –315 μm size fraction destined for flotation. An elevated pyrite content may adversely affect talc beneficiation, potentially compromising the whiteness of the flotation concentrate, which is undesirable in the final talc product. Therefore, it is imperative to comprehensively investigate pyrite behavior throughout flotation circuits. This involves analyzing pyrite recovery at various stages and discerning potential variations in results based on the different grinding stages employed. Table 3 shows the pyrite recovery values in the products from each flotation stage.

The data in Table 3 reveal negligible differences in pyrite content and recovery between the flotation products derived from feed samples ground under closed-cycle BM and those ground under closed-cycle RM. For both grinding circuits, the pyrite content in the final cleaner concentrate (Fc) is approximately 0.01% by weight, accounting for less than 1% of the pyrite recovery from the original feed. This demonstrates highly efficient rejection of pyrite to the tailings streams and minimal carry-over to the final concentrate.

Table 3. The yield of flotation stages products and the corresponding pyrite content and recovery values in relation to grinding media type.

Grinding Media type	Flotation Product	Yield (%)	Pyrite Content (%)	Pyrite Recovery (%)
Closed-Cycle BM	Rt	52.55%	0.76%	81.64%
	Ct1	26.23%	0.15%	15.80%
	Ct2	8.54%	0.02%	1.98%
	Fc	12.67%	0.01%	0.58%
Closed-Cycle RM	Rt	47.81%	0.48%	85.39%
	Ct1	31.88%	0.06%	10.68%
	Ct2	9.64%	0.02%	2.95%
	Fc	10.67%	0.01%	0.98%

Ultimately, the switch from RM to BM grinding is not expected to negatively impact pyrite contamination or whiteness of the final talc concentrate product achieved by the second cleaner stage of flotation, which maintained more than 96% talc purity under both types. The comparable pyrite deportment and final concentrate purities indicate that both grinding media are equally effective for liberating pyrite particles in the –315 μm size fraction.

4. Conclusions

This study investigated the effects of grinding media type in tumbling mill on talc ore processing in terms of particle size distribution, pyrite removal via dense media separation, and talc flotation performance. Through comprehensive experimental work involving single-stage batch tests and continuous closed-cycle grinding, key differences were delineated between the two milling types.

The results from batch grinding demonstrated that, compared with BMs, RMs exhibited superior early-stage grinding progression and selectivity toward coarse particles. However, BMs generated higher yields of fine particles. In closed-cycle grinding tests, RMs produced substantially more –1000+315µm particles amenable to dense media separation for pyrite rejection. Correspondingly, rod milling enabled higher recoveries of coarse pyrite particles. However, compared with rod milling, closed-cycle grinding ball milling increased the grinding capacity by 3% due to the greater amount of –315 µm fine particles produced.

While the ball milled talc showed slightly more hydrophobic character prior to frother conditioning, evidenced by a modestly less negative zeta potential, both talc samples experienced nearly identical shifts after exposure to frother, indicating similar adsorption capacities regardless of charge type. Since the type of milling does not appear to dramatically modify surface properties nor frother adsorption, observed differences in subsequent flotation behavior would likely originate from other factors.

During flotation, the highest talc recovery was achieved using BM feed due to the optimized particle size distribution. The reduced talc recoveries observed from RM ground product, compared to the BM product, can be attributed to the wider size distribution present in the RM flotation feed product. The RM feed contained approximately twice the proportion of coarse-fine (–315+100 µm) size fraction compared to the BM product. The increased quantity of this size fraction in the RM feed is correlated with lower liberation of the talc particles and less favorable flotation conditions, which together diminish the talc recovery. Pyrite contamination levels in the concentrates were low for both mills, indicating effective rejection.

Overall, this study elucidated the mechanisms and magnitude of key differences between grinding of this talc ore by rod or ball grinding media. While both grinding media types achieved the stipulated objectives, grinding with balls offered higher grinding stage capacities and talc flotation recoveries alongside the operational performance benefits. The approaches and findings may aid other operations in processing similar ores to make informed mill selection and beneficiation decisions.

Acknowledgement

The research work was supported by Project No 19007 - MineTALC. Backfill Mining Optimisation for Low- and Medium- Strength Deposits, EIT. The paper elaboration was carried out at the University of Miskolc, within the framework of the Thematic Excellence Program funded by the Ministry of Innovation and Technology of Hungary. We gratefully acknowledge the assistance and support of the Raw Materials Preparation and Environmental Technology research team, especially. Their diligent work in performing the experiments and collecting the data that underpins this research was invaluable. We thank them for their time, effort, and willingness to facilitate the completion of this project.

Disclosure statement

The authors report there are no competing interests to declare.

References

Ahmed, M. M., Ibrahim, G. A., & Hassan, M. M. A. 2007. Improvement of Egyptian talc quality for industrial uses by flotation process and leaching. *International Journal of Mineral Processing*, *83*(3–4), 132–145. https://doi.org/10.1016/j.minpro.2007.07.002

Ahmed, M. M., Ibrahim, G. A., & Hassan, M. M. A. 2011. Beneficiation of Talc Ore. *Earth and Environmental Sciences*. https://doi.org/10.5772/27935

Bazar, J. A., Rahimi, M., Fathinia, S., Jafari, M., Chipakwe, V., & Chehreh Chelgani, S. 2021. Talc flotation—an overview. *Minerals*, *11*(7), 8–13. https://doi.org/10.3390/min11070662

Beattie, D. A., Huynh, L., Kaggwa, G. B., & Ralston, J. 2006. Influence of adsorbed polysaccharides and polyacrylamides on talc flotation. *International Journal of Mineral Processing*, *78*(4), 238–249. https://doi.org/10.1016/j.minpro.2005.11.001

Boujounoui, K., Abidi, A., Baçaoui, A., El Amari, K., & Yaacoubi, A. 2020. Optimization of chlorite and talc flotation using experimental design methodology: Case study of the MCG plant, Morocco. *Journal of the Southern African Institute of Mining and Metallurgy*, *120*(12), 693–700. https://doi.org/10.17159/2411-9717/1186/2020

Brezáni, I., Zeleňák, F., & Zeleňák, M. 2013. Collectorless flotation of talc-magnesite ore with respect to particle size. *Acta Montanistica Slovaca*, *18*(3), 198–205.

Bulatovic, S. M. 2007. Handbook of Flotation Reagents: Chemistry, Theory and Practice. In *Handbook of Flotation Reagents: Chemistry, Theory and Practice* (Vol. 1, Issue April).

Camalan, M., & Hoşten, Ç. 2015. Ball-mill grinding kinetics of cement clinker comminuted in the high-pressure roll mill. *Mineral Processing and Extractive Metallurgy Review*, *36*(5), 310–316. https://doi.org/10.1080/08827508.2015.1004402

Chen, Z., Gu, G., Li, S., Song, S., & Wang, C. 2018. Influence of particle size in talc suppression by a galactomannan depressant. *Minerals*, *8*(4), 9–15. https://doi.org/10.3390/min8040122

Duroudier, J.-P. 2017. Size Reduction of Divided Solids. In *Size Reduction of Divided Solids*. Elsevier Ltd.

Feng, D., & Aldrich, C. 2004. Effect of ultrasonication on the flotation of talc. *Industrial and Engineering Chemistry Research*, *43*(15), 4422–4427. https://doi.org/10.1021/ie034057g

Gaudin, A. M., Schuhmann, R., & Schlechten, A. W. 1942. Flotation kinetics. II: The effect of size on the behavior of galena particles. *Journal of Physical Chemistry*, *46*(8), 902–910. https://doi.org/10.1021/j150422a013

Kuan, S. H., & Finch, J. A. 2010. Impact of talc on pulp and froth properties in F150 and 1-pentanol frother systems. *Minerals Engineering*, *23*(11–13), 1003–1009. https://doi.org/10.1016/j.mineng.2010.04.010

Kursun, H., & Ates, A. 2010. Adsorption and column flotation studies on talc using anionic and cationic collectors. *Korean Journal of Chemical Engineering*, *27*(6), 1922–1927. https://doi.org/10.1007/s11814-010-0298-0

Kursun, H., & Ulusoy, U. 2006. Influence of shape characteristics of talc mineral on the column flotation behavior. *International Journal of Mineral Processing*, *78*(4), 262–268. https://doi.org/10.1016/j.minpro.2005.11.003

Leterme, P., Gayot, A., Finet, G., Bizi, M., & Flament, M. P. 2005. Influence of the morphogranulometry and hydrophobicity of talc on its antisticking power in the production of tablets. *International Journal of Pharmaceutics*, *289*(1–2), 109–115. https://doi.org/10.1016/j.ijpharm.2004.10.023

Li, C., & Gao, Z. 2017. Effect of grinding media on the surface property and flotation behavior of scheelite particles. *Powder Technology*, *322*, 386–392. https://doi.org/10.1016/j.powtec.2017.08.066

Li, Z., Fu, Y., Yang, C., Yu, W., Liu, L., Qu, J., & Zhao, W. 2018. Mineral liberation analysis on coal components separated using typical comminution methods. *Minerals Engineering*, *126*(December 2017), 74–81. https://doi.org/10.1016/j.mineng.2018.06.028

Liu, M., Yu, H., Zhang, H., Wang, K., Tan, X., & Liu, Q. 2022. Roles of the hydrophobic and hydrophilic groups of collectors in the flotation of different-sized mineral particles. *Colloids and Surfaces A: Physicochemical and Engineering Aspects*, *637*(November 2021), 128262. https://doi.org/10.1016/j.colsurfa.2022.128262

Rácz, Á., Dolgos, F., Halyag, N., Mucsi, G., & Bokányi, L. 2021. *Optimization of existing grinding circuit – Conversion of an existing Rod Mill for obtaining a Ball Mill*.

Runge, K. C., Tabosa, E., & Jankovic, A. 2013. Particle Size Distribution Effects that Should be Considered when Performing Flotation Geometallurgical Testing. *The Second AUSIMM International Geometallurgy Conference*, *October*, 335–344.

Schubert, H. 2008. On the optimization of hydrodynamics in fine particle flotation. *Minerals Engineering*, *21*(12–14), 930–936. https://doi.org/10.1016/j.mineng.2008.02.012

Shoji, K., & Austin, L. G. 1974. A model for batch rod milling. *Powder Technology*, *10*(1–2), 29–35. https://doi.org/10.1016/0032-5910(74)85028-X

Simba, K. P., & Moys, M. H. 2014. Effects of mixtures of grinding media of different shapes on milling kinetics. *Minerals Engineering*, *61*, 40–46. https://doi.org/10.1016/j.mineng.2014.03.006

Steenberg, E., & Harris, P. J. 1985. Surface-chemical and mineralogical properties relevant to the flotation of talc and other layer silicates. *Report of the Council for Mineral Technology (South Africa)*, *M209*.

Trahar, W. J. 1981. A rational interpretation of the role of particle size in flotation. *International Journal of Mineral Processing*, *8*(4), 289–327. https://doi.org/10.1016/0301-7516(81)90019-3

U.S. Geological Survey. 2023. Mineral Commodity Summaries 2023. In *USGS Publications* (Issue 703). https://pubs.usgs.gov/publication/mcs2023

Vinnett, L., Grammatikopoulos, T., El-menshawy, A. H., & Waters, K. E. 2022. Justifying size-by-size flotation rate distributions from size-by-association kinetic responses. *Powder Technology*, *395*, 168–182. https://doi.org/10.1016/j.powtec.2021.09.042

Vizcarra, T. G., Wightman, E. M., Johnson, N. W., & Manlapig, E. V. 2011. The effect of breakage method on the shape properties of an iron-oxide hosted copper-gold ore. *Minerals Engineering*, *24*(13), 1454–1458. https://doi.org/10.1016/j.mineng.2011.07.007

Wang, D., & Liu, Q. 2021. Influence of aggregation/dispersion state of hydrophilic particles on their entrainment in fine mineral particle flotation. *Minerals Engineering*, *166*(March), 106835. https://doi.org/10.1016/j.mineng.2021.106835

Wonyen, D. G., Kromah, V., Gibson, B., Nah, S., & Chelgani, S. C. 2018. A review of flotation separation of Mg carbonates (Dolomite and magnesite). *Minerals*, *8*(8), 16–18. https://doi.org/10.3390/min8080354

Yehia, A., & Al-Wakeel, M. I. 2000. Talc separation from talc-carbonate ore to be suitable for different industrial applications. *Minerals Engineering*, *13*(1), 111–116. https://doi.org/10.1016/S0892-6875(99)00154-5

Yekeler, M., & Sönmez, I. 1997. Effect of the hydrophobic fraction and particle size in the collectorless column flotation kinetics. *Colloids and Surfaces A: Physicochemical and Engineering Aspects*, *121*(1), 9–13. https://doi.org/10.1016/S0927-7757(96)03942-8

Effect Of Deviation In The Unbalance Excitation On The Performance Of An Inclined Screen

Zehra Bayın [1]*, Engin Can Çelik [1]*, Vilaiat Alekperov [1], Ekrem Savaş [1], Tuncay Karaçay [2]

[1]MEKA Global Makine İmalat Sanayi ve Ticaret A.Ş.

[2]Gazi University

*Corresponding author: zbayin@mekaglobal.com (Zehra Bayın)

Abstract:

Inclined screens are widely used in mineral processing operations such as aggregate, mining and even food industries. Basic mechanical and working principles are thoroughly studied in the literature. Inclined screens are designed to produce circular vibrating motion with single unbalance excitation ideally placed at center of gravity. However, due to design and manufacturing constraints it is not easy to fully apply this concept in practice. In this study, the inclined screen is modeled as six degrees of freedom, and the deviation of unbalance excitation position with respect to the center of gravity is simulated. The distortion of the orbit profiles at the center of gravity, discharge, and feed positions are analyzed and discussed in terms of screening performance, which is defined as the capacity in terms of tons/hour, and simulations are performed using Rocky DEM software.

Keywords: *Inclined screen, vibration, screening performance, Rocky DEM, mathematical modelling*

1. Introduction

Vibrating screens are important machines used for grading by grain size (Zhao at al., 2011). The mechanisms that generate vibration in the machine are designed to provide linear, circular or elliptical motion (Krot et al., 2019). Inclined screens are the most preferred screen type in the mineral processing and aggregate industries. Inclined screens allow the material to move on the screen deck with circular motion. In order to provide circular motion, the drive system with unbalanced loads must be placed in such a way that it passes through the center of gravity of the machine. However, when placing the drive system during the manufacturing and assembly stages, deviations from the center of gravity may occur. In addition, in cases such as maintenance and replacement of spare parts, it may cause the assembly to fail to be exactly at the center of gravity. Mounting with a deviation from the center of gravity distorts the circular motion on the screen. This situation can lead to changes in the performance of the machine.

Dynamic models have been created to understand the motion of vibrating screen (Ramatsetse et al., 2017; Moncada and Rodriguez, 2018; Liu et al., 2019). There are many studies on the dynamic modeling of screens (Snyman at al., 1992; Peng at al., 2014; Lyan at al., 2021). The dynamic models created allows to understand the distortions that occur in the motion of screen to be clearly seen (Moncada and Rodriguez, 2018; Liu et al., 2019; Krot et al., 2019). Although a large part of these studies are aimed at examining the screen motion and creating the desired motion profile, a handful of studies on the distortion of the motion caused by the assembly misalignments in the screen drive system. Vibrating screen motion characteristics may deteriorate over time due to errors during manufacturing, environmental conditions or fatigue due to long working hours ((Ramatsetse et al., 2017). These distortions in the screen motion also affect the screen performance. Linhares et al. (2024) experimentally investigated the effects of manufacturing defects in the drive shafts on the screening trajectory of a top-driven vibrating screen with a double vibration motor. When the shaft part was examined, it was determined that there was a 1-degree manufacturing error between the drive slots between the two ends of the shaft, which caused synchronization failure in the screen (Linhares et al., 2024). Similarly, Jiang et al. investigated the effect of process parameters (screen inclination angle, feed ratio, drive coefficient, drive clearance) on screening performance in vibrating screen used in top-drive coal screening with 2 vibration motors. As a conclusion in the study, it was observed that the screen inclination angle was the

most effective parameter, and the maximum efficiency was achieved at 15 degrees with the increase of the inclination angle (Jiang et al., 2017).

In the study conducted by Nguyen et al., (2019), firstly the vibration motion of the screen and the random motion of the particles on the screen surface were mathematically modeled in a single point driven vibrating screen. Then, the effect of the position change of the vibration motor at a total of 4 different points on the front and back of the screen on the vibration amplitude was simulated in Matlab software. When the simulation results were examined, it was observed that the 0.3 m position change of the vibration motor in the +x direction (towards the front of the screen) maximized the vibration amplitude of the points on the front of the screen, while the 0.3m position change in the -x direction (towards the back of the screen) maximized the vibration amplitude of the points at the back (Nguyen et al., (2019).

Rocky DEM is used to evaluate the performance of screens whose dynamic behaviors are examined by mathematical modeling. It is a suitable method for the screening process because it can reflect dynamic processes such as particle separation, transition and transport by providing the necessary parameters (Harzanagh et al., 2018). The discrete element method enables the examination of particle behavior, and the performance of the system may be evaluated based on different performance definitions. Zhao Lala et al. (2017) investigated the effects of particle motion and various vibration parameters on the screen performance for a circular vibrating screen by DEM simulation. With this study, it was concluded that the average velocity of particles with complex movements on the screen increases along the screen deck, and that the very small vibration amplitude or inclination angle causes particle accumulation on the screen deck, but if it is too large, the screening efficiency decreases Zhao et al. (2017) investigated the effects of vibration parameters on screening using the Taguchi orthogonal experiment method for a circular vibrating screen using DEM simulation. The changes in the screening efficiency of particles with different particle sizes and shapes at average velocity and the combined effect of amplitude, frequency, and inclination angle on the screening efficiency were investigated (Zhao et al., 2017).

The dynamic behavior of screens can deteriorate over time for different reasons. There are quite a few studies on the performance evaluation of the screens affected by the unbalance mass position variation in the driving system. In this study, the dynamic behavior change of vibrating screens caused by deviation in the unbalance excitation is investigated. The screen is modeled as 6 degrees of freedom including translational and rotational freedoms and model is simulated for 3 different positions of the unbalance weight. In order to analyze screening performance, DEM simulations are performed in the Rocky DEM software using the motion results of the mathematical model. The results show that the small change in the position of the unbalance does not affect the performance of the screen severely.

2. Vibrating Screen Modelling

Vibrating inclined screens consist of the screen body fixed to the screen frame, screen decks, drive system, spring consoles and springs as a general structure. Large-scale vibrating screens are always inclined downwards at a certain angle to improve material particle flow from inlet to outlet with less energy consumption. The motion expected to occur in inclined screen is circular vibration motion. The eccentric weights on the single drive system placed in the screen body ensure that the screen motion is circular (Krot et al., 2019). In different industries such as mining, aggregate, food, etc., different inclined screens are used in terms of their scale and number of screen decks. In this study, in Figure 1, a three-decks MS2060-3 model screen with a scale of 2000x6000mm, manufactured and sold by Meka company, which is widely preferred in the mining sector, was used. The schematic image of the dynamic model of the vibrating screen in the standard design state is shown in Figure 2. Fundamental screen parameters and geometric quantities used in modeling have been manipulated to avoid directly affecting the results in this study because they are commercially preserving information. This screen is single-driven, three-decks, consists of body, spring consoles, feeding chute and discharge chute parts, and is designed to give circular vibration motion. The inclination angle of the screen in nominal operating conditions is 18°.



Fig. 1. General view of MS2060/3 inclined vibrating screen

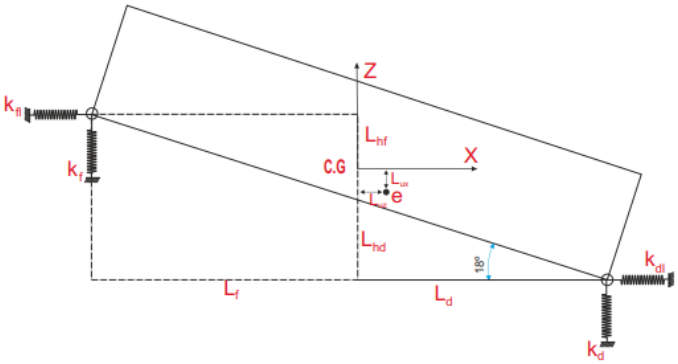


Fig. 2. Dynamic model schematic view of MS2060/3 inclined vibrating screen

2.1. Mathematical Modelling

In this study, an inclined vibrating screen is modeled as six degrees of freedom. The mass and moments of inertia are considered a rigid rectangle, and the spring support points are placed planar. The parameters used in the standard screen model given in Figure 2 are as follows; $l_d = 1700\ mm,\ l_f = 1800\ mm,\ l = 3500\ mm,\ M = 7500\ kg,\ m * e = 28500\ \text{kg.mm},\ k_d = k_f = 4 * 180\ \frac{\text{N}}{\text{mm}},\ k_{dl} = k_{fl} = 4 * 68\ \frac{N}{mm},\ l_{hf} = 82\ \text{mm},\ l_{uz} = 220\ mm,\ l_{ux} = 30\ mm,\ l_{hd} = 800\ mm,\ J = 2{,}7e + 10\ kg.mm^2.$ The parameters $l_{uz}\ and\ l_{ux}$ are changed according to simulation scenario. The basic calculation for the helical springs in the literature was used for the analysis of the spring stiffness of the screen (Bargetti and Villa, 2014). To calculate the lateral stiffness of this type of spring, the formulas were used. The equations of motion of the modeled screen are given below, and these differential equations are solved with the MATLAB software.

$$M\ddot{x} + x\left(k_{drx} + k_{dlx} + k_{flx} + k_{frx}\right) + \gamma\left(l_r k_{drx} - l_l k_{dlx} - l_l k_{flx} + l_r k_{frx}\right) = mr * er * \omega^2 * cos(wt) + ml * el * w^2 * cos(wt) \quad (1)$$

$$M\ddot{z} + z\left(k_{drz} + k_{dlz} + k_{flz} + k_{frz}\right) + \theta\left(l_d k_{drz} - l_d k_{dlz} - l_f k_{flz} + l_f k_{frz}\right) + \alpha\left(l_r k_{drz} + l_l k_{dlz} - l_l k_{flz} - l_r k_{frz}\right) = m * e * w^2 * sin(wt) + m * e * w^2 * sin(wt) \quad (2)$$

$$J_{yy}\ddot{\theta} + \left(k_{drz}\frac{l_{drz}^2}{cos\beta} + k_{dlz}\frac{l_{dlz}^2}{cos\beta} + k_{frz}\frac{l_{frz}^2}{cos\beta} + k_{flz}\frac{l_{flz}^2}{cos\beta}\right)\theta + \left(k_{drz}l_{drz} + k_{dlz}l_{dlz} - k_{flz}l_{flz} - k_{frz}l_{frz}\right)z + (k * lr + k * ll)\alpha = -m * e * w^2 * l_{uz} * cos(wt) + m * e * w^2 * l_{ux} * sin(wt) * 2 \quad (3)$$

$$M\ddot{y} + y\left(k_{dry} + k_{dly} + k_{fly} + k_{fry}\right) + \gamma\left(l_d k_{dry} + l_d k_{dly} - l_f k_{fly} - l_f k_{fry}\right) = 0.00N \quad (4)$$

$$J_{xx}\ddot{\alpha} + \left(k_{drz}\,l_{tdrz}^2 + k_{dlz}\,l_{tdlz}^2 + k_{frz}\,l_{tfrz}^2 + k_{flz}\,l_{tflz}^2\right)\alpha + \left(k_{drz}l_{tdrz} - k_{dlz}l_{tdlz} - k_{flz}l_{tflz} + k_{frz}l_{tfrz}\right)z + (kdr * lr * ld - kdl * ll * ld - kfr * lr * lf + kfl * ll * lf)\theta = m * e * w^2 * l_{re} * sin(wt) - m * e * w^2 * l_{le} * sin(wt) \quad (5)$$

$$J_{zz}\ddot{\gamma} + \left(k_{dry}\frac{l_{dry}^2}{cos\beta} + k_{dlz}\frac{l_{dly}^2}{cos\beta} + k_{fry}\frac{l_{fry}^2}{cos\beta} + k_{flz}\frac{l_{fly}^2}{cos\beta}\right)\gamma + \left(k_{dry}l_{dry} + k_{dly}l_{dly} - k_{fly}l_{fly} - k_{fry}l_{fry}\right)y + (klr - kll)x = m * e * w^2 * l_{re} * cos(wt) - m * e * w^2 * l_{le} * cos(wt) \quad (6)$$

2.2. Rocky-DEM Simulations

The discrete elements method (DEM) is a method used to analyze the screening process. The main benefit of using DEM is that this method allows all interactions between particles in the material flow and between particles and surfaces can be monitored (Davoodi et al., 2019). The solid model is drawn

in a simplified way, without fasteners, etc. This simplified body used for DEM simulations. The parameters and particle sizes used in DEM modeling are given in Table 1.

For DEM simulation, static friction, dynamic friction, coefficient of restitution, rolling friction coefficient, etc. parameters have been chosen around typical values according to the simulated particle material, considering the studies in the literature (Jahani et al., 2015; Yin et al., 2016; Zhao et al., 2017; Moncada and Rodriguez, 2018; Davoodi et al., 2019; Chen et al., 2019;). Preliminary tests were carried out for the simulation studies, and it was determined that the simulation times were too long if the small particles in the gradation were defined as particles of complex shape. For this reason, spherical shape was defined for particles smaller than 15mm, and polyhedron shape was defined for particles larger than 15mm in such a way as not to affect the bulk behavior and screening performance.

Particles of different sizes are fed to the screening surface simultaneously and whole material are fed to the screen within a specified time frame. Particles reaching the screen wire will either be screening or moving along the screen wire to the discharge chute.

Three simulation cases given in Table 2 are chosen to investigate the effect of vibration change to the screening performance. A total of four cubic space were placed under the screen in the simulation to measure the amount of screened material: four equal cubes at the feed and discharge of the screens and one at the discharge. Thus, it is also possible to analyze the amount of screened material in different parts of the screen with the change of screening motion. The performance change is measured with respect to the healthy/perfect condition of the screen.

Table 7. Modeling and simulation parameters of Rocky-DEM

Machine and Particle Parameters			
Screen Aperture	5x5 mm, 12x12 mm, 25x25 mm		
Amplitude (mm)	3,86		
Particles Shapes	15 mm < sphere, 15 mm > polyhedron		
Particles numbers	2566806		
Material Properties	**Poisson's Ratio**	**Young's Modulus (Gpa)**	**Density (kg/m³)**
Particle	0.3	78	2800
Screen	0.3	200	7850
Collision Properties	**Particle- Particle**	**Particle-Deck**	
Static Friction Coefficient	0.7	0.45	
Dynamic Friction Coefficient	0.7	0.3	
Rolling Resistance	0.01	0.01	
Restitution Coefficient	0.3	0.3	
Tangential Stiffness Ratio	1	1	

Particles of different sizes are fed to the screening surface simultaneously and whole material are fed to the screen within a specified time frame. Particles reaching the screen wire will either be screening or moving along the screen wire to the discharge chute.

Three simulation cases given in Table 2 are chosen to investigate the effect of vibration change to the screening performance. A total of four cubic space were placed under the screen in the simulation to measure the amount of screened material: four equal cubes at the feed and discharge of the screens and one at the discharge. Thus, it is also possible to analyze the amount of screened material in different parts of the screen with the change of screening motion. The performance change is measured with respect to the healthy/perfect condition of the screen.

Table 8. Simulation scenarios of Rocky-DEM

	1. Case	2. Case	3. Case
Distance change of x-axis standard position (l_{ux})	Healthy	300 mm	-400 mm
Distance change of z-axis standard position l_{uz}	Healthy	300 mm	-400 mm

3. Results and Conclusions

DEM analysis is performed for all three cases. Screening performance is defined based on the amount of material overflow at the deck exits, cube is placed in the application, as shown in Fig.3.

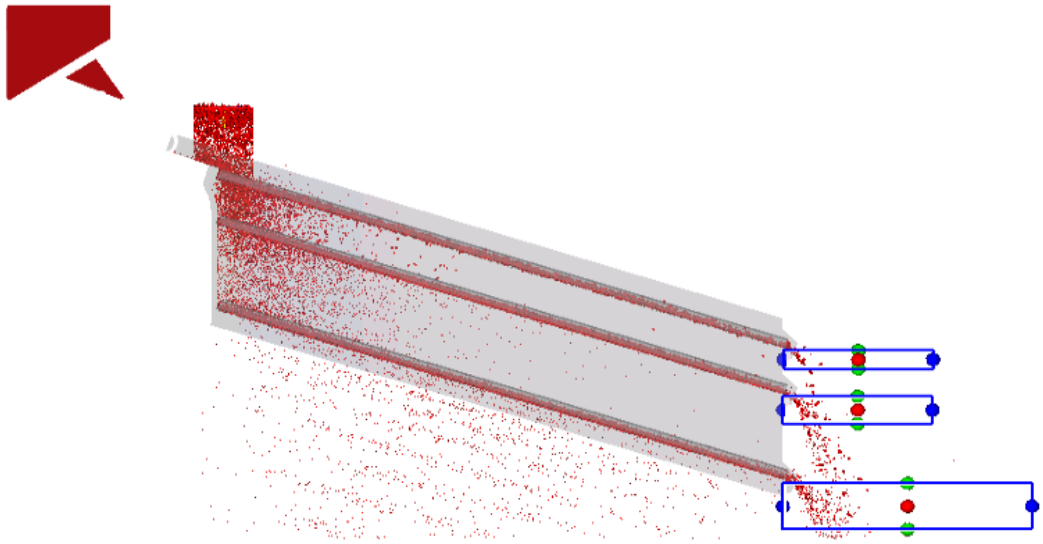


Fig. 3. The Rocky-DEM Model and cubes placement for the measurements

The overflow material of each deck was evaluated individually, and the results are given in below graphs.

In Fig. 4, for the top deck, there is no significant difference between case-1 and case-2. In case-3, approximately 5% of material was not screened.

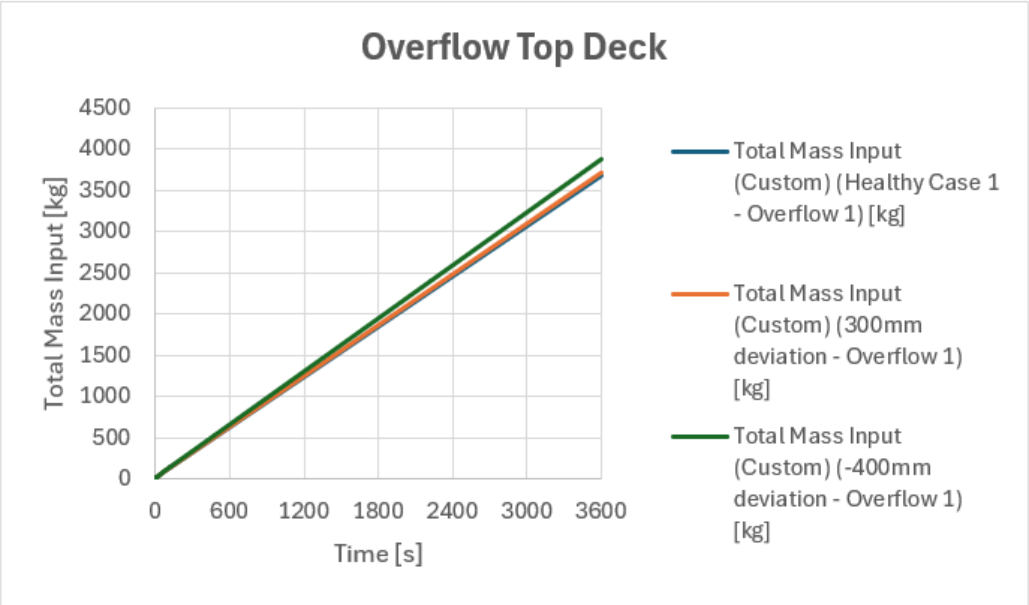


Fig. 4. Graph of top deck overflow.

In Fig. 5, for the second deck, there is no significant difference between cases-1 and case-2. In case-3, approximately 4% of material was not screened.

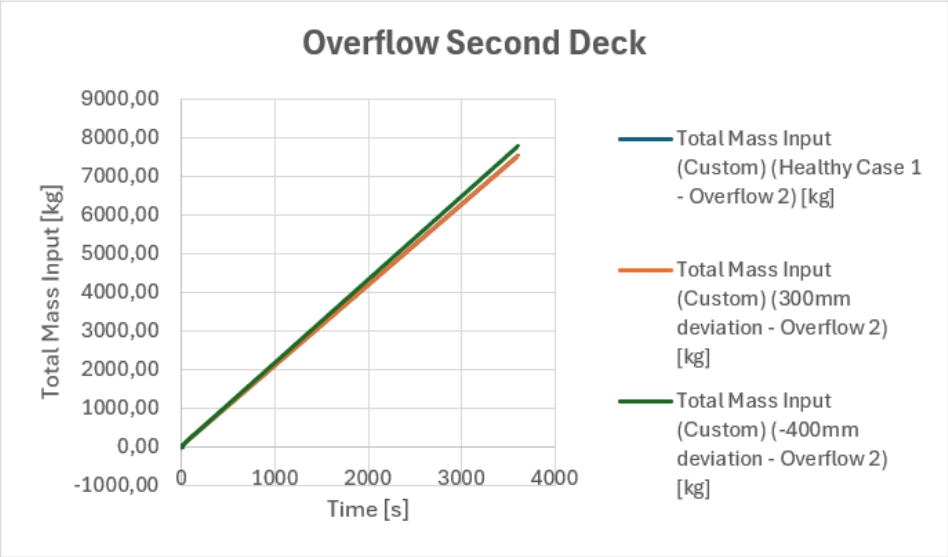


Fig. 5. Graph of second deck overflow

In Fig. 6, there is no significant difference between case-1 and case-3 at bottom deck. In case-2 , material approximately 2% of material was not screened.

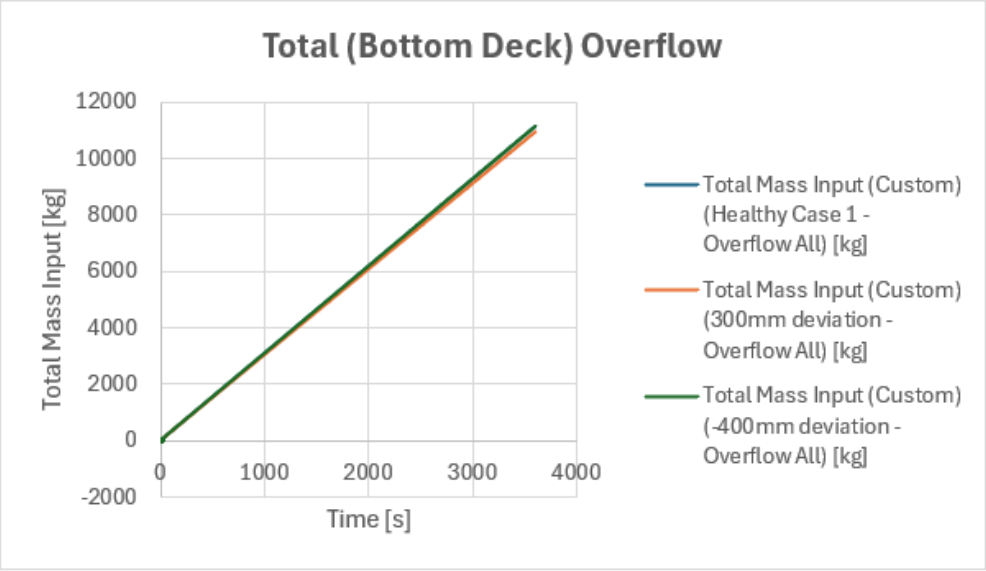


Fig. 6. Graph of bottom deck overflow

A dynamic model of an inclined screen was introduced with six degrees of freedom, and results were implemented in Rocky DEM software for particle simulation. Effects of unbalance excitation position on screening performance were obtained in terms of overflow mass for each deck. The results show that the small change in the position of the unbalance does not affect the performance of the screen severely. These outcomes result from dynamic characteristics changes of inclined screen due to described unbalaced excitation position.

Acknowledgments

We would like to express our gratitude to the Meka Global Makine İmalat Sanayi ve Ticaret A.Ş. family for their contributions and support to our work.

References

Baragetti, S., & Villa, F. (2014). A dynamic optimization theoretical method for heavy loaded vibrating screens. Nonlinear dynamics, 78, 609-627.

Chen, B., Yan, J., Mo, W., Xu, C., Zhang, L., & Tamma, K.K. (2019). DEM simulation and experimental study on the screening process of elliptical vibration mechanical systems. Journal of Vibroengineering, 21(8), 2025-2038.

Davoodi, A., Asbjörnsson, G., Hulthén, E., & Evertsson, M. (2019). Application of the discrete element method to study the effects of stream characteristics on screening performance. Minerals, 9(12), 788.

Harzanagh, A. A., Orhan, E. C., & Ergun, S. L. (2018). Discrete element modelling of vibrating screens. Minerals Engineering, 121, 107-121.

Jahani, M., Farzanegan, A., & Noaparast, M. (2015). Investigation of screening performance of banana screens using LIGGGHTS DEM solver. Powder Technology, 283, 32-47.

Jiang, H., Zhao, Y., Duan, C., Zhang, C., Diao, H., Wang, Z., & Fan, X. (2017). Properties of technological factors on screening performance of coal in an equal-thickness screen with variable amplitude. Fuel, 188, 511-521.

Krot, P., & Zimroz, R. (2019, November). Methods of springs failures diagnostics in ore processing vibrating screens. In IOP Conference Series: Earth and Environmental Science (Vol. 362, No. 1, p. 012147). IOP Publishing.

Linhares, T. B., & Vimieiro, C. B. S. (2024). Evaluation of the movement performance of a vibrating screen due to machining errors on the shaft. Engineering Failure Analysis, 161, 108260.

Liu, Y., Suo, S., Meng, G., Shang, D., Bai, L., & Shi, J. (2019). A theoretical rigid body model of vibrating screen for spring failure diagnosis. Mathematics, 7(3), 246.

Lyan, I., Panovko, G., & Shokhin, A. (2021). Creation and verification of spatial mathematical model of vibrating machine with two self-synchronizing unbalanced exciters. Journal of Vibroengineering, 23(7), 1524-1534.

Moncada M, M., & Rodríguez, C. G. (2018). Dynamic modeling of a vibrating screen considering the ore inertia and force of the ore over the screen calculated with discrete element method. Shock and Vibration, 2018(1), 1714738.

Nguyen, V. X., Nguyen, K. L., & Dinh, G. N. (2019, November). Study of the dynamics and analysis of the effect of the position of the vibration motor to the oscillation of vibrating screen. In Journal of Physics: Conference Series (Vol. 1384, No. 1, p. 012035). IOP Publishing.

Peng, L. P., Liu, C. S., Li, J., & Wang, H. (2014). Static deformation-based fault diagnosis for damping spring of large vibrating screen. Journal of Central South University, 21(4), 1313-1321.

Ramatsetse, B., Mpofu, K., & Makinde, O. (2017). Failure and sensitivity analysis of a reconfigurable vibrating screen using finite element analysis. Case studies in engineering failure analysis, 9, 40-51.

Snyman, J. A., & Vermeulen, P. J. (1992). The mathematical modelling of the motion of a horizontal vibrating screen supported by ROSTA oscillating mountings. R&D Journal, 8, 25-33.

Zhao, L., Zhao, Y., Bao, C., Hou, Q., & Yu, A. (2017). Optimisation of a circularly vibrating screen based on DEM simulation and Taguchi orthogonal experimental design. Powder Technology, 310, 307-317.

Zhao, L., Zhao, Y., Liu, C., Li, J., & Dong, H. (2011). Simulation of the screening process on a circularly vibrating screen using 3D-DEM. Mining Science and Technology (China), 21(5), 677-680.

The Beneficiation Studies of Barite-Florite from Eskisehir-Beylikova Ore by Gravity Separation Methods

Akar H.[1], Gunaydın, N. [1], Cugu S.[1], Sahin, Y.[1], Savran C*[1]., Gurkan, O.M.[1], Basturkcu, E.[1], Yuce, A.E.

[1] Department of Mineral Processing Engineering, Faculty of Mine, Istanbul Technical University, 34467 Istanbul, Turkiye.

*Corresponding author: savranc15@itu.edu.tr (Ceyda Şavran)

Abstract:

With increase in the production potential in the world, the demand for industrial raw materials is rising day by day. Fluorite, one of these minerals, produced worldwide and especially used in iron and steel metallurgy, due to its slag-making feature. Barite, another strategic industrial mineral also has several usage areas but mostly utilized in drilling mud. Flotation method is generally preferred for enrichment of barite and fluorite depending on particle size. However, gravity beneficiation is alternative, economical, and environmentally-friendly method even for lower particle sizes.

Eskisehir-Beylikova deposit is one of the potential sources for production of Barite and Fluorite in addition to REE in Türkiye. In the presented study, after classification of representative sample, Mozley table and Falcon were applied to evaluate the beneficiation potential of barite and fluorite with alternative gravity separation techniques. The effects of different particle fractions and alternative devices on the content and recovery of Barite-Flourite were investigated. At -150+106 µm and -106+38 µm, with the application of mozley table, barite content enhanced to 69,9% and 77,9%, respectively. On the other side, fluorite content in the light products were analyzed as 52% and 53%. Falcon separator was not successful comparing to mozley table. The content and recoveries were distributed almost equal for heavy and light products. In order to enhance the recovery and content, the effect of pulp ratio and G force can be investigated for further studies.

Keywords: *Barite, Fluorite, Falcon, Mozley table, Gravity separator*

1. Introduction

Barite is an important industrial raw material because being high density, is chemically inert, less corrosive, low solubility in water and acids, and no magnetic properties. Approximately 85% of barite is used in the petroleum industry, approximately 10% in the chemical industry and 5% in the filler industry. Although there are many barite ore deposits in our country, the deposits with significant reserves found in four regions: Alanya-Gazipaşa, Konya-Isparta, Muş and Kahramanmaraş. Additionally, there are barite formations that can be considered important in Giresun, Kocaeli and Kütahya regions. (MTA, 2021). According to the research, it has been determined that all barite resources in the world are approximately 2 million tons, but the detected barite resources are approximately 740 million tons. In the world; China, India and Morocco are among the leading countries in production of barite (USGS, 2023).

Fluorite (CaF_2) is another industrial mineral defined as strategic raw materials. While fluorite deposited in various geological environments, it is found in many regions of the world; China, Mexico, South Africa, Mongolia and Spain play a critical role in terms of reserves. The most important area of use of fluorite, to be used commercially in the acid industry, chemical industry or metallurgical industry. Due to its slag-forming feature, it has high utilization capacity in iron and steel metallurgy. Apart from these, fluorite is also used in the food industry, cement, glass, ceramics and optical industries. (MTA 2019; USGS 2023). In order to beneficiate and obtain salable concentrate quality of barite and fluorite, flotation is the preferred method because of the liberation size. However, with the development of technology, there are studies on the possibilities of enrichment of Barite-Fluorite by using new generation gravity

separators in fine size fractions by taking advantage of the density difference between them (Yıldız, 2016; Jordens et al., 2013; Yang et al.., 2015; Abaka-Wood et al., 2016).

One of the study performing with MGS (multi-gravity separator), the effects of different operating parameters such as the solids ratio, rotational drum speed, washing water flow rate and inclination angle were examined in detail to concentrate barite. The best results were achieved with a solids-in-pulp ratio of 25%, a drum speed of 190 rpm, an inclination angle of 5˚ and a washing water flow rate of 5 L/min. As a result of the experiments, barite concentrate with a grade of 92.55% $BaSO_4$ and a total barite recovery of 78.41% was obtained from barite residues containing 38.40% $BaSO_4$. (Deniz, V., 2020)

Bhattacharyya and Singh aimed to obtain a product containing >90% barium sulphate that can be reused from the ash of the plant producing Barium Carbonate (BaCO3). According to chemical and particle size analysis, it was decided to reduce particle size to 74 µm. In enrichment experiments using MGS, the solid ratio of pulp, slope, washing water ratio and rotation speed were examined. According to the optimum data obtained as a result of the experiments, it was possible to obtain $BaSO_4$ with approximately 53% efficiency and 90% $BaSO_4$ content (Bhattacharyya, Singh, 2011).

In this study; to investigate obtaining the pre-concentration of barite and fluorite from Eskisehir-Beylikova ore using gravity separation, Falcon concentrator and Mozley table were preferred and the effect of particle size with constant parameters was observed.

2. Material & Method

The sample was taken from Eskisehir-Beylikova Barite-Flourite-REE-Th deposit which is shown in Figure 1. The sample used in the experiments were prepared based on study performed by Basturkcu et al. (2022). After crushing, mechanical attrition and classification; -150+38 µm fraction was separated for experiments performed in this study.



Figure 1. Sample from Eskisehir-Beylikova deposit

The fractional analysis for Barite and Fluorite were presented in Table 1.

Table 1. The fractional analysis of Barite and Fluorite

Fraction	**Amount**	**$BaSO_4$**		**CaF_2**	
µm	**%**	**Content,%**	**Distribution, %**	**Content,%**	**Distribution, %**
-150+106	18,9	31,9	17,0	40,76	20,3
-106+75	26,4	26,76	20,0	41,45	28,7
-75+53	32,5	39,34	36,2	36,97	31,6
-53+38	22,2	42,79	26,8	33,22	19,4
Total	100,0	**35,37**	100	**38,03**	100,0

3. Results

The results of Falcon and Mozley table were presented based on -150+106 µm and -106+38 µm fraction.

3.1. The Results of Falcon

Sample classified between -150+106 µm were fed to falcon separator to investigate the barite-fluorite separation. Solid ratio in pulp was 25%; washing water was set at an average of 2 L/min. The force was arranged as 150G in the first stage of beneficiation, and the force was set to 300G in the 2nd and 3rd stages of the heavy product. According to analysis of sample obtained from experiments, the results were demonstrated in the metallurgical table in Table 2.

As a result of the enrichment experiments with Falcon in the size range of 150+106 µm, 4 products were obtained: Light 1, Light 2, and Heavy. When the test results were observed, a heavy product with 49.83% $BaSO_4$ content can be achived with 24.9% efficiency, while the light 2 product contained 41.04% CaF_2 content and 49.9% efficiency.

Table 2. The metallurgical table of Falcon experiments -150+106 µm

Products	Amount	$BaSO_4$, %		CaF_2, %	
	%	Content	Recovery	Content	Recovery
Heavy	15,1	49,83	24,9	33,33	11,9
Light 2	51,8	29,49	50,5	41,04	49,9
Light 1	33,1	22,58	24,6	49,21	38,2
Total	100,0	30,27	100,0	42,58	100,0

The sample in the size range -106+38 µm was fed to the Falcon separator. Similar to experiments performed with -150+38 µm size fraction, solid ratio in pulp was 25, the washing water was adjusted to an average of 2 L/min. While the force was arranged as 150G in the first feeding, the force was set as 300G in the 2nd and 3rd feeding of the heavy product.

Regarding the result of falcon experiments with the size fraction of -106+38 µm, Light 1, Light 2, and Heavy products were obtained. The results given in the Table demonstrated that heavy product included 39.79% barite and in the light product 39.37% fluorite was obtained which showed that there was no beneficiation in this fraction.

Table 3. The metallurgical table of Falcon experiments -106+38 µm

Products	Amount	$BaSO_4$, %		CaF_2, %	
	%	Content	Recovery	Content	Recovery
Heavy	14,6	39,79	16,6	37,31	14,0
Light 2	1,4	40,15	1,6	31,23	1,1
Light 1	84,0	34,05	81,8	39,37	84,9
Total	100	34,97	100	38,96	100

3.2. The Results of Mozley Table

The sample in the -150+106 µm size range was fed to the Mozley table, which was in an almost horizontal position. At the end of feeding, light and heavy product were separated. Heavy product was fed to cleaning stage with 6˚ inclination. The results of experiments were summarized in Table 4.

According to the test results performed at this size, the heavy product obtained with 69.93% $BaSO_4$ content with 31.5% recovery. The CaF_2 content of this product was 2.60%. In the same experiment, the CaF_2 content in the light product was 52.69% and the BaSO4 content was 22.51%.

Table 4. The metallurgical table of Mozley table experiments, -106+38 µm

Products	Amount	$BaSO_4$, %		CaF_2, %	
	%	Content	Recovery	Content	Recovery
Heavy	14,1	69,93	31,5	2,60	0,9
Middling	18,2	34,06	19,8	20,11	9,2
Light	67,7	22,51	48,7	52,69	89,9
Total	100,0	31,3	100,0	39,69	100,0

The sample classified between -106+38 µm was fed to mozley table and the parameters were same as applied in -150+106 µm size. In the experiment conducted with the Mozley Table in the -106+38 µm size range, three products were obtained: light, middling and heavy. While barite was obtained with 77.93% content and 44.2% recovery in the heavy product; and Fluoride content was 3.66%. In the light fraction, the fluoride content was 53.48% and the efficiency was 86.4%. It was observed that the barite content of this product was 15.15%.

Table 5. The metallurgical table of Mozley table experiments, -106+38 µm

Products	Amount	$BaSO_4$, %		CaF_2, %	
	%	Content	Recovery	Content	Recovery
Heavy	21,0	77,93	44,2	3,66	2,1
Middling	19,8	59,06	31,6	21,31	11,5
Light	59,2	15,15	24,2	53,48	86,4
Total	100,0	36,99	100,0	36,7	100,0

4. Conclusion & Discussion

In this study, the alternative methods were investigated to flotation for obtaining barite and fluorite concentrate from Eskisehir-Beylikova ore. The results obtained from experiments were summarized below.

The sample was classified as -150+106 µm and -106+38 µm after crushing, mechanical attrition, grinding and classification.

Falcon concentrator was used to enhance barite and fluorite for the classified products. Regarding the results; barite content was reached to almost 50%. Fluorite content was also obtained as 49% in the

fraction of -150+106 µm. However; in the fraction of -106+38 µm, there was not observed significant enrichment.

On the other hand, the experiments performed for the same groups had more favorable results with Mozley table comparing to Falcon concentrator. In the -150+106 µm size range; barite content was achieved with almost 70%. On the light fraction, CaF_2 content was 52.69%. Moreover; in the –106+38 µm size fraction, barite was reached to 78% and CaF_2 was obtained with 54% content.

Briefly; the pre-experiments which investigated the efficiency of alternative gravity methods for separation of barite and fluorite showed that there was a potential to obtain pre-concentrate before flotation. Especially the results of Mozley table was promising for obtaining barite as a pre-concentrate. In the further study, the details of parameters will be investigated to enhance the content and recovery of products.

References

Abaka-Wood, G., Addai-Mensah, J. ve Skinner, W. (2016). Review of flotation and physical separation of rare earth element minerals. 4th UMaT Biennial International Mining and Mineral Conference, pp. 55-62, Tarkwa.

Barit. (2022). MTA: https://www.mta.gov.tr/v3.0/bilgi-merkezi/barit

Bhattacharyya, P. &. (2011). Generation of Value Added Product by Beneficiation of Barite Waste.

Deniz, V. (2020). Prediction of barite recovery and grade by multiple linear regression (MLR) analysis in concentrating of barite tailings by using multi-gravity separator (MGS). Particulate Science and Technology.

Florit. (2022). MTA: https://www.mta.gov.tr/v3.0/bilgi-merkezi/florit

Jordens, A., Cheng, Y. P. ve Waters, K. E. (2013). A review of the beneficiation of rare earth element bearing minerals. Minerals Engineering, 4, 97-114.

Mıneral Commodıty Summarıes 2023.

Yang, X., Satur, J. V., Sanematsu, K., Laukkanen, J. ve Saastamoinen, T. (2015). Beneficiation studies of a complex REE ore. Minerals Engineering, 71, 55-64.

Yıldız, N. (2016). Nadir toprak elementleri. Ankara

Investigation of Operational Parameters for High Capacity – High Intensity Prototype Magnetic Separator (D:300 mm) to Produce A-Grade Egyptian Sand

B. E. Uğurlar [1]*, B. İbis [1], Ç. Ulusoy [1], H. Baştürkcü [2]

[1]MIKNATIS ARAŞTIRMA ve GELİŞTİRME A. Ş.

[2]Istanbul Technical University, Mineral Processing Engineering Department

*Corresponding author: isgelistirme@miknatis.net (Bekir Emre Uğurlar)

Abstract:

Silica sand imported from Egypt is used in glass industry in the particle size range of 100 - 600 µm. It is imported as Grade A with affordable costs. However, A-Plus import cost creates a significant difference compared to A Grade.

To achieve A-Plus quality, the composition should include at least 99.5% SiO_2 and Fe_2O_3 content should be lower than 100 ppm as recommended as with <200 ppm TiO_2 content. A-plus is used in the high permeability and ultra white and solar glass industry. Considering the investments in the solar glass sector, the enrichment of imported silica sand products has significant potential as added value for the glass industry.

The dry magnetic experiments were carried out with different feed capacities of 4 and 18 t/h, which is quite high as an industrial prototype. The device used in the experiments was designed by MIKNATIS ARGE which has the largest diameter of 300 mm made for the micronized mining industry in Türkiye.

The ongoing TÜBİTAK – 1507 R&D project carried out by MIKNATIS ARGE also makes tests for the 500 mm machine. This machine will be unique in the world with the highest capacity in the world. As part of the project, considering the capacity and quality expectations of the Diameter 500 machine, it is planned to make the settings by a semi-autonomous system instead of operator. It is aimed to reduce the demand of flotation process by replacing dry process. It has advantages in terms of CAPEX -OPEX, water consumption, and process applicability.

Keywords: Magnetic Separation, Dry Process, High Purity Silica Sand, Solar Glass

1. Introduction

Silica sand is a naturally occurring mineral widely used in various industrial and commercial applications worldwide. The history of silica sand dates back to ancient times. Initially used in glassmaking and construction, silica sand has evolved with technological and industrial advancements to find applications in numerous other fields. Today, it is extensively used in electronics, chemistry, ceramics, foundries, glass production, water filtration, and the construction industry. The applications of silica sand have continuously expanded due to its physical and chemical properties (Doremus, 2002; Richerson, 2006).

Silica sand is classified based on its purity level and iron content into different grades: A, B, and C. These grades represent the quality levels of silica sand:

- **A Grade Silica Sand**: This grade has the highest purity level with low iron content, making it suitable for use in industries requiring high purity, such as glass, electronics, and specialized applications.

- **B Grade Silica Sand**: This grade has medium iron content and is preferred in construction, ceramics, and chemical industries where purity is not as critical as in high-tech applications.

- **C Grade Silica Sand**: This grade has the highest iron content and is used in applications requiring less purity, such as in construction and concrete production.

Table 1. Grades of Silica Sand

Component, %	(Ultra)	(A)	(B)	(C)
SiO_2	99.75	99.6% min	99.0% min	99.0% min
Fe_2O_3	0.009	0.0135% max	0.025% max	0.035% max
Al_2O_3	0.046	0.15% max	0.4% max	0.5% max
TiO_2	0.012	0.016% max	0.035% max	0.035% max
CaO	0.007	0.021 max	0.03 max	0.03 max
Cr_2O_3	0.47 ppm	2.655 ppm	0.0005% max	0.0005% max
MgO	0.002	0.003% max	0.005% max	0.005% max
LOI	0.03	0.20%	0.25%	0.25%

Table 1 reflects the chemical composition of different grades of silica sand, from Ultra to Grade C, highlighting the variations in impurities and the purity level of SiO_2 across the grades.

This table highlights the variations in impurities and SiO_2 purity levels across different grades of silica sand.

Reynolds and Jones (2001) conducted a comprehensive study on the industrial uses of silica sand based on iron content. Their research highlighted the importance of low iron content silica sand for glass production, as iron can affect the color and purity of glass. Silica sand with moderate iron content is preferred in ceramics and chemical industries, where purity is less critical compared to glass production. High iron content silica sand is typically used in construction and concrete production, where color and purity are less important.

Table 2. Maximum Fe_2O_3 Content Limits for Different Glass Types

Glass Type	Max. Fe_2O_3 Content (ppm)
High-Tech Glass	50
Solar Glass	100
Tableware Glass	200
Glass Container	300
Flat Glass	500
Colored Glass	800

Türkiye is a significant consumer of silica sand, with high demand in construction, glass, ceramics, and foundry industries. The glass industry has driven the need for high-purity silica sand. The ceramics industry also uses this material extensively. The wide usage of silica sand in Türkiye continuously increases the demand for both local and imported sources.

Türkiye imports silica sand from various countries, including Egypt, Italy, India, and the USA. These imported sands are available in different purity levels and quality grades, catering to Türkiye's diverse

industrial needs. Silica sand imported from Egypt is particularly noted for its high purity and low iron content, making it ideal for precision industries like glass manufacturing (Sickafus & Schaefer, 2003).

Egyptian silica sand is considered one of the highest quality silica sands globally. Its high purity and low iron content make it indispensable in glass and electronics industries. Additionally, its homogeneous granule size and low moisture content make it a preferred material in many industries. These characteristics make Egyptian silica sand a low-processing material during enrichment (McCloy, 2003).

The enrichment process of silica sand aims to increase the material's purity for industrial use. In high-purity industries like glass and electronics, removing unwanted minerals such as iron is crucial. Enrichment not only improves product quality but also reduces environmental impact. High-quality silica sand production minimizes waste material, contributing to an environmentally friendly manufacturing process (Helman, 2002).

2. Material and methods

2.1. Material

The analysis of the silica sand sample imported from a local supplier in Egypt for a major tableware manufacturer in Türkiye reveals that the primary component is SiO_2 at 99.770% (Table 3). This high purity level indicates that the sample is largely composed of silica, making it highly valuable for applications in glass production.

Table 3. XRF Analyses of The Sample

Component	MgO	SiO_2	Al_2O_3	K2O	TiO_2	Fe_2O_3
%	0.011	99.77	0.124	0.003	0.031	0.015

Other components are present at very low levels:

- Na_2O (Sodium Oxide): Not detected (%0.000), indicating the sample is free of sodium, which is undesirable in glassmaking.
- MgO (Magnesium Oxide): At 0.011%, showing minimal contamination with magnesium.
- Al_2O_3 (Aluminum Oxide): Present at 0.124%, may negatively impact optical clarity and mechanical properties in glass applications.
- K_2O (Potassium Oxide): At 0.003%, nearly free of potassium.
- TiO_2 (Titanium Dioxide): At 0.031%, its low content suggests suitability for producing colorless glass.
- Fe_2O_3 (Iron Oxide): At 0.015%, low iron content is advantageous as iron can discolor glass.
- Overall, this analysis confirms the silica sand's high purity with minimal contaminants, ideal for high-purity industrial processes.

2.2. Method

The method used in this study is dry magnetic separation, a technique that removes unwanted magnetic impurities from minerals by using High Magnetic Intensity Roll Separator. Dry separation is preferred for materials with low moisture content and eliminates the need for water, reducing environmental impact. Magnetic impurities, such as iron, are effectively removed from silica sand using this technique.

"The MIKNATIS ARGE-Ø300X1100 Magnetic Roll Separator is designed specifically to separate magnetic components from silica sand. It features various adjustment mechanisms."

- Feed Roll Speed: Adjusts the feeding rate of the material, affecting processing capacity.
- Belt Speed: Determines the distance the product travels, which influences the efficiency of the separation process.
- Blade Adjustment: Controls the amount of product passing to the waste stream, optimizing product purity while minimizing material loss.
- Belt Type: 0.5 mm thickness PVC belt was chosen for its durability and effective separation.

Magnet Arrangement: The magnets are arranged with 9-2 mm spacing to create a strong magnetic field. Maximum magnetic flux density measured on surface of the roll is 13,000 ±5% Gauss, with 11,000 ±5% Gauss on the 0.5 mm belt, ensuring precise separation of magnetic impurities.

The enrichment process involves feeding the product through the feed roll, vibro tray, and finally through two-stage rolls. This multi-stage process ensures high efficiency and effective removal of magnetic impurities from silica sand.



Fig. 1. Industrial Prototype of Ø300 mm Roll Separator with Blade Distance and Feeding Mechanism.

3. Experimental Results

In this study, three different experiments were conducted to remove iron oxides from Egyptian Silica Sand B Grade to A Plus. The experiments varied in parameters such as feed roll speed and other settings, and the results and efficiency of each experiment were evaluated. The parameters and settings for each experiment are given in Table 4.

Table 4. Experimental Inputs

Experiment	Input Sample	Magnet Arrangement	Magnetic Flux Density	Capacity	Feed Roll Speed	Belt Speed	Blade Distance	Waste Ratio
Test 1	10 kg	9-2 mm	11,000 Gauss 0.5 mm Belt	4 t/h	15 Hz	27 Hz	5 cm	1.0%
Test 2	10 kg	9-2 mm		10 t/h	18 Hz	33 Hz	6 cm	0.8%
Test 3	10 kg	9-2 mm		18 t/h	20 Hz	38 Hz	7 cm	1.6%

Table 5. Chemical analyses of the tests

Component, %	Test 1 – Product	Test 1 - Waste	Test 2 - Product	Test 2 - Waste	Test 3 - Product	Test 3 - Waste
Na_2O	0.000	0.046	0.000	0.043	0.000	0.050
MgO	0.000	0.235	0.008	0.280	0.010	0.270
SiO_2	99.92	97.39	99.87	97.08	99.86	96.50
Al_2O_3	0.057	0.967	0.07	1,.3	0.065	1.10
K_2O	0.003	0.013	0.003	0.014	0.004	0.016
TiO_2	0.018	0.643	0.033	0.727	0.028	0.710
Fe_2O_3	0.003	0.517	0.007	0.560	0.010	0.600

The results of the experiments highlight the efficiency of magnetic separation in improving the quality of silica sand. Each experiment showed that the silica content in the product was maintained at high levels and the iron oxide content was significantly reduced.

- Experiment 1: With lower feed roll and belt speeds, and a standard blade distance, the results showed an increase in SiO_2 and a decrease in Fe_2O_3 in the product.
- Experiment 2: Increasing feed roll and belt speeds improved product efficiency and reduced Fe2O3 content further but resulted in a higher Fe_2O_3 ratio in the waste.
- Experiment 3: A balanced approach in parameters helped maintain product quality and keep Fe_2O_3 levels low.

Overall, each experiment demonstrated the impact of different parameters on the effectiveness of the separation process, suggesting that optimal settings can achieve the highest efficiency. These findings provide valuable insights for future processing and optimization efforts.

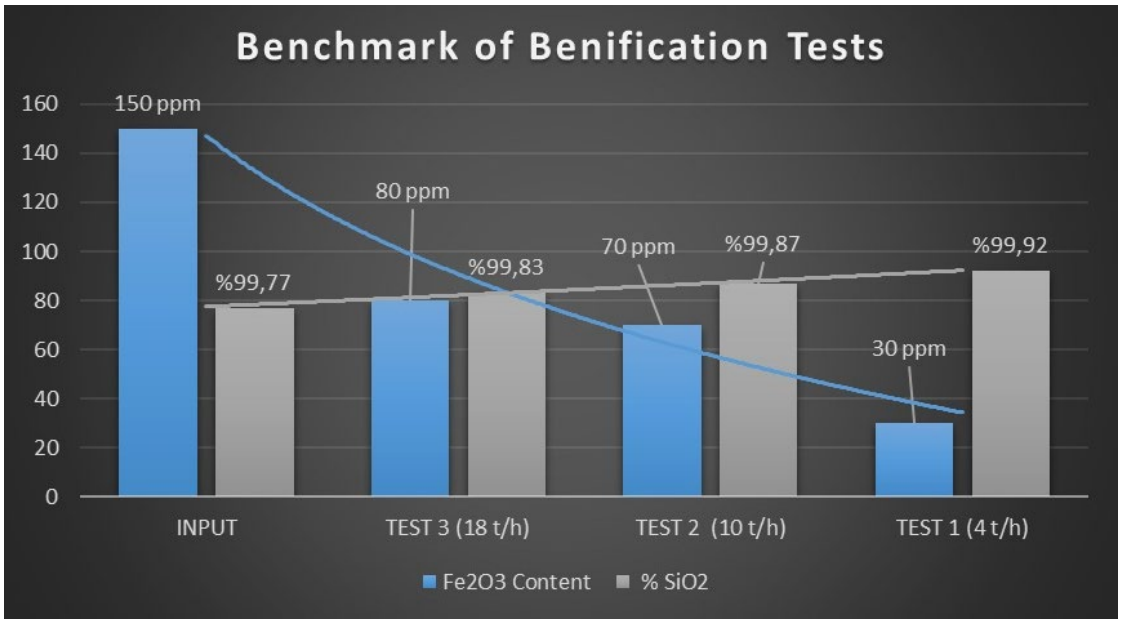


Fig. 2. Benchmark of Beneficiation Tests

4. Conclusion

4.1. Elimination of Flotation Needs

The experimental results have demonstrated that the magnetic separation process for Egypt Silica Sand A Grade to A Plus eliminates the need for flotation. Various parameters applied during the experiments (feed roll speed, belt speed, blade distance, etc.) achieved high-purity products and effectively separated iron oxides. Especially, the performance of dry magnetic separation in Test 1 led to the conclusion that a product quality close to that achieved through the flotation process can be obtained.

4.2. Environmental Benefits

The use of a single machine for magnetic separation has provided several environmental benefits:

- Energy Savings: The elimination of additional processes such as flotation has reduced energy consumption. The use of a single machine has increased process efficiency and consequently decreased environmental impact.

- Reduction in Chemical Use: Flotation typically involves chemical substances. By eliminating flotation, the use of chemicals has been avoided, contributing to a reduction in environmental pollution and toxic waste.

- Waste Management: Magnetic separation minimizes the amount of waste and controls its content. The reduction in waste volume has lessened the environmental impact associated with waste management and disposal.

4.3. Ultra Purity

The magnetic separation process with a single machine has achieved high cleanliness levels. Results from the best experiment shows that the SiO2 content in the products increased from 99.77% to 99.92%. Additionally, the Fe2O3 content was maintained at low levels (0.003% in Test 1, 0.007% in Experiment 2, and 0.010% in Experiment 3), confirming high cleanliness levels. These high cleanliness levels contribute to improved product quality and effective removal of unwanted contaminants. Especially in the first test, the product received an Ultra grade with excellent results.

5. Discussion

Advantages of Ø100, Ø150, Ø300 mm Roll Separators

The Ø100, Ø150, and Ø300 mm roll separators available in the market each offer various advantages to meet different needs:

- ✓ Ø100 mm Roll Separator: These machines are particularly suited for small-scale production facilities. The small diameter roll separators provide medium-precision separation and are typically used for low-capacity applications. They offer a low-cost investment, but to meet high-capacity needs, a large number of these machines would be required. This would result in significant space consumption and increased labor costs.

- ✓ Ø150 mm Roll Separator: The Ø150 mm separators are more suitable for medium-sized facilities, offering increased capacity and improved performance. These machines provide a broader range of applications compared to Ø100 mm models and are designed to meet medium-capacity production needs.

- ✓ Ø300 mm Roll Separator: Ideal for large-scale facilities and high-capacity applications, the Ø300 mm roll separators deliver high efficiency and quality, providing superior performance in separating large quantities of materials with less waste ratios than the other roll separators.

Their ability to achieve high capacities with a single machine offers advantages in terms of reduced labor, space savings, and cost efficiency.

Each model's development reflects a response to industrial needs and technological demands, showcasing continuous improvements in capacity, efficiency, and performance.

Reasons For Ø500 Production Decision

The decision to produce Ø500 mm roll separators is based on several strategic reasons:

- ✓ Quality and Capacity: The Ø500 mm roll separator is designed to upgrade the advantages of larger diameters and higher capacities, aiming to provide the highest quality and performance for high-capacity production processes. Larger diameter machines offer improved separation efficiency with lower waste and quality, enhancing industrial performance.

- ✓ Elimination of Flotation Needs: Ø500 mm roll separators offer the capability to achieve high-purity products without requiring additional processes like flotation. This simplifies the process and reduces costs. Additionally, it offers an environmentally friendly solution by reducing the environmental impacts and chemical use associated with flotation.

- ✓ Global Competitiveness: Ø500 mm roll separators are among the largest diameter machines available, providing a strong position in the global market. The production of this innovative machine aims to enhance competitive advantage and strengthen market leadership. The absence of Ø500 mm machines until now indicates a unique position in the market and fills an industry gap.

In summary, the decision to produce Ø500 mm roll separators is a strategic move to meet high-quality and capacity requirements. This new machine is considered a significant advancement in both industrial performance and environmental benefits.

References

Doremus, R. H. (2002). Chemistry of Glasses. Wiley.

Helman, J. J. (Ed.). (2002). Handbook of Glass Properties. Academic Press.

McCloy, M. J. (2003). Glass: Properties and Manufacturing Guide. CRC Press.

Reynolds, P., & Jones, M. (2001). Industrial Uses of Silica Sand. Industrial Minerals Research.

Richerson, D. W. (2006). Introduction to Glass Science and Technology. Wiley.

Sickafus, K. E., & Schaefer, M. W. (2003). Materials Science of Glass. Springer.

Pre-concentrate Production from Oolitic Iron Ore by Physical and Chemical Separation Methods.

Nassima Chebel [1]*, Djamel Nettour [1], Mohamed Chettibi [2]

[1]National Higher School of Technology and Engineering, Mines Metallurgy Materials Laboratory (L3M), 23005, Annaba, Algeria

[2]Department of mines, Mineral Resources Valorization and Environment Laboratory, Badji Mokhtar University, Annaba, Algeria

*Corresponding author: n.chebel@etu.ensti-annaba.dz (Nassima Chebel)

Abstract:

Oolitic iron ores are characterized by their fine-grained texture and high levels of phosphorus and gangue minerals, which pose challenges for their efficient beneficiation. The study discussed the feasibility of removing phosphorus (P), and other impurities such as silica and alumina, and improving the iron grade of an oolitic iron ore containing 56.08 % Fe and high phosphorus content (P ~ 0.8 %); using physical and chemical separation methods, including magnetic separation and flotation. Magnetic separation using wet low-intensity magnetic separation was employed for the selective removal of gangue minerals from the iron-bearing phases, and enhance the iron content of the ore, while flotation in the presence of starch and fatty acid was used to selectively separate phosphorus and other remaining impurity minerals from the iron minerals. The combination of these two methods resulted in a product containing 61.16 % iron and 0.69% phosphorus with a decrease in amounts of other gangue minerals. The results indicate that the iron recovery and dephosphorization of iron ore used in this work are ensured; Although, the process would be more effective with the addition of other separation technologies as roasting, and with further parameter optimization of the process to improve these findings.

Keywords: *Oolitic iron ore, Magnetic separation, Flotation, Dephosphorization, impurity removal*

1. Introduction

The efficient extraction and utilization of iron ore resources are pivotal for meeting the global demand for steel and other industrial applications. Among various iron ore types, Oolitic iron ore, characterized by its oolitic structure where iron oxide particles are bound within a matrix of gangue minerals, poses significant processing challenges due to its fine particle size and complex mineralogical composition (Chebel et al., 2023). Traditional beneficiation methods of oolitic iron ore containing phosphorus often face limitations due to the fine and complex nature of the ore, necessitating the development of advanced techniques to enhance the efficiency of ore concentration and to improve recovery rates and concentrate quality (Quast, 2018). The modern steel industry has limited the concentration of phosphorus in steel and considered it as an undesirable impurity in iron ore, and this is because phosphorus negatively affects the strength of the product, possibly causing hot shortness and/or temper embrittlement (Tang et al., 2013). The removal of phosphorus during the high temperature iron or steel making process is costly and the ores with a high content of phosphorus are less desirable or can be marketed with high penalties. As a result, phosphorus must typically be removed from phosphorus-rich iron ores before they can be used as feedstock for manufacturing iron (Li et al., 2015). Magnetic separation and flotation are two prominent techniques employed in iron ore beneficiation. Magnetic separation exploits the magnetic properties of iron-bearing minerals to separate them from non-magnetic impurities (Poloko, 2019). Flotation, on the other hand, leverages differences in surface chemistry to selectively separate valuable minerals from unwanted gangue (Nagaraj and Farinato, 2016). Both methods have been utilized separately with varying degrees of success in the treatment of oolitic iron ores. Seifelnassr et al. (2012) conducted magnetic separation tests on Wadi Halfa ore, achieving a concentrate grade of 42.4% Fe at 92.2% recovery with a 150–20 µm feed size. Repassing the

rougher magnetic concentrate yielded 63.5% Fe with 67.7% recovery, indicating the ore's suitability for processing by either tabling followed by magnetic separation or two-stage magnetic separation for high-grade concentrates. Sadawy (2013) tested dry, high-intensity magnetic separation on Aswan oolitic iron ore but found it ineffective for upgrading the ore. While coarse particles gave higher grades and fine particles had higher recoveries, no combination of field strengths (0.4–1.2 T) produced reasonable grades and recoveries. Qiu et al. (2013) used low (0.12 T) and high intensity (1.6 T) magnetic separation on oolitic hematite ore tailings (48.32% Fe, 14.92% SiO2), achieving 54.5% Fe at 77% recovery after low intensity separation. Fine grinding to 98.4% passing 74 µm reduced recovery, while four-stage processing yielded 52.95% Fe at 82.32% recovery. Zhang and Wang (2014) found that fatty acid increased the contact angle for limonite, oolitic hematite, and magnetite, but decreased it for hematite, indicating the need for a surfactant to achieve hydrophobicity for flotation. Fan et al. (2020) published a review focused on the reverse flotation of iron ores, and found that it is the most commonly used route in iron ore flotation, and the fatty acids are widely used as a collector in the reverse anionic flotation of iron ores. The integration of these techniques into a cohesive pre-concentration strategy could potentially address the ore's unique challenges more effectively (Chen et al., 2023). This study investigates the effectiveness of a combined approach involving magnetic separation and flotation for pre-concentrate production from oolitic iron ore. By optimizing the parameters for both techniques, we aim to achieve a high-grade pre-concentrate that can significantly enhance the efficiency of subsequent processing stages. The research addresses key aspects such as the magnetic properties of the ore, flotation reagents, and process conditions to determine the optimal conditions for pre-concentration. The findings are expected to contribute valuable insights into the development of more efficient and sustainable methods for the beneficiation of oolitic iron ores.

2. Material and methods

2.1. Material

The raw material used in this research was taken from the Gara Djebilet deposit in Tindouf province of Algeria. It is a high-phosphorus oolitic iron ore with (> 0.10% P). The chemical composition and iron ore texture are shown in Tables 1 and Figure 1.

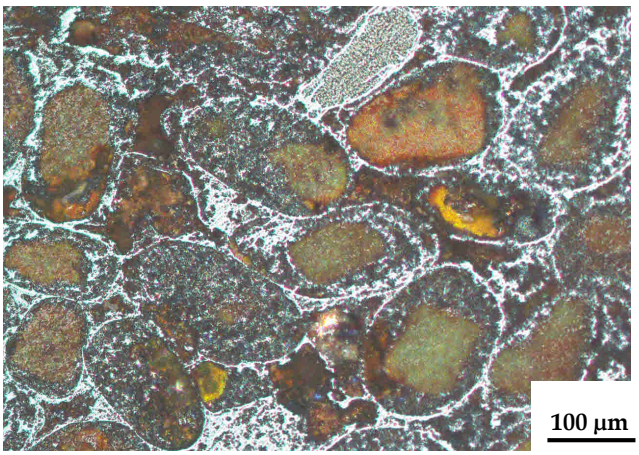


Fig. 1. The oolitic texture of GD oolitic iron ore.

Table 1. Chemical composition of GD high-phosphorus oolitic iron ore (%).

Element	TFe	Fe_2O_3	SiO_2	Al_2O_3	P_2O_5	K_2O	CaO	Na_2O	MgO	MnO	SO_3	LOI
Content (wt %)	56.08	80.19	6.72	5.47	0.77	0.05	0.99	0.05	0.34	0.63	0.06	4.31

* LOI mass lost on ignition at 1000 °C.

The ooids can be seen in Figure 1. Recent publication by the authors (Chebel et al., 2023) showed that hematite is the main iron bearing mineral in the ore; along with magnetite, goethite, chlorite, siderite.

And that silica, aluminum minerals and phosphorus are finely disseminated in the oolitic structure. Quartz has been observed inside and outside the ooids.

2.1.1. Sample preparation

The lumps were collected from the mine site and reduced to finer sizes using a sledgehammer. Sub-samples were further crushed to 5 mm using a jaw laboratory crusher, and then mixed and split by quartering technique to obtain a representative sample to produce a pre-concentrate of iron with low impurity.

2.2. Methods

A multi-stage process aimed to produce a pre-concentrate of high-grade iron suitable for further processing is illustrated in Figure 2.

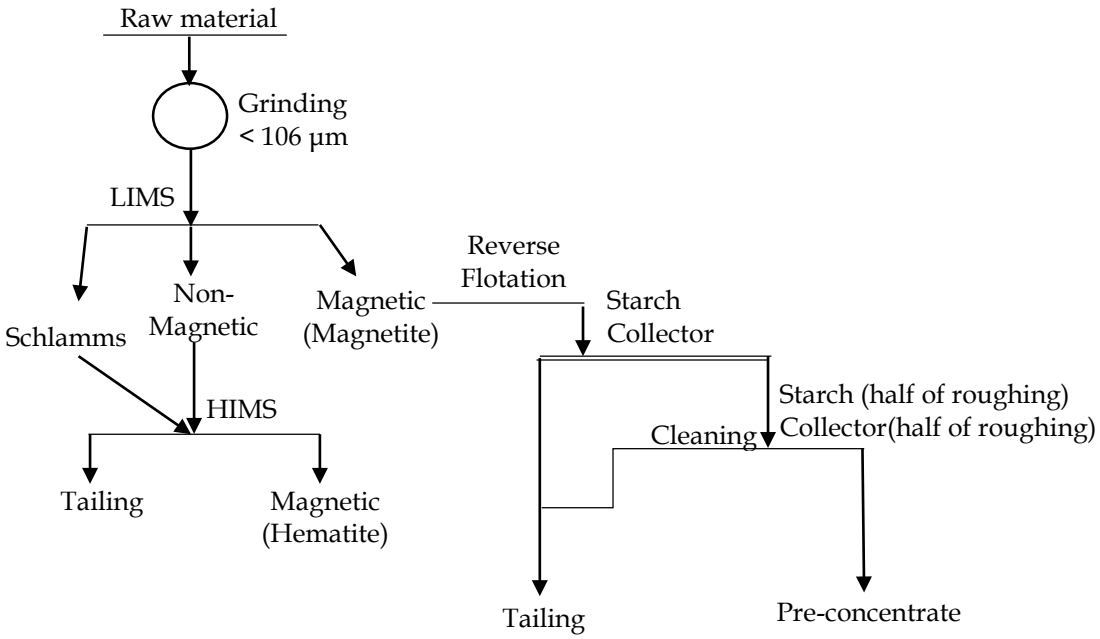


Fig. 2. The flowsheet of pre-concentrate production process.

2.2.1. Grinding

The crushed ore was subjected to grinding in a ball mill under wet conditions. The milling was performed for 15 minutes to reach the target particle size, monitored by sieve analysis. The ore was ground to achieve a particle size of 80% passing 74 µm, ensuring optimal liberation of iron-bearing minerals for subsequent separation processes. The ground material was collected for further processing in magnetic separation and flotation tests.

2.2.2. Magnetic Separation

Two stages of magnetic separation were conducted using a laboratory-scale wet drum magnetic separator. The ground ore was fed into the separator, and low-intensity magnetic fields (0.12 T) were applied to recover magnetic iron minerals. The magnetic fraction (pre-concentrate) was collected, while the non-magnetic tailings were set aside for (WHIMS) high intensity wet magnetic separation. The recovery and grade of the magnetic concentrate were determined using X-ray fluorescence spectroscopy (XRF), as well as the tailing product quality.

2.2.3. Flotation

The magnetic fraction from the magnetic separation stage was further processed using inverse flotation to remove any remaining impurity minerals. A flotation cell was employed, using a fatty acid-based collector (Potassium oleate (K-oleate)) to float gangue minerals (phosphorus ,silica…) from the oolitic iron ore. Tapioca starch (600 g/t) was used to depress the iron minerals, while the anionic collector was added at 400 g/t in the rougher stage and half of the original in cleaner stage, and that in a neutral medium (Ph = 7.2). The froth was collected as the gangue, and the remaining concentrate was analyzed for iron content and recovery.

2.2.4. Characterization of Products

All concentrate and tailing products were dried, weighed, and subjected to chemical analysis to determine iron, phosphorus and other impurity content. Particle size distribution of the ground material was also determined by fractional sieve analysis.

3. Results and discussion

The efficiency of grinding and particle size distribution of the studied iron ore were determined by the fractional sieve analysis. The result is shown in Figure 3.

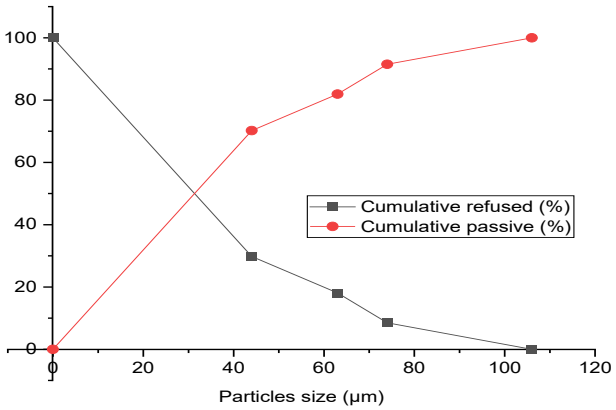


Fig. 3. Particle size distribution of the ground material.

The results of the sieve analysis shown that more than 80% by weight of the sample reported below 63 µm, with D50 (median particle size) = 32 µm. Sieve analysis confirmed that the target particle size was achieved, which is crucial for effective separation in both magnetic and flotation processes. The fine grinding ensured medium liberation of gangue minerals present in the oolitic iron ore due to their fine dissemination in the oolitic structure. Although overgrinding led to a small fraction of ultra-fine particles, which can negatively impact separation efficiency, especially in flotation.

Low-intensity magnetic separation (0.12 T) was conducted on the ground ore to recover magnetic minerals. Under these conditions, an iron concentrate with a grade of 61.33% Fe was produced, with a recovery of 73.75%. The magnetic separation successfully recovered the magnetite present in the ore, while the hematite and the non-magnetic tailings, mainly composed of quartz, were further processed by second stage of magnetic separation. To enhance the grade and recovery, high-intensity magnetic separation (1.6 T) was applied to the tailings of LIMS. This step resulted in an additional iron recovery of 14.75%, but the concentrate grade was lower (52.11% Fe), indicating that further grinding or adjustments to the magnetic field strength could improve performance. The combined process of low- and high-intensity separation produced a pre-concentrate with a total recovery of 88.5%, indicating the efficiency of the magnetic separation stages.

Reverse Flotation was performed on the magnetic fraction (Magnetite of LIMS) to remove any remaining impurity minerals, particularly phosphorus, silica and alumina. Using a fatty acid-based anionic collector (K-oleate) and starch as a depressant, flotation achieved a concentrate grade of 61.16% Fe with a recovery of 99.14% (Figure 4). The addition of starch at 600 g/t in the rougher stage and 300 g/t in the cleaner stage effectively suppressed the magnetite, preventing it from floating with the silicate gangue minerals. However, a challenge was observed with the fine particle fraction (<20 µm), where recovery rates were lower due to the "muddy" behavior of ultra-fines, which negatively affected both magnetic separation and flotation. This suggests that desliming prior to flotation may enhance concentrate quality and recovery.

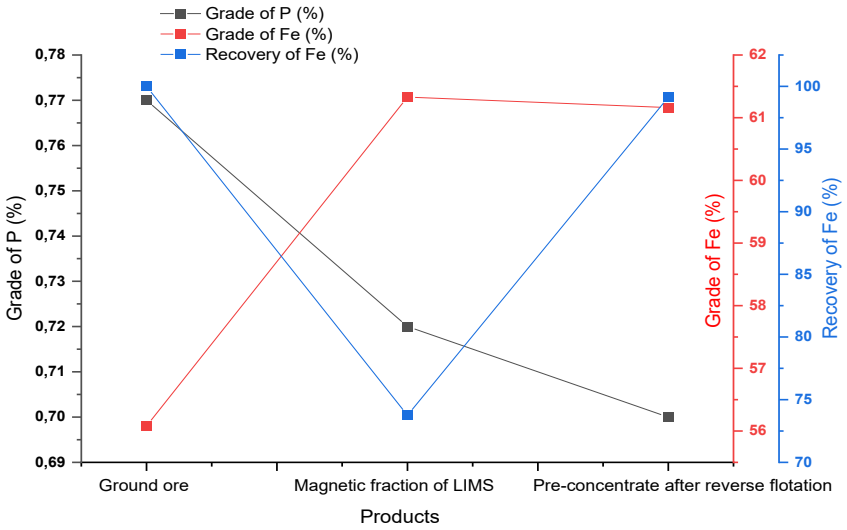


Fig. 4. Results of pre-concentrate production process.

Analysis of iron pre-concentrate product

The chemical composition of iron pre-concentrate product is shown in Tables 2. The results show that there is an increase in the iron content from 56.08% to 61.16% Fe, while the contents of the gangue minerals P, Si, Al and other impurity are decreased. Therefore, the combination of grinding, magnetic separation, and flotation techniques is effective, even though the flow sheet need further optimization to maximize iron recovery and concentrate grade.

Table 2. Chemical composition of iron pre-concentrate product (%).

Element	TFe	Fe_2O_3	SiO_2	Al_2O_3	P_2O_5	K_2O	CaO	Na_2O	MgO	MnO	LOI
Content (wt %)	61.16	87.45	3.68	3.33	0. 69	0.04	0.43	0.1	0.22	0.35	2.99

4. Conclusions

This study demonstrated the production of a high-grade iron pre-concentrate from oolitic iron ore using a combination of grinding, magnetic separation, and flotation techniques (an iron grade of 61.16% Fe from 56.08% Fe). The grinding was largely broken-down the oolitic structure of the iron ore, aiding the liberation of iron minerals. However, some hematite remained locked within silicate matrices, which could account for the minor losses during magnetic separation and flotation. While a poor liberation of gangue minerals mainly phosphorus due to its fine dissemination and distribution in iron ore structure and iron crystals. Low-intensity magnetic separation achieved a high recovery of magnetite, in return, reverse flotation was failed in removing the content of phosphorus. The integration of flotation after magnetic separation was removed a minor gate of phosphorus (0.02%P). However, further fine-tuning

of the reagent dosages, particularly for starch and anionic collectors, could help enhance the removal rate of phosphorus. Overall, this study provides a viable method for upgrading oolitic iron ore into a high-grade pre-concentrate suitable for further metallurgical processing; with the potential for further improvements through process optimization noting adjusting the reagent dosages, milling times, and magnetic field strengths to maximize iron recovery and concentrate grade.

Acknowledgments

The authors wish to thank Prof. Dr. Mehmet Sabri Çelik and Prof. Dr. Feridun Boylu, both from Istanbul Technical University, for the valuable and important discussion in carrying out this work and for their contribution during the execution of the magnetic separation tests. Prof. Dr. Gulay Bulut from the same university is greatly acknowledged for her professional and kind assistance in flotation. Res.Assis. Yunus Emre Çavdar from the same university, is greatly appreciated for his assistance in the laboratory test work.

References

Chebel, N., Nettour, D., Chettibi, M., Chaib, R., Khoshdast, H., & Hassanzadeh, A. (2023). Studying on mineralogical and petrological characteristics of Gara Djebilet oolitic iron ore, Tindouf (Algeria). *Physicochemical Problems of Mineral Processing, 59*(5), 178382. https://doi.org/10.37190/ppmp/178382

Chen, C.; Zhang, Y.; Zou, K.; & Zhang, F. (2023). Flotation Dephosphorization of High-Phosphorus Oolitic Ore. *Minerals,* (13), 1485. https://doi.org/10.3390/min13121485

Fan, G.; Wang, L.; Cao, Y.; & Li, C. (2020) .Collecting Agent–Mineral Interactions in the Reverse Flotation of Iron Ore: A Brief Review. *Minerals, 10* (8), 681. https://doi.org/10.3390/min10080681

Li, G., Rao, M., Ouyang, C., Zhang, S., Peng, Z., & Tao. (2015). Distribution characteristics of phosphorus in the Metallic Iron during Solid-State Reductive Roasting of Oolitic Hematite Ore. *ISIJ International, 55* (11), 2304–2309. DOI: https://doi.org/10.2355/isijinternational.ISIJINT-2015-212

Nagaraj, D.R., & Farinato, R.S. (2016). Evolution of flotation chemistry and chemicals: A century of innovations and the lingering challenges. *Minerals Engineering, Volumes* (96–97), Pages 2-14. https://doi.org/10.1016/j.mineng.2016.06.019

Physical separation methods, Part 1: A Review. IOP Conf. Series: Materials Science and Engineering, (641), 012023. doi:10.1088/1757-899X/641/1/012023

Poloko, N. (2019). *Physical separation methods, Part 1: A Review*. Paper presented at the Mineral Engineering Conference (MEC 2019), Kocierz, Poland.

Effect of particle fineness on the finely disseminated iron ore for beneficiation. Powders & Grains (AIP Conference Proceedings), (1542), 1294–1295. https://doi.org/10.1063/1.4812176

Qiu, T.S., Zhang, W.X., Fang, X.H., & Gao, G.K. (2013). *Effect of particle fineness on the finely disseminated iron ore for beneficiation*. Powders & Grains. Paper presented at the 7th International Conference on Micromechanics of Granular Media, Sydney, Australia.

Quast, K. (2018). A review on the characterization and processing of oolitic iron ores. *Minerals Engineering. (126),* 89–100. https://doi.org/10.1016/j.mineng.2018.06.018

Sadawy, M.M. (2013). Characterization and dry high intensity separation of Aswan iron ore. Proceedings, *Characterization of Minerals, Metals and Materials* (pp. 355–362): The Materials, Metals and Materials Society.

Seifelnassr, A.A.S., Moslim, E.M., & Abouzeid, A.-Z.M. (2012). Effective processing of low-grade iron ore through gravity and magnetic separation techniques. *Physicochem. Probl. Min. Process. 48* (2), 567–578.

Tang, H., Wang, J., Guo, Z., & Ou, T. (2013). Intensifying gaseous reduction of high phosphorus iron ore fines by microwave pre-treatment. *Journal of Iron and Steel Research International. 20* (5), 17-23. DOI: https://doi.org /10.1016/ S1006-706X(13)60091-6

Zhang, H., & Wang, F. (2014). Analysis of surface wettability of synthetic magnetite. *Journal of Wuhan University of Technology-Mater. Sci. Ed. 29* (4), 679–683. https://doi.org/10.1007/s11595-014-0979-3

Investigating the Use of Chromite Beneficiation Plant Data in Simulation Studies

Betül AYDOĞMUŞ [1], Yakup UMUCU [1] *, Halil İPEK [1]

[1]*Eskişehir Osmangazi University, Department of Mining Engineering, Türkiye,*

*Corresponding author: yakup.umucu@ogu.edu.tr (Yakup Umucu)

Abstract:

Chromite is an indispensable mineral in modern industrial applications. It plays a critical role in many areas, from stainless steel production to metal coating, from wood protection to catalyst production. Due to its properties such as high durability, corrosion resistance and chemical stability, chromite is considered an essential component in many areas of industry. Therefore, chromite mining and processing is of great importance to the world economy and industry.

The use of MODSIM in ore beneficiation studies enables processes to be analyzed and optimized in detail. This increases operating efficiency, cost effectiveness and environmental sustainability. It also supports the training and development of operators and engineers, minimizing risks and strengthening strategic decision-making processes.

The purpose of this study is to evaluate the operating efficiency of JIG by performing different separation intensities in the JIG unit used in the chromite enrichment facility. In addition, simulation studies were carried out on different separation densities used in JIG studies in MODSIM using facility data. In the light of the data obtained, it was determined that the parameters changed on the JIG did not have much effect on the separation. However, this study has shown that parameter changes in MODSIM affect the JIG simulation.

Keywords: *Chromite, beneficiation, jig, simulation, MODSIM*

1. Introduction

Chromite is a valuable mineral that has a wide range of uses in industry. Many industries, including stainless steel production, metal coating, ceramics, and the paint and varnish industry, widely use chromite. Chromite is a critical component in stainless steel production. Stainless steel is a corrosion-resistant, durable, and aesthetically appealing material. Stainless steel finds widespread use in automotive, construction, home appliances, and numerous other industrial applications. Chromite is a coating material frequently used in metal coating processes. It helps protect metal surfaces against corrosion, increase their durability, and provide an aesthetic appearance. Chromite plays an important role in the wood preservation industry. It is the main component of a chemical known as chromium picrate. Chromium picrate prevents wood from rotting and prevents insect damage, thus extending the life of the wood. Chromium plays a crucial role in the creation of catalysts. Many industrial processes, including petrochemical and chemical production, use catalysts to accelerate chemical reactions. The ceramic industry uses chromite in the production of refractory materials. It plays an important role in the production of ceramics that are resistant to high temperatures. Chromite is a valuable mineral that has a wide range of uses in industry and plays a critical role in many industrial applications. Numerous areas utilize it extensively, including the production of stainless steel, metal coating, wood protection, and catalyst production. Therefore, the industrial importance of chromite is constantly increasing with its large and diverse areas of use.

Piece ores containing more than 32–34% Cr_2O_3 can find a usage area. The industry needs to evaluate and enrich ores containing less than 32% Cr_2O_3 to bring them to the desired composition (Güney, 1990). The density of chromite is higher than that of the gangue minerals it coexists with. As long as the liberation grain size allows, the most suitable enrichment method is gravity enrichment. If the ore is

liberated in large sizes, separation can be done with heavy media or a jig. Enrichment with a shaking table can be preferred when liberation in finer sizes is achieved (Ağaçayak, 2004).

Simulation of chrome enrichment processes is important for efficient processing of chrome ores and optimum quality production of chrome concentrate. These processes typically consist of stages such as grinding, flotation, separation based on density differences, and concentrate cleaning. Simulation of chrome enrichment can help optimize these stages, evaluate process performance, and develop new operating strategies. Occasionally, the density difference separation method is the preferred method for enriching chrome ores. Simulation can assess the effectiveness of separation circuits and parameters in response to varying density differences, thereby enhancing the efficiency of the process. The obtained chrome concentrate must be cleaned and purified. Simulation can evaluate different cleaning stages and optimize the quality of chrome concentrate. Simulation can also be used as a tool for designing and optimizing process control systems for chrome enrichment plants. It can assess and improve automation systems' performance. Additionally, simulation can reduce operating costs and environmental impacts by ensuring more efficient use of energy and other resources (Aydoğmuş, 2024; Benzer, et. all., 2001; Umucu, 2015).

The impact of Eskişehir region chrome mining on Turkey's chrome mining is very significant. The fact that the ores of the Taştepe region are difficult to evaluate economically due to the low Cr/Fe ratio brought to the market by the mines operating in the region is a very important contribution. Thus, the mines operating in the region ensure the efficient evaluation of all chromium in Turkey. To maximize the efficiency of the run-of-mine ore from the mines, the ore enrichment facility consists of two sections. These sections are given table 1 (Aydoğmuş, 2024).

Table 1. Beneficiation stages available at the facility

For high-grade ore	For Low-Grade Ores
Hand selection (triage) Jig	24 main product shaking tables 6 intermediate product shaking tables

The study conducted grade and quantity measurements on products with varying densities using the facility's jig. Additionally, we established the same flow chart in MODSIM and created a simulation. The obtained data is presented in a comparative manner. The results are interpreted in detail.

2. Materials and Method

The ore used in the study was obtained from the Chrome Enrichment Plant located in Tepebaş District of Eskişehir Province. To examine and investigate the mineralogical structure of the ore, the sample was brought to Eskişehir Osmangazi University's Mining Engineering Mineral Processing Laboratory. The relevant ore was preserved under appropriate conditions, and mineralogical-petrographic analyses were performed.

In a zone extending 1300 meters southeast of Taştepe, there are four mineralizations. These mineralizations are most likely considered to be the continuation of each other. According to the production and manufacturing analysis results, the grade of the ore varies between 12 and 44% Cr_2O_3. The thickness of the mineralizations varies between 1 and 6 meters, and it generally includes banded, nodular, and massive types.

3. Experiments

3.1. Beneficiation with JIG and Plant Analysis

At this stage of the study, grade and quantity analyses were performed on the concentrate obtained at different separation densities on the JIG equipment in the enrichment plant. Prior to these studies, sieve analysis was performed on the ore feed to the JIG unit. The sieve analysis results obtained are given below. Beneficiation with JIG and Plant Analysis

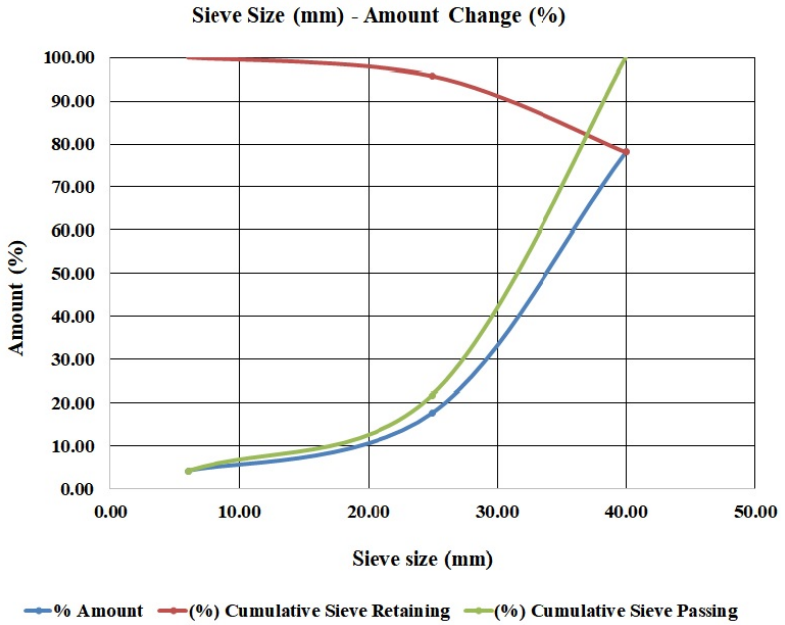


Figure 1. Changes in the quantities with the sieve size of the ore fed to the JIG.

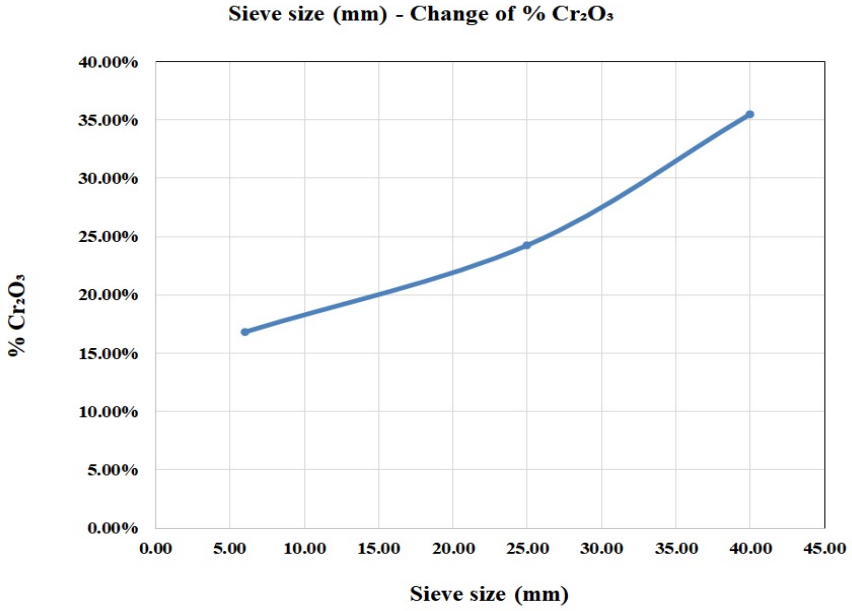


Figure 2. Grade changes with sieve size of the ore fed to the JIG.

The analysis revealed that the Cr% grade decreased as the grain size decreased. The analysis determined that the olivine ore within the chromite was released in fine grain sizes. In terms of comminution characteristics, it is understood that chromite is more difficult to comminute than olivine.

3.2. JIG plant analysis

Samples were taken from the concentrates obtained from the Bendalary JIG unit at different operating densities in the plant according to the sampling rules and the grade and quantity changes were determined. The operational conditions for the JIG are given in the table for each separation density, respectively.

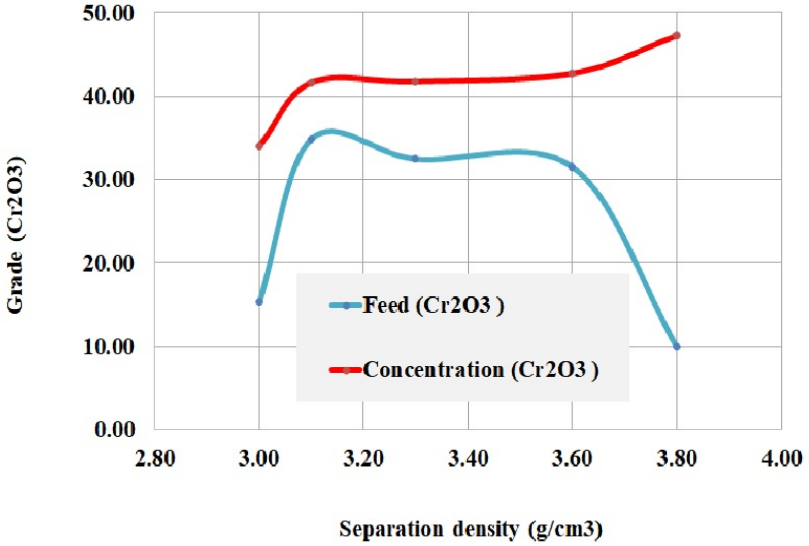


Figure 3. Illustrates the grade change for the concentrate fed and obtained at different separation densities for JIG.

4. Simulation Studies in MODSIM

MODSIM is a simulator that examines the mass balance in all its details for any mineral processing plant. The mass balance expression here includes the change in material grade, composition, grain size distribution, and total solid and liquid flow. In addition, MODSIM allows the use of standard and common models for crushing, grinding, and classification processes. It is a program with a completely modular structure that allows for model calculation for each process added to the simulator (Umucu et. all., 2016; Umucu, 2015).

As a result, the models can be adapted to any application and used in the simulation of the appropriate plant modification and development. With this characteristic feature, MODSIM allows the integration and development of research results carried out at any stage of mineral processing processes. Within the scope of the thesis study, MODSIM 3.6 was used.

The conditions in the studies carried out at the facility scale were taken as reference, and the separation densities remained the same in MODSIM, and 3.00-3.10-3.30-3.60-3.80 gr/cm3 separation densities were used, and simulation studies were carried out. The stages of the simulation studies in MODSIM are given in Figure 4-5 order. The MODSIM results and real-time data are presented in tables. At the start of the MODSIM simulation program, a flow chart is created regarding the process to be performed. Then, it is recorded in the system and defined (Figures 4-5).



Figure 4. MODSIM's main login platform

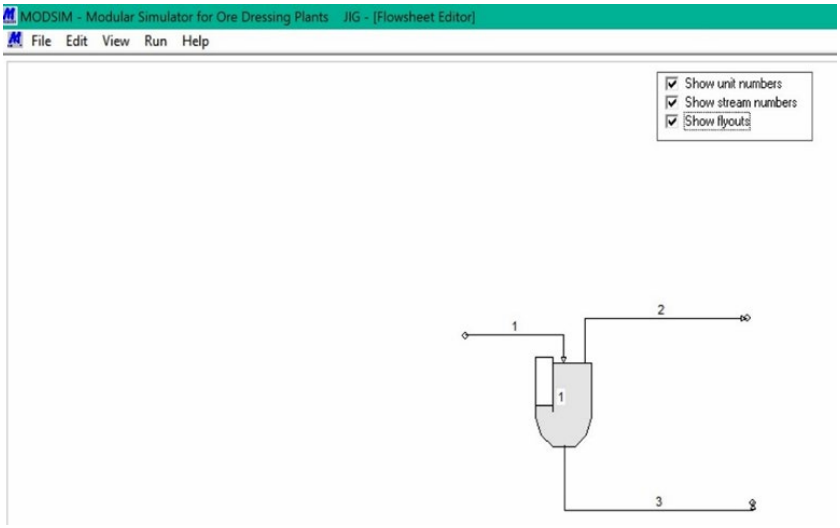


Figure 5. JIG simulation platform created in MODSIM

Once the flow chart has been defined, detailed information about the flow branches is entered. Data, such as density and grain size analysis, are defined.

The data obtained because of the simulation studies are given in Figures 6 – 7, respectively.

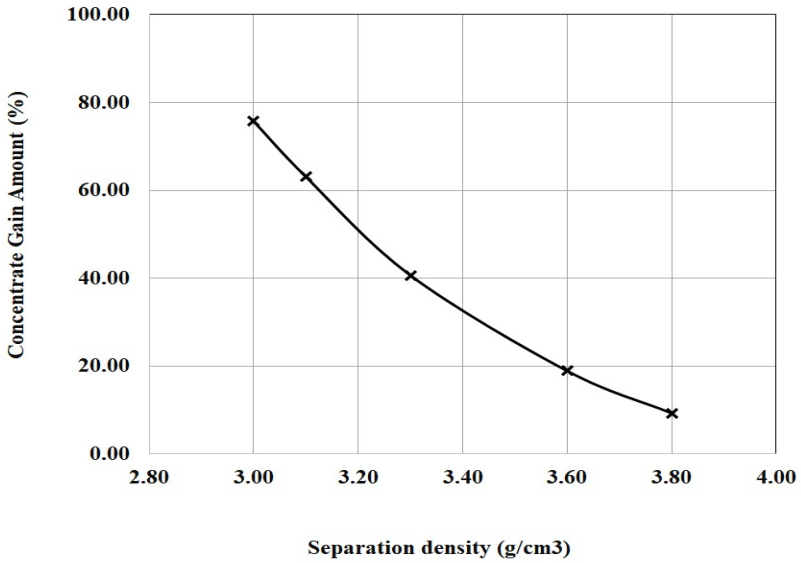


Figure 6. Change in the amount of concentrate gain obtained at different densities as a result of the simulation created for JIG in MODSIM.

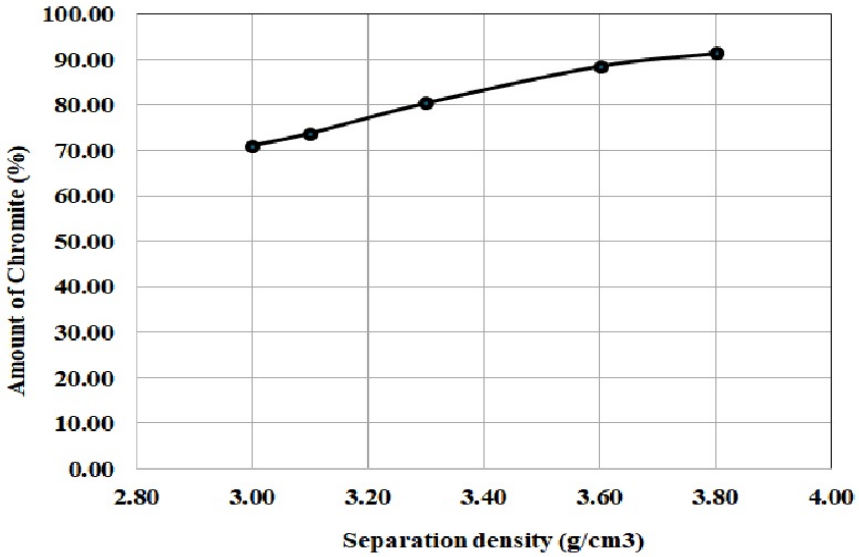


Figure 7: The relationship between chromium recovery efficiency and different densities that was found in the MODSIM simulation made for JIG.

As shown by the simulation results in Figures 8, as the density increases, the amount of concentrate decreases. In terms of quality, the gain in high-chromium-grade material actually increases. While the chromium in the fed material is being gained, a quantitative decrease occurs. On the other hand, it has been determined that the MODSIM simulation program reacts like a working JIG in reality.

4.1. Comparison of simulation and plant data

As shown in Figure 8, it has been determined that the simulation data and the JIG facility data are not compatible. The only thing that is compatible here is the decrease in quantity as density increases. It should be noted that theoretical calculations in simulation studies effectively utilize the density value. However, it has been determined that the structure of the ore and other operating conditions in the real-time JIG enrichment unit do not have much of an effect in applications.

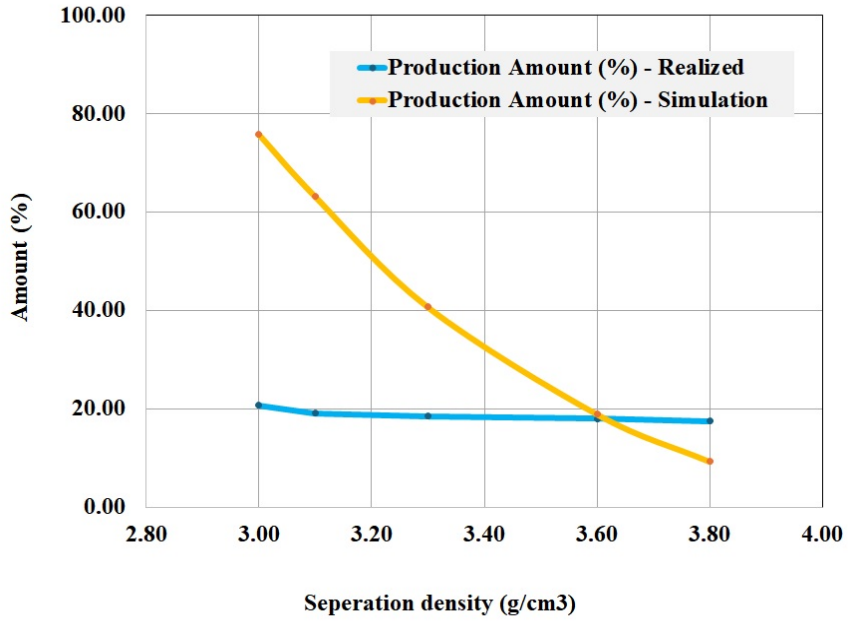


Figure 8. Change in the amount of concentrate gain obtained at different densities in MODSIM and the facility

5. Conclusion

The use of simulation and simulation techniques in mineral processing processes has become an important tool for increasing the efficiency and effectiveness of industrial operations. Simulation and simulation software provide the opportunity to perform detailed process analysis and evaluate the effects of various parameters and alternative process scenarios. The use of these techniques allows businesses to achieve significant gains in critical areas such as process optimization, cost reduction, energy efficiency, product quality, and environmental impact management. Simulation and simulation allow optimization of various mineral processing processes (e.g., grinding, flotation, gravity separation). By simulating process parameters, businesses can determine the most efficient operating conditions and improve process performance.

Within the scope of the study, it was determined from the data obtained in a JIG enrichment facility that the parameter change did not change the concentrate and concentrate grade obtained. However, it was seen that any parameter change had an effect on the results obtained in the simulation studies. The figure illustrates that the results of the simulation studies yielded a wealth of data. In addition to the concentrate amount, the quantitative distributions of different densities in the concentrate can also be determined. While it is a problem that these data cannot be accessed due to the difficult application of float-sink tests of metallic ores, many data can be easily accessed thanks to simulation programs.

The results of the simulation studies revealed a wealth of data, as illustrated in Figures 6-8. In addition to the concentrate amount, the quantitative distributions of different densities in the concentrate could also be determined. While it is a problem that these data cannot be reached due to the difficult application of float-sink tests of metallic ores, many data can be easily reached thanks to simulation programs.

References

Ağaçayak,T., 2004. Topraktepe (Yeşildağ Beyşehir-Konya) kromitlerinin zenginleştirme yöntemlerinin araştırılması, MSc Thesis, Selçuk Üniversitesi, Graduate School of Natural and Applied Sciences, Konya-Türkiye.

Aydoğmuş B., 2024. Investigating the Use of Chromite Beneficiation Plant Data in Simulation Studies, MSc Thesis, Eskişehir Osmangazi University, Graduate School of Natural and Applied Sciences, Eskişehir-Türkiye

Benzer, H., Ergun, L., Lynch, A.J., Oner, M., Gunlu, A., Celik, I.B., Aydogan N., 2001. Modelling cement grinding circuits, Minerals Engineering, Vol 14, Issue 11, pp 1469-1482.

Güney, A., 1990. Etibank Üçköprü krom zenginleştirme tesisi artıklarından küçük boyutlu kromitin zenginleştirilmesi, Istanbul Technical University, Graduate School of Natural and Applied Sciences, İstanbul-Türkiye

Umucu, Y., Deniz, V., Bozkurt, V., Çağlar, M.F., 2016. The evaluation of grinding process using artificial neural network. International Journal of Mineral Processing 146, 46-53.

Umucu, Y., 2015. Investigation of separation performance of dense medium cyclone using computer simulation, Physicochemical Problems of Mineral Processing 51 (1), 303-314.

Enrichment of Waste Printed Circuit Boards using a Zig-Zag Air Separator

Ersin Yener Yazici [1], Elif Yilmaz [1], Yunus Emre Cavdar [1, 2], Oktay Celep [1*], Haci Deveci [1]

[1]Hydromet B&PM Research Group, Mineral&Coal Processing Division, Department Mining Eng., Karadeniz Technical University (KTU), 61080, Trabzon, Türkiye

[2] Department of Mineral Processing Engineering, Istanbul Technical University (ITU), Istanbul, Türkiye

*Corresponding author: ocelep@ktu.edu.tr (Oktay Celep)

Abstract:

This study explored the enrichment of waste printed circuit boards (WPCBs) using a zig-zag air separator. After removing the fine fraction (-0.106 mm), the WPCB sample (-1 +0.106 mm) containing 19.8% Cu, 1.60% Fe, 425 g/t Ag, 120 g/t Au and 129 g/t Pd was used in the tests. The effects of air flow rate (5-15 m/s) on the separation of metals from size fractions (-1 +0.5 mm, -0.5 +0.106 mm) of WPCBs were studied. Increasing the flow rate from 5 to 10 m/s improved metal recoveries from the coarse fraction (-1 +0.5 mm). However, further increasing the flow rate to 15 m/s adversely affected Cu and Fe recoveries. Similarly, this high flow rate had also an adverse impact on metal recoveries from the fine fraction (-0.5 +0.106 mm). The results have shown that zig-zag air separation is more efficient in recovering metals at coarse particle sizes. At a 10 m/s air flow rate, a concentrate containing 52.3% Cu, 4.93% Fe, 1081 g/t Ag, 145 g/t Au and 161 g/t Pd was produced from the coarse fraction of -1 +0.5 mm with a relatively high recoveries: 97.9% Cu, 99.1% Fe, 98.3% Ag, 94.5% Au and 88.2% Pd, with 24.3% of the WPCB sample being separated as the tailings. These findings demonstrate the potential of zig-zag air separation in enriching the WPCB sample by removing non-metal materials.

Keywords: *WEEE, Printed circuit boards (PCBs), Recycling, Metals, Air Separation*

1. Introduction

Electronic waste or Waste of Electrical and Electronic Equipments (WEEE) is one of the fastest-growing waste streams worldwide owing to the rapid-developing digital technology (Ongondo et al., 2011, Shittu et al., 2021, Sun et al., 2016; Widmer et al., 2005). However, the ratio of collected and recycled WEEE is still low with only 22.3% in 2022 (Baldé et al, 2024). The improper disposal or treatment of WEEE can result in air, soil and water pollution, due to the release of potential pollutants such as Pb, Cd, Cr^{6+}, chlorinated/brominated flame retardants etc. (Jang and Townsend, 2003, Lincoln et al., 2007, Palanisamy et al., 2023, Robinson, 2009, Yazici et al., 2010, Yazici and Deveci, 2016). WEEE contains high base, precious and critical/strategic metals, making it a valuable resource with a high economic potential (Işıldar et al., 2018, Gulliani et al., 2023). Metals in WEEE are mostly present in printed circuit boards (PCBs), key components of EEE accounting for 3-5% of the total WEEE (Faraji et al., 2023).

The circular economy concept and growing environmental concerns necessitate the recovery of metals from WEEE. Recycling methods for WEEE can be broadly categorized into physical, hydrometallurgical/biohydrometallurgical, electrometallurgical and pyrometallurgical processes (Chauhan et al., 2018, Cui and Zhang, 2008, Deveci et al., 2019, Gulliani et al., 2023, Işıldar et al., 2019, Kaya, 2016, Sethurajan et al., 2019, Tuncuk et al., 2012). Recycling "high-value" WEEE, containing 400 g/t Au, is considered more economically feasible (Hagelüken, 2006). Based on this fact, industrial metallurgical plants prefer to process "high-value" WEEE for economic reasons (Hagelüken, 2006). The demand for some particular metals (e.g., Cu, Ag) contained in WEEE have been increasing for use in clean energy technologies (electric vehicles (EVs), renewable energy, etc.) (IEA, 2021). Copper has been recently identified as a strategic raw material (SRM) under the critical raw material (CRM) list published by the EU in 2023, due to its vital role in the green energy transition (European Commission, 2023). SRMs are defined as the raw materials essential for technologies supporting the green, twin and digital

economy transition, as well as for defence and aerospace applications. Copper is also listed as a CRM by Canada, South Africa and China (IRENA, 2023; Natural Resources Canada, 2022). Electric vehicles require 2.4-fold higher copper than cars with conventional internal combustion engines (ICE). Due to high copper demand, which is expected to increase by 28% by 2040 (IEA, 2021), a supply shortage is expected (European Commission, 2023). Also, the demand for silver is rising due to its use in solar photovoltaic panels (PVs) and other technologies (IEA, 2021).

Physical separation methods are often favoured due to their lower environmental impact, simplicity and low cost (Silva et al., 2019). These methods allow the separation of the metallic and non-metallic materials in WEEE, exploiting the differences in physical properties of materials (i.e., specific gravity, conductivity, magnetic susceptibility, brittleness, etc.). However, the use of physical separation methods in the recycling of WEEE is often hampered by relatively low metal recoveries and high metal losses, which can reach 10-35% (Goosey and Kellner, 2002; Yazici, 2012). One of the widely used physical separation methods, gravity separation can be employed to enrich metals by effectively rejecting non-metallic materials from WEEE, based on the relatively high specific gravity difference between metal and non-metal fractions (e.g., 8.93 g/cm^3 (Cu) vs. ≤2 g/cm^3 (most plastics in WEEE)) (Das et al., 2009, Li et al., 2007, MengPeng et al., 2004, Wen et al., 2005, Zhang and Forssberg, 1998, Zhao et al., 2004). Air separation/classification is a gravity separation method, effectively used in various industries such as agriculture, mineral processing and waste treatment (Wills and Napier-Munn, 2006). Air separators have been previously tested for the recovery of metals from WEEE (Eswaraiah et al., 2008, He et al., 2011, Ribeiro et al., 2019, Silva et al., 2019; Zhao et al., 2004). A zig-zag air separator is essentially a vertical air column (Fig. 1), in which upward-flowing air carries the light-fine particles into overflow whilst the heavy-coarse particles settle to underflow due to their high density and mass (Fig. 1).

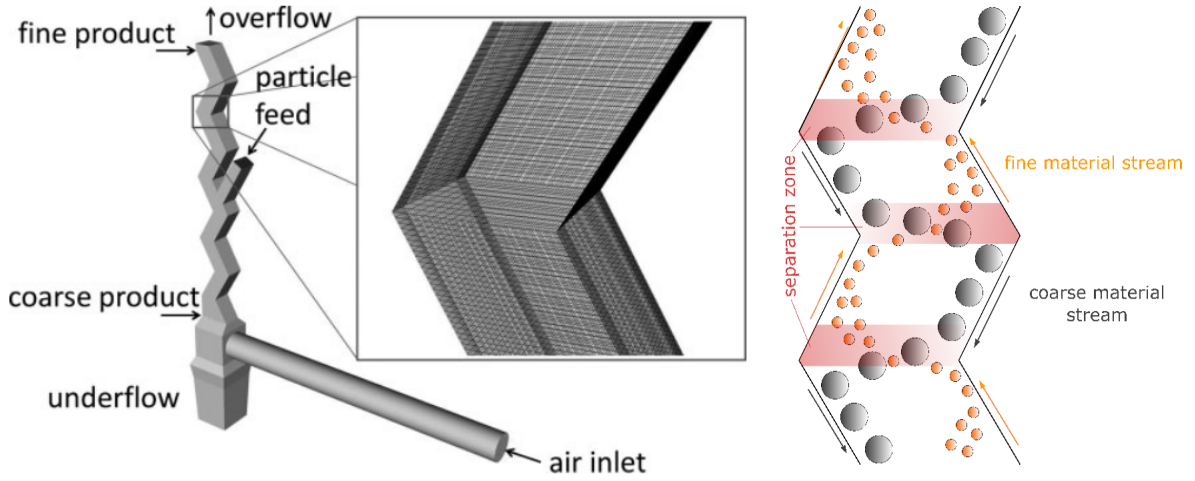


Fig. 1. General structure of a zig-zag air separator (left) (Hagemeier et al., 2014) and, material streams and separation zones of coarse-fine particles in the separator channels (right) (Kaas et al., 2022)

This study investigates the use of a zig-zag air separator as a simple, environmentally sound and cost-effective approach for the recovery of metals from crushed WPCBs to produce a metal-rich concentrate. The effect of air flow rate (5-15 m/s) on the separation of metals was studied from fine (- 0.5 +0.106 mm) and coarse (- 1 +0.5 mm) fractions. Separation efficiency (%), enrichment ratio and ratio of concentration were also calculated to evaluate the separation performance of the zig-zag air separator.

2. Material and methods

2.1. Material

Waste printed circuit boards (WPCBs) were collected from obsolete WEEE including computers, monitors etc. and reduced in size to -8 mm and then to 3.35 mm using a rotary cutting shredder (Fig. 2a,b). The product of two-stage shredding (-3.35 mm) was then ground to -1 mm using an ultra-centrifugal grinding mill (Retsch ZM 200). Based on the results of preliminary zig-zag air separation

tests which showed that separation of metals from fine fractions is not effective, the fine fraction (-0.1 mm) was removed and the -1 +0.106 mm fraction was used in the the zig-zag air separator. The feed material has a high copper content of 19.8% with an appreciable amount of precious metals (i.e., 120 g/t Au, 425 g/t Ag and 129 g/t Pd) and 1.60% Fe. This waste material can be classified as "medium-value" WEEE given that its gold content is between 100 and 400 g/t Au (Hagelüken, 2006).

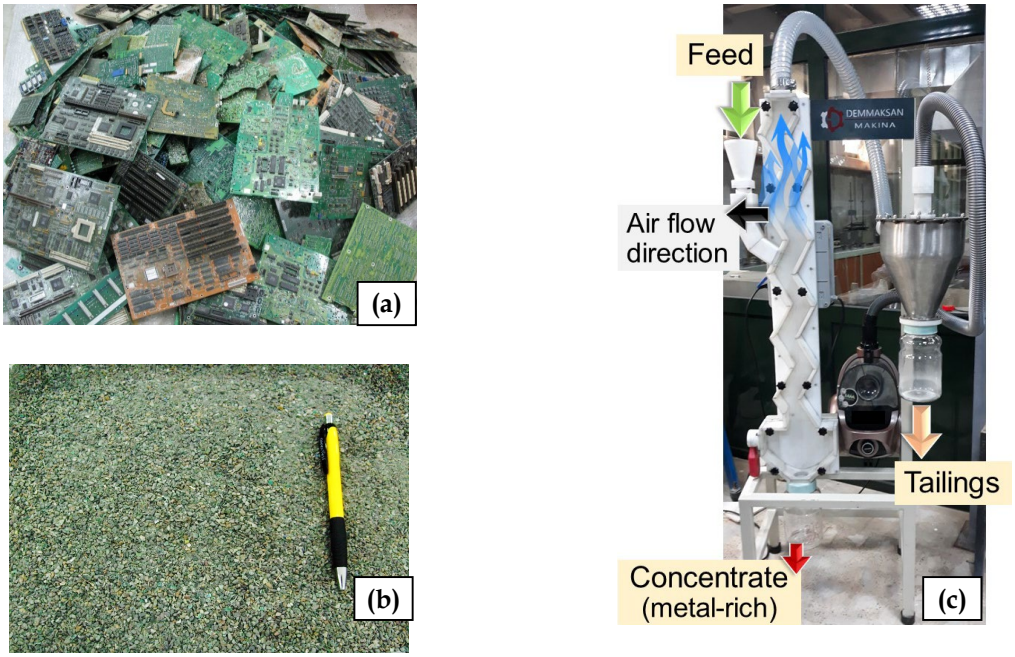


Fig. 2. Collected waste printed circuit boards (WPCBs) from WEEE (a); WPCBs (-3.35 mm) after two-stage size reduction (b); the zig-zag air separator used in the tests (c)

2.2. Method

A zig-zag air separator (DEMMAKSAN Machinery, Trabzon/Türkiye) was used in the separation tests (Fig. 2c). The effect of air flow rate (5-15 m/s) on the separation performance of metals from sized WPCBs (-1 +0.106 mm). A vacuum suction device was used to provide the flow of air upwards. The coarse-heavy material in which metals are enriched (i.e., metal concentrate) moves downwards and collects in the underflow stream. The tailings, rich in non-metallic materials (i.e., fine-light fraction) were reported to the overflow-collection bottle. A known amount of WPCBs (~50 g) was fed to the air separator operating at the tested air flow rate, metered by a digital flow meter. The concentrate and tailings collected from the separator were weighed and sieved through a 0.5 mm sieve to obtain fine (-0.5 +0.106 mm) and coarse (-1 +0.5 mm) fractions. These fractions are sampled and samples are digested in hot aqua regia ($HCl:HNO_3$=3:1 by volume) for analysis of metals by atomic absorption spectrometer (Perkin Elmer AAnalyst 400). The grade (%) and recovery (%) of each metal (i.e., Cu, Fe, Au, Ag, Pd) were calculated based on the concentrate and tailings assays.

Several formulas/indexes have been proposed to assess the separation efficiency of metals/minerals in mineral processing operations (Drzymala, 2007). One of the most commonly used indexes is "Separation efficiency (SE)" (Eq. 1), which takes into account the concentrate grade and recovery of the metals/minerals in physical and physicochemical separation processes (Schulz, 1969).

$$\text{Separation efficiency (SE; \%)} = R_m - R_g \quad (1)$$

where R_m and R_g are the recovery of the metal (e.g. Cu, Au, Ag, Pd or Fe) and the remaining material (other metals and non-metals) into the concentrate, respectively. "Enrichment ratio" and "ratio of concentration" were also calculated for these metals in the concentrate and tailings products obtained from the zig-zag separator. The enrichment ratio is the ratio of the metal grade of concentrate to that of feed (i.e., grade of Cu, Fe, Au, Ag, Pd). The ratio of concentration refers to the ratio of the amount of feed to that of the concentrate (Drzymala, 2007).

3. Results and Discussion

Fig. 3 illustrates the effect of air flow rate on the grade and recovery of each metal for the -1 +0.5 mm fraction. A decrease in the recovery of Cu and Fe was observed with an increase in the air flow rate from 5 to 15 m/s (Fig. 3). As a general trend, increasing the air flow rate resulted in the production of high-metal grades in the concentrate, with an exception of Ag. Despite the increase in the Ag grade of the concentrate by increasing the flow rate from 5 to 10 m/s, a further increase in the air flow rate led to a sharp decrease in the Ag grade. These results suggest that the most suitable air flow rate for the coarse particle size fraction is 10 m/s, particularly for Cu and Ag (Fig. 3). At this flow rate, 24.3% of the feed material was rejected as the tailings product while the recovery of metals into the concentrate was 97.9%, 99.1%, 98.3%, 94.5% and 88.2% for Cu, Fe, Ag, Au and Pd, respectively. The concentrate was determined to assay 52.3% Cu, 4.93% Fe, 1081 g/ton Ag, 145 g/ton Au and 161 g/ton Pd.

For the fine fraction (-0.5 +0.106 mm), a trend of decrease in the recovery was evident with increasing the air flow rate (Fig. 4), indicating that the zig-zag separator is more effective for the separation of metals from the coarse fraction. Fig. 5 shows the dependency of the separation efficiency (SE) of each metal from the coarse (-1 +0.5 mm) and fine fractions (-0.5 +0.106 mm) at the air flow rates tested. By increasing the air flow rate from 5 to 10 m/s, SE of all metals from the coarse fraction (-1 +0.5 mm) improved. A further increase in the flow rate to 15 m/s resulted in a further improvement in the SE for copper, silver and palladium, while adversely affecting the separation efficiency of iron and gold.

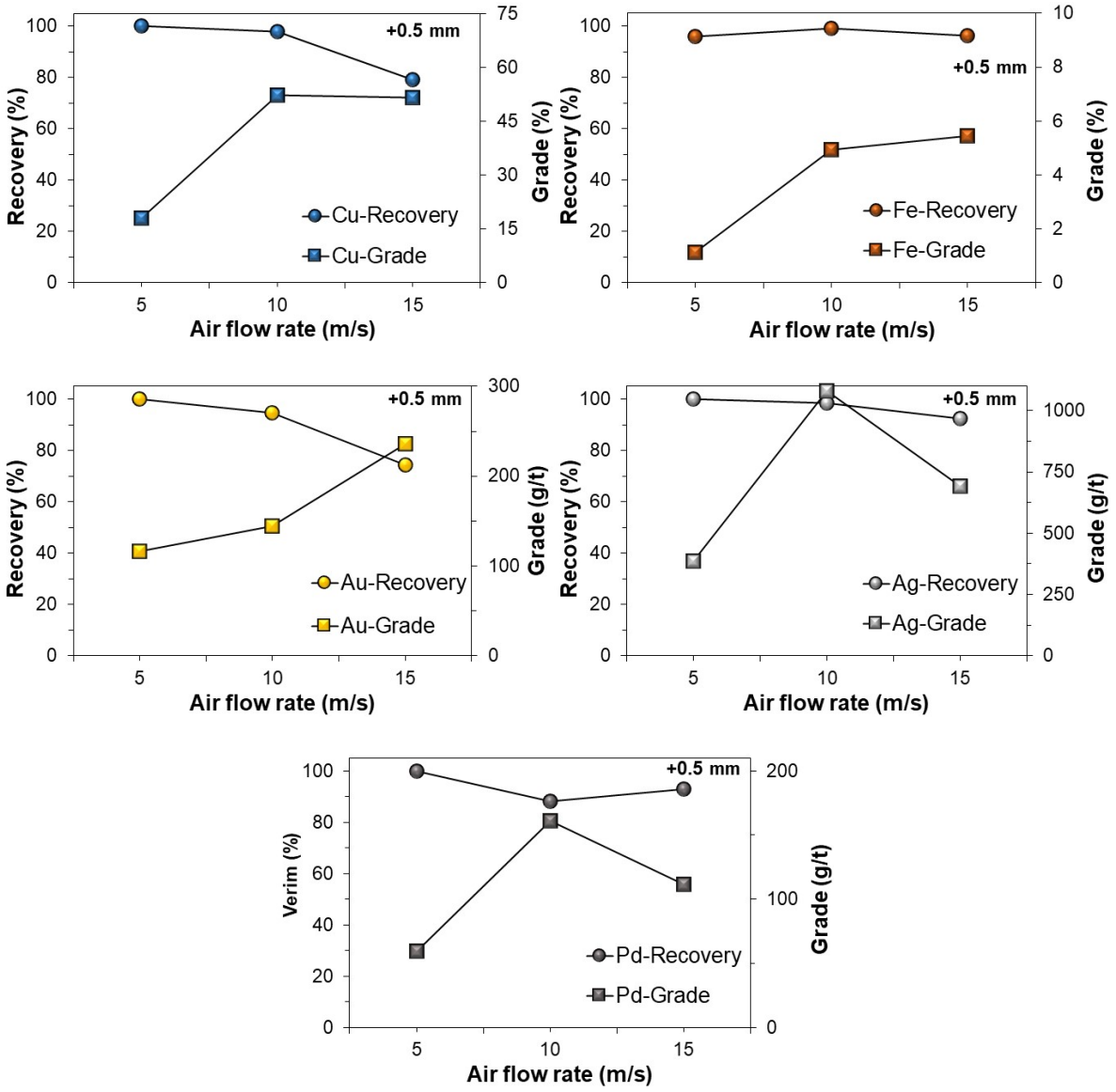
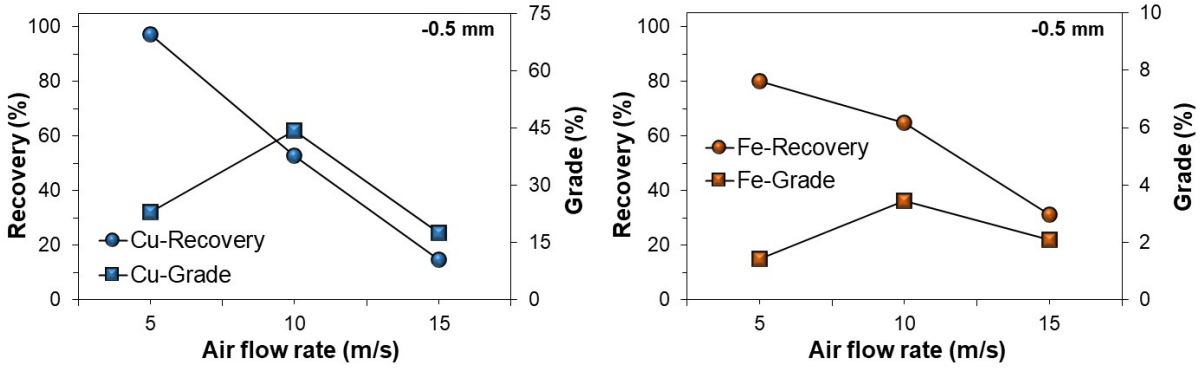


Fig. 3. Recovery (%) and grade (% or g/t) plots for metals at the coarse fraction (-1 +0.5 mm)

In contrast, for the fine fraction, the separation efficiency of metals was essentially minimally affected by increasing the air flow rate from 5 to 10 m/s. However, there was a significant reduction in the separation efficiency of all metals, as also observed for the coarse fraction, when the air flow rate was further elevated to 15 m/s.



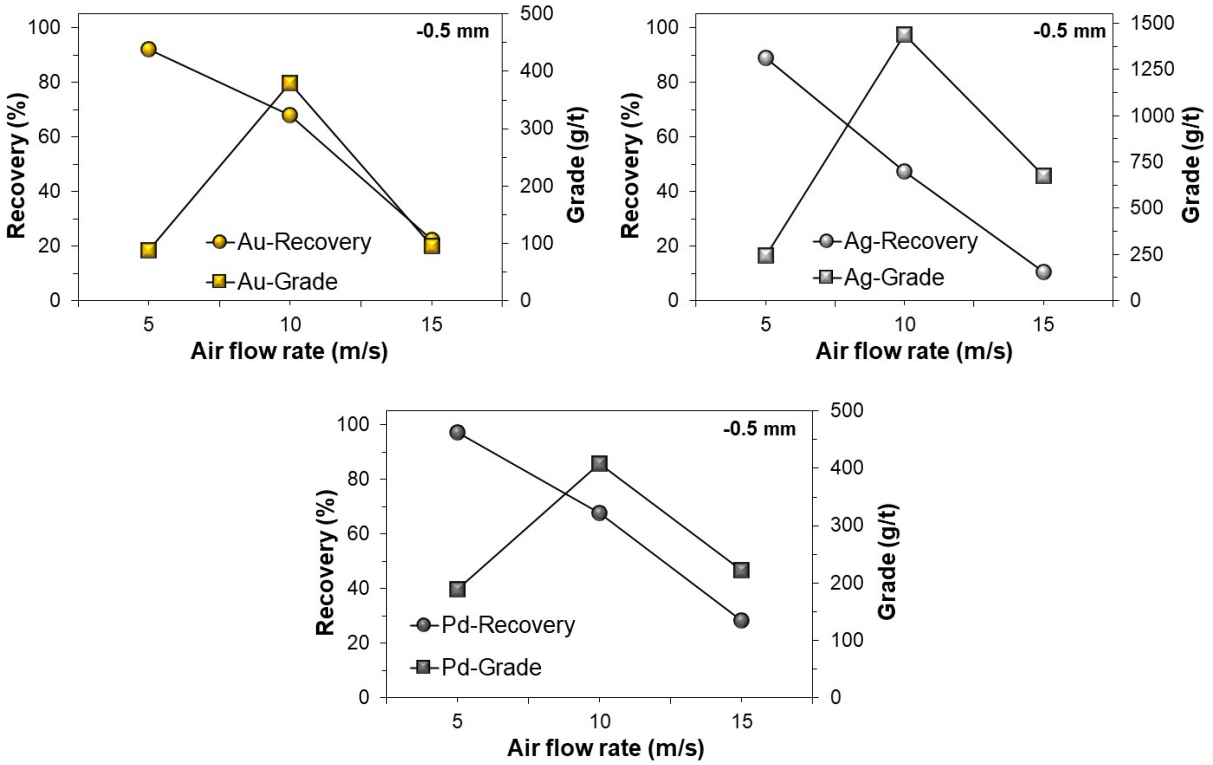


Fig. 4. Recovery (%) and grade (% or g/t) plots for metals at the fine fraction (-0.5 +0.106 mm)

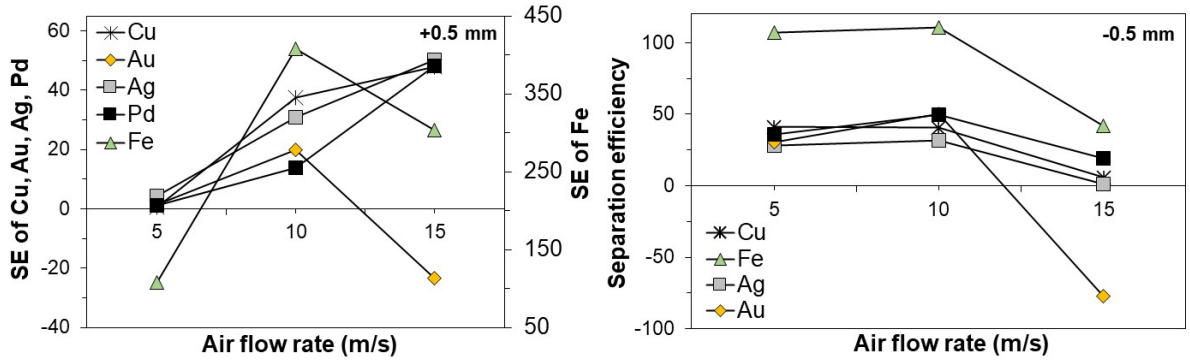


Fig. 5. Effect of air flow rate on separation efficiency of each metal

Fig. 6 also shows the effect of increasing air flow rate on the enrichment ratio of metals and the concentration ratio for fine and coarse fraction materials. Increasing the air flow rate improved the enrichment ratio for all metals at the coarse fraction (-1 +0.5 mm), leading to metal-rich concentrates. However, at the fine fraction, despite the improvement in the enrichment ratio with increasing the flow rate from 5 to 10 m/s, a reduction was observed at 15 m/s. The concentration ratio increased with the air flow rate, independent of the particle size (Fig. 6). This was consistent with the increased quantity of material collected in the overflow stream (i.e., tailings), as the air flow rate increased. Considering high metal, particularly gold, losses at a 15 m/s flow rate, an air flow rate of 10 m/s is the most appropriate for the air separation process.

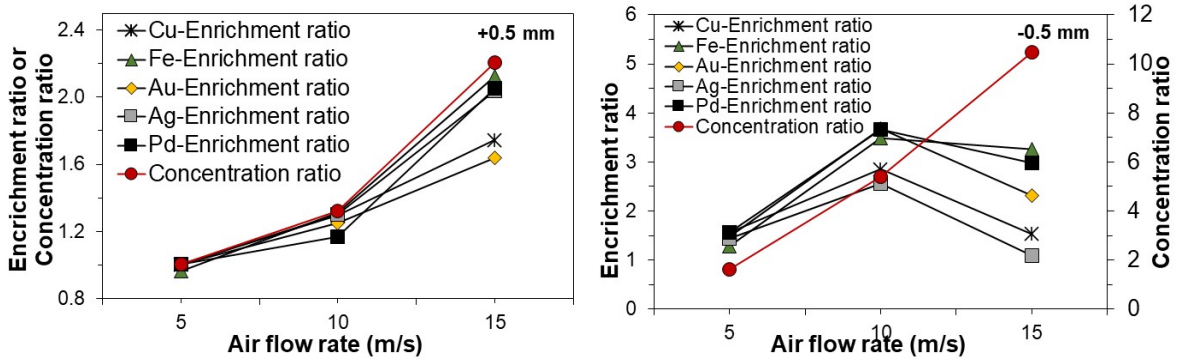


Fig. 6. Effect of air flow rate on enrichment ratio of each metal and concentration ratio

4. Conclusions

Air separation tests were carried out to enrich metals from waste printed circuit boards (WPCBs; -1 +0.106 mm) containing 17.9% Cu, 1.12% Fe, 110 g/t Au, 386 g/t Ag, and 60 g/t P, using a zig-zag air classifier. The results have shown that the separation process is most efficient from the coarse fraction (+0.5 µm) at a 10 m/s air flow rate. At this flow rate, 75.7 wt% of the material was recovered into the concentrate with high metal recoveries (88.2-99.1%). The concentrate contained 52.3% Cu, 4.93% Fe, 1081 g/t Ag, 145 g/t Au, and 161 g/t Pd. These findings demonstrated that a metal-rich concentrate can be produced by zig-zag air separation from WPCBs.

Acknowledgments

The authors would like to express their sincere thanks to the Office of Scientific Research Projects of Karadeniz Technical University for the financial support (Project no: FBA-2020-87865393).

References

Baldé, C. P. Kuehr, R., Yamamoto, T., McDonald, R., D'Angelo, E., Althaf, S., Bel, G., Deubzer, O., Fernandez-Cubillo, E., Forti, V., Gray, V., Herat, S., Honda, S., Iattoni, G., Khetriwal, D. S., di Cortemiglia, V. L., Lobuntsova, Y., Nnorom, I., Pralat, N. & Wagner, M. (2024). *Global E-waste Monitor 2024*. International Telecommunication Union (ITU) and United Nations Institute for Training and Research (UNITAR).Geneva, Bonn.

Chauhan, G., Jadhao, P. R., Pant, K. K. & Nigam, K. D. P. (2018). Novel technologies and conventional processes for recovery of metals from waste electrical and electronic equipment: Challenges and opportunities – A review. *Journal of Environmental Chemical Engineering*, 6 (1) 1288–1304.

Cui, J., Zhang, L. (2008). Metallurgical recovery of metals from electronic waste: A review. *Journal of Hazardous Materials*, 158 (2–3) 228–256.

Das, A., Vidyadhar, A. & Mehrotra, S. P. (2009). A novel flowsheet for the recovery of metal values from waste printed circuit boards. *Resources, Conservation and Recycling*, 53 (8) 464–469.

Deveci, H., Yazici, E. Y., Akcil, A., Erust, C. & Celep, O. (2019). *Physical separation and hydrometallurgical processes for treatment of WEEE*. XXIX. International Mineral Processing Congress, Paper No: 908, Russia.

Drzymala, J. (2007), *Mineral Processing - Foundations of theory and practice*, Wroclaw University of Technology, Poland.

Eswaraiah, C, Kavitha, T., Vidyasagar, S. & Narayanan, S. S. (2008). Classification of metals and plastics from printed circuit boards (PCB) using air classifier. *Chemical Engineering and Processing: Process Intensification*, 47 (4) 565–576

Eswaraiah, C. & Soni, R. K. (2015). Milling and classification of printed circuit boards for material recycling. *Particulate Science and Technology*, 33 (6) 659–665.

European Commission (2023). European Commission, Study on the critical raw materials for the EU 2023 – Final Report. Luxembourg.

Faraji, F., Golmohammadzadeh, R., & Pickles, C. A. (2022). Potential and current practices of recycling waste printed circuit boards: A review of the recent progress in pyrometallurgy. *Journal of Environmental Management*, 316, 115242.

Goosey, M. & Kellner, R. (2002). A scoping study: end-of-life printed circuit boards. Intellect and the Department of Trade and Industry, Makati City.

Gulliani, S.,Volpe, M., Messineo, A. & Volpe, R. (2023). Recovery of metals and valuable chemicals from waste electric and electronic materials: a critical review of existing technologies, *RSC Sustainability*, 1, 1085

Hagelüken, C. (2006). Recycling of Electronic Scrap at Umicore Precious Metals Refining. A*cta Metallurgica Slovaca*, 12, 111–120.

Hagemeier, T., Glöckner, H., Roloff, C., Thévenin, D. & Tomas, J. (2014). Simulation of Multi-Stage Particle Classification in a Zigzag Apparatus. *Chem. Eng. Technol.*, 37: 879-887.

He, Y., Duan, C., Wang, H., Zhao, Y. & Tao, D. (2011). Separation of metal laden waste using pulsating air dry material separator. *International Journal of Environmental Science & Technology*, 8 (1) 73–82.

IEA (2021). The role of critical minerals in clean energy transitions, International Energy Agency (IEA), Paris.

IRENA (2023). Geopolitics of the energy transition: Critical materials, International Renewable Energy Agency, Abu Dhabi.

Işıldar, A., Rene, E. R., van Hullebusch, E. D. & Lens, P. N. L. (2018). Electronic waste as a secondary source of critical metals: Management and recovery technologies. *Resources, Conservation and Recycling*, 135, 296–312.

Işıldar, A., van Hullebusch, E. D., Lenz, M., Du Laing, G., Marra, A., Cesaro, A., Panda, S., Akcil, A., Kucuker, M. & Kuchta, K. (2019). Biotechnological strategies for the recovery of valuable and critical raw materials from waste electrical and electronic equipment (WEEE) – A review. *Journal of Hazardous Materials*, 362, 467–481.

Jang, Y.-C. & Townsend, T. G. (2003). Leaching of lead from computer printed wire boards and cathode ray tubes by municipal solid waste landfill leachates. *Environmental Science & Technology*, 37 (20) 4778–4784.

Kaas, A., Mütze, T. &Peuker, U. A. (2022). Review on zigzag Air Classifier. *Processes*, 10 (4) 764.

Kaya, M. (2016). Recovery of metals and nonmetals from electronic waste by physical and chemical recycling processes. *Waste Management*, 57, 64–90.

Li, J., Xu, Z. & Zhou, Y. (2007). Application of corona discharge and electrostatic force to separate metals and nonmetals from crushed particles of waste printed circuit boards. *Journal of Electrostatics,* 65 (4) 233–238.

Lincoln, J. D., Ogunseitan, O. A., Shapiro, A. A. & Saphores, J.-D. M. (2007). Leaching Assessments of Hazardous Materials in Cellular Telephones. *Environmental Science & Technology*, 41 (7) 2572–2578.

Natural Resources Canada (2022). The Canadian critical minerals strategy - from exploration to recycling: powering the green and digital economy for Canada and the World. 9 Oct.

Ongondo, F. O., Williams, I. D. & Cherrett, T. J. (2011). How are WEEE doing? A global review of the management of electrical and electronic wastes. *Waste Management*, 31 (4) 714–730.

Palanisamy, K. & Subburaj, R.G. (2023). Integration of electronic waste management: a review of current global generation, health impact, and technologies for value recovery and its pertinent management technique. *Environ Sci Pollut Res,* 30, 63347–63367.

Peng, M., Layiding, W., Dong, X., Jiangang, G. & Guanghong, D. (2004). *A physical process for recycling and reusing waste printed circuit boards*. Proceedings of the International Symposium on Electronics and the Environment, IEEE Computer Society, 237–242.

Robinson, B. H. (2009). E-waste: An assessment of global production and environmental impacts, *Science of The Total Environment*, 408 (2), 183-191

Ribeiro, P. P. M., Santos, I. D. Dos & Dutra, A. J. B. (2019). Copper and metals concentration from printed circuit boards using a zig-zag classifier. *Journal of Materials Research and Technology*, 8 (1) 513–520.

Schulz, N. F. (1969). *Separation Efficiency*. Society for Mining, Metallurgy & Exploration, 69-B-44.

Sethurajan, M., van Hullebusch, E. D., Fontana, D., Akcil, A., Deveci, H., Batinic, B., Leal, J. P., Gasche, T. A, Kucuker, M. A., Kuchta, K., Neto, I. F. F., Soares, H. M. V. M. & Chmielarz, A. (2019). Recent advances on hydrometallurgical recovery of critical and precious elements from end of life electronic wastes - a review. *Critical Reviews in Environmental Science and Technology*, 49 (3) 212–275.

Shittu, O. S., Williams, I. D. & Shaw, P. J. (2021). Global E-waste management: Can WEEE make a difference? A review of e-waste trends, legislation, contemporary issues and future challenges. *Waste Management*, 120, 549–563.

Silva, M. de F. da, Dutra, A. J. B. & Borges, M. M. (2019). Enrichment of copper, lead, and tin by mechanical dry processing of obsolete printed circuit board residues. *Materials Research*, 22 (5) 1–7.

Sun, Z., Xiao, Y., Agterhuis, H., Sietsma, J. & Yang, Y. (2016). Recycling of metals from urban mines – a strategic evaluation. *Journal of Cleaner Production*, 112, 2977–2987.

Tuncuk, A., Stazi, V., Akcil, A., Yazici, E. Y. & Deveci, H. (2012). Aqueous metal recovery techniques from e-scrap: Hydrometallurgy in recycling. *Minerals Engineering*, 25 (1) 28-37.

Wen, X., Zhao, Y., Duan, C., Zhou, X., Jiao, H. & Song, S. (2005). *Study on metals recovery from discarded printed circuit boards by physical methods*. Proceedings of the International Symposium on Electronics and the Environment, IEEE Computer Society, 121–128.

Widmer, R., Oswald-Krapf, H., Sinha-Khetriwal, D., Schnellmann, M. & Böni, H. (2005). Global perspectives on e-waste. *Environmental Impact Assessment Review,* 25 (5) 436–458.

Wills, B. A., & Napier-Munn, T. (2006). *Wills' Mineral Processing Technology: An Introduction to the Practical Aspects of Ore Treatment and Mineral Recovery*. Butterworth-Heinemann.

Yazici, E., Deveci, H., Alp, I., Akçil, A. & Yazici, R. (2010). C*haracterisation of computer printed circuit boards for hazardous properties and beneficiation studies*, XXV. International Mineral Processing Congress, Brisbane, 4009-4015.

Yazici, E. Y. (2012). Recovery of metals from e-wastes by physical and hydrometallurgical processes, PhD Thesis, Karadeniz Technical University, Trabzon, Türkiye.

Yazici, E. Y. & Deveci, H. (2016). Economic potential and environmental characterisation of waste of printed circuit boards. *Scientific Mining Journal*, 55 (3) 35-44.

Zhang, S. & Forssberg, E. (1998). Mechanical recycling of electronics scrap - the current status and prospects, *Waste Management & Research*, 16 (2) 119–128.

Zhao, Y., Wen, X., Li, B. & Tao, D. (2004). Recovery of copper from waste printed circuit boards. *Minerals & Metallurgical Processing*, 21, 99-102.

The effect of grinding type on roughness and coagulation of magnesite particles

Halim Recep Kayabaşı [1], Arman Ehsani [1], Burçin Kaymakoğlu [2], Tuğba Deniz Tombal Kara [1], Onur Güven [1*]

[1]Adana Alparslan Türkeş Science and Technology University, Faculty of Engineering, Department of Mining Engineering, 01250, Adana

[2]Adana Alparslan Türkeş Science and Technology University, Faculty of Engineering, Department of Materials Engineering, 01250, Adana

*Corresponding author: oguven@atu.edu.tr (Onur Güven)

Abstract:

Coagulation is one of the most important processes for aggregating the fine particles in a dispersed system via different mechanisms. Many factors such as particle size, morphology, pH, coagulant type, and concentration may affect particle-particle interactions, which will then be effective on their coagulation characteristics. In this study, the effect of grinding type on the roughness of magnesite particles under 38 microns was evaluated for its role in the coagulation of particles under different salt types and concentrations. The results of grinding tests showed that rougher particles could be obtained with a rod mill compared to the particles ground in a ball mill. After grinding of particles, an increasing trend was obtained in terms of settling rate for different salts in an order of $NaCl<CaCl_2<AlCl_3$ during coagulation tests under all concentrations (10^{-3}, 10^{-2}, 10^{-1} and 1 M) at a constant pH value as 8.01±0.2. In sum, the results of this study clearly showed that adjusting the grinding conditions is not only effective on the size and morphology of the particles but also plays a significant role in particle-particle interactions and accordingly their coagulation characteristics.

Keywords: *Grinding, Roughness, Coagulation, Salt*

1. Introduction

Coagulation is a process of reducing the surface charge of particles to bring particles into closer contact in the form of bunches and aggregates. It is also of utmost importance in ore preparation and enrichment processes (Bratby et al., 2006). These processes enhance operational efficiency by facilitating the aggregation of very fine-sized particles, particularly before sedimentation and filtration (Khazaie et al., 2022). However, for the success of this process, not only chemical parameters but also the physical properties of particles should be considered (Uysal et al., 2021). While numerous studies in the literature focus on chemical parameters affecting coagulation efficiency, there is limited information available regarding the influence of particle morphology on these processes (Hassas et al., 2021).

As well known, during basic steps of mineral processing like grinding, the aim is to produce particles within a specific size range for future enrichment processes like gravity separation, flotation, leaching, etc. However, in addition to particle size, the changes in morphological properties of particles like shape and roughness will be effective for adjusting the enrichment of the aforementioned processes (Guven et al., 2015). Thus, advantageous roughness properties would improve the efficiency of processes such as the “coagulation” process at even lower coagulant concentrations. This approach is expected to yield positive results both technically and economically, and it is anticipated to contribute to the advancement of industrial processes.

In this context, the most common traditional laboratory procedure for assessing solid-liquid separation is the batch cylinder test. Batch settling tests (BSTs) are used to obtain detailed information on the sedimentation behavior (e.g. settling velocity) of suspensions. Generally, a suspension is flocculated within a measuring cylinder and the settling rate is determined from the rate of fall of the mud-line. With a given initial settling rate and the value of critical point, BSTs have been a major step in sizing thickeners and clarifies. These tests are important steps in estimating compressive yield stress and hindered settling function. It is also reported that the coagulation of particles before filtration increases the filtration efficiency (Hassas et al., 2016).

In this manner, the primary aim of this study is to provide a fresh perspective on the impact of particle morphology on coagulation processes in the literature and to translate this knowledge into practical applications. For this aim,

the effects of coagulant type and concentration will be examined experimentally along with the effects of particle roughness. Considering that, the main objective of this study is to obtain meaningful results for magnesite mineral by conducting coagulation experiments under the same conditions but with varying degrees of roughness.

2. Materials and Methods

Magnesite samples used in this study were obtained from KÜMAŞ Magnesite Co., Kütahya, Turkey. X-ray diffraction Analysis (XRD) using the Rigaku-Miniflex XRD unit determined the crystallinity of the sample. The radiation applied was CuKα from a long fine focus Cu tube, operating at 40 kV and 15 mA (i.e., 600 W x-ray tube) while the 2θ range (5-90°) and the scanning speed were adjusted to 2º/min. The XRD results of the sample revealed that the samples were mainly composed of magnesite with impurities in trace quantities (Figure 1).

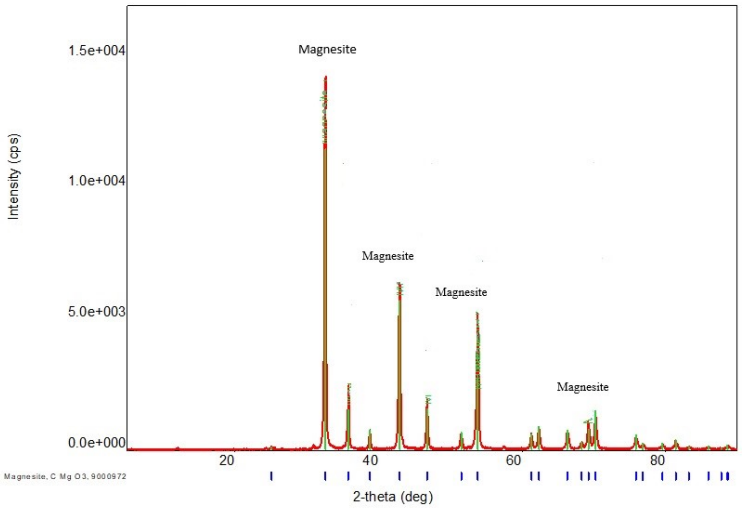


Figure 1. XRD peaks for magnesite sample.

Before grinding tests, the size distribution of the feed sample was determined via sieves with apertures of 1, 0.500, 0.212, 0.150, 0.106, 0.075, and 0.038 mm. As shown in Figure 2, the d_{80} of the sample was very close to 0.300 mm while the d50 of the sample was found as 0.150 mm. Considering these values, the particle size distribution) of crushed material indicated that the presence of fines (<0.038 mm) in the feed material was negligible. Following the determination of feed size, to adjust the size range suitable for coagulation tests, the sample was ground under 0.038 mm by adapting different grinding medium types such as rod and ball mill. In these tests, in addition to size reduction, the contribution of the grinding type on the roughness of the particles was investigated.

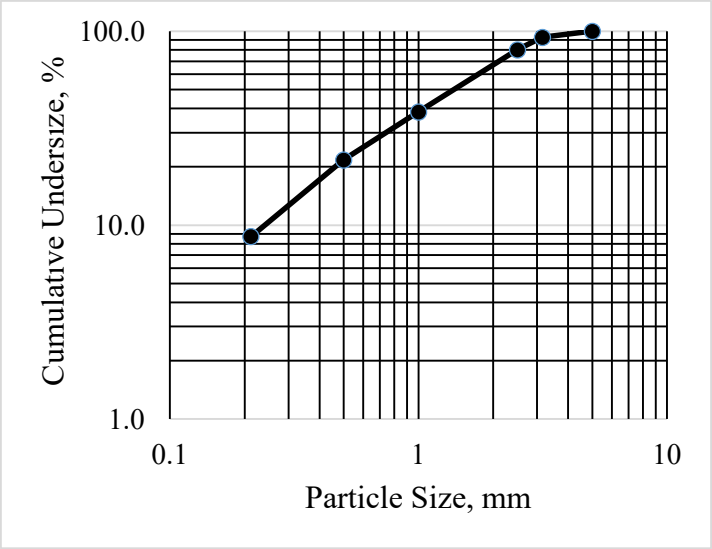
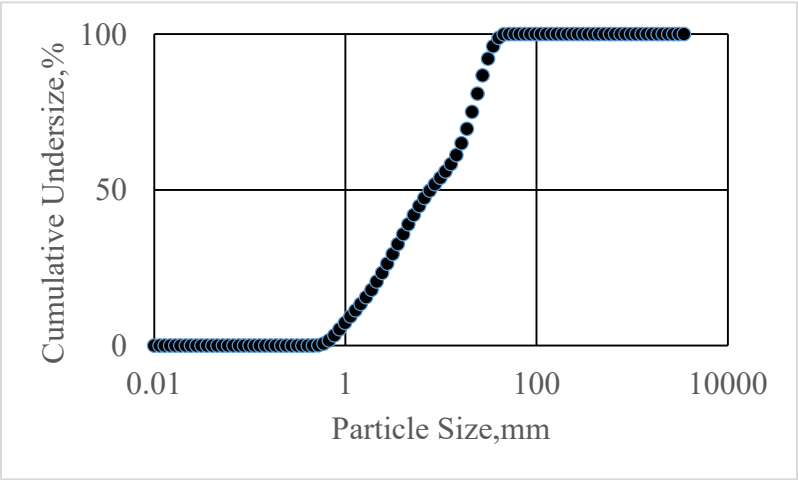


Figure 2. The size distribution of feed sample to grinding processes.

During these tests, a laboratory-type ball mill with a volume of 5224 cm^3 (D=19.5 cm, H=17.5 cm) was used with a mixture of steel balls (which were 30, 25, and 20 mm in diameter and 816 g in weight), and a laboratory-type rod mill with a volume of 7850 cm^3 (D=20 cm, H=25 cm) with steel rods (which were 31.7 mm, 24.6mm, 15.9 mm, and 9.8 mm in diameter). The mill feed sub-samples were ground for different durations under both grinding conditions, after which material below 0.038 mm was separated from each grinding step material using wet screening. Consequently, size analysis was performed using the Malvern Particle Sizer 3000 with a wet analysis unit.



As can be seen from the particle size distribution (PSD) graphics of ground particles in the ball and rod mill, while the d_{80} sizes were around 30 microns for each one, the d_{50} sizes of the particles were measured as 10 microns on average. From this point of view, it can be concluded that the roughness can be studied while the effect of size distribution can be dismissed during the evaluation of results.

2.1. Profilometer

The surface roughness values of pellets formed with the ground particles with different grinding mediums were determined with the contact profilometer device (Mitutoyo SV-2100 model, Japan). This instrument measures the average roughness (Ra) of surfaces by scanning across the surface of pellets made of − 38 sized particles. Thus,

pellets were prepared under constant conditions such as pelletizing pressure (10 bar) and time (5 min). To show the repeatability of the analysis, the average of at least 10 measurements was shown with standard deviation bars.



Figure 3. Rod and Ball Mill Ground Magnesite Particles in Pellets Formed

2.2. Settling Tests:

For each sedimentation test, 100 ml of deionized water was used at a solid concentration ratio of 1%. Sedimentation tests were applied to samples taken from two different mill outputs to observe the effect of grinding and morphology on coagulation. All tests had the same conditions for both ball and rod mill output samples. Parameters considered included pH and salts with different concentrations. These parameters were selected because coagulation primarily involves two mechanisms: neutralization of surface charge and double-layer compression. To induce coagulation and observe the effect of zeta potential, the pH of the prepared salt solutions were initially adjusted. Different salt types and concentrations were considered to observe the effect of the second mechanism on coagulation. In these tests, the pH was adjusted using NaOH to create basic conditions, with a pH value set at approximately 8. The second part of these tests involved different types of salts (NaCl, $CaCl_2$, and $AlCl_3$) at various concentrations. Sedimentation tests were conducted for all salt concentrations.

2.2.1. Settling rate tests

These tests were conducted in a specially designed cylindrical glass cell of 100 mL. In all experiments, the total solution (solid+liquid) was prepared in the form of 100 mL mixtures at a certain % solids by wt. as 1 % and salt concentrations at a natural pH of respective mineral suspensions using distilled water. A series of systematic experiments were carried out with samples of -38 µm particle size. For each test, freshly prepared salt solutions were prepared on a magnetic stirrer at a medium speed of 360 rpm for 5 min. The conditioned 100 mL sample was transferred into the cylindrical glass cell. Before starting the measurement, the cell was gently shaken laterally from right to left 5 times to ensure the dispersion of the particles. Observational measurements were made every 15 sec. The average values obtained were recorded for constructing distance-time curves. The average settling rate in that particular collector concentration and % solids by wt. was obtained from the slope of the curve, and concentration-dependent logarithmic “Sedimentation Rate” curves were drawn.

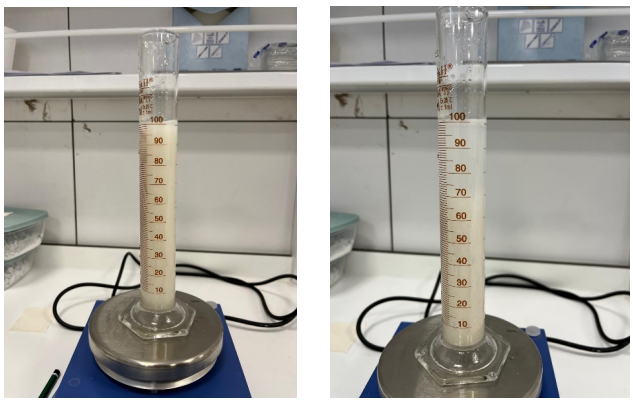


Figure 4. Settling Rate Experiments of Magnesite Particles.

3. Results and Discussion

3.1. Profilometer

Roughness characterization includes measurements such as average roughness (Ra) and other roughness parameters like skewness (Rsk) and kurtosis (Rku). While the average roughness value is generally used to express the roughness characteristics of materials, other parameters like skewness and kurtosis are used for more specific surface characterization. The roughness values of magnesite samples are provided in the table below.

Table 1. Roughness Values (Ra) of Magnesite samples

Material Type and Grinding Media	Average Roughness (Ra) Values (µm)
Magnesite (Rod Mill)	2,2391
Magnesite (Ball Mill)	1,8835

3.2. Coagulation Tests

Before tests for the effect of salt type, and salt concentration on the coagulation of fine-ground magnesite particles with varying roughness values, different series of tests were adapted as a function of pH and solid wt. % in the suspension with distilled water to determine the optimum conditions for targeted tests. In these primary tests, the settling method was used. The results of these tests are shown in Figure 5 respectively.

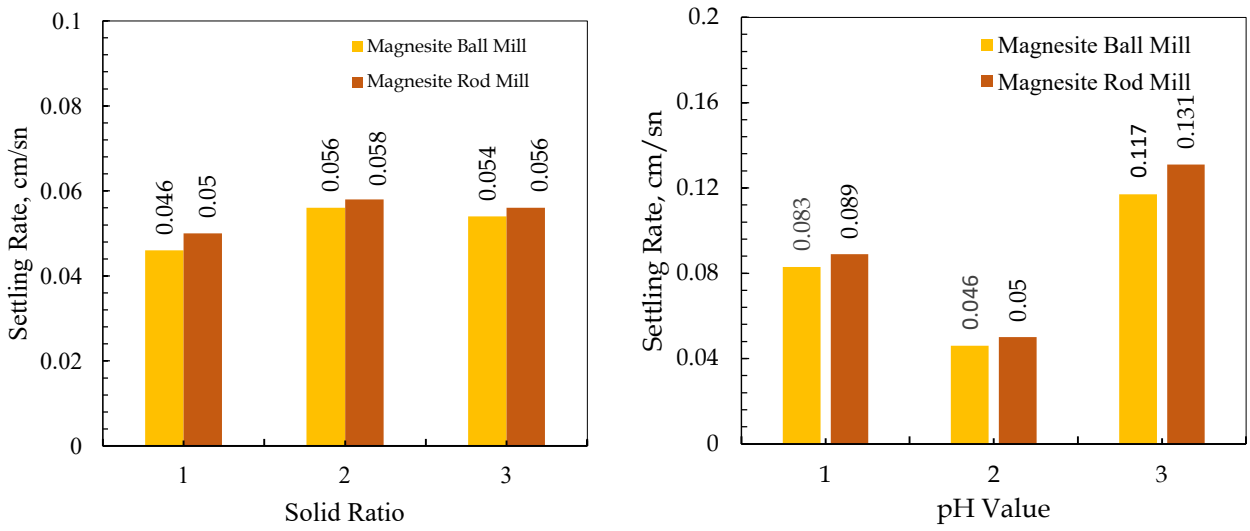


Figure 5. The effects of Solid Ratio and pH value on coagulation characteristics of magnesite samples ground in different grinding medium type

As can be seen from the results shown for ball and rod-milled samples, the general trend is that the rod-milled products settle faster than ball-milled products, which in turn is a function of their roughness values. On the other hand, considering the values obtained for different conditions as solid wt. percentage and pH, generally, the minimum values obtained in solid wt. percentage parameters were taken as a reference for future tests to show the contribution of salt concentration and accordingly the contribution of double-layer compression for coagulation efficiency and therefore particle-particle interactions. Although lower settling rate values were obtained within acidic pH range values, remaining tests were performed at the original pH values of the samples to prevent the possible compression effect of salts during the coagulation of particles. Hence, in this way, a better comparison could be obtained for different salt types and roughness values of particles.

As mentioned above, finely ground magnesite samples in different mills presented different roughness values. To calculate the settling rate based on roughness, solutions with different salt types molar values were prepared. These prepared solutions are respectively NaCl, $CaCl_2$, and $AlCl_3$ salt concentrations.

3.3. The Effect of Salt Type and Concentration on Settlement Rate of Magnesite

The effects of NaCl, $CaCl_2$, and $AlCl_3$ salts on the precipitation rates of magnesite sample are compared. In this comparison, the precipitation rates of products from ball mill and rod mill were analyzed using solutions with different molarities. The results of these tests is shown in Figure 6.

When distilled water is used, the lowest precipitation rates are observed. For magnesite, the underflow from the ball mill has a rate of 0.046 cm/s, and from the rod mill, it is 0.050 cm/s. These results indicate that natural water does not sufficiently reduce the electrostatic repulsion forces between particles, hence resulting in lower precipitation rates.

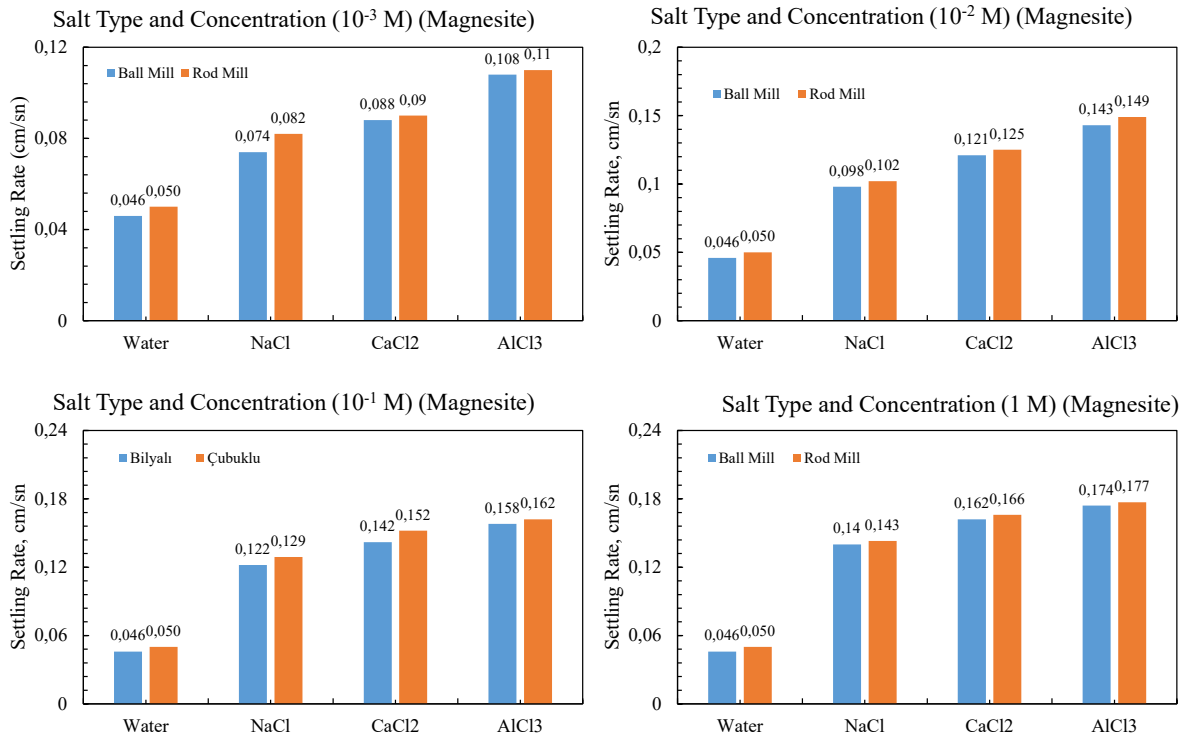


Figure 6. The effects of NaCl, $CaCl_2$, and $AlCl_3$ salts on the precipitation rates of magnesite samples

When NaCl solution is used, the precipitation rates increase compared to distilled water. As it can be seen from the Figure that the product from the ball mill has a rate of 0.074 cm/s, and from the rod mill, it is 0.082 cm/s. This increasing trend clearly shows that NaCl salt reduces the electrostatic repulsion forces between particles, thereby increasing the precipitation rate.

$CaCl_2$ solution provides slightly higher precipitation rates compared to NaCl solution. As it can be seen from the Figure that while the product from the ball mill has a rate of 0.088 cm/s, and the product from the rod mill, it is 0.090 cm/s. This indicates that $CaCl_2$ more effectively reduces double-layer compression than NaCl, resulting in faster precipitation.

Compared to other salt types, the highest precipitation rates are observed when AlC_3 solution is used. For magnesite, the underflow from the ball mill has a rate of 0.108 cm/s, and from the rod mill, it is 0.110 cm/s. $AlCl_3$ effectively reduces the electrostatic repulsion forces between particles, maximizing the precipitation rate.

In conclusion, the graph illustrates that the types of salts and mill types have significant effects on precipitation rates. $AlCl_3$ provides the highest precipitation rates, while $CaCl_2$ and NaCl also show significant improvements. Distilled water provides the lowest precipitation rates. Additionally, rod mill products generally have higher

precipitation rates than ball mill products, suggesting that rod mills can produce rougher particles and thus facilitate faster precipitation. These results demonstrate that salts and grinding methods are important factors in optimizing particle precipitation rates.

4. Conclusion

-The roughness values of magnesite particles increased with the usage of a rod mill compared to grinding with a ball mill.

- The settling rate of particles exhibited a minimum at low solid wt. % while an average value was obtained under the original pH values of particles.

- The addition of mono and multi-valent salts enhanced the coagulation of both rougher and smoother particles in the order of $NaCl<CaCl_2<AlCl_3$. However, rougher particles produced higher settling rates in the presence of the same salt concentration.

-In addition to settling tests, the same trend was also obtained as the results of jar test experiments.

-The overall results suggested that the adjustment of milling methods to obtain rougher particles is one of the key parameters to control the particle-particle interaction and accordingly their coagulation characteristics regardless of coagulant type.

Acknowledgments

This study is supported by The Scientific and Technological Research Council of Turkey (TUBITAK) with Project Number 2219A.

References

Bratby, J. (2006). Coagulation and Flocculation in Water and Wastewater Treatment. London: IWA Publishing.

Guven, O., Celik, M.S., Drelich, J. (2015). Flotation of methylated roughened glass particles and analysis of particle-bubble energy barrier. Mineral Engineering, pp. 125-132.

Hassas, B.V., Caliskan, H., Guven, O., Karakas, F., Cinar, M., Celik, M.S., (2016). Effect of roughness and shape factor on flotation characteristics of glass beads. Colloids and Surfaces A: Physicochemical and Engineering Aspects.

Hassas, B.V., Guven, O., Basturkcu, E., Celik, M.S., 2021. Morphological changes of glass bead particles upon an abrasive blasting as characterized by settling and flotation experiments. Physicochemical Problems of Mineral Processing, 57,2, 157-168.

Khazaie, A., Mazarji, M., Samali, B., Osborne, D., Minkina, T., Sushkova, S., Mandzhieva, S., Soldatov, A. (2022). A Review on Coagulation/Flocculation in Dewatering of Coal Slurry. Water, 14, 918.

Uysal, T., Guven, O., Ozdemir, O., Karaagaclioglu, I.E., Tunç, B., Celik, M.S., 2021. Contribution of particle morphology on flotation and aggregation of sphalerite particles. Minerals Engineering, 165, 106860.

Beneficiation Performance of Heterogenous Ore Grades from a REE-Carbonatite Deposit

Ezgi Akyildiz [1]*, Stefanie Lode [1], Camilo M. Silva [1], Kornel Tobiczyk [1], Pshem Kowalczuk [1]

[1] Norwegian University of Science and Technology (NTNU), Department of Geoscience and Petroleum, S.P. Andersens vei 15a, Trondheim, 7031, Norway

*Corresponding author: ezgi.akyildiz@ntnu.no (Ezgi Akyildiz)

Abstract:

Major economically exploitable rare earth element (REE) deposits in the world are related to igneous rocks, especially to carbonatites. Carbonatites are rich sources of REE and niobium, with a characteristic enrichment of light REE (LREE) over heavy REE (HREE). In this paper, sample materials were collected from a carbonatite-hosted REE deposit with the potential to be one of the largest REE resources across Europe. While bastnäsite and monazite are the primary REE minerals (REM) found in more than half of carbonatite related REE deposits, parisite is the predominant REM in the mineralized rock under investigation. Within the study, samples with two different ore grades (2.9 (feed-A) and 0.3 wt.% (feed-B) of total rare earth oxides – TREO) were evaluated through beneficiation tests. The feed materials were prepared and characterized using a chemical analysis method (portable X-ray fluorescence spectrometer-pXRF), alongside mineralogical characterization conducted via scanning electron microscopy-based automated mineralogy (SEM-AM). The beneficiation tests were tailored according to mineralogical data. The study aimed to evaluate the impact of mineralogical variations in REE beneficiation to determine potential separation alternatives. Automated mineralogy results revealed variability in target mineral concentrations within the deposit, indicating the need for tailored processing strategies. Preliminary tests using experiment-1, which excludes a pre-concentration step, showed that Feed-B required additional grinding due to its complex mineral matrix. Achieving a particle size below 150 µm was sufficient for high recovery and concentration of REE in Feed-A. For Feed-B, further grinding improved recovery rates and eliminated the need for an extra cleaning step, simplifying the process. A comparison of flotation performance and gravity concentration of REM with results from the Mozley table demonstrates that flotation of the finely ground feed-B is more efficient than both gravity separation and the combined experiment (experiment-3). Gravity separation primarily functioned only as a de-sliming step, as it removed fine particles and reduced REE recovery. The study concluded that fine particles (finer than 25 µm) do not negatively affect flotation, allowing efficient processing with adjusted flotation time.

Keywords: *Rare earth elements, rare earth minerals, critical raw materials, automated mineralogy, mineral processing*

1. Introduction

Rare earth elements (REE) are critical to numerous advanced technologies, making their extraction and efficient processing vital to meeting global demand. Most economically viable REE deposits are associated with igneous rocks, particularly carbonatites, which are notably rich in light REE (LREE) such as lanthanum (La) to europium (Eu) (Wang et al., 2020). Nine percent of carbonatites and alkaline-carbonatite complexes are actively or historically exploited and represent targets for exploration, not only REE but also other commodities (Simandl and Paradis, 2018). Of this fraction, three percent contain historic mines with significant potential for further exploration (Simandl and Paradis, 2018.). However, the overall grade of both currently exploited and newly discovered mineral deposits has been decreasing (Gandhi and Sarkar, 2016). This brings additional limits on potential processing methods due to more complex mineralogy and finer liberation size (Bradshaw, 2014). Exploiting economically important low-grade mineral deposits requires the development of processing flowsheets capable of handling fine particles effectively (Farrokhpay et al., 2021). The grinding step for adequate liberation

must be carried out carefully to avoid the production of ultra-fine particles. As particle size decreases to liberate finely distributed target minerals, the range of suitable processing techniques becomes more limited (Jordens et. al, 2013). Among these methods, froth flotation stands out as one of the most effective processing methods to handle fine particles (Wills, 2016). Physical pre-concentration methods, including gravity, magnetic, and electrostatic separation techniques, are often employed to remove unwanted gangue particles early in the separation process. These methods help to provide a relatively higher feed grade, thereby increasing the efficiency of subsequent processes (Abaka-Wood et al., 2021; Alsabbagh and Mustafa, 2023; Filippov and Filippova, 2016; Jordens et al., 2014) Gravity separation is one of the most common pre-concentration methods for REM with low capital and operational costs (Marion et. al, 2018). Due to recent advancements, centrifugal gravity concentrators can now treat particles as small as 15 µm, while air classifiers can handle particles down to 3 µm (Das and Sarkar, 2018).

In this study, the goal was to assess how mineralogical variations affect rare earth minerals (REM) beneficiation, with the intention of identifying potential separation alternatives. Preliminary experimental tests using experiment-1, which does not include a pre-concentration step, were applied to both feed materials. It was observed that Feed-B required additional grinding to effectively liberate REM from the gangue minerals, suggesting a more complex mineral matrix that demands finer grinding for optimal mineral separation. For Feed-A, reducing the particle size to below 150 µm was sufficient to achieve a high recovery rate and a substantial concentration of REEs through experiment-1. In contrast, for Feed-B, further grinding significantly enhanced both the recovery rate and concentration of REE. This improvement made it possible to eliminate an additional cleaning step, thereby simplifying experiment-1 and potentially lowering operational costs. Gravity separation was tested as a pre-concentration step for REM from the low-grade Feed-B prior to flotation. However, it primarily removed fine particles and negatively impacted the flotation process by discarding a significant amount of REE in the rejected light fraction, proving ineffective for its intended purpose. Comparing the results from different experiments, it was concluded that fine particles do not negatively affect the flotation process. This suggests that particles finer than 25 µm can be effectively processed without compromising the overall efficiency of mineral recovery, given adjustments to the flotation time.

2. Materials and methodology

2.1. Materials and reagents

Both feed materials were obtained from a historic Fe-Nb ore mine. The feed materials containing 2.9 and 0.3 wt.% of TREO will hereafter be referred to as feed-A and feed-B, respectively. The TREM content in feed-A is 3.9 wt.%, whereas in feed-B, it is 0.9 wt.%. Both materials were ground to a particle size below 150 µm, based on the preliminary flotation tests on various size fractions, for characterization and beneficiation tests. Following the flotation tests on feeds ground to below 150 µm, feed-B was further ground to ensure that 90% of its particles were below 88 µm to improve liberation.

Benzohydroxamic acid (BHA) and Aero® 6493 were used as collectors. Na-silicate, Na-carbonate, and citric acid were used as depressants while Brij 58 was used as frother. NaOH was used to adjust pH during flotation tests.

The feed materials were ground below 150 µm for the characterization and beneficiation tests ($d_{90,\ \text{feed-A}}$ =140 µm and $d_{90,\ \text{feed-B}}$ = 123 µm). Based on the flotation test results, further grinding studies were conducted on feed-B. It was ground in a ball mill for 15 (d_{90} = 151 µm), 30 (d_{90} = 88 µm), and 45 minutes (d_{90} = 72 µm), then sieved into fractions to determine the TREO distribution in different size fractions.

2.2. Methods

2.2.1. Beneficiation tests

Since the flotation method was effective in producing a concentrate with a satisfactory content for feed-A, gravity separation was carried out to assess the potential of this method as a pre-concentration step specifically for feed-B. A Mozley mineral separator was utilized under the following conditions: a wash

water flow of 4 liters/min, a speed of 110 rpm, and an amplitude of 6.3 cm. The conditions were determined based on the preliminary tests.

Based on previous experimental trials, the rougher flotation tests were run using a Maelgwyn mechanical flotation device with a 1.2 l cell, 2000 rpm, and an airflow of 150 l/h with a 20% solids ratio (Silva et al., 2023). The cleaner step was conducted with the same flotation device using a 0.6 l cell, 1600 rpm, and 50 l/h. During conditioning, after the addition of the depressants: Na-silicate, Na-carbonate, and citric acid, pH values were measured and adjusted for the best flotation performance. In experiment-1, flotation was performed with one rougher stage and two cleaner stages, without any pre-concentration step. In experiment-2, flotation involved one rougher stage followed by one cleaner stage. Experiment-3 included a pre-concentration step before flotation, which then proceeded with one rougher stage and one cleaner stage. Experiment-1 was applied to both feed materials, while experiment-2 and experiment-3 were conducted using only feed-B to enhance separation. All experiments were carried out twice. The products obtained by the beneficiation tests were filtered, dried at 80 °C for 12 hours, weighed, and analyzed via pXRF.

2.2.2. Particle size analysis

The particle size distribution of ground ores was measured by Malvern Panalytical Mastersizer 3000. Each sample was measured 10 times, and the average of these measurements was used to determine the particle size distribution.

2.2.3. Mineralogical analysis

SEM-based automated mineralogy (SEM-AM) for feed-A was performed in the Norwegian Laboratory for Minerals and Materials Characterization (MiMaC) at the Department of Geoscience and Petroleum, NTNU. Feed-B was analyzed at the Federal Institute for Geosciences and Natural Resources (BGR). The analyses were performed using a ZEISS Sigma 300VP field emission SEM equipped with two Bruker X-flash 6|60, 129 eV EDS detectors and ZEISS Mineralogic Software v.1.08.02, Mining plug-in. The following microscope settings were used: 8.5 mm working distance (WD), 20kV acceleration voltage, and an aperture of 120 µm. The step size was set to 2 µm due to fine intergrowths of various minerals. For the investigations via SEM-AM, grain mounts were prepared as polished blocks of samples mixed with epoxy (Logitech 2 Part Epoxy Resin Type 301) in pucks of 30 mm diameter.

2.2.4. Chemical analyses

All products obtained from flotation tests and the feed materials were analyzed via a Niton XL3t hand-held X-ray fluorescence spectrometer (pXRF) using the Ta/Hf calibration from Thermo Scientific on pressed powders. ICP-MS analyses of feed materials were done by using a PerkinElmer SCIEX — ELAN DRC-II spectrometer featuring axial field technology. Approximately 0.4 g of material from each sample was digested in HNO_3 solution at 85 °C for 20 hours for conducting ICP-MS analyses. Cerium oxide (Ce_2O_3), lanthanum oxide (La_2O_3), praseodymium oxide (Pr_2O_3), and neodymium oxide (Nd_2O_3) were used to calculate the total REO (TREO) with a conversion factor of 1.17 (Silva et al., 2023).

3. Results and discussion

3.1. Mineralogical analysis of the feed materials

3.1.1. Modal mineralogy

The mineralogical analysis revealed that parisite is the main and monazite is the secondary REM in both feeds. However, the relative amount of monazite in the feed-B is higher than in feed-A. TREM content in the feed-A is 3.9 wt.% while it is 0.9 wt.% for the feed-B. Mineral maps obtained by SEM-AM of ground ores with a particle size smaller than 150 µm are shown in Fig. 1. Ferroan dolomite, ankerite, and calcite are the main gangue minerals, with feed-B containing significantly more calcite than feed-

A. The modal mineralogy and the relative amount of REM in the ores are presented in Fig. 2. Table 1 provides the chemical formulas and densities of the minerals, sorted from the main REM to the gangue minerals. Considering the mineralogical distribution for developing a theoretical flowsheet, feed-B emerged as a promising candidate for a pre-concentration trial. The higher amount of calcite, a gangue mineral with the lowest density, suggests that gravity separation could be a potential step to produce a richer feed for flotation tests with feed-B. The mineralogical analysis of two distinct rock samples could show considerable variability in the concentration of target minerals across the deposit.

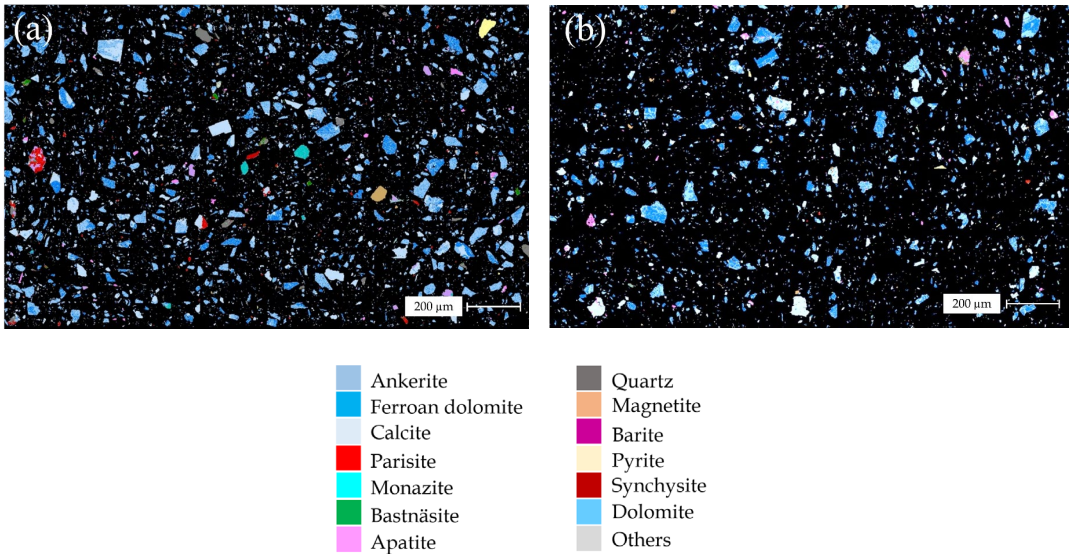


Figure 1. Mineral maps of ground feed-A (a) and feed-B (b) obtained by SEM-AM.

The concentration criterion (Δρ) for gravity separation can be calculated based on Eq. 1 where ρh is the density of the heavy mineral, ρl is the density of the light mineral, and ρf is the density of the fluid medium. The densities of the target minerals (parisite, monazite, bastnäsite, and synchysite) in both ores range from 3.9 to 5.7, while the densities of the main gangue minerals (ankerite, calcite, and ferroan dolomite) range from 2.4 to 2.8 g/cm ^{3}. Consequently, this yielded a concentration criterion of bigger than 2, based on Eq. 1, which is considered suitable for gravity separation (Wills, 2016). Therefore, gravity separation was applied to feed-B to assess the potential for producing a pre-concentrate for flotation and selective removal of gangue minerals with smaller densities.

$$\Delta\rho = \frac{\rho h - \rho f}{\rho l - \rho f} \quad (1)$$

$$\Delta\rho = \frac{4.5 - 1}{2.6 - 1} = 2.18$$

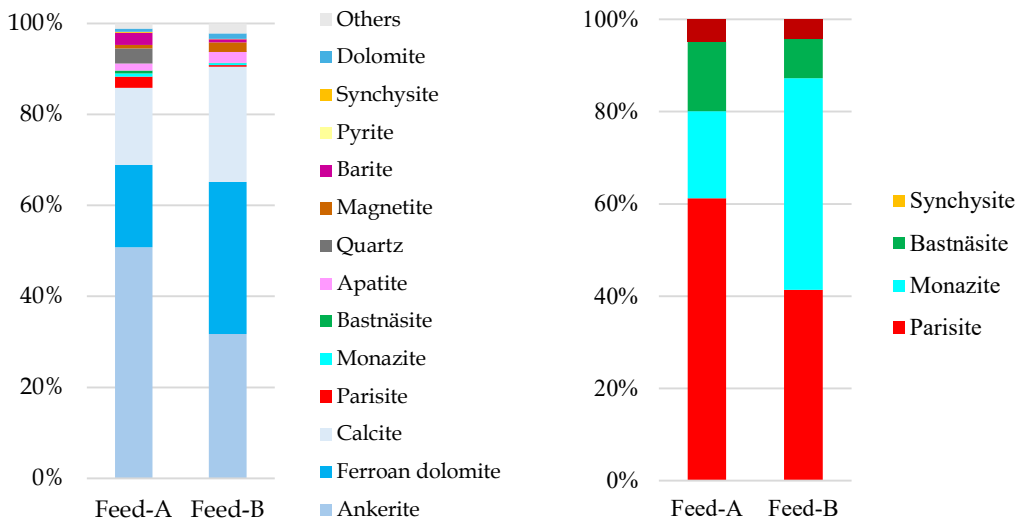


Figure 2. Modal mineralogy and relative amount of REM in the feeds.

Table 1. Chemical formula and densities of minerals sorted starting from the main REM and gangue minerals (Drzymala, 2007; Abaka-Wood et al., 2019).

Mineral name	Chemical formula	Density (g/cm^3)
Parisite	$Ca(Ce,La,Nd)_2(CO_3)_3F_2$	4.3
Monazite	$(Nd,La,Ce)PO_4$	4.6-5.7
Bastnäsite	$(Ce,La,Nd,Y)(CO_3)F$	4.9-5.2
Synchysite	$Ca(Ce,La,Nd)(CO_3)_2F$	3.9
Ankerite	$Ca(Fe,Mg,Mn)(CO_3)_2$	3
Calcite	$Ca(CO_3)$	2.7
Quartz	SiO_2	2.6
Barite	$BaSO_4$	4.5
Magnetite	Fe_3O_4	5.1
Apatite	$Ca_5(PO_4)_3(Cl,F,OH)$	3.1
Pyrite	FeS_2	5

3.2. Liberation analysis

Exposed particle perimeters were used to assess the liberation degree of the minerals in the ground rocks with a particle degree below 150 µm. The particles with an exposed perimeter of more than 90% were classified as liberated, the particles with an exposed perimeter between 90% - 30% were classified as composites and the particles with and lower than 30% of the exposed perimeter were classified as locked. The degree of liberation based on partial perimeter for main REM in the ores is given in Fig. 3. Liberation analysis revealed that less than 3% and less than 2% of parisite mineral particles were completely liberated in the mineralized rocks in feed-A and feed-B, respectively. Monazite, mostly in composite form, is more liberated than parisite in both feeds. The remaining REM were found to form complex composite particles with the gangue minerals, presenting potential challenges for physical separation. Liberation analysis results, along with the modal mineralogy, were used to develop the theoretical beneficiation flowsheet for the feed samples. Hence, feed-B was further ground to enhance the liberation of target minerals.

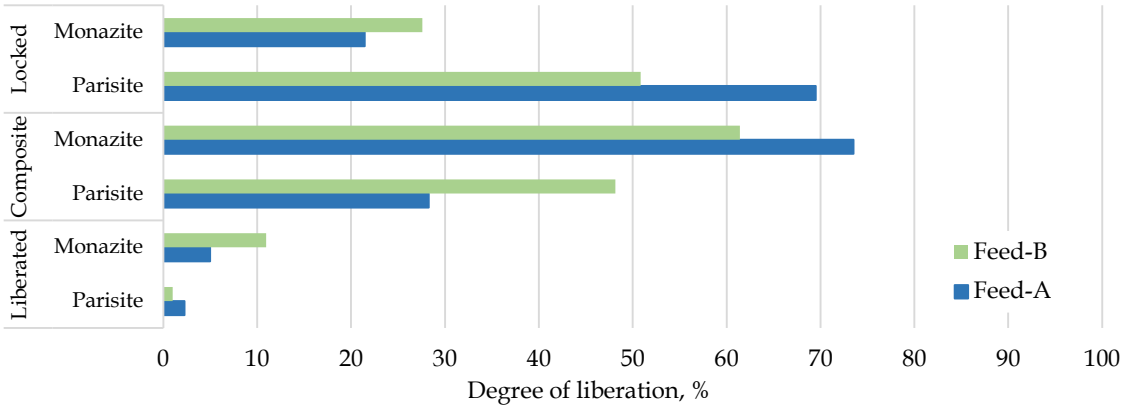


Figure 3. Degree of liberation based on partial perimeter for main REM in the ores. "Liberated" (≥90% liberated); "Composite" (30% to 90% liberated); "Locked" (≤30% liberated).

3.3. Chemical analysis of feed materials and beneficiation products

TREO wt.% of feed-A was 2.9 whereas feed-B contained %0.3. Cerium and lanthanum are the main REE in both mineralized rocks.

Both ores with a particle size below 150 µm were treated according to experiment-1, which included two cleaner flotation steps following the rougher stage. The flotation test on feed-A yielded a concentrate with 44.1 wt.% TREO and an 86% recovery rate, whereas feed-B yielded a concentrate with 7 wt.% TREO and a 39% recovery rate. This indicates the exposed surface of target minerals was insufficient for effective flotation and further improvement was possible for feed-B (Fig. 5). It was further ground to enhance the liberation, and then sieved into fractions to determine the TREO distribution in different size fractions. TREO distribution in these fractions was analyzed using pXRF, as depicted in Fig. 4. The 30-minute grinding time was chosen for beneficiation tests because it was found that most of the REM were concentrated in particles smaller than 74 µm.

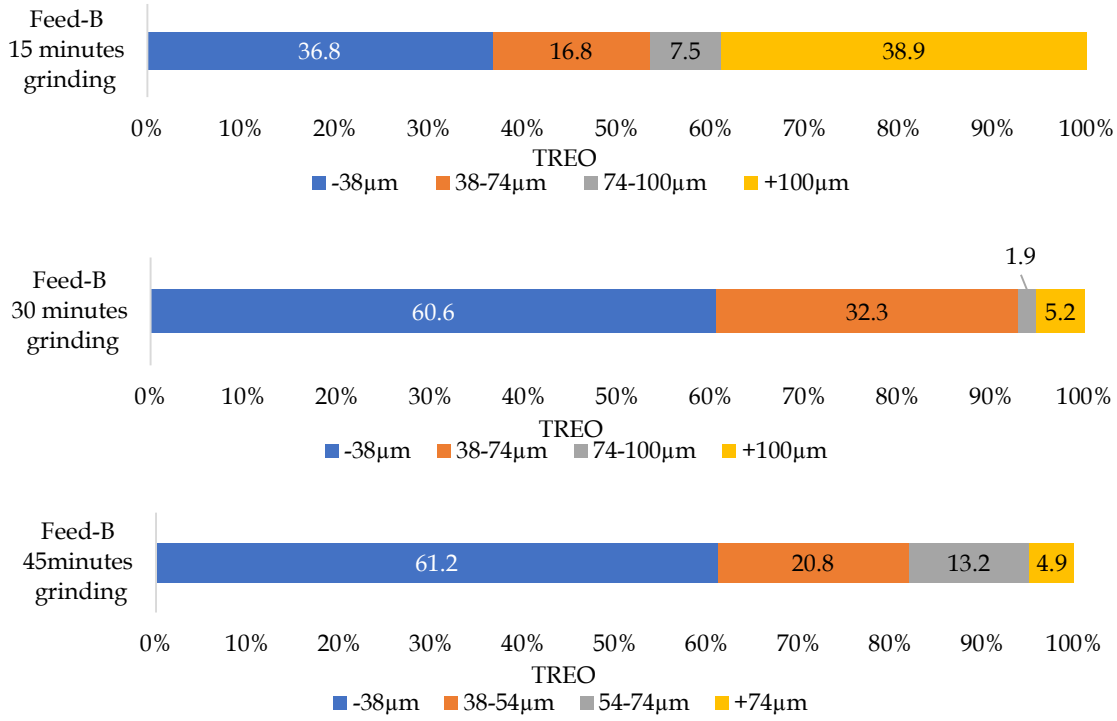


Figure 4. TREO % distribution via pXRF in different particle size fractions of feed-B ground for 15, 30, and 45 minutes in the ball mill (based on pXRF).

According to experiment-3, gravity separation was applied to feed-B using a Mozley mineral separator to remove barren gangue minerals. The feed sample was ground for 30 minutes and the test was conducted twice under the same conditions to minimize experimental error. In the first test, the light fraction contained 0.03 wt.% of TREO with a recovery rate of 4.8%, while the heavy fraction contained 0.14 wt.% of TREO with a recovery rate of 95%. In the second test, conducted under the same conditions, the light fraction had 0.04 wt.% of TREO with a recovery rate of 5.1%, and the heavy fraction had 0.16 wt.% of TREO with a recovery rate of 94%. The upgrading ratios of the two tests with the same conditions were 1.53 and 1.80. The products of gravity separation were allowed to undergo sedimentation to facilitate the subsequent process such as filtering and drying. It was observed that the particles in the light product remained suspended in the separation liquid for a longer period, whereas the particles in the heavy product settled immediately. This indicated that the particles in these products had different settling velocities, which were significantly influenced by particle size regardless of particle density (Abaka-Wood et al., 2019). Smaller particles have lower settling velocities, making gravity separation inefficient even if the concentration criterion is met (Das and Sarkar, 2018). During gravity separation, fine particles of target minerals were removed along with the light gangue mineral particles due to insufficient settling time. This negatively impacted the flotation process by causing a significant loss of REE in the discarded light fraction. Consequently, reducing particle sizes to improve liberation proved to be a limiting factor for gravity separation. According to the chemical and particle size distribution analysis, Mozley separation tests were only successful in desliming; thus, there was no enhancement in the flotation results (Fig. 5). Ninety percent of the particles in the light fraction were under 24 µm in size, while in the heavy fraction, this size was 162 µm. After grinding feed-B to achieve a d_{90} = 88 µm, experiment-2 was applied to determine if further grinding resulted in any enhancements. The content of the concentrate was 5.7 wt.% of TREO with a recovery of 46% and a mass yield of 1.2%. The recovery of TREO in the middlings was ca. 50%, so the flotation time was two-folded in the cleaning step to increase the fine particle recovery. The goal of extending the flotation time was to provide adequate residence time for fine particles besides increasing collision probability with the bubbles and as well as improving their attachment efficiency (Farrokhpay et al., 2021; Pease et al., 2006; Wills, 2016). As expected, with longer flotation time (experiment-2), a recovery of TREO was 73% in the concentrate with a grade of 5.1 wt.% was achieved.

Experiment-3 resulted in a concentrate with 3.4 wt.% TREO and a recovery of 64%. As discussed above, applying gravity separation to produce a relatively richer feed did not enhance the separation of target minerals through flotation.

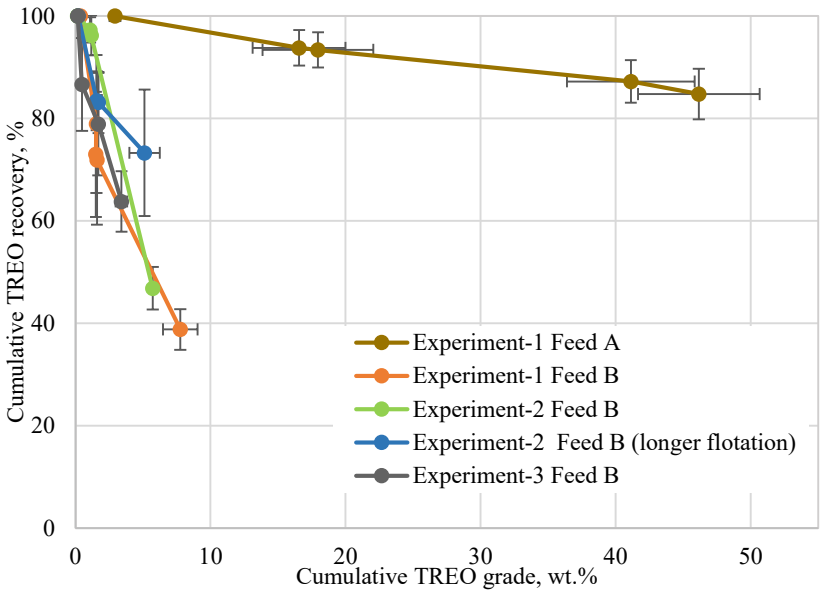


Figure 5. TREO grade-recovery curve for the flotation experiments with and without gravity pre-concentration (determined by pXRF).

4. Conclusions

The beneficiation performance of two different heterogenous ore grades from a REE-carbonatite deposit was evaluated in this study.

- The mineralogical characterization of two different rock samples demonstrated a potential variability in the concentration of target minerals throughout the deposit. This variation suggests that the distribution of valuable minerals is not uniform, requiring tailored processing approaches for different parts of the deposit.
- Preliminary experimental tests were conducted using experiment-1, which does not include pre-concentration step. This test was applied to both feed materials. It was observed that for feed-B, additional grinding was necessary to liberate the REM from the gangue minerals effectively. This indicates that feed-B has a more complex mineral matrix requiring finer grinding for optimal mineral separation.
- For feed-A, achieving a particle size below 150 µm was adequate to ensure a high recovery rate and a substantial concentration of REE via experiment-1.
- In contrast, for feed-B, further grinding significantly improved both the recovery rate and the concentration of the REE. This improvement allowed the elimination of an additional cleaning step, simplifying the experiment-1 and potentially reducing operational costs.
- Gravity separation was tested as a pre-concentration step of REM from the low-grade feed-B before flotation. However, it mainly removed fine particles and negatively impacted the flotation process by rejecting a significant amount of REE in the discarded light fraction, proving ineffective for the intended purpose.
- When comparing the results obtained from different experiments, it is concluded that fine particles do not impact the flotation process negatively. This suggests that particles finer than a certain size (finer than 25 µm) can be effectively processed without hindering the overall efficiency of mineral recovery with modified flotation time.

Acknowledgements

The authors would like to thank Rare Earths Norway, EIT Raw Materials for the financial support (Rare Green, project number: 21130), and Trond Watne (Rare Earths Norway AS) for providing the feed materials. We acknowledge the Research Council of Norway for the support of the Norwegian Laboratory for Mineral and Materials Characterization, MiMaC, project number 269842/F50. We would also like to express our thanks to Laurentius Tijhuis, senior engineer at IGP-NTNU, for performing the ICP-MS analyses and Kjetil Eriksen, engineer at IGP-NTNU, for preparing the polished blocks for SEM analysis.

References

Abaka-Wood, G., B., Quast, K., Zanin, M., Addai-Mensah, J., Skinner, W., 2019. A study of the feasibility of upgrading rare earth elements minerals from iron-oxide-silicate rich tailings using Knelson concentrator and Wilfley shaking table. Powder Technology 344, 897–913. https://doi.org/10.1016/j.powtec.2018.12.005

Abaka-Wood, G., B., Ehrig, K., Addai-Mensah, J., Skinner, W., 2022. Recovery of Rare Earth Elements Minerals from Iron-Oxide-Silicate-Rich Tailings: Research Review. Eng 2022, 3, 259–275. https://doi.org/10.3390/eng3020020

Alsabbagh, A., H., Mustafa, R., M., 2023. Wet gravity separation and froth floatation techniques for rare earth elements beneficiation from monazite ore in Jordan. Heliyon 9, e19597. https://doi.org/10.1016/j.heliyon.2023.e19597

Bradshaw, D., 2014. The role of 'process mineralogy' in improving the process performance of complex sulphide ores. Keynote Paper 932, IMPC 2014.

Coint, N., Dahlgren, S., 2019. Rare earth elements (REE) in two long drill-cores from the Fen Carbonatite Complex, Telemark, Norway.

Das, A., Sarkar, B., 2018. Advanced Gravity Concentration of Fine Particles: A Review. Mineral Processing and Extractive Metallurgy Review, 39, No. 6, 359–394. https://doi.org/10.1080/08827508.2018.1433176

Drzymala, J., 2007. Mineral Processing, Foundations of theory and practice of minerallurgy, Oficyna Wydawnicza PWr.

Farrokhpay, S., Filippov, L., Fornasiero, D., 2021. Flotation of Fine Particles: A Review. Mineral Processing And Extractive Metallurgy Review, Vol. 42, No. 7, 473–483. https://doi.org/10.1080/08827508.2020.1793140

Filippov, F., O., Filippova, Q., D., 2016. Rare earths (La, Ce, Nd) and rare metals (Sn, Nb, W) as by-products of kaolin production – Part 3: Processing of fines using gravity and flotation. Minerals Engineering 95, 96–106. http://dx.doi.org/10.1016/j.mineng.2016.06.004

Gandhi, S.M., and Sarkar, B.C., 2016. Essentials of Mineral Exploration and Evaluation. Chapter 1, Metals and Minerals: Global Trends, Outlook, and Mineral Exploration. Elsevier Inc. https://doi.org/10.1016/C2015-0-04648-2

Marion, C., Grammatikopoulos, T., Rudinsky, S., Langlois, R., Williams, H., Chu, P., Awais, M., Gauvin, R., Rowsonc, N.A., Waters, K.E., 2018. A mineralogical investigation into the pre-concentration of the Nechalacho deposit by gravity separation. Minerals Engineering 121, 1–13. https://doi.org/10.1016/j.mineng.2018.02.008

Jordens, A., Marion, Cheng, Y.P., Waters, KE., 2013. A review of the beneficiation of rare earth element bearing minerals. Minerals Engineering 41, 97–114. http://dx.doi.org/10.1016/j.mineng.2012.10.017.

Jordens, A., Sheridan, R., S., Rowson, N., A., Waters, K., E., 2014. Processing a rare earth mineral deposit using gravity and magnetic separation. Minerals Engineering 62, 9–18. http://dx.doi.org/10.1016/j.mineng.2013.09.011

Marien, C., Dijkstra, A. H., Wilkins, C., 2018. The hydrothermal alteration of carbonatite in the Fen Complex, Norway: mineralogy, geochemistry, and implications for rare-earth element resource formation. Mineralogical Magazine, Vol. 82(S1), pp. S115–S131. https://doi.org/10.1180/minmag.2017.081.070

Marion, C, Grammatikopoulosb, T., Rudinskya, S., Langloisa, R., Williamsa, H., Chua, P., Awaisc, M.,

Pease, J.,D., Curry, D.C. Young, M.F., 2006. Designing flotation circuits for high fines recovery. Minerals Engineering, 19, 831–840. https://doi.org/10.1016/j.mineng.2005.09.056

Simandl, G.J., Paradis, S., 2018. Carbonatites: related ore deposits, resources, footprint, and exploration methods. Applied Earth Science, VOL. 127, NO. 4, 123–152. https://doi.org/10.1080/25726838.2018.1516935

Silva, C., Lode, S., Aasley K., Kowalczuk, P., 2023. Early-stage application of process mineralogy methodologies for mineral tracking in flotation of rare earth elements (REE)-bearing minerals from a deposit in Norway. Minerals Engineering, 202,108268. https://doi.org/10.1016/j.mineng.2023.108268

Wang, Z., Fan, H., Zhou, L., Yang, K., She, H., 2020. Carbonatite-Related REE Deposits: An Overview. Minerals, 10, 965. https://doi.org/10.3390/min10110965

Wills, B., 2016. Wills' Mineral Processing Technology, Elsevier.

Flotation Research on Magnesite Tailings

F.Göktepe [1]*, B. Aydın [2], G.Bulut [2]

[1] Balıkesir University, Balıkesir/TURKEY

[2] Istanbul Technical University, Istanbul/TURKEY

*Corresponding : fgoktepe@balikesir.edu.tr (Ferihan Göktepe)

Abstract:

Magnesium is the eighth most abundant element in the Earht's crust and the third most plentiful element dissolved in seawater. Magnesium and magnesium compounds are produced from seawater, well and lake brines as well as from minerals such as magnesite, dolomite, brucite, and olivine. Heavy medium separation, magnetic separation, and flotation processes are used depending on the grade of the ore. Especially flotation processes have been successfully used for recovering magnesite from low-grade ores by two different well-known methods that are the direct flotation of magnesite and the reverse flotation of magnesite. Low-grade ores contain less than 10% MgCO3 besides magnesite tailings may have higher than this value depending on the applied beneficiation methods. As particle size determines the concentration method, produced tailings may have high MgCO3 content. In such cases, reprocessing these tailings is necessary to avoid resource waste and environmental pollution. This review will focus on the beneficiation of magnesite and the recovery of magnesite from tailings through flotation processes.

Keywords: *Magnesite, Tailings, Flotation*

1. Introduction

Magnesium (Mg) is a versatile element with numerous applications in modern society. It forms strong, lightweight metal alloys used in a variety of products, including aircraft and automotive components, laptops, televisions, mobile phones, portable power tools, bicycles, and other sporting equipment. Magnesite and magnesium-containing products are also primarily used as refractory materials in the cement and steel industries, as well as in metallurgy, construction, ceramics, glass fillers, catalysts in synthetic rubber manufacturing, raw materials in magnesium fertilizers, animal feed, and the chemical, pharmaceutical, and cosmetic industries. Additionally, they are applied in environmental protection, water, and effluent treatment, flue gas desulfurization, and heat-resistant linings (Bimplas & Anastassakis, 2020; Zhu et al., 2022; Shanmugasundaram && Shanmugam, 2021).

Magnesium is encountered in many minerals, both siliceous and non-siliceous. In the non-siliceous minerals, the following are included: the carbonate ones magnesite ($MgCO_3$) and dolomite ($CaCO_3.MgCO_3$), the hydroxylated form brucite [$Mg(OH)_2$] and the minerals of evaporate group carnallite ($KCl.MgCl_2.6H_2O$), bischofite ($MgCl_2.6H_2O$), kieserite ($MgSO_4.H_2O$) and brunerite, which is a solid solution of magnesium carbonate and iron carbonate, with its $FeCO_3$ content ranging between 5 and 30%. Among the siliceous minerals, olivine [$(MgFe)_2SiO_4$], talc [$H_2Mg_3(SiO_3)_4$] and serpentine [$H_4Mg_3Si_2O_9$] are the most important (Bimplas and Anastassakis, 2020). Among these, magnesite ($MgCO_3$) is a magnesium carbonate mineral that is the source of two-thirds of the world's magnesia (MgO). Magnesite–is white coloured, chemically inert, soft enough, and good absorbent. Because of that it is one of the most important basic raw materials for the production of refractories due to its high fire resistance. Magnesite specifications and characteristics can be summarised as;



- Mohs hardness: 3.5-4.5.
- Color: White, colorless, gray, yellow, brown, light pink, or lilac-rose.
- Crystal structure: Hexagonal (trigonal)
- Luster: Earthy, chalky, dull, or vitreous (glassy)
- Transparency: Transparent to opaque.
- Refractive index: 1.509-1.717.
- Density: 3.0-3.2 g/cm^3

The world reserve of magnesite is estimated to be 8.5 billion tonnes. China, Turkey and Russia are the largest magnesite producers, accounting for about 82% of the total world production, followed by Brazil, Austria, Greece, Spain, Australia, and India (Shanmugasundaram & Shanmugam, 2021).

From the magnesite rock mined, only a small part is used to produce magnesium metal while the great majority is directed to industrial uses, with magnesite being the most important mineral from the commercial point of view (Bimplas & Anastassakis, 2020). The most important magnesite products are raw magnesite, caustic calcined magnesia, dead-burnt magnesia, and refractory mass. When magnesite is heated up to 1400–1800 °C, the carbonates are removed as carbon dioxide and the magnesium oxide is produced. Magnesium oxide is an important refractory material that can be used to produce fire-resistant products widely used in metallurgy, chemical and ceramic industries. When magnesite mineral is heated up to 700–1000 °C, the resulting product can be used to produce soundproof materials, wear-resisting materials, insulating materials, as well as pharmaceutical products. It also has a high absorption capacity and can be used as an adsorbent for the removal of harmful gases from air which the absorption characteristics of magnesium oxide are directly related to the purity of magnesite ores (Chen & Tao, 2004). The main application of magnesite ore is used for refractory, but the impurities in it will break the fire resistance property of its product, so there is a rigid criterion of magnesite's impurities if it will be used for fireproofing (Santana & Peres, 2001). Magnesite resources usually contain large quantities of silicate minerals such as quartz and serpentine which make direct industrial smelting impossible therefore beneficiation is necessary.

2. Beneficiation Methods

Due to the huge demand for magnesite products and high- quality refractory materials, it has become necessary to develop a more efficient process for magnesite separation from associated gangue minerals to obtain higher-grade magnesite in recent years. Magnesite is usually associated with quartz, dolomite, and feldspar. Among these minerals, quartz is one of the most widely existing gangue minerals in the magnesite ores and other impurities such as CaO, Fe_2O_3, Al_2O_3 have a detrimental impact on the efficiency of the process and the properties of the refractories. Iron minerals in the magnesite can be pyrite, pyrrhotite, magnetite, and hematite, after weathering iron sulfide minerals can converted into limonite (Han et al., 2021). The magnesite raw materials with iron impurities have a great impact on fire resistance. Iron impurities react with CaO, generating a low-melting point material, while iron oxide is reduced to metallic iron, making refractory products in the formation of melting holes. The presence of iron impurity degrades magnesite products.

The chemical composition of raw magnesite, after mining or beneficiation, determines its suitability for various uses. From the quality point of view, the commercial specifications of magnesite are not standard. Magnesite for caustic calcined magnesia, which is the main feedstock for refractories, is considered commercial for MgO content higher than 40% (corresponding to 84.0% $MgCO_3$). Internationally, the specifications of commercial magnesite for refractories range between: MgO 40-47% (or $MgCO_3$ 84.0- 99.0), CaO 0-3.5%, SiO_2 0-7%, Fe_2O_3 + Al_2O_3 0-3% (Bimplas & Anastassakis, 2020).

Many processing techniques remove the impurities and upgrade the magnesia content of magnesite ore. These include optical sorting, magnetic separation, gravity separation, electric or electrostatic separation, and flotation. Each type of physical processing technique effectively removes one type or more of impurities. The optical sorting method targets all impurities depending on the mineral surface properties and can effectively remove (SiO_2), (Al_2O_3), (Fe_2O_3) and (CaO) from low-grade magnesite ore (Bilir & Akdaş, 2012). Iron impurities in magnesite, either from the raw ore or entrapped during crushing, can be partially removed using magnetic separation, though nonmagnetic and weakly magnetic iron are harder to separate. Strong magnetic separation is typically used to remove iron from magnesite. As the need for high-purity MgO has increased in recent years, more efficient methods for separating magnesite from gangue minerals are crucial. Bimplas and Anastassakis (2020) reported that hand-sorting for coarse particles and optical sorting for particles sized 4-10 mm is a common method to separate magnesite (white) from colored gangue minerals, such as serpentine. Magnetic separation is used to remove magnetic gangue, and gravity-heavy media separation for coarse particles (>1 mm) removes silicate minerals and dolomite. Magnesite can be effectively separated from silicate gangue minerals by flotation, but not from carbonates. The flotation method depends on the nature of the minerals in the ore. For ores with a high silicate content, reverse flotation with cationic collectors can produce high-quality magnesite, suitable for dead-burned magnesite production. Flotation is particularly useful for fine magnesite when a high-grade concentrate is required (Chen & Tao, 2004).

There are a few studies on the leaching of magnesite in hydrochloric acid solution, in organic acids such as acetic acid, lactic acid, and gluconic acid and it was found that the leaching process was controlled by resistance of chemical surface reaction and they reported that the dissolution rate of MgO was controlled by chemical surface reaction (Özdemir et al. 2009).

Therefore, due to the high commercial importance of magnesite, extensive scientific work has been carried out on magnesite beneficiation.

2.1. Flotation

Froth flotation was used for magnesite mineral processing as early as in 1930s by Doerner and Dwigh (Chen & Tao, 2004). For full utilization of low-grade magnesite resources, froth flotation is commonly used to reduce the silicon content and meet the industrial standard for smelting magnesite. The particle size distribution is a critical factor for the flotation performance to a great extent as it determines whether a mineral is completely liberated. However, it is almost impossible to accurately predict the flotation results when the feed particle size varies greatly (Fu et. al. 2020). The type of impurities and their proportion in the ore directly affect the flotation results. Because gangue minerals such as silicates, quartz, and iron oxides present different physicochemical behaviour during flotation in comparison to that of magnesite, therefore, their separation is relatively easy. Magnesite ($MgCO_3$) also often coexists with calcium gangue minerals such as dolomite and calcite which dolomite ($MgCa(CO_3)_2$) is one of the most common carbonate gangue minerals in magnesite. Calcium gangue minerals contained in magnesite can seriously affect the quality of refractory materials. During the melting process, calcium gangue minerals transform into calcium silicate, which may loosen in cooling and cause the refractory materials to collapse. So far, flotation is one of the most effective methods for separating magnesite and calcium gangue minerals. It has been reported that silicate minerals can be easily separated from magnesite in neutral pulps using alkyl sulfonate as a collector and caustic soda as a depressant. Although a lot of research has focused on magnesite flotation, the separation of magnesite away from dolomite remains a challenge. Due to the similar physical and chemical properties; such as surface wettability, surface charge properties; and crystal structures, it is difficult to separate magnesite from dolomite by flotation. Additionally, dissolved components from magnesite and dolomite can also influence flotation separation. Sodium hexametaphosphate, sodium silicate, starch, and carboxymethyl cellulose are commonly used depressants in carbonate flotation. These depressants not only inhibit gangue minerals but also significantly suppress magnesite flotation. Studies have shown that sodium hexametaphosphate and sodium silicate can be used together as an effective depressant, thus making them cooperate, strengthen the regulating functions, and in the best dosage, the sodium silicate is about 10 times the sodium hexametaphosphate. Both sodium hexametaphosphate and sodium silicate adsorbed on the surface of magnesite by chemical adsorption, which depresses magnesite and allows

for the collection of silicon by reverse flotation (Luo et al. 2024). To improve the selectivity of sodium silicate, metal ions such as Al^{3+}, Pb^{2+}, and Fe^{3+} have also been used to modify sodium silicate in the flotation process at pH 10.5 by Chen & Tao, (2004) because the dissolution behavior has a crucial effect on collector and modifier, thus affecting the mineral separation. The effect of metal ions on flotation generally occurs in two ways: metal ions adsorb onto the mineral surface, change the active sites with flotation reagents, and enhance or weaken the effectiveness of flotation reagents. For example, in direct flotation under acidic conditions, the dissolution of calcium-bearing ores releases Ca^{2+} ions into the solution. This alters the surface properties of minerals, impacting flotation behavior by promoting the adsorption of Ca^{2+} onto magnesite and quartz surfaces. This reduces the selectivity of the collector and weakens the selectivity of the collector (Chen & Tao, 2004).

Most of the dolomite and a small amount of quartz are often removed with an anionic collector by researchers. The common collectors are fatty acids and their salts which are used in carbonate flotation. Gence & Ozdag (1995) studied the surface properties of magnesite and serpentine in the presence of various collectors (oleic acid, sodium oleate, and Armoflote 14) and sodium silicate, as serpentine depressant during anionic flotation of magnesite. The study reported a slight improvement in concentrate with 70-80% magnesite recovery.

Reverse flotation is usually used when a high-grade magnesite concentrate is required. Amine collectors are widely used in the reverse flotation separation of magnesite from quartz and it is possible to achieve $CaO:SiO_2$ ratio between 0,32 and 5,79, which falls within acceptable limits for producing dead burned magnesia. Santana and Perez (2001) applied reverse flotation (silicates flotation) using amine collector and corn starch as magnesite depressant achieving high-purity magnesite concentrate with a quartz and other silicate content of - just 0,17% and weight recovery of approximately 92%. However, the loss of magnesite during reverse flotation is unavoidable as amine collectors have a certain ability to float magnesite. Mixed amine collectors have been found effective in magnesite flotation as magnesite, dolomite, and quartz exhibit noticeable surface differences, so through the reverse flotation method dolomite and quartz can be selectively floated, improving the separation process (Chen & Dai, 2020). Organic and inorganic depressants, such as sodium silicates, organic sulfate, sodium hexametaphosphate, citric acid and oxalic acid are commonly used to minimize the loss of magnesite during the reverse flotation separation of magnesite from quartz by selectively adsorbed on the surface of magnesite. Zhu et al. (2022) introduced a new environmentally friendly reagent, Carboxymethyl cellulose (CMC), which demonstrated efficient flotation separation of quartz and magnesite. Their findings suggest that CMC has the potential to act as a selective depressant in the magnesite−quartz separation.

In the literature, it has been reported that the combination of direct flotation (magnesite flotation) using anionic collectors (fatty acids) and reverse flotation using cationic collectors (amines) for separation of cryptocrystalline magnesite, with serpentine as major and hematite/ calcite as minor gangue minerals, provides concentrates with acceptable impurity levels however, reagent consumption has been reported to be high. Cationic reverse flotation is typically used to remove silicon and iron from magnesite ore followed by anionic flotation to remove calcium and some silicon when impurity levels are high (Han et al. 2021). Additionally, a combination of pre-concentration with high-intensity dry magnetic separation followed by reverse flotation (serpentine flotation) with cationic collectors has been reported to produce concentrates with acceptable levels of SiO_2 and Fe_2O_3 but not for CaO (Bimpilas & Anastassakis, 2020). Santana and Peres (2001) confirmed that the reverse flotation process can reduce the amount of siliceous inclusions to acceptable levels, achieving SiO_2 content lower than 0.20% (calcined basis). The use of corn starch as a depressant was found to be crucial for achieving 92% recovery, where SiO_2 content in the concentrate was reported to be rather low although it slightly increased of the iron grade in the concentrate.

Öz Aksoy et al. (2022) studied bioflotation using "surfactin," a biosurfactant derived from Bacillus subtilis, as a bio-collector in the flotation of magnesite, and compared its performance to that of oleate, a traditional magnesite collector. The study reported that while oleate has a significant cost advantage in terms of reagent expense, surfactin was used in much lower quantities per unit of ore. Additionally, it is eco-friendly that makes it more prominent.

2.2. Tailing Processing

Depletion of the high-grade and high-purity magnesite deposits along with the continuously increasing demand for magnesite products, has created an urgent need to focus on the processing lower-grade deposits and magnesite tailings. Large-scale magnesite exploitation has inevitably generated enormous amounts of tailings (Özdemir et al., 2009). These tailings not only occupy significant land–areas but also contribute to severe environmental pollution, including dust emissions, which can adversely affect agriculture, land use, and water bodies (Shanmugasundaram & Shanmugam, (2021). Many materials previously regarded as waste can now be considered raw materials. Froth flotation not only allowed the economical separation of fine-grained ores, but also significantly increased recoveries and concentrate grades (Brezani et. al. 2018).

Bimplas & Anastassakis, (2020) focused on the exploitation of the material with a particle size of -40 mm that had been deposited as tailings from previous separation. The tailings still contain a significant amount of usable magnesite, but at a very low grade (about 35% to 39% MgO) and these tailings contain large amounts of impurities such as talc, quartz, and dolomite. Consequently, it is highly desirable to utilize magnesite tailings to recover magnesium and avoid a storage problem. Applying the sorting method upgrades a magnesite waste by effectively removing SiO_2, CaO, Fe_2O_3, and Al_2O_3. Heavy media separation is effective in removing CaO gangue from the magnesite ore. Also, a multi-gravity separator has been utilized to reduce calcined magnesite (CaO) impurities. Electrostatic separation is also applied to magnesite ore, demonstrating suitable performance between carbonates and silicates. According to Chen et al. (2020), the SiO_2 and CaO impurities were reduced by approximately 0.6% for the high-grade magnesite ore and 10% for low-grade magnesite ore. Bozkurt et al. (1999) reported that süper- clean magnesite can be obtained from magnesite tailings by magnetic separation and oil agglomeration. These processes yielded a concentrate with a total recovery 86.09%, containing 0.48% SiO_2, 1.55% CaO, 0.21% Fe_2O_3 and 46.61% MgO, from ore that initially contained 7.98% SiO_2, 1.65% CaO, 1.32% Fe_2O_3 and 44.33% MgO.

The selective flotation of magnesite from magnesite tailings using anionic collectors is often inefficient, as both silica and silicate minerals are activated by Mg^{+2} ions. Therefore, the application of depressant reagents is necessary to achieve selective separation of carbonate minerals from gangue materials. Sodium silicate is one of the commonly used depressants. Gawel et al. (1997) demonstrated that strains of *Aspergillus niger* are effective in producing a series of depressant agents for magnesite flotation. The competition between the anionic collector and metabolites produced by *Aspergillus niger* explains the decrease of magnesite tailings floatability after one or two weeks of biotreatment.

Göktepe and Özdağ (2001) reported that flotation can effectively upgrade magnesite plant tailings with a particle size of -4 mm, utilizing both direct and reverse flotation techniques. The best results were achieved through direct flotation under the following conditions: pH 10.5, oleic acid at 4.5 kg/ton, AP 825 at 1 kg/ton as the collector, and Na_2SiO_3 at 1 kg/ton as the depressant for particles sized -150 microns. This process increased the MgO percentage from 40.8% to 44.5% with a recovery rate of 96%. However, it is important to note that the reagent consumption was relatively high. In another study, flotation concentrates with acceptable magnesite content were produced from secondary magnesite ore deposits using a single- stage reverse froth flotation process. The presence of naturally floatable talc particles and the hydrophilic nature of the magnesite surface contributed to the challenges of direct flotation, where the froth product yield could be very high. This would lead to an entrainment effect that negatively impacts the quality of the prepared concentrate, resulting in a significant reduction in the amount of produced tailings. The use of amine collectors is sufficient to achieve adequate results in terms of concentrate grade and yield when pH is adjusted. Additionally, the use of soluble starch can further increase the yield of magnesite concentrate while reducing impurity content. Although the natural floatability of magnesite is relatively low due to the hydrophilic surface, further depression of magnesite floatability is possible using starch (Brezani et al. 2018). Özdemir et al. (2009) also investigated magnesium recovery from magnesite tailings through leaching in hydrochloric acid solution, varying factors such as temperature, acid concentration, solid-to-liquid ratio, particle size, and stirring speed. They reported that about 92% of the magnesium in the magnesite tailings was recovered at a

temperature of 40 °C, with a 1.0 M acid concentration, a solid-to-liquid ratio of 10 g/L, a particle size of 100 μm, and a leaching time of 60 minutes.

3. Conclusions

As a non-renewable mineral resource, the reserves of high-grade magnesite ore have gradually decreased due to extensive mining in the past. This decline has made the utilization of low-grade magnesite ore increasingly critical; however, beneficiating magnesium ores presents challenges, as associated minerals often include other magnesium-containing ores with similar characteristics. To address these challenges, comprehensive research is essential, focusing on the physicochemical properties, manufacturing mechanisms, and applications of magnesite, as well as the optimization of processing technologies and conditions. Such research can help minimize resource waste and enhance the economic and environmental benefits of utilizing low-grade ore or magnesite tailings. By applying suitable mineral processing technologies, it is possible to produce high-quality magnesite concentrates, thereby maximizing the use of magnesite ore resources and improving the quality of magnesium products.

References

Bilir K. & Akdaş H. (2012), *Evaluation of Magnesite Wastes Using Optical Sorting Machine*, Conference: Proceedings of XIIIth International Mineral Processing Symposium, October 10-12, 2012, Bodrum, Turkey

Bimpilas G.M. & Anastassakis G.N., (2020), Magnesite benefiation methods; A Review, *Sustainable extraction and processing of raw mterials journal, 14-20*

Bozkurt V., Uçbaş Y. & Bilir K., (1999), Production of Super Clean Magnesite from Magnesite Tailings, *Cevher Hazırlama* 2- 37-45

Brezani I., Sisol M., Valkova M. & Marcın M., (2018), Processing of Magnesite Rich Flotation Waste Deposited on a Heap, *Styczen– Czerwiec, Journal of the Polish Mineral Engineering Society*

Chen G. & Tao D., (2004), Effect of solution chemistry on flotability of magnesite and dolomite, International Journal of Mineral Processing, *Volume 74,* Issues 1–4, Pages 343-357

Chen Z. & Dai S. (2015), An Experimental Study on the Flotation of a Magnesite Ore in Liaoning, *International Journal of Simulation: System, Science & Technology*, , DOI 10.5013/ IJSSST.a.17.30.32

Öz Aksoy D., Özdemir S., Koca S., Çakmak H., Aytar ÇELİK P., Çabuk A. & Koca H.,(2022), Modelling of Magnesite Flotations with two Different Collectors: Biocollector and Oleate, *ESOGÜ Müh Mim Fak Derg*., 30(1), 106-114

Fu Y., Yang B., Yingqiang M., Sun Q., Yao J., Fu W. & Yin W., (2020), Effect of particle size on magnesite flotation based on kinetic studies and machine learning simulation, *Powder Technology, 376,* 486–495

Gawel J., Maliszewska I. & Sadowski Z., (1997), he Effect of Biopretreatment on the Flotation recovery of Magnesite Tailings, *Minerals Engineering*, *Vol.10*, No 8, 813-824

Gence N. & Ozdag H. (1995), Surface properties magnesite and adsorption mechanisim, *International Journal of Mineral Processing*, 43, 37-47

Göktepe F. & Özdağ H., (2001), *Concentration of Magnesite Tailings by Froth Flotation*, Proceedings of 9th Balkan Mineral Processing Congress, İstanbul/Turkey, page 247-251

Han J., Li X., Dai S. & Liu G., (2021), "The Flotation Separation of Magnesite and Limonite Using an Amine Collector", *Adsorption Science & Technology, Volume 2021, 1-12*

Luo N., Shi J., Yan B.& Wang X., (2024), Flotation Separation of Magnesite from Dolomite Using Sodium Silicate Modified with Zinc Sulfate as a Selective Depressant" Minerals, 14*(4),* 355; https://doi.org/10.3390/min14040355

Özdemir M., Çakır D. & Kıpçak İ., (2009), Magnesium recovery from magnesite tailings by acid leaching and production of magnesium chloride hexahydrate from leaching solution by evaporation *International Journal of Mineral Processing*, *93,* 209–212

Santana A.N. & Peres A.E.C, (2001), Reverse magnesite Flotation, *Minerals Engineering, Vol.14,* 107-111

Shanmugasundaram V. & Shanmugam B., (2021) Characterisation of magnesite mine tailings as a construction material, *Environmental Science and Pollution Research* , *Volume 28,* pages 45557–45570

Zhu Y., Yang L., Hu X., Zhang X. & Zheng G., (2022) Flotation separation of quartz from magnesite using carboxymethyl cellulose as depressant", *Trans. Nonferrous Met. Soc.* China, 32, 1623−1637

Investigation of the collector effect on the chalcopyrite flotation

Adnan Ceylan [1]*, Gülay Bulut [2]

[1] Miryıldız Mining Company, Ortaklar köyü, Şehitkamil, Gaziantep,Turkey

[2] Istanbul Technical University, Faculty of Mines, Mineral Processing Department, 34469, Maslak, Istanbul, Turkey

*Corresponding author: adnanceylan1@hotmail.com (Adnan Ceylan)

Abstract:

In this study the effects of collector were investigated on chalcopyrite flotation with different collector amounts. The tests were performed with the ore in the laboratory and Etibakır Siirt-Madenköy plant scale. Effect of collector amounts was examined depending of the bubble size, froth thickness, Cu grade and recovery of concentrate. It was determined that copper recovery increased. While bubble size copper grade and froth thickness decreased depending on the increase collector amounts

According to the laboratory and plant studies, it was determined that the copper recovery increased. While bubble size,copper grade and froth thickness decreased depending on the increase collector amounts.When the laboratory and plant results of the collectors compared, it was determined that similar results were obtaiened.

Keywords: *Chalcopyrite flotation, froth, collector, pH*

1. Introduction

The collector is usually added to the slurry to enhance the surface hydrophobicity of the mineral particles, and the addition of this may also affect the bubble size. If a small amount of collector is present in the slurry, the collector molecules are easily adsorbed to the non-polar groups of the frother molecules, increasing the hydrophobic capacity of these, which makes these easier to adsorb at the gas-liquid interface and enhances the surface activity. However, with the increase of the collector addition, more collector molecules are adsorbed at the gas-liquid interface, resulting in the coadsorption, which affects the adsorption of the frother at the gas-liquid interface. This phenomenon may reduce the stability of the bubble and promote the breakup and coalescence, affecting the bubble size. This behavior has been reported by (Zhu et al., 2019).

Collectors are usually add to slurry to mix with the mineral particles by the fluid turbulent flow to enhance the surface hydrophobicity of valuable minerals. Moreover, a fluid turbulent flow is utulized to keep the mineral particles in suspension. Air is then introduced or forced into the flotation cell to form fine bubbles under the effect of turbulence, and the frothers are added to the slurry to inhibit the coalescence of bubbles and keep the bubbles stable. Subsequently, bubbles collide with the mineral particles in the flotation cell, and hydrophobic particles adhere to the bubbles, rising to form a froth layer, whereas the hydrophilic particles sink to the bottom of cell to form a tailing (Wang et al., 2019; Mesa and Brito-Parada, 2019; Rosa and Rubio, 2018).

The actual flotation process is a complex, multi-factor coupling separation process. The bubble size is synergistically affected by the frother, collector, slurry properties, mechanical energy input, and air flow rate in the flotation cell. The effect of multi-factor coupling on the bubble size should attract sufficient attention.(Wang et al., 2020).

Flotation performance is typically controlled by the addition of chemical reagents such as collectors and frothers. A frother has two main functions: generate and preserve small bubbles in the pulp phase; and provide stability to the froth phase. Three mechanisms of particle recovery into the froth have been proposed: by particlebubble attachment; by water entrainment; and by entrapment between attached particles (Wills and Finch, 2016)

The main function of a collector is to selectively adsorb on a mineral surface, altering its hydrophobicity such that bubble particle aggregation can take place for minerals which are not readily floatable in the absence of collector addition. A number of recent studies investigating the influence of collectors on flotation hydrodynamics have shown that amine and many oxhydryl collectors exhibit frother like properties (Espinosa Gomez et al., 1988; Laskowski, 1993; El-Shall et al., 2000; Atrafi et al., 2012; Ravichandran et al., 2013; Corona-Arroyo et al., 2015). Atrafi et al. (2012)

Flotation frothers are used to facilitate air dispersion into fine bubbles, and to stabilize the froth. According to Leja–Schulman's penetration theory (Leja and Schulman, 1954; Leja, 1956/57), frothers accumulate prefer entially at the air–water interface and interact with collector molecules adsorbed onto solid particles in the particle-to-bubble collision and attachment. The effect of frothers on bubble size has recently been extensively studied (Cho and Laskowski, 2002a,b; Laskowski et al., 2003a,b; Laskowski, 2003; Grau et al., 2005). It has been found that the effect of frothers on bubble size results from their ability to prevent bubble coalescence. The degree of bubble coalescence decreases with increasing frother concentration and at a particular concentration (known as critical coalescence concentration, CCC) for a frother, it reaches non-coalescence environment. Beyond the CCC, there is very little effect of the increase of frother concentration on the bubble size.

Numerous studies on the effect of collectors on solid's wettability and flotation have led to a well established conclusion that the major role of the collector is to render a treated mineral hydrophobic. The role of frother is not so clear; it is believed that it provides finer bubbles, stabilizes the froth and according to the Schulman Leja penetration theory (Leja and Schulman, 1954; Leja, 1956/57) enhances particle-to-bubble attachment.

The froth flotation process is a physicochemical separation process, which commonly requires a large variety of flotation reagents. Collectors and frothers are considered as important reagents. Collectors render the valuable minerals hydrophobic. Frothers are used for froth generation and also to facilitate the air dispersion into fine bubbles. According to Leja-Schulman's penetration theory (Leja and Schulman, 1954; Leja, 1956/57) frothers accumulate preferentially at the air–water interface and interact with collector molecules adsorbed onto solid particles in the particle-to-bubble collision and attachment.

Naturally hydrophobic minerals can be floated without the addition of surfactant. However, in most applications, collector is required to render valuable part of ore hydrophobic. On the other hand, frother is used to obtain stable froth to carry the hydrophobic mineral particles into the concentrate launder. Type and amount of collector and frother are strongly related with entrainment of gangue in froth and recovery of valuable minerals (Srıprıya et al., 2003)

Extensive research has confirmed that the frother and the collector can yield a synergistic effect on the bubble size, which is affected by the addition and performance of the frother and the collector. The mechanism of the synergistic effect of the frother and the collector requires further research to explore the best combination of the frother and the collector. In addition, the slurry viscosity increases with the increase in the addition of collector, preventing the deformation and coalescence of bubbles (Zhu et al., 2019).

The aim of this study is to examine the effect of collector amount on flotation in bubble size, froth height, copper grade and recovery were monitored in both laboratory and plant scale experiments.

2. MATERIAL AND METHOD

2.1. Material

The ore sample used in this study was obtained from Etibakır Siirt-Madenköy, Turkey. The chemical analysis of the sample is presented in Table 1. As a result of mineralogical analyses of the sample, which are the basis for experimental studies, pyrite mineralization containing chalcopyrite magnetite and sphalerite was determined in the ore composition. Pyrite was observed as the main component in polishing sections, both free and as a locked particle with all minerals in the ore. The other common mineral was chalcopyrite, usually, chalcopyrite phases locked with cataclastic pyrite structure, and

chalcopyrite was seen to fill in the fractures of pyrite as a matrix material as well as it showed a colloidal structure with pyrite. Figure 1 shows an example of the polishing section of the ore sample.

Table 1. Chemical analysis of Etibakır Siirt-Madenköy ore sample

Element	Etibakır Siirt-Madenköy Ore %
Cu	1.52
Pb	0.08
Zn	0.21
Fe	30.78
S	26.07
SiO_2	18.42

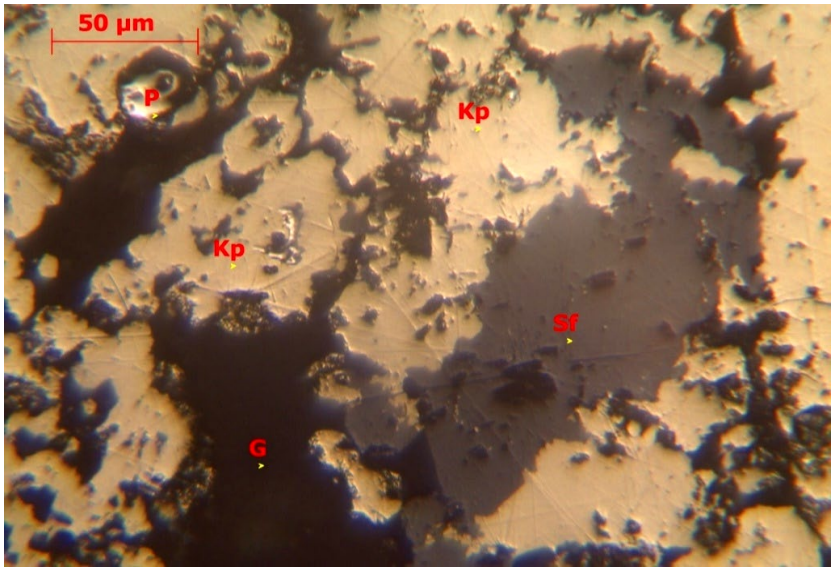


Figure 1. In the polishing section of the sample, small pyrite (P) and sphalerite (Sf) occurrences in scattered white, which appear white in the body of chalcopyrite (Kp) predominant coarse, dark-colored cracks are filled with gang (G) minerals

Etibakır Siirt-Madenköy copper plant ore content is around 1.5% Cu and a concentrate has been produced with 20%Cu by selective flotation. 1.6700.000 tons of ore are processed annually and 100.000 tons of copper concentrate is obtained. In the Etibakır Siirt-Madenköy copper plant, Aerophine 3418 A (collector), MIBC, (frother) sodium silicate (depressant), and lime (pH modifier) are used as the flotation reagents.

2.2. Method

In this study, some studies were carried out to measure bubble sizes during the flotation experiments, the flotation experiments were applied at pH 12, In order to examine the effect of amount of collector on copper grade and recovery, bubble size and froth height the studies were conducted on both laboratory and plant scales. Flotation experiments in the laboratory scale were carried out in a Denver flotation machine with a constant stirring speed at 1300 rpm. Aerophine 3418 A was used as the collector for two stages adding such as (25+25 g/t) in every experiment, and MIBC used as the frothers were used at two stages 12.5+12.5 g/t. Finally, the flotation products were collected for 5 min at pH 12, and

chalcopyrite was separated from pyrite and gang minerals, selectively. In the Etibakır Siirt-Madenköy copper plant, 20 m3 Outotec tank cells have been used in the rougher circuit while 10 m3 Outotec tank cells in cleaner circuits. All tests performed in the laboratory and plant scale were investigated on rougher circuits of chalcopyrite separation. The Image J analysis program has recently found wide fields of study in various sciences (Uslu and Tafakhori, 2013). During the experiments conducted on the laboratory scale, the photos of the bubbles were taken from the top of the flotation cell. The bubble sizes from these photos were measured using the Image J analysis measurement program Approximately 30 bubbles were measured for each condition. For these experiments, the experimental setup and procedure defined in a recent publication were used in the literature (Güven et al., 2020; Batjargal et al., 2021). Figure 2 shows the bubble size measurement method, and Figure 3 shows the images from the measurements with different collector amounts. Also, the bubble size measurements were made by the same method by taking a photograph in Etibakır Siirt Madenköy copper plant cells. The bubble size was measured selective-rougher circuit in the plant to be compatible with laboratory measurements.

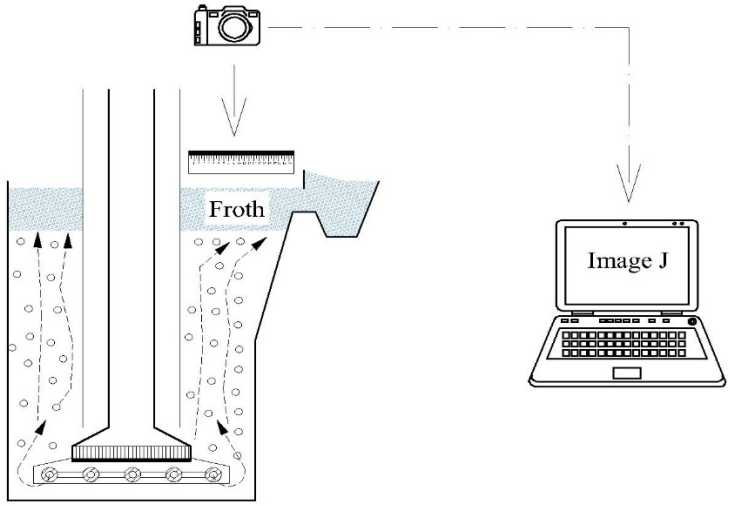


Figure. 2. Schematic presentation of bubble-size measurement



50 g/t 75 g/t 100 g/t

Figure 3. Images from measurements with different amounts of Aerophine 3418 A collector

3. RESULTS AND DISCUSSION

3.1. Effect of collector amounts

In these experiments, the amounts of collector effect on bubble size, concentrate grade and recovery were examined. The result was given Table 2 and shown in Figure 4,5.

Table 2. Effect of Collector amount on bubble size concentrate grade, and recovery

Experimental medium	Collector amounts, g/t	Bubble size, cm	Froth thickness, cm	Concentrate grade, % Cu	Concentrate Recovery %
Laboratory	50	0,579	2,1	6,46	85,8
	75	0,484	1,7	5,89	87,2
	100	0,414	1,5	5,41	89,5
	125	0,367	1,4	5,01	91,3
Plant	50	0,666	23	13,72	85,0
	75	0,554	20	11,69	86,7
	100	0,408	18	9,51	88,7
	125	0,357	15	8,36	90,3

As seen in Table 2, the average bubble size decrease as the amount of collector increased in laboratory scale experiments. When the amount of collector is increased from to 50 g/t to 125 g/t in all experiments, the average bubble size decrease by %63 It was observed.

In the plant scale study, the bubble size decreased by 54% as the amount of collector increased In addition, it was observed in both plant and laboratory scale experiments that the frother thickness decreased by 35% as the amount of collector increased. The increase in the amount of collector led to an increase in the material transport rate and thus a decrease in the frother thickness

Collector is typically added to the slurry to enhance the surface hydrophobicity of the mineral particles that might be one of the reasons for obtaining bubbles of smaller size at higher collector amounts. Extensive research has confirmed that the frother and the collector can yield a synergistic effect on the bubble size, which is affected by the introduction of the frother and the collector to slurry as well as their performance (Nguyen et all., 2006;Pienaar et all., 2019; Wang et all., 2020:Pan et all., 2022).

Flotation reagents include collectors and surface modifiers, frothers, and pH-regulators controlling physical and chemical conditions of solid, air, and liquid phases, respectively. The importance of frothers in flotation is widely acknowledged, particularly in terms of their role with respect to bubble size, and the stability and mobility of the froth phase. These factors play a significant role in the kinetic viability of the process, and the overall recovery and the grade that can be achieved from a flotation cell or circuit (Comley et all., 2002).

Frothers also interact with collectors resulting in a stronger and faster particle-bubble attachment (Leja et all., 1954)

The bubble size is influenced by several factors such as the frother, collector, slurry properties, mechanical energy input, and air flow rate. Thus far, numerous studies have focused on the effects of individual factors on the bubble size, particularly the frother. Using a suitable frother and increasing the frother concentration to CCC may effectively reduce the bubble size and improve the flotation recovery. Further studies are required to thoroughly understand the regulation mechanism of the bubble size in a flotation and develop bubble regulation technology (Wang et al., 2020).

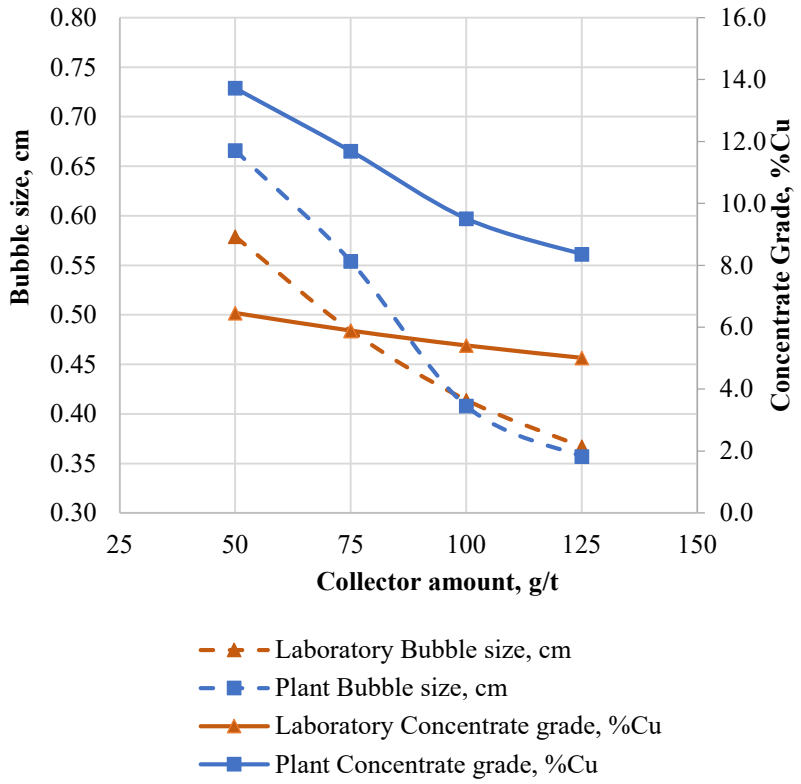


Figure 4. Effect of Collector amount on bubble size and concentrate grade

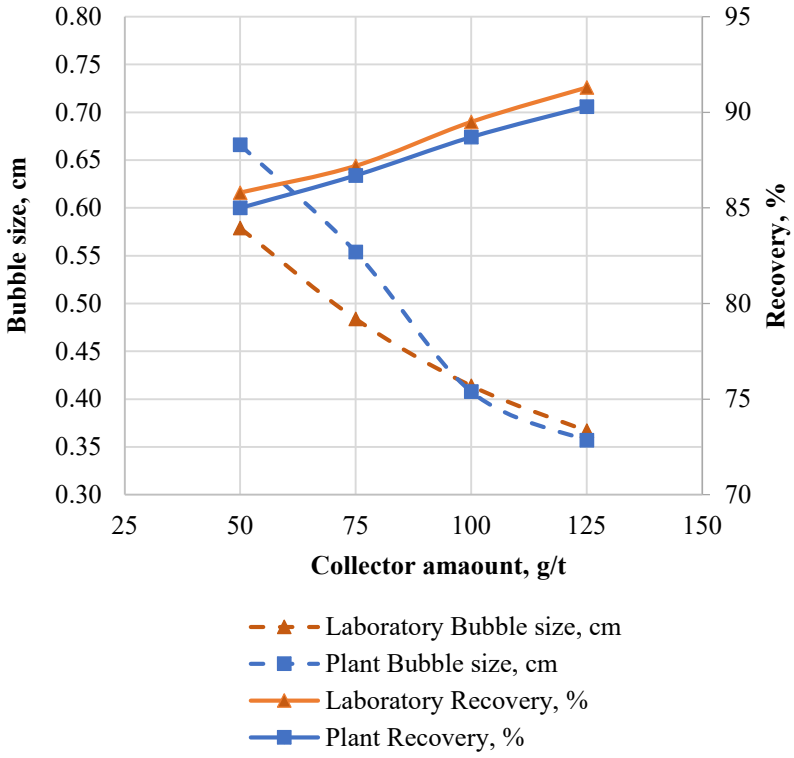


Figure 5. Effect of Collector amount on bubble size and recovery

The probability of bubble-particle collisions reduces as the particle size decreases and the bubble size increases.This implies that decreasing bubble size can improve the flotation rate and efficiency of the bubble-particle collision for fine particles (Waters et all., 2008)

Increasing the amount of collector led to a decrease in bubble diameter in both ores, As the collector amount increases the copper grades decrease and copper recoveries increase because wıth smaller bubbles the collision probability between copper mineral particles increases and also causes entrainment of gangue minerals, leading to low copper grade and high recovery (Ceylan et all., 2024).

4. CONCLUSION

In this study, the effect of collector amount were investigated on chalcopyrite flotation. In the flotation tests at the laboratory and plant scale, it was found that the bubble size changed as a function of the collector amounts. All flotation tests show that as the amount of collector increases the copper grade and bubble sıze decrease but copper recovery increase.

According to the laboratory and plant studies, it was determined that the copper grade of concentrate decreased and recovery increased due to the smaller bubble sızes for all collector amounts When the laboratory and plant results of the collector amounts were compared, it was determined that similar results were obtained.

REFERENCES

Atrafi, A., Gomez, C.O., Finch, J.A., Pawlik, M., 2012. Frothing behavior of aqueous solutions of oleic acid. Miner. Eng. 36–38, 138–144.

Batjargal, K., Güven, O., Özdemir, O., Karakashev, S., Grozev, N., Boylu, F., Çelik, M.S., 2021. Adsorption kinetic of varius frothers on rising bubbles of different sizes under flotation conditions, Minerals, 11,324, 1-16

Ceylan, A., Aydın, Ş.B.,Göktepe,F.,Bulut, G.,2024.Relation of bubble size,grade and recovery in the copper flotation systems. Colloids and Surfaces A; Physicochemical and Engineering aspects,692,133929

Cho, Y.S., Laskowski, J.S., 2002a. Effect of flotation frothers on bubble size and foam stability. Int. J. Miner. Process. 64, 69–80.

Cho, Y.S., Laskowski, J.S., 2002b. Bubble coalescence and its effect on dynamic foamability. Can. J. Chem. Eng. 80, 299–305.

Comley, B.A., Harris, P.J., Bradshaw,D.J., Harris, M.C.,2002.Frother characterization using dynamic surface tension measurements, Int. J. Miner. Process. vol. 64, pp. 81-100

Corona-Arroyo, M.A., Lopez-Valdiviesco, A., Laskowski, J.S., Encinas-Oropesa, A., 2015. Effect of frothers and dodecylamine on bubble size and gas holdup in a downflow column. Miner. Eng. 81, 109–115.

El-Shall, H., Abdel-Khalek, N.A., Svoronos, S., 2000. Collector-frother interaction in column flotation of Florida phosphate. Int. J. Miner. Process. 58, 187–199

Espinosa-Gomez, R., Finch, J.A., Bernert, W., 1988. Coalescence and froth collapse in the presence of fatty acids. Colloids Surf. 32 (3/4), 197–209.

Grau, R.A., Laskowski, J.S., Heiskanen, K., 2005. Effect of frothers on bubble size. Int. J. Miner. Process. 76 (8), 225–233.

Güven, O., Batjargal, K., Özdemir, O., Karakashev, S., Grozev, N., Boylu, F., Çelik, M.S., 2020. Experimental procedure for the determination of the critical coalescence (CCC) of simple frothers, Minerals, 10(7), 617,1-12

Laskowski, J.S., 1993. Frothers and flotation froth. Miner. Process. Extract. Metall. Rev.: Int. J. 12 (1), 61–89

Laskowski, J.S., 2003. Fundamental properties of flotation frothers. In: Lorenzen, L., Bradshaw, D.J. (Eds.), Proc. 22nd Int. Mineral Processing Congress, vol. 2. The South African Institute of Mining and Metallurgy, Cape Town, pp. 788–797.

Laskowski, J.S., Cho, Y.S., Ding, K., 2003a. Effect of frothers on bubble size and foam stability in potash ore flotation systems. Can. J. Chem. Eng. 81, 63–69.

Laskowski, J.S., Tlhone, T., Williams, P., Ding, K., 2003b. Fundamental properties of polyoxypropylene alkyl ether flotation frothers. Int. J. Miner. Process. 72, 289–299

Leja, J., Schulman, J.H., 1954. Flotation theory: molecular interactions between frothers and collectors at solid–liquid–air interfaces. Trans. AIME 199, 221–228

Leja, J., 1956/57. Mechanism of collector adsorption and dynamic attachment of particles to air bubbles as derived from surface chemical studies. Trans. IMM 66, 425–437

Mesa, D., Brito-Parada., P.R., 2019. Scale-up in froth flotation a state of the art review, Sep. Purif. Technol. 210, 950-962.

Nguyen, A.V., Phan, C.M.,Evans,G.M.,2006.Effect of the bubble size on the dynamic adsorption of frothersand collectors in flotation. Int.J. Miner. Process. 79,pp 18-26

Pan,Y., Gresham,I., Bournival, G., Prescott, S.,Ata, S., 2022.Synergistic effects of frothers, collector and salt on bubble stability, Powder Technol.397,117028.

Pienaar, D., Jordan, T., McFadzean, B., O'Connor, C.T., 2019.The Synergistic interaction between dithiophosphate collectors and frothers at the air- water and sulphide mineral interface.Miner.Eng.138, pp 125-132.

Ravichandran, V., Eswaraiah, C., Sakthivel, R., Biswal, S.K., Manisankar, P., 2013. Gas dispersion characteristics of flotation reagents. Powder Technol. 235, 329–335

Rosa, A.F., Rubio, J., 2018. On the role of nanobubbles in particle-bubble adhesion for the flotation of quartz and apatitic minerals, Miner. Eng. 127, 178-184.

Srıpriya, R., Rao P. V. T., Roy Choudhury, B., 2003. Optimisation of operating variables of fine coal flotation using a combination of modified flotation parameters and statistical techniques [J]. International Journal of Mineral Processing, 68, pp.109-127.

Uslu, I., Tafakhori, F., 2013. Image J program.

Wang, H., Yang, W., Yan, X., Wang, L., Wang, Y., Zhang, H., 2020.Regulation of bubble size in flotation:A review , Journal of Environmental Chemical Engineering B, 104070

Wang, H., Zhu, H., Zhu, J., Shao, S., Huang, D., Liu, J., Li, T., 2019. Effect of energy consumption on dispersion and recovery of coal slimes in a mechanical flotation cell. Energy Sources Part a Recovery Utilization and Environ. Effects 42, 1882-1990.

Waters, K.E.,Hadler, K., Cilliers, J.J., 2008.The flotation of fine particles using charged microbubbles, Miner.Eng. 21, 918-923

Wills, B.A., Finch, J.A., 2016. Wills' Mineral Processing Technology: An Introduction to the Practical Aspects of Ore Treatment and Mineral Recovery, eighth ed. Butterworth-Heinemann.

Zhu, H., Zhu, J., Valdivieso, L.A., Min, F., Wang, H., Xu, W,. Li, M., 2019.Effect of reagent blend on characteristics and dispersion of bubbles in a flotation column, J. China Coal Soc. 44, 1586–1592

Enrichment of Lead-Zinc Sulfide Ore of Bolkar-Tepeköy Deposit by Flotation

Oğuzhan Mert Gürkan [1]*, Buse Yılmaz [2], Ş. Beste Aydın [1], Alim Gül [1]

[1] Istanbul Technical University, Department of Mineral Processing Engineering, Maslak, İstanbul, TÜRKİYE

[2]Eti Gübre A.Ş., Mardin, 47700, TÜRKİYE

*Corresponding author: e-mail (Firstname Lastname)

Abstract:

This study investigates the enrichment of sulfide lead-zinc ore from the Bolkar-Tepekoy region using flotation. The ore sample, consisting of 0.67% Pb, 2.42% Zn, 1.63 g/t Au, and 40 g/t Ag, primarily contains pyrite, galena, and sphalerite as valuable minerals, with minor quantities of fahlerz, arsenopyrite, and chalcopyrite, alongside quartz as the primary gangue mineral. The main objective of this research is to optimize the selective flotation process to achieve the highest possible recoveries of lead and zinc, while also recovering gold and silver present in the ore. The tests focused on the effects of pH, particle size, and rotor speed on the flotation efficiency on the lead flotation. As a result of the flotation tests, the lead concentrate obtained with 52.27% Pb at a recovery of 50.4%, and a zinc concentrate with 48.77% Zn at a recovery of 84.4%. The silver was concentrated primarily in the lead concentrate with 2450 ppm Ag content, while gold was concentrated in the pyrite concentrate with 6.22 ppm Au content.

Keywords: *Flotation, galena, pH, particle size, rotor speed*

1. Introduction

Flotation is a crucial mineral processing technique used extensively for the beneficiation of sulfide ores, particularly those containing lead and zinc. The process exploits differences in the surface properties of minerals, allowing for the separation of valuable sulfide minerals from gangue (Fuerstenau, 1978). Lead and zinc are among the most essential industrial metals, used in a variety of applications including battery production, galvanization, and alloy manufacturing (Rodrigues et al., 2001). In nature, lead is predominantly found in the form of galena (PbS), while zinc occurs mainly as sphalerite (ZnS). Flotation is often the preferred method due to its high efficiency in processing low-grade ores and producing concentrates with high purity (Cytec Industries, 2002).

In Türkiye, a significant portion of the lead-zinc ore reserves are sulfide-based, which necessitates the use of flotation for their beneficiation (Ağaçayak & Yılmaz, 2021). The Bolkar-Tepekoy region, known for its rich mineral deposits, offers a substantial source of lead and zinc. However, the complex mineralogy of these ores, characterized by the presence of multiple sulfide minerals and trace amounts of precious metals such as gold and silver, poses challenges for efficient recovery (Fuerstenau, 1978). This study aims to optimize the flotation parameters to maximize the recovery of lead, zinc, gold, and silver from the Bolkar-Tepekoy ore, contributing to the broader understanding of sulfide ore processing

2. Material and Method

The ore sample used in this study was obtained from the Bolkar-Tepekoy region, containing 0.67% Pb, 2.42% Zn, 1.63 g/t Au, and 40 g/t Ag. Mineralogical analysis revealed that the sample primarily consisted of pyrite, galena, and sphalerite, with minor amounts of fahlerz, arsenopyrite, chalcopyrite, and quartz as the primary gangue mineral.

The ore was first subjected to comminution, where it was ground to a particle size below 74 µm using a laboratory ball mill at a 60% pulp solid ratio. The flotation tests were performed using a Denver laboratory-scale flotation machine. The effects of pH, particle size, and rotor speed on flotation

performance were investigated. The reagents used were selected based on their ability to optimize the separation process for sulfide minerals (Cytec Industries, 2002). The flotation test was conducted using 1 kg of ground ore in a 2.5 L flotation cell at a rotor speed of 1500 rpm. The lead flotation tests comprised of four-stage rougher flotation while zinc and pyrite flotation tests were made up of two-stage rougher flotation. The flotation reagents used in the lead circuit included sodium silicate (Na_2SiO_3) as a silicate depressant, zinc sulfate ($ZnSO_4$) as a sphalerite depressant, sodium metabisulfite ($Na_2S_2O_5$) as a sphalerite and pyrite depressant, and Aerophine 3418A as a selective collector for lead minerals (Cytec Industries, 2002). In zinc circuit, $CuSO_4$ and KAX were used as zinc activator and sphalerite collector, respectively. Besides, Tomamine-M73 was added as pyrite collector in pyrite circuit. Methyl Isobutyl Carbinol (MIBC) was used as the frother in all circuits (Rodrigues et al., 2001). The test conditions for rougher flotation are shown in Table 1.

Table 1. Rougher flotation test conditions

Rougher Circuit	Flotation Conditions	1.Stage	2.Stage	3.Stage	4.Stage
Pb Circuit	Na_2SiO_3, g/t	1000	-	-	-
	$ZnSO_4$, g/t	500	500	500	-
	$Na_2S_2O_5$, g/t	250	250	250	-
	Conditioning time, min	10	5	5	5
	Aerophine 3418A, g/t	5	5	5	5
	Conditioning time, min	3	3	3	3
	MIBC, g/t	20	10	10	10
	Flotation time, min	3	3	3	3
Zn Circuit	$CuSO_4$, g/t	200	100		
	Conditioning time, min	10	5		
	KAX, g/t	20	10		
	Conditioning time, min	3	3		
	MIBC, g/t	20	10		
	Flotation time, min	3	3		
Pyrite Circuit	Tomamine-M73, g/t	50	25		
	Conditioning time, min	3	3		
	MIBC, g/t	10	10		
	Flotation time, min	3	3		

3. Results and Discussion

3.1. Effect of pH

The first parameter investigated was the effect of pH on the flotation process. Flotation tests were conducted at three different pH values for the lead flotation circuit at natural pH (~8), pH 9, and pH 10. Lime (CaO) and sulfuric acid (H_2SO_4) were used to adjust the pH values in the flotation cell. In the zinc flotation, pH was adjusted at a fixed of 11.5 using lime, and the pyrite flotation was carried out at natural pH (~11.3) without any pH regulator. The tests were performed at 74 μm particle size. This test aims to determine the optimum pH that maximizes lead recovery while minimizing zinc and gangue mineral recovery in lead concentrate. The flotation results obtained based on the recoveries of the lead and zinc rougher concentrates are shown in Figure 1.

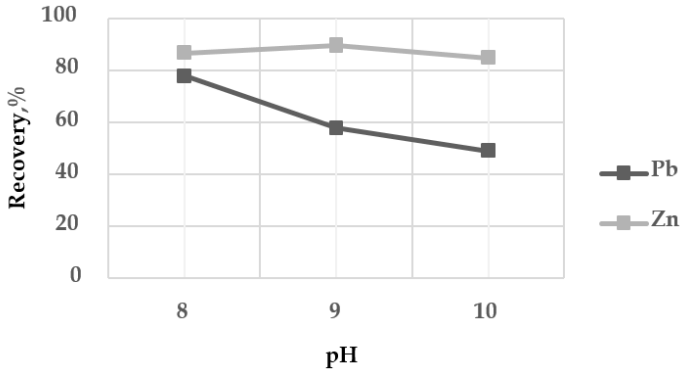


Figure 1. Effect on lead and zinc recoveries of different pH values used in lead flotation

According to the test results, lead recovery decreases with increasing pH in the lead circuit. Lead recoveries were obtained 77.9%, 58.0% and 49.1% at pH 8, 9 and 10, respectively. In addition, the lead flotation performed at different pHs did not provide a difference in terms of zinc recovery in the zinc circuit. Since the highest lead recovery was obtained at pH 8, the subsequent tests were carried out at this pH value.

3.2. Effect of Particle Size

Particle size plays a critical role in mineral liberation and therefore flotation efficiency (Fuerstenau, 1978). To investigate the effect of particle size, three different sizes were tested such as 74 µm, 63 µm, and 53 µm. The ore was ground at different times such as 25, 45, and 50 min for 74 µm, 63 µm, and 53 µm particle size using a ball mill and particle size analysis was performed using a Malvern Mastersizer Hydro 2000 MU. Flotation tests were conducted with the condition mentioned in Section 2. The aim was to determine the particle size at which the lead and zinc minerals were sufficiently liberated from the gangue to achieve maximum recovery. Flotation tests were performed on each particle size, and the results were indicated in Figure 2.

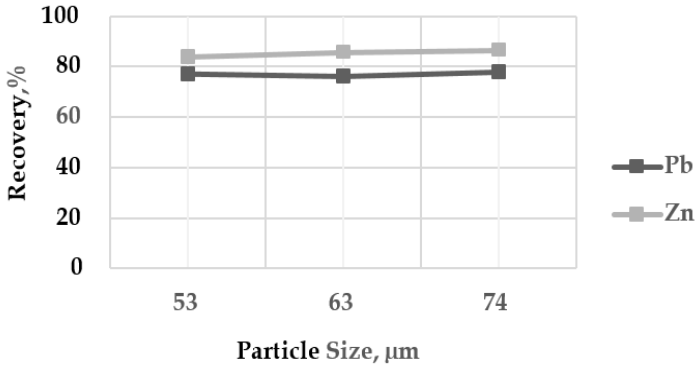


Figure 2. Effect on lead and zinc recoveries of different particle size in lead flotation

As a result of the tests, it can be said that there is not a significant difference in the lead recoveries as the particle size decreases, therefore there is no increase in the degree of liberation of the particles at particle sizes of 74 µm and below. Since grinding processes are always one of the most energy-consuming processes, the least costly conditions should be applied. Considering the grinding cost and energy consumption, the optimum particle size was determined as 74 µm.

3.3. Effect of Rotor Speed

The third parameter examined was the effect of rotor speed on flotation performance. Rotor speed affects the turbulence and mixing in the flotation cell, which in turn influences the attachment of mineral particles to air bubbles (Rodrigues et al., 2001). Two rotor speeds were tested as 1300 rpm and 1500 rpm.

The flotation tests were performed using the previously optimized pH and particle size conditions, and the rotor speed was varied to assess its impact on lead and zinc recoveries.

In the tests, the primary objective was to determine the rotor speed that provided the best balance between flotation kinetics and concentrate quality, minimizing the entrainment of gangue minerals while maximizing the recovery of lead and zinc (Rodrigues et al., 2001). As shown in Figure 3, while the lead recovery in rougher lead concentrate was obtained as 77.9% at 1500 rpm, it was acquired as 73.4% at 1300 rpm. According to the results, it was observed that as the rotor speed increased, the lead recovery was higher and thus the optimum rotor speed was found 1500 rpm.

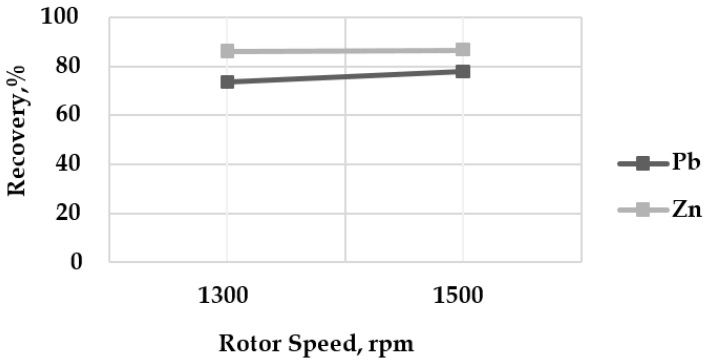


Figure 3. Effect on lead and zinc recoveries of different rotor speeds in lead flotation

3.4. Cleaning Flotation

Following the optimization of pH, particle size, and rotor speed, cleaning flotation was conducted to obtain saleable lead and zinc concentrates. The rougher flotation test conditions are given in Table 1. Before rougher flotation, 2 kg of sample was ground to below 75 µm and the test was carried out in a 5 L cell and the rotor speed was 1800 rpm. Lead flotation was carried out at natural pH (~8), zinc flotation was performed at pH 11.5. Cleaning flotation was carried out in cells with a rotor speed of 1000 rpm and a volume of 1.7 L. While two cleaning stages were performed on lead and zinc rougher concentrates, one cleaning stage was applied on pyrite rougher concentrate. Cleaning flotation conditions are given in Table 2 and the results of the test are shown in Table 3.

Table 2. Conditions of the cleaning flotation test

Circuits	Cleaning Flotation Conditions	Cleaning 1	Cleaning 2
Pb Cleaning Circuit	$Na_2S_2O_5$, g/t	250+0	125
	Conditioning time, min	5+0	2
	Aerophine 3418A, g/t	0+2.5	2
	Conditioning time, min	0+1	2
	MIBC, g/t	0+5	5
	Flotation time, min	2+2	3
Zn Cleaning Circuit	$Na_2S_2O_5$, g/t	500+0	250
	Conditioning time, min	5+0	5
	KAX, g/t	0+2.5	-
	Conditioning time, min	0+2	-
	MIBC, g/t	10+5	10
	Flotation time, min	3+2	3
Pyrite Cleaning Circuit	Tomamine-M73, g/t	0+10	
	Conditioning time, min	0+3	
	MIBC, g/t	0+10	
	Flotation time, min	3+3	

As a result of the cleaning flotation, lead concentrate containing 52.27% Pb content with 50.3% recovery and zinc concentrate containing 48.77% Zn content with 84.4% recovery were obtained. Besides, the lead concentrate assayed 2450 ppm Ag with a recovery of 38.4% while pyrite concentrate contained 6.22 ppm Au with a recovery of 50.1%.

Table 3. Results of the cleaning flotation tests (C: Concentrate, Mid: Middlings)

Products	Weight	Content				Recovery, %			
	%	Pb, %	Zn, %	Ag, ppm	Au, ppm	Pb	Zn	Ag	Au
Pb C.	0.6	52.27	5.01	2450	8.05	50.3	1.3	38.4	2.6
Pb Mid-1	0.4	11.21	3.94	681	4.34	7.2	0.7	7.1	0.9
Pb Mid-2	0.4	4.88	4.72	308	3.06	2.8	0.7	2.9	0.6
Pb Mid-3	1.4	3.86	4.27	174	2.43	8.9	2.7	6.5	1.9
Zn C.	3.9	0.53	48.77	123	1.30	3.3	84.4	12.6	2.7
Zn Mid-1	2.4	0.87	2.61	56	8.19	3.4	2.8	3.6	10.6
Zn Mid-2	1.7	0.48	0.86	32	5.01	1.3	0.6	1.4	4.6
Pyrite C.	15.1	0.35	0.25	29	6.22	8.5	1.7	11.5	50.1
Pyrite Mid.	5.5	0.24	0.33	11	0.60	2.1	0.8	1.6	1.8
Tailing	68.6	0.11	0.14	8	0.66	12.1	4.2	14.4	24.2
Total	100.0	0.62	2.27	38.19	1.87	100.0	100.0	100.0	100.0

4. Conclusions

Beneficiation studies by flotation were conducted on sulfide lead-zinc ore obtained from Niğde Bolkar-Tepeköy region. According to the results of the chemical analyses, the sample contains 0.67% Pb, 2.42% Zn, 1.63 g/t Au, and 40 g/t Ag. The mineralogical examinations showed that the representative ore sample comprised mainly pyrite, galena, and sphalerite. The study investigated the effect of pH, particle size, and rotor speed on lead flotation. While the best result was obtained regarding lead recovery at pH 8 (natural pH), significant decreases in lead recovery were observed as pH increased. A substantial change was not attained in the tests that examined particle size, considering energy consumption, the optimum particle size was determined as 74 µm. As the rotor speed increased, the lead recovery increased, therefore the rotor speed was determined as 1500 rpm. After the optimum parameters were obtained by rougher flotation, cleaning flotation was performed. As a result of cleaning flotation, a lead concentrate with 52.27% Pb content and a recovery of 50.4%, and a zinc concentrate with 48.77% Zn at a recovery of 84.4% were obtained. Besides, lead concentrate had 2450 ppm Ag content and pyrite concentrate contained 6.22 ppm Au. As a result, although the ore has a low lead content of 0.67%, the enrichment of gold and silver also shows that additional economic benefits can be obtained from the ore.

References

Ağaçayak, T., & Yılmaz, B. (2021). Optimum flotation conditions for the recovery of lead and zinc from Niğde-Ulukışla ore. Journal of Mineral Processing, 45(2), 125-132.

Cytec Industries. (2002). Aerophine 3418A promoter for selective flotation of lead and zinc minerals. Cytec Industries Technical Bulletin.

Fuerstenau, D. W. (1978). Sulfide mineral flotation. Mineral Processing and Extractive Metallurgy Review, 4(1-2), 167-197.

Rodrigues, R. T., Rubio, J., & Guo, W. (2001). Development of a new jet flotation system for laboratory and industrial applications. Minerals Engineering, 14(9), 1149-1156.

Investigation of the production of high carbon concentrate from Kütahya-Oysu graphite ores by flotation method

Gülşah Güven [1*], Hasret Demir [1], İbrahim Eren Püsür [1], Uğur Ulusoy [2], Fırat Burat [1]

[1]Istanbul Technical University, Mining Faculty, Mineral Processing Engineering Department, Maslak 34469, İstanbul, TÜRKİYE

[2]Sivas Cumhuriyet University, Faculty of Engineering, Chemical Engineering Department, Sivas 58140, TÜRKİYE

*Corresponding author: guveng15@itu.edu.tr (Gülşah Güven)

Abstract:

With the world keeping on moving from fossil fuels to renewable energy sources, battery metals—graphite included—are playing an ever-more-important role. Because high-grade graphite ores are harder to come by naturally, low-grade ores must be treated to boost their value in order to satisfy the growing demand, which is expected to rise by more than 700% by 2025 as a result of the widespread use of electric vehicles. New graphite occurrences in Eastern Türkiye reveal the hidden potential of mineralization, while on the other hand, the Menderes Massif metamorphic rocks in Western Türkiye host active graphite mining and potentially prove the existence of more graphite deposits. It was reported that the deposit contains 7.2 million tons of graphite and 125 million tons of potential graphite ore. Because graphite is hydrophobic by nature, low-grade ores are often beneficiated through flotation. The present research offers the first experimental investigation on the flotation method of graphite ore beneficiation in the Kütahya-Oysu region with the aim of optimizing some affecting variables in mechanical flotation. Oysu graphite ore containing 31% C was first ground to 300 microns and then a coarse concentrate was obtained by rougher flotation in a Denver flotation cell using kerosene as a collector, MIBC as a frother, and Na_2SiO_3 as a depressant. This combined process consisted of a rougher circuit applied to a graphite sample reduced to below 300 "microns, followed by cleaning and scavenger flotation circuits, resulting in a final concentrate containing 76.8% C, while after regrinding to below 200 microns, a scavenging circuit waste product containing 9.4% C was obtained.

Keywords: *Graphite, beneficiation, flotation, carbon*

1. INTRODUCTION

Graphite, which is a layered carbon material in which carbon atoms are arranged in a hexagonal pattern, plays a crucial role in various industries due to its unique combination of physical and chemical properties. These properties include high thermal and electrical conductivity, chemical inertness, and mechanical strength, making graphite indispensable in applications such as battery production, refractories, lubricants, and the manufacture of electrodes (Amnatsin et al., 2023; Kalyoncu and Taylor, 2000; Chang 2002; Kaya and Canbazoğlu, 2009). Since graphite is a mineral that is becoming more and more significant as we strive toward cleaner energy, the demand for graphite, a crucial component of battery materials used in electric vehicles (EVs), is expected to rise as EVs become more popular worldwide. 850,000 metric tons (Mt) of the commodity were produced in China in 2022, making up an astounding 65% of the global mine supply (Graphite Investing Outlook 2024). In addition, it was reported that the United States alone consumed about 72,000 Mt of graphite in 2022 (Karl et al., 2022). The European Union has classified graphite as one of the 14 essential raw minerals due to its strategic significance, which reflects the need for safe supply networks and the rise in worldwide demand. The recovery of graphite from primary sources, such as natural graphite ore, is essential to meet the increasing global demand. Natural graphite is mined from deposits where it exists as flakes, lumps, or amorphous forms, each varying in quality and suitability for different industrial applications (Jin et al.,

2018). Flake graphite, in particular, is highly sought after for its superior properties and is commonly used in high-technology applications, including lithium-ion battery anodes, where high purity and crystallinity are required (Vasumathi et al., 2023).

The flotation process, which leverages the natural hydrophobicity of graphite, is one of the most effective methods for concentrating graphite from natural ores. This process involves the separation of graphite particles from the surrounding gangue minerals, resulting in a high-purity concentrate that can be further processed for industrial use. Türkiye is a country with significant mineral wealth, including notable graphite deposits. The most prominent of these is the Kütahya-Oysu deposit, which is the only active graphite mine in the country. This deposit is of particular interest due to its potential to supply high-quality graphite for both domestic use and international markets. The strategic importance of developing Türkiye's graphite resources is underscored by the country's increasing focus on energy independence and technological innovation, particularly in sectors such as electric vehicles and renewable energy storage.

The deposit in Kütahya-Oysu is primarily composed of microcrystalline or amorphous graphite, which, despite being of lower quality compared to flake graphite, can be effectively used in various industrial applications following proper beneficiation (Tufan and Batar, 2015). The exploitation of these deposits is essential to making Türkiye a major player in the world graphite market and lowering its reliance on imported graphite.

Besides, China is the main supplier of graphite, accounting for 70% to 80% of the world's graphite production. Since China controls a large portion of the world's graphite production, it is well-positioned to influence global prices and supply dynamics. There are considerable reports that elucidate the application of gravity separation and flotation techniques to remove gangue materials from graphite (Li et al., 2015; Moradi and Botte, 2016).

Türkiye's graphite resources have been underutilized historically, partly due to the challenges associated with the small-scale dispersion and fine-grained nature of the deposits. On the other hand, new opportunities for the effective recovery and use of these resources have been created by recent developments in beneficiation technology, such as the optimization of flotation operations.

Although the beneficiation of Kütahya Oysu graphite ore by flotation was previously studied by Tufan and Batar (2015), this study is the first of its kind in terms of the studied chemicals and flotation stages.

Following the preparation of run-of-mine graphite ore with a 13.3% total carbon content in -300 micron size, butyl glycol was utilized as a frother, diesel oil as a collector, sodium silicate as a depressant, and S-9278 as a pH regulator. 76.89% concentrate grade and 71.59% flotation efficiency were attained as a consequence of this optimization study. Therefore, this study aims to optimize the recovery of graphite from primary sources using flotation. The research focuses on improving the purity and recovery of the graphite concentrate by process parameters, including particle size, collector dosage, and the use of depressants.

2. MATERIAL AND METHODS

2.1. Material

In this study, the graphite ore was obtained from the Kütahya region of Türkiye. Oysu region is of the microcrystalline and macrocrystalline graphite type. More accurately, it was formed within a crystalline series of an old coal level as a result of the metamorphism of this series. The ore sample, which underwent two-stage crushing at the facility, was sent to the ITU Mineral Processing Engineering Laboratory by company officials to be used in experimental studies. Firstly, the riffle sample splitter was utilized as part of the systematic sample reduction process before the grinding and particle size analysis experiments. After the screen analysis, the fractions and weight are determined, and the results are given in Table 1. The cumulative undersize curve (Fig. 1) showed that the d_{80} size of the representative sample was around 5.9 mm.

The proximate analysis and calorific value of the representative sample are given in Table 2. XRD studies were performed on the representative sample and presented in Fig. 2. According to the phase

composition, approximately 80% of the gangue minerals in the ore are calcite and the remaining amount is associated with silicates.

Table 1. Screen analysis of primary source graphite sample

Size (mm)	Weight (%)	Σ % undersize
13	2.3	100.0
-13+11	4.7	97.6
-11+9	5.3	93.0
-9+5.6	7.1	87.7
-5.6+4.70	4.8	80.7
-4.70+3.35	9.6	75.9
-3.35+2	12.9	66.3
-2+1	13.7	53.4
-1+0.5	8.9	39.7
-0.5+0.3	5.5	30.9
-0.3+0.212	3.7	25.3
-0.212+0.15	5.6	21.6
-0.15+0.106	4.6	16.0
-0.106+0.053	7.5	11.4
-0.053+0.038	2.9	3.9
-0.038	1.0	1.0
TOTAL	100.0	

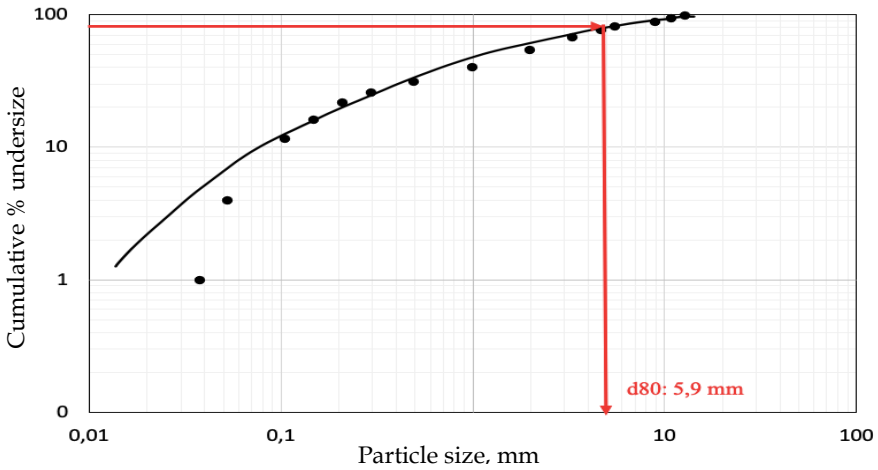


Fig. 15. The cumulative undersize curve of the representative sample

Table 2. Chemical analysis of the representative ore

Sample	Ash, %	C, %	S, %	Volatile, %	Fixed C, %	Calorific value, (kcal/kg)
Primary source	48.9	31.2	0.04	19.4	31.7	2614

2.2. Method

The steel ball mill with a volume of 5 L was used to grind the ore below 300, 250, and 200 microns. The dry grinding was carried out using 300 g of crushed sample. After the graphite was ground to the specific size, a Denver-type flotation cell (Fig. 3) was used to determine the optimum flotation parameters: feed size, kerosene, and Na_2SiO_3 dosage. MIBC (Methyl Isobutyl Carbinol) is also used as a frother. Impeller speed were kept constant at 1500 rpm. All chemicals used in experimental studies were provided by the Karabacak Mining Graphite Flotation Plant.

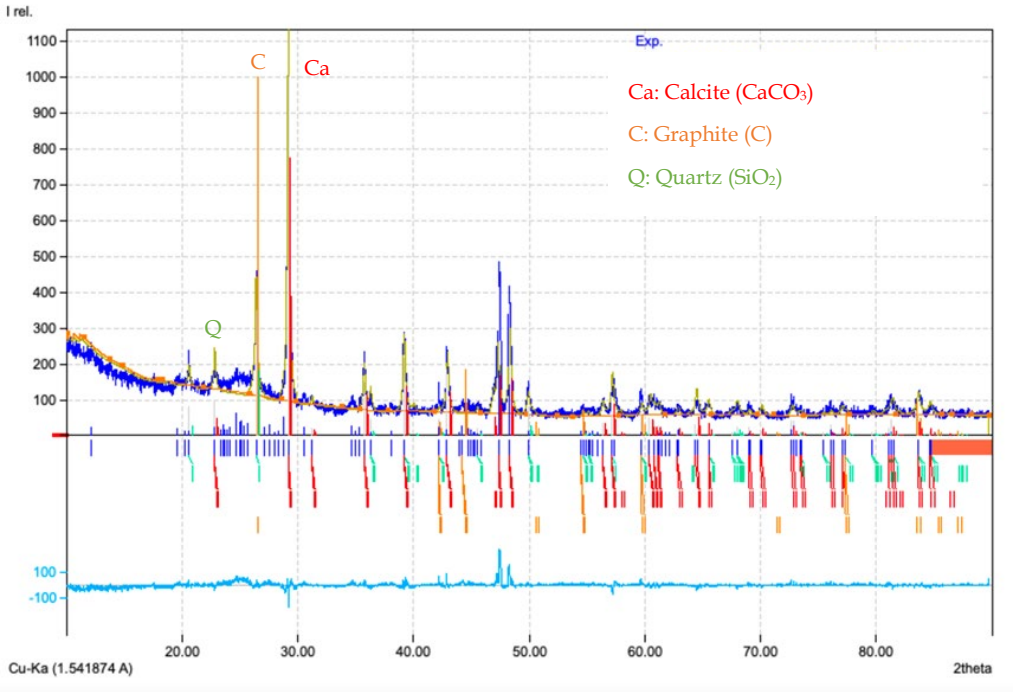


Fig. 16. XRD analysis result of the graphite sample



Fig. 17. Graphite Flotation Experiment in Denver Flotation Cell

Flotation tests were performed on ground ore below 300, 250, and 200 microns at constant collector and depressant dosages to determine the optimum feed size. Na_2SiO_3 was added to the pulp at different amounts (0, 1000, and 2000 g/t) to investigate the effect of dispersant agents for improved recovery of C. After the rougher flotation, the float product was sent to one-stage cleaning and the sunk material was transferred to two-stage scavenger circuits to obtain the graphite with high flotation efficiency. To determine the C content of all products, an Eltra CS 580 carbon-sulfur analyzer was used.

3. RESULTS AND DISCUSSION

3.1. Optimization of Feed Size on Flotation

The sample was ground in various fractions (-300, 250, and 200 microns) using a ball mill, and the effect of feed size on flotation was investigated. In flotation experiments, the amount of kerosene and MIBC was kept constant at 750 g/t and 100 g/t. 0+250+250+250+250 g/t kerosene and 50+20+20+10 g/t MIBC were added to the pulp at each stage of flotation. Conditioning and flotation times were determined as 3+3+3+3+3+3 minutes and 3+3+3+3+3 minutes, respectively.

Table 3. The effect of feed size on flotation

Feed Size, µm	Products	Weight, %	C, %	Recovery, %
-300	Float 1	10.4	46.5	15.1
	Float 2	25.8	67.7	54.8
	Float 3	16.5	29.5	15.3
	Float 4	10.7	11.0	3.7
	Tailing	36.6	9.7	11.1
	Total	100	31.9	100
-250	Float 1	13.3	40.3	17.0
	Float 2	31.3	63.4	62.9
	Float 3	12.7	19.5	7.8
	Float 4	9.2	10.6	3.1
	Tailing	33.4	8.6	9.1
	Total	100	31.6	100
-200	Float 1	3.8	45.6	5.5
	Float 2	12.6	63.6	25.8
	Float 3	27.0	55.9	48.4
	Float 4	15.0	18.3	8.8
	Tailing	41.6	8.7	11.6
	Total	100.0	31.2	100.0

As is seen in Table 3, the carbon content and recovery values of products obtained for the three different particle sizes were found relatively similar. However, taking into account the grinding costs, the - 300 micron particle size was chosen as the optimum feed size.

3.2. Optimization of Depressant Dosages

The initial Na_2SiO_3 dosage was examined between 0-1000-2000 g/t during optimization. The investigated amounts of Na_2SiO_3 were added to the pulp in four stages. Table 4 shows the effect of Na_2SiO_3 dosage on flotation.

As seen in Table 4, when no depressant was added the highest C-containing graphite concentrate (63.9%) was obtained. With the addition of Na_2SiO_3, the C content of Float 1 products decreased, while the C content of Float 2 products increased. The reason for this is thought to be that gangue minerals, which are still interlocked on large-sized graphite grains, gained wettable properties with the addition of the depressant and concentrated in Float 2 products. Accordingly, it was decided to conduct the subsequent experiments without the use of a depressant in the first two flotation stages. It was also planned to add a grinding step before the scavenger circuit to facilitate the release of locked particles in the middlings.

Similarly, in previous studies, Öney and Samanli (2016) who achieved a clean concentrate with 77.8% total carbon content from Kütahya Altıntaş region graphite ore with a total carbon content of 17.6% with a yield of 46.68% also concluded that the dosage of sodium silicate has a small effect on the total carbon content and total carbon recovery of the coarser graphite concentrate.

Table 4. The effect of depressant

Na_2SiO_3, g/t	Products	Weight, %	C, %	Recovery, %
0	Float 1	9.6	63.9	19.4
	Float 2	33.6	58.2	62.0
	Float 3	12.8	14.5	5.9
	Float 4	13.3	9.5	4.0
	Tailing	30.8	8.9	8.7
	Total	100.0	31.5	100.0
1000	Float 1	10.4	46.5	15.1
	Float 2	25.8	67.7	54.8
	Float 3	16.5	29.5	15.3
	Float 4	10.7	11.0	3.7
	Tailing	36.6	9.7	11.1
	Total	100	31.9	100
2000	Float 1	9.8	46.0	14.4
	Float 2	33.8	59.6	64.0
	Float 3	15.0	18.7	8.9
	Float 4	12.3	9.8	3.8
	Tailing	29.1	9.6	8.9
	Total	100.0	31.5	100.0

After the two coarse (-300 microns) flotation stages, the coarse tailings containing locked graphite and gangue minerals were re-ground (-200 microns) to achieve further particle liberation and increase carbon efficiency at the subsequent scavenger flotation.

Table 5. The effect of depressant on scavenger circuit

Na_2SiO_3, g/t	Products	Weight, %	C, %	Recovery, %
0	Concentrate	16.6	68.3	35.9
	Middling 1	23.9	51.5	38.8
	Middling 2	11.1	22.1	7.7
	Middling 3	12.1	14.6	5.6
	Tailing	36.3	10.5	12.0
	Total	100.0	31.7	100.0
300	Concentrate	24.1	70.3	54.0
	Middling 1	19.2	41.0	25.1
	Middling 2	13.3	18.1	7.7
	Middling 3	9.5	11.9	3.6
	Tailing	33.9	8.9	9.6
	Total	100.0	31.3	100.0

As seen in Table 5 the depressant has a limited effect on decreasing the C content of tailings. When no depressant was used, the C content of the tailings was found to be 10.5%, however, the C content decreased to 8.9% after 300 g/t Na_2SiO_3 in the scavenger circuit.

Table 6. The proximate analyses and calorific value of the concentrate and tailings after depressant addition on the scavenger circuit

Products	Ash, %	C, %	S, %	Volatile, %	Fixed C, %	Calorific value, (kcal/kg)
Concentrate	22.2	70.3	0.040	15.9	61.9	5059
Tailing	71.2	8.9	0.002	25.3	3.5	1014

Table 6 shows the proximate analysis and calorific value of the concentrate and tailings obtained in the experiments in which depressant was added in the scavenger circuit after re-grinding of tailings. The high level of volatiles indicates that these products may contain a carbonated structure. For this reason, XRD analysis was performed on the concentrate and tailings, and the results are shown in Fig. 4.

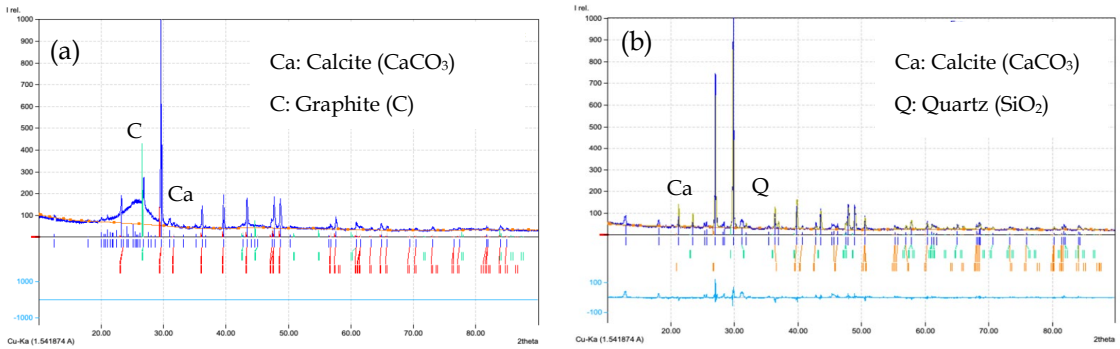


Fig. 18. XRD analysis result of7 graphite (a) concentrate and (b) tailings

Calcite is the dominant gangue mineral in the run-of-mine sample and presents mainly in the graphite concentrate, however, silicates could not be detected. Silicates that have hydrophilic features are generally found in fine sizes and liberated as clay form. According to the XRD results in Figure 4a, a large number of silica peaks were detected along with calcite. Therefore, it was understood that they remained in the cell and concentrated in the tailings at the end of the flotation process. When we look at the phase composition of the minerals that make up the tailings, approximately 70% calcite and 30% silicon dioxide are present. Especially due to the high calcite content in the concentrate, studies were carried out to evaluate the rough concentrate by cleaning flotation after re-grinding.

After the two stages of coarse flotation stages, 500 g/t depressant was added to the cleaning circuit without re-grinding. Thus, the effect of depressant addition on the cleaning circuit of the floating product with a size of -300 microns was investigated. As seen in Table 7, the addition of 500 g/t of Na_2SiO_3 in the cleaning circuit has a very positive effect on C content and recovery. With the dispersing and depressing effect provided by the depressant, calcite-dominant gangue minerals couldn't float and collected in the Middling 1 product. Consequently, a final concentrate assaying 76.8% C content was obtained with 69% recovery. The recommended flowsheet for graphite recovery is shown in Fig. 5.

Table 7. The effect of depressant on cleaning circuit

Na_2SiO_3, g/t	**Products**	**Weight, %**	**C, %**	**Recovery, %**
0	Concentrate	16.6	68.3	35.9
	Middling 1	23.9	51.5	38.8
	Middling 2	11.1	22.1	7.7
	Middling 3	12.1	14.6	5.6
	Tailing	36.3	10.5	12.0
	Total	100.0	31.7	100.0
500	Concentrate	34.4	76.8	69.0
	Middling 1	9.6	51.0	12.8
	Middling 2	11.2	18.7	5.5
	Middling 3	30.4	11.5	9.2
	Tailing	14.4	9.4	3.5
	Total	100.0	38.2	100.0

The previous study (Tufan and Batar, 2015) conducted with ore from the same region shows the following results. The highest concentrate grade and recovery were obtained as 76.89% and 71.59%, respectively, by enrichment of Kütahya, Oysu graphite ore containing 13.3% total carbon by flotation. Optimized conditions were obtained when 450 g/t butyl glycol was used as a frother, 1500 g/t diesel oil as a collector, 30 g/t Na_2SiO_3 as a suppressor and 250 g/t S-9278 (1%) as a regulator at pH 8-8.50 at -300 micron size.

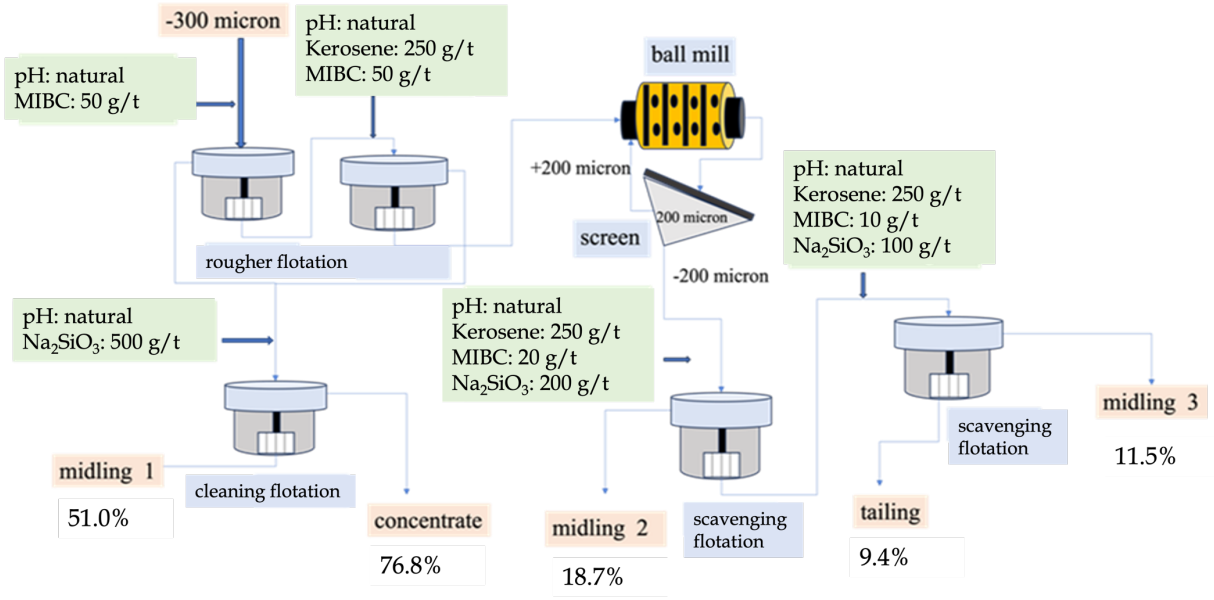


Fig. 19. Proposed flowchart for recovery of graphite

CONCLUSION

Graphite plays a crucial role as a key component in modern technology, especially in batteries. The importance of graphite in battery production lies in its excellent electrical conductivity, stability, and abundance, making it indispensable in ensuring the efficient performance of these energy storage systems. As the demand for energy storage solutions such as lithium-ion batteries continues to grow the importance of graphite will increase. In this study, graphite samples and flotation chemicals were obtained from Kütahya Oysu Graphite Beneficiation Plant, the only graphite beneficiation plant in Turkey. The samples were used to conduct various flotation experiments aimed at determining the optimal parameters for graphite recovery. Through the flotation studies, optimum conditions were determined, which led to significant findings. The material, reduced to below 300 microns at its natural pH (8-8.5), after two-stage coarse flotation and the addition 500 g/t depressant (Na_2SiO_3), a final concentrate with a carbon content of 76.8% was obtained with a 69% recovery. In the scavenging circuit, after grinding the sample to below 200 microns and adding 300 g/t Na_2SiO_3, a tailing with 9.4% carbon content and 3.5% recovery was obtained. The tailing was found to contain a high concentration of clay and calcium-based components, which contributed to the low carbon content.

However, the results of this study suggest that graphite recovery can be further improved in future studies so that high-quality concentrates can be recovered. Studies such as testing new chemicals and other enrichment methods combined with flotation may also be considered.

REFERENCES

Amnatsin, C., Kanlayakan, W., Lhosupasirirat, S., Verojpipath, N., Pragobjinda, B., Osotchan, T., Sirisinha, C., Srikhirin, T. (2023). Ultrafine Graphite Scrap and Carbon Blocks Prepared by High-Solid-Loading Bead Milling and Conventional Ball Milling: A Comparative Assessment, ACS Omega, *vol. 8*, no. 50, doi: 10.1021/acsomega.3c06164.

Chang, L. Y., (2002). Graphite. *In Industrial Mineralogy: Materials, Processes, and Uses* (L. L. Y. Chang, Ed.), Upper Saddle River, NJ: Prentice Hall, pp. 129–142.

Graphite Investing Outlook 2024, https://investingnews.com/free-report-online/graphite-investing-outlook-graphite-stocks-buy/

Jin, M., Xie, G., Xia, W., and Peng, Y. (2018). Flotation optimization of ultrafine microcrystalline graphite using a box-Behnken design. *International Journal of Coal Preparation and Utilization, vol. 38,* no. 6, pp. 281–289.

Kalyoncu, R. S., and Taylor, H. A. (2000). Natural graphite. *Kirk-Othmer Encyclopedia of Chemical Technology 39(11*): 31–34.

Karl, N. A., K, L. D., G, W. R.; Mauk, J. L., S, G. (2022). Graphite Deposits in the United States; U.S. Geological Survey Data Release: United States of America.

Kaya, Ö. and Canbazoğlu, M. (2009). Chemical demineralization of three different graphite ores from Türkiye. *Minerals and Metallurgical Processing, 26*, pp. 158–162.

Li, L., Qu, W., Zhang, X., Lu, J., Chen, R., Wu, F., Amine, K. (2015). Succinic acid-based leaching system: a sustainable process for recovery of valuable metals from spent Li-ion batteries. *J. Power Sources 282,* 544–551.

Öney, Ö., Samanli, S. (2016). Determination of optimal flotation conditions of low-grade graphite ore, E3S Web of Conferences 8, 01002, doi: 10.1051/e3sconf/20160801002 MEC2016.

Moradi, B., Botte, G.G. (2016). Recycling of graphite anodes for the next generation of lithium ion batteries. J. Appl. Electrochem. 46 (2), 123–148.

Tufan, B., and Batar, T. (2015). Oysu Grafit Cevheri Flotasyon Parametrelerinin İyileştirilmesi. *Süleyman Demirel University Journal of Natural and Applied Sciences vol. 19,* no. 3, pp. 17-25. doi: 10.19113/sdufbed.97179

Vasumathi, N., Sarjekar, A., Chandrayan, H., Chennakesavulu, K., Reddy, G. R., Kumar, T. V. V., El-Gendy, N. S., and Gopalkrishna, A. J. (2023). A mini Review on Flotation Techniques and Reagents Used in Graphite Beneficiation. *Hindawi International Journal of Chemical Engineering, vol 2023.* doi: 10.1155/2023/1007689

Enrichment of Yozgat Potassium Feldspar by Different Methods

Tülay Türk [1]*, Yunus Emre Çavdar [1], Murat Olgaç Kangal [1]

[1] Istanbul Technical University, Department of Mineral Processing Engineering, Maslak, İstanbul, TÜRKİYE

*Corresponding author: turktu@itu.edu.tr (Tülay Türk)

Abstract:

Feldspar, a crucial raw material in various industrial applications such as glassmaking, and ceramics, often contains iron impurities that can adversely affect the quality and color of the end products. Iron oxides in feldspar ores are particularly problematic in producing high-quality glass and ceramics, where even trace amounts of iron can lead to undesirable coloration and reduced transparency. Therefore, reducing iron content in feldspar ores is a significant process that enhances their suitability for high-end industrial uses. Potassium feldspar, in particular, holds substantial importance for Türkiye due to its extensive use in local industries. Despite Türkiye having considerable reserves of potassium feldspar, the country still relies on imports to meet the high demand in various sectors. Enhancing the quality of locally sourced potassium feldspar by reducing iron content can significantly reduce import dependency and strengthen domestic production capabilities. This study investigates the reduction of iron content in potassium feldspar ore sourced from the newly identified Sorgun, Yozgat Region reserve. The composition of the raw ore includes 6.2% K2O, 2.16% Na2O, 2.23% Fe2O3, 0.323% TiO2, and 71.13% SiO2. Both magnetic separation and flotation methods were applied to achieve a lower iron content. Magnetic separation did not reach optimal results regarding Fe2O3 reduction. However, the flotation method demonstrated promising outcomes. In the flotation experiments, varied parameters such as particle size (-300, -212, -106 µm), collector type (Derna-7, Derna-4, DAHC), and size fractions (-300+74, -300+53, -300+44, -300+38 µm) to optimize the potassium feldspar concentrate with the lowest possible iron content were systematically studied.

Keywords: *Potassium feldspar, magnetic separation, flotation, concentrate, iron reduction*

1. Introduction

Feldspar, a group of rock-forming minerals, is one of the most abundant constituents of the Earth's crust, comprising approximately 60% of it. This mineral group includes three main types: potassium feldspar (K-feldspar), sodium feldspar (Na-feldspar), and calcium feldspar (Ca-feldspar), each of which has distinct chemical compositions and properties. The industrial applications of feldspar are diverse, primarily due to its role as a flux in the ceramic and glass industries, where it significantly lowers the melting temperature of the raw materials, thereby enhancing the efficiency of the production processes (Gougazeh, 2022; Wang et al., 2018). One of the most common impurities found in feldspar ore is iron, typically present in the form of hematite or magnetite. The removal of iron is crucial, as even small amounts can lead to discoloration in ceramic and glass products. Various methods have been developed to address this issue, including magnetic separation, flotation, and chemical leaching (Yassin et al., 2023). Various studies have demonstrated that magnetic separation is an effective method for removing ferrous impurities from feldspar ore. These investigations show that both wet and dry magnetic separators can achieve high efficiency in separating iron oxide-containing impurities, significantly enhancing the quality of feldspar. The advantages of magnetic separation in eliminating iron-containing compounds and other paramagnetic impurities contribute to increasing the potential industrial applications of feldspar (Hillier and Hodson, 1997; Liu et al., 2013; Moura et al., 2019; Baila et al., 2023; Subari et al., 2024). Flotation techniques also play a significant role in the purification of feldspar. Reverse flotation, where impurities are selectively floated away from the desired feldspar, has been employed successfully. For example, the use of cationic collectors has been shown to enhance the separation of iron-bearing minerals from feldspar in various studies (Yushina et al., 2021; Isnugroho et al., 2019). The optimization of flotation conditions, such as pH and collector type, is essential for

maximizing the recovery of high-quality feldspar concentrates (Yushina et al., 2021). Additionally, the combination of flotation with other methods, such as magnetic separation, has been explored to achieve better results in impurity removal (Gougazeh, 2022). Chemical leaching is another approach that has gained attention for its ability to selectively dissolve impurities from feldspar ore. Acid leaching, particularly with citric acid or hydrochloric acid, has been investigated for its effectiveness in removing iron and other metallic impurities. The kinetics of these leaching processes are influenced by factors such as temperature, concentration of the leaching agent, and reaction time, making it crucial to optimize these parameters for efficient impurity removal (Venegas et al., 2014). Moreover, the integration of leaching with thermal treatments has been proposed to enhance the overall recovery of valuable components from feldspar ore (Zhong et al., 2016). In addition to traditional methods, recent advancements in technology have introduced novel approaches for feldspar purification. For instance, the development of dry vibrating high-gradient magnetic separators has shown promise in enhancing the efficiency of iron removal from potash feldspar ores. These innovative technologies not only improve the recovery rates of feldspar but also contribute to more sustainable mining practices by reducing water usage and minimizing waste generation (Xu et al., 2021).

The economic implications of removing impurities from feldspar ore are significant. High-purity feldspar commands a premium price in the market, making the investment in advanced beneficiation techniques economically viable. Furthermore, the recovery of critical raw materials, such as lithium and tantalum, from feldspar processing waste has been explored, adding an additional layer of value to the beneficiation process (Vrbický & Přikryl, 2021; Gougazeh, 2022). This dual focus on purity and resource recovery aligns with the growing demand for sustainable practices in the mining industry.

In this context, our primary objective is to produce a commercially saleable potassium feldspar concentrate with iron content below 0.5% Fe_2O_3 from the recently discovered deposit in the Sorgun/Yozgat region. In order to achieve this aim, magnetic separation and flotation methods were used in this study.

2. Material and Methods

2.1. Material

Feldspar sample was obtained from the Sorgun/Yozgat region for this study. In order to determine particle size distribution, sieve analysis performed to define d80 size of the raw ore. The results of the sieve analysis are given in Table 1 and Fig. 1. According to the sieve analysis results, d90, d80, d50, d10 sizes were found to be 1.62, 1.39, 0.77, 0.10 mm, respectively.

Table 1. Sieve analysis of the ore

Particle size, mm	Weight, %	US*, %
-2+1	35,7	100
-1+0,5	28,0	64,3
-0,5+0,3	12,7	36,3
-0,3+0,212	5,4	23,6
-0,212+0,106	4,7	18,3
-0,106+0,074	3,1	13,6
-0,074+0,053	2,2	10,5
-0,053+0,038	1,9	8,2
-0,038	2,0	6,3
Total	100,0	

*US: Cumulative undersize

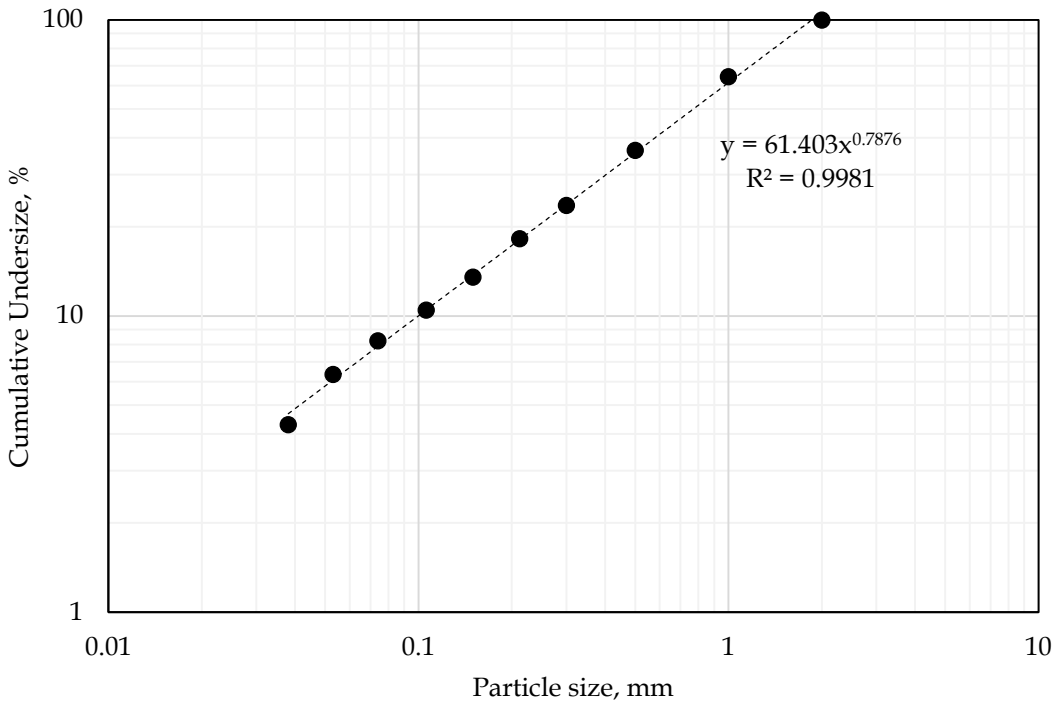


Fig. 1. Cumulative undersize graph of the ore

After determining the particle size, chemical and mineralogical analyses were conducted to further characterize the sample. The chemical composition of the raw ore was analyzed using the Inductively Coupled Plasma (ICP) method. The results, presented in Table 2, indicate that the ore contains 5.03% K, 1.53% Na, 1% Ca, and 1.4% Fe. To assess the oxide composition of the raw ore, X-Ray Fluorescence (XRF) analysis was performed. According to the XRF results, the ore is composed of 65.69% SiO_2, 17.62% Al_2O_3, 7.21% K_2O, 2.28% Fe_2O_3, 2.14% Na_2O, 1.66% CaO, 0.37% TiO_2, 0.36% MgO, with a loss on ignition of 2.62%.

Table 2. ICP analysis results of the representative raw ore

Component	Content, %	Component	Content, ppm	Component	Content, ppm
Al	6.41	As	14.4	Li	20.53
Ca	1	Ba	592.4	Mn	417.79
Fe	1.4	Be	5.82	Mo	9.94
K	5.03	Ce	86.03	*Ni	7.12
Mg	0.13	Co	7.39	*Pb	34.67
Na	1.53	Cr	61.11	Sb	7.57
P	0.04	*Cu	35.16	Sr	152.06
S	0.07	Ga	17.28	V	29.26
Ti	0.08	Hf	2.42	*Zn	49.12
		La	51.17	Zr	145.38

Following the chemical analysis, mineralogical characterization was performed using X-Ray Diffraction (XRD) analysis. This was conducted with a copper-sourced Panalytical X'Pert Pro diffractometer, and the PDF4/Minerals ICDD software was employed for mineral phase identification. The relative proportions of the mineral phases were determined using the Rietveld refinement method. The XRD graph is given in Fig. 2.

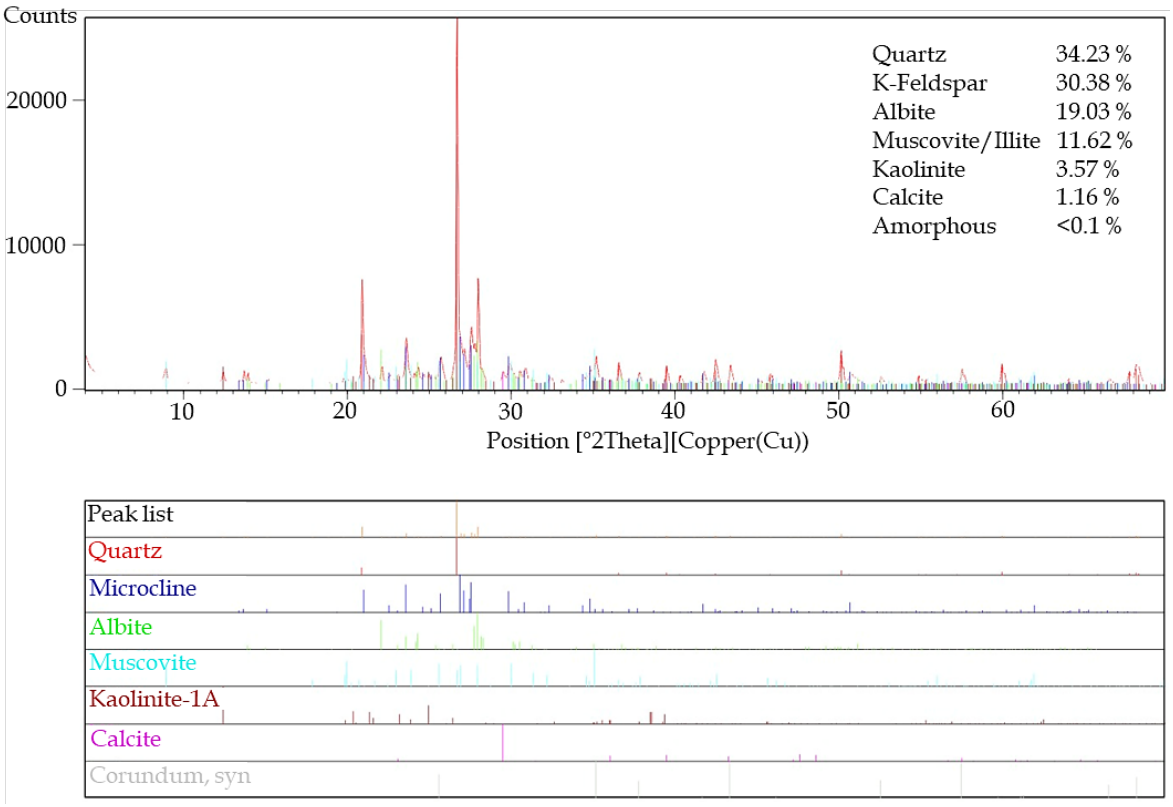


Fig. 2. XRD analysis result of the ore

The XRD pattern of the ore, displayed in Fig. 2, reveals that the ore primarily consists of quartz (SiO_2) and microcline ($KAlSi_3O_8$), alongside albite ($NaAlSi_3O_8$), muscovite ($KAl_2(Al_2Si_3O_{10})(OH)_2$), kaolinite ($Al_2Si_2O_5(OH)_4$), calcite ($CaCO_3$), and corundum ($Al_2O_3$).

2.2. Methods

For the enrichment of feldspar, both physical and physico-chemical methods were employed to obtain a saleable concentrate. The ore sample was initially classified into the following size fractions: -2+1 mm, -1+0.5 mm, -0.5+0.212 mm, and -0.212 mm. These size fractions were then subjected to magnetic separation experiments using high-intensity magnetic separators. For size fractions above 0.212 mm, a REMS magnetic separator (10,000 Gauss) was used, while a Carpco magnetic separator, operating between 6,000 and 9,200 Gauss, was used for fractions below 0.212 mm.

Following the magnetic separation experiments, flotation tests were conducted on the raw sample. The flotation experiments examined various parameters, including particle size (-300 µm, -212 µm, -106 µm), collector type (Derna-7, Derna-4, DAHC), and the size of the separated slurry (75 µm, 53 µm, 44 µm, 38 µm). After optimizing the flotation conditions, the non-magnetic fraction obtained from the magnetic separation process was subjected to flotation to enhance feldspar recovery.

3. Experimental Results

3.1. Magnetic separation experiments

For the magnetic separation experiments, the ore samples, previously divided into size fractions, were subjected to magnetic separation to reduce the iron content using REMS and Carpco devices. In the experiments utilizing the REMS separator, cleaning circuits were applied to the products when necessary. In the trials involving the Carpco separator, the magnetic field strength was maintained at a constant 5 A, and the magnetic product was cleaned in two stages. The results of the magnetic separation experiments are presented in Table 3.

Table 3. Results of magnetic separation experiments

Size fractions, mm	Sample	Amount, %	K_2O		Na_2O		SiO_2		Fe_2O_3		LOI, %
			C, %	D, %	C, %	D, %	C, %	D, %	C, %	D, %	
-2+1	Non-magnetic	92.2	6.9	93.6	2.19	92.1	69.81	93.3	1.56	73.5	2,31
	Midling	6.5	5.85	5.6	2.31	6.9	61.52	5.8	4.47	14.9	4,64
	Magnetic	1.3	4.26	0.8	1.73	1.0	49.41	0.9	17.66	11.6	6,19
	Total	37.9	6.80	37.2	2.19	37.2	69.01	38.9	1.96	34.4	2,51
-1+0.5	Non-magnetic	67.2	7.29	70.4	2.26	67.2	70.13	69.5	1.06	36.8	1,8
	Midling	28.7	6.47	26.7	2.35	29.8	64.40	27.3	2.73	40.4	3,52
	Magnetic	4.1	5.09	3.0	1.68	3.0	54.23	3.3	10.85	22.8	6,01
	Total	29.4	6.96	29.6	2.26	29.8	67.84	29.6	1.94	26.4	2,47
-0.5+0.212	Non-magnetic	44.5	7.07	45.7	2.47	47.4	71.18	47.3	0.8	17.0	1,68
	Midling	45.6	6.99	46.4	2.35	46.2	65.87	44.8	1.85	40.3	2,73
	Magnetic	9.9	5.51	7.9	1.5	6.4	53.54	7.9	9.07	42.7	6,24
	Total	15.2	6.88	15.1	2.32	15.8	67.02	15.1	2.09	14.8	2,61
-0.212	Non-magnetic	79.8	7.4	82.8	2.3	83.5	64.58	81.8	1.7	45.1	3,02
	Magnetic	20.2	6.08	17.2	1.8	4.5	56.61	18.2	8.16	54.9	5,01
	Total	17.5	7.13	18.0	2.20	17.2	62.97	16.4	3.01	24.4	3,42
TOTAL		100,0	6.92	100.0	2.23	100.0	67.30	100.0	2.16	100.0	2.67

C: Content , D: Distribution , LOI: Loss on ignition

According to the experimental results, the non-magnetic product with the lowest iron content was obtained in the -0.5+0.212 mm size fraction, with an Fe_2O_3 content of 0.8%. Additionally, the K_2O content of the non-magnetic product in this size group was determined to be 7.07%. Based on these findings, it was concluded that reducing the iron content to below 0.5% cannot be achieved solely through magnetic separation. Consequently, further experiments were carried out using the flotation method.

3.2. Flotation experiments

3.2.1. Effect of particle size

In the flotation experiments, the particle size parameter was evaluated first. The flotation process was conducted in two stages, beginning with oxide minerals, followed by the flotation of mica minerals. In the oxide flotation circuit, the pH was maintained at 9.5, and a total of 2500 g/t of Derna-7 (a mixture of oleic and linoleic acid, serving as an anionic collector) was used over five stages. Mica flotation was performed at a pH of 2.5, using a total of 200 g/t of DAHC (dodecylamine hydrochloride, a cationic collector) in two stages.

The experimental results for three size fractions (-300 µm, -212 µm, and -106 µm) are presented in Table 4. Analysis of these results shows that the lowest iron content, 0.69% Fe_2O_3, was achieved at the -300 µm particle size. Although finer particle sizes typically enhance separation efficiency due to increased liberation of the minerals, in the case of feldspar flotation, efficiency decreases as the particle size becomes finer. This decrease in flotation efficiency at smaller particle sizes can be attributed to several factors, including the increased surface area of fine particles, which leads to higher reagent consumption and less selective attachment of collectors. Consequently, the optimal result was obtained at the -300 µm size, which was identified as the most suitable particle size for feldspar flotation in this study.

Table 4. Results of particle size experiments

Size fractions, µm	Sample	Amount, %	K_2O		Na_2O		Fe_2O_3	
			C, %	D, %	C, %	D, %	C, %	D, %
-106	Float-1	20.9	6.23	19.1	1.87	18.7	3.76	37.1
	Float-2	16.4	6.83	16.4	2.01	15.7	2.9	22.4
	Float-3	15.8	6.96	16.1	2.12	16.0	1.87	14.0
	Float-4	9.7	6.95	9.9	2.12	9.8	1.51	6.9
	Float-5	8.2	6.99	8.4	2.2	8.5	1.18	4.5
	Float-6	2.1	8.18	2.5	1.76	1.8	1.95	2.0
	Float-7	2.0	7.84	2.3	1.75	1.6	2.13	2.0
	Sunken	24.9	6.96	25.3	2.35	27.9	0.95	11.1
	Total	100.0	6.83	100.0	2.10	100.0	2.12	100.0
-212	Float-1	9.5	5.96	8.1	1.65	7.7	4.08	19.3
	Float-2	14.9	6.6	14.1	1.82	13.3	3.67	27.2
	Float-3	10.7	6.91	10.6	1.96	10.3	2.7	14.4
	Float-4	11.7	7.15	12.0	2.02	11.6	1.84	10.7
	Float-5	14.7	7.19	15.1	2.11	15.2	1.3	9.5
	Float-6	4.6	7.74	5.1	1.69	3.8	2.18	5.0
	Float-7	1.0	7.79	1.1	1.84	0.9	2.44	1.2
	Sunken	32.9	7.2	33.9	2.31	37.2	0.78	12.7
	Total	100.0	6.99	100.0	2.04	100.0	2.01	100.0
-300	Float-1	23.3	6.63	22.7	1.86	20.3	3.42	40.5
	Float-2	13.4	6.91	13.6	1.98	12.5	3.03	20.6
	Float-3	8.9	7.12	9.3	2.01	8.4	2.6	11.8
	Float-4	4.9	6.94	5.0	2.15	4.9	2.51	6.2
	Float-5	5.9	6.79	5.9	2.35	6.5	1.61	4.8
	Float-6	0.9	8.23	1.1	2.36	1.0	1.77	0.8
	Float-7	0.5	8.15	0.6	2.07	0.5	1.99	0.5
	Sunken	42.2	6.73	41.8	2.32	45.9	0.69	14.8
	Total	100.0	6.80	100.0	2.13	100.0	1.97	100.0

C:Content , D:Distribution

3.2.2. Effect of collector type

In the experiments conducted to investigate the effect of different collectors, the conditions in the oxide flotation circuit were kept constant. In the mica flotation circuit, Derna-4, a collector capable of floating both mica and oxide minerals, was used in place of DAHC, a selective collector for mica minerals. During the experiments with Derna-4, the pH was maintained between 6 and 6.5, and a total of 60 g/t of the collector was applied in two stages. The results of the experiments using DAHC and Derna-4 are presented in Table 5.

Table 5. Results of collector type experiments

Collector type	Sample	Amount, %	K_2O		Na_2O		Fe_2O_3	
			C, %	D, %	C, %	D, %	C, %	D, %
DAHC	Float-1	23.3	6.63	22.7	1.86	20.3	3.42	40.4
	Float-2	13.4	6.91	13.7	1.98	12.5	3.03	20.7
	Float-3	8.9	7.12	9.3	2.01	8.4	2.6	11.7
	Float-4	4.9	6.94	5.0	2.15	4.9	2.51	6.2
	Float-5	5.9	6.79	5.9	2.35	6.5	1.61	4.8
	Float-6	0.9	8.23	1.1	2.36	1.0	1.77	0.8
	Float-7	0.6	8.15	0.7	2.07	0.5	1.99	0.6
	Sunken	42.2	6.73	41.8	2.32	45.9	0.69	14.8
	Total	100.0	6.80	100.0	2.13	100.0	1.97	100.0
Derna-4	Float-1	7.1	5.69	5.6	1.24	4.6	3.88	15.1
	Float-2	6.4	6.38	5.6	1.61	5.4	4.1	14.4
	Float-3	7.0	6.78	6.6	1.47	5.4	1.07	4.1
	Float-4	6.8	6.89	6.5	1.53	5.5	3.63	13.6
	Float-5	8.7	7.07	8.5	2.1	9.6	2.56	12.2
	Float-6	1.8	7.37	1.8	1.65	1.5	2.35	2.3
	Float-7	1.6	7.33	1.6	1.74	1.5	2.51	2.2
	Sunken	60.7	7.56	63.7	2.09	66.6	1.08	36.1
	Total	100.0	7.20	100.0	1.91	100.0	1.82	100.0

C:Content , D:Distribution

According to the results, the sinking product obtained with Derna-4 exhibited a higher iron content compared to that obtained with DAHC; however, the K_2O content was also higher in the Derna-4 experiment. It should be noted that in the experiments with Derna-4, the presence of fine particles in the slurry may have negatively impacted the yield. Despite this, Derna-4 was selected for use in subsequent experiments due to its favorable results.

3.2.3. Effect of the fine sizes

Due to the negative effect of fine particle sizes on feldspar flotation efficiency, subsequent flotation experiments were conducted by separating the fine fractions. Derna-7 was utilized for oxide flotation, while Derna-4 was used for mica flotation, under conditions same as the previous experiments. The ore sample, ground to below -300 microns, was further subdivided into particle size ranges of -300+75, -300+53, -300+44, and -300+38 microns, and each size fraction was subjected to flotation testing. The results of these experiments are presented in Table 6.

Upon analyzing the test results, it was observed that the lowest iron content was achieved with the sample fractionated at 53 microns, which was subsequently identified as the optimal particle size. The composition of the product obtained at 53 microns closely resembled that of the sinking product in the experiment conducted with DAHC.

Given that DAHC is a more expensive collector compared to Derna-4, the use of Derna-4 presents a more cost-effective alternative for subsequent flotation experiments. Despite the comparable performance of DAHC in achieving low iron content, the economic advantage of using Derna-4 makes it the preferred collector. This choice is particularly relevant in industrial applications, where the cost of reagents can significantly impact the overall efficiency and profitability of the process.

Table 4. Results of particle size experiments

Size fractions, µm	Sample	Amount, %	K_2O		Na_2O		Fe_2O_3	
			C, %	D, %	C, %	D, %	C, %	D, %
-300+38	Float-1	17.2	5.80	15.0	2.54	19.7	3.48	28.1
	Float-2	0.5	6.94	0.5	1.08	0.3	3.54	0.9
	Sunken	43.2	6.95	45.0	2.34	45.6	0.90	18.2
	Slime	39.0	6.75	39.5	1.95	34.4	2.89	52.9
	Total	100.0	6.67	100.0	2.22	100.0	2.13	100.0
-300+44	Float-1	19.2	6.05	16.5	2.21	20.6	3.10	28.7
	Float-2	0.8	7.80	0.9	1.42	0.6	2.81	1.1
	Sunken	38.4	7.33	40.2	2.25	42.1	0.78	14.5
	Slime	41.6	7.13	42.4	1.81	36.7	2.76	55.7
	Total	100.0	7.00	100.0	2.05	100.0	2.07	100.0
-300+53	Float-1	23.2	6.69	22.6	2.31	25.3	2.75	30.3
	Float-2	0.8	6.94	0.8	2.34	0.9	2.10	0.8
	Sunken	30.0	6.93	30.3	2.36	33.4	0.71	10.1
	Slime	46.0	6.92	46.3	1.86	40.4	2.70	58.8
	Total	100.0	6.87	100.0	2.12	100.0	2.11	100.0
-300+75	Float-1	8.2	5.95	7.1	2.28	9.2	3.55	14.2
	Float-2	0.5	7.04	0.5	1.88	0.5	2.38	0.6
	Sunken	25.1	6.77	24.9	2.32	28.8	0.74	9.1
	Slime	66.2	6.98	67.5	1.88	61.5	2.36	76.2
	Total	100.0	6.84	100.0	2.02	100.0	2.05	100.0

C:Content , D:Distribution

4. Conclusions

Turkey is a country abundant in feldspar resources; however, the majority of these deposits consist primarily of sodium feldspar. As a result, the exploration and beneficiation of potassium feldspar deposits hold significant importance. Currently, potassium feldspar suitable for industrial use must contain at least 10% K_2O and no more than 0.5% Fe_2O_3. In this study, the primary objective was to reduce the iron content through a combination of magnetic separation and flotation experiments. However, the lowest achievable iron content was 0.7% Fe_2O_3.

To further investigate why the iron content could not be reduced below this threshold, it is recommended that Mineral Liberation Analysis (MLA) be conducted. This would provide insights into the mineralogical constraints that may be limiting further iron reduction. Additionally, the K_2O content in the final product was found to be approximately 6.9%, which is lower than the desired level. This lower K_2O content is likely due to the high quartz content in the ore. To enhance the K_2O content, further processing through quartz flotation could be employed, offering a potential solution for increasing the potassium concentration in the feldspar product.

References

Baila, F., Labbilta, T., & Darmane, Y. (2023). Feldspar Purification from Iron Impurities: A Review of Treatment Methods. Mineral Processing and Extractive Metallurgy Review, 45(6), 564–572. https://doi.org/10.1080/08827508.2023.2217322

Gougazeh, M. (2022). Beneficiation and upgrading of low-grade feldspar ore in medina, saudi arabia. Journal of Ecological Engineering, 23(6), 271-277. https://doi.org/10.12911/22998993/147834

Hillier, S. & Hodson, M. E. (1997). High-Gradient Magnetic Separation Applied to Sand-Size Particles: An Example of Feldspar Separation from Mafic Minerals: RESEARCH METHOD PAPER. Journal of Sedimentary Research, 67(5), 975-977.

Isnugroho, K., Birawidha, D., & Amin, M. (2019). The potentials of improving mineral source additional values in lampung province – a preliminary study. Journal of Engineering and Scientific Research, 1(1), 1. https://doi.org/10.23960/jesr.v1i1.2

Liu, Y., Peng, H., & Hu, M. (2013). Removing iron by magnetic separation from a potash feldspar ore. Journal of Wuhan University of Technology-Mater. Sci. Ed., 28(2), 362–366. https://doi.org/10.1007/s11595-013-0696-3

Moura, L. C., André, F. P., Miceli, H., Neumann, R., & Tavares, L. M. (2019). Manufactured Feldspar-quartz Sand for Glass Industry from Gneiss Quarry Rock Fines Using Dry Rare-earth Magnetic Separation. Mineral Processing and Extractive Metallurgy Review, 40(5), 333–343. https://doi.org/10.1080/08827508.2019.1643341

Subari, S., Erlangga, B. D., Arifin, D. N., & Nugroho, T. (2024). Removal of iron contents from Banjarnegara serpentine by leaching process for ceramic purposes. In AIP Conference Proceedings (Vol. 3003, No. 1). AIP Publishing.

Venegas, P., Cruz, L., & Lapidus, G. (2014). Dissolution of iron from oxides in a solution of citric acid and sodium thiosulfate. Advanced Materials Research, 976, 114-118. https://doi.org/10.4028/www.scientific.net/amr.976.114

Vrbický, T. and Přikryl, R. (2021). Recovery of some critical raw materials from processing waste of feldspar ore related to hydrothermally altered granite: laboratory-scale beneficiation. Minerals, 11(5), 455. https://doi.org/10.3390/min11050455

Wang, W., Cong, J., Deng, J., Weng, X., Lin, Y., Huang, Y., & Peng, T. (2018). Developing effective separation of feldspar and quartz while recycling tailwater by hf pretreatment. Minerals, 8(4), 149. https://doi.org/10.3390/min8040149

Xu, J., Chen, J., Ren, X., Tao, X., Liu, K., & Song, S. (2021). A novel dry vibrating hgms separator for purification of potash feldspar ore. Separation Science and Technology, 57(3), 484-491. https://doi.org/10.1080/01496395.2021.1900250

Yassin, K., Ahmed, M., Khalifa, M. G. E., & Hagrass, A. A. (2023). Removing Iron Impurities from Feldspar Ore Using Dry Magnetic Separation (Part One). Archives of Mining Sciences, 68(1), 19–33. https://doi.org/10.24425/ams.2023.144315

Yushina, T., Thuy, N., Dumov, A., & Trong, N. (2021). Study of the possibility of selective flotation of quartz-feldspar ore of quang nam deposit (vietnam). Eurasian Mining, 49-54. https://doi.org/10.17580/em.2021.02.11

Zhong, Y., Gao, J., Chen, P., & Guo, Z. (2016). Recovery of potassium from k-feldspar by thermal decomposition with flue gas desulfurization gypsum and caco3: analysis of mechanism and kinetics. Energy & Fuels, 31(1), 699-707. https://doi.org/10.1021/acs.energyfuels.6b01915

Comparison of Amine Type and Xanthate Type Collectors in Pyrite Flotation

İbrahim GÖKTAŞ [1], Begüm ÖZDUR [1]*, Ahmet YAKAR [1], Gizem DEMİRDAĞ ÖZEL [1]

[1]ETİ BAKIR A.Ş., Research and Development Center, 55300, Tekkeköy, Samsun, Türkiye

*Corresponding author: begum.ozdur@etibakir.com.tr (Begüm ÖZDUR)

Abstract:

In this study, amine based collector Tomamine M73 (alkyl ether amine, an amphoteric surfactant) and xanthate type collectors SBX (Sodium Butyl Xanthate) and PBX (Potassium Butyl Xanthate) were employed in order to increase the recovery and grade values of pyrite concentrate produced at Eti Bakır

C.O. Küre Concentrate Plant. According to the flotation tests, pyrite concentrate containing 48,85% S with 88,85% recovery was obtained using Tomamine M73, pyrite concentrate containing 48,52% S with 72,70% recovery was obtained using SBX and pyrite concentrate containing 48,18% S with 93,25% recovery was obtained using PBX. Accordingly, it has been shown that xanthate type collectors can be effective in selective flotation of pyrite from chalcopyrite in alkaline pH ranges.

Keywords: *Pyrite, flotation, collectors, xanthate, amine*

1. Introduction

Pyrite is the most widespread and abundant of naturally occurring metal sulfides (Bicak et. al., 2007). It is usually associated with other valuable metal sulfides such as chalcopyrite, galena, sphalerite, etc. In the enrichment of these valuable minerals, the selective depressed of pyrite during flotation is necessary. One of the important properties of pyrite is that it is well depressed at an alkaline pH and its floatability increases significantly at an acidic pH.

Pyrite flotation is achieved using xanthate type collectors in a slightly acidic pH environment. Xanthates are thiol-type collectors that are widely used and are very important in the flotation of sulfide minerals. It reverses the positive surface charge of pyrite in acid pH pulps, and as the xanthate concentration increases, the surface gets more negative at neutral and alkaline pH ranges. (Fuerstenau et al.,1968; Jiang et al., 1998; Bulut et al., 2004; López Valdivieso et al., 2005). It is generally accepted that xanthates make pyrite hydrophobic adsorbing as dixanthogen and, meanwhile, the loss of positive charge is associated with the formation of surface ferric hydroxide, which results in an increase in the negativity of the zeta potential of pyrite. (Bulut et. al., 2021).

On the other hand, it was shown that amine-type collectors are effective in the selective flotation of pyrite from chalcopyrite in an alkaline pH ranges. Amines are organic compounds that have a positive charge in an aqueous environment and are cationic collectors based on pentavalent nitrogen, with a polar group that is a cation. (Bulatoviç, 2007). The adsorption mechanism of amine type collectors is proposed to be through columbic forces (Smith and Akhtar, 1976) between the polar group of the collector and the charged electrical double layer on the mineral surface. These forces determine the binding strength and selectivity of the collector to the mineral.

Eti Bakır Küre Plant produces 400,000 tons of pyrite concentrate annually. The produced pyrite concentrate is shipped to the Mazıdağı Metal Recovery and Integrated Fertilizer Plant for use in sulfuric acid production. In this context, sulfur recovery and grade are important. The aim of this study is to increase the grade and recovery values of pyrite concentrate with xanthate type collectors at high pH values.

2. Material and methods

2.1. Material

2.1.1. Sample

This study was conducted on a sulfide complex ore located within the boundaries of Küre District, Kastamonu Province. The main minerals of the Küre deposits are pyrite and chalcopyrite. The mineralogical analysis and chemical analysis results of the ore used in the experiments are given in Table 1 and Table 2.

Table 1. Modal mineralogy weight

Modal Mineralogy Weight

Mineral	Percentage, %
Quartz	7,15
K-Feldspar	0,67
Plagioclase	0,75
Muscovite	0,88
Montmorillonite (Na)	0,13
Montmorillonite (Ca)	1,17
Smectite	2,87
Beidellite-Saponite	0,34
Pyralspite Garnets	14,73
Olivine	0,54
Pyroxene	0,13
Calcite	2,01
Siderite-Magnesite	1,66
Dolomite-Ankerite	0,50
Pyrite	61,73
Pyrrhotite	1,20
Sphalerite	0,27
Chalcopyrite	0,35
Iron Spinel	1,42
Other	1,51

Table 2. Chemical analysis of the Kastamonu-Küre ore

Element	Cu	Co	Fe	S	Zn	Al	Ca

%	0,33	0,40	34,43	31,85	0,33	1,42	1,34

According to the mineralogical analyses, the ore contains major sulfide minerals including pyrite (FeS_2), chalcopyrite ($CuFeS_2$), sphalerite (ZnS), and pyrrhotite ($Fe_{1-x}S$). SEM image of the ore is shown in Figure 1.

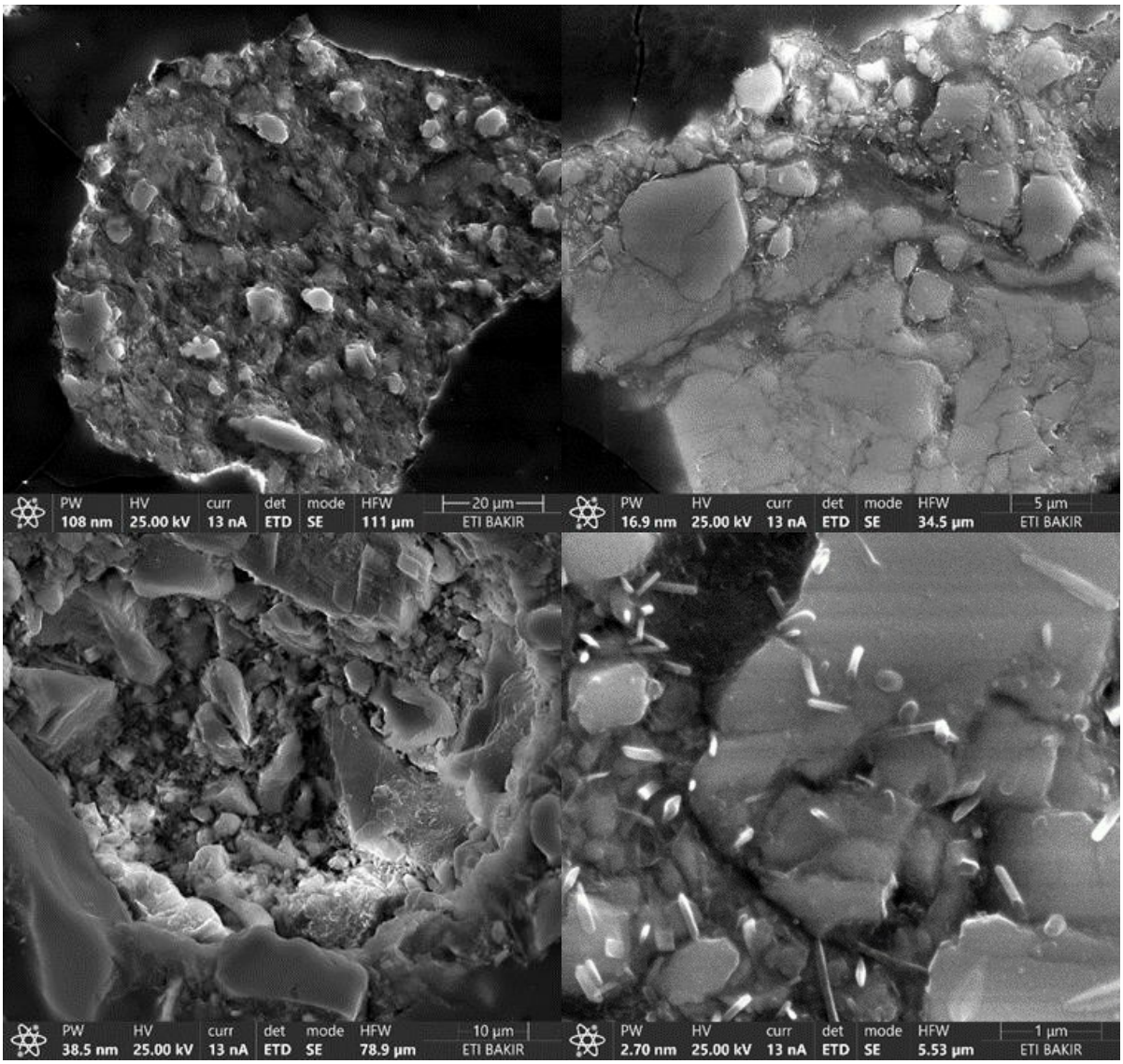


Figure 1. SEM images of the ore

2.1.2. Collectors

In this study, the effects of different collectors on pyrite flotation were investigated. The collectors used for flotation tests and their types are given at Table 3.

Table 3. Collectors that used in study

Collectors	**Collector Type**
Tomamine-M73	Amine
Sodium Butyl Xanthate (SBX)	Xanthate
Potassium Butyl Xanthate (PBX)	Xanthate

Tomamine M73, alkyl ether amine, is indeed an amphoteric surfactant commonly used in both alkaline and acidic cleaning formulations.

Potassium n-butyl xanthate (PBX) and sodium butyl xanthate (SBX) are thiol-type collectors for sulfide flotation. PBX, widely used in industrial applications to improve the flotation efficiency owing to its strong capture ability for target minerals. (Yan et al., 2016). The chemical structures of PBX and SBX are shown in Figures 2 and 3.

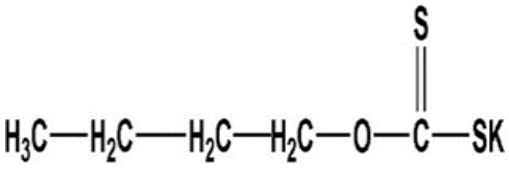


Figure 2. Chemical structure of PBX

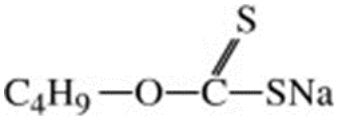


Figure 3. Chemical structure of SBX

2.2. Method

In the Küre Copper Plant, the feed for pyrite flotation is the tailings from the rougher copper flotation circuit. Before feeding the pyrite flotation, fine ore in the form of slurry is removed from the system using a hydrocyclone, and then the pyrite flotation is carried out. Pyrite flotation is carried out at high pH values (11.50-12.00) using Tomamine (M-73) as a collector and Dowfroth 250 as a frother. According to the plant conditions, laboratory-scale flotation tests were conducted using SBX and PBX reagents at different dosages with the cyclone underflow sample taken from the pyrite flotation circuit. Flotation tests were done with laboratory scale Denver type flotation machine. The tests conducted with a 1 kg sample in a flotation cell with a volume of 2.2 liters were adjusted to a solid ratio of 30-35%. Air feed was 2 l/min and impeller speed was 1100 rpm at pH: 10,5-10,8. The sample pH was adjusted to the desired level using lime. The conditioning time is 5 minutes for the collector and 1 minute for the frother. The collector dosages were set at 150 g/t for Tomamine-M73 reagent, and for SBX and PBX reagents, flotation tests were conducted using three different dosages (170 g/t, 190 g/t, and 210 g/t). Additionally, since SBX and PBX reagents do not have frothing properties, Dowfroth-250, which is used at the plant as a frother, was added at 30 g/t in the tests. The flowsheet of flotation tests is given in Figure 4.

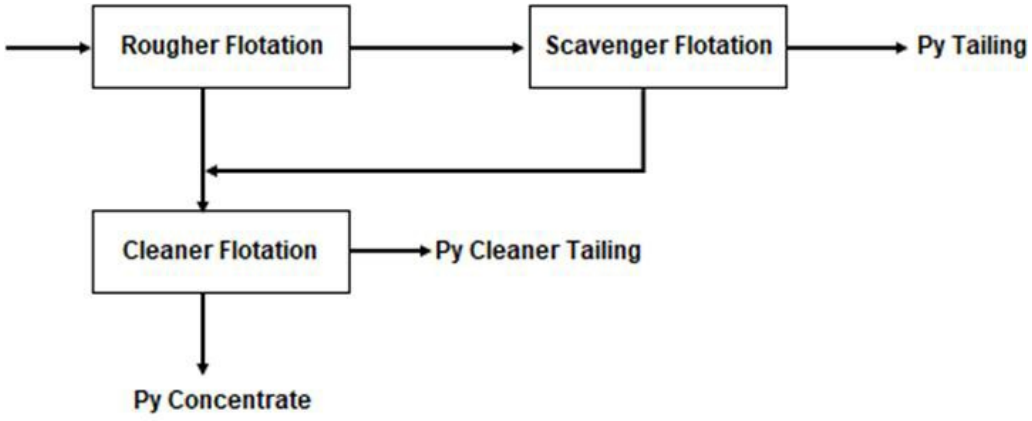


Figure 4. Flotation test flowsheet

3. Result and Discussion

3.1. The Effect of SBX

The results of the flotation tests conducted with the amine-based collector Tomamine-M73 and the xanthate-type collector SBX are given in Figure 5.

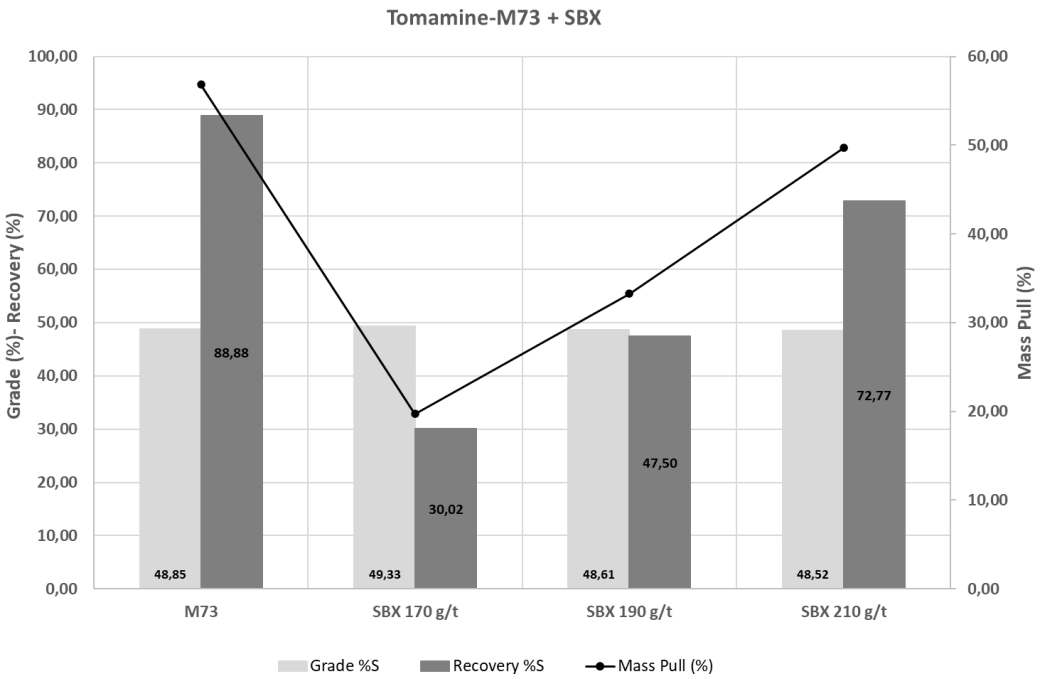


Figure 5. Pyrite concentrate recovery (%)- grade (%)- weight (%) graph

According to the flotation test results, the S grade was 48.85% and the recovery was 88.88% in the experiment conducted with Tomamine-M73 reagent. In experiments conducted with SBX, at a dosage of 170 g/t, the S grade was 49.33% and the recovery was 30.02%. At a dosage of 190 g/t, the S grade was 48.61% and the recovery was 47.50%. At a dosage of 210 g/t, the S grade was 48.52% and the recovery was 72.77%. It was observed that compared to Tomamine-M73 reagent, the SBX reagent acted more selectively, increasing the sulfur grade but resulting in a lower sulfur recovery in the pyrite concentrate.

3.2. The Effect of PBX

The results of the flotation tests conducted with the amine-based collector Tomamine-M73 and the xanthate-type collector PBX are given in Figure 6.

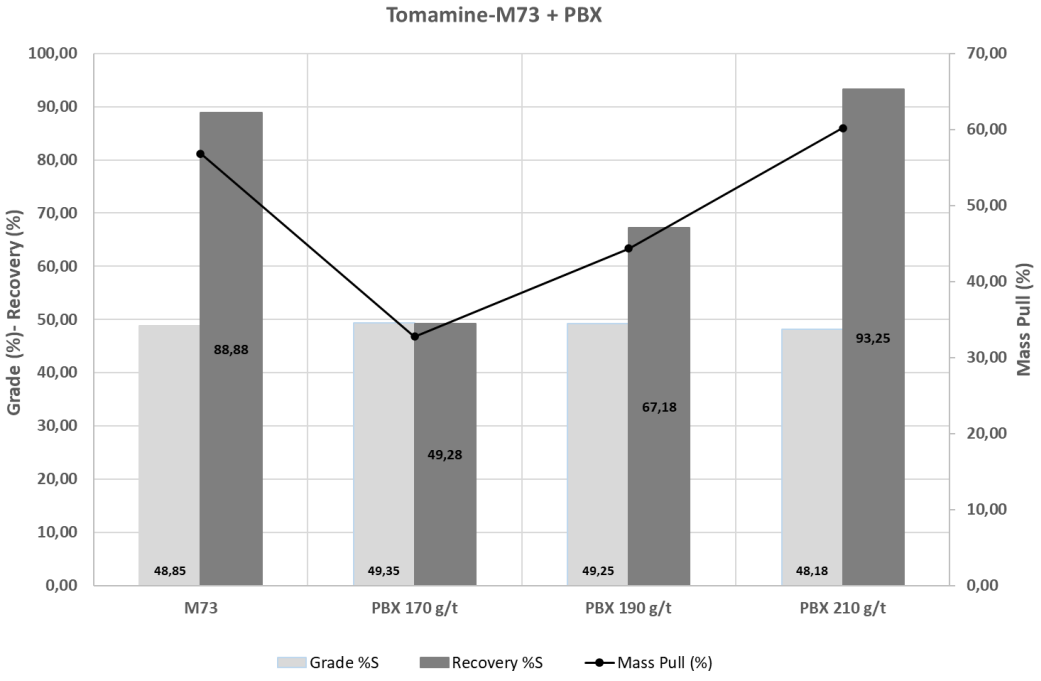


Figure 6. Pyrite concentrate recovery (%)- grade (%)- weight (%) graph

According to the flotation test results, the S grade was 48.85% and the recovery was 88.88% in the experiment conducted with Tomamine-M73 reagent. In experiments conducted with PBX, at a dosage of 170 g/t, the S grade was 49.35% and the recovery was 49,28%. At a dosage of 190 g/t, the S grade was 49,25% and the recovery was 67,18%. At a dosage of 210 g/t, the S grade was 48.18% and the recovery was 93,25%. Compared to Tomamine-M73, flotation tests conducted with PBX reagent yielded favorable results due to both higher sulfur grade and higher recovery of the concentrate. When comparing SBX and PBX, it is observed that the PBX reagent positively affects flotation kinetics and achieves higher sulfur recoveries.

4. Conclusions

In this study, the flotation behavior of pyrite was investigated using amine-based Tomamine-M73 as a cationic collector and xanthate-type SBX and PBX reagents as anionic collectors to enhance the recovery and grade values of the pyrite concentrate produced at the Küre Copper Plant. These experimental studies have shown that, unlike amine-type collectors, xanthate-type collectors are effective in pyrite flotation within alkaline pH ranges. With a dosage of 210 g/t PBX reagent, a pyrite concentrate with a grade of 48.18% was obtained with a recovery of 93.25%.

In industrial applications, the use of xanthate-type collectors, especially after copper flotation at alkaline pH ranges, leads to a decrease in pH for pyrite flotation, resulting in increased acid consumption. As a result of the experiments, processes where chalcopyrite and pyrite are recovered as separate products without the need to lower the pH for pyrite flotation will offer an advantage over conventional methods. This way, acid consumption will be prevented and the control of the flotation process will be simpler. Additionally, the lower cost of xanthate-type collectors compared to amine-type collectors will provide an advantage in reducing collector costs for flotation plants.

References

Bicak, O., Ekmekci, Z., Bradshaw, D.J., Harris, P.J., 2007. *Adsorption of guar gum and CMC on pyrite*. Minerals Engineering 20, 996–1002.

Bulatovıc, S. M, 2007. *Handbook of Flotation Reagents; Chemistry, Theory, Practice, Canada*, Elsevier Science, pp. 7- 33.

Bulut, G., Sirkeci, A.A., Arı B., 2021. *Comparison of anionic, cationic and amphoteric collectors used in pyrite flotation*. Physicochem. Probl. Miner. Process., 57(5), 15-22.

Bulut, G., Arslan, F., Atak, S., 2004. *Flotation behaviors of pyrites with different chemical compositions*. Minerals and Metallurgical Processing, 21, 86-92.

Fuerstenau, M. C., Kuhn, M.C. D. A. Elgillani, D.A. 1968. *The role of dixanthogen in xanthate flotation of pyrite*. SME Transaction, pp. 148-156

Jiang, C. L., Wang, X. H., Parekh, B. K., Leonard, J. W., 1998. *The surface and solution chemistry of pyrite flotation with xanthate in the presence of iron ions*. Colloids and Surfaces A: Physicochemical Engineering Aspects, 136, 51-62.

López Valdivieso, A., Sánchez López, Song, S., 2005. *On the cathodic reaction coupled with the oxidation of xanthates at the pyrite/aqueous solution interface*. International Journal of Mineral Processing, 77, 154-164.

Smith, R. W. Akhtar, S., 1976. *Cationic Flotation of Oxides and Silicates, vol. 1. Flotation A.M. Gaudin Memorial*, American Chemical Society, Washington, DC.

Yan, P., Chen, G., Ye, M., Sun, S., Ma, H., Lin, W., 2016. *Oxidation of potassium n-butyl xanthate with ozone: Products and pathways.* Journal of Cleaner Production 139, 287-294

Optimization of Stibnite Flotation Conditions In The Presence of Activator And Dispersant

Seyed Ramin Banihashemi [1], Mehdi Rahimi [1], Gholamreza Parvareh [1], Ziaeddin Pourkarimi [1*]

[1]Iran Mineral Processing Research Centre (IMPRC)

*Corresponding author: z.pourkarimi@imprc.ir (Ziaeddin Pourkarimi)

Abstract:

The antimony deposit in Razavi Khorasan province, Iran, contains 1.17% Sb in the mineral form of stibnite along with quartz, calcite, dolomite, and gypsum as the dominant gangue minerals based on XRD analysis and ZEISS polarizing microscope images. Stibnite can be extracted by froth flotation due to the sulfide nature and size of stibnite particles distributed in the ore according to liberation degree. In this work, the effects of the potassium amyl xanthate as the collector (150-500 g/t), MIBC as the frother (0.1-0.5 l/t), and pH (8-11) were investigated and the optimal conditions in rougher were obtained. Also, the effect of adding copper sulfate as the activator and sodium silicate as the dispersant on Sb grade and recovery have been evaluated, and their positive effects have been confirmed. The possibility of producing concentrate by 40% Sb grade was determined by conducting kinetic tests of the rougher and cleaner flotations. As well as, the optimization of scavenger flotation led to reducing its tail by about 0.15% Sb. Therefore, the main objectives of the research have been achieved to reduce the Sb grade of the tail of the scavenger to the proper range and produce a high-grade concentrate in cleaner.

Keywords: *Stibnite, Antimony, Froth Flotation, Kinetic Experiment*

1. Introduction

Antimony is a silvery, white, brittle, crystalline solid classified as a metalloid that exhibits poor conductivity of electricity and heat. The abundance of antimony in the earth's crust is approximately 0.2 mg/kg. Antimony is a chalcophile, occurring with sulfur and the heavy metals of copper, lead, and silver as a sulfosalt. It occurs as either a distinct antimony-bearing sulfide, such as stibnite (Sb_2S_3); sulfosalt minerals, such as tetrahedrite; rare antimonides, such as aurostibite; or as a minor or trace constituent in sulfides like arsenopyrite and pyrite (Dunne et al. 2019).

Overall, it is estimated that the distribution of antimony uses and consumption worldwide is flame retardants 72%, transportation including batteries 10%, chemicals 10%, ceramics and glass 4%, and other 4% (Dunne et al. 2019).

The beneficiation process of sulfide ores includes size reduction, classification, physical beneficiation processes, and/or flotation steps. Flotation is one of the most important methods used in the enrichment of sulfide ores and enrichment of minerals is carried out according to their buoyancy properties. In the flotation of a stibnite ore, stibnite has been declared as naturally hydrophobic in the presence of air or as partially hydrophobic on the basis of the critical surface tension of wetting (Ozcan, 1992; Popov, 1987). In addition, in practice, the particle shape, roughness and particle size, heterogeneous structure of the minerals to be flotation affect their surface properties and thus their buoyancy. In that sense, it has been a frequent practice to add collectors in order to improve the flotation rate of those minerals. The most common collectors for stibnite flotation have been alkyl xanthates, preferably those of long chains (4 or more carbon atoms) (Fuerstenau, 2007).

In the following, the flotation concentrate (30-40% Sb) undergoes hydro/pyrometallurgical processes to complete the Sb purification.

In this research, the purification of antimony from the low-grade ore by flotation method in the presence of the surfactants, and in three stages of rougher, cleaner and scavenger has been investigated.

2. Material and methods

2.1. Material

An Antimony-bearing sulfide ore containing 1.17% Sb from a deposit in Razavi Khorasan province, Iran, was used for all the experiments. The mineralogical properties of the ore sample were characterized based on optical mineralogy methods using the polished and thin sections by ZEISS polarizing microscope images and XRD analysis. XRD analysis showed that the ore contains calcite, dolomite, stibnite, quartz, and gypsum are present in the ore. For major elemental analysis, inductively coupled plasma (ICP), and X-ray fluorescence (XRF) were used (Tables 1 and 2).

Table 1. ICP analysis result

Sb (%)	Ca (%)	Al (%)	Fe (%)	Ba (%)	Mg (%)	Mg (%)	S (%)
1.17	12.88	3.62	1.90	1.87	1.44	1.44	1.26
Na (%)	K (%)	Sr (%)	Pb (%)	Zn (%)	Mn (%)	Ti (%)	P (%)
<1	<1	<1	<1	<1	<1	<1	<1

Table 2. XRF analysis result

SiO_2 (%)	Al_2O_3 (%)	CaO (%)	MgO (%)	TiO_2 (%)	SO_3 (%)	Fe_2O_3 (%)	BaO (%)	Sb_2O_3 (%)	K_2O (%)	L.O.I (%)
43.05	6.85	18.04	2.39	0.47	3.15	2.71	2.09	1.45	0.93	18.15

According to Table 3, the liberation degree of stibnite was studied in different-size fractions. Mineral liberation degree is the ratio of the number of unlocked particles of mineral to the sum of the number of locked and unlocked particles of mineral. The calculation formula is as follows:

$$df = \frac{n_1}{n_1+n_2} \times 100 \quad (1)$$

where *df* is the mineral liberation degree, n_1 is the unlocked content of the mineral, and n_2 is the content of locked particles.

The degree of liberation of stibnite has a value of 85% for size fraction (-90+63) μm, slightly increasing to the value of 90% for particles below 63 μm. As shown in Figure 1, gangue minerals are closely related to stibnite in coarse sections. With the decrease in the size of the grains, most of the minerals correlation has occurred in binary status, which includes types of correlation between stibnite and waste minerals such as stibnite-calcite, and stibnite-quartz.

Table 3. Degree of liberation of stibnite

size fractions (micron)	Stibnite degree of liberation (%)
+1400	10
-1400, +710	25
-710, +355	30
-355, +180	47
-180, +125	59
-125, +90	76
-90, +63	85
-63, +38	90

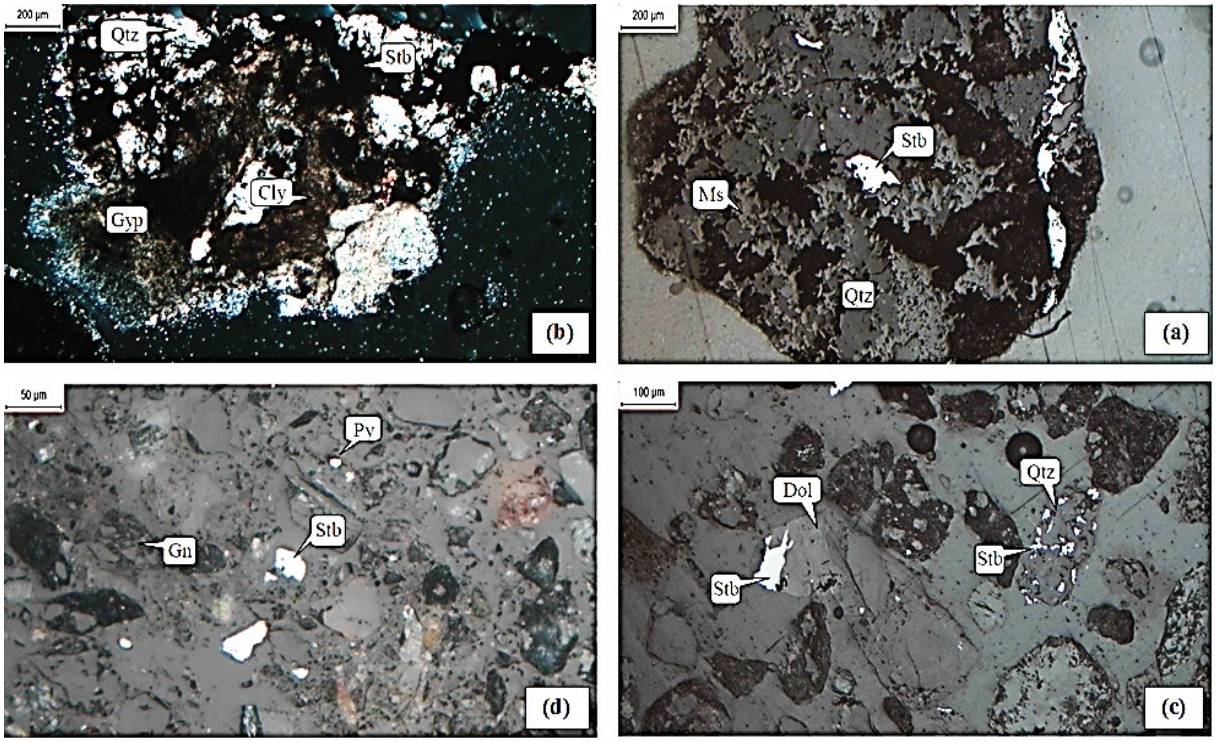


Fig. 1. Stibnite liberation in different size fractions. (a) Stibnite-muscovite-quartz correlation in (+1400 mic.) fraction (by plane polarized light), (b) Stibnite-gypsun-clay mineral-quartz correlation in (-1400, +710 mic.) fraction (by cross polarized light), (c) Stibnite-dolomite and stibnite-quartz correlations in (-180, +125 mic.) fraction (by plane polarized light), (d) Unlocked stibnite in (-90, +63 mic.) fraction (by plane polarized light).

2.2. Methods

Flotation tests have been conducted in two parts. The first part includes optimizing the values of collector, frother, and pH, as well as checking the presence of activator and dispersant in the rougher flotation process. In the second part, the cleaner and scavenger flotation processes have been done and evaluated.

The flotation rate is highly dependent on particle size (Trahar, 1981; McIvor and Finch, 1991), with the ore liberation as an underlying consequence of size. As shown in the previous section, At finer sizes, the particles will tend to be more liberated and will be less liberated at coarser sizes. Flotation recovery is reduced in the finer and coarser sizes. At the same degree of liberation, coarse particles floated more slowly than intermediate-sized particles but poorly liberated particles of optimum flotation size could float more rapidly than liberated coarse particles. As well as, the presence of fine particles (<38 mic.) in flotation due to sticking on coarse particles, will prevent the absorbtion of reagents and so reduces flotation efficiency. Thus, flotation performance depends on both size and liberation. Based on the liberation degree result, the flotation experiments were performed with feed that is ground under 150 microns (d_{80}: 75 microns).

Flotation studies were carried out using a Denver-type laboratory scale flotation machine at 1000 rpm using a 1-litre flotation cell. After dewatering, drying, and measuring the weight of the concentrate and tailings of each experiment, they were referred to the chemistry laboratory for Sb analysis. The recovery formula is calculated as follows:

$$R = \frac{Cc}{Ff} \times 100 \quad (2)$$

where R is the recovery percentage, C and F are masses of the concentrate and feed respectively, and c and f are the grades of the concentrate and feed respectively.

2.2.1. Optimization of consumption of collector and frother

There is a great body of literature on collectors and frothers for a sulfide/nonsulfide ore, but appropriate efficiencies have remained slanted toward a rather narrow set of conventional chemicals (e.g., xanthate/ MIBC/lime for a sulfide ore; fatty acid/soda ash for a nonsulfide ore).

A clear preference is observed towards long-chain xanthates, such as potassium amyl xanthate among others in the stibnite flotation process. Moreover, there seems to be a consistency in the superior performance of long-chain xanthates over short-chain xanthates for different pH values, at least in terms of antimony grade in the concentrate (Ealedona and Fujita, 2006; Richards, 1997). Therefore, potassium amyl xanthate (PAX) was selected as the collector in the flotation process. MIBC (methyl isobutyl carbinol) was considered as the frother in the flotation process, as well.

In the optimization flotation of collector dosage, the conditions given in Table 4 were kept constant, and experiments were carried out with PAX in different amounts (150, 200, 300, 400, 500 g/t). The evaluation was made according to the Sb contents of the concentrates and Sb recovery in concentrates obtained as a result of the flotation experiments with different collector amounts is given in Fig. 2. Achieving higher recovery is the main goal in the rougher flotation stage. According to the trendline of Sb recovery; in almost all PAX dosages, more than 75% Sb recovery was achieved.

Table 4. The conditions of rougher flotation were carried out to determine the effect of collector (PAX) dosage

Pulp Density (%)	30
pH, pH adjustor	9, lime
PAX condition time (min.)	5
Frother, dosage (l/t)	MIBC, 0.2
MIBC condition time (min.)	3
Flotation Time (min.)	5
Agitation speed (rpm)	1000

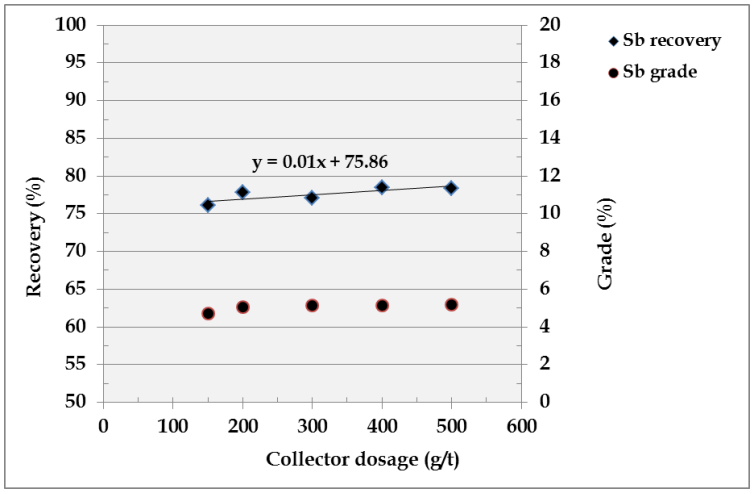


Fig. 2. The effect of PAX amount on Sb content and recovery of flotation concentrate

In the optimization flotation of frother dosage, 200 g/t PAX and other parameters (like Table 4) were kept constant. Experiments were performed with MIBC in various dosages (0.1, 0.2, 0.3, 0.4, 0.5 l/t). The result of the flotation experiments with different frother amounts is shown in Fig. 3. According to the test results; the highest Sb recoveries (approximately 80%) were obtained using more than 0.3 l/t MIBC.

At the end of the optimization of rougher flotation experiments, the condition of 200 g/t PAX and 0.3 l/t frother was introduced as an optimum dosage of the mentioned reagents. In the optimum condition, the Sb contents of the concentrates and Sb recovery in concentrates reached 5.15% and 79.7%, respectively. The tailings grade in optimization experiments was in the range of 0.15-0.25% in rougher flotation stage.

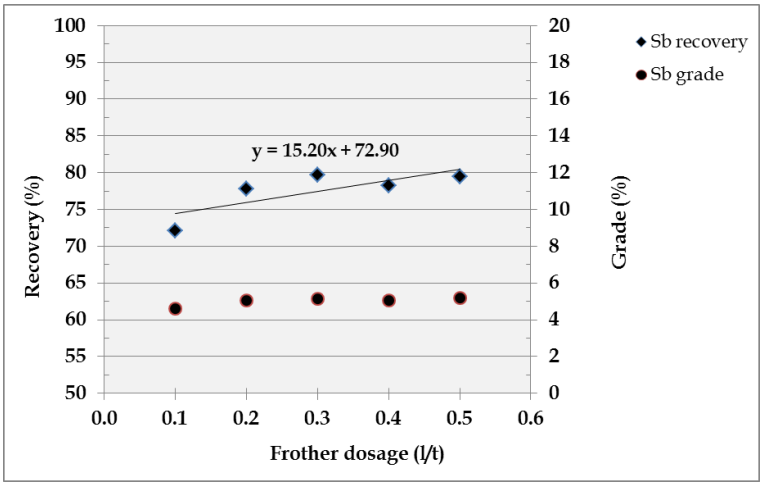


Fig. 3. The effect of MIBC amount on Sb content and recovery of flotation concentrate

2.2.2. pH optimization in flotation media

The pH of the pulp, which determines the surface charge of the minerals and the adsorption of the reagents on the minerals, plays a crucial role in froth flotation. In order to determine the appropriate pH of pulp in the flotation experiments, a series of tests were carried out by considering the different pH values as 7.8 (ambient), 9, 10, and 11. All the flotation tests were conducted single stage rougher flotation. During these tests, 200 g/t PAX and 0.3 l/t MIBC were used as collector and frother, respectively.

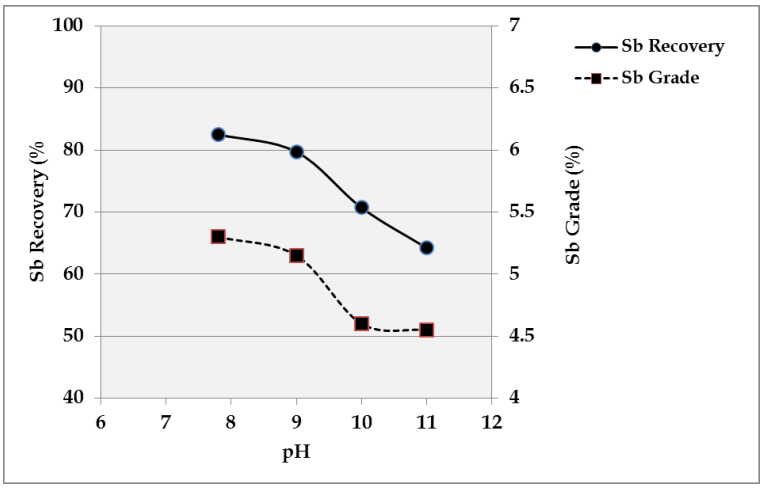


Fig. 4. The result of flotation experiments conducted to determine the optimum pH

According to the results given in Fig. 4, pH: 7.8 and 9 were found as an optimum pH value, considering the recovery and antimony content of the concentrate. These results also indicated that an increase in pH value resulted in increasing oxidation on the sulfur mineral surfaces and it can be also thought that competition between collector and hydroxyl ion occurs for absorption on the surface of the mineral.

2.2.3. Effect of presence of activator and dispersant

$CuSO_4$ is an effective stibnite flotation activator (Ye, 2019; Ai, 2018). Copper sulfate may promote stibnite flotation using a xanthate, possibly because Cu^{2+} is adsorbed on the lattice of stibnite, forming a complex hydrophobic layer comprising copper xanthan acid and antimony xanthan acid on the stibnite surface (Lager and Forssberg, 1989). Furthermore, Cu^{2+} is reduced on the stibnite surface to form a more hydrophobic Cu2S layer, facilitating the adherence of stibnite to the bubbles and thus improving its

recovery rate (Cao, 2018). The dispersion of the slurry is usually achieved by adding a special dispersant. One of the commonly used dispersants in flotation is sodium silicate (Na_2SiO_3).

The addition of 2000 g/t $CuSO_4$ as an activator in the presence and absence of 1000 g/t Na2SiO3 as a dispersant at pH values of 9 and 7.8 in four separated flotation tests were investigated. The flotation conditions are given in Table 5.

Table 5. The conditions of flotation carried out to determine the effect of activator and dispersant

Pulp Density (%)	30
pH, pH adjustor	7.8 and 9, lime
PAX dosage (g/t), and condition time (min.)	200, 5
MIBC dosage (l/t), and condition time (min.)	0.3, 3
Condition time of activator and dispersant (min.)	3
Flotation Time (min.)	5
Agitation speed (rpm)	1000

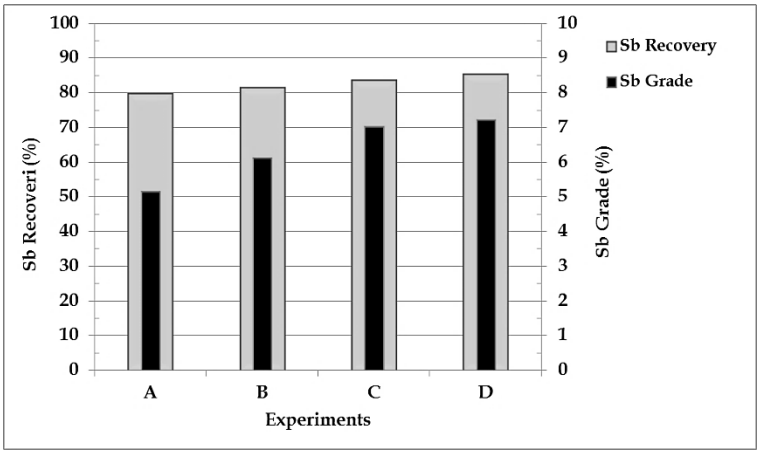


Fig. 5. The effect of MIBC amount on Sb content and recovery of flotation concentrate (Experiments; A: without activator and dispersant at pH: 9, B: with 2000 g/t $CuSO_4$ and without dispersant at pH: 9, C: with 2000 g/t $CuSO_4$ and 1000 g/t Na_2SiO_3 at pH: 9, C: with 2000 g/t $CuSO_4$ and 1000 g/t Na_2SiO_3 at pH: 7.8)

In accordance with Fig. 5., the Sb grade of concentrate grows up to 7.2% by using copper sulfate and sodium silicate at a pH value of 7.8. Not only usage of copper sulfate and sodium silicate change the Sb grade in the concentrate dramatically, but also antimony losses decreased in the obtained residue.

2.2.4. Kinetic studies in the rougher flotation stage

The batch flotation tests are evaluated according to recovery obtained at a specified time. Particles of the same minerals float at different rates because of different particle characteristics and cell conditions (Polat and Chander, 2000; Albijanic, 2015; Gupta and Yan, 2016). A flotation kinetic determines the variation of the rate of change of recovery with time. The test for determination of flotation kinetics was carried out with the optimum conditions obtained from previous tests (the addition of 2000 g/t $CuSO_4$, 1000 g/t Na2SiO3, 200 g/t PAX, and 0.3 l/t MIBC at pH 7.8 with 0.5 kg sample in a 1.3 L flotation cell). The total flotation time was fixed as 5 min; the five concentrates were floated at 1, 2, 3, 4, and 5 min. As a function of time, cumulative recoveries versus cumulative contents of antimony and cumulative recoveries versus cumulative weight recoveries calculated from the test are given in Figs. 6 and 7.

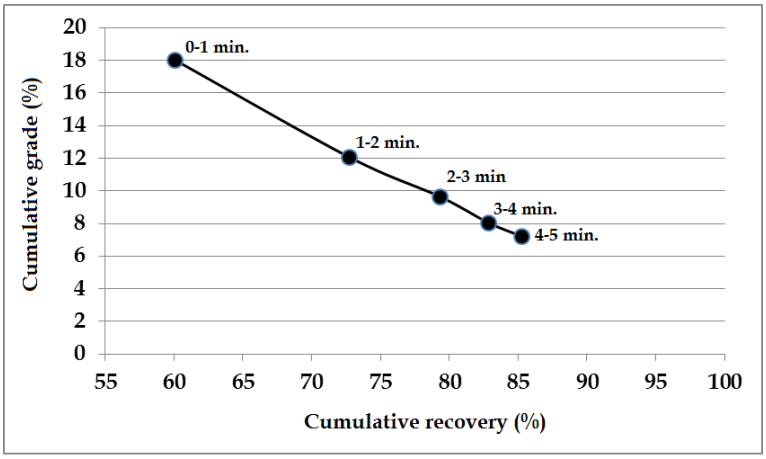


Fig. 6. cumulative Sb recovery versus cumulative content of antimony in concentrate

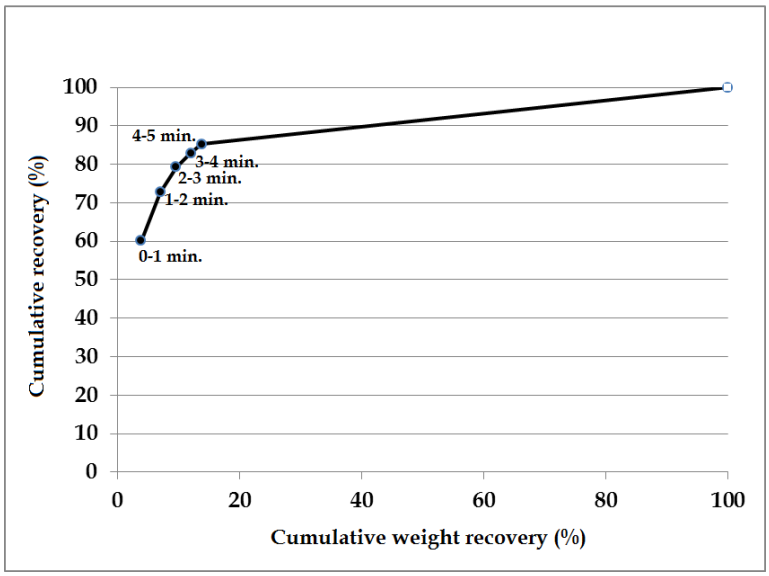


Fig. 7. Cumulative weight recovery versus cumulative recovery of antimony in concentrate

According to kinetic results, the drop in Sb grade after 1 minute is very high. In addition, about 80% of the antimony was recovered in the first 3 minutes. As the time increased from 3 min. to 5 min., although the recovery reached 85%, the concentrate grade decreased from 9.6 to 7.2%.

2.2.5. Cleaner and scavenger flotation stages

In order to produce a salable antimony concentrate, a cleaning flotation stage was applied on 5 min.-rougher-concentrate. In this flotation experiment, the pH was taken as 7.8 and the froth was scraped for 5 minutes with the addition of only 10 g/t PAX. The cleaning step was performed as a kinetic test to check its concentrates that floated in 1, 2, 3, 4, and 5 minutes. As shown in Table 6, more than 85% of Sb was recovered in the first 2 minutes with 33.4% Sb.

According to the kinetic experiments of the rougher stage in 5 minutes, the grade of Sb in the tailings has reached 0.2%. The scavenger flotation tests have been carried out with the aim of reducing the grade of tailings to the level of approximately 0.15%. During the 3 scavenger flotation tests, 20, 40, 60 g/t PAX and 0.1 l/t MIBC were used as collector and frother, respectively.

Table 6. kinetic test of cleaning flotation

cumulative weight recovery (%)	Average grade (%)	cumulative Sb recovery (%)	Sb recovery (%)	Sb grade (%)	weight recovery (%)	Time (min.)
14.83	40.67	71.22	71.22	40.67	14.83	0-1
21.71	33.38	85.57	14.35	17.67	6.88	1-2
26.20	29.16	90.18	4.61	8.70	4.49	2-3
30.14	26.09	92.84	2.66	5.71	3.95	3-4
33.85	23.53	94.05	1.22	2.77	3.71	4-5
100	-	100	5.94	0.76	66.15	Final tailings
-	-	-	100	-	100.00	Total

Table 7. result t of scavenger flotation

No.	PAX (g/t)	Section	Weight percent (%)	Sb grade (%)	Sb recovery (%)
1	20	Feed	100	0.20	-
		Concentrate	6.82	1.36	46.3
		Tailings	93.18	0.115	53.7
2	40	Feed	100	0.20	-
		Concentrate	6.18	1.20	37.1
		Tailings	93.82	0.134	62.9
3	60	Feed	100	0.20	-
		Concentrate	6.76	1.14	38.5
		Tailings	93.24	0.132	61.5

It is very acceptable to use 20 grams per ton of collector, which results in 0.115% antimony grade in the scavenger tailings. Scavenger concentrate is also suitable for returning to the rougher stage. The decrease in recovery at higher collector concentrations can be attributed to micelle formation.

3. Conclusions

In this study, The low-grade antimony sample contains 1.17% Sb in the mineral form of stibnite, which was utilized to find the optimum rougher flotation conditions. The effects of the potassium amyl xanthate as the collector (150-500 g/t), MIBC as the frother (0.1-0.5 l/t), and pH (8-11) were investigated and the optimal conditions in rougher were obtained under the following conditions;

a) Particle size(d100): 212 µm, b) pH: ambient (7.8), c) 200 g/t PAX, d) 0.3 l/t MIBC, e) 30% solids in pulp ratio f) flotation time: 5 minutes.

In the mentioned optimum condition, the Sb contents of the concentrates and Sb recovery in concentrates reached 5.3% and 82.5%, respectively. Using copper sulfate as the activator and sodium silicate as the dispersant on Sb grade and recovery have been evaluated and confirmed due to increasing the Sb grade and recovery up to 7.2% and 85.3%, respectively.

The kinetic result of rougher flotation showed that more than 79.3% of antimony was recovered in concentrate by 9.65% Sb only in 3 minutes.

in accordance with the cleaner flotation stage, more than 70% of Sb could be cleaned in the first minute with 40.6% Sb content in concentrate.

The effect of using PAX in different dosages (20,40,60 g/t) was studied in scavenger flotation. Using 20 grams per ton of collector, results in 0.115% antimony grade in the scavenger tailings.

Acknowledgments

This project was supported and carried out at Iran Mineral Processing Research Center (IMPRC)

References

Ai, M.; Xie, Y.; Xu, D. (2018) Reagent predictive control using joint froth image feature for antimony flotation process. *IFAC-PapersOnLine. 51*, 284-289. doi: https://doi.org/10.1016/j.ifacol.2018.09.433

Albijanic, B., Subasinghe, N., Park, C.H. (2015). Flotation kinetic models for fixed and variable pulp chemical conditions. *Minerals Engineering*, *78*, 66-68. doi: https://doi.org/10.1016/j.mineng.2015.04.010

Cao, Q.; Huang, Y.; Zou, H.; Wen, S. (2018). The surface features of activated stibnite surface with copper or lead ion %j physicochemical problems of mineral processing. *Physicochem. Probl. Miner. Process*. *54*, 763-770. doi: https://doi.org/10.5277/ppmp1884

Dunne, R., Komar Kawatra, S., & Young, C. (2019). Antimony production and commodities. *SME mineral processing and extractive metalurgy handbook*. (pp. 1557-1568): society for mining, metallurgy and exploration

Ealedona, N.S., Fujita, T. (2006). *Stibnite recovery from complex Tolukuma ore*. Paper presented at XXIII International Mineral Processing Congress. Istanbul.

Fuerstenau, M. C., Jameson, G., & Yoon, R. H. (2007). *Froth flotation: a century of innovation*. (891): Society for Mining, Metallurgy, and Exploration.

Gupta, A., and Yan, D.S. (2016). *Mineral Processing Design and Operations: An Introduction*. (689-741): Elsevier.

Lager, T.; Forssberg, K.S.E. (1989). Current processing technology for antimony bearing ores a review, part 2. *Minerals Engineering*, *2*, 543-556. doi: https://doi.org/10.1016/0892-6875(89)90088-5

McIvor, R.E., and Finch, J.A. (1991). A guide to the interfacing of plant grinding and flotation operations. *Miner. Eng. 4(1)*, 9–23. doi: https://doi.org/10.1016/0892-6875(91)90114-B

Ozcan, O. (1992). Classification of minerals according to their critical surface tension of wetting values. *Int. J. Miner. Process*, *34*, 191–204. doi: https://doi.org/10.1016/0301-7516(92)90073-6

Polat, M., Chander, S. (2000). First-order flotation kinetics models and methods for estimation of true distribution of flotation rate constants. *International Journal of Mineral Processing, 58*, 145–166. doi: https://doi.org/10.1016/S0301-7516(99)00069-1

Popov, S.R., Vucinic, D.R., Calic, N.M. (1987). Surface phenomena of antimonite in solutions of different flotation reagents. *Colloids Surf. 23*, 171–183. doi: https://doi.org/10.1016/0166-6622(89)80333-6

Richards, R.G. (1977). *Laboratory flotation of Endeavour Inlet, N. Z. Antimony ore*. Paper presented at Australas. Inst. Min. Metall.

Trahar, W.J. (1981). A rational interpretation of the role of particle size in flotation. *Int. J. Miner. Process. 8*, 289–327. doi: https://doi.org/10.1016/0301-7516(81)90019-3

Ye, L.; Ouyang, Z.; Chen, Y.; Chen, Y.; Xiao, L. (2019). Sulfur fixation and reduction roasting of stibnite for clean extraction of antimony by a combined metallurgy and beneficiation process. *Minerals Engineering*. *144*, 106049. doi: https://doi.org/10.1016/j.mineng.2019.106049

The Effect of Different Storage Times of Drilling Cores on Flotation Performance

Seda Özçelik [1]*, Cankut Çendik [1], Özlem Bıçak [1]

[1]Department of Mining Engineering, Hacettepe University, Beytepe, Ankara 06800, Turkey

*Corresponding author: sedaozcelik26@gmail.com (Seda Özçelik)

Abstract:

Sulfide minerals are unstable in the presence of aerated aqueous conditions and open atmosphere conditions because of the electrochemical interactions that occur between sulfide minerals and the solution species. Slight surface oxidation may enhance the flotation performance of the sulphide mineral but extensive oxidation results in high quantities of metal hydroxides on the mineral surface and may negatively affect flotation performance. The effects of oxidation on the flotation behavior of sulfide minerals may differ depending on mineralogy, ore genesis and the duration/degree of oxidation.

In this study, the effect of oxidation was investigated using core samples of a sulfide Cu-Zn ore that had been stored in the mining area for different periods of time. The ore sample contains chalcopyrite, sphalerite and pyrite as the major sulfide minerals. The core samples categorized according to their storage periods and were prepared in the laboratory for the tests. Flotation tests were performed under optimum conditions to determine the effect of oxidation for different periods and their effects on flotation performance. Accordingly, the period which the ore can be kept in the stockpile without adversely affecting the flotation performance has been determined. EDTA tests were performed to determine the degree of oxidation of the samples and the correlation between flotation performance and EDTA results was revealed.

Keywords: *oxidation, sulfide minerals, flotation, EDTA test*

1. Introduction

Sulfide minerals are readily oxidised in aerated aqueous conditions due to electrochemical interactions between the sulfide minerals and solution species. The oxidation of their surfaces plays a critical role, particularly in the flotation process, where the floatability of sulfide particles is directly influenced by the degree of surface oxidation (Fullston et al., 1999c; Peng and Zhao, 2011; Jacques et al., 2016).

Slight surface oxidation can enhance the flotation performance of sulfide minerals by improving their hydrophobicity. However, extensive oxidation leads to the formation of significant quantities of metal hydroxides on the mineral surface (Buckley and Woods, 1984; Smart, 1991; Smart et al., 1998; Vaughan et al., 1995). Additionally, the formation of sulfate or thiosulfate compounds reduces the hydrophobicity of the minerals. This lack of hydrophobicity decreases the floatability of sulfide minerals and negatively impacts their selectivity in the flotation process, making efficient separation more difficult (Rao et el., 1992; Senior and Trahar, 1991; Rumball and Richmond, 1991; Ekmekçi et al., 2005; Greet and Smart, 2002).

Surface oxidation may occur during in situ weathering of an ore body, or during the different extraction and processing stages (mining operations, stockpiling, crushing, milling, and flotation). Each ore type has a different tolerance to surface oxidation depending on the mineralogy and ore genesis. The rapid oxidation of complex sulfide ores, particularly the ores containing high amounts of electrochemically active pyrite and secondary copper minerals, is observed during the mining phase and in the stockpiles. In this paper, the aim was to determine the effects of oxidation on flotation performance using a sulfide copper-zinc ore fromTurkey. Core samples, which had been stored in core boxes for an extended period without any precautions (such as vacuum storage, freezing, or nitrogen purging) against oxidation, were used in the study. Within this scope, the core samples were categorized based

on their storage time/duration, from the most recent to the oldest, and the effects on flotation performance were evaluated.

2. Material and Methods

2.1. Ore Samples

The composites used in the study were selected from regions that are as lithologically and mineralogically as similar as possible. Core samples were classified into three groups, from the newest to the oldest, and three composite samples were formed.

- JM 1: Composite 1: 0-1 year old core samples
- JM 2: Composite 2: 1-2 year old core samples
- JM 3: Composite 3: 2-3 year old core samples

The core samples were combined, and each composite sample was crushed to -2 mm particle size by using jaw crusher and roller crusher. After homogenizing, the crushed samples were representatively split into 1.2 kg, vacuum-sealed to prevent oxidation, prepared for flotation tests and stored in a freezer.

The specific gravities of the composite samples used in the flotation tests were determined using a pycnometer. The specific gravity of JM1, obtained from 1-year-old core samples, is 3.47 g/cm^3, while the specific gravities of JM2 and JM3, obtained from 2- and 3-year-old core samples, are 3.15 and 3.11 g/cm^3, respectively.

The chemical analysis of the composites were determined using an XRF device, and the results are presented in Table 9. The Cu and Zn grades of the ore samples are high, while the Pb grade is very low. The copper and iron content of the 1-year-old core samples is higher compared to the copper content of the 2- and 3-year-old core samples. Additionally, the zinc content of the 1- and 3-year-old core samples is higher than that of the 2-year-old samples.

Table 9. Head assay of the ore samples used in the tests.

	Cu (%)	**Fe (%)**	**Pb (%)**	**Zn (%)**
JM 1	2.31	12.69	0.01	3.37
JM 2	1.23	10.22	0.01	2.58
JM 3	1.67	8.91	0.11	3.85

2.2. EDTA Tests

EDTA (Ethylenediaminetetraacetic acid) is a colorless, water-soluble, solid acetate. EDTA has the ability to dissolve the oxidation products of the sulfide minerals and form metal complexes but does not react with metal sulfides (Rumball and Richmond, 1996; Shannon and Trahar, 1986; Grano et al., 1988). Hence, EDTA extraction is used as a practical method for assessment of the surface oxidation of the sulfide minerals both in laboratory- and plant-scale applications. In this study, to determine the degree of oxidation of these samples, EDTA tests were conducted in duplicate for each of the three composite samples.

A representative 10 g ore sample ground to p80 = 38 µm (the grind size in the flotation tests) was used in the EDTA tests. The sample was stirred for 30 min in 3% w/w EDTA solution adjusted to a pH of 7.5 using NaOH. The sample was then filtered and passed through a 0.45 µm Millipore membrane. The pregnant solution was analyzed for Cu, Zn, and Fe using Atomic Absorption Spectrometry (AAS). Analytical-grade chemicals were utilized in this section.

Percentage of an oxidation for an element was calculated using the following equation:

$$\text{EDTA extractable M \%} = \frac{\text{mass of M in EDTA solution}}{\text{mass of M in solid}} \times 100 \quad (1)$$

where M is the metal (Rumball and Richmond, 1996). The EDTA values of Cu, Zn and Fe were used the for assessment of surface oxidation of the chalcopyrite, sphalerite, and pyrite, respectively.

2.3. Batch Flotation Tests

The batch-scale flotation tests were conducted to investigate the effects of oxidation. The flotation tests were performed with a feed particle size of P80: 38 microns. Grinding calibration tests were conducted using the JM3 sample, and it was determined that a grinding time of 17 minutes was required to achieve a P80 particle size of 38 µm. The same grinding duration was applied to the flotation tests of the other two composite samples as well.

In the flotation, 1.2 kg ore sample was ground at 60% w/w solids content in the presence of the depressants in a ball mill with high-chrome balls. The flotation was performed at 30% w/w using a Denver flotation machine and 2.5 L volume cell as sequential copper flotation and zinc flotation.

In the copper circuit, sodium metabisulfite (MBS) was used as a pyrite depressant in combination with a polymeric depressant, 7261 A. The ore contains a significant amount of fine material in the slime size range, which leads to the formation of a viscous pulp during flotation. To mitigate this, sodium silicate (Na Sil) was used as a clay dispersant. In the zinc circuit, copper sulfate was used as an activator.

The optimum flotation reagent scheme includes:

Copper Flotation

500 g/t Na Sil, 1000 g/t MBS, 100 g/t 7261 added in the mill

pH 11.5

35 g/t 3418A (a phospine based collector)

20 g/t MIBC (methly isobutyl carbinol, as frother)

Zinc Flotation

pH 11.5-12

500 g/t CuSO4

120 g/t KAX (Potassium Amly Xanthate, as collector)

Open-cleaner flotation tests were performed to determine the grade and recovery of the final copper concentrate. Three stages of cleaner flotation were applied with stage addition of depressants and collector addition.

3. Results and Discussion

3.1. Effects of Oxidation

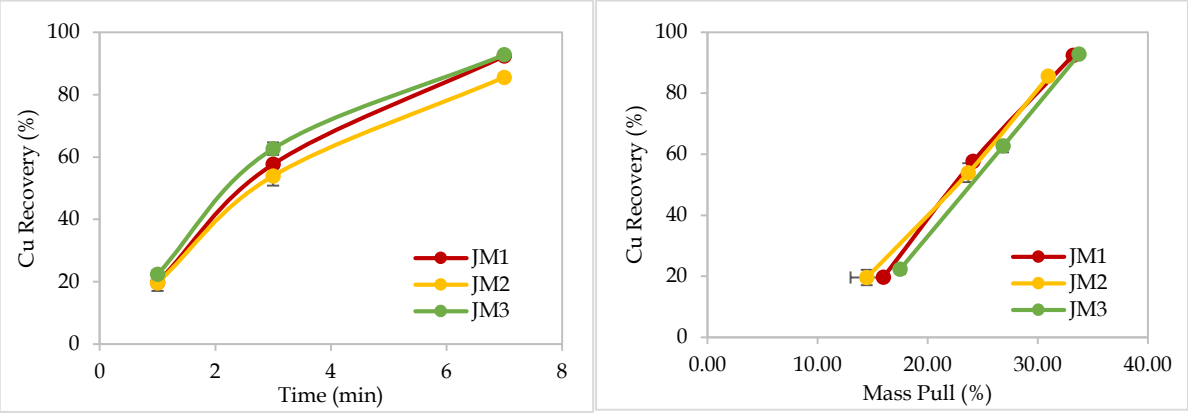
The EDTA tests were performed on the ore samples to measure the quantity of the oxidation products present on the mineral surfaces. In EDTA results, the Es value represents the ratio of dissolved copper to the total copper in the ore and is an indicator for determining of the degree of oxidation of individual metals, while the total Em value is an indicator of the ratio of dissolved metals to the entire ore, providing an overall measure of oxidation. Additionally, oxidation degrees were calculated on a percentage basis and are given in Table 10.

Table 10. EDTA test results of ore samples

	Es (mg/g)			Em (mg/g)	% Degree of Oxidation		
	Es Cu	Es Fe	Es Zn	Em Total	% Cu	% Fe	% Zn
JM1	7.16	9.39	5.88	1.68	0.72	0.94	0.59
JM1-Repeat	5.48	7.80	4.19	1.39	0.55	0.78	0.42
JM1-Average	6.32	8.60	5.04	1.54	0.64	0.86	0.51
JM2	13.47	10.90	7.12	1.51	1.35	1.09	0.71
JM2-Repeat	12.39	11.45	6.55	1.52	1.24	1.14	0.66
JM2-Average	12.93	11.18	6.84	1.52	1.30	1.12	0.69
JM3	9.72	14.04	4.52	2.35	0.97	1.40	0.45
JM3-Repeat	6.45	10.42	3.78	1.92	0.64	1.04	0.38
JM3-Average	8.09	12.23	4.15	2.14	0.81	1.22	0.42

According to the EDTA results, JM1 has the lowest degree of oxidation. This is expected, considering that the JM1 sample was prepared from the most recent drill cores. The oxidation levels of JM2 and JM3 were found to be similar to each other and higher than that of JM1. The EsFe values, which indicate oxidation based on the iron element, were higher for the second- and third-year core samples. This can be considered as an indication that pyrite has started to oxidize. Flotation tests were conducted to assess the impact of these differences on the flotation performance of the samples.

Rougher kinetic flotation tests were performed on ore samples under standard conditions. The JM2 and JM3 samples were tested in duplicate. As shown in Figure 20, although the flotation kinetics of the three composite samples differ, their ultimate Cu recoveries are not significantly distinct.



(a) (b)

Figure 20. Relationship between Time and Cu Recovery (a) and Mass Pull and Cu Recovery (b) in Cu Ro Stages.

The Zn recoveries in the Cu circuit for the JM1, JM2, and JM3 samples were 30.3%, 49.5%, and 53%, respectively. This indicates that nearly half of the Zn in the 2- and 3-year-old cores floated in the copper flotation circuit. Looking at the Cu-Zn separation selectivity curves (Figure 21a) showed that the trend curves were similar and above the reference line. However, the most selective separation was observed in the JM1 sample, followed by JM3, with the poorest separation occurring in JM2.

In the zinc circuit, after three stages of rougher flotation, Zn stage recovery values exceeded 95% for all samples (Figure 21b).

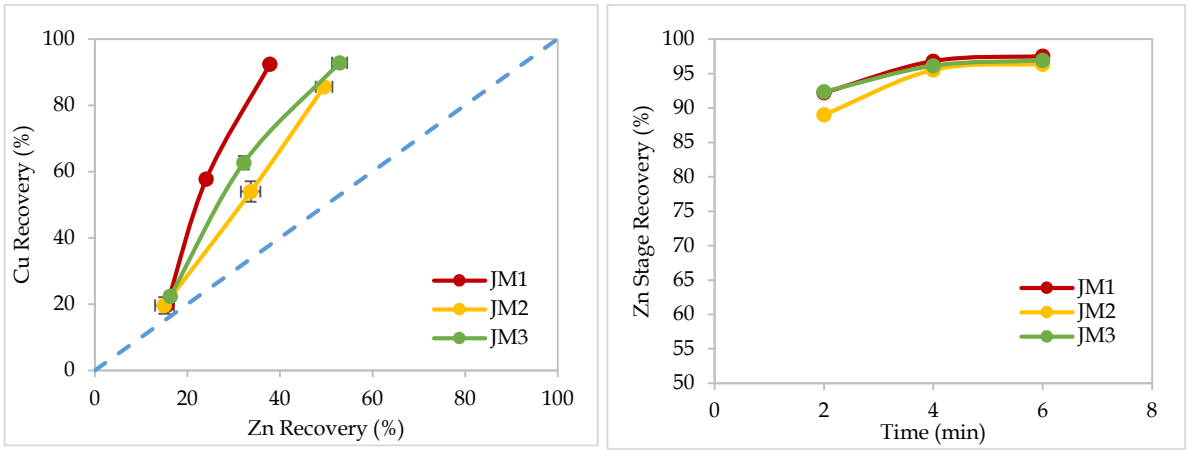


Figure 21. Relationship between Cu and Zn Recovery in Cu Ro Stages (a) and Time and Zn Recovery in Zn Ro Stages (b)

Cu-Zn selectivity was also evaluated using the Gaudin Selectivity Index (SI) (Figure 22), as the Selectivity Index considers both the recovery and grade of copper and zinc. The SI values were calculated using Equation (2), where Rm and Rg represent the recoveries of valuable and gangue minerals respectively (Wills and Finch, 2015).

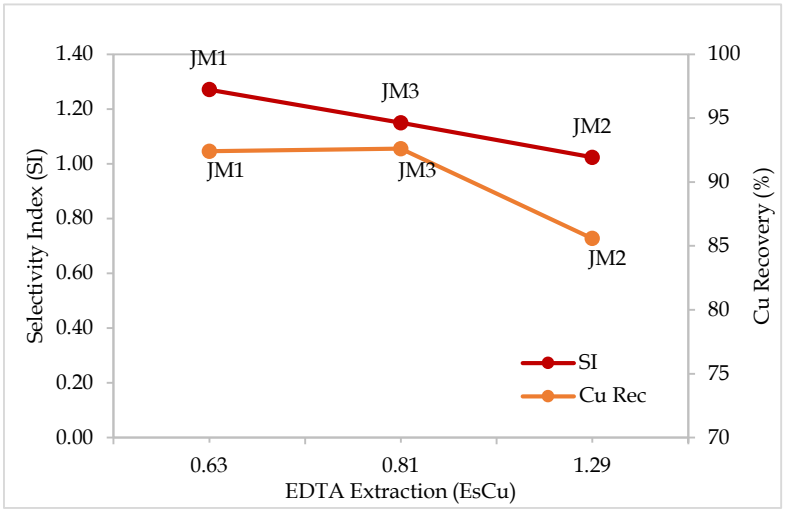


Figure 22. Gaudin Selectivity Index as a function of EDTA Extraction (EsCu)

Figure 22 illustrates the inverse relationship between EDTA extraction (EsCu) and the selectivity index (SI). As the EsCu value increased, the Cu-Zn selectivity index decreased. The oxidation of chalcopyrite and secondary copper minerals leads to the dissolution of Cu ions from the mineral surface, releasing metal hydroxides under alkaline conditions and forming a sulfur-rich metal layer on the surface (Owusu et al., 2011; Peng and Zhao, 2011; Von Oertzen et al., 2007; Todd et al., 2003). The presence of dissolved Cu ions promoted sphalerite flotation through Cu adsorption on its surface, negatively impacting the selectivity of copper flotation (Von Oertzen et al., 2007; Chandra and Gerson, 2009; Lascelles and Finch, 2002). With further oxidation, the amount of hydrophilic metal hydroxides increases, reducing mineral hydrophobicity and degrading the collector's selectivity, making it less selective for various sulfur minerals (Senior and Trahar, 1991; Clarke et al., 1995). However, in this case, the sulfide minerals were not significantly oxidized, as their total recoveries remained high and relatively similar.

$$SI^{2} = \frac{Rm\ x\ Rg}{(100-Rm)\ x\ (100-Rg)} \qquad (2)$$

Open cleaner flotation tests were conducted under standard conditions to determine the final copper and zinc concentrate qualities after three stages of cleaner flotation. The grades of the final concentrates obtained from the open cleaner tests are presented in Table 11. Accordingly, the highest grade and recovery were achieved with the JM1 sample, which corresponds to the 1-year-old cores. The copper concentrate with the lowest zinc and iron content was also obtained from the 1-year-old cores. JM1 was the best sample in terms of selectivity; however, JM2 and JM3 also produced saleable concentrates (over 20% Cu) when considering oxidation levels and flotation performance. The copper circuit recoveries for JM2 and JM3 were 85% and 92.7%, respectively, indicating high ore recoveries. Nonetheless, the iron and zinc content in the copper concentrates from JM2 and JM3 was higher than that of JM1. This indicates a decline in ore selectivity and suggests that the copper concentrates are starting to be contaminated with pyrite and sphalerite, reflecting early signs of oxidation.

Table 11. Comparison of the copper and zinc final concentrates produces from the different samples

			Grade %			**Recovery %**		
		Weights %	**Cu**	**Fe**	**Zn**	**Cu**	**Fe**	**Zn**
Cu Final Cons	**JM1**	3.53	33.91	25.21	1.51	54.43	7.12	1.54
	JM2	2.74	25.26	25.90	8.79	46.02	6.37	7.76
	JM3	3.64	29.66	25.44	5.81	59.10	9.31	4.82
Zn Final Cons	**JM1**	3.04	3.06	3.32	62.98	4.24	0.81	55.31
	JM2	1.78	3.93	4.93	59.72	4.66	0.79	34.28
	JM3	2.86	2.78	2.96	66.46	4.36	0.85	43.31

4. Conclusions

A core sample of a sulfide Cu-Zn ore was used to investigate the effects of storage duration on flotation performance. Core samples stored in the mining area for different periods were tested. EDTA tests, standard flotation tests, and open cleaner tests were conducted on the samples.

The oxidation levels of the samples are ranked from lowest to highest as follows: JM1, JM3 and JM2. Based on the years, JM3 was expected to have the highest oxidation level. However, due to the storage conditions the JM2 samples exhibited a higher oxidation value.

High-grade copper and zinc concentrates were produced from all three composite samples. Considering both rougher and cleaner concentrates, the highest grades and recoveries for both copper and zinc circuits were achieved with JM1, corresponding to the 1-year-old cores. The copper concentrate with the lowest zinc and iron content was also obtained from the 1-year-old cores. Therefore, while JM1 is the best sample in terms of selectivity, JM2 and JM3 were able to produce saleable concentrates with over 20% copper and over 55% zinc.

Oxidation negatively affected the Cu/Zn selectivity in the JM2 and JM3 samples, resulting in a Zn recovery of around 50% during the copper flotation stage. However, the zinc flotation stage was unaffected by surface oxidation, achieving Zn stage recoveries greater than 95%.

In conclusion, the higher iron and zinc content in the copper concentrates of JM2 and JM3 compared to JM1 indicates a decline in ore selectivity and suggests that the copper concentrates have begun to be contaminated with pyrite and sphalerite, signaling the onset of oxidation, though not at an advanced stage. Nevertheless, this level of oxidation did not hinder the production of high-grade copper and zinc concentrates.

Acknowledgments

The authors would like to thank Nakkaş Madencilik for their technical support.

References

Buckley, A.N.; Woods, R. 1984. An X-ray photoelectron spectroscopic study of the oxidation of chalcopyrite. *Aust. J. Chem.*, *37*, 2403–2413.

Chandra, A.P.; Gerson, A.R. 2009. A review of the fundamental studies of the copper activation mechanisms for selective flotation of the sulfide minerals, sphalerite and pyrite. Adv. Colloid Interface Sci., 145, 97–110.

Clarke, P.; Fornasiero, D.; Ralston, J.; Smart, R.S.C. 1995. A study of the removal of oxidation products from sulfide mineral surfaces. Miner. Eng., 8, 1347–1357.

Ekmekçi, Z.; Buswell, M.A.; Bradshaw, D.J.; Harris, P.J. 2005. The value and limitations of electrochemical measurements in flotation of precious metal ores. Miner. Eng., 18, 825–831.

Fullston, D., Fornasiero, D., Ralston, J. 1999c. Zeta potential study of the oxidation of copper sulfide minerals. Colloids Surf. A: Physicochem. Eng. Aspects 146, 113–121.

Grano, S.R.; Ralston, J.; Johnson, N.W. 1988. Characterization and treatment ofheavy medium slimes in the Mt. Isa mines lead-zinc concentrator. Miner. Eng., 1, 137–150.

Greet, C.; Smart, R.S.C. 2002. Diagnostic leaching of galena and its oxidation products with EDTA. Min. Eng., 15, 515–522.

Jacques, S., Greet, C.J., Bastin, D., 2016. Oxidative weathering of a copper sulphide ore and its influence on pulp chemistry and flotation. Miner. Eng. 99, 52–59.

Lascelles, D.; Finch, J.A. 2002. Quantifying accidental activation. Part I. Cu ion production. Miner. Eng., 15, 567–571.

Owusu, C.; E Abreu, S.B.; Skinner, W.; Addai-Mensah, J.; Zanin, M. 2014. The influence of pyrite content on the flotation of chalcopyrite/pyrite mixtures. Miner. Eng., 55, 87–95.

Peng, Y., Zhao, S., 2011. The effect of surface oxidation of copper sulfide minerals on clay slime coating in flotation. Miner. Eng. 24, 1687–1693.

Rao, S.R.; Labonte, G.; Finch, J.A. 1992. Electrochemistry in the plant. In Innovations in Flotation Technology; Springer: Dordrecht, The Netherlands, pp. 57–100.

Rumball, J.A.; Richmond, G.D. 1996. Measurement of oxidation in a base metal flotation circuit by selective leaching with EDTA. Int. J. Miner. Process., 48, 1–20.

Senior, G.D.; Trahar, W.J. 1991. The influence of metal hydroxides and collector on the flotation of chalcopyrite. Int. J. Miner. Processing., 33, 321–341.

Shannon, L.K.; Trahar, W.J. 1986. The role of collector in sulphide ore flotation. In Advances in Mineral Processing; Somasundaran, P., Ed.; Proc. Symp: Littleton, CO, USA, pp. 408–425.

Smart, R.S.C.; Amarantidis, J.; Skinner, W.; Prestidge, C.A.; La Vanier, L.; Grano, S. 1998. Surface analytical studies of oxidation and collector adsorption in sulphide mineral flotation. Scan. Microsc., 12, 553–583.

Smart, R.S.C. 1991. Surface layers in base metal sulfide flotation. Miner. Eng., 4, 891–909.

Todd, E.C.; Sherman, D.M.; Purton, J.A. 2003. Surface oxidation of chalcopyrite (CuFeS2) under ambient atmospheric and aqueous (pH 2-10) conditions: Cu, Fe L-and O K-edge X-ray spectroscopy. Geochim. Cosmochim. Acta, 67, 2137–2146.

Vaughan, D.J.; England, K.E.R.; Kelsall, G.H.; Yin, Q. 1995. Electrochemical oxidation of chalcopyrite (CuFeS2) and the related metal-enriched derivatives Cu4Fe5S8, Cu9Fe9S16 and Cu9Fe8S16. Am. Mineral., 80, 725–731.

Von Oertzen, G.U.; Skinner, W.M.; Nesbitt, H.W.; Pratt, A.R.; Buckley, A.N. 2007. Cu adsorption on pyrite (1 0 0): Ab initio and spectroscopic studies. Surf. Sci., 601, 5794–5799.

Wills, B.A.; Finch, J. 2015. Wills' Mineral Processing Technology: An Introduction to the Practical Aspects of Ore Treatment and Mineral Recovery: Butterworth-Heinemann; Elsevier: Amsterdam, The Netherlands.

Effects of Various Salts on Foam Stability of Surfactants

Yunus Emre Çavdar[1]*, Orhan Özdemir[1]

[1] *Department of Mineral Processing Engineering, Istanbul Technical University (ITU), Istanbul, Türkiye*

*Corresponding author: cavdar@itu.edu.tr (Yunus Emre Çavdar)

Abstract:

Froth flotation technology, developed in the early 20th century, remains integral to the enrichment of over 100 essential minerals (including copper, lead, zinc, nickel, silver, manganese, chromium, cobalt, titanium, quartz, feldspar, and coal), which serve as critical raw materials for a multitude of globally utilized products. In addition to its widespread use in mineral processing, this technology has been increasingly applied to various non-mining sectors, such as wastewater treatment. Flotation is a complex physico-chemical process, based on the separation of hydrophobic (water-repelling) particles from hydrophilic (water-attracting) particles using air bubbles. The efficiency of this process depends on the capacity of frothers to generate the appropriate size and quantity of air bubbles, which are capable of stably adhering to naturally hydrophobic particles. Foam formation and stability are therefore of paramount importance across a range of industries, including ore beneficiation, food production, cosmetics, and wastewater treatment. Surfactants, by adsorbing at the air-liquid interface, play a crucial role in modulating these interfacial properties. The presence of various dissolved ions in process water within industrial facilities can significantly impact foam characteristics. This study aimed to elucidate the effects of different ions on the stability of the surfactant-generated foam. Specifically, the investigation focused on the impact of Na^+ and Ca^{2+} ions on the foam stability of sodium dodecyl sulfate (SDS) solutions. The findings revealed that an increase in Na^+ concentration enhanced SDS foam stability, with marked improvements particularly evident at higher Na^+ concentrations. Conversely, the effect of Ca^{2+} ions on foam stability exhibited a negative correlation with the concentration; while minor improvements in the foam stability were observed at lower Ca^{2+} concentrations, a substantial decrease in stability occurred at higher concentrations.

Keywords: *Flotation, SDS, Salt, Foam, Dynamic Foam Stability*

1. Introduction

Dynamic foam stability is a critical aspect of flotation processes, particularly in mineral processing. The stability of foam directly influences the effectiveness of flotation, which relies on the separation of hydrophobic particles from hydrophilic ones. The fundamental principle behind flotation is the formation of bubbles that attach to the desired particles, allowing them to rise to the surface where they can be collected. However, the performance of this process is heavily dependent on the characteristics of the foam, including its stability, which is influenced by various factors such as reagent type, presence of various ions, concentration, and the physico-chemical properties of the solution.

Various methods have been developed to evaluate foam stability, which can generally be classified into two categories: dynamic tests and static tests. A dynamic test refers to a scenario where the foam reaches a dynamic equilibrium between its formation and decay rates. In contrast, a static test is one in which the foam formation rate is zero; after the foam is generated, it is allowed to collapse without further agitation or the introduction of gas for regeneration. The dynamic test is considered more representative of the conditions in an actual flotation system. In this test, air is continuously supplied to the solution, initiating foam formation at the bottom, which then rises upwards. The liquid flows downward, causing the foam quality to vary with height. Eventually, the top layer of the foam reaches a state of instability and collapses. These characteristics closely resemble the behavior observed in real flotation processes, making the dynamic method more likely to provide an accurate indication of foam stability during flotation testing (Farrokhpay, 2011). The dynamic foam stability factor was first proposed by Bikerman (1973). Bikerman defined the dynamic stability factor as the ratio of the maximum volume of foam

produced to the gas flow rate. In a study conducted by Mackay et al. (2018), the effects of particle size on dynamic foam stability were investigated, demonstrating the relationship between dynamic foam stability and flotation performance.

The role of foam stability extends beyond merely supporting the flotation of particles; it also impacts the overall recovery rates and the quality of the concentrate obtained. It is important to note that enhanced foam stability can significantly improve water recovery and the entrainment of solid particles, both of which are critical for maximizing the overall efficiency of the flotation process. Furthermore, the control of chemical additives can reduce the consumption of frothers while maintaining or enhancing flotation performance, indicating that foam stability can be optimized through careful chemical management (Pashkevich et al., 2023). This underscores the critical role of dynamic foam stability not only in ensuring effective flotation but also in advancing sustainable practices within the industry. By optimizing foam stability, resource consumption can be minimized, leading to more environmentally sustainable and cost-efficient operations.

In addition to the chemical composition of the flotation medium, the physical dynamics of foam significantly impact flotation efficiency. The stability of the foam, for instance, is largely determined by the size and distribution of bubbles, both of which are influenced by the choice and concentration of foaming agents. Stable foam plays a critical role by retaining floated materials at the water surface, enabling their collection at the optimal time. This process is essential for ensuring effective separation and maximizing flotation performance (Szyszka, 2018).

One of the key mechanisms by which salts affect foam stability is through the crystallization of surfactants. Research has demonstrated that the addition of salts, such as NaCl or KCl, to aqueous sodium dodecyl sulfate (SDS) solutions induces the formation of surfactant crystals during foam generation. This phenomenon occurs at intermediate salt concentrations, where the surfactant crystals obstruct the Plateau borders, subsequently reducing liquid drainage and enhancing foam stability (Binks & Shi, 2020).

Moreover, the presence of specific ions can significantly modify the adsorption behavior of surfactants at the air-water interface. Studies have shown that magnesium ions can stabilize ultrastable foams formed by flexible, bipolar-headed surfactants, indicating that certain cations can enhance foam stability by facilitating the formation of a multilayer surfactant structure within the foam film. (Li et al., 2013).

Furthermore, the choice of surfactant plays a crucial role in determining foam stability in saline environments. It has been observed that anionic surfactants, such as sodium dodecyl sulfate (SDS), can interact with divalent cations under high salinity conditions, leading to the formation of precipitates. This interaction negatively impacts foam stability, as the resulting precipitates disrupt the foam structure and reduce its effectiveness (Li et al., 2021).

Moreover, the interaction between salts and surfactants can give rise to more complex foam structures, which may be advantageous in certain applications. For example, it has been reported that the addition of high salt concentrations can result in the precipitation of surfactants onto bubble surfaces, leading to the formation of ultrastable foams. These foams have the potential to persist indefinitely under specific conditions, highlighting the role of salt-surfactant interactions in enhancing foam stability in targeted contexts (Zhang et al., 2015).

For this purpose, this study aimed to understand the effects of Na^{+} and Ca^{2+} ions on the stability of the SDS-generated foam using a dynamic foam analyzer.

2. Materials and methods

2.1. Materials

In the study, analytical-grade NaCl (Sigma Aldrich, Denmark) and $CaCl_2$ (Sigma Aldrich, Germany) salts were used. Sodium dodecyl sulfate (SDS) (≥ 99,0 $C_{12}H_{25}NaO_4S$, Sigma Aldrich, Japan) was employed as the surfactant.

2.2. Dynamic foam stability measurements

Foam stability measurements were conducted using a KRÜSS dynamic foam analyzer DFA100 (KRÜSS GmbH, Hamburg, Germany). This instrument measures foam formation and decay in liquids over time. The device primarily consists of a cell, which is a tempered glass column with a diameter of 40 mm and a height of 250 mm, optical sensors that monitor the cell, and a computer for data collection. The prepared solution is placed into the cell, and air is introduced through a filter plate with a pore size of 12-25 µm at the base of the cell to initiate foam formation. Airflow is maintained for a specified duration to generate foam, and upon cessation of airflow, foam decay is observed. Throughout the experiment, foam height is recorded by the optical sensors and transmitted to the computer. The experimental setup used in the tests is shown in Fig. 1.

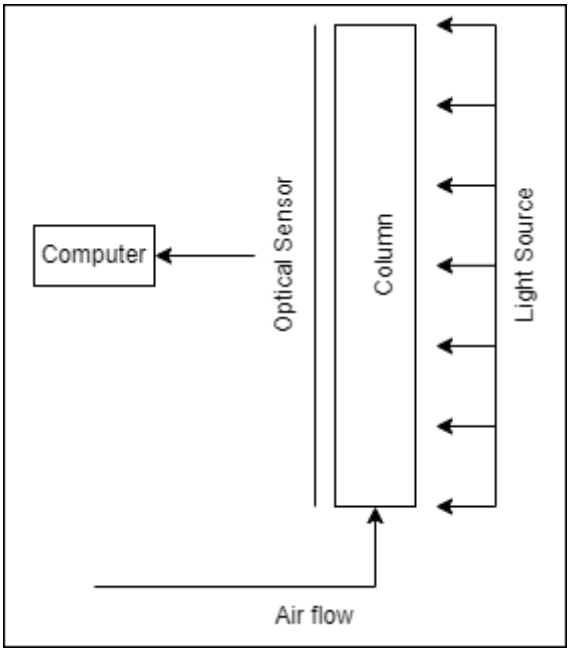


Fig. 1. Experimental setup for the foam stability experiments

In the experiments, various concentrations of salt solutions ($1 \cdot 10^{-3}$, $1 \cdot 10^{-2}$, $1 \cdot 10^{-1}$, 1 M) and SDS solutions ($1 \cdot 10^{-6}$, $5 \cdot 10^{-6}$, $1 \cdot 10^{-5}$, $5 \cdot 10^{-5}$, $1 \cdot 10^{-4}$, $5 \cdot 10^{-4}$, $1 \cdot 10^{-3}$, $5 \cdot 10^{-3}$, $8 \cdot 10^{-3}$) were used. Initially, each solution was prepared in 50 mL volumes and introduced into the cell, where foam generation and decay were measured (airflow rate: 0.2 L/min, foam formation time: 60 sec, foam decay time: 40 sec). Subsequently, to observe the change in foam height of SDS in the presence of salt, mixtures were prepared ($1 \cdot 10^{-4}$ M SDS + $1 \cdot 10^{-3}$ M, $1 \cdot 10^{-2}$ M, $1 \cdot 10^{-1}$ M, 1 M salt), and the foam generation and decay of these solutions were measured. Subsequently, using the measured foam heights, the dynamic foam stability for systems with different concentrations of SDS and SDS+salt was calculated using Eq. 1:

$$\Sigma = \frac{H_{max} \cdot A}{Q} \quad (1)$$

Where Σ is the dynamic foam stability factor (sec), H_{max} is the maximum foam height (cm), A is the cross-sectional area of column (cm^2) and Q is the gas flow rate (cm^3/sec).

3. Results and discussion

Foam height curves of the solutions prepared with NaCl and $CaCl_2$ without SDS are shown in Fig. 2. Upon examining Fig. 2, it is observed that NaCl does not form a stable foam at the specified

concentrations. By the 60th sec, when the air supply was cut off, the foam completely collapsed. A similar observation was also valid for $CaCl_2$, indicating that neither salt was capable of maintaining stable foam formation.

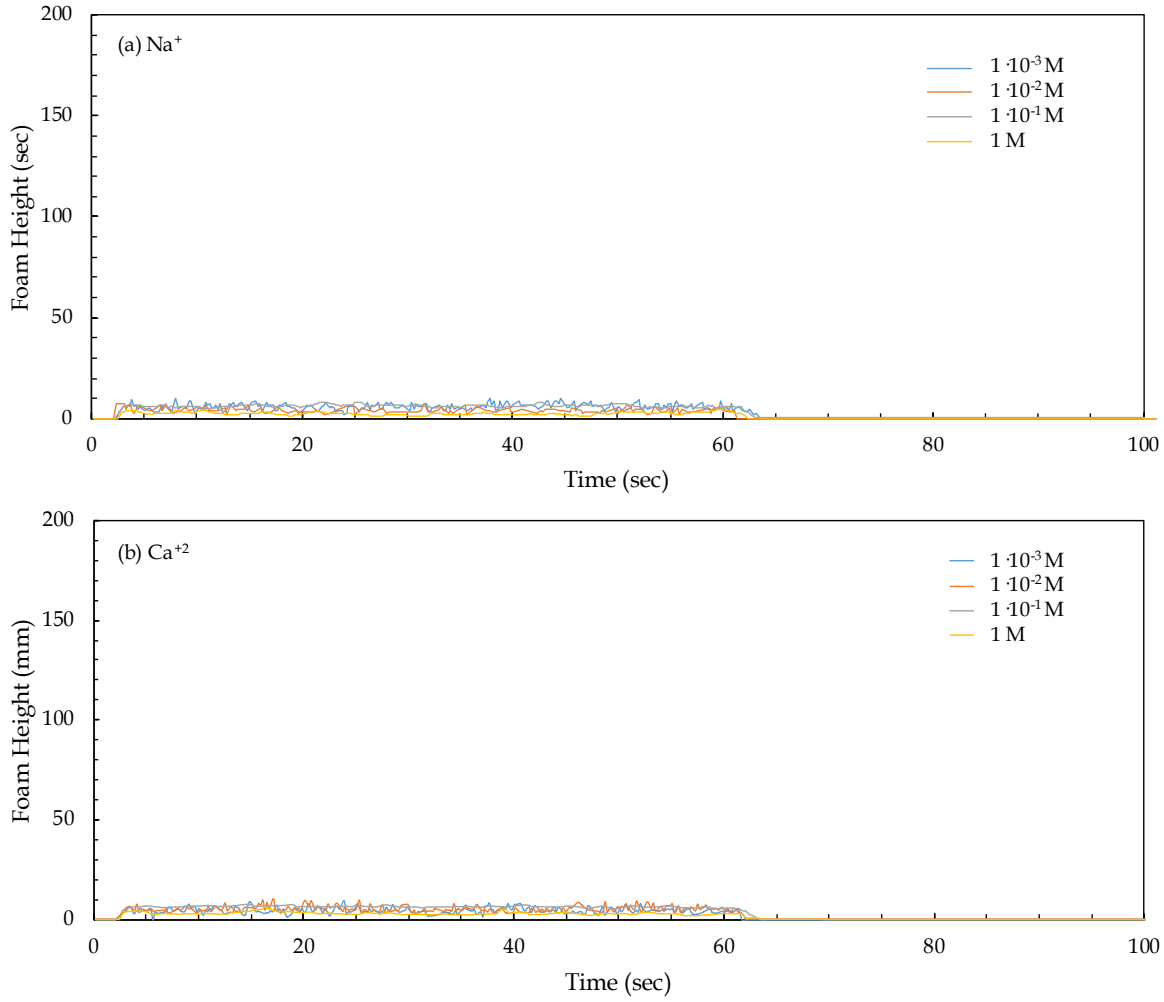


Fig. 2. Effect of NaCl (a) and (b) $CaCl_2$ on the foam stability

The foam stability in the presence of salt ions with SDS to evaluate the effectiveness of SDS in the presence of salt, the foam height was measured by adding salt solutions at varying concentrations ($1 \cdot 10^{-3}$ M, $1 \cdot 10^{-2}$ M, $1 \cdot 10^{-1}$ M, and 1 M) at $5 \cdot 10^{-5}$ M SDS solution. The data obtained are presented in Fig. 3. Upon examining Fig. 3, it is observed that the addition of $1 \cdot 10^{-3}$ M NaCl to the $5 \cdot 10^{-5}$ M SDS solution does not affect the foam-forming ability of SDS, with the foam height remaining constant at approximately 40 mm. However, as the NaCl concentration increases, the foam height rises to around 170 mm. In this context, it is determined that the addition of NaCl positively enhances the foam-producing capability of SDS. In contrast, the addition of $1 \cdot 10^{-3}$ M $CaCl_2$ to the $5 \cdot 10^{-5}$ M SDS solution increases the foam height from 40 mm to 120 mm. Nevertheless, as the concentration of $CaCl_2$ decreases, the foam-forming efficiency of SDS is adversely affected. Moreover, it has been observed that the addition of 1 M $CaCl_2$ almost completely inhibits SDS's ability to produce foam.

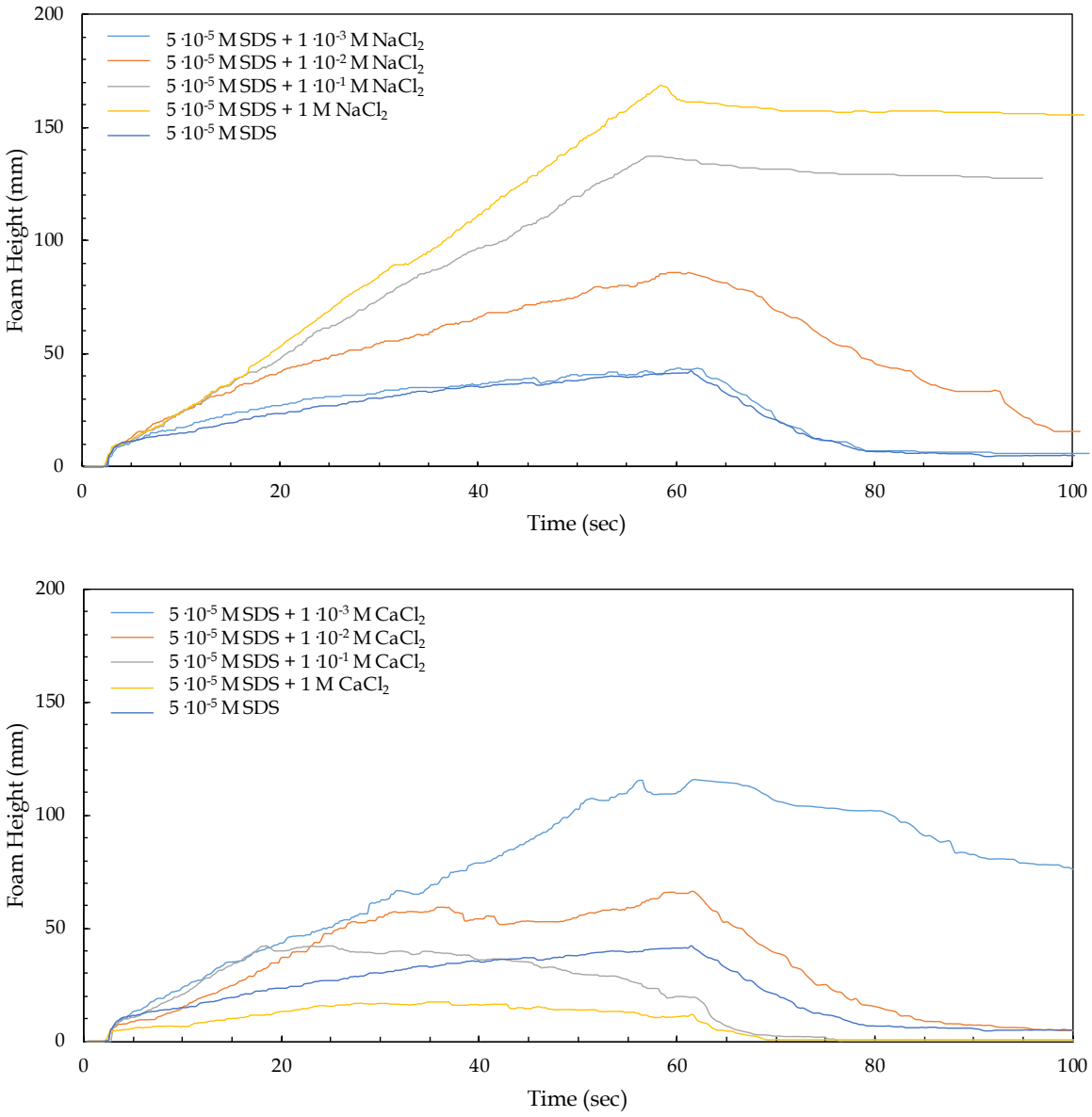


Fig. 3. Effect of addition of salt on foam height of SDS (a) addition of NaCl, (b) addition of $CaCl_2$

The foam stability curve of the solutions prepared by the addition of salt to the 5 ·10- 5 M SDS solution is presented in Fig. 4. The data presented in Fig. 4 reveal distinct effects of NaCl and $CaCl_2$ addition on the dynamic foam stability of a 5 ·10- 5 M SDS solution. The addition of NaCl leads to a concentration-dependent increase in foam stability. At a concentration of 1 ·10- 3 M NaCl, the foam stability is approximately 20 sec, which increases progressively with higher concentrations, reaching around 80 sec at 1 M NaCl. This indicates that NaCl significantly enhances the foam stability of SDS. In contrast, the addition of $CaCl_2$ showed a negative impact on the foam stability of SDS. While the foam stability is around 45 sec at 1 ·10- 3 M $CaCl_2$, it decreases steadily with increasing concentration, dropping to nearly zero at 1 M $CaCl_2$. Furthermore, when NaCl and $CaCl_2$ are added in the absence of SDS, the foam stability remains low across all concentrations, approximately 5 sec, suggesting that these salts alone are not effective in stabilizing foam. These findings demonstrate that NaCl has a positive effect on the foam stability of SDS, whereas $CaCl_2$ diminishes foam stability at higher concentrations.

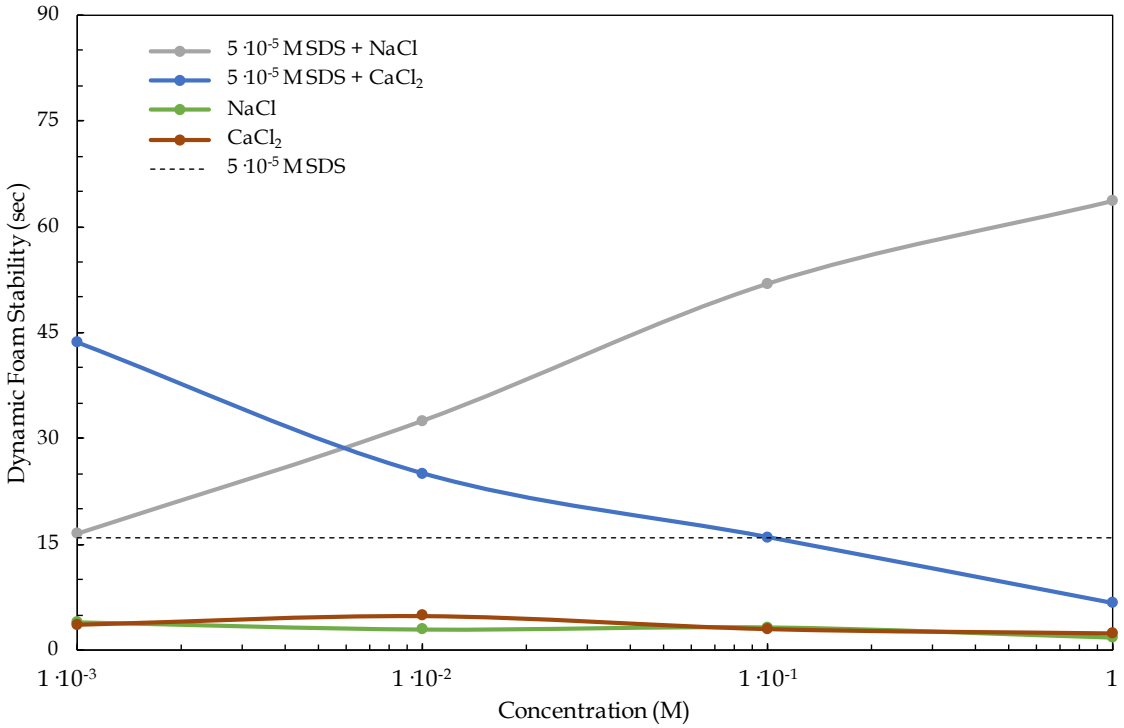


Fig. 4. Dynamic Foam Stability Of SDS In The Presence Of Salt

Conclusions

The results from this study indicated that the salts alone, even at concentrations up to 1 M, were unable to form stable foam.

The addition of NaCl to a $5 \cdot 10^{-5}$ M SDS solution does not significantly affect the foam formation ability of SDS at low concentrations. However, as the NaCl concentration increases, there is a notable increase in foam height. In contrast, the effect of $CaCl_2$ follows an opposite trend. At low concentrations, $CaCl_2$ enhances foam height, but as the concentration increases, it negatively impacts foam height, leading to a reduction in foam formation.

The presence of NaCl significantly enhances the foam stability of SDS as its concentration increases. Notably, at a concentration of 1 M NaCl, foam stability reaches approximately 80 sec. Conversely, the effect of $CaCl_2$ on SDS shows a reverse trend, with foam stability decreasing as the concentration increases. At a concentration of 1 M $CaCl_2$, foam stability is nearly eliminated. Furthermore, it has been observed that when NaCl and $CaCl_2$ are used alone, without SDS, the foam stability remains very low and does not show a significant increase despite changes in concentration. These findings indicate that while NaCl positively influences the foam stability of SDS, $CaCl_2$ has a detrimental effect on this stability.

Acknowledgments

The authors would like to express their sincere thanks and appreciation to the Office of Scientific Research Projects of İstanbul Technical University for the financial support (FHD-2024-45574).

References

Bikerman, J. J., 1973. *Theories of Foam Stability Sections, Foams*. Springer, New York, NY, USA, 231-244.

Binks, B. and Shi, H., 2020). *Aqueous foams in the presence of surfactant crystals*. Langmuir, 36(4), 991-1002. https://doi.org/10.1021/acs.langmuir.9b03862

Farrokhpay, S., Fornasiero, D., 2017. *Flotation of coarse composite particles: Effect of mineral liberation and phase distribution*. Advanced Powder Technology, 28(18), 49–54. doi:10.1016/j.apt.2017.03.012

Li, C., Liu, Y., Yuan, R., & Lv, W., 2013. *Study of the microcharacter of ultrastable aqueous foam stabilized by a kind of flexible connecting bipolar-headed surfactant with existence of magnesium ion*. Langmuir, 29(18), 5418-5427. https://doi.org/10.1021/la4011373

Li, W., Wang, K., & Zheng, W., 2021. *Static and flow behaviors of supercritical co2 foam stabilized with betaine surfactant for mobility control application*. Oil & Gas Science and Technology – Revue D'ifp Energies Nouvelles, 76, 58. https://doi.org/10.2516/ogst/2021040

Mackay, I., Mendez, E., Molina, I., Videla, A. R., Cilliers, J. J., Brito-Parada, P. R., 2018. *Dynamic froth stability of copper flotation tailings*. Miner. Eng. 124, 103–107.

Pashkevich, D., Li, R., Kökkılıç, O., & Waters, K., 2023. *Investigations of monomineralic flotation of galena, sphalerite, and pyrite at different temperatures.* Minerals, 13(5), 615. https://doi.org/10.3390/min13050615

Szyszka, D., 2018. *Critical coalescence concentration (CCC) for surfactants in aqueous solutions*. Minerals, 8(10), 431. https://doi.org/10.3390/min8100431

Zhang, L., Mikhailovskaya, A., Yazhgur, P., Muller, F., Cousin, F., Langévin, D. & Salonen, A., 2015. *Precipitating sodium dodecyl sulfate to create ultrastable and stimulable foams.* Angewandte Chemie, 127(33), 9669-9672. https://doi.org/10.1002/ange.201503236

Effect of sodium silicate, sodium tripolyphosphate, and sodium hexametaphosphate dispersants on particle size distribution of the halloysite, kaolinite, and quartz minerals in the dispersion process

Emrah Durgut [1], Yunus Emre Çavdar [2*], Mustafa Çınar [3], Osman Yavuz [4], Orhan Ozdemir [2]

[1] *Department of Mining and Extraction, Çan Vocational School, Çanakkale Onsekiz Mart University, Çanakkale, Türkiye*

[2] *Department of Mineral Processing Engineering, Istanbul Technical University (ITU), Istanbul, Türkiye*

[3] *Çanakkale Onsekiz Mart University, Department of Mining Engineering, Faculty of Engineering, Çanakkale, Türkiye*

[4] *Istanbul University-Cerrahpasa, Department of Mining Engineering, Faculty of Engineering, Büyükçekmece, İstanbul, Türkiye*

*Corresponding author: cavdar@itu.edu.tr (Yunus Emre Çavdar)

Abstract:

Kaolinite group clay minerals are generally formed by hydrothermal alteration of aluminosilicate minerals and have the chemical formula $Si_2Al_2O_5(OH)_4.nH_2O$. This group of ores is mainly composed of dickite, nacrite, kaolinite, halloysite, and other clay minerals, but may also contain impurities such as quartz, iron, titanium, and alunite. Halloysite is classified as harmless and a biocompatible material according to the Environmental Protection Agency (EPA 4A). However, the degree of purity determines the area where the halloysite will be used. In this respect, it is very important to determine the grade of halloysite mineral in the ore. Since halloysite mineral is chemically very similar to kaolinite mineral, it can be confused with each other in chemical and mineralogical analyses. Although the kaolinite and quartz minerals are found in the structure of halloysite ore besides halloysite mineral primarily, it is necessary to provide fine-size (-38 µm) particle liberation and to remove them from each other at these sizes to reach high purity. Within the scope of the study, the particle size differentiation of halloysite, kaolinite, and quartz suspensions was studied by dispersing in the presence of sodium silicate (SS), sodium tripolyphosphate (STPP) and sodium hexametaphosphate (SHMP) dispersants at fine particle size. In the dispersion experiments, a significant decrease in d_{90} values is observed as the dosage increases for all dispersants, while a partial decrease was observed in d_{50} and d_{10} values did not change significantly for halloysite and kaolinite minerals. In quartz mineral, the addition of dispersant did not affect the particle size importantly and d_{10}, d_{50}, and d_{90} values remained almost unchanged. Especially for halloysite and kaolinite minerals, no significant change was observed after 5 kg/ton dosage for each dispersant.

Keywords: *Halloysite, Kaolinite, Dispersion, Dispersant*

1. Introduction

Industrial raw materials are defined as rocks, minerals, or naturally occurring substances of economic value, except metallic ores, mineral fuels, and ornamental stones (Allaby, 2013). Such natural resources, which constitute an important part of daily lives, are mainly used in agriculture, ceramics, glass, refractories, metallurgy, and construction sectors; fillers, paints, fertilizers, chemicals, abrasives, gemstones, drilling muds, and electrical/electronic industries (Adekunle et al., 2015; Hamdi et al., 2018; Balde et al., 2021). In the past, pure sources found in nature could be used as they were extracted from the quarry. However, due to the depletion of pure resources, industrial raw materials are subjected to various preparation and enrichment processes nowadays (Murray, 1976; Mukherjee, 2011). In addition, with the developing analysis methods, the properties of industrial minerals can be examined in more detail and can be used in the production of new-generation nanomaterials (Zhou and Keeling, 2013; Ma et al., 2024).

Raw materials obtained from nature must be subjected to processes such as particle size reduction, classification, and mineral beneficiation to be used in related industrial fields. In this context, current

mineral processing and beneficiation methods are used in wet and dry medium. However, the selection of the mineral processing and beneficiation method to be applied is very important in order not to damage natural properties for the efficient use of such minerals in the field of nanotechnology (Takahashi, 1957; Takahashi, 1959). In addition, the processing method is of great importance in terms of ensuring particle size liberation according to the plastic and non-plastic character of the minerals. During mineral processing application, particle size reduction methods are applied in wet and dry environments in order to ensure particle size liberation. Afterward, the ore is separated into fine sizes by grinding or mixing processes depending on the plastic or non-plastic character. Mixing in aqueous media is used for the economic and technical separation of clay minerals into fine sizes. The high pulp density in this process is an important issue in terms of natural gas and water consumption in the drying stage (Wilson, 2007). The clay minerals have different effects on rheological properties during the industrial production steps (Khaydapova et al., 2015). Therefore, it is important to determine the rheological properties of clays used in wet systems. The rheological properties of clays depend on many parameters such as the solids ratio, chemical and mineralogical composition, particle shape and size distribution, dispersant type and dosage, pH, temperature, organic content, non-clay minerals, etc. (Chang et al., 1993; Maxwell and Dinger, 2008; Shoaib et al., 2022). During the dispersion of clay minerals, a small amount of inorganic or organic additives are added to the clay-water suspension to obtain a fluid mixture with high density. Such additives can be classified as deflocculants, binders, and plasticizers and are used to regulate the rheological behavior of suspensions. Sodium carbonate, sodium silicate, tetrasodium pyrophosphate, sodium tripolyphosphate, sodium polyacrylate, and sodium citrate are well-known dispersants. Binder additives are microcrystalline cellulose, ammonium alginate, and methylcellulose. Plasticizer additives are ethylene glycol, and glycerol (Tadros, 2005). Dispersion is the process by which solid colloidal particles move away from each other in the pulp such that they remain in suspension by repulsive electrostatic motion caused by the dispersant. Therefore, dispersants increase the fluidity of the suspension and reduce the apparent viscosity in aqueous suspensions (Landrou et al., 2018).

Today, understanding the fine structures of clay minerals is becoming increasingly important for the production of nanotechnological materials. Clay minerals have recently started to be used in the field of nanotechnology with various next-generation analysis methods and the unexplored properties of nano clay minerals have encouraged researchers to work on this subject. In this study, it was aimed to understand the particle size distribution of halloysite, kaolinite, and quartz suspension by dispersing in the presence of sodium silicate (SS), sodium tripolyphosphate (STPP), and sodium hexametaphosphate (SHMP).

2. Materials and methods

2.1. Materials

In this study, pure halloysite and quartz samples from Türkiye and pure kaolinite sample from Ukraine were used for dispersion experiments. The results for the mineralogical (XRD) analyses of the pure samples are shown in Fig. 1. As seen in Fig. 1a, the halloysite was composed of metahalloysite and halloysite, besides kaolinite and quartz (Fig. 1b and c) were formed as pure minerals.

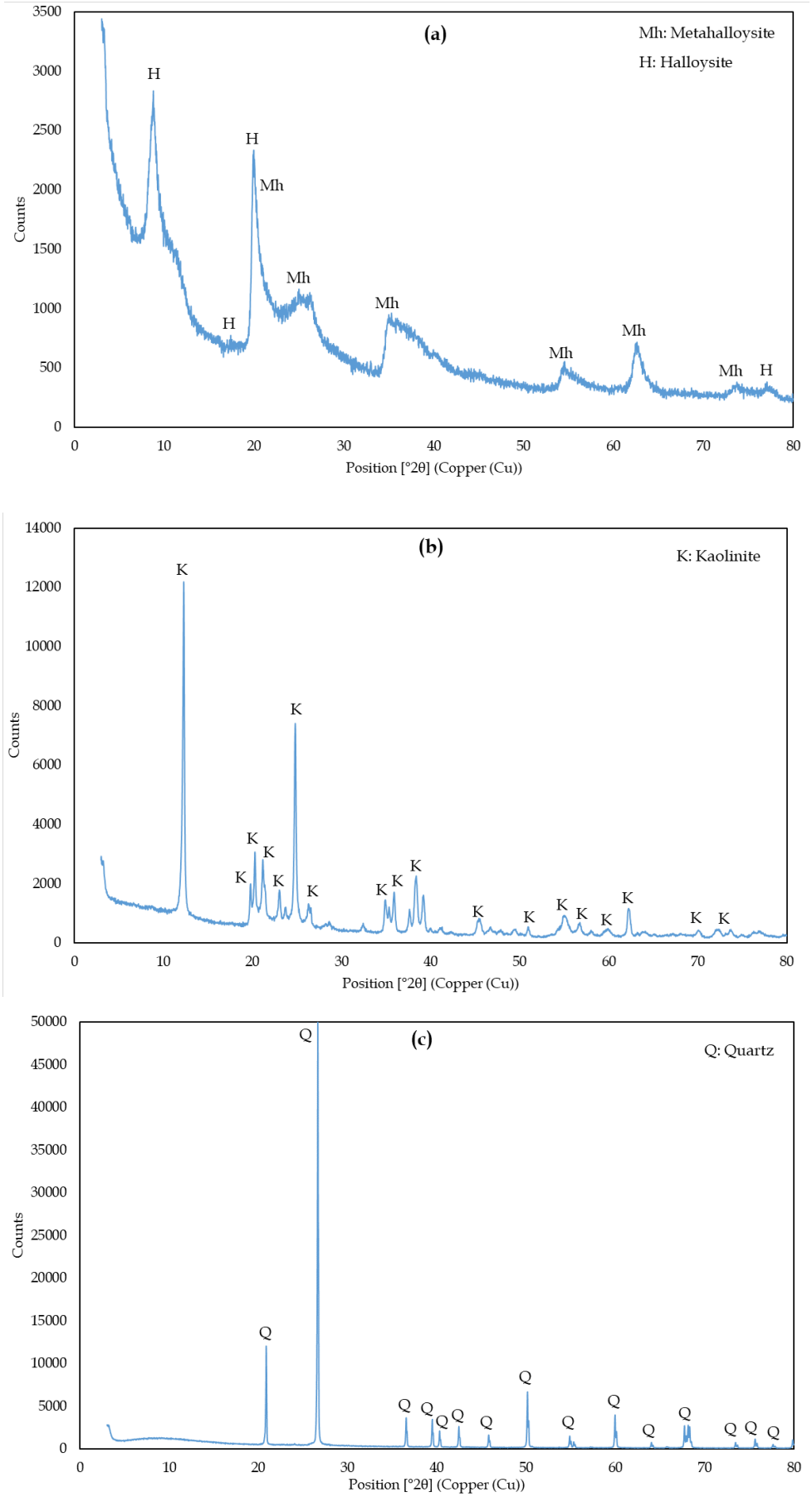


Fig. 1. The XRD patterns of (a) halloysite, (b) kaolinite, and (c) quartz samples

2.2. Dispersion experiments

Sodium silicate (SS) with a molecular weight of 184.04 g/mol and a density of 1.526 g/cm ^{3} obtained from Zag Kimya, sodium tripolyphosphate (STPP) with 94% purity obtained from TEKKİM Kimya, and extra pure sodium hexametaphosphate (SHMP) with a total phosphate content of 65-70% were used to perform the dispersing process of pure halloysite, kaolinite, and quartz samples. The experiments were carried out using dispersants at different dosages (2.5 kg/ton, 5 kg/ton, 10 kg/ton) for 30 min at 20% solids ratio in a magnetic stirrer operated at 600 rpm mixing speed. At the end of the experiment, the products were sieved with a 74 µm aperture sieve and the sieved products were analyzed in terms of particle size with a Malvern Mastersizer 2000 laser measuring device. Mastersizer measurements were performed by taking 5 drops with a pasteur pipette after the suspensions prepared at 5% solids ratio were mixed and homogenized in a magnetic stirrer for 5 min. The experimental setup for the dispersion experiment is shown in Fig. 2.

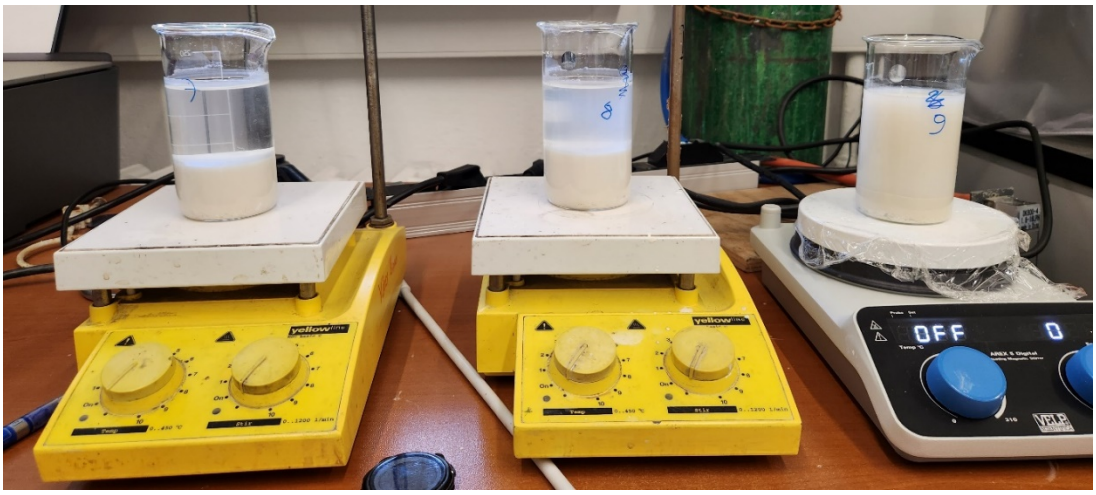


Fig. 2. Experimental set-up for dispersion experiments

3. Results and discussion

The d_{10}, d_{50}, and d_{90} values of the products of pure halloysite sample obtained from the dispersion processes at different dosages of selected dispersants (SS, STPP, SHMP) (2.5 kg/ton, 5 kg/ton, 10 kg/ton) are presented in Table 1 and shown in Fig. 3.

Table 1. d_{10}, d_{50}, d_{90} values of the products obtained by dispersing pure halloysite mineral at different dispersant dosages

	SS			**STPP**			**SHMP**		
Dosage (kg/ton)	d_{10} (µm)	d_{50} (µm)	d_{90} (µm)	d_{10} (µm)	d_{50} (µm)	d_{90} (µm)	d_{10} (µm)	d_{50} (µm)	d_{90} (µm)
0.0	3.2	27.8	74.8	3.2	27.8	74.0	3.2	27.8	74.0
2.5	3.1	21.7	74.0	2.8	21.7	64.0	2.6	21.7	63.5
5.0	2.5	18.1	60.1	2.7	17.6	61.6	2.3	15.0	50.8
10.0	2.6	19.6	63.8	2.7	16.5	57.5	2.3	15.8	54.7

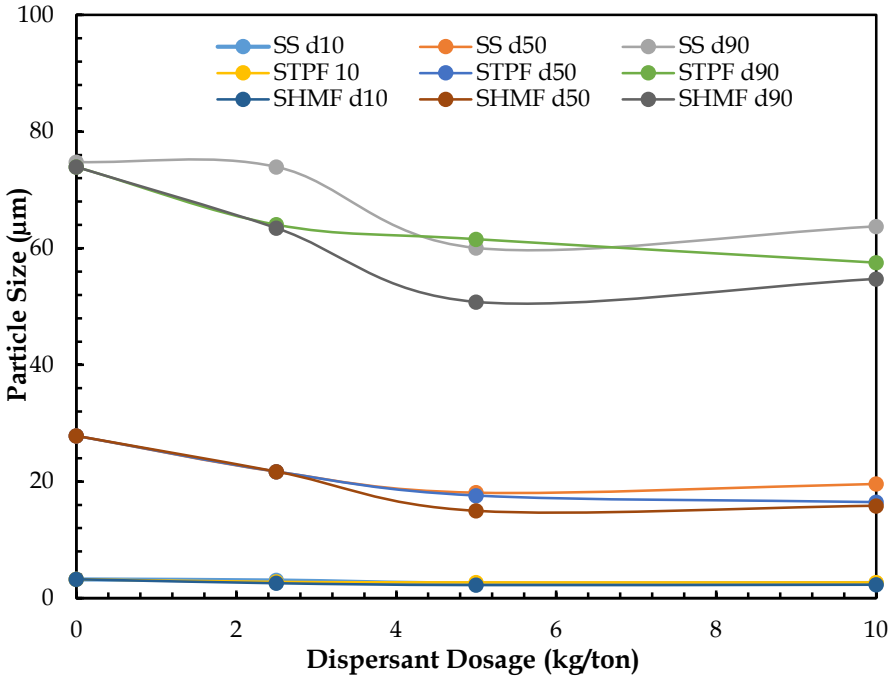


Fig. 3. d_{10}, d_{50}, d_{90} values of the products obtained by dispersing pure halloysite sample at different dispersant dosages

As d_{90} values were examined, the size value of pure halloysite sample without dispersant addition was 74.0 µm, while it decreased to 63.8 µm in the presence of 10 kg/ton SS, 57.5 µm in the presence of 10 kg/ton STPP, and 54.7 µm in the presence of 10 kg/ton SHMP. When d_{50} values were examined, while the size value of pure halloysite sample without dispersant addition was 27.8 µm, it decreased to 19.6 µm in the presence of 10 kg/ton SS, 16.5 µm in the presence of 10 kg/ton STPP and 15.8 µm in the presence of 10 kg/ton SHMP. When d_{10} values were examined, the size value of the dispersed pure halloysite sample without dispersant addition was 3.2 µm, while it decreased to 2.6 µm in the presence of 10 kg/ton SS, 2.7 µm in the presence of 10 kg/ton STPP and 2.3 µm in the presence of 10 kg/ton SHMP (Fig. 3).

The d_{10}, d_{50}, and d_{90} values of the products obtained by dispersing pure kaolinite sample at different dispersant dosages (2.5 kg/ton, 5 kg/ton, 10 kg/ton) are presented in Table 2 and shown in Fig. 4.

Table 2. d_{10}, d_{50}, d_{90} values of the products obtained by dispersing pure kaolinite sample at different dispersant dosages

	SS			**STPP**			**SHMP**		
Dosage (kg/ton)	d_{10} (µm)	d_{50} (µm)	d_{90} (µm)	d_{10} (µm)	d_{50} (µm)	d_{90} (µm)	d_{10} (µm)	d_{50} (µm)	d_{90} (µm)
0.0	1.6	8.7	50.7	1.6	8.7	50.7	1.6	8.7	50.7
2.5	1.7	8.7	42.0	1.9	9.9	42.1	1.3	7.7	28.6
5.0	1.6	8.3	39.3	1.8	9.4	40.0	1.4	8.0	27.2
10.0	2.1	9.3	34.3	2.0	9.4	36.0	1.4	7.9	26.3

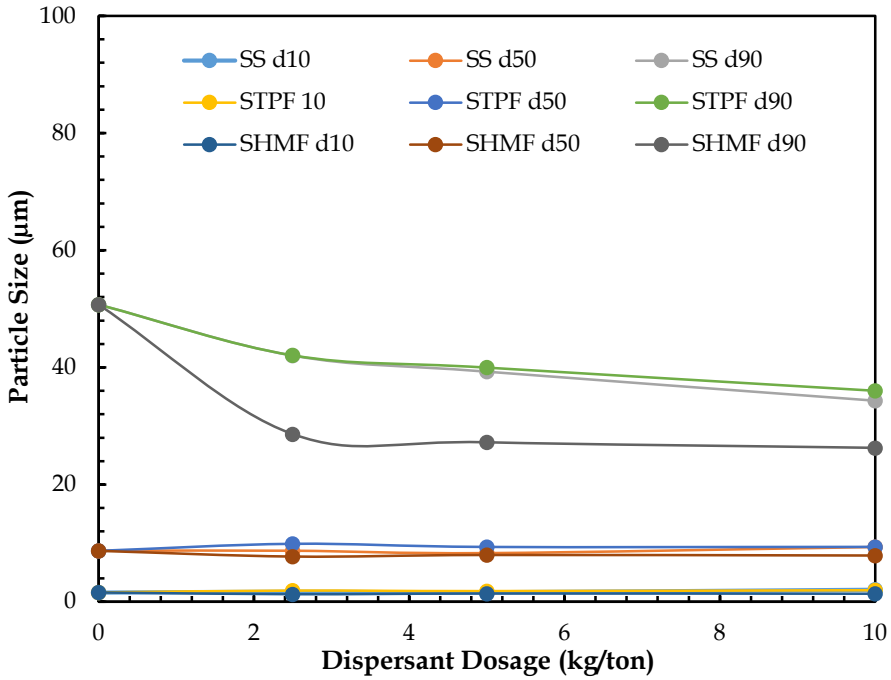


Fig. 4. d_{10}, d_{50}, d_{90} values of the products obtained by dispersing pure kaolinite sample at different dispersant dosages

As d_{90} values were examined, the size value of the dispersed pure kaolinite sample without dispersant addition decreased from 50.7 µm to 34.3 µm in the presence of 10 kg/ton SS, 36.0 µm in the presence of 10 kg/ton STPP, and 26.3 µm in the presence of 10 kg/ton SHMP. When the d_{50} values were examined, the size value of the dispersed pure kaolinite sample without dispersant addition was 8.7 µm, while it increased to 9.3 µm in the presence of 10 kg/ton SS, 9.4 µm in the presence of 10 kg/ton STPP and decreased to 7.9 µm in the presence of 10 kg/ton SHMP. When the d_{10} values were analyzed, the size value of the dispersed pure kaolinite sample without dispersant addition was 1.6 µm, while it increased to 2.1 µm in the presence of 10 kg/ton SS, 2.0 µm in the presence of 10 kg/ton STPP and decreased to 1.4 µm in the presence of 10 kg/ton SHMP (Fig. 4).

The d_{10}, d_{50}, and d_{90} values of the products obtained by dispersing pure quartz sample at different dispersant dosages (2.5 kg/ton, 5 kg/ton, 10 kg/ton) were given in Table 3 and Fig. 5.

Table 3. d_{10}, d_{50}, d_{90} values of the products obtained by dispersing pure quartz sample at different dispersant dosages

	SS			**STPP**			**SHMP**		
Dosage (kg/ton)	d_{10} (µm)	d_{50} (µm)	d_{90} (µm)	d_{10} (µm)	d_{50} (µm)	d_{90} (µm)	d_{10} (µm)	d_{50} (µm)	d_{90} (µm)
0.0	2.7	21.8	61.3	2.7	21.8	61.3	2.7	21.8	61.3
2.5	2.8	21.7	60.0	3.0	24.0	63.9	2.6	20.8	57.6
5.0	2.8	21.7	60.0	2.9	23.3	63.1	2.6	20.7	57.7
10.0	2.7	20.7	58.1	2.9	23.3	63.5	2.6	20.5	57.1

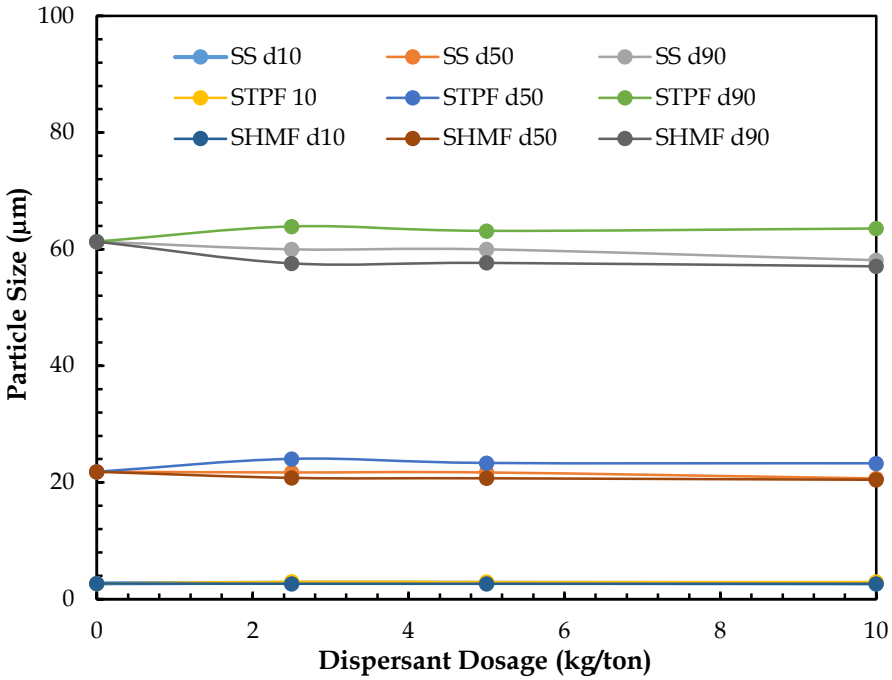


Fig. 5. d_{10}, d_{50}, d_{90} values of the products obtained by dispersing pure quartz sample at different dispersant dosages

As d_{90} values were examined, the size value of the dispersed pure quartz sample without dispersant addition changed from 61.3 µm to 58.1 µm in the presence of 10 kg/ton SS, 63.5 µm in the presence of 10 kg/ton STPP and 57.1 µm in the presence of 10 kg/ton SHMP. When the d_{50} values were examined, the size value of the dispersed pure quartz sample without dispersant addition was 21.82 µm, while it changed to 20.68 µm in the presence of 10 kg/ton SS, 23.27 µm in the presence of 10 kg/ton STPP, and 20.48 µm in the presence of 10 kg/ton SHMP. When the d_{10} values were examined, the size value of the dispersed pure quartz sample without dispersant addition was 2.7 µm, it stayed permanent in the presence of 10 kg/ton SS and changed to 2.9 µm in the presence of 10 kg/ton STPP and 2.6 µm in the presence of 10 kg/ton SHMP (Fig. 5).

4. Conclusions

In the dispersion experiments, a significant decrease in d_{90} values was observed with increasing dosage in all dispersants used for halloysite and kaolinite samples, while a partial decrease was observed in d_{50} values. d_{10} values do not change significantly. In quartz mineral, the addition of dispersant did not affect the particle size, and d_{10}, d_{50}, and d_{90} values remained almost unchanged. It was observed that there was no significant change after 5 kg/ton dosage in all dispersants used for halloysite and kaolinite minerals with dispersant addition. In this context, the optimum dispersant dosage was determined as 5 kg/ton. Besides, it was understood that SHMP produced finer-sized products compared to SS and STPP at the same dosage. In conclusion, it was understood that SHMP was a stronger dispersant than STPP and SS.

Acknowledgments

The authors would like to express their sincere thanks and appreciation to the Office of Scientific Research Projects of İstanbul Technical University for the financial support (Project no: MAB-2023-44800).

References

Adekunle, S., Ahmad, S., Maslehuddin, M., & Al-Gahtani, H.J., 2015. *Properties of SCC prepared using natural pozzolana and industrial wastes as mineral fillers*. Cement and Concrete Composites, 62, 125–133. https://doi.org/10.1016/j.cemconcomp.2015.06.001.

Allaby, M., 2013. *A Dictionary of Geology and Earth Sciences* (300): Oxford University Press.

Balde, M.Y., Djangang, C.N., Diallo, R.B., Blanchart, P., & Njopwouo, D., 2021. *Physicochemical characterisation for potential uses as industrial mineral of bauxite from Débélé, Guinea*. Journal of Materials Science and Chemical Engineering, 09(03), 9–22. https://doi.org/10.4236/msce.2021.93002.

Chang, S.H., Ryan, M.H., & Gupta, R.K., 1993. *The effect of pH, ionic strength, and temperature on the rheology and stability of aqueous clay suspensions*. Rheologica Acta, 32(3), 263–269. https://doi.org/10.1007/bf00434190.

Hamdi, N., Messaoud, I.B., & Srasra, E., 2018. *Production of geopolymer binders using clay minerals and industrial wastes*. Comptes Rendus Chimie, 22(2–3), 220–226. https://doi.org/10.1016/j.crci.2018.11.010.

Khaydapova, D., Milanovskiy, E., & Shein, E., 2015. *Rheological properties of different minerals and clay soils*. Eurasian Journal of Soil Science (Ejss), 4(3), 198. https://doi.org/10.18393/ejss.2015.3.198-202.

Landrou, G., Brumaud, C., Plötze, M.L., Winnefeld, F., & Habert, G., 2018. *A fresh look at dense clay paste: Deflocculation and thixotropy mechanisms*. Colloids and Surfaces a Physicochemical and Engineering Aspects, 539, 252–260. https://doi.org/10.1016/j.colsurfa.2017.12.029.

Ma, J., Jin, X., Lu, Y., Yang, M., Zhao, X., Guo, M., Zhang, H., Li, X., & Wang, B., 2024. *Preparation of modified halloysite nanotubes@Ag_3PO_4/polyacrylonitrile electrospinning membranes for highly efficient air filtration and disinfection*. Applied Clay Science, 253, 107361. https://doi.org/10.1016/j.clay.2024.107361.

Maxwell, C.B., & Dinger, D.R., 2008. *Effects of Ball-Clay processing on suspension rheology*. In Ceramic engineering and science proceedings (pp. 116–122). https://doi.org/10.1002/9780470313183.ch13.

Mukherjee, S., 2011. *Industrial mineralogy: mineral processing, beneficiations and other related mineral usage*. In Springer eBooks (pp. 428–489). https://doi.org/10.1007/978-94-007-1162-4_17.

Murray, H., 1976. *Beneficiation of selected industrial minerals and coal by high intensity magnetic separation*. IEEE Transactions on Magnetics, 12(5), 498–502. https://doi.org/10.1109/tmag.1976.1059070.

Shoaib, M., Cruz, N., & Bobicki, E., 2022. *Effect of pH-modifiers on the rheological behaviour of clay slurries: Difference between a swelling and non-swelling clay*. Colloids and Surfaces a Physicochemical and Engineering Aspects, 643, 128699. https://doi.org/10.1016/j.colsurfa.2022.128699.

Tadros, T.F., 2005. *Applied Surfactants: Principles and applications*. http://ci.nii.ac.jp/ncid/BA71909633.

Takahashi, H., 1957. *Effect of dry grinding on kaolin minerals*. Deleted Journal, 6, 279–291. https://doi.org/10.1346/ccmn.1957.0060121.

Takahashi, H., 1959. *Wet grinding on kaolin minerals*. Bulletin of the Chemical Society of Japan, 32(4), 381–387. https://doi.org/10.1246/bcsj.32.381.

Wilson, I., 2007. *Applied clay mineralogy. Occurrences, processing and application of kaolins, bentonite, palygorskite sepiolite, and common clays*. Clays and Clay Minerals, 55(6), 644–645. https://doi.org/10.1007/bf03406033.

Zhou, C.H., & Keeling, J., 2013. *Fundamental and applied research on clay minerals: From climate and environment to nanotechnology*. Applied Clay Science, 74, 3-9. https://doi.org/10.1016/j.clay.2013.02.013.

Investigation of the Effectiveness of Oleate in Fine-Sized Magnesite Flotation

S. Koca [1]*, D.O. Aksoy [1], H. Koca [2]

[1] Mining Engineering Department, Eskişehir Osmangazi University, Eskişehir, Turkey

[2] Porsuk Technical College, Eskisehir Technical University, Eskişehir, Turkey

*Corresponding author: deryaoz@gmail.com (Derya Oz Aksoy)

Abstract:

In this work, effectiveness of oleate in fine sized magnesite flotation was studied by froth flotation. In the flotation experiments, conditioning time, flotation time, air rate and particle size were kept constant while solid ratio, pH and collector dosage were varied. The experimental results revealed that a concentrate of over 43 % MgO content with nearly 75 % MgO recovery was obtained. The Si02 content of concentrate was around 4,92 % indicating 75 % reduction according to head sample.

Keywords: *Froth flotation, Oleate, Magnesite, Quartz.*

1. Introduction

Magnesite is one of the most important raw materials for many products, especially in the metal, glass and cement industries. Magnesite is largely used especially in the production of high temperature resistant products. The most important factor that limits its utilization is the impurities, it contains. While it can be economically enriched in large sizes with various physical enrichment methods; as the grain size becomes smaller, flotation comes to the fore as an enrichment method.

Oleate is commonly used as the collector in magnesite flotation particularly magnesite-dolomite separation. For example, in a study published by Zhong et al in 2020, magnesite and dolomite were separated by flotation by using α-chloro-oleate acid as collector. In this flotation study approximately 95% of magnesite was concentrated, while 82.5% of dolomite remained in waste. In another study (Sun et al., 2020) on the magnesite-dolomite separation, sodium oleate was used as a magnesite collector. Since oleate was also adsorbed on the dolomite surface, selectivity was achieved using sodium hexametaphosphate as depressant. A more recent study published by Luo et al., in 2024, separation of magnesite from dolomite was achieved by using sodium silicate modified with zinc sulphide as depressant.

Froth flotation is also used in the concentration of magnesite by reducing SiO2 content in a numerous of study. For example, in a study published by Sun and Yin in 2022, a specially designed cationic collector, palmitoyl trimethylammonium chloride was used to separate artificial mixtures of magnesite and quartz without the need of a depressant by using the -0,074+0,045 mm fine size fraction. In another study (Zhu et al., 2022) on the artificial mixtures of magnesite-quartz separation, carboxymethyl cellulose was used as depressant in froth flotation.

In the present study, the flotation separation of fine sized magnesite from quartz using sodium oleate was investigated without the help of a depressant.

2. Material and methods

2.1. Material

In this study, a mixture of pure magnesite (96,4% of purity) and pure quartz (98% of purity) was used, and the composition of this mixture was designed as 80% magnesite and 20% quartz by weight. Samples were purchased commercially and its particle size was 80% passing 0,100 mm. X-ray fluorescence (XRF

Panalytical Zetium, Malvern Panalytical Inc., UK) spectrochemical analysis was carried out in ESOGU ARUM laboratories to determine the elemental composition of the sample and products. The XRF results of the magnesite-quartz mixture to be used as flotation feed were given in Table 1.

Table 1. XRF analysis of flotation feed

Composition	Amount (%)
Al_2O_3	0,6
CaO	0,9
Fe_2O_3	0,2
K_2O	0,3
MgO	37,4
MnO	0,1
Na_2O	0,5
P_2O_5	<0,1
SiO_2	19,8
TiO_2	<0,1
Loss on ignition	40,1

Analytical grade sodium oleate salt (Sigma-Aldrich, Germany) was used as a collector in the classical magnesite flotation experiments. Since oleate has frothing properties, no frother was used in the experiments Analytical grade NaOH and H2SO4 (SigmaAldrich, Germany) were used to adjust pulp pH.

2.2. Method

Flotation experiments were carried out by using laboratory type mechanically stirred Denver Floatation machine with a volume of 1,5 liter cell at the Mineral Processing Laboratory of Eskisehir Osmangazi University. In the flotation experiments; solid ratio, pH and collector amount were varied to determine optimum separation conditions. Flotation was carried out at ambient temperature (26–28°C). In the experiments, conditioning time, flotation time and air rate were kept constant at 8 min, 150 secs, and 6 L/min, respectively.

After each flotation experiments, MgO grade and SiO2 content of the concentrates were determined by XRF analysis, the weight yield (WY) and MgO recovery were calculated according to equations 1-2, respectively.

$$WY = 100 * \frac{C}{F} \quad (1)$$

$$R_{MgO} = 100 * \frac{C * c_{mgO}}{F * f_{MgO}} \quad (2)$$

where C is the amount of concentrate; F is the amount of feed; cMgO is the MgO grade of concentrate; and fMgO is the MgO grade of feed (%).

3. Result and Discussion

The flotation experiments were carried out under the following conditions. Particle size, collector conditioning time, flotation time and air rate were kept constant while solid ratio, pulp pH and collector amount were varied.

Particle size : 80% passing 0,100 mm

Collector conditioning time : 8 min

Flotation time : 150 sec

Air rate: 6 L/min

Collector amount : 150-450 g/t

Solid ratio (w/w) : 25-35 %

Pulp pH : 7-10

The effect of collector amount:

The dosage of sodium oleate was varied between 150 and 450 g/ton, and results were illustrated in Figure 1. Figure 1 shows that as the collector amount increases both weight yield and MgO recovery increased significantly. It should be noticed that MgO content did not change up to 300 g/ton, slightly decreased afterwords. As the collector dosage increased, SiO2 content of the concentrate decreased up to 300 g/ton then increased significantly at high collector dosage. It is thought that high collector dosage caused the flotation of excess amount of materials along with magnesite particles. It is noteworthy to point out that weight yield and MgO recovery increased from 40,92 % to 82,15 % and from 54,76 % to 90,29 %, respectively while lowest SiO2 content was obtained at 300 g/ton collector dosage. A remarkable increase was obtained in MgO content of the concentrate according to head sample, ie from 37,4% to 43,37%.. Therefore 300 g/ton collector dosage was chosen as optimum value. At optimum conditions, MgO content, MgO recovery and SiO2 content of the concentrate were obtained as 43,37 %, 72,60 % and 4,92 %, respectively.

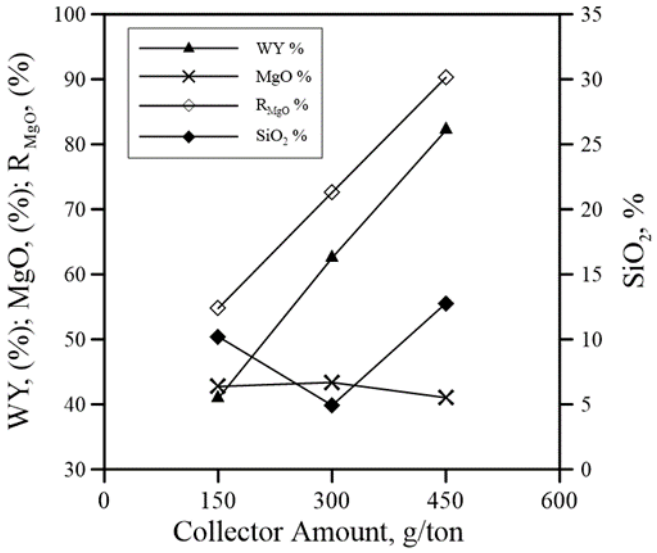


Fig. 1. The effects of collector amount on flotation.

The effect of solid ratio:

A series of flotation experiments were carried out to determine the solid ratio on flotation, and solid content was varied between 25-35 % while other conditions were kept constant. The results were given in Figure 2, and the best results obtained at 30 % solid ratio. At this point the lowest SiO2 content while acceptable MgO content and MgO recovery were obtained. It was observed that the selectivity was decreased at high solids content, causing a reduction in both WY and MgO recovery and SiO2 content in the concentrate fraction.

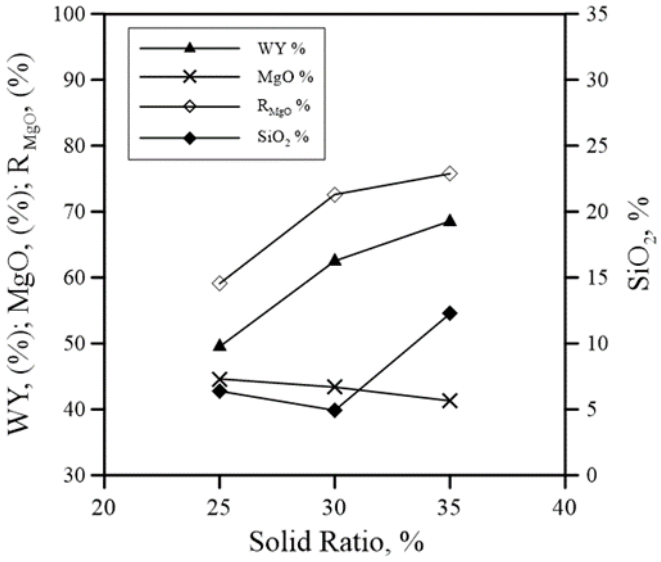


Fig. 2. The effects of solid ratio on flotation.

The effect of pulp pH

The effect of pH on MgO content and recovery and SiO2 content was investigated and the results are shown in Figure 3. As expected, variations in system pH effected all the response variables significantly. At low pH value (7), lowest WY and MgO recovery values were obtained. As pH increased from 7 to 10, WY and MgO recovery sharply increased. On the other hand, as the pH increased from 7 to 8.5 a slight decrease in SiO2 content while a slight increase in MgO content were observed. A further increase in pH from 8,5 to 10 SiO2 content of the concentrate increased significantly from 4,92 % to 17,66 % while MgO content decreased slightly.

It was proved in literature that sodium oleate is an effective collector in magnesite flotation at alkaline region (Luo et al., 2024). At the same study it was shown that the zeta potential of magnesite in the presence of sodium oleate has a large negative shift indicating sodium oleate adsorb onto magnesite's surface. The high recoveries at alkaline region are attributed to the chemisorptions of sodium oleate onto magnesite surfaces. Another study by Andrade et al showed that sodium oleate also adsorbed onto quartz surface at strong alkaline mediums and causes a remarkable increase in flotation recovery (Andrade et al, 2012).

The results obtained in this study are consistent with the results in the literature. At strong alkaline medium both magnesite and quartz were floated by sodium oleate that caused bulk flotation and resulted with a decrease in MgO and an increase in SiO2 contents.

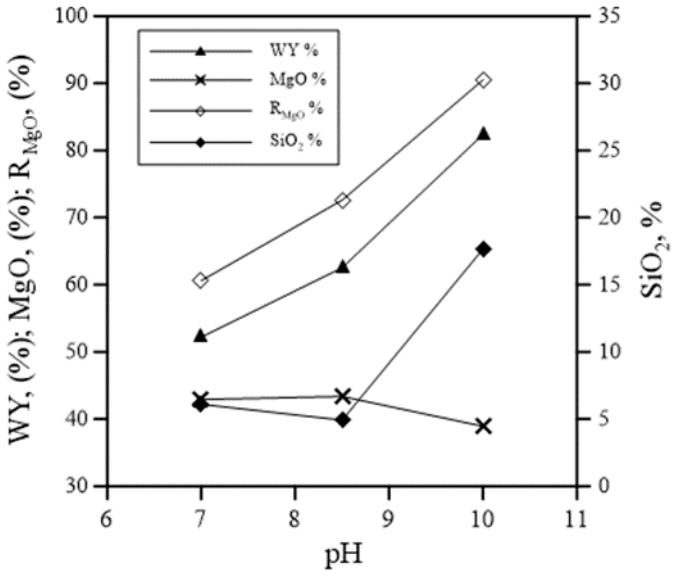


Fig. 3. The effects of pH on flotation.

4. Conclusions

The flotation of fine sized magnesite quartz by sodium oleate was investigated using a laboratory scale mechanical flotation cell. The experimental results revealed that at pH 8,5, the MgO content of concentrate was obtained as 43,37 % with 72,60 % MgO recovery and 4,92 % SiO2 content under the conditions of solid ratio of 30 %, Na oleate dosage of 300 g/ton.

It has been shown that in fine sized magnesite flotation, sodium oleate can be used as an effective collector. Apart from sodium oleate, other studied parameters, pH and solid ratio also affected the results significantly. It was concluded that the better results could be obtained if an effective quartz depressant would have been used. On the other hand, in oleate flotation, temperature should also be utilized as a parameter to increase MgO recovery.

References

Andrade, E.M., Costa, B. L. C. M., Alcantara, G. A. G. and Lima, R. M. F., 2012, Flotation of Manganese Minerals and Quartz by Sodium Oleate and Water Glass, Latin American Applied Research, 42, 39-43.

Luo, N., Shi, J., Yan, B. and Wang, X., 2024, Flotation Separation of Magnesite from Dolomite Using Sodium Silicate Modified with Zinc Sulfate as a Selective Depressant. Minerals, 14, 355.

Sun, H., Han, F., Yin, W.Z., Hong, J. and Yang, B., 2020, Modification of Selectivity in the Flotation Separation of Magnesite from Dolomite, Colloids and Surfaces A: Physicochemical and Engineering Aspects, 606, 125460.

Sun, H. and Yin W, 2022, Selective Flotation Separation of Magnesite from Quartz by Palmitoyl Trimethylammonium Chloride, Separation and Purificiation Technolgy, 295, 121201.

Zhong, W., Yin, W., Wang, Y. and Yao, J. 2020, Selective flotation of magnesite from dolomite using α-chloro-oleate acid as collector, Powder Technology, 2020, 373, 147–151.

Zhu, Y.G., Yang, L.F., Hu, X.X., Zhang, X.R. and Zheng G.B., 2022, Flotation Separation of Quartz from Magnesite Using Carboxymethyl Cellulose as Depressant, Transactions of Non ferrous Metals Society of China, 32, 1623-1637.

Characterization and Leaching Behavior of Mixed Oxide-Sulfide Zinc Ore from Hakkari-Türkiye

İlhan Ehsani [1]*, Arman Ehsani [2], Fatih Çavuşlu [3], Sadiye Kantarcı [1]

[1]Şırnak University, Mining Engineering Department, Şırnak, Türkiye

[2]Adana Alparslan Türkeş Science and Technology University, Mining Engineering Department, Adana, Türkiye

[3]Adana Alparslan Türkeş Science and Technology University, Material Science and Engineering Department, Adana, Türkiye

*Corresponding author: ilhanehsani@sirnak.edu.tr (Ilhan Ehsani)

Abstract:

Besides sulfide ores, non-sulfide and mixed oxide-sulfide zinc have become important resources for zinc. Prior to processing these types of ores using non-conventional methods, chemical, and mineralogical characterization is required. In this study the chemical and mineralogical characteristics of domestic mixed zinc ore were studied using optical microscopy, SEM, XRD, ICP-OES, XRF, FT-IR, and TG-DTA. The results of these analyses provide valuable information such as mineral composition, oxide percentage, grain size, mineral constituents, and thermal decomposition, which are essential for determining the mineral processing method. For instance, the ore mineralogy primarily consists of carbonate ($ZnCO_3$; smithsonite), and less sulfide (ZnS; sphalerite) and oxide (ZnO; Zincite). Besides, the dissolution behavior of the ore was investigated in both alkaline (NaOH and NH_4OH) and acidic (HCl and H_2SO_4) solutions ranging from 1 to 6 M concentrations, under constant conditions (-300 µm, 60 minutes leaching time, 25°C leaching temperature, and 1:10 solid:liquid ratio). In alkaline solutions, it was observed that the dissolution rate increased with higher concentrations; however, this increase was negligible in acidic solutions. The maximum leaching rates of zinc were achieved at 68.68%, 55.42%, 74.78%, and 75.45% for NaOH (4M), NH_4OH (6M), HCl (4M), and H_2SO_4 (4N) solutions, respectively.

Keywords: *Mixed Oxide-Sulfide Zinc Ore, Characterization, Acidic and Alkaline leaching,*

1. Introduction

The minerals of lead and zinc are commonly found together in three primary types of deposits: sulfide minerals, non-sulfide ores, and mixed sulfide-oxide ores. Sulfide minerals, which are mainly located in the primary sulfide ore bodies, undergo multiple stages of mineralization. Sphalerite (ZnS) and galena (PbS) are the major sulfide minerals of zinc and lead, respectively. Non-sulfide ores can be further categorized as hypogene or supergene weathering types, while mixed sulfide-oxide ores with complex mineralogy found in the transition zones within deposits. Notable examples of this type of deposits are the Angouran Zn-Pb ore deposit in Iran and the Lanping Pb-Zn mine in Yunnan province, China. Currently, sulfide and oxide ores are the main raw materials for zinc production, however as these supplies diminish, the exploitation of mixed sulfide-oxide ores is gaining importance. Despite their substantial reserves, the efficient utilization of mixed sulfide-oxide ores remains problematic due to challenges associated with their beneficiation (Gilg et al., 2006; Jia et al., 2016; Moradi and Monhemius, 2011).

Mixed sulfide-oxide zinc and lead ores have a complex mineralogy that includes sphalerite, smithsonite, hemimorphite, galena, cerussite, pyrite, goethite, hematite, limonite, calcite, dolomite, gypsum, quartz, feldspar, clays, and other minerals. Due to extraction difficulties caused by this complexity, they have been ignored for years but with the development of recent technologies, such as electrowinning (EW), solvent extraction (SX) and leach to chemical (LTC) the interest in these types of ores has increased (Hitzman et al., 2003; Jia et al., 2016; Moradi and Monhemius, 2011).

Acidic and alkaline solutions could be used for leaching. Alkaline systems including sodium hydroxide (NaOH), ammonium hydroxide (NH_4OH) and ammonia salts, have advantages because of high selectivity (due to the low iron leaching), low cost and easy generation. While acidic systems including

sulfuric acid (H_2SO_4), hydrochloric acid (HCl) and chlorides (Cl^-), nitric acid (HNO_3) and nitrates (NO_3^-) have high recovery, low cost and the possibility of solvent extraction and electrowinning method usage (Ehsani et al., 2019; Jia et al., 2016; Kaya et al., 2020; Moghaddam et al., 2005).

The aim of present research work was to comparatively investigate the dissolution behavior of Hakkari mixed Zn-Pb ore in both alkaline (NaOH and NH_4OH) and acidic (H_2SO_4 and HCl) media and evaluate the effect of leaching conditions.

2. Material and methods

2.1. Materials

The high-grade and mixed carbonate-sulfate zinc ore used in the experiments was obtained from Hakkari Province in Türkiye. The ore sample was crushed, milled and sieved until the size of all particles became under 300 µm ($d_{80} \approx 150$ µm). It was then homogenized and kept in the room for 10 days (moisture < 1%) and stored in airtight containers for further characterization analysis and leaching experiments.

2.2. Characterization and Analysis

The characterization of the ore sample was conducted by optical microscopy (Olympus), SEM-EDS (FEI/Philips), XRD (Rigaku, CuKα), ICP-OES (ACME Lab), XRF (Rigaku), FT-IR (Perkin Elmer) and TG-DTA (Setaram) analysis. To begin with, chemical composition of the of the sample was determined by ICP-OES and XRF. The results illustrated that the ore contains a high percentage of Fe (27.93%), Zn (11.86%), S (9.99%), Ca (7.10%) and C (4.71%), as well as smaller amount of Si (2.98%), Mg (1.29%), Pb (1.01%) Ba (0.84%), Al (0.61%) and 18.23% loss of ignition (Table 1).

Table 12 Chemical composition of Zn-Pb ore sample

Element	Fe	Zn	Ca	Mg	Pb	Ba	Al	S	C	LOI
Content (%)	27.93	11.86	7.10	1.29	1.01	0.84	0.61	9.99	4.71	18.23

X-ray diffraction (XRD) analysis of the ore sample has identified the main mineralogical phases included both sulfide and nonsulfide phases; i.e., zinc (Zn) appeared in smithsonite ($ZnCO_3$), sphalerite (ZnS) and zincite (ZnO) forms, associated with calcium is in the form of calcite ($CaCO_3$), dolomite ($CaMg(CO_3)_2$) and gypsum ($CaSO_4 \cdot 2H_2O$) forms. On the other hand, for iron (Fe), the most abundant element in the ore, only peaks belonging to goethite (FeOOH) could be detected while the peaks corresponding to siderite ($FeCO_3$) were not distinguishable due to their similarity to smithsonite. Additionally, a few small peaks belonging to quartz (SiO_2) occurred (Fig 1.).

Hakkari's supergene non-sulfide Zn-Pb deposit, from which the sample was taken, was formed by the oxidation (alteration) of both sulfide and hypogene non-sulfide deposits, which are often found in carbonate host rocks. Therefore, this type of ore contains Zn (smithsonite, hydrozincite, hemimorphite, and sauconite), Pb (cerussite and anglesite), and Fe (hematite and goethite) minerals as expected (Santoro et al., 2014).

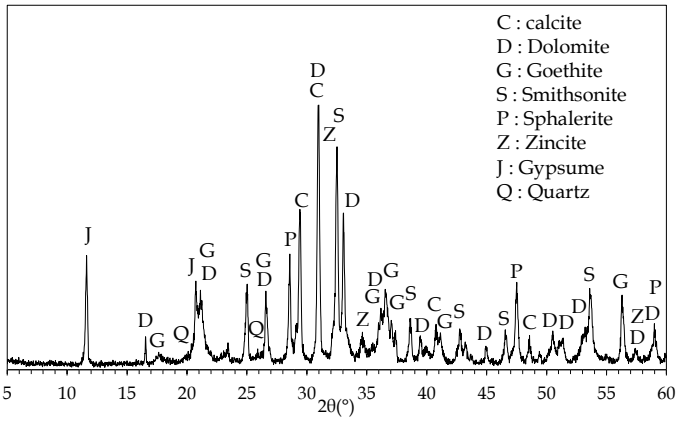


Fig 1. XRD pattern of Zn-Pb Ore sample

Thermal analysis was fulfilled on the sample at a rate of 10 °C · min^{-1}, TG curve displays weight loss regions. The first small one refers to the loss of moisture and water, the second one refers to the decomposition of gypsum between 110 and 150 °C (Paulik et al., 1992). The third weight loss region refers to the decomposition of goethite (Naono et al., 1987) and smithsonite (Zhang et al., 2014) which begin at about 200°C and finishes at about 450°C, the last one is observed at temperatures over 650 °C refer to calcite, dolomite (Olszak-Humienik & Jablonski, 2015) and sphalerite (Gulyaeva et al., 2018) thermal decompositions. Finally, the overall mass loss reaches 17.64% at 1000 °C.

According to DTA curve endothermic peaks probably assigned to decomposition reaction of gypsum (131 °C; Paulik et al 1997), goethite (283 °C), smithsonite (350 °C), calcite and dolomite (522 °C, 764 °C & 822 °C) and exothermic peaks relevant to the decomposition of sphalerite (554 °C & 783 °C; Baláž et al., 1992) accomplished with some undefined peaks at 434 °C, and 911 °C (Fig 2. Left).

In accordance with Fourier Transform Infrared (FTIR) spectrum of sample, the characteristic infrared band $ZnCO_3$ observed at 750 cm^{-1}, together with other vibration bands observed at 595 cm^{-1} (Fe-O), 668 cm^{-1} ($CaCO_3$), 799 cm^{-1} (FeOOH), 872 cm^{-1} (CO_3^{2-}), 1031 cm^{-1} (Zn-O), 1112 (SO_4^{2-}) 1416 cm^{-1} (CO_3^{2-}), 3180 and 3391 (OH^-) (Frost et al., 2008; Granados Oliver et al., 2020) indicate that ore sample consists of carbonate, oxide and hydroxide phases, which is in line with the results of previous mineralogical analyses (Fig 2. Right).

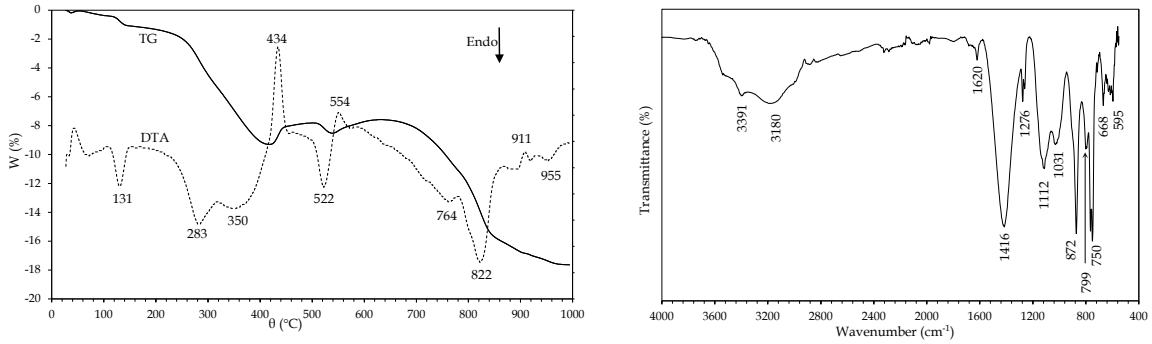


Fig 2. TG-DTA pattern (Left) and FT-IR Spectrum (Right) of Zn-Pb Ore sample

As can be seen from the optical microscope images, the ore sample consists of irregular and shapeless particles in varied sizes, mostly yellow or light brown while others are white, grey, black, dark blue or colorless. Additionally, most of the particles are matte, and rarely transparent or metallic sheen. Besides, in SEM-EDS spectroscopy of the sample, it is seen that some zinc-containing particles contain both C and S that means there are minerals in both carbonate and sulfate phases had existed (Fig 3.). Therefore, it is estimated that at least some of Zn containing particles consist of both carbonate (oxide) and sulfate mineral phases.

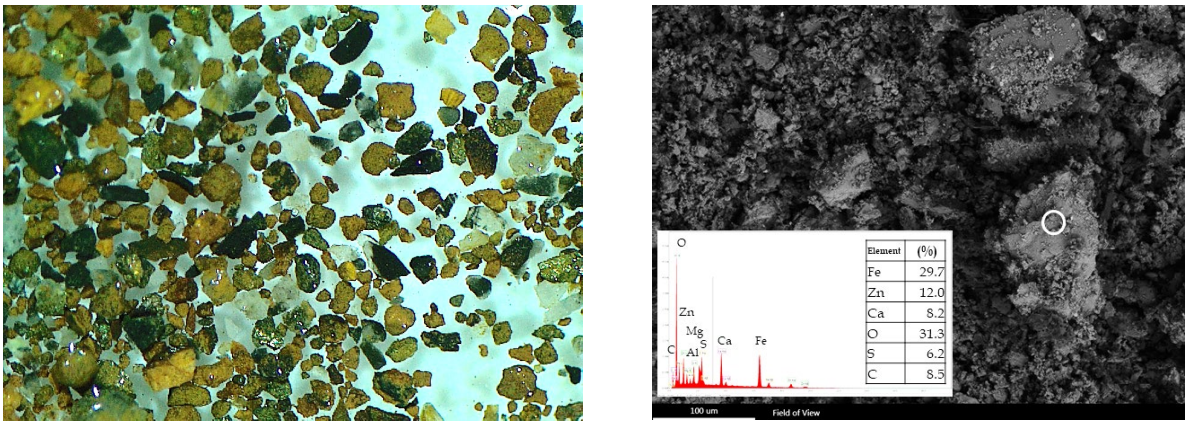


Fig 3. Optical microscope image (left), SEM-EDS spectroscopy (Right) of Zn-Pb Ore sample

2.3. Leaching Experiments

Four reagent grade chemicals (Merck), sodium hydroxide (NaOH; 99%), ammonium hydroxide (NH_4OH; 25%), hydrochloric acid (HCl; 37%), and sulfuric acid (H_2SO_4; 95%), which used in all experiments, diluted with distilled water for preparing leaching solution at desired concentrations (1M, 2M, 4M, and 6M). It should be mentioned that for equal comparison, 1N, 2N, 4N, and 6N concentrations of sulfuric acid, a divalent acid, were utilized in the study. Then, 40 g of the ore sample was added to 400 ml of solution in a 600 ml glass beaker and agitated with a magnetic stirrer. The experiments were conducted under constant conditions of solid:liquid (S/L) ratio of 1:10 g/ml, agitation speed of 650 rpm (which is enough to keep all particles in suspense), and room temperature (25 °C). These constant parameters were chosen because they provided operational convenience in the agitation and filtering stages, which have insignificant effects on zinc dissolution and were determined as optimum conditions in previous studies. Besides, the effect of leaching temperature was not examined in this comparative study due to the low boiling temperature of ammonium hydroxide solutions. In addition to reagent type, other influencing factors such as reagent concentration, leaching time, and particle size distribution of the ore have been examined. At the end, the residues were filtered and washed with distilled water, dried overnight at 105 °C then weighed, and kept for future analyses.

3. Results and Discussion

3.1. Effect of concentration on dissolution rate

The effect of alkaline and acidic solution concentrations was examined by measuring Zn, Pb, and Fe content of leaching residue. The dissolving ratio of metals was determined using Equation-1, where the M_i is the amount of Metal (%) in sample. Figure 4 shows leaching studies with various concentrations (1M, 2M, 4M, and 6M) for 60 min, S/L ratio of 1:10 g/ml, agitation speed of 650 rpm, particle size distribution of -300 µm, and ambient temperature of 25 °C.

$$Dissolving\ ratio\ of\ M\ (\%) = \frac{M_{Ore} - M_{residue}}{M_{Ore}} \times 100 \quad (1)$$

where M_{ore}: Metal content in the ore, $M_{residue}$: Metal content in the leach residue

The concentrations of acids have a negligible effect on Zn dissolution, the highest ratios were obtained as 75.32% for 4N H_2SO_4 and 74,78% for 4M HCl acid concentration. However, lead exhibits a different dissolution behavior, while it is slightly soluble in H_2SO_4 (max. 8.56% at 4N concentration), the dissolution in HCl increased with increasing concentration and reached 78.38% at 4 M concentration. In addition, it was also determined that acids dissolved almost all of the gypsum, calcite and dolomite in the ore (99% Ca and 95% Mg were dissolved).

The concentration of alkaline reagents (NaOH and NH_4OH) has a pronounced effect on the dissolution of zinc, as can be seen in Fig 4. The dissolution of zinc (Zn) increased with increasing concentration and reached the maximum rate of 68.68% and 55.42% in 6M concentration of NaOH and NH_4OH, while, for 4M concentration these are 68.60% and 49.46%, respectively. On the other hand, the dissolution rates of lead (Pb) and iron (Fe), as well as calcium (Ca) and magnesium (Mg), in alkaline solutions are negligible. For NaOH and NH_4OH solutions, the highest dissolution ratios were attained 3.99% for Fe, 14.19% for Pb and 1.74% for Fe, 3.27% for Pb, respectively.

The leaching ratios of Zn are consistently low in all cases. This is due to the low solubility of sphalerite and zincite in acidic and alkaline media (Jia et al., 2016). Additionally, Fe has lower solubility in alkaline solvents. This leads to the conclusion that alkaline solutions selectively dissolve zinc more effectively. Lead, on the other hand, was dissolved well only in HCl solutions, and at very low rates in other solvents.

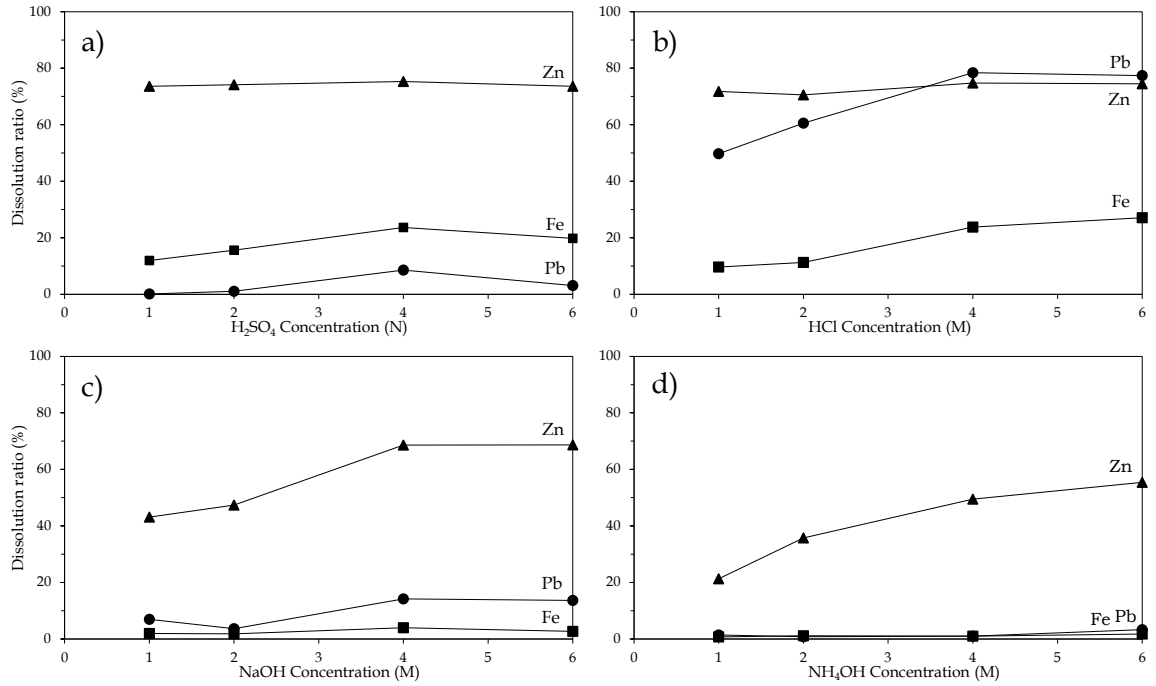


Fig 4. Effect of concentration on dissolution ratios (%) of Zn, Pb, and Fe (60 min, 25°C, 1:10 g/ml, -300 µm, and 650 rpm)

3.2. Effect of leaching time on dissolution rate

In this stage, the effect of leaching time on dissolution ratios of targeted metals was investigated. Figure 5 illustrates the dissolution ratios of Zn, Pb, and Fe over leaching times of 30, 60, and 120 minutes. These experiments were conducted with a concentration of 4M (4N for H_2SO_4), S/L ratio of 1:10 g/mL, temperature of 25°C, and stirring speed of 650 rpm. The results indicate that Zn and Pb leaching in H_2SO_4, HCl, and NH_4OH solutions are slightly improved by increasing leaching time, reaching their highest values for Zn at 78.79%, 76.95% and 54.83%, and for Pb at 15.72%, 81.71%, and 4.60% after 120 minutes of leaching time, respectively. Conversely, in NaOH solutions leaching time has a slightly negative effect on Zn and Pb leaching ratios which are 71.18%, 68.60%, 67.62% for Zn and 21.05%,14.19%, and 10.12% for Pb, at 30, 60, and 120 minutes of stirring time, respectively.

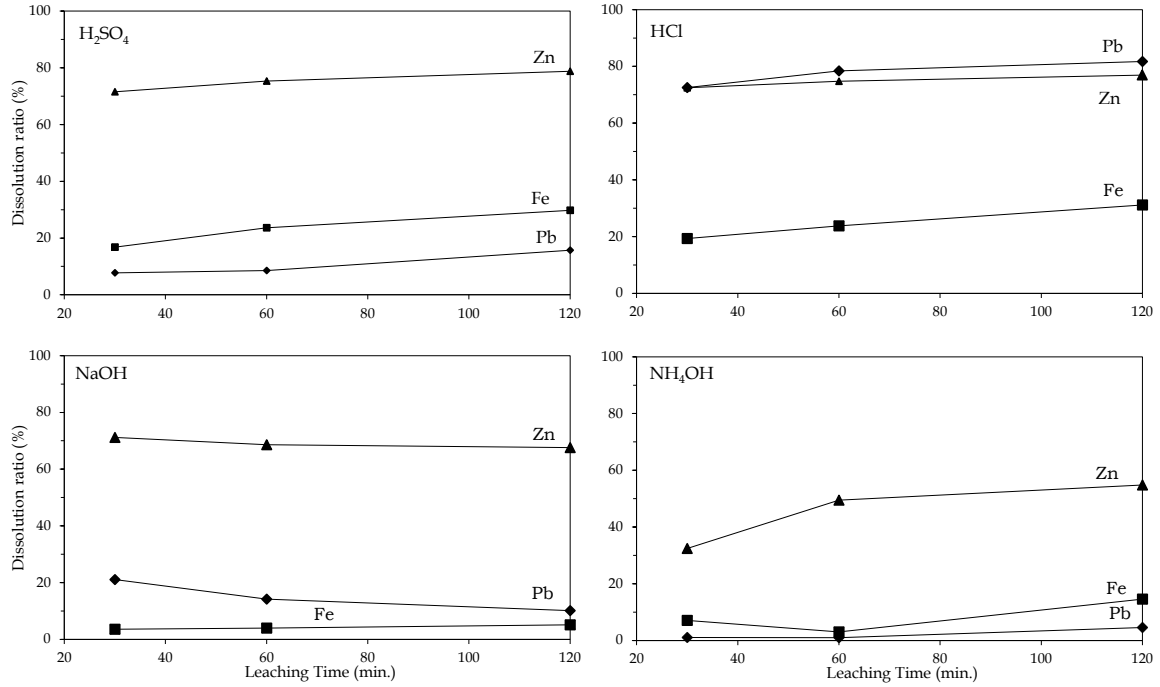


Fig 5. Effect of Leaching time (min.) on dissolution ratios (%) of Zn, Pb, and Fe (4 N, 25°C,1:10 g/ml, -300 µm, 650 rpm)

3.3. Effect of particle size on dissolution rate

The effect of the particle size distribution of ore on leaching efficiency was investigated for two different particle size: -300 µm (d_{80} ≈150 µm) and -106 µm (d_{80} ≈80 µm) under constant experimental conditions (4 N, 1:10 S/L, 60 min, 650 rpm, and 25°C). The results demonstrate that a reduction in particle size generally leads to a slight increase in the leaching ratios of Zn and Pb across all solutions, while simultaneously enhancing the leaching ratio of Fe. For particle size up to 106 µm leaching ratio of Zn, Pb and Fe are measured as 75.74%, 13.97%, and 24.38% for H_2SO_4; 75.58%, 81.01%, and 27.88% for HCl; 69.24%, 14.76%, and 5.03% for NaOH; and 53.17%, 1.99%, and 11.72% for NH_4OH solutions, respectively (Fig. 6).

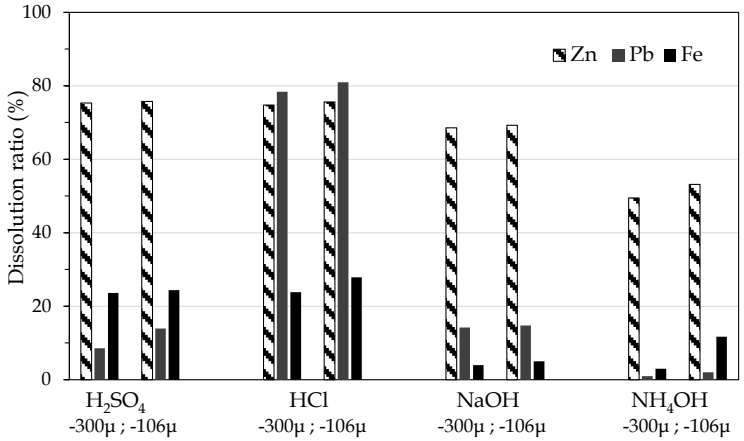


Fig 6. Effect of particle size (µm) on dissolution ratios (%) of Zn, Pb, and Fe (4 N, 60 min, 25°C, 1:10 g/ml, and 650 rpm)

4. Conclusions

In this study, the characterization of mixed carbonate-sulfate Zn-Pb ore from Hakkari and its leaching behavior in alkaline and acidic media was examined. The complex structure of the ore was determined by mineralogical and metallurgical analysis such as optical microscopy, SEM-EDS, XRD, XRF, ICP-OES, FT-IR, and TG-DTA. The results showed that the main Zn minerals in the ore are smithsonite, sphalerite and zincite, along with goethite, calcite, dolomite, gypsum, and quartz as gangue minerals.

The effects of leaching parameters, including concentration (1, 2, 4, and 6M (N for H_2SO_4)), leaching time (30, 60, and 120 min.), and particle size distribution (-300 and -106 µm) were investigated in four different leach solutions (NaOH, NH_4OH, HCl, and H_2SO_4). The concentration of the solution has a positive effect on dissolving up to 4M(N), but only in NH_4OH, dissolution ratios continue to improve even at the highest concentration of 6 M. Additionally, extending the leaching time slightly improves the dissolution ratios of Zn and Pb, except in NaOH solutions, where longer leaching times result in decreased dissolution ratios. Moreover, reducing the particle size of the ore beneficially affects the dissolution rates of Zn, Pb, and Fe across all solutions. Nonetheless, the inherent complexity of the ore presents challenges in achieving optimal metal dissolution rates. Therefore, to enhance dissolution efficiencies, it is advisable to explore thermal, chemical, or mechanical pretreatments, as well as pressure or oxidative leaching methods.

Acknowledgments

The work was financially supported by the Scientific Research Projects Coordination Unit of Şırnak University (ŞÜ, BAP, Project Number: 2022.FNAP.06.04.01). The authors also appreciate SEDEX Mining Co. for supplying the ore sample.

References

Baláž, P., Huhn, H. J., & Heegn, H. (1992). Differential thermal analysis of mechanically activated sphalerite. *Thermochimica Acta*, *194*(C), 189–195. doi: https://doi.org/10.1016/0040-6031(92)80017-Q

Ehsani, I., Ucyildiz, A., & Obut, A. (2019). Leaching behaviour of zinc from a smithsonite ore in sodium hydroxide solutions. *Physicochemical Problems of Mineral Processing*, *55*(2). doi: https://doi.org/10.5277/ppmp18150

Frost, R. L., Martens, W. N., Wain, D. L., & Hales, M. C. (2008). Infrared and infrared emission spectroscopy of the zinc carbonate mineral smithsonite. *Spectrochimica Acta - Part A: Molecular and Biomolecular Spectroscopy*, *70*(5), 1120–1126. doi: https://doi.org/10.1016/j.saa.2007.10.027

Gilg, H. A., Boni, M., Balassone, G., Allen, C. R., Banks, D., & Moore, F. (2006). Marble-hosted sulfide ores in the Angouran Zn-(Pb-Ag) deposit, NW Iran: Interaction of sedimentary brines with a metamorphic core complex. *Mineralium Deposita*, *41*(1), 1–16. doi: ttps://doi.org/10.1007/s00126-005-0035-5

Granados Oliver, J. A., Pérez, M. R., Teja Ruiz, A. M., Palacios Beas, E. G., Labra, M. P., Barrientos Hernández, F. R., Juárez Tapia, J. C., & Cobos Murcia, J. A. (2020). Characterization by FTIR of sphalerite obtained in the flotation without collector in the presence of ferric iron. *Minerals, Metals and Materials Series*, *PartF1*, 451–457. doi: https://doi.org/10.1007/978-3-030-36628-5_44

Gulyaeva, R. I., Selivanov, E. N., & Pikalov, S. M. (2018). Mechanism and Kinetics of the Thermal Oxidation of Natural Sphalerite. *Russian Metallurgy (Metally)*, *2018*(3), 221–227. doi: https://doi.org/10.1134/S0036029518030047

Hitzman, M. W., Reynolds, N. A., Sangster, D. F., Allen, C. R., & Carman, C. E. (2003). Classification, genesis, and exploration guides for nonsulfide zinc deposits. *Economic Geology*, *98*(4), 685–714. doi: https://doi.org/10.2113/gsecongeo.98.4.685

Jia, N., Wang, H. gang, Zhang, M., & Guo, M. (2016). Selective and Efficient Extraction of Zinc from Mixed Sulfide–oxide Zinc and Lead Ore. *Mineral Processing and Extractive Metallurgy Review*, *37*(6), 418–426. doi: https://doi.org/10.1080/08827508.2016.1233874

Kaya, M., Hussaini, S., & Kursunoglu, S. (2020). Critical review on secondary zinc resources and their recycling technologies. *Hydrometallurgy*, *195*(April), 105362. doi: https://doi.org/10.1016/j.hydromet.2020.105362

Moghaddam, J., Sarraf-Mamoory, R., Yamini, Y., & Abdollahy, M. (2005). Determination of the optimum conditions for the leaching of nonsulfide zinc ores (high-SiO2) in ammonium carbonate media. *Industrial and Engineering Chemistry Research*, *44*(24), 8952–8958. doi: https://doi.org/10.1021/ie050479+

Moradi, S., & Monhemius, a. J. (2011). Mixed sulphide-oxide lead and zinc ores: Problems and solutions. *Minerals Engineering*, *24*(10), 1062–1076. doi: https://doi.org/10.1016/j.mineng.2011.05.014

Naono, H., Nakai, K., Sueyoshi, T., & Yagi, H. (1987). Porous texture in hematite derived from goethite: Mechanism of thermal decomposition of geothite. *Journal of Colloid And Interface Science*, *120*(2), 439–450. doi: https://doi.org/10.1016/0021-9797(87)90370-5

Olszak-Humienik, M., & Jablonski, M. (2015). Thermal behavior of natural dolomite. *Journal of Thermal Analysis and Calorimetry*, *119*(3), 2239–2248. doi: https://doi.org/10.1007/s10973-014-4301-6

Paulik, F., Paulik, J., & Arnold, M. (1992). Thermal decomposition of gypsum. *Thermochimica Acta*, *200*(C), 195–204. doi: https://doi.org/10.1016/0040-6031(92)85115-C

Santoro, L., Boni, M., Rollinson, G. K., Mondillo, N., Balassone, P., & Clegg, A. M. (2014). Mineralogical characterization of the Hakkari nonsulfide Zn(Pb) deposit (Turkey): The benefits of QEMSCAN?? *Minerals Engineering*, *69*, 29–39. doi: https://doi.org/10.1016/j.mineng.2014.07.002

Zhang, Y., Deng, J., Chen, J., Yu, R., & Xing, X. (2014). The electrowinning of zinc from sodium hydroxide solutions. *Hydrometallurgy*, *146*, 59–63. doi: https://doi.org/10.1016/j.hydromet.2014.03.006

Investigation of arsenic removal from copper concentrates by alkaline sulphur leaching

Taha Boyraz [1, 2*], Tuğba Türk [1], İbrahim Alp [1, 2]

[1] Karadeniz Technical University, Dept. of Mining Engineering, 61080, Trabzon, Türkiye

[2] Ergold Innovation Eng. Srv. Ltd. Co., Trabzon Teknokent, No: 19/B No: 3301, 61080 Trabzon, Türkiye

*Corresponding author: tahaboyraz@ktu.edu.tr (Taha Boyraz)

Abstract:

This study investigated the removal of arsenic from copper concentrates by alkaline sulphur leaching. A first set of mineralogical investigations has been carried out as part of the study. It has been assessed that arsenic is present in the ore in the form of the mineral enargite and the minerals of the Fahlers group. Chemical analyses support these mineralogical findings. As was observed to be associated with Cu-Ag-Zn. Mineralogical tests indicated that the arsenic in the concentrate could not be removed by flotation. Na_2S and NaOH leaching (alkaline sulphur leaching) were carried out to remove arsenic from the flotation concentrate selectively. It was observed that the arsenic contained in the copper concentrate was recovered with high efficiency (>80%) after the alkaline sulphur leaching process. Furthermore, it was observed that arsenic recovery increased further (>90%) when the flotation concentrate was regrinded and alkaline leached under the same conditions. Finally, elemental sulfur (S) precipitated the arsenic from the leach solution. The production of arsenic in solid salt form (Na_3AsO_4) by precipitation is an advantage of the process investigated in this study, as it is environmentally friendly and has the potential to be used in different areas.

Keywords: *Copper concentrates, arsenic removal, alkaline sulphur leaching, Na_2S, NaOH*

1. Introduction

Arsenic occurs naturally in a number of minerals. The most important of these are arsenopyrite (FeAsS), orpiment (As_2S_3), realgar (As_2S_2) and those that occur in complex sulfide minerals, including enargite (Cu_3AsS_4), tennantite ($Cu_{12}As_4S_{13}$), and proustite (Ag_3AsS_3), among many others (Mandal and Suzuki, 2002). This study is concerned with the treatment of copper–iron–sulfide concentrates that contain arsenic in the forms of enargite (Cu_3AsS_4) and tennantite ($Cu_{12}As_4S_{13}$). These minerals are the most prevalent among the copper-bearing minerals with high copper content. However, this is unfortunately accompanied by a high arsenic content. The presence of this problematic element has a marked impact on the quality and physical characteristics of the copper product (Bujňáková et al., 2014). On the other hand, arsenic compounds have been identified as carcinogenic substances, and there is a growing body of evidence to suggest that repeated exposure to these compounds through industrial inhalation may contribute to an increased prevalence of certain cancers, particularly lung and skin cancer (Kitchin, 2001).

The atmospheric release of arsenic presents a significant environmental risk in the majority of copper smelting operations. Consequently, alternative hydrometallurgical processing routes for the treatment of such materials must be developed. A variety of approaches may be employed for enargite and tennantite treatment, including ammonia leaching (Gajam and Raghavan, 1983), bioleaching (Takatsugi et al., 2011), and acid leaching (Dutrizac and Morrison, 1984). Nevertheless, the most optimal method for the removal of arsenic from these minerals appears to be alkaline leaching (Curreli et al., 2009; Awe and Sandström, 2010). The selective leaching of arsenic from concentrates in sodium sulfide (Na_2S) solutions under highly alkaline reducing conditions is a consequence of the alkaline leaching process. The conversion or transformation of Cu_3AsS_4 or ($Cu_{12}As_4S_{13}$) to Cu_2S or CuS is represented by the following equations (1) and (2), respectively.:

$$2Cu_3AsS_4 + 3Na2S \rightarrow 3Cu2S + 2Na_3AsS_4 \quad (1)$$

$$Cu_{12}As_4S_{13} + 2Na_2S \rightarrow 5Cu_2S + 2CuS + 4NaAsS_4 \quad (2)$$

The leaching medium comprises two principal components, sodium sulfide and sodium hydroxide. The application of Na_2S generates a markedly reducing environment, exhibiting a potential of approximately -500 mV. This is in contrast to the effect of NaOH on pH values, which are maintained above 12.5. This property of NaOH prevents the hydrolysis of sulfide ions, which are known to be involved in the substitution of arsenic in enargite and tennantite (Tongamp et al., 2009). A further significant factor affecting the effectiveness of arsenic removal from enargite and tennantite is the impact of temperature. A higher temperature correlates with increased efficiency in this process (Curreli et al., 2009).

The removal of arsenic, which is dissolved in an alkaline solution (Na_2S–NaOH), from the pressure oxidation leaching of enargite, which occurs in the forms of $Ca_3(AsO_4)_2$ or $Fe_3(AsO_4)_2$, necessitates a reduction in the solution pH to a level below 2 in order for precipitation reactions to occur (Filippou et al., 2007). However, Tongamp and et al. (2010) present an alternative process for the removal of dissolved arsenic from the Cu_3AsS_4–NaHS–NaOH leaching system, whereby the arsenic is precipitated as Na_3AsS_4 without the necessity for pH adjustment.

The aim of this paper is to put forward a process for the treatment of arsenic-bearing copper concentrate that entails the precipitation of the arsenic-containing filtrate obtained after selective alkaline leaching. The proposed methodology represents a sustainable approach to the processing of these concentrates, whereby no residual dangerous waste is generated at the completion of treatment. All experiments were conducted in accordance with standard laboratory procedures.

2. Material and methods

2.1. Material

The present study was conducted on copper concentrate with the chemical composition presented in Table 1. A sieve analysis was conducted on the concentrate, resulting in the calculation of an average particle size (d_{80}) of 118 microns. The data indicate that 9.9% of the sample exhibits a size above 150 microns, while 29% of the sample is below 20 microns. Microscopic studies were conducted using a Nikon Eclipse polarizing microscope. The microscope is located in the Mineralogical Analysis Laboratory of the Mining Engineering Department of KTU. The ore microscopy studies revealed that the concentrate predominantly consists of chalcopyrite, bornite, sphalerite, pyrite, enargite, and minerals from the fahlers group.

Table 1. Elemental analysis values of the flotation concentrate

Element	Cu %	Zn %	Pb %	Fe %	As %	Au g/ton	Ag g/ton
Copper concentrate	13.9	17.5	0.22	34.1	1.8	2.44	83.2

The following chemicals were utilized in this study: sodium sulfide ($Na_2S.9H_2O$) (98% purity, Sigma Aldrich, USA), sodium hydroxide (NaOH) (>98% purity, Sigma Aldrich, USA), and sulfur (S) (99.5% purity, Sigma Aldrich, USA).

2.2. Methods

2.2.1. Sample Preparation for Mineralogical Analysis

An arsenic-containing copper concentrate sample was subjected to fractional analysis, employing the requisite sample preparation techniques. The sample was separated into six distinct fractions, each with a specific sieve size, using a sieve analysis technique. The fractions were as follows: <20 micron, 20-38

micron, 38-75 micron, 75-150 micron, and >150 micron. Subsequently, polished sections of each fraction were prepared for mineralogical analysis.

2.2.2. Alkaline Leaching Tests

The objective of this study was to investigate the feasibility of utilizing alkaline leaching techniques to remove arsenic from the flotation concentrate. Leaching experiments were conducted in a jacketed reactor. The reactors, with a nominal capacity of 250 mL, are equipped with vortex preventers on their inner walls. The temperature was regulated by means of a heating-cooling circulator, which circulated water through the jacket of the reactor. During the leaching experiments, the reactors were maintained in a sealed state with the application of suitable covers in order to prevent evaporation losses due to the ambient temperature. A mechanical mixer equipped with torque control and a digital speed display was employed in the mixing process. A Teflon (PTFE) coated impeller was employed to withstand leaching conditions, specifically high temperatures and alkalinity. The leaching system is illustrated in Fig. 1.



Fig. 7. Leaching System

In the experimental procedure, the initial solution volume was selected as 125 mL, and the solid ratio was selected as 20% weight/volume (w/v). Once the requisite temperature was reached, the flotation concentrate sample was introduced into the reactor, thereby initiating the experiment. The mixing speed was maintained at a constant value of 500 rpm. The temperature at which leaching occurred was maintained at 90 °C. The leaching time was maintained at a constant six hours. Furthermore, the impact of grain size on leaching efficiency was examined through the implementation of distinct experiments utilising concentrate particle sizes (d_{80}) of 118 and 57.8 µm, respectively. At designated intervals (15, 30, 60, 120, 240, and 360 minutes) throughout the leaching process, samples were taken (2-3 mL) and subjected to centrifugation at 4100 rpm for three minutes. This procedure facilitated the separation of solid and liquid phases. The solution obtained after centrifugation was diluted and subjected to metal analysis using atomic absorption spectrometry (AAS). Ultimately, following the completion of the leaching tests, the leach pulp was subjected to centrifugation at 4100 rpm for eight minutes with the objective of separating the loaded leach solution. Following centrifugation, the clear solution was transferred to sample storage bottles for subsequent analysis. The solid component was subjected to a hot distilled water wash and oven drying at 65 °C for a period of 12 hours. The leaching efficiencies were calculated by analyzing the amounts of metal in the pregnant solution at the end of the leaching process, the amounts of metal remaining in the waste material, and the amounts of metal in the sample prior to leaching.

2.2.3. Arsenic Precipitation Experiment

The arsenic concentration was adjusted to a level exceeding 35 g/L with the objective of precipitating arsenic through the use of elemental sulfur (S) derived from the alkaline leach solution that had been loaded. In order to achieve this outcome, two alkaline leaching tests were conducted under identical conditions using the same leaching solution. The results of the conducted tests demonstrated that a leach solution with a arsenic concentration of 40.3 g/L was produced. In this section, the solid (flotation concentrate) and liquid (arsenical alkaline leaching solution) phases were separated by solid-liquid

separation following alkaline leaching. The loaded leach solution was subjected to conditioning at a temperature of 90 °C for a period of 20 minutes. The initial 10 minutes of the 20-minute process were dedicated to mixing. Subsequently, at the outset of the second 10 minutes, elemental sulfur was introduced to the solution at a concentration of 1.5 times the arsenic. Following the addition of sulfur, the mixture was left to stand for a period of 10 minutes without agitation. Once the conditioning phase was concluded, the precipitation process was initiated by gradually reducing the temperature in a laboratory setting. Fig. 2 illustrates the process flow chart for the precipitation of arsenic from solution.

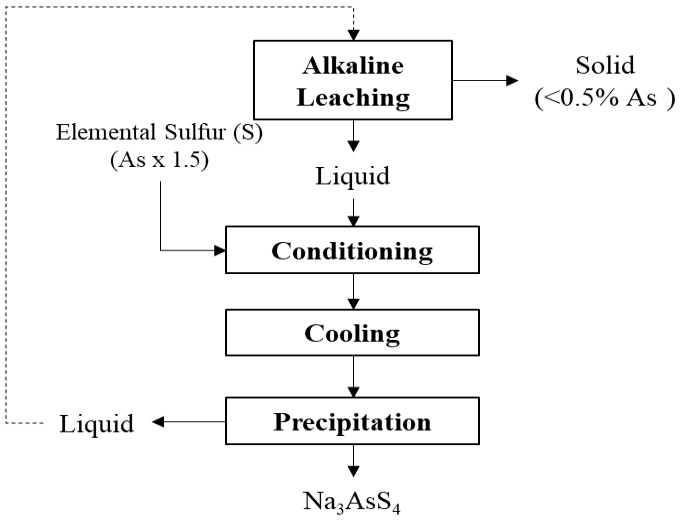


Fig. 8. The precipitation of arsenic from the leach solution

3. Results and Discussion

3.1. Mineralogical structure of cupper concentrate

When the particle size of 150 microns and above was examined, it was seen that chalcopyrite was the common mineral. Then the density of pyrite, bornite, sphalerite, chalcopyrite and chalcopyrite were determined. Grains of bornite, sphalerite, pyrite and chalcopyrite as large as 300×140 microns were observed. Fahlers and chalcopyrite compositions are also available (300×75 microns). The pyrite mineral is most often seen as a granular material within larger grains. In this particle size range, the texture of the substitution is overdetermined (Fig. 3a). While the replacement texture is abundant in this grain size range, it was also observed that the number of interlocked grains is quite high. Tennantite-tetrahydrite minerals were observed in this grain size range. It was also noted that enargite and luzunite were present in the Fahlers structure (Fig. 3b).

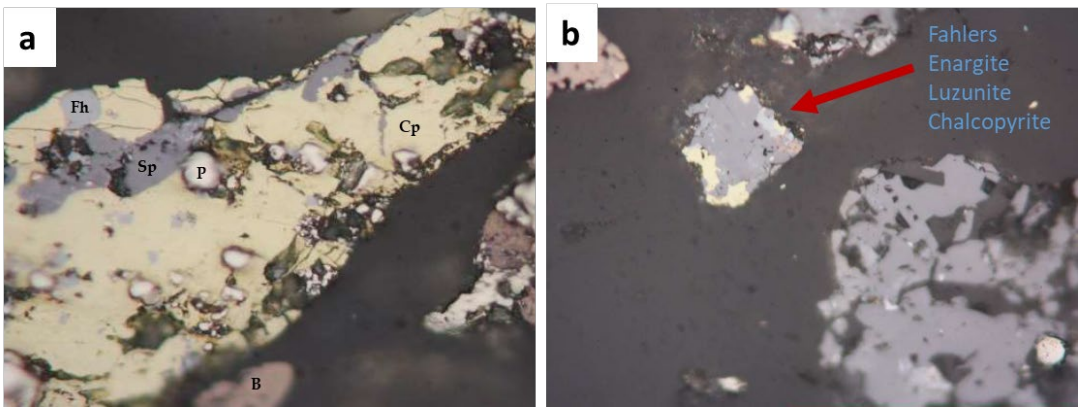


Fig. 9. Unliberated pyrite-chalcopyrite-sphalerite-fahlerite-bornite grain (Cp: Chalcopyrite, P: Pyrite, Sp: Sphalerite, B: Bornite, Fh: Fahlers) (a) Fahlers-enargite-luzunite-chalcopyrite granules (b)

Replacement minerals are quite abundant in grains between 75-150 microns. It was observed that chalcopyrite was extensively liberated in this particle size range, while only a part of the sphalerite was liberated. The minerals sphalerite, fahlers, bornite and covelin have been determined to be interlocked (Fig. 4a). It has been observed that the gangue minerals (especially quartz) are quite rare. It was determined that these sections were dominantly ore minerals.

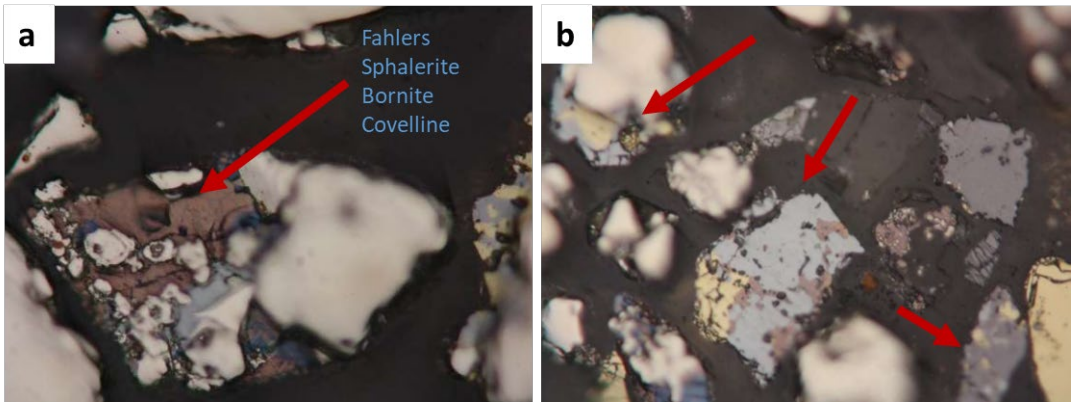


Fig. 4. Interlocking (bonded) sphalerite, fahler, bornite and covelline minerals (a) Interlocking sphalerite, fahlerite and bornite minerals (b)

In the microscopic examination of the particle between 38-75 microns, the composition of chalcopyrite, fahlers and sphalerite was observed. It was determined that grinding below 20 microns was required for liberation when the relevant mineral particle was examined (Fig. 4b). Additionally, it was observed that fahlers and chalcopyrite compositions interpreted as replacement textures are quite common. It is well known that the release of these replacement tissues is quite difficult.

Microscopic examination of particles between 20-38 microns was performed. It was noted that free chalcopyrite and pyrite granules are quite common in this section. The interlocking of chalcopyrite, fahlerite, sphalerite and pyrite that is seen in the larger grain sizes was also observed at this particle size. It was determined that some of the complex-bound grains (bornite, fahlers, sphalerite, pyrite) contained disseminated grains of pyrite less than 5 microns in size (Fig. 5a).

Microscopic examination of the fraction below 20 microns showed that most of the pyrite and chalcopyrite were liberated. Numerous free bornite and fahlers minerals were also observed. Although the number of bound particles was generally limited, the presence of a small number of chalcopyrite, sphalerite and chalcopyrite composite particles was identified (Fig. 5b).

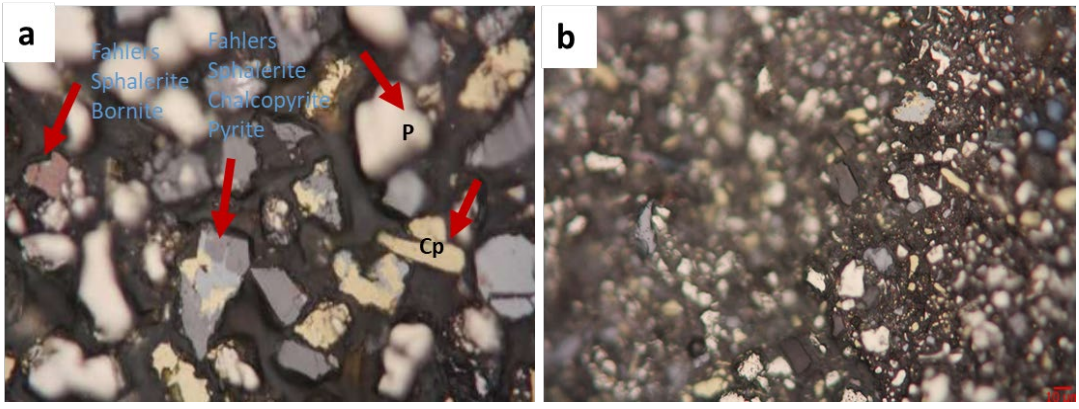


Fig.5. Free pyrite-chalcopyrite granules and bound fahlers-chalcopyrite-sphalerite-bornite granules (a) Predominantly free minerals and limited bound chalcopyrite and fahlers (<20 µm) (b)

3.2. Arsenic removal from copper concentrate

The copper concentrate used in this study was found to contain high levels of arsenic (Table 1). In marketable copper concentrates, the maximum arsenic content is 0.5%. Microscopic studies (Section 3.1.1) indicated that the arsenic in the concentrate could not be removed by flotation. Therefore, Na_2S and NaOH leaching (alkaline leaching) was used to selectively remove arsenic from the flotation concentrate and the leaching test results are discussed in this section.

As a result of hot (90 °C) alkaline leaching tests in which the flotation concentrate containing 17969 ppm (1.8%) arsenic was used directly at 200 g/L Na_2S and 50 g/L NaOH concentrations, the As content of the concentrate was 4700 ppm (0.47%) while 82.1% As removal efficiency was achieved. While the arsenic in the concentrate was removed to a significant extent, the time-leach efficiency graph in Fig. 6 shows that the other metals were not leached at all. The concentrate sample containing 17969 ppm (1.8%) arsenic was grinded (d_{80}: 57.8 µm) and the leaching test was repeated under the same conditions. At the end of 6 hours, the As content of the concentrate was 1802 ppm (0.18%), while the arsenic removal efficiency increased to 90% (Fig. 7). This situation showed that very fine arsenic minerals were present as inclusions and that leaching efficiency could be increased if the necessary liberation was achieved.

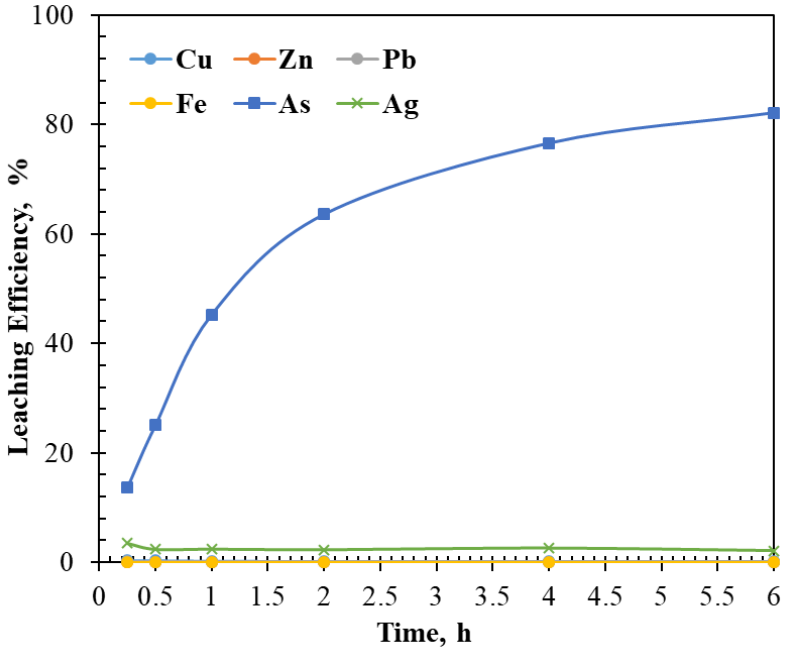


Fig. 6. Alkaline Leach Efficiency (unground concentrate) at 200 g/L Na_2S and 50 g/L NaOH concentrations, and 90°C

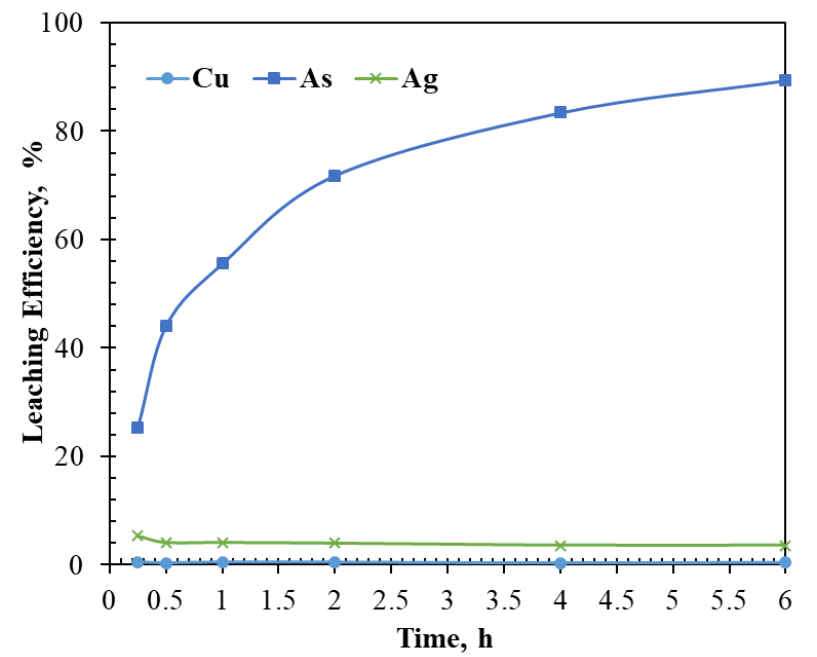


Fig. 7. Alkaline Leach Efficiency (ground concentrate) at 200 g/L Na_2S and 50 g/L NaOH concentrations, and 90°C

3.3. Arsenic precipitation

It was found that approximately 80% of the arsenic was precipitated from the loaded alkaline leach solution after the arsenic precipitation process described in test procedure. The alkaline solution that follows the precipitation process and contains a small amount of arsenic after the process can be reused in the leaching process. This process allows the alkaline solution to be recycled. It also makes it easier to manage the arsenic in the solution.

4. Conclusions

It was evaluated that arsenic in the copper concentrate examined in this study was present in the form of enargite mineral as well as fahlers group minerals. Maximum 0.5% arsenic is permitted in saleable copper concentrate. It is predicted that the arsenic contained in the copper concentrate cannot be removed by methods such as flotation due to its mineralogical structure. Therefore, Na_2S and NaOH leaching (alkaline leaching) was used to selectively remove arsenic from the cupper concentrate, and at the end of the process, the arsenic concentration in the concentrate was reduced below the allowable level in the saleable copper concentrate.

Arsenic removed from the flotation concentrate by alkaline leaching is in solution form. Recovery of arsenic in solid form from the leach solution is necessary due to the difficulty of storing the solution in systems such as tailings dams. In addition, there has recently been a demand for the use of arsenic as a raw material. For these reasons, it is important to recover high concentrations of arsenic in solution in solid form. As a result of the arsenic precipitation test performed in this study, a solid precipitate in the form of Na_3AsS_4 was obtained. Further research is needed to evaluate the arsenic sediments obtained both environmentally and economically.

Acknowledgments

The authors would like to thank Ergold Innovation Eng. Srv. Ltd. Co. for the financial support.

References

Awe, S. A., & Sandström, Å. (2010). Selective leaching of arsenic and antimony from a tetrahedrite rich complex sulphide concentrate using alkaline sulphide solution. Minerals Engineering, 23(15), 1227-1236. https://doi.org/10.1016/j.mineng.2010.08.018

Bujňáková,, Z., Baláž, P., & Zorkovská, A. (2014). Enargite concentrate processing by the combination of mechanochemical, hydrometallurgical and precipitation methods. International Journal of Mineral Processing, 127, 28-36. https://doi.org/10.1016/j.minpro.2013.12.008

Curreli, L., Garbarino, C., Ghiani, M., & Orrù, G. (2009). Arsenic leaching from a gold bearing enargite flotation concentrate. Hydrometallurgy, 96(3), 258-263. https://doi.org/10.1016/j.hydromet.2008.10.013

Dutrizac, J.E. & Morrison, R.M. (1984). The Leaching of Some Arsenide and Antimonide Minerals in Ferric Chloride Media. In: Bautista, R.G. (eds) Hydrometallurgical Process Fundamentals. NATO Conference Series, vol 10. Springer, Boston, MA. https://doi.org/10.1007/978-1-4899-2274-8_4

Filippou, D., St-Germain, P. & Grammatikopoulos, T. (2007). Recovery of Metal Values from Copper—Arsenic Minerals and Other Related Resources. Mineral Processing and Extractive Metallurgy Review, 28(4), 247-298. https://doi.org/10.1080/08827500601013009

Gajam, S., & Raghavan, S. (1983). A kinetic study of enargite dissolution in ammoniacal solutions. International Journal of Mineral Processing, 10(2), 113-129. https://doi.org/10.1016/0301-7516(83)90037-6

Kitchin, K. T. (2001). Recent Advances in Arsenic Carcinogenesis: Modes of Action, Animal Model Systems, and Methylated Arsenic Metabolites. Toxicology and Applied Pharmacology, 172(3), 249-261. https://doi.org/10.1006/taap.2001.9157

Mandal, B. K., & Suzuki, K. T. (2002). Arsenic round the world: A review. Talanta, 58(1), 201-235. https://doi.org/10.1016/S0039-9140(02)00268-0

Takatsugi, K., Sasaki, K., & Hirajima, T. (2011). Mechanism of the enhancement of bioleaching of copper from enargite by thermophilic iron-oxidizing archaea with the concomitant precipitation of arsenic. Hydrometallurgy, 109(1-2), 90-96. https://doi.org/10.1016/j.hydromet.2011.05.013

Tongamp, W., Takasaki, Y., & Shibayama, A. (2009). Arsenic removal from copper ores and concentrates through alkaline leaching in NaHS media. Hydrometallurgy, 98(3-4), 213-218. https://doi.org/10.1016/j.hydromet.2009.04.020

Tongamp, W., Takasaki, Y., & Shibayama, A. (2010). Selective leaching of arsenic from enargite in NaHS–NaOH media. Hydrometallurgy, 101(1-2), 64-68. https://doi.org/10.1016/j.hydromet.2009.11.020

Improvement in the Performance of Solvent Extraction Operation Using Solutions Spray System

Muhammad Zubair Rahim [1, 2], Ali Ihsan Arol [1,*]

[1] Department of Mining Engineering, Middle East Technical University, Ankara 06800, Türkiye

[2] Department of Chemical Engineering, Pakistan Institute of Engineering and Applied Sciences, Islamabad 45650, Pakistan

*Corresponding Author: arol@metu.edu.tr (Ali Ihsan Arol)

Abstract:

The solvent extraction (SX) technique is a widely used hydrometallurgical method for the extraction of metals from leach solutions. Conventional SX operations have limitations in terms of insufficient mass transfer between the immiscible solutions and slow process kinetics during solution mixing and separation. The solutions spray system is a new setup which is developed with the aim of increasing the mass transfer during extraction operation and reducing the mixing and separation times. The mono-sized micro-droplets produced in the mixing column generated a well-mixed emulsion of the two immiscible phases and improved the mass transfer between them. Furthermore, the new design of the settling section improved the phase separation and continually produced a fine quality product, fully separated from raffinate. This setup and the mixer-settler were used to extract La, Nd, and Eu from their synthesized chloride solutions while using DEHPA as an organic solvent. The maximum extraction of La, Nd, and Eu was 95.03%, 99.36%, and 99.98%, respectively, at 2.0 pH of feed solution and 0.303 M DEHPA with solutions spray system. Whereas the %E was 73.68%, 89.25%, and 98.60% for La, Nd, and Eu, respectively, with the mixer-settler system. Compared to the conventional mixer-settler, this new apparatus showed better mass transfer during extraction operation and quick phase separation because of the mono-sized micro-droplets and the special geometry of the settling column.

Keywords: *Solvent extraction, Solutions spray system, Mixer-settler, Rare earth elements, DEHPA*

1. Introduction

Solvent extraction is a widely used industrial process to recover valuable components or separate them from the gangues, especially in cases where higher purity or effective separation is required (Cantwell & Losier, 2002; Izzaty et al., 2004). In this technique, the two immiscible fluids (an aqueous feed and an organic solvent) come in contact with each other, resulting in the transfer of components from one solution to another. The desired components in the aqueous feed are transferred completely or partially to the organic phase depending on the distribution ratio of those components (Nicol et al., 2022; Poole, 2020; Stevens & Pratt, 2000; Weber, 2019).

Solvent extraction was reported back by the Romans, where this method was used for the separation of silver and gold from copper. In the 19th century, it was used in the petroleum industry, followed by the use in pharmaceutical and bioprocessing (Stevens & Pratt, 2000). Later, this technique proved more effective for the separation of radioactive elements in the nuclear industry, followed by its extensive use in the hydrometallurgical industry. Since then, this technique has been used for the extraction of different metals because of the increasing demand of pure metals to manufacture modern products and the synthesis of new solvents (Hashemi-Moghaddam, 2023; Ritcey, 2006; Stevens & Pratt, 2000).

A number of equipment have been designed (Todd, 2014) and are being used in solvent extraction operations for the extraction of rare earth elements (REEs), radioactive elements, and other industrial metals (M.A. Yelubay & S. R. Massakbayeva, 2017). The basic goals of these apparatuses are to improve the mass transfer between the immiscible feed streams, maximize the mass transfer rate, the separation of the product liquid phases, and control the loss of organic solvent (Hashemi-Moghaddam, 2023;

Parvizi et al., 2016; Stevens & Pratt, 2000; Weatherley, 2020). The selection of equipment depends on the initial and operating cost, simplicity of the operation, and the performance of that equipment. The Mixer-settler and the spray columns are the two common techniques used for the solvent extraction operation because of their simplicity and cost-effectiveness (Hashemi-Moghaddam, 2023; M.A. Yelubay & S. R. Massakbayeva, 2017; Stevens & Pratt, 2000).

The mixer-settler has separate mixing and separation sections. The feed streams are continuously mixed in the mixing chamber with the help of a mechanical mixer. This mixing generates the poly-sized droplets of the feed solutions, thus increasing the interfacial area, and hence mass transfer is increased between the two phases. The emulsion produced in this section is then transferred to the separation chamber, where the separation of the product streams takes place under gravity. In the mixing section, the equilibrium can be reached by adjusting the proper mixer speed and the retention time. The biggest advantages of this apparatus are its flexibility, efficiency, and simplicity. Whereas the biggest disadvantage is the bigger size of the settling chamber, the longer residence time for complete phase separation, and the loss of organic solvent (Duhamet & Commission, 2015; Gharehbagh & Mousavian, 2009; Hadjiev & Paulo, 2005; Kothari et al., 2012; Troshkin, 1996). Some work has been done to improve this separation through the phase inversion technique for certain specific cases, and it needs further investigation (Hadjiev & Paulo, 2005; Paulo & Hadjiev, 2006), and by changing different variables with the help of computational fluid dynamics simulation (Ye et al., 2020).

The spray column is one of the oldest devices used for the solvent extraction operation (Frank Seibert & Fair, 1988; Hixson, 1950; Johnson et al., 1957; Pasteur & Koch, 2020). In this device, the mixing and the separation/settling takes place in a single unit (Izzaty et al., 2004; Weatherley, 2020). One of the feed phases is continuous, and the other is introduced in the form of droplets to enhance the interfacial area for quick mass transfer. Normally, the aqueous feed enters from the top of the column as a continuous phase, and the organic phase is injected from the bottom of the column in the form of droplets, which are generated with the help of a sparger (Hashemi-Moghaddam, 2023). The organic phase flows in the upward direction and the aqueous phase in the downward direction because of the density difference between the two immiscible phases. During their counter-current flow, the mass transfer takes place between the immiscible phases, and the organic product is recovered from the top outlet and the aqueous raffinate from the bottom outlet. The biggest advantage of this equipment is the production of uniform-sized micro-droplets with the help of a distributor (Stevens & Pratt, 2000). The major disadvantage of the spray column is the back mixing of the liquid phases (Pasteur & Koch, 2020; Sovilj et al., 2019; Todd, 2014). During the upward flow of organic droplets, a volume of the continuous phase also attaches to these droplets and causes axial mixing. This mixing reduces the performance of the overall extraction operation. This back-mixing is controlled by introducing different internals in the spray column, thus enhancing the droplets' coalescence-breakage cycle and mass transfer (Stevens & Pratt, 2000).

To overcome the problems faced by these conventional equipment, a new apparatus was devised to enhance the performance of solvent extraction operation (Zubair Rahim & Ihsan Arol, 2024) and was studied in the previous work. This system showed promising extraction values along with the swift separation of the product phases. In this study, this setup will be studied along with the mixer-settler, and the two setups will be compared for the extraction of rare earth elements (REEs).

2. Materials and Method

2.1. Materials

The aqueous feed was synthesized by dissolving lanthanum oxide (La_2O_3), neodymium oxide (Nd_2O_3), and europium oxide (Eu_2O_3) (supplied by NATEN, Türkiye) in 1.0 M HCl (37%). The concentration of REEs in the feed was 1.0 g/L of each REO. Di-(2-ethylhexyl) phosphoric acid (DEHPA) (supplied by NATEN, Türkiye) was used as an organic solvent without further purification and mixed with kerosene (supplied by Etibakir A.S. Türkiye) at a volume ratio of 10:90 (i.e. 10% DEHPA) to decrease its viscosity. pH of the feed solution was adjusted from 0.50 to 2.0 with the help of NaOH.

2.2. Equipment and Method

In this study, the newly designed "solutions spray system" and the "mixer-settler" were used to extract REEs. The results of percent extraction were compared for these two techniques.

2.2.1. Solutions spray system

In the present work, a solutions spray system was studied with the objective of producing uniformly sized micro-droplets of the feed streams. These uniform-sized droplets not only improve the mass transfer in the mixing section but also enhance the phase separation and the quality of the product (Shimogouchi et al., 2019).

This setup (**Hata! Başvuru kaynağı bulunamadı.**) consists of two separate sections, the mixing and the settling/separation section. In the mixing section, the two immiscible feed streams are sprayed counter-currently with spray nozzles. These spray nozzles produce micro-sized droplets of uniform size, which, on mixing, form an emulsion in this mixing section, and the mass transfer takes place. This emulsion is then sent to the settling column under gravity where the separation of the two product phases is accelerated by the sudden increase in the diameter of the upper and lower sections. Furthermore, when the emulsion enters the settling column, the partial segregation between the two product streams takes place in such a way that the aqueous phase droplets move in the downward direction and organic droplets in the upward direction because of their density difference. During their upward flow, the organic droplets become bigger because of their collision and coalescence. The velocity of these droplets suddenly falls to a minimum on reaching the increased cross-sectional area, and meanwhile, the droplets behind them collide with the already-reached ones, and this collision results in the coalescence and the formation of the continuous organic phase, which is completely free from the aqueous raffinate. Similarly, the aqueous raffinate, completely free from the organic phase, is collected from the bottom outlet. For the product stream droplets to flow in the opposite direction in the separation column, the lower half of the settling column is filled with the aqueous and the upper with the organic solvent before starting any experiment.

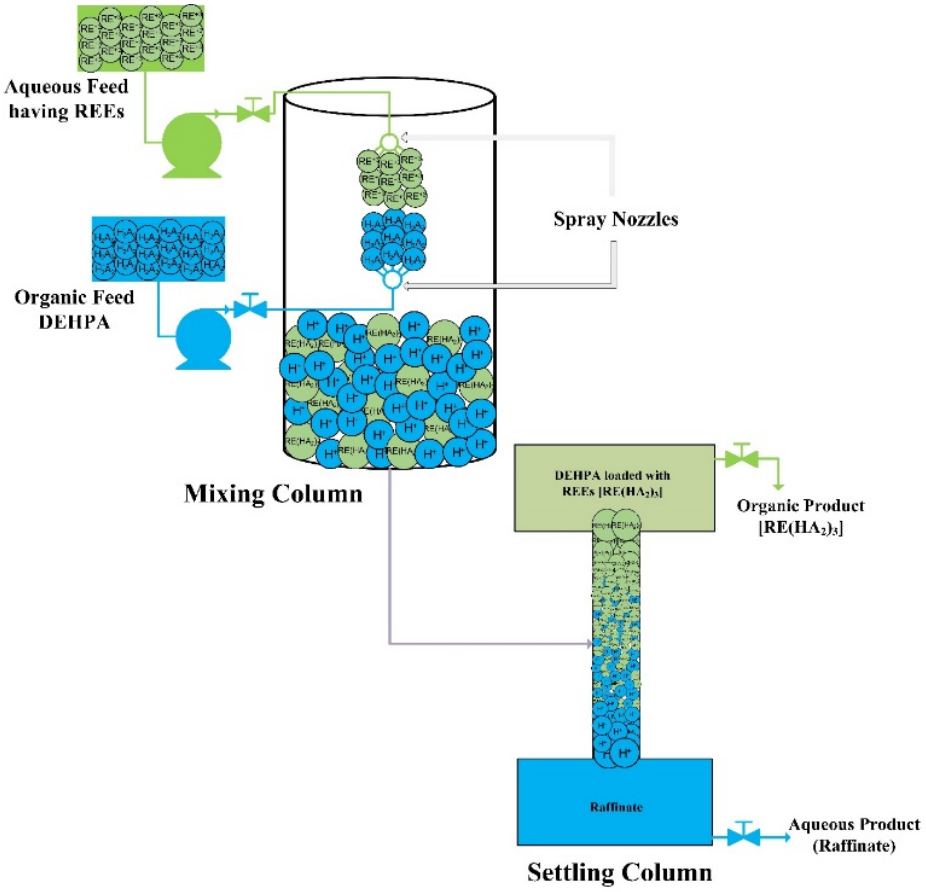


Fig. 10. Solutions spray system

In these experiments, 200 mL of aqueous and organic feed solutions were sprayed having a flow rate of 150 mL/min, and the product solutions (DEHPA loaded with REEs and the aqueous raffinate) were collected in a continuous manner. The pH of the synthesized feed solution was varied from 0.50 to 2.0 with NaOH to see the pH effect on REEs' extraction.

2.2.2. Mixer settler

A mechanical mixer was also used to mix the two immiscible phases and compare the results of the percent extraction of REEs with the solutions spray system. In this method, aqueous and organic feeds were mixed in a beaker with a mechanical mixer at 1400 rpm. It took 10 minutes to mix the two immiscible solutions, and it took almost 4.0 hours to completely separate the product solutions.

Similar to the solutions spray system, the constants in this technique included 100 mL of each feed stream and 1.0 g/L of each REO in the aqueous feed solution. Whereas the pH was changed from 0.50 to 2.0 with the addition of NaOH.

2.3. Characterization and evaluation of the experimental data

The percentage extraction of REEs was measured to see the performance of these techniques and calculated by the following equation.

$$\%E = \frac{[RE]_{in} - [RE]_{eq}}{[RE]_{in}} X\ 100 \quad (1)$$

Here, [RE]in and [RE]eq represent the initial and equilibrium concentrations of rare earth ions in the aqueous feed and raffinate. The concentrations of these elements in the aqueous solutions were measured with inductively coupled plasma optical emission spectroscopy (ICP-OES 5900). The pH of

the aqueous feed and raffinate was determined with a pH meter (pH 211 microprocessor, Hanna instruments).

3. Results and Discussion

3.1. Effect of pH on the extraction of REEs for the two mixing techniques

The organic solvent used in this study was di-(2-ethylhexyl) phosphoric acid (DEHPA), which is an acidic solvent. During the contact of DEHPA with the aqueous feed solution having RE^{3+}, a cation exchange process takes place in such a way that H^+ from DEHPA is replaced by RE^{3+} from the aqueous solution according to the Equation **Hata! Başvuru kaynağı bulunamadı.**).

$$RE_{aq}^{3+} + 3H_2A_2 \rightleftharpoons RE(HA_2)_3 + 3H_{aq}^{+} \quad (2)$$

Equation **Hata! Başvuru kaynağı bulunamadı.**) represents that the reaction will move in the reverse direction with the increase in the acidity of the system, thus inhibiting DEHPA deprotonation and REEs' extraction from the aqueous solution.

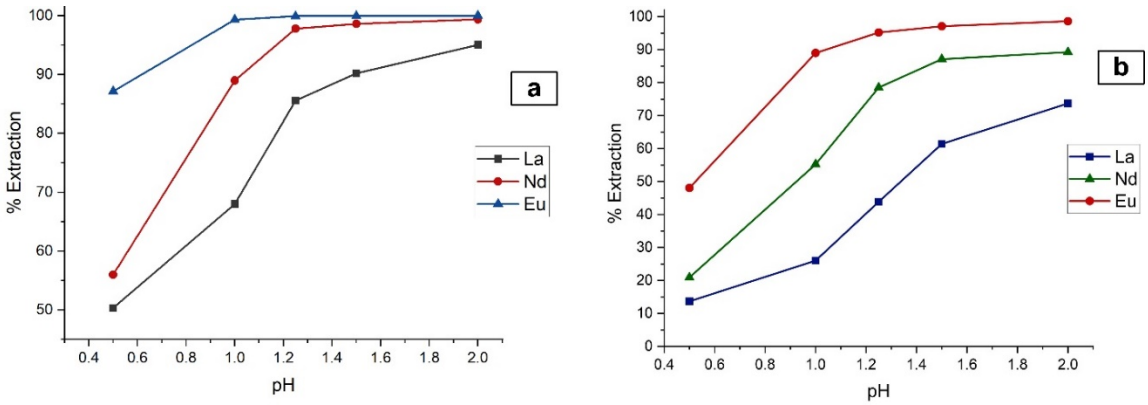


Fig. 11. pH effect on REEs' extraction while using a) solutions spray system, b) mixer-settler

The influence of pH on the DEHPA-based La, Nd, and Eu extraction for the two systems under investigation is shown in **Hata! Başvuru kaynağı bulunamadı.**. In both cases, in accordance with Equation **Hata! Başvuru kaynağı bulunamadı.**, the %E increased as pH rose. Furthermore, due to the variations in their ionic radii, Eu was extracted to the greatest extent in both situations, followed by Nd and La. Additionally, due to the variations in their ionic radii, Eu was extracted to the greatest extent in both situations, followed by Nd and La. Eu has the highest affinity to form a connection with DEHPA among the elements examined because of its smaller ionic radius (0.950 Å), followed by Nd (0.995 Å) and La (1.061 Å) (Bautista, 1995; Han et al., 2014; Kislik, 2012). **Hata! Başvuru kaynağı bulunamadı.**(a) shows the extraction of REEs while using the solutions spray system. It is evident from the figure that the extraction of Eu increased on raising pH from 0.50 to 1.0 and it was almost completely extracted at 1.0 pH. After that, its extraction remained almost independent of the aqueous pH. On the other hand, Nd recovery increased steeply with the increase in pH up to 1.25, and after that, the increase in extraction was very small with the rise in pH. Finally, it can be seen that the extraction of La increased continuously with the increase of pH and achieved maximal recovery at 2.0 pH. The maximum values of %E achieved at 2.0 pH were 95.03% for La, 99.36% for Nd, and 99.98% for Eu. **Hata! Başvuru kaynağı bulunamadı.**(b) shows the extraction of REEs for the mechanical mixer system. Here, Eu extraction steeply increased up to 1.0 pH and then the rise in extraction was gradual with the increase in pH, achieving maximal extraction at 2.0 pH. Whereas La and Nd extraction rose steadily with the increase in pH with highest values at 2.0 pH. The maximum extractions with this mixer-settler system, achieved at 2.0 pH, were 73.68% for La, 89.25% for Nd, and 98.60% for Eu. A bar chart is also plotted and shown in **Hata! Başvuru kaynağı bulunamadı.** to illustrate a comparison of these recoveries for the two solvent extraction techniques.

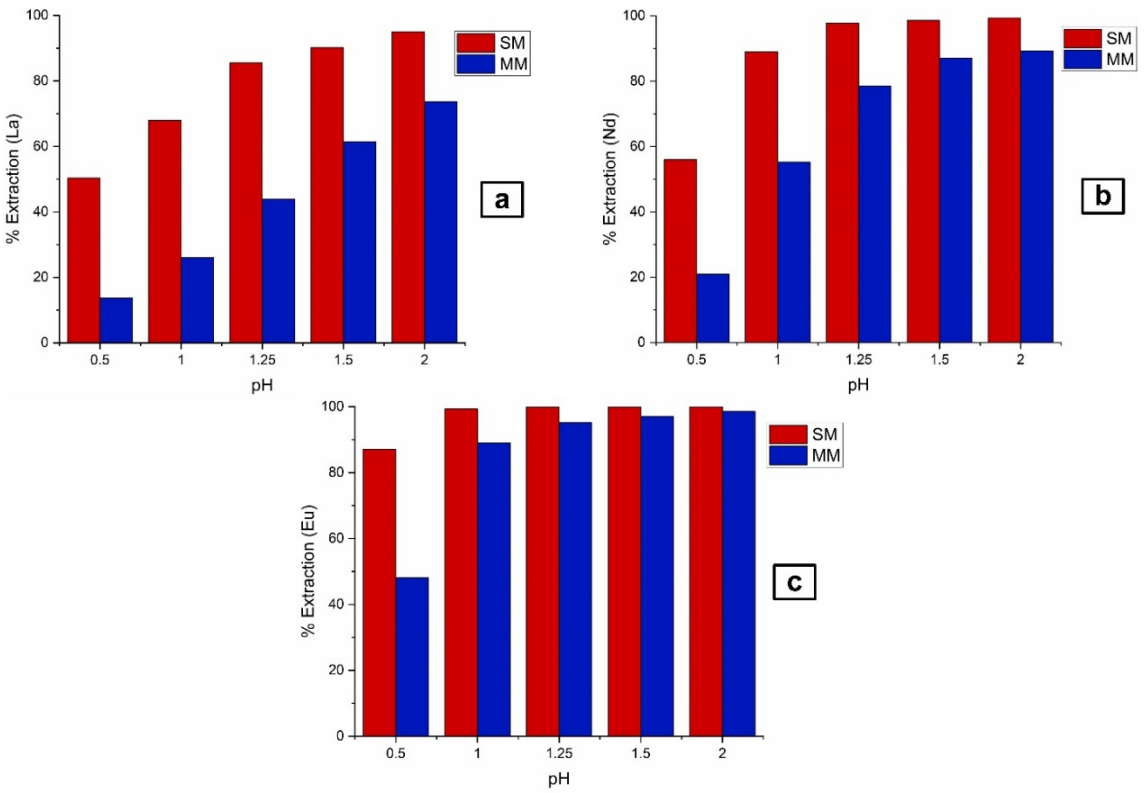


Fig. 12. Comparison of the spray mixing (SM) and mechanical mixing (MM) for the extraction of a) La, b) Nd, c) Eu

Hata! Başvuru kaynağı bulunamadı.(a) represents the extraction of La for spray mixing by solutions spray system and mechanical mixing. It is evident from the figure that the recovery of La was superior in the case of the solutions spray system compared to the mechanical mixing. The difference in the extraction for the two systems was higher at the lower pH values because of the competition of RE^{3+} against the higher concentration of H^{+} for the ion exchange process. Similarly, the solutions spray system showed greater extraction values for Nd compared to the mixer-settler technique, as shown in **Hata! Başvuru kaynağı bulunamadı.**(b). Finally, **Hata! Başvuru kaynağı bulunamadı.**(c) shows the extraction for Eu, where the difference in the performance of the two techniques is not very prominent because of the very high affinity of the Eu with DEHPA.

The higher recoveries of the REEs with the solutions spray system compared to the mixer-settler technique are because of the generation of mono-sized micro-droplets in the case of the solutions spray system as shown in **Hata! Başvuru kaynağı bulunamadı.** (Shimogouchi et al., 2019).

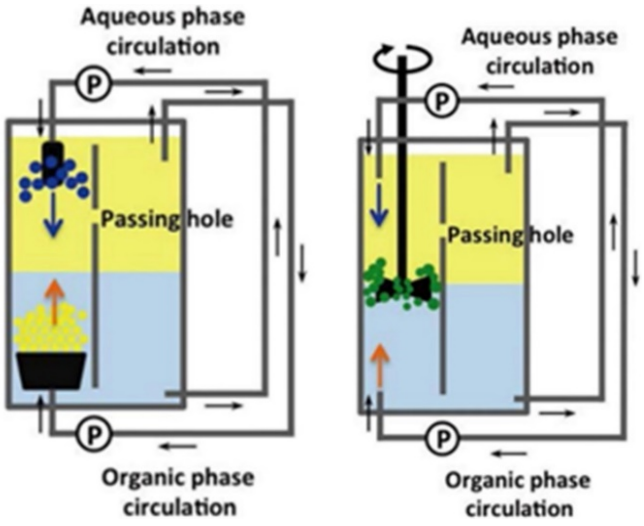


Fig. 13. Spraying system vs Mechanical stirring system (Shimogouchi et al., 2019)

Upon spraying a liquid, the monodispersed droplets generated by the sparger undergo densification, randomly agglomerate together, and form emulsion. The aqueous product in the settling section is constantly transparent and free of organic droplets, making it possible to rapidly separate and clean product streams (**Hata! Başvuru kaynağı bulunamadı.**). While, it is challenging to differentiate between the many phases of the mixture created by the mechanical stirrer, and this is because of the generation of poly-dispersed droplets of both phases (Shimogouchi et al., 2019). These poly-sized droplets not only create problems in mass transfer in the mixing section but also hinder the phase separation because of the very small settling velocities of small droplets compared to the larger ones and require a large cross-sectional area or a very long time for phases to be fully separated.

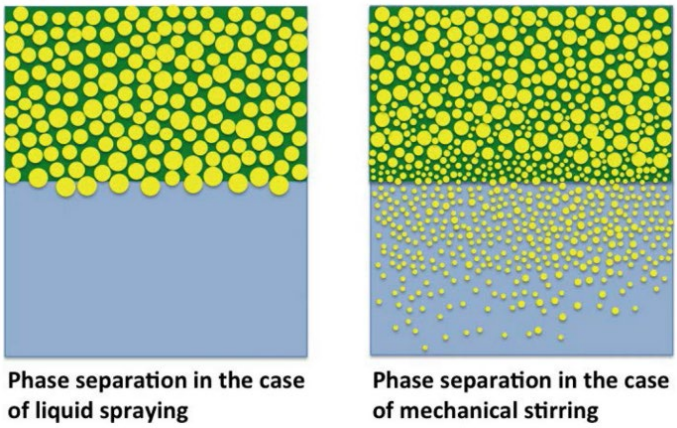


Fig. 14. Difference in the phase separation between droplets generated by spraying and mechanical mixing (Shimogouchi et al., 2019)

3.2. McCabe Thiele Diagrams for solutions spray system

The solutions spray system was further studied to find the theoretical stages to completly extract REEs from the aqueous solution. For this purpose, McCabe Thiele diagrams were plotted against aqueous:organic (A:O) phase ratios of 1:2 to 5:1. These diagrams were generated by drawing the reaction isotherms at equilibrium, and the operating lines were plotted against A:O phase ratio of 2:1.

Hata! Başvuru kaynağı bulunamadı.(a) represents the number of theoretical stages for the extraction of La while using a 2:1 A:O ratio in the case of the solutions spray system. It is shown that a four-stage counter-current operation gave complete recovery of La from the aqueous feed to DEHPA. Whereas the two-stage counter-current operation is sufficient to completely extract Nd from the aqueous phase, as shown in **Hata! Başvuru kaynağı bulunamadı.**(b). Finally, a single-stage operation is adequate for the

extraction of Eu with only 3.0 mg/L in the raffinate, as shown in **Hata! Başvuru kaynağı bulunamadı.**(c).

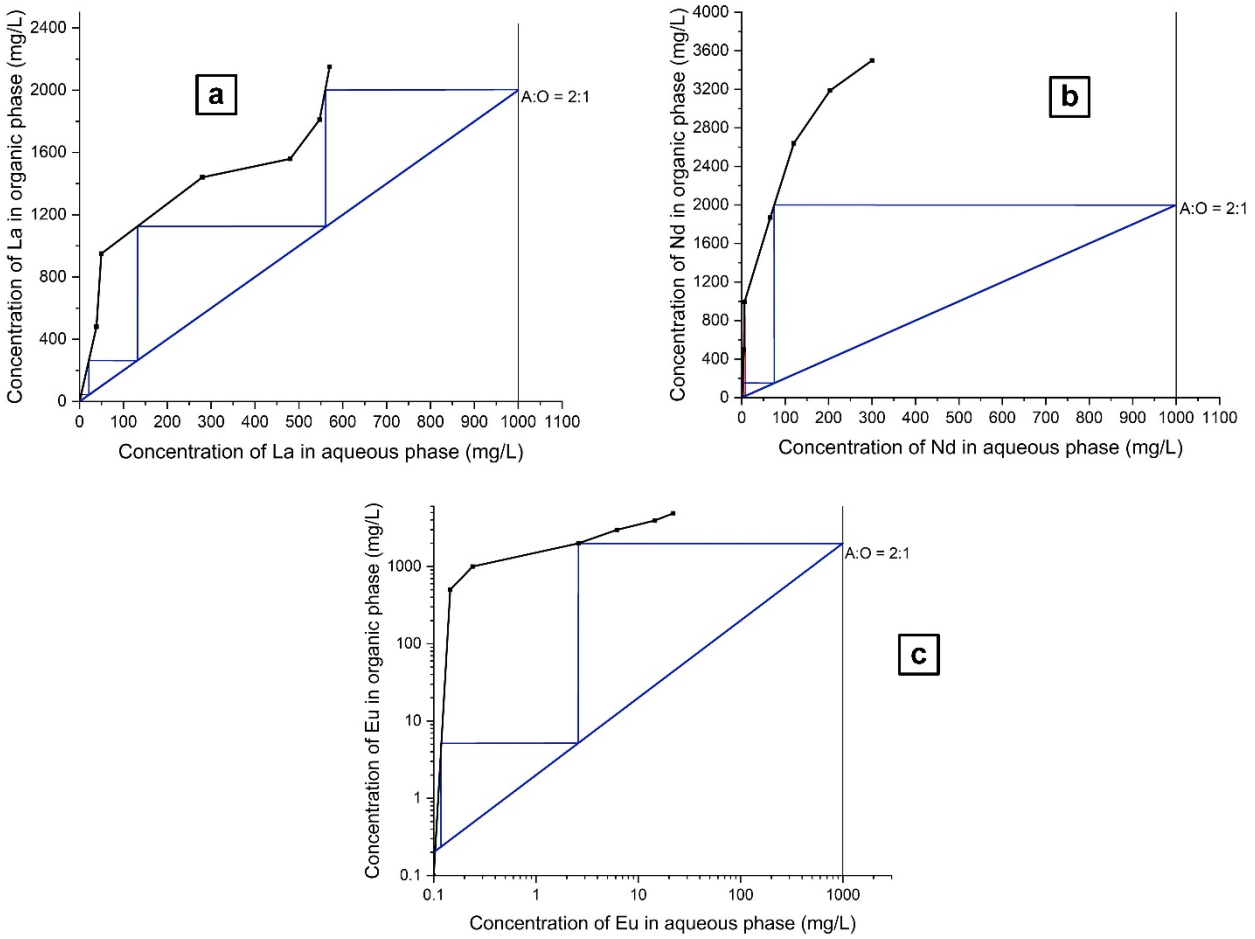


Fig. 15. McCabe Thiele diagram for the extraction operation in the case of the solutions spray system

4. Conclusion

In this study, a recently developed solutions spray system was compared with the mixer-settler while extracting REEs from a synthesized solution. The solutions spray system showed better extractions of REEs compared to the mechanical mixer. This better performance was because of the generation of mono-sized micro-droplets in the solutions spray system which not only improved the mass transfer but also enhanced the phase separation and the product quality.

The two solvent extraction techniques were studied to extract lanthanum, neodymium, and europium from an aqueous feed having 1.0 g/L of each REO. The pH of the feed solution was changed from 0.50 - 2.0 with the addition of NaOH. The organic solvent used was DEHPA having 0.303 M concentration. The feed solutions flow rate was 150 ml/min in the case of the solutions spray system, and the product solutions were received continuously from the separation column. Whereas, for the mixer-settler operation, the agitation speed was 1400 rpm, and it took 10 minutes to mix the two immiscible feed solutions and 4.0 hours for their complete separation.

In the case of the solutions spray system, the maximum extraction values were 99.98% for Eu, 99.36% for Nd, and 95.03% for La. Whereas these values were 98.60% for Eu, 89.25% for Nd, and 73.68% for La, in the case of mixer-settler. The better results with the solutions spray system are because of the production of mono-sized micro-droplets in the mixing section and the special design of the settling section, which enhanced the separation of the product streams and improved the quality of the

products. Finally, the McCabe Thiele diagrams showed the number of theoretical stages for the complete extraction of REEs against an A:O phase ratio of 2:1 for the solutions spray system.

Acknowledgments: The authors acknowledge Nadir Toprak Elementleri Araştırma Enstitüsü for providing REOs and DEHPA, and AR-GE laboratory, Eti Bakir a.ş, Türkiye, for conducting ICP-OES analysis.

Funding: This research did not receive any specific grant from funding agencies in the public, commercial, or not-for-profit sectors.

Declaration of competing interest: The authors declare that they have no known competing financial interests or personal relationships that could have appeared to influence the work reported in this paper.

References

Bautista, R. G. (1995). Chapter 139 Separation chemistry. *Handbook on the Physics and Chemistry of Rare Earths*, *21*, 1–27. https://doi.org/10.1016/S0168-1273(05)80108-4

Cantwell, F. F., & Losier, M. (2002). Liquid-liquid extraction. *Comprehensive Analytical Chemistry*, *37*, 297–340. https://doi.org/10.1016/S0166-526X(02)80048-4

Duhamet, J., & Commission, A. E. (2015). *40 Years of experience with liquid-liquid extraction equipment in the nuclear industry 40 YEARS OF EXPERIENCE WITH LIQUID-LIQUID EXTRACTION MIXER-SETTLERS*. *January 2003*.

Frank Seibert, A., & Fair, J. R. (1988). Hydrodynamics and mass transfer in spray and packed liquid-liquid extraction columns. *Industrial and Engineering Chemistry Research*, *27*(3), 470–481. https://doi.org/10.1021/ie00075a017

Gharehbagh, F. S., & Mousavian, S. M. A. (2009). Hydrodynamic characterization of mixer-settlers. *Journal of the Taiwan Institute of Chemical Engineers*, *40*(3), 302–312. https://doi.org/10.1016/j.jtice.2008.07.016

Hadjiev, D., & Paulo, J. B. A. (2005). Extraction separation in mixer-settlers based on phase inversion. *Separation and Purification Technology*, *43*(3), 257–262. https://doi.org/10.1016/j.seppur.2004.11.006

Han, K. N., Kellar, J. J., Cross, W. M., & Safarzadeh, S. (2014). Opportunities and challenges for treating rare-earth elements. In *Geosystem Engineering* (Vol. 17, Issue 3, pp. 178–194). Taylor & Francis. https://doi.org/10.1080/12269328.2014.958618

Hashemi-Moghaddam, H. (2023). Liquid-liquid extraction in the food industry. In *Extraction Processes in the Food Industry*. Elsevier Inc. https://doi.org/10.1016/B978-0-12-819516-1.00006-5

Hixson, A. N. (1950). *Mass Transfer Coefficients in an Extraction t l. June*.

Izzaty, R. E., Astuti, B., & Cholimah, N. (2004). Solvent Extraction: Principles and Practice. In *Angewandte Chemie International Edition, 6(11), 951–952.* (2nd ed.).

Johnson, A., Minard, G. W., Huang, C., Hansuld, J. H., & Mcnamara, V. M. (1957). Spray-ex traction-tower Studies. *A.I.Ch.E. Journal*, *3*(1), 101–110.

Kislik, V. S. (2012). *Solvent Extraction: Classical and Novel Aproaches* (1st ed.).

Kothari, D. C., Renge, V. C., Padma, B., Rao, S., Raidas, R., & Pitt, M. J. (2012). Advanced Separation Techniques for Industrial Effluents. *Indian Chemical Engineer*, *54*(4), 262–270. https://doi.org/10.1080/00194506.2012.766004

M.A. Yelubay, & S. R. Massakbayeva. (2017). *Mass Transfer Devices*.

Nicol, M., Welham, N., & Senanayake, G. (2022). Solvent extraction. In *Hydrometallurgy*. https://doi.org/10.1016/b978-0-323-99214-5.00007-3

Parvizi, S., Keshavarz Alamdari, E., Hashemabadi, S. H., Kavousi, M., & Sattari, A. (2016). Investigating Factors Affecting on the Efficiency of Dynamic Mixers. *Mineral Processing and Extractive Metallurgy Review*, *37*(5), 342–368. https://doi.org/10.1080/08827508.2016.1218868

Pasteur, L., & Koch, R. (2020). *1. Introduction 1. Introduction* (Vol. 74, Issue 2020).

Paulo, J. B. A., & Hadjiev, D. E. (2006). Mixer-settler based on phase inversion: Design of the mixing zone. *Industrial and Engineering Chemistry Research*, *45*(11), 3821–3829. https://doi.org/10.1021/ie050133z

Poole, C. F. (2020). *Liquid phase Extraction*.

Ritcey, G. M. (2006). Solvent extraction in hydrometallurgy: Present and future. *Tsinghua Science and Technology*, *11*(2), 137–152. https://doi.org/10.1016/S1007-0214(06)70168-7

Shimogouchi, T., Naganawa, H., Nagano, T., Grambow, B., & Nagame, Y. (2019). Size distribution of droplets in a two liquid-phase mixture compared between liquid spraying and mechanical stirring. *Analytical Sciences*, *35*(9), 955–960. https://doi.org/10.2116/analsci.18P508

Sovilj, M. N., Nikolovski, B. G., & Spasojević, M. D. (2019). Hydrodynamics in spray and packed liquid-liquid extraction columns: A review. *Macedonian Journal of Chemistry and Chemical Engineering*, *38*(2), 267–282. https://doi.org/10.20450/mjcce.2019.1519

Stevens, G. W., & Pratt, H. R. C. (2000). Solvent extraction equipment design and operation: Future directions from an engineering perspective. *Solvent Extraction and Ion Exchange*, *18*(6), 1051–1078. https://doi.org/10.1080/07366290008934722

Todd, D. B. (2014). Solvent Extraction. In *Fermentation and Biochemical Engineering Handbook: Principles, Process Design, and Equipment: Third Edition* (Third Edit). Elsevier Inc. https://doi.org/10.1016/B978-1-4557-2553-3.00012-X

Troshkin, V. P. (1996). Investigation of the hydrodynamics of extraction processes. *Chemical and Petroleum Engineering*, *32*(5), 403–406. https://doi.org/10.1007/BF02416568

Weatherley, L. R. (2020). *Intensi fi cation of Liquid – Liquid Processes* (Issue May).

Weber, M. (2019). Practical Experience in Design and Operation of Liquid-Liquid Extraction Processes. *Chemie-Ingenieur-Technik*, *91*(11), 1515–1521. https://doi.org/10.1002/cite.201800174

Ye, S., Tang, Q., Wang, Y., & Fei, W. (2020). Structural optimization of a settler via CFD simulation in a mixer-settler. *Chinese Journal of Chemical Engineering*, *28*(4), 995–1015. https://doi.org/10.1016/j.cjche.2020.01.010

Zubair Rahim, M., & Ihsan Arol, A. (2024). Solvent extraction of La, Nd, and Eu using a newly designed solutions spray system. *Minerals Engineering*, *216*(April), 108909. https://doi.org/10.1016/j.mineng.2024.108909

Acidic Dissolution of Metals from Waste Printed Circuit Boards

Şule Ilgın [1], Nazlım İlkyaz Dinç [1], Fırat Burat [1], Arslan* [1]

[1] Istanbul Technical University, Mining Faculty, Mineral Processing Engineering Department, 34469, Maslak, Istanbul, Türkiye

*Corresponding author: *arslanf@itu.edu.tr (Fatma Arslan)

Abstract:

Developing technology and increasing population have created the waste problems. There is increasing concern about the volume of end of life electronics due to creating huge landfills and environmental dirtiness. The limited availability of landfill and the need to adopt a more sustainable approach to materials consumption has led to greater attention being given to the problems associated with end of life electronics. With growing pressure to recycle more end of life Printed Circuit Boards (PCBs) there is a clear need to develop and implement integrated recycling methodologies. In this experimental study, dissolution of metallic values (Cu, Zn, Ni, Fe) from secondary sources was investigated. Waste computer circuit boards subject to this experimental study contained 26.56% Cu, 1.05% Zn, 0.49% Fe, 0.23% Ni, 0.02% Pb, 1.31% Al, 281 ppm Ag, and 27 ppm Au. The total metal content of the material was determined as 57.99% as a result of the dissolution with aqua regia. In the leaching experiments, the effects of acid type and concentration, addition of H2O2 as an oxidizing agent, and leaching time on metal dissolution efficiencies were investigated. At the end of 5 h leaching, 65.52% Cu, 77.26 % Zn, 85.14 %Fe, and 72.37 % Ni leaching efficiencies are found. In using 8 M H2SO4, 53.60 % Cu, 51.35 %Zn, 41.29 %Ni, and 79.10 %Fe leaching efficiencies are reached in one hour leaching time. In the tests with 8 M HCl, 74.24 %Ni, 51.92 %Fe, 80.61 %Zn leaching efficiencies whereas in the tests with 1 M HNO3, 56.64 %Ni, 54.9 %Fe, 55.24 %Zn leaching efficiencies are achieved. Since different acids dissolve different metals selectively, as a result, stepwise leaching processes can be applied by considering experimental results carried out in different test conditions.

Keywords: *Waste Printed Circuit Board, Acidic Dissolution, Copper, Zinc, Nickel, Iron*

1. Introduction

There is increasing concern about the volume of end of life electronics due to creating huge landfills and environmental dirtiness. The limited availability of landfill and the need to adopt a more sustainable approach to materials consumption has led to greater attention being given to the problems associated with end of life electronics (Goosey & Kellner, 2003). Additionally, emerging legislation such as the waste from electrical and electronic equipment (WEEE) directive, will necessitate the increasing recovery and recycling of materials found in scrap electronics because of having valuable metals as shown in Table 1. As seen from the table copper il the leading one among the metals. With growing pressure to recycle more end of life Printed Circuit Boards (PCBs) there is a clear need to develop and implement integrated recycling methodologies (Goosey & Kellner, 2002). General routes which may be followed for recycling comprise (Chatterjee, 2012): (a) Component recycling via disassembly, (b) Materials recycling via mechanical processing, pyrometallurgy, hydrometallurgy or a combination of these techniques.

Table 1. Composition of populated PCBs (Goosey & Kellner, 2002).

Materials	Content %	Materials	Content %
Non-metal (epoxy, glass, etc.)	70	Silver	0.05
Copper	16	Gold	0.03
Solder	4	Palladium	0.01
Nickel	2	Others (bismuth, antimony, tantalum, etc)	0.01
Iron, ferrite (from transformer cores)	3		

All existing and potential treatment approaches involve mechanical or mechanical/ hydrometallurgical methods (Goosey & Kellner, 2002, 2003). Due to the nature of the input material base, even the most sophisticated hydrometallurgical treatment models involve a level of mechanical treatment. It should be noted, however, that hydrometallurgical approaches do offer a genuine treatment alternative to smelting and the possibility of realizing higher metal recovery yields. This is of great significance when dealing with high value scrap PCBs and the inherent loss from process of precious metals which may be evident within a mechanical route. Mechanical approaches are (a) Primary coarse size reduction, (b) Coarse ferrous metal separation, (c) Pulverization, (d) Classification, (e) Electrostatic separation, and (f) Further size reduction. In some cases, gravity separation methods are also included (Goosey & Kellner, 2003). Hydrometallurgical approaches offer a viable methodology in maximizing the recovery of intrinsic metal value, particularly precious metals. No single treatment approach will be appropriate for the handling of all scrap PCBs due to their diversity and varying intrinsic worth. Rather, an integrated hierarchy of approaches which encompasses disassembly, mechanical and hydrometallurgical methodologies will be needed.

Hydrometallurgical process for selective metals recovery from the waste-printed circuit boards (WPCBs) using a combination of conventional and time-saving methods: leaching, cementation, precipitation, reduction and electrowinning (Silvas et al, 2015). Aiming WEEE recycling and the recovery of metallic fraction, several treatment techniques can be applied. Generally, it consists of three basic stages:

- Pre-treatment: includes the processes of manual disassembling of electronic components,
- Processing/Concentration: can includes processes of comminution, granulometric classification, magnetic and electrostatic separation, pyrometallurgical processing and hydrometallurgical processing,
- Recovery/purification: can be used solvent extraction processes, precipitation/cementation, electrowinning/electroplating.

Among hydrometallurgical processes that can be applied, leaching is the leading technique based on the principle of solid component solubility by through of contact with leaching agent. Different factors can influence the leaching process, such as: pH, temperature, concentration and oxidation–reduction potential (ORP). Metallic fraction dissolution is related with pH/ORP rate and can be studied by Pourbaix Diagrams plotted for metal/leaching systems at determined temperatures (Doyle, 1987). Several leaching agents can be used in PCBs recycling processes (Birloaga et al., 2013; Tuncuk et al 2012). Acids are the most used and their concentration depends which metal is being solubilized, as well as the acid class: HNO_3, H_2SO_4, HCl. Addition to these acids, a wide variety of reagent systems (e.g. iodide, ammonia, cyanide, thiourea and thiosulphate) in the presence of a suitable oxidant (e.g. H_2O_2, O_2, Cu(II), Cl_2 etc.) have been tested for leaching of metals from WPCBs (Kim et al., 2010; Madenoğlu, 2005; Tuncuk et al., 2012; Yazici, 2012; Yazici and Deveci, 2013).

The aim of this experimental study is to recover metallic values from waste printed circuit boards (PCBs) in electronic wastes (WEEE). Experiments include preparation, physical and chemical analyses, and hydrometallurgical tests.

2. Material and Method

In the experiments 2.2 kg waste PCBs under 1 mm in size is used. Screen analysis results are showed that d_{50} and d_{80} values are found as 0.31 and 0.64 respectively. Chemical analysis of the sample according to particle size ranges is given in Table 2. According to the results, waste computer circuit boards subject to this experimental study contains 26.56% Cu, 1.05% Zn, 0.49% Fe, 0.23% Ni, 0.02% Pb, 1.31% Al, 281 ppm Ag, and 27 ppm Au.

In order to find the metal content of the sample according to particle size ranges, all samples are dissolved in aqua regia (HNO_3+3HCl) and results are given in Table 3. As seen from the table, metal content of the sample increased while plastic content of the sample decreased with decreasing particle size range. Total metal content was found as 57.99% and the plastic content was 42.01%.

In leaching experiments, the effects of acid type and concentration, oxidizing agent addition and leaching time on metal leaching efficiencies were investigated.

Table 2. Chemical anaysis results of the sample used in the tests.

Particle Size Range (mm)	Weight (%)	Metal Content (%)					ppm		
		Cu	Fe	Ni	Zn	Al	Pb	Au	Ag
-1+0.85	5.0	38.13	0.21	0.24	2.20	0.14	0.02	15	250
0.85+0.5	25.2	49.50	0.28	0.28	2.12	0.14	0.03	13	260
0.5+0.3	21.0	2.30	0.71	0.13	0.05	2.61	0.01	25	250
0.3+0.212	7.8	8.10	0.62	0.21	1.32	1.44	0.02	60	150
0.212+0.106	11.6	24.88	0.33	0.24	0.08	0.95	0.02	31	360
0.106+0.053	7.9	48.30	0.18	0.26	0.11	0.92	0.01	18	330
0.053+0.038	13.5	1.98	0.75	0.14	0.06	2.70	0.02	36	310
-0.038	7.9	51.48	0.72	0.43	3.30	0.70	0.03	38	360
Total	100.0	26.56	0.49	0.23	1.05	1.31	0.02	27	281

Table 3. Total metal and plastic contents of the sample according to size ranges.

Particle Size Range (mm)	Weight (%)	Metal Content (%)	Plastic Content (%)
-1+0.85	5.0	33.02	66.98
-0.85-0.5	25.2	39.51	60.49
-0.5-0.3	21.0	48.03	51.97
-0.3-0.212	7.8	47.02	52.98
-0.212-0.106	11.6	71.94	28.06
-0.106-0.053	7.9	82.71	17.29
-0.053-0.038	13.5	83.23	16.77
-0.038	7.9	81.75	18.25

Total	100	57.99	42.01

3. Experimental Results and Discussions

In the leaching tests, effect of acid (H_2SO_4) concentration, oxidizing agent (H_2O_2) addition, leaching time and different acid types (H_2SO_4, HCl, HNO_3) on metal leaching efficiencies was investigated.

In the first group of experiments, effect of acid (H_2SO_4) concentration on Cu and Zn dissolution efficiencies were investigated. Experimental conditions were used as 10% solid/liquid ratio, 60°C temperature (as found in our earlier study (Arslan et al, 2022), 600 rpm stirring speed, 1 h leaching time and different acid concentrations between 1-8 M. Results are shown in Table 4. Increasing acid concentration had an increasing effect on Cu, Zn, Fe dissolution efficiencies and had almost no effect on Ni leaching efficiency. In using 8 M H_2SO_4, 53.60 % Cu, 51.35 %Zn, 41.29 %Ni, and 79.10 %Fe leaching efficiencies were reached.

Table 4. Effect of acid concentration on metal leaching efficiencies.

H_2SO_4 (M)	**Weight Loss (%)**	**Metal Dissolution Efficiency (%)**			
		Ni	**Fe**	**Zn**	**Cu**
1	1.36	44.79	10.54	6.80	10.47
2	1.41	52.65	12.00	7.10	11.70
3	3.83	61.53	35.80	18.73	28.38
4	3.74	42.24	37.60	20.18	29.06
8	8.26	41.29	79.10	51.35	53.60

In the second group of experiments, the effect of oxidizing (H_2O_2) addition on metal leaching efficiencies were investigated. Experimental conditions are used as 10% solid/liquid ratio, 60°C temperature, 600 rpm stirring speed, 1 h leaching time, different acid concentrations between 1-8 mole/L, and 10-20% H_2O_2 addition. Results are shown in Table 5 and it is seen that oxidizing agent addition had an increasing effect on metal dissolution efficiencies. Leaching efficiencies of Zn and Cu are increased from 6.80 % and 10.47 % (Table 4) to 13.51% and 33.68 % (Table 5) with 10% H_2O_2 addition. 22.35 %Zn and 62.68 %Cu leaching efficiencies are reached with 20 % H_2O_2 addition. Similar results are also found in the literature studies. In an earlier study on the extraction of copper from scrap TV boards by Deveci et al (2010), it was found that Cu dissolution was also increased with H_2O_2 addition (0.3 M, 1-4 hours) in sulfide media. Oh et al. (2003) proposed sulfuric acid (H_2SO_4) leaching of PCBs in the presence of H_2O_2 as a first stage process where Cu, Fe, Zn, Ni, and Al were extracted at high recoveries of >95%. In the second stage, they targeted the recovery of precious metals using ammoniacal thiosulfate ($CuSO_4$-NH_4OH-$(NH_4)_2S_2O_3$) as lixiviant. Quinet et al. (2005) also considered sulfuric acid leaching as the first stage process at which various oxidants including H_2O_2, O_2, and Fe^{3+} were tested for the extraction of copper.

Table 5. Effect of H_2O_2 addition on different acid concentrations.

H_2SO_4 (M) +%10 H_2O_2	**Weight loss (%)**	**Metal Dissolution Efficiency (%)**			
		Ni	Fe	Zn	Cu
1	21.65	46.72	76.02	13.51	33.68
2	32.41	59.44	79.78	22.39	37.85
3	21.3	61.45	94.92	30.05	42.68
4	25.87	77.96	92.83	36.16	53.37
8	26.48	82.35	78.65	46.09	57.79
8M H_2SO_4 + %20 H_2O_2	28.05	41.29	79.11	52.35	62.68

In the third group experiments, effect of leaching time on metal dissolution efficiencies. Experimental conditions are used as 8 M H_2SO_4 concentration, 10% solid/liquid ratio, 60°C temperature, 600 rpm stirring speed, 1 h leaching time, and 10% H_2O_2 addition at different leaching durations (1-5 hours). Results are summarized in Table 6. Metal leaching efficiencies are increased with increasing leaching time. At the end of 5 h leaching, 65.52% Cu, 77.26 % Zn, 85.14 %Fe, and 72.37 % Ni leaching efficiencies are found.

Table 6. Effect of leaching time on metal leaching fficiencies.

Time (h)	Weight loss (%)	Metal Leaching Efficiency (%)			
		Ni	Fe	Zn	Cu
1	28.05	41.29	79.11	25.35	62.68
2	27.62	24.72	83.66	32.98	61.14
3	32.82	14.01	73.99	41.37	78.16
4	28.45	79.97	83.84	53.63	72.22
5	23.24	72.37	85.14	77.26	65.52

In the last group experiments effect of different acids (H_2SO_4, HCl, and HNO_3) are tested. Constant experimental conditions are 60°C temperature, 600 rpm stirring speed, 10 % solid/liquid ratio and 1 h leaching time. 4M HCL, 8M HCl, and 1M HNO_3 are used and results are given in Table 7 and Figure 1.

Table 7. Effect of different acids on metal leaching efficiencies

Type of Acid	Metal Leaching Efficiency (%)				
	Pb	Ni	Fe	Zn	Cu
8 M H_2SO_4	-	41.29	79.10	51.35	53.60
8M H_2SO_4+ %10 H_2O_2	-	46.72	82.35	46.09	57.79
8M H_2SO_4+ %20 H_2O_2	-	59.44	74.10	52.35	62.68
1M HNO_3	13.28	56.64	54.90	55.24	35.76
4M HCl	9.88	63.95	31.51	62.21	8.21
8M HCl	14.14	74.24	51.92	80.61	31.63

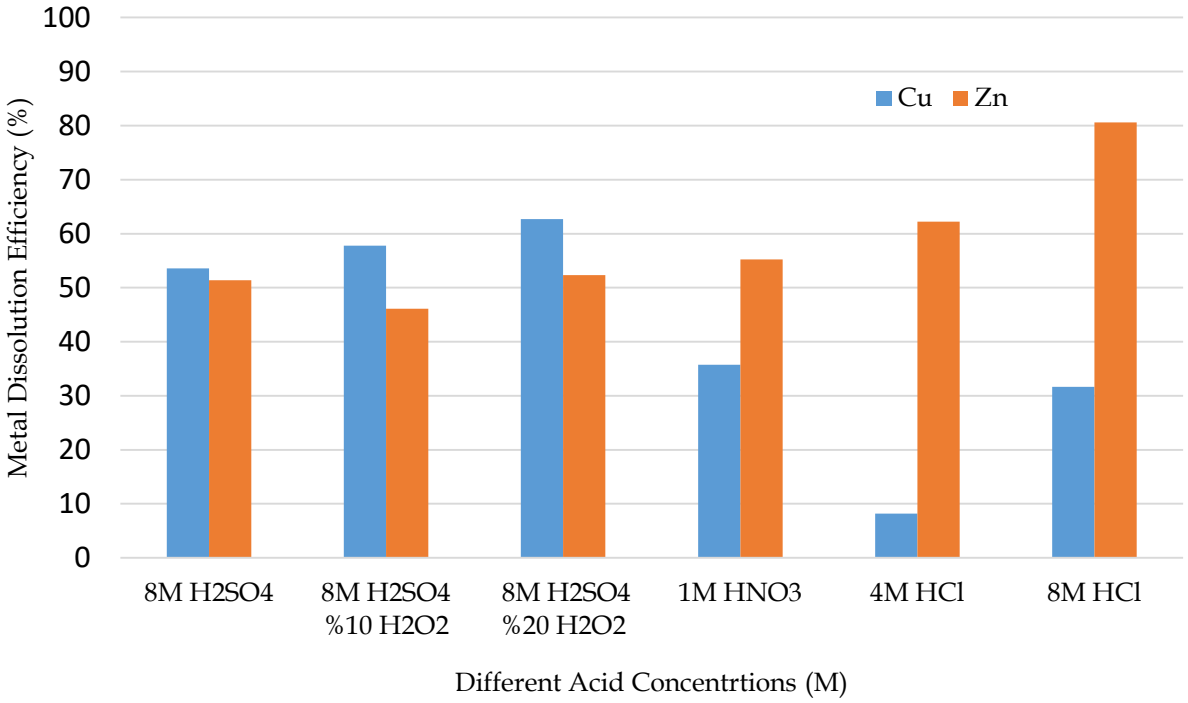


Figure 1. Effect of different acids on Cu and Zn leaching efficiencies.

According to Table 7, in the tests with 8 M HCl, 74.24 %Ni, 51.92 %Fe, 80.61 %Zn leaching efficiencies whereas in the tests with 1 M HNO_3, 56.64 %Ni, 54.9 %Fe, 55.24 %Zn leaching efficiencies are achieved. The highest Ni and Zn leaching efficiencies are observed with 8 M HCl is used. In terms of HNO_3 use, higher metal leaching efficiencies may be observed with increasing acid concentrations. In terms of H_2SO_4 use, metal dissolutions can be increased by adding oxidizing agent during leaching as seen from Table 7.

As given in the literature studies, acid leaching is often used as the first stage leaching for the extraction of base metals, copper in particular. Acid leaching of metals from e-waste has been extensively investigated using various mineral acids and oxidants (HCl, H_2SO_4, HNO_3/H_2O_2, $HClO_4$, NaClO) (Deveci et al, 2010). Bacterial leaching is also studied (Brandl et al. 2001) and ferric ion addition during bioleaching increased Cu extraction to >99% according to Yang et al. (2009). In the studies done by Mecucci & Scott (2002) high Cu and Pb extractions (>85%) were observed by nitric acid (HNO_3) leaching.

In our earlier study (Arslan et al, 2022) with PCBs of waste mobile phones, in the experiments using HNO_3, higher Co, Ni, and Pb leaching efficiencies, and in the experiments using HCl, higher Pb, Co, Al, and Fe leaching efficiencies are observed while Cu leaching efficiency was still low in all cases with different types of acids. Castro and Martins (2009) similarly reported that Cu extraction from PCBs found <0.01 % in sulfuric acid leaching supporting our results and about 30% in cases of H_2SO_4+HCl, HCl, and HCl+HNO_3 solutions. According to Madenoğlu's report (2005) the highest extraction of Cu and Au from PCBs was also obtained by using HNO_3/HCl media (e.g. Aqua regia) as expected.

4. CONCLUSIONS

Waste computer circuit boards subject to this experimental study contains 26.56% Cu, 1.05% Zn, 0.49% Fe, 0.23% Ni, 0.02% Pb, 1.31% Al, 281 ppm Ag, and 27 ppm Au while the total metal content of the material was determined as 57.99%. In the leaching experiments, the effects of acid type and concentration, addition of H_2O_2 as an oxidizing agent, and leaching time on metal dissolution efficiencies were investigated. At the end of 5 h leaching, 65.52% Cu, 77.26 % Zn, 85.14 %Fe, and 72.37 % Ni leaching efficiencies are found. In using 8 M H_2SO_4, 53.60 % Cu, 51.35 %Zn, 41.29 %Ni, and 79.10

%Fe leaching efficiencies are reached in one hour leaching time. In the tests with 8 M HCl, 74.24 %Ni, 51.92 %Fe, 80.61 %Zn leaching efficiencies whereas in the tests with 1 M HNO_3, 56.64 %Ni, 54.9 %Fe, 55.24 %Zn leaching efficiencies are achieved. As a result, stepwise leaching processes can be applied by considering experimental results carried out in different test conditions. In conclusion, sequential leaching with different acids is recommended for the effective leaching of all metals. Precious metals can be dissolved by using cyanide, thiourea, and aqua regia. For metal recoveries from leach solutions solvent extraction/ion exchange, precipitation, cementation, and electrowinning depending on metal types and compounds can be used.

References

Arslan, F., Perek, K. T., Arslan, C., Çuhadar, İ. E., Altun, A. (2022). Studies on Acidic Leaching of Waste Mobile Phones, International Journal of Mineral Processing and Extractive Metallurgy, 7(2): 36-42, doi: 10.11648/j.ijmpem.20220702.11

Birloaga, I., Coman, V., Kopacek, B., Vegliò, F., 2014 An advanced study on the hydrometallurgical processing ofwaste computer printed circuit boards to extract their valuable content of metals. Waste Manag., 34, 2581–2586. doi: 10.1016/j.wasman.2014.08.028

Brandl, H., Bosshard, R., Wegmann, M., 2001. Computer-munching microbes: metal leaching from electronic scrap by bacteria and fungi. Hydrometallurgy 59, 319– 326. Doi: 10.1016/S0304-386X(00)00188-2

Castro, L.A., Martins, A.H., 2009. Recovery of tin and copper by recycling of printed circuit boards from obsolete computers. Brazilian Journal of Chemical Engineering 26 (4), 649–657.

Deveci, H., Yazıcı, E.Y., Aydın, U., Yazıcı, R., Akcil, A., 2010. Extraction of copper from Scrap TV boards by sulphuric acid leaching under oxidizing conditions. In: Proceedings of Going Green-CARE INNOVATION 2010 Conference, 8–11 November, Vienna, Austria, p.45.

Doyle, F.M., 1987. Hydrometallurgical extraction and reclamation. By E. Jackson, Ellis Horwood Limited, Halsted Press, Chichester, 1986, 266 pp., $4 1.95. AIChE J. 33. doi: 10.1002/aic.690330923, 1580–1580.

Goosey, M., Kellner, R. (2002), A scoping study end-of-life printed circuit boards, The Department of Trade and Industry, Shipley Europe Limited.

Goosey, M., Kellner, R. (2003), Recycling technologies for the treatment of end of life printed circuit boards (PCBs), Circuit World, Vol. 29, Iss: 3, pp. 33-37.

Kim, E., Kim, M., Lee, J., Jeong, J., Pandey, B.D. (2010). Leaching behavior of copper using electro-generated chlorine in hydrochloric acid solution. Hydrometallurgy 100, 95–102. doi: 10.1016/j.hydromet.2009.10.009

Madenoglu, H. (2005). Recovery of Some Metals from Electronic Scrap. Ege University, Graduate School of Natural and Applied Sciences, Department of Chemical Engineering, Master Thesis, 138 pp.

Mecucci, A., Scott, K. (2002). Leaching and electrochemical recovery of copper, lead and tin from scrap printed circuit boards. Journal of Chemical Technology and Biotechnology 77, 449–457. doi: 10.1002/jctb.575

Oh, C.J., Lee, S.O., Yang, H.S., Ha, T.J., Kim, M.J. (2003). Selective leaching of valuable metals from waste printed circuit boards. Air & Waste Management Association 53, 897–902. doi: 10.1080/10473289.2003.10466230

Quinet, P., Proost, J., Van Lierde, A. (2005). Recovery of precious metals from electronic scrap by hydrometallurgical processing routes. Minerals Metallurgical Process 22, 17–22.

S. Chatterjee, (2012), Sustainable Electronic Waste Management and Recycling Process, American Journal of Environmental Engineering, 2(1): 23-33. Doi: 10.5923/j.ajee.20120201.05

Silvas, F.P.C., Correa M.M.J., Caldas M.P.K., Moraes V.T., Espinosa D.C.R., Tenorio J.A.S. (2015). Printed circuit board recycling: Physical processing and copper extraction by selective leaching. Waste Management, 46(4). http://dx.doi.org/10.1016/j.wasman.2015.08.030

Tuncuk, A., Stazi, V., Akcil, A., Yazici, E.Y., Deveci, H. (2012). Aqueous metal recovery techniques from e-scrap: hydrometallurgy in recycling. Miner. Eng. 25, 28–37. http://dx.doi.org/10.1016/j.mineng.2011.09.019

Yang, T., Xu, Z., Wen, J., Yang, L. (2009). Factors influencing bioleaching copper from waste printed circuit boards by Acidithiobacillus ferroxidans. Hydrometallurgy 97, 29–32. doi: 10.1016/j.hydromet.2008.12.011

Yazici, E. Y., Deveci, H. (2013) Extraction of metals from waste printed circuit boards (WPCBs) in H_2SO_4-–$CuSO_4$–NaCl solutions, Hydrometallurgy, 139,30–38. doi: 10.1016/j.hydromet.2013.06.018

Yazici, E. Y., Deveci, H. (2014). Ferric sulphate leaching of metals from waste printed circuit boards, International Journal of Mineral Processing, Vol 133, pp 39-45. doi: 10.1016/j.minpro.2014.09.015

Yazici, E.Y., Deveci, H. (2010). Factors affecting decomposition of hydrogen peroxide. XII. International Mineral Processing Symposium (IMPS), 6–8 September, Cappadocia, Turkey.

Leaching Behaviour of Base and Precious Metals During Cyanide Leaching of a Pyrite Concentrate

Oktay Celep[1], Ersin Yener Yazici[1],Hacı Deveci [1]*, Murat Mercimek[2], Alper Gönen[2], Cumhur Demirel[2], Melih Cingöz[2], Hüseyin Kömürcü[2], Serkan Çakmak[1]

[1]1Hydromet B&PM Research Group, Mineral&Coal Processing Division, Mining Eng. Dept., Karadeniz Technical University, 61080, Trabzon, Türkiye

[2] Yıldız Bakır Madencilik A.Ş., 29100, Gümüşhane, Türkiye

*Corresponding author: hdeveci@ktu.edu.tr (Hacı Deveci)

Abstract:

In this study, cyanide leaching tests were carried out to investigate the effects of the concentration of cyanide (1.5-7 g/L NaCN), particle size (d_{80}= 28-55 µm) and solids ratio (40-60%) on the leaching behaviour of gold/silver and other metals (Cu, Zn, Fe) from the concentrate. In the tests, pulp samples (60% solids ratio) obtained from the plant were used. XRD analysis confirmed the dominant presence of sphalerite, pyrite and chalcopyrite minerals in the concentrate. Chemical analysis showed that the concentrate contained 10.6 g/ton Au, 42 g/ton Ag, 0.21% Cu, 3.57% Zn and 31% Fe. The results showed the concentrate is highly refractory considering the low gold recovery (37%) obtained at 1.5 g/L NaCN over 24 h. Increasing the cyanide concentration to 7 g/L improved the gold recovery to 73% at the expense of increased cyanide consumption by 3.64-fold. Copper dissolution varied between 25-32%. Slow and limited copper dissolution was ascribed to its occurrence mainly as chalcopyrite. No significant leaching of zinc was found, indicating the relative inertness of sphalerite in cyanide leaching. Particle size (d_{80}= 28-55 µm) did not significantly affect the gold recovery. Low solids ratios allowed higher gold recoveries i.e., 37% Au vs. 51% Au at 60% and 40% solids ratios, respectively, over 24 h. These results showed that the concentrate is highly refractory and not amenable to cyanide leaching under typical conditions. High cyanide concentrations seem to be required to improve, to some extent, gold extraction conveniently at low solids ratios (40%).

Keywords: *Gold, Cyanide leaching, Pyrite, Cyanicides, Refractoriness*

1. Introduction

Cyanide leaching is a widely used hydrometallurgical technique employed primarily in extracting gold and silver from ores. The process involves the dissolution of these precious metals in an aqueous cyanide solution, forming metal-cyanide complexes that can be easily recovered from pregnant leach solutions by activated carbon adsorption or zinc cementation (Marsden & House, 2006). Due to its numerous advantages, efficiency and cost-effectiveness, cyanide leaching has become the dominant industrial practice for gold extraction from ores (Adams, 2016). However, the presence of cyanicides, substances that consume cyanide without contributing to precious metals recovery, presents a significant challenge to the process's overall efficiency and cost.

Cyanide leaching is not essentially a selective process. Accordingly, known as cyanicides, metals other than gold (copper, zinc, nickel, iron, etc.) dissolve from the carrier minerals in the ore by forming metal cyanide complexes (e.g. $Cu(CN)_2^-$, $Zn(CN)_4^{2-}$, $Ni(CN)_4^{2-}$, $Fe(CN)_6^{4-}$ etc) at varying extents (Table 1) (Wang et al., 2017). This leads to increased cyanide and oxygen consumption and economic and technical problems (Bas et al., 2012, 2015; La Brooy et al., 1994; Marsden and House, 2006). Excessive reagent consumption makes it difficult to recover gold in the leaching circuit due to its interfering effect. In addition, these dissolved metals adversely affect post-cyanide leaching purification (adsorption), metal recovery and tailings rehabilitation processes (Sceresini, 2005). The presence of cyanicides can therefore increase the operational costs of cyanide leaching due to higher reagent consumption and more complex treatment of tailings (Gong et al., 2015).

Tablo 1. Solubility of some minerals in cyanide solutions (Habashi, 1967).

Mineral			**Dissolution in 24 h (%)**
Gold Minerals	Calaverite	$AuTe_2$	Readily soluble
Silver Minerals	Argentite	Ag_2S	Readily soluble
	Cerargyrite	AgCl	Readily soluble
	Proustite	Ag_3AsS_3	Sparingly soluble
	Pyrargyrite	Ag_3Sbs_3	Sparingly soluble
Copper Minerals	Azurite	$2\ CuCO_3.Cu(OH)_2$	94.5
	Malachite	$CuCO_3.Cu(OH)_2$	90.2
	Chalcocite	Cu_2S	90.2
	Cuprite	Cu_2O	85.5
	Bornite	$FeS.2\ Cu_2S.CuS$	70
	Enargite	$3\ CuS.As_2S_3$	65.8
	Tetrahedrite	$4\ Cu_2S.Sb_2S_3$	21.9
	Chrysocolla	$CuSiO_3$	11.8
	Chalcopyrite	$CuFeS_2$	5.6
Zinc Minerals	Simitsonite	$ZnCO_3$	40.2
	Zincite	ZnO	35.2
	Hydrozincite	$3\ ZnCO_3.\ 2\ H_2O$	35.1
	Franklinite	$(Fe, Mn, Zn)\ O.\ (Fe, Mn)_2\ O_3$	20.2
	Sphalerite	ZnS	18.4
	Galemine	$H_2.Zn_2SiO_4$	13.4
	Willemite	Zn_2SiO_4	13.1
Iron Minerals	Pyrrhotite	FeS	Readily soluble
	Pyrite	FeS_2	Sparingly soluble
	Hematite	Fe_2O_3	Practically insoluble
	Magnetite	Fe_3O_4	Practically insoluble
	Siderite	$FeCO_3$	Practically insoluble
Arsenic Minerals	Orpiment	As_2S_3	73
	Realgar	As_2S_2	9.4
	Arsenopyrite	FeAsS	0.9
Antimony Minerals	Stibnite	Sb_2S_3	21.1
Lead Minerals	Galena	PbS	Soluble at high alkalinity

Understanding the behaviour of cyanicides and mitigating their impact is critical for improving the overall efficiency of cyanide leaching processes. This paper explores the mechanisms through which cyanicides affect cyanide consumption, their impact on metal recovery, and potential strategies to minimize their influence, ensuring more sustainable and cost-effective cyanide leaching practices.

In this study, the leaching behaviour of base and precious metals during cyanide leaching of a gold-bearing pyrite flotation concentrate was investigated. The effects of increasing the concentration of cyanide (1.5-7 g/L NaCN), particle size (d_{80}= 28-55 µm) and solids ratio (40-60%) on the leaching behaviour of gold/silver and other metals (Cu, Zn, Fe) from the concentrate were studied.

2. Material and methods

2.1. Material

A sample of gold-bearing pyrite concentrate in the form of pulp (≈60% solids density by weight) was kindly provided by Yıldız Bakır Mining Inc. The size distribution of the concentrate sample was analysed using Malvern Mastersizer Hydro 2000MU. It was found to have an 80% passing size of 28 µm (d_{80}). The chemical composition of the concentrate, which was determined using fire assay and wet chemical analysis methods, is shown in Table 2. The concentrate sample which contains 11 g/ton Au and 46 g/ton Ag, is classified as a high-grade gold-silver material. The XRD analysis of the concentrate sample, which was conducted using a PANalytical X-Pert3 Powder difractometer (Cu Kα 1.54 Å, detector Pixel 1D, 5-140°, 45 kV, and 40 mA) has revealed that pyrite, sphalerite and quartz are the most common phases present, accompanied with galena, chalcopyrite, and clay as minor phases (Fig. 1).

Table 2. The precious and base metal content of the concentrate sample used in this study (Deveci et. al,2023)

Metal	Au, (g/ton)	Ag, (g/ton)	Zn, (%)	Fe, (%)	Cu, (%)	Pb, (%)
Content	11	46	3.06	31.0	0.18	0.02

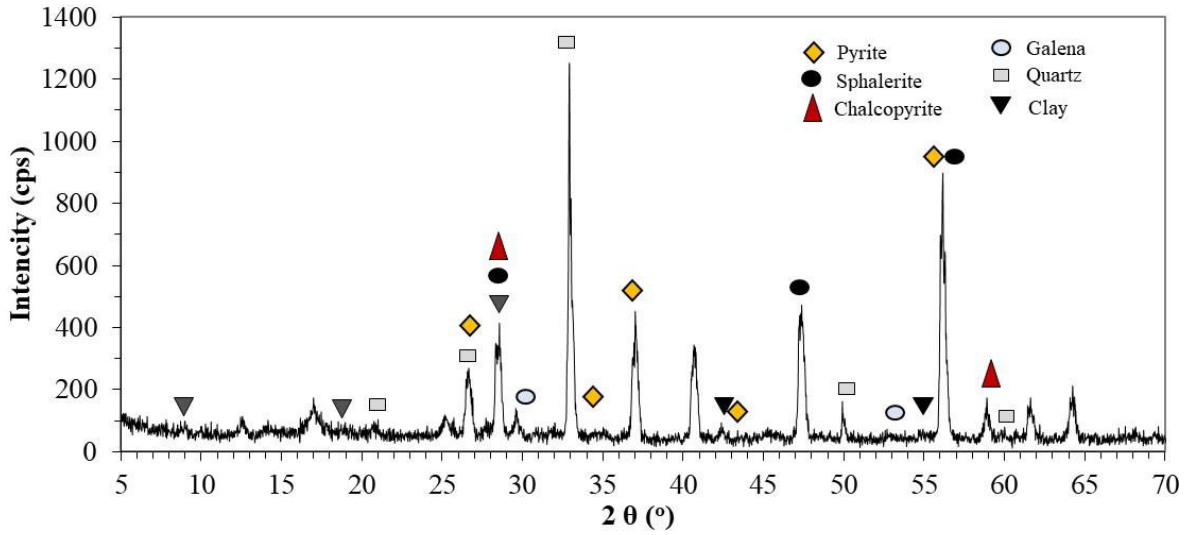


Figure 1. XRD pattern of the concentrate sample used in this study (Deveci et. al, 2023)

2.2. Method

A multi-port experimental set-up was employed to conduct cyanide leaching tests in 1-L glass reactors, each equipped with pitched-blade turbine impellers operating at 600 rpm. Table 3 summarises the fixed experimental conditions, the variables studied such as NaCN concentration, solids ratio and particle size, along with their ranges. During the tests, the initial concentration of cyanide was maintained, if consumed, by adding cyanide from a stock solution (5% NaCN). The cyanide consumption was recorded. Similarly, the pH was also monitored and adjusted if necessary, to control within ~pH 10.5-11 by lime addition.

Samples were collected at predetermined intervals over the course of each test. These samples were centrifuged at 4100 rpm for 5 min. to obtain clear aliquots for analysis. The aliquots were used to monitor the leaching of metals, measure the free CN^- concentration via silver nitrate titration using p-dimethylaminobenzalrhodanine (0.02% (w/w) in acetone) as the indicator, and check the pH.

Upon completion of a leaching test, the solid residues were recovered by vacuum filtration and subsequently analysed for their metal content. The analysis of residue was carried out by wet chemical

analysis and involved digestion with four acids (HCl, HNO_3, $HClO_4$, and HF), before metal concentration was determined usin atomic absorption spectroscopy (AAS). The residual metal content in solids residue, along with the leached metal into solution, was used to establish a mass balance and calculate the extent of metal extraction.

Table 3. Experimental conditions for cyanidation of the flotation concentrate

Parameter	Unit	Value
NaCN concentration	g/L	1.5-3-3.5-5-7
Solid ratio (by weight)	%	40-50-60
Particle size (d_{80})	µm	28-55
Temperature	°C	Room temperature
Leach time	hour	24
Stirring speed	rpm	600
Air flow rate	L/min.	1.5
pH	-	10.5-11

3. Results and Discussion

3.1. Effect of Cyanide Concentration

Fig. 2 illustrates the effect of cyanide concentration on the leaching of Au, Ag, Cu and Zn. Increasing the cyanide concentration improved both gold and silver extractions. To illustrate, increasing the cyanide concentration from 1.5 g/L to 7 g/L enhanced gold extraction significantly from 37% to 73% (Fig. 2). In addition, the dissolution of gold appears to continue, albeit at a slower rate. A similar enhancement was also observed for silver. However, a decrease in the extraction of silver occurred after 8 h at 1.5 g/L NaCN. This may be attributed to the free cyanide concentration (1.5 g/L) not being sufficient for silver dissolution. It is known that sulphide minerals such as pyrite have adsorbing ('preg-robbing') properties in the presence of insufficient cyanide in the medium (Celep et al., 2010).

The dissolution of copper at different cyanide concentrations is also shown in Fig. 2. In general, copper dissolved rapidly at the beginning (first 2-4 hours); thereafter, its rate of dissolution remarkably slowed down. The dissolution of copper, although slow, continues in a time-dependent manner. In other words, it increases as the retention time increases. In the plant case, the long retention times can lead to high copper levels. In this regard, copper concentrations as high as 2000 mg/L have been reported in the plant solutions.

In addition, the data obtained in the leaching tests carried out within the scope of this study showed that the copper dissolution efficiency increased with the increase in cyanide concentration (1.5-7 g/L), while 25% of copper was dissolved at 1.5 g/L NaCN concentration at the end of 24 hours leaching time. It reached 32% at 7 g/L NaCN (Fig. 2). In effect, the relatively slow dissolution of copper from the concentrate is consistent with the occurrence of copper, as chalcopyrite is the only copper phase detected in the XRD analysis (Fig. 1), with its inherent resistance to cyanide leaching (Table 1).

Zinc and iron were found to be dissolved to an insignificant extent (≤0.45% and ≤0.21%, respectively) (Fig. 2). This may be attributed to the relatively low solubility of sphalerite and pyrite minerals, as the dominant zinc and iron phases present, in cyanide solutions (Table 1).

Figure 3 presents the effect of increasing NaCN concentration on its consumption. Cyanide consumption increased from 2.83 kg/tonne to 12.1 kg/tonne (3.3 times) with increasing cyanide concentration from 1.5 g/L to 7 g/L NaCN. The increase is most significant above 3 g/L NaCN.

3.2. Effect of Particle Size

In cyanide leaching processes, it is generally sufficient for high gold recovery to grind the ore in such an extent, as to ensure the contact of precious metals (Au, Ag) with cyanide solutions, without the need for complete liberation of gold grains. However, in refractory gold ores, gold is generally sub-micron sized and is found in association with carrier minerals such as pyrite, and as an inclusion in the mineral

lattice of these minerals. In some pyritic/arsenopyritic refractory gold ores, a limited improvement in gold extraction can be achieved by extremely fine grinding.

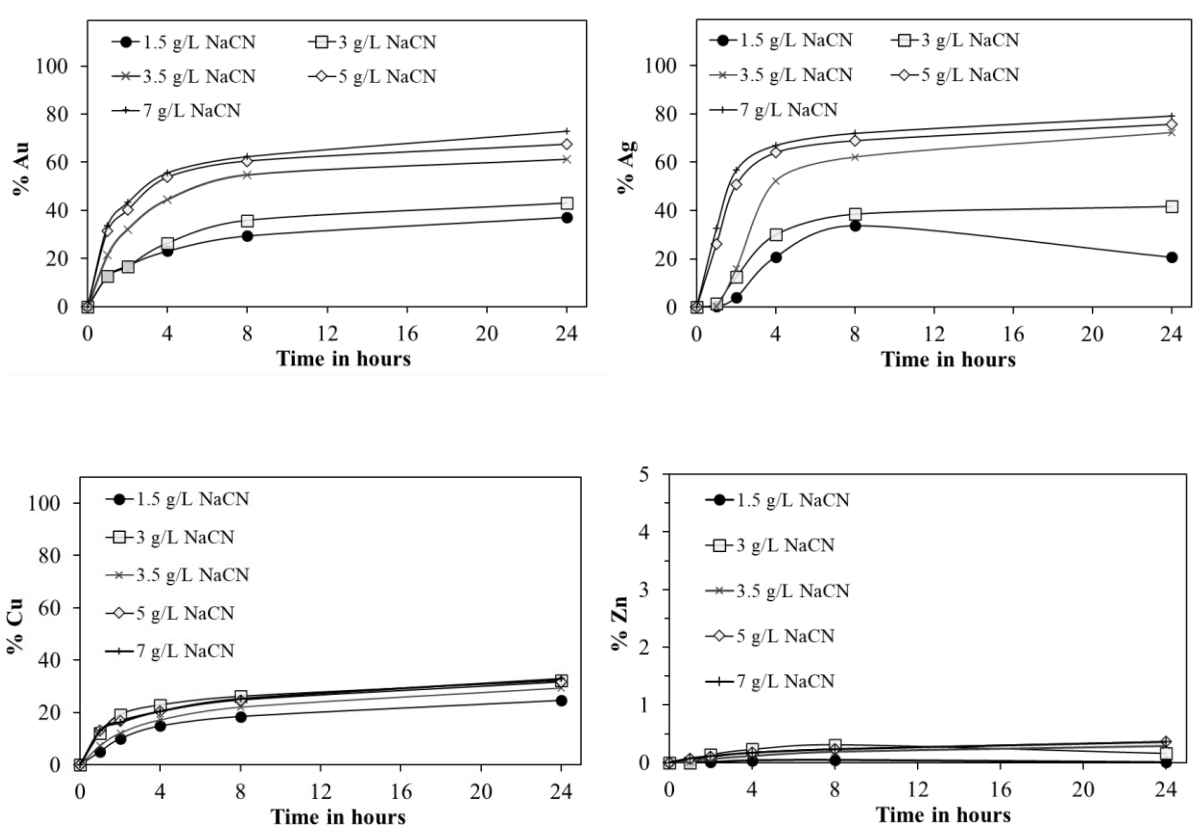


Figure 2. Effect of concentration of cyanide on the leaching of metals

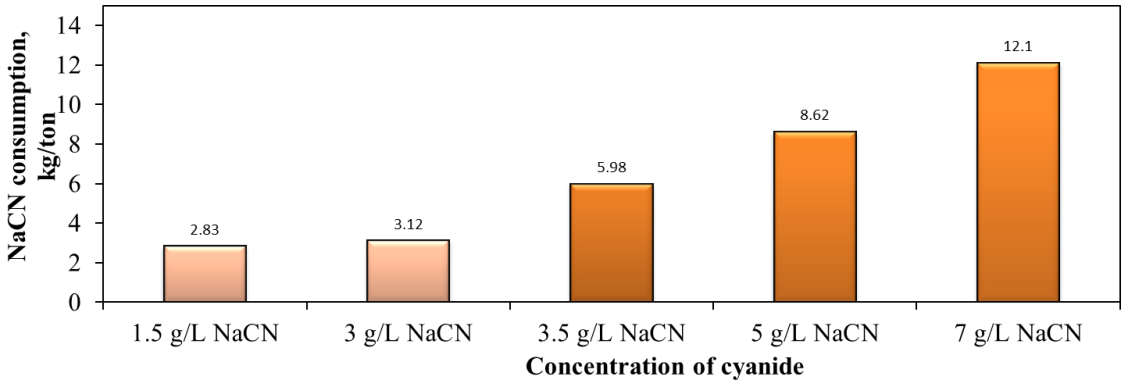


Figure 3. Cyanide consumption at different initial cyanide concentrations (pH 10.5-11, 60% w/w solids, 1.5 L/min air, d_{80}: 28 µm)

To evaluate the effect of particle size on gold extraction, samples taken from the inlet and outlet of the ball mill where fine grinding was performed were subjected to cyanide leaching and the results are shown in Figure 4. The particle size (80% passing size, d_{80}) of the samples taken from the inlet and outlet of the mill was determined as 55 µm and 28 µm, respectively. Cyanide leaching tests were carried out under typical plant conditions at a NaCN concentration of 1.5 g/L. It was observed that gold dissolved faster initially (in the first 8 hours) by reducing the particle size from 55 µm to 28 µm. However, around 7% lower gold leaching efficiency was obtained from finely ground ore at the end of 24 hours of leaching

time (Fig. 4). Similarly, a significant decrease in silver leaching from 68% to 38.7% was recorded when reducing the particle size of the concentrate down to 28 µm (Fig. 4). On the other hand, no change with almost identical leaching profile was observed in copper extraction (24-25%) with decreasing particle size (Fig. 4). In addition, only negligible zinc dissolution occurred (≤0.25%) (Fig. 4) from both fine and ultrafine samples. Reducing size had a negligible effect on cyanide consumption (data not shown).

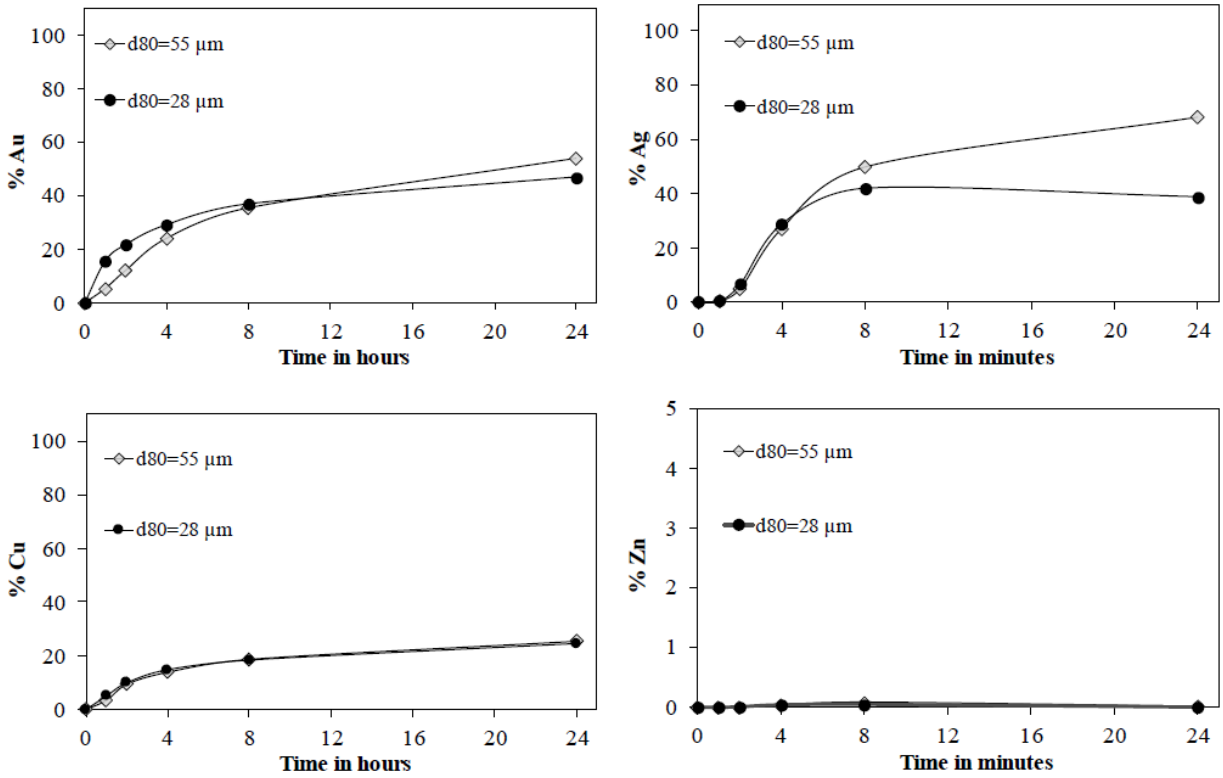


Figure 4. Effect of fine grinding on the extraction of Au, Ag, Cu and Zn from the pyrite concentrate (pH10.5-11, 60% w/w solids, 1.5 L/min air, d_{80}: 28 µm).

These findings suggest that fine grinding does not significantly enhance gold and silver recovery under the tested conditions. Given that fine grinding is an energy-intensive process, a more detailed evaluation of its effects is warranted, particularly at finer particle sizes (<28 µm), where the potential for improved gold and silver extraction could be greater.

3.3. Effect of Pulp Density

In cyanide leaching tests, the effect of the solids ratio on metal recovery was significant, particularly for gold, silver, and copper (Fig. 5). Gold extraction improved from 37% to 51%, as the solids ratio was reduced from 60% to 40% w/w, indicating that a lower solids ratio enhanced the leaching of gold from the concentrate.

A more pronounced increase in silver recovery was observed compared to gold, with its extraction rising significantly from 20% to 72% (Fig. 5). Notably, no delay in silver leaching was detected during the initial stages, and no loss of silver from the solution occurred at solids concentrations of 40-50% w/w, compared to 60% w/w solids. Additionally, copper leaching also increased as solids content decreased, while zinc dissolution remained minimal (≤0.15%) (Fig. 5). Furthermore, lower cyanide consumption was recorded at higher solids ratios (Fig. 6), likely attributed to reduced metal leaching efficiency under these conditions.

The positive impact of reducing solids ratio on metal extraction could be ascribed to improved contact between the cyanide solution and the gold particles, better oxygen transfer, and reduced viscosity of

the slurry at lower solids content. In other words, as the solids ratio increases, reagent and oxygen consumption also rise, and mixing efficiency and oxygen transfer deteriorate due to increased slurry viscosity.

Typically, cyanide leaching plants operate at solids ratios of 40-50%. The current findings suggest that operating at lower solids content (e.g., <50%) could enhance the overall performance of the leaching circuit.

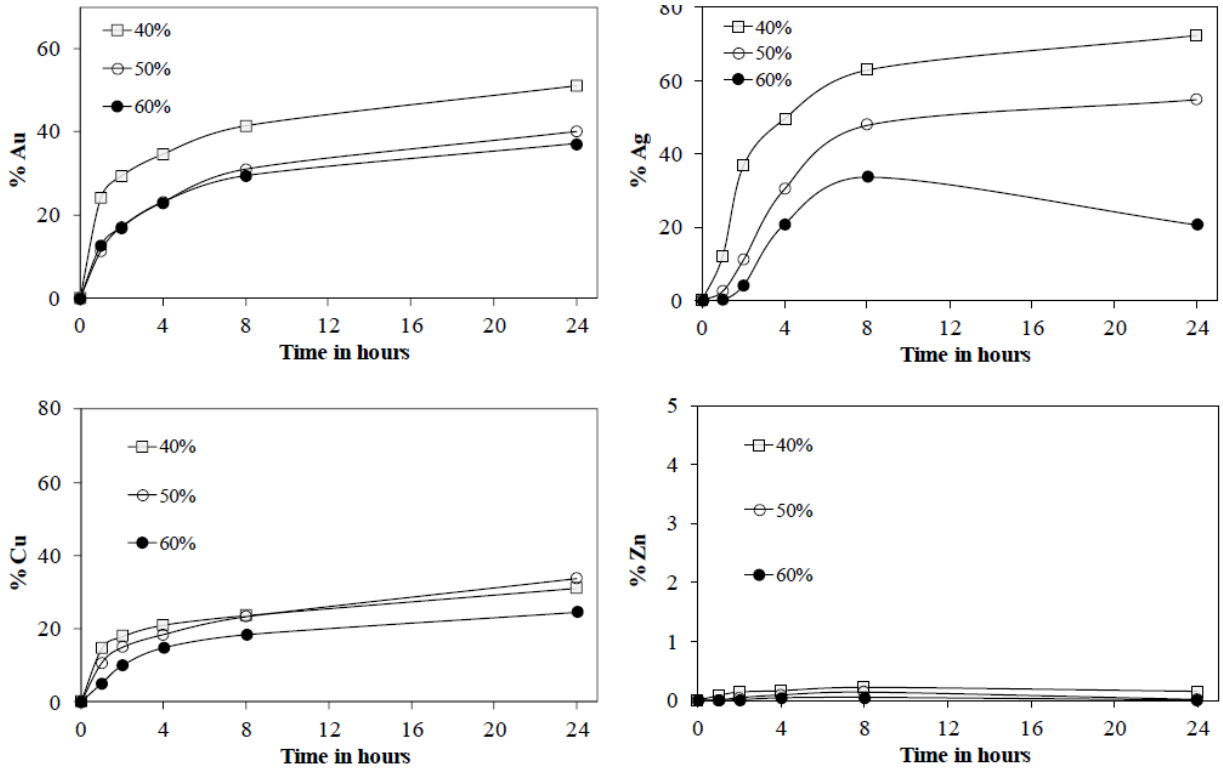


Figure 5. Effect of pulp density on the extraction of Au, Ag, Cu and Zn from the pyrite concentrate (pH10.5-11, 1.5 g/L NaCN, 1.5 L/min air, d_{80}: 28 µm).

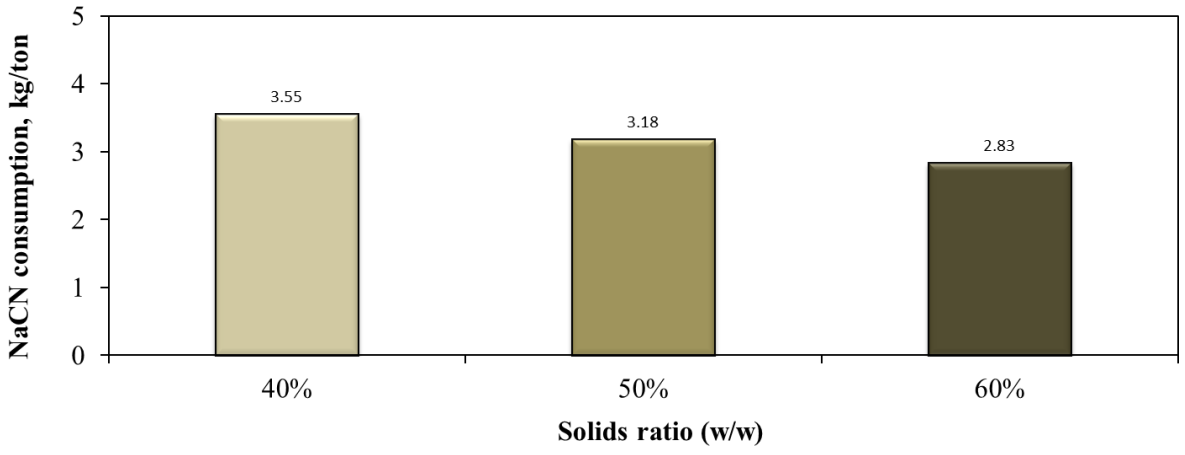


Figure 6. Effect of pulp density on cyanide consumption (pH 10.5-11, 1.5 g/L NaCN, 1.5 L/min air, d_{80}: 28 µm).

4. Conclusions

In this study, the effect of process conditions on the leaching of precious and base metals from a pyrite concentrate was studied to provide insights into the accumulation of cyanicides (copper in particular) in the leaching and adsorption circuit in the plant. The results have revealed that increasing cyanide concentration enhances the extraction of gold and silver. Gold extraction improves significantly when

cyanide concentration is increased from 1.5 g/L to 7 g/L, with gold recovery rising from 37% to 73%. Silver extraction follows a similar trend but exhibits sensitivity to cyanide concentration, particularly with a drop in recovery at low cyanide levels. However, copper dissolution also increases slowly with time and cyanide concentration, while zinc and iron dissolution remains minimal. However, higher cyanide concentrations incur significantly increased cyanide consumption.

Fine grinding improves the initial rate of gold dissolution but does not yield better overall gold recovery after 24 hours. On the contrary, finer grinding reduces silver recovery by a substantial margin. Copper and zinc extractions remain unaffected by particle size reduction. Given the energy demands of fine grinding, these findings suggest that fine grinding to 28 µm may not be justifiable under the current conditions, although ultrafine grinding (<28 µm) could be explored for potential improvements in gold extraction.

Reducing the solids ratio from 60% to 40% significantly enhances the extraction of gold and silver. The most substantial improvement was observed for silver extraction, rising from 20% to 72%. The enhanced leaching of metals by lowering solids ratio could be due to the improved contact between the cyanide solution and the metal or mineral particles, improved oxygen transfer, and reduced slurry viscosity. The results suggest that operating at lower solids ratios (<50%) may improve the performance of the leaching circuit.

Acknowledgments

The authors would like to express their sincere thanks and appreciation to Yıldız Bakır Mining Inc. for the financial support.

References

Adams, M. D. (2016). Gold ore processing: Project development and operations: Elsevier.

Bas, A.D., Yazici, E.Y., Deveci, H. (2012). Treatment of a Copper-Rich Gold Ore by Ammonia Assisted CyanideLeaching. Paper presented at the XXVI International Mineral Processing Congress (IMPC), New Delhi, India.

Bas, A.D., Koc, E., Yazici, E.Y., Deveci, H. (2015). Treatment of copper-rich gold ore by cyanide leaching, ammonia pretreatment and ammoniacal cyanide leaching. Transactions of Nonferrous Metals Society of China, Vol.25, 597-607.

Celep, O., Yazıcı, E.Y., Bölük, D., Deveci, H., Alp. İ. (2010). Evaluation of Preg-robbing Potential of RefractoryGold Ores. Paper presented at the XIIth. International Mineral Processing Symposium), Cappadocia, Nevşehir, Türkiye.

Deveci, H., Yazici, E. Y., Celep, O., Mercimek, M., Demirel, C., Çakmak, S., Cingöz, M. B., Kavlu, Ö. H. & Kömürcü, H. (2023). Effects of Lead Nitrate and Pre-aeratıon on the Deportment of Base/Precious Metals in Cyanide Leaching of a Pyritic Refractory Gold Concentrate. Physicochemical Problems of MineralProcessing, 59(5), 166259. DOI:10.37190/ppmp/166259.

Gong, C., Xu, B., Wang, Y., & Wu, S. (2015). The impact of cyanicides on cyanidation of gold and its treatment methods. Hydrometallurgy, 155, 75-83.

Habashi, F. (1967). Kinetics and mechanism of gold and silver dissolution in cyanide solution. Montana Bureau of Mines Geological Bulletin, No. 59, 1-42.

La Brooy, S.R., Linge, H.G. & Walker, G.S. (1994). Review of Gold Extraction from Ores. Mineral Engineering, 7(10), 1213-1241.

Marsden, J., & House, C. (2006). The chemistry of gold extraction: SME.

Sceresini, B. (2005). Gold-copper ores. Developments in Mineral processing (Mike D. Adams and B.A. Wills (Ed.)): Elsevier (pp. 789–824).

Wang, Y., Zhu, Y., Li, S., & Chen, Y. (2017). Effect of cyanicides in the gold cyanidation process: A review. Minerals Engineering, 105, 64-73.

Cu Zn and Co Recovery from Pyrite Calcine at Atmospheric and Pressure Sulfuric acid leaching: Investigation of Reactions

Mehmet Canbazoğlu [1]*, Arzu Yılmaztürk [1], Fatih Özel [1], Sezer Kabaoğlu [1], Gizem Demirdağ Özel [1]

[1]Etibakır AŞ. R&D Center, Samsun/ TURKEY

*Corresponding author: Mehmet.canbazoglu@etibakir.com.tr (Mehmet Canbazoğlu)

Abstract:

In this study, it was aimed to recover the Cu, Zn and Co contained in Calcine by dissolving it with H_2SO_4 under atmospheric conditions(AAL) and high temperature and oxygen pressure(POX). In this context, pyrite calcine from Eti Bakır Aş. Mazıdağı facility was used. Atmospheric leaching conditions were: leaching temperature 90 ^oC; Acid concentration (75-150 g H_2SO_4/L) and leaching time were taken as 8 hours. Solid/Liquid ratio is fixed and 1/4 is taken. The results reveal that high rates of dissolution occur in the first 2 hours and then the leaching kinetics slow down and reach equilibrium. In optimum conditions; 95% of copper; 91% of zinc and 90% of cobalt could be dissolved, with a acid consumption was 370 kg H_2SO_4 /Ton Calcine.

Despite these results, the results of sulfuric acid under oxidative pressure leaching conditions (220 ^oC; 5 Bar O_2 and 3 hours leaching time) of the Mazidağı facility were found to be close to atmospheric acid leaching conditions. However, during leaching under pressure, iron remains in the leach cake by forming hematite.

In this study, the results obtained during atmospheric and pressure leaching of calcine and the reactions that occur are presented. Additionally, the advantages of these two methods in terms of both metal recovery and economics are discussed.

Keywords: *Calcine, Sulfuric acid, Pressure oxidative leaching, Reactions analysis*

1. Introduction

As is known, massive sulphur ores containing Cu-Zn-Pb have a complex structure and the main gangue mineral is pyrite. However, pyrite can also contain important elements such as Co-Au-Ag in its crystal structure. The Küre-Kastamonu/Turkey ore structure is the most recent example of this. Common practice is to enrich these ores by flotation and, depending on their conditions, produce copper-zinc-lead concentrates and leave the pyrite in the waste. In such a case, the economically valuable elements contained in pyrite, if any, cannot be recovered. This situation was valid for Küre ore, which is recorded to have been operated since the time of the Genoese, until pyrite concentrate was produced from flotation waste and a new roasting + pressure leaching (POX) + solvent extraction (SX) facility was established in Mazıdağı and put into operation in 2018.

Extensive information about the development of Mazıdağı has been presented in recent publications (Canbazoğlu et all., 2019; Haavanlammi et all., 2019). The facility currently produces sulfuric acid from the SO_2 gas formed after burning pyrite and phosphoric acid to be combined with phosphate concentrates and various phosphate-nitrogenous fertilizers. However, cathode Cu and, Zn and Co carbonate can be obtained from calcin formed as a result of roasting of pyrite by applying hydrometallurgical method (POX + SX), and Au and Ag can be obtained from the remaining leach cake by cyanidation process. The remaining result is cake as iron raw material, which can be given directly or as pellets to the iron and steel industry. As a result, unusable pyrite and obtainable elements are recovered and offered to the economy. By utilizing pyrite in this way, there is no waste left in this facility.

Is the leaching process of calcine with sulfuric acid sometimes carried out under atmospheric conditions? It is debated whether it would be better to do it under pressure. In this context, during roasting, the main elements contained in calcine are hematite, magnetite and silica. However, the trace elements that are subjected to the process and desired to be recovered can be found in metallic, sulfur, sulfate and oxide forms. Below are possible reactions (Savikangas et all., 2014; Schlesinger et all., 2011):

Acid leaching reactions of metal oxides can be written as follows (Me: Refers to +2 valued elements):

$$MeO_{(s)} + H_2SO_{4(aq)} \longrightarrow MeSO_{4(aq)} + H_2O_{(l} \quad (1)$$

Acid leaching reactions of metal sulfides can be written as follows:

$$MeS_{(s)} + 2\,O_{2(g)} + H_2SO_4 ,, \longrightarrow MeSO_4 + H_2SO_{4(aq} \quad (2)$$

Me^{+2} (Cu, Co, Zn, Fe) sulfate dissolution:

$$MeSO_{4(s)} \longrightarrow Me^{+2}{}_{(aq)} + SO_4{}^{-2}{}_{(aq)} \quad (3)$$

Me^{+3} (Al, Fe) sulfate dissolution:

$$Me_2(SO_4)_{3(s)} \longrightarrow 2Me^{+3}{}_{(aq)} + 3SO_4{}^{-2}{}_{(aq)} \quad (4)$$

Ferrous iron oxidation to ferric iron:

$$Fe^{+2}{}_{(aq)} + 2H^+{}_{(aq)} + \tfrac{1}{2}\,O_{2(g)} \longrightarrow Fe^{+3}{}_{(aq)} + H_2O_{(l)} \quad (5)$$

Ferric iron precipitation to hematite:

$$2Fe^{+3}{}_{(aq)} + 3H_2O_{(l)} \longrightarrow Fe_2O_{3(s)} + 6H^+{}_{(aq)} \quad (6)$$

Trivalent arsenic oxidation to pentavalent arsenic:

$$As^{+3}{}_{(aq)} + 2H^+{}_{(aq)} + \tfrac{1}{2}\,O_{2(g)} \longrightarrow As^{+5}{}_{(aq)} + H_2O_{(l)} \quad (7)$$

Arsenic precipitation as ferric arsenate:

$$As^{+5}{}_{(aq)} + Fe^{+3}{}_{(aq)} + 4H_2O_{(l)} \longrightarrow FeAsO_{4(s)} + 8H^+{}_{(aq)} \quad (8)$$

Calcine, which is formed as a result of roasting of pyrite concentrates at high temperatures between 650°C and 850°C, contains very complex compounds such as oxide - sulfur - sulfate metallic etc. The dissolution of the desired elements such as Cu-Zn-Co contained in the calcine in sulfuric acid medium occurs according to the reactions summarized above (no. 1 to 8). However, since the oxidation process in leaching under pressure is included in the system with oxygen pressure, ferrous cations are oxidized to ferric cations, and +3-valued arsenic is oxidized to +5-valued compounds.

2. Material And Method

Pyrite Calcine was obtained from Mazıdağı Facility that is using Küre pyrite concentrate including some economical metals. The grain size of the sample is d80 46 microns. Calcine chemical analysis was given in Table 1. The calcine contains significant fractions of Cu Zn Co Fe S and Au and Ag. This material, shows a complex mineralogical structure also. Significant amounts of hematite, magnetite, quarts, gypsum, copper sulphide, pyrite, sphalerite and galena were detected by Outotec (Savikangas et all 2014)(Table 2).

The tests were carried out in the laboratories of ETI BAKIR AŞ R&D Directorate. Atmospherically leaching conditions are as follows: Magnetic mixer and heater with contact thermometer and 1000 ml leaching balloon were used in the tests. The resulting water vapor was controlled by a serpentine back

cooling system placed on top of the balloon. The parameters examined were leaching temperature (50-70-90 oC), And acid concentration(75 -150 g H2SO4/L) and leaching time was taken for 8 hours. The Solid/Liquid ratio is constant and 1/5 is taken. While pressure leaching was realized in 2 lt Parr Autoclave in Mazıdağı Facility leaching conditions as follows: S/L ¼ ; Sample 200 g; H_2SO_4 70 g/L; O_2 over pressure 7 Bar.

Table 1. Chemical Composition of Mazıdağı Calcine

Elements	%
Cu	0.349
Fe	61.34
Zn	0.346
Co	0.778
S	0.58
Pb	0.013
Na	0.035
Ca	0.27
Mg	0.20
As	0.064
Sb	0.004
Au (g/t)	1.5
Ag (g/t)	4.15
Specific gravity (g/cm3)	4.79

Table 2. Mineralogical composition of Mazıdağı Calcine

Determined Minerals	%
Hematite	87.54
Magnetite	7.20
Quarts	3.90
Gypsum	0.74
Cu- Sulphide	0.35
Pyrite	0.19
Sphalarite	0.05
Galena	0.03

3. Experimental Results And Discussion

Leaching test studies conducted under atmospheric (AAL) and pressure (POX) conditions are given and discussed under two separate headings.

3.1. Atmospherically Sulphuric Acid Leaching of Pyrite Calcine

The conditions and results of the dissolution of calcine in atmospheric conditions with acid concentration are given in Table 3 and Figure 1 below. Calcine acid leaching was done at concentrations of 75 – 150 g H_2SO_4/L and for 8 hours. According to these results;

1. As the acid concentration increases, the amount of calcine dissolved by weight also increases. While the total dissolved amount is at the level of 12% when 75 g/L acid is used, the total dissolved amount reaches 23% when 150 g/L acid is used. However, in terms of the amount of acid consumed, when the condition of using 75 g/L acid and 150 g/L acid are compared, the acid consumption per ton of leached calcine increases rapidly and reaches from 174 kg to 370 kg.

Table 3. Effect of Acid Concentration

(S/L ¼ ; Samples 200 g; Leaching temperature, 90 °C; Leaching time 8 hours)

Acid Concentration H_2SO_4 g/L	Total Dissolved %	Dissolutions, %				Acid Consumption (kg/t Calcine)
		Cu	Fe	Zn	Co	
75	12.12	89.40	21.73	87.38	73.94	174.31
100	16.82	93.30	26.00	88.93	84.87	239.26
125	14.70	94.01	24.88	89.37	87.95	309.02
150	23.65	95.35	32.02	91.74	90.73	370.85

2. Depending on the acid concentration, in parallel with the increase in the total dissolved amount from calcine, the valuable elements copper, cobalt and zinc found in calcine are also dissolved. In the case of increasing the acid amount from 75 g/L to 150 g/L; Copper dissolves from 89.40% to 95.35%, Cobalt from 73.94% to 90.73%, Zinc from 87.38% to 91.74%, while Iron dissolves from 21.73% to 32.02%.

3. Depending on the acid concentration (from 75 g/L to 150 g/L), the dissolved copper and zinc ratios are very close to each other and partially increase as the amount of acid increases, while cobalt and iron are more effected and soluble at higher acid concentrations.

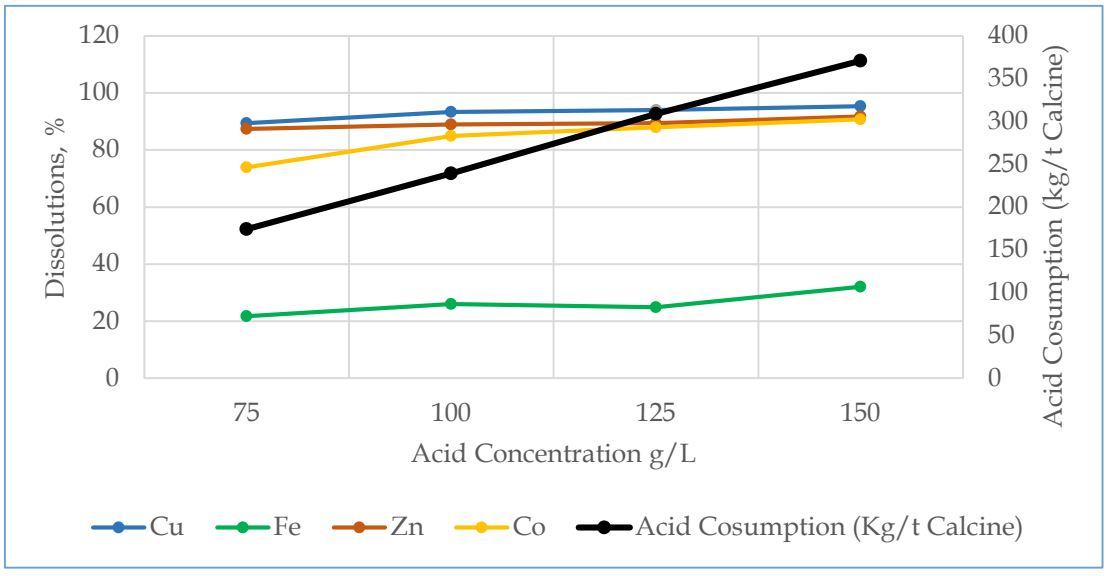


Figure 1. Effect of Acid Concentration

4. It was concluded that it would be appropriate to use 125 g/L H_2SO_4 as the optimum acid concentration, both to dissolve less iron and to consume less acid for determining leaching time tests.

Atmospherically leaching time is very important for to compare with pressure leaching and 2, 4, 6 and 8 hour leaching times were chosen in tests with conditions given in Table 4 and Figure 2 below;

1. Depending on the leaching time, copper, zinc and cobalt dissolution also partially increases. On the other hand, the dissolved iron rate was not affected by the leaching time during the 8-hour leaching period examined and was dissolved at a rate of 25%.

Table 4. Effect of Leaching Time

(Acid Concentration 125 g H_2SO_4/L; S/L 1/4; Samples 200 g; Leaching temperature, 90 °C)

Leaching Time hours	Total feed Dissolved %	Dissolutions, %				Acid Consumption (kg/t Calcine)
		Cu	Fe	Zn	Co	
2	N.D	88.63	24.67	85.61	76.54	N.D
4	N.D	91.94	25.77	87.49	83.68	N.D
6	N.D	92.97	25.12	88.12	86.46	N.D
8	14.70	94.01	24.88	89.37	87.95	309.2

N.D: Not determined

2. At the end of the leaching time of 2 hours, copper and zinc from calcine were significantly dissolved (Copper 88%, Zinc 85.61%), while cobalt was remained lower at a yield of 76.54%.

3. Copper, zinc and cobalt dissolution reached acceptable values after 8 hours of leaching: 94% copper, 89% zinc and 88% cobalt. Acid leaching under atmospheric conditions can only reach acceptable dissolution efficiencies under long-term leaching and concentrated acid use conditions.

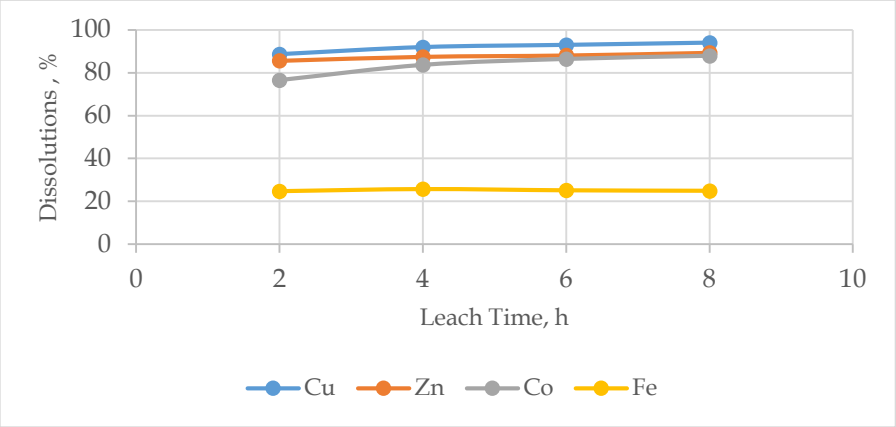


Figure 2. Effect of Leaching Time

3.2. Pressure Sulphuric Acid Leaching of Pyrite Calcine

Leaching application of calcine in sulfuric acid medium under oxygen pressure(POX) in Eti Bakır AŞ, Mazıdağı Facilities started in 2017. The application continues successfully (Canbazoğlu et al., 2019; Haavanlammi et al., 2019). Laboratory POX test results performed under facility conditions are given in Table 5 and Figure 3. Accordingly;

Table 5. Pressure Leaching of Mazıdağı Calcine: Effect of Leaching Time

(Leaching Conditions: S/L ¼ ; Sample 200 g; H_2SO_4 70 g/L; O_2 Over Pressure 7 Bar)

Leaching Time hours	Total feed Dissolved %	Dissolutions, %					Acid Consumption (kg/t Calcine)
		Cu	Fe	Zn	Co	S	
1.5	N.D	87.86	6.44	93.49	88.79	N.D	N.D
2	N.D	93.00	4.96	93.49	88.79	N.D	N.D
3	9.87	93.03	5.50	93.23	88.44	39.39	184.67

N.D: Not determined

1. Current Mazıdağı Facility POX results and laboratory POX test results were highly compatible. Copper, cobalt and zinc dissolution efficiencies are the same. However, it is seen that not all of the iron was converted into hematite and therefore 5% remained in the leach solution. This rate is much lower in the facility and is due to the pre-leaching processes carried out before autoclaving.

2. Apart from copper, it has been observed that 1.5 hours of leaching time for zinc and cobalt provides maximum dissolution under oxygen pressure laboratory test.

3. Pressure leaching results show that after 3 hours of leaching, copper was dissolved with 93.03%, cobalt with 88.44% and zinc with 93.23% efficiency. The amount of acid consumed was 184.67 kg/t calcine.

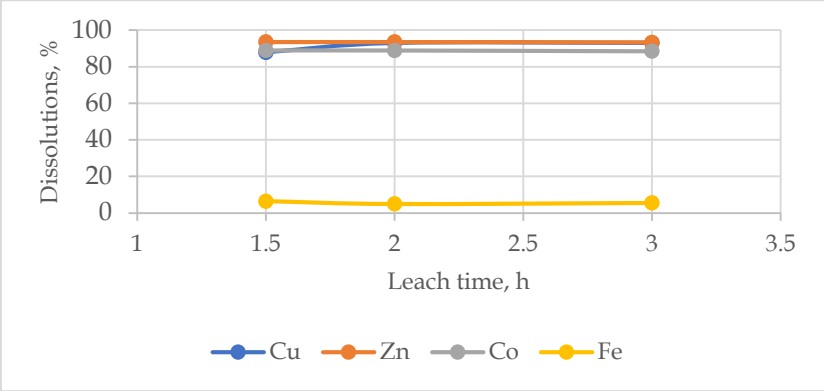


Figure 3. Pressure Leaching of Mazıdağı Calcine: Effect of Leaching Time

4. Conclusions

The leaching evaluation of calcine using sulfuric acid under atmospheric (AAL) and oxygen pressure (POX) is summarized in Table 6 below. According to these evaluation results, the most important advantage of using POX is that the iron dissolved in the leaching stage is oxidized and converted into hematite and precipitated, and therefore, it does not cause metal loss since the impurities in the pregnant solution are reduced.

Table 6. AAL vs POX

Leaching	Elements dissolution	Leach Process	
		Atmospherically (AAL)	Pressure (POX)
	Cu	Close value-Same	Close value-Same
	Co	Close value-Same	Close value-Same
	Zn	Close value-Same	Close value-Same
	Fe	More	Very low
	Time	Too long	1-2 hours
	Acid Consumption	1/3 more than POX	185 kg/t Calcine
	Oxygen	Any	Is being used
Pregnant solution purification	Iron ions	Ferrous iron needs to be oxidized and all iron removed	After copper SX, iron, aluminum and others can be removed
	Filtration	Difficult, (larger filtration group)	Easier
	Metal loss	Losing some copper	Any

Acknowledgments

The authors acknowledge ETİ BAKIR Company Bosses Mr. Şeref CENGİZ and Mr. A. Osman CENGİZ, and Our Research and Developing Center Management for giving us their support during this study.

References

Canbazoğlu, M., Kayışoğlu, E., Şengül, B., & Laitala, H. (2019). Pressure leaching and solvent extraction of Cu-Co-Zn at Mardin Mazıdağı-Turkey: Calcine processing plant, IMPC-Eurasia, 1st Regional Mineral Processing Conference, 3 Oct- 2 Nov., Antalya-Turkey, pp 1004-1015

Haavanlammi, K., Laitala, H.,& Canbazoğlu, M.,(2019). Pressure leaching of copper-cobalt-zinc containing calcine with the Outotec pressure oxidation process, COM Copper, Vancouver- Canada, 20 August.

Savikangas,J., Ekman. E., Kravtsov, T., Vesa, L., & Huuhilo, T., (2014), Mazıdağı Test Work for Recovery of Co Cu Au and Ag from Calcine, Outotec Research Center,Pori, Confidential report, 14047-OCR-T, June 193 pages.

Schlesinger M.E., King M. J., Sole K. C., & Davenport W. G.,(2011) Extractive Metallurgy of Copper, FİFTH EDITION, Elsevier, 417 pp, 89-110

Optimization of Alkaline Pre-Treatment in Zarshuran Gold Mine for Enhancing Gold Recovery

Seyed Hossein Hashemi [1], Ziaeddin Pourkarimi [1], Faraz Soltani [2], Qolamreza Parvareh [1], Mehdi Rahimi [1]

[1]Iran Mineral Processing Research Centre (IMPRC)

[2] Arak University of Technology

*Corresponding author: rahimi.mehdi@imprc.ir (Mehdi Rahimi)

Abstract:

The Zarshuran gold mine is one of Iran's significant gold reserves. This ore is refractory due to sulfide and arsenic phases that trap gold and increase chemical consumption. To mitigate these effects and release the encapsulated gold, an alkaline pre-treatment is used at 70-80°C with ammonia, lime, sodium chloride, and aeration. this process typically takes up to 36 hours and occasionally extends to 72 hours. This study aims to optimize the operational parameters of this pre-treatment process.

Initially, sampling was conducted from 32 extraction steps of open pit mine, in a grid pattern. All samples were characterized and classified into four types based on sulfur content. High-sulfur samples from the mine were used for laboratory-scale optimization tests of the oxidation process parameters. One of the key parameters examined was the aeration rate and bubble size. Previous experiences have suggested that nano-bubbles are effective in flotation processes, leading to the hypothesis that bubble size could also impact oxidation processes. However, no research in Iran has previously investigated the effect of bubble size on oxidation. A micro-nanobubble generator was used to reduce bubble size in a closed system with other additives. Results showed that the use of micro- reduced oxidation time by 20% compared to laboratory tests and by 45% compared to industrial conditions. Additionally, with a 2.5% increase in the gold dissolution rate in the cyanidation process, the gold dissolution reaches 79.5%, which is nearly the threshold for the dissolution of non-refractory gold.

Keywords: Refractory Gold, alkaline oxidation, nano-bubbles

1. Introduction

The cyanidation process, combined with gold adsorption onto activated carbon, is the most effective method for extracting gold, accounting for about 92% of global extraction in the past two decades. However, when gold is associated with minerals like arsenic, antimony, tellurium, mercury, and others, only a small portion of gold dissolves during cyanidation. These ores are known as "refractory gold ores" due to their resistance to standard cyanidation. This issue is common in sulfide gold ores, where gold is trapped within the sulfide mineral structure, making direct cyanidation ineffective. Therefore, a pre-treatment process is required to release the gold for leaching(Marsden,J, 2006;Adams,2016) .

Various pre-treatment methods for sulfide ores include pre-aeration, chlorination, roasting, pressure oxidation, bio-oxidation, ultra-fine grinding, and chemical oxidation(Li et.al 2009). This study investigates the use of alkaline oxidation before cyanide leaching and its impact on the cyanidation process. It examines the factors influencing sulfide ore oxidation to maximize gold recovery during cyanidation. The Zarshuran gold mine in Takab city, West Azerbaijan,Iran, serves as the case study for this researh.

1.1. Zarshuran gold ores

The Zarshuran gold deposit, is the largest gold reserve in Iran and the Middle East, with over 105 tons of gold. The Zarshuran gold processing plant includes seven main units and several auxiliary units designed to produce 3,060 kilograms of gold and 1,278 kilograms of silver annually in its first phase.

These units cover crushing, homogenization, grinding, oxidation, leaching, elution, gold recovery, and filtration, along with a tailings dam(Soltani et al.2019).

The mine features various ore types with significant variations in sulfide mineral content and associated gangue. Due to this diversity, a practical classification system for the ore is challenging. Consequently, ore types are classified based on the amownt of gold-sulfide minerals. Despite its large reserves, exploitation has been delayed due to the refractory nature of the ore. The plant has struggled to reach its expected capacity and recovery rates. Research findings aim to identify factors affecting low recovery rates and enhance plant performance(Soltani et al.2019).

1.2. literature review

Due to the decrease in oxidized gold resources over the past century, recent research has focused on recovering gold from refractory ores, which have low metal recovery rates and high chemical consumption when using traditional processing methods. The Zarshuran gold mine in Iran is a high-sulfide deposit with low gold recovery because the gold is encapsulated in sulfide minerals. To improve recovery, pre-treatment methods like chemical or biological oxidation or alternative leaching agents are needed (Marsden,J, 2006;Adams,2016). Studies by Mehrabi classify the Zarshuran deposit as a Carlin-type ore, where gold is primarily associated with minerals like orpiment, realgar, and arsenopyrite, making extraction challenging (Mehrabi et al.2006). Aazami examined the impact of various parameters on gold recovery using a thiosulfate solution, finding that while certain conditions improved recovery, the maximum gold recovery was still below 70%, which is not economically feasible for the Zarshuran deposit (Aazami et al.2014). Soltani studied the impact of oxidative pre-treatment (using ammonia) and lead nitrate addition on the cyanide leaching of refractory Zarshuran gold. Using lead nitrate improved gold recovery by up to 10% and that oxidative pre-treatment reduced the negative effects of arsenic and the need for lead nitrate. The oxidation process converts arsenic to arsenate, which forms a stable precipitate with calcium, reducing cyanide consumption and thus lowering costs (Soltani et al.2019). In the study by Mahmoodi and Azizi, alkaline oxidation pre-treatment for refractory Zarshuran gold was investigated, focusing on the effects of solution pH, aeration rate, stirring speed, temperature, and oxidation time (Mahmoodi and Azizi 2018). None of these studies examined the effect of air bubble particle size. This research will investigate this effect.

2. Material and methods

2.1. Sampling and sample conditions

In the study, sampling began on March 17, 2020, and lasted for one month, covering all levels of the Zarshuran mine from 2680 meters to 2390 meters elevation. Samples were collected from 30 benches, with a total of 7,500 kilograms gathered in 380 individual samples. Sampling distances ranged from 5 to 190 meters, and samples were taken only from the bench walls to avoid contamination and ensure they were fresh and unoxidized.

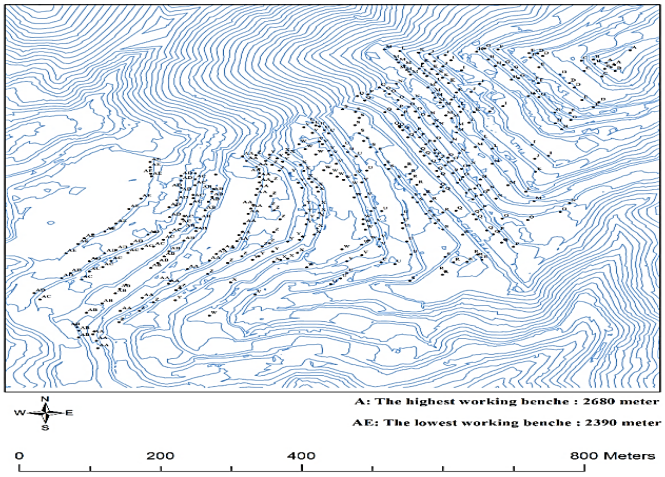


Figure 23: Coordinates and Specifications of Sampling Conducted on the Extraction Benches at Zarshuran Mine

The 380 samples collected from the Zarshuran mine underwent a two-stage crushing process. Initially, a 6-mesh screen (3.35 mm) was used to segregate smaller particles and prevent over-crushing, thereby enhancing efficiency. In the first stage, large samples were manually fed into a Fritsch jaw crusher. After initial crushing, particles larger than 6 mesh were further processed using an Allis Mineral Systems cone crusher, resulting in all samples being reduced to a particle size of less than 3.35 mm. Subsequently, the samples were categorized, and half of each category was combined to produce a representative sample for each type. These were designated as ZT1 to ZT4 for types 1 to 4, respectively. For the analysis of major elements, the alkaline fusion method and the XRF method were employed. Trace elements were analyzed using the ICP-MS method and ICP-OES. Gold content was determined using the Fire Assay method.

2.2. Oxidation Method

Hydrodynamic cavitation using Venturi tubes was employed to produce MN-b (Micro-Nano bubbles) for better distribution and mixing of Air in the Solution. Details of MN-b generation is described in our previous work, so this study provides only a brief overview. Figure 2 illustrates the connection of the Venturi tube to the oxidation circuit in our laboratory. A slurry, with air added from a compressor, is delivered to a mechanically stirred closed oxidation cell via a centrifugal pump. Between the pump and the Venturi tube, the solution passes through a linear mixer (for generating millimeter-sized air bubbles), a water flow meter, and a set of manometers (to monitor the pressure of the incoming flow to the cavitation tube). The Venturi tube, which contains the "air-oxygenated solution from the Venturi tube outlet," is directly connected to a laser particle size analyzer (LPSA, Malvern Mastersizer 2000) for online measurement and analysis of bubble size according to BS ISO 13320_09 standards. The LPSA measurements involve initially measuring the background of the dispersed medium. Then, with the addition of the sample, particle or bubble size is measured in the two-phase environment. Measurements are configured to automatically repeat over time, with over 200 continuous repetitions during these tests, and the average size is reported. Additionally, the refractive index (RI) is a critical optical parameter for determining particle and bubble sizes. In all experiments, the RI of the bubble sample (air) was 1, and the RI of the dispersing water was 1.33. Two Venturi tubes with inlet diameters of 2.2 mm and 1.5 mm were used in parallel configuration for circulating the aerated solution or slurry to achieve stable NB production and reproducible results when needed (z.pourkarimi et.al 2021).

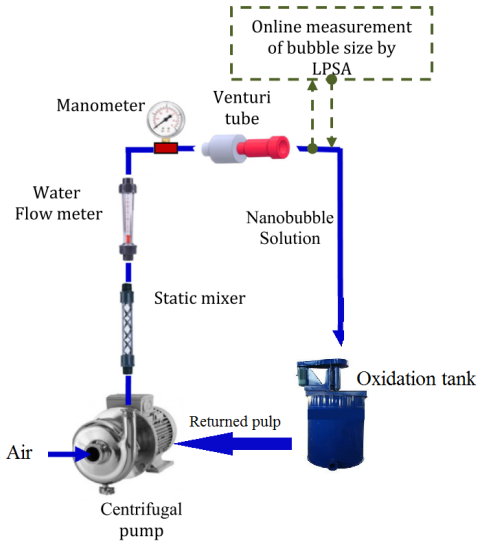


Figure 24: Schematic diagram of the laboratory micro-nanobubble oxidation

The laser particle size analyzer indicated that the particle size of MN-b was measured at 87 micrometers. This measurement reflects the average diameter of the particles, which is crucial for understanding the material's behavior and performance in various applications. The accuracy and precision of the laser particle size analyzer are essential for ensuring that the particle size data is reliable and consistent.

3. Results and Discussion

The summary of the chemical analysis results for the four different sample types from the Zarshuran mine indicates that the gold content is 1.6, 3.6, 3.87, and 5.69 grams per ton for types 1 to 4, respectively.

Table 13: Chemical analysis of representative samples of 4 types

Composition	ZT1	ZT2	ZT3	ZT4	Composition	ZT1	ZT2	ZT3	ZT4
Au (g/t)	1.6	3.6	3.87	5.69	MnO (%)	0.16	0.1	0.07	0.15
SiO2 (%)	12.58	30.19	48.57	41.09	P2O5 (%)	0.06	0.13	0.12	0.2
CaO (%)	42.97	28.92	12.81	14.87	Na2O (%)	0	0.06	0.08	0.06
Al2O3 (%)	2.54	5.84	9.09	7.64	BaO (%)	0	0.22	0.1	0.13
Fe2O3 (%)	2.91	4.04	4.52	5.06	Zn (ppm)	5461	7141	4671	3646
MgO (%)	1.49	1.59	3.16	2.86	Cu (ppm)	54	84	129	95
As (%)	0.61	1.32	1.52	3.38	Ag (ppm)	1.28	2.01	3.99	1.92
SO3 (%)	0.33	0.98	3.04	3.4	Ni (ppm)	170	106	40	33
K2O (%)	0.58	1.4	2.27	1.74	Pb (ppm)	300	668	908	573
TiO2 (%)	0.18	0.75	0.44	0.55					

Types 1 and 2 have higher calcium content, while types 3 and 4 have higher silicon content. Calcite is the most abundant mineral in types 1 and 2, whereas quartz is the most abundant in types 3 and 4(XRD methode). Arsenopyrite, as a secondary mineral with a frequency of 2 to 10 percent, is consistent across all types. Additionally, orpiment and pyrite increase with each type, appearing as secondary or minor minerals in types 3 and 4.

The gold leaching efficiency in the stirred leaching tests for types 1 to 4 is 92.6%, 91.7%, 75.7%, and 41.3%, respectively, and in other tests, it is 94.48%, 93.1%, 74.08%, and 35.31%, respectively. Cyanide

consumption is relatively lower in types 1 and 2, around 1.12 and 2.09 kg/t, but exceeds 5 kg/t in types 3 and 4. These results indicate that all four types exhibit refractory characteristics, necessitating optimization to reduce cyanide consumption and increase leaching efficiency. This is especially true for types 3 and 4, which both require significant improvement.

To investigate the effect of oxidation under the current plant conditions and nano-micro bubbles on leaching efficiency, type 4 was selected as the most refractory sample. Initially, nine experiments were conducted under typical Zarshuran plant conditions to optimize parameters such as aeration rate (1 to 5 liters per minute), solid percentage (25 to 35%), time (16 to 24 hours), and temperature (40 to 80 °C). The pH of all samples was adjusted to 11.5–11.7 using hydrated lime. Additionally, 15 grams per kilogram of ammonia and 20 grams per kilogram of NaCl were added to all samples. After completing the oxidation tests, all pulp samples were cyanided under identical conditions for 24 hours, using 3000 grams of cyanide per ton of solid at a solid percentage of 35%. Finally, a kinetic test was performed under conditions similar to the conventional plant setup to assess the impact of nano-bubble production on enhancing the gold oxidation-dissolution process.

Table 14: Conditions and results of gold dissolution with conventional oxidation conditions of the plant

Std	Run	Air (Lit/min)	Solid Ratio (%)	Time (h)	Temperature (°C)	Au Leaching efficiency (%)
4	1	2	25	20	80	77.24
3	2	1	35	24	80	75.59
1	3	1	25	16	40	55.27
8	4	5	30	16	80	75.4
2	5	1	30	20	60	68.87
9	6	5	35	20	40	67.76
7	7	5	25	24	60	77.09
5	8	2	30	24	40	68.08
6	9	2	35	16	60	70.05

The proposed software model is a linear model with an F-value of 10.40 and a P-value of 0.0217, indicating the model's statistical significance. Among the four tested parameters, oxidation time and temperature have a more substantial effect compared to aeration rate and solid percentage. This is also reflected in the software's suggested equation, where the coefficients for factors C (oxidation time) and D (temperature) are significantly higher than those for parameters A (aeration rate) and B (solid percentage) when the parameters are coded.

Table 15: Model conditions provided by experiment design software

	Sum of		Mean	F	p-value	
Source	Squares	df	Square	Value	Prob > F	
Model	352.9413	4	88.2353	10.4025	0.0217	significant
A-A	53.95201	1	53.9520	6.3607	0.0652	
B-Solid Ratio	2.406667	1	2.4067	0.2837	0.6225	
C-Time	66.9336	1	66.9336	7.8911	0.0484	
D-Temperature	229.6491	1	229.6491	27.0745	0.0065	
Residual	33.92848	4	8.4821			
Cor Total	386.8698	8				

Based on the fitted model, the following empirical equation for gold dissolution is presented:

Au Recovery= +71.07 + 2.88A +0.63B +3.34C + 6.19D (1)

Optimal conditions for maximum gold recovery were determined as follows:

- Aeration rate: 4.25 liters per minute
- Pulp solid percentage: 35%
- Oxidation time: 24 hours
- Oxidation temperature: 65°C

Figure 3 illustrates the effect of time on the gold oxidation process and consequently, the gold dissolution efficiency achieved through cyanidation.

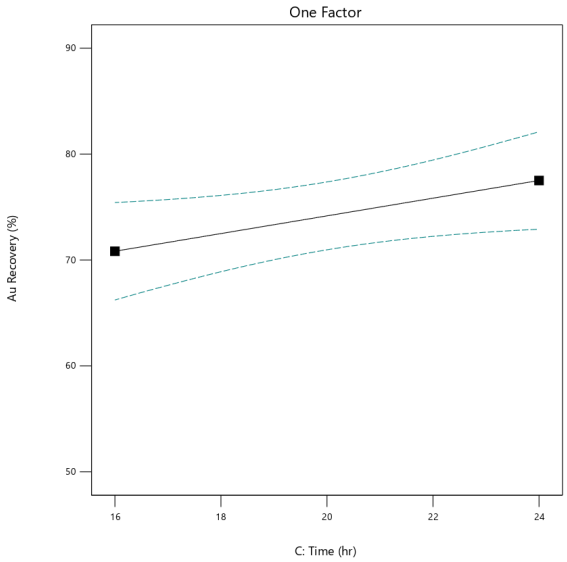


Figure 25: Effect of time on the Gold recovery

The summary of the results presented in the figure 3 is shown in Table 4. According to the presented results, under the usual plant conditions, by increasing the oxidation time from 16 hours to 24 hours, the gold dissolution efficiency increased from 70.80% to 77.5%.

Table 16: The summary of the results presented in the figure related to the effect of time on the oxidation process (oxidation temperature: 70 degrees Celsius, 30% solids, and an aeration rate of 3 liters per minute).

Row	Time (hour)	Gold Recovery (%)
1	16	70.8
2	18	72.6
3	20	74.0
4	22	75.9
5	24	77.5

The other conditions remained constant at an aeration rate of 3 liters per minute, 30% solids, and a temperature of 70°C. Under the same conditions, the tests were repeated using a nano-bubble generator, and the results are presented in the graph below.

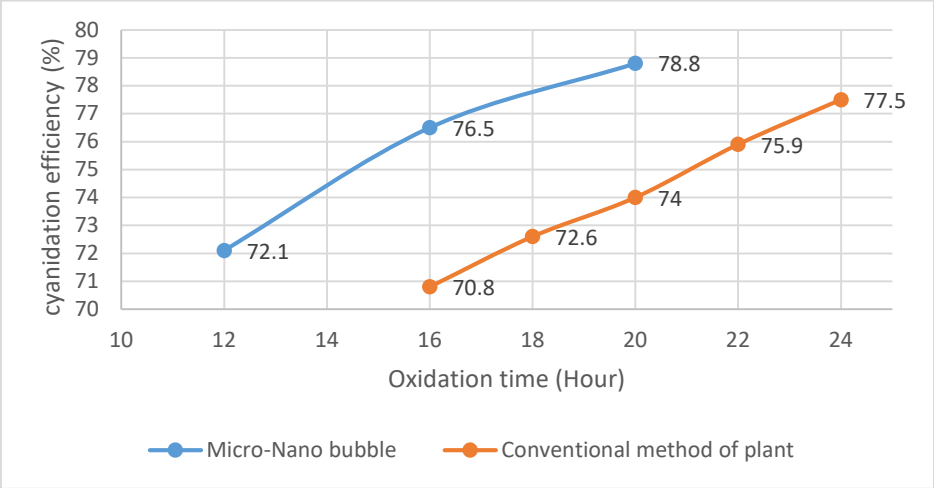


Figure 26: chart comparing gold recovery using two different methods (the conventional method used in the plant and the method of increasing air injection through micro-bubble generation) (oxidation temperature: 70 degrees Celsius, 30% solids, and an aeration rate of 3 liters per minute).

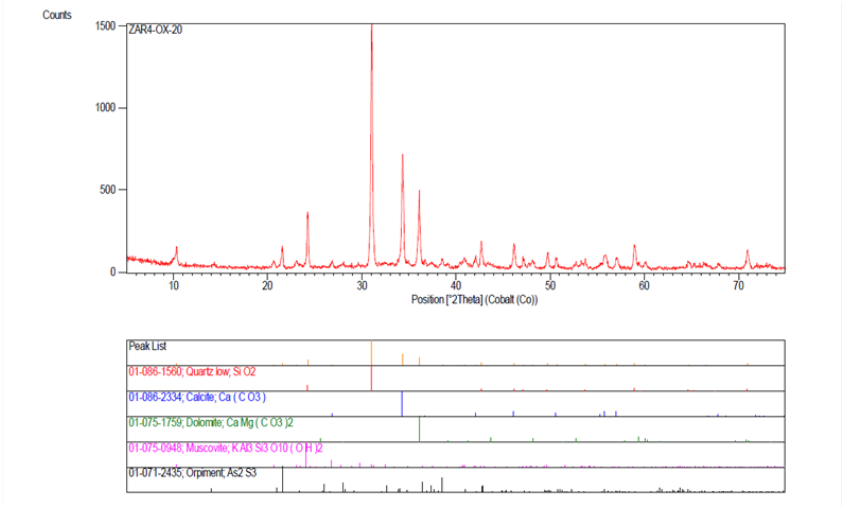


Figure 27: XRD diagram of oxidation test residue using micro-nanobubbles

As shown in the figure 5, when nano-bubbles are used (under conditions similar to those of a conventional reactor), the oxidation kinetics of gold have significantly increased. The creation of nano-bubbles is not a complex or costly process, which makes it feasible for industrial-scale implementation.

Figure 5 shows the XRD graph of the sample after 20 hours of oxidation. As indicated in the figure, most of the sulfide minerals in the sample have been removed, and pyrite, as the main component of the sample, is absent in the graph. This indicates the success of the oxidation process using nano-bubbles.

4. Conclusion

This research revealed that the Zarshuran gold ore is classified as refractory. Furthermore, the study found that employing the micro-nano bubble oxidation method significantly improves the dissolution of gold in the cyanidation process, achieving higher gold recovery in a shorter period. The enhanced efficiency of the process is primarily due to the smaller size of the air bubbles generated by this method. Smaller bubbles lead to improved selectivity and more uniform distribution of air bubbles within the pulp. This improved dispersion enhances the interaction between the cyanide solution and the gold particles, thereby facilitating more effective gold extraction during cyanidation.

Acknowledgments

This project was supported by and conducted at the Iran Mineral Processing Research Centre (IMPRC). We extend our sincere gratitude to IMPRC for their invaluable support and resources, which were essential for the successful completion of this research.

References

Aazami, M., Lapidus, G., Azadeh, A.J.I.J.o.M.P., 2014. The effect of solution parameters on the thiosulfate leaching of Zarshouran refractory gold ore. 131, 43-50. DOI:10.1016/j.minpro.2014.08.001

Adams, M. D. (Ed.). (2016). Gold ore processing: project development and operations. Elsevier.

Li, Q., D. Li, and F.J.H. Qian, Pre-oxidation of high-sulfur and high-arsenic refractory gold concentrate by ozone and ferric ions in acidic media. 2009. 97(1-2): p. 61-66. DOI:10.1016/j.hydromet.2009.01.002

Mahmoodi, F., Azizi, A.J.M.R.E., 2018. Optimizing the alkaline oxidation pretreatment of a refractory gold ore using taguchi orthogonal array method. 5(12), 126516. DOI:10.1088/2053-1591/aae196

Marsden, J., House, I., 2006. The chemistry of gold extraction. SME.

Mehrabi, B., Mohammadzadeh, S., & OliYazadeh, M. (2006). Identification and analysis of gold distribution in Zarshuran gold ore using diagnostic leaching method. Proceedings of the 10th Conference of the Geological Society of Iran, Tehran.

Soltani, F., Marzban, M ,.Darabi, H., Aazami, M., Chegeni, M.H.J.J., 2020. Effect of Oxidative Pretreatment and Lead Nitrate Addition on the Cyanidation of Refractory Gold Ore. 72(2), 774-781. DOI:10.1007/s11837-019-03859-0

Z. Pourkarimi, B. Rezai, M. Noaparast, A.V. Nguyen, S. Chehreh Chelgani,2021. Proving the existence of nanobubbles produced by hydrodynamic cavitation and their significant effects in powder flotation,Advanced Powder Technology, https://doi.org/10.1016/j.apt.2021.03.039.

Effect of refractory ore character on silver recovery by acidified sodium chloride-hypochlorite leaching

Ömer Canıeren [1]*, Cengiz Karagüzel [1]

[1] Kütahya Dumlupınar University, Engineering Faculty, Mining Engineering Department, Kütahya, TÜRKİYE

[2]Affiliation 2

*Corresponding author: omer.canieren@dpu.edu.tr (Ömer Canıeren)

Abstract:

Eti Gümüş Corporation aims to recover silver from different ore formations in the Kütahya-Türkiye region. It has also been contributing to its country's economy by continuing its activities since 1980 in the silver plant, where the ore structure has changed over the years. An average of 85 ppm silver is still recovered from refractory ores such as sulfate, oxide, clayey ores etc., by cyanide leaching. The Eti Gümüş silver plant is also considering making process ore containing 100 ppm silver in the tailings pond. In this study, Kavacıkdere I ore with high quartz, Kavacıkdere II ore with high barite, Aktepe ore with moderately high quartz and the sample taken from the tailings pond were subjected to sodium chloride-hypochlorite leaching separately. The obtained results showed that while the recovery efficiency of Kavacıkdere II ore was 60,47%, silver could be recovered with 55,29%, 31,34% and 23,99% efficiencies for Aktepe, Kavacıkdere I, and tailings pond samples, respectively. Correspondingly, it was determined that Kavacıkdere II ore and Aktepe ore were classified as moderately refractory. In contrast, Kavacıkdere I and tailings dam samples were found to be highly refractory ore.

Keywords: *Silver leaching; sodium chloride; hypochlorite; classification of refractory ores*

1. Introduction

There has been a growing interest in the consumption of silver metal in the world. At the same time, hydrometallurgical processes are generally used to recover silver metal. Hydrometallurgy is a technique within the field of mineral processing, the obtaining of metals from their ores. Hydrometallurgy involves the use of aqueous solutions for the recovery of metals from ores, concentrates, and recycled or residual materials. In addition, hydrometallurgical processes consist of four basic stages such as pre-leaching preparation, dissolution, solid-liquid separation and recovery from solution (Habashi, 2009).

In the dissolution of precious metals by hydrometallurgical methods, cyanide reagent is mainly preferred worldwide because of its effective leaching performance and being more economical (De Michelis et al., 2013; Estay et al., 2013). Solvents with effective leaching performance and lower toxicity include thiosolvents; [thiosulfate ($S_2O_3^{-2}$), thiourea ($CS(NH_2)_2$), thiocyanate (SCN^-)], and halogens; [chloride (Cl_2), bromide (Br_2), iodide (I_2)]. Among these leaching methods, thiosulfate is more costly than cyanide due to its high reagent consumption and high oxygen requirement. Likewise, thiourea has higher reagent consumption than cyanide.

In addition, gold/silver recovery from thiourea leach solutions is quite difficult. Thiocyanate, despite its fast leaching kinetics, forms insoluble compounds with metals such copper, so it is not preferred in the recovery of silver (Celep, 2011).

Another alternative reagent that is not as toxic as cyanide and stands out with its fast leaching kinetics and effective leaching performance is halogens. In recent studies, leaching systems using halogen salts and sodium hypochlorite as oxidants have been suggested as an alternative to cyanide in the recovery of gold and silver (Hasab vd., 2014; Lampinen vd., 2017).

When the existing studies in the literature on this subject are examined, it is seen that the chloride solution (Cl_2) stands out among the halogen salts because its unit cost is very affordable. In the chlorination process, the air and oxygen given to the environment is oxidized silver from Ag^0 to Ag^+. It dissolves as $AgCl_2^-$, $AgCl_3^{-2}$ by forming a complex with free chlorine. The general solubility reactions of gold and silver with chlorine are expressed in Equations (1), (2) and (3) (Puvvada and Murthy, 2000).

$$Ag^0 + 1/2O_2 + 2HCl + Cl^- \rightleftharpoons AgCl_3^{-2} + H_2O \quad (1)$$

$$Au^0 + 1/2O_2 + 2H^+ + 4Cl^- \rightleftharpoons 2AuCl_2^- + H_2O \quad (2)$$

$$Au^0 + 3/2O_2 + 6H^+ + 8Cl^- \rightleftharpoons 2AuCl_4^- + 3H_2O \quad (3)$$

As expressed in Equation (4), silver dissolves in the form of an ($H^+AgCl_2^-$) as a result of the addition of NaOCl and HCl to the system to facilitate the anodic dissolution of silver (Olteanou vd., 2014).

$$NaOCl + Ag + 4HCl \rightleftharpoons 2(H^+AgCl_2^-) + H_2O + NaCl \quad (4)$$

In recent years, high-grade and probable precious metal deposits are rapidly depleting. It is anticipated that placer types, especially those containing free coarse grains, which can be easily enriched, will be completely depleted in the future. Therefore, refractory ores in which silver is disseminated into the lattice structures of other minerals and also require pre-enrichment treatment such as pressure leaching, roasting, ultra-fine grinding, etc., have gained great importance. The conditions that cause refractoriness in the ore are the encapsulation of the precious metal in structures such as sulfide, oxide, silicate, etc., the adsorption of the metal from the solution by carbon-containing materials (preg-robbing), the passivation of the silver surface due to the formation of a chemical layer, and the consumption of the solvent reagent by other metals in the ore (La Brooy, 1994; Şeflek, 2019). The degree of refractoriness of an ore varies depending on the mineralogy and metal recovery of that ore. The refractoriness degrees of the ores, which vary depending on their metal recovery, are classified as shown in Table 1.

Table 1. Classification of ore refractoriness (La brooy et al., 1994).

Metal recovery (%)	Refractoriness level
<50	Highly refractory
50-80	Moderately refractory
80-90	Mildly refractory
90-100	Non refractory (free milling)

It is undeniable that the beneficiation of refractory ores has gained great importance nowadays, and the mining industry needs more research on this subject. In this study, the chemical enrichment of refractory silver ores taken from different formations in the mine and a complex structured tailings pond sample under oxidizing NaOCl and acidified NaCl solution was investigated. Moreover, the refractoriness degrees of the ores were also determined in terms of silver recovery.

2. Material and methods

2.1. Material

In this study, ore samples were taken from three different formations of the Kütahya Gümüşköy region in the silver mine, and the tailings pond sample was used. Firstly, some of the silver ores are separated for chemical analysis. The remaining part was crushed to less than 4 mm in the primary jaw crusher. Then, the samples were ground to -15 µm particle size with the help of an agate mill. The ground samples were reduced by applying coning-quartering and gridding methods, and some of them were

separated to be used in experimental studies while the remaining part was stockpiled. The four different samples used in the experiments are named Aktepe, Kavacıkdere I, Kavacıkdere II and tailing pond sample. Chemical analysis of representative silver ore samples was performed by X-ray fluorescence spectrometry. XRF results of silver ore are given in Table 2.

Table 2. XRF results of the ores used in the experiments

Sample Name	SiO_2 (%)	CaO (%)	Al_2O_3 (%)	MgO (%)	Na_2O (%)	BaO (%)	K_2O (%)
Aktepe	44,03	8,66	9,49	4,56	-	3,88	3,71
Kavacıkdere I	64,43	1,56	8,33	0,87	0,22	7,4	3,08
Kavacıkdere II	28,15	7,56	2,68	3,5	0,92	27,6	0,69
Tailing pond	45,72	4,95	6,32	2,25	0,26	10,2	1,58

As seen in Table 2, as a result of XRF analysis, it is seen that Aktepe, Kavacıkdere I ores and the sample taken from the tailings pond contain quartz in amounts varying between 44-65%. In comparison, Kavacıkdere II ore contains 28.25% quartz as well as a large amount of 27.6% barite. The elements included in the ores used as feed samples in the experiments at ppm level are given in Table 3.

Table 3. ICP-OES results of the ores used in the experiments

Sample Name	Ag (ppm)	Cu (ppm)	Pb (ppm)	Zn (ppm)	Fe (ppm)	Mn (pm)	Ni (ppm)	Sb (ppm)	As (ppm)	S (ppm)
Aktepe	85	73	4854	13785	20910	3642	33	1977	3855	5679
Kavacıkdere I	65,5	98	3180	6350	31433	2284	107	1092	2789	4605
Kavacıkdere II	176,6	153	5366	28833	13000	1841	164	1864	8351	15185
Tailing pond	94,4	118	9975	15842	26918	5565	0	4616	8982	10810

As a result of chemical analysis performed with ICP-OES, it was determined that Kavacıkdere II, Aktepe, Kavacıkdere I, and tailings dam samples contained 176.6 pm, 85 ppm, 65.5 ppm, 94.4 ppm silver, respectively. At the same time, the samples are seen to be rich in iron, lead, arsenic and manganese. Additionally, sulfur (S) contents of the ores were determined as 15185 ppm, 5679 ppm, 4605 ppm and 10810 ppm, respectively.

2.2. Method

In this study, chemical dissolution tests were carried out with NaCl solution under atmospheric conditions for silver recovery from refractory-type ore. Leaching experiments were carried out depending on time; pulp samples were taken at the end of 5-15-30-60-120 minutes, and the pulp was filtered. The obtained loaded leach solution and residues were chemically analyzed by atomic absorption spectrometer (AAS). The experimental setup and operating parameters used in the experiments are given in Fig. 1 and Table 3. As seen in Fig. 1, the experimental setup consists of a low-evaporation dissolving vessel, a magnetic stirrer, and an air pump used to provide oxygen to the system.



Fig. 1. The experimental setup used in the experiments

In the leaching studies, the optimum conditions specified in Canıeren and Karagüzel., 2019, were taken into account. pH and Eh measurements were carried out throughout the experiments, and the parameters that were kept under control and whose effects were examined are given in Table 4.

Table 4. The parameters investigated and kept under control.

Parameters	Unit	Quantity
Sample amount	g	100
Particle size	80%,	-15
pH	-	5-7
Mixing speed	rpm	750
NaCl	molarity	2
NaOCl	molarity	0,1
HCl	molarity	0,25
Leaching time	min	5-15-30-60-120
Solid ratio	%	30
Temperature	°C	24,5
Air	bar	0,5

3. Result and discussion

In this investigation, comparing the silver recovery efficiencies of ores with different mineralogy, the ores were dissolved for 120 minutes by periodically taking samples under optimum conditions: 2 molarity of NaCl, 0.1 molarity of NaOCl, solid ratio 30%, 0.25 molarity of HCl, particle size -15 µm. The experimental results are given in Fig. 2.

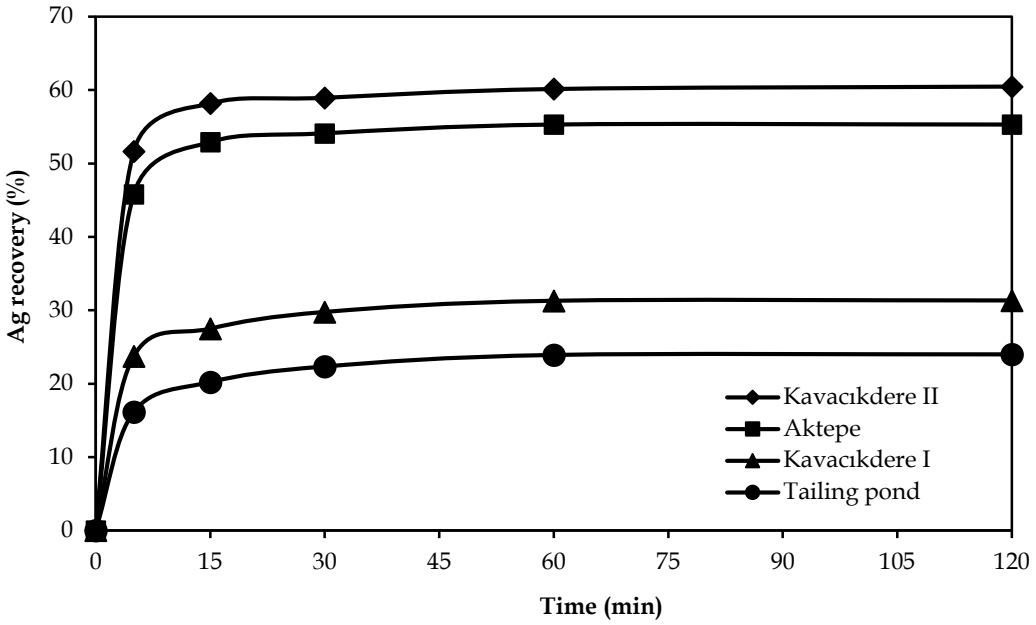


Fig. 2. Comparison of silver recovery efficiencies of different ores

As seen in Fig. 1, in leaching experiments where NaOCl/NaCl was used as the solvent, it is seen that the silver solubility increased in all samples up to 15 min, after which point the solubility started to stabilize. In the experiment of Kavacıkdere II ore with high barite was dissolved, the highest amount of Ag was recovered at 60.47%. While 55.29% Ag was recovered in the leaching experiment using Aktepe ore with moderately high quartz, 31.34% and 23.99% Ag were recovered in the experiments where high quartz Kavacıkdere I ore and tailings dam samples were dissolved, respectively. According to the refractoriness classification given in Table 1, it was determined that Kavacıkdere II ore and Aktepe ore (50-80%) were classified as moderately refractory. At the same time, Kavacıkdere I and the tailings pond samples were found to be highly refractory ore. The varying amount of Ag recoveries can related to possible mineral encapsulations. These results also agree with the previous studies of Arık, 2002 and Canıeren and Karagüzel., 2021 that Gümüşköy silver ore was encapsulated in barite, quartz, chalcedony, and dolomite matrices. It is estimated that Kavacıkdere II ore contains more free silver grains than Kavacıkdere I ore compared to Aktepe ore, and this affects the Ag recoveries. The complex structure of tailing pond sample also caused lowest silver recovery in the experiments.

4. Conclusions

In this study, the enrichability of four different silver ores belonging to the Kütahya Gümüşköy region in an acidified NaCl/NaOCl medium by atmospheric leaching method was investigated. As a result of leaching studies carried out under optimum conditions, the highest rate of Ag was recovered at 60.47% in the experiment of Kavacıkdere II ore. In the leaching experiment using Aktepe ore, 55.29% of Ag was recovered. Additionaly, 31.34% of Ag and 23.99% of Ag were also recovered in the experiments of Kavacıkdere I ore and tailings pond samples, respectively. At the same time, according to the classification of La brooy et al., 1994, it was determined that Kavacıkdere II ore and Aktepe ore were moderately refractory, while Kavacıkdere I ore and tailings dam samples were highly refractory.

The application of different processes to different ore formations in our country, where new precious metal deposits are discovered every day, will enrich the processes. This study emphasizes the significance of the recovery of refractory silver ores using different leaching methods as an alternative to cyanide. With the advanced technique in this field, the recovery of refractory ores will make higher contributions to the mining economy and employment in the short and mid-term.

Acknowledgments

The authors gratefully acknowledge the Scientific Research Projects of Kütahya Dumlupinar University for the financial support received through the research project 2018-35. We also thank the Eti Silver Mining Industry Co., Ltd. for providing the raw material and laboratory supports.

References

Arik F (2002) *Geochemical modeling of the Gumuskoy (Kutahya) silver deposit*. Doctoral dissertation, Selcuk University, Konya, 335p.

Canıeren, Ö., & Karagüzel. (2019). *Ambient leaching of gümüşköy refractory silver ın hypochlorite-chloride media*, Paper presented at International Mineral Processing Congress, Antalya.

Canıeren, Ö., & Karagüzel, C. (2021). Silver Metal Extraction from Refractory Silver Ore Using Chloride-Hypochlorite and Hydrochloric Acid Media Under High Pressure. Mining, Metallurgy & Exploration, 38(2), 1215-1223. doi: https://doi.org/10.1007/s42461-021-00389-9

Celep, O. (2011). *Application of alkaline pretreatments for gold and silver recovery from refractory ores,* Doctoral dissertation, KTU Fen Bilimleri Enstitüsü, Trabzon, 167p.

Estay, H., Ortiz, M., & Romero, J. (2013). A novel process based on gas filled membrane absorption to recover cyanide in gold mining. Hydrometallurgy, 134, 166-176. doi: https://doi.org/10.1016/j.hydromet.2013.02.012

Habashi, F. (2009). Recent trends in extractive metallurgy. Journal of Mining and Metallurgy, Section B: Metallurgy, 45(1), 1-13.

Hasab, M. G., Rashchi, F., & Raygan, S. (2014). Chloride–hypochlorite leaching and hydrochloric acid washing in multi-stages for extraction of gold from a refractory concentrate. *Hydrometallurgy*, *142*, 56-59. doi: https://doi.org/10.1016/j.hydromet.2013.11.015

La Brooy, S. R., Linge, H. G., & Walker, G. S. (1994). Review of gold extraction from ores. Minerals Engineering, 7(10), 1213-1241. doi: https://doi.org/10.1016/0892-6875(94)90114-7

Lampinen, M., Seisko, S., Forsström, O., Laari, A., Aromaa, A., Lundström, M., & Koiranen, T., (2017). Mechanism and kinetics of gold leaching by cupric chloride. *Hydrometallurgy*, 169, 103–111. doi: https://doi.org/10.1016/j.hydromet.2016.12.008

De Michelis, I., Olivieri, A., Ubaldini, S., Ferella, F., Beolchini, F., & Vegliò, F. (2013). Roasting and chlorine leaching of gold-bearing refractory concentrate: Experimental and process analysis. *International Journal of Mining Science and Technology*, *23*(5), 709-715. doi: https://doi.org/10.1016/j.ijmst.2013.08.015

Puvvada, G. V. K., & Murthy, D. S. R. (2000). Selective precious metals leaching from a chalcopyrite concentrate using chloride/hypochlorite media. *Hydrometallurgy*, *58*(3), 185-191. doi: https://doi.org/10.1016/S0304-386X(00)00083-9

Şeflek, C., (2019). *Rinding and cyanide leaching of bolkardag gold andsilver ores*, Doctoral dissertation, Çukurova Üniversitesi, Fen Bilimleri Enstitüsü, Adana, 218p.

Olteanu, A. F., Dobre, T., Panturu, E., Radu, A. D., & Akcil, A. (2014). Experimental process analysis and mathematical modeling for selective gold leaching from slag through wet chlorination. *Hydrometallurgy*, *144*, 170-185. doi: https://doi.org/10.1016/j.hydromet.2014.02.011

Optimization of nickel and cadmium leaching process from spent batteries

Mohsen Mirzaei [1]*, Mohammad Ali Moradzadeh [1], Ziaeddin Pourkarimi [1], Mehdi Rahimi [1], Seyed Javad Mousavi [1]

[1]Iran Mineral Processing Research Centre (IMPRC)

*Corresponding author: m.mirzaei@imprc.ir (Mohsen Mirzaei)

Abstract:

The rapid growth of the battery industry, environmental pollution, and the value of metal content, necessitate the recycling of spent nickel-cadmium batteries. In this study, the leaching of nickel and cadmium from spent batteries was investigated. XRF analysis revealed that the cadmium content in the cathode and nickel in the anode were 55.25% and 53.57%, respectively. Iron was the highest impurities in the cathode, as well as potassium, sodium, and iron were the highest impurities in the anode. through experimental design, the effects of acid concentration, time, temperature, L/S ratio, and agitation speed on nickel and cadmium recovery were studied. The variance analysis table highlighted that temperature, acidity, time, and the solid-to-liquid ratio (L/S) significantly impacted the leaching process, and agitation speed had a minor effect. Based on the optimal conditions, a recovery rate of 92% for nickel was achieved with a leaching time of 4 hours, a temperature of 80°C, an acid concentration of 3 Molar, an L/S ratio of 20 ml/g, and an agitation speed of 236 rpm. Additionally, the results from the variance analysis table indicated that the L/S ratio and time had a greater impact on cadmium recovery improvement compared to agitation speed, temperature, and acidity. Finally, under the optimal conditions, a cadmium recovery rate of 98% was obtained with a leaching time of 4 hours, a temperature of 80°C, an acid concentration of 3.05 Molar, an L/S ratio of 20 ml/g, and an agitation speed of 236 rpm. Validation tests have confirmed the results.

Keywords: *optimization, leaching, experimental design, nickel, cadmium*

1. Introduction

Each year, a significant volume of batteries is produced and consumed globally, with these batteries playing a crucial role in daily human activities. Once these batteries reach the end of their useful life, they become degraded and lose their ability to generate electrical energy. Consequently, a substantial amount of spent batteries is produced, requiring considerable storage space and posing serious risks to both human health and the environment. Additionally, the battery production process generates a large quantity of waste, which, if released directly into the environment in solid or liquid form, could have detrimental and destructive effects. Moreover, valuable materials would be wasted without being recycled (Nogueira & Margarido. 2004).

The increasing adoption of nickel-cadmium (Ni-Cd) batteries in applications ranging from portable electronics to industrial equipment has led to significant environmental and economic challenges related to their disposal. Spent Ni-Cd batteries comprise valuable components including approximately 43% cathode and anode materials composed of nickel and cadmium, 5% plastic separators, 27% steel casing, and 25% nickel mesh serving as a substrate for the anode powder. effective recycling is crucial to mitigate potential environmental hazards and recover valuable metals (Assefi et al. 2020; Rana et al. 2023; Hung et al. 2018).

Recent advancements in the recycling of spent Ni-Cd batteries have explored various methods to enhance metal recovery and minimize environmental impact. For example, thermal separation processes have demonstrated successful metal recovery, yielding slag, bullion, and flue gas, with the bullion containing 514,000 mg/kg of iron and 245,000 mg/kg of nickel (Hung et al. 2018). Vacuum metallurgy separation has achieved a near-total cadmium recovery efficiency of 99.98% under optimal

conditions (Huang et al. 2010). Electrochemical methods have also been investigated, with electroassisted leaching and electrodeposition showing current efficiencies of up to 73% for cadmium recovery (Hazotte et al. 2016).
In the context of multi-battery recycling, the simultaneous processing of lithium-ion and nickel-metal hydride batteries has led to over 98% recovery of lithium, cobalt, and nickel (Liu et al. 2019). Modeling studies on solvent extraction have improved nickel and cadmium separation efficiencies by optimizing the synergistic effects of different solvents (Vahidi et al. 2016). Pyrometallurgical techniques, while effective, remain energy-intensive, with significant advancements in improving their sustainability (Assefi et al. 2020).
Innovative leaching techniques using sulfuric acid and formic acid have shown promising results, with formic acid-based methods achieving up to 98% cadmium recovery and 81% nickel recovery under optimal conditions (Polychronopoulou et al. 2022; Rana et al. 2023). Hydrometallurgical methods, including leaching and electrowinning, have demonstrated high recovery rates of up to 96% for nickel and 99.5% for cadmium (Randhawa et al. 2016; Rudnik & Nikiel 2007). Recent reviews emphasize the need for continued development of more efficient and environmentally friendly recycling technologies (Blumbergs et al. 2021; Wang et al. 2022).

Overall, the diverse range of methods explored—from thermal and electrochemical processes to advanced hydrometallurgical techniques—demonstrates the ongoing efforts to enhance the sustainability and efficiency of battery recycling. These studies collectively contribute to a comprehensive understanding of the challenges and advancements in the field, highlighting the need for continued innovation and optimization in recycling practices.

2. Material and methods

For this study, samples were collected from spent nickel-cadmium batteries with metal casings. The required powder for the experiments was obtained by removing the powders from the anode and cathode plates. A 20 kg sample of cadmium was extracted from these batteries for the experiments. The leaching of the nickel-cadmium batteries was performed in several stages.

Initially, it is crucial to use safety equipment, including acid-resistant gloves, goggles, and laboratory coats. All leaching tests were conducted under a fume hood to mitigate exposure to the toxic fumes produced during the leaching process, and masks were used whenever possible.

In the first stage, the outer surface of the batteries was cut open, and the battery electrolyte was drained. The anode and cathode were then removed from the battery, and the anode and cathode plates were separated from the terminal section. The powder inside the anode and cathode plates was separately extracted. Sulfuric acid was used to identify the anode and cathode: sulfuric acid was poured into two separate beakers, and portions of the extracted powder were added to the sulfuric acid. The green color indicated nickel (anode), while the reddish color indicated cadmium (cathode). Fig. 1 shows the separation and identification of the anode and cathode using sulfuric acid.



Fig. 1. Overview of the Preparation of Powder Required for Testing from Cathodes

2.1.1. Mineralogical Studies of the Sample

To determine the composition of the sample, an X-ray fluorescence (XRF) analysis was conducted. The XRF analysis revealed that the Ni and Cd concentrations were approximately 53.5% and 55.25%, respectively (Table 1 and 2).

Table 1: XRF Analysis Results of Cathode Sample

Cd	L.O.I. (%)	Na_2O (%)	Al_2O_3 (%)	SiO_2 (%)	P_2O_5 (%)	SO_3 (%)	Cl (%)	Fe_2O_3 (%)	Ni (%)	Cu (%)	Cd (%)
	11.11	0.745	0.063	0.343	0.006	0.988	0.042	31.377	0.093	0.02	55.251

Table 2: XRF Analysis Results of Anode Sample

Ni	L.O.I. (%)	Na_2O (%)	MgO (%)	Al_2O_3 (%)	SiO_2 (%)	SO_3 (%)	Cl (%)	K_2O (%)	Fe_2O_3 (%)	Co (%)	Ni (%)
	31.75	2.401	0.072	0.3	0.338	0.483	0.056	7.179	1.474	0.361	53.572

Cu (%)	Zn (%)	Sr (%)	Cd (%)	Ba (%)
0.062	0.073	0.036	0.445	1.399

2.1.2. Factor Levels and Variation

In this study, five parameters were examined for leaching experiments, as shown in Table 3. Another significant parameter that affects the leaching rate and metal concentration in the solution is the use of hydrogen peroxide. However, due to the high corrosion rate of the equipment used in the process, hydrogen peroxide was excluded as a variable.

Table 3: Factors and Their Effect on Leaching

Factor Levels	Factor Under Study
1, 2, 3, 4	Acid Concentration (M)
25, 45, 65, 85	Temperature (°C)
1, 2, 3, 4	Time (h)
200, 300, 400, 500	Stirring Speed (RPM)
5, 10, 15, 20	L/S (Liquid to Solid Ratio)

3. Results

3.1. Experimental Design and Analysis

For the leaching experiments, the Taguchi method and the L16 orthogonal array were chosen for design and analysis of the factors affecting the recovery rates. The analysis was conducted using Design Expert software. In these experiments, five factors were selected and nickel recovery was considered as the response variable (Table 4). The analysis of variance (ANOVA) for nickel and cadmium recovery during the process is shown in Tables 5 and 6.

Table 4. Results of Leaching Experiments

Experiment No.	Time (h)	L/S (ml/g)	Acid Concentration (M)	Stirring Speed (RPM)	Temperature (°C)	Cd Recovery (%)	Ni Recovery (%)
1	1	5	1	200	25	78	62
2	2	10	2	300	25	88.6	72.4
3	3	15	3	400	25	90.7	77
4	4	20	4	500	25	98.8	90
5	4	15	2	200	45	94	80
6	3	20	1	300	45	79.2	78
7	2	5	4	400	45	80	77
8	1	10	3	500	45	84	75
9	2	20	3	200	65	87	92
10	1	15	4	300	65	93	82
11	4	10	1	400	65	88.6	79
12	3	5	2	500	65	80	77.5
13	3	10	4	200	85	94	86
14	4	5	3	300	85	86	81
15	1	20	2	400	85	92	85
16	2	15	1	500	85	90	80

Table 5. ANOVA for Nickel Recovery

Source	Sum of Squares	df	Mean Square	F Value	p-value
Model	682.20	5	136.44	22.19	<0.0001
Temperature	157.64	1	157.64	25.64	0.0005
Stirring Speed	1.83	1	1.83	0.30	0.5973
Acid Concentration	174.35	1	174.35	28.36	0.0003
L/S	277.89	1	277.89	45.20	<0.0001
Time	70.50	1	70.50	11.47	0.0069
Residual	61.48	10	6.15		
Total	743.68	15			

Table 6: ANOVA for Cadmium Recovery

Source	Sum of Squares	df	Mean Square	F Value	p-value
Model	417.75	5	83.55	6.59	0.0058
Temperature	1.89	1	1.89	0.15	0.7075
Stirring Speed	2.08	1	2.08	0.16	0.6940
Acid Concentration	13.37	1	13.37	1.05	0.3288
L/S	327.65	1	327.65	25.84	0.0005
Time	72.77	1	72.77	5.74	0.0376
Residual	126.82	10	12.68		
Total	544.57	15			

3.2. Normal Distribution of Residuals

Residuals are the differences between the actual values (measured in experiments) and the predicted responses for each point. A normal distribution of residuals is confirmed if the points follow a straight line in the normal probability plot. If residuals do not follow a normal distribution, a transformation on the response data may be necessary to achieve a valid mathematical model (Fig. 2 and 3).

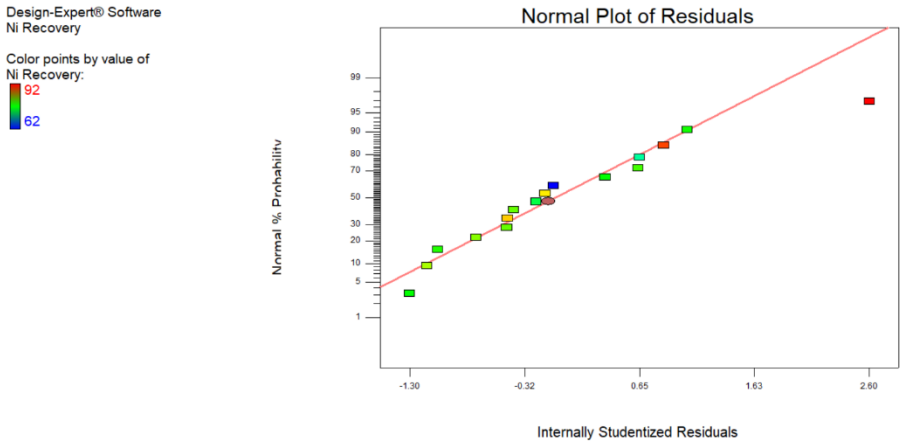


Fig. 2. Normal Distribution Curve of Nickel Recovery Residuals

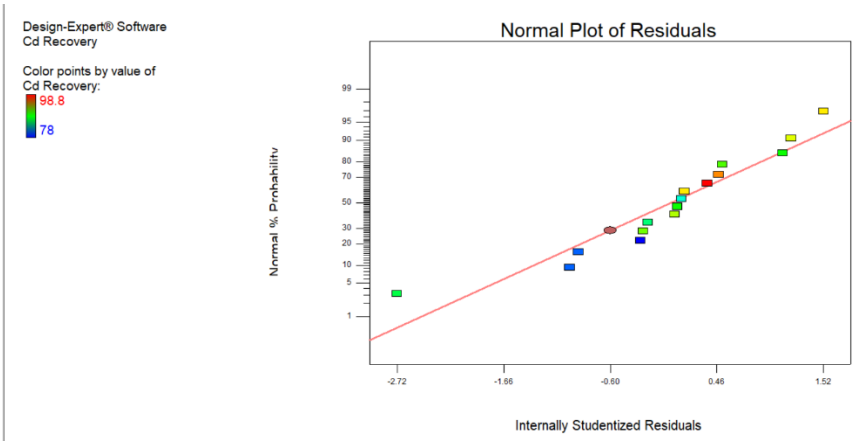


Fig. 3. Normal Distribution Curve of Cadmium Recovery Residuals

3.3. Effect of the Parameters on Nickel Recovery

Effect of Contact Time: As shown in the Fig. 4, nickel recovery increases from 77% to 84% as the contact time increases from 1 hour to 4 hours. This increase is due to the consumption of remaining acid in the solution, enhancing nickel extraction (Fig. 4 (a)).

Effect of Temperature: The rate of nickel extraction increases linearly with temperature. Nickel extraction rises from 76% at 25°C to 84% at 85°C. This can be due the fact that higher temperatures reduce solution viscosity, decreasing mass transfer resistance and increasing extraction efficiency (Fig. 4 (b)).

Effect of L/S Ratio: At a low L/S ratio (5 ml solution per 1 g solid), nickel recovery is 74%, while at a high L/S ratio (20 ml solution per 1 g solid), recovery increases to 85.5%. More solution per unit of solid increases sulfuric acid availability, improving nickel extraction (Fig. 4 (c)).

Effect of Stirring Speed: Stirring speed does not significantly impact nickel recovery. The critical control step in leaching is likely the chemical reaction at the particle surface, which is primarily influenced by temperature (Fig. 4 (d)).

Effect of Acid Concentration: Nickel recovery improves from 76% at 1 M sulfuric acid to 84% at 4 M. Higher acid concentrations provide more exposure of acid to metal ions, thus enhancing recovery (Fig. 4 (e)).

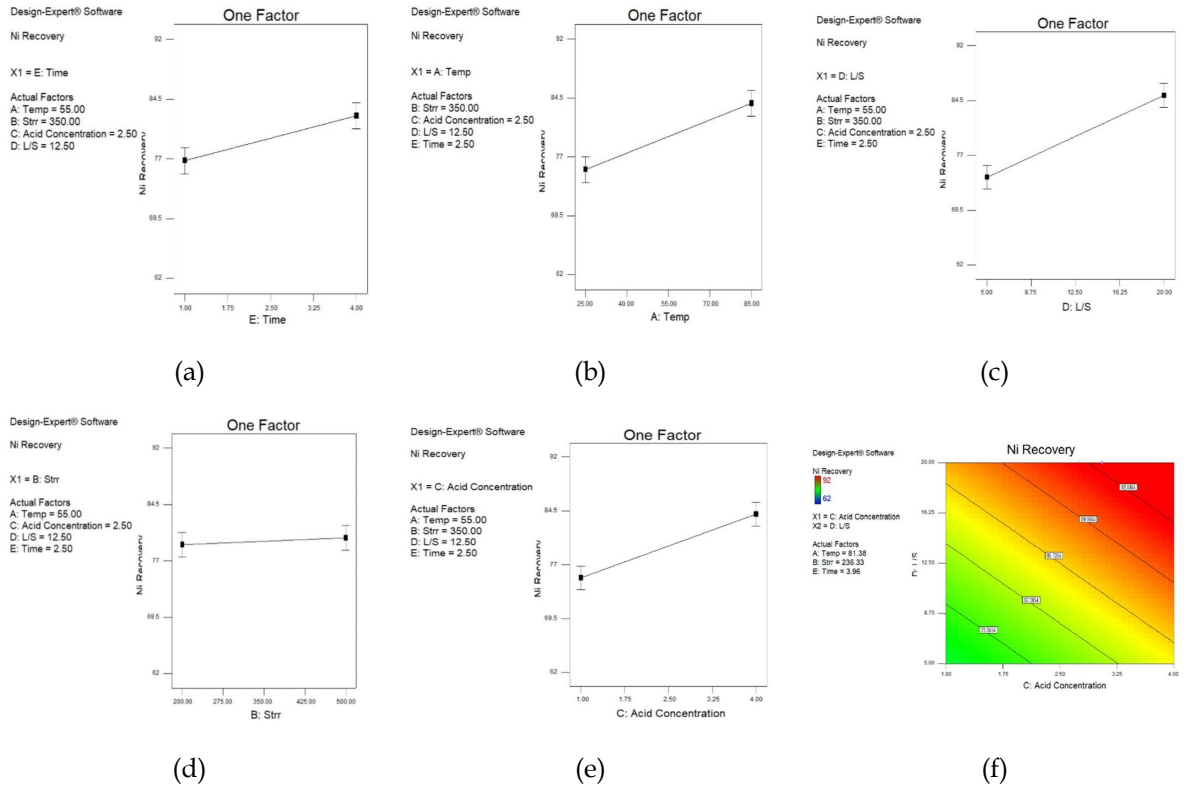


Fig. 4. Effects of Parameters on Nickel Recovery

3.4. Effect of the Parameters on Cadmium Recovery

Effect of Acid Concentration: Cadmium recovery is relatively independent of acid concentration. Recovery improves from 88% at 1 M sulfuric acid to 91% at 4 M. This is due to the ease of dissolution of all cadmium phases, which does not heavily rely on acid concentration (Fig. 5 (a)).

Effect of Contact Time: Cadmium recovery increases from 85% to 91.5% as contact time extends from 1 hour to 4 hours, due to the consumption of residual acid (Fig. 5 (b)).

Effect of Temperature: Cadmium recovery shows minimal dependence on temperature, with a slight increase from 85.5% at 25°C to 86.5% at 85°C. This suggests that cadmium dissolution is less temperature-sensitive compared to nickel (Fig. 5 (c)).

Effect of L/S Ratio: At a low L/S ratio (5 ml solution per 1 g solid), cadmium recovery is 83%, and it increases to 94% at a high L/S ratio (20 ml solution per 1 g solid). Increased L/S provides more sulfuric acid per unit of solid, enhancing recovery (Fig. 5 (d)).

Effect of Stirring Speed: Stirring speed does not significantly affect cadmium recovery, similar to nickel, indicating that the primary control step is likely the chemical reaction at the particle surface (Fig. 5 (e)).

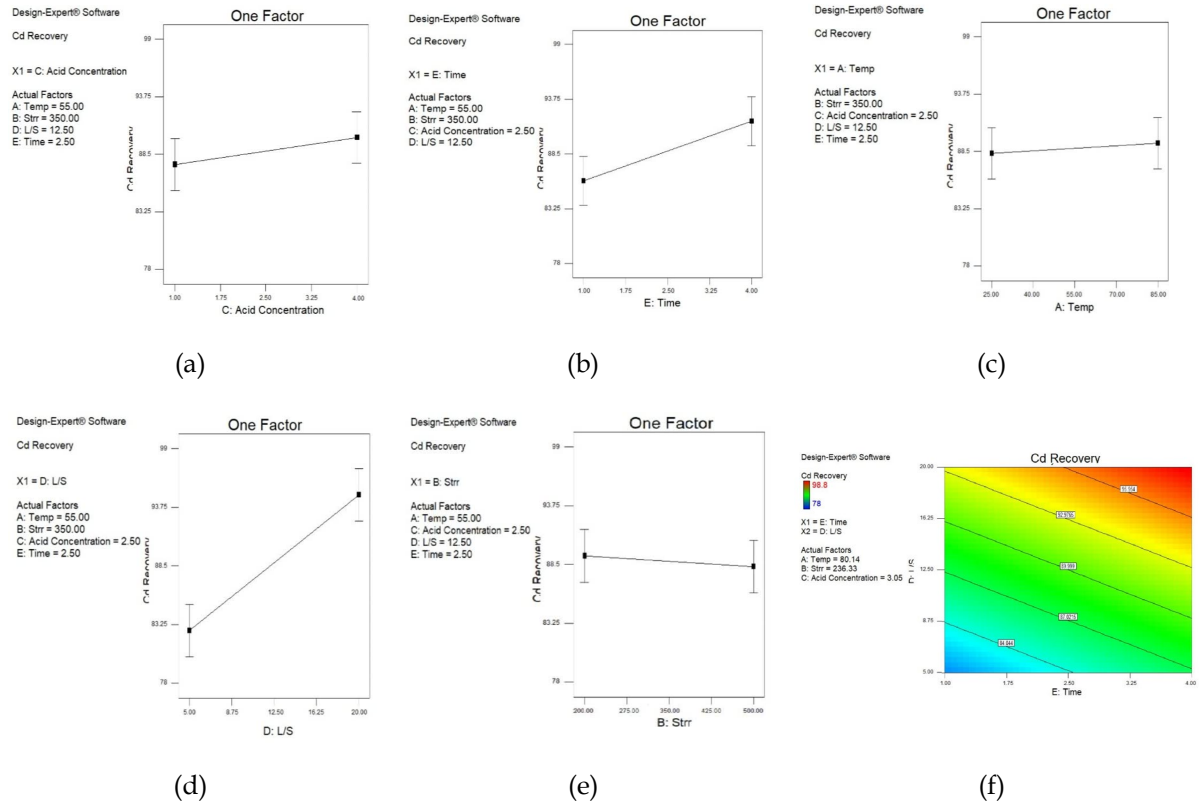


Fig. 5. Effects of Parameters on Cadmium Recovery

3.5. Modeling

Based on the models fitted by the software for nickel and cadmium recovery responses, a linear model is proposed. The following equations were derived to estimate the recovery rates of nickle and cadmium respectively.

$$Ni \text{ Recovery} = 50{,}4500 + 2{,}8075 \times \text{temp} + 0{,}3025 \times \text{strr} + 2{,}9525 \times \text{acid cons} + 3{,}7275 \times \text{L/S} + 1{,}8775 \times \text{time} \quad (1)$$

$$Cd\ Recovery = 71{,}9000 + 0{,}3075 \times temp - 0{,}3225 \times strr - 0{,}8175 \times acid\ cons + 4{,}0475 \times L/S + 1{,}9075 \times time \quad (2)$$

These linear models can be used to predict recovery rates based on the varying experimental conditions.

3.6. Optimization of Nickel and Cadmium Leaching Conditions

To optimize the leaching process, it is essential to select process responses as objectives. The DX7 software uses default upper and lower limits for response ranges, which may not meet practical requirements. Therefore, specific goals for the responses must be set to obtain acceptable results from the software. Given that the primary goal of the leaching operation is the maximum recovery of nickel and cadmium, the objective was set to maximize the process recovery (Table 7 and 8).

Table 7: Optimization of Nickel Leaching

Parameter	Time (h)	Temperature (°C)	Acid Concentration (M)	Stirring Speed (RPM)	L/S (ml/g)	Ni Recovery (%)
Optimal Value	4	80.14	3.05	236.33	20	92.7

Table 8: Optimization of Cadmium Leaching

Parameter	Time (h)	Temperature (°C)	Acid Concentration (M)	Stirring Speed (RPM)	L/S (ml/g)	Cd Recovery (%)
Optimal Value	4	80.14	3.05	236.33	20	98.78

These optimal conditions represent the settings that maximize the recovery of nickel and cadmium in the leaching process based on the analysis performed by the software. Two tests were conducted under the optimal conditions, and similar recovery results were achieved.

4. Conclusions

The design and analysis of experiments to evaluate the effects of selected factors were performed using the Taguchi method and the L16 orthogonal array, with the help of Design Expert software. In this series of experiments, five factors were selected, and nickel recovery was considered as the response variable. A linear model was fitted to the experimental data, and error analysis was conducted.

The results from the analysis of variance table for nickel recovery indicate that the factors L/S, temperature, acid concentration, and time have a more significant impact on improving nickel recovery compared to other parameters. Stirring speed had the least effect. Optimization aimed to adjust the factor levels to achieve the most desirable experimental response, which in this study was the maximization of nickel recovery. The results show that the highest nickel recovery was achieved under the conditions of 3 M acid concentration, 4 hours of leaching time, 240 RPM stirring speed, L/S ratio of 20, and 80°C temperature.

Regarding cadmium, XRF analysis revealed that the nickel-cadmium battery powder used in this study contained a significant amount of cadmium, approximately 2.55%. Identifying and understanding the parameters involved in the leaching process is crucial. Parameters such as time, temperature, acid concentration, L/S ratio, and stirring speed were each examined at four different levels. For cadmium recovery, the analysis of variance results indicated that L/S ratio and time had a more substantial effect on improving cadmium recovery, while stirring speed, temperature, and acid concentration had less influence.

Acknowledgments

This research was made possible with the support and resources provided by the Iran Mineral Processing Research Centre (IMPRC). We sincerely thank IMPRC for their crucial contribution to the successful execution of this project.

References

Nogueira, C. A., & Margarido, F. (2004). Leaching behaviour of electrode materials of spent nickel cadmium batteries in sulphuric acid media. Hydrometallurgy, 72(1-2), 111-118.

Assefi, M., Maroufi, S., Yamauchi, Y., & Sahajwalla, V. (2020). Pyrometallurgical recycling of Li-ion, Ni–Cd and Ni–MH batteries: A minireview. Current Opinion in Green and Sustainable Chemistry, 24, 26-31.

Rana, M., Khan, M. I. H., Nshizirungu, T., Jo, Y. T., & Park, J. H. (2023). Green and sustainable route for the efficient leaching and recovery of valuable metals from spent Ni− Cd batteries. Chemical Engineering Journal, 455, 140626.

Hung, Y. Y., Yin, L. T., Wang, J. W., Wang, C. T., Tsai, C. H., & Kuo, Y. M. (2018). Recycling of spent nickel–cadmium battery using a thermal separation process. Environmental Progress & Sustainable Energy, 37(2), 645-654.

Huang, K., Li, J., & Xu, Z. (2010). Characterization and recycling of cadmium from waste nickel–cadmium batteries. Waste management, 30(11), 2292-2298.

Hazotte, C., Leclerc, N., Meux, E., & Lapicque, F. (2016). Direct recovery of cadmium and nickel from Ni-Cd spent batteries by electroassisted leaching and electrodeposition in a single-cell process. Hydrometallurgy, 162, 94-103.

Liu, F., Peng, C., Porvali, A., Wang, Z., Wilson, B. P., & Lundströ̈m, M. (2019). Synergistic recovery of valuable metals from spent nickel–metal hydride batteries and lithium-ion batteries. ACS Sustainable Chemistry & Engineering, 7(19), 16103-16111.

Vahidi, E., Babakhani, A., Rashchi, F., & Zakeri, A. (2016). Modeling of synergistic effect of Cyanex 302 and D2EHPA on separation of nickel and cadmium from sulfate leach liquors of spent Ni-Cd batteries. REWAS 2013: Enabling Materials Resource Sustainability, 262-271.

Polychronopoulou, E., Oustadakis, P., Tsakiridis, P., Betsis, K., & Xenidis, A. (2022). Sulphuric Acid Leaching of Spent Nickel Metal Hydride Car Batteries. Materials Proceedings, 5(1), 126.

Randhawa, N. S., Gharami, K., & Kumar, M. (2016). Leaching kinetics of spent nickel–cadmium battery in sulphuric acid. Hydrometallurgy, 165, 191-198.

Rudnik, E., & Nikiel, M. (2007). Hydrometallurgical recovery of cadmium and nickel from spent Ni–Cd batteries. Hydrometallurgy, 89(1-2), 61-71.

Blumbergs, E., Serga, V., Platacis, E., Maiorov, M., & Shishkin, A. (2021). Cadmium recovery from spent Ni-Cd batteries: a brief review. Metals, 11(11), 1714.

Wang, J., Zhang, Y., Yu, L., Cui, K., Fu, T., & Mao, H. (2022). Effective separation and recovery of valuable metals from waste Ni-based batteries: A comprehensive review. Chemical Engineering Journal, 439, 135767.

Zinc Recovery From Flue Dust of Blast Furnace and Arc Furnace Plants in Iron and Steel Industry

Onur ATAŞ [1]*, Mehmet BİLEN [2],

[1]Kardemir A.Ş. Karabük

[2] Zonguldak Bülent Ecevit University, Engineering Faculty, Department of Mining Engineering

*Corresponding author: onatas@kardemir.com (Onur ATAŞ)

Abstract:

Blast furnace dust (BFD) is a potentially hazardous waste and an important source of zinc with large annual productions. BFD is a by-product of the iron production process and consists of particles carried by blast furnace gas through the dust removal system. BFD is a fine-grained material containing significant amounts of zinc, iron and carbon, with variable amounts of calcium, silicon, aluminum, chlorine and alkali metals. Direct recycling of BFD is hindered by the presence of zinc, chlorine and alkali metals. Due to its low boiling point nature, its prolonged accumulation is detrimental to the blast furnace, corroding the furnace lining and disrupting the blast furnace tuyere, gas flow and shortening the life of the blast furnace. Therefore, certain treatment methods need to be adopted to remove zinc, chlorine and alkali metals from the BFD. In our country, 80% of steel production is carried out in Electric Arc Furnaces (EAF) using scrap as raw material. During steel production in electric arc furnaces, 10-15 kg of flue dust containing 25-45% Zn is formed per 1 ton of steel depending on the composition of the scrap. In this study, it is aimed to protect the Zn in the flue dust from damage to nature and to separate it and turn it into usable pure raw material.

Keywords: *Blast furnace dust, Zinc, recycle, hydrometallurgy, pyrometallurgy*

1. Introduction

Zinc is one of the most important non-ferrous metals used in society. Its properties that protect steel against corrosion provide tremendous economic and environmental impacts [1]. However, as zinc has been used since ancient times, the increasing demand for this metal may limit its availability [2,3]. In ancient Indian writings, the first descriptions of processes to produce metallic zinc from ores have been found [4]. Sources report that at this time this smelter could produce 60,000 tons of metallic zinc [5] and about one million tons of metallic zinc and zinc oxide [6]. William Champion developed and patented the production of zinc in vertical retorts. In 1743, the first zinc smelter was built in Bristol with an annual capacity of about 200 tons [7]. Zinc production in the United States began in 1850. In 1917, a process for the electrolysis of zinc was developed (roasting-leaching-electrolysis). Another change in the zinc production process was the introduction of pressure leaching in the 1980s [8].

The description presented of zinc production in the ancient days points to the problems associated with its extraction. With the development of civilization, there was a leap in the industry's interest in zinc, which led to the need to develop rational and efficient methods of obtaining it, which ultimately made this metal one of the most important metals used in technology today. Zinc is a component of many alloys, including brass, aluminum zinc alloy. Rolled zinc sheets with titanium added are used in roofing. It is used in electrical cells and in the form of zinc compounds. Zinc oxide ZnO (zinc white) is produced from primary zinc and is used in the chemical industry as an additive to paints and varnishes and as a filler and stabilizer for rubber and plastics. Zinc sulfate has strong anti-inflammatory properties. Although zinc has been used in medicine for thousands of years, it was not until 1957 that zinc was officially recognized as one of the essential micronutrients [9]. In industry, zinc is most commonly used to coat steel products to protect them against corrosion. Coatings produced by hot-dip galvanizing (HDG) are the oldest known method of producing anti-corrosion coatings, patented in 1836 [10], and are currently the most economical and effective anti-corrosion protection.

Zn is an essential non-ferrous metal required for a variety of applications in batteries, solder, dielectric materials and piezoelectric materials. High grade Zn ores are becoming increasingly scarce and to meet today's demand for Zn, it is necessary to develop economical and environmentally safe metallurgical technologies that utilize secondary materials such as leach tailings and EAF powders from Zn concentrates. The Zn in most of these tailings exists as zinc ferrite (franklinite, $ZnFe_2O_4$), which is stable and insoluble in most acidic and alkaline solutions. Various pyrometallurgical and hydrometallurgical processes have been proposed for the processing of $ZnFe_2O_4$. Pyrometallurgical methods are costly due to high energy consumption and toxic gas emissions pose an environmental problem. Hydrometallurgical methods are preferred for process economics and environmental reasons [11].

2. Iron and Steel Production in Turkey and Arc Furnace System

In 1925, the Ministry of Economy (Ministry of Treasury and Finance) began to examine whether an iron and steel industry could be established. Experts were brought from abroad to examine oil deposits, coal and iron ore. The expert Dr. Granigg conducted studies on the suitability of the country for the industry, the structure of coal and where the industry could be established. Until 1932, work was suspended, but resumed with the Russian delegation's examinations and the establishment of the Iron and Steel Industry. In the joint research conducted by Sümerbank and Erkan-ı Harbiye in order to determine the location of the establishment of the heavy iron industry and to examine other problems, a final decision was taken and Karabük region was found suitable as the location of the establishment. The reasons for the preference of Karabük were that it was close to coal mines, it was a railway transportation facility, the workers of the region could be accommodated and its geological structure was suitable for the establishment of heavy facilities [12].

Steel was first produced in Kırıkkale in 1928. In 1939, Kardemir, the first integrated iron and steel plant was opened, followed by the Ereğli Iron and Steel Plant (ERDEMİR) to meet Turkey's demand for flat steel production. Then, in 1977, Iskenderun Iron and Steel Plant (ISDEMIR), Turkey's third integrated iron and steel plant, started to produce long steel products [13].



Figure 1. Steel Production in Turkey [13].

There are 40 crude steel production facilities in Turkey. As can be seen in Figure 1, 26 of them are electric arc furnace (EAF), 11 are induction furnace and 3 are BOF production facilities [14].Turkey produced 8.7 percentage points less than the world production in 2022 and production decreased by 12.9% to 35.1 million tons. In January 2023, Turkey's crude steel production decreased by 17.6% to 2.6 million tons compared to the same month of the previous year [13].

Of the 22 million tons/year of iron and steel produced in Turkey, 16 million tons are produced in factories with arc furnaces. The production of high value-added products such as alloyed steel and flat products by plants with arc furnaces requires a separate investment. Since the investment cost of arc furnace plants is much lower than that of integrated plants producing from ore, arc furnace plants are more preferred in our country. The chemical reaction that occurs during the process takes place at high temperatures. The iron and steel industry involves obtaining iron by processing pure iron ore or scrap in various ways and then producing steel by reducing and/or increasing the oxidation present in the

iron, reducing and/or increasing the molecules present in it but undesirable in the alloy. When we briefly examine electric arc furnaces (EAO) in terms of their general formation, the main parts are; EAO lining with a casting hole, the lower casting hole, which is often used in today's industry, and the slag gate. In addition, the movable upper part, the wall plates made of cooled refractory bricks, the electrodes, which are usually graphite with electrode carrier arms, other parts carrying electricity in the furnace and finally the tilting mechanism-piston group can be seen as the main parts. In electric arc furnaces, the casting weight starts at a few kilograms and can reach up to 350 tons if the furnaces created in laboratories for testing purposes are taken into account. Approximate casting weight is between 80-120 tons [15]. An EAF is shown schematically in Figure 2.

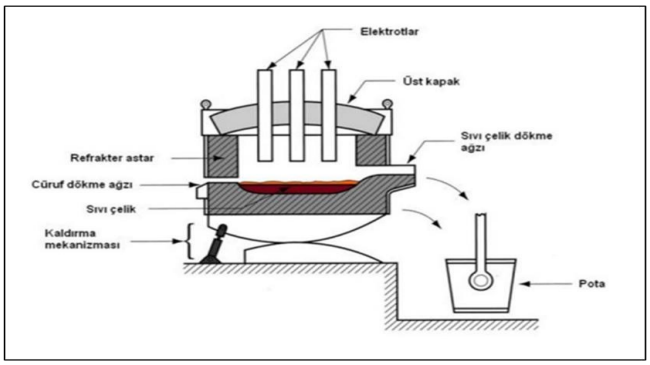


Figure 2. General view of an electric arc furnace.

The main reasons for the high preference of electric arc furnaces compared to blast furnaces are ease of production, installation costs, fast start-up and shutdown compared to blast furnaces. While 60% of the world's steel production is carried out in integrated production sites and 40% in EAFs, when this ratio is analyzed for our country, 34% of the steel production is carried out in integrated production facilities and 66% in EAFs. The main reasons why electric arc furnaces take the majority of the production are the low initial investment cost and the ease of material procurement since scrap is used as raw material [16]. In today's industry, scrap metallurgy has been developed and combined with secondary metallurgy, and with this advantage, it has emerged as the leading role in the production of steel types with a wide product range and comparatively heavy tonnage steel types such as carbon and structural steels.

3. Zinc Production from Secondary Sources

Zinc-containing products, e.g. galvanized steel, are used as a source of raw materials for recycling. These products are collected and processed according to scrap availability, alloy composition (e.g. purity, etc.) and ease of processing [17]. Today, more and more zinc is being produced, resulting in the generation of a large amount of zinc-containing waste (new scrap) at various stages of production. Table 1 shows the generation of new and old zinc scrap at different stages of zinc production and Figure 3 shows the material cycle in zinc recycling.

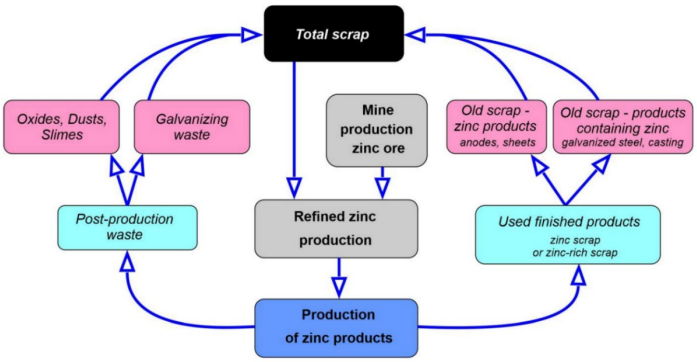


Figure 3. Material cycle in zinc recycling.

Table 1. Sources and types of zinc scrap. Sources and types of zinc scrap, calculated according to [17].

Scrap Source	Scrap Type			Recovery Process
	Skimming-New Scrap	Finished Products-Old Scrap	Steel Dust- Old Scrap	
Brass/Bronzes	Yes	Yes	No	Remelting
Zn-Al alloys	No	Yes	No	Remelting
Galvanizing	Yes	No	Yes	New Scrap-remelting, old scrap-refining
Rolled zinc - Zn-Ti sheets	No	Yes	No	Remelting
Other	Yes	Yes	Yes	New Scrap-remelting, old scrap-refining

The primary energy intensity of zinc production ranges from 49 to 55 GJ/ton. Energy savings from recycling steel (especially in the case of galvanized steel) and zinc can range from 60 to 75% [18]. Worldwide, about 20% of zinc is converted into new scrap in batch and continuous galvanizing processes.

Zinc concentrates have a relatively constant chemical composition, while the resulting zinc waste contains varying amounts of zinc. Table 2 shows the characteristics of zinc precipitates generated in industry and in the production process. Galvanized steel is the main source of secondary zinc, both in the galvanizing process and in the remelting of galvanized steel. The specificity of the hot-dip galvanizing process results in lower zinc utilization efficiency compared to other areas of zinc production and consumption. Zinc consumption depends not only on the thickness of the coating, but also on losses due to the peculiarities of the technology, namely the formation of hard zinc and galvanizing ashes, oxidation of the bath surface and the formation of solidified zinc precipitates. Studies have shown that one ton of zinc used in the hot-dip galvanizing process generates 147.6 kg of hard zinc and 139.3 kg of zinc ash. The average zinc content in hard zinc ranges from 94 to 96 wt%, while the average zinc content in galvanizing ashes ranges from about 70 wt%. This means that for every tonne of SHG zinc delivered to the galvanizing plant, on average about 240 kg of zinc is inefficiently used to generate waste in the form of hard zinc and zinc ashes [19]. These are zinc-rich by-products, which are of course the raw material for secondary zinc production.

Table 2. The properties of various zinc wastes generated in industry and in the production process, based on the studies [18, 20, 21].

Waste	Source of Formation	Chemical Composition
Zinc ashes	Oxide surface on galvanizing bath	60–80% ZnO, 2–12% Cl, 0.2–1.5% Fe, <0.3% Al, small amounts of alloy additives for the bath Pb, Bi, Sn
Hard zinc	Particles of the intermetallic phases of the Fe-Zn system that fall to the bottom of the galvanizing bath	96% Zn, 4% Fe
Zinc slimes	Wet flux on the surface of the galvanizing bath	5.6% Zn, 48.1% $ZnCl_2$, 27.4% ZnO, 3.1 $AlCl_3$, 15.8% NH_4Cl and Fe and other oxides
Other waste from hot dip galvanizing process	Residues after finishing and cleaning products from infiltrations and thickenings of zinc	81% Zn, 16% ZnO, 0.3% Fe, small amounts of alloy additives Pb, Bi, Sn for the galvanizing baths
Brass skimming	An insoluble alloy that sinks to the bottom of the brass bath	41–42% Zn, 41–42% Cu, 1–2% Fe, 1–2% SiO_2, 0.1–0.5% Cl
Brass ashes	Volatile oxide surface on brass bath	20–30% ZnO, 4–8 Cu, 1.5–2.5 Fe, 0.25–20% SiO_2, 0.1–0.3% Cl
EAF kiln dust	Dust from the EAF furnace collecting above the bath	19.4% Zn, 24.6% Fe, 6.8% Cl, 4.5% Pb, 2.2% Mn, 1.2% Mg, 1.4% Si, 0.42% Cu, 0, 4% Ca, 0.3% Cr, 0.1% Cd
Waste after precipitation	Zinc metallurgical residues from purification of the electrolytic solution	9.5% Zn, 1.44% Co, 2.3% Fe, 5.27% Mn, 1.1% Cu, 0.16% Cd
Sludge from the washing process of rayon	Precipitated solution after washing rayon	18–40% $Zn(OH)_2$, 60–82% $CaCO_3$, others

Zinc oxidation on the surface of the galvanizing bath forms zinc oxide (galvanizing ash) contaminated with flux decomposition products. The need to clean the bath surface before each dip and the emergence of the charge creates a significant amount of galvanizing ash. Ensuring a high quality coating requires constant cleaning of the bath surface and periodic removal of galvanizing ash. During the collection of ashes, it is also inevitable that a significant amount of "pure" zinc is removed from the surface. Galvanizing ashes are therefore a zinc-rich waste. The hot-dip galvanizing process also provides zinc-rich waste left over from the purification of finished products. Surface zinc thickening and drips are removed by mechanical grinding and the removed zinc is remelted. Zinc-rich wastes are also the zinc sludge produced when wet fluxing is used. However, wet galvanizing is now used much less frequently.

Another important source of zinc is electric arc furnace (EAF) dust. The EAF furnace is estimated to produce 15-25 kg of dust per ton of crude steel, with zinc content ranging from 10 to 40%. The minimum zinc content required for the zinc recovery process from steelmaking dust to be profitable depends on various factors such as proximity of steel mills, energy costs, slag cost, etc., but should be around 15% [22]. Zinc is also present in steelmaking dust from the conversion process (BOF). However, the zinc content in it ranges from only 0.5% to 6%. This value is too low for profitable recovery of zinc from these dusts. Zinc cannot be recovered from BOF process dusts; the recommended solution in this case is to collect galvanized sheet scrap and send it to the EAF process or to de-zincify steel scrap [23, 24, 25].

Hydrometallurgical production of zinc produces deposits, leaching and purification residues. In the production of rayon fiber yarn, zinc is used as a modifier for cellulose regeneration. After the rayon is made, it is washed and the solution contains 30-50 ppm zinc, which precipitates in the form of zinc hydroxide [21].

Studies on the recycling of galvanized steel scrap are mainly concerned with alkaline dezincification, i.e. the dissolution of zinc with hot caustic soda (NaOH) into sodium zincates (Na2ZnO2 and $NaHZnO_2$)-Figure 4a. Zinc is recovered electrolytically in powder form, while uncoated steel is easily used for remelting [26]. Acid dezincification has recently become very popular - Figure 4b. Typically very low acid concentrations make the process safe and the dissolution reaction takes place spontaneously without the need for heating or using an external electrical source. The advantage of using dilute acids is that the zinc coating is completely dissolved with little or no attack on the steel substrate; the zinc is eventually recycled while the zinc is recovered from the solution in metallic form or as a metal salt, depending on the type of acid used.

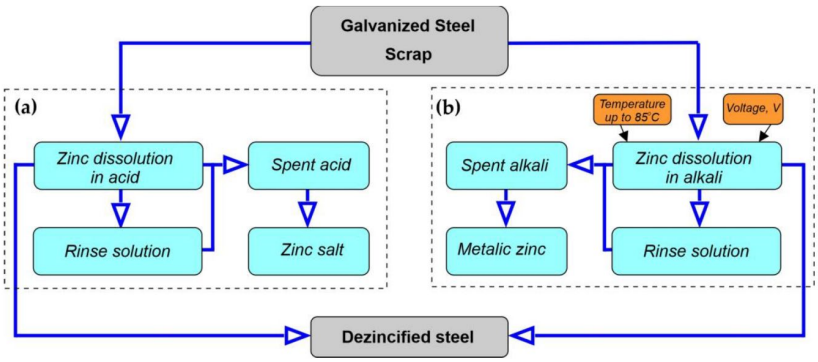


Figure 4. Scheme: (a) acidic and (b) alkaline dezincification of galvanized products.

In the case of the acid dezincification process, it has been found that more concentrated acids (more than 10%) tend to accelerate the dezincification rate, but also have an intense effect on the dissolution of the steel substrate. Dilute acids (2% or less) reduce the dissolution rate, but tend to partially or even ineffectively dezincification [26].

In summary, hydrometallurgical processes can produce precious metals with high mass fraction. The energy consumption of the processes is low due to their low temperatures. Unfortunately, these methods require devices to have high corrosion resistance. The slag obtained after leaching is also problematic due to its complex composition and cannot meet the storage requirements of environmental protection law. Pyrometallurgical methods are also used for dezincification (for example, in Japan there are two plants based on this solution), but they are much more expensive. They focus on steel scrap and the recovery of zinc products is practically low [27]; moreover, these processes are highly energy intensive and require large equipment.

Figure 5 shows the flow of recycled zinc, taking into account the hot-dip galvanizing process and finished products withdrawn from circulation [28]. Currently, about 70% of zinc comes from primary refining of zinc ores (including 10-15% from recycling sources) and about 30% from directly recycled zinc (corresponding to 80% of the zinc available for recycling). The long lifetime of galvanized steel products in the construction sector makes their appearance in waste streams difficult to predict.

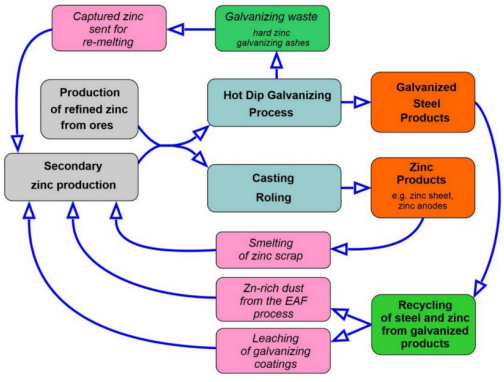


Figure 5. Recycling zinc flow. Recycling zinc flow, including the hot-dip galvanizing process and finished products withdrawn from circulation.

In the case of zinc, the following two recycling rates are used: end-of-life (EOL) and recycled content (RC). The EOL indicator offers a very comprehensive approach, taking into account recycling efficiency, product life and past production patterns; it measures the value of zinc actually recovered and recycled into new metallic zinc at the end of the product's life ('old scrap'). It is estimated that around 45% of the zinc present at the end of the life of various zinc-containing products is recovered and actually recycled (Table 4). In developed regions such as Europe and North America, the EOL rate can be 50% or more. In developing regions, it is 30-40% due to the lack of developed recycling networks and regulatory initiatives aimed at reducing industrial waste [21]. Recycled content RC is a measure of the recycled content in a product. The recycled content for refined zinc is currently around 8% (scrap combined with concentrate as raw material in the smelter).

Table 4. Recycling process indicators [21].

Indicator	Description	Estimated Global Recycling Rate
Recycled content (RC)	Zinc scrap fraction (new and old) in the total use of metal in production	25%
Ratio of old scrap	Zinc fraction from old scrap in the general recycling loop	70%
EOL recycling rate	Fraction of recycled zinc in relation to the amount of zinc available at the end of its life	45%

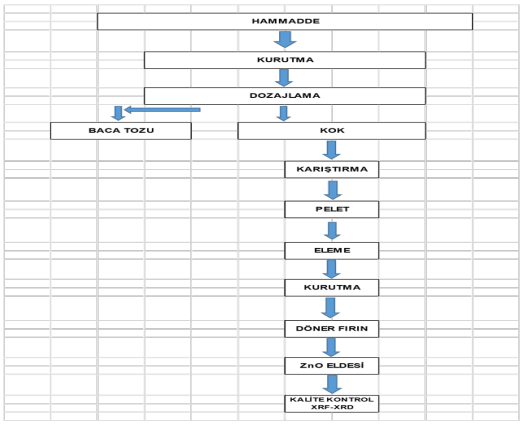
Table 4 shows the production of zinc, taking into account the method of obtaining it. Over the years, more emphasis has been placed on the amount of recycled zinc. However, the lifetime of zinc-containing products is variable. This is especially true for galvanized products, where zinc is used to extend their durability. The durability of zinc coating protection depends on the needs of the market and the application. For example, in the case of the service life of automobiles or household appliances, the service life can be between 10 and 15 years. Although the zinc in these products still fulfills its protective role, these products are scrapped due to corrosion of other elements and subassemblies. The situation is different in the case of corrosion protection of steel structures and products operated in an atmospheric environment with different corrosive aggressiveness. The aggressiveness of the atmospheric environment depends on many factors such as temperature, humidity and the content of aggressive components, e.g. chlorides, sulfur compounds, weather factors, etc. The aggressiveness of the natural atmospheric environment may change over time. In this case, the durability of galvanized elements varies from a few to 100 years and is difficult to predict.

Table 5. Total zinc production, disaggregated into primary and secondary zinc production and unbundled production, in thousands of tons, based on data in [29, 30, 31].

Year	1991	1995	2000	2005	2010	2015	2017
Primary production, thous. tone	4370	4160	4330	4680	4810	12,600	12,700
Secondary production, thous. tone	376	345	348	298	279	409	447
Undistinguished production, thous. tone	2570	2980	4460	5770	7710	711	691

4. Material and Method

The most promising solvent reagents, namely NH_3 + NH_4Cl, H_2SO_4, and HCl, were chosen following a thorough literature review.



(a)



(b)

Figure 6. (a) Experimental Flowsheet, (b) Leaching setup

In terms of the beneficiation of the blast furnace dust, 3 types of experiments were carried out. In this study, the feasibility of pivot-scale ZnO production from EAF flue dusts was investigated and the desired studies are given in Figure 6 (a) respectively.

Rigaku Ultimate IV brand XRD device at Karabük University Iron and Steel Institute will be used for phase analysis of the flue dust before and after the Waelz oxide process. The visual of this device is shown in Figure 7 (a). Rigaku Primus II - X-Ray brand XRF device located in Karabük University Iron and Steel Institute in Figure 7 (b) will be used for elemental analysis.



(a)



(b)

Figure 7. (a) XRD Analysis Equipment, (b) XRF Analysis Equipment

5. Results and Discussion

Leaching in ammonia-ammonium chloride

Experiments were performed to evaluate the effectiveness of ammonium chloride leaching. The objective of these experiments was to identify the optimum NH_3 consumption for achieving maximum zinc extraction.

However, as depicted in Figure 9, zinc recovery rate is only up to 17%, which is significantly below the desired benchmarks for successful implementation of the technology. These findings suggest that the ammonia-chloride leaching method does not offer optimal conditions for treating this particular type of dust.

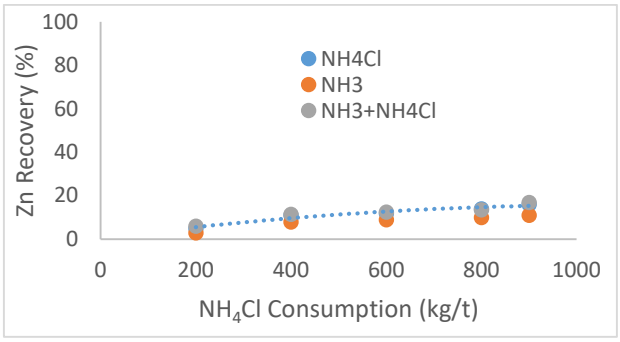


Figure 9. NH_3 (kg/t) consumption vs. Zn recovery (%).

Leaching in sulfuric acid

A similar series of experiments was conducted for sulphuric acid leaching. The results showed that while sulfuric acid consumption increases, the rate of Zn recovery increases up to 85 %. (See Figure 10).

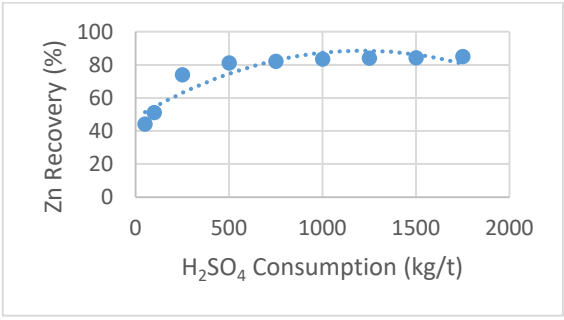


Figure 10. H_2SO_4 (kg/t) consumption vs. Zn recovery (%).

Leaching in hydrochloric acid

Similar experimental procedure was employed for testing hydrochloric acid leaching. As it can be depicted in Figure 11, the most favourable choice would be to use an acid quantity of 400 kg/t. With this flow rate, zinc extraction of up to 95% can be achieved. This acid consumption allows for a relatively high level of acid regeneration.

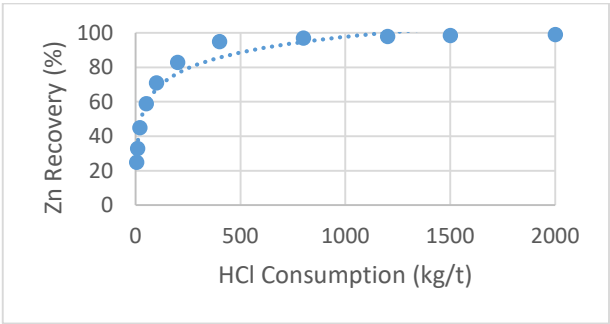


Figure 11. HCl (kg/t) consumption vs. Zn recovery (%).

6. Conclusions

Considering the environmental impact and sustainability aspects, hydrometallurgical technology emerged as the more favourable option. This technology offers reduced environmental impact, a small carbon footprint, easy recovery of by-products, and the ability to regenerate components. To determine the optimal method, the mineralogical and chemical composition of the sludge was thoroughly analysed. It was found that the sludge contained a low amount of poorly soluble zinc ferrite and mainly zinc in oxide form, which influenced the selection of the leaching reagents. Leaching experiments were conducted to determine the optimum parameters for each process. Hydrochloric acid leaching emerged

as the most successful method, achieving a remarkable 95% recovery of zinc at an optimum HCl consumption of 400 kg/t. Based on this finding, a new process for blast furnace dust processing in terms zinc recovery can be developped specifically for hydrochloric acid leaching.

In conclusion, the findings presented in the context of this study provides a valuable contribution to the field of blast furnace sludge recycling. The developed technology for hydrochloric acid leaching offers a practical and sustainable solution for zinc recovery from sludge. The findings of this study are promoting a more environmentally friendly and economically viable approach to waste management and resource recovery.

References

[1]. Sverdrupa, H.U.; Olafsdottira, A.H.; Ragnarsdottir, K.V. On the long-term sustainability of copper, zinc and lead supply, using a system dynamics model. Resour. Conserv. Recycl. 2019, 4, 100007.

[2]. Ragnarsdottir, K.V.; Sverdrup, H.; Koca, D. Substitution of metals in times of potential supply limitations: What are the mitigation options and limitations? In In Proceedings of the 2015 World Resources Forum, Davos, Switzerland, 11–15 September 2015.

[3]. Graedel, T.E.; Erdmann, L.Will metal scarcity impede industrial use? Met. Res. Soc. Bull. 2012, 37, 325–333.

[4]. Gandhi, S.M. Ancient mining and metallurgy in Rajasthan. In Crustal Evolution and Metallogeny in the Northwestern Indian Shield: A Festschrift for Asoke Mookherjee; Deb, M., Ed.; Alpha Science Int. Ltd.: Oxford, UK, 2000; pp. 29–51. ISBN 1-84265-001-7.

[5]. Emsley, J. Nature's Building Blocks: An A-Z Guide to the Elements; Oxford University Press: Oxford, UK, 2001; pp. 499–505. ISBN 978-0-19-850340-8.

[6]. Habashi, F. Zinc—The Metal from the East. Bull. Can. Inst. Min. Met. 2001, 94, 71–76.

[7]. Ostrowska-Popielska, P.; Sorek, A. Przegla˛d i wste˛pny dobór technologii odzysku cynku ze szlamów i pyłów stalowniczych. Pr. Inst. Metal. Z˙ elaza 2012, 64, 39–46. (In Polish)

[8]. Zhang, C., Zhuang, L., Wang, J., Bai, J. & Yuan, W. (2016). Extraction of zinc from zinc ferrites by alkaline leaching: enhancing recovery by mechanochemical reduction with metallic iron. J. S. Afr. Inst. Min. Metall. 116(12), 1111-1114.

[9]. Kalpaklı, A., Ayaz, Ş., İlhan, S., & Zorağa, M. (2020). Tehlikeli atık sınıfında olan elektrik ark fırını baca tozlarından hidrometalurjik yöntemler kullanılarak çinkonun geri Güncel değerlendirmeler. Journal of Anatolian Environmental and Animal Sciences, 5(3), 274-282.

[10]. Morcali, M. H., Yucel, O., Aydin, A., & Derin, B. (2012). Carbothermic reduction of electric arc furnace dust and calcination of waelz oxide by semi-pilot scale rotary furnace. Journal of Mining and Metallurgy, Section B: Metallurgy, 48(2), 173-184.

[11]. Antuñano, N., Cambra, J. F., & Arias, P. L. (2019). Hydrometallurgical processes for Waelz oxide valorisation–An overview. Process Safety and Environmental Protection, 129, 308-320. 2) Process Safety and Environmental Protection

[12]. Yang, J., Huang, R., He, X., Lv, X., Zhu, R., Jin, H., & Deng, X. (2023). Research for the recovery of Zn and Pb from electric arc furnace dust through vacuum carbothermal reduction. Process Safety and Environmental Protection, 170, 960-970.

[13]. Wang, J., Zhang, Y., Cui, K., Fu, T., Gao, J., Hussain, S., & AlGarni, T. S. (2021). Pyrometallurgical recovery of zinc and valuable metals from electric arc furnace dust–a review. Journal of Cleaner Production, 298, 126788.

[14]. Grogan, J. Dezincing of Galvanized Steel. Ph.D. Thesis, Colorado School of Mines, Golden, CO, USA, 2015.

[15]. Langill, T. North American Galvanizers process Survery. In In Proceedings of the 19th International Galvanizing Conference, INTERGALVA 2000, Berlin, Germany, 1–8 March 2000; EGGA: Berlin, Germany, 2000; pp. 1–7.

[16]. Jha, M.; Kumar, V.; Singh, R.J. R. Review of hydrometallurgical recovery of zinc from industrial wastes. Resour. Conserv. Recycl.2001, 33, 1–22.

[17]. Sahu, K.K.; Agrawal, A.; Pandey, B.D. Recent trends and current practices for secondary processing of zinc and lead. Part II: Zinc recovery from secondary sources. Waste Manag. Res. 2004, 22, 248–254.

[18]. Palimąka, P., Pietrzyk, S., Stępień, M., Ciećko, K., & Nejman, I. (2018). Zinc recovery from steelmaking dust by hydrometallurgical methods. Metals, 8(7), 547.

[19]. Lin, X., Peng, Z., Yan, J., Li, Z., Hwang, J. Y., Zhang, Y., ... & Jiang, T. (2017). Pyrometallurgical recycling of electric arc furnace dust. Journal of Cleaner Production, 149, 1079-1100.

[20]. Abanades, S., Charvin, P., & Flamant, G. (2007). Design and simulation of a solar chemical reactor for the thermal reduction of metal oxides: Case study of zinc oxide dissociation. Chemical Engineering Science, 62(22), 6323-6333.

[21]. Masson, N., & Briol, P. (2017). A brief summary of zinc oxide processing methods available for the Bongara deposit. PBSIM & BFS Consulting Engineering, Published by ZINC ONE RESOURCES INC, 1-11.

[22]. Kurka, V., Jonšta, P., Kotásek, O., & Mlčoch, P. (2021). Reducing the content of zinc in metallurgical waste in a rotary kiln. In Proc. WASTE (p. 78).

[23]. Ye, F., Li, M., Su, S., Xia, H., Wei, C., Li, X., & Deng, Z. (2024). Separation and recovery of zinc from blast furnace dust via coordination leaching of Cl− and hydrolysis of NH4+. Separation and Purification Technology, 330, 125361.

[24]. Muica, V. T., Ozunu, A., & Török, Z. (2021). Comparative life cycle impact assessment between the productions of zinc from conventional concentrates versus Waelz oxides obtained from slags. Sustainability, 13(2), 580.

[25]. Antuñano, N., Cambra, J. F., & Arias, P. L. (2017). Development of a combined solid and liquid wastes treatment integrated into a high purity ZnO hydrometallurgical production process from Waelz oxide. Hydrometallurgy, 173, 250-257.

[26]. Peltekov, A. B., Boyanov, B. S., & Markova, T. S. (2014). Behavior of arsenic in hydrometallurgical zinc production and environmental impact. Polish Journal of Chemical Technology, 16(4), 80-86.

[27]. Iureva, G. (2023). Hydrometallurgical Recovery of Zinc from Blast Furnace Sludge.

[28]. Ijomah, M.N.C.; Ijomah, A.I. Chemical recycling of galvanized steel scrap. Indian J. Chem. Technol. 2003, 10, 159–165.

[29]. Kania, H., & Saternus, M. (2023). Evaluation and current state of primary and secondary zinc production—a review. Applied Sciences, 13(3), 2003.

[30]. Gock, E.; Vogt, V.; Schonfelder, I.; Carlowitz, O.; Zeller, T.; Sauter, A.; Pilkahn, H. Process for the Acid Pre-Dezincification of Steel Scrap. In In Proceedings of the XXVI International Mineral Processing Congress, New Delhi, India, 24–28 September 2012. No. 729.

[31]. Xiao, X., Zhang, S., Sher, F., Chen, J., Xin, Y., You, Z., ... & Qiu, G. (2021). A review on recycling and reutilization of blast furnace dust as a secondary resource. Journal of Sustainable Metallurgy, 7(2), 340-357.

Valuable Metals dissolution from Flash Furnace Electrostatic Precipitators (ESP) Dust by atmospherically Sulfuric acid leaching

Mehmet Canbazoğlu [1]*, Arzu Yılmaztürk [1], Gizem Demirdağ Özel [1]

[1] Etibakır AŞ. R&D Center, Samsun/ TURKEY

*Corresponding author: Mehmet.canbazoglu@etibakir.com.tr (Mehmet Canbazoğlu)

Abstract:

In this study, it was aimed to separate and recover the Cu and Zn contained in the Electrostatic Precipitators (ESP) dust by dissolving it with H2SO4 under atmospheric conditions. In this context, Eti Bakır AŞ. Samsun facility Flash smelting ESP dust was used in the studies. The parameters examined were leaching temperature (50-70-90 oC); Acid concentration (100-150 g H2SO4/L) and leaching time were taken from 2 to 8 hours. Solid/Liquid ratio is fixed and taken as 1/5. The results reveal that optimum dissolution can be achieved in the first 2 hours. 85% of the copper in the feed; It was revealed that 70.90% of zinc and 51.33% of iron could be dissolved, the acid consumption was 76 kg H2SO4 / t dust and 71.90% of the dust was dissolved. This result shows that if the remaining cake after the acid leaching process is fed back to the smelter, processing the dust in the smelter system with acid leaching processes can increase the capacity of the smelter.

Keywords: *Flash Smelter, ESP dust, Sulfuric Acid, Atmospheric leaching*

1. Introduction

Copper is produced by the pyrometallurgical method, mostly by using the 'flash and converter' smelting method (Schlesinger et all, 2011; Hanniala et all, 1999). Naturally, the dust formed during smelting in the flash furnace and converter is moved by air circulation in the waste heat boiler, cyclones and ESP, and is kept and recovered in the system by circulating in the existing system showed in Figure 1. In these processes, the excess of impurities in the composition of the powders reduces the furnace capacity.

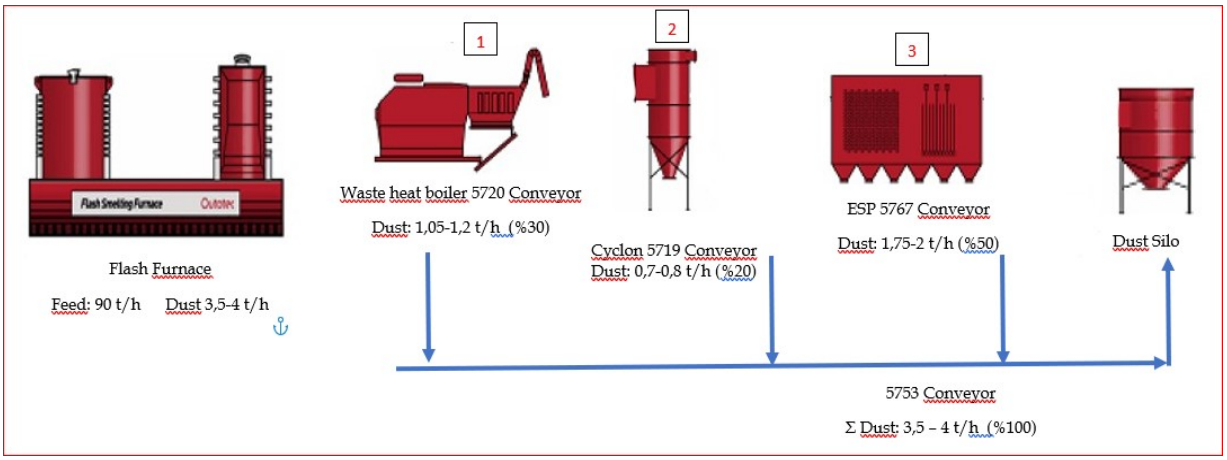


Figure 1. Flash furnace dusts

The most important parameter that determines the properties of powders in the classical flash furnace system is Pb, Zn, As, Sb and similar minerals found in small or large amounts in the copper concentrate fed to the furnace. Another important parameter is the oven regime. The parameters such as furnace feed amount, furnace air and/or oxygen feed rate, control of exothermic temperatures and so on are very important in terms of characterization of the dust to be formed. In addition, the dust contains partially reacted, oxidized, drifted sulfur minerals whose mineralogical composition has changed, as

well as unreacted, unoxidized sulfur minerals. The minerals that make up these dusts are new minerals that are partially or completely oxidized and are not minerals with a characteristic structure formed geologically. The copper minerals formed may contain iron, arsenic, lead and similar elements in different proportions (Okanihbe et all, 2017).

Just as the dusts obtained from each copper smelter have different element tenor and mineralogical composition, it is seen that different approaches have been developed in the economic evaluation of these dusts and, accordingly, different methods have been considered. Atmospheric Sulfuric acid leaching was the first notable method to be tried in leach Temperature from 50 ^{o}C to 90 ^{o}C (Caplan et all, 2021). On the other hand, acid leaching of the powders under pressure at 210 ^{o}C and 7 bar was also tested (Zhi-feng XU et all, 2010). Another remarkable way is the evaluation of powders by agglomeration (Ryan et all, 1999).

Acid leaching reactions of metal oxides can be written as follows(*Me*: Refers to +2 valued elements):

$$MeO_{(s)} + H_2SO_{4(aq)} \longrightarrow Me^{2+} + SO_{4(aq)}{}^{2-} + H_2O_{(l)}$$

Acid leaching reactions of metal sulfides can be written as follows (Schlesinger et all, 2011):

$$MeS_{(s)} + 2\ O_{2(g)} + H_2SO_{4(aq)} \longrightarrow MeSO_{4(aq)} + H_2SO_{4(aq)}$$

The purpose of this study is to examine whether more concentrate can be fed to the flash furnace if the ESP dust rotating in the flash furnace - Waste heat boiler - Cyclones - Electrofilter is removed from the system. For this reason, the necessary parameters have been determined if acid leaching can be applied.

2. Material And Method

Flash Furnace Electrostatic Precipitators (ESP) Dust samples was taken from ETİ BAKIR A.Ş. Samsun Copper Smelter. This sample, which was taken at intervals for 3 days while the facility was ringing, was prepared by reducing it for tests in the laboratory. The grain size of the sample is d96 20 microns. The ESP chemical analysis was performed in Table 1. The powder contains significant Fractions of Cu Zn Fe S and As. This powdered material, which is exposed to high temperature in a flash furnace, also shows a complex mineralogical structure. Significant amounts of Zinc Iron oxides, Copper oxides and sulfides, as well as Iron sulfide minerals were detected by XRD(Table 2).

Table 1 . Chemical composition of Flash Furnace Electrostatic Precipitators (ESP) Dust

Elements	%	Elements	%
Cu	12.29	Bi	0.14
Zn	10.14	Cd	1.17
Pb	3.92	Co	0.67
Fe	19.91	Ba	0.36
As	4.84	S	6.93
Sb	0.06	SiO2	1.34

Table 2 . Mineralogical composition of Flash Furnace Electrostatic Precipitators (ESP) Dust

Determined Minerals by XRD	%
Zinc iron oxide, Franklinite	27.4
Copper oxides/sulphates	11.8
Copper sulfide	8.2
İron sulfide, Pyrrhotite	20.0
İron oxide,	19.0
Copper Lead Antimony Sulfide, Zinkenite	6.8
Aluminum Arsenate Hydroxide Hydrate Bettertonite	6.8

The tests were carried out in the laboratories of ETI BAKIR AŞ R&D Directorate. Magnetic mixer and heater with contact thermometer and 1000 ml leaching balloon were used in the tests. The resulting water vapor was controlled by a serpentine back cooling system placed on top of the balloon. The parameters examined were leaching temperature (50-70-90 oC), Acid concentration (100-150 g H2SO4/L) and leaching time was from 2 to 8 hours. The Solid/Liquid ratio is constant and 1/5 is taken.

3. Experimental Results And Discussion

3.1. Effect of Leach Temperature

The solubility of Cu, Zn, Fe, As, Pb, Bi, Sb found in ESP dust was studied by leaching with sulfuric acid at 3 temperatures for 8 hours. The Fractions of Cu, Zn, Fe, As, Pb, Bi, Sb were analyzed. The results are given in Table 3 and Figure 2.

Table 3. Effect of leaching temperature (S/L 1/5; Samples 125 g; Leaching time 8 hours; Acid concentration 150 gH_2SO_4/L.)

Temperature °C	Total dissolved %	Dissolved elements %								Acid Cosumption (kg/t ESP)
		Cu	Zn	Pb	Fe	Bi	As	Sb	S	
50	59.48	74.28	51.56	0.32	21.62	19.25	95.70	21.85	89.53	23.63
70	63.57	78.23	57.72	1.47	32.59	28.17	97.79	36.34	89.54	40.12
90	71.90	85.02	70.90	2.68	51.33	51.57	98.60	58.35	90.27	13.60

The findings obtained reveal the following determinations:

1.As the temperature increases from 50 ° C to 90 ° C, the total solute weight of ESP dust also increases from 59.48% to 71.90%. On the other hand, acid consumption is increasing rapidly from 23.63 at 50 oC to 131.60 kg H2SO4/t ESP at 90 oC.

2.The dissolution of elements from ESP dust occurs when the leaching temperature is increased from 50 oC to 90 oC.; dissolved elements were increased as Copper from 74% to 85%, Zinc from 51% to 70%, iron from 21% to 51%, Bismuth from 19% to 51%, Antimony from 21% to 58%, Arsenic from 95%-98% and Sulfur from 89%-90%.

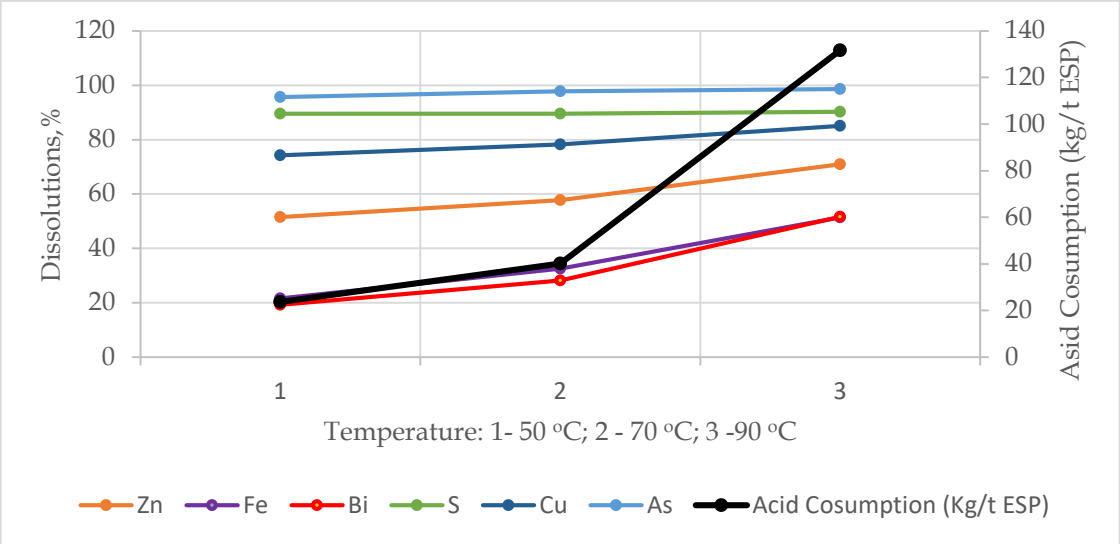


Figure 2. Effect of Leach temperature

3.2. Effect of Acid Concentrations via leach time

Leaching test was performed on two different sulfuric acid concentration. In these experiments, samples were taken from leach ballon and analyzed at 2-hour intervals. The results obtained are given in Table 4 and Figure 3.

The findings obtained reveal the following determinations:

1.As the acid concentration increases from 100 to 150 g H2SO4/L, the total dissolved weight of ESP dust also increases from 61.21% to 71.90% after 8 hours leaching. On the other hand, acid consumption is increasing rapidly from 34.14 at 100 g/L to 131.60 kg H2SO4/ton ESP at 150 g H2SO4/L.

2. It is seen that 2 hours of leaching time is sufficient for both acid concentrations examined and there is no significant increase when the leaching time is increased. On the other hand, metal solubility increases slightly with increasing acid.

Table 4. Effect of Acid Concentration via leaching time. (S/L 1/5; Samples 125 g; Leaching Temperature 90 °C)

Acid concentration (g H_2SO_4/L)	Time Hour (h)	Dissolved %								Acid Consumption (kg/t ESP)
		Total Weight	Elements							
			Cu	Fe	Zn	Pb	Bi	As	Sb	S	
100	2	61.21	76.71	30.64	64.21	9.23	54.61	92.02	26.57	88.92	34.14
	4		76.98	30.21	63.38	5.25	52.95	94.70	27.96		
	6		75.63	29.98	63.88	9.03	56.26	95.50	29.34		
	8		77.17	30.00	64.30	3.00	48.55	94.40	29.34		
150	2		84.23	47.54	68.64	24.92	59.74	98.14	52.32		
	4		84.20	50.28	69.12	17.91	58.34	98.30	53.83		
	6		84.83	51.45	69.85	9.14	58.54	98.50	56.84		

8	71.90	85.02	51.33	70.90	2.68	51.57	98.60	58.35	90.27	131.60

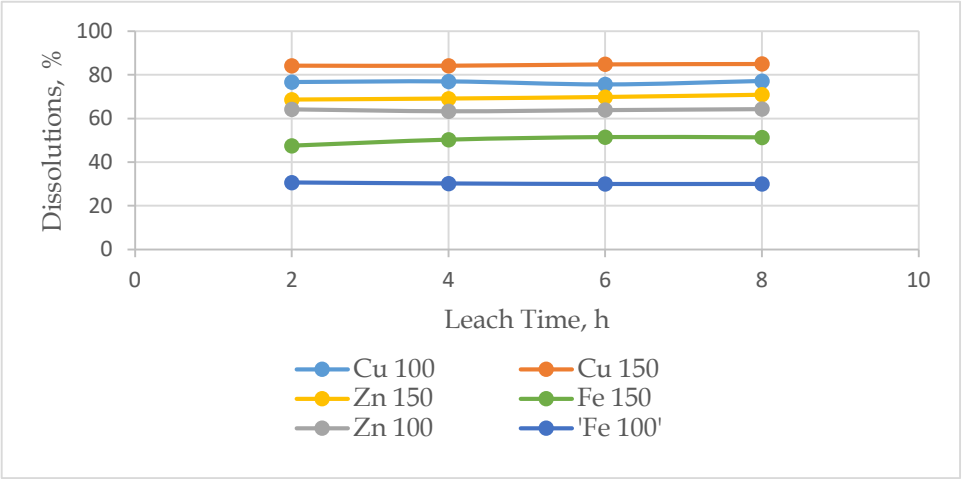


Figure 2. Effect of Acid Concentration via leach time

In conclusion under current operating conditions, approximately 3-5% of the amount fed into the Flash furnace circulates in the system as dust. 50% of these dusts are ESP dust. Naturally, taking these dust from the flash furnace results in more concentrated feeding. However, since the amount of dust dissolved in acid leaching is 70%, the insoluble part will be mixed into the feed as a cake and fed back to the smelter. However, the smelter feed amount increases as the dissolved dust increases. In this recommended current diagram, there is no loss of copper, gold and silver. On the other hand, a significant amount of zinc metal can be produced.

4. Conclusion

Optimum acid leaching conditions for ESP dust are found 2 hours leaching at 90 °C, Solid/Liquid 1/5, Acid concentration 150 g H_2SO_4/L. The amount of acid consumed is 131 kg/t ESP dust and the total amount of dissolved ESP dust is 71%. Under these conditions, the amount of copper dissolved in ESP dust is 84.23%, while the amount of zinc is 68.64%. Bismuth is taken into solution at 59.74%, Antimony at 52.32% and Arsenic at 98.14%. Along with these soluble elements, a significant amount of iron is also dissolved (47.54%).

An acid leaching facility can be established where ESP powder and other flash furnace powders can be evaluated together. It seems possible to apply the following flowchart in this new facility. Accordingly;

1. Powder acid leaching facility will be established. Cake-pregnant solution separation will be made. The cake will be sent to the copper concentrate feed blend. The loaded solutions will be sent to the Solvent Extraction (SX) facility.

2. Copper solution suitable for electrowinning can be produced from pregnant leaching solutions by solvent extraction (SX), and electrowinning (EW) EW unit and cathode copper can be produced.

3. Fe, As, Sb and other impurities will be removed by precipitation.

3. Zinc can be recovered as cathode zinc in the SX + EW facility to be established.

Acknowledgments

The authors acknowledge ETİ BAKIR Company Bosses Mr. Şeref CENGİZ and Mr. A. Osman CENGİZ, Samsun Facility General Menager Mr. Ali YILMAZ, Samsun Quality and Control Menager Mrs. Gülgün ÖZCAN and Our Research and Developing Center Management for giving us their support during this study.

References

Hanniala, P., Helle, L. and Kojo, I.V. (1999). Competitiveness of the Outokumpu flash smelting technology in the third millennium. In Copper 99-Cobre 99 Proceedings of the Fourth International

Conference, Vol. V Smelting Operations and Advances, ed. George, D.B., Chen, W.J., Mackey, P.J. and Weddick, A.J., TMS, Warrendale, PA, 221 238.

Schlesinger M. E., King M. J., Sole K. C., & Davenport W. G., (2011). Extractive Metallurgy of Copper, Fifth Edition, Elsevier , 417 pp, 89-110

Caplan M., Trouba J., Anderson C., & Wang S.,(2021). Hydrometallurgical Leaching of Copper Flash Furnace Electrostatic Precipitator Dust for the Separation of Copper from Bismuth and Arsenic, Metals, 11, 371, pp 1-18

DO Okanihbe, API Popoola , AA Adeleke.,(2017). Characterization of copper smelter dust for copper recovery, Int. Conference on Sustainable Mineral Processing And Manufacturing SMPM 2023-2025 January , Manufacturing 7, pp 122-126

Ryan, P., Smith, N., Corsi, C. and Whiteus, T., (1999). Agglomeration of ESP dusts for recycling to plant smelting furnaces," In Copper 99-Cobre 99 Proceedings of the Fourth International Conference, Vol. V Smelting Operations and Advances, ed. George, D.B., Chen, W.J., Mackey, P.J. and Weddick, A.J., TMS, Warrendale, PA, 561 571.

XU Zhi-feng , LI Qiang , NIE Hua-ping ., (2010). Pressure leaching technique of smelter dust with high-copper and high-arsenic, Transactions of Nonferrous Metals Society of China, Volume 20, Supplement 1, Pages s176-s181

Pipeline Leaching of Poor Ferrous Zinc Tailings following Microwave Tube Radiation - Cu and Zinc Recovery

Yıldırım İ. TOSUN [1*],

[1*]Şırnak University, Engineering Faculty, Mining Eng. Dept, Şırnak

*Corresponding author: yildirimismailtosun@gmail.com (Yıldırım İsmail Tosun)

Abstract:

The heap or column leaching of low-grade complex ores causes great danger to environment. Due to simultaneous integrated oxidative leaching and extraction of copper and zinc metals during pipeline haulage of tailings fine of Hakkari ferrous zinc tailings containing 14,7% Zn and Pb and Cu were investigated using a small-scale pipeline leaching column in the laboratory scale and aqueous sulphuric acid (2M) in aqueous solutions was performed at pH 4.5 as an dissolved electrolyte. The results showed sufficient leaching yields for zinc and Cu from the ores by pipeline leaching. The zinc concentration of the leach liquor in the first leaching–extraction circuit was 11.5 g/L, and in the 2th cycle the zinc concentration was 9.2 g/L and 0,4 g/L after the pipeline leaching cycled at giving higher 86% and 53% Cu extraction. The thickened and filtrated zinc sulfate solution provided high metal recoveries at ecah pipe line leaching cycle for zinc extraction.

Keywords: *Cu and Zinc Recovery, Microwave Leaching, Pipeline Leaching, Ferrous Zinc Tailings*

1. Introduction

In larger operations heap leaching and tank leaching methods commonly work in time dependent cycled line flows for dissolution of poor metal contents or wastes. This leaching method is requiring the production of sulphuric acid in the pyrite roasting, which provides the leaching agent required in the hydrometallurgical recovery of zinc and copper.(Canbazoğlu etal 1988, Keane 1987, Dayton 1987) However, in recent decades several major advancements in the field have allowed the hydrometallurgical recovery of copper to be increasingly competitive in certain circumstances. The hydrometallurgical recovery of zinc and copper bearing waste ores or tailings has advantages in both economic and environmental considerations.

There are two methods for solving copper and zinc; acid or basic amine dissolution showing longer kinetics (Hanilçi etal 2012). Higher rate of dissolution processing requires the reactive the zinc and copper-bearing minerals(Wang 2019, Ye et al 2017), followed by settling or electrolysis with which there are cathodic multi metal recoveries and subsequent refining. Short dissolution of waste Cu and Zn bearing ores processing commonly requires leaching using sulphuric acid, upgrading of copper using redox settling and subsequently electrowinning (Wang etal. 2020, Bodas 2019. Girgin and Kırşan 1990).

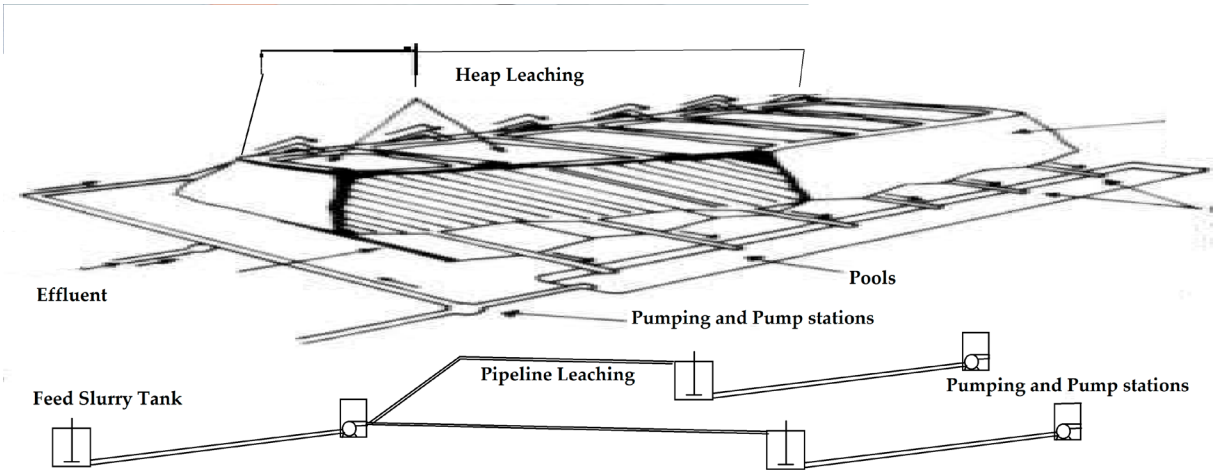


Fig. 1. Heap Leaching and Pipeline leaching on the comparison of the way of practice flow diagrams.(Tosun 2022)

Microwave heated mill slurries of Hakkari ferrous poor zinc ores used in this study. The studied process compromised a microwave heated leaching tube and pipe transferring in a modified type of the pressurized pipes at 5 bar. (Fig. 1) The leachate was transferred 10 mins time following microwaved slurry-water jet at 1 bar and then pressurized the slurry for pipeline transfer to the cycling leaching vessel. The tube leaching and pipe transfer leaching used for ultrafine particles, conventional type of ball mill used in cement materials.

1.1. Poor Oxide Ore Leaching

Heap leaching is the process of selectively taking the desired component into solution by sending solvent to the material on an impermeable ground. This process is applied in two main ways: prepared heap leaching and direct dump leaching. The importance of heap leaching applications is that they allow the economic evaluation of low-grade ores and tailings that cannot be evaluated with conventional methods. Zinc oxide ore is an important source of zinc metal after zinc sulfide ores. the zinc and copper-bearing minerals such as cuprite (CuO), gothite [$FeO \cdot H_2O$] and smithsonite ($ZnCO_3$), etc., have become an important source of zinc (Canbazoğlu, 1988). These applications are gaining increasing importance day by day, especially in the evaluation of low-grade and small-reserve deposits that are very far from the facilities where production is made with conventional methods. In addition, applications are often made for high-grade and small-reserve deposits. Currently; research and applications on this subject, especially gold and silver, copper and uranium ores, are being successfully continued (Dayton, 1987; Keane and Chase, 1987; Pizarro et al., 1987). In our country, in 1974, a preparatory heap leaching application was carried out for uranium ores in a pilot facility established by the MTA Institute(Girgin etal 1990 , Canbazoğlu etal 1988). In addition, Canbazoğlu (1988) completed laboratory column test studies on open-pit waste oxidized copper ores and they have reached the stage of starting a pilot-scale heap leaching application in Ergani Copper Enterprises.

Acid or alkaline leaching can be used to recover zinc ore waste by dissolving it. Alkaline reagents such as sodium hydroxide, ammonium hydroxide and sodium carbonate can selectively take the desired Zn and Cu metals into solution while Fe and other metals remain in the residue.(Santoro et al 2020, Santoro 2013) Conventionally, stirred leaching or pressure leaching, and stirred tank leaching after microwave pretreatment have been applied.(Tosun 2015, Tosun 2022) However, the recycling rate of Zn from ore wastes containing zinc and Cu, Mn, Cd and Pb was found to be at lower levels.(Kaya etal 2019). Additionally, ammonia solution and ammonia were used for poor copper-zinc ores. Recoveries were lower below 40%.

Acidic solutions such as sulfuric acid, hydrochloric acid and nitric acid dissolved Cu and Zn metals from poor ore wastes at certain saturation rates into salts dissolved in aqueous

environment.(Canbazoğlu, 1988) Sulfuric acid is the lowest cost among these acids and is widely used in the recovery of zinc-containing ore wastes by leaching [Kaya 2019]. Factors affecting sulfuric acid leaching efficiency include acid concentration, pH, leaching time, temperature, solid-liquid ratio.

1.2. Microwave Leaching

Zinc oxide ores can be dissolved under microwave radiation by acidic leaching processes (Bodas, 1996). However, zinc is dissolved following the dissolution of many other metals such as Fe, Ca, Mg. Pipe line transfer was preferred for slurries haulage in mining. This method will facilitate of leaching poor zinc ores before sending to solution plants from the mining areas of Hakkari reaching over 15-22 different mining areas widely spread in the province. Topographic conditions were also was creating a great problem for haulage of ore at minus 50 mm to processing plant area. However the poor ore stacks was reaching million of tons tailing heaps in the region. Additionally, heap leaching will be great threat for environmental concerns if used for poor ferrous zinc ores.

2. Material and methods

Ore waste dust containing Zinc and Copper contains approximately 0.05% Cu. A homogeneous solid solution was mixed in 1500 mL of solution at 600 rpm for 10 minutes without microwave effect to create a biochar suspension. Then, 20% biochar was added at a rate of 20% solid solution for 10 minutes while stirring at 300 rpm. Surface biochar interaction was carried out by microwave effect and then the suspension was filtered. The resulting residue was analyzed as a post-leach solution using a two-step HCl leaching wash.

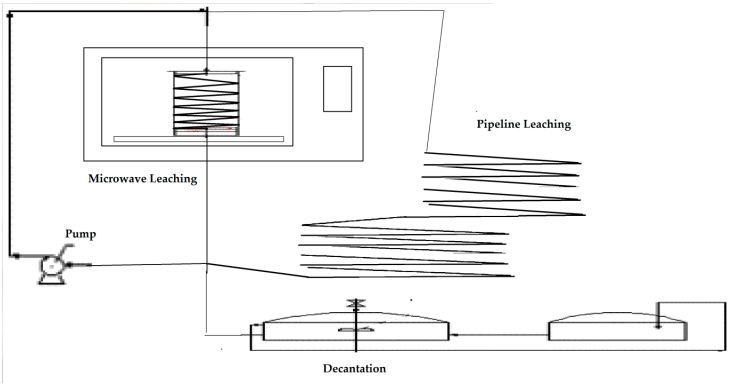


Fig 2. Following Microwave radiated leaching for Pipeline leaching Method of poor Zn Ores.

During the dissolution of these ore tailings, the aim was to separate metallic copper and zinc oxide through solid-liquid separation of solid copper and liquid zinc sulfate from acidic leachate. The dissolution process was carried out using diluted sulfuric acid with a waste solid concentration of 20%, keeping the pH at 5, and stirring at 300 rpm at both room temperature and 60° for 1 hour. The low pH and low leaching temperature of sulfuric acid solutions in dissolving poor zinc ores reduced the leaching of other undesirable metals. Biochars were washed by adjusting the pH to 2.0 using biochar HCl solution. After solid-liquid separation occurred, the pH level of the copper sulfate and zinc sulfate solution was analyzed by diluting it with water.

Then, secondary selective acidic leaching was carried out in lower pH solutions to dissolve copper, 1.5 and 2, and other low-concentration heavy metals. After applying a similar dissolution process, popped rice, corn and cotton biochars were tested by adding the same biochar solid ratio and using a 10-minute microwave interaction and adjusting the values to 2.0, 2.5 and 3.0. After the solid-liquid separation, the other low concentration metal filtrate obtained from the second selective acidic leaching was separated from the liquid. The biochars were washed twice with HCl and the filtrate and solutions were analyzed.

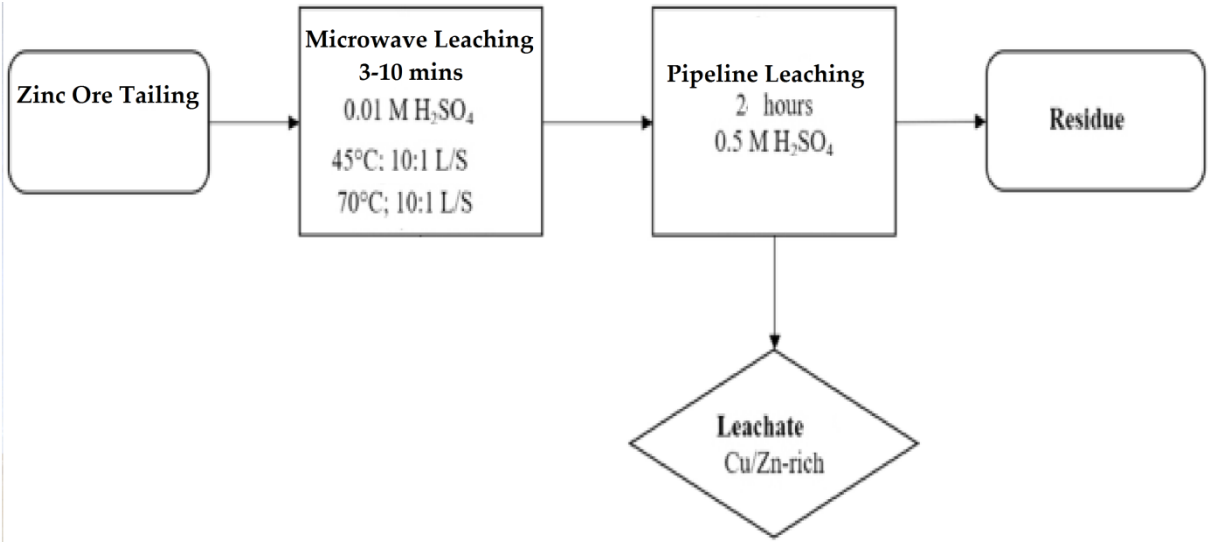


Fig 3. Experimental Method for Pipeline leaching of por Zn Ores.

Table 1. Chemical composition of the poor zinc oxide ores of Hakkari as taken from the Tailing Heaps

Element %	Zn	Pb	Cd	Cu	Fe	MgO	CaO	SiO_2
Tailing A	11.4	7.5	0.05	0.04	24.2	1.5	3.4	26.2
Tailing B	14.2	0.5	0.03	0.06	20.9	1.3	3.4	29.3
Tailing C	9.7	9.5	0.35	0.04	29.8	1.2	5.4	26.29

Zn concentration tailings A, Zn concentration tailings B, Ferrous zinc tailings C samples are taken from the heap stocks in the mining area of Hakkari Zn tailings field, collected and dumped from time to now.

As a metal recovery process, waste powder samples containing copper were stored in plastic containers by hydrometallurgical dissolution in sulfuric acid. The pH of the waste ore after dissolution was measured. Total concentrations of metals such as Zn, Cu, Fe, Si, Cd, Mn, and Pb in the ore tailings after dissolution and washing were determined using AAS.

3. Results and Discussion

During low-frequency microwave treatment, copper-zinc-containing poor ferrous ore powder is produced every approximately 10-30 min. Hakkari ferrous poor ores have a wide metal content, and the ore dust contains elements such as iron, zinc in some mines, manganese, calcium, magnesium in some, silicon, lead, sulfur, copper, and sometimes cadmium and arsenic in some mines. For this reason, Various poor ore stock wastes were collected from the quarries in the Hakkari region. In addition, enrichment facility wastes are stacked according to their metal content, resulting in millions of tons of waste piles. In order for these wastes to be evaluated, they must be adequately characterized and evaluated appropriately without harming the environment and the metals must be recovered.

Zn ores are enriched by the Hakkaride flotation method: (1) crushing and crushing process; With this process, the ore is reduced to powder size, which enables enrichment by flotation and the liberation of

the zn ore. (2) Flotation is also used and the poor ore is enriched to powder size and sold. However, precious metals such as Pb and Cu are disposed of in waste and cannot be recycled, and their recovery by flotation is particularly costly;

In this study, acid or base solution was used to dissolve and recover zinc by dissolving Zn ore waste in powder size by hydrometallurgical method. In this recovery process, the recovery rate can exceed 80%, but it is necessary to prevent waste solution pollution. Cementation of metals in solution or retention with active carbon is the most practical method. In addition, pyrometallurgically, the production of Zn oxide in facilities containing the widely used Waelz Furnaces is a costly process and is not suitable for waste. Fig. 4 showed higher leaching performance rates reaching 80-79% for Zn at the micrpwave timing of 10 minutes.

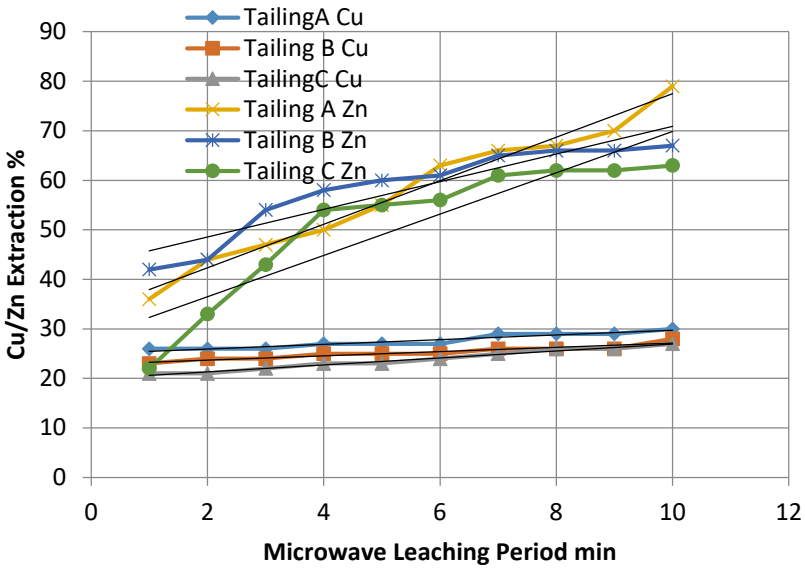


Fig 4. Microwave Duration Effect of Pipeline Leaching of Zinc Ore.

Fig. 5 showed higher leaching performance rates reaching 80-75% for Zn at the microwave leaching temperature of 75 ◦C.

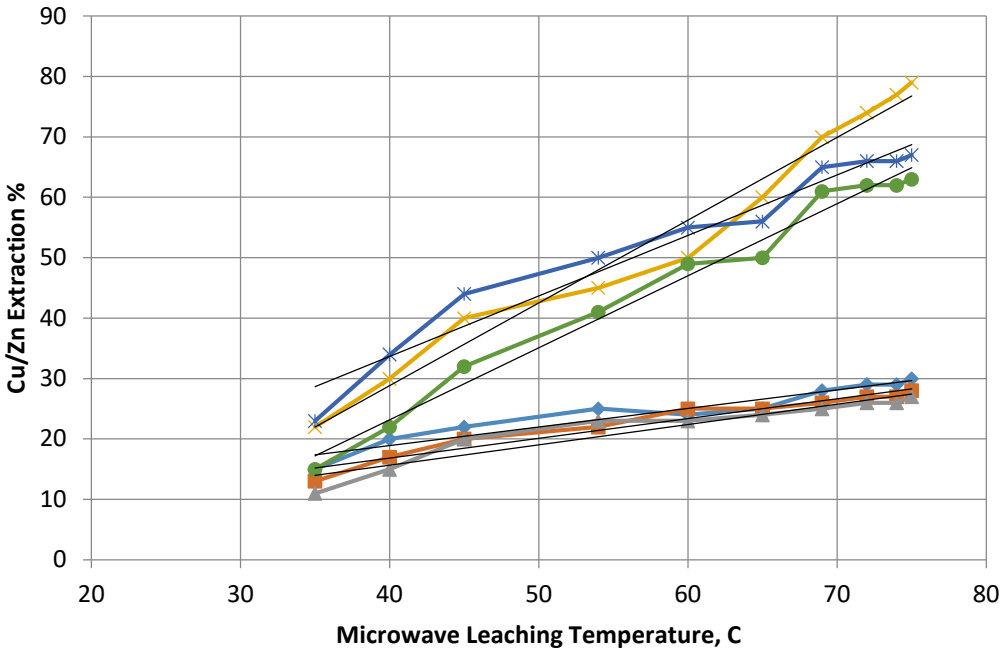


Fig. 5. Temperature Effect of Pipeline Leaching of Zinc Ore.

Fig. 6 showed higher leaching performance rates reaching 70-65% for Zn at the microwave leaching pressure of 1 bar.

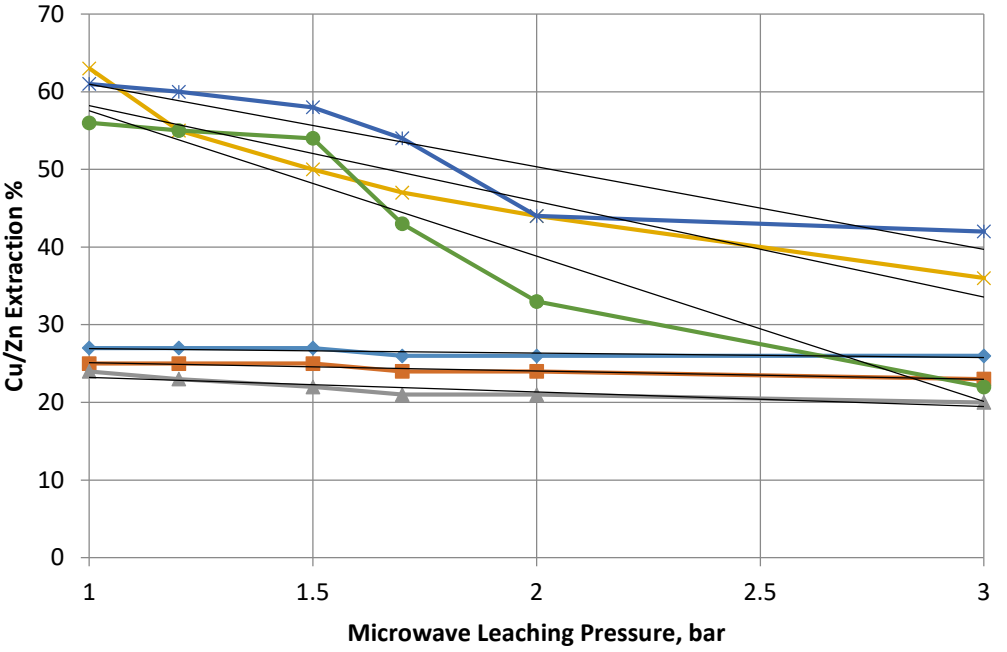


Fig 6. Pressure Effect of Pipeline Leaching of Zinc Ore.

Fig. 7 showed higher leaching performance rates reaching 89-78% for Zn at the microwave leaching cycling of 10.

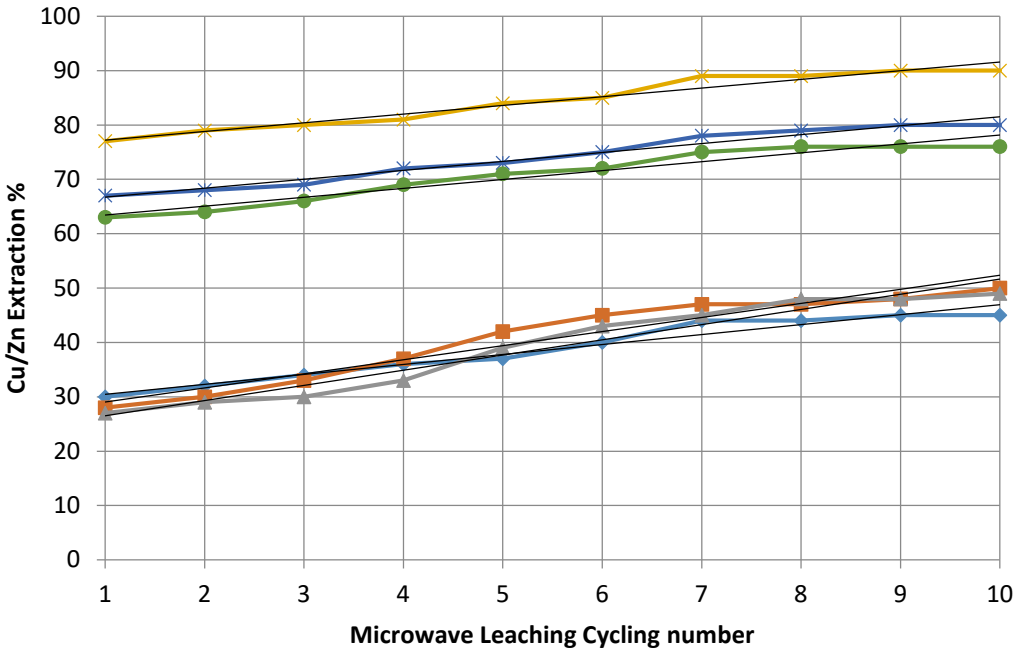


Fig. 7. Cycling Effect of Effluent in Pipeline Leaching of Zinc Ore.

4. Conclusions

In this study, the retention of poor ferrous copper zinc ores with powdered biochar and activated carbon was investigated. In this way, the recovery of copper and zinc is improved by providing the cheapest and highest pulp flow. Copper and Zn concentrations in low Zn and Cu grade ferrous ore dust were resolved by sulfuric acid dissolution in Hakkari ore deposits. Therefore, it is advantageous to dissolve such low-grade ores in low acid concentrations and keep them with biochar in tubes. Copper and Zn recovery rates were determined to be still lower due to iron content of feed below 50-45%for Cu and 80-89% for Zn at even the microwave heating and leaching stage used in our experiments.

In this study, the zinc and copper retention percentages in pipeline haulage time were found to be sufficient to recover metals approximately 84%Zn and 56%Cu, respectively. Talings of Hakkari Concentration Plant were used to recover whole other Cu Co metal-containing acid discharge effluents and to recover waste metal resources. In the first stage, pH values were controlled at 4.0-5.0 and the solid/liquid ratio was 20%. The results showed that the zinc retention efficiency was higher than 89% by microwave radiation. A proposed microwave acid leaching process was used to recover the copper content. In the second stage, in the pipeline haulage leaching process, 2 N sulfuric acid was added to the suspension and the pH value was kept at 2.0, solubilization was made and retained in the biochar samples. Solutions were formed by washing the biochars and then they were cemented and recovered. Zinc and copper yields were 88-92% and 72-78% respectively.

References

Behnajady B, Moghaddam J, Behnajady MA, Rashchi F (2012) Determination of the optimum conditions for the leaching of lead from zinc plant residues in NaCl–H_2SO_4–$Ca(OH)_2$ media by the Taguchi method. Ind Eng Chem Res. https://doi.org/10.1021/ie202571x

Bodas, M.G. (1996),Hydrometallurgical treatment of zinc silicate ore from Thailand,Hydrometallurgy, Volume 40, Issues 1–2, p 37-49, https://doi.org/10.1016/0304-386X(94)00076-F.

Canbazoğlu, M., Zengin, M., Arıtaş, N., (1988) Heap Leaching Studies at Eti bank Ergani Copper Works, II. Uluslararası Cevher Hazırlama Sempozyumu, Izmir, 653-662

Dayton, S.H., (1987), Gold Processing Update, Engineering and Mining Journal, 25,29

Dutrizac JE (1992) The leaching of sulphide minerals in chloride media. Hydrometallurgy. https://doi.org/10.1016/0304-386X(92)90004-J

Farahmand F, Moradkhani D, Safarzadeh MS, Rashschi F (2009) Brine leaching of lead-bearing zinc plant residues: Process optimization using orthogonal array design methodology. Hydrometallurgy. https://doi.org/10.1016/j.hydromet.2008.07.012

Girgin I., Kırşan H İ,(1990), Yığın Liçi Uygulamaları ve Ekonomik Açıdan Önemi, MADENCİLİK Dergisi, Eylül1990, Cilt 30, Sayı 3, 30-43

Hanilçi N, Öztürk H, Banks, D (2020) Geological, geochemical and microthermometric characteristics of the Hakkari region Zn-Pb deposits, SE Turkey. Ore Geology Reviews, 125. Elsevier BV. 103667 doi:10.1016/j.oregeorev.2020.103667

Kaya M, Gul E, Kursunoglu S, Hussaini S (2019) Leaching of oxidized Turkish Pb–Zn flotation tails by inorganic acids, IMPC-Eurasia-2019 Congress, Antalya-Turkey

Keane, J.M., Chase, CK., 1987 Evaluation of Copper Dump and Heap Leaching situations, Mining engineering, 197-200.

Lundström M, Liipo J, Aromaa J (2012) Dissolution of copper and iron from sulfide concentrates in cupric chloride solution. Int J Miner Process. https://doi.org/10.1016/j.minpro.2011.11.005

Ruiz MC, Montes KS, Padilla R (2011) Chalcopyrite leaching in sulfate–chloride media at ambient pressure. Hydrometallurgy. https://doi.org/10.1016/j.hydromet.2011.05.007

Santoro L. , M. Boni, R. Herrington, A. Clegg,(2013),The Hakkari nonsulfide Zn–Pb deposit in the context of other nonsulfide Zn–Pb deposits in the Tethyan Metallogenic Belt of Turkey, Ore Geology Reviews,Volume 53,p 244-260,https://doi.org/10.1016/j.oregeorev.2013.01.011.

Santoro, Licia, Putzolu, Francesco, Mondillo, Nicola, Boni, Maria, Herrington, Richard (2020) Influence of Genetic Processes on Geochemistry of Fe-oxy-hydroxides in Supergene Zn Non-Sulfide Deposits. Minerals, 10 (7) 602 doi:10.3390/min10070602

Santos SM, Machado RM, Correia MJN, Reis MTA, Ismael MRC, Carvalho JMR (2010) Ferric sulphate/chloride leaching of zinc and minor elements from a sphalerite concentrate. Miner Eng. https://doi.org/10.1016/j.mineng.2010.02.005

Wang, P.; Sun, Z.H.; Hu, Y.N.; Cheng, H.F. (2019) Leaching of heavy metals from abandoned mine tailings brought by precipitation and the associated environmental impact. Sci. Total Environ. 2019, 695, 133893

Ye M, Yan P, Sun S, Han D, Xiao X, Zheng L, Huang S, Chen Y, Zhuang S (2017) Bioleaching combined brine leaching of heavy metals from lead-zinc mine tailings: transformations during the leaching process. Chemosphere. https://doi.org/10.1016/j.chemosphere.2016.10.095

Zhang R, Hedrich S, Römer F, Goldmann D, Schippers A (2020) Bioleaching of cobalt from Cu/Co-rich sulfidic mine tailings from the polymetallic Rammelsberg mine, Germany. Hydrometallurgy. https://doi.org/10.1016/j.hydromet.2020.105443

Ivrindi Gold And Silver Mine Permeability Testwork

Melis N. ERDEM [1*]

[1] Tümad Madencilik San. ve Tic A.Ş, Barbaros Mah. Buğday Sk. No:9, Ankara, Türkiye

*Corresponding author: melis.erdem@tumad.com.tr (Melis N. ERDEM)

Abstract:

The heap leaching method is a commonly used economic hydrometallurgical process for the treatment of low-grade ores. In this study, the tests used in the design and operation of heap leaching were explained and studies were carried out in order to increase the efficiency of the plant with the permeability tests carried out within the scope of the heap leaching process in İvrindi plant. In the study, tests were carried out using different cement types and different dosages and the effect on permeability and cost was investigated. As a result, it was determined that operating costs can be reduced by using different cements that provide the same permeability at lower dosages.

Keywords: *Gold, Heap Leach Design, Metalurgical Testwork, Permeability Testwork*

1. Introduction

The heap leaching process is a hydrometallurgical method widely used in mining to economically process low-grade ores. This method, particularly preferred for the extraction of metals such as gold, silver, copper, and uranium, has become increasingly favored due to its lower environmental impact and cost-effectiveness.

The heap leaching method has some important advantages and disadvantages compared to other leaching methods. Its advantages include low initial investment cost, short startup time, simple waste management, and the ability to directly obtain the final product (dore metal). This method is attractive for small-scale operations due to its low capital requirements and its ability to be quickly initiated. Additionally, its flexible structure allows it to easily adapt to varying production and operational conditions.

However, when compared to other leaching methods, heap leaching also has some disadvantages. Mismanagement of the process can lead to increased environmental risks. Factors such as the lengthening of the metal recovery process, high clay content, or mineralogy can hinder the penetration of the solvent, further reducing efficiency. Therefore, careful evaluation and the establishment of appropriate management strategies are necessary before implementing the heap leaching method.

Due to heap leach design, as the heap height increases, the homogeneous distribution of the solvent and metal solubility become more difficult. In order to determine the impact on solution permeability, efficiency and cost, percolation testing is currently used to simulate field conditions in a laboratory environment and allow optimization of the applied process.

1.1. HEAP LEACH PROJECT DESIGN

Heap leaching is the process of feeding an appropriate leaching solution to heap prepared on an impermeable ground with a solution collection system, allowing valuable metals to leach into the effluent.

Determining the suitability of the ore for heap leaching requires a comprehensive evaluation of the ore's physical and chemical properties, as well as environmental factors. The steps as follows:

- The ore characterisation with geology,
- The liberation characteristics of the ore should be examined.

- The presence of refractory minerals should be investigated.
- The optimal particle size for heap leaching should be determined.
- It should be ensured that the crushed ore has sufficient solution permeability.
- Metallurgical test studies should be conducted to determine the parameters for leaching kinetics. (IBRT, column percolation, etc.)
- The chemical properties of the ore should be determined (the presence of carbon-containing minerals, impurities, optimal pH value).
- Geotechnical and hydrogeological assessments should be conducted to understand the stability of the ore and the flow characteristics of the solution (ore moisture content, compaction, solution flow, and drainage).
- The environmental and legal compliance process should be managed (potential environmental impacts such as leakage, dust formation should be evaluated, and compliance with local, regional, and national standards should be ensured).
- The investment and operational costs required for heap leaching should be calculated, and a cost-benefit analysis should be performed for the corresponding metal recovery and revenue.
- Technical, environmental, and economic risks should be identified, and necessary precautions should be taken to minimize these risks.

1.2. TESTS USED IN HEAP LEACH DESIGN

Various tests are conducted during the heap leach design process to determine the suitability of the ore for this method and to establish operational parameters. These tests play a critical role in determining the metal recovery rate, the effective penetration of the leaching solution into the ore, and the amount of reagents to be consumption in the process. The tests and their applications are as follows:

- *IBRT (Bottle Roll Tests):* This test is used to quickly assess the metal solubility and recovery rate by mixing the ore with the leaching solution. The ore sample is typically mixed with the leaching solution for 24-72 hours, and the metal solubility and leaching kinetics are determined. This allows for a preliminary evaluation of leaching time, reagent consumption, and metal recovery rate.
- *Column Leach Tests:* This test method provides a larger-scale simulation of the leaching process and offers more detailed information. It is used to optimize process parameters.
- *Cyanide Consumption Tests:* This test is conducted to determine how much cyanide, or other reagents, will be used during the heap leach process. Determining cyanide consumption is important for controlling operational costs.
- *Acid Consumption Tests:* This test is conducted to determine sulfuric acid consumption during the leaching of metals such as copper. The ore sample is contacted with an acid solution to determine acid consumption. This test is performed to optimize acid usage or evaluate alternative acids.
- *Percolation Tests:* This test is conducted to determine the flow rate and distribution of liquid within the heap. It identifies factors that need to be optimized to ensure permeability and homogeneous distribution of the solution within the heap.
- *Compacted Permeability Tests:* The compact permeability test study is used to examine the permeability of a material under different compaction loads (heap heights). The vertical loading of the test material is used to simulate the increasing pressure obtained when the heap is loaded to successive heights. Characteristics such as flow rate, percentage of slump, percentage of pellet breakdown, and the color and clarity of the solution also contribute to the evaluation process of whether the test is considered “passed” or “failed.”

- *Geotechnical Tests:* These tests are conducted to evaluate heap stability, compaction behavior, and drainage properties. They provide information on how the heap will behave under load, ensuring protection from collapse, erosion, and other events.

2. PERMEABILITY TESTS AT IVRINDI GOLD AND SILVER MINE

The permeability tests conducted in the Metallurgy Laboratory of the İvrindi Facility aim to control ore permeability in site operations and increase the efficiency of the extraction process by ensuring the homogeneous distribution of the solution. For this purpose, the test results are evaluated based on the design criteria established during the comissioning phase. When necessary, parameters are optimized and applied to site operations.

3. CASE STUDY OF THE IVRINDI PROCESS PLANT

At the İvrindi Plant, a test study was initiated to reduce the cost of operation and optimize the process by considering the design parameters. In this study, cements samples were used, and the aim was to determine the impact of these cements on ore permeability and cost when used in different dosages.

The test carried out in two stages. In the first stage, percolation tests were conducted using the existing cement in the heap leach process and other cement samples (with different clinker ratios) at the same dosage, and their permeability was recorded. Annual costs were calculated based on consumption per ton.

In the second stage, percolation tests were performed by reducing the dosage of these cement samples, and percolation rates were recorded. Costs were calculated based on consumption per ton.

The permeability results obtained with the same dosage of different cement samples in the test study carried out are as shown in Table 1:

Table 1: Test Results from Different Cement Sample+Same Dosages

Sample I.D.	H_1(mm)	H_2(mm)	H_3(mm)	Auto Slump	Tapped Slump	Water Volume (ml)	Time (sec)	Percolation Rate L/h/m2	pH
CEM I	463	463	444	0,00%	1.90%	400	3,61	64.015,68	12,42
CEM II	453	453	442	0,00%	2.10%	400	4,32	68,179.77	12,40
CEM III	458	458	445	0,00%	2.16%	400	4,33	62,040.79	12,62
CEM IV	453	453	442	0,00%	3.01%	400	4,32	60.179,77	12,40

* CEM1: Currently used cement, CEM II, CEM III, CEM IV are different cement samples

When the results in Table 1 are evaluated, it is stated that the permeability and slump values of the cements used in the test are at an acceptable level according to the literature and design criteria.

Table 2: Test Results for Different Cement Sample + Different Dosages

Sample I.D.	H_1(mm)	H_2(mm)	H_3(mm)	Auto Slump	Tapped Slump	Water Volume (ml)	Time (sec)	Percolation Rate L/h/m2	pH
CEM I	455	455	438	0,00%	3.82%	400	4,58	62,763.45	12,17
CEM II	453	453	439	0,00%	4.02%	400	4,17	66,344.51	12,18
CEM III	455	455	440	0,00%	5.36%	400	4,64	56.029,44	12,42
CEM IV	453	453	439	0,00%	5.45%	400	4,17	54,344.51	12,18

*CEM1: Currently used cement, CEM II, CEM III, CEM IV are different cement samples

The results obtained when the dosage of the cement samples was reduced and the effect on permeability was investigated are shown in Table 2. According to these results, it is seen that there is a 2% decrease

in slump and permeability values in the use of low dosage of CEM 2 sample. In the same way, cost calculation made considering the annual consumption of cements.

When all the data obtained from the percolation experiments were examined, it was seen that 4 kg of cement consumed per ton could be saved in the operation without compromising the percolation quality.

4. RESULTS

The conclusion of the document reveals that permeability tests conducted at the İvrindi Gold and Silver Mine evaluated the impact of different cement samples on permeability and costs. The study found that the CEM 2 cement sample provided sufficient permeability even at lower dosages. As a result, it was observed that the amount of cement used per ton could be reduced, leading to a significant decrease in operational costs.

The tests demonstrated that costs could be optimized without compromising percolation quality, even at lower dosages. Consequently, it was decided to use the CEM 2 cement sample at the İvrindi facility to reduce operational costs. This decision resulted in a cost advantage while maintaining process efficiency.

REFERENCES

Orman, M. E., & Criley, K. (1997). Ore permeability testing for heap leach design. Paper presented at the SME Annual Meeting, Denver, CO, February 24-27, 1997. Society for Mining, Metallurgy, and Exploration, Inc.

Kappes, D. W. (2002). Heap Leaching of Gold and Silver Ores. In M. C. Fuerstenau, T. P. Battle, & P. C. Ludington (Eds.), Developments in Mineral Processing (Vol. 15, pp. 1-38). Elsevier.

Free, M. L., Moats, M., Davenport, W., & Stankiewicz, J. D. (2013). Hydrometallurgy: Fundamentals and applications. John Wiley & Sons.

Marsden, J., & House, I. (2006). The chemistry of gold extraction (2nd ed.). Society for Mining, Metallurgy, and Exploration.

Society for Mining, Metallurgy, and Exploration (SME). (2014). Design and operation of heap leach pads. SME Technical Paper.

Simons, P. A. (2005). Evaluation of heap leach projects for precious metals (Doctoral dissertation, Colorado School of Mines).

Smith, M. E. (1997). Gold Heap Leach Operations: Methods and Economics. In Proceedings of the Annual Meeting - Society for Mining, Metallurgy, and Exploration, Inc. (SME).

Aygun, A., U., 2006. Ovacık cevherleri için adsorbsiyonda farklı aktif karbon tipleri uygulaması ile optimum seçeneğin tespiti. İTÜ Cevher Hazırlama Anabilim Dalı, Bitirme Tezi, İstanbul, pp. 11-20

Girginc, I., 1989. "Düşük Tenörlü Cevherlerden Yığın Liç Yöntemiyle Altın ve Gümüş Kazanımı", Madencilik, Volume XXVII., Sayı No 1, pp 35-39.

Fuzzy Logic Estimation of Coal Recovery by Knelson concentrator

Sevgi Karaca[1], Ali Uçar[1]*, Oktay Şahbaz[1]

[1]Kutahya Dumlupinar University, Department of Mining Engineering, Kutahya, Turkey

*Corresponding author: ali.ucar@dpu.edu.tr (Ali UÇAR)

Abstract:

The use of centrifugal gravity concentrators is more effective than conventional concentrators in recovering fine-grained coal tailings. The Knelson concentrator study investigated ash content and combustible recovery estimation using fuzzy logic. The sample taken from the Western Coal Enterprise (WCE) tailings dam was divided into -1+0.038, -1+0.212 and -0.212+0.038 mm size groups. Flow rate (2, 3 and 4 l/min) and centrifugal force (20, 30, 40 and 50 G) were used as input variables in the estimation studies. Finally, the fuzzy logic estimation results were compared with the actual values, and it was shown that the fuzzy logic system could be successfully applied to Knelson concentrator enrichment results.

Keywords: *Coal tailing, Knelson concentrator, Fuzzy logic*

1. Introduction

Coal production processes generate significant amounts of unrecovered fine-grained waste material. Wastes are generally categorized into three groups based on coal characteristics and the operational and technological processes applied (Fecko et al., 2013):

1. Coal produced during the extraction and preparation of coal from the mine,

2. Fine-sized coal discharged in beneficiation processes (e.g. shorting, washing, crushing),

3. Coal wastes from the production processes of commercial products.

Effective recovery and utilization of these coal wastes are important for sustainable coal mining operations. However, recovering coal from fine waste is very costly. However, with appropriate strategies and utilization methods, it is possible to bring these wastes into the economy and prevent environmental pollution. With the development of technology, fine-sized coal can be recovered effectively by gravity methods utilizing centrifugal force and flotation. However, environmental problems arise with extra reagent costs in the flotation method and performance decreases in oxidized coals (Ghaffari and Farzanegan, 2017; Kökkılıç et al., 2015; Peer et al., 2002; Uslu et al., 2012). For this reason, centrifugal separators are becoming increasingly important in the recovery of fine coals, the amount of which is increasing every year and causing environmental problems.

There are many studies in which the Knelson concentrator (KC), one of the centrifugal separators, has been used in coal recovery. In these studies, the operating parameters of the equipment, such as water flow rate, centrifugal force, and feed rate, have been investigated by various researchers. Sabah and Koltka (2014) obtained clean coal containing 30.51% ash with a weight of 81.18% by KC enrichment of the material with 42.6% ash content in the -0.5+0.038 size group obtained from samples taken from the waste pool of ELI Soma Enterprise. Majumder et al. (2007) showed that this equipment can produce a clean coal product with 17% ash content at 40% efficiency from the feed having 36.13% ash. Honaker et al. (1996), in their study, obtained clean coal with 8% ash content with 85% combustible recovery by beneficiation of 21% ash material of -0.6+0.210 mm size in KC. Again, Honaker and Das (2004) obtained 8% ash clean coal with 70% efficiency by beneficiation of coal with 22% ash content in the size range of -0.150+0.044 mm in pilot KC. According to the study conducted by Öney and Tanrıverdi (2016) with KC on the beneficiability of Amasra coals in the size range of -1+0.15 mm and containing 34.30% ash, clean coal with 16.28% ash was obtained with 67.82% efficiency.

Coal recovery is a complex process consisting of a large number of factors, including material parameters such as particle size, ash content, as well as equipment operating parameters. Traditional approaches to modeling and optimizing this process are usually based on deterministic techniques, which cannot adequately account for the existing uncertainties and non-linear relationships. Fuzzy logic, on the other hand, is a powerful tool for dealing with imprecise and ambiguous information and has been successfully applied in various ore recovery processes (Abkhoshk et al., 2010; Ali et al., 2018; Cai et al., 2021; Li et al., 2012; Saravani et al., 2014).

Fuzzy logic, a decision-making mechanism, was first introduced by L.A.Zadeh (1965). Fuzzy logic is used to mathematically model expressions that cannot be explained using known methods. Fuzzy logic is one of the methods to give computers the ability to make decisions. In fuzzy logic, input data is expressed in many levels in the range of 0-1, not in two stages of 0 and 1 as in classical logic. Membership values, which define the level of membership between sets, are in the close range [0,1] and a value of 1 indicates that membership is fully accepted and vice versa. Fuzzy logic consists of three stages: Defuzzification, inference, and stabilization. Fuzzification is the process of transforming normal input variable values into linguistic expressions. Inference involves matching inputs with linguistic output values using fuzzy if-then rules and logical operations. The computer's decision-making criteria are determined by creating a rule table. In the output unit, the fuzzy output values are rinsed again and digitized (Fig 1).

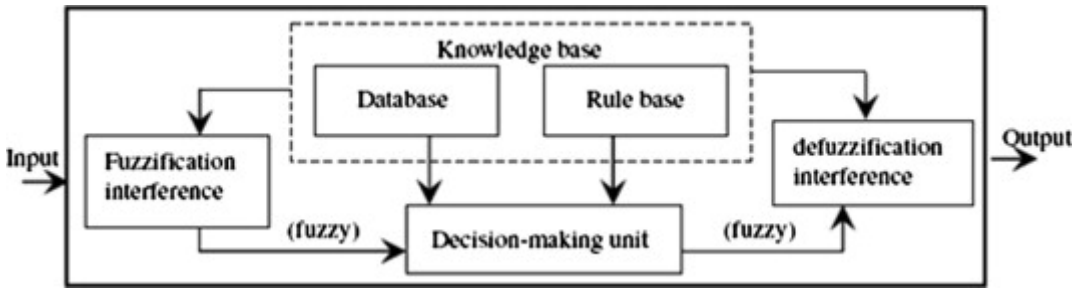


Fig 1. Fuzzy inference system (Jain and Martin, 1998)

This study aims to develop a fuzzy logic-based approach to predict the ash content, weight, and combustible recovery of coal recovery from the pond wastes of Turkish Coal Enterprises Garp Lignileri İşletmesi (TKİ GLİ) using a Knelson concentrator. Thus, the inherent uncertainties and challenges of the device and coal encountered in the coal recovery process can be effectively accounted for through this approach. Furthermore, a series of experiments were conducted to prove the effectiveness of the approach and provide a more robust and accurate decision-making tool.

2. Material and methods

2.1. Material

The materials used in the experiments were taken from the waste pond No. 4 of the WLE Plant. These materials were taken from the tailings pond by the operating engineers and brought to DPU Mining Engineering Department Laboratory and homogenized by mixing separately. The 400 kg sample was divided by sample splitting procedures and stored for experimental studies. Analyses were performed to determine the material's properties to be used in the experiments (Fig 2 and Table 1). The material was divided into -1+0.212, -0.212+0.038, and -1+0.038 mm size groups and subjected to beneficiation experiments with a laboratory-type Knelson concentrator.

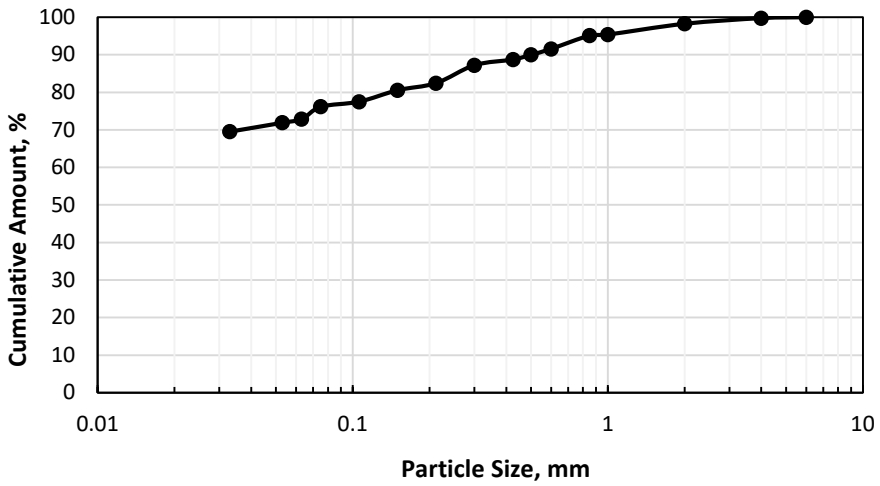


Fig. 2. Particle size distribution of the sample

Table 1. The results of moisture, sulphur, ash content, LCV and UCV of the sample

Particle Size (mm)	Ash (%)	UCV (Kcal/kg)	LCV (Kcal/kg)	Sulphur (%)	Moisture (%)
+4	27.25	5191	4763	1.07	3.80
-4+2	24.83	5441	4944	1.16	4.70
-2+1	20.41	5731	5233	1.19	4.30
-1+0.85	25.45	5170	4710	1.23	4.30
-0.85+0.6	22.31	5468	4980	1.24	4.40
-0.6+0.5	26.00	5260	4803	1.28	4.20
-0.5+0.425	26.66	5031	4564	1.26	4.60
-0.425+0.3	33.64	4859	4451	1.20	4.00
-0.3+0.212	40.04	4519	4133	1.33	4.20
-0.212+0.150	37.78	4670	4251	1.33	4.60
-0.150+0.106	47.10	3933	3680	1.43	2.20
-0.106+0.075	48.03	3358	3086	1.39	3.10
-0.075+0.063	40.07	3598	3263	1.31	3.90
-0.063+0.053	50.69	3127	2870	1.12	3.10
-0.053+0.038	58.81	2531	2333	1.11	2.50
-0.038	81.91	-	-	0.34	1.70
Total	68.01	-	-	0.62	2.35

2.2. Methods

The study is divided into two parts: conducting KC experiments and predicting the obtained data using fuzzy logic. In the first stage, a series of experiments were conducted in all three size fractions to determine the effect of centrifugal force and wash water flow rate. The experiments were carried out with a laboratory type Knelson concentrator at centrifugal forces of 20, 30, 40 and 50 G and wash water flow rates of 2, 3 and 4 L/min. In these experiments, the feed flow rate and solids content were kept constant.

In the second part of the study, the estimation of ash content, combustible recovery and clean coal weight, which are important in coal beneficiation, were determined using fuzzy logic. Mamdani method was used in the study using the fuzzy logic module of MATLAB program. The Mamdani method, one of the two most widely used inference methods (the other is the Takagi-Sugeno-Kang (TSK) method), was chosen because it is more familiar to human perception, relatively easy and easy to interpret. Centrifuge force and wash water flow rate were taken as input (independent) variables in the modeling process. The output (dependent) variable is the coal recovery parameters that we estimate. Figure 3 shows the input and output variables used in the model.

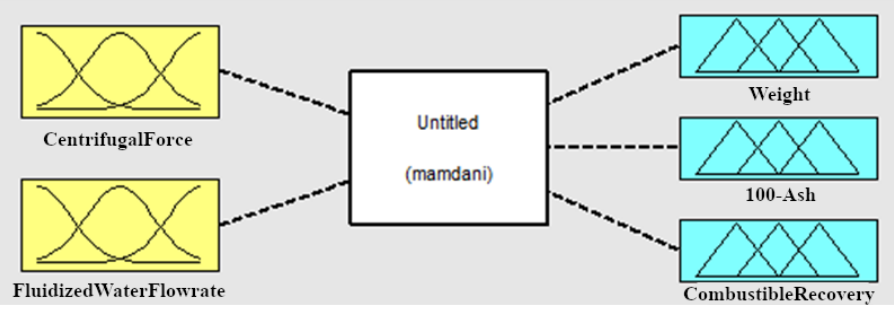


Fig. 3. Input and output variables

Membership functions define fuzzy sets. Membership degrees are calculated according to the shape of the membership set. The triangular method was used in the study because it gave the best results, and the membership degree was calculated using Equation 1. The membership function names of the parameters are given as weak, medium, strong, and very strong for the centrifugal force and low, normal, high, and very high for the washing water flow rate (Fig 4) The centrifugal force is given as weak, medium, strong and very strong, and the washing water flow rate is given as low, normal, high and very high. In Figure 4, it used to interpret what exactly the range of weak-medium-strong-very strong centrifugal force would be for the user designer of this system. The positioning of the language values in these ranges is a completely subjective interpretation. It is not possible for the researcher to determine the values here in the same way. In addition, the use of fuzzy logic generates real data from subjective interpretations. Hence, depending on the material used in your actual experiment, you define a range that can be widened or narrowed depending on the output results obtained with varying parameters.

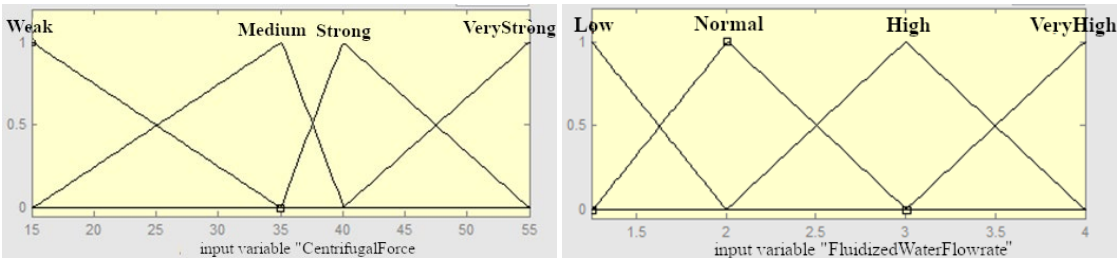


Fig. 4. Membership functions of parameters

$$\mu_a(X) = \begin{cases} 0, & x < a_1 \\ \frac{x-a_1}{a_2-a_1}, & a_1 \le x \le a_2 \\ \frac{a_3-x}{a_3-a_2}, & a_2 \le x \le a_3 \\ 0, & x > a_3 \end{cases} \quad (1)$$

The rule table defines the linguistic relations between input variables and output variables. All relations between input variables in the rule table are formed with the conjunction "and". The conjunction "and" here indicates the assignment of the smallest value of the input membership degrees in assigning the membership degree of the output set. The number of rules is determined by multiplying the number of

each function of two input variables. In this study, 16 association rules were created for each fraction (Fig 5).

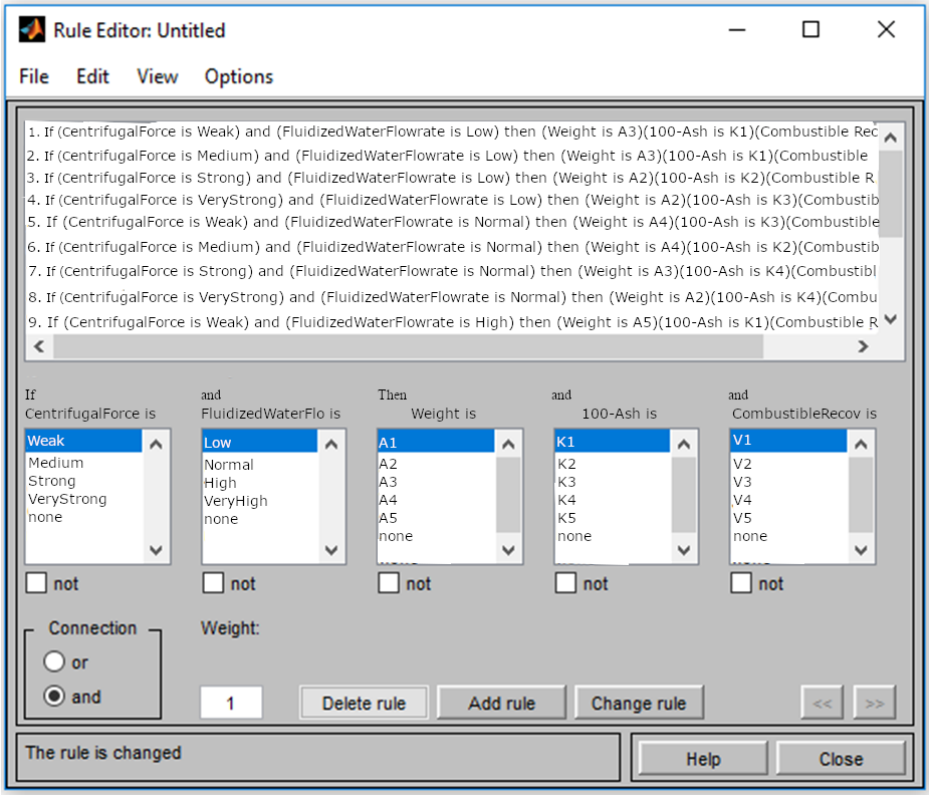


Fig. 5. Model Rules

The inference process was based on the "min-max" inference rule. The centroid of gravity (COG) method, which is widely used for rinsing, was used in the study.

In this study, the fuzzy logic method was applied to the experimental results of three different sizes of waste coal beneficiated using a Knelson concentrator. In order to determine the size at which the Knelson concentrator gave the best results in three different sizes, an absolute fraction of variance (R^2), mean absolute percentage error (MAPE), and root mean squared (RMS) error criteria were used for comparison (Özcan et al., 2009). These values were then calculated in excel.

$$R^2 = 1 - \left(\frac{\sum_{i=1}^{N}(t_i - o_i)^2}{\sum_{i=1}^{N}(o_i)^2}\right) \quad (2)$$

$$RMS = \sqrt{\frac{1}{N}\sum_{i=1}^{N}|t_i - o_i|^2} \quad (3)$$

$$MAPE = \frac{1}{N}\sum_{i=1}^{N}\left|\frac{t_i - o_i}{o_i}\right| * 100 \quad (4)$$

3. Experimental Studies

With the Mamdani model developed in this study, which aims to predict ash ratio, combustible recovery, and clean coal weight with fuzzy logic, the shape and number of membership functions belonging to both input and output variables and the rule table created were completely determined according to the closeness of the results to be obtained. By entering the data into the model created accordingly, a certain level of weight, 100-ash, and combustible recovery estimation could be achieved. The results obtained experimentally were divided into two groups and 10% of the total number of

experiments were used for testing purposes. Based on the prediction results of the model run, it can be seen in Figures 7, 9, and 11 for three size ranges.

In the -1+0.212 mm size, which is obtained by removing the fine-sized product, the material coming to the concentrate increases as the centrifugal force decreases, without the importance of the fluidized water flow rate. However, the other two sizes, which contain fine-sized material, are affected by the fluidized water flow rate, and the material coming to the concentrate decreases considerably with increasing centrifugal force (Figure 7).

In Figure 9(a), similar results were obtained with the amount of material coming to the concentrate in the size range of -1+0.212 mm. As the centrifugal force decreased, the ash in the clean coal was removed. In Figure 9(b), the clean coal with the least ash was obtained at the lowest centrifugal force and the highest fluidized water flow rate. In Figure 9(c), the fluidized water flow rate does not affect the 100-ash value at a low centrifuge value. However, with the increase in centrifugal force, ash leakage to clean coal occurs due to the effect of the force acting on a wide range of particles. The clean coal with the least ash at 4 L/min fluidized water flow rate was obtained at 30-40 G centrifugal force.

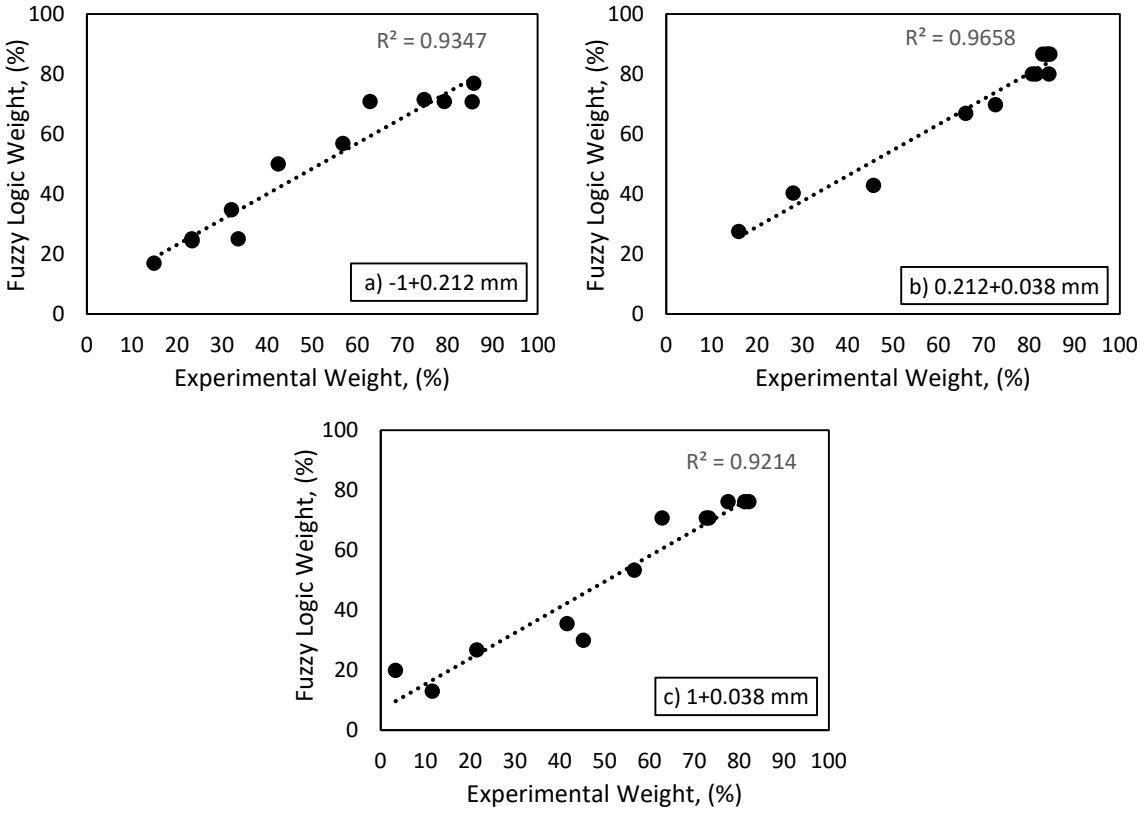


Fig. 6. Distribution of weight experimental results and fuzzy results for experiments with (a) -1+0.212 mm, (b) 0.212+0.038 mm and (c) 1+0.038 mm

Figure 11(a)' The combustible recovery value for the range -1+0.212 mm increases with decreasing centrifugal force without any significance of the fluidized water flow rate. However, as a result of the loss of selectivity of the separation, the ashy material is also introduced into the clean coal, which increases the combustible recovery value. In Figure 11(b) and (c), the combustible recovery value is the highest as the centrifugal force decreases and the fluidized water flow rate increases.

Both experimental and fuzzy logic results are given in Figures 6, 8 and 10 for weight, 100-ash and combustible recovery values. R^2 values are also given above the graphs. The results in the -0.212+0.038 mm size range show that the experimental results are the most consistent with the fuzzy logic results. The dimension with the least agreement is -1+0.038 mm.

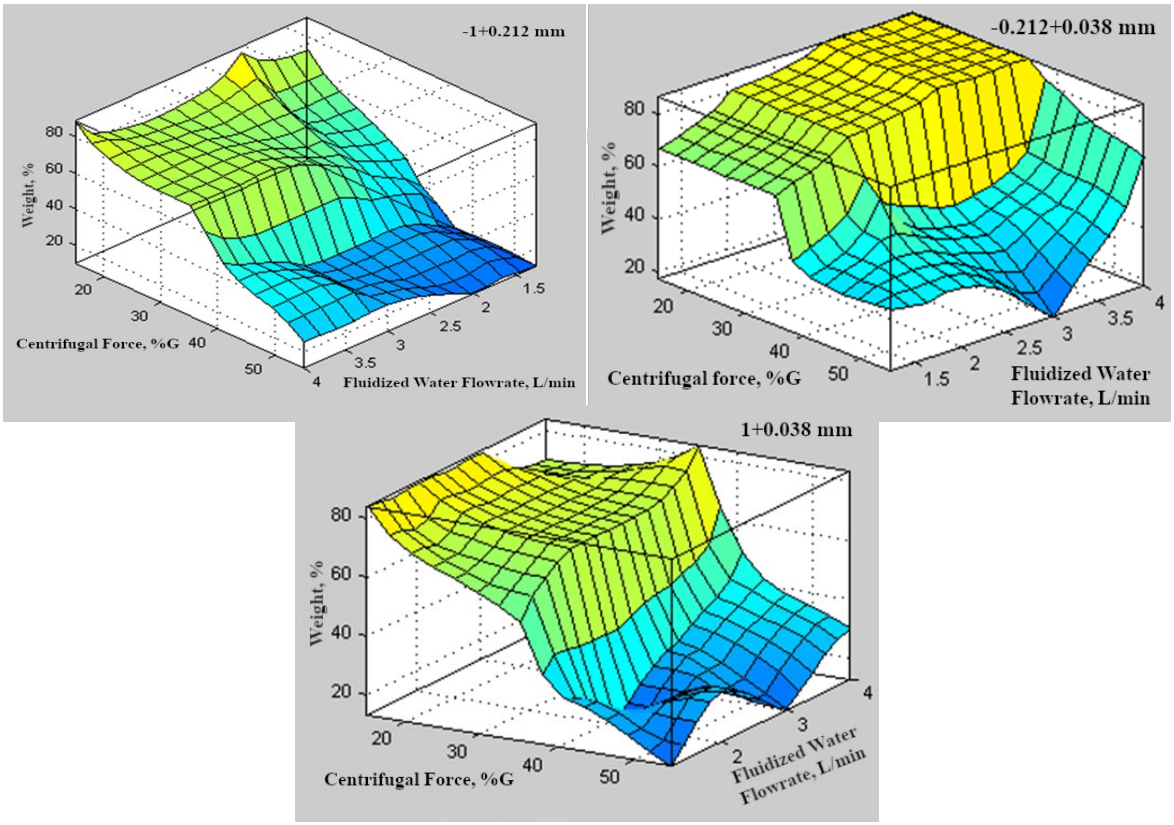


Fig 7. Weight plots of experiments performed at (a) -1+0.212 mm, (b) 0.212+0.038 mm and (c) 1+0.038 mm

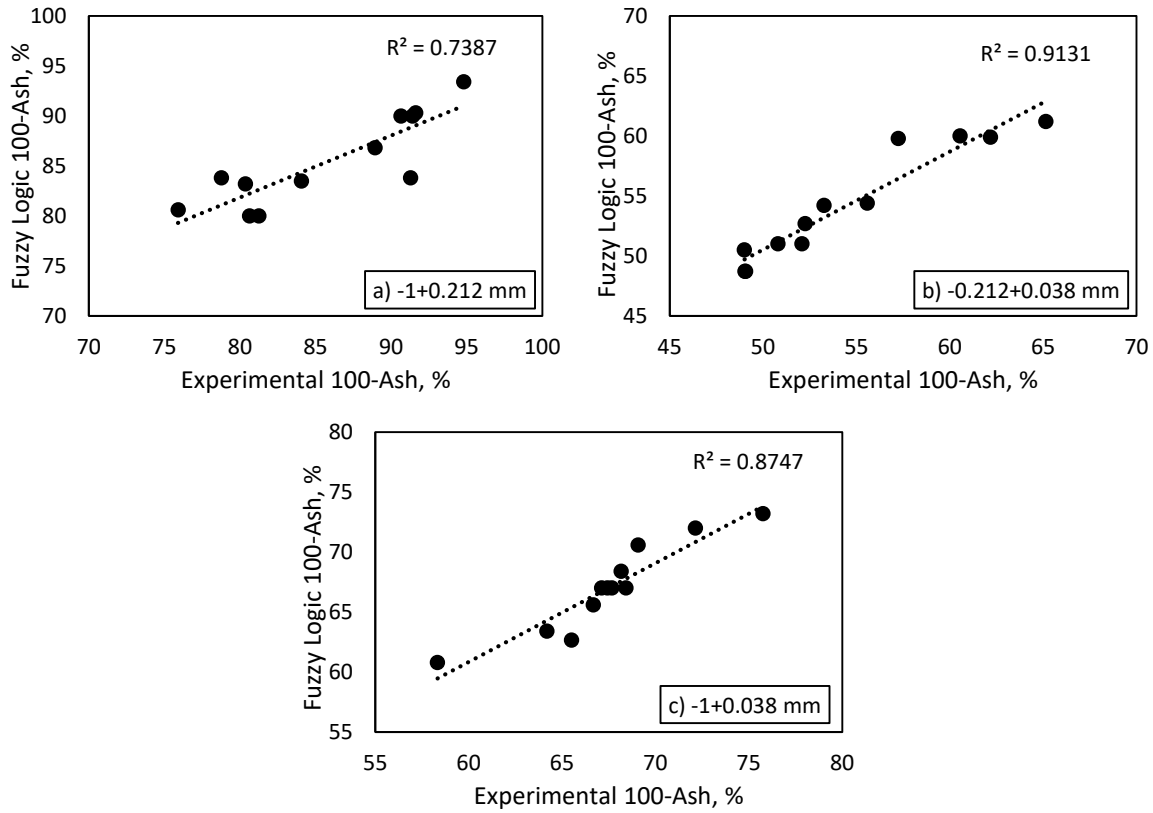


Fig 8. Distribution of 100-ash experimental results and fuzzy results for (a) -1+0.212 mm, (b) 0.212+0.038 mm and (c) 1+0.038 mm

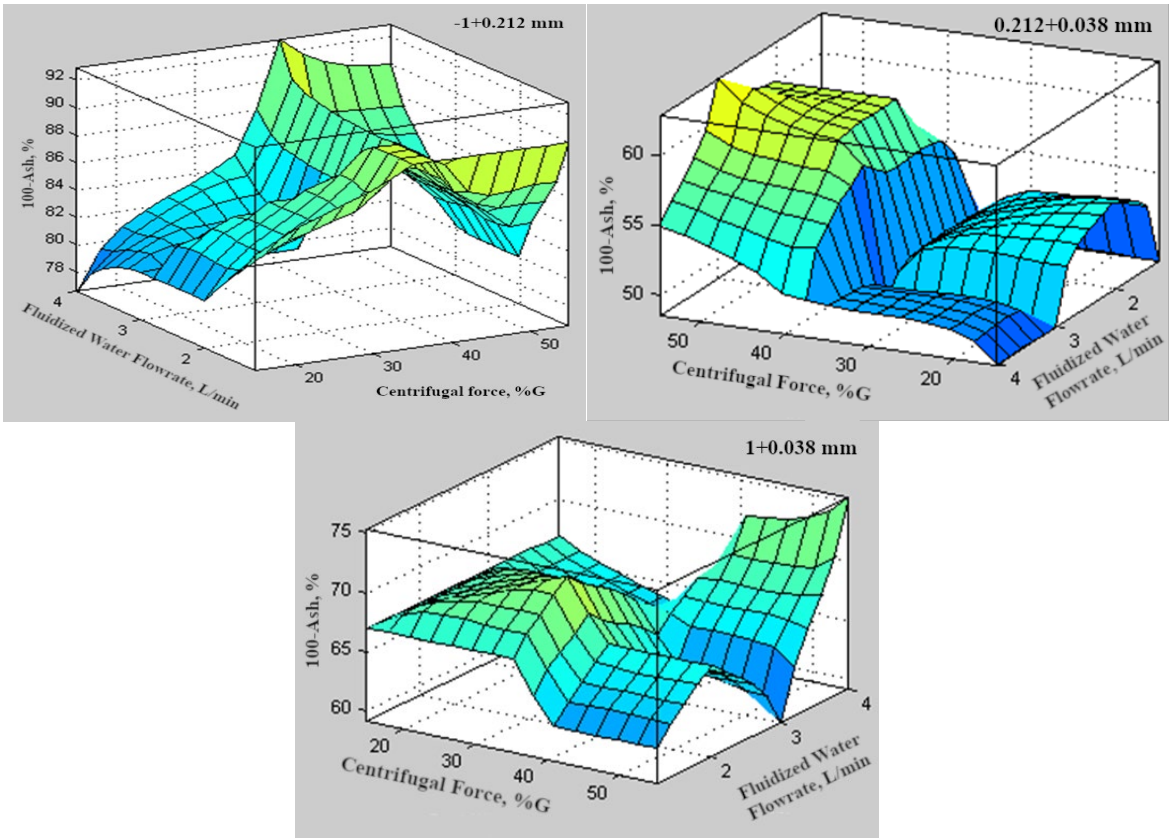


Fig 9. 100-Ash plots for experiments performed at (a) -1+0.212 mm, (b) 0.212+0.038 mm and (c) 1+0.038 mm

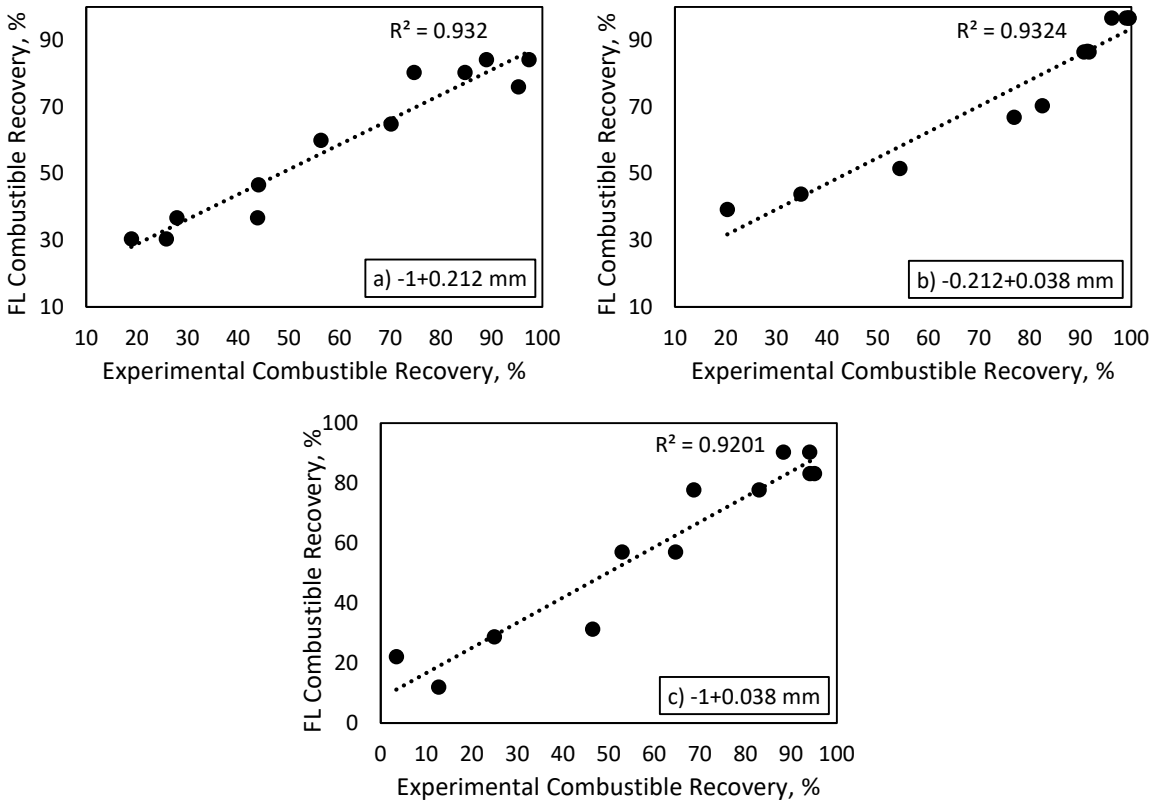


Fig 10. Distribution of combustible recovery experimental results and fuzzy results for the experiments performed at (a) -1+0.212 mm , (b) 0.212+0.038 mm and (c) 1+0.038 mm

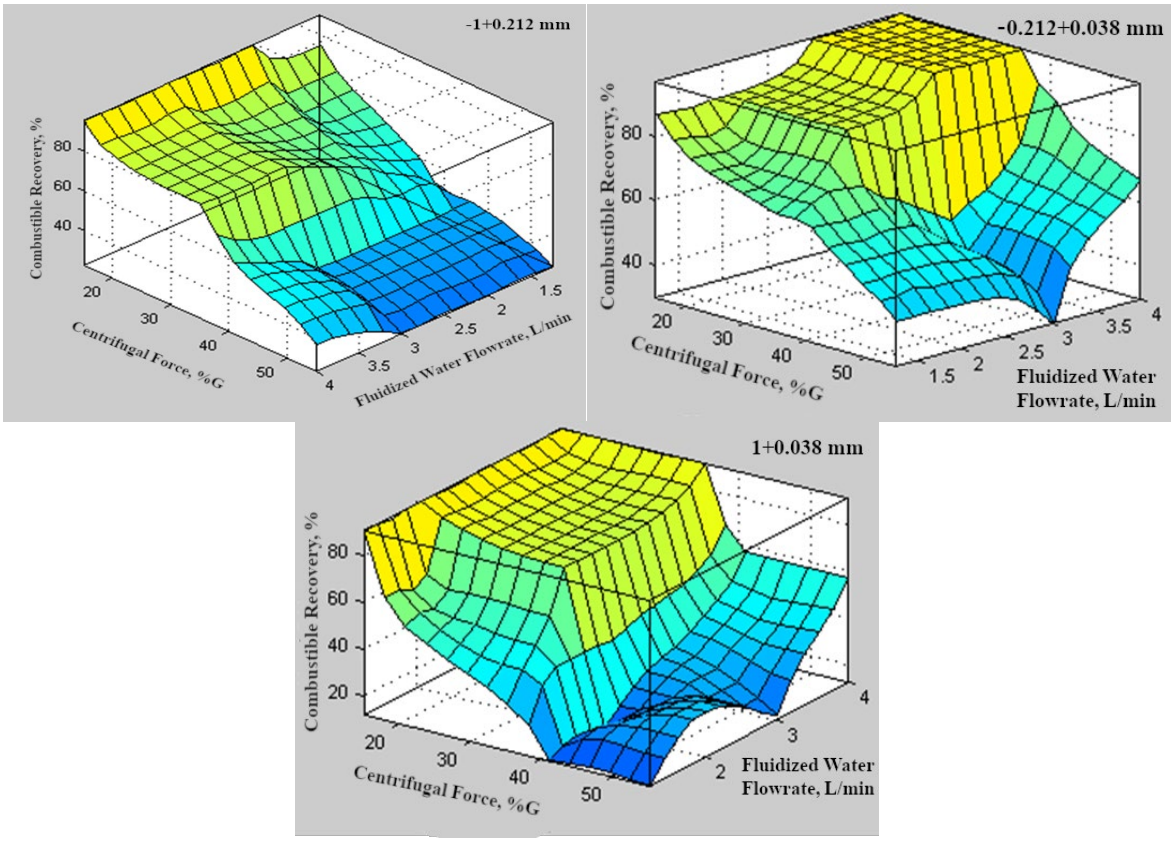


Fig 11. Combustible recovery graphs for experiments performed at (a) -1+0.212 mm, (b) 0.212+0.038 mm and (c) 1+0.038 mm size

R^2, RMS, and MAPE values for all dimensions are given in Table 2. The coefficient of determination (R^2) and error variance criteria (RMS and MAPE) were considered in determining the best-fitting particle size. Accordingly, the model with high R^2 and low RMS and MAPE values was considered as the best method. According to the results obtained from the evaluations, high R^2 values of weight and combustible recovery were generally obtained in all particle sizes. However, the R^2 values of 100-ash were low.

Table 2. Determining the agreement between the actual value and the model prediction

Particle Size (mm)	Outputs	R^2	RMS	MAPE
-1+0.212	Weight (%)	0.9347	7.0149	11.0467
	100-Ash (%)	0.7387	3.2159	2.9007
	Combustible Recovery (%)	0.9320	8.8860	16.5312
-0.212+0.038	Weight (%)	0.9658	5.4583	12.4416
	100-Ash (%)	0.9131	1.6758	2.2288
	Combustible Recovery (%)	0.9324	8.0691	14.6385
-1+0.038	Weight (%)	0.9214	7.749	51.9848
	100-Ash (%)	0.8747	1.5149	1.7821
	Combustible Recovery (%)	0.9201	9.3900	55.4473

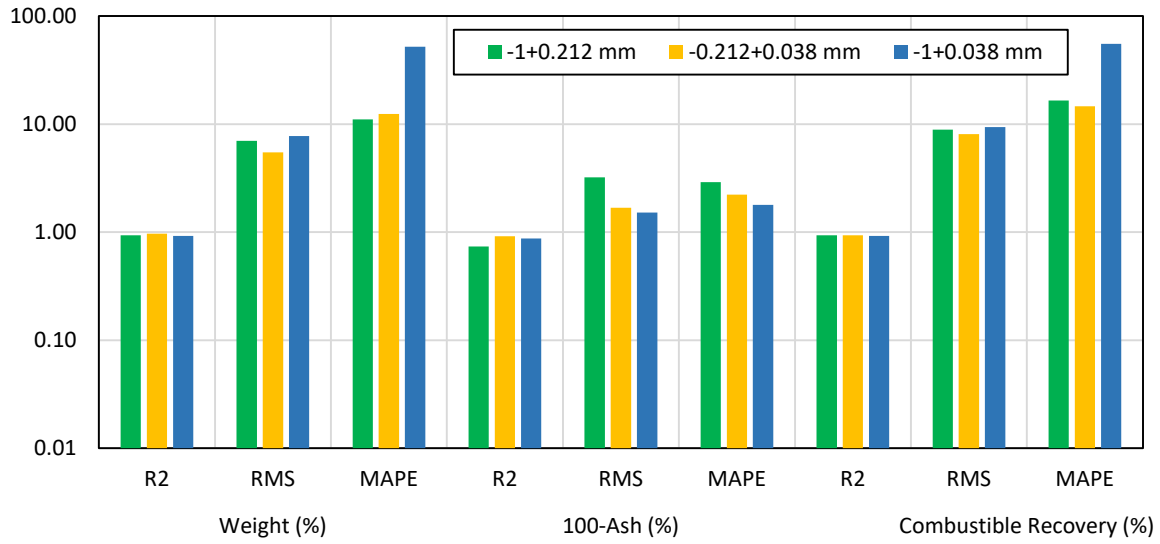


Fig 12. Agreement values of output parameters depending on particle size

The size range with the highest R^2 values obtained in the study is -0.212+0.038 mm. The lowest R^2 value was obtained at the 100-Ash value and was obtained as 0.9131. The MAPE and RMS values of 100-Ash values are 2.2288 and 1.6758, respectively, indicating that the prediction results are highly accurate.

The high MAPE and RMS values obtained in fuzzy logic for weight and combustible recovery of the experiment conducted at -1+0.038 mm indicate that the prediction is of low accuracy. This can be explained by the fact that the results obtained from the Knelson experiments are quite scattered. This may be due to the wide size range.

4. Conclusions

In this study, the fuzzy logic method was applied to the experimental results of three different sizes of waste coal concentrated using a Knelson concentrator. According to the results, experimental and fuzzy logic results are very close to each other in the size range of -0.212+0.038 mm. This is also seen with the statistical values of R^2, RMS and MAPE.

The results obtained from the evaluations showed high R^2 values in general in each size range. However, it is seen that the -0.212+0.038 mm size range gives higher R^2 values than the -1+0.038 mm size range, and the error values are lower.

Findings indicate that the fuzzy logic method is beneficial in the prediction of ash content, combustible recovery and clean coal weight, which are important in coal beneficiation. In addition, this method can minimize the both time and financial cost losses during the studies at various equipment conditions and particle sizes.

The low amount of data used in the evaluation also affects the error rate, and it is thought that more satisfactory results will be obtained if the amount of data is increased.

Acknowledgments

We thank to Turkish Coal Enterprises WLE (TKİ GLİ) for providing information and samples.

References

Abkhoshk , E., Kor, M., & Rezai, B. (2010). A study on the effect of particle size on coal flotation kinetics using fuzzy logic. *Expert Systems with applications*, *37*(7), 5201-5207.

Cai, X., Zhang, J., Ning, Z., Cui, Z., & Chen, J. (2021). A many-objective multistage optimization-based fuzzy decision-making model for coal production prediction. *IEEE Transactions on Fuzzy Systems*, *29*(12), 3665-3675.

Ali, D., Hayat, M. B., Alagha, L., & Molatlhegi, O. K. (2018). An evaluation of machine learning and artificial intelligence models for predicting the flotation behavior of fine high-ash coal. *Advanced Powder Technology*, *29*(12), 3493-3506.

Eyüp, S., & Selçuk, K. (2014). Separation Development Studies on the Beneficiation of Fine Lignite Coal Tailings by the Knelson concentrator.

Fecko, P., Tora, B., & Tod, M. (2013). Coal waste: handling, pollution impacts and utilization. In *The coal handbook: towards cleaner production* (pp. 63-84). Woodhead Publishing.

Ghaffari, A., & Farzanegan, A. (2017). An investigation on laboratory Knelson concentrator separation performance: Part 1: Retained mass modeling. *Minerals Engineering*, *112*, 57-67.

Honaker, R. Q., & Das, A. (2004). Ultrafine coal cleaning using a centrifugal fluidized-bed separator. *Coal Preparation*, *24*(1-2), 1-18.

Honaker, R. Q., Wang, D., & Ho, K. (1996). Application of the Falcon concentrator for fine coal cleaning. *Minerals Engineering*, *9*(11), 1143-1156.

Jain, L. C., & Martin, N. M. (Eds.). (1998). Fusion of neural networks, fuzzy systems and genetic algorithms: industrial applications (Vol. 4). CRC press.

Kökkılıç, O., Langlois, R., & Waters, K. E. (2015). A design of experiments investigation into dry separation using a Knelson concentrator. *Minerals Engineering*, *72*, 73-86.

Li, J. W., Sun, C. Y., Yin, W. Z., & Yuan, C. (2012). Effect of particle size on galena flotation kinetics using fuzzy logic. *Journal of Northeastern University (Natural Science)*, *33*(2), 279.

Majumder , A. K., Tiwari, V., & Barnwal, J. P. (2007). Separation characteristics of coal fines in a Knelson concentrator-A hydrodynamic approach. *Coal preparation*, *27*(1-3), 126-137.

Öney, Ö., Tanrıverdi, M., (2016). *Investigation of the Beneficiability of Zonguldak Fine Coals in Knelson concentrator*. Turkey 20th Coal Congress, TMMOB, Zonguldak, 375-383.

Ozcan, F., Atis, C. D., Karahan, O., Uncuoglu, E., & Tanyildizi, H. (2009). Comparison of artificial neural network and fuzzy logic models for prediction of long-term compressive strength of silica fume concrete. *Advances in Engineering Software*, *40*(9), 856-863.

Peer, F., Mongwe, A., & Van Heerden, J. H. P. (2002). A preliminary investigation into the metallurgical efficiency of an enhanced gravity separator. *Journal of the South African Institute of Mining and Metallurgy (South Africa)*, *102*(4), 251-253.

Saravani , A. J., Mehrshad, N., & Massinaei, M. (2014). Fuzzy-based modeling and control of an industrial flotation column. *Chemical Engineering Communications*, *201*(7), 896-908.

Uslu, T., Sahinoglu, E., & Yavuz, M. (2012). Desulphurization and deashing of oxidized fine coal by Knelson concentrator. *Fuel Processing Technology*, *101*, 94-100.

Zadeh, L. A. (1965). Fuzzy sets. Information and control, 8(3), 338-353.

Utilization of TTK Armutçuk Region Coal in Sectors Other Than General Consumption

Faik ALP [1]*, Serdar YILMAZ [2], İhsan TOROĞLU [2], Mehmet BİLEN [2]

[1] TTK Genel Müdürlüğü, Zonguldak-TURKIYE

[2] Zonguldak Bülent Ecevit University, Engineering Faculty, Department of Mining Engineering

*Corresponding author: faikerim@hotmail.com (Faik ALP)

Abstract:

Zonguldak Coal Basin North West of Turkey region. Most of the coal in the basin is of good quality. high volatile bituminous bituminous coal with coking properties (FSI value 7-9) Although in the eastern part of the Basin in the Amasra Region, the Coking feature unavailable (FSI value 0-1) coals in Armutçuk Region in the north-western part. There are bituminous coals with poor coking properties (FSI value 2-4).

Today, Turkish Hard Coal Authority (TTK) Armutçuk TIM's raw coal is produced by Baum Jiği at the Armutçuk Lavuar plant, which was established by McNally in 1960 with a capacity of 200 tons/hour. washed, 150-18 mm size range lump charcoal domestic fuel, 18-10 mm and 10-0.5 mm size range The clean coal is marketed as industrial coal and the 0.5 mm size is marketed as power plant coal. The coal obtained as a result of washing in the Armutçuk Laver, which has completed its operational life, and When the ash of 18-0.5 mm sized clean coal marketed as industrial coal ash values above the project value and decreases in plant performance over time is observed.

Keywords: *Turkey, Zonguldak, Armutçuk, Hard coal, Foundry sand carbon additive, PCI, Activated Carbon, Barbuki Coal, Hookah Coal*

1. Introduction

Although most of the coals in the Zonguldak Coal Basin, located in the north-western region of Turkey, are high volatile bituminous coal with good coking properties (FSI value 7-9), there are coals with no coking properties (FSI value 0-1) in the Amasra Region in the eastern part of the Basin and bituminous coals with poor coking properties (FSI value 2-4) in the Armutçuk Region in the north-western part of the Basin. The main purpose of this study is to investigate the possibilities of utilizing the coal produced in the underground mines of the Armutçuk Hard Coal Enterprise of the Turkish Hard Coal Authority (TTK) by transforming all of it into high value-added products other than traditional consumption places.

2. Zonguldak Coal Basin

Zonguldak Coal Basin is the only coal region in Turkey where hard coal is available. The hard coal produced in the basin is of two different qualities: coking and non-coking. The reserves suitable for direct metallurgical coke production are located in the working areas of Kozlu, Üzülmez and Karadon Enterprises, while the coal produced in Armutçuk operation is semi-coking and Amasra coals are non-coking (Öztürk, 2014). Coaly units in the basin start with the Alacaağzı formation belonging to the Namurian of the Upper Carboniferous, and are completed by the Lower Westphalian A aged Kılıç formation, the Kozlu formation belonging to the Upper Westphalian A and the Westphalian B-C-D aged Karadon formation. There are 46 coal seams with different structures and properties within these formations in the basin, and production activities are currently carried out in 18 seams that can be operated economically. Production is mainly carried out in the productive seams within the Kozlu formation. Fig. 1 shows the Zonguldak hard coal basin and Armutçuk Enterprise.

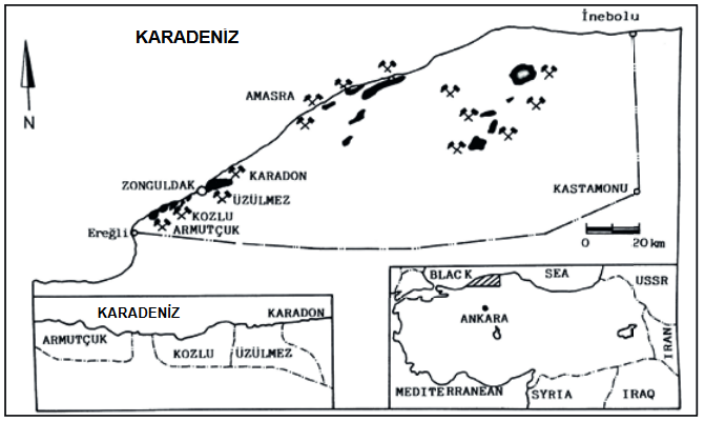


Fig. 1. Zonguldak Hard Coal Basin and Armutçuk Enterprise (Didari et al., 2015)

The calculated geological reserve of the basin up to a depth of -1200 m is approximately 1.354 billion tons, of which 42% is considered as visible reserve. The slopes of the coal seams vary between 0-90° and the thickness of the seam varies between 0.8-3.5 m. Armutçuk Establishment The thickness of the large seam reaches up to 25 m. The steep and nearly steep vein slopes have caused the pits to deepen rapidly. The average production depth increases by approximately 12 m every year. In Karadon and Kozlu mines, production and preparation works are carried out at a depth of -540 and -630 m, respectively, and preparation for deep coal mining is carried out with wells deepened to -1000 m (Öztürk, 2014).

In Zonguldak Hard Coal Basin, production is carried out with advancing-driven longwall methods in seams with 0-45° inclination and with reversing-driven longwall methods in fire-prone seams (Armutçuk and Kozlu Establishments). In seams with a slope greater than 45°, pneumatic blasting excavation method is applied and production is carried out with the intermediate layer caving method. In addition, in Kozlu Plant, tumbling chimney method, which is a different type of chamber heel method, is also applied in steep seams. Numerous large and small faults and squeezes in the basin prevent the application of mechanized methods. Production is still largely dependent on manpower (Öztürk, 2014).

Table 1. Information on the enterprises producing in the basin (Öztürk, 2014)

Association	Reserve (106 ton)	Average Depth of Production (m)
Armutçuk	**33**	**550**
Amasra	407	236
Karadon	412	373
Kozlu	159	488
Üzülmez	305	200
Toplam	1316	

Basin Coals were formed in the Carboniferous Period. Bituminous coal is produced in Armutçuk, Kozlu, Üzümez, Karadon and Amasra Plants of Turkish Hard Coal Corporation. Bituminous coal containing high volatile matter with good coking properties (FSI value 7-9) is produced in Kozlu, Üzülmez and Karadon Plants. Bituminous coal containing high volatile matter with poor coking properties (FSI value of 2-4 and Lustrous carbon (bright coal) value of 8-12) is produced at Armutçuk Plant. Bituminous coal containing high volatile matter with coking properties (FSI value 0-1) is produced at Amasra Plant.

3. TTK Armutçuk Association

TTK Armutçuk Hard Coal Enterprise is located 35 km west of Zonguldak province in Kandilli Town (the western border of Zonguldak Hard Coal Basin). The Establishment carries out its activities in an area of 100 km2 in total, of which 54 km2 is on land and 46 km2 is in the sea, containing approximately 22 million tons of reserves. In addition, around 12 million tons of reserves in the field are operated under royalty. The Big vein constitutes ~ 76% of the total reserves. All of the production activities of the enterprise are located in the Büyük vein with a thickness ranging between 3 and 25 m (average 6 m),

which constitutes the boundary between the Westphalian A aged Kozlu formation and Namurian aged Alacaağzı formation (Didari et al., 2015; TTK, 2021).

3.1. TTK Armutçuk Coal Preparation Plant

The Armutçuk Lavatory, where the raw coal belonging to TTK Armutçuk TIM is washed, was established in 1960 by McNally Company (American). The plant has a capacity of 200 tons/hour and was built in such a way that 0-150 mm size range can be enriched with one Baum Jet, 0,5-6 mm size range can be enriched with 8 shaking tables and 0-0,5 mm size can be enriched by flotation method. The shaking table and flotation units in the fine circuit of the plant were deactivated for various reasons. After the cancellation of these units, the ash value of the 0-10 mm sized clean coal increased to 20-25% from time to time, problems were encountered in the marketing of the product and a significant decrease in its economic value occurred. As a result of the studies carried out, it was determined that the ash content can be reduced to 5-10% if the coal is washed in a modern lavuvar to be newly established and that it has the properties that can be used in the production of PCI, casting sand carbon additive, barbecue and hookah charcoal production and activated carbon production.

4. Use of Armutçuk Coal as Foundry Sand Additive

Two types of binding agents are generally used to hold the sand together during the metal casting process. Depending on the type of binder used, casting sands are classified as clay-binder sand (greensand) and chemical binder sand used for high temperature processes. Clay-bonded (greensand) sands consist of natural materials blended together, such as high quality silica sand (85-95%), bentonite clay (4-10%) as binder, a carbonaceous additive (2-10%) to improve casting surface smoothness, and (2-5%) as binder. Coal powders with low ash content and high Lustrous Carbon: a carbonaceous additive added to bentonite-based molding sands to reduce oxidation in the casting mold, minimize casting sand adhesion during shaking, improve casting surfaces and combat the formation of casting defects. The most important feature sought in the coals that can be used for this purpose is the amount of lastrous carbon (bright carbon) of the coal and this amount is desired to be above 10% (La Fay et al., 2009; Türkeli, 2016; PS, 1998). Chemical properties such as ash, moisture, volatile matter (UM), sulfur (S), nitrogen (N) content should also be taken into consideration when selecting hard coal and carbonaceous additives. A coking property (FSI) of 2-4 is preferred. Bentonite-based sands used in the construction of casting molds are considered ecological. Molds made of sands doped with organic matter (additives that lead to the formation of bright carbon during high-temperature pyrolysis of organic matter) are volatile organic compounds (VOCs) that are released from the mold after pouring liquid metal into it, and polycyclic compounds of aromatic hydrocarbons (PAHs) and benzol hydrocarbons (BTEX) are not involved in the thermal reactions of polycondensation, and polymerization is particularly harmful and has carcinogenic, mutagenic and teratogenic effects. For this reason, despite the high content of Lustrous Carbon, organic materials are not preferred in foundry sands because they are not ecological and their prices are very high (Chakherlou et al., 2011; Kwasnıewska-krolikowska, 2013; Kaminska et al., 2021; Kaminska et al., 2023)

Of the 1040 organizations operating in the foundry sector in Turkey, 1024 are private sector and 16 are public and military organizations. The Turkish foundry sector has an important place both in Europe and in the world. Most of the castings produced in the European Union (76%) are based on conventional molding sands (Greensand system), which contain bentonite-bright carbon carrier (coal) (Fig. 2). The most popular carbon additive is still coal. In the world, there are very few coal mines with a Lustrous Carbon percentage between 10-15%, low ash and chemical properties (volatile matter, sulfur, nitrogen, coking) that can be added in conventional molding sands (Greensand system) (Izdebska-Szanda et al., 2009; Kwasnıewska-krolikowska et al., 2013; Holtzer et al., 2013). The coals produced in TTK Armutçuk Coal Plant have physical and chemical properties suitable for the demand of this sector. The volatile matter content of Armutçuk coal varies between 30-40%. Lustrous carbon (bright carbon) is between 8-12 and the sulfur content of the coal is around 0.5 on average (Gedikli, 2019; Baran, 2022).

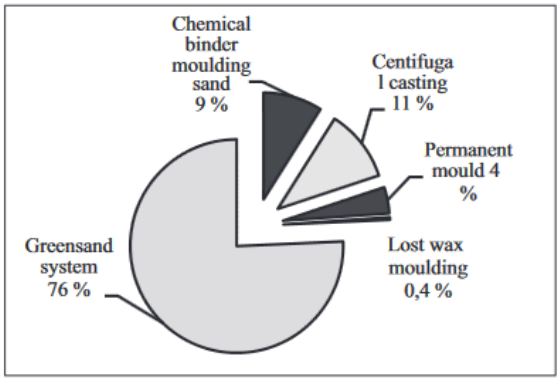


Fig. 2. Greensand System molding allowance (Kaminska, 2023)

5. Use of Injection Coal In Blast Furnace

Pulverized coal injection (PCI) is an additional fuel injection system in blast furnaces in order to reduce the metallurgical coke ratio, to provide ease of process control, to increase furnace efficiency and ultimately to provide cost savings. The factors affecting the combustion efficiency of pulverized coal in blast furnace can be listed as coal type, ash, volatile matter content, moisture content, fixed carbon content, sulphur content, mineral structure and grain size (PS, 1988).

European countries and Japan started to use pulverized coal injection in the early 1980s. With the injection of coal into the Blast Furnace; By replacing metallurgical coke, the coke ratio is reduced and the cost of Blast Furnace liquid raw iron production is greatly reduced. The application of the Pulverized Coal Injection into Blast Furnace (PCI) system is given in Fig. 3.

In Turkey and the countries in the region, the only coal source that can be used as Pulverized Coal Injection (PCI) in terms of moisture, ash, volatile matter, fixed carbon, sulfur content and mineral properties of the coal is Armutçuk coal region. When the ash content is reduced below 10% after the washing process in the lavuar, it can be used as pulverized coal injection to the Blast Furnace at the maximum rate.

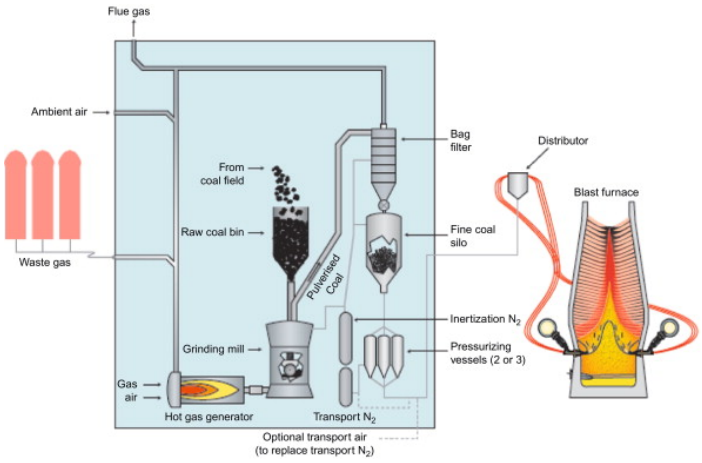


Fig. 3. Schematic view of pulverized coal injection in blast furnace

6. The Use of Armutçuk Coal in Activated Carbon Production

Activated carbon is a material with high porosity. Since high porosity causes high absorption capacity, activated carbons are widely used in the removal of impurities contained in many gases and liquids. It is preferred in gas mask making, air purification systems, some poisoning, water filters for the separation of harmful microbes, substances and elements. Activated carbons are divided into three groups as micropores (<2 nm), mesopores (2-50 nm) and macropores (>50 nm) by the International Union of Pure and Applied Chemistry (IUPAC) according to the radius (size) of the pores they contain.

In activated carbons, micropores generally constitute 95% of the total surface area. Activated carbon is produced from highly carbon-containing materials that are abundant and cheap. Some of these materials are wood, coal, peat, coconut shells, various fruits and agricultural wastes. The properties of the raw materials from which activated carbon is produced have a direct impact on the quality and properties of the activated carbon produced. One of the raw materials commonly used in activated carbon production is coal. Coal is one of the most important energy sources in the world. It is known that there will be significant restrictions on the use of coal in this sector in the near future (Döngel, 1997; Demir and Elbinsoy, 2019).

TTK Armutçuk coal has shown that it can be used as raw material in activated carbon production when the ash content is reduced below 5-6% after washing in the lavuar. Studies with Armutçuk coal have shown that it can be used especially in the production of granulated activated carbon. As a result of the activation studies carried out at prototype scale, granulated activated carbon with a BET surface area of 1250-1519 m2/g was produced and the physical and chemical properties of this activated carbon showed that it can be used as a filter in gas masks that allow the retention of toxic organic gases/vapors. Fig. 4 shows the coal-based activated carbon used in toxic gas filters.



Fig. 4. Coal-based activated carbon in toxic gas filters

7. Use of Armutçuk Coal in Barbecue and Barbuki Coals

It has been shown that the tüvenan hard coal produced in Armutçuk coal pit can be used in the production of barbecue and barbuki coal when the ash content is reduced below 5-6% after the washing process in the lavuar. Successful results have been obtained in the studies on the possibilities of using Armutçuk coals in the production of barbecue and barbecue charcoal. The representations of smokeless barbuki coal of coal origin are given in Fig. 5.



Fig. 5. Coal-based smokeless barbuki coal

8. Conclusion

In Turkey, Armutçuk coal is the most important coal source that can be used as an additive in casting sand, PCI coal, activated carbon, barbecue and hookah coal production. In the countries of the region, coal resources similar to Armutçuk coal are limited and their needs are met by importing from Far East

countries such as China. Armutçuk coals are known to be used in the production of injection coal for blast furnaces and as an additive to casting sand. However, there is very little information about its use as a raw material in activated carbon production and as an additional additive in the production of barbecue and barbuki coal. Armutçuk coal needs to be washed in a modern lavvar in order to transform it into coal with high added value. Established in 1960 and considered to have completed its economic-technological life, it is possible to replace the TTK Armutçuk lavatory with a new lavatory and utilize all of the coals produced from the lavatory as high value-added products mentioned above.

Armutçuk coals should be washed as strategic coal that can be used in sectors other than energy production (domestic and steam production) and marketed in these sectors, since coal deposits with this coal feature are limited in the world and especially in European countries.

References

Baran, F, (2022). Dökümhanelerde kullanılan kalıp ve maça kumları kaynaklı döküm hataları ve önlenmesi, Yüksek Lisans Tezi, Sakarya Üniversitesi, Fen Bilimleri Enstitüsü, 79 s.

Chakherlou, N.T. et. al., (2011). Studies of mechanical and technological parameters and evaluation of the role of lustrous carbon carriers in green moulding sands with hybrid bentonite in bentonite mouldig sands. *Materials&Desgn, 32*, pp.162-169.

Demir, U and Elbinsoy S, 2019 Investigation of the Usability of High Sulfur Coal in Activated Carbon

Didari, V Oskan M and Barış K, 2015 TTK Armutçuk Müessesesi Büyük damar gaz içeriğinin doğrudan ölçme yöntemiyle belirlenmesi Bilimsel Madencilik Dergisi, Cilt 54, sayı 2, s.3-12.

Dike, Ö.S., 2008. Pulverize kömür enjeksiyonu kullanımının yüksek fırın çalışmasına etkileri. Yüksek Lisans Tezi, Cukurova Üniversitesi, Fen Bilimleri Enstitüsü, 74 s. Adana.

Döngel, B 1997 Zonguldak kömürlerinden aktif karbon üretimi, Zonguldak Karaelmas Üniversitesi, Fen Bilimleri Enst. Yüksek Lisans Tezi, Zonguldak, 76 p.

Holtzer, M. et. al., (2013) Harmfulness assessment of resin used as lustorous carriers in bentonite mouldig sands, Archives of metallurgy and materials, Vol.58, 79-84.

Izdebska-Szanda, I. et. al., (2009) Effect of additives promoting the formation of lustrous carbon on the knocking out properties of foundry sands with new inorganic binders, Archives of foundry engineering, Vol9, Issue1, 17-20.

Gedikli, M., (2019) Dökümhanelerde oluşan atık döküm kumunun geri kullanım yöntemlerinin incelenmesi, Yüksek Lisans Tezi, Sakarya Üniversitesi, Fen Bilimleri Enstitüsü, 57 s.

Kaminska, J. et. al., (2021) Research on selected Types of lustrous carbon carriers after the high temperature pyrolysis, Vol.21,Issue1, pp.566-62

Kaminska, J. et. al., (2023) Studies of mechanical and technological parameters and evaluation of the role of lustrous carbon carriers in green moulding sands with hybrid bentonite in bentonite mouldig sands, Archives of metallurgy and materials, https//doi.org/10.1007/s43452-022-00550-1

Kwasnıewska-krolikowska, D. et. al., (2013) Selection criterıa of lustrous carbon carriers in the aspect of properties of 4greensands system, Matalurgua, 52, (2013) 1 pp.62-64.

LaFay, V.S., et. al., (2009) Three methods of redacing seacoal by adding grahite into greensand molds, AFS Transaetions, 117, 798-806.

Öztürk, M, (2014) Taşkömürü Havzası Damar Gaz İçerikleri Tespit Çalışmaları, Zonguldak Türkiye Taşkömürü Kurumu İş Sağlığı Güvenliği ve Eğitim Daire Başkanlığı, 71.

Polish Standard, The content of lustrous carbon, Polish standard no.BN-88/4024-09.

Türkeli, A., 2016 Sentetik kalıp kumuyla yapılan dökümde kömür tozu kullanımının azaltılması, kömür tozuna alternative teknoloji, 8. Uluslararası Döküm Kongresi, İstanbul

TTK, (2021) Türkiye Taşkömürü Kurumu 2021 yılı faliyet raporu

Performance Of Sequential Gas Scrubber Systems At High Sulfur Dioxide (SO_2) Concentration

Furkan Enes ÖZEL [1]*, Arzu Sinem SATILMIŞ [2],

[1]ASOS Proses Makina San. Ve Tic. A.Ş.

[2] ASOS Proses Makina San. Ve Tic. A.Ş.

*furkanenes@asos.com.tr (Furkan Enes ÖZEL)

Abstract:

The release of sulfur dioxide (SO_2) into the atmosphere is an air pollution problem with significant environmental and human health impacts. SO_2 gas is found in the flue gas of thermal power plants and plants that process sulfurized ore. Failure to remove sulfur dioxide (SO_2) results in acid rain (sulfurose acid (H_2SO_3) and sulfuric acid (H_2SO_4)). Acid rain is harmful to human health and the environment. SO_2, which causes air pollution, is removed through the desulfurization process. Desulfurization systems are devices that remove sulfur dioxide (SO_2) from flue gas by scrubbing it with lime solutions ($CaCO_3$ or CaO solutions). While the amount of sulfur dioxide (SO_2) in the flue gas of thermal power plants is in the range of 2,500-3,500 ppm, the amount of sulfur dioxide (SO_2) in the flue gas of the roasting plant established and commissioned by ASOS Proses Makina San A.Ş. in Konya region is in the range of 25,000-35,000 ppm.

The removal of sulfur dioxide (SO_2) gas, which is approximately 28,000 ppm in the "Inline Flue Gas Washing Plant" installed in the roasting plant, is provided to reduce the removal to 70 ppm and below. This removal is calculated to be 99.75%. When compared with the desulfurization systems used in thermal power plants, it was found that the removal is at the level of 95-97%. Comparing the system used in thermal power plants with the in-line flue gas scrubber, this study shows that it works with higher removal and efficiency.

Keywords: *Scrubber, calcination, SO_2, gas scrubbing systems, desulfurization*

1. Introduction

The major component of the sulfur oxides produced by the high-temperature calcination of sulfur fuels or sulfur-containing minerals is SO_2 gas. It has been found that some of the SO_2 in the air is converted to SO_3 by catalysis by sunlight or solid particles, or oxidation by complex reactions on water droplets, and then leaves the atmosphere by wet or dry precipitation. The emitted SO_2 gas combines with water vapor to form sulfuric acid (H_2SO_4), leading to serious environmental effects known as acid rain. Acid rain disrupts the pH balance of the soil, damaging vegetation and agricultural production. Acid rain also has a devastating effect on water resources, forests and buildings. It reduces agricultural productivity and weakens natural vegetation. It also causes an acidic pH in water sources, threatening the survival of aquatic life in ecosystems such as lakes, rivers, and oceans. Fish and other aquatic life are severely affected and biodiversity is reduced. When SO_2 in the air exceeds certain levels, it can cause respiratory disease, especially lung failure, and can be fatal for respiratory patients (Müezzinoğlu, A. (1987)).

Table 1. Classification of Gaseous Air Pollutants (De Nevers, 2000).

Form	Primary Pollutants	Secondary Pollutants
Sulfur-Containing Compounds	SO_2, H_2S	SO_3, H_2SO_4, MSO_4
Nitrogen-Containing Compounds	NO, NH_3	NO_2, MNO_3
Organic Compounds	H-C Compounds	Ketones, aldehydes, O_3, acids, organics, aerosols
Carbon Oxides	CO, CO_2	-
Halogen Compounds	HCl, HF	-
Photochemical Oxidants	-	O_3, NO_3, H_2O_2, peroxyacetyl nitrate

Desulfurization processes are required to minimize the impact of SO_2 gases on the environment. Table 1 shows the impact of sulfur-based compounds on air pollution and the role of other waste gases. The history of desulfurization dates back to the 19th century. During this time, with the growth of coal-fired industries, sulfur dioxide (SO_2) emissions into the atmosphere became a serious environmental problem. Particularly during the Industrial Revolution in the UK, problems such as acid rain and air pollution led to the need to control sulphur-containing gases. In the 20th century, desulfurization technologies developed rapidly as environmental awareness increased and stricter environmental regulations were introduced. Flue gas desulfurization (FGD) systems, which became widespread in the 1970s, especially in power plants, were an important step in reducing sulfur dioxide emissions. (De Nevers, N., 2000)

Increasing demand for raw materials is leading to the use of sulfur ores that could not previously be economically processed. During the processing of these ores, SO_2 is released through high-temperature processes such as roasting. For economic reasons, the processing of low-grade, high-sulfur ores is preferred, which increases SO_2 emissions.

The development of FGD systems is an important milestone in the beneficiation of sulphur-bearing ores. The control of SO_2 emissions, the reduction of environmental impact and the availability of sulfur ores on a larger scale demonstrate the critical role of FGD technologies in this process. This development enables more efficient, economical and environmentally friendly production processes in the mining industry. The right design will ensure that the system operates at high efficiency, costs are optimized and by-products are managed effectively, which is important for both the business and the environment.

Table 2. Emission limits for gas-fired combustion plants. (Çevre ve Orman Bakanlığı, (2010))

FUEL TYPE	FUEL HEAT POWER	EMISSION LIMIT VALUES (mg/Nm^3)			
		DUST	SO_2	NO_2 (NO VE NO_2)	CO
General Situation Natural gas, fuel gas, LPG, etc.	50 MW ≤ Fuel thermal power <300 MW	5	35	150	100
	Fuel thermal power ≥300 MW			100	
Blast Furnace Gas		10	200	200	
Gases that are produced in the iron and steel industry and can be used elsewhere		30	400* 200**		
Liquefied gas		5	5		
Low-calorie gases formed in the coke oven		30	400		

Low-calorie gases formed in blast furnaces		10	200		

* Low-calorie gases formed in coke ovens

** Low-calorie gases formed in blast furnaces

Table 2 presents data on the emission values of gas-fired plants installed in the Republic of Turkey according to the "Regulation on Large Combustion Plants" published in 2010. The plant to be constructed by Asos Proses will be built using blast furnace gas within the scope of this regulation and designed to keep SO_2 emission value below 200 mg/Nm^3.

2. Materials and Methods

The LECO analysis result of the ore provided for the determination of process values is given in Table 3.

Table 3. Ore content subjected to roasting process

LECO ANALYSIS RESULTS			
Analysis Method	Sample Description	C	S
LECO	AS-1	0,20%	7,06%
LECO	AS-2	0,19%	7,06%
LECO	AS-3	0,21%	7,57%
LECO	AS-4	0,20%	7,18%
LECO	AS-5	0,20%	7,23%
LECO	AS-6	0,20%	7,07%
LECO	AS-7	0,20%	7,33%
LECO	AS-8	0,19%	7,11%
LECO	AS-9	0,20%	7,11%
LECO	AS-10	0,18%	7,37%

When LECO determination was performed on ore samples taken at different times, it was found that there was sulfur in the range of 7.06%-7.37% as seen in Table 3. Sulfur is removed from the ore treated with high temperature air in the roasting plant and leaves the system as sulfur dioxide gas with the air. Asos Proses Makina San. ve Tic. A.Ş. in Konya region, SO_2 gas in the range of 25,000-35,000 ppm is formed as a result of processing the ore at high temperatures.

Table 4 shows the amount of SO2 that will theoretically occur in case of production with a capacity of 50 tons/h of ore with sulfur analysis results between 7,06% and 7,37% and the calculation required to keep the emission values within the legal limit.

Table 4. Calculation of ppm value and removal amount of SO_2 gas in flue gas with 50 tons/h capacity ore feeding

FGD REMOVAL CALCULATION		
Ore inlet amount	50.000,00	Kg/h
Ore inlet %S	7,50	%
Ore outlet %S	0,00	%
Inlet S amount	3.747,50	Kg/h
Ore without S	46.252,50	Kg/h
Outlet ore S	0,00	Kg/h

S to be removed	3.747,50	Kg/h
SO2 to be removed	7.495,00	Kg/h
Air mass	115.405,00	Kg/h
Stack Emission	82.805,12	mg/Nm^3
	28.981,79	ppm
Regulation limit value	200,00	mg/Nm^3
Removal	99,758	%

The roasting or calcination of sulfur-containing ores is a process of removing sulfur, especially sulfated minerals, by heating them at high temperatures in the presence of oxygen. This process usually takes place in the temperature range of 500-1000 °C and results in the oxidation of sulfurous minerals to release precious metals (especially gold and other metals). Sulfur dioxide (SO_2) gas, an important by-product, is released during roasting.

For example, sulfur in minerals such as pyrite (FeS_2) reacts with oxygen to form SO_2 gas. Meanwhile, the metal components of the mineral (e.g. iron) are oxidized to iron oxide (FeO), a form suitable for beneficiation. This chemical reaction is as follows (1);

$$2FeS_2(s) + 5O_2(g) \rightarrow 2FeO(s) + 4SO_2(g) \quad (1)$$

In this reaction, iron oxide and sulfur dioxide are released when pyrite reacts with oxygen. Similar reactions occur in other sulphated minerals and SO_2 gas is produced as a result. When this gas is released into the atmosphere, it can cause environmental pollution. For this reason, emissions are controlled by using flue gas treatment systems in modern plants.

Asos Proses Makina San. ve Tic. A.Ş. in Konya region, wet washing units were connected in series in order to keep emissions under control and below the emission limit of 200 mg/Nm^3. The series connection of these multiple wet scrubber systems makes it more effective to keep flue gas emissions below legal limits and facilitates the management of the process. In addition, by applying this method, the lifetime of the equipment used is extended and maintenance costs are kept to a minimum.

The choice of the chemical to be used for the removal of emissions in the wet washing system depends on the utilization potential of the by-products. Considering the economic analyses in the literature and field studies, the use of calcium oxide (CaO) and calcium carbonate ($CaCO_3$) are determined as the most appropriate solutions in terms of cost and benefit. In case of desulphurization with CaO solution, reactions (2), (3), (4) and with CaCO3, reactions (5), (6), (7) will take place in the reaction tank of the scrubber system. The use of these chemicals provides both effective results in emission control and advantages in terms of utilization of by-products.

$$SO_2(g) + H_2O(aq) \rightarrow H_2SO_3(aq) \quad (2)$$

$$H_2SO_3(aq) + CaCO_3(s) \rightarrow CaSO_3(s) + CO_2(g) + H_2O(aq) \quad (3)$$

$$2CaSO_3(s)(s) + O_2(g) + 4H_2O(aq) \rightarrow 2CaSO_4(s) \cdot 2H_2O(s) \quad (4)$$

$$CaO(s) + H_2O(aq) \rightarrow Ca(OH)_2(s) \quad (5)$$

$$Ca(OH)_2(aq) + SO_2(g) \rightarrow CaSO_3(s) + H_2O(aq) \quad (6)$$

$$2CaSO_3(s) + O_2(g) + 4H_2O(aq) \rightarrow 2CaSO_4 \cdot 2H_2O(s) \quad (7)$$

(Takashina and others (2001))

3. Results

Effective removal of SO_2 gas released during the roasting process is of great importance in terms of preventing environmental pollution. In the plant established by Asos Proses Makina San. ve Tic. A.Ş.,

wet washing units were connected in series in order to keep emissions under control, high efficiency was achieved and flue gas emissions were effectively limited. With the designed and manufactured equipment, the results of the plant after commissioning were realized with a 99.758% removal rate from 28,981.79 ppm SO2 emission value as shown in Table 4. While this value is between 95-97% in the thermal power plant, which is another facility where desulphurization systems are used, this value is exceeded in the sequential washing systems. The calcium carbonate ($CaCO_3$) or calcium oxide (CaO) chemicals used play an effective role in SO_2 removal and allow the utilization of by-products. The reaction of these chemicals with SO_2 in aqueous environment provides both high performance in emission control and beneficial use of by-products. As a result, these systems offer a significant advantage in terms of environmental sustainability and economic efficiency.

Acknowledgements

Thank you to Asos Proses Makina San. ve Tic. A.Ş. and our managers and colleagues for their moral and material support and contributions.

References

Biondo, S. J. and Marten, J. C., (1977) A History Of Flue Gas Desulfurization Systems Since 1850, *Journal of the Air Pollution Control Association, 27:10,* 948-961, DOI: 10.1080/00022470.1977.10470518

Çevre ve Orman Bakanlığından (2010); BÜYÜK YAKMA TESİSLERİ YÖNETMELİĞİ BİRİNCİ BÖLÜM;Amaç, Kapsam, Dayanak ve Tanımlar Sayı:27605 https://www.resmigazete.gov.tr/eskiler/2010/06/20100608-4.htm

De Nevers, N., (2000), *Air Pollution Control Engineering*, McGraw-Hill Chemical Engineering, NewYork.

Müezzinoğlu, A., (1987) *Hava Kirliliği ve Kontrolünün Esasları*, (No: 0908): Dokuz Eylül Üniv. Yayınları

Takashina, T., Honjo, S., Ukawa, N. and Oishi, T., (2001) Effect of Limestone Concentration and Particle Size on SO2 Absorption in Wet FGD Process, *Journal Chemical Engineering of Japan, 34,* 810-818 DOI:10.1252/jcej.34.810

Detailed Mass Balance Development of a Heap Leaching Operation Using Modelling and Simulation

Manuel Gonzalez [1]*, Tuğcan Tuzcu [2], Marie-Veronique Durance [1], Stephane Brochot [1]

[1]CASPEO, France

[2]MPES Engineering, Turkey

*Corresponding author: m.gonzalez@caspeo.net (Manuel Gonzalez)

Abstract:

Heap leaching is one of the most used techniques to extract valuable metals from the ore. The heap leach operations are carried out for the gold ores having gold grade lower than 1 ppm and the heap leach operations are cheaper than other gold leaching operations OPEX wise. The dynamic heap body encompasses several challenges such as permeability and different time dependency of the processes included in the flowsheet, especially in the cases of treating gold ores. These challenges make mass balance arduous to carry out. This work will explore how, using modelling and simulation, it is possible to create a full mass balance of a gold heap leaching operation and how the translation between dynamic and batch processes is done so everything is combined in a steady state process simulator.

Keywords: *heap leaching, mass balance, modelling, simulation*

1. Introduction

Leaching is the key operation to process a wide spectrum of oxide ores to produce metals like copper, cobalt, gold, silver, uranium…When the grade of the ore is not high enough to counterbalance the OPEX of an agitated leaching operation, heap leaching is the selected process to extract the metal from the ore.

Heap leaching is a low CAPEX and OPEX technology that enables the valorization of low grade deposits. The only downside, and it is not a small one, is that this technology is not easy to handle. Indeed, it is difficult to know what is happening inside the heap at a given time, and that means that it is difficult to predict how much metal (and money) the operation is generating over time.

A lot of research efforts has been made in the past to create mathematical models capable of predicting the metallurgical performance of a heap leaching operation. Different simulation techniques have been used, like CFD or phenomenological modelling. This paper illustrates how, using the appropriate modelling techniques, it is possible to build a process simulator of a gold hydrometallurgical plant integrating at the same time steady state and dynamic processes in the steady state simulation platform USIM PAC.

2. Building the simulator

A process simulator has three main components: the flowsheet, the material model and the mathematical models describing the equipment. Each of these elements has its importance and will be discussed hereafter.

2.1. Flowsheet description

The flowsheet selected, shown in Figure 28, is a classic hydrometallurgical flowsheet designed to process an oxide gold ore. It includes crushing, agglomeration, heap leaching, carbon in column, elution and electrowinning.

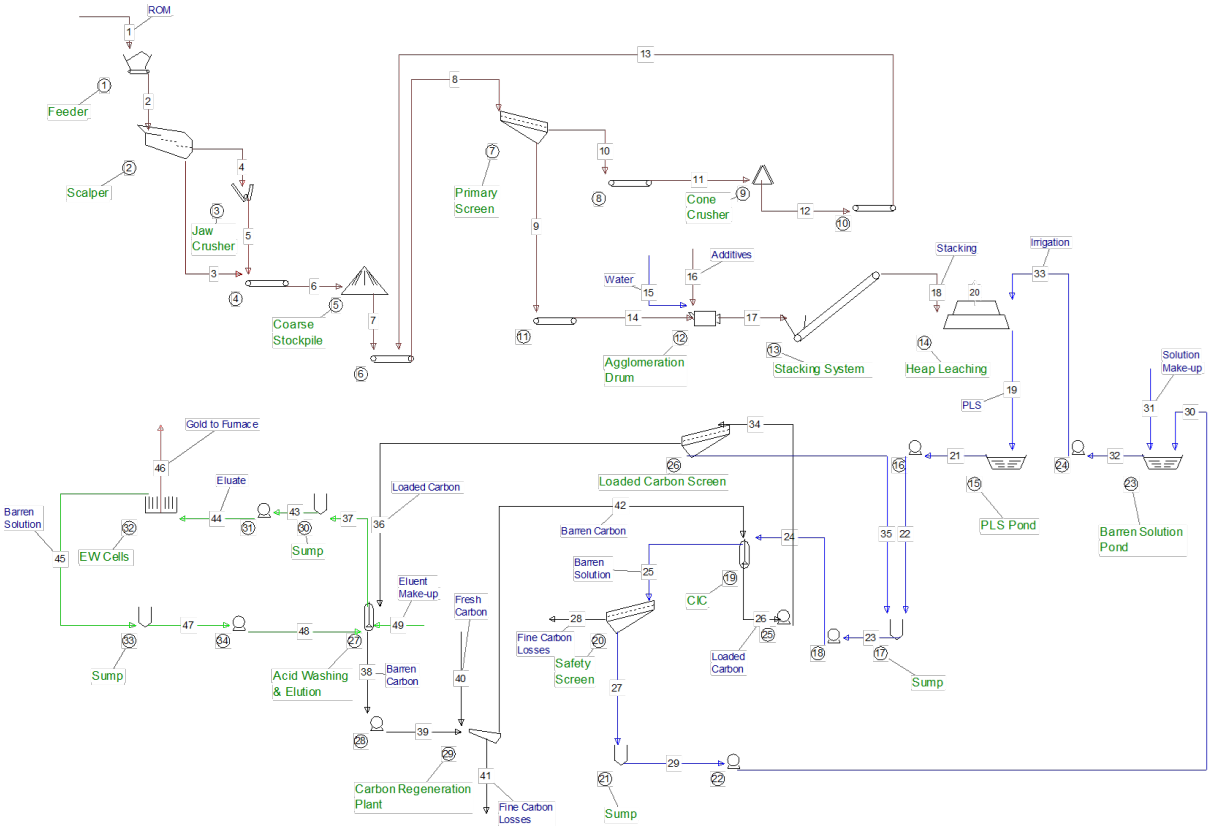


Figure 28. Gold processing flowsheet

Although some of the items included in the flowsheet, like the pumps and the belt conveyors, are not relevant for the metallurgical behavior of the process, they will allow the process engineers to estimate the power needed to run them.

One of the particularities of the flowsheet is how the different inventories are handled. In the case of the heap leaching, the Heap Leach icon includes a second exit called Heap Inventory, which gives the inventory of the heap. The example is shown in Figure 29. This approach can also be used to model the ponds, but it has been decided to assume that both ponds are run at constant level and there are not inventory variations.

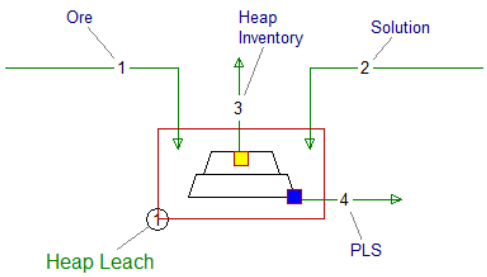


Figure 29. Heap Leaching dedicated icon

2.2. Material modelling

When a complete flowsheet of a gold hydrometallurgical plant is handled in a process simulator, different phases must be included: a solid phase to describe the gold ore, a liquid phase to describe water and leaching solution, a solid phase to describe the activated carbon, a liquid phase to describe the eluent and a solid phase to describe the doré/gold bars. And, in this case, we assume that the different reagents used in the process can be assimilated to a component of one of these phases.

The material model selected is shown in Figure 30. The Ore phase is of type "Ore" and is described by its particle size distribution (PSD) and its composition per size class in terms of components "Gold" and "Ore", the latter grouping all other minerals. The Solution phase is of type "Liquid" and is used to describes the moisture content of the ROM, the process water for agglomeration and the leaching solution. It manages composition in terms of components "Gold" and "Water", the latter containing all other elements, including reagents. Both are constituting the Slurry allowing to manage its density and %-solids. The Carbon phase is of type "Solid" and is described by its composition regarding "Gold" and activated "Carbon". The Eluent phase is like the Solution and the Gold phase is "Solid" with only one component "Gold". For the sake of simplicity, only gold is considered as leach metal, knowing other metals like silver and copper can also be present up to the final product.

$$\begin{cases} Slurry\ (P)\begin{cases} \text{Ore (O)}\begin{cases} \text{PSD} \\ \text{Composition per size class} \end{cases} \\ \text{Solution (L)}\{Composition \end{cases} \\ Carbon\ (S)\{Composition \\ Eluent\ (L)\{Composition \\ Gold\ (S)\{Composition \end{cases}$$

Figure 30. Material model

An additional key item to the material model is the link between the different components around the flowsheet. Indeed, to limit the number of possibilities, it is necessary to describe, for instance, how the gold goes from a solid phase (the ore) to a liquid phase (the Pregnant Leaching Solution - PLS).

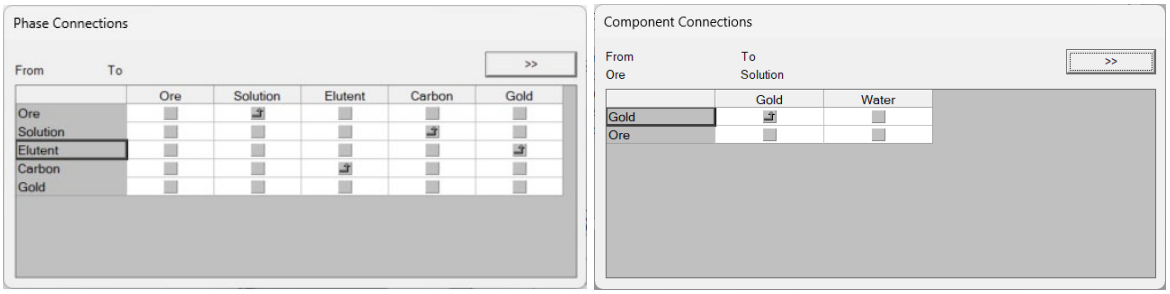


Figure 31. Phase Connections interface (left) and Component Connections interface (right)

The Phase Connections interface shown in Figure 31 (left) allows the user to define how the different components can be transferred from one phase to another. For example, there is a transfer of components from the Ore to the Solution which will represent the leaching of gold in the heap, the transfer of gold from the Solution to the Carbon that represents the gold adsorption taking place in the carbon columns or the desorption of gold from the Carbon to the Eluent taking place in the elution column, and finally the gold precipitation from Eluent to Gold cathode during electrolysis. Similarly, to indicate which component in a phase becomes which component in another phase, the Component Connections interface shown in Figure 31 (right) links, for example, the Gold component in the ore to the Gold component in the solution

2.3. Model selection

The selection of the mathematical models representing the equipment performance during the construction of the process simulator depends on the available data and the objectives of the simulator being built. In this case, the objective of the simulator is to generate a complete mass balance of the plant, so mainly performance models will be used. Hereafter, the models associated with the key units are presented.

2.3.1. Classification equipment

To accomplish the main objective of the simulator, generate a full mass balance around the plant, it is not necessary to choose complex models to represent the different screens present in the circuit. It has been decided to use the model Screen (0), which parameters are shown in Figure 32.

Parameters of Equipment #2 - Scalper - Screen (0)

Parameters	Values	Units
Screen openings	50	mm
Efficiency (%)	90	
Short circuit of fines (%)	0	
Percent solids in the coarse stream (%)	96.1538	

Figure 32. Screen (0) model parameters

This model calculates the screen outputs using, as main parameter, the screen openings size and the classification performances in terms of the efficiency and the short circuit. The liquid partition is calculated using the last parameter.

2.3.2. Crushing equipment

The flowsheet includes primary and secondary crushing stages, using a jaw crusher and a cone crusher respectively. In this case, the Crusher from Database model is used. This model contains a database of crushers and their associated typical size distribution curves for different settings.

Parameters of Equipment #3 - Jaw Crusher - Crusher from Database

Parameters	Values	Units
Number of crushers in parallel	1	
Closed side setting	75	mm
Adjustment of capacity according to material properties	1	
Database file name - C:\ProgramData\Caspeo\PAS English 3.3\Crusher.dat	Edit	
Order in database - C3054 jaw crusher granite	Edit	
Work index per component	Edit	
Power with Bond formula	Edit	
Power with Magdalinovic formula	Edit	
Calculated parameters	Edit	

Figure 33. Crusher from Database model parameters

If the user inputs the Work Index of the material, the model is also capable of calculating the power consumption of the crusher using the Bond´s or Magdalinovic´s formula.

2.3.3. Heap leaching

The heap leaching is the key process of the flowsheet, from which the value of the ore is recovered or lost. The used model to represent the heap leaching is still under testing and the interface shown (Figure 34) is an alpha version. The mathematical model is based on the Botz and Marsden recovery curves (Botz & Marsden, 2019). The model has been extended to work with different particle sizes and metals at the same time using, if it can be measured, kinetics per size class and metal.

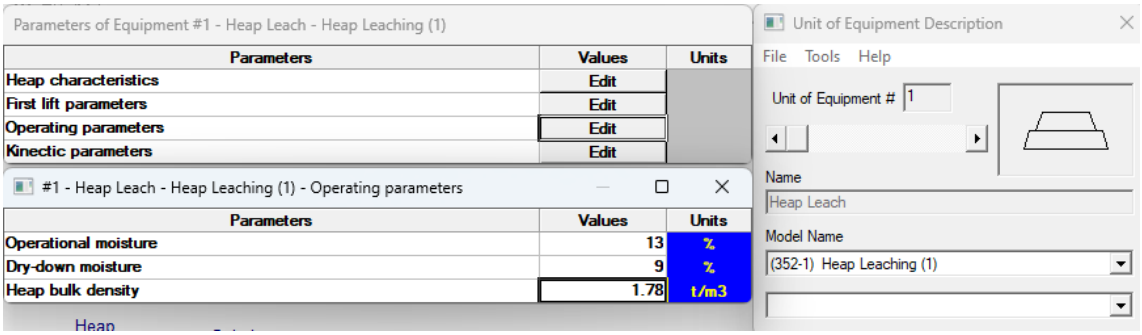


Figure 34. Heap Leaching (1) model parameters

The model has been designed with two objectives in mind: the first one is to calculate the average value of the PLS flowrate and grade over a period of time; the second one is to analyze the impact of the different heap parameters on the PLS produced and, later on, on the whole plant.

The first objective is the way to be able to integrate the model in a static simulator. As the PLS flowrate and grade change over time, depending on the cycle, the capacity to calculate average values helps the engineers to analyze how the downstream process behaves.

2.3.4. Carbon in column and Elution

As the structure of the models used to simulate the carbon in column (CIC) and the elution are quite similar, they are discussed together. These models are rather simple and utilize only the maximum recovery of the components and the mass conversion between phases.

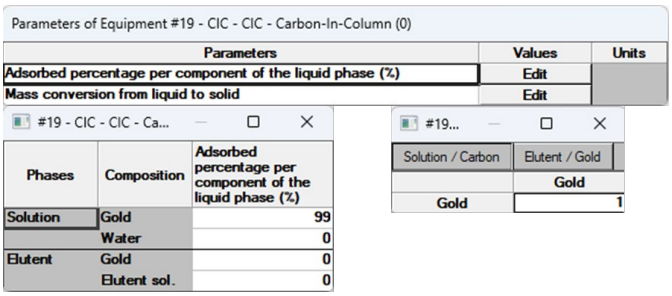


Figure 35. CIC - Carbon-In-Column (0) model parameters

Although the name of the model is not the same, the CIC and the elution models share the main structure, both using a parameter to define the performance and another one to take into account the reactions and the selected material model.

2.3.5. Electrowinning

The selected electrowinning model proposes the parameters needed to produce a very detailed mass balance around this operation. In this case, it has been decided to build the balance in the simplest possible way, so the assumption that the produced metal is completely dry has been made, using only the second and third parameters shown in Figure 36.

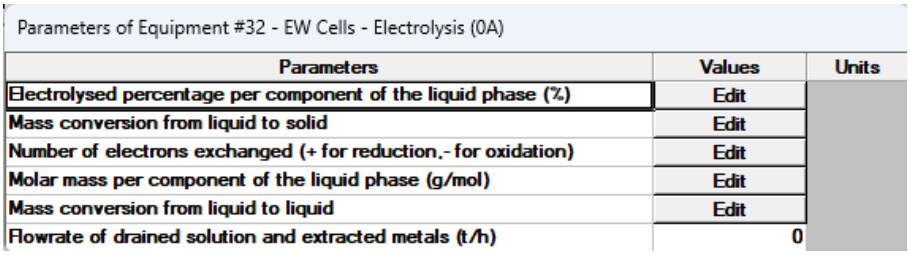


Figure 36. Electrolysis (0) model parameters

Using this model, all the eluate is recirculating and the produced gold cathode is completely dry. This behavior can be altered using the last parameter of the model, Flowrate of drained solution and extracted metals (t/h).

3. Mass balance results

The simulator described in the previous paragraphs was run using the parameters shown in Table 17.

Table 17. Main simulation parameters

Variable	Value
ROM feedrate, dry (t/h)	1,000
ROM top size (mm)	500
Crushing product d80 (mm)	16.3
Leaching recovery (%)	75
Irrigation (l/h/m2)	10
CIC recovery (%)	99
Elution recovery (%)	99.5

As the plant is expected to work 8,000 h/year, simulation results are shown in Table 18 and Table 19 for the grades and the flowrates, respectively.

Table 18. Selected simulation results - grades

Stream	Grade
Ore (ppm)	0.75
Barren Solution (g/m3)	0.004
PLS (g/m3)	0.51
Loaded carbon (g/t)	3,501.6

Table 19. Selected simulation results - flowrates

Stream	Flowrate
PLS (m3/h)	960.6
Loaded carbon (t/y)	1,115.6
Gold (oz/y)	124,963

The key operation on the flowsheet is the heap leaching, which, by means of the selected model, allows to predict the mean values of the PLS over long periods (1 year, for instance) and then use the results to simulate the rest of the circuit.

In the case of a CIC batch technology, the number of required cycles can be calculated knowing the carbon capacity of the columns, then the number of needed columns knowing the inter-cycle time.

4. Conclusions

Creating a mass balance of a heap leaching operation can become a difficult task if a lot of details are needed. For example, when kinetics per metal and per size class are used to accurately describe the behavior or the ore in the leaching pad, or if several metals are tracked across a full flowsheet.

A process simulator can help to alleviate the work related to complex mass balance during the process development stage. Such a simulator is based on three main items: flowsheet, material model and mathematical models. The mix of these elements, into the USIM PAC process modelling and simulation platform, allows the user to describe in detail what is happening with the valuable metals in each process unit, what are the characteristics of each stream and what are the key performance indicators of the process. Furthermore, as previously shown, combining the right modelling techniques, it is even

possible to integrate dynamic processes, as the heap leaching or the CIC, in a steady state simulator to produce a full, detailed mass balance of the complete flowsheet of a gold hydrometallurgical plant.

References

Botz, M. & Marsden, J. (2019). Heap Leach Production Modelling: a Spreadsheet-Based Technique. *Mining, Metallurgy & Exploration*, *Volume* 36, Pages 1041-1052. DOI: 10.1007/s42461-019-00129-0

Investigation of the rheological behavior of acid-leached sepiolite

Kemal Bilir [1],* and Utku Çağlar [2]

[1]Eskişehir Osmangazi University, Department of Mining Engineering

[2]Kütahya Construction Chemicals

*Corresponding author: bilirk@gmail.com (Kemal Bilir)

Abstract:

This study investigates the rheological behavior of acid-leached sepiolite, focusing on improving its properties through mechanical activation and nitric acid treatment. Sepiolite from the Türktaciri region of Sivrihisar was mechanically activated using a rotor-stator homogenizer to disperse the fiber bundles. The activated sepiolite was then subjected to nitric acid leaching to remove dolomite impurities. The effects of varying acid concentrations on sepiolite enrichment were examined using X-ray fluorescence (XRF) and X-ray diffraction (XRD) analyses. Results showed that the sepiolite content could be increased from 84.4% to 91.9% using a nitric acid molar ratio sufficient to dissolve 80% of the dolomite present. However, exceeding this ratio led to a rapid decrease in sepiolite content. The study found that at a 40% molar ratio, the sepiolite grade increased to 88% with 92% enrichment efficiency, while at an 80% molar ratio, the sepiolite grade reached 92% with 82% enrichment efficiency. These findings provide insights into optimizing the acid leaching process for enhancing sepiolite's rheological properties, which is crucial for its industrial applications.

Keywords: *Sepiolite, Rotor-stator homogenizer, Mechanical activation, Nitric Acid Leaching*

1. Introduction

Sepiolite is a natural hydrated magnesium silicate clay mineral. Its structure is made up of tetrahedral and octahedral oxide layers stacked on top of each other. Along the fibers, there are channel cavities (Rodriguez et al., 1994). Sepiolite is useful in many ways because it has a large surface area, a fibrous structure, porosity, surface activity, and the ability to form stable suspensions with high viscosity at low concentrations. Its sorptive, catalytic, and rheological properties are also useful in technology (Galan, 1996).

Sepiolites deposited in sedimentary layers are generally earthy, fine-grained, and slippery in appearance. They contain sepiolite minerals exceeding 90% in their structure, and the accompanying minerals are generally dolomite and smectite group clays and magnesite, palygorskite, and detrital minerals. The main component other than sepiolite is dolomite mineral, and illite, detrital quartz, and volcanic glass are found in varying proportions here and there. In cases where the sepiolite content falls below 50%, the material acquires the quality of sepiolite dolomite. However, in materials at the main sepiolite level, sepiolite is usually present in the composition at 10% or more (Sabah and Çelik, 1998). Sepiolite with a sepiolite content below 50% needs to be enriched to improve its rheological properties.

The rheological properties of sepiolite suspensions depend on the purity of the sepiolite used, the fiber size, and the degree of liberation of the fibers. In mechanical activation studies conducted to improve the rheological properties of sepiolite, the use of high-energy transfer devices resulted in the deterioration of the fiber structure and stability of sepiolite and the collapse of the tubular structure at different rates (Vučelić et al., 2002). For this reason, it is emphasized in the studies that the use of a low energy transfer activation method that creates more shear force effect instead of high energy transfer size reduction techniques will yield more effective results. By mixing the solid and liquid parts, high-shear rotor-stator homogenizers make emulsions with a high viscosity that stay stable (Myers et al., 1999).

The dispersion quality, gel stability, change in particle size distribution and apparent viscosity of sepiolite suspensions that will be mechanically activated with rotor-stator homogenizers will all provide direct or indirect comments on the degree of liberation and quality of sepiolite fibers.

In this study, it was aimed to determine the amount of nitric acid in the mole ratio that will be needed to dissolve 80% of dolomite in sepiolite mechanically activated with rotor-stator homogenizer and to enrich it in order to improve its rheological properties.

2. Material and methods

2.1. Material

A brown sepiolite sample supplied by Akmin Madencilik operating in the Türktaciri region of Sivrihisar was used in the experiments. The sample was made ready for use in the experiments after the following steps.

- Drying for 24 hours at 70 °C in a drying oven
- Crushing the sample below 5 mm in the laboratory-type jaw crusher
- Crushing the sample below 2 mm in the laboratory-type hammer crusher
- Sample reduction and division
- Samples' packaging and coding

The sepiolite sample was characterized using particle size distribution, specific surface area, X-ray diffraction (XRD), and X-ray fluorescence (XRF) methods. Chemical and mineralogical analyzes of the samples were made in the laboratory of Eskişehir Ceramic Research Institute. The results are given in Tables 1, Table 2, and Fig. 1, respectively.

Table 20 Chemical analysis of sepiolite sample

Chemical Composition	SiO_2 %	Al_2O_3 %	Fe_2O_3 %	MgO %	CaO %	K_2O %	LOI %	Total %
Content	52.78	0.91	0.49	23.75	4.57	0.20	17.30	100

Table 2 Mineralogical analysis of sepiolite sample

Mineral Name	Formula	Content (%)
Sepiolite	$Mg_4Si_6O_{15}(OH)_2{+}6H_2O$	84.00
Dolomite	$CaMg(CO_3)_2$	13.50
Other	-	2.50

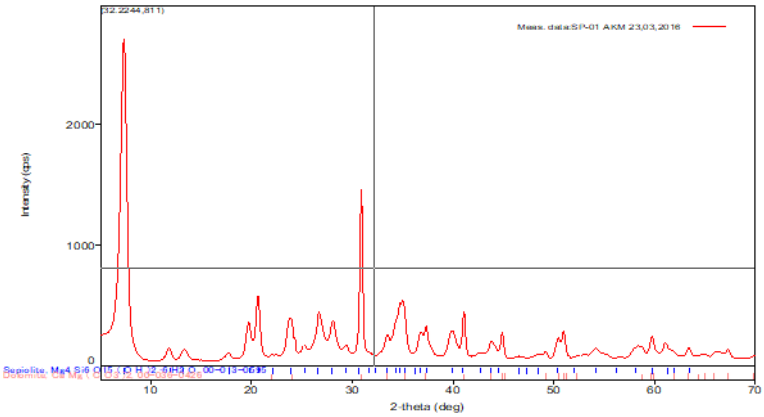


Figure 1 XRD pattern of sepiolite sample

The particle size distribution of sepiolite was obtained with a Mastersizer 2000 particle size analyzer (Malvern. UK). The particle size distribution of sepiolite is shown in Figure 2. In the measurements,

D90: 1211 µm, d50: 503 µm, d10: 19.74 µm, weighted average by volume (VWA): 556 µm, and specific surface area (SSA) was determined as 0.165 m2/g.

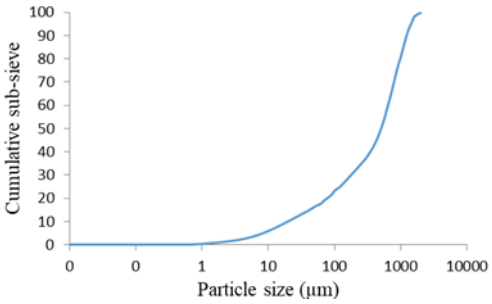


Figure 2 The particle size distribution of the sepiolite sample

2.2. Method

Sepiolite consists of bundles of fibers with impurities trapped between them. Researchers have used methods such as grinding, dispersing, and mixing to break up these bundles and release the impurities. These methods have resulted in various outcomes including increased specific surface area, decreased fiber size, thinning of the fibers due to surface erosion, and disruption of the tubular structure (Myers et al. 1999). Myers et al. (1999) recommend the use of low-energy transfer activation procedures that produce greater shear force effects instead of high-energy transfer size reduction approaches that produce impact, compression, and abrasion effects. According to Myers et al. (1999), rotor-stator homogenizers effectively disperse solid and liquid phases and produce stable emulsions with high viscosity. Sepiolite is particularly difficult to activate mechanically and efficiently due to its high viscosity at low concentrations.

Considering the difficulties and disadvantages of mechanical removal of high dolomitic impurities from the sample and the efficiency and capacity of enrichment, the acid leaching method, which is one of the chemical enrichment techniques, is a good option (Çağlar, 2019).

Sepiolite acid treatment tests were not carried out for enrichment, but mainly to examine the changes in surface area and adsorption capacity and to improve these properties. Within the scope of this study, when the findings of previous studies (Jiménez-López et al., 1978; Campelo et al., 1987; Rodriguez et al., 1994; Myriam et al., 1998; Franco et al., 2014; Çınar et al., 2009; Dékány et al., 1999) were evaluated, nitric acid (HNO3), which was found to cause the least damage to sepiolite morphology, was selected, and the washing time was determined as one hour.

2.3. High-pressure homogenization method

Substantial dispersion energy is necessary to produce sepiolite suspensions with high rheological properties. However, the type of dispersion mechanism plays an important role here. According to a 2011 study by Xu et al., the high-pressure homogenization method opened sepiolite bundles successfully without affecting the micro-morphological properties. Within the scope of the studies, it is stated that instead of high-energy size reduction techniques, the use of the low-energy activation method, which creates a greater shear force effect, will yield more effective results. Based on these results, it was thought that rotor-stator homogenizers, which have a high shear force and low energy transfer, would work well for the tests, and studies were continued. Rotor-stator homogenizers mix solid and liquid phases to produce stable emulsions and dispersions with high viscosity.

The operating principle of these machines is based on the compression of a solid-liquid mixture under high shear forces through a narrow gap of approximately 100–3000 µm between the moving rotor and the stationary stator. The peripheral speed of the rotor varies between 10 and 50 m/s, and the material is subjected to shear forces of up to 100,000 s-1 as it passes through the gap between the rotor and the stator (Atiemo-Obeng and Calabrese, 2004).

2.4. Rheological character and gelation properties of sepiolite

Sepiolite's surface characteristics, free cation content, and fibrous and needle-like mineral structure all have a significant impact on its rheological behavior. Sepiolite minerals, which consist of needle-shaped bundles of different lengths and thicknesses, do not swell when exposed to water due to their low cation exchange capacity and chain-like structure.

When fiber bundles are mechanically activated and dispersed in a polar solvent, a large number of particles are released from these bundles. These free particles, together with other free particles, form a three-dimensional network structure, trapping water in the medium. As a result, the dispersion acquires a viscous structure that is resistant to flow. Continuous and more intensive mechanical mixing (high energy transfer) reduces the size and number of these bundles, causing the number of free particles to increase further and a more complex multiple network to form. This increases the resistance to flow, i.e., viscosity, and increases the water retention capacity (Alvarez, 1984; Çınar, 2005).

The schematic representation of the mechanism is given in Figure 3.

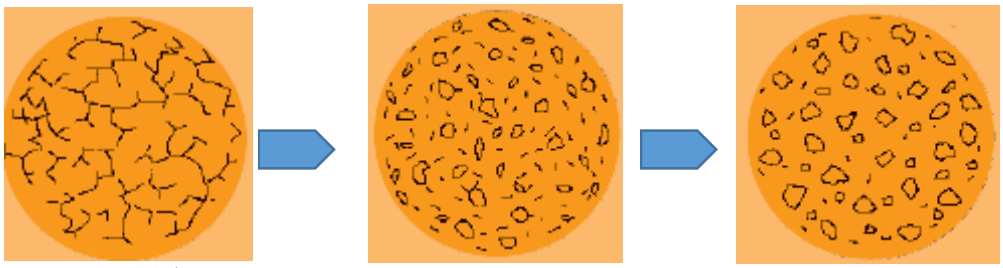


Figure 3. Schematic representation of mechanical activation and gelation behavior of sepiolite

Sepiolite bundles that are mechanically activated and released in water prevent collapse by supporting each other (Santaren, 1993; Simonton et al., 1988). Van der Waals forces and hydrogen bonds between the silanol groups, each with a different strength, hold the resulting network structure together. Sepiolite is used as a suspension material due to this feature. If there are other particles in the suspension besides sepiolite, these additional particles become trapped in the network where the sepiolite fibers form. Large grains other than sepiolite in the suspension remain suspended due to the strong forces between the particles that maintain the sepiolite network structure.

Sepiolite suspensions produce high viscosity (pseudo plastic) at low shear rates and low viscosity (thixotropic) at high shear rates. The gelation mechanism of sepiolite is quite different from the gelation mechanism of layered silicates due to the differences in physicochemical properties. Layered silicates have negatively charged surfaces due to the cationic content in their crystal structures. Clays containing Na^+ as a cation between the layers separate into layers due to the osmotic swelling effect that occurs in the solution when placed in solutions with low electrolyte concentration. Normally, the hydration energy of the cations is large enough to overcome the electrostatic attraction of the clay layers. When the clay layers are separated from each other by osmotic swelling, gelation occurs even at low clay concentrations due to the asymmetry of their particles. The negatively charged surfaces of the clay layers in the planar structure attract the positively charged edges and form a structure, and gelation occurs (Santaren, 1993).

Sepiolites do not exhibit osmotic swelling behavior because they are not layered. The particles forming the fibrous bundles are held together very strongly by Van der Waals forces and hydrogen bonds. The release and separation of the fiber bundles from each other is possible only by mechanical methods, as it does not occur as a result of hydration of the displaced interlayer cations as in layered clays. Therefore, the bundles must be activated in polar solvents with special methods to disperse them into free fibers without damaging the fibers. These properties of sepiolite provide great advantages over other clays (Santaren, 1993; Simonton et al., 1988).

The interaction between particles and the gelation mechanism of sepiolite-type fibrous clays have not yet been fully explained. It is thought that silanol groups play an important role in holding the fibers together and that this affects the rheological properties of sepiolite suspensions. It has been determined

that fiber lengths and thicknesses affect the rheological properties of sepiolite suspensions, and suspensions prepared with sepiolites with long fiber lengths have higher viscosity values and a stable gel structure (Simonton et al. 1988).

2.5. Mechanical Activation Studies

Before the nitric acid leaching process, the correct mechanical activation time and criteria must be determined. At the point where sufficient mechanical activation and kinetic energy transfer are provided, the fibers and impurities will be liberated, and an environment will be created that will increase the efficiency of the next step, the enrichment process.

Although the degree of liberation of sepiolite and the fiber size increase the gel stability and viscosity of sepiolite suspensions, it is also possible that the fiber structure and stability will deteriorate as a result of high energy-transferred mechanical activation forces.

At this point, it was determined that the determination and selection of a system with high shear force and low energy transfer would yield more accurate results, and as a result of the research conducted, it was determined that rotor-stator homogenizers could be suitable for this process, and the studies were continued within this scope.

In the study, two different designs of rotor and stator heads were used for dispersion evaluation with an optical microscope, gel stability with thermal aging, apparent viscosity with a viscometer, and grain size change with the laser diffraction method.

3. Results and Discussion

3.1. Acid Leaching Experiments

Sepiolite suspensions were prepared in accordance with the operating and mechanical activation parameters according to previous studies. The determined nitric acid concentrations were obtained by mixing the mechanically activated sepiolite suspension with a magnetic stirrer at a stirring speed of 300 rpm, continuously controlling the pH, and gradually adding nitric acid.

As a result of preliminary studies, the mixing time was determined as 1 hour and was applied in the experiments. After 1 hour of mixing, the reaction product was washed with distilled water, dried after neutralizing the pH, and ground with a ceramic mortar to perform XRF chemical analysis and XRD mineralogical analysis. The enrichment efficiency was calculated according to the obtained XRF chemical analysis and XRD mineralogical analysis results.

The enriched solid product obtained after the experiments was named as “SP01AKM-X%” in the experiments. The “X” in the name represents 4 times the molar ratio of HNO3 that would be needed to dissolve 1 mole of dolomite. This “4” factor was obtained from the chemical reaction equation below.

$$CaMg(CO_3)_2 + 4HNO_3 \longrightarrow Ca(NO_3)_2 + Mg(NO_3)_2 + 2CO_2 + 2H_2O$$

For example, the expression “SP0AKM-%100” indicates that the amount of HNO3 required to dissolve all dolomite in sepiolite was used in the experiment, while the expression “SP01AKM-%40” indicates that the amount of HNO3 required to dissolve 40% of dolomite in sepiolite was used in the experiment.

The amount of nitric acid required to remove dolomite, the main impurity of sepiolite, was calculated based on the XRF chemical analysis data in Table 2 and the above calculation model. The results of the experimental study are shown in Tables 3, 4, 5, and 6.

Table 3. Nitric Acid Leaching pH values and Solid Recovery Rates

SP01AKM-X% (X%=)	0%	40%	60%	80%	100%	140%
pH	7.72	7.22	6.91	6.44	5.51	2.45
Solid Recovery Amount (% by weight)	100.00	88.30	84.66	75.75	67.50	33.20

As seen in Table 3, the pH decreases with the increase in acid concentration. Depending on the increasing amount of acid, solid recovery decreases. Given that the dolomite content in SP-01 AKM is

13.5%, it is evident that when mass losses exceed this threshold, sepiolite, which is undesirable for dissolution in the system, also sustains damage. It is observed that mass losses increase very rapidly when the pH value drops below 6. This is by the sepiolite dissolution diagrams reported in the literature (Tomura et al., 1995; Özdemir and Kıpçak, 2004; Çınar, 2005).

The purpose of the leaching process in this study is to reach the minimum impurity value at the maximum solid concentration. The chemical analysis results of the recovered solid and the solution liquid obtained after washing are given in Tables 4 and 5.

Table 4. XRF analysis results of the recovered concentrated solid

SP01AKM-X% (X%=)	0%	40%	60%	80%	100%	140%
Chemical Content			%			
SiO_2	52.80	55.68	58.10	60.30	62.29	71.40
Al_2O_3	0.91	0.88	0.89	0.90	0.89	0.80
Fe_2O_3	0.49	0.50	0.50	0.51	0.50	0.41
MgO	23.75	23.68	23.61	23.43	22.54	17.32
CaO	4.57	2.91	1.53	0.39	0.11	0.03
K_2O	0.18	0.19	0.19	0.19	0.19	0.11
LOI	17.30	16.17	15.18	14.28	13.49	9.93

The XRF analysis of the concentrated solid that was recovered shows that as the acid concentration rises, the silicon dioxide ratio goes up while the calcium oxide and magnesium oxide components go down. On the contrary, there is a rapid increase in magnesium and calcium elements in the waste solution (Table 4).

Table 5. AAS Chemical Analysis Results of Waste Solution

SP01AKM-X% (X%=)	0%	40%	60%	80%	100%	140%
Chemical Content			ppm			
Al_2O_3	0,15	1,34	1,85	2,44	1,97	92,60
Fe_2O_3	0,59	0,59	0,60	0,61	0,69	91,59
MgO	1,79	779,72	1275,70	1826,39	2608,56	12597,36
CaO	2,14	2745,22	4386,48	5088,32	5155,31	5170,98

Table 5 shows that the acid concentration was higher than the molar ratio needed to dissolve all the dolomite in the mineral. In addition, the results of the SP01AKM-140% coded experiment clearly show that the silicon oxide ratio went up quickly and the magnesium oxide ratio went down quickly.

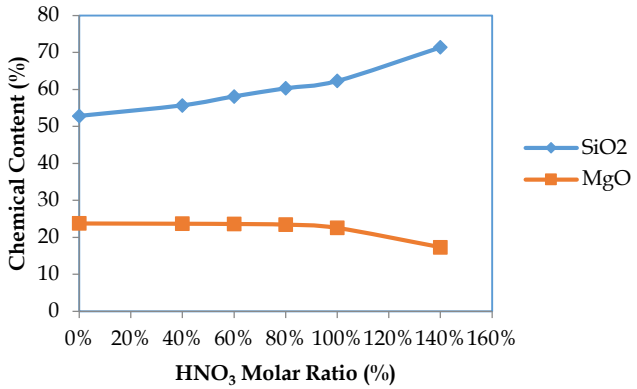


Figure 4 HNO3 Molar Ratio, Magnesium Oxide and Silicon Oxide Content Change in Enriched Concentrated Solid

As seen in Figure 4, as the acid concentration increases, there is a decrease in magnesium oxide compounds and an increase in silicon dioxide. On the contrary, there is a rapid increase in magnesium elements in the waste solution. The SP01AKM-140% coded experiment data shows that the acid

concentration was higher than the molar ratio needed to dissolve all the dolomite in the mineral. This caused magnesium oxide and silicon oxide to drop quickly.

This sudden change is similar to the solid recovery rate and is interpreted as the dolomite content in the mineral having decreased to a minimum level and the acid molecules having started to damage the sepiolite structure.

It is not possible to comment on the enrichment performance with only solid recovery rates and chemical analysis data. For this reason, quantitative XRD analysis was performed on enriched samples (Table 6).

Table 6. XRD Mineralogical Analysis Results of Enrichment Samples

SP01AKM-X% (X%=)	0%	40%	60%	80%	100%	140%
Mineralogical Content			%			
Dolomite	9.5	5.9	3.0	1.0	0.0	0.0
Sepiolite	84.4	87.7	90.3	91.9	88.3	65.6
Other (Free Silica etc.)	6.1	6.4	6.7	7.5	11.6	34.4
Total	100.0	100.0	100.0	100.0	100.0	100.0

It was found that nitric acid could raise the molar ratio needed to dissolve 80% of the dolomite in sepiolite from 84.4% to 91.9% when the chemical and mineral analysis data were evaluated together. When this molar ratio was exceeded, the sepiolite content dropped quickly, reaching 65.6% in the SP01AKM-140% sample.

As the nitric acid concentration increased from 60% to 80% molar ratio, the dolomite content decreased in parallel, and the free silica content increased along with the sepiolite content (Table 6). When this result was interpreted together with the chemical analysis results, it was determined that from a 60% molar ratio, nitric acid molecules began to damage the structure of sepiolite, and the free silica mineral phase began to increase in the environment.

Table 7 Acid leaching efficiency after enrichment

Sample Name	Concentrate Solid Amount (%)	Sepiolite Grade (%)	Enrichment Yield (%)
Raw Material	100	84	0
SP-01 AKM-40	88	88	92
SP-01 AKM-60	85	90	91
SP-01 AKM-80	76	92	82
SP-01 AKM-100	68	88	71
SP-01 AKM-140	33	66	26

As can be seen in Table 7, when the molar ratio is at 40%, the sepiolite grade increases to 88% and the enrichment efficiency reaches 92%. When the molar ratio is at 80%, the sepiolite grade increases to 92% and the enrichment efficiency decreases to 82%. When the molar ratio exceeds 80%, both the enrichment efficiency and the sepiolite grade decrease.

4. Conclusions

This study has demonstrated the effectiveness of combining mechanical activation via rotor-stator homogenizers with nitric acid leaching to enhance the rheological properties of sepiolite. The key findings are:

1. Rotor-stator homogenizers proved to be an effective method for mechanically activating sepiolite suspensions, providing the necessary shear force while minimizing damage to the sepiolite structure.
2. Nitric acid leaching successfully increased the sepiolite content from 84.4% to a maximum of 91.9% when using a molar ratio sufficient to dissolve 80% of the dolomite impurities.
3. The optimal range for acid concentration was identified: at 40% molar ratio, sepiolite grade increased to 88% with 92% enrichment efficiency, while at 80% molar ratio, sepiolite grade reached 92% with 82% enrichment efficiency.
4. Exceeding the 80% molar ratio led to a rapid decrease in both sepiolite content and enrichment efficiency, likely due to acid-induced damage to the sepiolite structure.
5. The process of dolomite removal and sepiolite enrichment was accompanied by an increase in free silica content, particularly noticeable above 60% molar ratio of nitric acid.

These results provide valuable insights for optimizing the acid-leaching process in sepiolite enrichment. The findings can be applied to improve the quality and rheological properties of sepiolite for various industrial applications. Future research could focus on further refining the mechanical activation process and investigating the effects of different acids or combinations of acids on sepiolite enrichment.

References

Alvarez, A., 1984, *Sepiolite: Properties and uses, Developments in sedimentology*, A. Singer ve E. Galan, Elsevier, 37, 253-287.

Atiemo-Obeng, A, V., Calabrese, R. V., 2004, *Rotor-stator mixing devices*, E. L. Paul, V. A. Atiemo-Obeng ve S. M. Kresta, John Wiley & Sons, Inc.: Hoboken, NJ, 479-505.

Campelo, J. M., Garcia, A., Luna, S., Marinas, J. M., 1987, *Catalytic activity of natural sepiolites in cyclohexene skeletal isomerization*, Clay Minerals 22(2), 233-236.

Çağlar, U., 2019. *Enrichment of sepiolite by wet grinding and acid leaching methods and modelling of its rheological behavior*. Fen Bilimleri Enstitüsü, ESOGÜ, Doktora Tezi.

Çınar, M. (2005). *Sepiyolitin reolijik özelliklerinin belirlenmesi ve su bazlı sepiyolit üretimi*. Fen Bilimleri Enstitüsü, İTÜ, Doktora Tezi.

Çınar, M., Can, M. F., Sabah, E., Karagüzel, C., Çelik, M. S., 2009, *Rheological properties of sepiolite ground in acid and alkaline media*, Applied Clay Science 42(3), 422-426.

Dékány, I., Turi, L., Fonseca, A., Nagy, J. B., 1999, *The structure of acid treated sepiolites: Small-angle x-ray scattering and multi mas-nmr investigations*, Applied Clay Science 14(1), 141-160.

Franco, F., Pozo, M., Cecilia, J. A., Benítez-Guerrero, M., Pozo, M., vd.,, 2014, *Microwave assisted acid treatment of sepiolite: The role of composition and "crystallinity"*, Applied Clay Science 102, 15 – 27.

Galan, E. (1996). *Properties and applications of palygorskite-sepiolite clays*. Clay Minerals, 31(4), 443-453.

Jiménez-López, A., López-González, J. d. D., Ramīrez-Sāenz, A., Rodrīguez-Reinoso, F., Valenzuela-Calahorro, C., vd.,, 1978, *Evolution of surface area in a sepiolite as a function of acid and heat treatments*, Clay Minerals 13(4), 375-385.

Myers, K. J., Reeder, M. F., Ryan, D., Daly, G., 1999, *Get a fix on high-shear mixing*, Chemical engineering progress 95(11), 33-42.

Myriam, M., Su, M., M. Mart, J., 1998, *Structural and textural modifications of palygorskite and sepiolite under acid treatment*.

Özdemir, M., & Kıpçak, İ. (2004). *Dissolution kinetics of sepiolite in hydrochloric acid and nitric acid*. International Journal of Mineral Processing, 75(1-2), 91-99.

Rodriguez, M. V., Gonzalez, J. d. D. L., Munoz, M. B., 1994, *Acid activation of a spanish sepiolite: Physico-chemical characterization, free silica content and surface area of products obtained*, Clay Minerals 29(3), 361-367.

Sabah, E., & Çelik, M. S. (1998). *Sepiyolit: Özellikleri ve Kullanım Alanları*. 3. Endüstriyel Hammaddeler Sempozyumu, İzmir, Turkey.

Santaren, J., 1993, *Sepiolite: A mineral thickener and rheology additive*, Modern Paint and Coatings 98, 72.

Simonton, T. C., Komarneni, S., Roy, R., 1988, *Gelling properties of sepiolite versus montmorillonite*, Applied Clay Science 3(2), 165-176.

Tomura, S., Inukai, K., Miyawaki, R., 1995, *Purification of sepiolite and palygorskite*, Journal of the Society of Materials Engineering for Resources of Japan 8(1), 90-98.

Vučelić, D., Simić, D. S., Kovačević, O., Dojčinović, M. M., Mitrović, M., 2002, *The effects of grinding on the physicochemical characteristics of white sepiolite from golesh*, Journal of the Serbian Chemical Society 67(3), 197-211.

Xu, J., Zhang, J., Wang, Q., Wang, A., 2011, *Disaggregation of palygorskite crystal bundles via high-pressure homogenization*.

Enhanced Hydrophobic Sensing Using Hydrophobized Halloysite Biocomposite Fillers: Ball Milling vs. Surfactant

Mervenur Kirazoğlu [1], Birgül Benli [2*]

[1]Istanbul Technical University, Graduation School, Nanoscience and Nanoengineering Program, 34469 Maslak, Türkiye

[2]Istanbul Technical University, Mining Faculty, Department of Mineral Processing Engineering, 34469 Maslak, Türkiye

*Corresponding author: benli@itu.edu.tr

Abstract:

Biosensors and biomedical applications transform patient care, treatment, and diagnosis in modern healthcare. There is a growing demand for nanofillers that enhance bio-nanocomposites' properties, including biocompatibility, biodegradability, non-toxicity, and low immunogenicity. Fat-based components like Vitamin D are common in biomedical applications, particularly in dietary supplements and drug formulations. Due to the low stability and wide dispersibility of lipophilic Vitamin D, there is a need for nanofillers and nanocarrier systems. Biopolymers' performance can be further improved with suitable nanofillers. Halloysite nanotubes (HNTs), derived from natural clays, present opportunities due to their tubular morphology and active sites.

This study examines hydrophobized halloysite for sensing Vitamin D by comparing two modification methods: Ball milling and amine-type surfactant Hexadecyltrimethylammonium bromide (HTAB) modification. During the 3-hour milling process, the potential of HNTs changed from -19.33 ± 1.25 to 0.095 ± 0.12 mV. However, after HTAB modification, the zeta potential showed a higher positive value of about 29.44 ± 0.50 mV.

In studies with alginate biocomposites, the Langmuir model was most suitable for describing Vitamin D_3 adsorption. The Langmuir constants were close; for instance, the q_{max} values for Ball milling and HTAB modification are 5318.108 and 5935.263, respectively, indicating higher adsorption capacity with HTAB. Conversely, the K_L values for Ball milling and HTAB modification are 0.48 and 0.23, respectively, indicating higher binding affinity with Ball milling. These findings suggest that HTAB modification enables higher loading capacity, while Ball milling ensures more stable binding, impacting Vitamin D delivery efficiency and stability. This is supported by desorption studies.

Keywords: *Biosensors, Hydrophobized Alginate, Vitamin D Adsorption, Nanofillers, Ball Milling and Surfactant Modification*

1. Introduction

Patient care, therapy, and diagnosis in the contemporary healthcare industry are being revolutionized by biomedical applications, highlighting the necessity of utilizing biocomposites to enhance the biocompatibility, biodegradability, non-toxicity, and low immunogenicity of bio-nanomaterials [Arif et al., 2023]. A notable challenge in this context is the incorporation of lipophilic components, such as vitamin D, which are widely used in dietary supplements and medication formulations. Despite its recognized health benefits, vitamin D suffers from poor stability and dispersibility, particularly in formulations where maintaining potency and bioavailability is crucial [Khadilkar et al., 2012]. The global market for vitamin D supplements reflects substantial consumption and a critical need for innovative delivery systems to address these formulation hurdles [Chugh et al., 2012]. This market is experiencing robust growth, with its value projected to rise from approximately $1.1 billion in 2020 to an estimated $1.9 billion by 2027, indicating a compound annual growth rate (CAGR) of about 7.1%. This expansion is driven by increasing consumer awareness of vitamin D's vital role in bone health, immunity, as evidenced by global consumption exceeding 100,000 metric tons annually, including

various forms integrated into fortified foods and dietary supplements. These trends underscore a growing preference among consumers for products that enhance nutritional intake, amplifying the demand for effective delivery methods that ensure optimal absorption [Jakobsen et al., 2024].

The development of biocomposites is a promising advancement in biomedical research, particularly for encapsulating lipophilic compounds like vitamin D to enhance stability and bioavailability. Halloysite nanotubes (HNTs) have emerged as a leading candidate due to their unique tubular structure, which allows efficient encapsulation and controlled release of bioactive molecules, thereby improving therapeutic efficacy. These natural clay nanotubes are biocompatible and biodegradable, reducing toxicity concerns and offering a safe delivery platform [Boraei et al., 2024]. Their surface chemistry can be modified for targeted delivery, making them ideal for enhancing vitamin D's effectiveness in healthcare applications. There are also different types of Vitamin D. In our study, we chose vitamin D_3 (cholecalciferol) because of its superior bioavailability and well-documented metabolic effects compared to D_2, aiming for more reliable and consistent outcomes [Zhou et al., 2024].

Halloysite, a natural mineral clay, is recognized for its unique physicochemical properties and wide range of applications. Its hollow, stacked alumina-silica layers form nanotubes that range from a few micrometers to several hundred micrometers in length, with inner diameters typically between 10-30 nanometers (Fig. 1). This high aspect ratio allows HNTs to enhance stability and bioavailability in various applications, including drug delivery [Joussein et al., 2005]. HNTs are also used in cosmetics and pharmaceuticals for their ability to encapsulate and release active ingredients in a controlled manner. Hydrophobic modification further improves their performance and release control, enhancing functionality across applications [Saif et al., 2018].

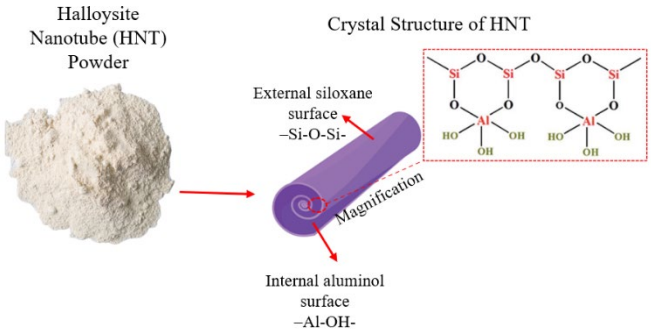


Fig. 1. Crystal structure of Halloysite nanotube.

Halloysite nanotube organomodification involves chemically altering their surface with organic compounds to improve compatibility with polymers and enhance mechanical, thermal, and barrier properties [Kausar et al.,2017]. A common method is coating with organic surfactants that have both hydrophilic and hydrophobic parts, which stabilize the nanotubes and reduce aggregation in polar solvents. Cationic surfactants bind to the negatively charged surfaces of halloysite, improving dispersion and suspension stability. HTAB is particularly noted for enhancing the dispersibility and mechanical properties of polymer composites. Additionally, ball milling can modify the structure and properties of halloysite nanotubes by breaking them into smaller segments, increasing their surface area and reactivity. This process can introduce defects or functional groups, creating active sites for chemical reactions or anchoring points for functional molecules [Cavallaro et al., 2015]. By adjusting milling conditions, such as time and speed, the modifications can be tailored for specific applications, resulting in enhanced properties like improved dispersibility, increased adsorption capacity, and better drug delivery characteristics [Massaro et al., 2018]. The choice between organomodification and ball milling for halloysite nanotubes depends on specific application goals. Organomodification enhances compatibility and dispersibility by attaching organic functional groups, while ball milling uses mechanical grinding to alter its structure [Lun et al., 2014]. In this study, both methods were employed to modify halloysite nanotubes, with subsequent comparisons of their characterizations.

This study modified halloysite nanotubes through surfactant treatment and ball milling to enhance compatibility in biocomposite, aiming to improve Vitamin D_3's bioavailability through better adsorption, stability, and release mechanisms for use in food and pharmaceutical applications.

2. Material and methods

2.1. Material

The halloysite clay nanotubes were supplied by ESAN, Eczacıbaşı (Türkiye). HTAB was obtained from Merck. Methanol 99,99% and Ethanol 95% were obtained from EMSURE. Poly (diallyldimethylammonium chloride) solution (PDDA) and silane were obtained from Sigma Aldrich. Deionized water was used throughout the experiments.

2.2. Methods

2.2.1. Preparation of hydrophobic alginates

Hydrophobic Alginates were prepared by reacting sodium alginate with HTAB through esterification in the presence of formic acid derived from a previous study [Nomura et al., 1982]. To perform the formylation process, 1 g of alginate was mixed with 10 mL of formic acid and stirred for 10 minutes at 25°C. 8 mL of HTAB solution was then added dropwise. The reaction mixture was then heated to 50°C for 20 min. The reaction was stopped at the end by adding 100 mL of 95% v/v ethanol, and the mixture was then filtered to extract the solid phase. After repeatedly washing the solid phase with 95% v/v ethanol, it was vacuum-dried at room temperature [Neumeister et al., 1990].

2.2.2. Surfactant treatments of halloysite nanotubes

HNTs were dried at 110 °C for 3 h [Yue et al., 2019]. Aqueous surfactant solution was prepared by dissolving 4 g of HTAB in 500 cm^3 of water-ethanol mixture (1:1 v/v). Then, 8 g of HNTs was added, and the obtained dispersion was stirred for 48 h. The functionalized material was recovered by centrifugation at 700 rpm for 40 min. Excess surfactant was removed by washing with water. The obtained powder was dried at 80 °C for 7 days [Cavallaro et al., 2018].

2.2.3. Modified halloysite nanotubes via ball milling

HNTs were dried for one hour at 67 °C. They were altered by grinding them for 0.5, 1, 2, 3, and 4 hours at room temperature using a planetary ball miller (OPT-SFM3, OPTOSENSE LLC) at 300 rpm (Fig. 2). A 10 mL ball mill jar (OPTOSENSE LLC) filled with zirconia beads received 1g of HNTs. The jar walls were activated by the heat and shear force produced during the milling operation [Tan et al., 2022].



Fig. 2. High-speed vibrating ball mill.

2.2.4. Preparation of biocomposites

Vitamin D_3 contained in an oral solution (1 mL) was extracted with 1 mL methanol. In the label declaration, the concentration of vitamin D_3 in the Oral Solution is given as 300.000 IU (7.5 mg/mL) in 1 mL. The amount of vitamin D_3 in the drug, which is 7.5 mg/mL, is 1.95 x 10^{-2} M when calculated in terms of molarity (Vitamin D_3 MA: 384.65 g/mol). Vitamin D_3 was extracted from the oral solution using the basic liquid-liquid extraction method with methanol. To prepare nanocarriers, a certain amount of hydrophobic-modified halloysite nanotubes were mixed with vitamin D_3 solutions. They continuously stirred until all contents were homogeneously dispersed. To reduce vitamin D_3 breakdown during preparation, all these studies were carried out in complete darkness [Kaygusuz et al., 2015]. All biocomposites were prepared in this method.

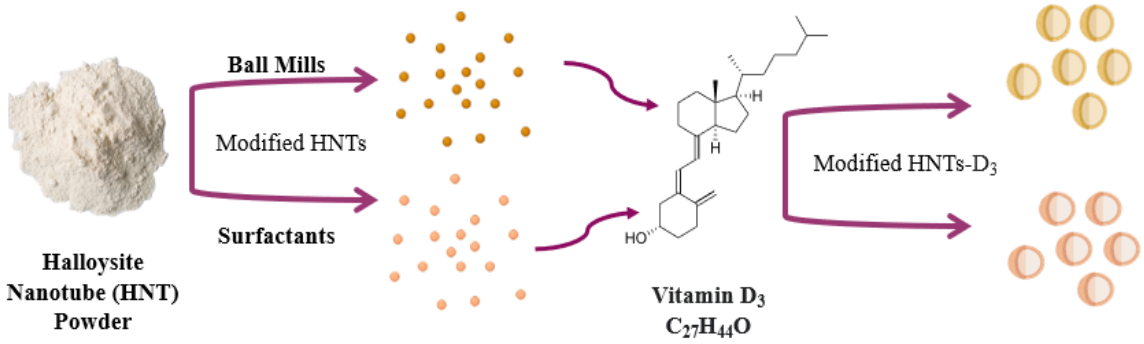


Fig. 3. Schema of Modified HNTs with two approaches

Adsorption experiments of vitamin D_3 solutions on biocomposites.

Adsorption experiments were performed to determine the material that retained the most vitamin D_3. For testing the loading capacity of the mixed hydrophobic halloysite-alginate biocomposites towards sorbing Vitamin D_3 and understanding the interaction mechanism, equilibrium batch adsorption experiments were conducted.

Experimentally, batch experiments were performed inside a series of 20 mL glass vials, and the same amount of adsorbent (0.1 g) was added to each vial. Then, each vial was loaded with 6 ml of the different concentrations (53.576 ng/mL, 42.456 ng/mL, 37.503 ng/mL, 18.751 ng/mL, 9.876 ng/mL) of Vitamin D_3. The vials were tightly sealed and shaken at 200 rpm for 1 hour to allow adsorption to take place. Subsequently, the samples were centrifuged at 3000 rpm for 5 minutes, and the resulting solution was passed through a 45-micron PTFE filter. At predetermined contact times, solid/ solution phases were separated, and residual supernatant concentrations inside each vial were determined by using UV-Vis spectrophotometry at 265 nm. Then, the adsorbed amounts of Vitamin D_3 (q_e) in mg/g can be calculated by applying the mass balance equation as follows:

$$q_e = \frac{V}{m}(C_o - C_e) \quad (1)$$

where V is the volume of the solution (mL), m is the mass of hydrophobic halloysite-alginate biocomposite as an adsorbent (g), Ce is the concentration at equilibrium (mg/mL), and Co is the initial concentration of the Vitamin D_3, which was used at the beginning of the experiment. According to the adsorption mechanism of Vitamin D_3 on the surface of the hydrophobic halloysite-alginate biocomposite, generally used adsorption isotherms such as Langmuir, Freundlich [Burmeister et al., 2013].

Langmuir Isotherm

It assumes that the adsorbent forms a monolayer homogeneous layer on the adsorbent surface. In this model, it is assumed that all areas are equal, and the adsorption of each molecule has equal activation energy and equal affinity. Once an adsorbent molecule occupies a location, no further adsorption processes can occur in that location. The adsorbent has a limited capacity for the adsorbed substance [Kuziora et al., 2014]. Langmuir equation is included in Equation 2:

$$q_e = \frac{q_{ml} K_L C_e}{1 + K_L C_e} \quad (2)$$

q_{ml} refers to the maximum adsorption capacity (mg/g) and KL refers to the Langmuir constant (L/mg).

Freundlich Isotherm

The Freundlich isotherm is one of the oldest known relations described for reversible and non-ideal adsorption that is not limited to monolayer formation. According to Freundlich, the adsorption areas on the surface of an adsorbent are heterogeneous, that is, they are composed of different types of adsorption areas. This experimental relationship can be used for multilayer adsorption, where the adsorption heat and interest are not distributed evenly on the heterogeneous surface [Suryanarayana, 2001]. The Freundlich equation is included in Equation 3:

$$q_e = K_f * Ce^{1/nf} \quad (3)$$

Kf is the Freundlich constant (L/g) and nf^{-1} is the adsorption density. This isotherm shows the relative energy distribution and surface heterogeneity of the adsorbent sites. Adsorption is considered suitable if nf^{-1} is between zero and 1 ($0 < nf^{-1} < 1$). When nf^{-1} is greater than 1, the adsorption process is negative and when $nf^{-1} = 1$, it is irreversible.

2.2.5. Desorption experiments of vitamin D_3 solutions on modified HNTs and biocomposites.

PBS solution was used at pH 7.4 to simulate intestinal fluid for the desorption experiment. Modified HNTs and 0.1 g Biocomposites were prepared with vitamin D_3 solutions (42 ng/mL). Samples were mixed until homogeneous. About 150 µL of the solution was placed on a glass plate (area about 4 cm^2) and spun at 2000 rpm for 10 min by using a spin coater. Repeated 10 times for each sample. These films were then dried in a heater at 50 °C temperature. The films were then placed in 20 mL PBS in pH 7.4 solutions. Releases were observed depending on time at an absorbance value of 265 nm wavelength.

3. Result and Discussions

3.1. Characteristics of untreated and modified HNTs and biocomposites

Zeta potential analysis was used to examine changes in the surface charge of HNTs to verify surfactant alteration. The electronegative surfaces of the pure HNTs are largely composed of siloxane groups on their outer surface. It is clear from Table 1 that surfactant modification modifies the negative zeta potential of pure HNTs (-19.33 ± 1.25) [Dong et al., 2018]. The HNTs with HTAB alteration showed a positive zeta potential of about 29.44 ± 0,50 mV [Abhinayaa et al., 2019]. The change in the potential of sodium alginate during modification increased the potential of negatively charged alginate from -31.67 ± 0.75 [Loosli et al., 2015] to -6.68 ± 2.14 mV. (Table 1) This result suggests a reduction in the inter-particle electrostatic repulsion.

Table 1. HNTs, modified HNTs, alginate, modified alginate, and biocomposites at pH 7: Zeta Potential

Samples	Zeta Potential (mV)
HNTs	-19.33 ± 1.25
HNTs-60 min Ball milling	-18.03 ± 0.17
HNTs-120 min Ball milling	-5.49 ± 0.28
HNTs-180 min Ball milling	0.095 ± 0.12
HNTs-200 min Ball milling	0.0029 ± 0.287
HNTs-240 min Ball milling	-15.76 ± 0.205
HNTs-HTAB	29.44 ± 0.50
Alginate	-31.67 ± 0.75
Modified Alginate	-6.68 ± 2.14
MBHA (Ball mill halloysite + modified Alg)	-10.83 ± 0.17
MHHA (HTAB-halloysite + modified Alg)	0.041 ± 0.52

A groundbreaking two-step approach for attaching long alkyl chains to sodium-alginate via ester functionality is reported, which does not need the use of organic solvents for alginate dissolution before

modification [98]. The first step in the method includes dissolving sodium-alginate in formic acid. In this stage, formate esters are synthesized in situ. The formate esters are critical in lowering hydrogen bonding between alginate chains, allowing more hydroxyl groups to be accessible. Then, HTAB, a highly reactive reagent, is introduced to create hexadecyl alginate esters with high degrees of substitution by reacting with the accessible hydroxyl groups. Since formate esters are inherently unstable, they hydrolyze at the end of the reaction, leaving pure HTAB esters of alginate.

The formation of an ester linkage between sodium alginate and hexadecyl was confirmed by FT-IR. The FT-IR spectra of pure alginate and hexadecyl alginate ester (HAE), which are shown in Figure 2, suggest the presence of an ester bond and hexadecyl group. The reduced peaks at 1593.02 cm^{-1} represented asymmetric stretching of carboxyl groups and the increased peaks at 1722.69 cm^{-1} represented C=O stretching vibration showing the presence of the C=O component of an ester bond [Vu et al., 2019]. The increased peaks at 1223.26 cm^{-1} and 1402.81 cm^{-1} exhibited the presence of hexadecyl group. The peak at 1223.26 cm^{-1} was identified as the stretching vibration of C-C [Thanos et al., 2006], and the peak at 1402.81 cm^{-1} was identified as a deformation vibration of CH_2 [Li et al., 2007].

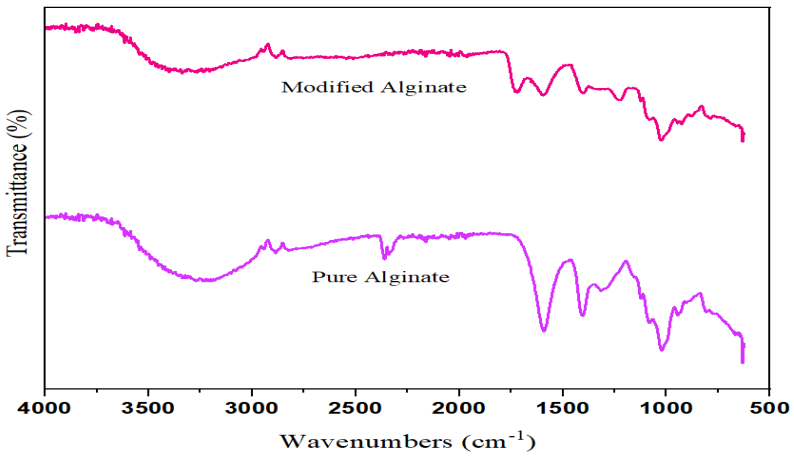


Fig. 4. The pure alginate and modified alginate FT-IR spectra.

3.2. Adsorption Isotherms Experiments of Vitamin D_3 Solutions on Biocomposites

Equilibrium relationships between adsorbent and adsorbate are described by adsorption isotherms which are usually the ratio between the quantity adsorbed and the remaining in solution at a fixed temperature at equilibrium. Adsorption models of vitamin D_3 exchanged biocomposites were determined through batch experiments. According to the adsorption mechanism of Vitamin D_3 on the surface of the biocomposites, generally used adsorption isotherms such as Langmuir, and Freundlich. Linear plots were analyzed for the regression coefficients of the Langmuir, and Freundlich models (Fig. 6 and Table 2), and Langmuir models were determined as the best fitting models for vitamin D_3.

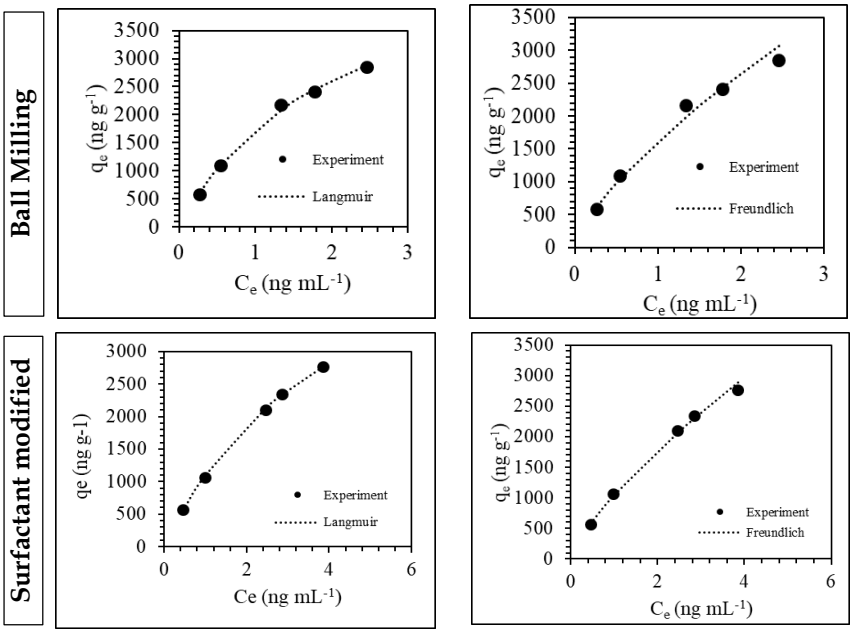


Fig. 6. Adsorption isotherm behavior of different concentrations of vitamin D_3 adsorption on Alg-Hal biocomposite.

Tablo 2. Absorption isotherm models constants of vitamin D_3 adsorption on biocomposites.

	Langmuir Model			Freundlich Model		
	q_{max}	K_L	R^2	K_F	n	R^2
MBHA	5318.108	0.48	0.9916	1611.169	1.4	0.9891
MHHA	5935.263	0.23	0.9980	1048.538	1.33	0.9975

3.3. Desorption Experiments of Vitamin D_3 Solutions on Modified HNTs and Biocomposites

The in vitro release profile of modified HNTs and biocomposites for 2 days were monitored in PBS (simulated intestinal fluid) with 7.4, respectively. 32% of the vitamin D was released in the first 3 h from halloysite nanotubes (with a ball mill) and then the release rate slowed significantly as shown in Figure 7. Vitamin D_3 was released with increasing time, and 21 % of the encapsulated vitamin D_3 was released after 48 hours of the test. 30 % of the vitamin D_3 was released in the first 3 h from the halloysite nanotubes (with HTAB), and then the release rate slowed. 20.04 % of the encapsulated vitamin D_3 was released after 48 hours of the test. This result may be attributed to the lack of specific binding affinity between the free Vitamin D_3 and the HNTs' comparatively high surface area. The prolonged discharge in the later part of the time came after the first outburst.

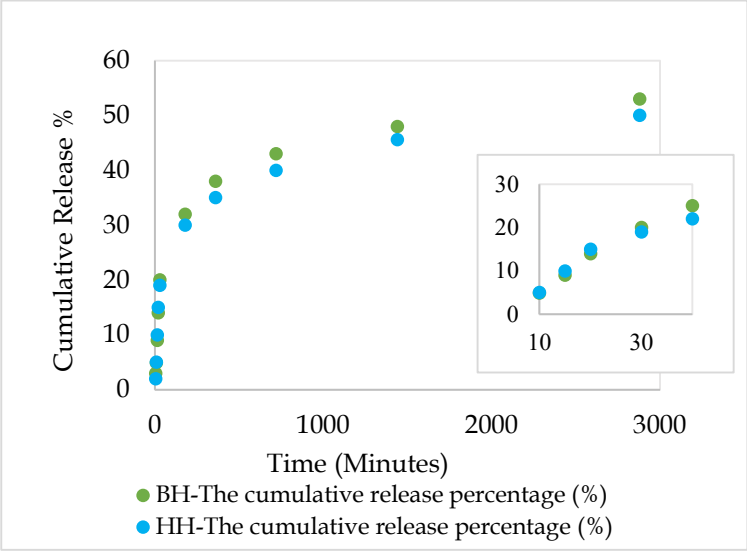


Fig. 7. Vitamin D_3 release % from modified halloysite nanotubes

On the other hand, 42% of the vitamin D_3 was released from the biocomposite MBHA in the first 30 minutes. After that, the release rate dramatically decreased. After 48 hours of the test, 48% of the encapsulated vitamin D_3 was released. Vitamin D_3 was released gradually over the course of the 48 hours. 30.79 % of the vitamin D_3 was released in the first 30 min from MHHA and then the release rate slowed. 50% of the encapsulated vitamin D_3 was released after 48 hours of the test. The outcome suggests that the biocomposites may achieve a prolonged release in the fluid of the gastrointestinal tract.

4. Conclusions

In this study, the preparation and coating properties of sodium alginate modified with hydrophobic groups and hydrophobic halloysite structured composite-based material were investigated. This biocomposite that can adsorb vitamin D_3 was examined. Sodium alginate and halloysite nanotubes were successfully modified. Two methods were tried in modifying the halloysite nanotubes. Halloysite nanotubes were hydrophobized in 200 minutes using the Ball mill method, decreasing the zeta potential from -19 mV to 0.0029 mV. Similar results were obtained by grinding methods for up to 200 minutes using a Ball mill and by adding 0.4 mM concentration of HTAB in the method mentioned. Composites were successfully prepared and monitored via FTIR through hexadecyl bonding. According to adsorption isotherms, it was determined that the binding of Vitamin D_3 was monomolecular and followed Langmuir isotherm. Release studies were monitored through desorptions, findings showed similarity with fluctuations in PBS body fluid.

References

Arif, Z. U., Khalid, M. Y., Noroozi, R., Hossain, M., Shi, H. H., Tariq, A., ... & Umer, R. (2023). Additive manufacturing of sustainable biomaterials for biomedical applications. Asian Journal of Pharmaceutical Sciences, 18(3), 100812

Khadilkar, A., Kadam, N., Chiplonkar, S., Fischer, P. R., & Khadilkar, V. (2012). School-based calcium–vitamin D with micronutrient supplementation enhances bone mass in underprivileged Indian premenarchal girls. Bone, 51(1), 1-7.

Chugh, P. K., & Lhamo, Y. (2012). An assessment of vitamin supplements in the Indian market. Indian journal of pharmaceutical sciences, 74(5), 469.

Jakobsen, J., & Jensen, M. B. (2024). Vitamin D in food—Compounds, stability, sources. In Feldman and Pike's Vitamin D (pp. 77-96). Academic Press.

Boraei, S. B. A., Eshghabadi, F., Hosseinpour, R., Zare, Y., Munir, M. T., & Rhee, K. Y. (2024). Halloysite nanotubes in biomedical applications: Recent approaches and future trends. Applied Clay Science, 253, 107346.

Zhou, F., Jamilian, A., Prabahar, K., Hernández-Wolters, B., Kord-Varkaneh, H., & Bai, D. (2024). The effect of vitamin D2 supplementation on vitamin D levels in humans: A time and dose–response meta-analysis of randomized controlled trials. Steroids, 109394.

Joussein, E., Petit, S., Churchman, J., Theng, B., Righi, D., & Delvaux, B. J. C. M. (2005). Halloysite clay minerals—a review. Clay minerals, 40(4), 383-426.

Saif, M. J., Asif, H. M., & Naveed, M. (2018). Properties and modification methods of halloysite nanotubes: a state-of-the-art review. Journal of the Chilean Chemical Society, 63(3), 4109-4125.

Kausar, A. (2018). Review on polymer/halloysite nanotube nanocomposite. Polymer-Plastics Tech and Engineering, 57(6), 548-564.

Cavallaro, G., Lazzara, G., Milioto, S., & Parisi, F. (2015). Hydrophobically modified halloysite nanotubes as reverse micelles for water-in-oil emulsion. Langmuir, 31(27), 7472-7478.

Massaro, M., Cavallaro, G., Colletti, C. G., Lazzara, G., Milioto, S., Noto, R., & Riela, S. (2018). Chemical modification of halloysite nanotubes for controlled loading and release. Journal of Materials Chemistry B, 6(21), 3415-3433.

Lun, H., Ouyang, J., & Yang, H. (2014). Natural halloysite nanotubes modified as an aspirin carrier. RSC advances, 4(83), 44197-44202.

Nomura, T., & Okuhara, M. (1982). Frequency shifts of piezoelectric quartz crystals immersed in organic liquids. Analytica Chimica Acta, 142, 281-284.

Neumeister, J., Thum, R., & Lüder, E. (1990). A SAW delay-line oscillator as a high-resolution temperature sensor. Sensors and Actuators A: Physical, 22(1-3), 670-672.

Yue, X., Yang, X., Li, H., Zhang, R., & Qin, D. (2019). Quaternary Ammonium Compounds-Modified Halloysite and Its Antifungal Performance. In Physics and Techniques of Ceramic and Polymeric Materials: Proceedings of Chinese Materials Conference 2018 19th (pp. 121-131). Springer Singapore.

Cavallaro, G., Lazzara, G., Milioto, S., Parisi, F., Evtugyn, V., Rozhina, E., & Fakhrullin, R. (2018). Nanohydrogel formation within the halloysite lumen for triggered and sustained release. ACS applied materials & interfaces, 10(9), 8265-8273.

Tan, C., Zhao, P., Zhou, Y., & Liu, M. (2022). Hydrophobic halloysite nanotubes via ball milling for stable pickering emulsions: Implications for food preservation. ACS Applied Nano Materials, 5(8), 11289-11301.

Kaygusuz, H., Uysal, M., Adımcılar, V., & Erim, F. B. (2015). Natural alginate biopolymer montmorillonite clay composites for vitamin B2 delivery. Journal of Bioactive and Compatible Polymers, 30(1), 48-56

Burmeister, C. F., & Kwade, A. (2013). Process engineering with planetary ball mills. Chemical Society Reviews, 42(18), 7660-7667.

Kuziora, P., Wyszyńska, M., Polanski, M., & Bystrzycki, J. (2014). Why the ball to powder ratio (BPR) is insufficient for describing the mechanical ball milling process. International journal of hydrogen energy, 39(18), 9883-9887.

Suryanarayana, C. (2001). Mechanical alloying and milling. Progress in materials science, 46(1-2), 1-184.

Dong, C., Zhang, M., Xiang, T., Yang, L., Chan, W., & Li, C. (2018). Novel self-healing anticorrosion coating based on L-valine and MBT-loaded halloysite nanotubes. Journal of materials science, 53, 7793-7808.

Abhinayaa, R., Jeevitha, G., Mangalaraj, D., Ponpandian, N., & Meena, P. (2019). Toxic influence of pristine and surfactant modified halloysite nanotubes on phytopathogenic bacteria. Applied Clay Science, 174, 57-68.

Loosli, F., Vitorazi, L., Berret, J. F., & Stoll, S. (2015). Towards a better understanding on agglomeration mechanisms and thermodynamic properties of TiO2 nanoparticles interacting with natural organic matter. water research, 80, 139-148.

Vu, A. A., & Bose, S. (2019). Effects of vitamin D3 release from 3D printed calcium phosphate scaffolds on osteoblast and osteoclast cell proliferation for bone tissue engineering. RSC advances, 9(60), 34847-34853.

Thanos, C. G., Bintz, B. E., Bell, W. J., Qian, H., Schneider, P. A., MacArthur, D. H., & Emerich, D. F. (2006). Intraperitoneal stability of alginate–polyornithine microcapsules in rats: an FTIR and SEM analysis. Biomaterials, 27(19), 3570-3579.

Li, Y. Y., Chen, X. G., Liu, C. S., Cha, D. S., Park, H. J., & Lee, C. M. (2007). Effect of the molecular mass and degree of substitution of oleoylchitosan on the structure, rheological properties, and formation of nanoparticles. Journal of agricultural and food chemistry, 55(12), 4842-4847.

Investigation of Aluminum Concentrate Production Potentials from Bauxite Ore with High Iron Content

Zeynep ÜÇERLER-ÇAMUR*, Tülay TÜRK, Yusuf Enes PURAL, Mahmut Emre Çoban, Murat Olgaç KANGAL

Istanbul Technical University, Faculty of Mines, Mineral Processing Engineering Department, Maslak, Istanbul, Türkiye, 34469

*Corresponding author: ucerler@itu.edu.tr (**Zeynep Üçerler-Çamur**)

Abstract:

Almost all of the aluminum metal production is provided from bauxite ores, which are classified as critical raw materials. Metal production is carried out with the Bayer process worldwide and in our country. For this, the ore must have the appropriate size and chemical content. This production meets only 10% of the country's needs. In our country, metal production is being carried out from ores containing high alumina and low silica in the Konya Seydişehir region. Apart from Seydisehir, significant bauxite reserves are located in the Southeastern Anatolia Region in Alanya, Mersin, Iskenderun, and Gaziantep regions and around the Taurus Mountain Range. However, these ores do not appear to be operable ores due to their high silica content and fine-size liberation. Within the scope of the study, studies were carried out using bauxite ore from the Iskenderun region. Experiments were carried out using magnetic separation, flotation, and roasting methods. Magnetic separation and flotation experiments were carried out at -300, -212, -106, and -75 micron sizes, while roasting experiments were carried out at -53 micron size. As a result of the experiments, it is aimed to obtain high-value-added aluminum concentrate.

Keywords: *Bauxite, Magnetic separation, Flotation, Roasting*

1. Introduction

The main reasons for the high demand for aluminum are its lighter weight than other metals, strength, high corrosion resistance, high thermal and electrical conductivity, easy shaping and applicability of heat treatments. Due to these properties, it has become a raw material in demand in many fields such as construction, automotive, packaging, defense industry, paint and transportation. Considering these properties, it has become the most widely used metal after iron and steel. If aluminum is produced from ore, the type of ore used is bauxite ores. Although there are many methods for aluminum production from bauxite ores, the most widely used method is the Bayer method presented by Carl Bayer. This process includes two stages, the first stage is the production of alumina (Al_2O_3) from the ore and the second stage is the production of aluminum metal from alumina by electrolysis. With this method, if 4 tons of bauxite is fed to the process, 2 tons of alumina is produced and 1 ton of aluminum is produced from the 2 tons of alumina produced, and aluminum metal production is approximately a quarter of the fed material (Eroğlu ve Şahiner, 2018). According to their mineralogical compounds, bauxites are divided into three types; diasporic bauxites (γ-$Al_2O_3.3H_2O$), boehmitic bauxites (γ-$Al_2O_3.H_2O$) and gibbsitic bauxites(α-Al_2O_3.H2O). In addition, another important issue in the grouping of bauxites is their silica modulus and iron content. Those with Al_2O_3/SiO_2 ratios greater than 20, between 10-20 and between 4-10 are grouped as high-alumina ores, aluminous ores and siliceous ores, respectively, while those with Fe_2O_3 content greater than 25, between 10-25 and less than 10 are divided into three groups as very ferrous ores, ferrous ores and low ferrous ores, respectively (Gök, 2019). In order to realize the Bayer process economically, the lower limit of the silica modulus (Al_2O_3:SiO_2) of the ore should be 7-8 on average, depending on the ore type and technical-economic conditions. In the case of a high quality bauxite ore, this value is above 10 (Birinci and Gök, 2018). Bauxite ore obtained from deposit types with a silica modulus below 7-8 cannot be directly subjected to the Bayer process due to its high silica content. The silica content in the ore must be reduced. Otherwise, the process cannot be economical because the caustic consumption will be too high. Therefore, before the Bayer process, it is necessary to carry out a

whole set of processes defined as pre-desilication, which can be applied to remove silica, for an economic production. For this purpose, for example, the flotation process can be used to remove the silica content in the ore (Kangal, 2024). Besides, the iron content from ferrous bauxite ores should be decreased.

For the reduction of iron content, processes such as gravity separation, magnetic separation for the removal of hematite, flotation of iron oxide contents and carbothermal reduction, the transformation of Fe_2O_3 to Fe_3O_4 and magnetic separation of magnetite can be applied (Pickles et al., 2012; Sadler and Venkataraman, 1991). Anionic collectors are typically employed in the flotation of iron oxides. These collectors can be categorized into two main types: sulfhydryl and oxyhydryl. Oxyhydryl collectors are predominantly utilized for minerals containing iron oxides, carbonates, and sulfur groups. Among the most frequently used collectors for the flotation of iron oxides are fatty acids, soaps, as well as alkyl sulfates and sulfonates, which demonstrate high efficiency in this application. These reagents selectively interact with the iron oxide surfaces, facilitating their separation from other mineral phases during flotation processes (Nakhaei and Irannajad, 2018).

In this study, the material was not classified as siliceous bauxite ore due to its silica modulus being 8.01. However, given its iron oxide content ranging between 10-25%, it was identified as ferrous bauxite ore. To reduce the iron oxide content, in the experimental works, various methods were employed, including gravity separation through a shaking table, high-intensity wet and dry magnetic separation processes, the physicochemical process, flotation, and finally, the pyrometallurgical process, roasting. Each of these methods aimed at effectively lowering the iron content in the ore.

2. Materials and Method

The representative sample was originated from İskenderun-Hatay. The chemical analysis of run-of mine by X-ray Fluorescence (XRF) was demonstrated in Table 1. Based on the chemical analysis of a representative sample, the silica modulus (Al_2O_3/SiO_2) was determined to be 8.01. To further assess the mineralogical properties of the sample, X-ray diffraction (XRD) patterns were examined, and the findings from the modal mineralogy analysis were presented in Figure 1 and Table 2, respectively.

Table 21. The chemical analysis of run-of mine by XRF

Compound	**%**	**Compound**	**%**
Al_2O_3	53.54	P_2O_5	0.11
Fe_2O_3	14.40	Cr_2O_3	0.11
TiO_2	11.65	V_2O_5	0.061
SiO_2	6.68	K_2O	0.01
CaO	0.91	Co_3O_4	0.005
MgO	0.54	Na_2O	< 0.01
MnO	0.113	CuO	< 0.005
LOI	11.72	NiO	< 0.003

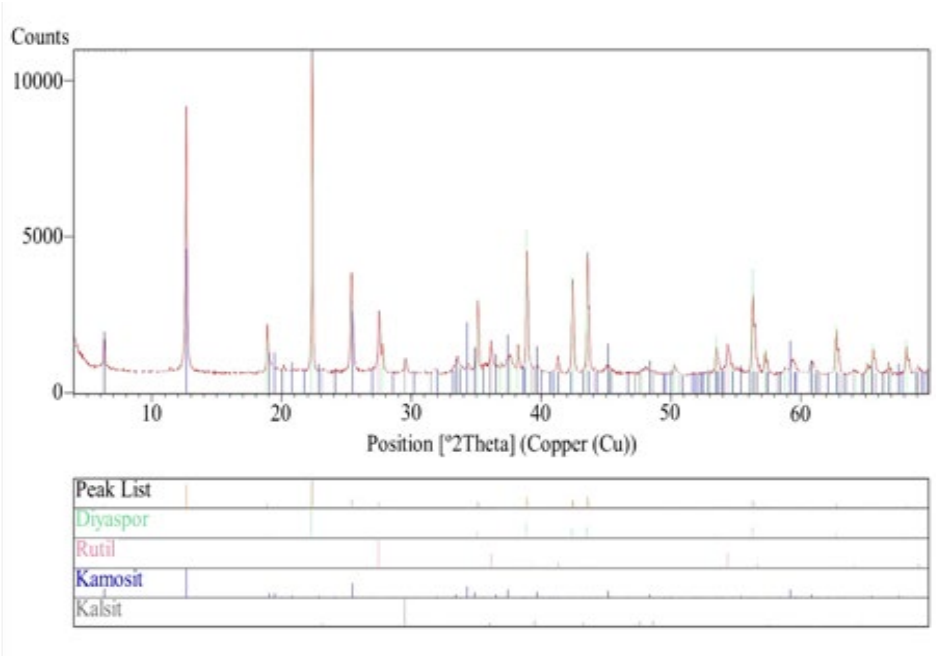


Figure 37. XRD peaks of run-of mine

Depending on the XRD peaks, it was determined that the run-of mine consisted of 13.6% chloride, 41% diaspore, 6.9% rutile and 37% amorphous.

Table 22. The modal mineralogy analysis of run-of mine

Mineral	%	Mineral	%
Pyrite	0.13	Amfibole	0.03
Diaspore	35.12	Mica	0.15
Lateric Diaspore	24.52	Pyroxen	0.01
Iron Oxide/Hydroxide	8.24	Chloride	9.27
Magnesium Hydroxide	0.04	Si-Al Clays	4.57
Rutile	9.80	Apatite	0.27
Altered Ilmenite	4.37	Calcite	1.23
Zircon	0.09	Dolomite	0.53
Quartz	0.19	Others	1.34
Feldspar	0.09		

Mineralogical analysis revealed that the sample was predominantly composed of diaspore, comprising 35.12% diaspore and 24.52% lateritic diaspore with low Fe-Ti content. The primary minerals presented, aside from diaspore, included rutile, Fe oxide/hydroxide, and altered ilmenite, in decreasing order of abundance. Diaspore served as the principal aluminum carrier within the sample. A significant portion of the diaspore was finely intergrown with TiO_2, was texturally discernible, and exhibited an amorphous or weakly crystalline structure. The term "low Fe-Ti lateritic diaspore" referred to a fine-grained mixture of diaspore with rutile and ilmenite, where ilmenite was observed to be altered and amorphous or poorly crystalline.

Scanning Electron Microscope (SEM) was used to analyze the images of the sample and the results were given in Figure 2. The images obtained through SEM corroborated the findings of the mineralogical analyses.

Particle size analysis were conducted for the most abundant minerals in the raw sample—diaspore, rutile, and ilmenite—to determine their size distribution. The results were presented in Table 3, and the size distribution was shown in Figure 3. To determine the liberation size, a Mineral Liberation Analysis (MLA) was performed, with the findings displayed in Figure 4. Besides, in Figure 5, the results of size liberation analysis were demonstrated.

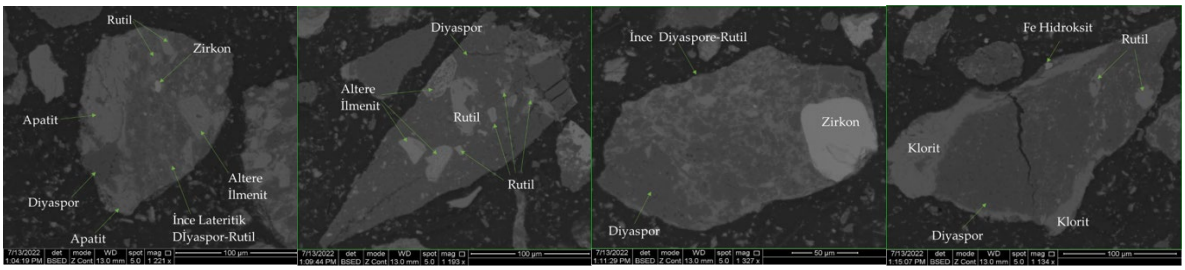


Figure 38. The image analysis of run-of mine

Table 23. The size distribution of diaspore, rutile and ilmenite

Particle Size, µm	Diaspore	Rutile	Ilmenite
3	0	0	0
5	3	10	27
7.5	6	23	56
10	9	34	72
13.25	13	48	88
18.75	22	67	96
26.5	35	87	100
37.5	52	98	100
53	70	98	
75	89	99	
106	97	100	
150	100		

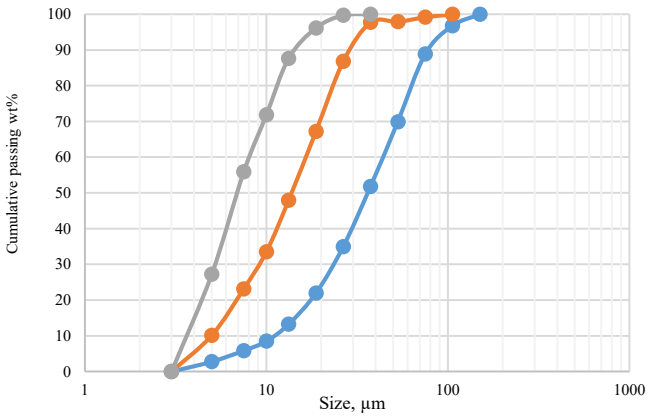


Figure 39. The particle size curve of diaspore, rutile and ilmenite

To obtain a bauxite concentrate with low Fe-Ti oxide content, various beneficiation methods, including gravity separation, magnetic separation, and flotation, were explored. For gravity separation, a shaking table was employed. High-intensity dry magnetic separation was performed using a rare earth magnetic separator (REMS) and a rotary disc magnetic separator. Additionally, high-intensity wet magnetic separation was carried out using Carpco magnetic separator. Dry magnetic separation and shaking table processes were carried out by classifying the size fractions of the raw ore, all of which were reduced below 1 mm, into -1+0.5 mm, -0.5+0.212 mm and -0.212+0.038 mm size fractions. However, the wet magnetic separation method using the Carpco separator and flotation processes were applied individually to the raw ores at particle sizes of -300 µm, -212 µm, -106 µm, and -75 µm. The flotation tests were carried out by using DERNA 7 as collector at pH 9.5. In addition, calcination processes were also investigated for the removal of iron oxides and calcination temperatures (600-700-900-1000°C) and calcination times (2-4-6-8 hours) were optimized.

3. Experimental Studies

3.1. Shaking Table

Shaking table tests were performed on three different size fractions of the run-of-mine ore (-1+0.5 mm, -0.5+0.212 mm, and -0.212+0.038 mm) following desliming, with the objective of reducing the iron and titanium oxide content in the bauxite concentrate. The results were analyzed in terms of Al_2O_3%, SiO_2%, Fe_2O_3%, TiO_2%, and silica modulus. The outcomes for the size fractions -1+0.5 mm, -0.5+0.212 mm, and -0.212+0.038 mm were presented in Table 4.

Table 24. The experimental results of shaking table tests

Size, mm	Products	Weight, %	Al_2O_3, %		SiO_2, %		Fe_2O_3, %		TiO_2, %		Silica Modulus, %
			C	D	C	D	C	D	C	D	Al_2O_3/SiO_2
-1+0.5	Heavy	30.5	55.30	30.3	4.85	29.6	14.62	31.4	12.73	31.8	11.40
	Middling 1	23.5	56.28	23.8	4.75	22.4	13.75	22.7	12.18	23.6	11.85
	Middling 2	23.4	55.82	23.6	5.02	23.6	14.00	23.1	12.23	23.6	11.12
	Middling 3	11.7	55.72	11.7	5.13	12.0	13.92	11.4	11.45	11.0	10.86
	Light	10.9	53.86	10.6	5.68	12.4	14.78	11.4	11.18	10.0	9.48
	Total	100.0	55.54	100.0	4.99	100.0	14.21	100.0	12.16	100.0	11,13
-0.5+0.212	Heavy 1	1.1	56.27	1.1	4.21	1.0	14.47	1.2	12.68	1.2	13.37
	Heavy 2	2.6	55.46	2.6	4.22	2.3	15.62	2.9	12.74	2.8	13.14
	Middling 1	33.6	57.22	34.3	4.45	31.2	13.32	32.3	12.2	34.0	12.86
	Middling 2	21.8	55.86	21.7	4.47	20.4	14.24	22.4	12.16	22.0	12.50
	Middling 3	23.0	56.01	23.0	5.05	24.2	13.68	22.7	11.99	22.8	11.09
	Light	17.9	54.23	17.3	5.6	20.9	14.35	18.5	11.59	17.2	9.68
	Total	100.0	56.05	100.0	4.79	100.0	13.86	100.0	12.05	100.0	11.70
-0.212+0.038	Heavy 1	1.7	53.42	1.6	4.01	1.3	17.72	2.0	12.87	1.9	13.32
	Heavy 2	2.9	52.74	2.8	4.06	2.2	18.40	3.6	12.71	3.1	12.99
	Middling 1	23.6	56.13	24.3	4.49	19.9	14.07	22.4	12.35	25.0	12.50
	Middling 2	15.6	54.28	15.6	4.79	14.1	15.12	16.0	12.61	17.0	11.33
	Middling 3	21.5	54.56	21.7	5.56	22.5	14.50	21.3	11.61	21.6	9.81

Middling 4	20.4	55.07	20.7	5.72	21.9	14.07	19.4	11.09	19.4	9.63
Light	14.3	50.64	13.3	6.77	18.1	15.91	15.3	9.78	12.0	7.48
Total	100.0	54.36	100.0	5.32	100.0	14.78	100.0	11.63	100.0	10.21

C: Content, D*: Distribution*

The experimental results indicated that, although there were no significant differences in terms of Al_2O_3% content in the products from the three size fractions, the most effective removal of iron and titanium oxides was achieved with the -0.212+0.038 mm size fraction. The slime fraction contained 51.17% Al_2O_3, 7.25% SiO_2, 16.38% Fe_2O_3, and 8.66% TiO_2.

3.2. High-Intensity Dry Magnetic Separation

High-intensity dry magnetic separation was conducted on the material classified into -1+0.5 mm and -0.5+0.212 mm size fractions using REMS, with the objective of reducing iron content to produce a bauxite concentrate with low Fe-Ti oxide content. Additionally, the experimental conditions were assessed by performing magnetic separation on the -0.212+0.038 mm size fraction using a rotary disc magnetic separator. The results were shown in Table 5.

Table 25. The experimental results of high intensity dry magnetic separation

	Products	Weight, %	Al_2O_3, %		SiO_2, %		Fe_2O_3, %		TiO_2, %		Silica Modulus, %
			C	D	C	D	C	D	C	D	Al_2O_3/SiO_2
-1+0.5	Magnetic	63.3	53.54	60.9	5.65	71.8	16.42	73.1	11.84	60.8	9.48
	Non-Mag.	36.7	59.19	39.1	3.82	28.2	10.4	26.9	13.18	39.2	15.49
	Total	100.0	55.61	100.0	4.98	100.0	14.21	100.0	12.33	100.00	11.17
-0.5 +0.212	Magnetic 1	3.8	44.55	3.1	6.29	4.9	29.51	7.9	8.17	2.5	7.08
	Magnetic 2	10.0	41.00	7.4	10.90	22.5	29.22	20.8	6.89	5.6	3.76
	Magnetic 3	6.7	44.67	5.4	8.33	11.6	24.86	11.9	9.64	5.3	5.36
	Non-Mag.	79.5	58.41	84.1	3.71	60.9	10.53	59.4	13.36	86.6	15.74
	Total	100.0	55.22	100.0	4.84	100.0	14.08	100.0	12.27	100.0	11.41
0.212+0.038	Magnetic 1	5.5	41.88	4.2	5.68	5.9	31.85	11.8	8.87	4.2	7.37
	Magnetic 2	15.5	41.41	11.8	10.51	30.9	28.08	29.5	7.78	10.3	3.94
	Non-Mag.	79.0	57.93	84.0	4.22	63.2	10.99	58.7	12.63	85.5	13.73
	Total	100.0	54.49	100.0	5.28	100.0	14.78	100.0	11.67	100.0	10.33

C: Content, D*: Distribution*

The magnetic separation process conducted on the -1+0.5 mm size fraction resulted in the highest Al_2O_3 content in the non-magnetic product. In contrast, the -0.212+0.038 mm size fraction achieved the highest Al_2O_3 recovery efficiency at 84%, despite the Al_2O_3 content being 57.93%.

-0.212+0.038 mm size fraction also exhibited the highest iron oxide content, with Fe_2O_3 content of 31.85%, although the yield of the magnetic product in this fraction was relatively low. In comparison, the iron oxide content in the -1+0.5 mm size fraction was 16.42%, which was lower than that of the finer fractions, yet this fraction demonstrated the highest recovery efficiency at 73.1%. However, Fe_2O_3 content in the non-magnetic product remained consistent across all size fractions.

3.3. High-Intensity Wet Magnetic Separation

High-intensity magnetic separation process was carried out with Carpco device and was carried out over four different top sizes; -300 micron, -212 micron, -106 micron and -75 micron. In all size groups, firstly magnetic and non-magnetic product was obtained with 0.4 Ampere (A) and then the non-magnetic product was subjected to three stages of scavenging at 1A, 3A and 5.8A magnetic field. The metallurgical balance table of the final magnetic and non-magnetic products is given in Table 6.

Table 26. The experimental results of high intensity wet magnetic separation

Size, µm	Products	Weight, %	Al_2O_3		SiO_2		Fe_2O_3		TiO_2		Silica Modulus, %
			C	D	C	D	C	D	C	D	Al_2O_3/SiO_2
-300	Magnetic	40.1	52.39	37.8	5.89	47.0	17.27	49.5	11.80	39.6	8.89
	Non-Mag.	59.9	57.58	62.2	4.45	53.0	11.78	50.5	12.05	60.4	13.06
	Total	100.0	55.50	100.0	5.03	100.0	13.98	100.0	11.95	100.0	11.04
-212	Magnetic	30.0	50.77	27.5	6.03	36.7	19.51	40.7	11.42	28.5	8.43
	Non-Mag.	70.0	57.33	72.5	4.45	63.3	12.13	59.3	12.26	71.5	12.92
	Total	100.0	55.36	100.0	4.92	100.0	14.34	100.0	12.01	100.0	11.25
-106	Magnetic	34.7	52.92	32.8	5.24	39.0	17.75	44.4	11.41	33.0	10.12
	Non-Mag.	65.3	57.76	67.2	4.35	61.0	11.82	55.6	12.36	67.0	13.33
	Total	100.0	56.08	100.0	4.66	100.0	13.88	100.0	12.03	100.0	12.04
-75	Magnetic	25.1	50.11	22.7	5.73	28.7	20.07	34.7	11.65	25.0	8.87
	Non-Mag.	74.9	57.02	77.3	4.76	71.3	12.67	65.3	11.75	75.0	12.04
	Total	100.0	55.28	100.0	5.00	100.0	14.52	100.0	11.72	100.0	11.05

C: Content, D*: Distribution*

Upon examining the size-dependent trends, it was observed that -106 µm fraction deviates from the overall trend. This discrepancy could be attributed to the agglomeration of material used during the experiment. In terms of the silica modulus, better results were achieved with coarser size fractions. A similar trend was observed in experiments conducted using the rotary disc magnetic separator for the -1+0.038 mm fractions. Additionally, the silica modulus value in the run-of-mine ore was approximately 11, which was sufficient for the BAYER process (modulus >7). Although the iron content in the non-magnetic product decreased, silica modulus remained relatively high (>9%). This could be due to most of the ilmenite being locked within the matrix.

The titanium content did not change significantly with magnetic separation. This was probably because most of the ilmenite and rutile were present in very fine locked forms. Moreover, a portion of the rutile was probably found in binary associations with diaspore, while another fraction was present in more complex ternary associations.

3.4. Flotation

Flotation experiments were conducted at a pH of 9.5 with a solid-in-pulp ratio of 25%, and a pulp mixing speed of 1200 rpm. The collector, Derna 7, was used in a three-stage flotation process at a dosage of 500+250+250 g/t. Conditioning times for each stage were 5+5+5+3 minutes, while the flotation times were 2+2+2+2 minutes. Throughout the experiments, the flotation conditions were kept constant, and the influence of varying upper particle sizes—specifically, -300 µm, -212 µm, -106 µm, and -75 µm—was systematically evaluated. The results were presented in Table 7.

Table 27. The experimental results of flotation tests

Size, µm	Products	Weight, %	Al_2O_3		SiO_2		Fe_2O_3		TiO_2		Silica Modulus, %
			C	D	C	D	C	D	C	D	Al_2O_3/SiO_2
-300	Float 1	17.9	52.68	17.0	5.87	20.2	16.04	20.0	9.31	14.5	8.97
	Float 2	15.0	54.12	14.7	5.69	16.4	15.38	16.1	9.66	12.6	9.51
	Float 3	7.3	52.55	7.0	6.16	8.8	16.77	8.6	10.84	6.9	8.53
	Sink	59.8	56.72	61.3	4.73	54.6	13.28	55.4	12.65	65.9	11.99
	Total	100.0	55.30	100.0	5.18	100.0	14.34	100.0	11.47	100.0	10.67
-212	Float 1	16.7	54.29	16.3	5.39	17.8	15.43	17.7	9.19	13.5	10.07
	Float 2	15.1	54.09	14.8	5.52	16.5	15.50	16.0	9.80	13.0	9.80
	Float 3	9.7	53.15	9.4	5.88	11.3	16.44	11.0	10.95	9.4	9.04
	Sink	58.5	56.32	59.5	4.71	54.4	13.81	55.3	12.49	64.1	11.96
	Total	100.0	55.34	100.0	5.04	100.0	14.55	100.0	11.38	100.0	10.94
-106	Float 1	16.9	54.82	16.8	5.07	16.9	15.00	17.1	9.71	14.0	10.81
	Float 2	14.7	55.55	14.9	5.20	15.1	14.51	14.3	9.85	12.3	10.68
	Float 3	21.3	54.76	21.2	5.39	22.6	15.29	21.8	11.14	20.2	10.16
	Sink	47.1	54.84	47.1	4.88	45.4	14.81	46.8	13.32	53.5	11.24
	Total	100.0	54.92	100.0	5.07	100.0	14.90	100.0	11.74	100.0	10.84
-75	Float 1	16.3	55.38	16.5	5.10	16.2	14.51	16.0	9.84	13.9	10.86
	Float 2	16.7	54.91	16.7	5.18	16.8	14.70	16.4	10.26	14.7	10.60
	Float 3	12.8	55.07	12.9	5.21	13.0	14.77	12.8	10.30	11.4	10.57
	Sink	54.2	54.39	53.9	5.11	54.0	15.01	54.8	12.79	60.0	10.64
	Total	100.0	54.73	100.0	5.13	100.0	14.85	100.0	11.57	100.0	10.66

C: Content, D*: Distribution*

Due to the possibility that the particles were associated in very fine sizes, there was no significant change in any content, including the silica modulus. Considering the results, an increase of 1.5-2% was observed in the sink product in terms of TiO_2 content.

3.5. Roasting

Physical and physicochemical processes were not successful in achieving bauxite concentrate. Therefore, it was aimed to transform Fe_2O_3 content into Fe_3O_4 content by reduction by pyrometallurgical method and then to reduce the iron content by low field strength magnetic separation. In this respect, the material predicted to be liberated in fine size was ground to -53 micron size with a ball mill. Firstly, the effect of different temperatures (600-700-900-1000°C) was investigated in a single constant time of 1 hour. Following the optimization of the temperature, the effect of 2-4-6-8 hours was examined under the optimized temperature. Optimization was carried out depending on the Fe_3O_4(%) content of the obtained products by means of Satmagan analysis. The effects of different temperatures on Fe3O4 reduction in terms of chemical by XRF (X-ray Fluorescence) and Satmagan analysis on the product were demonstrated in Table 8.

Table 28. The experimental results of roasting temperature

Temperature (°C)	Al_2O_3, %	SiO_2, %	Fe_2O_3, %	Fe_3O_4, %	TiO_2, %	CaO, %	KK, %
600	60.71	5.58	16.54	0.08	12.57	1.05	2.17
700	59.99	5.69	16.88	0.09	12.83	1.07	2.16
900	60.92	5.65	16.86	0.07	12.77	1.06	1.47
1000	61.16	5.68	17.19	0.07	13.10	1.09	0.51

No significant Fe_2O_3-Fe_3O_4 reduction was observed. However, it was concluded that the optimum temperature was at 700 °C.

Thermal treatment at 700 °C for 2-4-6-8 hours respectively was performed for a considerable aimed Fe_2O_3-Fe_3O_4 reduction. The chemical analysis of the end-product by XRF was shown in Table 9.

Table 29. The experimental results of roasting times

Compound (%)	Time (hours)			
	2	4	6	8
Al_2O_3	59.84	59.79	58.75	59.31
BaO	0.01	0.01	0.01	0.01
CaO	1.18	1.21	1.26	1.22
Cr_2O_3	0.15	0.15	0.16	0.15
Fe_2O_3	17.62	17.70	18.69	18.05
Fe_3O_4	0.43	0.46	0.24	0.22
K_2O_3	0.01	0.01	0.01	0.01
MgO	0.77	0.77	0.72	0.76
MnO	0.11	0.11	0.12	0.11
Na_2O	<0.01	<0.01	<0.01	0.03
P_2O_5	0.48	0.47	0.51	0.50
SO_3	0.29	0.08	0.08	0.08
SiO_2	6.34	6.38	6.07	6.34
SrO	0.01	0.01	0.01	0.01
TiO_2	13.09	13.21	13.51	13.33

Based on the results of Satmagan analysis and XRF analysis, it could be observed that Fe_2O_3-Fe_3O_4 reduction increased approximately five times as a result of 2 and 4 hour experiments. While Fe_2O_3 ratio of the ore fed to the experimental step where the temperature was kept constant and the time was kept variable was 0.09 at the initial stage, it could be increased up to the highest value of 0.46 at the end of 4 hours. It was indicated that the optimum temperature of 700 °C was determined and the optimum time was 4 hours. However, within this information, it was concluded that the process was not considered to be successful. In Figure 6, the sample before and after heat treatment was shown.



Figure 40. The image of the sample before and after heat treatment

4. Conclusion

In this study, the enrichment of a diasporic bauxite ore with 53.54% Al_2O_3 content and removal of iron oxide content was investigated through various separation methods. These methods included gravity separation using a shaking table, high-intensity dry magnetic separation using the REMS and rotary disc magnetic separators, high-intensity wet magnetic separation with the Carpco magnetic separator, flotation, and the roasting process. The effects of these processes on removal of iron oxide and the improvement of the ore's quality were evaluated. However, the processes conducted did not yield successful results, most likely due to the liberation of ilmenite, rutile, and diaspore at very fine particle sizes. This fine-grained liberation likely impeded the effective separation and enrichment of the desired minerals, reducing the overall efficacy of the applied methods.

References

Birinci, M., & Gök, R. (2018). A current review on bauxite beneficiation processes for pre-desilication. *Sicentific Mining Journal, 57*(3), 197-218. DOI: 10.30797/madencilik.457373 (in Turkish)

Gök, Ramazan. Investigation of beneficiation possibilities of low modulus metallurgical bauxite ores. Master Thesis, İnönü Üniversitesi, 2019. (in Turkish)

Kangal, M.O. (2024). Mineral reserves and beneficiation methods. *Lithium ion batteries in electric vehicles* (pp. 17-84): Otomotiv Teknolojileri Platformu. (in Turkish)

Nakhaei, F., & Irannajad, M. (2018). Reagents types in flotation of iron oxide minerals: A review. *Mineral processing and extractive metallurgy review*, *39*(2), 89-124. DOI: 10.1080/08827508.2017.1391245

Pickles, C. A., Lu, T., Chambers, B., & Forster, J. (2012). A study of reduction and magnetic separation of iron from high iron bauxite ore. *Canadian Metallurgical Quarterly*, *51*(4), 424-433. DOI: 10.1179/1879139512Y.0000000038

Sadler, L. Y., & Venkataraman, C. (1991). A process for enhanced removal of iron from bauxite ores. *International Journal of Mineral Processing*, *31*(3-4), 233-246. DOI: 10.1016/0301-7516(91)90028-H

An Investigation into the Prevention of Black Core Formation in Ceramic Bodies

M. Uğur Taşkıran [1], Kağan Kayacı [1], A. Ali Sirkeci [2], Hatice Turgut [2], Barış Darcan [2]

[1]Kaleseramik Research and Development Center, Çan, Çanakkale, TÜRKİYE

[2]Istanbul Technical University, Dept. of Mineral Processing Engr.

*Corresponding author: sirkecia@itu.edu.tr (Ayhan Ali Sirkeci)

Abstract:

Ceramics Industry is the major consumer of industrial raw materials including various types of clay minerals. The existence of impurities in ceramic raw materials is a challenging issue to produce high quality ceramics. Coloring impurities such as Fe and Ti cause discoloration within the ceramic bodies and they have to be kept below certain limits. Organic carbon present in clay rocks leads to another aesthetic problem within fired ceramic bodies referred to as "black core". During biscuit firing process organic carbon in the body composition slowly burns out. Burning requires oxygen and that oxygen is robbed out of Fe_2O_3, which is another impurity, reducing it to FeO. During the ongoing burning process FeO then melts, interacts penetrates within the surrounding matrix creating the so-called black core structures. Black core formation is not desired from the aesthetic point of view; however, it strengthens the ceramic body making it durable to mechanical shocks. In this investigation experimental studies have been conducted to reduce the black core formation in the ceramic bodies where organic carbon rich clay sources are used in the recipe. Test results have proven that black core formation could be greatly reduced to negligible levels by the chemical treatment of the clay raw material containing organic carbon as the impurity.

Keywords: *Black Core, Ceramic Bodies, Hydrogen Peroxide Leaching.*

1. Introduction

Ceramic tile production is a complex process where aesthetics and structural durability must be optimized together. In this process, production parameters must be managed precisely in order to obtain high-quality products. However, various defects encountered during the production process can seriously affect the quality of the products. One of these defects is the "Black Core" that causes both aesthetic and structural weaknesses because of a dark core formed the inside the ceramic tiles. It has been stated in the literature that the "Black Core" defect accounts for 15% to 20% of ceramic tile production flaws worldwide (Johnson & Smith, 2020; Gupta & Rao, 2019).

The "Black Core" is usually caused by glitches in the firing process. Failure to provide adequate air circulation during firing causes a lack of oxygen in the interior of the tile, which leads to the accumulation of unburned carbon residues. This has been observed especially in ceramics fired at high temperatures (Martinez & Lopez, 2021). Additionally, improper firing time or temperature may cause the clay to not sinter fully, which may trigger the "Black Core" error (Chen & Lee, 2018).

Another important factor affecting the occurrence of defects is the quality of the raw materials used. Failure to mix raw materials homogeneously may result in the formation of carbon-rich areas in some areas. In this case, sufficient combustion does not occur in these zones during firing, resulting in a "Black Core" formation (Kim & Park, 2022). This risk increases particularly in clays with high organic matter content. Studies show that a 2% deviation from homogeneity in the clay mixture can increase the incidence of the "Black Core" by up to 12% (Chen & Lee, 2018). The effect of this defects on ceramic tiles is not limited to aesthetic deterioration; It also negatively affects the mechanical durability of the tiles. In a study by Martinez and Lopez (2021), it was reported that the mechanical durability of tiles with the "Black Core" defect can decrease by up to 10%. This situation emerges as a serious problem in the

construction industry, which wants to provide a long-lasting and durable surface, especially in tile applications.

In this context, ceramic tile manufacturers need to establish a careful control mechanism in their production processes to minimize the "Black Core" error. Optimizing firing parameters, meticulously monitoring the quality of the raw materials used and ensuring homogeneity in the production line are key factors in preventing this defect. In addition, continuous monitoring of production processes and making necessary improvements will contribute to both increasing product quality and reducing manufacturing costs.

2. Material and methods

In this study, clay obtained from the Şile region was used. Hydrogen Peroxide (H_2O_2) was used as a chemical in leaching experiments. A magnetic stirrer with heating capability was used during the leaching tests. Leach temperature was kept at 55 ^oC employing a thermocouple thermostat system connected to the stirrer. At the end of the leaching experiments the liquid phase was filtered off and the solid residue was dried for analysis. A carbon-sulfur analysis device was used to assay carbon contents of the test samples. The test sample was soaked for 24 hours and then sieved through 53 μm sieve and the undersize fraction was used in all leach experiments. 25 g of dry samples was used in all tests where agitation speed and duration were 400 rpm and 3 hours respectively.

The chemical and mineralogical analyses of the test sample are presented in Tables 1 and 2. Chemical and mineralogical analyses of the sample were carried out using Axios Maxmodel X-ray Spectrophotometer device (XRF, PANalytical) and X'pert Pro MPD X-ray Diffractometer (XRD, PANalytical). Rietveld method was used to determine the quantitative XRD results. XRD pattern of the test sample is given in Figure 1.

Table 1. Results of the chemical analysis of the test sample

	L.O.I.	SiO_2	Al_2O_3	TiO_2	Fe_2O_3	CaO	MgO.	Na_2O	K_2O
Şile Region Clay	6.79	64.45	21.27	1.23	2.62	0.27	0.61	0.11	2.37

Table 2. The mineralogical composition of the test sample

Mineral	Weight, %
Quartz	33.33
Chlorite	2.24
Illite	23.58
Kaolinite	40.85

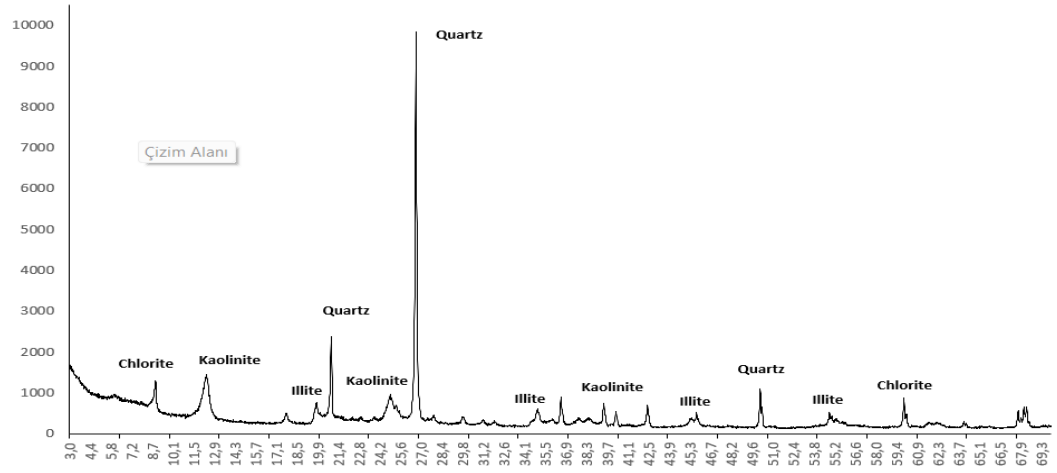


Figure 1. XRD Pattern of the test sample.

Prior to the firing tests the test sample was dried using an infrared lamp, milled to eliminate coarse particles and the ground powder was added water to achieve a moisture content of 5.5 wt% and pressed at a pressure of 300 kg/cm². Cylindrical tablet samples, measuring 40 mm in diameter and approximately 5 mm in thickness, were then sintered using an industrial porcelain tile firing curve at 1185 ^{0}C in the fast-firing industrial roller kiln.

3. Results

The test sample was sieved using a number of screen sizes and the results are given in Table 3.

Table 3. The results of screen analyses.

Size Fraction mm	Weight %	Cum. Undersize %	C %
1	3.72	100.00	18.91
-1 +0.5	5.12	96.28	4.15
-0.5 +0.212	7.91	91.16	1.76
-0.212 +0.106	5.12	83.26	1.19
-0.106 +0.053	6.51	78.14	0.65
-0.053 +0.038	4.19	71.63	0.52
-0.038	67.44	67.44	0.57
Feed	100		1.56

The carbon analyses performed on the size fractions show that C content below 53 µm considerable reduces. Therefore, leach tests were carried out using -53 µm size fraction.

In the leaching experiments hydrogen peroxide was added at varying amounts keeping the total liquid volume constant. Leach conditions are given in Table 4.

Table 4. Leach conditions adopted in the tests.

Test #	H_2O_2 Addition, ml	Distilled Water, ml
1	2.5	47.5
2	5	45
3	10	40
4	15	35
5	20	30

The size fraction below 53 μm contains around 0.57% C. A biscuit was prepared using the -53 μm size fraction sample and fired at 1185°C to see the black core formation within the untreated sample. In Figure 2. the black core formation inside the test sample is clearly seen.



Figure 2. Black core formation inside untreated -53 μm test sample.

The results of leach tests in terms of C content are presented in Table 5.

Table 5. Carbon contents after leaching tests.

Test #	C, %
1	0.26
2	0.30
3	0.22
4	0.27
5	0.26

The results of carbon analyses conducted on the samples show that C content in all test varies between 0.22 and 0.3%, in other words it does not change a lot and remains around 0.26 %. However, some amount of decrease in carbon content from 0.57% is clear. In order to see the effect of reduction in carbon on the black core formation a biscuit was prepared using the test sample assaying 0.26% C and fired. The result of firing test is given in Figure 3.



Figure 3. Black core formation inside -53 μm test sample after H_2O_2 leaching.

4. Conclusions

In this investigation leach tests were carried out to reduce organic carbon content in ceramics clays that causes black core formation inside ceramics bodies. In the tests H_2O_2, which is a strong oxidizing agent, was employed. Leaching trials showed that the carbon content of the test sample was reduced from about 0.57% to around 0.26%. The reduction in the carbon content prevented the formation of black core inside the ceramic bodies to a great extent.

References

Johnson, L., & Smith, M. (2020). Ceramic Tile Defects: Analysis and Mitigation. *Journal of Materials Processing Technology*, 276, 116401.

Gupta, P., & Rao, K. (2019). Thermal Behavior in Ceramic Manufacturing: A Study of Common Defects. *Journal of Ceramic Processing Research*, 20(3), 294-300.

Martinez, R., & Lopez, A. (2021). Mechanical Properties of Defected Ceramic Tiles: The Impact of Firing Errors. *Materials Science and Engineering: A*, 789, 139589.

Chen, Y., & Lee, S. (2018). Influence of Firing Conditions on Defects in Ceramic Tiles. *Journal of the European Ceramic Society*, 38(14), 4825-4834.

Kim, J., & Park, H. (2022). Material Homogeneity and Its Impact on Ceramic Tile Quality. *Ceramics International*, 48(5), 6321-6328.

Development Of Alternative Wall Tile Compositions By Using Different Industrial Wastes

M.Uğur Taşkıran [1], Kağan Kayacı [1*], Enrique Sanchez Vilches [2], Vicente Sanz Solana [2]

Şenay Türk [1], Ş. Can Genç [3, 1], Javier Castellano Brull [2]

[1] Kaleseramik Research and Development Center, Çan, Çanakkale, TÜRKİYE

[2] Instituto Universitario de Tecnología Cerámica (IUTC), Universitat Jaume I (UJI), Castelló, SPAIN

[3] Istanbul Technical University, Faculty of Mines, Geological Engineering Department, Maslak, Istanbul, TÜRKİYE

*Corresponding author: ugurtaskiran@kale.com.tr (Uğur Taşkıran)

Abstract

Effective utilization of industrial wastes plays an important role in reducing environmental impacts and efficient use of natural resources. In this context, it is important to investigate the usability of industrial waste materials in different application areas. In Türkiye, there are a huge amount of boron resources, and its mining wastes, together with the cutting wastes of the marble and/or limestones cutting factories. Beside these, fly ashes from the coal-burning thermic power plants, silica-rich raw material wastes used by the glass industry are in high amounts in some companies. Additionally, ceramic tile scraps of the ceramic tile manufacturers were also an important industrial waste. In this study, the potential of using boron mineral wastes from NW Anatolian boron deposits, Marmara Island limestone/dolomitic marble wastes, fly ashes obtained from Karabiga and sand wastes of the glass industry from Bilecik region in wall tile production was studies.

The waste materials were sampled on site and firstly their characterizations were carried out in the laboratory. Mineralogical properties (XRD), chemical composition (XRF), % water absorption, moisture expansion analyses and firing behaviours in wall tile regime were investigated. Considering the results obtained in the later stages of the study, alternative wall tile compositions in which boron, fly ash, sand and marble wastes were used at a ratio of 50% were realized. The different body compositions were fired separately and their firing behaviours, moisture expansion, water absorption characteristics were tested and the most suitable recipe for wall tiles was revealed. The production of wall tiles using different industrial wastes will provide sustainable raw material management by providing less use of natural raw materials on the one hand, and it will reduce raw material costs and ultimately reduce CO_2 emissions.

Keywords: *mining wastes, boron mineral wastes, marble wastes, sand wastes, fly ashes, CO_2 emission*

1. Introduction

The fact that the ceramic raw material resources in Türkiye are diminishing and the energy input is expensive is pushing technologists to search for alternative raw material resources. Instead of the standard raw materials used in the production of wall tiles, there is an increasing number of studies on the reuse of waste materials resulting from the production process or raw materials from other industries, the so-called secondary raw materials (Kayacı et al, 2014; Kayacı et al, 2019; Rahmannan et al, 2013; Torres et al, 2007; Tarhan et al, 2017). Efficient reuse of the wastes in the economy and reduction of their quantities are very important in terms of both economic and environmental problems. However, when evaluating wastes, not only their disposal should be considered, but also their use in areas with high added value. It is well known that a standard wall tile composition consists of a mixture of clay-kaolin, calcite and quartz raw materials in certain proportions. Each of these raw materials plays a different role in the composition (Sousa & Hollanda, 2005). Therefore, in the production of ceramic wall tiles, the design of the composition, the selection and the ratio of the raw materials that make up the composition must be adjusted with great precision Kayacı et al, 2010).

Clays are used to increase plasticity and raw strength in the shaping stages of wall tile compositions. Another important group of raw materials used in the production of wall tiles are carbonates (Garcia et al, 2008; Traore et al, 2007). The decomposition of carbonates in the composition formulation results in open pores and water absorption. The reactions of the resulting oxides with other materials to form new crystalline phases (such as anorthite and gahlenite) affect important properties of the final product such as dimensional stability and moisture expansion. In this study, the potential of using boron mineral wastes from NW Anatolian boron deposits, Marmara Island limestone/dolomitic marble wastes, fly ashes obtained from Karabiga and sand wastes of the glass industry from Bilecik region in wall tile production was studied. The potential for using secondary industrial wastes in different proportions in wall tile compositions has been demonstrated. In particular, it has been shown that wall tile products made from such different industrial wastes are potential raw materials for the ceramic industry.

2. Material and methods

2.1. Material

The wastes of the raw materials include boron mineral wastes from NW Anatolian boron deposits, limestone/dolomitic marble wastes from Marmara Island, fly ash obtained from Karabiga, and sand wastes from the glass industry in the Bilecik region. The chemical and mineralogical analyses of these secondary wastes are presented in Tables 1 and 2. For raw material characterization, Chemical and mineralogical analyses of the sample were carried out with Axios Maxmodel X-ray Spectrophotometer device (XRF, PANalytical) and X'pert Pro MPD X-ray Diffractometer (XRD, PANalytical). Duplicate analysis was done for each sample, and the average values were taken into account**.**

Table 1. Chemical analysis results of the Waste Materials (XRF)

	L.O.I.	SiO_2	Al_2O_3	TiO_2	Fe_2O_3	CaO	MgO	Na_2O	K_2O	B_2O_3
Marble Dust	42.6	2.5	0.8	-	0.3	53.0	0.3	-	0.1	-
Fly Ash	8.2	54.7	21.5	0.8	5.5	3.7	1.6	0.8	1.9	-
Tile Scraps	0.5	66.7	17.6	0.7	1.5	7.2	1.1	1.1	2.1	-
Sand Waste	5.0	76.4	14.9	0.4	1.2	0.3	-	-	1.3	-
Boric Waste	31.1	18.5	1.3	0.2	0.3	15.6	19.7	4.0	0.7	7.3

Table 2. Mineralogical compositions of the Waste Materials (XRD)

Material	Mineral			
Ball Clay	Quartz	Kaolinite	Illite	
Marble Dust	Calcite	Quartz		
Fly Ash	Amorphous phase	Mullite	Quartz	Hematite
Tile Scraps	Anorthite	Quartz	Amorphous phase	
Sand Waste	Quartz	Kaolinite		
Boric Waste	Dolomite	Ulexite		

2.2. Result and Discussions

2.2.1. Design And Preparation of Proposed Compositions

To maximize the use of waste raw materials, a development study for wall tile formulations was carried out. The new formulations are shown in Table 3 as WWT1, WWT2 and WWT3.

The different compositions were prepared on a laboratory scale using the standard processing method for ceramics, which included wet milling, drying, pressing, and firing in an electric kiln. Grinding was performed in planetary mills with ball loading for 10 minutes. The slurry was dried using infrared lamps and then milled dry to produce a fine powder. This powder was mixed with water to achieve a moisture content of 5.5 wt% and pressed at a pressure of 300 kg/cm². Cylindrical samples, measuring 40 mm in diameter and approximately 5 mm in thickness, were fired using a cycle that involved a rapid

heating ramp up to 500 °C, a temperature increase of 25 °C/min from 500 °C to the maximum temperature, and a dwell time of 6 minutes at the peak temperature. The firing temperatures were set at 1100 °C 1120 °C 1140 °C and 1160 °C. Additionally, a spray-dried powder composition corresponding to wall tile STD was prepared for comparative purposes. The laboratory-fired samples were analyzed by measuring their linear shrinkage and water absorption. Linear shrinkage was computed by comparing the diameters of the specimens before and after firing, using a caliper to measure these dimensions, and reporting this parameter on a dry basis. Water absorption was assessed using the vacuum method in accordance with the ISO 10545-3:2018 standard.

Moisture expansion is a property that should be minimized in fired wall tiles (Sanchez et al, 1990). Typically, this characteristic is assessed by measuring dimensional changes directly. However, due to the very small magnitude of expansion, measuring it by weight gain is preferred for greater precision. Therefore, moisture adsorption (MAd) was determined by the increase in weight (m_f–m_i) of the specimens after subjecting them to an autoclave cycle at a pressure of 10 kg/cm² for 5 hours, as described in Equation (1). Prior to measuring the final weight (m_f), the specimens were dried in an oven at 110 °C for 20 minutes (Sanchez et al, 2024).

$$MAd\ (‰) = (m_f - m_i)/m_i * 1000 \quad Eq \qquad (1)$$

Table 3. Alternative body formulations

Material	Formulations			
	STD	WWT1	WWT2	WWT3
Ball Clay	45	45	45	45
Kaolin	35			
Marble	15			
Marble Dust		15	15	15
Fly Ash		20	20	10
Tile Scraps	5	20	10	10
Sand Waste		-	10	15
Boric Waste		-	-	5

2.2.2. Evaluation of the Obtained Results

In order to investigate the mineral phases of the fired bodies of the standart and WWT1 To WWT3, we have carried out the XRD analysis. The XRD results showed the main mineral phases of the standart body was quartz + anorthite + diopsite + hematite + quartz + anorthite + gehlenite + amorphous phases for the WWT1 to WWT3 (Figure 1a, d). The gehlenite was probably crystallized from the high alumina contents of the fly ash and the tile scraps. It is crystallized from the metakaolinite and calcium bu the reaction of $Al_2Si_2O_7$ + (2+n) CaO→$Ca_2Al_2SiO_7$ + n$CaOSiO_2$. Later the anorthite formed from gehlenite, aluminium and silicon remaining from the metakaolinite and the quartz via the equation as follows; $Ca_2Al_2SiO_7$ + 3SiO_2 + Al_2O_3 →2$CaAl_2Si_2O_8$ (Traore et al, 2003, and the references therein). Absence of the mullite phase in the fired bodies is possibly due to the our body compositions are near to the anorthite field (Figure 2).

Table 4 represents, the technical properties of fired bodies. The interplay between waste material types, their proportions, and firing temperature significantly influences the technical properties of the ceramic bodies. As the firing temperature increases, linear shrinkage (LS) and bulk density (ρ) generally rises across all samples. Likewise, water absorption (WA) decreases consistently with rising temperature, reflecting improved vitrification and reduced porosity across all samples.

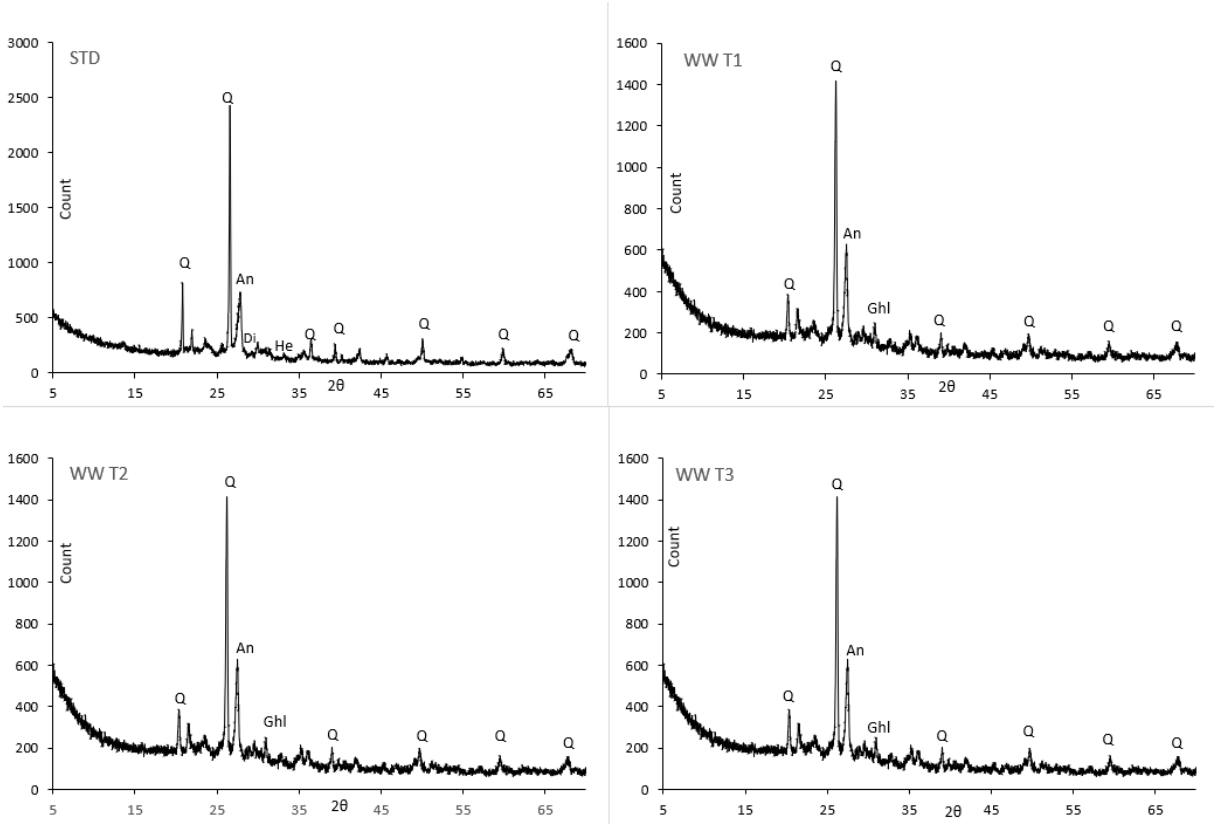


Figure 1. Mineral phases of the STD and WWT1 to WWT3 (XRD Cu Kα)

Meanwhile moisture expansion (MA), a critical factor in the durability of ceramics, is most pronounced at lower firing temperatures and in compositions with higher fly ash content, as seen in WWT1 and WWT2. This suggests that while fly ash aids in densification, it may also increase moisture sensitivity unless adequately vitrified at higher temperatures. In contrast, WWT3, which incorporates boric waste and a reduced amount of fly ash, shows significantly lower moisture expansion, particularly at higher firing temperatures. This indicates that boric waste effectively enhances moisture resistance, likely due to its fluxing properties that promote early vitrification and reduce porosity.

For better comparison, Figure 3a represents, the Moisture adsorption behaviour of formulations prepared with different waste materials.

The type of waste material used is a crucial factor in determining how the material behaves across different temperature ranges. As discussed, WWT1 and WWT2 show high moisture adsorption at lower temperatures, while it is minimised for comparison WWT3. These findings emphasize the importance of carefully selecting waste materials based on the desired moisture expansion properties for specific applications.

Figure 3b represents the relationship between temperature and two key properties, linear shrinkage and water absorption, for the different ceramic formulations: STD, WWT1, WWT2 andWWT3.

All formulations exhibit an increase in linear shrinkage as the temperature increases from 1100°C to 1160°C. This is expected as higher temperatures typically cause more significant densification in ceramics, leading to greater shrinkage. WWT3 formulation shows the similar linear shrinkage with the STD, particularly at 1160°C. However, the behaviour for WWT1 and WWT2 seems even better than that for STD, with a very stable shrinkage over the whole temperature range and similar values to STD in the central zone (1120-1140 °C).

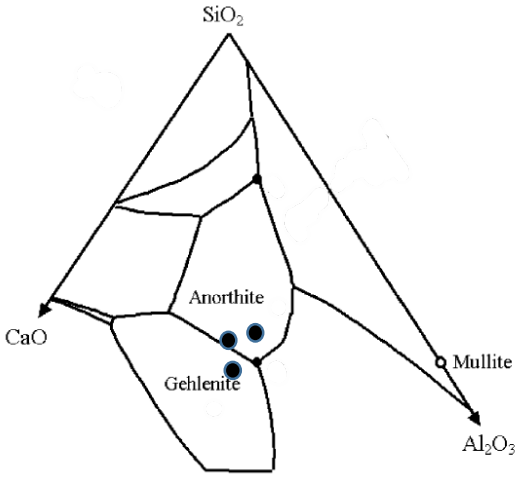


Figure 2. Ternary phase diagram of the SiO_2-CaO-Al_2O_3 (Osborn and Muan, 1960) and the stability fields of the gehlenite and the anorthite. Black dotes denote the general composition of the body recipes.

Table 4. Technical Properties of Fired Bodies (Temp: Temperature, L.S.: Linear Shrinkage, W.A.: Water Absorption, M.A.: Moisture Adsorption, D: Density)

Body	Temp. (°C)	L.S. (%)	W.A. (%)	M.A. (%)	ρ (g/cm3)
STD	1100	0.5	21.8	5.1	1.68
	1120	0.7	21.3	4.6	1.69
	1140	1.1	20.1	2.7	1.71
	1160	2.2	17.6	0.0	1.77
WWT1	1100	0.7	20.1	8.1	1.71
	1120	0.8	19.9	6.1	1.71
	1140	0.9	19.6	4.0	1.71
	1160	1.2	18.4	1.0	1.73
WWT2	1100	0.9	18.7	9.3	1.72
	1120	0.9	18.8	6.0	1.72
	1140	0.9	18.4	4.3	1.73
	1160	1.1	17.3	0.9	1.74
WWT3	1100	1.0	19.3	1.8	1.72
	1120	1.2	19.1	0.9	1.73
	1140	1.5	18.2	0.0	1.75
	1160	2.3	15.6	0.0	1.80

On the other hand, the water absorption percentage generally decreases as the temperature increases for all formulations. This is due to the reduction in porosity as the material densifies, reducing the capacity to absorb water. The standard formulation (STD) has the highest water absorption across all temperatures, indicating that it remains more porous than the formulations containing waste materials. Anyway, all the compositions have a water absorption higher than that specified for porous wall tiles (10%).

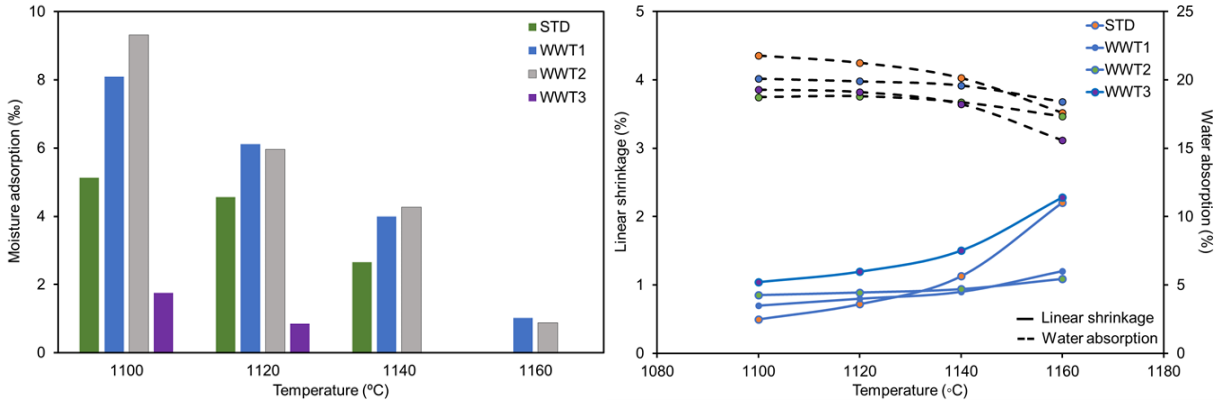


Figure 3a, b. Moisture Adsorption of Fired Bodies (a), Water Absorption and Linear Shrinkage Of Fired Bodies (b)

3. Conclusions

Model wall tile formulations were developed by simply using different industrial wastes and appropriate amount of clays. These new formulations show similar firing behaviour and consequently technological properties to the traditionally industrial compositions. Concretely, linear shrinkage, water absorption, bulk density and moisture adsorption of laboratory test pieces have been characterized as a function of the maximum firing temperature.

New recipes are expected to provide ease of operation, reduce company cost and contribute to environmental sustainability of the manufacturing process. However, further modifications on shaping and sintering conditions and also trials are required in order to confirm the suitability of new recipes for industrial applications.

Acknowledgments

This research has been performed at Kaleseramik Tile Factories and Kaleseramik Research and Development Center that was supported by Ministry of Science, Industry and Technology, Republic of Turkey.

References

Garcia, R.A., Domingues, R.C., Aguilar-Elguezabal, A., Bocanegra, B.M. (2008). *Use of thermally treated bentonitic clay in ceramic tile formulation.* X World Congress on Ceramic Tile Quality, QUALİCER 2008, Castellón (Spain).

Kayacı, K., Ergin, H., Altıntaş, A., Genç, Ş.C., Eker, A., Türek, Ş., Kılıç, M., Durgut, E. (2014). *The Recycling of Ceramic Sludge Waste to Produce Alternative Eco-Products.* Eurasia Waste Management Symposium, 153-162.

Kayaci, K., Küçüker A.S., Genc, S.C., Kara, A. (2010). *Utilization of a sandy clay in double – fired wall tile bodies.* Industrial Ceramics, 30(1), 7-15.

Kayacı, K., Yıldırım, Y., Genç, Ş.C., Keskin, A., Çırpın, A. (2019). *Investigation of the Possibilities of Using Cake and Ceramic Sanitary Ware Fired Cracked Wastes in Porcelain Tile Bodies of Ceramic Tile Factories.* Afyon Kocatepe University Journal of Science and Engineering, 19, Special Issue, 353-358.

Osborn, E.F., A. Muan, A. (1960). *System SiO2–CaO–Al2O3. Phase equilibrium diagrams of oxide systems, Fig. 630,* Am. Ceram. Soc.

Rahmannan, B., Sundaram, C.K, Viruthagiri, G., Shanmugam N. (2013). *Effects of fly ash addition on the mechanical and other properties of ceramic tiles*. International Journal of Latest Research in Science and Technology, 2(1), 486–491.

Sanchez, E.; GAarcia, J.; Sanz, V.; Ochandio, E. *Raw material selection criteria for the manufacturing of ceramic paving and tiling*. I World Congress on Ceramic Tile Quality, QUALICER 1990, Castellón (Spain)

Sanchez, E.; Sanz, V.; Castellano, J.; Sima, A.; Caillet, S.; Poilly, C.; Azar, M. (2024). *Design Of Hypocarbonic Wall Tile Compositions Based on Talc*. XVIII World Congress on Ceramic Tile Quality, QUALICER 2024, Castellón (Spain)

Sousa, S.J.G., Holanda, J.N.F. (2005). *Sintering behavior of porous wall tile bodies during single firing process.* Materials Research, 8(2), 197-200.

Tarhan, B., Tarhan, M., Aydin, T. (2017). *Reusing sanitary ware waste products in glazed porcelain tile production.* Ceramics International, 43(3), 3107-3112.

Torres, P., Manjate, R.S., Quaresma, S., Fernandes, H.R., Ferreira, J.M.F. (2007). *Development of ceramic floor tile compositions based on quartzite and granite sludge.* Journal of the European Ceramic Society, 27(16), 4649–4655.

Traore, K., Kabre, T.S., Blanchart, P. (2003). *Gehlenite and anorthite crystallisation from kaolinite and calcite mix*. Ceramics International, 29, 377–383.

Traore, K., Quedraogo, G.V., Blanchart, P., Jenot, J.P., Gomina, A.P. (2007). *Influence of calcite on the microstructure and mechanical properties of pottery ceramics obtained from a kaolinite-rich clay from Burkina Faso*, Journal of The American Ceramic Society, 75(5), 84-86.

Comparison of Gravity and Flotation Methods for Gold Recovery from Pyrite Ores

Ceyda Şavran [1]*, Tülay Türk [1], Alim Gül [1], M.Olgaç Kangal [1]

[1]Istanbul Technical University, Department of Mineral Processing Engineering, Maslak, İstanbul, TÜRKİYE

*Corresponding author: savranc15@itu.edu.tr (Ceyda Şavran)

Abstract:

The evaluation of pyrite ores and the recovery of valuable metals from these residues are becoming more important in gold mining. Therefore, the effective processing of pyrite ores offers significant economic and environmental advantages. Recovering gold from pyrite ores extends the lifespan of mining sites while providing sustainable solutions for waste management. In this study, experiments were conducted to characterize pyrite tailings from Kazakhstan and recover high-content gold (Au) concentrates. Following characterization, various gravity methods and flotation experiments were conducted. The chemical analysis of the run-of-mine ore revealed that it contained 71.40% SiO_2, 6.81% Al_2O_3, 6.04% Fe_2O_3, and 0.765 ppm Au. In the experiments, gold recovery was investigated using a shaking table for particles below 1 mm, and Falcon, Knelson concentrators for particles below 100 microns, based on specific gravity differences and flotation experiments on particles below 100 microns. The gold contents in the shaking table, Falcon, and flotation processes were calculated to be 5.79 ppm, 8.79 ppm, and 16.2 ppm, with recoveries of 68.2%, 86%, and 86.5%, respectively. The results indicated that the optimal outcome in terms of content and recovery was achieved with the Knelson concentrator. Experiments using the Knelson concentrator resulted in a concentrate with a gold content of 19.8 ppm and a recovery rate of 81%, while 95.8% of the material, containing 0.21 ppm Au, was removed as tailing. Based on the optimal flow sheet, it was deemed appropriate to use a two-stage Knelson concentrator to obtain high-content Au concentrate from the pyrite tailings in Kazakhstan.

Keywords: *pyrite, gold, physical enrichment, flotation*

1. Introduction

Pyrite, commonly referred to as “Fool’s gold,” is one of the most abundant sulfide minerals in the Earth's crust, with the chemical formula FeS_2. It typically exhibits a cubic crystal structure, though it can also occur in densely packed, spherical aggregates known as framboids [1][2]. Pyrite formation is prevalent in hydrothermal, metamorphic, and sedimentary deposits. In hydrothermal environments, pyrite is often found in association with other sulfide minerals, oxides, quartz, and other silicates. In metamorphic rocks, it frequently forms as a product of metamorphism, while in sedimentary settings, such as coal seams and sedimentary deposits, pyrite often occurs as massive accumulations, nodules, or lenticular bodies, its formation closely tied to the presence of organic matter [3]. Pyrite (FeS_2) is also a significant host for gold (Au) in various hydrothermal gold deposits. Gold is commonly found in "invisible" form within arsenian pyrite, where arsenic (As) substitutes for iron (Fe) or sulfur (S) within the pyrite lattice. This substitution induces lattice distortions, especially when As replaces S, which plays a critical role in the incorporation of gold, likely due to surface speciation and associated structural modifications [4][5]. In flotation concentrates derived from beneficiation plant tailings, typical compositions include 3 to 5 g/t of gold, 0.7–2.0% copper, and 2–3% zinc. These gold-bearing sulfide concentrates are predominantly composed of pyrite and arsenopyrite, with gold occurring primarily in finely disseminated form, closely associated with the sulfide minerals. Only a small proportion of the gold exists in free form [6]. Gravity concentration techniques are frequently employed for the recovery of free gold and gold associated with dense minerals such as sulfides and titanium-bearing minerals. The use of centrifugal concentrators, including Knelson and Falcon units, has significantly improved recovery efficiency. Flotation, often employed as a pre-concentration method before cyanide leaching or oxidative pretreatment, uses xanthates as the primary collectors for gold- and silver-bearing sulfides.

The development of specialized collectors, such as dithiophosphates, has further enhanced gold extraction in many applications. A combination of gravity concentration and flotation proves particularly effective for ores with a wide range of gold particle sizes [7]. Separation methods based on specific gravity and flotation are the most commonly employed techniques for the pre-enrichment of gold. In this study, experimental work was conducted using tailings from a beneficiation plant processing sulfide ores from the Kazakhstan region. Physical methods, including shaking tables, Falcon concentrators, and Knelson concentrators, as well as physico-chemical methods, such as flotation, were utilized to pre-enrich the gold content before proceeding with chemical beneficiation.

2. Material & Method

2.1. Material

In this study, pyrite tailings obtained from the Kazakhstan region was examined. Initially, a sieve analysis was conducted to determine the particle size of the sample. The sieve analysis data and graph are presented in Table 1 and Figure 1, respectively.

Table 1. Sieve analysis of the ore

Particle size, mm	Weight, %	Undersize, %
+1	1.0	100.0
-1+0.5	4.5	99.0
-0.5+0.42	2.4	94.5
-0.42+0.3	18.8	92.2
-0.3+0.212	14.3	73.4
-0.212+0.106	29.4	59.1
-0.106+0.074	6.7	29.7
-0.074+0.038	7.0	23.0
-0.038	16.1	16.1
Total	100.0	

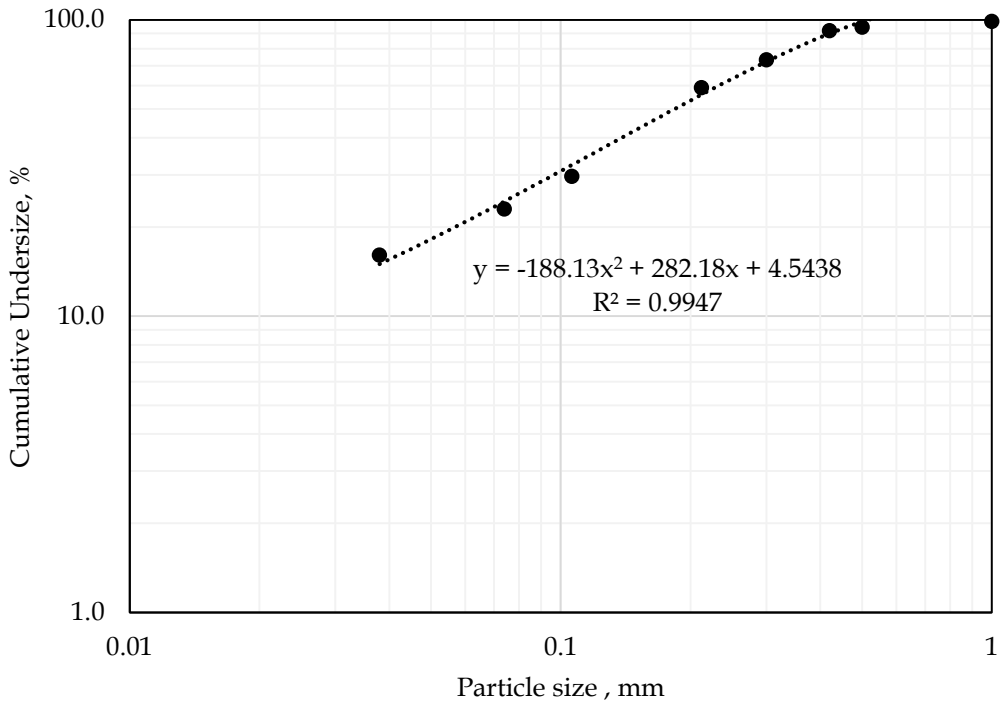


Figure 1. Cumulative undersize graph of the ore

Upon examining the sieve analysis graph, the d_{80} size of the material was determined to be about 348 micron. Subsequently, an ICP analysis was performed to identify the chemical composition of the sample. The results of this analysis are presented in Table 2.

Table 2. Chemical Analysis Results of the Representative Sample Measured by ICP Analysis

Component	Content, %	Element	Content, ppm	Element	Content, ppm
SiO_2	71.4	Au	0.765	Rb	70
Al_2O_3	6.81	Ag	11.2	Sb	25.1
Fe_2O_3	6.04	As	57	Sc	6.3
MnO	0.12	Ba	7260	Sr	164
MgO	3.54	Cd	39.3	Th	5.2
Cao	1.78	Co	12	V	35
Na_2O	0.22	Cr	27	Y	22
K_2O	1.83	Cu	927	Zn	9680
TiO_2	0.27	Hf	3.6	Zr	98
P_2O_5	0.06	Mo	26	La	18.9
LOI	4.98	Ni	30	Ce	38
S	3.30	Pb	2600	Nd	27

The chemical analysis revealed that the material contains 71.40% SiO_2, 6.81% Al_2O_3, and 6.04% Fe_2O_3. Additionally, the ore contains 0.765 ppm Au and 11.2 ppm Ag. For the mineralogical analysis of the sample, the MLA method was employed. According to the results, the sample contains altered Fe hydroxide with low Si content. Smithsonite appears to be altered, containing low amounts of Ca and Fe. Minerals that ore is contained are in Table 3. Based on the table, the most abundant mineral is quartz.

In addition, 8.30% of the ore consists of pyrite, 7.27% of feldspar, and 5.38% of Kammererite. SEM and BSE images are presented in Figure 2.

Table 3. Minerals that ore is contained

Mineral	Quantity, %	Mineral	Quantity, %
Electrum	<0.01	Flogopite/Biotite	2.31
Achantite	<0.01	Muscovite	4.41
Chalcopyrite	0.14	Kammererite	5.38
Sphalerite	0.51	Illite	1.30
Tenantite/Enargite	0.00	Si-Al Clays	0.25
Pyrite	8.30	Epidote	0.25
Galena	0.18	Zircon	0.00
Barite	4.48	Apatite	0.10
Fe Ox./Hydrox.	0.14	Calcite/Dolomite	3.49
Rutile	0.32	Siderite	0.59
Quartz	56.87	Seruzite	0.08
Feldspar	7.27	Smithsonite	1.67
Talc	1.08	Sulfide-Silicate structure	0.35
Pyroxene	0.07	Others	0.45
		Total	100.00

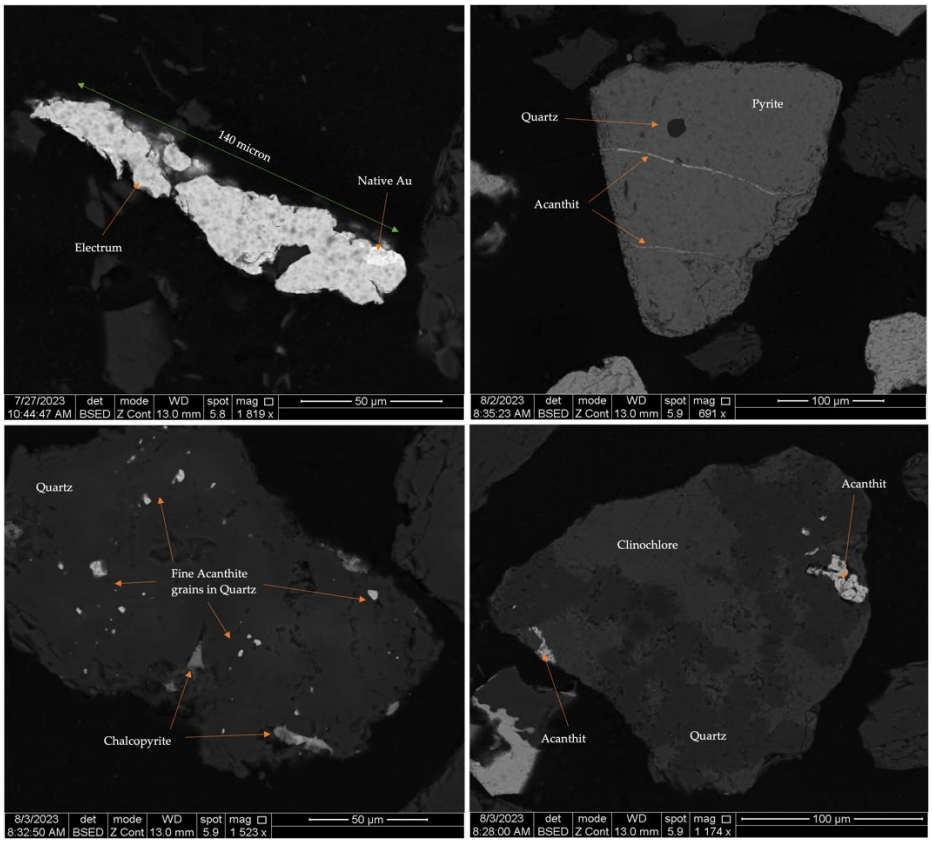


Figure 2. BSE images of gold and achantite particles

One nugget gold grain is seen in BSE images. In addition to Electrum, Ag appears as Acanthite as well. The EDS analyses (Figure 3) conducted on the representative sample clearly show the presence of Au and Ag peaks.

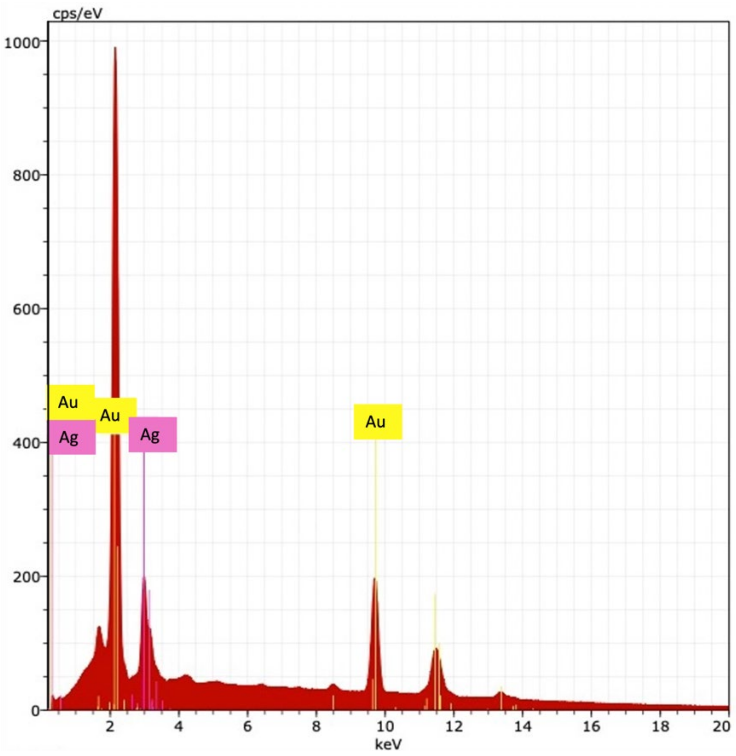


Figure 3. EDS analyses of gold and silver

2.2. Method

Two different beneficiation methods were applied to the ore: gravity separation and flotation. For the gravity experiments, a shaking table was used for coarse particle sizes, while centrifuge-based Knelson and Falcon devices were chosen for finer particle sizes. The original sample, with 99% by weight under 1 mm, was classified into size fractions of -1+0.3 mm, -0.3+0.106 mm, and -0.106+0.038 mm, and then subjected to shaking table experiments.

For the experiments with the Falcon concentrator, the sample was ground under controlled conditions in a ball mill for 20+25 minutes to achieve a particle size of less than 100 microns. The variable parameters in the experiments were determined as "G" values (centrifugal force) and wash water flow rates. The heavy product, which was planned to be collected as the concentrate, was subjected to cleaning stages at centrifugal forces of 300, 200, and 100 G, respectively. During these stages, wash water was applied at flow rates of 3, 2, and 1.8 L/min. For the scavenging process applied to the light product, three stages of scavenging were performed at 300, 300, and 200 G, with wash water flow rates of 3.2, 2.8, and 2.8 L/min.

The Knelson concentrator tests were conducted with a representative sample that was ground under controlled conditions to achieve a particle size of below 100 microns. These tests were performed at 60 G values and with a wash water pressure of 3 psi.

For the flotation experiments, the same ground sample was used. The tests were carried out under different stages and conditions. A flotation scheme consisting of one rougher stage and two cleaning stages was applied. Sodium silicate (Na_2SiO_3) was used as a dispersant, while Aero 3418A and Aero 238 were used as collectors, and MIBC was used as a frother. In the flotation tests, Aero 238 and Aero 3418A collectors were used in a 1:1 ratio, with a total dosage of 250 g/t in the rougher circuit. In the cleaning stages, the use of collectors continued, but the dosage was reduced to 50 g/t in the first cleaning and 25

g/t in the second cleaning. pH is kept 5 in all stages. The concentrate was floated for a total of 12 minutes in the rougher stage, 9 minutes in the first cleaning stage, and 6 minutes in the second cleaning stage.

3. Results&Discussion

3.1. Results of Shaking Table Experiments

The results of the experiments conducted using the shaking table for different size fractions are presented in Table 4.

Table 4. Results of shaking table experiments according to feed

Particle size, mm	Products	Weight, % (Tot.)	Au Content, ppm	Recovery, % (Tot.)
+1	**Total**	1.2	0.68	0.8
-1+0.3	Concentrate	0.7	19.65	13.4
	Middling	3.1	1.56	5.0
	Tailing	20.5	0.39	8.2
	Total	**24.2**	**1.06**	**27.4**
-0.3+0.106	Concentrate	6.0	5.62	34.8
	Middling	1.6	0.27	0.5
	Tailing	41.1	0.12	5.2
	Total	**48.8**	**0.80**	**40.5**
-0.106	Concentrate	4.7	4.09	20.0
	Middling	2.0	3.22	6.7
	Tailing	9.8	0.17	1.8
	Total	16.5	1.66	28.5
Slurry	**Total**	**9.3**	**0.37**	**3.6**
TOTAL		**100.0**	**0.97**	**100.0**

Upon examining the results, it is observed that the particle size of -1+0.3 mm achieved the highest Au content (19.65 ppm), though the recovery remained at 13.4%. Additionally, the Au content in the concentrates from other size fractions was obtained as 5 and 4 ppm with the recovery of 35% and 20%, respectively. When all the concentrates were combined, a product with 5,85 ppm Au content was obtained with a total recovery of 68,2%. Therefore, it can be concluded that the shaking table did not yield the expected results. The insufficient liberation at larger particle sizes and the encapsulation of gold are considered to be the probable reasons for the low recovery rates.

3.2. Result of Falcon Concentrator Experiments

In the experiments conducted using the Falcon centrifugal separator, concentrate, intermediate product, and tailings were obtained as a result of three stages of cleaning and scavenging processes. After the middling products have been allocated to concentrate and tailings based on calculations, the content and recoveries of the products are presented in Table 5.

Table 5. Results of Falcon concentrator experiments

Products	Weight, %	Au Content, ppm	Recovery,%
Concentrate	11.0	7.47	86.3
Tailing	89.0	0.146	13.7
TOTAL	100.0	0.95	100.0

The concentrate with an Au content of 7.47 ppm was recovered with an efficiency of 86.3%, while a total of 89% of the material obtained as a tailing with the Au content of 0.146 ppm. Despite an improvement in recovery rates following size reduction after the shaking table process, the Au content remained below the desired levels with Falcon concentrator.

3.3. Results of Knelson Concentrator Experiments

Using the Knelson concentrator, three stages of cleaning and one stage of scavenging were performed. The G values and water flow rates in the concentrator were kept constant at 60 G and 3 psi, respectively.

Table 6. Results of Knelson concentrator experiments

Products	Weight, %	Au Content, ppm	Recovery,%
Concentrate	4.2	19.80	80.9
Tailing	95.8	0.21	19.1
TOTAL	100.0	1.03	100.0

The concentrate obtained showed an Au content of 20 ppm, with a recovery of 81%. Additionally, the Au content in the tailings was reduced to a low value of 0.21 ppm (see Table 6). Despite the increase in Au loss in the tailings, the Au content obtained in the concentrate was higher compared to other devices. Additionally, the recovery rate remained at the desired level.

3.4. Results of Flotation Experiments

In the flotation experiments, the floated product was planned to be collected as the concentrate. Two stages of cleaning were applied to the floated product. The content and recoveries of the products obtained from the experiments are presented in Table 7.

Table 7. Results of flotation experiments

Products	Weight, %	Au content, ppm	Recovery, %
Concentrate	7.1	16.20	86.5
Middling 1	1.1	1.13	0.9
Middling 2	6.8	0.50	2.6
Tailing	85.0	0.16	10.0
TOTAL	100.0	1.32	100.0

The results indicate that, from flotation tests conducted with material ground to below 100 microns, a concentrate was obtained with 7.1% yield, an Au content of 16.2 ppm, and an Au recovery of 86.5%. Although higher recovery rates were achieved with flotation compared to Knelson, the content did not reach the same level.

In the project focused on the evaluation of pyrite tailings, various gravity separation and flotation methods were applied. According to the results obtained, the most optimal outcome in terms of content and recovery was achieved using the Knelson concentrator. The experiments conducted with the Knelson concentrator yielded a concentrate with 19.8 ppm Au content and a 4.2% weight yield, with an Au recovery of 81%, while the tailings with 0.21 ppm Au content and 95.8% weight were effectively removed from the system.

Based on these results, the proposed flow sheet for the most economical recovery of Kazakh pyrite tailings is shown in Figure 4. When all methods are compared, the experiments using the Knelson concentrator and flotation achieved the highest content and recovery. The Knelson gravity method, being less costly compared to flotation, was therefore preferred. As illustrated by the optimal flow sheet, a 2-stage Knelson concentrator is required to obtain a high-grade Au concentrate from Kazakh pyrite tailings.

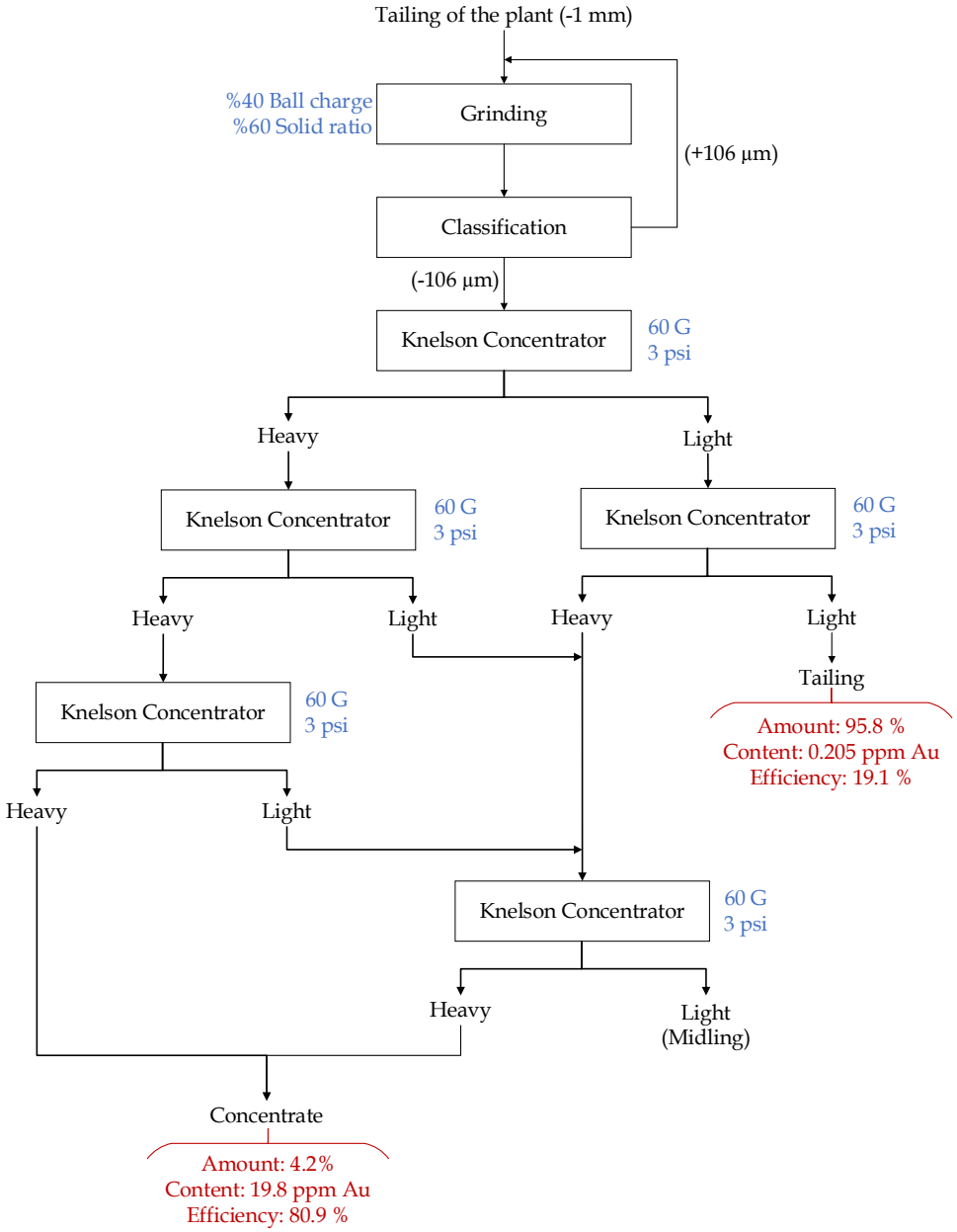


Figure 4. Proposed flowsheet

Pyrite is commonly found in the processing residues of sulfide ores. In cases where this pyrite contains gold, the recovery of gold holds significant economic and environmental importance. This recovery process facilitates the optimal utilization of enriched ore deposits and promotes the efficient management of natural resources. Additionally, the treatment and recovery of waste materials contribute to minimizing environmental impacts.

4. Conclusion

As mining activities continue to generate increasing volumes of waste and valuable mineral resources become more limited, there is a growing focus on environmentally sustainable and economically viable approaches to mineral processing. Gold, particularly when present in ultrafine particles, is typically recovered using chemical methods. However, in some gold processing plants, ores with low gold content undergo pre-enrichment to improve recovery efficiency. Pre-enrichment techniques commonly involve the use of flotation methods or centrifugal concentrators, such as the Knelson concentrator. This study aimed to explore strategies for both the utilization of mining waste and the creation of alternative sources for the recovery of valuable minerals. The results demonstrated that the Knelson concentrator yielded the most optimal outcome when compared to other methods tested. Although the gold content in the final product was insufficient for direct gold production, the pre-concentrated material was found to be suitable for further chemical processing. This provides a viable pathway for the recovery of valuable minerals while contributing to more sustainable mining practices.

4. References

[1] Craig, J. R., Vokes, F. M., & Solberg, T. N. (1998). Pyrite: physical and chemical textures. *Mineralium Deposita*, *34*, 82-101.

[2] Wilkin, R. T., Barnes, H. L., & Brantley, S. L. (1996). The size distribution of framboidal pyrite in modern sediments: an indicator of redox conditions. *Geochimica et cosmochimica acta*, *60*(20), 3897-3912.

[3] Ma, S., Shi, M., Zhang, C., & Cao, Q. (2023). Mineralogical Characteristics and Genetic Types of Pyrite with Different Occurrence: Constraints from Spectroscopy, Geochemistry and δ34S Stable Isotopes. *Minerals*, *14*(1), 52.

[4] Large, R. R., & Maslennikov, V. V. (2020). Invisible gold paragenesis and geochemistry in pyrite from orogenic and sediment-hosted gold deposits. *Minerals*, 10(4), 339.

[5] Wu, Y. F., Evans, K., Hu, S. Y., Fougerouse, D., Zhou, M. F., Fisher, L. A., ... & Li, J. W. (2021). Decoupling of Au and As during rapid pyrite crystallization. *Geology*, 49(7), 827-831.

[6] Surimbayev, B., Akcil, A., Bolotova, L., Shalgymbayev, S., & Baikonurova, A. (2024). Processing of refractory gold-bearing sulfide concentrates: A review. *Mineral Processing and Extractive Metallurgy Review*, *45*(6), 573-591.

[7] Young, C. A. (2019). *SME mineral processing and extractive metallurgy handbook*. Society for Mining, Metallurgy & Exploration.

Research and Application of Enrichment Methods for Gold in Refractory Form Found in Pyrite and Arsenopyrite Minerals

Alperen KÖLE [1]*, Ahmet YAKAR [1], Kutay AYDINBURUN [1], Hande Burçin HARMANCI [1], Begüm ÖZDUR [1], Mustafa ÖZTÜRK [1], İbrahim GÖKTAŞ [1]

[1] ETİ BAKIR Research & Development Center

*Corresponding author: alperen.kole@etibakir.com.tr (Alperen KÖLE)

Abstract:

Gold can be found within different mineralogical formations. These different formations determine theenrichment method of gold. Nowadays, gold enrichment is mainly done by the cyanidation (leach) method. However, if gold is found in refractory form within pyrite and arsenopyrite, it cannot be directly extracted with the leach method. In order to enrich the gold found in arsenopyrite and pyrite, a pre-enrichment process is applied using the flotation method followed by pyrometallurgical or hydrometallurgical processes.

Refractory gold ores can be encountered in facilities currently operating with the leach method. Although these ores have high gold grades, when fed into the leach system, they cause a decrease in recovery efficiency. In order to extract the gold that cannot be obtained with the existing enrichment system, revisions and changes may be necessary in the plant process flow diagram.

In this study, experiments were conducted for the enrichment of the Prevanly gold ore belonging to ETICopper Inc.'s Tereksay Operation. As a result of studies conducted with optical and scanning electron microscopes, native gold was not found. It was determined that gold was refractory in sulfide minerals.Additionally, gangue minerals in the ore are mainly composed of quartz, muscovite, and dolomite mineral structures. Samples that reached gold recovery efficiencies of 20-25% through bottle-roll tests were subjected to flotation. After flotation tests, gold recovery efficiency was achieved as 90-95%. The concentrate is planned to be sent to the smelter. Therefore, the high gold content in the concentrate is important in terms of transportation and smelting costs.

Keywords: *Gold, refractory gold, pyrite, arsenopyrite, flotation, hydrometallurgy, pyrometallurgy*

1. Introduction

Eti Bakır A.Ş. Gold mining operations are carried out using the tank leaching method at the Kyrgyzstan Tereksay plant. However, the gold ore found in a certain part of the region cannot be obtained directly by the leaching method because it is in refractory form. First, representative samples were prepared by mixing the samples taken from the relevant region in proportion to their weight. As a result of chemical and mineralogical analyses, it was determined that the ore contained 2.99 ppm gold. When the ore microscope and SEM-MLA results were examined, 70-75% free pyrite and arsenopyrite minerals were found. In the samples where 20% recovery efficiency was achieved in the bottle tests, 85% gold recovery efficiency was achieved after the flotation process.

In this study, it was aimed to enrich the Prevanly ore by flotation method and make it marketable. Flotation experiments were carried out to determine the ideal flotation conditions of samples taken from the relevant region. As a result of two locked-cycle tests, the concentrate with 27.45 ppm gold grade was produced with 81.86% recovery, and the concentrate with 32.03 ppm gold grade was produced with 65.48% recovery.

2. Material and methods

2.1. Material

Samples taken from Prevanly Region were crushed with the help of laboratory type crushers. All samples reduced to under 3.35 mm were divided homogeneously. ristics of experimental sample

2.2. Characteristics of experimental sample

2.2.1. Chemical analysis results

As a result of the analysis, it was determined that the sample contained high amounts of clay and silicate minerals. Gold determination by cupellation method determined that the sample contained 2.99 g/t gold. The graphic showing the analysis results is given in Figure 1.

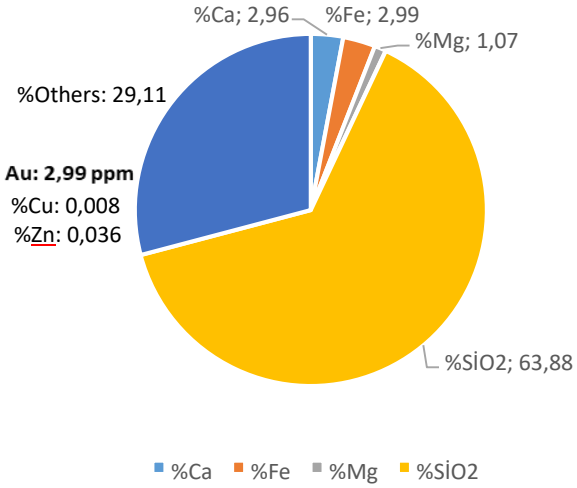


Fig. 1. Chemical analysis results of Prevanly feeding sample

2.2.2. Mineralogical analysis results

Microscope images show that in Figure 2 pyrite and arsenopyrite minerals are liberated in coarse sizes.

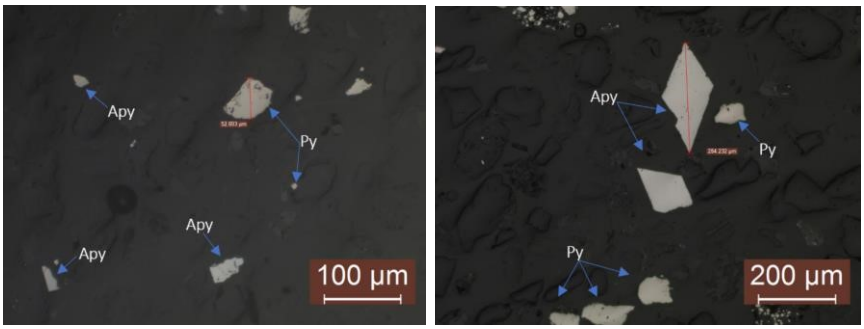


Fig. 2. Microscope images of sample

Samples separated into size fractions were poured into molds and separate bakelite was prepared for each fraction. After the surface of the prepared bakelite was coated with carbon, mineralogical examinations were carried out with the help of scanning electron microscope (SEM).

To determine the liberation degrees of the minerals in the sample, MLA (Mineral Liberation Analysis) software within the scanning electron microscope was used.

As seen in Table 1 and Table 2, pyrite and arsenopyrite minerals are completely liberated at the rates of 65-75% in all size fractions.

Table 1. Pyrite liberation degrees according to size fractions

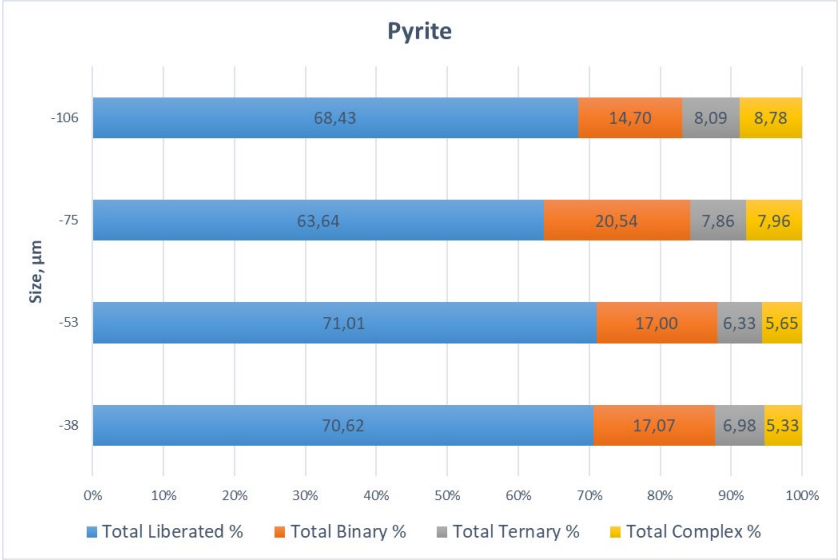
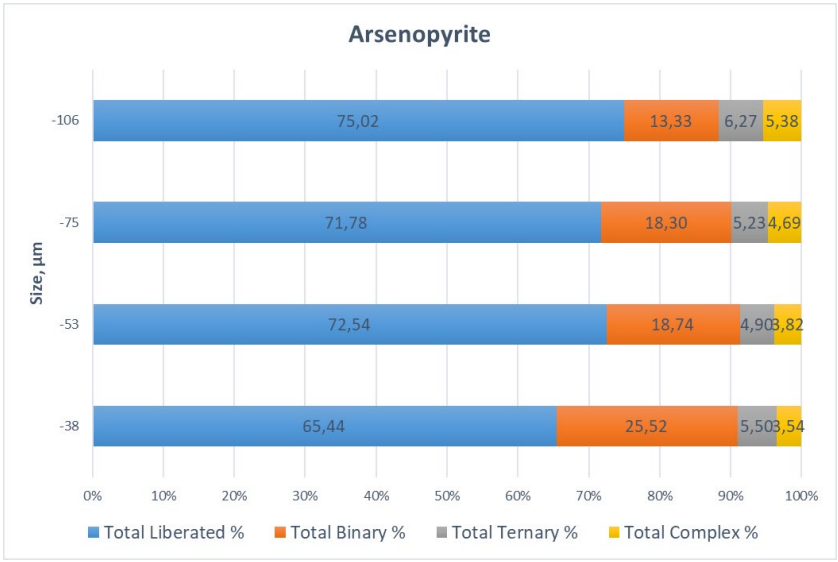


Table 2. Arsenopyrite liberation degrees according to size fractions



2.3. Method

2.3.1. Flotation test procedure

In the experiments, Denver-type flotation cells of the Ünal brand were utilized. Xanthate (SBX) was used as the collector, MIBC as the frother, and Aero MaxGold900 gold collector was employed with the aim of enhancing gold recovery efficiency. The particle size determined from the experiments was d80: 106 microns. All tests were conducted at natural pH (8.40–8.60). The collector dosages were set at a total of 125 g/t of SBX and 60 g/t of MIBC.

2.3.2. Locked – cycle flotation tests

In open circuit experiments, after determining all parameters, two closed circuit flotation tests were conducted. The closed-circuit tests were performed to obtain values closer to the operational conditions of the facility. Both tests were completed in six cycles. In the first test, the MaxGold900 gold collector was used, while in the second test, only xanthate was employed as the collector. These experiment's flowsheet is shown in Figure 3.

To increase the concentrate grade and reduce transportation costs, the aim was to reduce the amount of concentrate. Consequently, a decision was made to conduct a second closed circuit flotation test in pursuit of this objective. The experimental results indicated that while the MaxGold 900 gold collector improved recovery, it reduced selectivity. Therefore, in the second test, only SBX collector was used. It was observed that flotation kinetics slowed when no gold collector was used, which led to an extension of the rougher flotation time.

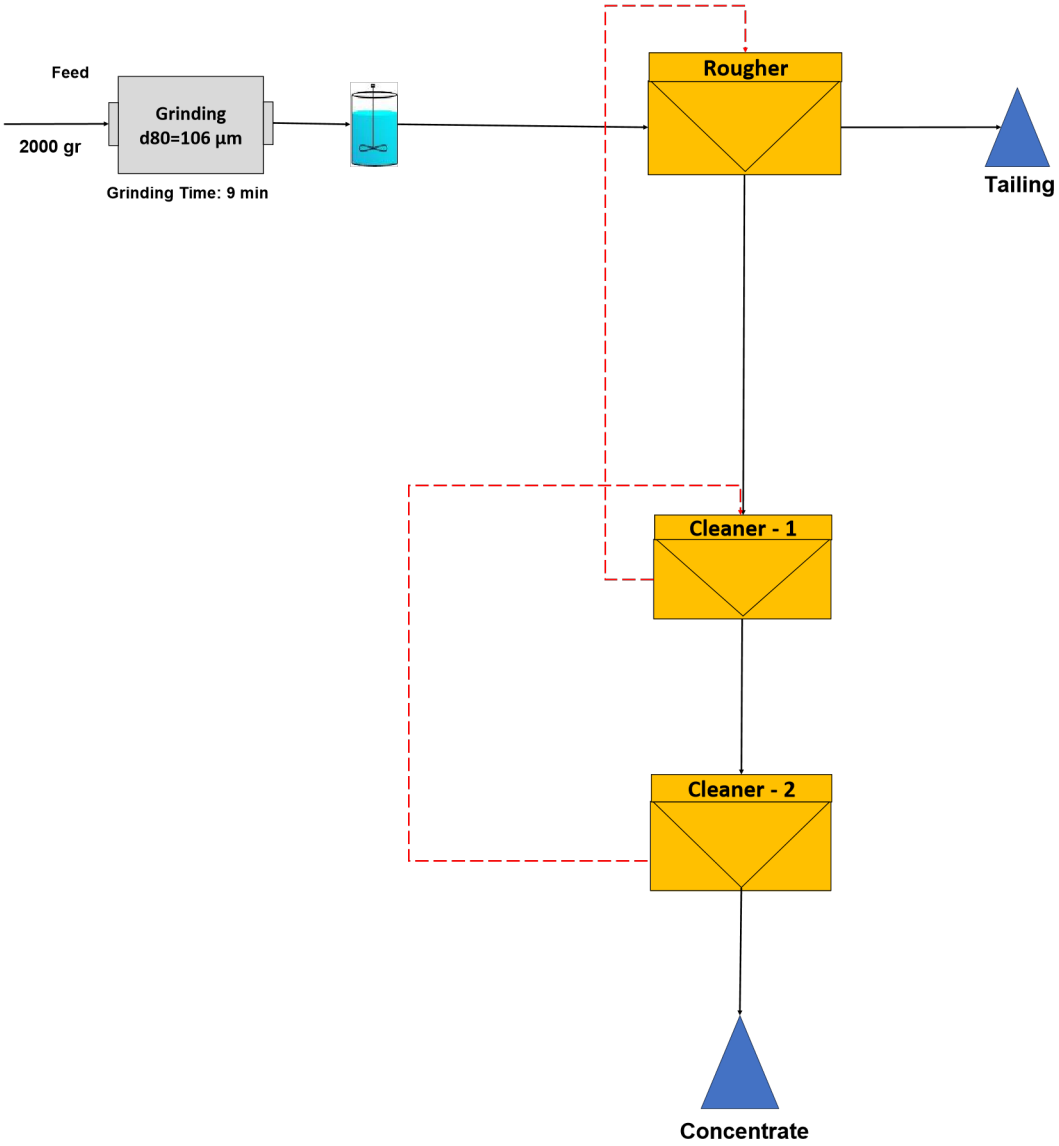


Fig. 3. Locked – cycle test's flowsheet

2.3.3. Bottle – roll tests

To recover the gold remaining in the flotation circuit tailings, laboratory-scale cyanide leaching tests were performed. Bottle tests were conducted separately on the tailings from each of the two closed circuit flotation experiments. Given that the flotation process particle size (d80) is 106 microns, particle size reduction trials were also carried out during the leaching process. In this context, the particle size was reduced different particle sizes and experiments were conducted accordingly. Bottle-roll tests were conducted for a total of 48 hours each. In all experiments, the solid ratio was maintained at 40%.

3. Results

3.1. Locked – cycle flotation tests

The results of the first experiment, as shown in Table 1, indicate that a concentrate containing 27.45 ppm gold was achieved with a gold recovery efficiency of 81.90%.

Table 3. The results of first locked-cycle flotation test

Mass, %	Grade		Ppm, %		Products
	S (%)	Au (ppm)	S	Au	
8,41	10,704	27,450	87,08	81,90	Concentrate
91,54	0,146	0,558	12,94	18,12	Tailings
100,0	**1,034**	**2,820**	**100,0**	**100,0**	

In the second experiment, the omission of the gold collector led to a reduction in recovery efficiency, while the gold content of the concentrate increased. As presented in Table 4, a concentrate with a gold concentration of 32.03 ppm was obtained, corresponding to a gold recovery rate of 65.48%.

Table 4. The results of second locked-cycle flotation test

Mass, %	Grade		Ppm, %		Products
	S (%)	Au (ppm)	S	Au	
5,30	19,248	33,619	82,20	65,39	Concentrate
94,70	0,233	0,945	17,80	34,61	Tailings
100,0	**1,241**	**2,677**	**100,0**	**100,0**	

When comparing the two experiments, it is evident that the use of the gold collector resulted in significant changes in the outcomes, as illustrated in Figure 4.

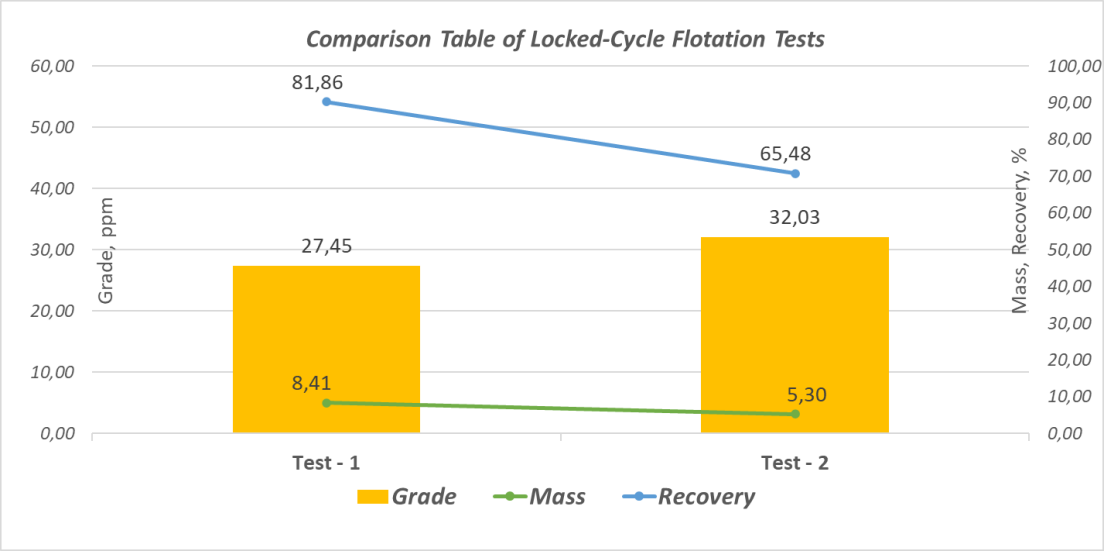


Fig 4. Comparison table of locked-cycle tests

3.2. Bottle – roll test's results

The first locked – cycle test's tail contains 0.558 ppm gold. Tests were conducted using three different particle sizes of bottle tests (d80: 106, 75, 53 microns) to recover the remaining gold from the waste. Experiments were conducted with 750 grams of solid material and a solid content ratio of 40%, with a cyanide dosage set at 1 g/L. The experiments lasted a total of 48 hours. Analysis of the results in Figure 5 reveals that the gold recovery efficiency ranged between 10-13%, and it was observed that as the particle size reduced, the gold recovery efficiency also decreased.

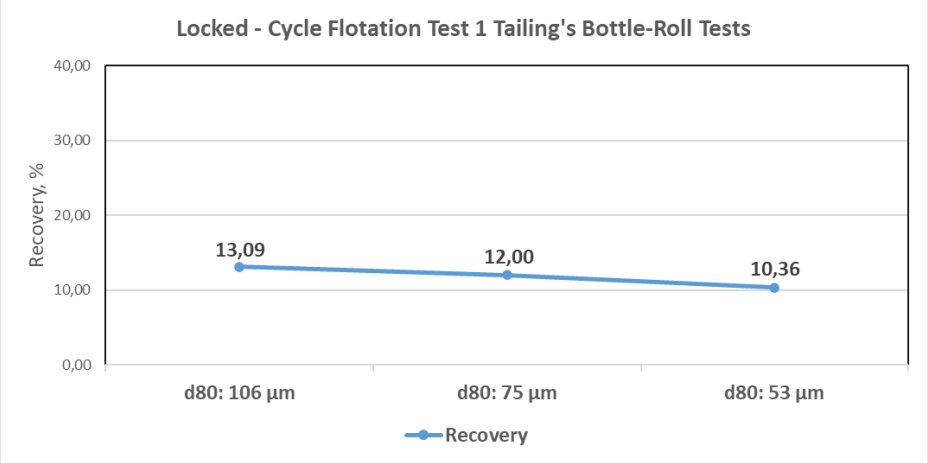


Fig. 5. First locked-cycle test's bottle-roll test's results

Tails from the second closed-circuit experiment, with a gold content of 0.945 g/t, were subjected to two bottle tests with d80 particle sizes of 106 and 45 microns, respectively. All other parameters were consistent with those used in the previous tests. Analysis of the results presented in Figure 6 indicates that the gold recovery efficiencies ranged from 10% to 10.5%.

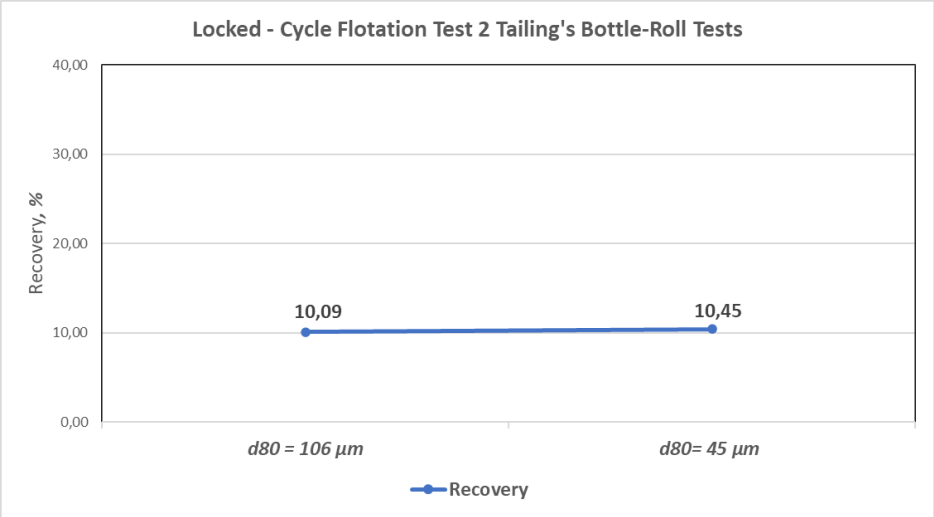


Fig. 6. Second locked-cycle test's bottle-roll test's results

4. Conclusion

In this study, it was observed that the flotation method significantly concentrated the pyrite, arsonopyrite and the gold contained within these minerals. Although the gold collector plays a crucial role in increasing efficiency, it complicates the production of high-grade concentrates. The concentrate requires transportation and further purification through various metallurgical processes. Therefore, the goal is to produce concentrates with high gold content to reduce the cost per ton. In scenarios where the gold collector is not used, the recovery efficiency remains low, resulting in reduced financial returns. The results from the bottle tests on flotation tailings were lower than expected. These experiments aimed to achieve maximum gold recovery efficiency using a flotation + leaching system. However, it has been observed that achieving higher gold recovery efficiencies is not feasible without disrupting the structure of the sulfide minerals in the ore.

Production Of Porphyry Copper Ore Containing Gold And Silver By The Sart Process Method

Gökçe Çıkın [1]*, Sercan Sevgül [1], Serhat Biçer [1], Ruveyda Nur Aytop [1]

[1]Aoza Gold Corporation

*Corresponding author gokce.cikin@kozagold.com (Gökçe Çıkın)

Abstract:

The recent increase in precious metal prices has significantly reduced the ore grades available for extraction, while the occurrence of oxidized gold ores in their pure form has diminished. This has led to a rise in the production of refractory and porphyry-type gold ores.

In this study, the recovery conditions and application areas for gold and silver extraction from a high-copper gold-silver ore using the SART process have been investigated. The high copper content in the ore can be recovered through the SART process, which helps to prevent cyanide consumption that may occur during direct leaching.The core of the process involves the precipitation of copper as Cu_2S by adding sodium hydrosulfide (NaHS) or sodium sulfide (Na_2S) to the leach solution under acidic conditions (pH 4-5). Following this step, the solid material is neutralized, and the production of gold and silver is carried out by adding sodium cyanide (NaCN) under alkaline conditions (pH 10.5-11). Additionally, pilot-scale studies were conducted to examine the chemical principles affecting process performance, along with an analysis of the investment and operating costs associated with the process.

Keywords: *Gold, Silver, Copper, SART Process, Cyanide Recovery*

1. Introduction

In modern mining, the most commonly applied industrial method for gold recovery from ores is cyanide leaching. Particularly in recent years, gold recovery from porphyry-type ores has been increasing. Generally, gold ores that are liberated through grinding can be processed using simple gravity techniques or direct cyanide leaching. When ores from which gold is easily liberated are subjected to leaching for 20–30 hours at a cyanide concentration of 100–250 mg/L and a pH of around 10, gold recoveries exceeding 90% can be achieved. The high solubility of copper minerals in cyanide solutions increases reagent consumption and leads to several technical issues, notably negatively affecting gold recovery (Sceresini and Breuer, 2016; Yılmaz, E., 2018). Due to high cyanide consumption, the use of appropriate cyanide recovery methods for such ores is a technical and economic necessity (Fleming, 2011; Yılmaz, E., 2018). However, the technical challenges encountered in recovering cyanide from high-concentration copper-containing solutions limit the methods applied on an industrial scale.

The SART process (Sulphidisation, Acidification, Recycling, and Thickening) is an industrial method that allows for the recovery of cyanide from high-copper cyanide solutions while also producing copper as a by-product. This process is implemented in various facilities both globally and in our country (Botz et al., 2011; Adams, 2013; Estay, 2018; Yılmaz, E., 2018).

In this study, the behavior of copper minerals in cyanide solutions, the SART process, and pilot-scale applications using different leaching methods have been examined. Additionally, the characteristics and technical performance of industrial-scale SART facilities are presented.

The SART (Sulfidization, Acidification, Recycling, and Thickening) process, used to remove copper from ore, is an effective method particularly for processing oxidized ores in copper production. This method efficiently eliminates unwanted copper from the solution during gold production via cyanide leaching. The SART process reduces cyanide consumption by facilitating the separation of copper from the solution phase and enabling its recovery. The key stages of the SART process are as follows:

Sulphidization: A sulfur-based reagent (usually sodium sulfite or sodium hydrosulfide) is added to the cyanide solution. This reagent reacts with the copper ions in the solution to form copper sulfide (CuS). Copper sulfide is an insoluble compound and precipitates out of the solution.

Acidification: The solution is acidified to stabilize the formed copper sulfide precipitates and ensure the reagent functions effectively. This acidification process is typically carried out by adding sulfuric acid, which completes the precipitation of copper.

Recycling: The precipitated copper sulfide is separated from the solution phase using mechanical or chemical methods. The separated copper sulfide undergoes further purification processes to recover metallic copper. Additionally, cyanide in the solution can also be recovered at this stage and reused in the process.

Thickening: The recovered solution undergoes a thickening process to reduce the amount of water and concentrate it further. This process enhances the recovery efficiency of valuable metals in the solution and allows it to be fed back into the process.

A flowchart illustrating the key steps of the process is presented in Figure 1. During the sulfidization stage, Na_2S or typically NaHS is added to the cyanide solution. Hydrogen sulfide (H_2S) gas can also be used as a sulfur source.

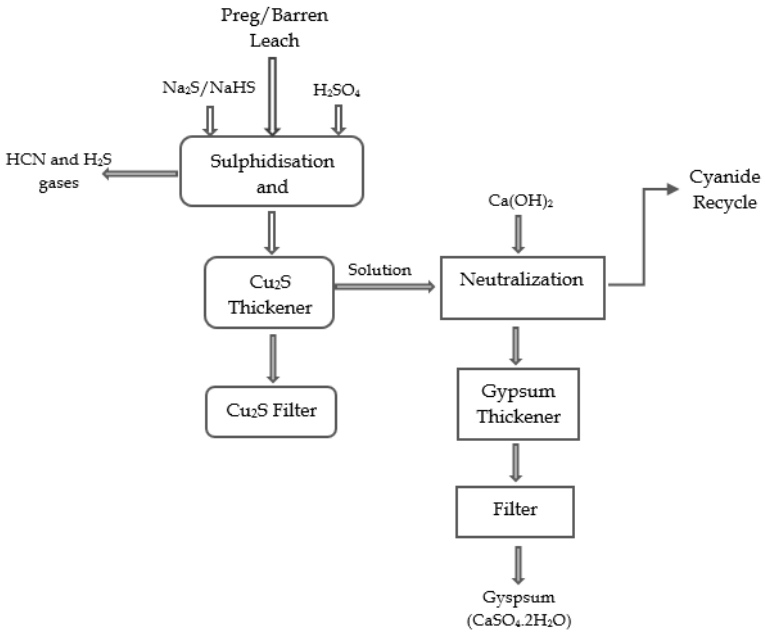


Fig. 1. General Flowsheet Of The SART Process (Nodwell vd.,2012, Yılmaz, E., 2018)

Following the addition of sulfur, the solution is acidified with H_2SO_4 to achieve a pH of 4-5, resulting in the precipitation of copper as Cu_2S (synthetic chalcocite) (logK=34.60) (Zhang et al., 1997; Yılmaz, E., 2018). To prevent environmental issues that may arise from the HCN and H_2S gases generated during the acidification stage, the process is conducted in sealed, leak-proof tanks, and the resulting gases are transferred to a gas scrubbing system for neutralization (pH 10-11) (Ford et al., 2008; Yılmaz, E.,2018).

$$2Cu(CN)_3^{-2} + 3H_2SO_4 + S^{-2} \rightarrow Cu_2S_{(s)} + 6HCN_{(aq)} + 3SO_4^{-2} \quad (1)$$

After the acidification process, Cu_2S precipitates are separated from the acidic solution through solid/liquid separation (thickening + filtration). In the SART process, instead of direct filtration, the solids are first thickened to increase the solids content to 10-15%, significantly reducing the required

pulp volume for filtration (Sceresini and Breuer, 2016). This filtration facility is important for minimizing high initial investment costs.

After the solid/liquid separation, lime is added to raise the solution pH to 10.5-11. The lime consumption (typically 0.5-0.9 kg $Ca(OH)_2/m^3$) varies depending on the sulfate and carbonate ions in the solution (Estay, 2018). During this process, the generated HCN is absorbed in the alkaline solution, allowing for the recovery of cyanide in the form of $Ca(CN)_2$ (7) (Figure 3) (Fleming, 2011; Estay et al., 2012; Xie et al., 2013; Yılmaz, E., 2018).

The key parameters affecting the SART process include NaHS concentration (S;Cu ratio), pH, cyanide concentration (CN:Cu ratio), and duration. For effective precipitation, sulfur must be added in an appropriate amount. Generally, the NaHS addition is chosen to be stoichiometrically above the requirement (110-120%) depending on the concentration of other metals present in the solution besides copper (Ford et al., 2008; Yılmaz, E., 2018).

2. Applications

2.1. Experimental Studies

Experimental studies conducted prior to the SART process have been investigated, with the aim of determining the consumption of H_2SO_4, NaHS, and lime, as well as calculating the cyanide recovery efficiency. These stages provide essential information for the engineering and design of a full-scale SART facility. The results of experimental studies conducted by Kevan J.R. Ford and colleagues regarding the NaHS addition ratio, using samples from a heap leaching operation, are presented below.

Table 1 Effect Of NaHS Addition In The SART

Feed Solution	Feed Cu ppm	Feed d NaCN (F) ppm	NaHS Addition %Of Stochiometric	%Cu Recovery to Cu_2S Precipitate	Final Solution Cu ppm	Final Solution NaCN F
Preg Solution 0.3 mg/L Au	288	238	80	58,3	120	368
	288	238	90	75,7	70	453
	288	238	100	86,1	40	538
	288	238	120	96,5	10	570
Barren Solution < 0.1 mg/L Au	248	174	80	63,7	90	260
	248	174	90	75,8	60	326
	248	174	100	83,9	40	376
	248	174	120	96	10	410

During the sulfidization stage, Na_2S or typically NaHS is added to the cyanide solution. Hydrogen sulfide (H_2S) gas can also be used as a sulfur source. It is possible to produce hydrogen sulfide by reducing elemental sulfur or sulfate through biological processes (Lawrence and Lopez, 2011). To evaluate the effect of the NaHS addition ratio (stoichiometric % required for Cu precipitation) on copper and cyanide recovery, bench-scale tests were conducted at pH 5 (Table 1). As shown in Table 1, copper recovery is directly proportional to the NaHS addition ratios. If sufficient sulfur ions are present at pH 5 to complex Cu and precipitate Cu_2S, high copper recoveries of 96.0% or more can be achieved.

Since sulfur ions are consumed by other metal cations such as Zn, Ag, Ni, and Fe, and due to other complexation reactions in the solution that consume S ions and complexes in the feed solutions of the SART facility, stoichiometric NaHS addition ratios exceeding 100% (depending on the available Cu) are necessary. If excessive sulfur is added, thiocyanate (SCN) formation will occur, reducing the available cyanide for gold leaching. Therefore, while it is important to provide sufficient sulfur ions for the recovery of Cu and other valuable metals in the SART process, it is equally crucial to avoid creating

thiocyanate or other sulfur species that could reduce free cyanide recovery and delay gold leaching during heap leaching recycling (Ford et al., 2008).

Following the addition of sulfur, the solution is acidified with H_2SO_4 to achieve a pH of 4-5, facilitating the precipitation of copper as Cu_2S (synthetic chalcocite) (logK=34.60) (Zhang et al., 1997).

Table 2 Effect Of Ph On The SART

Feed Solution	Feed Cu ppm	Feed NaCn(F) ppm	NaHS Addition %Of Stochiometric	pH in Cu Precipitation Reactor	%Cu Recovery to Cu_2S Precipitat e
Preg Solution 0.3 mg/L Au	290	265	100	5	86,2
	290	265	120	5	96,6
	290	265	100	4	89,7
	290	265	100	3	93,1
Barren Solution < 0.1 mg/L Au	220	147	100	5	81,8
	220	147	120	5	95,5
	220	147	100	4	90,9
	220	147	100	3	96,4

The effect of pH on Cu_2S precipitation has been investigated and is presented in the table. At a NaHS addition of 100, a lower pH enhances the recovery of Cu from the solutions. However, at pH 5 with a NaHS addition ratio of 120%, high Cu recoveries are achieved for Cu_2S. To reduce acid costs, pH 5 has been selected for further testing.

Table 3 SART Process H_2SO_4 and NaOH Consumption

Feed Solution	NaHS Addition % Of Stochiometric	H_2SO_4 Consumption kg/m3	NaOH Consumption kg/m3
Preg Solution 0.3 mg/L Au	80	0,44	370
	90	0,45	375
	100	0,47	375
	120	0,51	378
Barren Solution < 0.1 mg/L Au	80	0,38	378
	90	0,4	370
	100	0,47	368
	120	0,52	365

2.2. SART Process

Gold production from high-copper ores is increasing in our country (Yılmaz et al., 2018). During the recovery of gold from such ores, technical and economic challenges are encountered (Corrans and Kyle, 2000; Fleming, 2011). Therefore, the SART process has been implemented in some facilities to control the negative effects of copper (Botz et al., 2011; Nodwell et al., 2012). A detailed flowchart of the Mastra/Gümüşhane Gold Mine is presented in Figure 2.

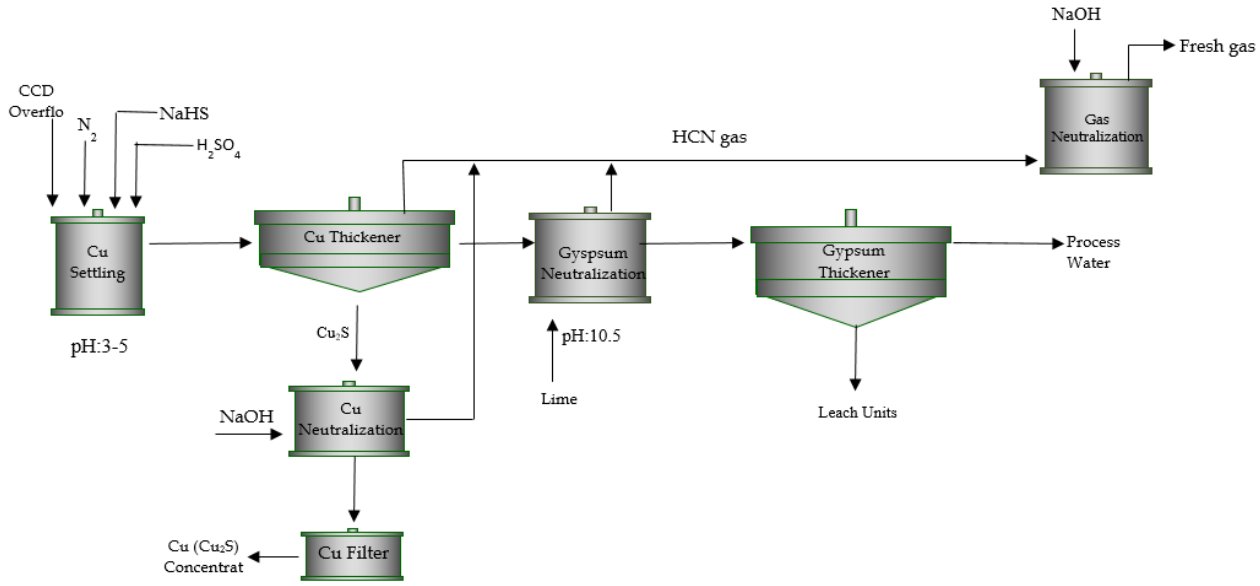


Fig. 2. Flowsheet Of The SART Process Applied In Mastra (Gümüşhane) Gold Mine

The development of the SART process from the past to the present is summarized in Table 4. The SART process was developed in the 1990s by SGS Lakefield Research (Canada), with initial research results from pilot-scale tests (Lobo-Marte project) published by MacPhail et al. (1998) (Fleming and Melashvili, 2016). The process was first implemented on an industrial scale at the Telfer gold mine in Australia (Ford et al., 2008). In subsequent years (2006-2013), SART facilities became operational in various countries (Table 3). Due to the relatively new nature of the SART process, the number of industrial-scale SART facilities remains below ten (Baker et al., 2017; Estay, 2018; Yılmaz, E., 2018).

Table 4 Timeline Of Milestones In The SART Process's History (Estay,2018, Yılmaz, E., 2018)

Years	Process Development
1986	(Potter and co-workers.) patented the MNR process, the base of SART process.
1998	(MacPhail and co-workers.) published the firstpaper of the SARTprocess, about pilot plant of Lobo
2001	(Barter andco-workers.) published the paperabout testing and pilot plant of Telfer SART process, the first SART plant constructed.
2006	The first SART plant is commissioned inTelfer plant, Australia. This plant was designed to treat 60 m3/h of PLS
2008	The largest SART plant to date is commissioned inYanacocha, Perú.This plant was designed to treat1400 m3/h of PLS
2008	The SART plant of Luvia deOro, Mexico is commissioned. This plant use sulfidebio-generation.
2009	The SART plant of Gedabek,Azerbaijan is commissioned. This plant was designedto treat 140 m3/h of PLS.
2010	The SART plant of Mastra,Turkey is commissioned. This plant was designedto treat 120 m3/h of Barren solution.
2012	The second largest SART plantto date is commissioned in Maricunga, Chile.This plant wasdesigned to treat750 m3/h of PLS.
2013	The last SART plantinstalled to date is commissioned inCopler, Turkey. This plant was designedto treat 380 m3/h of PLS.

2.3. Process Economics

The recovery of cyanide is an economic necessity, especially for high-copper ores. An economic assessment presented in Table 6 clearly indicates that the implementation of recovery processes (such as SART) is more advantageous than cyanide destruction in facilities processing high-copper gold ores (SGS, 2013). The sale of copper as a by-product provides additional income for operations. Due to the economic advantages provided by the SART process, SART facilities can finance their initial investment costs within a few years. For example, the payback period for a SART facility processing a solution containing 380 mg/L Cu at a capacity of 750 m^3/hour is estimated to be 1.5-2 years (Fleming, 2003; Ford et al., 2008).

One significant parameter affecting the investment cost of a SART facility is the distance of the site from the mining area. If the gypsum thickener underflow is not subjected to dewatering, both investment

and operating costs can be significantly reduced. SART gypsum waste can be utilized by being spread as a capping layer in heap leaching and mixed with feed before the CIP/CIL circuit (Baker et al., 2017).

One of the significant parameters affecting the operating cost of the SART process is the amount of "copper soluble in cyanide (CN-dissolved Cu)" in the ore (Fleming, 2011).

A comparison of cyanide destruction and recovery costs for a facility processing Au-Cu (with cyanide consumption of 1 kg/ton NaCN and dissolved copper of 0.4 kg/ton, based on 2005 prices) is presented in Table 5 (SGS, 2013).

Table 5

Cyanide destruction	Cost($)	Cyanide Recovery	Cost($)
New NaCN	1,50	Operating	0,60
Destruction	1,00	Capital	0,30
	2,50$	Subtotal	0,90
		Cu credit	0,40
		Total ($/t)	0,50

The operating costs of SART facilities consist of various items such as reagents (acid, base), transportation, energy, etc. Based on laboratory/pilot-scale tests for a SART facility, the distribution of operating expenses has been determined (Figure 4) (Ford et al., 2008). According to this, the largest share of operating expenses is attributed to NaSH costs, which account for 28%. The combined share of base (NaOH and lime) and acid (H_2SO_4) costs is also 29% (Ford et al., 2008). Similarly, another study shows that the highest share among operating expenses (27%) is attributed to NaSH used in the precipitation stage (Stewart and Kappes, 2012). In the same study, the costs associated with acidification and neutralization processes account for 40% of the expenses.

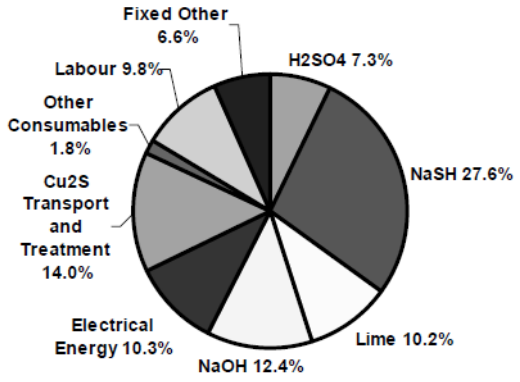


Fig. 3. SART Plant Operating Costs Distribution (Ford vd.,2008, Yılmaz, E., 2018)

3. Conclusion

To achieve economical gold recoveries from high-copper ores (>%0.5 Cu), leaching must be conducted at high cyanide concentrations (CN:Cu>4), followed by the recovery of cyanide from the leach solution and the extraction of copper as a by-product using the SART process. This process, suitable for copper-bearing solutions, significantly reduces cyanide destruction costs. However, due to its relatively new technology, the number of industrial facilities remains limited. Industrial SART plants can achieve high cyanide recoveries (>80%) under appropriate conditions. To obtain a high-quality Cu_2S precipitate that allows for easy solid/liquid separation, excessive sulfur addition should be avoided (the Sratio should not exceed 0.50), the settling time should be minimized at pH 3-5, contact with oxygen should be prevented, and the SART process should be operated continuously rather than in batch or semi-batch modes. Otherwise, copper may precipitate as CuS and CuCN, or dissolve as copper-cyanide complexes,

decreasing the purity of the copper precipitate and increasing reagent consumption. Currently, the number of SART facilities worldwide is below ten, and since some of these are small, batch-operated facilities far from mining sites, more continuous SART plants are needed to gain clearer insights into process costs, operability, and metallurgical performance. As the copper content soluble in cyanide increases, the economic return of the SART process also rises, with an estimated payback period of 1.5-2 years for initial investments. While the SART process offers significant technical and economic advantages for the recovery of cyanide (and copper as a by-product) from Au-Cu ores, some technical issues encountered in industrial applications indicate a need for further knowledge and experience regarding the process.

Acknowledgments

We would like to thank Koza Gold Corporation, Kaymaz Gold Mine Operations Manager Kemal Öcal, and Process Superintendent İlkay Handırı for their support in this study.

References

Adams, M. D., 2013. Impact of recycling cyanide and its reaction products on upstream unit operations, Minerals Engineering, 53, 241-255.

Baker, B., Rodriques, F., Littlejohn, P., 2017. SART implementation at gold mines in Latin America, The Conference of Metallurgists (COM), Ağustos 27-30, Paper No: 9489, Canadian Institute of Mining, Metallurgy and Petroleum, 8.

Botz, M., Kaczmarek, A., Orser, S., 2011. Managing copper in leach solution at the Çöpler gold mine: laboratory testing and process design,

Corrans, I.J., Kyle, J.H., 2000. An overview of unit operations and processes used for treating gold and copper ores, Editör: Adams, M.D., Proc. of the Oretest Colloquium 99, 10 November, Oretest Pty Ltd, Perth, Avustralya, 3–16.

Estay, H., 2018. Designing the SART process – A review, Hydrometallurgy, 176, 147–165.

Ford, K., Fleming, C., Henderson, R., 2008. Application of the SART process to heap leaching of gold-copper ores at Maricunga, Chile. In: 40th Annual Meeting of the Canadian Mineral Processors, Ottawa, January 22-24.

Koza Gold Corporation, Mastra Gold Mine, Process presentation, November 2011.

Lawrence, R. W. ve Lopez, O., 2011. Improving the economics of gold-copper ore projects using SART technology.

Lopez, O., Petrovic, N., Krashenina, S., 2014. Copper and cyanide recovery from barren leach solution at the gold processing plant, XXVII. International Mineral Processing Congress (IMPC 2014), Santiago, Şili, 11.

Nodwell, M., Kratochvil, D., Lopez, O., 2012. Risk management and mitigation for the SART copper cyanide recovery process, HYDROPROCESS 2012, 4th International Seminar on Process Hydrometallurgy, 12-13 Temmuz, Santiago, Şili, 1-7.

Sceresini, B. ve Breuer, P., 2016. Gold-copper ores, Gold Ore Processing, 2nd Edition, Chapter 43, Editör: Adams, M. D., Elsevier.

SGS, 2008. Application of the SART process to heap leaching of gold-copper ores at Maricunga, Chile, SGS Minerals Services Technical Paper 2008-51.

SGS, 2009. Cyanide Recovery, Technical Paper, No. T3 SGS 019, SGS Minerals Services.

SGS, 2013. Cyanide recovery, SGS Minerals Services – T3 SGS 019, 11-2013.

Stewart, M. ve Kappes, D., 2012. SART for copper control in cyanide heap leaching, SAIMM, 112, 1037–1043.

Xie, F., Dreisinger, D., Doyle, F., 2013. A review on recovery of copper and cyanide from waste cyanide solutions, 34:6, 387-411.

Yılmaz, E., Yazıcı, E. Y., Celep, O., Deveci, H., 2018. Recovery of cyanide from effluents: Sart Process.

Zhang, Y., Fang, Z., Muhammed, M., 1997. On the solution chemistry of cyanidation of gold and silver bearing sulphide ores, A critical evaluation of thermodynamic calculations, Hydrometallurgy, 46, 251-269.

Gold Recovery With Cyanide Leaching: Tank Leaching Application

Mert Kuzu [1]*, Ali Uluturk [1]

[1] TÜMAD Lapseki Gold-Silver Enrichment Facility, ÇANAKKALE

*Corresponding author: mert.kuzu@tumad.com.tr (Mert Kuzu)

Abstract:

Cyanide leaching method has been widely used in gold production for many years. In recent years, cyanide leaching has been applied in many facilities producing gold in Turkey. Tank leaching is the most commonly used cyanide leaching method. In tank leaching, the dissolution kinetics of gold is affected by the mineralogy of the ore, particle size, pulp solid ratio, free cyanide concentration, dissolved oxygen concentration, other soluble metals in the ore, and sulfur minerals. At TUMAD Mining Lapseki Gold and Silver Enrichment Facility, ore production is carried out using the tank leaching method. The waste from ore production is dewatered in the filtration unit before being sent to dry waste storage.

Keywords: *Gold, Leaching, Cyanide, Cyanidation, Tank Leaching, Leaching Kinetics*

1. Introduction

Today, the most common method used in gold production is cyanide leaching, as it is both economical and provides high metal recovery. Cyanide leaching has been used as the basic method for recovering gold from ores for over a century (Lima et al., 2006). Over the years, with the decrease in ore resources that allow gold recovery with gravity methods, which is a more basic enrichment method, cyanide leaching has found a wide range of application. As a result of electrochemical reactions, gold is oxidized and turned into a more stable and complex ion, oxygen is reduced and hydrogen peroxide is released (Lima, 2005). This process is carried out in the pH range of 10.5-11 and in an environment containing dissolved oxygen in order to prevent the conversion of cyanide molecules in the liquid phase to hydrogen cyanide, which is the gas phase. After the gold is taken into the solution phase, it is commonly absorbed onto active carbon, the carbon loaded with gold is subjected to a stripping (elution) process using sodium hydroxide and sodium cyanide solutions, and then it is ensured to stick to the cathodes by the electrowinning method. The gold particles accumulated in the cathodes are washed and filtered and then dried in a drying oven. The dried material is finally melted in a crucible and poured in the form of dore. At TUMAD Mining Lapseki Gold and Silver Mine Mineral Processing and Enrichment Facility, the run-of-mine ore produced from open pits and underground mines is reduced to the 90 micron particle size determined for the leach circuit. After metal recovery in the leach and adsorption circuits, the plant waste coming out of the circuit is subjected to chemical degradation and then dewatered in the Filter Unit and sent to the Dry (Solid) Tailing Storage (DTS) Site.

2. Use of Gold

When we look at the production method and usage area of gold in the early ages, it has been revealed by many historical excavations that it was used in the production of objects that were natural needs of people. Due to its resistance to corrosion and the fact that it did not tarnish in open natural conditions, it began to be used in the production of ornaments and jewelry over time. This precious metal, which has many unique features, has been used for 7000 years as an investment, savings, ornament and exchange tool. The oldest gold producers were the Egyptians, who began to mint standard gold bars and use them as a payment tool in 3100 BC (Küçük, 2012). Since gold can be shaped very easily in general, it is used especially in jewelry, in jewelry making, and in the coating and decoration of porcelain and glass surfaces.

3. Gold Mining in the World and in Our Country

With new developments in gold ore enrichment technology, gold mining in the world has been growing rapidly since the 1970s. In the last 15 years, there has been a ≅ 30% increase in world gold production. With these developments, while known gold ores are being put into operation, an intensive period of exploration and investment continues in the world to find new gold deposits (Gold Miners Association, 2019).

While world gold reserves were approximately 42,000 tons during the 2000s, as a result of exploration and reserve development studies carried out in Australia, Peru, South Africa and the USA, the world's gold reserves reached 57,000 tons as of 2017. The countries of Australia, Russia, South Africa, the USA, Indonesia and Peru have the largest share in these reserves.

Our country attracts great attention in terms of its gold potential in the light of world gold mining. The gold deposits known and under exploration in Turkey are concentrated in the Aegean, Eastern Black Sea, Inner Western Anatolia and Eastern Anatolia regions.

According to the latest statistics announced by the Turkish Gold Miners Association in 2019, organizations producing gold in our country have invested over 4.6 billion dollars to date, including 1.1 billion dollars for exploration and 3.5 billion dollars for production facilities. In 2018, the gold produced contributed 1.1 billion dollars to our country's economy. Approximately 9,000 people are employed in the developing gold mining businesses in our country.

4. Gold Extraction Methods from Ores

Gold ores are commonly enriched by methods such as gravity and flotation. Alkaline cyanide leaching is the most common method used for gold recovery from ores/concentrates (Petruk, 2000). In today's gold mining practices, gold production from ores is carried out according to physical, chemical and metallurgical methods, and the type, grade and structural properties of the ore deposit are taken into account in determining the method to be applied (Yildiz, 2010).

It is known that a concentrate with a high gold content is obtained before cyanide leaching by using enrichment methods for ores with coarse particle sizes, taking into account the particle size in the enrichment processes of gold-bearing ores. Hydrometallurgical methods are applied for ores with fine particle sizes.

5. Cyanide Leaching

In today's gold mining, almost without exception, cyanide reagent is used as a leaching chemical in hydrometallurgical gold recovery processes. Cyanide has been used in the recovery of metals since 1887 and is currently used and managed safely throughout the world in gold recovery. In cyanidation, the ore is subjected to leaching with a low-concentration alkaline cyanide solution (Yildiz, 2010). There are various methods that can be used in cyanide leaching of gold-bearing ores. These methods are;

- Tank leaching
- Heap leaching
- In situ leaching
- Vat leaching

6. Tank Leaching Method

The tank leaching method has been used for over 200 years to process various ores. This method is applied by mixing the ground ore with cyanide solution in a cylindrical or conical tank. The mixing process can be done by air, with the help of a mechanical impeller or a combination of the two. In the tank leaching method, an efficiency of over 80% is generally obtained and the leaching period can vary between 16-48 hours (average 24 hours) (Stange, 2006). Due to the high grinding, reagent and other costs, this method is generally preferred for high-grade ores. However, it is also seen that it is applied

to relatively low-grade gold ores due to the increase in the economic value of gold in today's conditions. The factors affecting metal recovery in the tank leaching method are as follows. In tank leaching, the dissolution kinetics of gold is affected by factors such as the mineralogy of the ore, particle size, pulp solid ratio, free cyanide concentration, dissolved oxygen concentration, other soluble metals in the ore, and sulphide minerals.

6.1. Factors affecting metal recovery in tank leaching

6.1.1. Particle size

Tank leaching is a method that requires grinding. Therefore, the ore must be ground to the optimum particle size determined according to the yield-grinding cost calculation. The dissolution rate generally increases with the decreasing particle size, the liberation of the gold and/or gold particle surfaces. The material to be leached is ground to a particle size that optimizes gold recovery and size reduction costs, typically between 80% < 45-150 µm. Tank leaching is rarely applied at sizes larger than approximately 150 µm due to the difficulty of keeping the pareticles in suspension and the increased wear rates in the equipment. With the developments in very fine grinding equipment (e.g. Xstrata IsaMill and Metso SMD), the application of very fine in tank leaching is also increasing.

6.1.2. Solid density

Leaching is generally carried out at sludge densities between 35% and 50% solids, depending on the specific gravity of the solids, particle size and the presence of minerals (e.g. clay minerals) that affect sludge viscosity. The mass transfer phenomenon is at its highest at low sludge densities; on the other hand, as the density increases, the residence time of the solid in a fixed volume leaching equipment also increases. In addition, as the sludge density increases, reagent consumption decreases and optimum concentrations are obtained at lower doses since the volume per unit mass of the material decreases (House et al., 2006).

6.1.3. pH

To prevent excessive cyanide gasification and removal from the system as a result of hydrolysis, alkali is always added to the medium before cyanide addition and to provide protective alkalinity. In most leaching systems, pH operates between 10.5 and 11. In order to maintain the desired working pH value, especially during the processing of ores containing components that lower pH, gradual base addition may be required throughout the leaching cycle (House et al., 2006).

6.1.4. Cyanide concentration

Cyanide can be added to agitated leach systems before the leaching phase, i.e. during grinding or in the first stage of the leaching process. Cyanide can also be added in the later stages of leaching to maximize gold dissolution. If there are no cyanide-consuming minerals in the ore or concentrate to be leached, cyanide concentrations used in practice range from 0.05 to 0.5 g/L NaCN, with typical values of 0.15-0.30 g/L NaCN. Typical cyanide consumption in agitated tank leaching systems for easily processed ores ranges from approximately 0.25 to 0.75 kg/t.

Cyanide concentrations are usually monitored by manual titration techniques or, less commonly, by online cyanide analyzers based on titrimetric, colorimetric, potentiometric and ion-specific electrode techniques (House et al., 2006).

6.1.5. Oxygen concentration

The oxygen requirement for the leaching process is usually met by air supply to the tanks. This supply is sometimes applied as the primary mixing method and sometimes as pure oxygen supply in mechanically stirred tanks. In cases where there are ores containing oxygen-consuming minerals, pure oxygen and hydrogen peroxide can be added in addition to simple air systems to increase the oxygen

concentration (Cathro and Walkey, 1961; Cathro, 1963). The amount of dissolved oxygen in leaching systems is usually monitored as 20-30 mg/L, which will positively affect the leaching kinetics.

6.1.6. Duration time

Residence time requirements vary depending on the leaching properties of the material being processed and are determined by test studies. In practice, leaching times vary from a few hours to several days. Leaching is usually carried out in 4-10 stages, where the volume and number of stages of each stage depend on the sludge flow rate, the required residence time and the efficiency of the mixing equipment used (House et al., 2006).

6.1.7. Temperature

Gold solubility increases with increasing temperature due to the increase in diffusion rate. However, oxygen solubility in solution decreases with increasing temperature.

6.1.8. Mixing speed

The gold dissolution rate also depends on the diffusion layer thickness and the mixing properties. Increasing the mixing speed increases the gold dissolution rate due to the decreased diffusion layer thickness and better homogeneity provided.

6.2. Gold recovery with CIP method in tank leaching method

In the CIP (carbon in pulp) method, after the dissolution period of the gold in the leach tanks is completed, the pulp is transferred to the tanks used for carbon adsorption and the adsorption process takes place. This method is generally applied for ores with high grade and/or long leaching time. The rate at which activated carbon adsorbs the gold-cyanide complex depends on the gold concentration in the solution, the free cyanide concentration, the organic solvents in the solution, the pH value, the ionic strength, the solution temperature, the particle size of the carbon and the mixing efficiency (Fleming and Nicol, 1984). In the tank leaching method, the adsorption tanks are positioned after the leach tanks. The carbon in contact with the loaded solution has the highest gold content, while the carbon in the last stage has the lowest gold content.

7. Tumad mining Lapseki Gold-Silver enrichment facility tank leaching application

The pulp with low solid content coming out of the Grinding Unit is brought to the targeted 45% solid density for leaching with the help of a thickener and flocculant. Excess water is transferred from the upper flow of the thickener to the process water tank to be reused. The lower flow of the thickener is transferred to the Leaching Unit (Fig. 1-2), which consists of 8 tanks and has a processing time of 48 hours, with the help of pumps. Cyanide solution is fed to the first tank. The sludge in the tanks passes to the other tank by its own gravity. Pure oxygen is given into the tank in order to increase the reaction efficiency. Gold recovery efficiency of over 95% can be achieved.

The most important environmental parameter to be controlled in the Leaching Unit is the HCN gas concentration. The aim is to prevent the formation of HCN gas. For this purpose, the pH of all pulps and solutions containing cyanide is adjusted to 10.5-11. pH is automatically adjusted under computer control by adding lime or caustic.



Figure 1. View of leach tanks

During cyanide leaching of gold ores, gold-silver is taken into the solution phase by forming stable complexes with cyanide (Mordoğan, 1997). The reaction occurring in the cyanidation process was first described by Elsner in 1846 in Equation 1 (Yüce, 1995). According to the reaction, gold in the ore dissolves in alkali cyanide (NaCN or KCN) solution in the presence of an oxidant (oxygen) as the aurocyanide complex [Au(CN) ^{2}]- (Hiçdönmez, 1997; Kakı, 1995). The dissolution rate of gold depends on the diffusion of oxygen and cyanide in the boundary layer.

$$4\ Au + 8\ CN^- + O_2 + 2\ H_2O \rightarrow 4\ Au(CN)_2^- + 4\ OH^-\ (basic) \quad (1)$$

Gold and silver dissolve in alkaline cyanide solution (pH 10.5-11) in the presence of oxygen. In gold mining, dilute sodium cyanide solutions containing 0.01%-0.05% cyanide are generally used (Longsdon et al., 2002). The solution containing gold is called "pregnant leach solution".

After the gold and silver are dissolved with the cyanide solution added to the leach tanks, the resulting loaded leach solution is sent to the rotary type CIP circuit, which consists of nine tanks and has a total processing time of 2 hours. Each tank contains 2 tons of activated carbon, in which gold and silver are adsorbed. The gold and silver dissolved with the carbon in the adsorption tanks are taken from the pulp. The sedimentation of the pulp is prevented by the mechanical mixers in all tanks. In addition, in-tank sieves are placed at the outlets of the adsorption tanks to prevent the passage of activated carbon. The carbon loaded with gold is subjected to the elution process, in which sodium hydroxide and sodium cyanide solutions are used, and then it is ensured to stick to the cathodes by the electrowinning method. The gold particles accumulated in the cathodes are washed and filtered and then dried in the drying oven. The dried material is finally smelted in the crucible and poured in the form of dore.



Figure 2. General view of Lapseki Gold-Silver Enrichment Facility

8. Conclusion

In Lapseki Gold-Silver Enrichment Facility, tank leaching process, which is a cyanide leaching method, is applied. In leaching tanks, pulp, which is generally kept at 45% solids, is mixed with cyanide and oxygen to ensure that the gold passes into solution. In tank leaching, gold recovery efficiencies of over 95% can be achieved by the application of grinding and the release of fine gold particles in the ore to a large extent. The tailing sludge generated after production is subjected to cyanide degradation process using INCO SO_2-Air process. Then, the waste sludge is turned into cake in filters and stored with Dry Tailing Storage method.

The main advantages of this method are listed below;

1. Short leaching time and quick visibility of the intervention
2. Obtaining high efficiency metal recoveries.
3. Providing high dissolution kinetics for some refractory ores.
4. Obtaining high yields at low cyanide concentrations.

References

CA Fleming, and Mj Nicol, The Adsorption of Gold Cyanide onto Activated Carbon. III. Factors Influencing the Rate of Loading and the Equilibrium Capacity, Journal - South African Institute of Mining and Metallurgy, 1984.

Cathro, K. J. and Walkey, A., The Cyanidation of Gold, CSIRO, Melbourne, 1961.

Cathro, K.J., The Effect of Oxygen in the Cyanide Process for Gold Recovery, Australasian Institute of Mining & Metallurgy, 1963.

Gold Miners Association, 2019

Hiçdönmez, Ş., 1997. Gold Mining in Turkey, 2nd National Toxicology Congress Panel Notes, Antalya, 75-84.

House, John O. Marsden and C. Iain, The Chemistry of Gold Extraction, Society of Mining, Metallurgy and Exploration, Inc., 2006.

Kakı, E., 1995. A New Method for the Solution of Gold, Master's Thesis, Marmara University, Institute of Science, Istanbul.

Küçük, S., 2012. Development of International Financial Markets and Forex Markets: Situation in Turkey, Master's Thesis, Çukurova University, Institute of Social Sciences, Adana.

Longsdon, MJ, Hagelstein, K. and Mudder, TI, 2002. Cyanide method in gold production, International Council on Metals and the Environment (ICME), 40.

LRP de Andrade Lima, D. Hodouin, Optimization of Reactor, 2005

LRP de Andrade Lima, D. Hodouin, Simulation Study of the Optimal distribution of Cyanide in a Gold Leaching Circuit, Minerals Engineering , 19, 1319-1327, 2006.

Mordoğan, H., 1997. Use of Cyanide in Mining, Chemistry and Treatment Methods, National Toxicology Congress Panel Notes, Antalya, 55-74.

Stange, W., The Process Design of Gold Leaching and Carbon in Pulp Circuits, Journal - South African Institute of Mining and Metallurgy, 1999.

Yildiz, N., 2010. Mineral Processing and Enrichment, Ertem Printing Publishing Distribution Industry and Trade Limited Co., Ankara.

Yüce, AE, 1995. Gold and Silver Recovery from Gold-Silver-Containing Sulphide Copper-Pyrite Ores by Thiourea Leaching, PhD Thesis, ITU, Institute of Science, Istanbul.

Zenit Mining, Kızıltepe Gold Plant Cyanide Destruction Circuit

Yıldız GÖKTAŞ [1], Nursun ŞİRVANCI [1]

[1]Zenit Mine Inc., Kızıltepe Gold Plant

*Corresponding author: y.goktas@zenitmadencilik.com (Yıldız GÖKTAŞ)

Abstract:

Tailings from the process plant is subjected to a cyanide detoxification process and the final tails is discharged to the tailings dam after cyanide destruction. During the feasibility stage of the project, cyanide destruction tests were conducted to identify suitable detox requirement. Cyanide destruction testing has shown that acceptable levels of residual cyanide can be achieved using the Inco SO_2/Air method. According to the test work results, the designed retention time for cyanide destruction reactor is 60 minutes at 50% solids by weight and result in final cyanide (WAD) in tailings of less than 1 ppm.

Since the process plant was commissioned in 2016 March, the weak acid dissociable (WAD) cyanide in tailings has been measured 0.8 ppm in project to date average. So, the cyanide destruction circuit has been operated better than designed criteria of 10 ppm in the Kızıltepe Gold Mine.

This study aims to investigate the key performance indicator of the Cyanide Detoxification Circuit in the Kızıltepe Gold Plant and provide the relationship between the operational parameters in detox circuit

Keywords: *Gold, CIL, Detox, WAD CN*

1. Introduction

In the Kızıltepe Gold Mine, the gold ore is mined using open-pit methods and hauled to the ROM stockpile. The ROM in the stockpile is fed to the ore preparation and enrichment plant consists of the following circuits;

- *Crushing and Classification Circuit (Jaw Crusher, SAG Mill, Ball Mill and Thickeners)
- Leach and Adsorption Circuit (Pre-Leach Tanks, CIL Tanks)
- Carbon Stripping Circuit
- Electrowinning and Refining Circuit
- Carbon Washing and Carbon Reactivation Circuit
- Cyanide Destruction Circuit (INCO SO_2/Air Process)

The ROM ore is fed to the jaw crusher through a grizzly feeder. The crushed ore is conveyed to a Ø5.5 x 3.2 m SAG Mill at a feed rate of 50 tph and the SAG Mill discharge is pumped to the primary cyclones for classification. The cyclone underflow reports to a Ø3.2 x 5 m Ball Mill for regrinding purposes and Ball Mill discharge is pumped to the secondary cyclones. BM cyclones are operated in closed circuit with the ball mill. Both primary and secondary cyclones overflows at P_{80} of 75 µm is split into two 8 m diameter grinding thickeners, via a vibrating trash screen. The overflow from the thickeners is stored in the process water tanks to be re-circulated in the system. The underflow from the grinding thickeners at ~50%solids by weight is pumped to the first of two agitated and aerated pre- leach tanks with a volume of 750 m^3 each in series. The average cyanide concentration in the pre-leach tanks is maintained in the range of 250-400 ppm NaCN and the gold recovery is in the range of 75% and 85% Au. The slurry from pre-leach tanks is transferred to the Carbon in Leach (CIL) tanks for both leaching and adsorption. There are 7 CIL tanks with a volume of 315 m^3 each. The retention time in pre-leach and CIL tanks at 50 tph and 50% solid is 54 hours. The discharge from the last CIL tank reports to a vibrating carbon safety screen with a 500 micron slot.

In CIL circuit, the activated carbon is moved from one tank to another in counter current with the slurry until the recovery of the loaded carbon in the first tank. The loaded carbon mixed with slurry is pumped from the first CIL tank to the loaded carbon de-sliming screen then the loaded carbon reports to carbon stripping circuit after the acid wash and neutralization process. The hot (<90°C) pregnant strip solution flows through two electrowinning cells in series. The precious metal sludge recovered as filter cake is dried in an electrical drying oven at 450°C then smelted in a tilting induction furnace and cast into moulds after mixed with fluxes. As a result of the enrichment processes, the dore bars are dispatched to a gold refinery for further processing to achieve the required purity for market release.

The CIL leach residue from the underflow of the carbon safety screen is pumped to the detoxification reactors for cyanide destruction (INCO SO_2/Air) and then it is pumped to the Tailings Management Facility (TMF). As the slurry of leach residue is piped into the dam, the solids settle to the bottom and the water is recycled to be used in the process plant again.

Kızıltepe Process Plant produces gold and silver dore using the tank leaching method. Due to the technical and economic requirements of this process, the use of cyanide is mandatory. Consequently, a cyanide detoxification process is necessary to address environmental and legal obligations. Therefore, at the end of the gold and silver enrichment process, the tailings are processed through the INCO SO_2/air detoxification circuit.

The simplified flow diagram of the process plant and the cyanide destruction circuit is shown in the Figure 1 below.

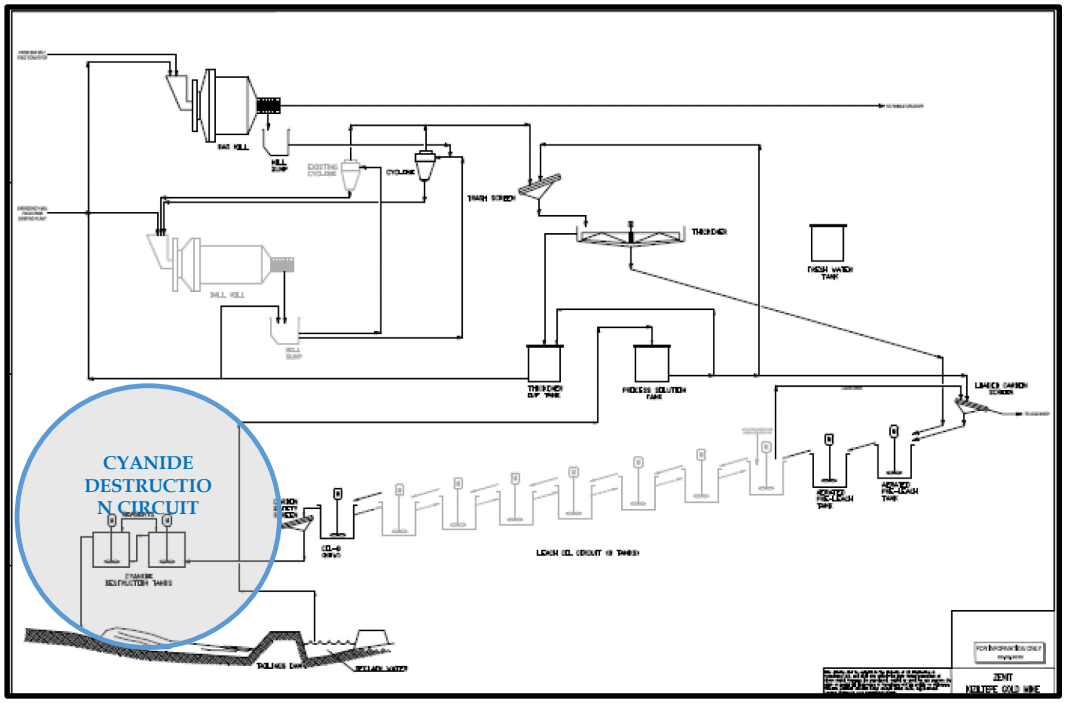


Figure 41: Simplified Process Flowsheet of Kızıltepe Gold Mine

2. Cyanide Destruction Methods

Cyanide is represented as free cyanide, WAD cyanide, and total cyanide (Young & Jordan, 1995; Mudder & Botz, 2004), as shown in the Figure 2. The detoxification process primarily aims to convert cyanide complexes in the waste into cyanate. Also, the natural degradation of cyanide by volatilization and UV destruction, proceeds in tailing dam (Marsden & Sass, 2014)

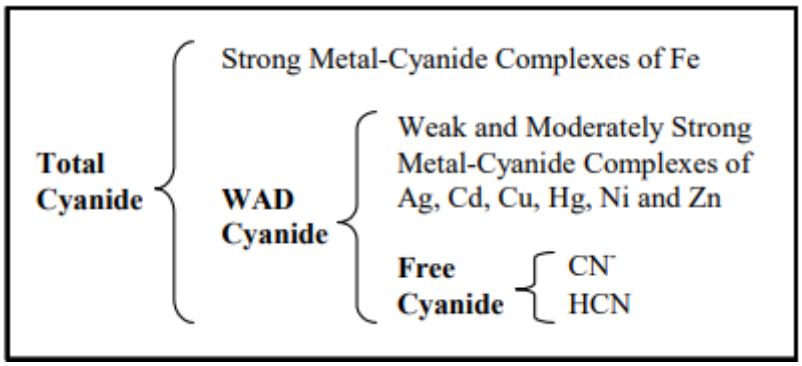


Figure 42: Classifications of Cyanide

Although various detoxification methods exist, the most well-known methods are as follows (Mudder, Botz, & Smith, 1991):

- INCO SO_2/Air

Free cyanide and WAD compounds in leach residues react with oxygen and sulfite ions in the presence of copper cations (Cu^{2+}), transforming into cyanate (OCN^-) and sulfate (SO_4^{2-}) ions. Theoretically, in the process, 2.46 gr of SO_2 required per gr of CN^- oxidized. However, in practice it is in the range of 3.5 to 5.0 gr SO_2 per gr of CN^- (Botz, Mudder, & Akcil, 2016). The process is the most commonly used cyanide destruction method and it occurs according to the following chemical equation.

$$\boldsymbol{SO_2 + O_2 + H_2O + CN^- \xrightarrow{Cu^{+2}\ Catalyst} OCN^- + SO_4^{-2} + 2H^+} \quad (1)$$

If the slurry contains heavy metals, Iron-Cyanide Precipitation may be considered as a continuation process after the INCO SO_2/Air process.

The precipitation process can be used in situations where the reactions can be controlled and the precipitate can be separated and properly disposed of. In the past, this process was used for direct detoxification, but today it is primarily used to reduce the total cyanide concentration to values between 1 and 5 mg/L. The reactions related to the process is shown in Equation 2 and Equation 3.

$$\boldsymbol{Fe^{+2} + 6CN^- + {}^1\!/_4\, O_2 + H^+ \rightarrow Fe(CN)_6^{-3} + {}^1\!/_2\, H_2O} \quad 2)$$

$$\boldsymbol{4Fe^{+2} + 3Fe(CN)_6^{-3} + {}^1\!/_4\, O_2 + H^+ \rightarrow Fe_4[Fe(CN)_6]_3 + {}^1\!/_2\, H_2O} \quad (3)$$

- Hydrogen Peroxide

In this process, which exhibits a similar reaction to the INCO SO_2/Air process, hydrogen peroxide is used instead of sulfur dioxide and air, and the reaction shown in Equation 4 takes place.

$$\boldsymbol{H_2O_2 + CN^- \xrightarrow{Cu^{+2}\ Catalyst} OCN^- + H_2O} \quad (4)$$

- Caro's Acid

In the Caro's Acid process, which can be considered relatively new, peroxymonosulfuric acid (H_2SO_5) is used, and the reaction shown in Equation 5 takes place. However, because of the fact that peroxymonosulfuric acid has a highly corrosive structure, it might be a handling issue of the reagent in the plant.

$$\boldsymbol{H_2SO_5 + CN^- \rightarrow OCN^- + SO_4^{-2} + 2H^+} \quad (5)$$

- Alkaline Chlorination

This process, which primarily occurs in two stages, is now rarely used due to the emergence of other processes alongside technological advancements and economic issues stemming from high reagent consumption. The reaction equations related to the process are presented as Equation 6 and Equation 7.

$$Cl_2 + CN^- \rightarrow CNCl + Cl^- \quad (6)$$

$$CNCl + H_2O \rightarrow OCN^- + Cl^- + 2H^+ \quad (7)$$

Biological treatment, activated carbon polishing, natural destruction, etc. lso being used in some processes.

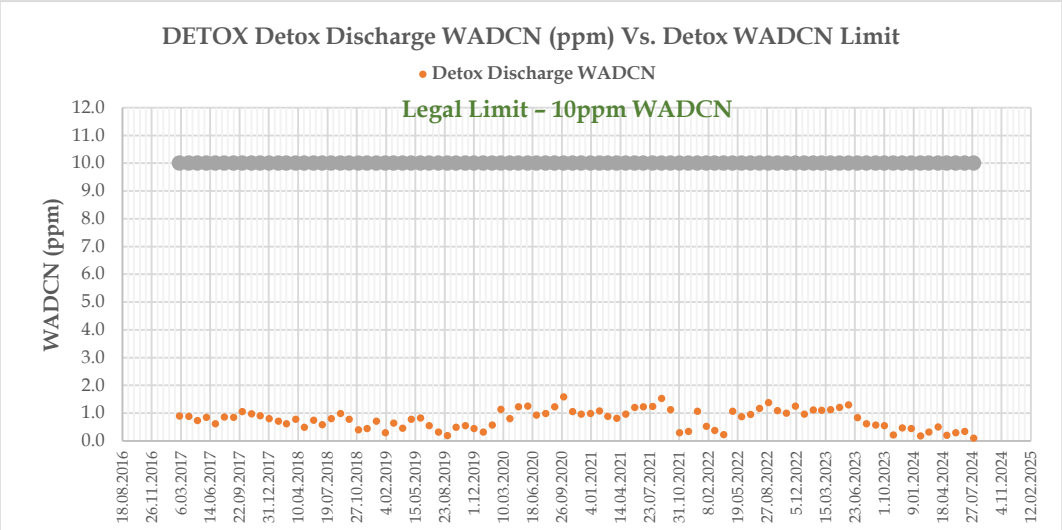
3. Evaluation of the Operating Parameters in Detox Circuit

In the INCO SO_2/Air cyanide destruction process sodium metabisulfite ($Na_2S_2O_5$) is used as an oxidation agent, copper sulfate ($CuSO_4$) as a catalyst, sulfuric acid (H_2SO_4) as a pH stabilizer, and air is supplied as an oxygen source in the detox reactors.

There are two reactors in the detoxification circuit with a volume of 31.6 m³ each. The leach residue is pumped to the first detox reactor after the CIL process. In the meantime the dosing pumps of the detox reagents report to the first reactor to be commenced the cyanide destruction process. The slurry in the first detox reactor overflows to the second detox reactor to complete the oxidation reaction and time for the cyanide destruction process to meet acceptable discharge levels.

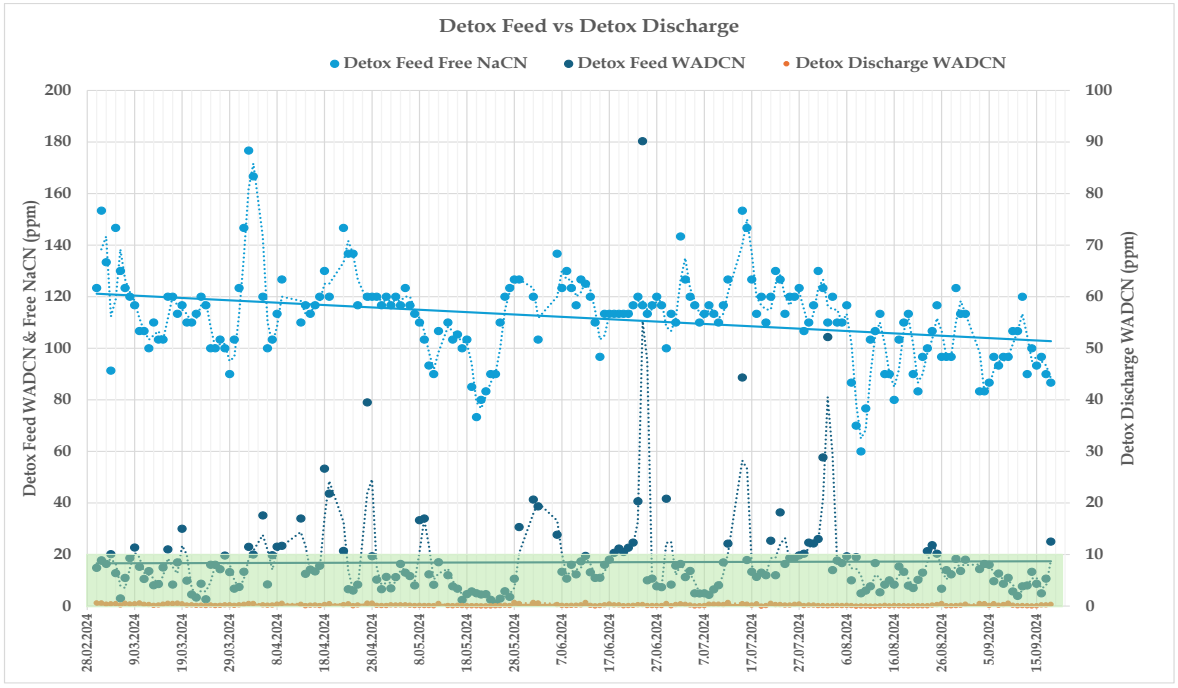
The WADCN content in the leach residue is reduced from 61 ppm to 0.8 ppm in the circuit and then pumped to the tailings dam for further cyanide destruction process. As a result of the close circuit water management system, the recycle water from the tailings dam is pumped back to the process plant with a WADCN concentration of 0.1 ppm.

Due to the environmental effects of cyanide and legal restrictions, the maximum allowable WAD cyanide level in the leach residue stored in the tailings dam is 10 ppm WADCN. Analyses conducted on the regular hourly samples are collected from the output of the detoxification circuit. Since commissioning of the process plant, the WAD cyanide in the leach residue transferred to the tailings dam consistently remained well below the legal limit of 10 ppm with the average of 0.8 ppm, as shown in the Graph 1.



Graph 1: Project to Date Average Data of Detox Discharge WADCN Vs. Detox WADCN Legal Limit

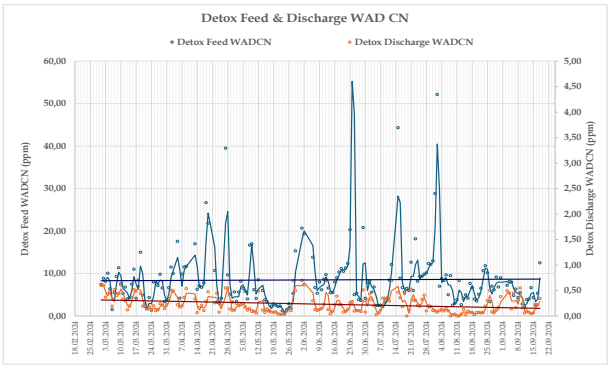
According to the database generated from the cyanide detoxification circuit from March to September 2024, the linear trend for the free NaCN and the WAD CN in the detox feed is almost parallel as shown in the Graph 2. So while the free cyanide is decreased, the WAD CN is decreased in the detox feed. As a result of this, the WADCN in the detox discharge is decreased.



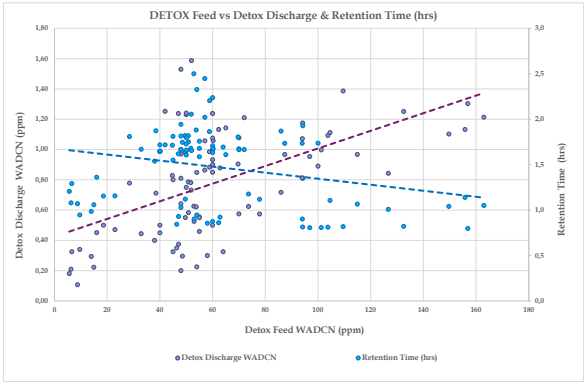
Graph 2: Detox Feed Free Cyanide and WADCN and Detox Discharge WADCN

As shown in the Graph 3, between March and September 2024, the WADCN in the detox feed is in the range of 90 to 1 ppm, while the WADCN of detox discharge is in the range of 0 to 1.6 ppm. So, as long as the retention time of the detox circuit remains at around 48 minutes, WAD CN of detox discharge tends to decrease by decreasing of detox feed WAD CN.

The retention time of the detox circuit is one of the key parameters for a steady state operation. The retention time to complete cyanide oxidation might be variable, depending on the composition of the detox feed to be treated, but generally it is in the range of 30 minutes to 2 hours. According to the design criteria, the detox circuit retention time for the Kızıltepe ore type is around 1 hour. Because the flow fluctuation in the CIL operation due to mill feed reduction causes low flow or additional flows from the spillage sumps, stripping circuit, etc, the detox feed would rise or drop for a certain time of period. As shown in the Graph 4 the retention time is in the range of 48 minutes to 2.5 hrs while the average WADCN in the discharge is 0.8 ppm which is well below of the legal limits of WADCN of 10ppm. As seen in the Graph 4, while WADCN in the detox feed is decreased, the WADCN in the detox discharge is decreased during the retention time between 48 minutes and 2.5 hours.



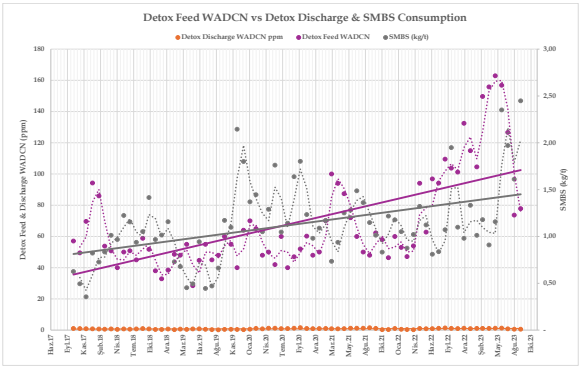
Graph 3: Detox Feed and Discharge WAD Cyanide



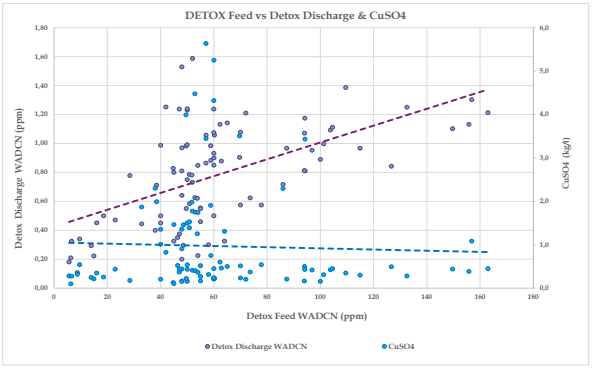
Graph 4: Detox Feed vs Discharge & Retention Time

In the process plant, the oxidising agent consists of air and Sodium Metabisulphite ($Na_2S_2O_5$) in liquid at a concentration of 10% for the O plus SO. Other reagents include $CuSO_4$ in liquid at a concentration of 10% to serve as a catalyst, and H_2SO_4 for pH control. The oxygen via air ring placed at the bottom of

the reactor and the reagents are dispersed in the leach residue using a well-agitated mixer. The reagent consumption of destruction process varies depending on the conditions. The WADCN in the detox feed slurry and the retention time of detox are the key parameters affect the reagent consumption. In the process plant, the SMBS consumption is in the range of 0.3 to 3.0 kg/t dry ore with a project to date consumption of 1.3 kg/t dry ore. Besides the Copper Sulfate consumption is between 0.1 and 5.64 kg/t dry ore with a project to date consumption of 1 kg/t dry ore.



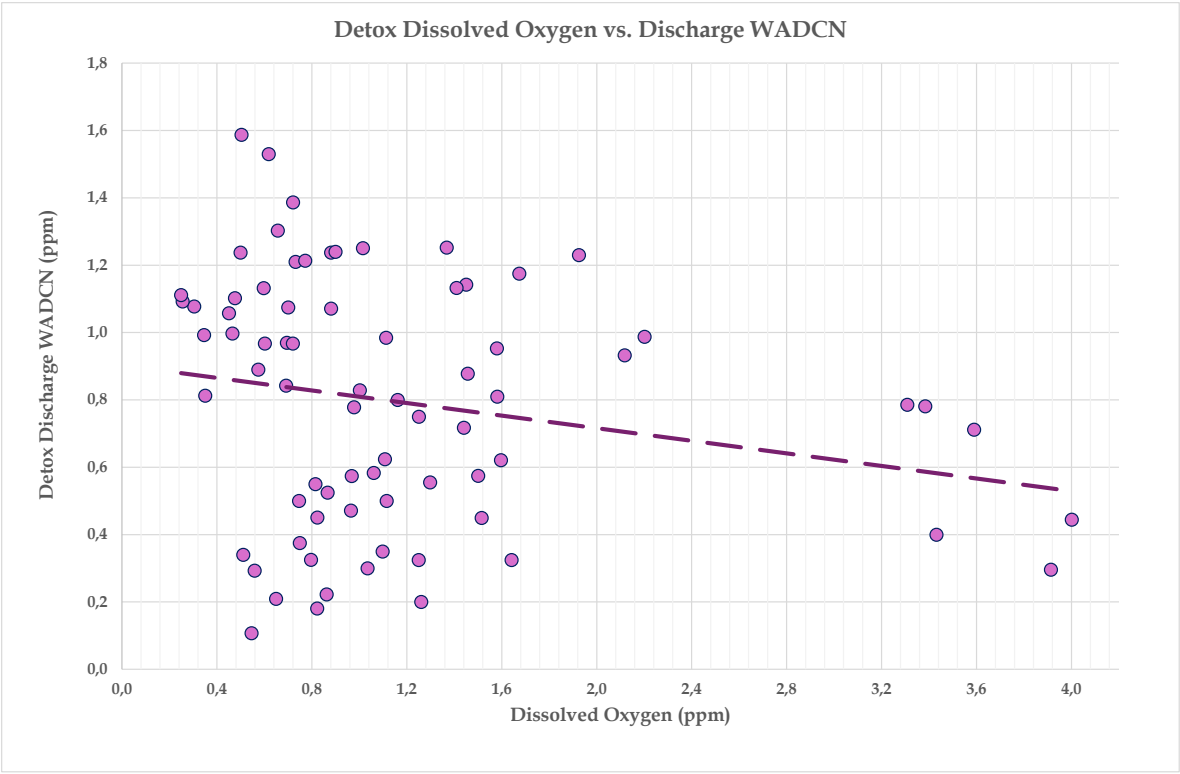
Graph 5: Detox Feed vs Discharge WADCN and SMBS



Graph 6: Detox Feed vs Discharge WADCN & $CuSO_4$

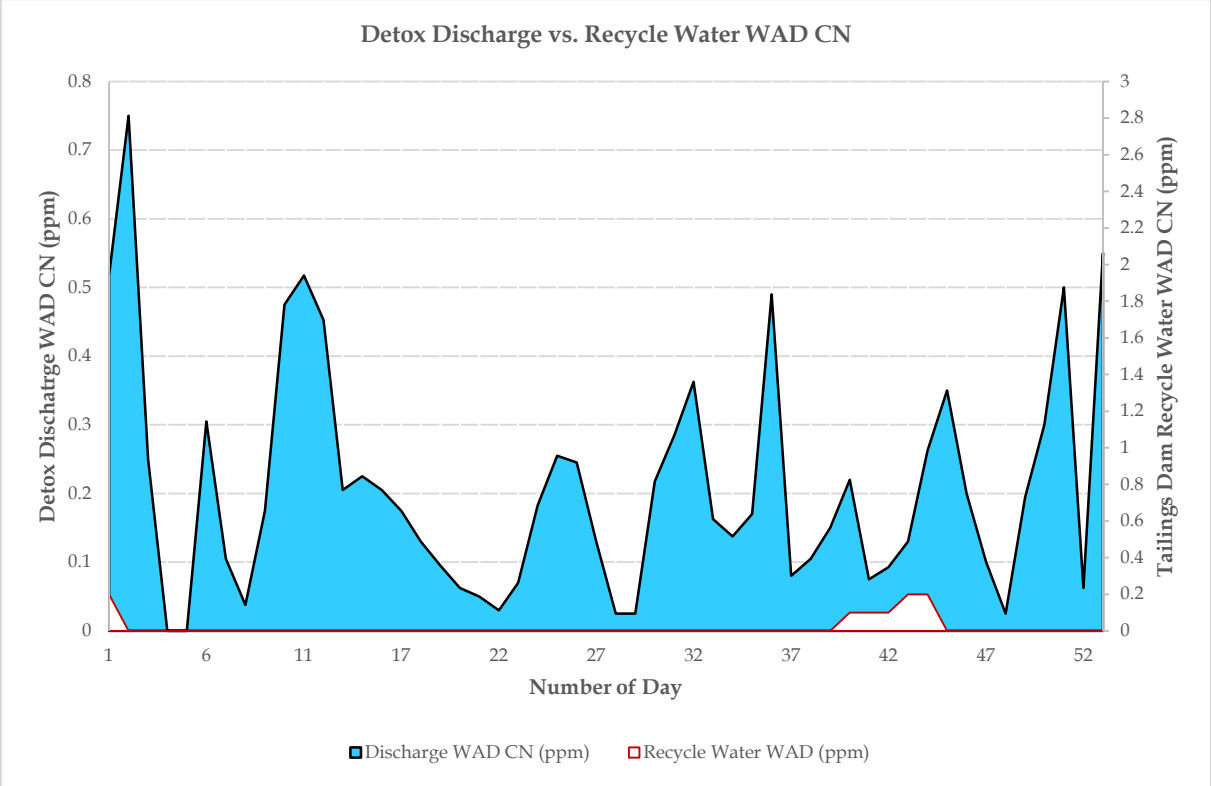
As shown in the Graph 5, when the WADCN in the detox feed increases, the SMBS consumption is increased and as a result of this the WADCN in the detox discharge is decreased as expected.

The WADCN in the detox feed vs the copper sulfate consumption is shown in the Graph 6 indicates that the Copper sulfate addition tends to remain constant as it is being used as a catalyst in the detox circuit. On the other hand, when the WADCN in the detox discharge slurry increases unexpectedly, the Copper Sulfate might be added in powder to reduce the retention time of the detoxification reaction in order to reduce the WADCN in the discharge.



Graph 7: Dissolved Oxygen vs Discharge WADCN

As stated in Equation 1, the cyanide destruction process is an oxidation reaction and the oxygen source would be suppled from either liquid oxygen generator as liquid or an air compressor as gaseous. In the process plant, air is supplied from an air compressor and delivered to the slurry via a ring sparger placed to the bottom of the reactor. The use of air as the oxygen source in the cyanide destruction circuit is the most economical option for the process operation as long as it meets the targeted WADCN in the discharge. The relationship between the dissolved oxygen and the WDCN in the detox discharge is shown in the Graph 7. While the dissolved oxygen is increased, the WAD CN in the discharge is decreased.



Graph 8: Detox Discharge & Recycled Water WAD CN

As shown in the Graph 8, the recycled water pumped back from TMF, generally contains less than 0.1 ppm WADCN and it does not exceed 0.2 ppm WADCN. So, this indicates that the natural cyanide destruction process continues in the tailings dam. As result of the this the WAD Cyanide in the leach residue is reduced to between 0.1 ppm (0.00001%) and 0.2 ppm after the treatment and this process does not produce any toxic material.

4. Conclusions And Discussions

Considering all the data;

- Because the WADCN content in the detox feed is the one of the key operating parameters of the detox circuit to maintain the WADCN concentration in the detox discharge under the legal limits of 10 ppm.

- As long as the cyanide addition to the leach circuit is maintained steady as required for the leaching recovery, the remaining cyanide in the leach residue would be controlled properly. This will also reduce the reagent consumption and operational cost for both the leach and detox circuit.

- The retention time is also an essential parameter for the cyanide detoxification process. So, the

capacity of the detox reactors should be designed properly to generate a steady state operation.

- It is observed that the WAD cyanide concentration in the detox discharge slurry is decreased when the SMBS consumption is increased. Also, the consumption of the copper sulfate tends to remain constant as it is used as a catalyst in this reaction. Therefore, the reagent consumption should be monitored and optimized as required to manage the operating cost.

- Because the natural cyanide destruction process continues in the tailings dam, the recycle water is being used in the process plant contains less than 0.2 ppm WADCN although the WADCN concentration in the detox discharge pumped to the tailings dam is in the range of 0 to 1.6 ppm.

- The detox reactions, as described in Equation1, require about 2.46 g of SO per gram of WAD cyanide stoichiometrically. The WAD Cyanide in the leach residue is reduced to between 0.1 ppm (0.00001%) and 0.5 ppm after the treatment and this process does not produce any toxic intermediaries.

References

Botz, M. M. (N.A.). Overview of Cyanide Treatment Methods.

Botz, M. M., Mudder, T. I., & Akcil, A. U. (2016). Cyanide Treatment: Physical, Chemical, and Biological Processes. In M. D. Adams, *Gold Ore Processing* (pp. 619-645).

Marsden, J. O., & Sass, S. A. (2014). Innovations in Gold and Silver Extraction and Recovery. In *Mineral Processing And Extractive Metallurgy-100 Years of Innovation*. Society for Mining, Metallurgy & Exploration.

Mudder, T. I., & Botz, M. M. (2004). Cyanide and Society: A Critical Review. *The European Journal of Mineral Processing and Environmental Protection*, 62-74.

Mudder, T. I., Botz, M. M., & Smith, A. (1991). Chemistry and Treatment of Cyanidation Wastes.

Razanamahandry, L. C., Andrianisa, H. A., & Karoui, H. (2017). Bioremediation of Soil and Water Polluted by Cyanide: A Review. *African Journal of Environmental Science and Technology*, 272-291.

Young, C. A., & Jordan, T. S. (1995). Cyanide Remediation: Current and Past Technologies. *Proceedings of the 10th Annual Conference on Hazardous Waste Research*, (pp. 104-129).

Heap Leaching Stability and Monitoring in İvrindi Gold and Silver Mine

Burak KAYACIK [1]*, Ali B. AKTAS [1], Alper ARUER [1], Yahya K. UZUNER [1], Serhat OZDOGAN [1]

[1] Tümad İvrindi Altın ve Gümüş Madeni, Değirmenbaşı Köyü No:422, İvrindi, Balıkesir, Türkiye

*Corresponding author: burak.kayacik@tumad.com.tr (Burak KAYACIK)

Abstract:

At TÜMAD Mining's İvrindi Gold and Silver Processing Plant, ore production is carried out using the heap leaching method. Under current economic conditions, low-grade gold ores have become processable due to advancements in size reduction systems and gold extraction techniques. One of the most important parameters to ensure the stability of the heap leach area is to operate in accordance with the design. To monitor the stability of the ore stacked according to the design, data from piezometers and moisture sensors installed in the heap leach area must be evaluated. For tracking surface deformations in the heap area, GeoRadar data is monitored simultaneously with prisms, and the collected data is analyzed and evaluated.

Keywords: *Heap Leaching, Geomembrane , Stabilite, Geomos, Georadar*

1. Introduction

The mining sector, which plays a crucial role in contributing underground resources to the national economy, inherently operates closely with nature. However, to ensure environmental health and safety, it is necessary to make significant efforts and apply sustainable and safe mining practices using the most suitable engineering methods. In this study, the stability of the heap leach area and its monitoring management practices will be discussed.

At TÜMAD Mining's Ivrindi Gold and Silver Mine Ore Processing and Enrichment Facility, run-of-mine ore produced from open pits is crushed in the crushing and screening circuit and reduced to the particle size specified for the leaching circuit. The crushed ore is then processed in the heap leach and CIC (Carbon in Column) circuits for metal recovery. The leaching process takes place in the heap leach area, where topography is prepared before the stacking process. The prepared area is isolated with an impermeable geomembrane. Once stacking is completed in the isolated area, the necessary monitoring and tracking procedures are carried out.

2. Heap Leach Design and Implementation

The most important aspect in practice is to ensure that activities are carried out in accordance with the design. Therefore, the following parameters are meticulously monitored:

- In the stacking process, the step design is made with a slope ratio of 3H:1V, and the step width is measured at 17 meters. Full compliance with these design criteria is ensured during implementation (Figure 1).

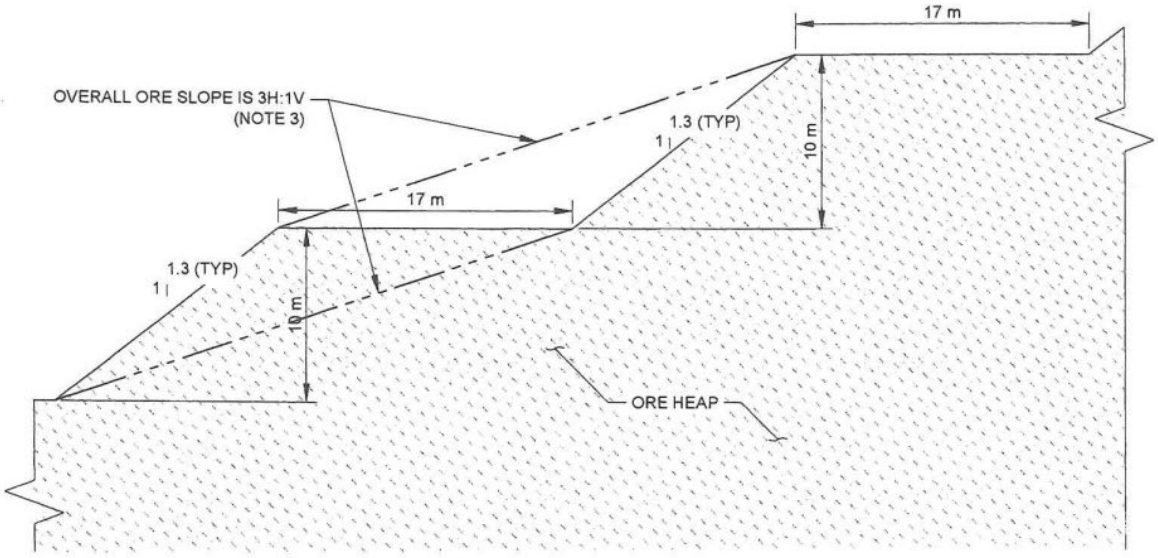


Figure 1. General Slope Gradient and Bench Width

- The quality of agglomeration is controlled by samples taken during each shift and is observed instantly using the "snowball test."
- The cement and water dosage is monitored in real-time through the SCADA system. Particularly in slope areas, ore heaps are agglomerated using cement dosages above the design requirements, thus enhancing slope stability.

3. Interlift Operations

Interlift operations are conducted in heap areas where the depth of the crushed and stacked ore reaches 40 meters. These operations aim to minimize solution accumulation in the lower levels of the heap and prevent water load formation at the base, thereby maintaining stability. The area designated for interlift is first prepared using bulldozers and is shaped with a slope of at least 1% and at most 3%. The sloped surface is connected to collection channels. Corrugated pipes are laid at regular intervals on this prepared surface, and a specific thickness of basalt is spread on top. This process prepares the area for the stacking of ore. (Figure 2).



Figure 2. Interlift operations

4. Piezometer and Moisture Sensor Operations

Heap leaching is monitored using piezometers and moisture sensors, with the data collected being analyzed and reported on a weekly and monthly basis. These sensors monitor the fluid pressure within

the heap, helping to detect potential stability issues such as water accumulation or pressure increases. Preventive actions are taken to address any identified issues. In line with the heap leach operation plan, the number of sensors in the field is increased based on project design and geotechnical studies carried out on-site, in parallel with production.

Measurement values are obtained in the heap area based on the no-load solution feed into the cell where the piezometer is located. When the solution feed is stopped, a decrease in the values indicates that no water load has formed within the ore in the field (Figure 3)

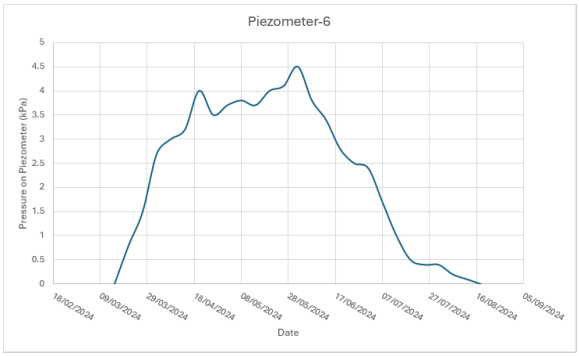


Figure 3. Piezometer and Moisture Sensor Operations

5. GeoMos and GeoRadar Operations

The slopes in the heap leach area are monitored 24/7 using the GeoMos and GeoRadar systems. GeoMos and GeoRadar work in conjunction with each other, continuously validating one another to ensure accurate monitoring (Figure 4).



Figure 4. GeoMos and GeoRadar4.1 GeoMos

5.1. GeoMos

GeoMos is a deformation monitoring system that tracks measurements using prisms. It can be accessed through any web-based device. In the field, fixed prisms located on slopes are continuously monitored 24/7 through automatic measurements taken by a total station (Figure 5)

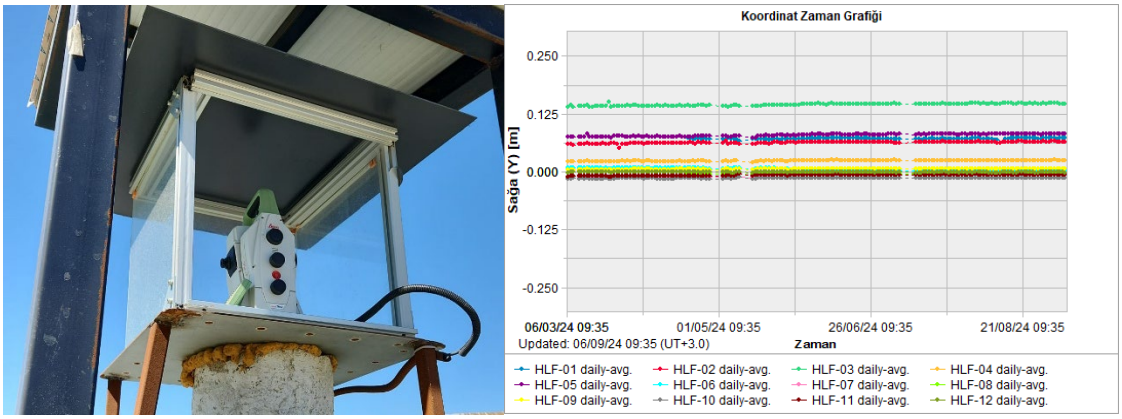


Figure 5. GeoMos

5.2. GeoRadar

GeoRadar is a deformation monitoring system that operates using radio waves. It is monitored with a device that has high speed, long range, and full 360-degree coverage. The surface of the slopes in the field is continuously monitored 24/7 through automatic measurements (Figure 6).

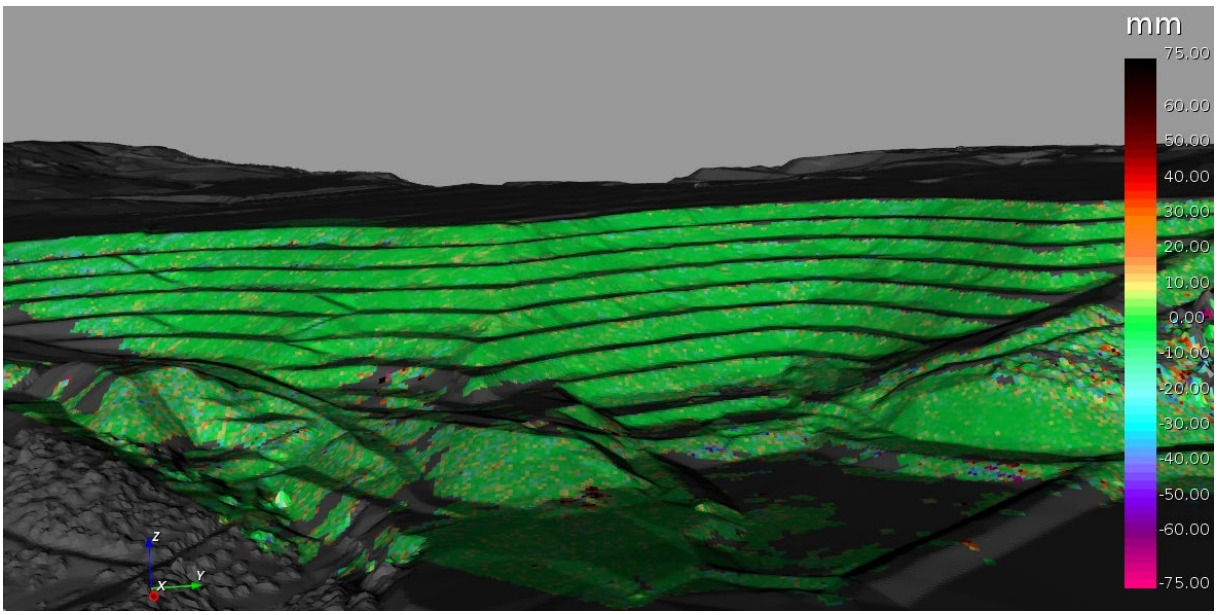


Figure 6. GeoRadar

6. 5. Geotechnical Studies.

Several geotechnical studies are conducted during and after the ore heap leaching process to measure the water load within the heap. These tests are listed below.

- **Electrical Resistivity Tomography (ERT Geophysics);** The purpose of this method is to create a moisture map within the heap leach area based on the electrical properties (resistivity) of the heap. In the graph below, the high moisture content on the interlift and the lower moisture content in the lower region indicate that the interlift is functioning effectively (Figure 7).

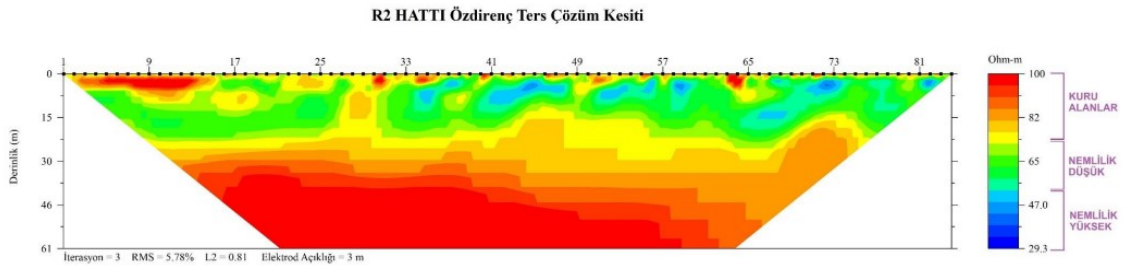


Figure 7. ERT generated graph

- **Cone Penetration Test (CPT):** Tip resistance and pore water pressure are monitored.
- **Seismic Cone Penetration Test (SCPT);** Tip resistance, pore water pressure, and seismic data are compared.
- **Resistivity Cone Penetration Test (RCPT);** Tip resistance, pore water pressure, and electrical conductivity data are compared.

In all three tests, lateral pressures are also monitored.

7. Conclusion

In the heap leaching operations at the İvrindi Gold and Silver Processing Plant, monitoring studies conducted with piezometers and moisture sensors have enabled the detection of water pressure and fluid accumulation, ensuring heap stability. Additionally, continuous slope deformation monitoring using GeoRadar and GeoMos systems has allowed for the early identification of potential risks in the heap area and the implementation of necessary preventive measures.

Geotechnical tests have shown that the water load in the heap area is under control and stability is maintained. In particular, interlift operations have improved heap stability by preventing water accumulation beneath the heap. In conclusion, heap leaching processes at the İvrindi Gold and Silver Mine are carried out in accordance with the design, and site stability is effectively monitored. As a result, metal recovery is achieved in a safe and economical manner, ensuring the sustainability of mining operations

References

M.E.Orman, K.Criley, February24-27,1997 ''Ore permeability Testing for Heap Leach Design''

Hasan KARAASLAN, Ali SİLAHTAR, December 2023, '' Elektrik Rezistivite Tomografi (ERT) ve yüzey dalgası analiz yöntemleriyle aktif bir heyelan alanının incelenmesi''

M.A. Styler, P.W. Mayne, D.McGowan, J.T.Sharp, July 23, 2018 '' Predicting changes in static liquefaction susceptibility using cone penetration test results''

Pascual Perazzo, Gabriella Vaschetti, Sep29,2023, '' Performance of a geomembrane faced tailings dam''

H.İbrahim KIRŞAN, İsmail GİRGİN,Sep 1990,'' Yığın Liçi Uygulamaları ve Ekonomik Açıdan Önemi''

Safe Use of Cyanide in Gold Production: International Cyanide Management Code

Bilge KÜÇÜKAYTAN [1]*

[1] Tümad Madencilik San. ve Tic A.Ş, Barbaros Mah. Buğday Sk. No:9, Ankara, Türkiye

*Corresponding author: e-mail (Bilge KÜÇÜKAYTAN)

Abstract:

Cyanide is a chemical widely used in the extraction of valuable and industrially important metals such as gold, silver, and copper. With the rise of gold mining in Turkey in the 2000s, the safe use of cyanide became a significant public concern. To establish principles for the safe use of cyanide and ensure its control, the International Cyanide Management Institute (ICMI) was established, headquartered in Washington, under the umbrella of the United Nations. The institute has developed 9 core principles regulating the processes of cyanide production, transportation, use, storage, operational use, mine closure, worker safety, emergency preparedness, training, disposal, and communication with stakeholders. Compliance with these principles is voluntary but requires full adherence to 29 standards and 238 criteria defined in the verification guide. Compliance is assessed through on-site audits conducted by independent auditors accredited by the institute. Information regarding these audits conducted on behalf of the International Cyanide Management Institute is transparently shared with the public at www.cyanidecode.org.

Keywords: *Safe Usage of Cyanide in Gold Mining, TÜMAD International Cyanide Management Code Application, Stakeholder Communication and Environmental Safety*

1. Introduction

Cyanide is the most preferred chemical for gold recovery. It is one of the few chemicals that dissolves gold in water and is a low-cost option widely used in the industry. Due to both technical and economic reasons, cyanide is considered the most suitable chemical for extracting gold from ores. Cyanide has been used in metal extraction since 1887 and is still safely used and managed in gold recovery worldwide today. Gold mining operations typically use very dilute sodium cyanide solutions, with concentrations ranging from 0.01% to 0.05% (100 to 500 ppm) (Mudder, 1999).

Other chemicals, such as halogens, thiocarbamide, and thiosulfate, are available for gold extraction, but they form less stable complexes with gold and require more aggressive conditions and oxidants for dissolving gold. These alternative chemicals are generally more expensive and pose similar or even greater risks to the environment and human health compared to cyanide. The industry continues its efforts to find environmentally friendly and more cost-effective alternatives to cyanide. Although alternative leaching agents have been researched for decades, a chemical system that is safer, more cost-efficient, and more effective than cyanide has yet to be found (Akcil, 2010).

1.1. Cyanide Management and Applications:

To ensure the safe use of cyanide in mining, the International Cyanide Management Institute (ICMI), a non-profit organization based in Washington, D.C., was established. It is responsible for promoting the application of the Cyanide Code and developing knowledge about cyanide management practices. The International Cyanide Management Code is one of the most established standards in the mining sector and serves as a security mechanism for stakeholders in the industry.

The International Cyanide Management Code is one of the most mature and established standards in the mining industry, serving as a mechanism of assurance for stakeholders in the sector. In 2000, following a dam breach accident caused by frozen water blocks during the sludge excavation process

in the Aural Gold Mine's tailings dam in Baia Mare, Romania, approximately 100,000 m^3 of sludge waste was discharged into the Tisza River, which is connected to the Danube River. As a result, fish deaths occurred along the Tisza River. Following this event and subsequent demands for restrictions or a complete ban on the use of cyanide in mining and the gold industry, the United Nations Environment Programme (UNEP) and the International Council on Metals and the Environment (ICME, now the International Council on Mining and Metals) organized a multi-stakeholder workshop in Paris in May 2000 to determine how cyanide management in gold mining could be improved. These initiatives led to the development of the international voluntary "Cyanide Code Implementation Guidelines" through collaboration between UNEP, the World Bank, voluntary environmental groups, and mining companies and producers (Akcıl, A., 2018).

The initial implementation of the Cyanide Code by 14 companies in 2005 has now grown to over 200 companies officially implementing it in more than 300 operations worldwide. The aim of the Cyanide Code is to improve the management of cyanide used in gold and silver mining, ensuring better protection of human health while reducing the environmental impact of accidental releases or exposures to the chemical. The Cyanide Code establishes a management system based on principles and standards to ensure the safe management of cyanide throughout its life cycle—from production to transportation, handling, use, recycling, and disposal at mining sites (www.cyanidecode.org). Since its inception, certified operations have reported "0 deaths and 0 major environmental disasters" caused by cyanide (ICMI, 2023 Annual Report, pp. 38).



Figure 1. Principles of the International Cyanide Code

According to the data in the 2023 annual report published by ICMI, approximately 133 mining operations worldwide comply with the detailed requirements of the Cyanide Code for managing cyanide. It is anticipated that 139 mines will be members of the code by 2024. In 2023, 70 certificates were renewed, and 281 companies were reported as Cyanide Code Certified. By the end of 2023, 100 cyanide code-certified mining operations continued in 26 countries.

Mining operations participating in the program are required to purchase cyanide from certified producers, and the cyanide must be transported using certified transport operations and supply chains. Certified producers and transporters manage cyanide shipments over long, regulated supply routes. The certification of transporters mandates full responsibility for the railroads, ports, and sea transportation routes chosen and used in their supply chains. Before a transport route can be included, all transportation routes, ports, railroads, and sea routes must undergo a due diligence and verification process to ensure safe cyanide transportation. Cyanide Code processes have been successfully implemented in various mining operations across developing and developed countries under different conditions and climates worldwide.

Gold and silver mining companies that use cyanide in their production, as well as cyanide producers and transporters, can initially join the program by becoming signatories to the Cyanide Code. The Cyanide Code consists of two primary components: the core principles and implementation standards. The core principles encompass comprehensive commitments to manage cyanide responsibly, while the implementation standards define the performance objectives and goals that must be met to fulfill the requirements of each principle. Guidance on how to achieve these goals is provided through questions defined in the guide.

To verify the implementation of the Cyanide Code, independent third-party auditors authorized by the International Cyanide Management Institute conduct audits every three years. Companies that fully comply with the principles, standards, and guidelines laid out by the code are granted full certification by the lead auditor. After reviewing the audit recommendation, the Institute issues a "FULL COMPLIANCE" certificate.

If a company demonstrates a good-faith effort to comply with the Cyanide Code and any identified deficiencies do not pose an immediate or serious threat to worker or public health or the environment, the auditor may find the company in "SUBSTANTIAL COMPLIANCE." In such cases, the certification is conditional, requiring the company to prepare a Corrective Action Plan (CAP) and implement it within one year to achieve full compliance. Actions taken by companies operating under substantial compliance are shared with the lead auditor and the institute, and corrections are published on the Cyanide Code website. This process provides a mechanism to ensure better protection of human health and the reduction of potential environmental impacts. The certification cannot exceed one year without full compliance.

Once certified, a company becomes accountable to the Institute. Significant cyanide-related incidents—such as spills, exposure, unauthorized discharges into natural surface waters, or wildlife deaths—must be reported to the ICMI within 72 hours. This includes transportation incidents or cyanide theft. In cases where non-certified cyanide is purchased or transported due to supply chain disruptions or emergency purchases, companies must notify ICMI within 72 hours, explaining the reasons and estimated time for restoring certified cyanide supply. Additionally, any changes to the transporters or elements of the supply chain must be reported within 72 hours.

The International Cyanide Code strengthens a company's operations and its standing with stakeholders, demonstrating that cyanide management is conducted with greater precision, transparency, reliability, and at a high level. It serves as a globally recognized reference point for the responsible use of cyanide. The Code confirms the implementation of best practices that support and align with regulatory compliance requirements. It enhances process improvements and cost savings. Adherence to the Cyanide Code provides an immediate opportunity for improvement in how cyanide is managed at facilities. Certified operations in compliance with the Cyanide Code significantly limit the potential for cyanide use to negatively impact human health or the environment. After alignment with the Code, the risks of potential accidents and environmental hazards related to cyanide are greatly reduced. The Cyanide Code can have a positive effect on corporate culture and behavior by enhancing a company's management practices and reputation for transparency. It motivates continuous improvement through the three-year audit and re-certification process. The Cyanide Code demonstrates a company's commitment to the environment, human health, and safety, provides a framework for community engagement, and supports the company's social license to operate. The Cyanide Code reduces liabilities by protecting workers, the public, living organisms, and the environment (Akcıl, A., 2014).

2. TÜMAD Mining

TÜMAD Mining is a Turkish mining company conducting exploration and operational activities in precious and base metals. Since 2017, the company has been running two mining operations in the districts of Lapseki in Çanakkale and İvrindi in Balıkesir, using tank and heap leaching methods. As a part of its vision, TÜMAD committed to operating in accordance with the requirements of the International Cyanide Code when it received its Environmental Impact Assessment (EIA) approval in 2015. The financing process was managed with the European Bank for Reconstruction and Development

(EBRD), which includes the requirement to obtain the International Cyanide Code certification within its sustainability criteria. As a result, the processes were aligned with the Code from the construction phase onward, and in 2017, the Code awareness training and certification process started with the T1 and T2 training programs.

The Lapseki Gold and Silver Mine operates using the tank leaching method. After the enrichment process carried out in the tanks, the cyanide present in the mine waste is chemically treated and degraded to below one ppm (<1ppm) using the INCO sulfur dioxide and air process. The mine waste is then filtered and pressed to solid waste at a rate of 82%, and is spread and compacted in a Dry Waste Storage area constructed with 50 cm of compacted clay, 2 mm of high-density geomembrane, and geotextile, whose impermeability has been independently verified. The Lapseki Gold Operation is the world's best available technology mine, where all these methods are applied together to ensure the highest level of operational safety.

With the commissioning of the Lapseki operation, a "Gap Analysis" was conducted to assess the operation's compliance with the Code requirements. The gap analysis, conducted in a full audit format, involved questioning all nine principles, 29 implementation standards, 238 questions, and requirements on-site, identifying gaps, and assigning actions to address them. Through corrections and corrective actions, the operation was brought into full compliance with the Cyanide Code requirements.

2.1. Cyanide Code Audit, Production, and Transport Loading/Unloading

In March 2021, a cyanide code audit was carried out at the Lapseki Gold Mine by a team composed of John Lambert, a lead auditor with over 30 years of technical experience, and Prof. Dr. Ata Akçıl, Turkey's only Cyanide Code auditor. The audit process starts by verifying that the cyanide is procured from a certified company listed on the ICMI website as an "approved producer." The audit checks whether the sodium cyanide is purchased in compliance with both legal and ICMC requirements, and agreements with the supplier on matters such as the Turkish safety data sheet, the labels on sodium cyanide boxes, the inclusion of coloring agents, and the labeling indicating "For Industrial and Commercial Use Only" in Turkish.

Transporters responsible for moving cyanide must also have an approved ICMC certification. During the contracting phase, certificates are requested from transport companies by the supply chain department. For cyanide transport within Turkey, the transport route must be determined and evaluated, and the transport must be carried out by a company with an ICMC certificate, according to an agreed route plan that includes the ports and crossing points. Risk assessments for all the ports and routes are conducted.

During transportation, to manage any potential emergencies, the transport process is overseen by trained personnel from the contracted company, who are specialized in responding to chemical spills. The entire transportation process continues until the cyanide-loaded containers arrive at the mine site entrance. Drivers are informed and trained on emergency procedures and safety measures. Traffic on shipment routes is halted, and equipment like forklifts and mobile cranes are inspected as part of job safety analyses before unloading operations begin. Working permits for height are issued, and the cyanide containers are suspended using a guide rope by personnel wearing parachute-type safety harnesses, with the help of a mobile crane. The truck is removed from the fenced cyanide storage area, and the container is lowered to the ground.

Seal numbers and box numbers throughout the supply chain process are carefully cross-checked, seals are cut and stored, and hydrogen cyanide (HCN) gas is measured twice using a mobile gas detector. Cyanide crates are stacked in a closed, leak-proof, epoxy-coated storage facility in a way that allows air circulation, following the manufacturer's guidelines for load capacity. Flammable, explosive, oxidizing, or acidic materials are not stored in the cyanide storage area.

Even though the storage facility is equipped with both natural and forced ventilation systems, a fixed HCN gas detector is installed in the closed storage to monitor potential gas formation. Values are continuously monitored via an automated system, and concentrations inside the facility are also tracked on screens located outside the building for easy remote observation.

2.2. Implementation of the Cyanide Code in Operational Activities

Cyanide code operations require the establishment and strict application of well-structured management systems. This includes setting up and maintaining a strong documentation system in line with the requirements of quality, environmental, and occupational health and safety management systems. Such systems ensure the control of operations through management plans, procedures, and instructions, the implementation of change management processes, operation of permit systems, and the execution of preventive processes like area control, monitoring, reporting, incident response, corrective actions, and training. Waste and water management, risk and opportunity identification, and calibration tracking are also essential parts of these processes.

During cyanide preparation at the facility, the cyanide boxes are first visually inspected for integrity. The "First In, First Out" (FIFO) rule is applied when taking cyanide boxes from the storage. To prevent other boxes from being punctured by the forklift during handling, the length of the forklift's forks is set at a maximum of 1200 mm. Additionally, the cyanide preparation unit tanks are equipped with level indicators, and alarms are set for 86-90% and 75-85% levels to prevent overflows, leaving at least a 0.5 m^3 air gap in the tanks.

At all stages, workers in the area use mobile gas detectors to monitor potential HCN gas formation (A1: 47 ppm, A2: 10 ppm). For possible emergencies, an emergency stop switch is integrated into the automation system, which triggers a warning on the control room screens when used by the workers. After cyanide preparation, wooden crates are broken up and stored in a closed warehouse to prevent any other use. Contaminated packaging waste, like big bags and disposable personal protective equipment, is disposed of by licensed carriers under national regulations.

Once the preparation is complete, all areas where cyanide solutions are supplied through pipelines are covered with concrete flooring to prevent any leakage from directly contacting the natural ground. Pipelines containing cyanide solution are double-walled, and the solution is dyed according to protocol for easy identification in case of leakage. Additionally, all pipelines are labeled with the type of liquid inside and the flow direction. Cyanide is transported in "purple-colored" pipelines within the facility. Secondary containment measures are in place in all areas where cyanide solutions may come into contact to prevent potential spills from contaminating groundwater. All cyanide units are carefully inspected during audits to verify that they are constructed in accordance with accepted engineering standards and technical specifications. Moreover, detailed water management plans are in place to maintain control over water management. Monitoring programs are conducted to observe the potential impacts of the activity on wildlife and surface and groundwater (WAD cyanide), with findings included in monitoring reports.

2.3. Closure of Mining Operations and Cyanide Management

The closure of mining operations requires the preparation of safe mine closure and safe decommissioning plans to protect human and environmental health against the possibility of unexpected causes, natural disasters, bankruptcy, or commercial needs. These plans are signed off after closure budgets are established by an independent competent third party. The calculations include unit quantities of concrete, pipes, steel materials, and equipment contaminated with cyanide at the facility, the costs of decontaminating these materials, the disposal of remaining cyanide stock, and engineering disposal amounts for monitoring. The costs of safe closure or unexpected closure must be secured with a financial institution. This can be achieved through methods such as bank guarantees, setting aside cash reserves, or obtaining insurance for the specified amount.

2.4. Protection of Employees and Training

Risk assessment studies encompassing all activities are conducted to protect employees from cyanide exposure. In shift-start training, a participatory approach is adopted by considering the views, requests, and suggestions of employees. Personal protective equipment to be used in areas containing cyanide is determined, and training is provided for the use of this equipment. All employees receive "Occupational Health and Safety (OHS) Induction and Chemicals Training," and those who pass are allowed to enter

the work area. Additionally, detailed cyanide training provided by the facility division is mandatory in areas containing cyanide.

2.5. Emergency Plans and Intervention Methods Practices

Response methods for potential cyanide-related emergencies have been established. Emergency plans are tested throughout the year via drills based on scenarios, and corrective actions are initiated to address any shortcomings. The search and rescue and medical teams carry out necessary interventions using equipment available at the facility. In cases where the impact of emergencies is significant, external support is sought by coordinating with relevant institutions. The search and rescue team is designed with scenarios involving the use of chemical substances in mind, and the equipment is kept ready for use, with monthly checks.

Cyanide spills are categorized into two groups: solid and liquid. Solid spills are easier to control due to their immobility, while liquid spills require more serious precautions. Spills must be neutralized to a basic state using substances like caustic soda or lime.

In the event of possible cyanide exposure, fast and effective first aid is crucial to increase the chances of survival after cyanide poisoning. For this reason, an adequate supply of cyanide antidotes is kept on hand and can be administered with oxygen by the workplace physician when necessary. Emergency response kits are available in areas containing cyanide, and these kits are kept in clearly marked, easily accessible locations. The kits include oxygen breathing apparatus, chemical-resistant gloves, protective goggles, and first aid procedures.

2.6. Stakeholder Engagement and Dialogue

In line with the requirements outlined in the stakeholder engagement plans, all stakeholders are identified, starting with nearby communities. Focus group meetings are held with stakeholders to discuss the transportation, use, and disposal of cyanide, sharing information to address frequently asked questions and concerns. Following the principle of transparency, cyanide-related spills are included in annual sustainability reports, ensuring the publication of global data and statistics. Additionally, information about cyanide antidotes for emergency use is shared with all public institutions, organizations, and local hospitals in the region. Visual and written materials are prepared to provide information on the use of cyanide and the International Cyanide Code.

3. Conclusion

The International Cyanide Code is an important certification based on voluntary principles, ensuring the safety of cyanide chemicals used in gold production by validating and certifying compliance with nine main principles, 29 standards, and a list of 238 questions, reflecting a complete life cycle involving producers, transporters, and end-users. It is regarded as a foundational reference for other internationally recognized integrated management system certifications and questions its existence. According to statistics published by the International Cyanide Institute, since the inception of the Cyanide Code, there have been "0 deaths and 0 major environmental disasters" in operations certified under the Code.

With its certification, the Cyanide Code enhances operational process improvements and cost savings. Compliance with the Cyanide Code provides urgent opportunities for improvement in the management of cyanide in facilities. Activities certified in accordance with the Cyanide Code significantly limit the potential negative impacts of cyanide use on human health and the environment. After achieving compliance with the Code, the potential accidents and environmental risks associated with cyanide are greatly reduced. The Cyanide Code positively affects a company's management practices and its reputation regarding transparency, contributing to the improvement of corporate culture and behavior. It motivates continuous improvement through three-year audits and re-certifications.

TÜMAD Mining has achieved great success as the first Turkish mining company to fully comply with the international cyanide code requirements for both tank leaching and heap leaching operations, certifying both operations with "zero non-copliences" Additionally, for the Lapseki operation, it has

successfully completed the second three-year re-certification process, demonstrating that it has continued to manage the safe use of cyanide, from procurement to transport, while maintaining effective emergency protocols and dialogue mechanisms with stakeholders.

REFERENCES

Akcıl,.A, (2018) Altın ve Gümüş Madenciliğinde "Bağımsız Denetleme Kültürü, P138-145

Akçıl, A, (2014) Siyanür Yönetilebilir bir kimyasal mı?

Akçıl, A. (2010). 'A New Global Approach of Cyanide Management: International Cyanide Management Code for the Manufacture, Transport, and Use of Cyanide in the Production of Gold', *Mineral Processing and Extractive Metallurgy Review*, 31(3), 135–149.

Akcil, A. (2006). "Managing cyanide: health, safety and risk management practices at Turkey's Ovacik gold-silver mine." *Journal of Cleaner Production*, 14, 727–735.

Akçıl, A. (2006). "Managing cyanide: health, safety and risk management practices at Turkey's Ovacik gold-silver mine." *Journal of Cleaner Production*, 14, 727–735.

Mudder, T. (1999). *The Management of Cyanide in Gold Extraction*.

https://cyanidecode.org/newsroom/#reports

https://cyanidecode.org/the-cyanide-code/#1615236112177-0770fca3-213b

https://cyanidecode.org/wp-content/uploads/2021/06/14-Mining-Verification-Protocol-JUNE-2021.pdf

https://cyanidecode.org/wp-content/uploads/2024/07/2023_Annual_Report_Secure2.pdf

[Siyanür Süreçlerinde İSG Yönetimi El Kitabı (TMD_LAP_İSG_ELK.003)].

Sogut Gold Mine: Gravity + CIL Processing Plant Overview

Fehmi Can Süter [1]

[1]Affiliation 1

[2]Affiliation 2

*Corresponding author: e-mail (Firstname Lastname)

Abstract:

.

Keywords: *Keyword1, Keyword2, Keyword3*

1. Introduction

Optimization of Rare Earth Element Recovery from Kızıldağ (Karaman-Türkiye) Shale Ore Using Response Surface Methodology

Turan Uysal [1]*, Ceren Erüst Ünal [2], Muhammed Esat Akça [3], Hikmet Sis [4], Murat Erdemoğlu [4]

[1] Gumushane University, Mining Engineering Department, Gumushane, Türkiye

[2] Munzur University, Rare Earth Elements Application and Research Center, Tunceli, Türkiye

[2] Istanbul Technical University, Department of Mineral Processing Engineering, Istanbul, Türkiye

*Corresponding author esat.akca721@gmail.com (Muhammed Esat Akça)

Abstract:

In this study, the usability of bauxite-related shale ore, rich in rare earth elements (REE), to produce REE, which have high added value and critical importance, was investigated. In this context, Kızıldağ (Karaman-Turkey) shale ore, was prepared for tests through size reduction and sampling processes. HCl leaching was performed at different acid concentrations, leaching times, leaching temperatures, and liquid/solid ratios to determine the optimum leaching conditions for the milled ore. The modeling and optimization parameters related to leaching efficiency were investigated using the response surface method. The results were evaluated using analysis of variance, three-dimensional graphs were drawn, and the accuracy of the models was discussed. Accordingly, optimum values were found, and the REE leaching efficiency corresponding to these optimum values was 49.13%. It was concluded that the optimization results were compatible with the experimental results, and the average error rate (6.35%) was low.

Keywords: *Shale, Rare Earth Element, Acid Leaching, Optimization, Response Surface Methodology*

1. Introduction

Considering the global supply and demand for commodities, the European Commission has identified 34 critical raw materials for 2023, with rare earth elements (REEs) ranking at the top of the list (European Commission, 2023). REEs consist of 17 elements, including the lanthanide group, scandium, and yttrium, all of which exhibit similar chemical properties. These elements, with an ionic valence of +3, are categorized as light and heavy rare-earth elements based on their atomic numbers and frequency of occurrence in nature. REEs are widely used in the production of many high-tech devices and equipment, such as electric/hybrid vehicles, wind turbines, solar panels, aircraft, and electronic devices, including cell phones, computers, rechargeable batteries, and modern medical devices, such as MRI devices (Binnemas et al., 2013; Krishnamurthy and Gupta, 2016; Ünal et al., 2023). With the widespread use of electric vehicles, wind turbines, and solar panels, demand for REEs has increased.

The Kızıldag and Kemiklitepe bauxite mineralizations in Turkey are in the Bolkar Mountain Bauxite Province. The protolith, the source rocks of the Bolkar Mountain bauxite mineralization, was defined as shale by Hanilçi (2013). Heavy REE enrichment is typical in these deposits, and bauxite deposits and their source rocks and shales contain high amounts of REEs that can be potential sources. Researchers (Hanilçi et al., 2013; Hepvidinli, 2019; Öztürk et al., 2019) have studied the formation of REE in bauxite-related deposits in the Bolkar mountain region and found that clay minerals formed during the lateritic weathering process balance the lack of electrostatic charge on their outer edges with ions, such as Ca^{2+}, Na^{+}, and REE_3^{-}. Thus, REEs were enriched by adsorption on the outer surface of the clay. These REE-rich clays were formed by the addition of bauxite. It is necessary to investigate the recoverability of REE from these bauxites with REE potential in the Bolkar Mountain region using a sustainable method. In this context, this study investigated and optimized the recovery of REEs from REE-rich shales which is considered unproductive because of their high silica and iron contents.

2. Material and Methods

2.1. Material

Shale samples were obtained from bauxite mines in the Ayrancı district of Karaman (Türkiye), owned by Demireller Inc. As analyzed by X-ray diffractometer (Figure 1), the ore contains mainly paragonite, muscovite, quartz, pyrophyllite, kaolinite, and halloysite. The chemical composition of the bauxite-related shales is presented in Table 1 which exhibits a good agreement with XRD results.

Table 1. Major oxide content of Kızıldağ shale ore, %

SiO_2	Al_2O_3	Fe_2O_3	CaO	MgO	Na_2O	K_2O	TiO_2	MnO	P_2O_5	LOI
42.7	28.8	4.29	5.69	0.56	3.04	3.04	1.41	0.025	0.05	9.49

Table 2. REE content of Kızıldağ shale ore. ppm

Ce	La	Y	Nd	Nb	Sc	Pr	Dy	Er	Gd	Sm
115.7	82.8	83.8	59.2	31.6	28	15.7	11.65	7.46	10.42	10.75
Yb	**Ho**	**Lu**	**Eu**	**Tb**	**Tm**	**∑REE**	**Rb**	**Th**	**U**	**-**
7.06	2.52	1.04	1.88	1.73	1.09	473	112	21.7	4.39	-

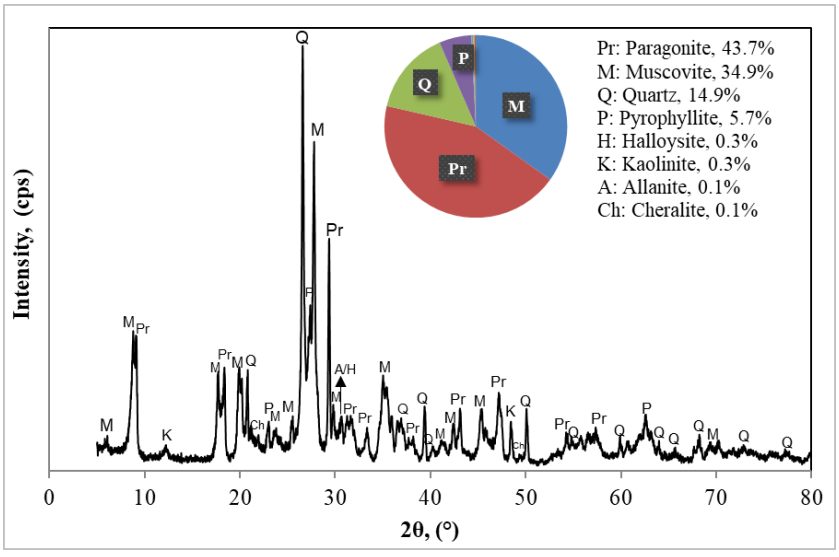


Figure 1. XRD pattern of Kızıldağ shale ore

2.2. Methods

Mineral processing

Shale ore was systematically crushed to a length of -4.75 mm with a Pulverisette I model (Fritsch) jaw crusher with an adjustable exit opening. Half of the crushed samples were separated into reference samples using a riffle sample splitter. The other half was crushed by jaw crusher to a length of -2 mm. Later, the samples were crushed to ~ 2 mm in size and divided into small batches (approximately 40 g) using a rotary sample divider. Then the samples were dried at 105 °C for 60 min before the leaching experiments.

Acid leaching

The leaching process was carried out in a 500 cm^3 glass flask placed in a flask heater device (Weightlab) with a bed volume of 500 cm^3, using a 200±10 cm^3 solution that could be mixed with a magnetic stirrer under reflux, with a mechanism set up in a fume hood, where the solution temperature was constantly monitored. Because the balloon heater also has magnetic stirring, an external stirrer was not required for the mixing process. At the end of the leaching period, the heating and mixing mechanisms were stopped immediately, and solid-liquid separation was performed by vacuum filtration of the loaded leaching solution. After recording volume of the liquid samples, they were placed in lidded plastic containers and stored in a refrigerated cabinet, whereas solid samples were placed in another lidded plastic container after weighing.

Experimental design

A set of leaching tests was carried out to simulate the leaching process of rare earth elements and determine the optimal conditions for producing a pregnant solution with the highest rare earth ion concentration. The response surface methodology (RSM) and Box-Behnken design were used for the mathematical modeling and optimization of leaching. In this study, optimization of the leaching parameters of shale samples was carried out using the response surface method with four independent variables: acid concentration, leaching temperature, leaching time, and liquid/solid ratio by weight. The effects of these parameters on the leaching recovery were examined using the Box-Behnken design, and mathematical models were developed. This method provides an experimental study and repetition opportunity, excluding the main points. With this design, the change and interaction of all the variables can be examined using the same process. Statistical analyses were performed using the Minitab 22 software. The results were statistically tested with a 95% reliability rate using analysis of variance (ANOVA). A total of 27 experiments were performed for the four factors according to the Box-Behnken method. When the response data were obtained from the experimental studies, regression analysis was performed to determine the coefficients, standard deviations, and magnitudes of the response model. The second-degree polynomial equation used to explain the dependent variables is given in Equation 1.

$$Y = \beta_0 + \sum_{i=1}^{k} \beta_i X_i + \sum_{i<j}^{k} \beta_{ij} X_i X_j + \sum_{i=1}^{k} \beta_{ii} X_i^2 + \quad (1)$$

In Eq. 1, y is the dependent variable (leaching recovery) and is a function of the independent variables coded in terms of x_1, x_2 and x_3. β_0 is the regression coefficient, ε is the error, β_i is the linear coefficient, β_{ii} is the quadratic coefficients and β_{ij} are the pairwise interaction coefficients.

Characterization techniques

The inductively coupled plasma atomic emission spectrometry (ICP-AES) for major oxides and inductively coupled plasma mass spectroscopy (ICP-MS) for REEs used to determine the chemical

composition in ALS Global Analytical Laboratories (İzmir, Türkiye). X-ray diffractometer (XRD) analysis was used to determine which minerals the calcined and over-ground products in Kızıldağ shale ore consist of and to monitor the change in the crystal properties of these minerals with calcination and grinding. XRD patterns were obtained with Rigaku MiniFlex 600 model XRD device (Munzur University) at CuKα (λ=1.5405 Å) irradiation, at a scanning speed of 2°/minute and at diffraction angles ranging from 5-80°. The International Center for Diffraction Data Powder Diffraction File (ICDD-PDF) database was used for mineral identification.

3. Results and discussion

3.1. Analysis of variance

The multiple determination coefficients and standard deviation values for the dependent variables of the REE recovery are listed in Table 3.

Table 3. Summary statistical values provided by Box-Behnken design

Factor	S	R-sq	R-sq (adj)	R-sq (pred)
REE	3.49	91.32%	81.18%	56.76%

S: Std. Deflection **R-sq**: Determination coefficient -R^2, **R-sq (adj):** Adjustable R^2, **R-sq (pred):** Estimated R^2

As shown in Table 3, the multiple determination coefficient of the second-degree regression equation R^2 was calculated to be 91.98%. The fact that these values approach each other and equal 1 indicates the success of the model. In addition. the R^2 and adjusted R^2 values were compatible with each other. This indicated that the model fit was high. The regression results showed that R^2 values greater than 80% were obtained for the responses, and based on this the Response Surface Methodology (RSM) model has the ability to correctly determine the effect on the leach recovery responses. In addition to RSM a variance analysis (ANOVA) was applied to determine whether there was a significant difference between the means of the factors. The ANOVA results are given in Table 4.

Table 4. Analysis of variance for REE leaching recovery (ANOVA)

Source	Degree of freedom	Adj SS	Adj MS	F-Value	P-Value
Model	14	1538.80	109.914	9.01	0.000
Linear	4	579.93	144.983	11.89	0.000

HCl concentration, M	1	11.12	11.121	0.91	0.358
Temperature, °C	1	322.83	322.828	26.47	**0.000**
Leaching time, h	1	257.29	257.291	21.10	**0.001**
Solution-Ore ratio, l/kg	1	2.19	2.192	0.18	0.679
Squares	4	186.20	46.549	3.82	0.032
Concentration*Concentration	1	18.38	18.379	1.51	0.243
Temperature*Temperature	1	27.34	27.336	2.24	0.160
Time*Time	1	54.24	54.238	4.45	**0.057**
Sol/Ore*Sol/Ore	1	66.24	66.241	5.43	0.038
2-Way Interaction	6	1120.75	186.791	15.32	0.000
Concentration*Temperature	1	78.85	78.848	6.47	**0.026**
Concentration*Time	1	31.51	31.508	2.58	0.134
Concentration*Sol/Ore	1	210.66	210.655	17.27	**0.001**
Temperature*Time	1	14.49	14.487	1.19	0.297
Temperature*Sol/Ore	1	511.99	511.987	41.98	**0.000**
Time*Sol/Ore	1	368.89	368.892	30.25	**0.000**
Error	12	146.34	12.195	-	-
Lack-of-Fit	7	74.38	10.626	0.74	0.656
Pure Error	5	71.96	14.392	-	-
Total	26	1685.14	-	-	-

Adj SS = Adjusted sum of squares; Adj MS = Adjusted mean squares

The most important criteria to consider in the ANOVA table were the F-value and P-value. A larger F value indicated more effective factor. The F-statistic is used together with the P-value when deciding whether the overall results are significant. The P-value is determined by the F statistic and expresses the probability that the results occur by chance. For a factor to influence the response, the P-value must be less than 0.05 (Şimşek and Uslu. 2020). P-values greater than 0.05 mean that the parameter is insignificant or has no effect on the response. Table 4 shows that the leaching recovery values had a significant effect on the response in linear terms. It was determined that the leaching temperature and leaching time P-values were less than 0.05, and the F value was high; therefore, they were the most effective parameters. It was also concluded that the temperature is more effective than the leaching time because of the higher F-value and lower P-value. In addition, when the binary interactions were examined, it was determined that the concentration×temperature, concentration×solution/ore, temperature×solution/ore, and time×solution/ore values were lower than 0.05 and that they were effective together. The estimated second-degree polynomial model equation suggested by the software program for the leaching recovery response value is given by Eq. 2. An estimate can be made using this equation and the experimental results can be compared with the model estimate.

$$\text{REE Recovery, \%} = -58.1 + 31.33*\text{Concentration} + 0.921*\text{Temperature} - 6.08*\text{Time} + 9.65*\text{Sol/Ore} - 1.093*\text{Concentration}^2 + 0.00294*\text{Temperature}^2 + 0.0528*\text{Time}^2 - 0.15*\text{Sol/Ore}^2 - 0.1745*\text{Concentration*Temperature} + 0.385*\text{Concentration*Time} - 1.531*\text{Concentration*Sol/Ore} + 0.0113*\text{Temperature*Time} - 0.0917*\text{Temperature*Sol/Ore} + 0.2755*\text{Time*Sol/Ore} \quad (2)$$

Pareto analysis is a bar chart used to separate important leaching parameters from relatively less important parameters. The Pareto chart is shown in Figure 2, and the contour maps showing the interdependent interactions of the parameters are shown in Figure 3.

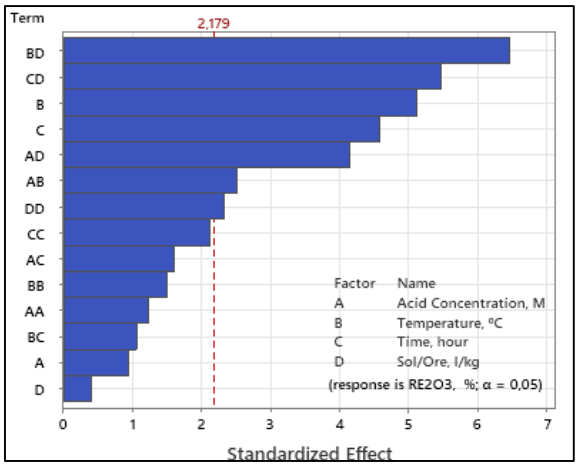


Figure 2. Pareto plot of standardized effects (α: 0.05)

In the Pareto chart, the factors to the left of the dashed red line are ineffective for the response while those to the right have a significant effect on the response. Accordingly, it can be observed that the leaching temperature and leaching time are effective for both responses. The standardized effect value was 2.179 for both the responses. When the 2-way interaction and squared interaction are examined, it is seen that the values solution/ore^2, temperature×time, temperature×solution/ore, time×solution/ore, concentration×temperature, and concentration×solution/ore are effective for the response.

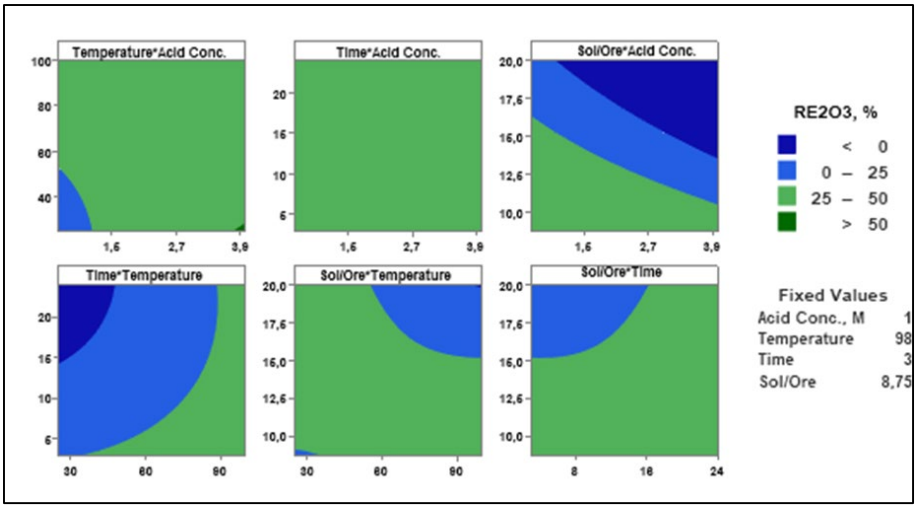


Figure 3. Contour maps showing the relationship between leaching parameters

Contour maps show the regions with low and high recovery, their boundaries, and the operating parameters of these regions using color scales. The parameters kept constant in the contour maps were the optimum leaching parameters. For example, for an REE recovery value between 25-50%, it is necessary to work in the green areas, that is, above 1 M HCl concentration and approximately above 55 °C. according to the temperature×concentration maps, at the specified fixed values. Three-dimensional graphs showing the relationship between the REE recovery and the leaching parameters are shown in Figure 4.

As seen in Figure 4.a, as the leaching temperature increased, the REE recovery increased significantly. When examined depending on the HCl concentration. a rapid increase was observed up to a certain concentration (approximately 2.5 M), and no change was observed after this concentration. According to this graph, the highest leaching recovery was determined by the low-concentration and high-temperature parameters. In Figure 4. b, as the leaching temperature increased. The REE recovery increased rapidly; no significant change was observed with increasing leaching time.Here, it is observed that the efficiency is high at high temperatures and short leaching times. Thus, by working with a short

leaching time, the process will be more economical and the leaching selectivity will be higher. When Figure 4.c is examined, while the REE recovery increases rapidly with temperature, the REE recovery decreases as the solution-ore ratio increases. From the ANOVA analyses, it was determined that the effect of the solution-ore ratio on leaching recovery was weak. Here, it is observed that the efficiency increases when working at a high temperature and low solution-ore ratio. When Figure 4.d was examined, the increase in the leaching time did not significantly increase. The recovery has a significant effect on the increase in leaching time because the amount of acid used per unit ore decreases over time, and accordingly, the significant effect of the leaching time decreases. In addition, working at a low solution-ore ratio, that is, under conditions where the amount of acid used per unit ore is low, both reduce operating costs and provide ease of operation.

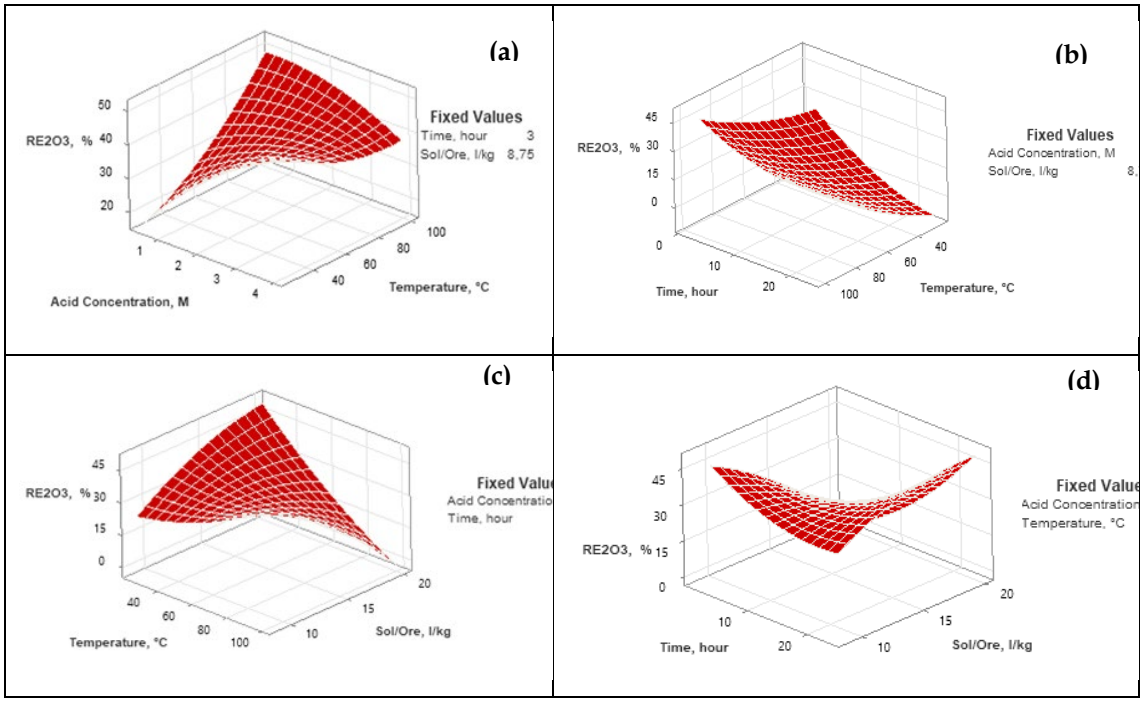


Figure 4. Change of REE recovery value depending on different leaching parameters

3.2. Optimization and Verification

The purpose of optimization is to obtain optimum leaching parameters that correspond to high leaching recovery. Accordingly, a 55.00% recovery value was targeted for the recovery value. This value was determined preferentially according to the highest recovery value of 46.00%. When the 55.00% recovery value was targeted, the optimum leaching parameters determined according to the Box-Behnken design method and the response values according to these results are given in Table 5.

Table 5. Optimum leaching parameters determined according to the Box-Behnken design method

Parameter	HCl. M	Temperature. °C	Time. h	Solution-Ore	%REE
Optimization	1.18	98.41	3.00	8.75	48.40

The REE recovery was determined by the model as 48.40% in response to these optimum values. In addition, the estimated results obtained by the model were compared with the experimental results to verify the experimental results. The error rates in this verification study were calculated according to Eq. 3, and since the average error value was 6.35% and below 10%, it is considered that the optimization study was successful. In the optimization studies in the literature, there are studies that optimized with a similar level or higher error rate (Kumar et al., 2020). In summary, it was determined that the values optimized by RSM were significant.

Error, % = [(Experimental result - Estimated result) / Experimental result]*100 (3)

4. Conclusion

The optimization and modeling of the raw ore depending on different leaching parameters were investigated using the Box-Behnken full design method. The effects of the independent variables acid concentration, leaching temperature, leaching time and solution-ore ratio on the dependent variable leaching recovery were investigated and the optimum leaching parameters were determined. Accordingly, the optimum leaching parameters were determined as; 1 M HCl concentration, 98 °C leaching temperature, 3 hours leaching time, 8.75 l/kg solution-ore ratio. It was concluded that the experimental results were compatible with the estimated results determined by the model, the average error rate was 6.35% and was at an acceptable level. In addition, it was determined that R^2 values greater than 80% were obtained in the regression results obtained and the RSM model fit created based on these was high. In addition, the effectiveness of the leaching parameters as a result of the leaching optimization was determined as; leaching temperature> leaching time> HCl concentration> solution-ore ratio, respectively.

Acknowledgment

The authors thank the Scientific and Technological Research Council of Turkey (TÜBİTAK) for financially supporting this study via Project No 122M810 and Demireller Mining Inc. for providing shale ore samples from Ayrancı (Karaman, Türkiye).

References

Binnemans, K., Jones, P.T., Blanpain, B., Van Gerven, T., Yang, Y., Walton, A., Buchert, M. 2013. Recycling of rare earths: A critical review, J. Clean. Prod. 51. 1-22.

European Commission. 2023. https://op.europa.eu/en/publication-detail/-/publication/57318397-fdd4-11ed-a05c-01aa75ed71a1. Accessed date: 25 May 2024.

Hanilçi, N. 2013. Geological and geochemical evolution of the Bolkardağı bauxite deposits. Karaman. Turkey: Transformation from shale to bauxite. Journal of Geochemical Exploration 133, 118-137.

Hepvidinli, B. 2019. Investigation of the Rare Earth Element Content of Kızıldağ and Kemiklitepe (Ayrancı-Karaman) Bauxite Mineralizations and Related Source Rocks. Master's Thesis. Istanbul Cerrahpaşa University, Department of Geological Engineering, Istanbul.

Kumar, A.N., Kishore, P.S., Raju, K.B., Ashok, R., Vignesh, A.K., Jeevanantham, K., Nanthagopal, and Tamílvanan, A. 2020. Decanol proportional effect prediction model as additive in palm biodiesel using ANN and RSM technique for diesel engine. Energy, vol. 213, 119072.

Krishnamurthy, N., Gupta, C.K. 2016. Extractive Metallurgy of Rare Earths (Second Edition). CRC Press-Taylor & Francis Group.

Öztürk. H., Hanilçi, N., Altuncu, S., Kasapçı, C. 2019. Rare earth element (REE) resources of Turkey: an overview of their characteristics and origin. Bulletin of the Mineral Research and Exploration 159: 143-129.

Ünal, E.C., Karacahan, M., Uysal, T., 2023. Hydrometallurgical roadmaps and future strategies for recovery of rare earth elements. Mineral Processing and Extractive Metallurgy Review, https://doi.org/10.1080/08827508.2022.2073591.

Green Chemistry Approaches in Mineral Processing with Deep Eutectic Solvents: A case of NdFeB magnets

Birgül Benli [1]*, Mert Sarıkaya [1]

[1]Istanbul Technical University, Mining Faculty, Mineral Processing Engineering Department, Maslak, Turkiye

*Corresponding author: benli@itu.edu.tr (Birgül Benli)

Abstract:

The widespread use of magnets in fields ranging from computer technology and electric vehicles to wind turbines and the space industry has driven the demand for high-capacity magnet production. The limited availability of natural resources has increased the importance of recycling magnets that have reached the end of their life cycle. This thesis aims to recover metals from permanent magnets using pyrometallurgical and hydrometallurgical methods, considering economic and environmental impacts to support a sustainable economy and planet. Initially, demagnetization and size reduction processes were applied to the magnet obtained in a magnetized state. Caustic digestion applied to fine particles of magnets to oxidize fully. Deep eutectic solvents (DES) synthesized from ethylene glycol, boric acid, citric acid and oxalic acid. In the leaching stage, NdFeB magnets leached with industrial acids and DESs. The Fe dissolution behavior of DESs and industrial acids was examined and compared in the leaching experiments. Eutectic freeze crystallization, antisolvent crystallization, and precipitation with Na2SO4 were applied to the pregnant solutions obtained from industrial acids to produce Nd and Fe based salt crystals.

Keywords: *NdFeB magnets, DES, Leaching, Crystallization*

1. Introduction

In today's world, depending on the development of technology, NdFeB magnets meet the requirements of many different high-tech applications, from hard disk drives to engines in vehicles or electric generators in wind turbines, and are used in many clean energy applications (Walton et al., 2015). Neodymium, an important rare earth element, plays a critical role in the production of permanent magnets, which are essential in many industrial processes due to their high efficiency and performance. However, these magnets can lose their functionality over time due to breakage and corrosion. The economical and sustainable benefits of neodymium recovery, particularly through hydrometallurgical methods, have led to increasing interest, as neodymium is a key component in green technologies such as electric vehicles, wind turbines, and various electronic devices, presenting significant economic and environmental potential for future sustainable energy solutions.

Deep eutectic solvents (DES) represent an innovative class of green solvents that facilitate selective leaching, providing effective solutions for sustainable and eco-friendly practices. As illustrated in Fig. 1, these solvents not only enhance the extraction efficiency of valuable materials but also minimize environmental impact, showcasing their potential in advancing sustainable resource management. DESs, first introduced by Abbott et al. (2003), consist of a eutectic mixture formed from at least two components: a hydrogen bond donor and a hydrogen bond acceptor, combined in a specific ratio. These solvents are prepared from a blend of Lewis or Brønsted acids and bases, encompassing a variety of anionic and cationic species, which contribute to their unique properties and applications in various fields. There are various classifications to understand the components of these alternative solvents. DES is based on the general formula $Cat^{+}X^{-}zY$, where: Cat^{+} represents a cation, typically, an ammonium, phosphonium, or sulfonium; X^{-} denotes a Lewis base, usually a halide anion; Y signifies a Lewis or Brønsted acid; z indicates the number of Y molecules that interact with the corresponding anion.

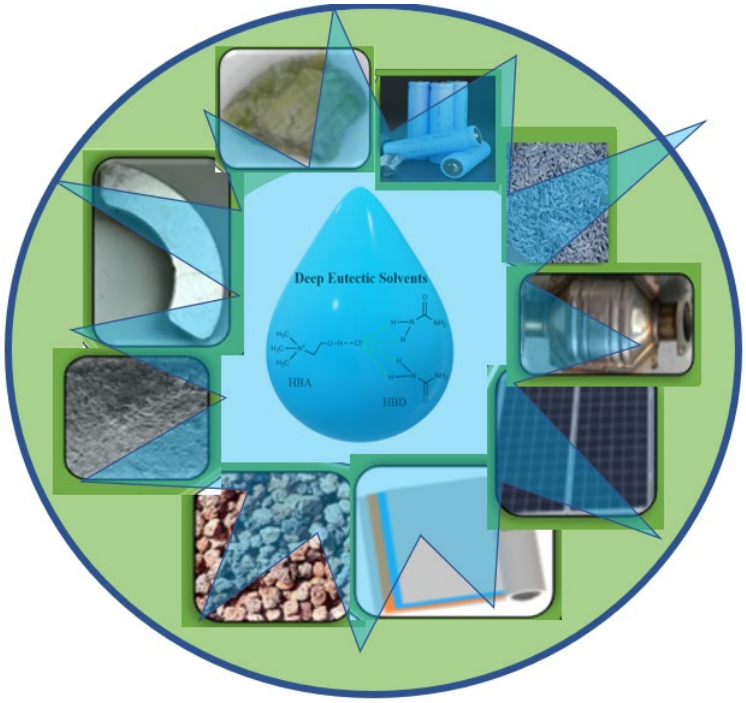


Fig. 1. Integrating Deep Eutectic Solvents (DES) Enhanced Recycling of Secondary Resources

In recent years, there has been a notable increase in studies utilizing DESs, which are capable of selectively dissolving various metal oxides based on their specific composition. This property makes DESs particularly suitable for the dissolution of end-of-life NdFeB magnets, whose composition can vary depending on the application. One successful study involved the selective leaching of spent NdFeB permanent magnets using DES synthesized from guanidine hydrochloride and lactic acid. Neodymium metal was precipitated with oxalic acid as $Nd_2(C_2O_4)_3$, followed by calcination of the leach solution to yield Nd_2O_3, achieving an impressive recovery rate of 99% in the form of neodymium oxide (Liu et al., 2020). In another investigation, spent magnets with a grain size below 100 microns were treated with a DES made from choline chloride and lactic acid. The selective leaching process was performed at 70 °C for 24 hours, successfully separating cobalt, iron, boron, neodymium, and dysprosium metals through solvent extraction with ionic liquids. The resulting Nd and Dy metals were precipitated using oxalic acid and then calcined at 950 °C for 3 hours, producing Nd_2O_3 with a purity of 99.87% and Dy_2O_3 with a purity of 99.94% (Riaño et al., 2017). To leach NdFeB in a selective way, the oxidizing process is fatal.

Heo et al. (2024) showed that by NaOH digestion process DESs leaching efficiencies increased. Firstly, demagnetized NdFeB magnets grinded and NaOH digestion applied then oxidative roasting is applied at 450°C for 3h. After that DES which is synthesized by ethylene glycol and maleic acid used in leaching of roasted magnet. Analysis showed that Nd and Fe leaching efficiencies were 97.3% and 0.7% respectively. Shuping et al. (2024) used DESs which components were tetraethylammonium chloride as HBA and levulinic, malonic, L-lactic and glycol acids as HBD. End of life NdFeB magnet leached with different DESs, Nd and Fe leaching efficiencies were 97.63% and 0.435% respectively. These studies underscore the effectiveness of DESs in the selective recovery of valuable metals from NdFeB permanent magnets, highlighting their potential for sustainable resource management. DESs are not using for leaching only NdFeB magnets but also other secondary resources such as batteries, photovoltaic panels, catalytic converters, fly ashes and metalic slags. Tang et al. (2022) used ethylene glycol and oxalic acid dihydrate DES to leach spent LIB cathode material, Li leaching efficiency was 94.4% and Ni, Mn and Co metals leaching efficiencies were 1%. Dong et al. (2023) also leached spent LIB cathode material with ethylene glycol-malonic acid DES with 100% Li, Ni, Co and Mn efficiencies. Yu et al. (2022) used ChCl-glycerol to leach spent LIB cathode material with 95.7% Co efficiency. Zhang et al. (2022) used ChCl-Urea DES to recover silver by leaching process with 98%. Topçu et al. (2021) also used ChCl-Urea DES to leach copper converter slag, leaching efficiencies of Cu and Zn were 90% and 65% respectively. In

this context, our study investigates the impact of ethylene glycol-based DESs on the selective separation of neodymium.

2. Material and methods

2.1. Material

Magnetic nickel coated NdFeB magnets (Fig 2.) were gently obtained from Magneteksan Co. (Turkiye) and used for the studies after demagnetized thermally in a muffle furnace at 450 ºC for 1 hour. Following this, the magnets were crushed in a mortar and ground in a ring mill for 55 seconds. Monoethylene glycol (EG) was used as the hydrogen bond acceptor (HBA), while citric acid monohydrate (S), boric acid (B), and oxalic acid dihydrate (O) were selected as hydrogen bond donor (HBD) components in various molar ratios. These mixtures were prepared in a glycerin bath at a constant temperature of 80 °C for 1 hour and completely homogeneous. Na_2SO_4 and ethyl alcohol were used as precipitating agents. The characterizations of samples were analyzed by particle size analyzer (Malvern mastersizer 3000), XRD analysis (PANalytical-AERIS), and Atomic absorption spectroscopy (VARIAN).

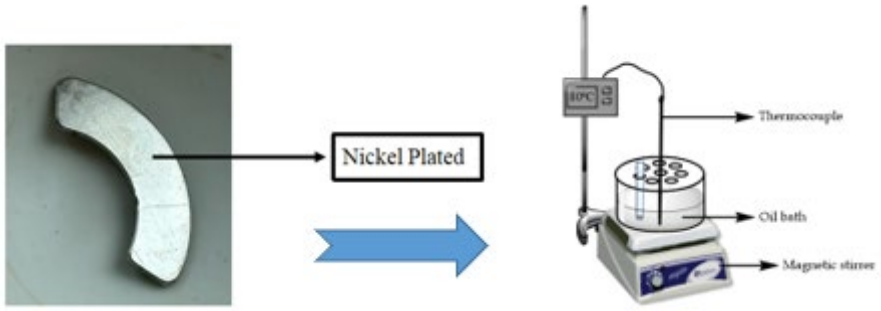


Fig. 2. (a) Magnets and (b) experimental set-up used in the study.

3. Results and Discussion

3.1. Demagnetization

In the demagnetization experiments, waste NdFeB magnets were subjected to heating at 450 °C for 1 hour. After this pretreatment, the magnets were crushed in a mortar and then ground in a ring mill for 55 seconds, as illustrated in Fig. 3. Its characterization was performed using the X-ray diffraction (XRD) pattern shown in Fig. 4, revealing high levels of $GaNd_3O_6$ and NdFeBCo structures.

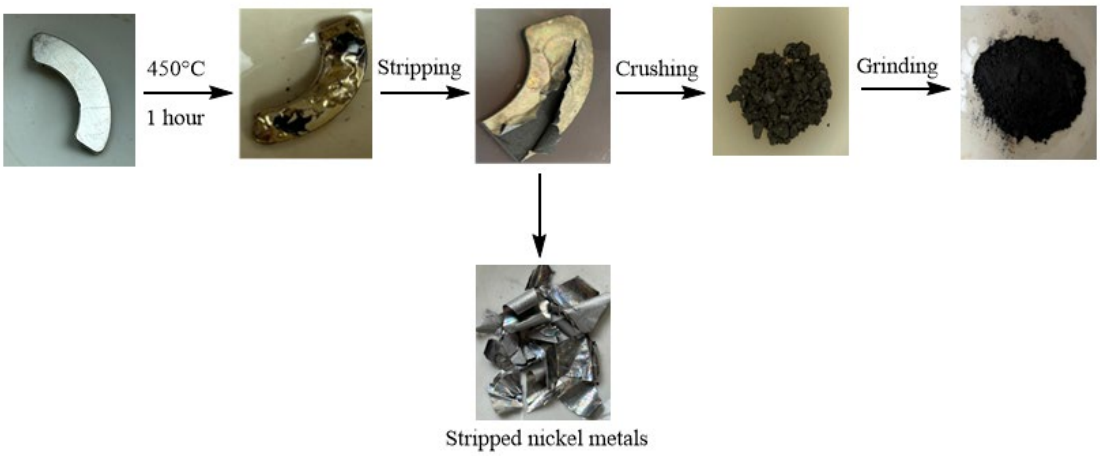


Fig. 3. The preparation procedures applied to the magnets.



Fig. 4. XRD analysis of waste NdFeB magnet.

3.2. DES leaching

To investigate the behavior of the solvents, DESs were synthesized with varying ratios of each component. The results indicated that DESs with high mole ratios exhibited high viscosities, leading to the decision to reduce the mole ratios of the hydrogen bond donor (HBD) groups used in the DES synthesis. Table 1 presents the most effective low-viscosity DESs.

In the leaching experiments, the performance of these DES was investigated. The Fe concentrations of the solutions obtained from the leaching processes were determined and low Fe and high Fe dissolution efficiencies were compared using the results of atomic adsorption spectrum (Figure 5 and Figure 6, respectively). In this comparison, the iron dissolution efficiency of sulfuric acid was considered to be 100%, serving as a benchmark for evaluating the efficiency of the DESs.

Table 1. Low viscosity DESs.

DES	HBA	HBD 1	HBD 2	HBD 3	Molar Ratio	Temperature	Time
1	Ethylene Glycol	Oxalic Acid	Boric Acid	-	1:0.50:0.25	80°C	1 hour
2	Ethylene Glycol	Oxalic Acid	Citric Acid	-	1:0.50:0.25	80°C	1 hour
3	Ethylene Glycol	Oxalic Acid	Boric Acid	Citric Acid	1:0.50:0.25:0.25	80°C	1 hour
4	Ethylene Glycol	Oxalic Acid	Citric Acid	Boric Acid	1:0.50:0.125:0.125	80°C	1 hour

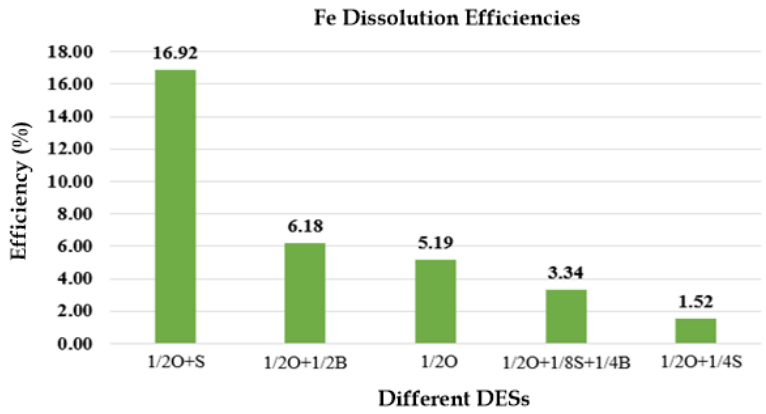


Fig 5. Comparison of Ethylene glycol based- DESs and sulphuric acid that dissolve Fe with low efficiency.

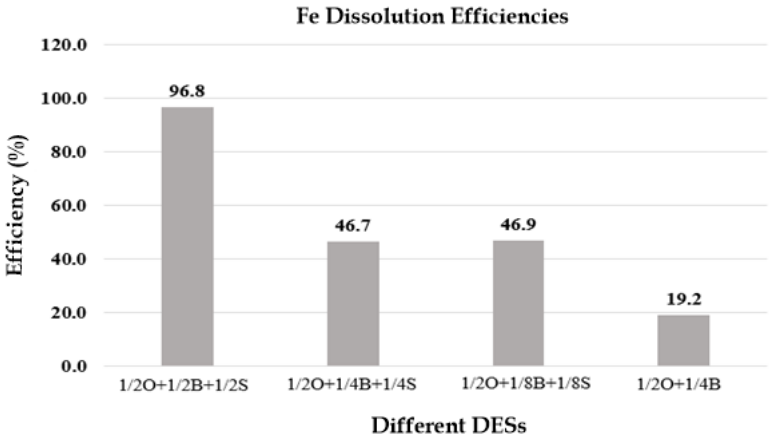


Figure 6. Comparison of DESs and sulphuric acid that dissolve Fe with high efficiency.

3.3. Crystallization and precipitation experiments

In the anti-solvent crystallization experiments, crystals containing iron were obtained. XRD analysis revealed that the anti-solvent crystals were $Fe_2(SO_4)_2.8H_2O$ (in Fig. 7). $NaNd(SO_4)_2.H_2O$ precipitation was made to the solution in which a large amount of $Fe_2(SO_4)_2.8H_2O$ was precipitated as a result of antisolvent crystallization and to the pregnant sulfuric acid solution. XRD analysis was conducted on the crystals obtained following precipitation (Fig. 8). The precipitation behaviors of the solutions at different temperatures were examined, with 1M Na_2SO_4 was added to the solutions at 80ºC and at room conditions. While the precipitation process at 80°C occurred within 10 minutes, the precipitation of the solution at room temperature took about 1 day. The reason for this difference in behavior is the decrease in the solubility of $Nd_2(SO_4)_2$ at high temperatures. Additionally, since DES experiments were conducted on a small scale, no crystallization process was performed, and only the dissolution behavior was examined.

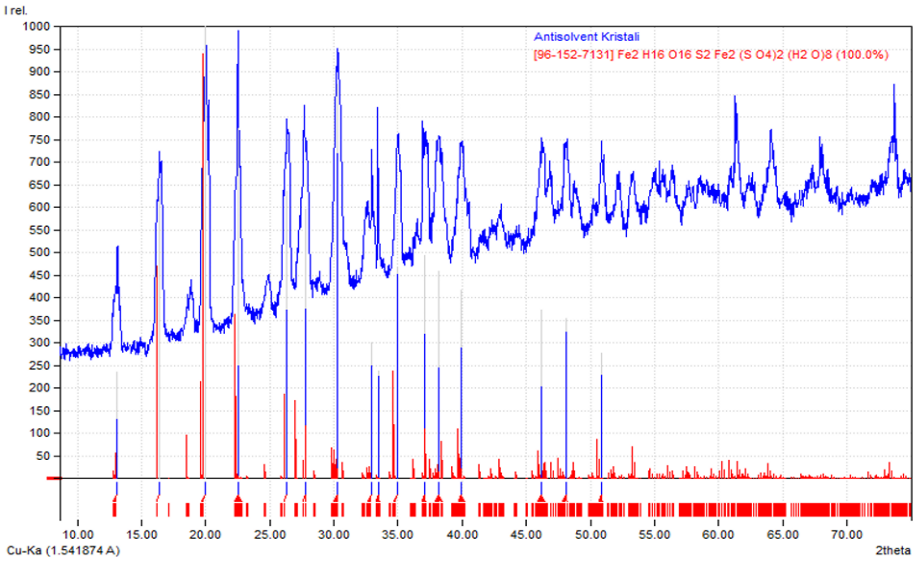


Fig. 7. Anti-solvent crystals of $Fe_2(SO_4)_2 \cdot 8H_2O$.

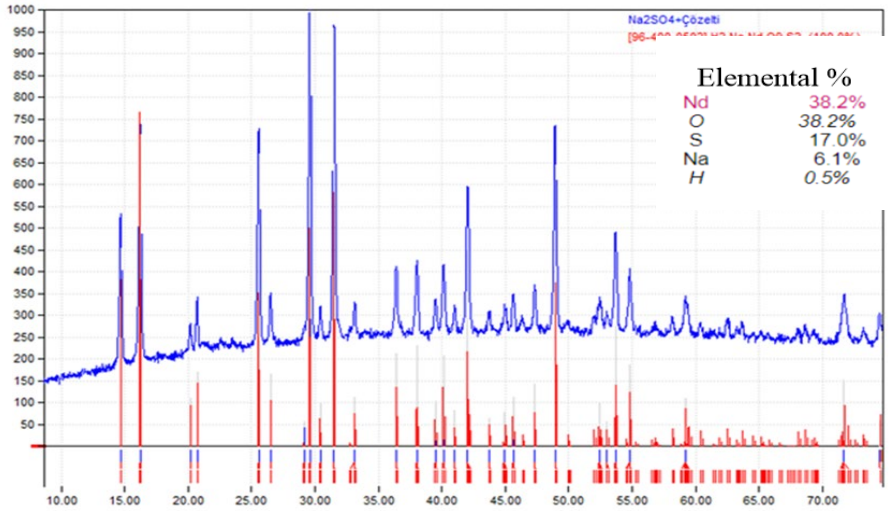


Fig. 8. $NaNd(SO_4)_2.H_2O$ crystals by adding Na_2SO_4

4. Conclusions

In this study, where we applied DES leaching and anti-solvent crystallization for the recovery of Nd and separation Fe, the following main results were obtained.

The predicted Fe dissolution behaviour in leaching experiments was examined for both strong acids and DES, DES was formed with EG+ $^{1}/_{2}$O+ $^{1}/_{4}$S ratios and Fe dissolution behaviour was evaluated as the most efficient DES with the lowest. It dissolved 100 times less Fe compared to strong acids. This shows that the synthesis of the desired DES was achieved within the scope of the thesis.

- As a result of the DES experiments conducted with strong acids, Nd-based crystals were obtained. In addition, precipitation was performed again with Na_2SO_4 at high temperature and $NaNd(SO_4)_2.H_2O$ crystal was obtained.

- As a result of the leaching experiments conducted with strong acids, the excess amount of iron ions passing into the solution were precipitated by antisolvent crystallization and $Fe_2(SO_4)_2.8H_2O$ was obtained.

- After the stripping process following the demagnetization process, approximately 0.80 grams of pure nickel metal was obtained from one magnet.

Acknowledgments

The authors would like to thank the ITU BAP unit for supporting the research conducted as part of the thesis within the general research project named "MGA-2023-45070 High Efficiency Recovery of Rare Earth Elements from Permanent Magnetic Materials, Deep Eutectic Solvents and Eutectic Freeze Crystallization Investigation".

References

Abbott, A. P., Capper, G., Davies, D. L., Rasheed, R.K., & Tambyrajah, V. (2003). Novel solvent properties of choline chloride /urea mixtures. Chemical communications (1), 70-71.

Dong, L., Li, Y., Shi, P., Ren, Z., & Zhou, Z. (2023). Low-viscosity acidic deep eutectic solvent for extraction of valuable metals from spent NCM. Journal of Power Sources, 582, 233564.

Heo, S., Kim, R., Yoon, H. S., Kim, C. J., Chung, K. W., & Lee, S. (2024). Effect of pretreatment methods on the selective leaching of rare earth elements from NdFeB permanent magnets using deep eutectic solvents. Hydrometallurgy, 226, 106284.

Liu, C., Yan, Q., Zhang, X., Lei, L., & Xiao, C. (2020). Efficient recovery of end-of-life NdFeB permanent magnets by selective leaching with deep eutectic solvents. Environmental Science & Technology, 54(16), 10370-10379.

Riaño, S., Petranikova, M., Onghena, B., Vander Hoogerstraete, T., Banerjee, D., Foreman, M. R. S., ... & Binnemans, K. (2017). Separation of rare earths and other valuable metals from deep-eutectic solvents: A new alternative for the recycling of used NdFeB magnets. Rsc Advances, 7(51), 32100-32113.

Shuping, C., Zhihan, Z., Dong, W., Wenjing, Z., Tao, Q., Zhi, W., ... & Guobiao, L. (2024). Selective leaching and recovery of rare earth from NdFeB waste through a superior selective and stable deep eutectic solvent. Separation and Purification Technology, 128498.

Tang, S., Feng, J., Su, R., Zhang, M., & Guo, M. (2022). New bifunctional deep-eutectic solvent for in situ selective extraction of valuable metals from spent lithium batteries. ACS Sustainable Chemistry & Engineering, 10(26), 8423-8432.

Topçu, M.A., Rüşen, A., & Küçük, Ö. (2021). Treatment of copper converter slag with deep eutectic solvent as green chemical. Waste Management, 132, 64-73.

Walton, A., Yi, H., Rowson, N. A., Speight, J. D., Mann, V. S. J., Sheridan, R. S., ... & Williams, A. J. (2015). The use of hydrogen to separate and recycle neodymium–iron–boron-type magnets from electronic waste. Journal of Cleaner Production, 104, 236-241.

Yu, H., Wang, S., Li, Y., Qiao, Q., Wang, K., & Li, X. (2022). Recovery of cobalt from spent lithium-ion battery cathode materials by using choline chloride-based deep eutectic solvent. Green Processing and Synthesis, 11(1), 868-874.

Zhang, C., Jiang, J., Ma, E., Zhang, L., Bai, J., Wang, J., ... & Wang, R. (2022). Recovery of silver from crystal silicon solar panels in Self-Synthesized choline Chloride-Urea solvents system. Waste Management, 150, 280-289.

The Use of a Reflux Classifier for Chromite Ores: Assessment of Different Circuit Alternatives at Pilot Scale

Özgür ÖZCAN [1]*

[1]Hacettepe University Department of Mining Engineering

*Corresponding author: ozgurozcan@hacettepe.edu.tr (Özgür Özcan)

Abstract:

A series of tests were conducted with single replication and statistically designed by using a pilot scale REFLUX™ Classifier (RC300) on three different streams of an operating plant. The RC300 was tested shaking table concentrate, spiral concentrate and spiral feed samples obtained during the steady state operation of plant. In the present work, fluidization water rate and pressure set point was considered. Other variables which are, feed rate and feed solid content kept constant and are not studied.

Based on the mass balanced test results, RC300 underflow stream was concentrated from 40.46% Cr_2O_3 up to 47.63% Cr_2O_3 with a mass yield of 77.63% and a recovery of 91.39% by using a single stage RC300 at shaking table concentrate. The chemical analyses revealed that a grade of 18.70% Cr_2O_3 could be concentrated up to 46.18% Cr_2O_3 by using spiral concentrate stream. Based on the test results obtained spiral feed stream, the feed concentrated from 9.10% Cr_2O_3 to 18.18% Cr_2O_3 with 39.72% mass yield and an 79.34% recovery.

According to results, dragon tables which manually concentrates the shaking table concentrate can be replaced with a RC and the final concentrate routed directly to a newly installed RC. A new flowsheet can be designed by using the spirals and the RC. This would eliminate the need for both shaking tables and dragon tables and the required footprint. The spiral feed test results revealed that RC is a suitable device as a rougher concentration.

Keywords: *Reflux™ Classifier, chromite, gravity concentration, teetered bed separator*

1. Introduction

The low-grade chromite ores found around the world are mined and beneficiated by using several gravity concentration methods. Density-based separations are the most convenient and cost effective methods for chromite beneficiation. Assessing the performance of density-based separation processes is an ongoing challenge in the mineral processing applications, particularly for high-density minerals. In the process of improving the efficiency of classification/separation, an equipment that has been gaining popularity in recent years is the teetered or hindered bed separator. As an evolved version of hydraulic classifiers, there are several types of equipment in the industry with different commercial names: floatex density separator (FDS), cross flow separator (CFS), reflux classifier (RC), allflux classifier (AC), etc. These units have been used in mineral sand ((Zhou et al., 2006, Tripathy et al., 2015), low-grade iron ore (Amariei, et al., 2014), chromite (Kari et al., 2006), pyrite (Remes et al., 2011) and the coal preparation industry (Hyde et al., 1988, Mankosa et al., 1995, Das et al., 2009, Sarkar et al., 2008).

The RC, is a new type of hydraulic classifier for separating particles on the basis of either size or density. The device can be compared to a hindered settling column or TBS (Galvin et al., 1999), basically a fluidized bed in which slower settling particles report to the overflow and faster settling particles to the underflow. However, the reflux classifier (RC) contains sets of parallel inclined plates that significantly increase the throughput of the device to a level many times higher than can be achieved in the more conventional system (Galvin et al., 2002, Galvin et al., 2009).

The RC is an innovative device, a hybrid between a fluidized bed separator (vertical part) and a lamella settler (inclined part). The separation within the vertical part is mainly governed by the hindered settling mechanisms and thus by the terminal velocities of the particles (which are closely related to

their size and density). The relative inefficiency of this part for fine heavier particles and coarse lighter particles that have the same terminal velocity is compensated for by the inclined part. The role of this part is firstly to increase the sedimentation surface area of separation (Amariei, et al., 2014). A schematic representation and a photo of the RC used for the tests are presented in Fig. 1.

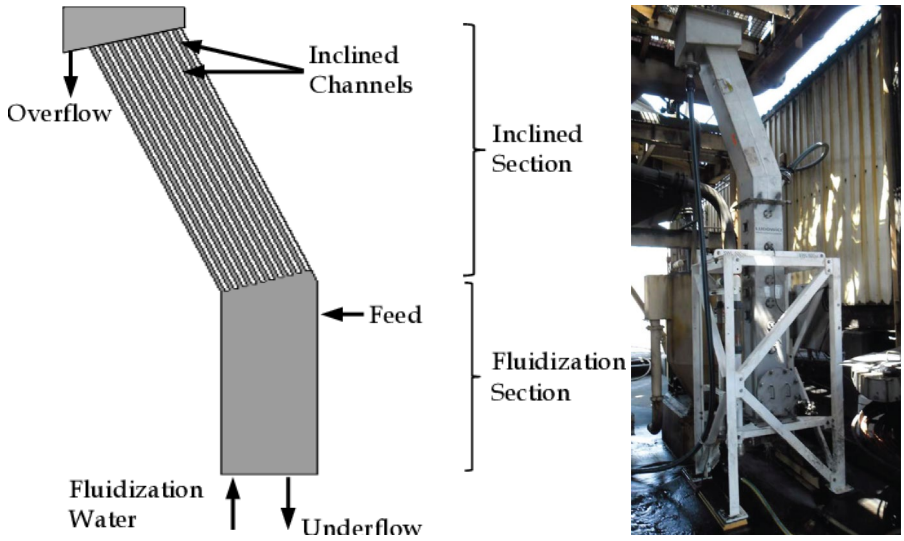


Fig. 1. Schematic of the Reflux Classifier

The main aim of this study is to present a series of results obtained using a pilot scale RC popularly known as the RC300. The main focus of the study is determining the relationship between operational variables and performance parameters of the device for chromite concentration, the consistency of its operation, and its response to changes in the operating conditions in an operating chromite beneficiation plant.

This paper describes the first pilot scale trial of the RC at a chromite concentration plant in Türkiye, in which the device is used to investigate grade and yield improvement opportunities at the operating spiral-shaking table plant as well as a further opportunity for the new expansion project.

2. Experimental

2.1. Chromite Beneficiation Plant

The simplified flowsheet of the plant and Reflux test streams are shown in Figure 2. In the beneficiation circuit, screen undersize stream is fed to de-sliming cyclone and cyclone overflow rejects as slime. Cyclone underflow stream is fed to spiral concentration circuit to obtain a pre-concentrate. The spiral concentration circuit consist of a rougher, a scavenger and three stage cleaner spirals. The tailing of the spiral concentration circuit is spiral tailing. Spiral concentrate fed to teetered bed separator (TBS) to obtain two narrow size fractions for shaking table circuit. TBS underflow is fed to coarse tables and TBS overflow stream is fed to fine tables. The total table concentrate is around 40-42% Cr_2O_3 fed to dragon tables, where by use of manual labor, the material is upgraded to 46-48% Cr_2O_3.

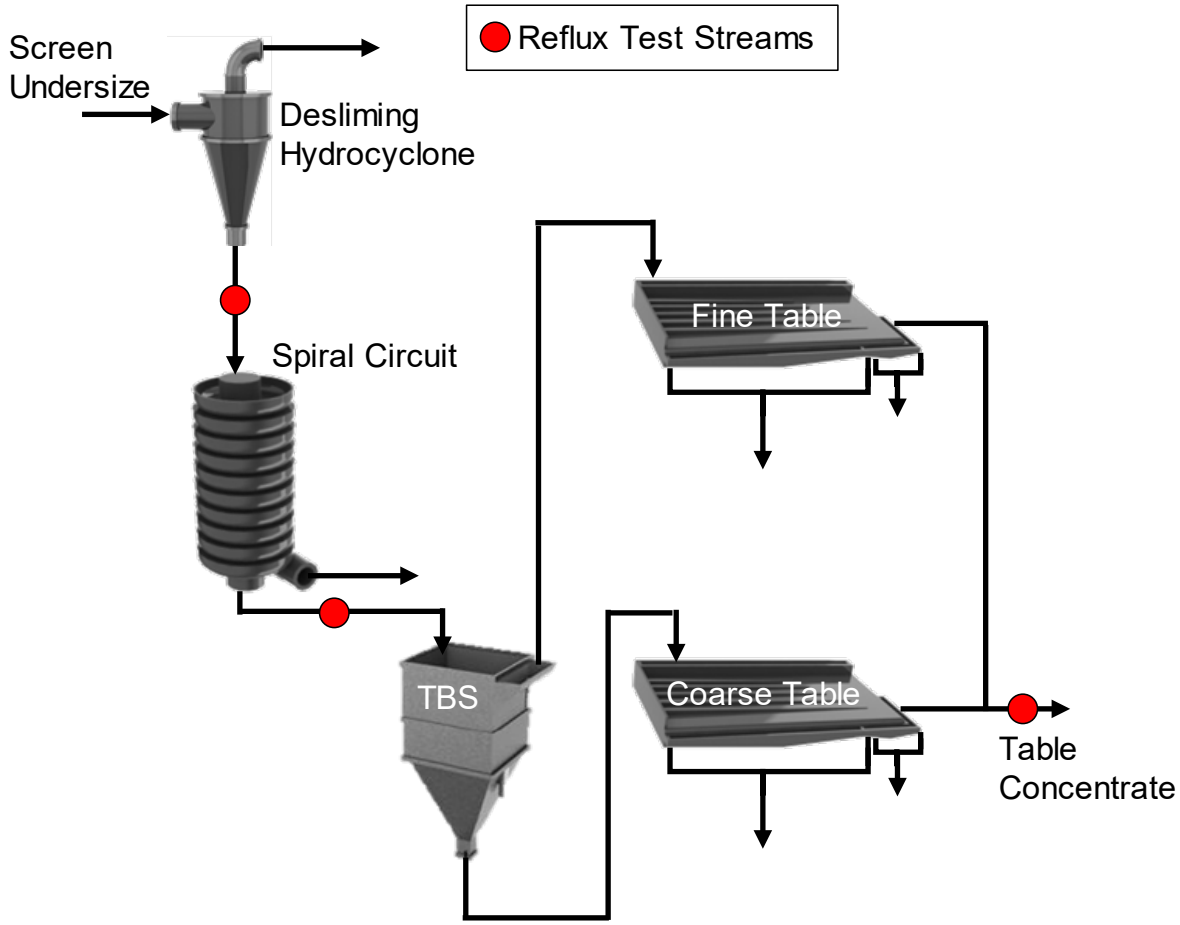


Fig. 2. Simplified flowsheet of chromite concentration plant and test streams

2.2. Pilot Scale Reflux Classifier (RC300)

A pilot scale Reflux Classifier (RC300), consisting of a series of parallel inclined channels below a fluidized bed, was used. The inclined section consisted of 1.2 m long inclined channels. A system with 38 channels was formed from 37 plates with a perpendicular spacing of 6 mm. A 2.7 m long inverted fluidized bed with cross sectional area of about 0.300 m × 0.300 m was located above the inclined section. Two pressure sensors were used to measure the suspension density down the vertical fluidized bed section, providing a basis for controlling the discharge rate of product to the underflow. A fluidization water chamber was installed above the fluidized bed section, distributing the spray water with a 2.5 mm spray nozzle size. The space between the inclined channels is 6 mm.

2.3. Sample Characterization

Three stream were tested with the RC300 from FLSmidth-Ludowici. Sample A was spiral circuit feed whereas sample B was spiral concentrate and sample C was shaking table concentrate (Fig. 2). Before the pilot scale study a detailed sampling campaign has been performed to collect RC300 feed samples. To obtain representative samples for each stream a long period sampling has been performed. Sampling campaign was completed in a shift (8 hours). About 15 m^3 of each sample were collected at original solid content to perform the RC tests. The main characteristics of the RC feeds (samples A, B and C) are tabulated in Table 1.

Table 1. Main characteristics of the Reflux Classifier feeds

Sample Name	Density	P80	Solid	Grade (%)					
	(g/cm^3)	(µm)	(%)	Cr_2O_3	Fe_2O_3	Al_2O_3	MgO	SiO_2	CaO
A (Spiral Feed)	3.52	268	35.45	9.10	9.52	1.89	37.05	30.06	0.92
B (Spiral Concentrate)	3.96	295	40.18	18.70	10.70	1.02	30.08	28.46	0.57
C (Table Concentrate)	4.52	255	28.16	40.46	13.46	0.67	23.43	17.39	0.24

As it can be seen in Table 1 that sample B has the coarsest particle size distribution while sample C has the finest particle size distribution. Sample C had a highest Cr_2O_3 content as expected. For the sake of simplicity in this paper, the fractional assays of Cr_2O_3 represent the valuable mineral in samples. Fractional Cr_2O_3 grades and distribution are shown in Fig 3.

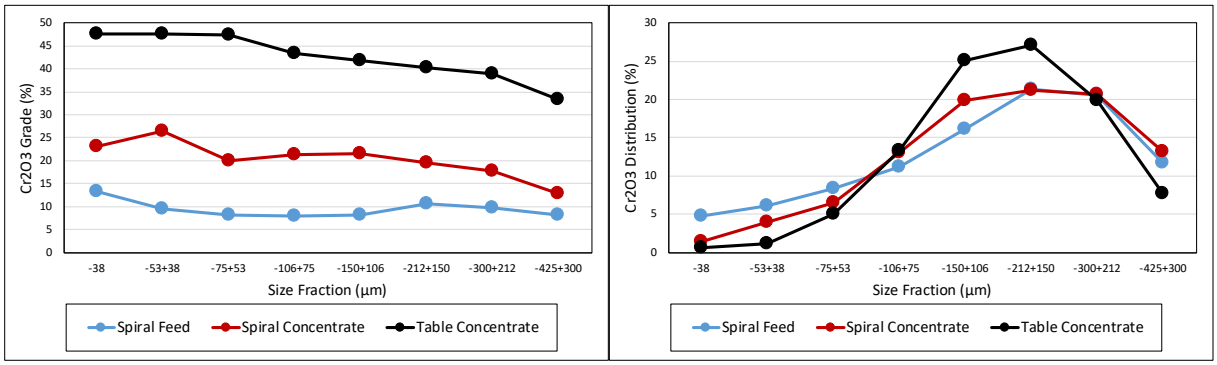


Fig. 3. Fractional Cr_2O_3 grade and distribution of RC feed samples

2.4. Reflux Classifier Tests

The flowsheet used for the RC tests is presented in Fig. 4. As illustrated, a homogeneous pulp with original solid content was prepared in the conditioner and then pumped in the RC unit at a constant flowrate by the aid of an adjustable speed pump. Water fluidization flow rates were adjusted between 0.8-1.3 m^3/h according to Cr_2O_3 grades. Six tests were carried out with each sample. The U/F product (the concentrate) and the O/F product (the tailings) was discharged and timed representative samples were collected under steady-state conditions (each sampling time of about 30 s) for each test. All products then submitted to a Cr_2O_3 analysis.

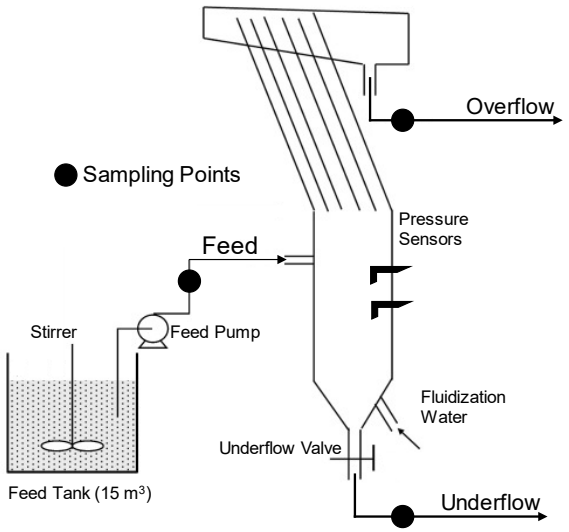


Fig. 4. Simplified flowsheet for the Reflux Classifier tests.

The RC tests were performed at around 2 tph dry feed tonnage. According to equipment brochure (REFLUX™ Classifier, 2024) this capacity is around which is 60%solid capacity of RC300 HC at -300+75 µm. The density of the fluidized bed and the water fluidization flow rate were varied throughout the tests. The RC300 unit was operated with an automatic PI controller set to maintain the average density in the column at a specified value. During the tests, changing the set point took over 20 min for the density to stabilize; steady state operation was assumed to have settled in after another 20-min delay. Detailed experimental conditions for all the samples are presented in Table 2.

Table 2. Pilot scale RC test conditions

Test	Sample A		Sample B		Sample C	
	Density set point (kg/m3)	Fluidization Rate (m3/h)	Density set point (kg/m3)	Fluidization Rate (m3/h)	Density set point (kg/m3)	Fluidization Rate (m3/h)
1	1500	0.8	1700	0.9	1700	1.0
2	1700	0.8	1900	0.9	1900	1.0
3	1900	0.8	2100	0.9	2100	1.0
4	1500	1.2	1700	1.2	1700	1.3
5	1700	1.2	1900	1.2	1900	1.3
6	1900	1.2	2100	1.2	2100	1.3

3. Results and Discussions

Table 3 presents the results of the mass balanced RC tests performed on samples A, B and C. It can be observed from Table 3 that the underflow stream was concentrated up to 43.50% Cr_2O_3 for sample A, 46.18% Cr_2O_3 for sample B and 53.91% Cr_2O_3 for sample C. The underflow chromite recovery decreases significantly depending on the increase in fluidization water rate (FW) and density set point (SP) for all samples. Higher FW and higher SP resulted in a high concentration of chromite in the TBS underflow stream. Moreover, the some of the O/F products showed reasonable Cr_2O_3 losses: lower than 6% for sample B and sample C, lower than 19% for sample A.

The Cr_2O_3 analyses of sample A revealed that a feed grade of 9.10% Cr_2O_3 could be concentrated up to a salable product grade of 43.50% Cr_2O_3. Results also showed that concentrate grade increases with increasing SP while recovery decreases. The mass yield to U/F at the optimum set point of 1500 was 45.34% at a tailing grade of 3.09% Cr_2O_3 while the concentrated grade was at 16.35% Cr_2O_3.

The Cr_2O_3 analyses of Sample B revealed that a feed grade of 18.70% Cr_2O_3 could be concentrated up to a final concentrate grade of 46.18% Cr_2O_3. The underflow mass yield at the optimum set point of 1700 was 78.73% at a tailing grade of 5.18% Cr_2O_3.

The Cr_2O_3 analysis of sample C revealed that a feed grade of 40.46% Cr_2O_3 could be concentrated a product grade between 46-54% Cr_2O_3. The U/F of RC had a mass yield between 58.98-83.05%. The optimum results were obtained where the RC received a feed of 40.46% Cr_2O_3 producing a salable concentrate 46.18% Cr_2O_3 with a mass yield of 83.05% and a recovery of 94.79%.

Table 3. Pilot scale RC test results

Sample	Test	Feed Cr_2O_3 (%)	Underflow (U/F)			Overflow (O/F)		
			Mass (%)	Cr_2O_3 (%)	Recovery (%)	Mass (%)	Cr_2O_3 (%)	Recovery (%)
A	1	9.10	45.34	16.35	81.44	54.66	3.09	18.56
	2		30.98	20.20	68.76	69.02	4.12	31.24
	3		18.34	29.99	60.44	81.66	4.41	39.56
	4		39.72	18.18	79.34	60.28	3.12	20.66
	5		25.04	23.87	65.66	74.96	4.17	34.34
	6		10.79	43.50	51.58	89.21	4.94	48.42
Sample	Test	Feed Cr_2O_3 (%)	Underflow (U/F)			Overflow (O/F)		
			Mass (%)	Cr_2O_3 (%)	Recovery (%)	Mass (%)	Cr_2O_3 (%)	Recovery (%)
B	1	18.70	78.73	22.35	94.11	21.27	5.18	5.89
	2		55.20	28.97	85.53	44.80	6.04	14.47
	3		43.32	33.48	77.57	56.68	7.40	22.43
	4		65.22	25.25	88.08	34.78	6.41	11.92
	5		44.56	33.04	78.74	55.44	7.17	21.26
	6		27.94	46.18	69.02	72.06	8.04	30.98
Sample	Test	Feed Cr_2O_3 (%)	Underflow (U/F)			Overflow (O/F)		
			Mass (%)	Cr_2O_3 (%)	Recovery (%)	Mass (%)	Cr_2O_3 (%)	Recovery (%)
C	1	40.46	83.05	46.18	94.79	16.95	12.44	5.21
	2		73.17	49.29	89.14	26.83	16.38	10.86
	3		65.18	51.63	83.18	34.82	19.55	16.82
	4		77.63	47.63	91.39	22.37	15.58	8.61
	5		68.31	50.91	85.95	31.69	17.94	14.05
	6		58.98	53.91	78.59	41.02	21.12	21.41

In order to determine the interactional effects of studied operational variables on performance parameters, the relationship between operational variables (TW, SP) and performance parameters were fitted in the form of a partition surface by using MATLAB software. The plots of yield to underflow as a function of TW and SP is shown in Figure 5.

Experimental results revealed a generally linear relationship between the studied operational variables and yield to underflow for all samples. The yield to underflow is decreasing with increasing TW and SP. Maximum yield to under flow can be achieved by maintaining low TW and SP. The upward water velocity which is a function of the teeter water flow rate and cross sectional area of the separation column, counters the downward settling velocities of the particles. Particles entering the column, which have a settling velocity that is less than that of the upward water velocity, are carried to the overflow stream. So with increase in the teeter water velocity, more amount of solids reports to the overflow stream in turn decreasing the yield to the underflow (Sarkar, 2008). Similarly, as the SP increases, the bed height also increases in the column. Therefore, more packed and viscous bed prevents material motion to the underflow. In this case, only coarser and heavier (denser) particles can report to underflow and more amount of particles are report to overflow.

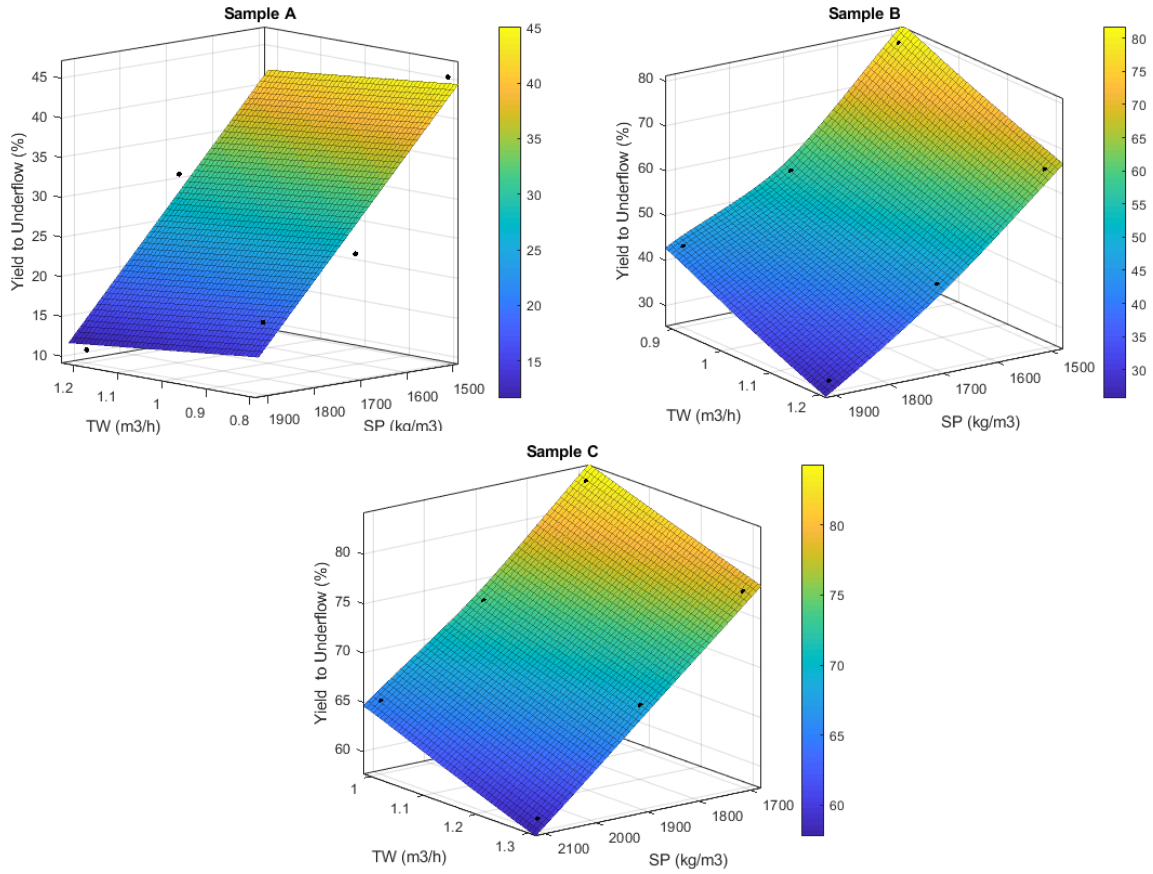


Fig. 5. Effect of studied process variables on yield to underflow

The plots of U/F Cr_2O_3 grade as a function of TW and SP is shown in Figure 6. It can be seen from Figure 6 that, as the TW and SP increases, the U/F Cr_2O_3 grade also increases. SP has major effect on the U/F Cr_2O_3 grade, followed by TW for the studied ore. The highest grade can be obtaining by maintaining highest levels of both variables. It is known that SP determines the accumulation of the deposited material inside the unit and hence the bed height inside the hindered bed separators. The bed height increases with the increase in bed pressure setting. As the bed height increases the average density and viscosity of the suspension goes up increasing the resistance for the particles to settle. In this condition less material can be report to U/F and these particles have a higher density and Cr_2O_3 characteristics.

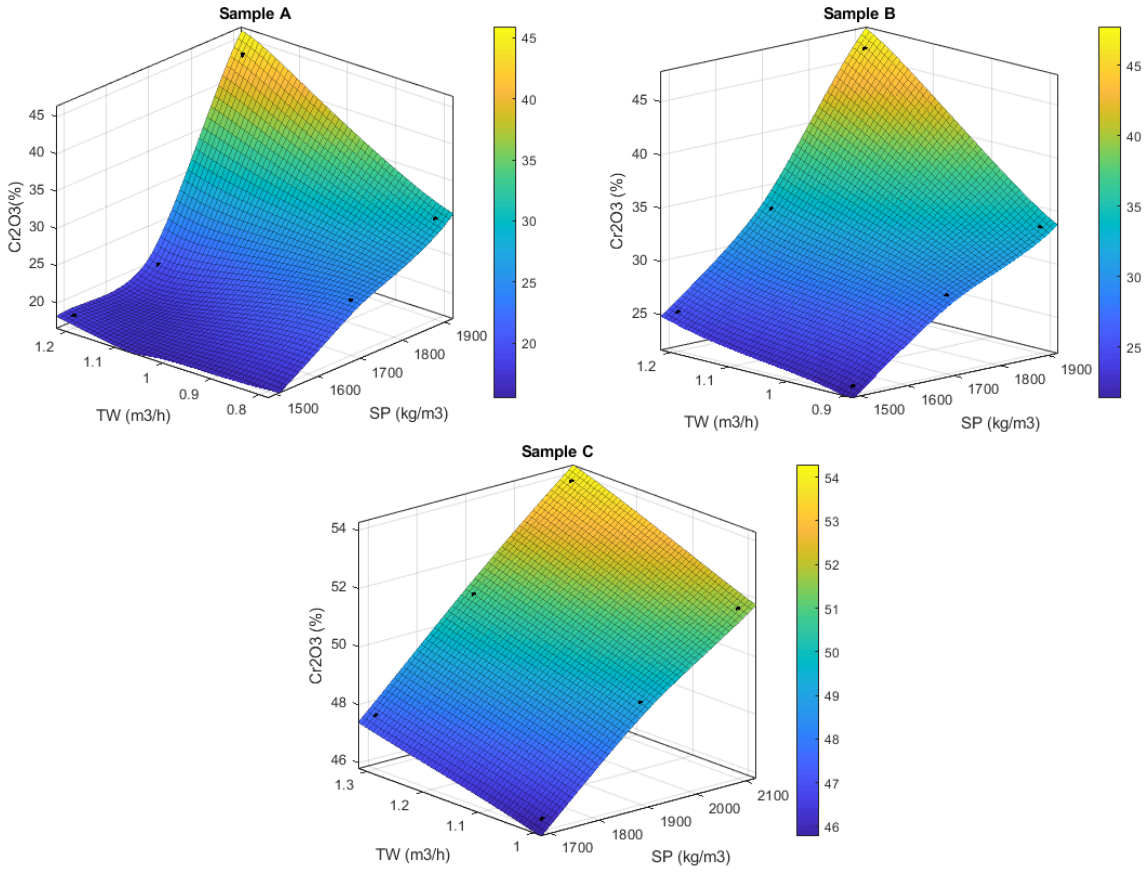


Fig. 6. Effect of studied process variables on U/F Cr_2O_3 grade

The plots of U/F Cr_2O_3 recovery as a function of TW and SP is shown in Figure 7. It can be seen from Figure 7 that, as the TW and SP increases, the U/F Cr_2O_3 recovery decreases, while Cr_2O_3 grade increases with the TW and SP. At lower bed pressures, the hindered bed classifiers merely act as a classifier (Das et al., 2009) and hence only the finer and less denser particles report to the overflow. On the contrary, at high SP, the suspension is denser and higher TW increases the upward hydraulic transport force. Moreover, denser (high chromite content) particles can also be diverted to the overflow irrespective of the SP. The relative movement of fine material to the underflow fraction is decreases because of more closed bed and higher upward hydraulic transport force which results some of the fine and locked chromite particles to move O/F and decreased recovery in the U/F.

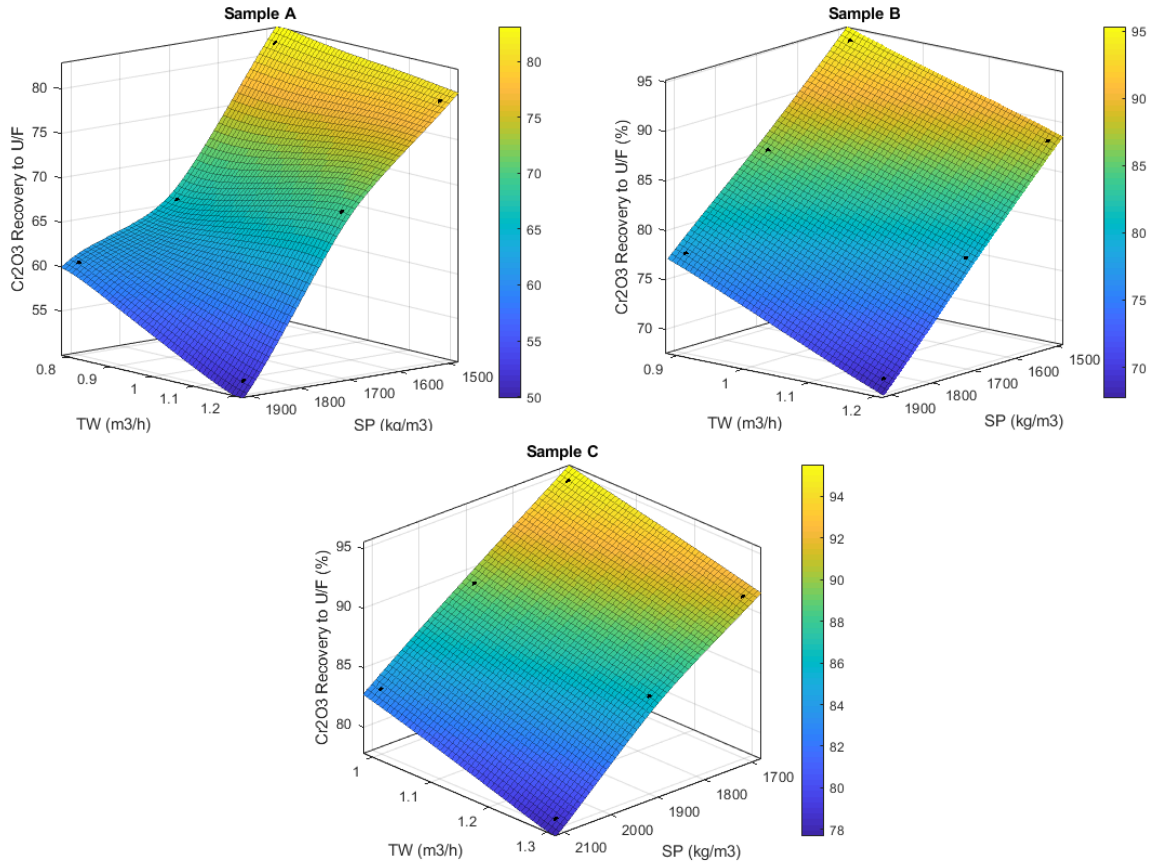


Fig. 7. Effect of studied process variables on U/F Cr_2O_3 recovery

4. Conclusions

Plotting the test results at the U/F against the bed density for samples shows that the mass yield and Cr_2O_3 recovery decreased, while Cr_2O_3 grade increased with the SP followed by TW. The decrease in U/F mass recovery observed upon increasing the SP and TW can be attributed exclusively to gangue removal from the concentrate. It can be assumed that the experimental conditions at intermediate and higher SP values were more efficient in reporting chromite to U/F and gangues to O/F. Further increase of the SP to 1900 kg/m^3 led to a U/F product with highest Cr_2O_3 grade and possibly lower gangue grades for all samples. The lower mass recovery at U/F recorded above these SP values can be attributed not only to gangue removal but also loss some of the finer chromite particles to O/F. This is also reflected in the Cr_2O_3 recovery at the U/F, for which a significant decrease was observed.

Density based separation was found more effective at the fluidization rate of lower than 1 m^3/h. The increase in TW decreased both yield to U/F and Cr_2O_3 recovery at the U/F for all samples. This can be explained by considering that in teetered beds, the separation of particles by density rather than size is promoted at low fluidization flow rates whereas increasing this variable promotes the inversion phenomenon (Galvin, 2003 and Moritomi et al., 1982). Galvin (2003) further showed that at low superficial liquid velocity, a high density suspension is produced, with the finer high density particles laying below the coarser low density particles. As the fluidization rate increases, the bed becomes more mobile (Galvin et al., 2005), and mixing occurs. Therefore, as the fluidization rate appears to be a very significant variable, an optimum should be sought according to the ore characteristics such as size, grade, amount of near density material etc. The same observation was made by Doroodchi et al. (2006) in their study on coal.

References

Amariei, D., Michaud, D., Paquet, G., Lindsay, M. (2014). The use of the Reflux Classifier for iron ores: assessment of fine particles recovery at pilot scale. Miner. Eng. 62, 66–73.

Das, A., Sarkar, B., Mehrotra, S.P., (2009). Prediction of separation performance of Floatex Density Separator for processing fine coal particles. Int. J. Miner. Process., 91(1), 41–49.

Doroodchi, E., Zhou, J., Fletcher, D.F., Galvin, K.P., 2006. Particle size classification in a fluidized bed containing parallel inclined plates. Minerals Engineering 19, 162–171.

Galvin, K.P., Pratten, S.J., Nicol, S.K. (1999). Dense medium separation using a teetered bed separator. Miner. Eng., Vol. 12 (9), pp. 1069–1081

Galvin, K.P., (2003). On the phenomena of hindered settling in liquid fluidized beds. In: Honaker, R.Q., Forest, W.R. (Eds.), Advances in Gravity Separation. SME Inc., Littleton, pp. 19–38.

Galvin, K.P., Doroodchi, E., Callen, A.M., Lambert, N., Pratten, S.J. (2002). Pilot plant trial of the reflux classifier. Minerals Engineering 15, 19–25.

Galvin, K.P., Callen, A., Zhou, J., Doroodchi, E., (2005). Performance of the reflux classifier for gravity separation at full scale. Minerals Engineering 18, 19–24.

Galvin, K.P., Walton, K., Zhou, J. (2009). How to elutriate particles according to their density. Chemical Engineering Science 64, 2003–2010.

Galvin, K.P., Zhou, J., Walton, K. (2010). Application of closely spaced inclined channels in gravity separation. Minerals Engineering 23, 326–338.

Hyde, D.A. Williams, K.P. Morris, A.N. Yexley, P.M. (1988). The beneficiation of fine coal using the hydrosizer. Mine and Quarry, Vol. 17 (3), pp. 50–54.

Kari, C. Kapure, G. Rao, S.M. Rao, N.D. (2006). Predicting the chromite mineral upgradation in floatex density separator using hindered settling models. ISIJ International, 46: 966–973.

Mankosa, M.J., Kohmuench, J.N., Eisenmann, M.D., Luttrell, G. H. (1995). Testing of Hydrofloat separator for coal cleaning application, Virginia Polytechnic Institute and State University, Blacksburg, Virginia

Moritomi, H., Iwase, T., Chiba, T., 1982. A comprehensive interpretation of solid layer inversion in liquid fluidized beds. Chemical Engineering Science 37 (12), 1751–1757.

REFLUX™ Classifier Fine particle technology 2024, accessed 01 September 2024, < https://www.flsmidth.com/en-gb/products/centrifugation-and-classification/reflux-classifier>.

Remes, A.; Tuikka, A.; and Kovio, H. (2011). Simulation and pilot experiments on pyrite concentrate separation in a floatex density separator. Minerals & Metallurgical Processing, 28: 62–70.

Sarkar B., Das A., Mehrotra SP., (2008). Study of separation features in floatex density separator for cleaning fine coal. Int. J. Miner. Process., 86, 40–49.

Tripathy, S.K., Bhoja, S.K., Kumar, C.R.; Suresh, N. (2015). A short review on hydraulic classification and its development in mineral industry. Powder Technology, Vol. 270, pp. 205–220.

Zhou, J., Walton, K., Laskovski, D., Duncan, P., Galvin, K.P. (2006). Enhanced separation of mineral sands using the Reflux Classifier. Miner. Eng. 19, 1573– 1579.

Scale, Deposit and Corrosion Control in Mineral Processing Growing Challenges and Emerging Solutions

Brian Danyliw [1]*

[1] Mine Water Service Inc.

[2]Affiliation 2

*Corresponding author: brian@minewaterservice.com (Brian Danyliw)

Abstract:

The mineral processing world has long relied on specialty chemicals and water treatment suppliers to provide solutions to control scale and deposit formation in plant water circuits. Without these treatment solutions many mineral processing water circuits would experience maintenance needs and downtime to a degree that could challenge the economic viability of the operation.

As the mining industry evolves water treatment challenges are also evolving. Lower grade ores, less accessibility to fresh water, less desirable ores containing more impurities and stricter environmental regulations are driving a need to reimagine the water treatment landscape for mineral processors.

This paper will discuss innovative technologies and approaches to scale, deposit, and corrosion control in modern water treatment for mineral processing operations. Specifically, the paper will focus on challenges presented by the adaptation of modern technologies by mineral processors.

- Water chemistry challenges presented by oxidative processes including pressure oxidation of sulfide gold ores and pressure acid leaching.
- The impact of higher water reuse rates and particularly the impact of implementation of dry stack tailings management.

A discussion of the water chemistry impacts of newer mineral processing adaptations leads to a discussion regarding innovations in chemical treatment approaches. Specialty chemical suppliers will need to focus on innovation in raw materials used in specialty water treatment chemical formulations to address these challenges. In some cases, this innovation is already taking place and will impact future treatment approaches.

A final discussion of the evolution of membrane filtration technologies (microfiltration, ultrafiltration, nanofiltration and reverse osmosis) for treatment and remediation of process waters in the mining industry will be included..

Keywords: *Water Reuse, Scale Control, Specialty Chemicals, Water Treatment, Membranes*

1. Introduction

The purpose of this paper is to explore the impacts of new and evolving practices in the mining and mineral processing industry on specific aspects of water treatment for these operations. Much of the work cited in this paper has been conducted by the author as a researcher and consultant working directly with mining companies that are dealing with the challenges being presented by industry changes. Discussion regarding innovations in the specialty chemical field as they pertain to emerging challenges in mining and mineral processing contained in this paper are based on actual work the author has and continues to conduct with these chemical producers. In these cases, application of new and innovative chemistries to the specific conditions and challenges emerging in mining and mineral processing is the basis for this collaboration.

This paper can serve as a guide for consideration of the impact of some operational options to mining and mineral processing plant operators on the water circuits and water chemistry in their plants. It is

the authors hope that through this paper and ongoing discussions on this subject mining and mineral processing operators can be better prepared to proactively address impacts on water systems resulting from processing of less desirable ore and/or adoption of new technologies.

2. Mining – An Evolving Industry

Mining faces considerable challenges as the global industry adjusts to changing world views. The industry has been dealing with challenges associated with lower grade ore and lower quality ore (higher impurities, more complex, more difficult to process) for many years. This, often coupled with ore bodies located in more remote and less climate friendly locations, have also put pressure on mining companies from a cost, manpower and staffing perspective. More recently ever-increasing pressure with respect to environmental stewardship has exasperated the pressures on mining companies. In its annual review of risks and opportunities for the mining and metals sector EY Canada lists ESG (Environment, Social and Governance) challenges as the number one challenge, in the same spot as last year ([1], Earnst and Young, 2024). Of the seventeen subsections of ESG respondents to the EY survey of mining operators and executives rated tailings and waste management and water stewardship both in the top three most important spots.

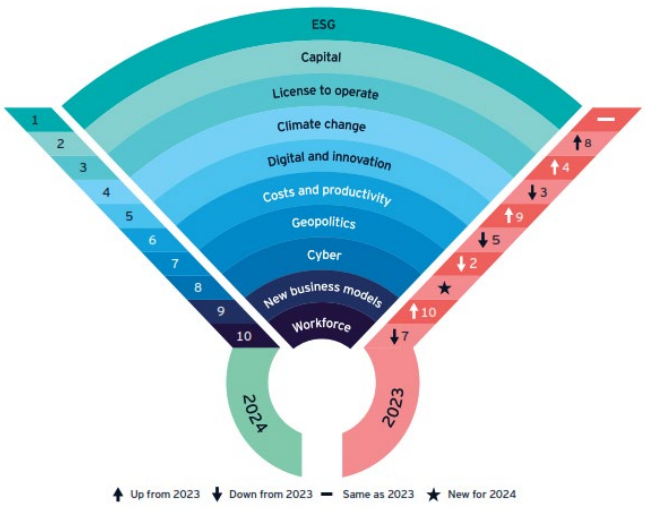


Figure 1, E&Y Canada Top Risks and Opportunities for the Mining Sector

Ultimately, from the perspective of this discussion, the top challenges facing the mining industry with respect to operational impacts on water quality can be summarized as follows:

Lower grade ores resulting in higher tonnage operations and lower profit margins driving operating cost containment

Lower quality ores resulting in higher content of unwanted materials that can adversely impact water quality (and in some instances recovery)

Less access to fresh water resulting in higher water recycle rates

Stricter environmental discharge limits add to the need to reduce fresh water use to reduce the volume of water discharged to the environment

1 EY Canada, Top 10 Business Risks and Opportunities for Mining and Metals 2024, https://www.ey.com/en_ca/mining-metals/risks-opportunities

3. Challenges to the Mine operator

When new operations are built to process less than desirable ore, or existing operations advance the mining operations to the point that ore quality changes the impact on the process water system is seen in an increase in soluble species associated with the new ore. In many instances the ore quality issues are associated with a higher sulfide content which results in the installation of oxidative processes. These oxidative processes can take the form of roasters, pressure oxidation (POX/HPAL) utilizing autoclaves or bio-oxidation. Both roasters and autoclave plants are far more common than bio-oxidation and for the purposes of this discussion are the two methods that will be discussed. In both cases the fundamental purpose of oxidizing sulfide species results in the formation of large amounts of sulphate which is added to the process water stream.

When mineral processing plants address concerns over freshwater volumes and effluent volumes it can take on two forms. Initially most operations will attempt to utilize a higher volume of tailing reclaim water to displace fresh water. This often takes the form of utilizing either TSF (tailings storage facility) recycle water or process water where fresh water has been traditionally used such as:

Reagent make down water

Reagent dilution water

Gland seal water

Scrubber water (gas or dust scrubbers)

Fire water in charged fire suppression systems

In many new construction situations and in some existing operations as a retrofit, dry stack tailings disposal is now being utilized. Dry stack tailings utilize filter presses to dewater plant tailings prior to disposal in the tailings storage area. This process allows recycling of very high percentages of process water, thereby reducing fresh water requirements significantly and correspondingly reducing discharge to the environment proportionally. While this is a very beneficial undertaking from an ESG perspective the impact on process water can be catastrophic if not properly understood and planned for due to the concentration of dissolved solids which accumulates in the process water under such high water recycle conditions.

This results in process water chemistry that is vastly different from other mining processes. The differences can be categorized as follows (based on a cross section of process water chemistry from 30 mining operations[2]:

Table 1. Characteristic Water Chemistry for Oxidative and Dry Stack Operations

Species	Units	Typical Values – Non Pox/HPAL/Dry Stack	POX/HPAL Values	Dry Stack Values
Conductivity	mS/m	775 – 6700	9800 – 20000	9500 - 20000
pH	Units	6.8 – 11.1	7.5 – 9.0	8.5 – 10.5
Sulphate	Mg/l as SO_4	140 - 3100	3000 – 4200	2575 - 5400
Calcium	Mg/l as $CaCO_3$	10 – 1050	1700 – 3400	1150 - 1900
Chloride	Mg/l Cl^-	36 – 490	43 – 6100	1100 - 2500
Trivalent Metals (Fe, Cu, Zn, Al, Mn)	Mg/l as species	0.5 – 42	50 – 110	5 – 40

[2] Mine Water Service Inc., Corporate files.

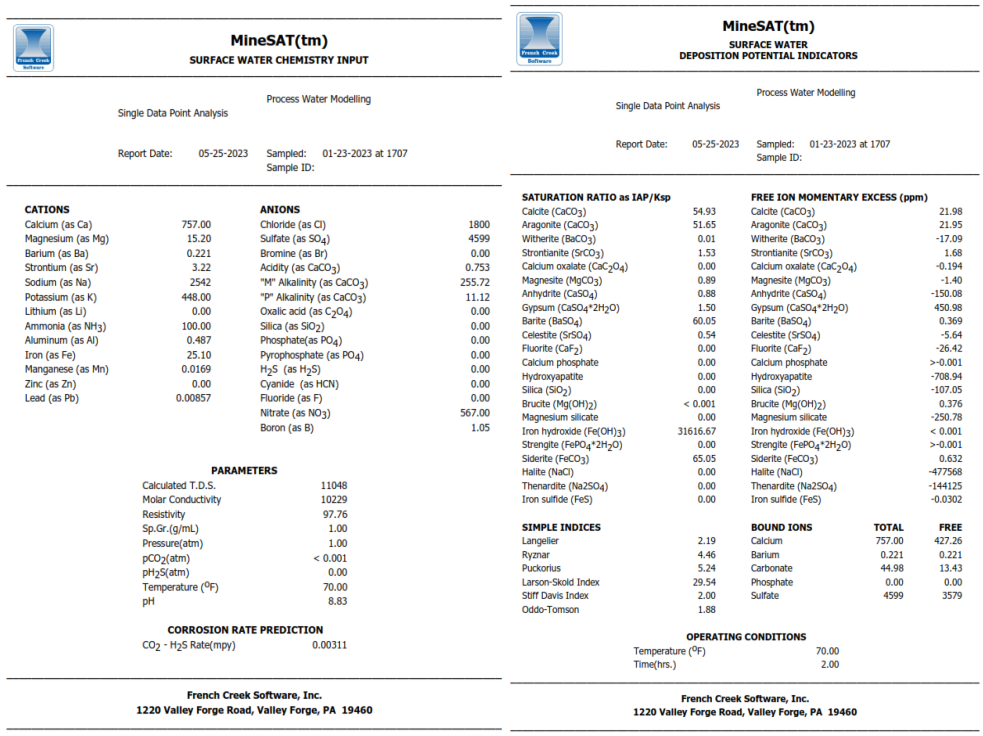
4. Impacts on Water Chemistry

The impacts on water chemistry shown in Table 1 point to the need to understand and anticipate these changes and to be prepared to deal with the accompanying operational challenges. The typical increase in total dissolved solids (as indicated by much higher conductivity) accompanied by dramatic increases in both dissolved calcium and sulphate point to much higher overall scale formation tendencies and a likely shift from calcium carbonate as the dominant scale forming species to calcium sulphate. Higher overall trivalent metal concentrations as well as much higher calcium concentrations also demonstrate the need to understand both the calcium tolerance and potential for poisoning of antiscalant ingredients by dissolved metals. Finally, the typical increase in conductivity, sulphate and chloride points to much higher corrosion potential in water systems associated with both oxidative and dry stack operations.

Calcium Sulphate formation in systems associated with both oxidative and dry stack operations is common. Calcium sulphate solubility is impacted by process and water quality variables with perhaps the most important variable being the concentration of monovalent ions. Species such as sodium and chloride have a significant impact on calcium sulphate solubility due to an effect known as ion pairing. This phenomenon is the result of high concentration of dissolved monovalent ions (in the case of calcium sulphate primarily sodium) stabilizing the salt in solution in this case $Ca^{+2}SO4^{-2}$) by pairing with the divalent sulphate radical.

In most of these systems the operator and water treater rely on a process known as controlled precipitation to maintain a calcium sulphate saturation level at a metal-stabile level above but close to theoretical saturation. Controlled precipitation refers to operation of the water circuit(s) and water treatment program in such a manner that critical areas of the system(s) can be maintained scale and deposit free while precipitation of oversaturated salts such as calcium carbonate and calcium sulphate is allowed to occur in locations where this precipitation is deemed to be least harmful or troublesome (such as in a leach train). The author has completed ion mass balances, including sulphate balances on both oxide and sulfide base metal dry stack operations and these mass balances support the hypothesis that controlled precipitation is the phenomenon that results in relatively stabile water chemistry.

Use of advanced modeling programs such as PHREEQC geochemical calculation software (available for free download from the U.S. Geological Survey) or proprietary software such as MineSAT™ (available from French Creek Software) becomes critical to understand potentially scale forming species solubilities in these highly stressed waters. Use of these programs provides insight into the adjusted saturation potential for salts based on the ion pairing effect and provides valuable insight into corrosion potential by calculating fully informed corrosion indices. In particular, the use of the Larson Skold index to predict the corrosive nature of high TDS, high chloride and high sulphate content waters is valuable.



MineSAT(tm)
SURFACE WATER CHEMISTRY INPUT

Process Water Modelling
Single Data Point Analysis

Report Date: 05-25-2023 Sampled: 01-23-2023 at 1707
Sample ID:

CATIONS		ANIONS	
Calcium (as Ca)	757.00	Chloride (as Cl)	1800
Magnesium (as Mg)	15.20	Sulfate (as SO_4)	4599
Barium (as Ba)	0.221	Bromine (as Br)	0.00
Strontium (as Sr)	3.22	Acidity (as $CaCO_3$)	0.753
Sodium (as Na)	2542	"M" Alkalinity (as $CaCO_3$)	255.72
Potassium (as K)	448.00	"P" Alkalinity (as $CaCO_3$)	11.12
Lithium (as Li)	0.00	Oxalic acid (as C_2O_4)	0.00
Ammonia (as NH_3)	100.00	Silica (as SiO_2)	0.00
Aluminum (as Al)	0.487	Phosphate(as PO_4)	0.00
Iron (as Fe)	25.10	Pyrophosphate (as PO_4)	0.00
Manganese (as Mn)	0.0169	H_2S (as H_2S)	0.00
Zinc (as Zn)	0.00	Cyanide (as HCN)	0.00
Lead (as Pb)	0.00857	Fluoride (as F)	0.00
		Nitrate (as NO_3)	567.00
		Boron (as B)	1.05

PARAMETERS

Calculated T.D.S.	11048
Molar Conductivity	10229
Resistivity	97.76
Sp.Gr.(g/mL)	1.00
Pressure(atm)	1.00
pCO_2(atm)	< 0.001
pH_2S(atm)	0.00
Temperature (^{0}F)	70.00
pH	8.83

CORROSION RATE PREDICTION

CO_2 - H_2S Rate(mpy) 0.00311

French Creek Software, Inc.
1220 Valley Forge Road, Valley Forge, PA 19460

MineSAT(tm)
SURFACE WATER
DEPOSITION POTENTIAL INDICATORS

Process Water Modelling
Single Data Point Analysis

Report Date: 05-25-2023 Sampled: 01-23-2023 at 1707
Sample ID:

SATURATION RATIO as IAP/Ksp		FREE ION MOMENTARY EXCESS (ppm)	
Calcite ($CaCO_3$)	54.93	Calcite ($CaCO_3$)	21.98
Aragonite ($CaCO_3$)	51.65	Aragonite ($CaCO_3$)	21.95
Witherite ($BaCO_3$)	0.01	Witherite ($BaCO_3$)	-17.09
Strontianite ($SrCO_3$)	1.53	Strontianite ($SrCO_3$)	1.68
Calcium oxalate (CaC_2O_4)	0.00	Calcium oxalate (CaC_2O_4)	-0.194
Magnesite ($MgCO_3$)	0.89	Magnesite ($MgCO_3$)	-1.40
Anhydrite ($CaSO_4$)	0.88	Anhydrite ($CaSO_4$)	-150.08
Gypsum ($CaSO_4*2H_2O$)	1.50	Gypsum ($CaSO_4*2H_2O$)	450.98
Barite ($BaSO_4$)	60.05	Barite ($BaSO_4$)	0.369
Celestite ($SrSO_4$)	0.54	Celestite ($SrSO_4$)	-5.64
Fluorite (CaF_2)	0.00	Fluorite (CaF_2)	-26.42
Calcium phosphate	0.00	Calcium phosphate	>-0.001
Hydroxyapatite	0.00	Hydroxyapatite	-708.94
Silica (SiO_2)	0.00	Silica (SiO_2)	-107.05
Brucite ($Mg(OH)_2$)	< 0.001	Brucite ($Mg(OH)_2$)	0.376
Magnesium silicate	0.00	Magnesium silicate	-250.78
Iron hydroxide ($Fe(OH)_3$)	31616.67	Iron hydroxide ($Fe(OH)_3$)	< 0.001
Strengite ($FePO_4*2H_2O$)	0.00	Strengite ($FePO_4*2H_2O$)	>-0.001
Siderite ($FeCO_3$)	65.05	Siderite ($FeCO_3$)	0.632
Halite (NaCl)	0.00	Halite (NaCl)	-477568
Thenardite ($Na2SO_4$)	0.00	Thenardite ($Na2SO_4$)	-144125
Iron sulfide (FeS)	0.00	Iron sulfide (FeS)	-0.0302

SIMPLE INDICES		BOUND IONS	TOTAL	FREE
Langelier	2.19	Calcium	757.00	427.26
Ryznar	4.46	Barium	0.221	0.221
Puckorius	5.24	Carbonate	44.98	13.43
Larson-Skold Index	29.54	Phosphate	0.00	0.00
Stiff Davis Index	2.00	Sulfate	4599	3579
Oddo-Tomson	1.88			

OPERATING CONDITIONS

Temperature (^{0}F)	70.00
Time(hrs.)	2.00

French Creek Software, Inc.
1220 Valley Forge Road, Valley Forge, PA 19460

Figure 2. MineSat™ Data from a Dry Stack Gold Operation with Sulfides

Figure 2 shows MineSat™ models for a stabile process water from a dry stack gold operation with sulfide content in the ore. The models show a stabile saturation level for calcite at ~55 and gypsum at ~1.5. From a corrosion perspective the Larson Skold index at 29.54 predicts potential for excessive corrosion which has in fact been experienced at this operation. Analysis of this operations entire circuit and sulfate and calcium balances across until operations and the full water circuit showed pick up of sulphate and calcium at various point in the process accompanied by loss of sulphate and calcium (controlled precipitation) at other points in the process. It is important to have a good knowledge of the entire mineral processing circuit and to consider not only impacts from the ore being processed but also calcium and sulphate inputs from reagents. In this specific case reagents used in various unit operations included lime, which is the main contributor of calcium and both sodium metabisulfite and copper sulphate which are significant contributors of sulphate in spite of oxidation of sulfide from the ore being the largest contributor.

This detailed mass balance demonstrates the valuable insight into opportunities to control scale and deposition in the process water circuit through strategic addition of antiscalant compounds coupled with controlled precipitation to ensure calcium carbonate and calcium sulphate saturations are maintained at natural levels based on the overall water chemistry.

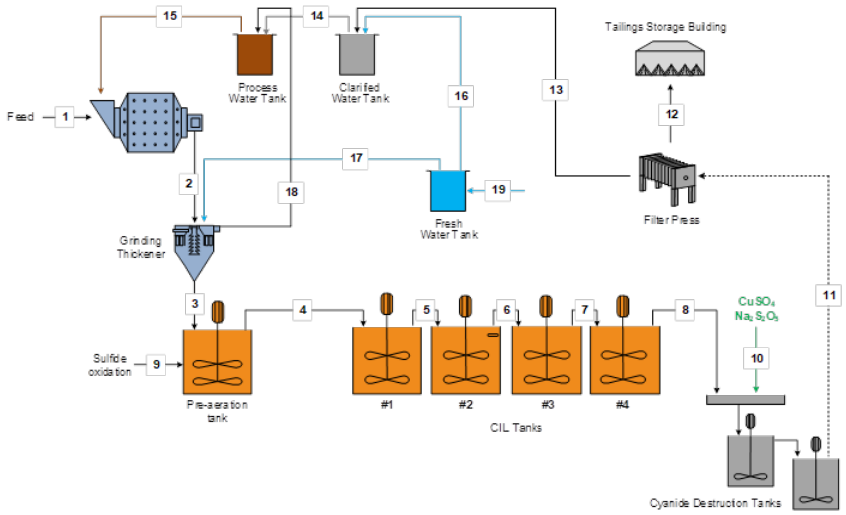


Figure 3. Flowsheet – Dry Stack Gold Mill

Table 2. Detailed Sulphate Balance – Dry Stack Gold Operation

Start Point	End Point	Average Sulfate Increase (mg/l)
#15 – Process Water	#3 – Grind TK Underflow	-385
#3 – Grind TK Underflow	#4 – Pre-aeration Discharge	+443
#4 – Pre-aeration Discharge	#8 – CIL Tails	-191
	NET	-133
#8 – CIL Tails	#11 – CN Detox Discharge	+604
#11 – CN Detox Discharge	#14 – Clarified Water Tank	-526
#14 – Clarified Water Tank	#15 – Process Water	55
	NET	+133
Total Circuit	NET	0

5. Chemical Industry Innovation

As an overview into the functionality of raw materials used in formulation of scale, deposit and corrosion control products for the mining and mineral processing industry the main groups of raw materials include:

- Scale control products that function through one or more of the main functional pathways
  - Threshold inhibition – meaning the ability to artificially increase salt solubility
  - Crystal distortion – meaning the ability to distort the crystal structure of precipitated salts
  - Dispersion – meaning the ability to disperse precipitate material and other solids in the water
- Corrosion control products based on traditional cathodic, anodic or combined cathodic and anodic corrosion control mechanisms

- Multifunctional materials that provide both scale and corrosion control

Historically innovation in the water treatment field was driven by attempts to improve performance in mainly cooling water systems due to the widespread use of cooling water across all industries. While this approach benefited water treatment and specialty chemical companies from a revenue potential perspective it did not address inherent idiosyncrasies of water treatment in the mining industry. Mining process water have traditionally been much more difficult to treat than cooling water due to higher calcium, sulphate, alkalinity, pH and dissolved solids levels. The advent of oxidative processes and higher water recycle rates, particularly with the introduction of dry stack tales only exacerbated these issues. Calium sulphate inhibition was never a strong focus in the cooling water treatment market as it is seldom encountered. The ability of raw materials to be effective in extremely high calcium environments was also not a concern in cooling water to the degree seen in mining. The lack of focus on calcium tolerance has resulting in the development and application of many raw materials that will not withstand the calcium concentrations seen in some mining waters. This results in precipitation of the inhibitor as a calcium salt rendering it ineffective and resulting in catastrophic failure on scale and deposit control programs in mining applications.

Recently a few innovative companies have begun to focus on development of molecules that can address both the calcium tolerance and calcium sulphate efficacy shortfalls. Innovative multi-component terpolymers and poly-carboxylic acid (PCA) based inhibitors are becoming available that offer improved performance under the high stress conditions seen in mining. Refinement of historically utilized molecules to add properties more aligned with the needs of the mining industry is also taking place.

An example of this kind of innovation is demonstrated by the following data representing comparative performance studies of a new and innovative raw material (EXP) and three historically utilized antiscalant raw materials.

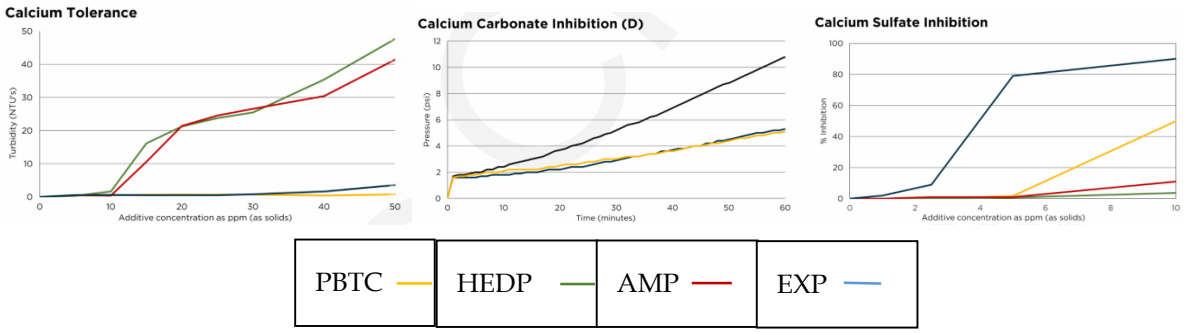


Figure 4. Comparative Testing of New Antiscalant Molecule[3]

This particular raw material, which is now commercially available, shows calcium tolerance equal to one of the current best in class molecules while providing superior inhibition performance for both calcium carbonate and calcium sulphate. This same molecule also provides vastly improved dispersion of both clay (~4X better) and iron oxide (~2.5X).

Examples of modifications made to existing molecules to impart improved performance include an improved version of an existing molecule which was able to provide a 40% improvement in calcite inhibition in dynamic testing and a 2X to 4X improvement in dispersive properties when compared to the previous generation molecule. This same molecule was shown to provide enhanced corrosion control in laboratory testing with a reduction in corrosion rates of approximately 50% when applied alone and approximately 30% when applied in combination with zinc as a cathodic inhibitor compared to the previous generation.

[3] Proprietary laboratory studies

The utilization of new and innovative raw materials in antiscalants, deposit control agents and corrosion control treatments for mining and mineral processing is allowing innovative water treaters to address new and emerging unmet needs. Those who are investing in research and development and working in partnership with raw material suppliers who are also investing in R&D and innovation will bring new products to market which promise to vastly improve the performance of water treatment programs for their mining clients.

6. Membrane Advances; The Holy Grail of Process Water Treatment?

Membrane filtration technologies encompass micro filtration, ultra filtration, nano filtration and reverse osmosis processes. Membrane filtration can be utilized to remove a host of impurities from water, down to the atomic level, producing a permeate (filtrate) of exceptionally low dissolved solids content. Membrane systems utilizing a combination of available technologies have been used in mining operations for many years as a means of treating water for discharge to the environment. Historically these plants were costly, both from a CAPEX and OPEX perspective and recovery, which is the volume of treated water (permeate/filtrate) relative to the amount of water that was wasted back to the plant feed source was quite low (often <50%).

Ongoing innovation in membrane filtration processes has resulted in a significant reduction in CAPEX and OPEX and allowed for significant improvements in recovery rates with many modern plants achieving recovery of >75% (often as high as 90% with a brine retreatment stage). One would assume then that these membrane systems could address many of the issues that modern oxidative processes and dry stack mining operations experience with water quality. This assumption would be correct in some ways but requires a detailed understanding of membrane system technologies and the potential impacts on membrane system efficacies based on typical and in some cases extreme mining water quality.

While it is true that membrane systems can separate undesirable constituents from a feed water these constituents are not eliminated but concentrated in the plant reject water. Treatment of a process water may very effectively reduce many undesirable ions such as calcium, sulphate and metals including copper, iron, nickel and zinc. These constituents are however concentrated in the membrane plant reject water and must be dealt with in some way. Most installed membrane plants, which are still mainly for effluent treatment, return the brine to the TSF either directly from the membrane plant or after a precipitation stage where calcium, sulphate and possibly metals are reduced via precipitation.

In a process water treatment scenario, the installation of a membrane plant to improve process water chemistry, typically with the use of a brine treatment to precipitate unwanted species such as sulphate, is in general simply replacing the controlled precipitation that is already taking place at various locations in the process plant unit operations. Removal of calcium, sulphate and in many instances, metals may not have an overall impact on the concentrations of these species in the process water. A careful analysis of the inputs to the process water of these species is required to understand the replacement rate via the ore being processed or reagent inputs. Additionally, consideration need to be given to the method by which these unwanted species will be precipitated in a membrane system brine treatment step. In many instances reagents used to precipitate species, such as the use of calcium chloride to precipitate gypsum, will result in an ongoing increase in monovalent ion concentration in the process water which will impact calcium sulphate solubility and could result in even more significant scale and deposit formation in certain parts of the process water circuit (not to mention increased chloride and associated corrosion). It should also be noted that in the case of oxidative gold processes the introduction of chloride in any form is normally avoided at all costs due to the potential for gold chloride in the oxidation process and resulting gold losses to tails.

While the use of membrane processes certainly does have its place in the mining industry careful consideration should be taken before attempting to utilize this technology specifically for process water treatment. In instances where recovery of metals from solution provides a valuable revenue stream or where careful mass balance calculations identify species replacement rates below removal rates offered by membrane technology then the option should be considered. In many instances however these conditions will not be met.

Removal of Anions (SO42- , S2O32- and SCN-) from Gold Mining Process Water by Membrane Capacitive Deionization Process

Yasemin Ozturk [1]*

[1]Hacettepe University, Mining Engineering Department, Beytepe, Ankara

*Corresponding author: yozdil@hacettepe.edu.tr (Yasemin Ozturk)

Abstract:

In this study, the removal of sulfate, thiosulfate, and thiocyanate (SO_4^{2-} , $S_2O_3^{2-}$ and SCN^-) by membrane capacitive deionization (MCDI) process was studied. For this purpose, an electrochemical cell containing an anion exchange membrane and a cation exchange membrane placed on a carbon paper electrode as anode and cathode was fabricated.

Batch mode experiments were conducted by recirculating single salt solutions of SO_4^{2-} , $S_2O_3^{2-}$, and SCN^- to determine the maximum removal efficiency. The amount of residual ions was determined by ion chromatography at various time intervals. Removal efficiency was determined at an operating voltage of 1.2 V at a constant flow rate of 1.5 ml of influent solution per minute. The electrodes removed 8600 mg SO_4^{2-}, 9850 mg $S_2O_3^{2-}$, and 9350 mg SCN^- per m^2 of the electrode.

Batch mode experiments were also performed in mixed salt solution containing 100 mg/L SO_4^{2-}, $S_2O_3^{2-}$, and SCN^- to observe the effect of co-ions on the removal efficiency. In the adsorption phase, salt removal efficiency percentages were determined to be 57% for SO_4^{2-}, 57% for SCN^-, and 88% for $S_2O_3^{2-}$ at 1.2 V. In the desorption phase, the electrodes were regenerated by reversing the operating voltage to -5.0 V. At the end of one-hour desorption, 92% of SO42-, 14% of S2O32-, and 28% of SCN^- were recovered.

The findings of the study suggest that MCDI is a promising tool for the treatment of gold mining process water. However, further research is required to assess its efficiency.

Keywords: *Water Treatment, Gold Mining Process Water, Membrane Capacitive Deionization (MCDI), Sulfide Minerals.*

1. Introduction

Cyanidation is a widely used process in gold extraction, particularly for ores containing sulfide minerals. During the process, cyanide reacts with elemental sulfur and polysulfides to produce thiocyanate, as shown in reactions (1)-(3) (Adams 1990).

$$S^0 + CN^- \leftrightarrow SCN^- \quad (1)$$

$$2S^{2-} + 2CN^- + O_2 + 2H_2O \leftrightarrow 2SCN^- + 4OH^- \quad (2)$$

$$S_2O_3^{2-} + CN^- \leftrightarrow SCN^- + SO_3^{2-} \quad (3)$$

Thiocyanate is a common contaminant in gold mining effluent. It can undergo oxidation reactions and always oxidized to sulfate (Gauguin 1951; 1949). It is a strong complexing agent, forming compounds with the first group transition metals via nitrogen and with the second and third group transition metals via sulfur (Gould et al. 2012). Thiocyanate, a hydrophilic species, can form compounds with metal sulfides such as Fe, Cu etc. and suppress their flotation (Wang and Forssberg 1996).

In the processing of sulfide minerals, thiosalts are produced by the oxidation of the sulfide group (e.g., pyrite, FeS_2 and pyrrhotite, FeS) by oxygen. They occur as partially oxidized sulfoxy anions like thiosulfate ($S_2O_3^{2-}$), trithionates ($S_3O_6^{2-}$), and tetrathionates ($S_4O_6^{2-}$) as shown in the reactions (4)-(7):

$$2FeS_2 + 1/2O_2 + H_2O \rightarrow 2Fe^{2+} + 2OH^- + 4S° \quad (4)$$

$$4S° + 6OH^- \rightarrow 2S^{2-} + S_2O_3^{2-} + 3H_2O \quad (5)$$

$$3S_2O_3^{2-} + 2O_2 + H_2O \rightarrow 2S_3O_6^{2-} + 2OH^- \quad (6)$$

$$4S_2O_3^{2-} + O_2 + 2H_2O \rightarrow 2S_4O_6^{2-} + 4OH^- \quad (7)$$

These anions are metastable species and oxidize or disproportionate to more stable sulfate, as described by following reactions (8)-(10), (Rao, 2011):

$$S_2O_3^{2-} + 2O_2 + H_2O \rightarrow 2SO_4^{2-} + 2H^+ \quad (8)$$

$$S_3O_6^{2-} + 2O_2 + 2H_2O \rightarrow 3SO_4^{2-} + 4H^+ \quad (9)$$

$$S_4O_6^{2-} + 7/2O_2 + 3H_2O \rightarrow 4SO_4^{2-} + 6H^+ \quad (10)$$

Products of these chemical reactions enter the process water and result in a reduction in water quality (Rao, 2011).

In recent years, Capacitive Deionization (CDI) has emerged as a robust, energy efficient, and cost effective technology for desalinating low to medium salinity water (Anderson et al., 2010). It operates on the principle that ions move towards porous electrodes when low potentials (< 1.5 V) are applied (Oren, 2008). It is a two-phase water treatment process. The first phase involves an ion electrosorption process that adsorbs ions on pairs of carbon electrodes to desalinate water. The second phase involves regenerating the electrodes by releasing the adsorbed ions (Porada et al. 2013).

The membrane capacitive deionization (MCDI) process is a modification of the CDI process utilizing ion-exchange membranes. Membranes are placed in front of the electrodes. During operation, the membranes prevent co-ions from leaving the electrode region during adsorption, improving the salt adsorption capacity (Biesheuvel and Van der Wal, 2010).

This study investigated the removal of SO_4^{2-} , $S_2O_3^{2-}$, and SCN^- by membrane capacitive deionization process. An electrochemical cell containing carbon paper electrodes and ion exchange membranes was used. Batch experiments with single salt solutions were conducted to determine the adsorption capacity of the electrodes for each ion at operating voltages of 0 V and 1.2 V. The process efficiency for mixed salt solution was also studied. In addition, regeneration of the electrodes was carried out by reversing the operational voltage to -5.0 V. The removal efficiency was evaluated by total salt removal (SR) and salt removal efficiency (SRE%).

2. Materials and Methods

2.1. Materials

Carbon paper (Sigracet GDL 39AA) was obtained from SGL Carbon. It has a total thickness of 280 µm. Anion exchange membrane (AEM Type 10, exchange capacity: 1.8 meq/g) was obtained from Fuji Film. Cation exchange membrane (CEM, exchange capacity: 2.0 meq/g) was supplied by Shanghai Shanghua.

Analytical grade chemicals were used to prepare the salt solutions. Ammonium thiocyanate (NH_4SCN) was obtained from Carlo Erba. Sodium thiosulphate ($Na_2S_2O_3.5H_2O$) was purchased from Sure Chem. Sodium sulfate (Na_2SO_4) was provided by Merck. Deionized water (Heal Force Smart) was used throughout the study.

2.2. Desalination Experiments

Schematic representation of bench-scale membrane capacitive deionization test setup is given in Figure 43. The feed solution was pumped with a peristaltic pump (Cole Parmer, Masterflex) through a flow by

type capacitive deionization cell. A potential was applied by using a potentiostat (Gamry PCI-4750) during process.

The MCDI cell consisted of two electrodes: an AEM placed on top of carbon paper as the anode, and a CEM placed on top of carbon paper as the cathode. A titanium sheet was used as a current collector. The sizes of current collectors and electrodes were 10X50 mm. The electrodes were separated from each other by a nylon separator. In all experiments, the flow rate of the solution was maintained at 1.5 mL per minute.

Batch mode experiments were performed to determine the removal efficiency of SO42- , S2O32-, and SCN- by membrane capacitive deionization method. 25 ml sulfate solution at various concentrations; 30 mg/L, 100 mg/L, and 200 mg/L was recirculated through the MCDI test setup for 3 hours at 0 V.

Single salt solutions containing 200 mg/L of SO42- , S2O32-, and SCN- with a volume of 25 ml were recycled through the test setup at 0 V and 1.2 V for 3 hours to observe the effect of voltage on desalination performance.

Treatment of 25 mL of a mixed salt solution including 100 mg/L of SO42- , S2O32-, and SCN- was carried out at 1.2 V for 3 hours at a flow rate of 1.5 ml/min. Concentration of residual ions was measured using ion chromatography (IC, Dionex ICS 3000) at various time intervals during the process.

For the regeneration of the electrodes, treated water produced from mixed salt solution test was recirculated through the system at an operating voltage of -5.0 V at a flow rate of 1.5 ml/min for 1 hour.

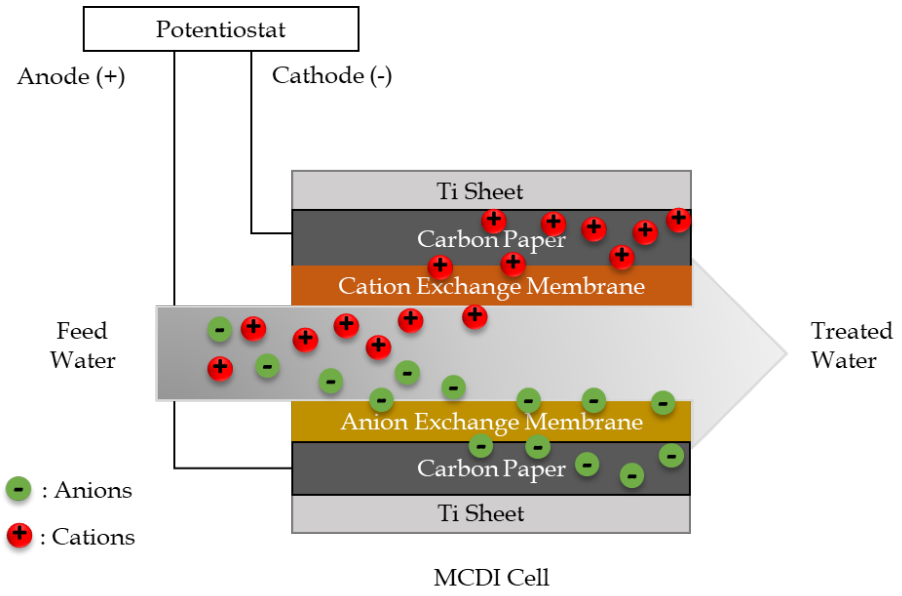


Figure 43. Schematic representation of membrane capacitive deionization test setup.

Process efficiency was determined by the amount of total salt removed (SR, mg/m2 (eq11)) and salt removal efficiency % (SRE %, (eq12)).

$$SR = \frac{(C_i - C_f)V}{A_e} \quad (11)$$

$$SRE[\%] = \frac{(C_i - C_f)}{C_i} x100\% \quad (12)$$

Ci: initial concentration (mg/L); Cf: final concentration (mg/L); V: volume (L); Ae: effective frontal area of the anode (m^2).

3. Results and Discussion

3.1. Single Salt Solution Studies

Batch recirculation tests of sulfate solutions at varying concentrations of 30- 100- 200 mg/L with a volume of 25 mL were conducted at a constant flow rate of 1.5 mL/min for 3 hours without applying voltage. The concentration of residual sulfate was continuously measured throughout the process to determine the maximum level of adsorption achieved at 0 V.

Figure 44 illustrates the total amount of sulfate per square meter of the electrode removed during the operation. The results indicated that the electrodes achieved maximum adsorption at a sulfate concentration of 200 mg/L, resulting in a total sulfate removal of 5600 mg/m^2 in 60 minutes. As a results, 200 mg/L concentration level was chosen for thiosulfate and thiocyanate ions. The experiment was performed using single salt solutions of 200 mg/L thiosulfate and thiocyanate ions at 0 V.

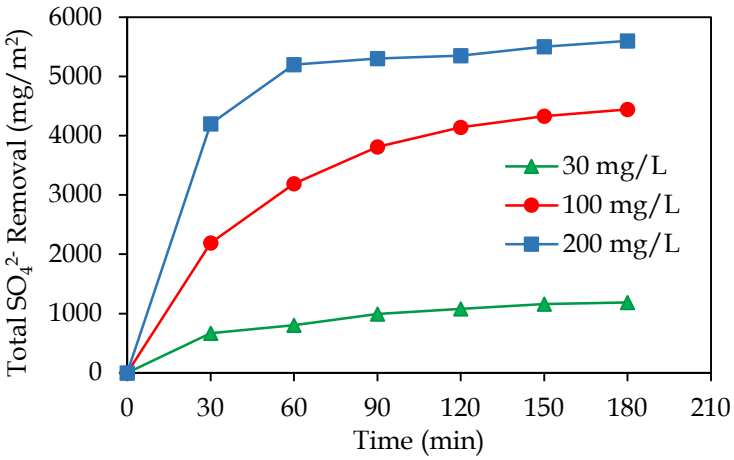


Figure 44. Total sulfate removal at varying concentrations in a 25 ml solution at 0 V with a flow rate of 1.5 mL/min.

In this phase of the study, the impact of voltage on desalination efficiency was investigated by applying 1.2 V to 200 mg/L single salt solutions of SO42- , S2O32-, and SCN-. The solutions were pumped at a rate of 1.5 mL per minute for 3 hours.

A comparison was conducted to assess the total salt removal for each ion at both 0 V and 1.2 V voltages. The results are presented in Figure 45 for the SO42- ion, Figure 46 for the S2O32- ion, and Figure 47 for the SCN- ion. The results indicated a significant increase in sulfate removal from 5600 mg/m^2 to 8600 mg/m^2 when the potential is applied, as shown in Figure 3. In addition, thiosulfate removal was enhanced from 7800 mg/m^2 to 9850 mg/m^2 (Figure 4), while thiocyanate levels increased from 6150 mg/m^2 to 9350 mg/m^2 (Figure 5). Based on the results, it can be concluded that removal efficiency of thiosulfate was greater than sulfate and thiocyanate ions.

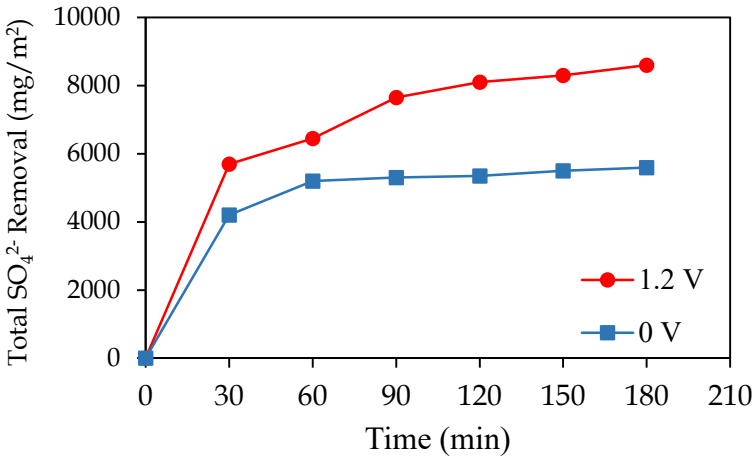


Figure 45. Total sulfate removal from a 25 ml, 200 mg/L sulfate solution at 0 V and 1.2 V with a flow rate of 1.5 mL/min.

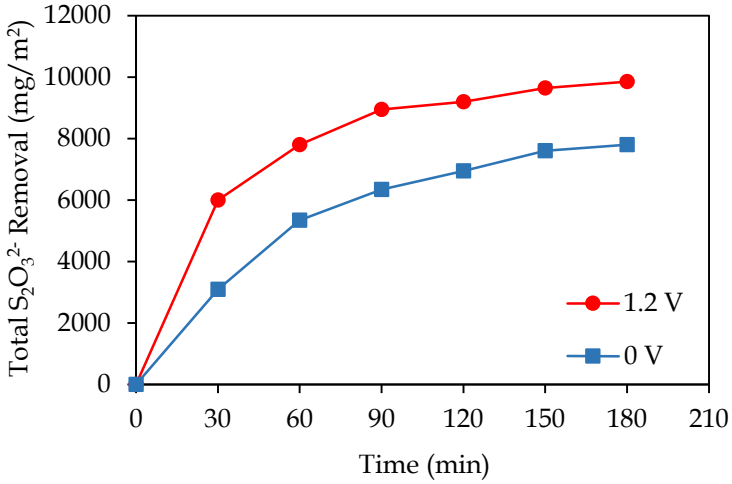


Figure 46. Total thiosulfate removal from a 25 ml, 200 mg/L thiosulfate solution at 0 V and 1.2 V with a flow rate of 1.5 mL/min.

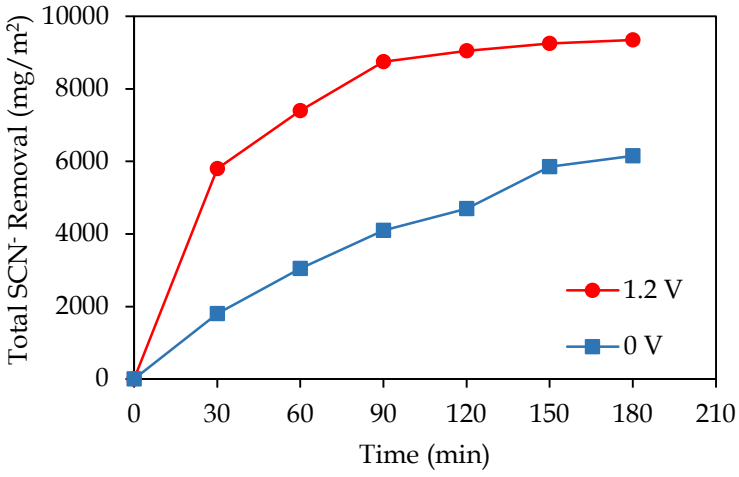


Figure 47. Total thiocyanate removal from a 25 ml, 200 mg/L thiocyanate solution at 0 V and 1.2 V with a flow rate of 1.5 mL/min.

3.2. Mixed Salt Solution Studies

The batch experiment of a mixed salt solution containing 100 mg/L SO_4^{2-}, 100 mg/L $S_2O_3^{2-}$, and 100 mg/L SCN^- was also performed to investigate the impact of co-ions on the removal efficiency. For this purpose, a 25 ml solution was pumped with a flow rate of 1.5 ml/min at an operating voltage of 1.2 V for 3 hours.

The total salt removal of each ion is presented in Figure 48. The results showed that the electrosorption of sulfate and thiocyanate reached an equilibrium state after 60 minutes of operation. The total salt removal was 2600 mg/m^2 for sulfate and 3150 mg/m^2 for thiocyanate. In contrast, thiosulfate demonstrated a higher salt removal of 5350 mg/m^2. The electrodes removed a total of 11100 mg/m^2 of salt throughout the process.

Figure 49 illustrates the salt removal efficiency percentages of the ions. The results indicated that the electrodes removed 57% of sulfate and thiocyanate, as well as 88% of thiosulfate within 3 hours of operation.

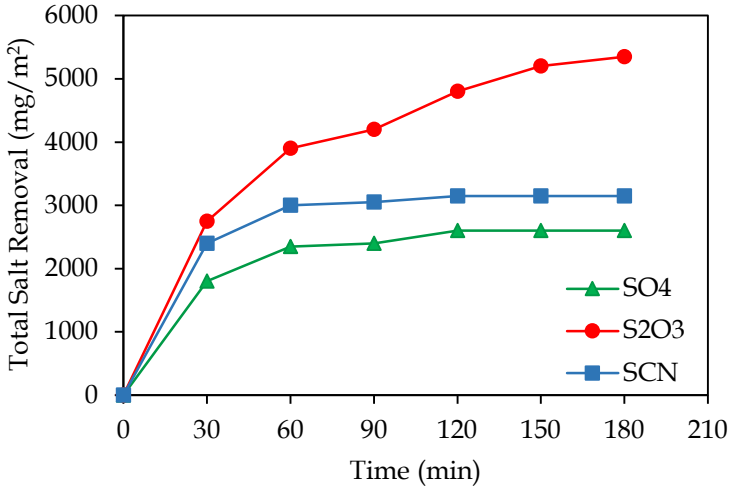


Figure 48. Total salt removal from a 25 ml mixed salt solution containing 100 mg/L SO_4^{2-}, $S_2O_3^{2-}$, SCN^- at 1.2 V with a flow rate of 1.5 mL/min.

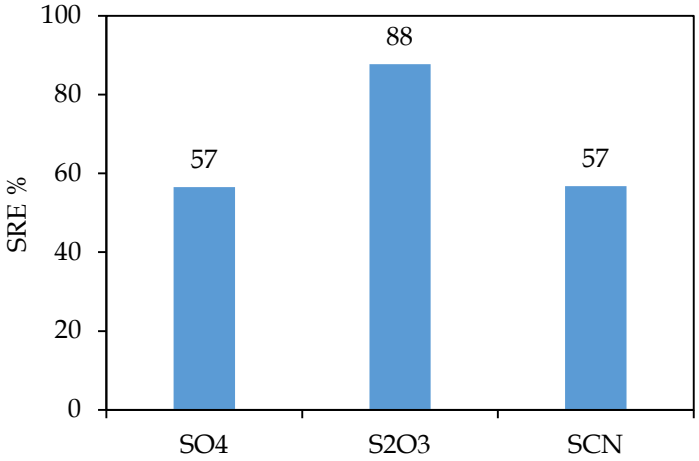


Figure 49. Salt removal efficiency % of 25 ml mixed salt solution containing 100 mg/L SO_4^{2-}, $S_2O_3^{2-}$, SCN^- at 1.2 V with a flow rate of 1.5 mL/min.

3.3. Regeneration of the Electrodes

When the electrodes reached their maximum adsorption capacity, the potential is reversed to facilitate the desorption of the adsorbed ions, resulting in the regeneration of the electrodes. For this purpose, 25 ml of treated water obtained from the mixed salt solution experiment was recirculated through the MCDI test setup at an operational voltage of -5 V with a flow rate of 1.5 ml/min for 1 hour.

The amount of adsorbed and desorbed ions in the electrosorption and desorption phases are compared in Figure 50. According to the results, 2600 mg/m^2 of sulfate was adsorbed by the electrodes in the electrosorption phase and 2400 mg/m^2 was desorbed in the desorption phase, corresponding to 92% recovery. However, 750 mg of thiosulfate and 900 mg of thiocyanate were recovered corresponding to recoveries of 14% and 28%, respectively. This could be attributed to the oxidation of desorbed thiosulfate and thiocyanate at high voltage in the desorption stage. During the desorption process, the electrodes desorbed 36.5% of the total adsorbed ions.

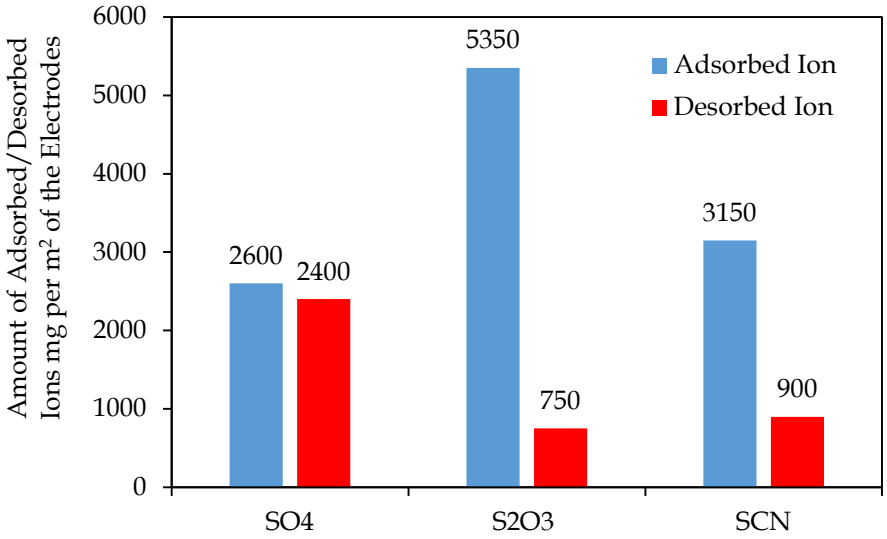


Figure 50. Amount of adsorbed and desorbed ions in the electrosorption and desorption phases.

3.4. Conclusion

The results obtained from this study were summarized below:

During the electrosorption process, 8600 mg of SO_4^{2-}, 9850 mg of $S_2O_3^{2-}$, and 9350 mg of SCN^- were removed per square meter of the electrode. This was achieved by recirculating 25 mL of 200 mg/L single salt solutions of each ion at a flow rate of 1.5 mL per minute and applying a voltage of 1.2 V for 3 hours.

2600 mg/m^2 sulfate, 3150 mg/m^2 thiocyanate, and 5350 mg/m^2 thiosulfate were removed from 25 ml of the mixed salt solution containing 100 mg/L of SO42-, S2O32-, and SCN- at 1.2 V for 3 hours. SRE% was determined to be 57% for SO_4^{2-}, 57% for SCN^-, and 88% for $S_2O_3^{2-}$.

Regeneration studies were performed by recirculating the treated water produced from mixed salt solution at a flow rate of 1.5 ml/min at an operating voltage of -5.0 V for 1 hour. The electrodes were regenerated with a recovery of 92% of SO42-, 14% of S2O32-, and 28% of SCN-.

- The study highlights the potential of MCDI for the treatment of gold mining process water. However, further research is needed to evaluate its efficiency. Operating parameters such as adsorption/desorption cycle times, applied voltage, and flow rate in continuous mode operation should be investigated. In addition, the long-term performance and stability of the electrodes should be monitored to assess their overall effectiveness.

References

Adams, M.D. 1990. The chemical behaviour of cyanide in the extraction of gold. 2. Mechanisms of cyanide loss in the carbon-in-pulp process. T*he Southern African Institute of Mining and Metallurgy,* 90 (3), 67-73.

Anderson, M.A., Cudero, A.L., Palma, J., 2010. Capacitive deionization as an electrochemical means of saving energy and delivering clean water. Comparison to present desalination practices: will it compete? Electrochimica Acta, 55, 3845–3856.

Gauguin, R. 1951. Oxydation electrochimique de l'ion thiocyanique. Application aux dosages et ä l'*étude* des reactions. Analytica Chimica Acta, 5, 200–214.

Gauguin, R. 1949. Remarques sur l'oxydation des thiocyanates par l'iodate. Analytica Chimica Acta, 3, 272–276.

Gould, W.D., King, M., Mohapatra, B.R., Cameron, R.A., Kapoor, A., and Koren, D.W. 2012. A critical review on destruction of thiocyanate in mining effluents. Minerals Engineering, 34:38–47.

Porada S, Zhao R, Van der Wal A, Presser V, Biesheuvel PM. 2013. Review on the science and technology of water desalination by capacitive deionization. *Progress in Materials Science,* 58, 1388–1442.

Oren, Y. 2008. Capacitive deionization (CDI) for desalination and water treatment — past, present and future (a review). Desalination, 228, 10–29.

Biesheuvel, P.M., van der Wal, A., Membrane capacitive deionization, Journal of Membrane Science, 346 (2010) 256–262.

Rao, S.R., 2011. Resource Recovery and Recycling from Metallurgical Wastes. Waste Management. Elsevier Science Ltd., Waste Management Series 7, pp. 473-475, ISBN-13: 9780080463209.

Wang, X.H., and Forssberg, K.S.E. 1996. The Solution Electrochemistry of Sulfide Xanthate-Cyanide Systems in Sulfide Mineral Flotation. Minerals Engineering, 9(5): 527-546.

Recovery of metals from coal power plant fly ashes via hydrometallurgical route

K. Tahsin Perek [1]*, Esra Baştürkcü [1], Mustafa Özer [1], Y. Enes Pural [1], Fatma Arslan [1]

[1] Istanbul Technical University, Mining Faculty, Mineral Processing Engineering Department, 34469 Maslak, Istanbul, Türkiye

*Corresponding author: perek@itu.edu.tr (K.T. Perek)

Abstract:

Combustion of coal for generation of electricity in thermal power plants (TPPs) produces a complex mixture of pollutants in the atmosphere namely acid gases, organic compounds and solid wastes such as fly ash, bottom ash, and flue gases. It is desirable to recover metals from TTPs solid wastes and production of high value compounds from such wastes. They usually contain a quantity of valuable metals and they are actually a secondary resource of metals. By applying mineral processing technologies, hydrometallurgical and bio-hydrometallurgical processes, it is possible to recover metals (C, S, Co, Fe, Ni, V, Zn, etc.) from TPP solid wastes. Fly ash is the finely divided mineral residue resulting from the combustion of ground or powdered coal in electric generating plant. It consists of inorganic, incombustible matter present in the coal, and during combustion partially some of the components transform into a glassy, amorphous structure. In this experimental study, after the physical, chemical, and mineralogical properties of the fly ash were determined, hydrometallurgical processes were applied in order to recover the metallic values (Co, Mo, Fe, V, Ni). In the leaching experiments, effects of type and concentration of leaching agent (H_2SO_4, HCl, HNO_3, and NaOH), temperature, solid/liquid ratio, and duration on metal (V, Co, Ni, Mo, Fe) leaching efficiencies were investigated, and optimum leaching conditions were found as 1/10 solid/liquid ratio, 400 g/L H_2SO_4, 80^{o}C temperature, and 60 min leaching time. Metal leaching efficiencies for Fe, Mo, V, Ni, and Co at optimum conditions were 74.6, 90.5, 100, 76.9 and 42.8% respectively and a conceptual flowsheet is produced.

Keywords: *Fly ash, gravity separation, hydrometallurgical processes, acidic dissolution*

1. Introduction

Due to the increasing amount of coal ash being underutilized and its substantial trace metals amount, it can be used as a secondary resource for metal extraction for further industrial application. In thermal power plants, low-calorie coals that are not generally used in industry are burned. Fly ash is obtained as a by-product of solid fuel-fired thermal power plants that produce electricity. Fly ash typically contains 34-58% SiO2, 20-40% Al_2O_3, 4-24% Fe_2O_3, 2-27% CaO, 1-6% MgO, 0.5-4% SO_3, and 2-6% water-soluble alkalis. (Bradlo et al, 2015, Meawad et al., 2010)

Most of the coal fly ash is typically used in brick production, cement and concrete production, lightweight aggregate production, road construction and geotechnics, gas concrete production, ceramic and glass production, casting sand, wall mortars, cleaning metal surfaces by spraying, as an anti-slip agent on asphalt road surfaces, drilling of oil wells, production of synthetic zeolites, recovery of metals such as Al, Ti, Ni, Au, etc. (JHA et al, 2008, Sahoo et al., 2016)

In recent studies on fly ash, main elements (Al, Si, Fe, and Ti), trace elements (V, Ga, Ge, Se, Li, Mo, U, Au, Ag, Pt group, and rare earth metals), and magnetic materials, cenospheres, and unburned carbon have been focused on. Research has particularly concentrated on recovery efficiency, issues in metal extraction, selective recovery, and purification. The recovery of Al and Ti, which are among the main metals from fly ash, is performed using acidic leaching (HCl, H_2SO_4, HNO_3, HF, etc.), basic leaching (NaOH), and pyrometallurgical methods. After hydrometallurgical methods, techniques such as precipitation, solvent extraction, re-crystallization, and electrolysis are employed (Meawad et al., 2010).

In the recent years, new and innovative green technology is emerging called bioleaching or biological leaching (Pangayao et al., 2015).

In this research, hydrometallurgical processes were applied in order to recover the metallic values (Co, Mo, Fe, V, Ni). In the leaching experiments, effects of type and concentration of leaching agent (H2SO4, HCl, HNO3, and NaOH), temperature, solid/liquid ratio, and duration on metal (V, Co, Ni, Mo, Fe) leaching efficiencies were investigated.

2. Material and methods

2.1. Material

The aim of this project is to recover the metallic values in the composition of fly ash obtained as a by-product from the Şırnak Thermal Power Plant (Turkey). The laboratory studies include (a) sample preparation and material characterization, (b) physical enrichment studies for preliminary enrichment, (c) leaching experiments for the recovery of metallic values.

The chemical composition of the sample used in the experiments were 3.33% Fe, 0.23% Mo, 0.38% V, 0.30% Ni, 0.002% Co, 0.72% C, and 6.65% S. The result of sieve analysis of the fly ash sample are given in Table 1. The fly ash sample, which is actually very fine particles under normal conditions, was distributed as coarse particle sizes due to agglomeration of very fine particles. When the distribution of metallic values by size range was examined as a result of dispersion with a scrubber and subsequent classification by size, it was observed that the metals were highly enriched in the size range of -38 microns. According to the mineralogical analysis performed with XRD, nearly 85 % of the sample consists of silicates, and the metals in the fly ash were oxidized form due to heat treatment.

Table 1. The results of sieve analysis I

Particle Size Range (mm)	Weight (%)	Total Oversize Weight (%)	Total Undersize Weight (%)
+3.36	12.8	12.8	100.0
-3.36+2	8.6	21.4	87.2
-2+1.41	6.7	28.1	78.6
-1.41+0.5	10.8	38.8	71.9
-0.5+0.125	8.9	47.7	61.2
-0.125	52.3	100.0	52.3
Total	100.0		

2.2. Method

The physical enrichment methods (particle size distribution and classification, and gravity separation) were employed in preliminary enrichment studies. However, notable efficiencies in selective separation were not achieved in the experiments. In leaching experiments, the effects of type and concentration of leaching agency (H_2SO_4, HCl, HNO_3, and NaOH), dissolution time, temperature, and solid/liquid ratio on the dissolution efficiencies of metals (V, Co, Ni, Mo, Fe) were investigated. According to the results obtained under optimal conditions, the iron precipitation experiment conducted at pH 4-4.5 by using NaOH. Metal analyses were performed using an Atomic Absorption Spectrophotometer (AAS) from the solution.

2.2.1. Effect of Type of Leaching Agent

Experiments were conducted using H_2SO4, HCl, and HNO_3 acids at concentrations of 100, 200, 300, and 400 g/L, and NaOH at concentrations of 100 and 400 g/L. The constant parameters for the experiments are given in Table

2. The results of the experiments conducted with each acid are presented graphically for H_2SO_4, HCl, and HNO_3 in Figure 1.

Table 2. Constant Experimental Parameters of the Leaching Experiments

S/L ratio	1/10
Leaching Agent Concentration(g/L)	300
Temperature (°C)	60
Leaching time (min.)	60

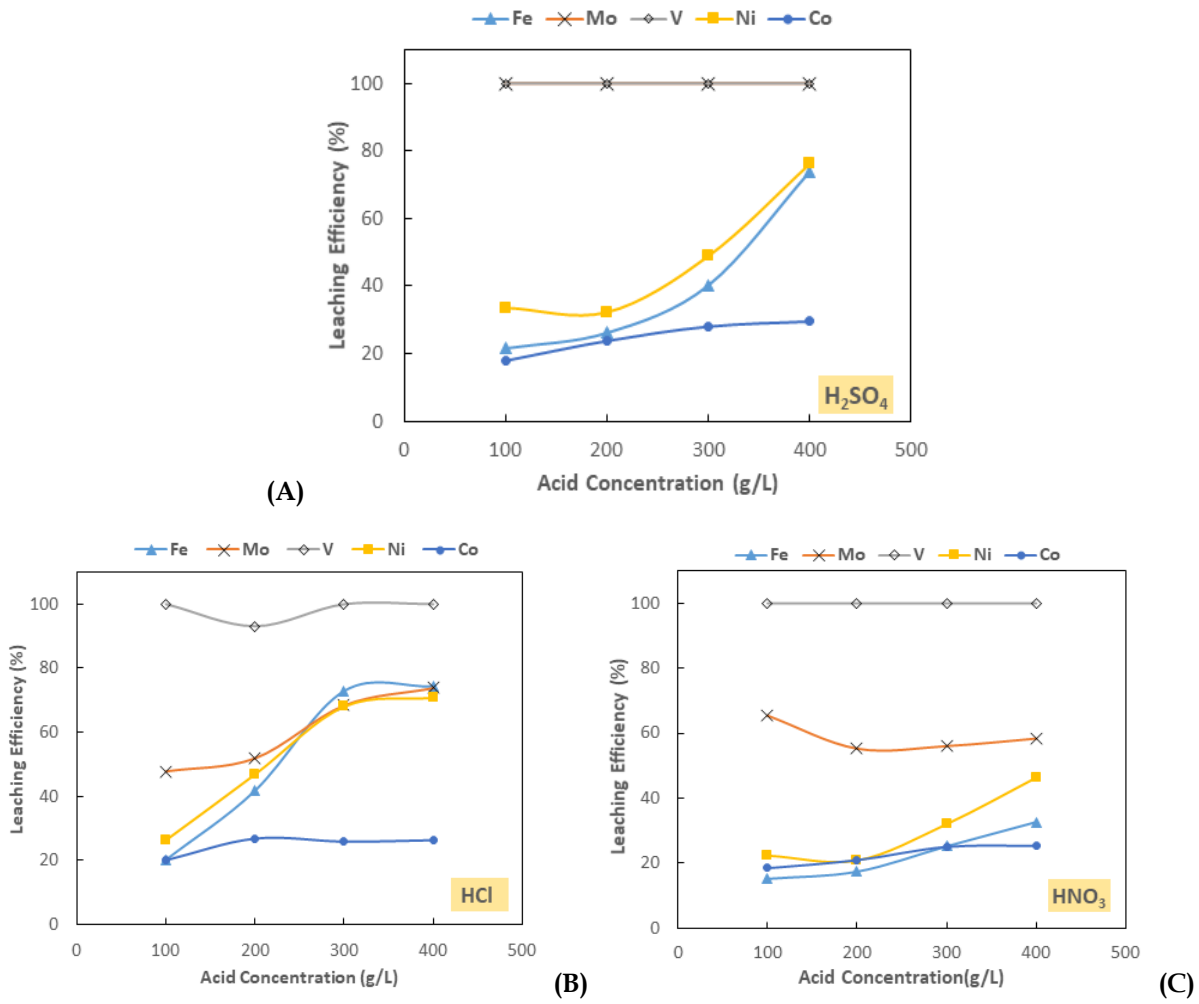


Fig. 1. Effect of acid concentration on metal dissolution efficiencies (a) H_2SO_4, (b) HCl, (c)HNO_3 .

As a result of the acid leaching experiments with different acids to examine the effect of leaching agent type, the highest dissolution efficiencies were obtained in the experiments conducted with H_2SO_4. Therefore, this acid was used in subsequent experiments. The highest dissolution efficiencies were achieved at an acid concentration of 400 g/L. HCl and HNO_3 are expensive agents in terms price of acid and large evaporative losses make these processes largely uneconomic. The processes also constitute an environmental hazard. In the experiments conducted with NaOH, lower yields were obtained compared to the acids. A slight increase in yields was observed with the increase in NaOH concentration.

2.2.2. Effect of Dissolution Time

The experiments investigating the effect of dissolution time were conducted at a concentration of 400 g/L H_2SO_4, at a temperature of 60°C, and a solid/liquid ratio of 1/10 for durations of 60, 120, and 180 minutes. The results obtained from these experiments are presented in Figure 2.

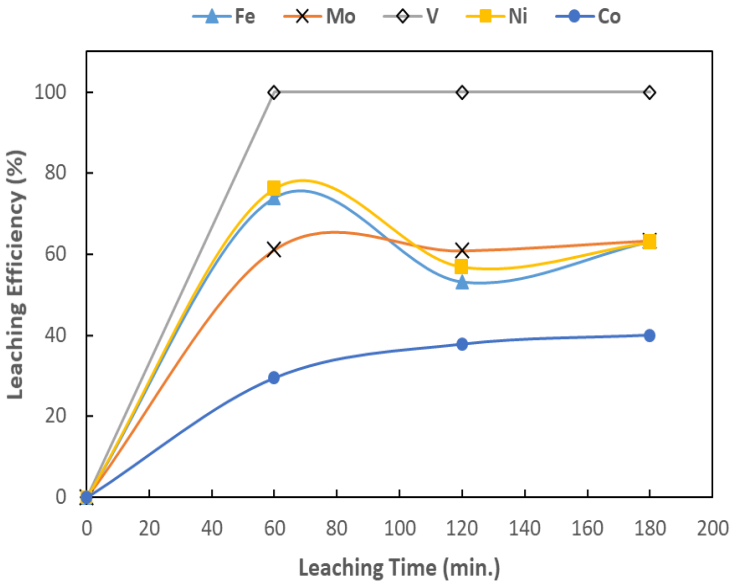


Fig. 2. Effect of dissolution time on metal dissolution efficiencies at 400 g/L H_2SO_4, at a temperature of 60°C

According to the results, an increase in dissolution time leads to an increase in the dissolution efficiencies of the metals. For metals like Ni and Fe, fluctuations in efficiency were observed beyond 60 minutes of dissolution. Therefore, since a 60-minute dissolution time was found to be sufficient for all metals, this duration was used as a basis for subsequent experiments.

2.2.3. Effect of Dissolution Temperature

The experiments were carried out at temperatures of 40, 60 and 80°C, taking the H_2SO_4 concentration as 400 g/L, the dissolution time as 60 minutes, and the Solid/Liquid ratio as 1/10. In order to examine the effect of dissolution temperature, the results are given in Figure 3. An increase in metal dissolution efficiency was observed due to the increase in temperature, and the optimum dissolution temperature was taken as 80°C.

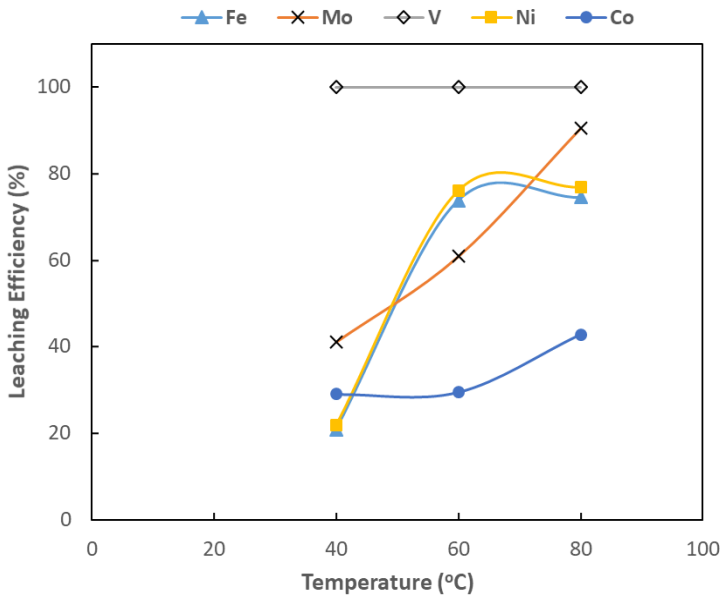


Fig.3. Effect of dissolution temperature on metal dissolution efficiencies

2.2.4. Effect of Solid/Liquid Ratio

In the experiments examining the effect of the Solid/Liquid ratio, experiments were carried out at 1/3, 1/5 and 1/10 Solid/Liquid ratios under constant conditions which were H_2SO_4 concentration of 400 g/L, leaching time of 60 minutes, and dissolution temperature of 80°C. Experimental results are given in Figure 4.

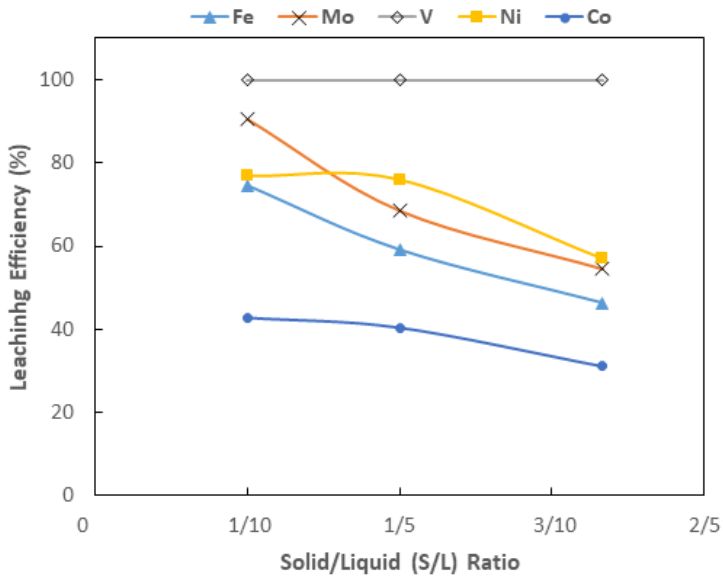


Fig. 4. Effect of Solid/Liquid ratio on metal dissolution efficiencies

In experiments examining the solid/liquid ratio change, it is seen that dissolution efficiency decreases as the S/L ratio value goes from 1/10 to 1/3. Accordingly, it can be seen that the S/L ratio value where the best dissolution efficiency obtained is 1/10. As a result of the leaching experiments, the following optimum experimental conditions were determined:

Acid Type : H_2SO_4

Acid Concentration : 400 g/L
Dissolution Temperature : 80°C
Dissolution Time : 60 min
Solid/Liquid (S/L) ratio : 1/10

Another experiment was carried out under the optimal conditions and the amount of acid consumption was determined. According to the results of chemical analysis, the dissolution efficiencies of Fe, Mo, V, Ni and Co were 74.6%, 90.5%, 100%, 76.9% and 42.8%, respectively. The acid consumption was calculated approximately 3700 kg/ton fly ash.

3. Conclusions

The chemical composition of the sample used for the experiments was found to be 3.33% Fe, 0.23% Mo, 0.38% V, 0.30% Ni, 0.002% Co, 0.72% C, and 6.65% S. As a result of sieve analysis, it was observed that the metals largely accumulated in the -38 micron size range.

In preliminary enrichment studies, no significant selective separation was achieved by using physical beneficiation methods (dispersion, classification by size, and gravity separation) and therefore direct leaching experiments with fly ash were conducted.

In the leaching experiments, the effects of type (H_2SO_4, HCl, HNO_3, and NaOH) and concentration of leaching agent, leaching time, temperature, and solid/liquid ratio on the dissolution efficiencies of metals (V, Co, Ni, Mo, Fe) were investigated. The following optimal leaching conditions were found: acid concentration:400 g/L H_2SO_4, leaching temperature: 80°C, leaching time: 60 minutes, S/L ratio: 1/10. At these optimal conditions, the dissolution efficiencies for Fe, Mo, V, Ni, and Co were found to be 74.6%, 90.5%, 100%, 76.9%, and 42.8%, respectively, with the acid consumption of approximately 3700 kg/ton fly ash.

Fe is an undesirable metal in the recovery of non-ferrous metals from solution and can be removed by precipitation. Then, it would be more appropriate to selectively recover the metals from the solution by solvent extraction (SX) or ion exchange (IX) methods with appropriate reagents/organics and then precipitate the Fe ions. After SX/IX, metals can be recovered in the form of metals or compounds by precipitating from concentrated solutions using appropriate methods.

Fly ashes generally contain 20-40% Al_2O_3 that we did not consider in this study. In most studies, Al recovery is taken into account as the main element, while other elements are evaluated in trace amounts and recovered as by-products. Aluminum can also be taken into solution hydrometallurgically by acidic or basic dissolution. In the following studies, Al and other metals that also go into solution need to be investigated. A conceptual flowsheet evaluated as a result of this study is given in Figure 5.

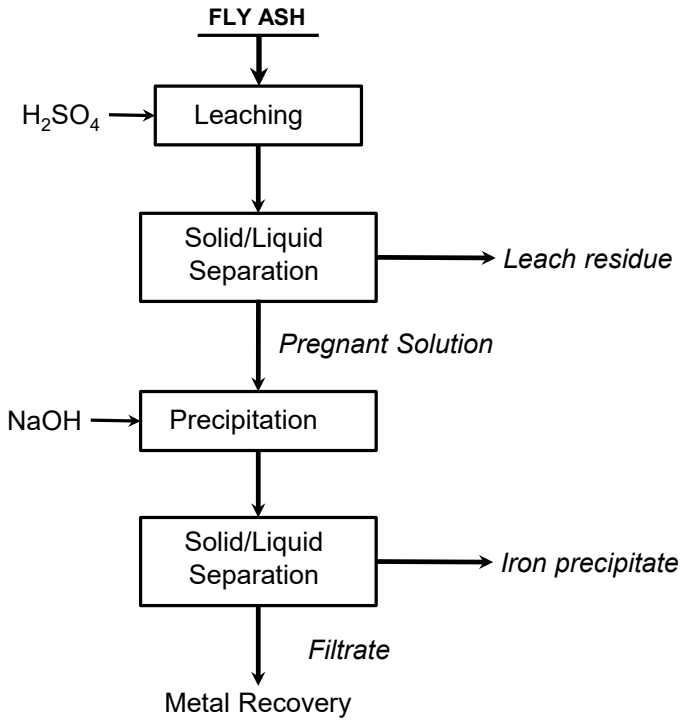


Fig.5. The General Flowsheet of produced as a result of this study.

References

Bradlo, D., Zukowski, W., Czuprynski, P., Witkowski, K., (2015). Potential of metal recovery from coal combustion products. Part II. Leaching of selected elements. *Inzynieria Mineralna*. 16. 163-170.

Jha, V. K., Matsuda, M., Miyake , M., (2008) , Resource recovery from coal fly ash waste: an overview study, , *Journal of the Ceramic Society of Japan*, 116[2],167-175.;

Meawad, A.S., Bojinova, D.Y., Pelovski, Y.G.,(2010), An overview of metals recovery from thermal power plant solid wastes, *Waste Management,*Volume 30, Issue 12, Pages 2548-2559, ISSN 0956-053X,

Pangayao, D. C., van Hullebusch, E. D., Gallardo, S. M., Bacani, F. T., (2015) Bioleaching of trace metals from coal ash using mixed culture of Acidithiobacillus albertensis and Acidithiobacillus thiooxidans, *Journal of Engineering Science and Technology,* Special Issue on SOMCHE 2014 & RSCE 2014 Conference, 36–45,

Sahoo, P.K., Kim, K., Powell, M.A. et al., (2016). Recovery of metals and other beneficial products from coal fly ash: a sustainable approach for fly ash management. *Int J Coal Sci Technol* 3, 267–283.

Effective Removal of Boron and Arsenic from Industrial Wastewater Using Coagulation and Electrocoagulation Methods

Buğra ÖZDEMİR [1]*, Tolga GÜLSEVER [1]

[1]ASOS Proses Makina San. Ve Tic A.Ş.

*bugra@asos.com.tr (Buğra ÖZDEMİR)

Abstract:

Heavy metals resulting from industrial processes contaminate soil, water, and the atmosphere, affecting living organisms and causing environmental pollution. Although boron is not classified as a heavy metal, it is recognized as an essential nutrient for plants. However, excessive amounts of boron are toxic to both plants and human health. Since boron and heavy metal ions in wastewater are not biologically degradable, they accumulate in organisms and enter food chains, necessitating treatment processes to meet standard regulations. Among the most common methods for this purpose are chemical coagulation and precipitation, as well as electrochemical coagulation.

In this study, the aim was to remove boron and heavy metal content from a high-boron-containing (4000 ppm) solution in wastewater from a boric acid production facility using chemical coagulation and electrocoagulation methods. The sulfate content in the wastewater is 4500-5000 ppm. The research focused on parameters such as pH, current density, type of plates, chemicals used, and time. A total of 8 different chemicals were used during the experiments.

After a total of 12 experiments, the maximum boron removal achieved was 90%. Under optimal operating conditions, boron removal was observed to be 82%. Arsenic removal was observed to be 100% as a result of the study. Other heavy metals in the wastewater were reduced to trace amounts after treatment. The water treated for boron and heavy metal content via chemical coagulation was rendered suitable for further advanced treatment processes (ultrafiltration, reverse osmosis)

Keywords: Boron, Wastewater Treatment, Coagulation, Electrocoagulation

1. Introduction

Turkey, holding 72% of the world's boron reserves, is the largest producer and supplier of this strategic resource. These reserves in Turkey primarily consist of valuable minerals such as colemanite ($2CaO.3B_2O_3.5H_2O$), tincal ($Na_2O.2B_2O_3.10H_2O$) and ulexite ($Na_2O.2CaO.5B_2O_3.16H_2O$) concentrated in specific regions like Balıkesir-Bigadiç, Kütahya-Emet, Bursa-Kestelek, and Eskişehir-Kırka. Globally, around 230 different boron compounds exist, playing a critical role in various industries such as nuclear energy, glass, detergents, pharmaceuticals, fertilizers, and paints. In addition to boron's wide range of applications, its environmental and health risks are of great importance. While boron acts as an essential micronutrient for plants at low concentrations, it can cause toxic effects if found in irrigation or drinking water at high concentrations. In boron-rich soils, like those in Turkey, when irrigation is done with boron-containing water, the element accumulates quickly, reaching toxic levels. This situation poses significant threats to environmental and human health due to complexes formed by boron compounds combining with heavy metals in the soil. (Selimoğlu ve Boncukoğlu, R. (2019))

The World Health Organization (WHO) considers a daily intake of 1-13 mg of boron for an adult to be safe. However, excessive boron intake can lead to health problems such as headaches, vomiting, diarrhea, nervous system disorders, and more severe neurological issues in children. While the WHO sets an upper limit of 0.3 mg/L for boron concentration in drinking water, the European Union (EU) has established this limit at 1 mg/L. In many water sources in Turkey, boron levels exceeding these limits have been detected, making the effective removal of boron from water a crucial necessity. Removing boron from water is essential to minimizing environmental impacts and protecting water resources. (Yilmaz ve diğerleri (2005))

Conventional biological treatment methods are generally insufficient for removing boron from water, which has led to the development of advanced treatment techniques such as chemical precipitation, adsorption, ion exchange, reverse osmosis, and electrocoagulation. This study focuses on chemical coagulation and electrocoagulation methods, using calcium hydroxide ($Ca(OH)_2$), sodium hydroxide (NaOH), ferric chloride ($FeCl_3$), polyaluminum chloride (PAC) to effectively remove boron from industrial wastewater. The ultimate goal of these efforts is to contribute to sustainable water management by minimizing the environmental impacts of boron while optimizing chemical and energy consumption. In this context, it is crucial for both the conservation of natural resources and the development of environmentally responsible industrial practices.

The wastewater studied, which contains a high concentration of boron, originates from boric acid production. Treatment of this waste is necessary to prevent environmental harm during its disposal. The efficiency of coagulation and filtration systems used in treatment depends significantly on the composition of the wastewater, the chemicals applied, and the specific requirements of the chosen methods. For efficient and regular operation of filters prior to advanced filtration, it is crucial to bring the wastewater composition to the required levels. Coagulation methods are particularly effective in meeting the necessary conditions for advanced filtration, offering high efficiency and low costs.

In the study, the removal of arsenic and heavy metals from the wastewater, in addition to boron, is also aimed. Although lime (calcium hydroxide) provides highly efficient results in raising the pH for removal efficiency, the high calcium content can become a concern. Therefore, experiments combining lime with other chemicals are considered more suitable for industrial applications to avoid excessive calcium levels while maintaining effective removal efficiency.

2. Material and Method

In the studies, wastewater from the processing of colemanite boron ore was used as the raw water. Despite variations in the wastewater content due to changes in ore processing and ore grade at industrial facilities, high efficiencies in boron removal were achieved. These variations did not hinder the effectiveness of the treatment processes, demonstrating the robustness of the methods used for boron removal.

2.1. Chemical Coagulation

In the chemical coagulation method, chemicals were used to adjust the pH, and floc formation was achieved with the precipitation of anionic polymer.

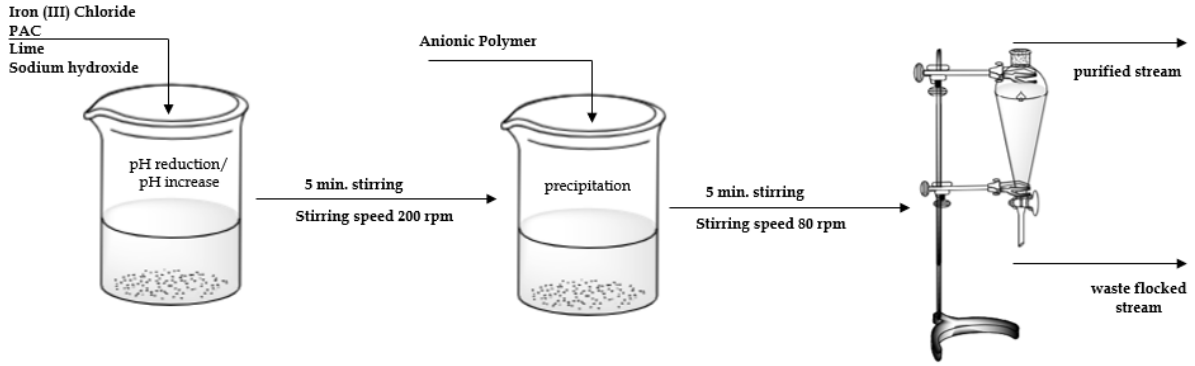


Fig. 1. Chemical Coagulation System

In the experiments, 1 kg of wastewater was placed in a beaker and mixed at 200 rpm while the necessary chemicals for pH adjustment were added. Sequentially, if a pH reduction process was needed according to the prescribed recipe, it was done first, and then the pH was raised. When the appropriate pH level was reached, the wastewater was subjected to a 5-minute mixing period. Afterward, polymer was added until settling occurred. After sufficient polymer addition, mixing was continued at a low rpm (80 rpm) for 5 minutes. After polymer addition, the wastewater in the beaker was transferred to a separating

funnel, and after 5 minutes of waiting, the settled portion was removed from the solution. The remaining solution was analyzed as treated water. As seen in the ICP analysis results, the desired removal efficiencies were achieved.

Table 1. Chemicals Used in Chemical Coagulation Experiments and the Resulting pH Levels

		pH Reduction		pH Increase				Flocculant
Experiment ID	Wastewater pH	Ferric Chloride $FeCl_3$	Polyaluminum Chloride PAC	Sodium Hydroxide NaOH	Calcium Hydroxide $Ca(OH)_2$	Calcium Oxide CaO	Sodium Carbonate $NaCO_2$	Anionic Polymer
R-1	6,75	-	3,99	9	-	-	-	+
R-2	6,75	-	4	7	8	-	-	+
R-3	7,01	-	3,99	7	9	-	-	+
R-4	6,75	-	4,01	7,01	9,02	-	10	+
R-5	6,75	3,99	-	7,04	10,01	-	-	+
R-6	6,87	-	-	-		12,51	-	+
R-7	6,87	-	-	-	12,51	-	-	+

Table 2. esults of Chemical Coagulation Analysis

Experiment ID	B_2O_3 (mg/l)	B (ppm)	Na (ppm)	Ca (ppm)	Mg (ppm)	Mn (ppm)	Fe (ppm)	SO_4 (ppm)	As (ppm)
Wastewater	12.130	3.767,57	283	744	695	4	0,005	3.793	4,22
R-1	5.810	1.804,58	8.727	397	793	0,3	0,005	2.731	<0,2
Removal Efficiency	52%	52%	-2.984%	47%	-14%	93%	0%	28%	100%
R-2	7.020	2.180,41	8.984	204	576	0,2	0,005	2.824	<0,2
Removal Efficiency	42%	42%	-3.075%	73%	17%	95%	0%	26%	100%
R-3	5.220	1.621,33	10.216	78	288	0,01	0,005	2.536	<0,2
Removal Efficiency	57%	57%	-3.510%	90%	59%	100%	0%	33%	100%
R-4	7.250	2.251,85	4.431	2.170	1.154	0,9	0,005	3.088	<0,2
Removal Efficiency	40%	40%	-1.466%	-192%	-66%	78%	0%	19%	100%
R-5	3.949	1.226,55	960	730	410	0,3	0,005	2.274	<0,2
Removal Efficiency	67%	67%	-239%	2%	41%	93%	0%	40%	100%
R-6	1.484	460,93	960	730	0,005	0,005	0,005	3.250	<0,2
Removal Efficiency	88%	88%	-239%	2%	100%	100%	0%	14%	100%
R-7	1.211	376,32	220	1.800	0,005	0,005	0,005	1.524	<0,2
Removal Efficiency	90%	90%	22%	-142%	100%	100%	0%	60%	100%

2.2. Electrocoagulation

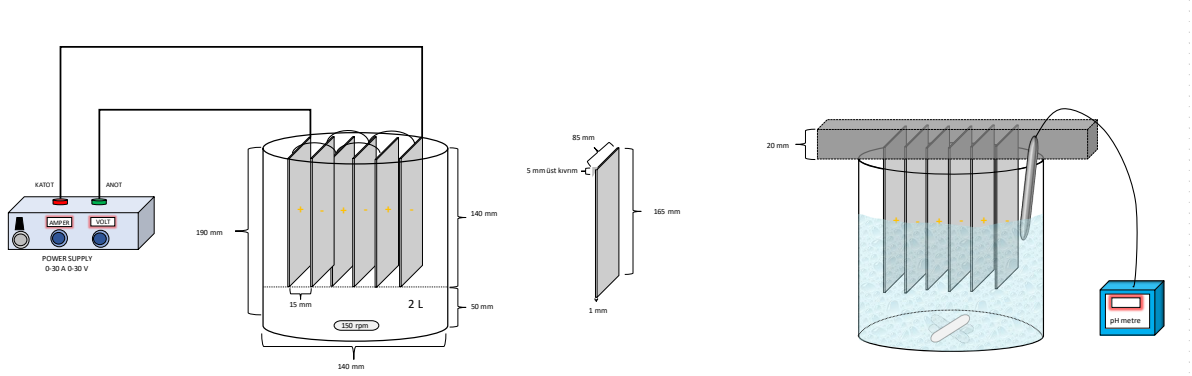


Fig. 2. Electrocoagulation System

In the electrocoagulation system, an adjustable 0-30 V DC power supply, a 2 L beaker, and 6 plates were used. The current to be supplied from the power source was determined according to the following formula:

$$j = I/A \quad (1)$$

j= Current Density mA/cm^2

I= Current mA

A= Effective Area cm^2

Effective Area: The total area of the anode plates in contact with the solution

In the experiments, conditioning was applied to the wastewater. The parameters tested include the conditioning chemical, plate type, residence time, and the amount of current supplied to the plates.

Two liters of wastewater in a beaker are mixed at 150 rpm while adjusting the pH to the specified level using the chosen chemicals. The selected plates are positioned inside the beaker with a fixed distance between them. The plates are connected in series to the power supply, and the required power is provided to achieve the specified current density. After the work is completed for a certain period, the current is cut off, and the system is allowed to rest for a short time. After settling, the upper layer of the solution is analyzed as treated water.

Tablo 3. Chemicals used in Electrocoagulation Experiment and Resulting pH Levels

Experiment ID	Type of Plate	Current (mA/cm^2)	pH	Residence Time (min)	pH Booster	Distance Between Plates (cm)	Stirrer RPM
R-8	Al	30	9	15	NaOH	1,5	150
R-9	Al	30	9	15	$Ca(OH)_2$	1,5	150
R-10	Fe	30	9	15	$Ca(OH)_2$	1,5	150
R-11	Fe	0,5	9	15	$Ca(OH)_2$	1,5	150
R-12	Al	30	9	30	NaOH	1,5	150

Tablo 4. Results of Electrocoagulation Analysis

Experiment ID	B_2O_3 (mg/l)	B (ppm)	Na (ppm)	Ca (ppm)	Mg (ppm)	Mn (ppm)	Fe (ppm)	SO_4 (ppm)	As (ppm)
Wastewater	15.990	4.965,58	295	869	944	0,005	0,005	4.678	4,5
R-8	11.270	3.499,82	4215	95	323	0,005	0,005	4.347	<0,2
Removal Efficiency	30%	30%	-1.329%	89%	66%	0%	0%	7%	100%
R-9	2.890	897,46	279	1.245	335	0,005	0,005	3.208	<0,2
Removal Efficiency	82%	82%	5%	-43%	65%	0%	0%	31%	100%
R-10	2.860	888,15	261	1.330	339	0,005	0,005	3.060	<0,2
Removal Efficiency	82%	82%	12%	-53%	64%	0%	0%	35%	100%
R-11	2.980	925,41	254	1.280	499	0,005	0,005	3.364	<0,2
Removal Efficiency	81%	81%	14%	-47%	47%	0%	0%	28%	100%
R-12	9.690	3.009,16	4.010	30	47	0,005	0,005	3.716	<0,2
Removal Efficiency	39%	39%	-1.259%	97%	95%	0%	0%	21%	100%

3. Results

Based on the results of the studies, when examining the effects of parameters, it was observed that in chemical coagulation, the removal efficiency increased as the pH value rose in the comparison between R-2 and R-3. In the comparison between R-1 and R-3, it was observed that the use of lime was more efficient than the use of caustic soda. In the R-7 study, it was observed that a removal efficiency of 90% was achieved with lime alone at a pH value of 12. In the R-8 and R-12 electrokoagulation studies, it was observed that an increase in residence time positively affected the efficiency.

In the electrocoagulation system, it was found that treatment was effective with lime conditioning. It was observed that efficiency was directly proportional to the current applied and the residence time.

The boron removal efficiency data from the studies can be seen in the graphs below.

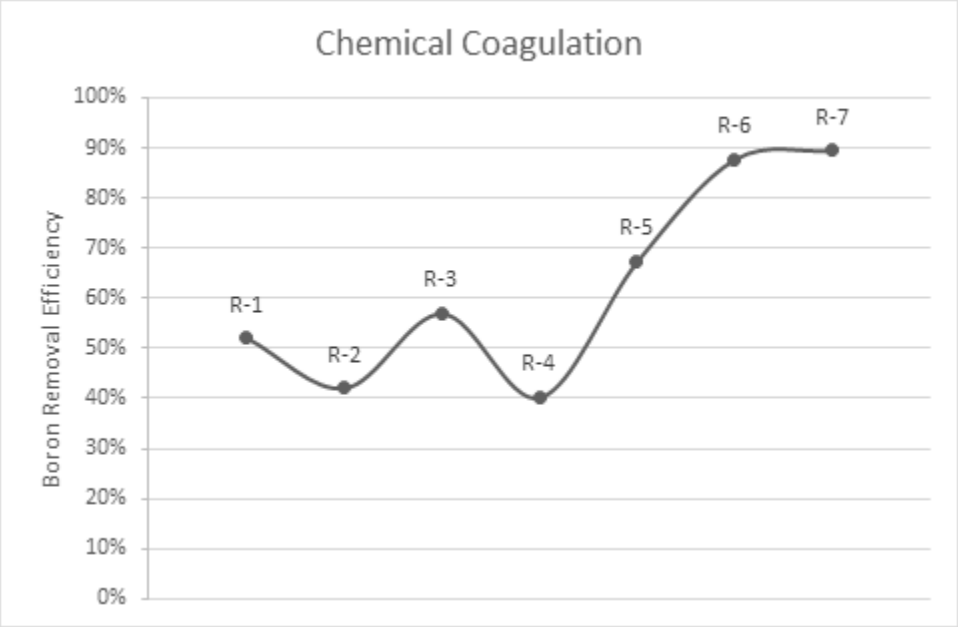


Fig. 2. Chemical Coagulation Boron Removal Efficiency

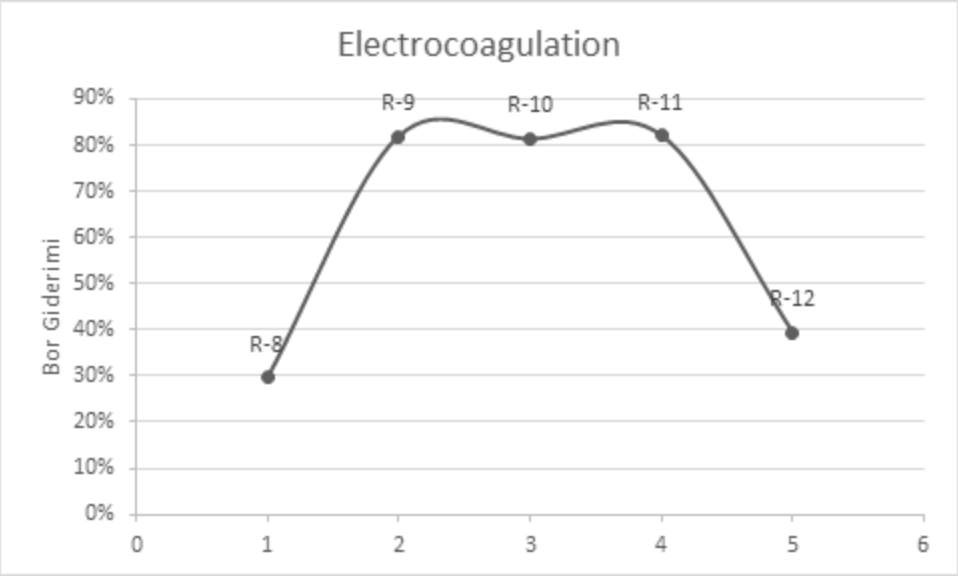


Fig. 3. Electrocoagulation boron removal efficiency

This study results, the effectiveness of chemical coagulation and electrocoagulation methods in removing boron and heavy metal pollution from wastewater derived from Turkey's rich boron reserves. The results demonstrate that these advanced treatment techniques achieve high efficiency in removing environmentally and health-risk elements such as boron and arsenic from water. Ensuring that water treated through chemical and electrocoagulation is suitable for further purification processes is a significant step towards sustainable water management. It plays a critical role in preserving Turkey's natural resources and developing environmentally friendly industrial practices. In this context, the study offers effective and practical solutions to minimize the negative impacts of industrial wastewater on the environment and human health.

Acknowledgements

We thank Asos Proses and our colleagues within the organization for their financial and moral support and contributions.

References

Khaoula, M., Wided B., Chiraz H., Béchir H. (2013). Boron Removal by Electrocoagulation. Journal of Water Resource and Protection, 2013, 5, 867-875 ,10.4236/jwarp.2013.59088

Qian Jianga, J., Grahama, N., Andrea, C., Kelsallc, G., Brandon, N. (2002). Laboratory study of electro-coagulation–flotation for water treatmentx**.** *Water Research 36 (2002) 4064–4078*

Selimoğlu, V., Boncukoğlu, R. (2019). Removal Of Boron From Boron Solutions By Chemical Precipitation. *Journal of the Institute of Science and Technology, 9(3): 1343-1350,* 1344**.** DOI: 10.21597/jist.515526

Yilmaz , E., Boncukcuoglu, R., Kocakerim, M., Keskinler, B. (2005). The investigation of parameters affecting boron removal by electrocoagulation method. *Journal of Hazardous Materials B125 (2005) 160–165*

Zeboudji , B., Drouiche, N., Lounici, H., Mameri, N & Ghaffour, N. (2013). The Influence of Parameters Affecting Boron Removal by Electrocoagulation Process. *Separation Science and Technology, 48:8, 1280-1288*, DOI: 10.1080/01496395.2012.731125

Techno-Economic and Environmental Assessments for Hydrometallurgical Treatment of Waste Lithium-Ion Batteries (LIBs): The ELiMINATE Project

E. Y. Yazici [1]*, H. Deveci [1], O. Celep [1], F. Ahlatci [1], E. Esen [1], C. Dorfling [2], R.F. van Schalkwyk [2], G. Akdogan [2], L. Louw [3], R. F. Maritz [2], M. W. J. Kuhn [3], D. T. Vooght [2], E. Emilsson [4], A. Wu [4], N. Elginoz [4], J. Ots [4], A. N. Ozturk [4], M. Petranikova [5], E. Cuhadar [6], C. Eyupoglu [6], E. Eken Torunoglu [6]

[1]Hydromet B&PM Research Group, Division of Mineral & Coal Processing, Department of Mining Engineering, Karadeniz Technical University (KTU), 61080, Trabzon, Türkiye

[2]Department of Chemical Engineering, Stellenbosch University (SUN), Stellenbosch, South Africa

[3]Department of Industrial Engineering, Stellenbosch University (SUN), Stellenbosch, South Africa

[4]IVL Swedish Environmental Research Institute, Sweden

[5]Department of Chemistry and Chemical Engineering, Chalmers University of Technology (CUT), Gothenburg, Sweden

[6]EXITCOM Recycling, Kocaeli, Türkiye

*Corresponding author: eyazici@ktu.edu.tr (Ersin Yener Yazici)

Abstract:

The generation of end-of-life (EoL) lithium-ion battery (LIBs) waste is increasing rapidly due to the growing demand for consumer electronics and electric vehicles (EVs), in particular. Recovering the critical and strategic metals through hydrometallurgical treatment of LIBs offers several benefits over pyrometallurgical treatment. ELiMINATE is a multi-disciplinary project aimed at evaluating various hydrometallurgical process alternatives for the recovery of metals from the "black mass". The project also focused on integrating these processes into the value chain, identifying the environmental impacts and material flows. The work plan involved data collection and mapping of EU LIB recyclers, as well as life cycle assessment of hydrometallurgical processes using mineral acids (HCl, H_2SO_4) and organic acids to determine the environmental impact of different cathode active materials. Material mapping and logistic network modelling for the recycling of EoL LIBs were developed for the South African and European contexts, which were used to determine optimal locations for collection centres and processing plants. Experimental studies were carried out to develop novel recycling processes for EoL LIBs. Inorganic and organic acid solutions were used to leach metals in the presence of various reducing agents. Downstream processes were also developed to selectively recover metals from the pregnant leach solutions in the form of different salts/compounds. Pilot scale tests for the developed process schemes were also performed at EXITCOM Recycling facilities. Findings have demonstrated that efficient leaching of metals can be achieved under suitable conditions, and pregnant leach solutions can be treated using appropriate methods to recover metals selectively.

Keywords: *Lithium-ion battery (LIB), Life Cycle Assessment (LCA), Material Flow Analysis (MFA), Hydrometallurgy, Recycling*

1. Introduction

In recent years, the push for a green transition has intensified, leading to an increase in the use of renewable energy technologies, which is expected to play a key role in reducing the dependency on oil (European Commission, 2019). A major development in this context has been the rise in the production of electric vehicles (EVs), which offer a sustainable alternative to conventional vehicles powered by internal combustion engines (ICE) (IEA, 2021). The shift towards EVs reflects broader efforts to decarbonise the transportation sector and meet global climate targets. The critical part of the EVs is lithium-ion batteries (LIBs), which allow energy storage by electrochemical reactions between cathode

and anode. LIBs have already been commonly used in portable electronic devices, including cell phones, laptops, etc. However, the increasing demand for EVs is driving a significant rise in the production of LIBs. This surge in production brings challenges related to the disposal and recycling of these batteries at the end of their life cycle.

Critical/strategic raw materials (CRM/SRM) play a crucial role in the green transition due to their essential use in the production of green technologies, including LIBs in EVs (European Commission, 2023; IRENA, 2023). Considering the high CRM/SRM content in LIBs (e.g., lithium, cobalt, etc.) and the potential environmental impact in the case of their disposal, recycling end-of-life (EoL) LIBs is crucial from the circular economy and environmental perspectives (Baum et al., 2022; Celep et al., 2023).

Developing environmentally friendly, technically and economically viable recycling processes for EoL LIBs is essential for reducing environmental concerns, conserving natural resources and lowering the dependency on CRM and SRM. Among various extractive metallurgical methods, hydrometallurgical processes have several advantages, including relatively low to medium costs and high operational flexibility. Although several hydrometallurgical processes have been proposed to recover metals from EoL LIBs, techno-economic viability of these processes, their potential environmental impact and the scale-up issues remain significant barriers to widespread implementation (Celep et al., 2023; Jung et al., 2021; Musariri et al., 2019; Neumann et al., 2022; Pinegar and Smith, 2019; Rouquette et al., 2023). Addressing these challenges through innovative solutions with a low environmental footprint is essential for improving the LIB recycling industry and achieving a circular economy. Therefore, there is still a need for R&D&I projects to develop environmentally acceptable processes with high technical performance and low cost.

In this context, the ELiMINATE project (End-of-life Li-ion battery management integration and technology evaluation) aims to deliver an implementation framework for establishing recycling facilities for the recovery of metals from end-of-life lithium-ion batteries (van Schalkwyk et al., 2023; Wu, 2022; Yazici et al., 2023). The project is supported under ERA-MIN 2 Call and coordinated by Stellenbosch University (SUN; South Africa) with consortium partners from Sweden (IVL Swedish Environmental Institute and Chalmers University of Technology (CUT)) and Türkiye (Karadeniz Technical University (KTU) and EXITCOM Recycling as the SME partner). The ELiMINATE project covers (i) the comparison of alternative hydrometallurgical process routes from a technical and environmental impact perspective for the recovery of metals from waste batteries, (ii) market analyses & business development to understand value chain integration for processes within a European context and South African context, (iii) performing material flow analyses and reverse logistics optimization to improve resource efficiency of the recycling industry within European and South African contexts and (iv) development of novel alternative hydrometallurgical processes at laboratory scale and their demonstration at pilot scale. This study presents the key findings of the research conducted throughout the project.

2. Material and methods

The project's work plan was implemented within six work packages. IVL & CUT, and SUN conducted studies to understand how the market is structured and likely to develop in European and South African contexts. The business case development followed a needs-approach-benefit-competition framework, evaluating (1) a mineral acid-based process, (2) an organic acid-based process and (3) a thermal pre-treatment process, all with an emphasis on value creation. Using the literature data, nine flow sheets were established and modelled based on the use of three lixiviants (i.e., HCl, H_2SO_4 and citric acid) chosen for three different downstream treatments i.e., sequential precipitation, direct production of mixed NMC, and sequential precipitation with solvent extraction (SX). A tenth flowsheet, which involves H_2SO_4-based leaching of black mass (NMC) with thermal pretreatment, was also evaluated. The black mass feedstock was assumed to be a mixture of LIB types, including NMC, LCO and LFP.

Life cycle assessment (LCA) studies were carried out for the selected flow sheets, incorporating multivariate uncertainty analyses and weak point analyses to identify preferred processes and alternative processing technologies. Screening LCAs was performed to evaluate and determine the best process options among the various flowsheets. A full LCA was carried out for the selected processes in

European and South African contexts to pinpoint critical process units for development and assess compliance with environmental policies.

Novel hydrometallurgical processes were developed and tested by KTU at a laboratory scale using the black mass sample (~120 kg) obtained from various brands of cell phones at EXITCOM Recycling facilities (Fig. 1). The black mass sample was produced through a pre-treatment step involving size reduction, screening to remove impurities, and the elimination of electrolyte. The chemical analysis of the black mass sample revealed that it contained 3.25 % Li, 23.6 % Co, 2.06 Ni, 8.36 Mn, 1.78 % Al, 0.92 % Cu, and 0.28 % Fe. The novel hydrometallurgical processes employed either mineral acid (i.e., sulphuric acid (H_2SO_4)) or organic acid leaching in the presence of hydrogen peroxide (H_2O_2) or sodium metabisulphite ($Na_2S_2O_5$) as reducing agents. This was followed by metal recovery from PLSs using the solvent displacement crystallisation (SDC) method. Pilot scale tests of these novel processes were conducted at EXITCOM Recycling facilities.



(a) (b) (c)

Fig. 1. The black mass produced by EXITCOM Recycling from EoL LIBs and used by KTU for hydrometallurgical test work (a); photos from the pilot plant (b, c) of EXITCOM

3. Results and Discussion

3.1. Value chain integration

Market analyses were conducted to assess the recycling industry in South Africa (SA) and the European Union (EU) to establish a business case strategy for best positioning a LIB recycling process. Strategies were also developed to integrate recycling companies into the existing value chain. The market analysis in South Africa (2022-2030) revealed that the source of waste LIB will come mainly from laptops and mobile phones to a lesser extent, while the contribution of EVs will be limited. This suggests that the battery type of LIB will be LCO, which has a high cobalt content. Currently, there are no LIB recycling plants in South Africa. Future estimations showed that the recovery rate of the waste LIB should be at least 37% for the economically viable treatment of a single recycling facility.

In Europe, assessments showed that the current and future state of the battery recycling market in terms of EoL LIBs generation, pre-processing and material processing capacity is increasing. European policies support this increasing trend by securing the supply of critical raw materials in Europe. The increased EoL EVs will also drive growth. Nickel-based cathode chemistries for EVs are expected to increase. The prime locations for establishing recycling centres were either Nordic countries or Germany. The ideal number of facilities to construct varies between one and four, depending on the chosen technology and the associated transportation costs. The comparison of battery markets in Europe and South Africa is shown in Table 1. For the South African context, among nine hydrometallurgical processes, H_2SO_4-H_2O_2 leaching followed by the precipitation of a nickel-cobalt-manganese-hydroxide (NMC) mixture was determined to be the best process option in terms of economics and environmental footprint. The NMC and lithium carbonate produced in the process can be used in precursor cathode active material (pCAM) production. The process was found to have the lowest environmental impact (as quantified via LCA) and the most straightforward implementation regarding plant operability (Kuhn, 2023; Ozturk, 2024). The economic feasibility and business development of two novel hydrometallurgical LIB recycling processes for cathodes (developed and tested at pilot plant scale as part of the ELiMINATE project) were evaluated. Three different business model scenarios were created

in the European context, and a techno-economic assessment was conducted for each of the novel process technologies. Different business model scenarios significantly impacted the profitability of the two novel recycling processes. The most profitable scenario for both technologies was when battery manufacturers had an in-house recycling facility and offered a buy-back option for their batteries.

Table 1. Comparison of battery markets in Europe and South Africa

	Europe	South Africa
Battery recycling market	Pre-processors and material recovery recyclers	No recyclers on the market (yet?)
Future applications (+10 years)	Electric vehicles	Portable devices
Dominant chemistries	Nickel-based	LCO-based
Battery regulation	EU Battery Regulation: to set targets for material recovery and min. recycled content in new batteries	Extended producer responsibility (since May 2021), ban on battery waste landfilling (from Aug 2021)

3.2. Process modelling and life cycle assessment (LCA) of hydrometallurgical processes

Simplified process flow diagrams were established, and modelling studies were performed using modelling/simulation software (Fig. 2). The results showed that the processes with an SX stage were generally the worst from an environmental impact viewpoint, considering the lowest endpoint values (Mariz et al., 2022; Maritz, 2024) (Table 2). Thermal pretreatment was also found to increase the environmental impact of the process. Depending on the screening LCA results, full LCAs were carried out for selected four flowsheets (i.e., H_2SO_4 – mixed NMC precipitation, HCl – mixed NMC precipitation, citric acid – mixed NMC precipitation and H_2SO_4 sequential precipitation) and novel hydrometallurgical processes developed by KTU. The findings of the full LCA studies showed that the H_2SO_4 – mixed NMC process has a slightly lower environmental impact than the novel technologies that were experimentally developed in the project in each EU and SA context (Ozturk, 2023). In addition, the H_2SO_4-based novel process was more economical (i.e., lower OPEX) than the organic acid-based novel process due to the lower costs of chemicals and waste treatment operations (Ozturk, 2023). LCAs were evaluated for the following impact categories of abiotic depletion (ADP elements), acidification potential (AP), eutrophication potential (EP), global warming potential excluding biogenic carbon (GWP), and ozone layer depletion potential (ODP) covered by Centrum voor Milieuwetenschappen (CML) 2001 methodology. Geographically, the EU showcased better environmental performance than SA because electricity is the primary source of adverse impact in South Africa (Maritz, 2024).

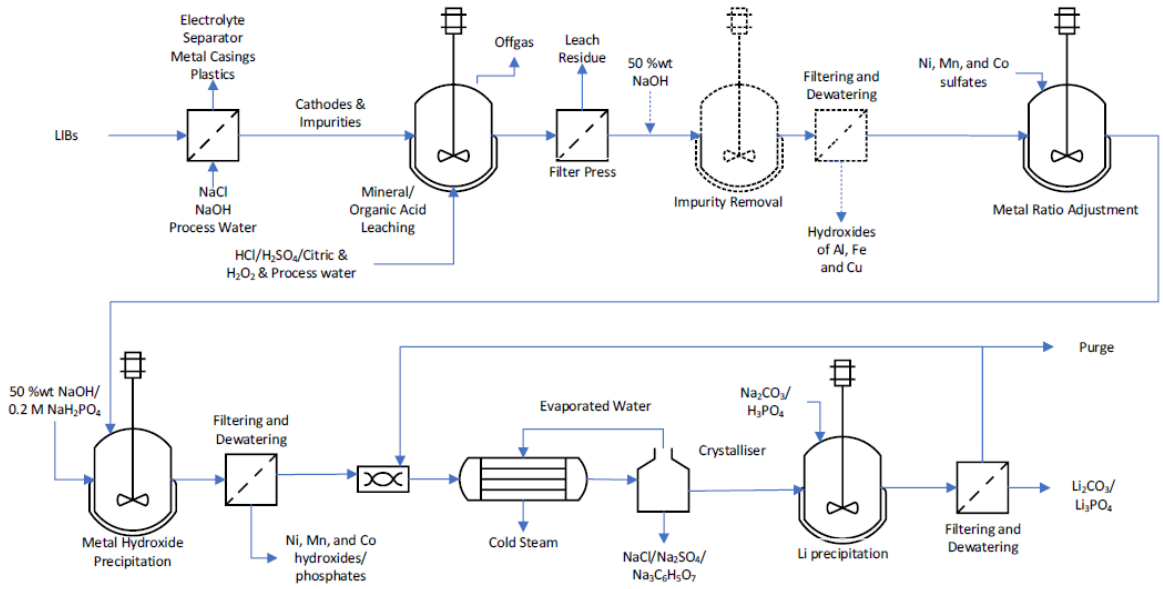


Fig. 2. Simplified process flow diagram for the recycling of waste LIBs using mixed NMC precipitation (Maritz, 2024)

Table 2. Endpoint values for the nine hydrometallurgical flowsheet options considered (Maritz, 2024)

Process Type	Endpoint Value (Pt)	Standardised Value
Hydrochloric acid - NMC	-5.44E-09	169%
Hydrochloric acid - Sequential	-3.22E-09	100%
Hydrochloric acid - SX	-3.97E-09	123%
Sulphuric acid - NMC	-5.83E-09	181%
Sulphuric acid - Sequential	-5.01E-09	155%
Sulphuric acid - SX	-2.08E-09	64%
Citric acid - NMC	-3.88E-09	120%
Citric acid - Sequential	-3.35E-09	104%
Citric acid - SX	-1.47E-09	46%

3.3. Material flow analysis and reverse logistics network modelling & optimisation

Material flow analysis and reverse logistics network modelling and optimisation in the South African and European contexts were conducted by IVL & CUT and SUN (Figs. 3-5). To minimise economic burden, the best network setup was determined in the optimisation studies for a single- or multi-facility network by considering the pretreatment and one of the novel hydrometallurgical processes developed. The results demonstrated that the potential savings from optimising the number of facilities ranged from 1-41% to over 100% of the minimum value. A reverse logistics network model, including the locations and capacities of collection points, dismantling centres, and pre-treatment and processing options, was established for EoL LIB recycling (Figs. 4 and 5).

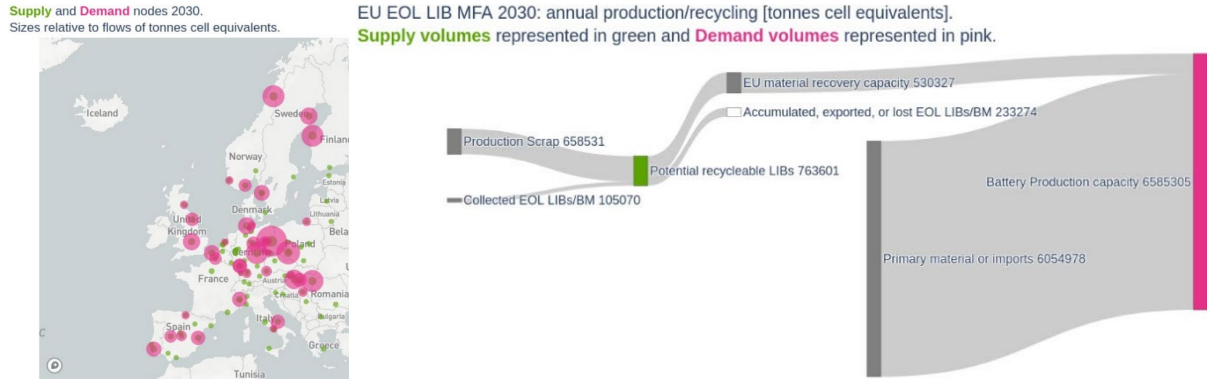


Fig. 3. The forecast (2030) capacities and demands in the LIB reverse supply chain within the EU in map (left) and Sankey chart (right) (Emillson and Ozturk, 2023)

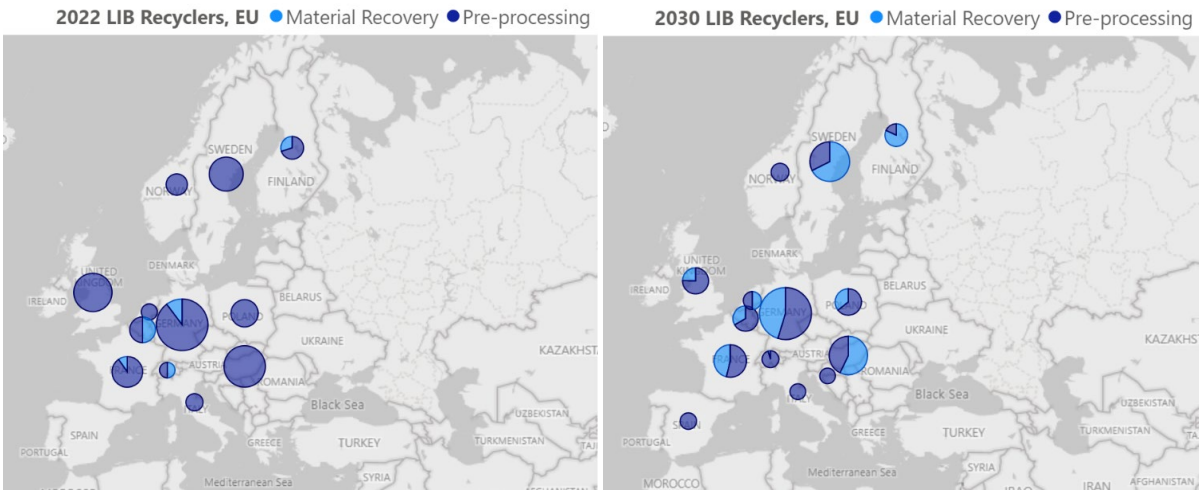


Fig. 4. Mapping of current and forecasted EoL LIB flows within EU

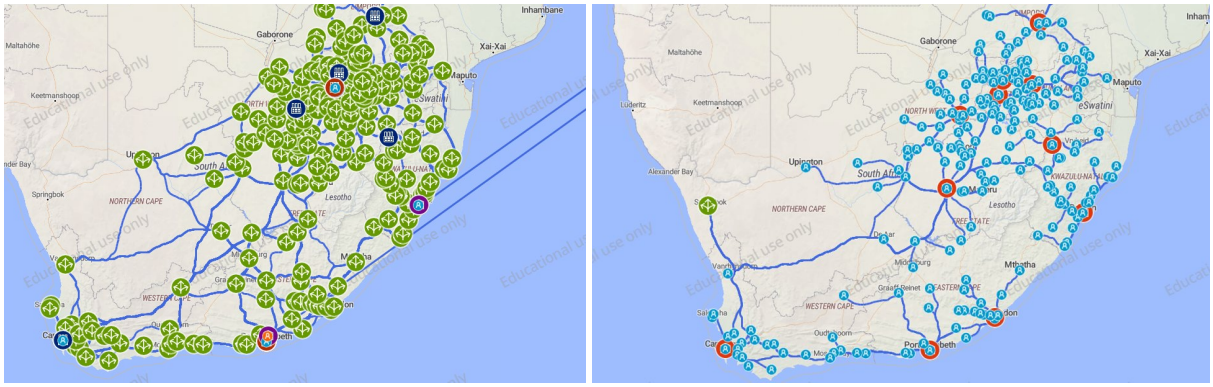


Fig. 5. Reverse logistic network simulations of EoL LIB collection centres (left) and local WEEE customers (right) in South Africa context

The assessment indicated that the best strategy for an efficient recycling network is to establish collection and e-waste dismantling centres throughout the country and operate a single recycling facility in Johannesburg. To increase profit, LIBs should be pre-treated at the dismantling facilities. The sale of e-waste from dismantling facilities has the potential to enhance profitability significantly. The discounted payback period and predicted internal rate of return (IRR) were estimated to be 11 years and 16.73 %, respectively, strongly depending on feed composition and LIB collection rates.

3.4. Development and scale-up of novel hydrometallurgical processes

KTU developed novel hydrometallurgical processes to recover critical/strategic metals from spent LIBs at a laboratory scale (Fig. 6). In the leaching stage, high recoveries (i.e., >90 %) were achieved for metals, independent of the acid or reducing agent under suitable conditions. However, H_2O_2 was selected as the most suitable reducing agent, considering the high selectivity in the downstream recovery of metals from leach solutions. Several solid products were produced from these hydrometallurgical processes, including manganese dioxide, mixed Co-Ni-sulphate, cobalt (III) oxy/hydroxide, cobalt oxide (Co_3O_4), nickel hydroxide and lithium carbonate (Li_2CO_3). Two of the developed hydrometallurgical processes were successfully demonstrated at a pilot scale in an operation campaign carried out with the collaboration of KTU and EXITCOM Recycling R&D Department at the company's facilities in Türkiye (Fig. 7). Patent applications for the developed novel hydrometallurgical processes are being processed.

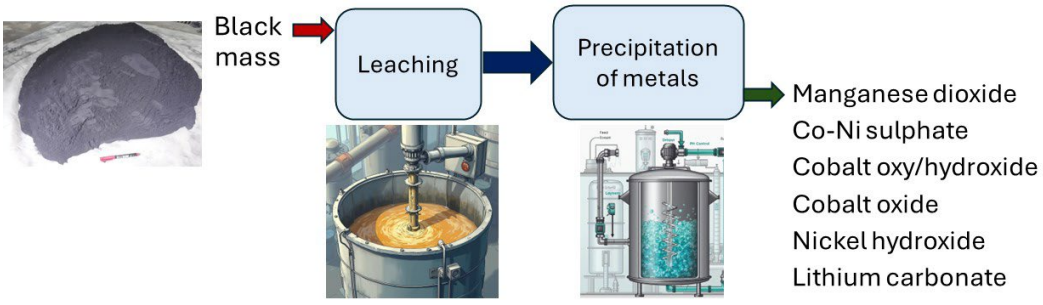


Fig. 6. Main stages and products of the developed H_2SO_4-based novel hydrometallurgical process

4. Conclusions

The ELiMINATE project is a multidisciplinary project that evaluated several hydrometallurgical processes for metals recovery from black mass, their value chain integration, environmental impacts, and reverse logistic networks (RLNs). These results were combined to create consolidated frameworks with guidelines for creating LIB recycling industries in South Africa and Europe. Market analyses have confirmed that the demand for recycling will increase. LCA studies showed that hydrometallurgical processes involving an SX stage generally had a higher environmental impact than those without an SX stage. Techno-economic and LCA studies also revealed that the best processes in terms of economics and environmental impacts were acid leaching followed by a mixed NMC precipitation. The findings also revealed that the novel processes developed had a slightly higher environmental impact than the

H_2SO_4 – mixed NMC precipitation process. Novel hydrometallurgical processes developed at the laboratory scale were successfully demonstrated at a pilot scale, reaching a high TRL.

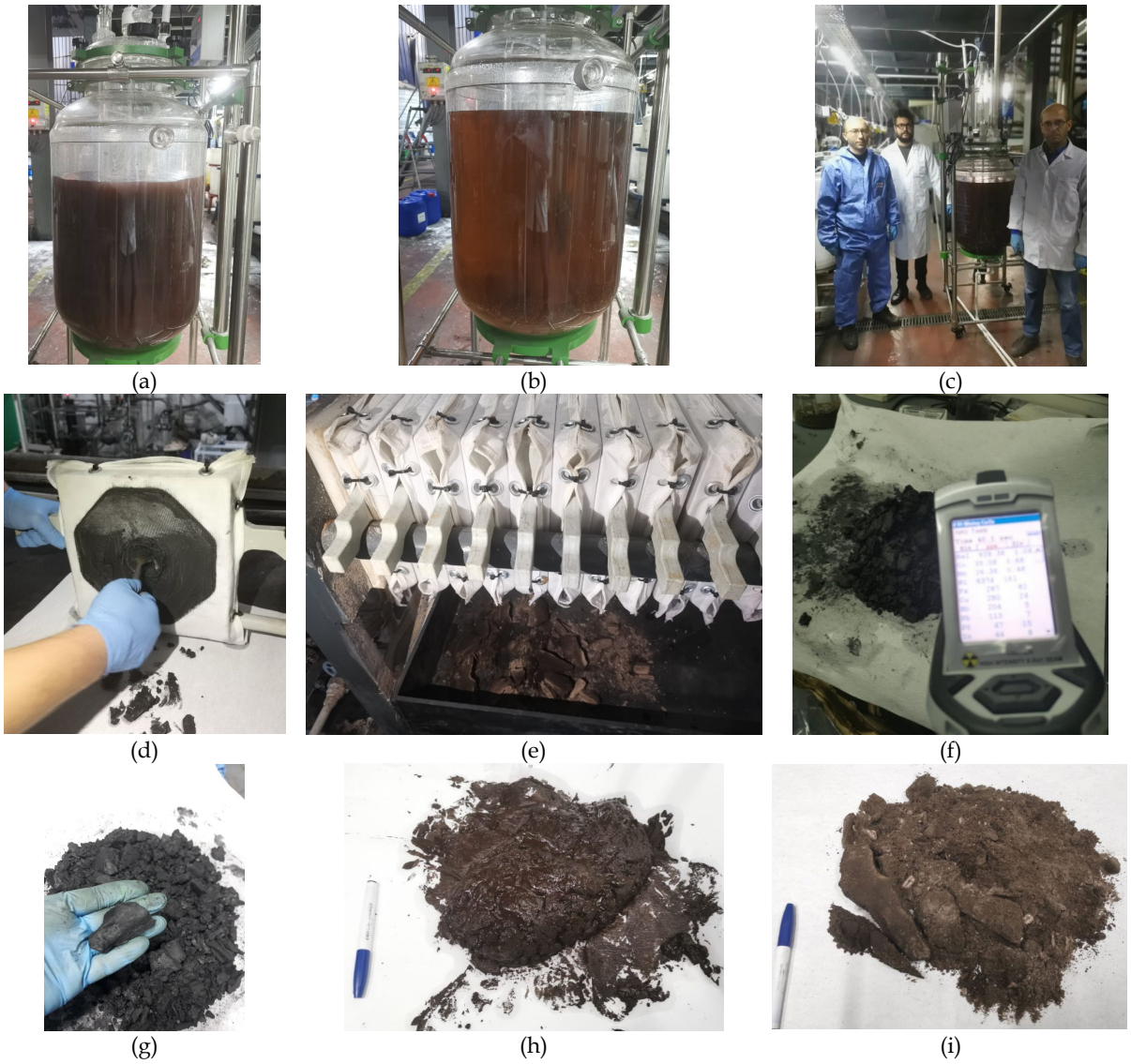


Fig. 7. Photos from different stages of pilot scale tests at EXITCOM Recycling facilities (a, b, c, d, e, f) and some products obtained from novel hydrometallurgical processes after pressure filtration (graphite (g), manganese dioxide (h), mixed Co-Ni sulphate (i))

Acknowledgments

The authors would like to appreciate ERA-MIN 2, co-funded by the Horizon 2020 program of the European Union, and national funding organisations; TÜBİTAK (Türkiye; Project No: 120N275), DSI (South Africa), Vinnova (Sweden), for the financial support for "End-of-life Li-ion battery management integration and technology evaluation (ELiMINATE)" Project.

References

Baum, Z.J., Bird, R.E., Yu, X., Ma, J. (2022). Lithium-ion battery recycling—overview of techniques and trends. ACS Energy Lett 7, 712–719. https://doi.org/10.1021/acsenergylett.1c02602

Celep, O., Yazici, E.Y., Deveci, H., Dorfling, C. (2023). Recovery of lithium, cobalt and other metals from lithium-ion batteries. Pamukkale Univ Muh Bilim Derg 29, 0. https://doi.org/10.5505/pajes.2022.98793

Emilsson, E., Ozturk, A. N. (2023). Optimizing Resource Recovery of Lithium-Ion Battery Recycling, IVL Swedish Environmental Research Institute, Report no: C801

European Commission (2019). Communication from the Commission to the European Parliament, The European Council, The Council, The European Economic And Social Committee And The Committee Of The Regions – The European Green Deal, European Commission, Brussels, 11.12.2019, 24, https://eur-lex.europa.eu/legal-content/EN/TXT/?qid=1588580774040&uri=CELEX%3A52019DC0640

European Commission (2023). European Commission, Study on the critical raw materials for the EU 2023 – Final Report. Luxembourg.

IEA (2021). The role of critical minerals in clean energy transitions, International Energy Agency (IEA), Paris.

IRENA (2023). Geopolitics of the energy transition: Critical materials, International Renewable Energy Agency, Abu Dhabi.

Jung, J.C.Y., Sui, P.C., Zhang, J. (2021). A review of recycling spent lithium-ion battery cathode materials using hydrometallurgical treatments. J Energy Storage 35, 102217. https://doi.org/10.1016/J.EST.2020.102217

Kuhn, M. W. J. (2023). Towards a business model for lithium-ion battery recycling in South Africa, MSc thesis, Department of Industrial Engineering, Stellenbosch University

Maritz, R.F., (2024). Comparing the environmental impact of different hydrometallurgical processes for the recycling of lithium-ion batteries using a life cycle assessment approach, PhD thesis, Department of Chemical Engineering, Stellenbosch University

Maritz, R.F., vanSchalkwyk, R.F., Elginöz, N., Akdogan, G., Dorfling, C. (2022). Investigating options for reducing the environmental impact of lithium-ion battery recycling plants using life cycle assessment, Circular Materials Conference, 14-15 September, Skellefteå, Sweden.

Musariri, B., Akdogan, G., Dorfling, C., Bradshaw, S. (2019). Evaluating organic acids as alternative leaching reagents for metal recovery from lithium ion batteries. Miner Eng 137, 108–117. https://doi.org/10.1016/J.MINENG.2019.03.027

Neumann, J., Petranikova, M., Meeus, M., Gamarra, J.D., Younesi, R., Winter, M., Nowak, S. (2022). Recycling of lithium-ion batteries—current state of the art, circular economy, and next generation recycling. Adv Energy Mater, 2102917. https://doi.org/https://doi.org/10.1002/aenm.202102917

Ozturk, A. N. (2023). Techno-economic assessment and business development of two novel Li-ion battery recycling technologies, MSc thesis, Uppsala University

Pinegar, H., Smith, Y.R. (2019). Recycling of end-of-life lithium ion batteries, part I: commercial processes. Journal of Sustainable Metallurgy 5, 402–416. https://doi.org/10.1007/s40831-019-00235-9

Rouquette, L.M.J., Petranikova, M., Vieceli, N. (2023). Complete and selective recovery of lithium from EV lithium-ion batteries: Modeling and optimization using oxalic acid as a leaching agent. Sep Purif Technol 320, 124143. https://doi.org/10.1016/J.SEPPUR.2023.124143

van Schalkwyk, R., Yazici, E. Y., Ots, J., Emilsson, E., Petranikova, M., Eken Torunoglu, E., Wu, A., Deveci, H., Akdogan, G., Louw, L., Elginöz Kanat, N., Maritz, R., Vooght, D., Kuhn, T., Ozturk, A. N., Lassesson, H., Dorfling, C. (2023). End-of-life li-ion battery management ıntegration and technology evaluation. 2nd International Conf. on Raw Materials and Circular Economy (RawMat 2023), 28 August- 2 September, Athens, Greece

Wu, A. (2022). The ELiMINATE project: How to integrate battery recycling innovations in future society?, Circular Materials Conference, 14-15 September, Skellefteå, Sweden.

Yazici, E. Y., Deveci, H., Celep, O., Dorfling, C., van Schalkwyk, R. F., Emilsson, E., Wu, A., Petranikova, M., Eken Torunoglu, E., Cuhadar, E., Eyupoglu, C. (2023) Preliminary findings of the ERA-MIN 2 project (ELiMINATE) on the management and treatment of end-of-life lithium ion batteries, The 5th

International Conference of Materials and Engineering Technology (TICMET'23), 13-16 November, Trabzon, Türkiye

The Recovery of Graphite from Black Mass using Centrifugal and Magnetic Separation

Halide Nur Dursun [1, 2]*, Argun Çiper [1], Doğukan Akardaş [1], Emircan Uysal [2], Beril Tanç Kaya [3], Fırat Burat [1]

[1]Department of Mineral Processing Engineering, Istanbul Technical University, Türkiye

[2]Department of Metallurgical and Materials Engineering, Istanbul Technical University, Türkiye

[3]Department of Geological Engineering, Istanbul Technical University, Türkiye

*Corresponding author: dursunh17@itu.edu.tr (Halide Nur Dursun)

Abstract:

Graphite is a strategic material with unique characteristics, leading to its inclusion as one of the 14 critical raw materials identified in the European Union's Critical Raw Materials report. As global demand for graphite increases, it is necessary to develop effective techniques to obtain higher efficiency of graphite-containing concentrates. Graphite recovery from secondary sources, mainly from Li-ion batteries, has emerged as a crucial endeavor in addressing the challenges of consuming natural resources. With the escalating global demand for graphite, driven primarily by the rapid growth of electric vehicles and renewable energy technologies, there is a pressing need to develop efficient and environmentally responsible techniques for graphite recovery. Various advanced physical enrichment methods can be utilized to recover graphite from secondary sources, such as gravity, magnetic, and electrostatic separation. The physical enrichment techniques are crucial in the recovery process due to their environmental benignity, absence of hazardous chemicals, and relative simplicity in implementation. This study investigates the recovery of graphite from secondary sources using physical enrichment methods. The anode and cathode current collector foils and battery powders directly obtained from shredded batteries were classified through screening. Graphite, the anode active material, was efficiently separated from the cathode active material using centrifugal gravity separation and magnetic separation, achieving high efficiency.

Keywords: *Graphite recovery, Recycling, Centrifugal Gravity Separation, Black Mass*

1. Introduction

Lithium-ion batteries (LiBs) play a crucial role in advancing toward a sustainable energy future, as they power a wide range of devices, from smartphones to electric vehicles. The significance of LIBs as power sources is evident in their steadily rising production rates and expanding market share (Velázquez-Martínez et al., 2019). While critical metals such as lithium, cobalt, and nickel are vital for these batteries, the significance of graphite, a key material in battery anodes, should not be ignored. Benchmark Mineral Intelligence's authoritative data indicates that by 2030, global demand for graphite in the battery industry will grow at an annual rate of 30% (Zhu et al., 2023). Environmental concerns are significant, as improper disposal of LiBs can create hazardous waste, making recycling crucial for recovering resources and minimizing ecological impact while also reducing the environmental burden of ore mining and metal processing by incorporating recycled materials and avoiding the harmful effects of other disposal methods (Mrozik et al., 2021). Effective recycling methods can retrieve valuable materials, reduce the reliance on new mining, and support a circular economy, which is essential for sustainable development.

Recycling lithium-ion batteries involves several techniques to recover valuable materials while minimizing environmental harm. These processes are typically categorized into three main groups: physical methods (such as dismantling, comminution, classification, gravity separation, magnetic separation, and electrostatic separation)(He et al., 2021), hydrometallurgical methods (including acidic leaching, alkaline leaching, solvent extraction, chemical precipitation, and electrochemical techniques)

(Chu et al., 2021), and pyrometallurgical methods (which involve thermal treatment and roasting) (Meng et al., 2019). Physical and physiochemical separation methods play a crucial role in recycling by offering cost-effectiveness and high energy efficiency, thereby reducing environmental impacts and achieving substantial energy savings (Mennik et al., 2023). Physical techniques include many methods, such as mechanical, magnetic separation, and gravity separation, which are effective for enriching metals from battery waste. Centrifugal gravity separation methods, like Knelson and Falcon concentrators, utilize centrifugal force to enhance the separation of materials according to their density. Research has demonstrated that when mechanically extracted from spent batteries and subsequently reutilized, graphite anodes exhibit properties analogous to those of primary graphite (Harper et al., 2019). This study focuses on recovering graphite from lithium-ion batteries using centrifugal gravity separation and magnetic separation methods, emphasizing their role in enhancing recovery rates and reducing the environmental impact of recycling processes.

2. Material and methods

2.1. Material

In this study, end-of-life (EoL) LiBs (LCO and NCM) from mobile phones were obtained in a shredded form by the Exitcom company in Türkiye. XRF (X-ray Fluorescence) analysis was conducted on the representative battery powder sample to characterize and determine the composition of anode and cathode active materials. SEM (Scanning Electron Microscope) analysis examined its morphological structure. EDS (Energy Dispersive X-ray Spectroscopy) analysis was also conducted on the SEM images to obtain elemental distribution data regionally. To investigate the effect of particle size on enrichment, the battery powder was subjected to grinding.

LiBs have five essential components: cathode, anode, electrolyte, separator, and collectors. Most materials constituting the components of EoL LiBs consist of harmful elements and compounds for the environment and human health. Therefore, the recovery of these components is of great importance. To obtain these components, preliminary preparation and size reduction processes must be carried out carefully. The flowchart of the sample pre-preparation and size reduction processes is illustrated in Figure 1.

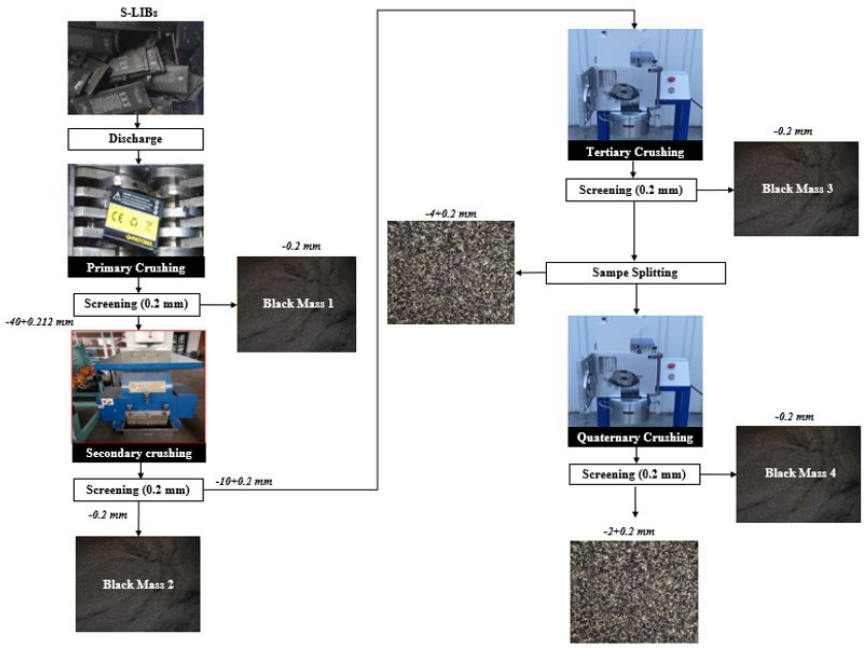


Fig. 1. Flowchart of sample preparation and size reduction processes

Before the commencement of the experimental studies, LiBs were discharged and shredded by Exitcom Recycling to mitigate the risk of explosion and fire. After the full discharge process, The EoL LiBs sample was subjected to primary crushing, and the particles were reduced to below 40 mm. After the first crushing, the material was screened through a 0.2 mm sieve. The materials on the sieve included mostly anode and cathode current collector foils, plastics, and case materials. In contrast, the under-screen fraction, mainly fine-size active anode and cathode materials, was named 'Black Mass 1'. The material above the sieve (-40+0.212 mm) was subsequently reduced below -10 mm using a shredder. The shredder (NET PLASMAK brand) has six blades on the rotor that chip off small pieces with each impact, reducing the size of the material. Below the single-shaft cutter is an adjustable sieve, which can be replaced with sieves of different hole diameters to achieve the desired size reduction. The hydraulic pusher system ensures continuous and uniform shredding by pressing the material against the blades.

The over-screen product (coarse fraction) was fed to a four-blade cutting mill (RAM200 model manufactured by Rantek Co.) designed to crush the elastic, medium-hard, soft, fibrous, and heterogeneous materials uniformly. The size of the crushed material was adjusted by selecting the suitable replaceable sieve in the lower compartment of the grinder. Subsequently, sieving with 0.2 mm was performed again, and 'Black Mass 2' was obtained as an under-screen product. Similarly, the foils in the -10+0.2 mm fraction were shredded using the Cutting Mill by equipping 4 mm and 2 mm screens. The -0.2 mm fractions obtained from these processes were named 'Black Mass 3' and 'Black Mass 4'. All four black masses were combined for the final product and used in the beneficiation studies. Subsequently, characterization methods were applied to the battery dust sample to determine its physical and chemical properties before the enrichment processes.

To investigate the effect of particle size on the enrichment processes, the obtained battery powder was ground in a planetary mill at 1000 rpm for 45 minutes, reducing the d_{80} size to below 35 microns. During production, grinding is used to achieve particle liberation due to the agglomeration that occurs due to binding the anode and cathode active materials with a binder at a particle size of 20 microns. The size-reduced sample was then subjected to centrifugal gravity separation for enrichment purposes.

2.2. Physical and Chemical Properties of the Sample

The sieve analysis was performed to determine the physical properties of the sample. The chemical analyses were conducted at the ITU Geochemistry Analysis Laboratory and the Department of Metallurgy and Materials Engineering.

2.2.1. Physical Properties

After the staged size reduction processes, the sieve analysis was conducted using an electric screen shaker to determine the size distribution properties of the graphite-containing battery powder. The particle size distribution (PSD) curve is shown in Figure 2. The graph shows the particle size distribution of black mass from EoL phone batteries, plotted as a cumulative undersize percentage against particle size in millimeters on a logarithmic scale. In lithium-ion batteries, cathode, and anode powders are usually produced with fine particle sizes. Moreover, the particle size of graphite powder produced through recycling typically ranges from 10 to 50 µm (Yi et al., 2020). However, according to the PSD curve, the d_{50} and d_{80} values of the battery powder were obtained as 0.1 mm and 0.17 mm, respectively. In contrast to the sizes used during production, an increase in particle size distribution was observed, which is likely attributed to the binders used in the batteries.

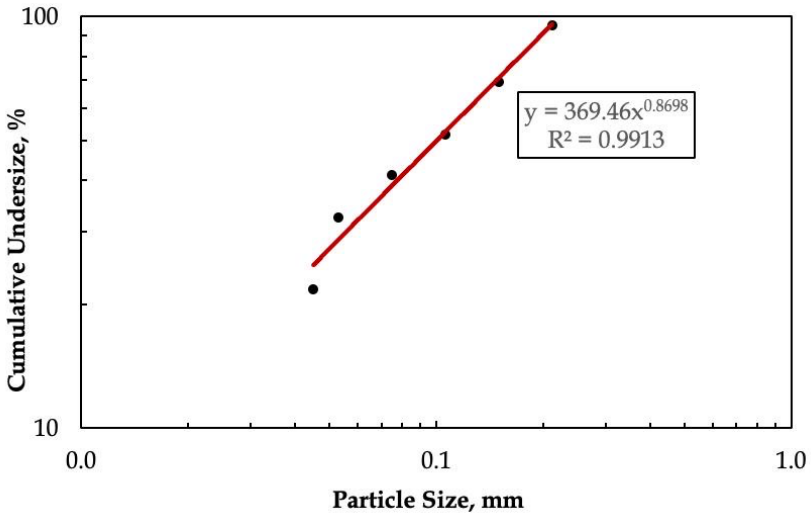


Fig. 2. Particle size distribution curve of battery powder

A size reduction process was performed using a planetary mill to prevent adverse effects in experiments caused by the anode and cathode active materials agglomerated due to the binder. After milling, the particle size analyzer (Mastersizer 2000, Malvern) indicated d_{50} and d_{90} values of 12.3 and 32 microns, respectively.

2.2.2. The chemical properties of the sample

XRF and SEM-EDS analyses were conducted at the ITU Geochemistry Analysis Laboratory and the Department of Metallurgy and Materials Engineering to determine the physical and chemical properties of the battery powder sample used in the enrichment experiments. The contents obtained from the chemical analysis of the raw material are shown in Figure 3. Cobalt (Co) is the most prevalent element in the battery powder obtained from spent batteries, accounting for up to 41.55%, followed by carbon (C) in graphite, which constitutes 38.45%.

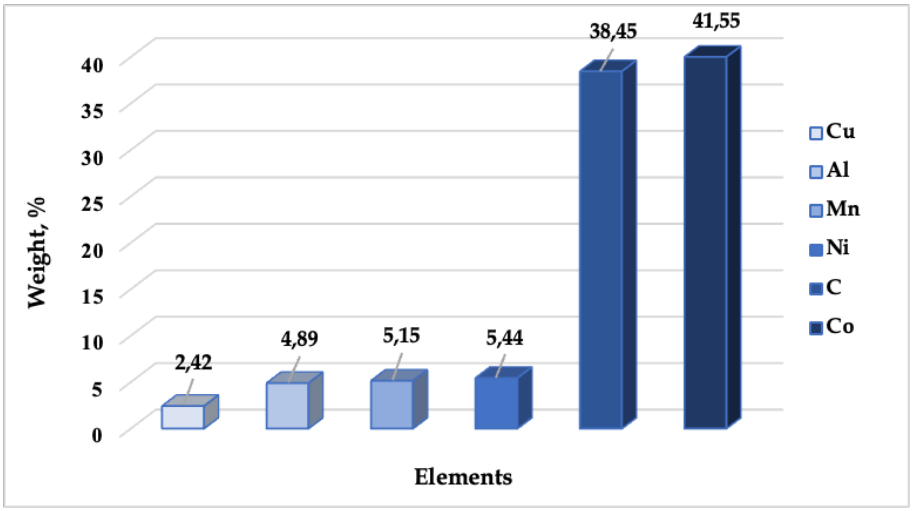


Fig. 3. The content of the black mass sample

2.2.3. SEM-EDS analysis

Particle morphology and size significantly impact physical enrichment steps (Chen et al., 2019). SEM analysis was conducted to determine the particles' morphology and size, and the image of the particles at 1000x magnification is presented in Figure 4a. It was observed that the particles exhibit a near-spherical but heterogeneous morphology. Additionally, the particles were found to have an average

diameter of approximately 38 µm. To better understand the elemental distribution of the particles, EDS analysis was performed, with the resulting EDS maps provided in Figure 4b (without carbon) and Figure 4c (including carbon). The EDS maps reveal the presence of free graphite within the anode section. Furthermore, it is evident from the EDS maps that the cathode materials retain their integrity but are coated with graphite on their surfaces.

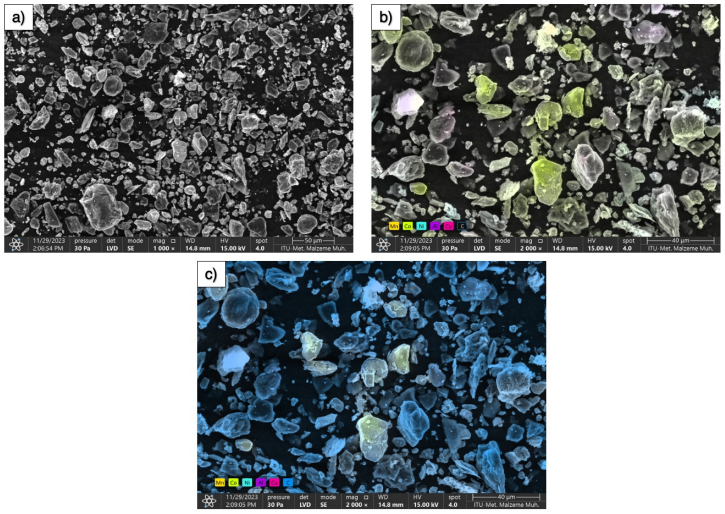


Fig 4. SEM image of the particles at 1000x magnification a), EDS map of the particles without carbon inclusion b), and EDS map of the particles with carbon inclusion c).

2.3. Method

Multistage size reduction and sieving processes were used to recover graphite with high content and recover it from EoL LiBs. Subsequently, centrifugal gravity separators, specifically the Knelson and Falcon concentrators, which separate particles according to their specific gravity differences, were used to concentrate graphite particles in the light product and cathode materials in the heavy product. After centrifugal gravity separation, magnetic separation was performed using the Carpco magnetic separator, taking advantage of the magnetic properties of the materials.

2.3.1. Knelson concentrator

The Knelson Concentrator's advantages are simplicity, high separation efficiency, and low cost. The specific gravity of graphite, the lightest element in the battery powder apart from lithium, is 2.2 g/cm³. The specific gravities of other components are Al 2.7 g/cm³, Co, and Cu 8.9 g/cm³. The densities of other non-metallic plastics and polymers are below 2 g/cm³. Centrifugal force in a conical chamber creates a disabled collapse environment that separates the grains from one another. Interspersed throughout the cone are protrusions that facilitate the disabled collapse. A conical chamber with a diameter of up to 75 cm is possible. Force of up to 60 G is produced by rotation on the vertical axis, which has a maximum speed of 400 rpm. Within the chamber are water jackets under pressure. The layer relaxes in pressured water, allowing heavy minerals to dissolve and become fluid. Since the d80 size of the material is 35 µm and below and there is a high specific gravity difference between metal-plastic materials, it was decided to use a Knelson Separator.

2.3.2. Falcon concentrator

The working concept of the Falcon concentrator is remarkably similar to that of the Knelson device. Unlike the Knelson, the Falcon has no pressurized water jacket and a centrifugal force of up to 300G. Centrifugal force causes it to travel upward and toward the chamber walls. Specific gravity and centrifugal force are the two fundamental forces at work. Centrifugal force causes an upward movement

while the particles in the hindered collapse environment are arranged in layers based on specific gravity. Light and fine particles are overflowing with upward motion.

2.3.3. Carpco magnetic separator

Carpco magnetic separator was used in experimental studies to produce magnetic and non-magnetic products. Paramagnetic metals include copper, lead, gold, and silver, whereas ferromagnetic metals include iron, nickel, and cobalt. Non-ferrous metals and other non-magnetic wastes are recovered using low-density/intensity magnetic separators. Based on the strength of the magnetic field, two types of magnetic enrichment devices are distinguished: high field and low field. Magnetic separators with modest magnetic fields are enough for minerals and materials with strong magnetic characteristics. Another parameter in device selection is grain size. While dry magnetic separation is preferred for large sizes, wet magnetic separators are used for materials below 500 microns. Carpco magnetic separator is a wet separator and includes matrices. The magnetic field strength can be adjusted by changing the amperage value.

3. Results and Discussions

3.1. Knelson concentrator

The gravity separation process with Knelson Concentrator was carried in 4 different psi values: 0.5, 0, 2, and 4 psi. A sample of battery powder below 38 µm was fed into a Knelson Concentrator operating at 0.5 psi, producing light and heavy products. The light product was fed back into the concentrator without adding water (0 psi), resulting in light and heavy products. The heavy product from the initial 0.5 psi process was fed into the concentrator at 2 psi, yielding a light product and another heavy product. This heavy product was further processed at 4 psi, producing a light and heavy product. The flowsheet of the process is presented in Figure 5.

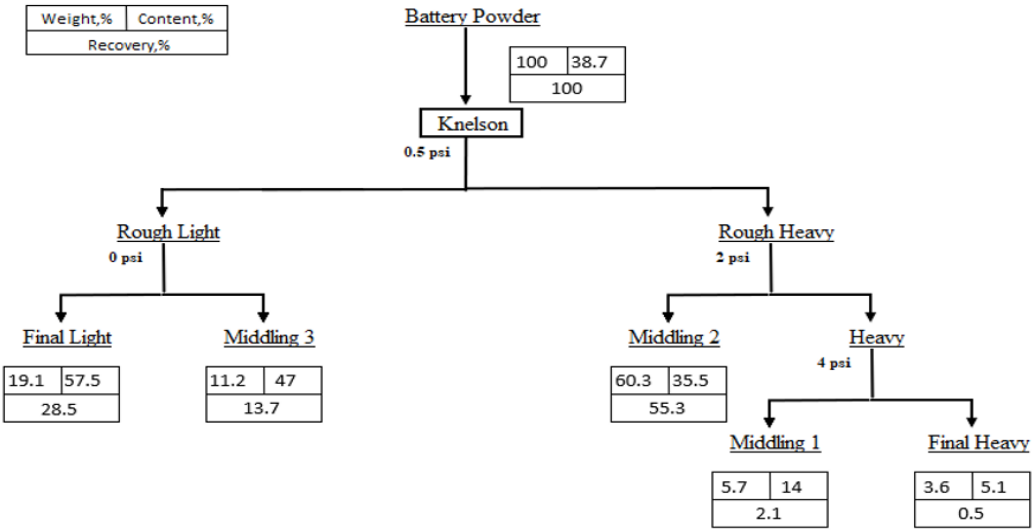


Fig. 5. The flowsheet of the Knelson concentration experiments

Table 2 illustrates the separation of black mass utilizing a Knelson concentrator, thereby elucidating substantial insights into the distribution and recovery of diverse elements. In centrifugal gravity separation experiments conducted with the Knelson concentrator, carbon content was obtained with 33.74% and 54.08% in Middling 2 and Final Light products, respectively. Furthermore, these fractions exhibited considerable cobalt concentrations of 45.6% and 17.3%. On the other hand, the Final Heavy fraction, representing 3.6% of the total weight, has high aluminum and cobalt content. Middling 2, which constitutes 60.3% of the total weight, exhibits the highest recovery rates for aluminum, manganese, cobalt, copper, nickel, and carbon, indicating a significant concentration of these elements in this fraction. The Final Light fraction, making up 19.1% of the total weight, has a notable carbon

content. These results suggest that the Knelson separator concentrates valuable metals, particularly in the Middling 2 fraction, which should be the focus for further processing. Additionally, high graphite presence in the Final Light fraction may necessitate process adjustments to reduce carbon losses and improve separation efficiency. This demonstrates the Knelson separator's capability to optimize the recycling process by segregating elements based on their densities.

Table 1. The results of Knelson concentrator experiments

Products	W, %	Al		Mn		Co		Cu		Ni		LOI	
		C, %	R, %	C, %	R, %	C, %	R, %	C, %	R, %	C, %	R, %	C, %	R, %
Final Heavy	3.6	6.0	5.8	5.6	3.7	58.4	5.2	12.8	25.4	6.7	4.1	3.48	0.3
Middling 1	5.7	4.2	6.5	5.7	6.0	60.2	8.6	1.7	5.2	4.7	4.6	9.43	1.5
Middling 2	60.3	4.0	64.5	5.3	58.8	45.6	68.6	1.5	48.6	5.1	52.7	33.74	55.6
Middling 3	11.2	3.3	10.0	5.7	11.6	33.4	9.3	1.3	8.1	6.6	12.7	46.74	14.4
Final Light	19.1	2.6	13.2	5.7	19.9	17.3	8.3	1.2	12.6	8.0	26	54.08	28.3
Total	100	3.7	100	5.5	100	40.1	100	1.8	100	5.9	100	36.6	100

W: Weight, C: Content, R: Recovery

3.2. Falcon concentrator

The gravity separation process with Falcon Concentrator was carried out using 3 different G force values: 300, 200, and 100. A sample of battery powder below 38 microns was fed into a Falcon Concentrator operating at 300 G, producing light and heavy products. The heavy product was then processed again in the concentrator at 200 G, yielding a light product and another heavy product. This heavy product underwent a third concentration at 100 G, resulting in a light and heavy product. The flowsheet of the process is presented in Figure 6.

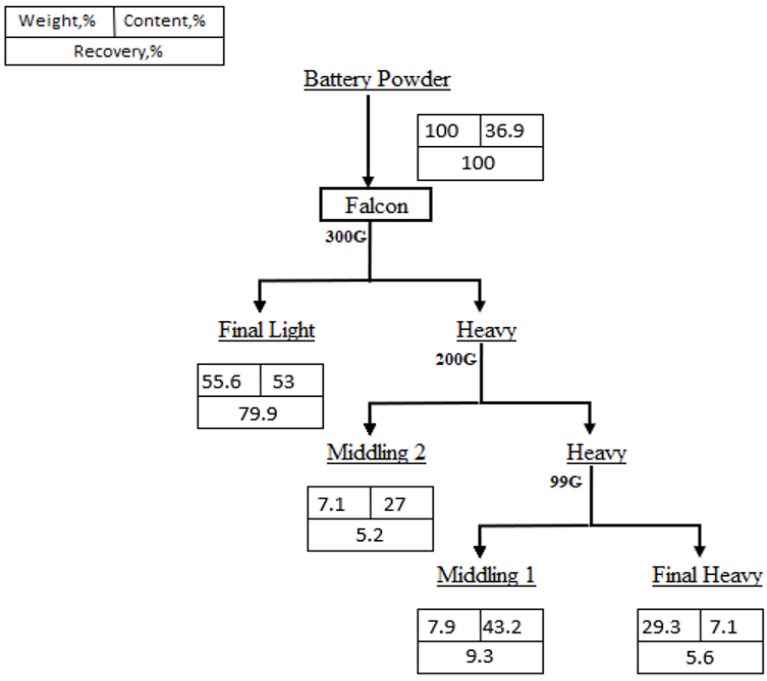


Fig. 6. Falcon process flowsheet

Table 2 shows black mass separated using a Falcon separator, revealing significant insights into the distribution and recovery of various elements. Results from the Falcon concentrator indicated that the Final Light product attained a carbon content of 53.16% with a recovery rate of 83.4%. Approximately

80% of the black mass is thought to originate from LCO ($LiCoO_2$) type batteries, and the rest are NCM ($LiNiCoMnO_2$) type batteries. The analysis shows that the Final Heavy fraction, comprising 29.3% of the total weight, has high contents and recoveries of cobalt and copper. In contrast, the Final Light fraction, making up 55.6% of the total weight, shows high recovery rates for aluminum, manganese, nickel, and carbon, indicating these elements are more concentrated in the lighter fractions. The Middling fractions exhibit intermediate values for all elements. The high carbon content in the Final Light fraction suggests graphite particles are being trapped during the separation process. To improve carbon recovery and minimize losses, increasing the number of feed stages and performing a more frequent and detailed cleaning of the separation equipment is recommended. These findings demonstrate the Falcon separator's effectiveness in segregating elements based on density, which can optimize the recycling process by allowing targeted treatments for heavy and light fractions, enhancing metal recovery and purity.

Table 2. The results of Falcon concentrator experiments

Products	W, %	*Al*		*Mn*		*Co*		*Cu*		*Ni*		*LOI*	
		C, %	R, %	C, %	R, %	C, %	R, %	C, %	R, %	C, %	R, %	C, %	R, %
Final Heavy	29.3	3.2	29.3	4.6	24.7	73.0	51.6	3.0	49.3	3.1	16.0	4.51	3.7
Middling 1	7.1	2.3	5.1	5.2	6.9	47.9	8.2	0.7	3.0	4.4	5.6	21.21	4.3
Middling 2	7.9	2.6	6.3	5.9	8.7	30.3	5.8	1.0	4.6	7.0	9.8	38.58	8.6
Final Light	55.6	3.4	59.2	5.8	59.7	25.7	34.4	1.4	43.1	6.9	68.6	53.16	83.4
Total	100	3.2	100	5.4	100	41.5	100	1.8	100	5.6	100	35.4	100

W: Weight, C: Content, R: Recovery

3.3. Carpco magnetic separator

The magnetic separation process with Carpco Magnetic Separator was carried out in 3 different ampere values: 6,4, and 2. A sample of battery powder below 38 microns was fed into a Carpco magnetic separator operating at 6 Amp, resulting in nonmagnetic and magnetic products. The nonmagnetic product was processed again at 6 Amp, yielding nonmagnetic and magnetic products. Both magnetic products from the 6 Amp process were combined and fed to the separator at 4 Amp, producing a nonmagnetic and magnetic product. This magnetic product was further processed at 2 Amp, resulting in a nonmagnetic and magnetic product. When examining the results, it can be observed that the manganese and nickel content is very high in the magnetic product. While most cobalt is collected in the non-magnetic fraction, a significant amount is also found in the magnetic sample. The nickel-cobalt-manganese trio in NCM-type batteries forms a spinel structure, causing nickel and manganese to drag cobalt into the magnetic fraction. Since LCO batteries, which comprise 80% of the black mass, do not contain nickel and manganese, the remaining cobalt ends up in the non-magnetic fraction as expected. The flowsheet of the process is shown in Figure 7.

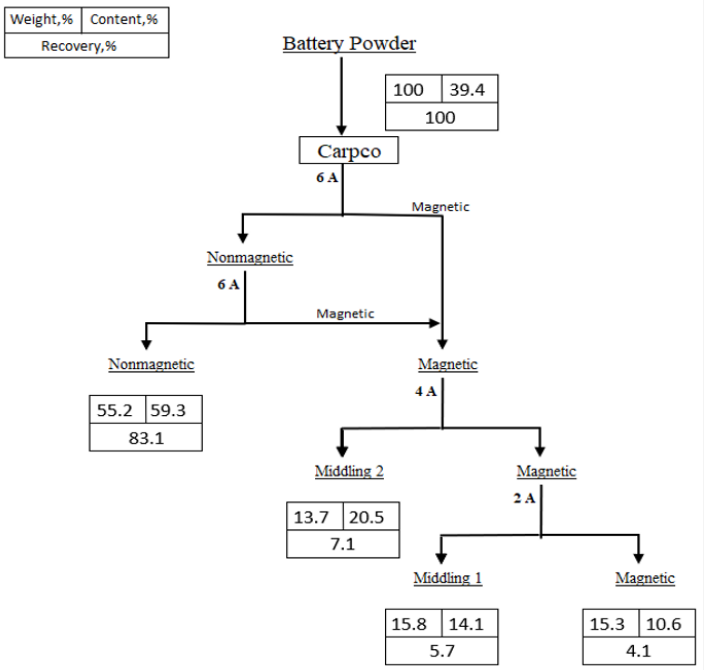


Fig. 7. Carpco process flowsheet

The magnetic susceptibilities of LCO and NCM-type batteries are shown in Table 3. In the Carpco magnetic separation experiments, a non-magnetic product was achieved with a carbon recovery of 56.0% and an efficiency of 89%. As anticipated, aluminum and copper are not affected by magnetic separation. Although the carbon content of the non-magnetic fraction is high, some losses have occurred. This is due to graphite particles getting trapped between the ball matrices in the Carpco device. Feed stages should be increased to reduce carbon loss, and cleaning should be done more frequently and thoroughly.

Table 3. The results of Carpco magnetic separator experiments

Products	W, %	Al		Mn		Co		Cu		Ni		LOI	
		C, %	R, %	C, %	R, %	C, %	R, %	C, %	R, %	C, %	R, %	C, %	R, %
Magnetic	15.3	4.4	20.1	21.7	56.7	41.1	15.8	1.5	12.8	17.8	44.9	4.49	2.0
Middling 1	15.8	4.7	22.5	8.6	23.3	55	22	1.8	16.3	10.7	28	6.55	3.0
Middling 2	13.7	4.3	17.6	4.3	10.0	57.6	19.9	1.8	14.2	6.1	13.7	15.39	6.1
Non-Magnetic	55.2	2.4	39.8	1.1	10.0	30.4	42.3	1.8	56.7	1.5	13.4	56.06	89.0
Total	100	3.3	100	5.8	100	39.6	100	1.7	100	6.1	100	34.8	100

W: Weight, C: Content, R: Recovery

4. Conclusions

In this original study, the characterization and the selective production of metal concentrates from EoL LIBs by physical methods including centrifugal and magnetic separation. The results from graphite recovery experiments conducted on NMC-LCO mixed black mass indicate that LCO recovery is more efficient in centrifugal gravity separation methods, whereas NMC recovery performs better in magnetic separation processes. The recovery of carbon from black mass through centrifugal gravity separation using Falcon and Knelson concentrators and magnetic separation methods represents a novel approach. Implementing physical pre-concentration techniques before chemical processing effectively mitigates the environmental and economic impacts of chemical processes. Consequently, the findings in this study suggest alternative physical processes to recover graphite from cathode active materials. With all

this information, further tests, including cleaning and scavenging stages, are strongly recommended to improve the quality of the products.

Acknowledgments

The present study is based on the results of the BAP (Scientific Research Project) Department with the project code MGA-2022-43640 at the Istanbul Technical University. The authors sincerely thank the Mineral Processing Department of Istanbul Technical University for providing laboratory equipment and analysis for this research. We are grateful to Rantek Co. for their support in crushing battery samples to fine size by cutting mill. We would like to thank Mr. Murat Ilgar and Mr. İlyas Emir Çuhadar in Exitcom Recycling Company for the supply of samples.

References

[1] Velázquez-Martínez, O., Valio, J., Santasalo-Aarnio, A., Reuter, M., & Serna-Guerrero, R. (2019). A critical review of lithium-ion battery recycling processes from a circular economy perspective. *Batteries*, *5*(4), 68.

[2] Zhu, X., Chen, Y., Xiao, J., Xu, F., Su, F., Yao, Z., ... & Zhong, Q. (2023). The strategy for comprehensive recovery and utilization of the graphite anode materials from the end-of-life lithium-ion batteries: Urgent status and policies. *Journal of Energy Storage*, *68*, 107798.

[3] Mrozik, W., Rajaeifar, M. A., Heidrich, O., & Christensen, P. (2021). Environmental impacts, pollution sources, and pathways of spent lithium-ion batteries. *Energy & Environmental Science*, *14*(12), 6099-6121.

[4] He, Y., Yuan, X., Zhang, G., Wang, H., Zhang, T., Xie, W., & Li, L. (2021). A critical review of current technologies for the liberation of electrode materials from foils in the recycling process of spent lithium-ion batteries. Science of The Total Environment, 766, 142382.

[5] Chu, H., Lie, J., & Liu, J. C. (2021). Rapid leaching of valuable metals from spent lithium-ion batteries with microwave irradiation using organic and inorganic acid. Journal of Sustainable Metallurgy, 7(2), 630-641.

[6] Meng, X., Hao, J., Cao, H., Lin, X., Ning, P., Zheng, X., ... & Sun, Z. (2019). Recycling of LiNi1/3Co1/3Mn1/3O2 cathode materials from spent lithium-ion batteries using mechanochemical activation and solid-state sintering. *Waste management*, *84*, 54-63.

[7] Mennik, F., Dinç, N. İ., & Burat, F. (2023). Selective recovery of metals from spent mobile phone lithium-ion batteries through froth flotation followed by magnetic separation procedure. Results in Engineering, 17, 100868.

[8] Harper, G., Sommerville, R., Kendrick, E., Driscoll, L., Slater, P., Stolkin, R., ... & Anderson, P. (2019). Recycling lithium-ion batteries from electric vehicles. *nature*, *575*(7781), 75-86.

[9] Yi, C., Yang, Y., Zhang, T., Wu, X., Sun, W., & Yi, L. (2020). A green and facile approach for regeneration of graphite from spent lithium ion battery. *Journal of Cleaner Production*, *277*, 123585.

The Recycling of End-of-Life Crystalline Silicon Solar Panels

Nazlım İlkyaz Dinç[1]*, Tülin Ulucan, Fırat Burat[1]

[1]Istanbul Technical University, Mining Faculty, Mineral Processing Engineering Department, 34469, Maslak, Sarıyer, Istanbul, Türkiye

*Corresponding author: dincnaz@itu.edu.tr (Nazlım İlkyaz Dinç)

Abstract:

Recently, there has been an increase in worldwide energy demand, mainly driven by a significant increase in population. Suppose policymakers towards renewable energy take ambitious steps. In that case, the cost of accessing the type of energy of interest will decrease and at the same time lead to a more energy-secure world. As the effects of global warming and CO_2 emissions increase, renewable energies take on a greater role in reducing the environmental impacts of conventional energies. Harnessing sunlight to generate electrical energy has proven to be one of the most promising solutions to the world's energy crisis. The device that converts solar energy into electrical energy, the solar cell, must be reliable and cost-effective enough to compete with traditional sources. Since solar energy is a newer energy source compared to non-renewable energy sources, it is considered the fossil fuel of the future for producers and users due to its rapid development in the market and ease of use. Although solar panels are generally considered relatively safe, occupational health issues related to the increasing number of hazardous substances used in the Photovoltaics (PV) industry warrant an all-encompassing occupational health and safety approach to ensure an optimal balance with sustainability. Given the limited lifespan of PVMs and the expected increase in solar panel waste, current recycling methodologies and associated challenges must be solved. This study examines the growing need for efficient recycling of crystalline silicon photovoltaic modules in the context of global solar-energy adoption and the characterization of components after mechanical treatment.

Keywords: *Photovoltaic module recycling, Recycling, Silicon*

1. Introduction

As of 2019, the most widely used energy sources depend highly on non-renewable resources (around 84%) (Opeyemi, 2021). Soon, it will not be possible to keep pace with non-renewable resources, both economically and resource-wise. According to Hirsch et al. (2007), world oil demand will increase by up to 40% by 2025. At this rate, future generations will be deprived of a sustainable world. As discussed in the previous sections, solar energy is the leader among renewable energy sources. The main reasons for this are that the cost of obtaining energy is low compared to other types, and the technological know-how in the sector moves and develops very quickly compared to different kinds of energy.

Moreover, from a consumer perspective, solar technologies create a positive energy gain context for energy security, renewables, and economic aspects. As a reminder, the 2030 targets refer to the Sustainable Development Goals set by the UN, while the 2050 targets refer to the European targets set by the EU (Nerini et al., 2017). Due to its low CO2 emissions, solar energy from photovoltaic panels (PV) is a high-priority option because it is one of the cleanest forms of energy. While fossil fuel-based electricity emits 400–1000 g CO_2-eq/kWh, the electricity produced by crystalline silicon PV panels is 23–81 g CO_2-eq/kWh, which is 5–8% of fossil fuel-based emissions (Louwen et al., 2015). Photovoltaic modules (or panels) are important power generators with a limited lifetime. Modules contain known pollutants and valuable materials such as silicon, silver, copper, aluminum, and glass. Recycling such waste is, therefore, of great importance. According to the International Renewable Energy Agency, 8 million tons of EoL modules will be considered waste in 2030 and 80 million tons by 2050 (IRENA, 2016).

This means that PV module waste could increase about tenfold in 20 years and has the potential to account for about 10% of the world's total electronic waste. Although methods such as landfilling seem feasible when analyzed in a circularity framework, it is not a reasonable, economical, and environmentally friendly method (Kokul and S. Bhowmik, 2021). It is of great importance to know how to handle PV modules from the design stage to the end-of-life point when examining them in terms of CE strategies (reject, rethink, reduce, reuse, repair, renew, remanufacture/reuse, recycle, and recover) (Morseletto, 2020).

2. Photovoltaic Module

A photovoltaic module (or PV module) is a structure consisting of solar cells that convert sunlight into electrical energy without needing a heat engine or rotor equipment. These modules work on the principle of the photovoltaic effect, converting solar energy into electrical energy. Photovoltaic modules are used in applications ranging from residential and commercial power generation to large-scale solar power plants. Modules typically consist of components such as a glass cover, back sheet, frame, and junction box, and these components are designed to increase the durability and efficiency of the module (Pastuszak and Węgierek, 2022).

There are different types of photovoltaic panels, among which silicon panels are the most common worldwide, with 85%–90% of PVs on the market. In general, 77.41% of such panels are composed of glass, 1.6% of metal filaments, 6.77% of solar cells, and 14.06% of polymers (Sah et al., 2022). Its structure contains elements such as copper (0.8 mg/g), silver (2.2 mg/g), zinc (12 wt%), aluminum (10 wt%), and silicon (20 wt%) (Pagnanelli et al., 2017; Belsky et al., 2022). The range of available technologies for the production of photovoltaic modules is divided into three generations. First-generation photovoltaic modules contain crystalline silicon (c-Si), which can be monocrystalline or polycrystalline, and have efficiencies between 15% and 20%. Second-generation photovoltaic modules, which include amorphous thin-film silicon (a-Si), cadmium telluride (CdTe), multi-junction cells (a-Si-µc-Si), copper indium gallium diselenide (CIGS), and copper indium diselenide (CIS), are cheaper to manufacture than first-generation panels. However, their efficiencies are approximately 9% and 15% lower, respectively. Third-generation photovoltaic modules include concentrator photovoltaic (CPV) and emerging technologies such as dye-sensitized solar cells, organic solar cells, hybrid cells, passivated emitter back contact (PERC), and passivated emitter back local diffusion (PERL). They have higher efficiency but high manufacturing costs (Paiano, 2015, Xu et al., 2018; Rahman et al., 2021). Currently, the majority (around 90%) of worldwide production consists of crystalline silicon cells (first generation) (Sica et al., 2018). A PV module typically consists of tempered glass, an anti-reflective coating frame, a silicon layer, lamination material such as Ethylene Vinyl Acetate (EVA) (Sisanth, 2017), a back sheet, a junction box, and aluminum frame units. The typical structure of c-Si PV modules is shown in Figure 1 (Heath et al., 2020).

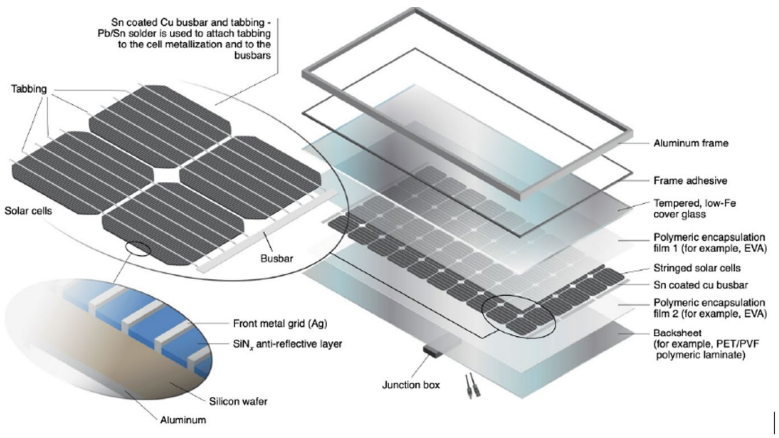


Figure 1. The typical structure of c-Si PV modules (Heath et al., 2020).

According to Radziemska (2014), crystalline silicon PV modules are manufactured from glass, aluminum frames, EVA (ethylene-vinyl acetate) copolymer transparent encapsulating layers,

photovoltaic cells, installation boxes, Tedlar protective foil, and mounting bolts, respectively. Metallic electrodes are placed on the front and back of the silicon cell. The front electrodes are typically made of silver, while the back electrodes are made of silver and aluminum (Pinho and Galdino, 2014). In this era of energy production, there has been a simultaneous rapid increase in the efficiency of solar modules. While the efficiency level used to be around 1%–5%, today there are different types of technologies with record efficiency levels of 20%–40.1% or even 47.1% achieved in solar modules (He et al., 2021; Geisz et al., 2020). Due to the faster and more feasible development of solar PV technologies compared to other renewable energy sources, the energy transition in terms of the 2030 and 2050 sustainability goals can be defined by solar energy.

2.1. Recycling of Waste Photovoltaic Modules

PV modules become solid waste (e-waste) at the end of their life. First-generation PV modules have a lifespan of about twenty years, and due to the growth of the solar industry, about one million tons of PV modules are expected to be disposed of in 2035 (International Energy Agency, 2013).There are several strategies to secure the silicon supply chain, which is the backbone of the PV industry. The European Union and global silicon supply chains aim to mitigate the risks associated with purchasing power and price fluctuations by reducing dependence on China and establishing supply chains with a lower carbon footprint. In this context, there is a particular need to strengthen silicon supply chains in Europe. The sourcing of raw materials and the development of advanced technologies capable of processing these materials play a critical role in supporting the circular economy.

In 2016, more than 45,000 tons of end-of-life PV modules were produced. Due to their limited lifespan of 25-30 years, photovoltaic waste will increase significantly, from 1.7 to 8 million tons by 2030 and from 60 to 78 million tons by 2050. The large number of end-of-life PV modules poses serious risks to the environment and human health (Xu et al., 2022; Weckend et al., 2016; Nain and Kumar, 2021). Moreover, recycling of these wastes is socially and environmentally negligible (Wang et al., 2023). In addition to these risks, it is also considered a source of raw materials for the recycling of Si and metals such as Ag, Cu, Pb, Al, and Sn (Xu et al., 2022; Jung et al., 2016; Chen et al., 2021).

The PV module recycling process begins with the removal of the EVA resin after the aluminum frame is separated. Chemical dissolution (nitric acid dissolution) and thermal decomposition (usually pyrolysis) are used to remove the sticky EVA layer. These processes allow for more efficient recovery of tempered glass, silicon cells, and copper strips (Xu et al., 2022; Bruton, 1994; Kim and Lee, 2012; Tammaro et al., 2015).

Several studies have been investigated to recover silicon, glass, and copper from PV modules. In the recycling of photovoltaic panels, many authors suggest different methods focusing on the recovery of precious metals and/or solar cells, divided into mechanical, chemical, and thermal processes (Lim et al., 2022).

The extraction of precious metals benefits from the use of material shredding techniques. Nevala et al. (2019) proposed electrohydraulic shredding (EHF) as an alternative to conventional shredding methods. They found that EHF reduces contamination and minimizes environmental impact compared to the residual dust produced by traditional shredding methods. In this approach, researchers place pieces of photovoltaic c-Si (12x18 cm) into a water-filled EHF reactor, where shock wave technology separates and fragments the photovoltaic layers while concentrating the target metals into specific particle sizes. This method has shown promise as a technique for preparing materials for subsequent precious metal extraction.

Kang et al. (2012) studied a three-stage recovery process to optimize the recovery of silicon and tempered glass from waste poly-silicon (p-Si) solar panels. They used toluene for organic solvent separation of tempered glass and PV cells. Toluene was found to effectively swell and dissolve EVA resin. As the temperature increased to 90 °C, it increased the swelling and dissolution rates of EVA and enabled the successful separation of tempered glass within 2 days. To clean the EVA, the swollen EVA resin was completely removed by heating at 600 °C in an argon atmosphere for 1 hour. This process prevented the carbonization of EVA, and clean PV cells were obtained. For the recovery of silicon and other metals, the clean PV cells obtained were subjected to etching in an acidic solution containing HF,

HNO_3, H_2SO_4, and CH_3COOH. The highest silicon yield of 86% was obtained with an etching time of 20 minutes and 20% surfactant. Surfactant was found to facilitate the removal of metal contaminants and increase the silicon yield. The purity of the recovered silicon was measured as 99.999%.

One way to recover various precious metals such as Ag, Si, and Al from photovoltaic c-Si is to combine different processes that help extract different metals. Dias R.P. et al. (2016) identified the materials used in photovoltaic panels and investigated techniques to separate these materials to enable recycling. They studied three different methods of component separation. Mechanical crushing, followed by sieving, and chemical separation with sulfuric acid allowed the separation of semiconductor materials by immersing the material in containers of 98% sulfuric acid for 5 days. They also suggested that pyrolysis before the separation of the material would degrade the EVA and reduce the toxicity of the chemical process by allowing the layers bound by the adhesive material to separate. Thermogravimetric analysis showed that all polymeric fractions present degraded at 773.15 ˚K.

Silver in solar cell modules is considered an important resource both economically and environmentally. In this study, the location and amount of silver in the modules were determined by various characterization methods and confirmed by X-ray fluorescence (XRF). The results show that the silver concentration in the modules is 0.0635%. Two different processes were evaluated for the extraction of silver; the first one is mechanical and hydrometallurgical (grinding and dissolution with nitric acid), while the second one aims to remove organic materials by adding a pyrolysis process. However, pyrolysis was found not to increase silver recovery and was found to be less efficient than conventional methods, with additional energy costs. These results show that silver can be effectively recovered by solubilization methods alone and emphasize that the recycling potential of solar panels represents a significant opportunity for the circular economy (Dias et al., 2016).

Lee et al. (2013) proposed a hydrometallurgical process for the recovery of silicon (Si), silver (Ag), and aluminum (Al) from waste silicon solar cells. Under optimal leaching conditions, 100% recovery of Al and Ag was achieved. Aluminum was recovered by crystallization from a leach solution with H2SO4 at 363.15 K. To recover silver from a leach solution with HNO_3 reagent, HCl was specifically used as a precipitant. Electrolysis was performed at different time intervals to recover some of the Ag by extracting the electrolyte at different temperatures. Then, part of the Ag-containing solution was taken and contacted with Zn plates and the exchange reaction was developed for 3 hours. Finally, 100% of the cadmium and precious metals were recovered in the silicon solution. It was concluded that these methods can be used to recover various precious metals from solar panels to achieve recycling targets.

High-voltage pulsed discharge technology was used as an environmentally friendly method for selective recovery of waste photovoltaic (PV) modules. As a result of the processes performed at 160 kV voltage, 300 pulse number, and 192.99 J/g energy consumption, PV modules were reduced to an average size of 4.1 mm. The results of the study showed that after the high-voltage pulsed shredding process, 95% of copper and 96% of silver were concentrated in particles smaller than 1 mm in diameter; 85% of aluminum, 85% of lead, and 87% of tin were collected in particles smaller than 0.5 mm in diameter. According to the results of another study, there are significant differences in the selectivity of different constituents during high-voltage pulsed comminution. These differences are due to the large variability in the dielectric constants of the materials. The selectivity of the materials is Ag > Si > glass, from high to low. High-value elements are generally concentrated in fine particles, and the purity of the comminuted products in the range of 0.5–4 mm reaches over 98%. These results indicate that high-voltage pulse technology can effectively separate and enrich waste PV modules, and this technology offers significant development prospects for harmless recycling processes (Wang et al., 2024; Song et al., 2020; Zhao et al., 2020).

The characterization of a crystalline solar panel was studied at ITU Mineral Processing Engineering Department (see Figure 2). The Al frame constitutes approximately 10% of the total weight. After the connection cables and Al frame were removed from the panel, size reduction processes were carried out. In size reduction processes, the entire material was reduced to -10 mm using the shredder. Sieve analysis was performed to determine the size distribution characteristics of the representative sample. The particle size distribution is given in Table 1 and the images of the products obtained by sieve analysis are given in Figure 3.



Figure 2. Solar panels used in the studies.

Table 1. Particle size distribution of the representative sample.

Size Fraction, mm	Amount, %	Σ Undersize, %
-10 + 5.60	14,3	100,0
-5.60 + 3.35	22,1	85,7
-3.35 + 2	26,4	63,6
-2 + 1	17,7	37,2
-1 + 0.5	8,6	19,5
-0.5 + 0.212	6,6	10,9
-0.212	4,3	4,3
Total	100,0	

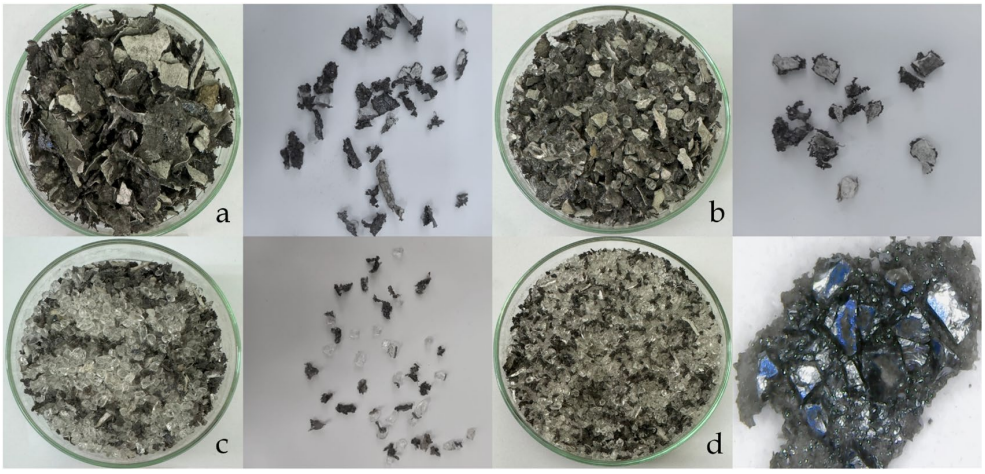


Figure 3. Images of the products obtained by a sieve analysis (a) -10+5.60 mm, b) -5.60+3.35 mm, c)-3.35+2 mm, d) -2+1 mm).

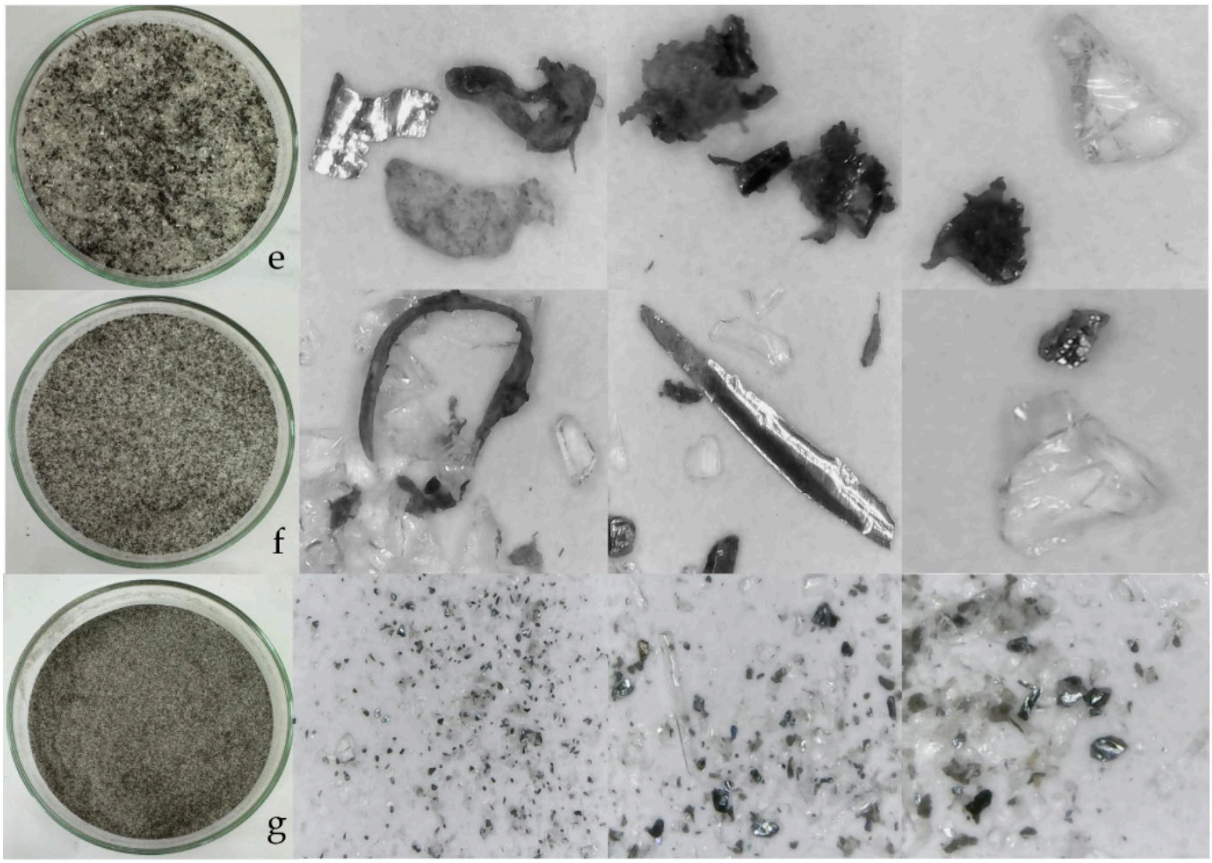


Figure 3. (continued) Images of the products obtained by sieve analysis (e) -1+0.5 mm, f) -0.5+0.212 mm, g)-0.212 mm).

According to the sieve analysis, the d_{80} size of the material was approximately 5 mm. When the images in Figure 3 are examined, it is seen that the components of solar panel particle liberation start to occur especially below 1 mm. With the size reduction process, it is seen that the glass part passes to fine fractions more easily.

Pasin (2013) proposed a glass recycling process for PV. Specifically, the PV is fed onto the conveyor belt and brought into the maneuvering zone created between two toothed rollers. These rotate in opposite directions, and when the end of the panel enters the working area, the rollers pull the whole panel (PF), where the teeth of the pair of rollers perform the first crushing operation, allowing the outer panel to separate. Thus the glass layer of the panel is removed, about 25-30% of the glass, then 70%, until the remaining glass is removed, causing a third crushing and separation of the outer glass layer of the panel.

Zambon and Cerchier (2022) proposed a combined method to economically separate glass from silicon and PV panels through mechanical separation and heat treatment. The PV panel was placed on a conveyor belt passing through an oven at a temperature above 773.15 ˚K, sufficient to break the insulating bond plates and the back sheet, and the glass was separated from the PV cells. After exiting the furnace, the glass is gravity-fed to the drop point. The falling process causes the glass (usually in pieces), metal contacts, and elements of the silicon photovoltaic cells to separate and fall into a collection bin with a grid at the top. The size range of this bin allows the passage of glass and silicon fragments but prevents the passage of metal contacts. At the bottom of the conveyor, due to the morphological difference between the parts and the fluid dynamic behavior, there must be some kind of medium that creates an airflow that allows the materials to pass into two separate compartments after the glass and silicon fall.

2.2. Challenges in Recycling Photovoltaic Panels

The photovoltaic panel industry is still an emerging sector, facing numerous challenges during the recycling stages. These challenges include the complexity of the methods used in the recycling process and the costs associated with the necessary equipment. Additionally, the economic value derived from recycled glass and polymers can often exceed the costs of the recycling process itself. The pyrolysis of polymers such as EVA can release toxic gases, posing risks to both environmental and human health. Technical difficulties related to the separation of materials and energy consumption are also significant hurdles (Wang et al., 2022; World Trade Report, 2021; Deng et al., 2019; Xu et al., 2018).

One of the most challenging aspects of this process is the reduction of the solar panel size due to the presence of polymers like EVA. While EVA provides flexibility to the panel, it can render shredding machines ineffective in reducing the size of the panels (Nain and Kumar, 2022). Selected studies propose various alternatives; however, it is essential to reduce the costs associated with this process by eliminating the need for high temperatures and other additives that make it more expensive. Developing specialized machinery for this task is a potential avenue for further research. Additionally, exploring the development of a more easily processed polymer type that could replace EVA may be a viable option (Isherwood, 2022).

Thermal processes, despite their high efficiency, are characterized by significant energy consumption and substantial environmental impacts, particularly in terms of air pollution. Consequently, hydrometallurgical methods present a considerable advantage. The use of more environmentally friendly solvents for the recovery of valuable metals from solar panels and minimizing the risk of contamination during the recycling process are among the primary challenges in hydrometallurgical processing. These green solvents have been utilized in other studies for the purification of ores and electronic waste, demonstrating promising dissolution efficiencies for successful application across various matrices.

One of the limitations of this analysis or review is the lack of detailed information from companies, which stems from the fact that their processes are currently of great interest as industrial secrets. This limitation constrains the analysis. Therefore, while some advancements in the research may be implemented or complemented by existing industrial-scale processes, the lack of information prevents more concrete recommendations for practical applications.

3. Conclusion

Most studies on photovoltaic (PV) panel recycling identify three main treatment types: mechanical, chemical, and thermal processes. Mechanical processing is particularly complex due to the flexibility of the panels, with techniques such as electrohydraulic fragmentation (EHF) and high-voltage fragmentation (HVF) being explored to reduce the size of PV components and achieve higher selectivity ratios in subsequent separation processes.

Chemical processes primarily involve dissolving EVA with specific reagents to recover valuable materials. While these methods can yield high recovery rates, the significant consumption of chemicals and the generation of liquid and gaseous waste complicate their industrial application and increase costs.

Thermal methods like pyrolysis can separate layered structures and facilitate EVA removal but produce undesirable gaseous byproducts, such as acetic acid and methane, which must be managed to minimize environmental impact.

Most patented technological advancements in PV recycling combine mechanical separation with chemical or thermal treatments. However, uncertainties arise from undisclosed aspects of these processes, as they are often treated as trade secrets. A major challenge in recycling is achieving sufficient particle liberation to effectively remove and separate EVA.

Given the expected increase in obsolete photovoltaic panels in the coming years, it is crucial to continue researching and patenting methods for PV recycling that minimize environmental and economic impacts while enhancing resource recovery.

Acknowledgment

We would like to express our sincere thanks to TÜMAKÜDER and Haşimoğlu Entegre Geri Dönüşüm Şirketi A.Ş. for their support in providing solar panels to the Istanbul Technical University Mineral Processing Engineering Department.

References

Andrea Pasin, A. (2013). "A method and machine to assist recycling of photovoltaic panels.," Available: https://patents.google.com/patent/WO2013057035A1/en

Belsky, A. A., Glukhanich, D. Y., Carrizosa, M. J., & Starshaia, V. V. (2022). Analysis of specifications of solar photovoltaic panels. *Renewable and Sustainable Energy Reviews*, *159*, 112239. doi: 10.1016/J.RSER.2022.112239.

Bruton, T. M. (1994). Re-cycling of high value, high energy content components of silicon PV modules. In *Proceedings of the 12^< th> EC Photovoltaic Solar Energy Conference* (pp. 303-304).

Cerchier, P., & Zambon, A. (2019). Method and plant for recycling photovoltaic panels. Available: https://patents.google.com/patent/WO2019087111A1/en

Chen, W. S., Chen, Y. J., Lee, C. H., Cheng, Y. J., Chen, Y. A., Liu, F. W., ... & Chueh, Y. L. (2021). Recovery of valuable materials from the waste crystalline-silicon photovoltaic cell and ribbon. *Processes*, *9*(4), 712. doi: 10.3390/pr9040712.

Deng, R., Chang, N. L., Ouyang, Z., & Chong, C. M. (2019). A techno-economic review of silicon photovoltaic module recycling. *Renewable and Sustainable Energy Reviews*, *109*, 532-550. https://doi.org/10.1016/j.rser.2019.04.020.

Dias, P. R., Benevit, M. G., & Veit, H. M. (2016). Photovoltaic solar panels of crystalline silicon: Characterization and separation. *Waste Management & Research*, *34*(3), 235-245. doi: 10.1177/0734242X15622812.

Dias, P., Javimczik, S., Benevit, M., Veit, H., & Bernardes, A. M. (2016). Recycling WEEE: Extraction and concentration of silver from waste crystalline silicon photovoltaic modules. *Waste management*, *57*, 220-225.

Fuso Nerini, F., Tomei, J., To, L. S., Bisaga, I., Parikh, P., Black, M., ... & Mulugetta, Y. (2018). Mapping synergies and trade-offs between energy and the Sustainable Development Goals. Nature Energy, 3(1), 10-15.

Geisz, J. F., France, R. M., Schulte, K. L., Steiner, M. A., Norman, A. G., Guthrey, H. L., ... & Moriarty, T. (2020). Six-junction III–V solar cells with 47.1% conversion efficiency under 143 Suns concentration. *Nature energy*, *5*(4), 326-335.

He, X., Chen, J., Ren, X., Zhang, L., Liu, Y., Feng, J., ... & Liu, S. (2021). 40.1% record low-light solar-cell efficiency by holistic trap-passivation using micrometer-thick perovskite film. *Advanced Materials*, *33*(27), 2100770.

Heath, G. A., Silverman, T. J., Kempe, M., Deceglie, M., Ravikumar, D., Remo, T., ... & Wade, A. (2020). Research and development priorities for silicon photovoltaic module recycling to support a circular economy. *Nature Energy*, *5*(7), 502-510.

Hirsch, R. L., Bezdek, R., & Wendling, R. (2007). Peaking of world oil production and its mitigation. In *Driving climate change* (pp. 9-27). Academic Press.

International Energy Agency (2013). Photovoltaic Power Systems Programme – Trends 2013 in Photovoltaic Applications.

IRENA (2016). End-Of-Life Management: Solar Photovoltaic Panels. International Renewable Energy Agency and the International Energy Agency Photovoltaic Power Systems.

Isherwood, P. J. (2022). Reshaping the module: the path to comprehensive photovoltaic panel recycling. *Sustainability*, *14*(3), 1676. doi: 10.3390/SU14031676.

Jung, B., Park, J., Seo, D., & Park, N. (2016). Sustainable system for raw-metal recovery from crystalline silicon solar panels: from noble-metal extraction to lead removal. *ACS Sustainable Chemistry & Engineering*, *4*(8), 4079-4083. doi: 10.1021/ acssuschemeng.6b00894

Kang, S., Yoo, S., Lee, J., Boo, B., & Ryu, H. (2012). Experimental investigations for recycling of silicon and glass from waste photovoltaic modules. *Renewable Energy*, *47*, 152-159.

Kim, Y., & Lee, J. (2012). Dissolution of ethylene vinyl acetate in crystalline silicon PV modules using ultrasonic irradiation and organic solvent. *Solar energy materials and solar cells*, *98*, 317-322. doi: 10.1016/j.solmat.2011.11.022.

Klugmann-Radziemska, E. (2014). *Recycling of Photovoltaic Solar Cells and Modules-Te State-of-Art* (pp. 1-53). Lambert Academic Publishing.

Kokul, S. R., & Bhowmik, S. (2021). Recycling of crystalline silicon photovoltaic solar panel waste to modified composite products. *Progress in Rubber, Plastics and Recycling Technology*, *37*(4), 327-339.

Lee, C. H., Hung, C. E., Tsai, S. L., Popuri, S. R., & Liao, C. H. (2013). Resource recovery of scrap silicon solar battery cell. *Waste management & research*, *31*(5), 518-524. doi: 10.1177/0734242X13479433.

Louwen, A., Van Sark, W. G. J. H. M., Schropp, R. E. I., Turkenburg, W. C., & Faaij, A. P. C. (2015). Life-cycle greenhouse gas emissions and energy payback time of current and prospective silicon heterojunction solar cell designs. *Progress in Photovoltaics: Research and Applications*, *23*(10), 1406-1428. doi: 10.1002/PIP.2540.

Morseletto, P. (2020). Targets for a circular economy. *Resources, conservation and recycling*, *153*, 104553.

Nain, P., & Kumar, A. (2021). Understanding metal dissolution from solar photovoltaics in MSW leachate under standard waste characterization conditions for informing end-of-life photovoltaic waste management. *Waste Management*, *123*, 97-110. doi: 10.1016/j.wasman.2021.01.013

Nain, P., & Kumar, A. (2022). A state-of-art review on end-of-life solar photovoltaics. *Journal of Cleaner Production*, *343*, 130978. doi: 10.1016/J.JCLEPRO.2022.130978.

Nevala, S. M., Hamuyuni, J., Junnila, T., Sirviö, T., Eisert, S., Wilson, B. P., ... & Lundström, M. (2019). Electro-hydraulic fragmentation vs conventional crushing of photovoltaic panels–Impact on recycling. *Waste management*, *87*, 43-50. doi: 10.1016/J.WASMAN.2019.01.039.

Opeyemi, B. M. (2021). Path to sustainable energy consumption: The possibility of substituting renewable energy for non-renewable energy. *Energy*, *228*, 120519.

Pagnanelli, F., Moscardini, E., Granata, G., Atia, T. A., Altimari, P., Havlik, T., & Toro, L. (2017). Physical and chemical treatment of end of life panels: An integrated automatic approach viable for different photovoltaic technologies. *Waste management*, *59*, 422-431. doi: 10.1016/J.WASMAN.2016.11.011.

Paiano, A. (2015). Photovoltaic waste assessment in Italy. *Renewable and Sustainable Energy Reviews*, *41*, 99-112.

Pastuszak, J., & Węgierek, P. (2022). Photovoltaic cell generations and current research directions for their development. *Materials*, *15*(16), 5542.

Pinho, J. T., & Galdino, M. A. (2014). Engineering manual for photovoltaic systems retrieved from Rio de Janeiro: CEPEL—CRESESB. *Manual de engenharia para sistemas fotovoltaicos*, 14.

Rahman, M. M., Khan, I., & Alameh, K. (2021). Potential measurement techniques for photovoltaic module failure diagnosis: A review. *Renewable and Sustainable Energy Reviews*, *151*, 111532. doi: 10.1016/J.RSER.2021.111532.

Sah, D., Chitra, Lodhi, K., Kant, C., Srivastava, S. K., & Kumar, S. (2022). Extraction and analysis of recovered silver and silicon from laboratory grade waste solar cells. *Silicon*, *14*(15), 9635-9642. doi: 10.1007/S12633-022-01715-505 6.

Sica, D., Malandrino, O., Supino, S., Testa, M., & Lucchetti, M. C. (2018). Management of end-of-life photovoltaic panels as a step towards a circular economy. *Renewable and Sustainable Energy Reviews*, *82*, 2934-2945.

Sisanth, K. S., Thomas, M. G., Abraham, J., & Thomas, S. (2017). General introduction to rubber compounding. In *Progress in rubber nanocomposites* (pp. 1-39). Woodhead Publishing.

Song, B. P., Zhang, M. Y., Fan, Y., Jiang, L., Kang, J., Gou, T. T., Zhang, C.L., Yang, N., Zhang, G.J., Zhou, X. (2020). Recycling experimental investigation on end of life photovoltaic panels by application of high voltage fragmentation. Waste Management, 101, 180-187. doi: 10.1016/j.wasman.2019.10.015.

Tammaro, M., Rimauro, J., Fiandra, V., & Salluzzo, A. (2015). Thermal treatment of waste photovoltaic module for recovery and recycling: Experimental assessment of the presence of metals in the gas emissions and in the ashes. *Renewable Energy*, *81*, 103-112. doi: 10.1016/j.renene.2015.03.014

Wang, J., Feng, Y., & He, Y. (2024). The research progress on recycling and resource utilization of waste crystalline silicon photovoltaic modules. *Solar Energy Materials and Solar Cells*, *270*, 112804.

Wang, X., Tian, X., Chen, X., Ren, L., & Geng, C. (2022). A review of end-of-life crystalline silicon solar photovoltaic panel recycling technology. *Solar Energy Materials and Solar Cells*, *248*, 111976.

Wang, X., Xue, J., & Hou, X. (2023). Barriers analysis to Chinese waste photovoltaic module recycling under the background of" double carbon". *Renewable Energy*, *214*, 39-54.

Weckend, S., Wade, A., & Heath, G. A. (2016). *End of life management: solar photovoltaic panels* (No. NREL/TP-6A20-73852; T12-06: 2016). National Renewable Energy Laboratory (NREL), Golden, CO (United States).

World Trade Organization (2021). Economic Resilience and Trade. https://www.wto.org/english/res_e/booksp_e/wtr21_e/00_wtr21_e.pdf.

Xu, X., Lai, D., Wang, W., & Wang, Y. (2022). A systematically integrated recycling and upgrading technology for waste crystalline silicon photovoltaic module. *Resources, Conservation and Recycling*, *182*, 106284.

Zhao, P., Guo, J., Yan, G., Zhu, G., Zhu, X., Zhang, Z., & Zhang, B. (2020). A novel and efficient method for resources recycling in waste photovoltaic panels: High voltage pulse crushing. *Journal of Cleaner Production*, *257*, 120442. doi: 10.1016/j.jclepro.2020.120442.

Efficient Photocatalytic Degradation of Textile Dye Contaminants Using Novel Materials: Thermally Exfoliated Boron Doped Graphitic Carbon Nitride

Haldun Kurama [1]*, Halit Levent Hoşgün [2], Ayşe Gül Türe [2]

[1] Eskişehir Osmangazi University, Mining Engineering Department, Eskişehir-Türkiye

[2] Bursa Technical University, Department of Chemical Engineering, Bursa Türkiye

*Corresponding author: hkurama@ogu.edu.tr (Haldun Kurama)

Abstract:

In this study, the basic features of the environmentally friendly Photocatalytic method are briefly reviewed within the scope of sustainable water management in order to prevent the increasing threat to wastewater as a result of the increased use of dyestuffs in the textile industry.

As an example application, a mixture of boron-doped, thermally exfoliated g-C3N4 photocatalyst, melamine and boron oxide was synthesized. For the synthesis process, the bulk g-C3N4 catalyst obtained by heating melamine at 600 C for 4 hours with a heating rate of 10 C/min was then thermally exfoliated by mixing with boric acid The structure of the prepared samples was analyzed by X-ray diffraction (XRD and N2 adsorption-desorption isotherms (BET)). The results obtained clearly showed the positive effects of the exfoliation process compared to the bulk sample.

Keywords: *Wastewater, Photocatalysis, g-C3N4, Boron*

1. Introduction

In recent years, globalization, technological advances, combined with people's evolving fashion preferences have contributed significantly to the increase in textile and clothing production. Textile industry products such as fabrics, clothing, and home furnishings are an indispensable part of the modern world. Textile products undergo numerous chemical processes from raw materials to final products. Dying, bleaching, mercerization, and finishing can be given as an example of most used chemical processes. Most of them consume large amounts of water and produce wastewater (Khanzada et al. 2020; Holkar et al. 2016). The most important organic matter in these wastewaters is dyestuffs. These dyestuffs have negative effects on the environment and human health. Numerous studies have been conducted on the treatment of textile wastewater and this issue still maintains its importance. Numerous treatment methods, including physical, chemical, and biological, have been the subject of these studies. The method selection depends on the characteristics of textile wastewater and industrial processes. Coagulation, electrocoagulation, adsorption, photocatalysis, ion exchange, microwave irradiation, ozonation, membrane separation, Fenton oxidation, sonication, and bioremediation methods are recommended as a treatment option for textile wastewater. (Abdelshafi and Sadik 2021; Ahmed et al. 2022)

Photocatalytic methods are one of the advanced oxidation processes used in textile wastewater treatment. In a broader sense, advanced oxidation processes encompass a set of photocatalytic chemical reactions that produce highly reactive species. These reactive species can rapidly react with or degrade any organic species (pollutant/contaminant) present in water. In the presence of ultraviolet (UV) or visible light, magnetic nanocomposites, additive nanocomposites, polymer-based nanocomposites, and heterojunction photocatalysts are used to produce highly reactive species that can degrade and remove pollutants. Photocatalysis is a process involving the formation of electron-hole pairs and the participation of this pair in the reaction. Semiconductor nanomaterials in particular have the potential for new applications related to dye degradation. In the photocatalytic degradation process, there are various factors affecting the performance, such as the light source, the nature of the effluent, the type of

photocatalyst, the semiconductor, the pathway, the reactor accessories, and the additives. Photocatalysts with narrow band gaps absorb more photons of visible light. How the reactor design separates the photogenerated electrons is also important because the bulk recombination of charge carriers reduces catalyst efficiency. Once successfully separated, these charge carriers can directly reduce/oxidize the pollutants or form various reactive species that then accelerate the pollutant degradation process. For example, free electrons can directly generate hydroxyl radicals or oxygen can absorb free electrons to form superoxide radicals (O_2^-), which eventually convert to hydroxyls. (Bhatkhande et al. 2002; Gaya et al. 2008)

One of the most important application parameters in photocatalytic purification processes is the use of the appropriate reactive matter. In this context graphitic carbon nitrides for photocatalytic oxidation have become attractive new photocatalyst candidates in recent years. g-C_3N_4 has a layer-by-layer structure and these layers are connected by van der Waal force. g-C_3N_4 crystal structure is an N-substituted graphite framework consisting of conjugated graphite planes, each plane consists of nitrogen and carbon alternately bonded by sp2 hybridization. (Yang et al. 2020). Due to its medium band gap structure, numerous studies have been conducted in the literature on the synthesis and application of graphitic carbon nitride (g-C_3N_4) as a environmental safe metal-free catalyst. Graphitic carbon nitride, generally known as g-C_3N_4, is considered the most stable allotrope among various carbon nitrides under ambient conditions. Melon is a linear polymer consisting of interconnected components. tri-s-triazines are in the form of 2D sheets consisting of tri-s-triazines connected to each other via secondary nitrogens, and g-C_3N_4 is in the form of tertiary amines via tri-s-triazines. (Paul and Nehra, 2021) In particular, the use of g-C_3N_4 for photocatalysis was first reported by Wang et al. for water splitting as a visible light photocatalytic method. Unlike TiO2, which is only active in the UV region, g-C_3N_4 has a band gap of approximately 2.7 eV. This makes it a visible light active photocatalyst for a range of reactions. Graphite carbon nitride can be made by polymerization of urea, cyanamide, dicyandiamide, or melamine. The initial polymeric g-C_3N_4 structure leads to more condensed and less defective g-C_3N_4 species based on tri-s-triazine (C_6N_7) units as basic building blocks by calcination. The electrons generated by photoexcitation in g-C_3N_4 exhibited a higher thermodynamic potential to facilitate the reduction of various organic compounds to H_2O and CO_2. g-C_3N_4 can be prepared by various methods such as thermal polymerization, solvothermal, template-assisted, sol-gel methods, and green synthesis. The thermal polymerization method is the most widely used in the preparation of g-C_3N_4 because it requires a simple and easy technology. (pattanayak, 2022) The most commonly used organic precursors in the synthesis of g-C_3N_4 are urea, melamine, thiourea, cyanamide, dicyandiamide, etc. The bulk g-C_3N_4 has several disadvantages such as limited specific surface area and accelerated recombination rate. There are reports in the literature that the photocatalytic performance of bulk g-C_3N_4 is increased by making composites with metal oxides, quantum dots, and heterojunction structures. Therefore, exfoliation of g-C_3N_4 by physical methods (e.g. heat treatment) or chemical methods (e.g. acid etching) is an attractive option to improve its photocatalytic performance, mainly by this and by increasing its surface area through the formation of porous structures. Among these, thermal exfoliation is the most environmentally friendly option currently being researched. (Bhanderi et al. 2023). In this study, based on these applications suggested in the literature, two different reagents, namely bulk and exfolied form, were synthesized and the advantages of the exfoliation application were compared with the characterization tests performed on the final material properties.

2. Materials and Methods

The melamine used in this study is 99% pure (CAS 108-78-1) and Methylene blue is a Merck brand. Protherm brand muffle furnace was used in g-C_3N_4 production experiment. The bulk g-C_3N_4 catalyst obtained by heating melamine at 600 ^oC for 4 hours with a heating rate of 10 C/min was then thermally exfoliated by mixing with boric acid.

3. Results

The XRD analysis of bulk and thermally exfoliated g-C_3N_4 are shown in Fig. 1 a and b

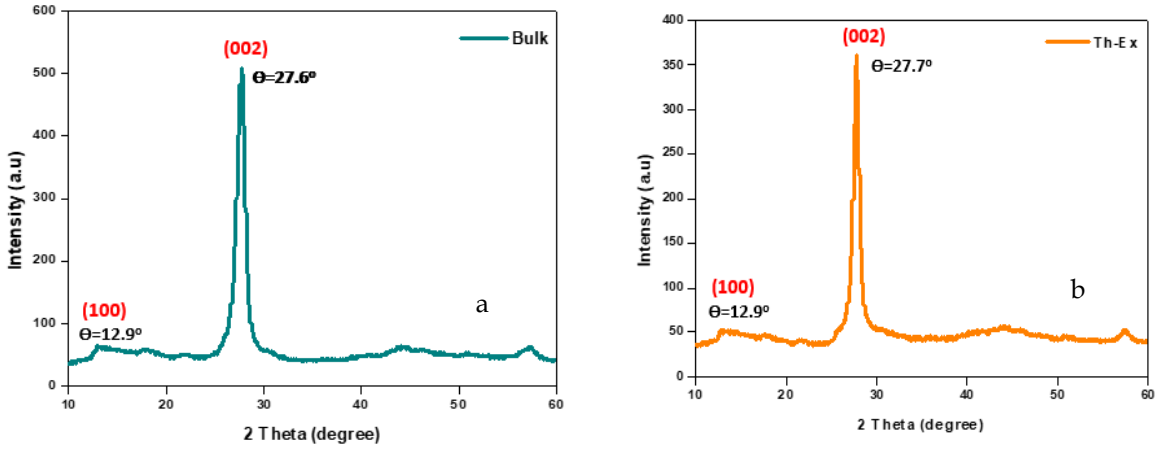


Fig 1 XRD patterns of a) Bulk and b) thermally exfoliated g-C_3N_4

XRD patterns show peaks around 13.1 (100) and 27.4 (002) as characteristic peaks of g-C_3N_4. These results clearly confirmed that the bulk material properties are preserved after the exfoliation process.

Textural properties of the catalysts are listed in Table 1. When the results are examined, it can be suggested that the significant increase on surface area can be obtained by surface activation (88.877 m^2/g) compared to the bulk catalyst (14.95 m^2/g), which clearly shows the effect of the exfoliation process. Similarly, Pore volume increases from 0.123 m^3/g to 0.478 m^3/g.

Table 1 Surface area, pore volume and pore size of catalysts.

Catalysts	**Surface Area (m^2/g)**	**Pore Volume (cm^3/g)**	**Pore Size (Å)**
Bulk g-C_3N_4	14,955	0,123	431,44
Th-Ex g-C_3N_4	88,877	0,478	265,97

References

Khanzada H, Khan MQ, Kayani S (2020) Cotton Based Clothing. pp 377–391. https://doi.org/10.1007/978-981-15-9169-3_15

Holkar CR, Jadhav AJ, Pinjari DV et al (2016) A critical review on textile wastewater treatments: possible approaches. J Environ Manag 182:351–366. https://doi.org/10.1016/j.jenvman.2016.07.090.

Abdelshafi NS, Sadik MA (2021) Environment-friendly processes: electrocoagulation and activated carbon filtration for reuse of textile wastewater. Egypt J Chem 64:3997–4003. https://doi.org/10.21608/ejchem.2021.63363.3358

Ahmed FS, Alsaffar MA, AbdulRazak AA (2022) One-step synthesis of magnetic fly ash composites for methylene blue removal: batch and column study. Environ Sci Pollut Res. https://doi.org/10.1007/s11356-022-23491-x

Bhatkhande, D. S.; Pangarkar, V. G.; Beenackers, A. A. C. M. Photocatalytic degradation for environmental applications–a review. Journal of Chemical Technology & Biotechnology: International Research in Process, Environmental & Clean Technology 2002, 77 (1), 102– 116, DOI: 10.1002/jctb.532

Gaya, U. I.; Abdullah, A. H. Heterogeneous photocatalytic degradation of organic contaminants over titanium dioxide: a review of fundamentals, progress and problems. Journal of photochemistry and

photobiology C: Photochemistry reviews 2008, 9 (1), 1– 12, DOI: 10.1016/j.jphotochemrev.2007.12.003

Yang Y., X. Li, C. Zhou, W. Xiong, G. Zeng, D. Huang, C. Zhang, W. Wang, B. Song, X. Tang, X. Li, H. Guo, Recent advances in application of graphitic carbon nitride-based catalysts for degrading organic contaminants in water through advanced oxidation processes beyond photocatalysis: a critical review, Water Res., 184 (2020), Article 116200, 10.1016/j.watres.2020.116200

Paul D.R., Nehra S.P. Graphitic carbon nitride: a sustainable photocatalyst for organic pollutant degradation and antibacterial applications, Environ. Sci. Pollut. Res., 28 (2021), pp. 3888-3896, 10.1007/s11356-020-09432-6

Pattanayak D.S., D. Pal, J. Mishra, C. Thakur, Noble metal–free doped graphitic carbon nitride (g-C3N4) for efficient photodegradation of antibiotics: progress, limitations, and future directions, Environ. Sci. Pollut. Res. (2022), 10.1007/s11356-022-20170-9

Bhanderi D., P. Lakhani, C.K. Modi Graphitic carbon nitride (g-C3N4) as an emerging photocatalyst for sustainable environmental applications: a comprehensive review RSC Sustain, 2 (2023), pp. 265-287, 10.1039/d3su00382e

Physico-Chemical Bases of Selective Extraction of Metals from Dust Concentrate of Blast Furnaces by Organic Acids. I. General conception

Vitaly Prokopenko [1], Volodymyr Chernenko [1], Olena Tsyganovich [1], Igor Volobaiev [1]

[1] F.D. Ovcharenko Institute of Biocolloid Chemistry, National Academy of Sciences of Ukraine, 42 Vernadsky av., 03142 Kyiv, Ukraine

*Corresponding author: chvy039@gmail.com (Volodymyr Chernenko)

Abstract:

The dust concentrate of the metallurgical enterprise "Arselor Mital Galati" (Romania) was chosen as the object of the study - a typical industrial waste of metallurgical production. Special attention was focused on the extraction of iron, from which it is possible to obtain commercially significant products, and on the extraction of heavy metals - zinc and lead. Considering the fact that the annual accumulation of dust waste from one blast furnace is about 300 thousand tons, there is no doubt in the logical conclusion about the practical value of such research. According to the obtained data of X-ray fluorescence and X-ray phase analyzes of dust concentrate samples, it is clear that its composition includes a significant number of chemical elements. Among the metals, iron (16.1 wt.%) and zinc (2.2 wt.%) are the most common. According to the mineral-phase analysis, the main mineral phases in the dust concentrate are: amorphous carbon (32.78%), iron oxides (II, III) – hematite (aFe_2O_3), magnetite ($FeFe_2O_4$), goethite ($aFeO(OH)$) and reduced iron (^0Fe) (total 23.01%), silicon oxide (7.39%) and calcium sulfate (4.25%). Attention is also drawn to the phases from which zinc can be extracted - zinc oxide (ZnO) and reduced fine-dispersed zinc (^0Zn), which make up a total of 2.73%. Some concern is the high content of toxic compounds such as lead oxide (0.8%), manganese (IV) oxide (0.63%) and arsenic (V) oxide (0.03%), which requires additional measures to prevent pollution environment by these elements. The average content of cobalt, copper and cadmium oxides is: CoO - 0.025%, CuO - 0.012%, CdO - 0.011%, the preparative extraction of which is not commercially profitable. The criterion for the selection of technology for processing dust concentrate was its chemical composition.

Keywords: *metallurgical wastes proceeding, dust concentrate leaching, acetic acid, lactic acid, oxalic acid*

1. Introduction

The main goal of this study was to find possible options for implementing the principles of modern "green chemistry" in the field of disposal of toxic waste from the metallurgical industry, namely, the use of organic acids produced by microorganisms and which can be obtained from renewable raw materials (from plant biomass) on an industrial scale. The latter include, first of all, such organic acids as acetic, lactic, and oxalic. All these acids belong to the class of carboxylic protogenic acids, which are capable of actively interacting under certain conditions with metals, and oxalic acid - selectively with iron oxides (FeO, Fe_2O_3) (Campbell, 1970). Since dust emissions from blast furnaces contain a fairly high concentration of finely dispersed metals and their oxides, the selection of the research object was focused on this material. In addition, we would like to draw the attention of the management of metallurgical enterprises to the fact that dust concentrates are an economically attractive off-balance sheet raw material for the repeated extraction of iron and other metals (for example, zinc). In our previous publication (Prokopenko et al., 2019), we reported on one of the possible methods of disposal of dusty waste from blast furnace gases of metallurgical production - by the method of regenerative roasting at temperatures of 750 °C.

2. Theory

2.1. The mechanism of formation of dust particles during the blast furnace processes

Dust concentrate is formed during metallurgical processes, in particular in the blast furnace, and is a material that is formed in the process of cooling and filtering waste gases (Coudurier et al., 1985; Campbell, 1970]. Modern metallurgical processes are based not only on the processing of natural ores, but also on the processing of a significant amount (up to 30%) of secondary iron-containing raw materials. A significant amount of the latter is made up of secondary materials, which contain, in addition to iron and its compounds, also non-ferrous metals, the overwhelming majority of which is zinc, much less tin, nickel, chromium and others. Taking into account the fact that the temperature regime in modern metallurgical processes reaches 1500 $^{\circ}C$ and higher, the gases formed (Table 1) initially contain vapor or a liquid phase - aerosols of the corresponding non-ferrous metals, and as they cool - their condensed phases.

Table 1. Composition of blast furnace gases

Type of metallurgical product	Contents, %				
	CO_2	CO	CH_4	H_2	N_2
Pig iron	12 - 18	24 - 30	0,2 – 0,5	1,0 – 2,5	55 - 59
Cast iron	8 - 14	28 - 32	0,2 – 0,5	1,5 – 3,0	56 - 59
Ferroalloys	4 - 8	31 - 35	0,2 – 0,5	2,0 – 3,5	56 - 59

As can be seen from Table 1, the amount of CO_2 and CO in its mass can total up to 48%, other reactive gases make up an insignificant share. Moreover, the amount of CO, as a rule, almost doubles the amount of CO_2. As is known, under the described conditions, the Boudoir reaction occurs in smoke emissions (Berdnikov and Gudim, 2020; Campball, 1970; Lapidus et al., 2011):

$$2CO \leftrightarrow \overset{0}{C} + CO_2 \ (\Delta H^0_{298} = -172{,}5 kJ \cdot mol^{-1}), \quad (1)$$

because at a temperature of about 872 °C, this disproportionation reaction has an unhindered course in the direction of the formation of a condensed phase of carbon ($\overset{0}{C}$), which, according to our data, makes up a fairly significant share (32.78 mass%) in the composition of the dust concentrate. Subsequently, at a temperature of condensation of zinc vapor to the liquid state under normal pressure is about 906 °C, and to the metallic state - about 420 °C. For tin, the solid phase formation temperature is 232 °C, for nickel 1455 °C. Therefore, dispersed particles (condensed phases) of the corresponding metals are formed in the waste gases that have a temperature at the exit from the melting furnace of 300-600 °C, and then - with a decrease in temperature to the temperature of the surrounding environment (~25 °C). Moreover, the process of phase formation depending on the gas flow rate, local concentrations of vapors of the corresponding metals, as well as, in different temperature zones, determines the dispersion of the formed phases, as evidenced by light stereomicroscopy (Fig. 2) and electronic images (Fig. 3). As can be seen from them, the dust concentrate contains polydisperse particles carbon phase with a "de novo" iron particles formed on its surface - from nanosized, less than 100 nm (Fig.3a), to quite voluminous - up to 100 μm phases (Fig.3b). The chemical composition of an individual particle at the point marked in Fig. 3b as "+1" is given in Table 2. The main element of this metal phase is iron (98.92%).

2.2. Redox reactions of the blast furnace process that generate finely dispersed particles of dust waste

The process that takes place in the conditions of a working blast furnace, that is, at a high temperature (1500 °C), is accompanied by the formation of liquid iron ($\overset{0}{Fe}$) and zinc ($\overset{0}{Zn}$), liquid slag - calcium silicate ($CaSiO_3$), and gaseous carbon oxide (IV) and carbon oxide (II) (Kovzun et al., 2007). At the same

time, a cascade of redox reactions takes place with the participation of carbon and mineral phases present in the dust waste:

$$\overset{+2}{Fe}O\cdot\overset{+3}{Fe}_2O_3 + 4SiO_2 + 10\overset{0}{C} + CaCO_3 \xrightarrow{T,1800\,^\circ C,+20e^-}$$

magnetite

$$3\overset{0}{Fe}\overset{0}{Si} + \mathrm{CaSi}O_3 + 10\overset{+2}{C}O\uparrow + CO_2\uparrow$$

ferrosilicon , (2)

$$\overset{0}{C} + \overset{0}{O}_2\uparrow \xrightarrow{T,1500\,^\circ C,-4e^-} \overset{+4}{C}\overset{-2}{O}_2\uparrow , \quad (3)$$

$$\overset{+4}{C}\overset{-2}{O}_2\uparrow + \overset{0}{C} \xrightarrow{T,1500\,^\circ C,+2e^-} 2\overset{+2}{C}\overset{-2}{O}\uparrow , \quad (4)$$

$$3\overset{+3}{Fe}_2O_3 + \overset{+2}{C}O\uparrow \xrightarrow{T,1500^\circ C,+2e^-} 2\overset{+2}{Fe}O\cdot\overset{+3}{Fe}_2O_3 + \overset{+4}{C}O_2\uparrow$$

hematite *magnetite* , (5)

$$\overset{+2}{Fe}O\cdot\overset{+3}{Fe}_2O_3 + \overset{+2}{C}O\uparrow \xrightarrow{T,1500\,^\circ C,+2e^-} 3\overset{+2}{Fe}O + \overset{+4}{C}O_2\uparrow$$

magnetite *iron (II) oxide* , (6)

$$\overset{+2}{Fe}O + \overset{+2}{C}O\uparrow \xrightarrow{T,1500^\circ C,+2e^-} \overset{0}{Fe} + \overset{+4}{C}O_2\uparrow , \quad (7)$$

$$\overset{+3}{Fe}_2O_3 + 3\overset{0}{C} \xrightarrow{T,1500\,^\circ C,+6e^-} 2\overset{0}{Fe} + 3\overset{+2}{C}O\uparrow , \quad (8)$$

$$\overset{+2}{Zn}O_{(solid)} + \overset{0}{C} \xrightarrow{T,750\,^\circ C,+2e^-} \overset{0}{Zn}_{(liquid)} + \overset{+2}{C}O\uparrow , \quad (9)$$

In addition, during reduction firing, amorphous carbon ($\overset{0}{C}$) can interact with silica (SiO_2), forming elemental silicon ($\overset{0}{Si}$) and silicon oxide (II) (SiO):

$$\overset{+4}{Si}O_2 + 2\overset{0}{C} \xrightarrow{T,1500\,^\circ C,+4e^-} \overset{0}{Si} + 2\overset{+2}{C}O\uparrow , \quad (10)$$

$$\overset{+4}{Si}O_2 + \overset{0}{C} \xrightarrow{T,1500\,^\circ C,+2e^-} \overset{+2}{Si}O + \overset{+2}{C}O\uparrow . \quad (11)$$

In turn, the products of reactions (10) and (11), actively interact with reduced iron ($\overset{0}{Fe}$) - the product of reactions (7) and (8), forming a new product - ferrosilicon ($\overset{0}{Fe}\overset{0}{Si}$), in which both iron and silicon have an oxidation state of "0" (Campbell, 1970):

$$\overset{0}{Fe} + 2\overset{+2}{Si}O \xrightarrow{T,2000\,^\circ C,-2e^-} \overset{0}{Fe}\overset{0}{Si} + \overset{+4}{Si}O_2 . \quad (12)$$

The final reaction of the process of reductive burning of iron (III) oxide in dust concentrate has the following form:

$$\overset{+3}{Fe}_2O_{3(solid)} + 3\overset{+2}{C}O\uparrow \xrightarrow{T,1500\,^\circ C,+6e^-} 2\overset{0}{Fe}_{(liqud)} + 3\overset{+4}{C}O_2\uparrow . \quad (13)$$

In addition, it is worth adding that carbon itself ($\overset{0}{C}$), as a reducing agent, is not very effective, since both it and iron oxide are solid phases, and the contact between them is not very effective. Therefore, carbon is effective only in combination with oxygen (O_2) in the combustion process (with oxygen blowing). At the same time, carbon oxides are formed, first - $\overset{+4}{C}O_2$, then - $\overset{+2}{C}O$. It is gaseous carbon dioxide (II) at a high temperature (1500 $^\circ C$) that provides rapid reduction to (reactions 5, 6, 7). From the point of view of the expediency of applying the preliminary thermochemical recovery of the carbon-containing composite, the fact that the newly formed Iron phases ($\overset{0}{Fe}$) and Zink phases ($\overset{0}{Zn}$) - the product of reactions (7), (8), (13), and (9), respectively - is quite actively involved in the redox reaction with molecules of organic acids – acetic, lactic, and oxalic, both in aqueous and non-aqueous solutions.

2.3. Selective leaching of metal phases and oxides of non-ferrous metals

2.3.1. Regenerative roasting of dust concentrate

From the metallurgical point of view, we consider dust waste stored in thousand-ton tailings dumps of metallurgical enterprises as secondary raw materials suitable for the extraction of metals - iron, zinc, lead, manganese, molybdenum and other useful elements. Reductive roasting of dust concentrate is a mandatory process for its preparation for subsequent enrichment by hydrometallurgical processing. In this case, three main goals are pursued: removal of unwanted impurities (primarily amorphous carbon and silicon oxide), change of mineralogical composition and conversion of iron oxides into magnetic form for its subsequent extraction (enrichment) by magnetic separation (Shumakov, et al., 2007). In order to ensure the metallurgical value of the dust concentrate, taking into account the classification of ores by iron content: rich (60 - 65%), medium (45 - 60%) and poor (less than 45%), implementing such processes as preliminary roasting and magnetic separation of the iron-containing fraction, it is possible to obtain a substance containing about 70% of iron in the form of its oxides - $FeO\cdot Fe_2O_3$ and $Fe_2O_3\cdot nH_2O$. In order to correctly perform the procedures for extracting the target elements (Iron (III) and Zinc) from the dust concentrate, we performed several options for pre-treatment of the samples with the aim of maximally effective separation and concentration of iron-containing and zinc-containing phases. The expediency of using the restorative roasting of the dust concentrate in order to pre-enrich the content of the metal phases ($\overset{0}{Zn}$, $\overset{0}{Pb}$, $\overset{0}{Mo}$, etc.) in it and to ensure the maximum extraction of iron and other non-ferrous metals from the waste (out-of-balance metal source) is due to the fact that the concentrate contains 32.78% of amorphous carbon ($\overset{0}{C}$), which can be used as an effective pyrometallurgical reducer of Zinc oxides, Lead and Molybdenum (Coudurier et al., 1985).

2.3.2. Leaching with organic acids

2.3.2.1. Leaching of the non-magnetic fraction with weak acids

The mechanism of leaching of metal phases of dust waste by weak organic acids is basically the same as that of strong mineral acids (for example, sulfuric, nitric or hydrochloric). And even such a weak acid as acetic acid is capable of leaching active metals with the formation of acetate and hydrogen gas:

$$\overset{0}{Mg} + 2CH_3COO\overset{+1}{H} \xrightarrow{T,-2e^-} \overset{+2}{Mg}(CH_3COO)_2 + \overset{0}{H}_2\uparrow , \quad (14)$$

and also dissolve oxides of alkaline earth metals with the formation of acetate and water:

$$CaO + 2CH_3COOH \rightarrow Ca(CH_3COO)_2 + H_2O\,. \quad (15)$$

However, acetates formed in the presence of a stronger acid than acetic acid are quickly transformed (converted) into a salt of the stronger acid. That is, the anions of weak acetic acid

(CH_3COO^-) are displaced from their salt by the proton (H^+) of a stronger acid. When a proton interacts with an acetate anion, the latter changes from a solvated state to a non-dissociated molecular form of acetic acid:

$$CH_3COO^- + H^+ \rightarrow CH_3COOH\,. \quad (16)$$

Traditionally, the strength of an acid is determined by the degree of its dissociation in a dilute aqueous solution and is determined by the ionization constant and the concentration of the acid ($mol \cdot (dm^3)^{-1}$). If the degree of acid is unknown, then it can be determined by the conductometric method, including even in non-aqueous solvents (Fialkov, et al., 1973; Fuoss, 1935; Fuoss, 1957). Knowing the values of and for the corresponding solutions of acids, it is possible to determine the degree of their dissociation α (in %) in this solution and the concentration of Hydrogen ions [H^+] ($mol \cdot (dm^3)^{-1}$), formed during the dissociation of acid molecules. Since organic acids belong to weak electrolytes, the degree of their dissociation and, accordingly, the concentration of ions in an aqueous solution are determined by the following formulas:

$$\alpha = \sqrt{\frac{K_\alpha}{C}} \cdot 100\,, \quad (17)$$

and

$$[H^+] = \sqrt{K_\alpha \cdot C}\,. \quad (18)$$

Accordingly, the degree of dissociation of lactic acid in water is:

$$\alpha_{C_3H_6O_3} = \sqrt{\frac{K_{\alpha(C_3H_6O_3)}}{C_{C_3H_6O_3}}} \cdot 100 = \sqrt{\frac{1{,}4 \cdot 10^{-4}}{1{,}0}} \cdot 100 = 1{,}183\%\,, \quad (19)$$

the concentration of ions H^+ in an aqueous solution of 1M lactic acid is:

$$[H^+] = \sqrt{K_{\alpha(C_3H_6O_3)} \cdot C_{C_3H_6O_3}} = \sqrt{1{,}4 \cdot 10^{-4} \cdot 1{,}0} = 1{,}183 \cdot 10^{-2}\ mol \cdot (dm^3)^{-1}\,. \quad (20)$$

In turn, the concentration of ions affects the pH of the medium, which depends on the course of reactions of selective dissolution (leaching) of metal phases in the dust concentrate:

$$pH = -\lg\left[H^+\right]. \quad (21)$$

Accordingly, if for a 1.0 M solution of lactic acid in water, the ionization constant of which is $K_{\alpha(C_3H_6O_3)} = 1.4 \cdot 10^{-4}$, and the concentration of hydrogen ions reaches $[H^+] = 1.183 \cdot 10^{-2}$ $mol \cdot (dm^3)^{-1}$, then the equation is used to find the pH value of such a solution :

$$pH = -\lg\left[H^+\right] = -\lg\left(1{,}183 \cdot 10^{-2}\right) = 1{,}927,$$

from which it follows that a solution of $1\,M \cdot (dm^3)^{-1}$ of lactic acid in an aqueous solution should have a pH of 1.927 ($[H^+] = 0{,}012\ mol \cdot (dm^3)^{-1}$). According to our data, in the medium of glacial acetic acid 1M lactic acid has a pH of 1.0 (!). That is, under these conditions, the concentration of protons in the acetic acid medium is $[H^+] = 0{,}1\ mol \cdot (dm^3)^{-1}$. To calculate the concentration of hydrogen ions $[H^+]$ in a solution with a known pH, the equation is used:

$$[H^+] = 10^{-pH}, \tag{22}$$

where $[H^+]$ is the concentration of hydrogen ions in $mol \cdot (dm^3)^{-1}$; pH - indicator of acidity of the solution. For $pH = 1.0$ the calculation is performed as follows:

$$[H^+] = 10^{-pH} = 10^{-1} = 0{,}1\ mol \cdot (dm^3)^{-1},$$

which is almost 10 times more than in the aqueous solution. And this parameter of the system is of essential importance, since the concentration of hydrogen ions $[H^+]$ ensures effective leaching of metals by organic and mineral acids (Karavayko, et al., 1989). Despite the fact that acetic acid is a rather weak electrolyte ($\varepsilon_{C_2H_4O_2}$ 6,19) compared to a similar indicator of water

(ε_{H_2O} 78,0), the use of acetic acid as a solvent for lactic acid ($\varepsilon_{C_3H_6O_3}$ 22,0) made it possible to achieve effective dissolution of such metal phases as iron, zinc , and lead (reaction equations (15), (16), (17)). Experimental attempts to use aqueous solutions of each of these acids separately for leaching metal phases from the dust waste turned out to be inconclusive.

During the leaching of reduced (atomic) metals with 1 M lactic acid in glacial acetic acid, a complex of oxidation-reduction reactions occurs, consisting of two half-reactions - anodic and cathodic types. The anodic reaction, or the reaction of metal dissolution, occurs with the loss of electrons by the iron atom, while in the associated cathodic reaction, the proton acts as an electron acceptor, resulting in the formation of molecular hydrogen. An example of these two reactions is presented in equations (1) and (2). In this case, iron is oxidized to iron II ions (1), while hydrogen ions are reduced, forming molecular hydrogen (2).

$$\overset{0}{Fe} \xrightarrow{-2e^-} Fe^{2+}, \tag{23}$$

$$2H^+ \xrightarrow{+2e^-} \overset{0}{H}_2 \uparrow. \tag{24}$$

It is quite remarkable that the reaction products formed in this case - acetates (salts of acetic acid) and lactates (salts of lactic acid) have high solubility in aqueous solutions. For example, lead acetate ($Pb(C_2H_3O_2)_2 \cdot 3H_2O$) has a solubility of 55 g in 100 cm^3 of water at 25 °C , and zinc acetate ($Zn(C_2H_3O_2)_2$) - 30 g in 100 cm^3 of water at 20 °C , 44.6 g at 100 °C , and in alcohol - 166 g in 100 cm^3 of ethanol at 70 °C (Nikolsky, 1971). A similar situation is observed with metal lactates. For example, iron (III) lactate ($Fe(C_3H_5O_3)_3$) is highly soluble in water - more than 50 g in 100 cm^3 at 20 °C , and iron (II) lactate ($Fe(C_3H_5O_3)_2 \cdot 3H_2O$) - 2.1 g at 10 °C and 8.5 g at 100 °C in 100 cm^3 of water. The opposite situation is observed with metal oxalates. Lead oxalate (PbC_2O_4) has a solubility of 0.00016 g at 18 °C , zinc oxalate (ZnC_2O_4) - 0.00057 g at 10 °C , iron (II) oxalate ($FeC_2O_4 \cdot 2H_2O$) - 0.097 g at 25 °C in 100 cm^3 of water. However, iron (III) oxalate ($Fe(HC_2O_4)_3 \cdot nH_2O$) has an abnormally high

solubility in water – similar to that of iron (III) lactate, and it is this property that we used for the selective extraction of iron from its oxides (Fe_2O_3 , $FeO \cdot Fe_2O_3$) present in the dust concentrate.

2.3.2.2. Leaching of the magnetic fraction with oxalic acid

Since lactic and acetic acids are unable to dissolve iron oxides ($FeO, Fe_2O_3, \mathrm{FeO \cdot Fe_2O_3}$) - according to thermodynamic parameters, acetic and lactic acids are quite weak acids, therefore the magnetic fraction of the dust concentrate, which contains 98% of iron-containing phases, is leached only with a 1.0 M solution of oxalic acid (9% aqueous solution, pH 0.85) at a temperature of 105 - 110 °C for 16 - 18 hours with active vibration activation. In this case, the solution consists of approximately 27% hydrooxalate ($HC_2O_4^-$) and 73% molecular form ($H_2C_2O_4$) oxalic acid (Saltykov, et al., 2001; Saltykov, et al., 2004), therefore, the resulting products are iron (II) hydroxalates - a water-insoluble salt ($Fe(HC_2O_4)_2$), and iron (III) - a highly soluble salt ($Fe(HC_2O_4)_3$). A typical redox reaction between iron and oxalic acid, accompanied by hydrogen reduction, occurs according to the following equation:

$$\overset{0}{Fe} + 2\overset{+1}{H}_2C_2O_4 \xrightarrow{pH \le 1{,}0, T, 105°C, -2e^-} \overset{+2}{Fe}(HC_2O_4)_2 \downarrow + \overset{0}{H}_2 \uparrow, \quad (25)$$

The product of this reaction is a water-insoluble salt - iron (II) hydrooxalate. In the case of interaction of 1M oxalic acid (pH 0.85) with iron oxide at a temperature of 105 $°C$ for 16-18 hours, with active mechanical stirring of the mixture (120 rpm), the following reaction occurs:

$$Fe_2O_3 \cdot nH_2O_{(solid)} + 6H_2C_2O_{4(liquid)} = 2Fe(HC_2O_4)_{3(liquid)} + (3+n)H_2O \quad (26)$$

Oxalic acid is the only organic acid capable of selectively removing iron (III) from its oxides, forming only one water-soluble salt - iron (III) oxalate, according to equation (26). After treatment of the magnetic fraction of the dust concentrate with oxalic acid, only impurity particles of silicon oxide (SiO_2) and ferrosilicon ($FeSi$) (less than 71 μm in size), indifferent to the action of the organic acid, remain in the residue.

2.3.2.3. Leaching with glycerol - alkaline extractant

In the conditions of a laboratory experiment, it was proved that by the method of glycerol-alkaline leaching (Solozhenkin and Nebera, 2003) of non-separated dust concentrate in a magnetic field: glycerol - 300.0 g/dm^3; NaOH - 60.0 g/dm^3; H_2O - up to 1.0 dm^3; pH > 12.0) according to the ratio "solid phase : liquid = 1 : 4", at a temperature of 105 $°C$ and with active stirring (120-240 rpm) within 16 hours, selective "dissolution" of non-ferrous metals, primarily zinc, occurs. It is quite interesting that the ratio of extracted metals in the form of glycerates is "Zn : Pb : Fe : Mo = 4 : 3 : 2 : 0,6" (Zn – 39.70%; Pb – 31.61%; Fe – 22, 42%; Mo – 6.25%). In addition, if necessary, it is possible to increase the quality of extraction of zinc, lead and other metals in glycerol - an alkaline medium under active vibroactivation - by mixing the components under the action of ultrasonic cavitation (within 10-15 minutes at a temperature of 105 $°C$) (Deng et al., 2024). Glycerates of iron, zinc, molybdenum and others are considered very promising precursors for the production of highly effective catalysts, including for the electrolytic production of hydrogen and oxygen (Larcher, et al., 2003). The use of such a leaching method seems to us to be very promising, however, before its application it must be preceded by a stage of reducing roasting and magnetic separation in order to maximize the extraction of metallic phases of iron and its magnetically sensitive oxides.

3. Experimental

3.1. Metal phases, their oxides and amorphous carbon in blast furnace smoke emissions

The data of X-ray fluorescence and X-ray phase (table 4) analyzes indicate that the dust concentrate contains a significant amount of chemical elements. Among non-metals, the most common are amorphous carbon (32.78%) and silicon oxide (5.8%), among metals - iron (16.1 wt.%) and zinc (2.2 wt.%).

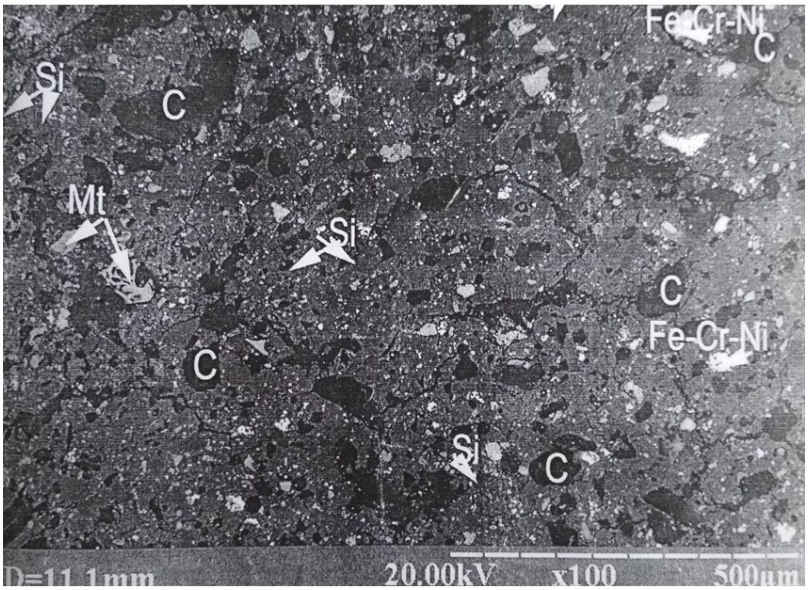
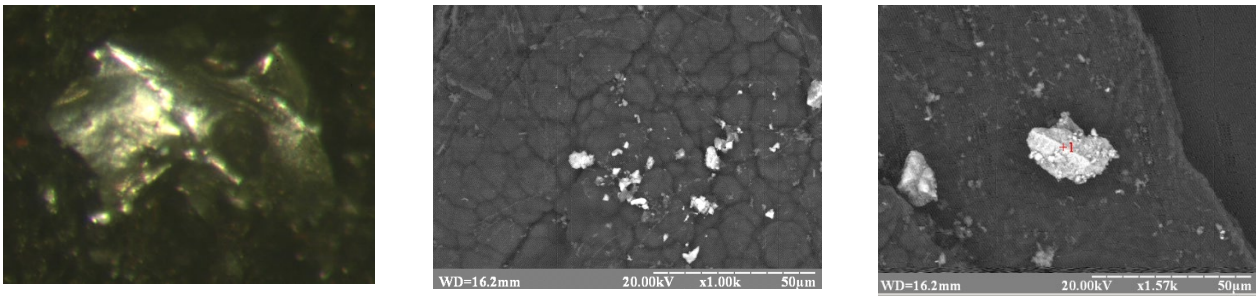


Fig. 1. X-ray phase analysis of dust concentrate. The main condensed phases: (C) – amorphous carbon, (Si) – silicon, (Mt) – magnetite ($FeFe_2O_4$), ($Fe-Cr-Ni$) - nano- and microdisperse polymetallic phases (magnification 100x)

When examining the dust concentrate by light microscopy (magnification 112x), the presence of particles with an abnormally bright metallic luster is observed, which, having a weak magnetic sensitivity, and during magnetic separation significantly lag behind the speed of movement of ferromagnetic particles of the type $Fe_2O_3 \cdot 2H_2O$ (hematite) or Fe_3O_4 (magnetite) (Fig. 2). According to X-ray structural analysis, these particles are aggregates of molten carbon (bright metallic luster), on the surface of which particles of metal phases formed "de novo" are condensed - iron, zinc and other elements that evaporate during the pyrometallurgical process.



a b c

Fig. 2. Particle of molten carbon (bright metallic luster, measuring 130 x 150 µm). a - Light stereomicroscopy (112x) of a molten carbon particle on the surface of which metal particles are adsorbed; b, c - SEM image of the same particle, with metal phases formed "de novo" on its surface (magnification 1000x and 1570x, respectively)

Electron microscopic studies (with X-ray spectral analysis of the constituent components) of the carbon phase indicate that ultradisperse (nanosized) particles of metals - iron and zinc, which do not aggregate with each other - are adsorbed on its surface. Moreover, these particles are represented in a wide size range - from tens of nanometers to several tens of micrometers. In Fig. 2b, 2c shows the structure of the carbon matrix on which metal particles are adsorbed, confirming the XRF data that it consists of amorphous carbon, which has a spongy structure. The chemical composition of an individual particle at the point marked in Fig. 2c as "+1" is given in Table 2. The main element of this metal phase is iron (98.92%).

Table 2. The chemical composition of particle at the point marked in Fig. 2c as "+1".

Element	Content, %
Fe	98.92
Zn	0.40
Si	0.39
Cr	0.19
Al	0.10
Total	100.00

3.2. Technological stages of preparation for leaching of metals from mineral phases present in dust concentrate

In fig. 3 shows the sequence of technological methods used in the processing of the original dust concentrate that was stored for a long time in the tailings repository and was exposed to the environment (rain and snow water, wind, solar radiation).

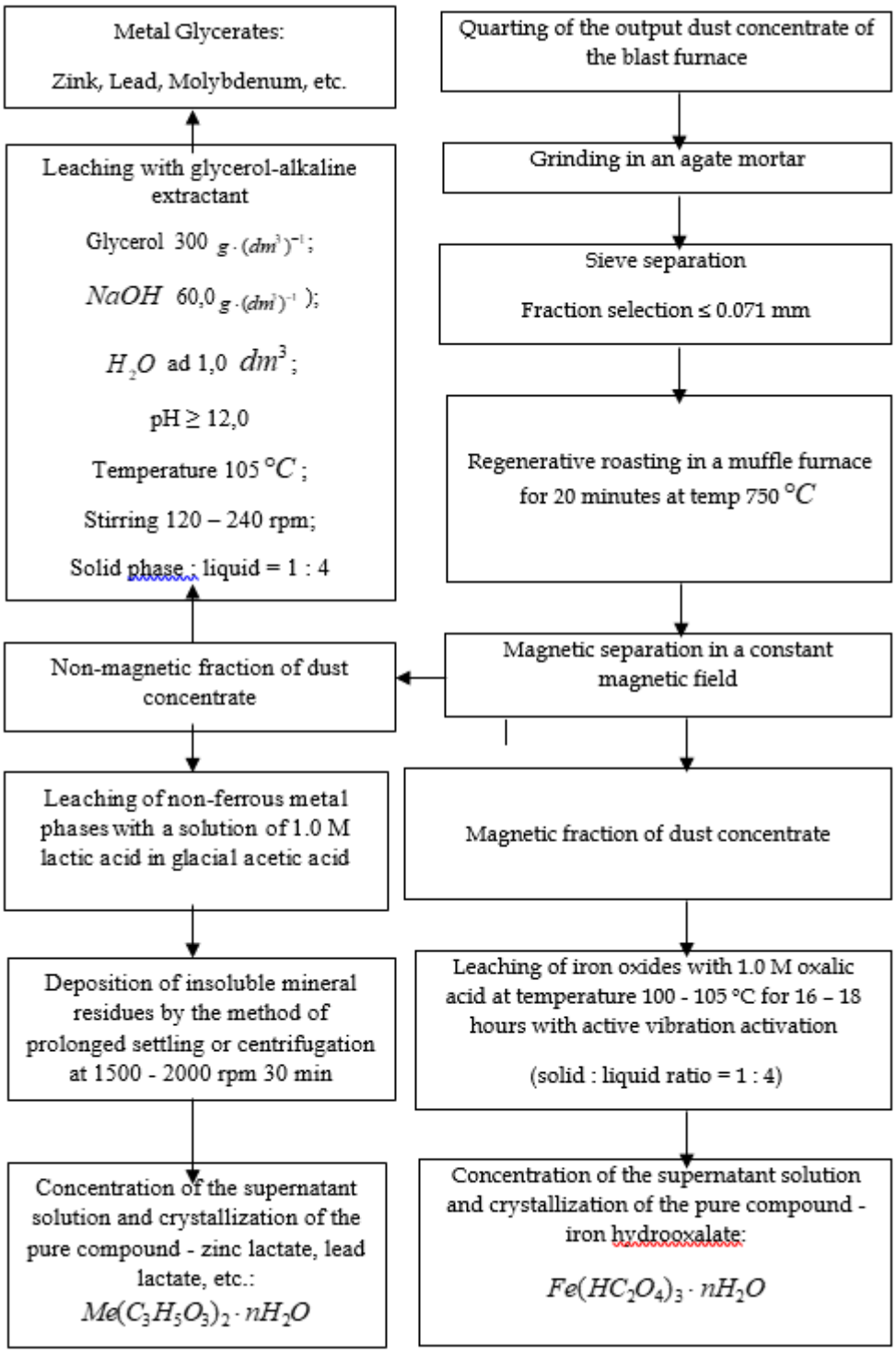


Figure 3. The sequence of technological techniques used in the processing of the original dust concentrate that was stored for a long time in the tailings repository

In order to ensure the maximum possible access of the liquid leaching agent (organic acid solution) to the surfaces of the target mineral phases, it is first necessary to grind solid massive conglomerates of the dust concentrate, which were formed during repeated contact with water (of rain and snow origin). We used an agate mortar for grinding, after which the material was sieved using a set of analytical sieves until 100% grinding was achieved with a mineral particle size of ≤ 0.071 mm. In all subsequent procedures for the processing of the dust concentrate, the material was only of such a degree of dispersion.

3.3. Regenerative roasting - magnetic separation

In a ceramic crucible, 100 g of the dust concentrate fraction with a particle size of ≤0.071 mm previously crushed in an agate mortar and sifted through a sieve complex were placed. Firing was performed in a muffle furnace (SNOL) at a temperature of 750 °C for 20 minutes. The fried product was cooled to room temperature and weighed on a scale to determine the mass of the remains.

67.0 g of the remains were transferred to 600 cm^3 of bidistilled water, a surface-active substance (surfactant) - sodium dodecyl sulfate (SDS) was added to a concentration of 0.01% and an aqueous suspension was formed. Magnetic separation was performed in a glass Petri dish using a permanent magnet. Separately collected magnetic and non-magnetic fractions were filtered and dried in an oven (ShS-250) at a temperature of 120 °C for 1 hour. The results of magnetic separation were evaluated by the weight method - the ratio of magnetic and non-magnetic fractions was approximately 1:1 (31.5 g and 33.2 g, respectively).

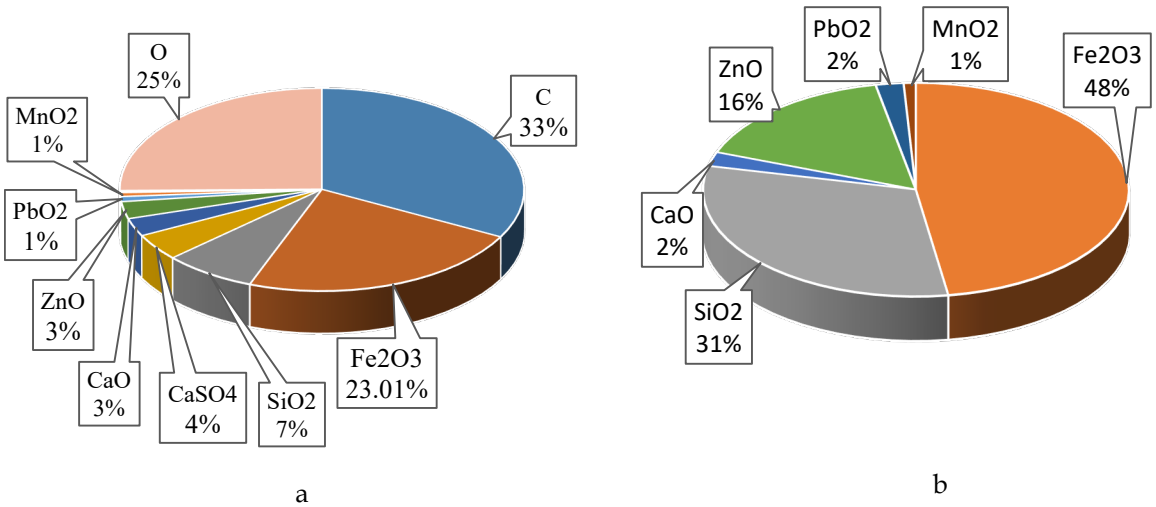


Fig. 4. Mineral composition of dust concentrate: a - before roasting; b - after reduction roasting (750 °C)

Preliminary roasting of the dust concentrate made it possible to significantly change the chemical and mineral composition of the residue - amorphous carbon ($\overset{0}{C}$) was completely removed, and the content of iron oxides (FeO, Fe_2O_3) increased from 23.01% to 47.56%, zinc oxides (ZnO) from 2.73% to 16.26%, lead oxide (PbO_2) from 0.8% to 2.11%, silicon oxide

(SiO_2) from 7.39% to 31.0% (Fig. 4). In addition, we took into account the oxygen content as an independent element (25%) included in the composition of hydrates and hydroxides of mineral phases present in the original dust concentrate. A significant change in the mineral and elemental composition after the reducing roasting made it possible to determine three major components - Fe_2O_3 (48%), SiO_2 (31%), and ZnO (16%) (Fig. 4b), as well as three minor fractions - PbO_2 (2%), CaO (2%), and MnO_2 (1%). Considering the fact that iron oxides in this mineral residue make up 48% of the total mass, it was quite logical to use magnetic separation to extract iron-containing phases. Table 3 shows the chemical composition of the magnetic fraction, which indicates that the iron content in it is 96.9% by weight, and impurity elements - Si (1.312%), Ca (1.203%), Mn (0.308%), Zn (0.129%), Sn (0.062%), and S (0.042%), respectively. Obviously, as a result of the phase transformations that occur during the reductive roasting of oxides of metals such as zinc and lead, the content of the metal phases of these metals increases, taking into account the roasting temperature (750 °C). From the point of view of the expediency of using preliminary reductive roasting of carbon-containing dust concentrate, the fact that

finely dispersed phases of metals formed in this process - iron, zinc, lead and manganese - can react quite actively with organic acids - acetic, lactic and oxalic is attractive.

Table 3. The elemental composition of the magnetic fraction of mineral phases after reductive roasting of dust concentrate (X-ray luminescence analysis)

Chemical element	Content, wt%	Analytical deviation, %
Fe	96,944	0,156
Si	1,312	0,121
Ca	1,203	0,096
Mn	0,308	0,031
Zn	0,129	0,014
Sn	0,062	0,015
S	0,042	0,016

3.4. Leaching of metals of the non-magnetic fraction with a solution of lactic acid in glacial acetic acid

After the primary reducing roasting and magnetic separation of the dust concentrate, when the enriched mixture of phases of reduced metals and their oxides is concentrated in the residue, the primary process is leaching with a mixture of weak organic acids - 1 M solution of lactic acid in glacial acetic acid. This combination of acids allows metals to be extracted from reduced metallic phases due to the oxidation-reduction reactions given in equations (7), (8), and (9), but does not allow them to extract iron from its oxides. To perform such a process, this tandem does not have sufficient chemical potential, therefore, at the next technological stage - leaching iron from its oxides concentrated in the magnetic fraction, oxalic acid only is used, which is capable of selectively extracting iron (III) from its oxides, forming only one water-soluble salt - iron (III) oxalate, according to equation (26). In order to predict which metal-containing phases will be reactive towards organic acids, we analyzed all the components of the dust concentrate in its initial state and after reductive roasting. Table 4 presents all the mineral phases of the dust concentrate.

Table 4. The content of mineral phases (wt.%) in the initial concentrate of blast furnace dust emissions and after its roasting at temperature of 750 °C

Mineral phase	The main chemical element of the phase	In the primary dust concentrate	After roasting the dust concentrate
Amorphous Carbon	C	32,78	0
A mixture of iron-containing mineral phases: hematite (αFe_2O_3), magnetite ($FeFe_2O_4$), goethite ($\alpha FeO(OH)$), and reduced iron ($\overset{0}{Fe}$)	Fe	23,01	47,56
SiO_2	Si	7,39	31,0
$CaSO_4$	S	4,245	0
CaO	Ca	2,868	2,15
ZnO	Zn	2,738	16,26
PbO_2	Pb	0,808	2,11
MnO_2	Mn	0,633	0,92
P_2O_5	P	0,229	0
As_2O_5	As	0,030	0
CoO	Co	0,025	0
CuO	Cu	0,012	0
CdO	Cd	0,011	0

According to the obtained data of X-ray phase analyzes of dust concentrate samples, it is clear that its composition includes a significant number of chemical elements. Among metals, iron (16.1 wt.%) and zinc (2.2 wt.%) are the most common. The main elements are carbon ($\overset{0}{C}$) and oxygen (O_2) in the composition of metal oxides, hydrates, and hydroxides, the contents of which were 32.78 and 37.57 mass%, respectively. The content of metals in the form of metal phases or their oxides was: *Fe* – 16.1; *Zn* – 2.2; *Ca* – 3.3; *Pb* – 0.7; *Mn* – 0.4; *Co* – 0.02; *Cu*, *As*, and *Cd* – 0.01wt%. The content of sulfur (*S*), and phosphorus (*P*) was 1.0 and 0.1 wt.%, respectively. The selective extraction of metals from the dust concentrate consists in their sequential "*step by step*" dissolution with organic acids in the order of increasing ionic strength of the acids - starting with the weakest pair "*acetic acid - lactic acid*" ($K_{1\,C_2H_4O_2} = 1.75 \cdot 10^{-5}$ (Harned, Murphy, 1931); $K_{1\,C_3H_5O_3} = 1.4 \cdot 10^{-4}$ (Martin, Tartar, 1937)), which allows leaching of metallic phases - iron, zinc and lead, and finishing the process of extracting metals from their oxides with *oxalic acid* - the strongest organic acid. Its ionization constant in an aqueous solution (an indicator of the ionic strength of the acid) is $K_{1\,C_2H_2O_4} = 5.6 \cdot 10^{-2}$, which exceeds the similar indicator of phosphoric acid ($K_{1_{H_3PO_4}} = 8.0 \cdot 10^{-3}$) by seven times. When processing finely dispersed metal particles of dust concentrate with 1.0 M lactic acid in an acetic acid solution (pH ≈1.0) at a temperature of 105 °C, hydrogen displacement reactions occur from lactic acid by finely dispersed metal particles with the formation of corresponding salts - lactates of these metals. Under such conditions, lactic acid is able to "dissolve" even particles of iron ($\overset{0}{Fe}$), zinc ($\overset{0}{Zn}$) and lead ($\overset{0}{Pb}$) with the formation of the corresponding water-soluble lactates (Prokopenko et al., 2019):

$$\overset{0}{Me} + 2CH_3CH(OH)COO\overset{+1}{H} \xrightarrow{T,105°C,-2e^-,CH_3COOH} \overset{+2}{Me}(CH_3CH(OH)COO)_2 + \overset{0}{H}_2\uparrow, \quad (27)$$

where $\overset{0}{Me}$ is the metallic phases of iron ($\overset{0}{Fe}$), zinc ($\overset{0}{Zn}$) or lead ($\overset{0}{Pb}$), respectively.

3.5. Thermodynamic characteristics of the reaction of formation of iron (III) hydrooxalate from iron (III) oxide of the magnetic fraction

Based on the thermodynamic properties of the starting compounds and reaction products (26), given in Table 4, it is possible to perform the following calculations of the thermodynamic parameters of this reaction. In conclusion $p = const$, the thermal effect of the reaction (26) indicates a change in the enthalpy ($\Delta H^0_{f,298,15}$) of the system:

$$\Delta H^0_{298,15\,(equation\,26)} = \sum \left(n_i \Delta H^0_{f,298,15_i}\right)_{products} - \sum \left(n_i \Delta H^0_{f,298,15_i}\right)_{(source\,components)} . \quad (28)$$

And if the chemical reaction (26) is described taking into account the stoichiometric indices, then we get the following equation:

$$\Delta H^0_{298,15(equation\,26)} = (2 \cdot \Delta H^0_{f,298,15\,Fe(HC_2O_4)_3} + 3 \cdot \Delta H^0_{f,298,15\,H_2O}) - (\Delta H^0_{f,298,15\,Fe_2O_3} + 6 \cdot \Delta H^0_{f,298,15\,H_2C_2O_4}). \quad (29)$$

That is, the thermal effect of the chemical reaction (18) is equal to the algebraic sum of the heats of formation of the reaction products minus the algebraic sum of the heats of formation of the initial components:

$$\Delta H^0_{298,15\,(equation\,26)} = \left(2 \cdot \left(-2567{,}05\right) + 3\left(-285{,}83\right)\right) - \left(1 \cdot \left(-822{,}16\right) + 6 \cdot \left(-829{,}94\right)\right) = -189{,}79\ kJ \cdot mol^{-1}. \quad (30)$$

Table 4. Thermodynamic constants of oxalic acid, iron (III) oxide, and their interaction products

The formula of a substance (phase state in the reaction)	Molar mass	$\Delta H^0_{f,298,15}$ $\frac{kJ}{mol}$	$S^0_{298,15}$ $\frac{J}{mol \cdot K}$	$\Delta G_{f,298,15}$ $\frac{kJ}{mol}$	$C^0_{p,298,15}$ $\frac{J}{mol \cdot K}$	Coefficients equation $C^0_p = f(T)$		
						a	$b \cdot 10^3$	$c' \cdot 10^{-5}$
$H_2C_2O_{4(liquid)}$	90,036	-815,04	152,41	-695,88	109,00	-	-	-
$Fe_2O_{3(solid)}$	164,69	-822,16	87,45	-740,34	103,76	97,7	72,1	-12,8
$Fe(HC_2O_4)_{3(liquid)}$	328,97	-2500,94	42,13	-2069,96	300,80*			
$H_2O_{(liquid)}$	18,01	-285,83	69,95	-237,23	75,30	39,0	76,6	11,9

Note: * - calculated theoretically, according to the Dulong-Petit law

This value of the thermal effect ($\Delta H^0_{298,15\,(18)} = -189{,}79\ kJ \cdot mol^{-1}$) indicates that the reaction is exothermic and can occur spontaneously - without additional external factors.

In addition, it is possible to calculate the amount of heat generated in the process of converting

1 kg of roasted iron (III) oxide (Fe_2O_3) into iron (III) oxalate ($Fe(HC_2O_4)_3$) according to reaction (26):

$$Q = n \cdot \left|\Delta H^0_{298,15\,(18)}\right|, \quad (31)$$

where n is the number of moles of the substance: $n = g \cdot M^{-1}$; g - mass of substance, g; M - molar mass of a substance, $g \cdot mol^{-1}$. In accordance: $n = \frac{g_{Fe_2O_3 \cdot 2H_2O}}{M_{Fe_2O_3 \cdot 2H_2O}} = \frac{1000}{195,72} = 5,1\,mol$; and if $g_{Fe_2O_3 \cdot 2H_2O} = 1000g$, then $M_{Fe_2O_3 \cdot 2H_2O} = 195,72\ g \cdot mol^{-1}$; where $Q = 5,1 \cdot \left|-189,79\right| = -967,92\,kJ$.

This indicator shows that the reaction is exothermic and can occur independently, without the use of additional factors. To process 1 kg (5,1 mol) of iron (III) oxide, 30.6 mol (2755 g) of oxalic acid is used; at the same time, 10,2 mol (or 3293,8 g) of water-soluble oxalate of iron (III) ($Fe(HC_2O_4)_3$) and 25.5 mol (459 g) of H_2O are formed. From this amount of iron oxalate, it is possible to produce 5,1 mol (about 284 g) of nanodispersed pyrophoric iron (Cha et al., 2006; Chekli, 2015; Prokopenko, 2019), or 5,1 mol (804,5 g) of lithium iron phosphate $LiFePO_4$ for the production of anode materials for power cells of electric vehicles (Padhi et al., 1997a; Padhi et al., 1997b). However, to this it is necessary to add such important information: the products of this reaction are environmentally safe substances that are non-toxic both to technical personnel and to the environment.

4. Conclusions

The process of selective leaching of metals from roasted dust concentrate, proposed by our research group, is based on separate (step-by-step) extraction of metals from their metallic phases and from phases containing metal oxides. This approach is of fundamental importance, since the leaching products should not be mixed with each other in one leaching solution, which significantly simplifies their subsequent purification from impurity elements at the stage of large-scale preparative production of pure metal or its salt. And depending on the commercial demand for certain products, it is possible, accordingly, to produce salts of target metals - lactates, oxalates, or acetates of iron, zinc, lead, etc. (Chernenko and Astrelin, 2010; Chernenko et al., 2018;). In this work, dedicated to the selective leaching of metal-containing phases from the dust concentrate with organic acids, reductive roasting was carried out in order to remove impurities of amorphous carbon. Changes in the mineral and chemical composition were recorded using light and electron microscopy ("scanning electron microscope - energy dispersive spectrometer" complex SEM-EDS) and X-ray diffraction (XRD), which made it possible to propose a new idea and technical support for effective and environmentally friendly use of dust waste of a metallurgical enterprise. Research on selective extractants of iron and non-ferrous metals from dust concentrate is ongoing.

Acknowledgments

This work was financially supported by the scientific project No. 88/19 H of the National Academy of Sciences of Ukraine.

References

BERDNIKOV, V.I., GUDIM Yu.A. 2020. *Chemical reactions during iron reduction from oxides.* Ferrous Metallurgy, 63, 842-847.

CAMPBELL, J.A. 1970. Chemical Systems: Energetics, Dynamic, Structure. Harvey Mudd College, Claremont, California. W.H. Freeman and Co., San Francisco.

COUDURIER, L., HOPKINS, D.W., WILKOMIRSKY, I. 1985. Fundamentals of Metallurgical Processes, Second edition, Pergamon Press, 349-354.

CHERNENKO, V.Yu., ASTRELIN, I.M. 2010. *Thermodynamic basis of environmentally-friendly technology of dissolution of carbonic polyminerals by biogenic agents.* Research bulletin of the National Technical University of Ukraine "Kyiv Polytechnic Institute", 5 (73), 145-152.

CHERNENKO, V.Yu., ASTRELIN, I.M., TOLSTOPALOVA, N.M. 2018. *Enrichment and leaching of non-ferrous metal ores and phosphate ores with organic acids.* International Scientific and Technical Internet Conference "Innovative Development of Resource-Saving Technologies of Mineral Mining and Processing", Book of Absytracts, Petroşani, Romania, UNIVERSITAS Publishing, 185-188.

CHERNENKO, V.Yu., ASTRELIN, I.M., SHECHUNOVA, S.B. 2013. *Study of the mechanism of decarbonization of Zhvaniv phosphorite by lactic acid.* The latest energy- and resource-saving chemical technologies without environmental problems. VI international scientific and technical conference, theses of scientific papers, September 9 - 13, 2013, Odesa, Ukraine, 2, 217-219.

CHERNENKO, V.Yu., SHEKHUNOVA, S.B., CHYGYRYNETS, O.E., STADNICHENKO, S.M. 2018. *Innovative technology of phosphorites processing.* Resource and resource-saving technologies in mineral mining and processing. Multi-authored monograph. Petroşani, Romania, UNIVERSITAS Publishing, 351-362.

CHA, H.G., KIM, Y.H., KIM, C.W., KANG, Y.S. 2006. *Preparation of aqueous dispersion of colloidal a-Fe nanoparticle by phase transfer.* Sensors and actuators, B, 126, 221-225.

CHEKLI, L., BAYATSARMADI, B., SEKINE, R., SARKAR, B., MAOZ SHEN, A., SCHECKEL, K.G., SKINNER, W., NAIDU, R., SHON, H.K., LOMBI, E., DONNER, E. 2015. *Analytical characterization of nanoscale zero-valent iron: An illustrated methodological review.* Analytica Chimica Acta, https://doi:10.1016/j.aca.2015.10.040

DENG, J., LUO, D., BAI, J., RONG, K. 2024. *Effect of ultrasonic pretreatment on flotation purification of quartz.* Physicochem. Probl. Miner. Process, 60(3), 190008, https://doi:10.37190/ppmp/190008

FIALKOV, Yu.Ya., ZHITOMIRSKY, A.N., TARASENKO, Yu.A. 1973. Physical chemistry of non-aqueous solutions, Leningrad, Chemistry, 376.

FUOSS, R.M. 1935. *Solution of the conductance equation.* J. Am. Chem. Soc., 57, 488-489.

FUOSS, R.M. 1957. *Ionic association. I. Derivation of constants from conductance data.* J. Am. Chem. Soc., 79, 3301-3303.

HARNED, H.S., MURPHY, G.M. 1931. *The temperature coefficient of dissociation of acetic acid in potassium and sodium chloride solutions.* J. Am. Chem. Soc., 53, 8-17.

KARAVAYKO, G.I., ROSSI, J., AGATE, A. 1989. Biogeotechnology of metals. Practical guide, M: Center for International Projects of the State Committee on Science and Technology, 1-375

KOVZUN, I.G., KOVALENKO, I.T., PROTSENKO I.T. 2007. *Influence of chemical-mineralogical and disperse composition of ferrous metallurgical slimes on their physical and chemical properties.* Nanosystems, nanomaterials, nanotechnologies, Kyiv, UA, 5 spec. iss., pt. 1, 209-216.

LAPIDUS, A.L., ELISEEV, O.L., KRYUCHKOV, M.V. 2011. *Bell-Boudoir and water gas Schift reactions under conditions of the Fischer-Tropsch synthesis.* Solid Fuel Chemistry, 45, 313-315.

LARCHER, D., SUDANT, G., PATRICE, R., TARASCON, J.-M. 2003. *Some insights on the use of polyols-based metal alkoxides powders as precursors for tailored metal-oxides particles.* Chem. Mater., 15, 3543-3551.

LEE, S. 2005. *Dissolution of iron oxides by oxalic acid.* A thesis submitted for the degree of Doctor of Philosophy. The University of New South Wales, Sydney, Australia, 1-209.

MARTIN, A.W., TARTAR, H.V. 1937. *The ionization constant of lactic acid, 0 – 50°, from conductance measurements.* J. Am. Chem. Soc., 59, 2672-2675.

NIKOLSKY, B.P., GRIGOROV, O.N., POZIN, M.E., PORAI-KOSHITS, B.A., RABINOVICH, V.A., RACHINSKY, F.Yu., ROMANKOV, P.G., FRIEDRICHSBERG, D.A. 1971. Chemist's Handbook. Basic Properties of Inorganic and Organic Compounds, Leningrad, Chemistry, 2, 1168.

PADHI, A.K., NANJUNDASWAMY, K.S., GOODENOUGH, J.B. 1997a. *Phospho-olivines as positive-electrode materials for rechargeable lithium batteries.* J. Electrochem. Soc., 144, 1188-1194.

PADHI, A.K., NANJUNDASWAMY, K.S., MASQUELIER, C., OKADA, S., GOODENOUGH, J.B. 1997b. *Effect of structure on the* Fe^{3+} / Fe^{2+} *redox couple in iron phosphates.* J. Electrochem. Soc., 144, 1609-1613.

PROKOPENKO, V.A., CHERNENKO, V.Yu., TSYGANOVICH, O.A., ASTRELIN, I.M. 2019. *Production of nanostructured iron compounds from metallurgical wastes.* Traditions and innovations of resource-saving technologies in mineral mining and processing. Multi-authored monograph. Petroşani, Romania, UNIVERSITAS Publishing, 416-424.

SALTYKOV, S.N., MAKAROV, G.I., TOROPTSEVA E.L. 2001. *Mechanism of anodic dissolution of armco iron and high-strength cast iron on a ferrite base in an oxalate medium.* Protection of Metals, 37, 186-191.

SALTYKOV, S.N., MAKAROV, G.V., TOROPTSEVA, E.L., FILATOVA, Ya. B. 2004. *Anodic behavior of white iron phases in oxalic media.* Protection of Metals, 40, 62-67.

SOLOZHENKIN, P.M., NEBERA, V.P. 2003. *Biohydrometallurgy of antimony gold-bearing ores and concentrates.* Biohydrometallurgy: a sustainable technology in evolution. XVth International Biohydrometallurgy Symposium (IBS 2003), September 14 – 19, 2003, Athens, Hellas, 1, Bioleaching applications, 107-115.

SHUMAKOV, N.S., DMITRIEV, A.N., GARAYEVA, O.G. 2007. Raw materials and blast furnace fuel, Ekaterinburg, Institute of Metallurgy, Ural Branch of the Russian Academy of Sciences, 1-392.

YUROV, V.M., LAURINAS, V.Ch., GUCHENKO, S.A. 2019. *Estimation of the melting temperature of some metal oxides nanoparticles.* International Journal of Applied and Fundamental Research, 1, 38-42.

Microwave Tube Radiated CIP Process Using Active Carbon of Popped Corn/Rice /Cotton in Leaching of Poor Ferrous Zinc Tailings

Yıldırım İ. TOSUN [1*],

[1*]Şırnak University, Engineering Faculty, Mining Eng. Dept, Şırnak

*Corresponding author: yildirimismailtosun@gmail.com (Yıldırım İsmail Tosun)

Abstract:

Biochar types used in this study were the popped rice, popped corn and cotton carbonized after popping at 300 ˚C received in nitrogen medium at 9 minutes kept on glass pan for popping and 30 minutes carbonization to obtain active carbon as biochar carbon, at 700 ˚C. 50 gr samples were tested for slurry mixing with acidic solutions. The cotton carbonized at 700 ˚C as control active carbon the various critical parameters affect on adsorption levels and performance data for fixed and dynamic slurry mixing fraction of 10% leachate and 10% carbonized bio chars for activated matter washed. Washing treatment carried out for adsorbed metal ions and dissolved ion change in liquid effluent matter shows capturing activity as 34,2 gr/lt for Zn in the carbon tube. The different types of contaminated slurries mixing parameters particle size and density are becoming so critical in metal adsorption in CIP tube in the microwave furnace.

Keywords: *Microwave Radiated CIP, CIP Process, Active Carbon, Popped Corn, Popped Rice, Cotton, Cu Leaching*

1. Introduction

Zn ores are enriched by the Hakkari zinc concentration plant of Ölmez Holding which preferred crushing and flotation method (Canbazoğlu et al., 1988; Kaya et al., 2019):

(1) Crushing and crushing process; with this process, the ore is reduced to powder size, which enables enrichment by flotation and the liberation of the zinc ore (Kaya et al., 2019; Santoro et al., 2020).

(2) Flotation is also used and the poor ore is enriched to powder size and sold. However, precious metals such as Pb and Cu are disposed of in ore waste (Santoro et al 2020) and cannot be recycled, and their recovery by flotation is particularly costly. Later leaching of zinc is proposed for zinc and other metal extraction (Girgin and Kirşan, 1992; Bodas, 1996, Wang et al., 2019; Wadnerkar et al., 2015).

In this study, acid or base solution was used to dissolve and recover zinc by dissolving Zn ore waste in powder size by hydrometallurgical method. (Dayton, Keane, and Chase Girgin)In this recovery process, the recovery rate can exceed 80%, but it is necessary to prevent waste solution pollution. Cementation of metals in solution or retention with active carbon is the most practical method. The pyrometallurgical process comprises the production of Zn oxide in facilities containing the widely used Waelz Furnaces, which is a costly process and is not suitable for waste processing.

1.1. Biochars as Active Carbon of Popped Corn /Rice and Cotton

Biochar of popped rice and corn were having much more surface active sites an holes with the great surface area of 120 m^2/gr as high capturing capacity and great meta adsorption activity on char carbon bu surface electrical apolar end and polar hole matters so that high efficient Cu and. Zn adsorption yield at 76 and 88 % received.

Active carbon is commonly used in Gold adsorption from cyanide solutions in CİP method in pachuca tanks. The adsorption period is becoming much ın parameter in adsorption and activity and carbon density of Pachuca tank.

There is a great concern over gold and cobalt recovery by surface adsorption on active carbon highly stable in CN basic solutions with high level iron cyanide and even Zn, Cu CNs (De Andrade Lima et al., 2016; Dutrizac, 2013; Farahmand et al., 2019). The metals in cyanide leachate recoveries at amount over 40 mg/l, 10 mg/l Cu streams in pipe CIP tanks could be adsorbed at 67% performance yield with 3% deteriorating active carbon strength (Wadnekar et al., 2015). The cost of materials such as cotton, popped rice and corn bio active carbons and microwave processing related acid charging or decaying technologies were also investigated at low cost (Tosun, 2022); The microwave radiated CIP lab tests at cycled matter with regarded a unit packed system during decaying time of hours to a day. The cost of designed operation flow sheets demonstrated that lower popped rice carbon load at vol. 30% to aliquate was advantageous at few hours time over copper adsorption. The CN leaching of complex Cu ore is usually evaluated as illustrated in Fig. 1.

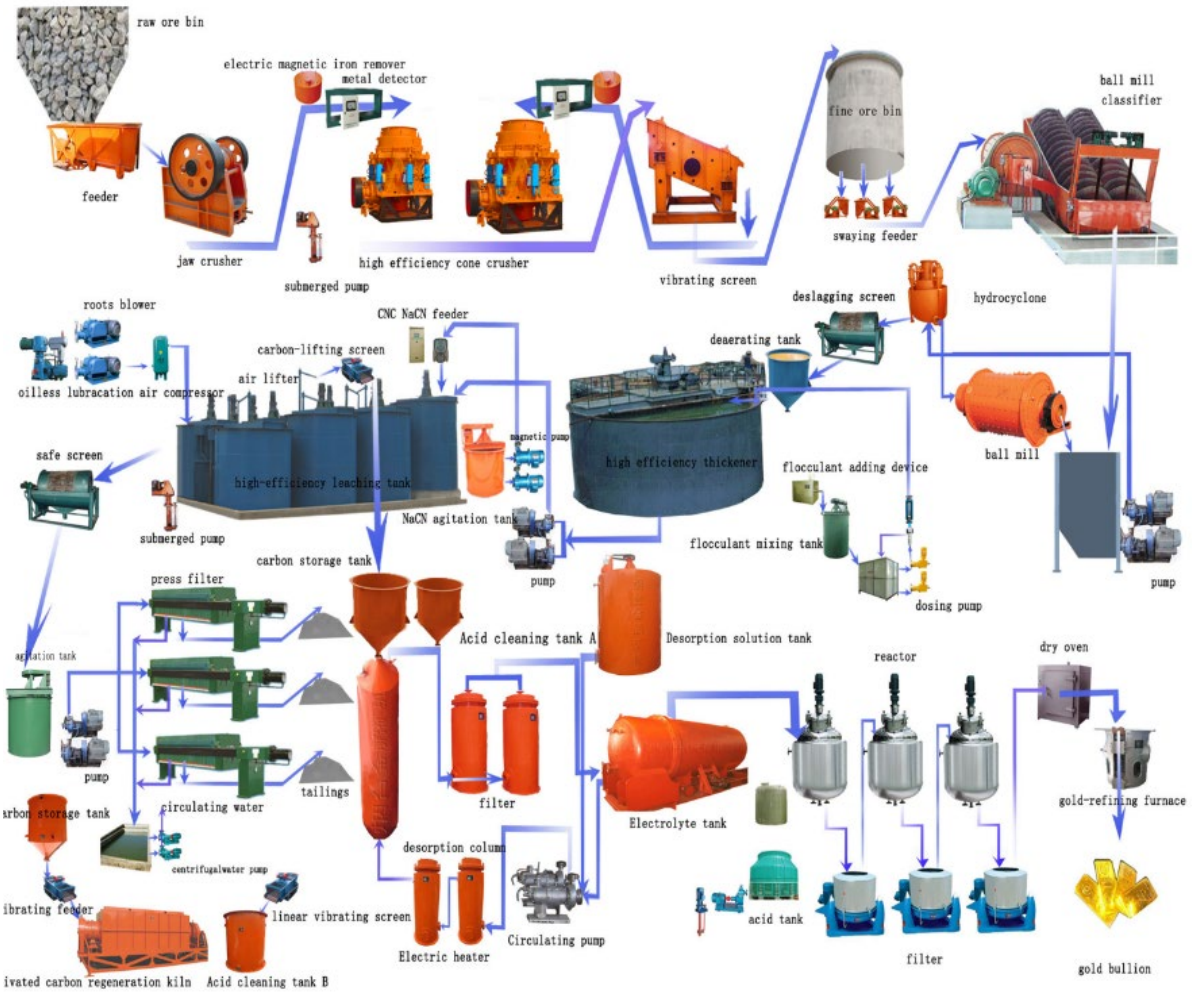


Fig. 1. 2500 t/d copper CIL/CIP plant with leaching CN solutions for Cu and Au.

The production flow sheet for Cu and Zn and CIL(CIP) process (Behnajady et., al 2012), had advantageous parameters in production using recycling char. The microwave processing parameters were also defined for metal leaching (Tosun, 2915). As a result of the experiments using microwave on zinc ore wastes with high iron content was efficient. The waste stocks reaching over 3 million tons in the mine site were carried out at laboratory dissolution pipeline unit established. Model dissolution unit was an efficient design on long search over the waste quality using a very well-time dependent leaching on the parametric analysis of efficiencies.

1.2. CIL/CIP Process in Poor Ore Leaching

CIL process is contain the units of decontaminate , concentrate before leaching , leaching and adsorption , desorption and electrowinning , hydrometallurgy , regeneration of activated carbon , tailings filling , waste water treatment defined as follows;

Decontaminate impurity ：remove the impurity like the bits of mood before cyanide adsorption, avoid the bits of mood adsorb the gold from slurry, avoid the bits of mood block the carbon separator. Counter current flows for metal extraction and adsorption of metal ions might be managed as shown in Fig. 2.

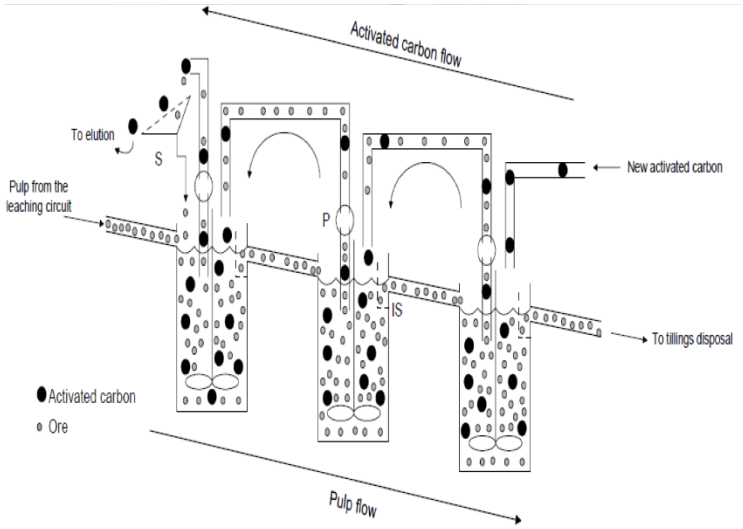


Fig. 2. Carbon in-Leach CIL/Carbon in-Pulp CIP flow with leaching effluents for extraction.

Concentrate before leaching, usually to reach a suitable leaching concentrate, the slurry should be dewatered through the thickener before leaching , the concentration could influence the leaching time and influence the float of activated carbon (Zhang et al., 2019; Wang et al., 2020).

Leaching and adsorption: put the slurry after decontaminated and concentrated into the high-efficiency leaching tank (Mannin and Kappes etal 3030, Hanilçi 2013), there are 5-8 tanks normally , add cyanide solution into the former two tanks , add activated carbon into the other five tanks , activated carbon adsorb gold become the loaded gold carbon , the loaded gold carbon lift into the lifting screen by air lifter , the lifting screen separate activated carbon and slurry .

Desorption and electrowinning : the desorption of activated carbon and electrowinning the liquid gold are completed in a closed system , in a high temperature and high pressure , activated gold carbon after desorption and electrowinning become gold pulp and barren carbon . Main equipment including : desorption column , acid tank , heater , filter , desorption tank , electrowinning tank.

Application of the regenerated activated carbon : the activated carbon after desorption make acid washing to remove the carbonate accumulate , after times of using that need heating activated to regenerate the carbon , then for recycling . Main equipment including activated carbon regenerated tank , water quench tank , fine carbon separate screen .

1.3. Microwave CIL/CIP

Zinc oxide ores can be dissolved under microwave radiation by acidic leaching processes. However, zinc is dissolved following the dissolution of many other metals such as Fe, Ca, Mg. Pipe line transfer was preferred for slurries haulage in mining (Tosun, 2022). This method will facilitate of leaching poor zinc ores before sending to solution plants from the mining areas of Hakkari reaching over 15-22 different mining areas widely spread in the province. Topographic conditions were also was creating a great problem for haulage of ore at minus 50 mm to processing plant area. However the poor ore stacks

was reaching millions of tons heap. Additionally heap leaching will be great threat for environmental concerns if used for poor ferrous zinc ores.

2. Material and Methods

Microwave heated mill slurries of Hakkari ferrous poor zinc ores used in this study. The studied process compromised a microwave heated leaching tube and pipe transferring in a modified type of the pressurized pipes at 5 bar. The leachate was transferred 10 mins time following microwave radiated slurry on the-water jet at 1 bar and then pressurized the slurry for pipeline transfer to the cycling leaching vessel. The tube leaching and pipe transfer leaching used for ultrafine particles, conventional type of ball mill used in cement materials.

In this study, the microwave activated char dust is treated the in the leach liquor in cycling tube flow as minor dissolved Cu and Zn passes through the secondary activated Pachuca cycling dissolution. Cycled pipe in tube sized as tube bags at that junction to each under 2 mm sized coagulates at total of feed size over 74 microns in dissolution process. (Fig. 3)

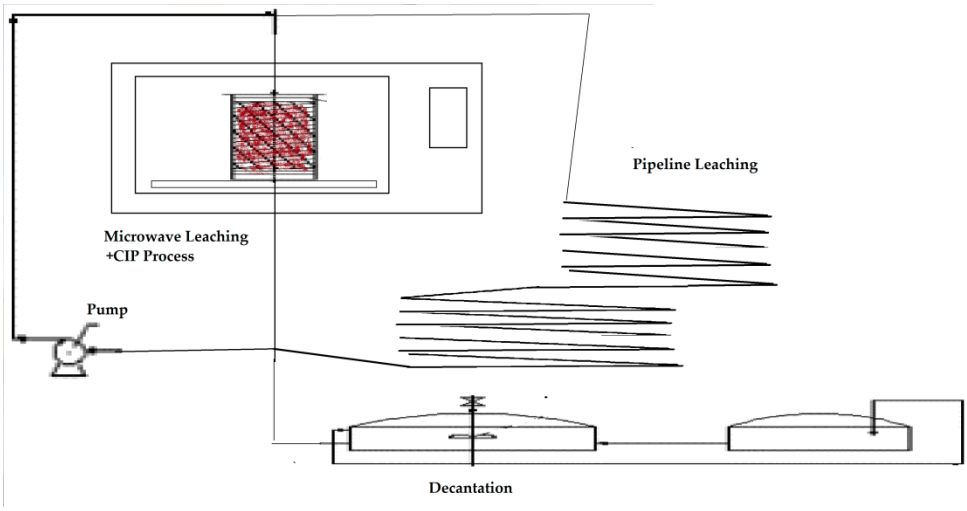


Fig. 3. CIP Biochar adsorption model with microwave effect.

Table 1. Chemical composition of the poor zinc ores, Zinc Tailing Heaps of Hakkari

Element *w*/%	Zn	Pb	Cd	Cu	Fe	MgO	CaO	SiO_2
Tailing A	11.24	7.25	0.05	0.04	24.12	1.5	4.4	26.2
Tailing B	14.24	0.25	0.03	0.06	20.12	1.3	3.4	29.3
Tailing C	9.24	9.25	0.35	0.04	29.12	1.2	5.4	26.29

3. Results and Discussion

The adsorption characteristic performed in biochar adsorption tests determines the results of the dissolution test. The dissolution efficiency of Zinc and Copper is used in the classification for the identification of fair ore wastes; Dissolution amounts of cadmium, lead and Fe remained low. Therefore, ore waste must be processed by an appropriate method to avoid negative environmental impacts. According to this dissolution, CIP biochars at pH levels between 1 and 2 are bleached for metal washing. Fouling of biochars with Fe during CIP dissolution and adsorption of metals on biochar with Fe contents between 6% and 17.8%. It was found to be suitable. The amount of zinc showed similar results to previous studies, but that of iron was determined to be relatively high due to the microwave effect, and that of copper was also relatively high. It showed that the zinc concentration for Hakkari ore tailings in CIP Zn washed aliquots was between 139.7 and 144.4 mg/L. Cu values were lower at the levels of 59

to73 mg/L. These figures prove that zinc and copper recovery efficiency can be maintained in biochar between 83% for Zn and 72% for Cu metal recovery. This showed it was possible to potentially efficient biochar capture for Zn and Cu, even other valuable metals in biochar in the second stage recovery.

3.1. Adsorption on biochar CIP

Hakkari poor Zn ores contain 7.6–18% Fe; Therefore, dilute sulfuric acid was used to dissolve in thawing processes, and high pH thawing and microwave thawing and biochar were also subjected to metal adsorption. The observed results showed that the Zn and Cu adsorbed values in washed aliquate, for the active carbons as biochars of the popped corn, rice and cotton were determined as follows: Basicly, first stage pH 4 is used for Zn extraction, the second stage leaching of pH1.5 is used for Cu extraction.

The main purpose of the pH 4 microwave acidic leaching process in the first stage for Zn and the secondly lower pH1,5 was applied for the separation and extraction of solid copper residue and liquid zinc sulfate and copper. Tailing B leaching is carried in CIP leaching below pH 2 under microwave radiation. After separation, zinc sulfate was subjected to microwave effective adsorption on biochar. As the temperature increased and the pH level decreased, the dissolution rate of Zn and Cu increased. In this first stage, the leaching rate of Zn remained between 88% and 96%, and that of Cu remained between 4% and 5%. It contained a pH level of 2.5; Zinc ion was retained in the biochar in the greatest amount, and metallic lead and copper remained in the least amount. Fig. 4 showed the high Zn extraction yields decreased by increasing leaching pH in CIP.

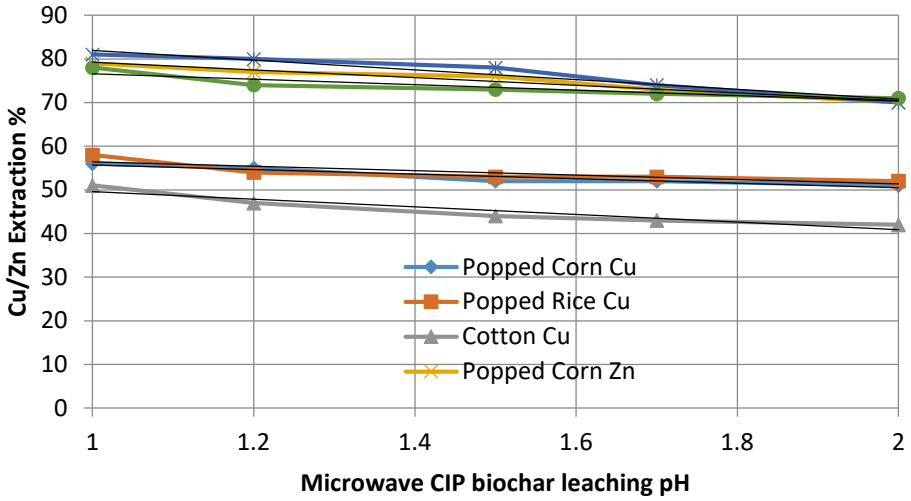


Fig. 4. Zinc and copper recovery during microwave radiated CIP leaching versus leaching pH levels for second stage Cu extraction

Fig. 5 showed the high Zn extraction yields reached by increasing CIP leaching period in 9 and 10 minutes under microwave radiation at pH 4.

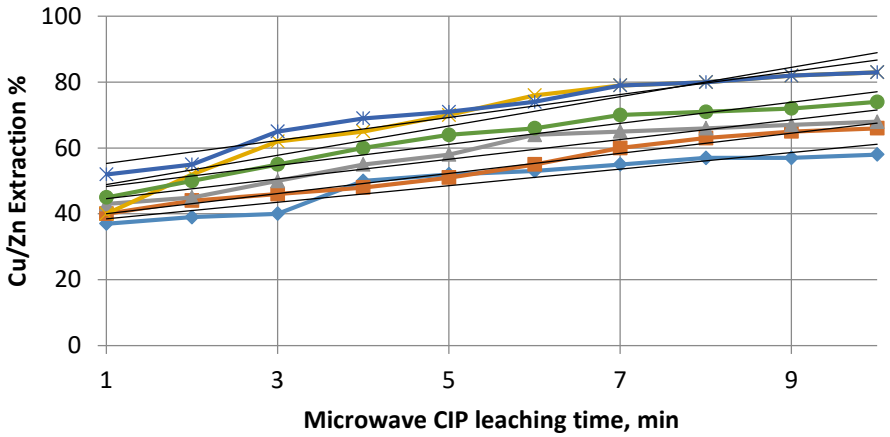


Fig. 5. Zinc and copper recovery during microwave raiated CIP leaching versus time at pH 4.

After Tailing B, the solid copper residue was leached again using bleaching in the second stage. After Tailing B, at various temperatures and pH levels. It shows the results of solid copper residue in the S4 row in the As the temperature increased and the pH level decreased, the recycling rate of Cu increased regarding Tailing B. Meanwhile, the leaching rate of Cu phase was 47.0% and Zn phase was 82.4%.

After Tailing B and biochar CIP bed of popped corn, metallic copper was recycled and Zn was bleached in the smallest amount. Optimal conditions for Tailing A included a temperature of 60°C and a pH level of 1.5; metallic copper was recycled in the largest amount and zinc ion was leached in the smallest amount; This approaches the extraction for Zn of flotation tailings at finer size of below 150 micron sized.

As a result, the use of biochar and microwave effective adsorption in the processing of poor zinc ore wastes, while the leaching time of zinc with sulfuric acid leaching was changed between 30 and 40 minutes, while the leaching temperature (80 °C), liquid/solid ratio at 25% and stirring speed (500 rpm). It was determined to be suitable.

4. Conclusions

The adsorption characteristic performed in biochar adsorption tests determines the results of the dissolution test. The dissolution efficiency of Zinc and Copper is used in the classification for the identification of fair ore wastes; Dissolution amounts of cadmium, lead and Fe remained low due to usage pH 4 leaching electropotential with lower oxidation matter in CIP liquid. Therefore, ore waste must be processed by biochar types such as cotton carbon, rice and corn carbon with low cost, that is an appropriate method to avoid negative environmental impacts.

The Zn and Cu adsorption efficiency and kinetics of Hakkari poor Zn ferrous and ore waste with biochar after dissolution proved that this method is suitable for poor ferrous ores. During this process, metal recovery such as Pb, Mn and Cd is also possible. Acidic leaching of such ores and industrial wastes can be carried out using diluted sulfuric acid, without causing environmental problems. The dissolution method in aqueous environments can be chosen gradually. While Zn is recovered in the first stage, copper recovery can occur in biochar in the second stage. For this purpose, the diluted sulfuric acid dissolution process can be done in two stages.

References

Behnajady B, Moghaddam J, Behnajady MA, Rashchi F (2012). Determination of the optimum conditions for the leaching of lead from zinc plant residues in NaCl–H_2SO_4–$Ca(OH)_2$ media by the Taguchi method. Ind Eng Chem Res. https://doi.org/10.1021/ie202571x

Bodas, M.G. (1996). Hydrometallurgical treatment of zinc silicate ore from Thailand,Hydrometallurgy, Volume 40, Issues 1–2, p 37-49, https://doi.org/10.1016/0304-386X(94)00076-F.

Canbazoğlu, M., Zengin, M., Aritaş, N., (1988). Heap Leaching Studies at Eti bank Ergani Copper Works, II. Uluslararası Cevher Hazırlama Sempozyumu, Izmir, 653-662

Dayton, S.H., (1987). Gold Processing Update, Engineering and Mining Journal, 25,29

De Andrade Lima, L. R. P. (2007) Dynamic simulatıon of the carbon-inpulp and carbon-in-leach processes, Brazilian Journal of Chemical Engineering, Vol. 24, No. 04, pp. 623 - 635

Dutrizac, J.E., (1992). The leaching of sulphide minerals in chloride media. Hydrometallurgy. https://doi.org/10.1016/0304-386X(92)90004-J

Farahmand F, Moradkhani D, Safarzadeh MS, Rashschi F (2009). Brine leaching of lead-bearing zinc plant residues: Process optimization using orthogonal array design methodology. Hydrometallurgy. https://doi.org/10.1016/j.hydromet.2008.07.012

Girgin I., Kirşan H İ,(1990). Yığın Liçi Uygulamaları ve Ekonomik Açıdan Önemi, MADENCİLİK Dergisi, Eylül1990, Cilt 30, Sayı 3, 30-43

Hanilçi N, Öztürk H, Banks, D (2020). Geological, geochemical and microthermometric characteristics of the Hakkari region Zn-Pb deposits, SE Turkey. Ore Geology Reviews, 125. Elsevier BV. 103667 doi:10.1016/j.oregeorev.2020.103667

Kaya M, Gul E, Kursunoglu S, Hussaini S (2019). Leaching of oxidized Turkish Pb–Zn flotation tails by inorganic acids, IMPC-Eurasia-2019 Congress, Antalya-Turkey

Keane, J.M., Chase, CK., (1987). Evaluation of Copper Dump and Heap Leaching situations, Mining engineering, 197-200.

Manning, T.J., Kappes, D.W. (2016). Chapter 25 - Heap Leaching of Gold and Silver Ores, Editor(s): Mike D. Adams, Gold Ore Processing (Second Edition), Elsevier, 2016,Pages 413-428, ISBN 9780444636584, https://doi.org/10.1016/B978-0-444-63658-4.00025-6.

Santoro L. , M. Boni, R. Herrington, A. Clegg, (2013). The Hakkari nonsulfide Zn–Pb deposit in the context of other nonsulfide Zn–Pb deposits in the Tethyan Metallogenic Belt of Turkey, Ore Geology Reviews,Volume 53,p 244-260,https://doi.org/10.1016/j.oregeorev.2013.01.011.

Santoro, L., Putzolu, F., Mondillo, N., Boni, M., Herrington, R. (2020). Influence of Genetic Processes on Geochemistry of Fe-oxy-hydroxides in Supergene Zn Non-Sulfide Deposits. Minerals, 10 (7) 602 doi:10.3390/min10070602

Stange W., (1999). The process design of gold leaching and carbon-in-pulp circuits,he Journal of The South African Institute of Mining and Metallurgy, FEBRUARY 1999,14-26

Wadnerkar D., M. O. Tade, V. K. Pareek, R. P. Utikar, (2015). Modeling and optimization of Carbon in leach (CIL) circuit for gold recovery, Minerals Engineering,Volume 83, 2015, p 136-148, https://doi.org/10.1016/j.mineng.2015.09.001.

Wang, P., Sun, Z.H., Hu, Y.N., Cheng, H.F. (2019). Leaching of heavy metals from abandoned mine tailings brought by precipitation and the associated environmental impact. Sci. Total Environ. 2019, 695, 133893

Zhang, R., Hedrich S., Römer, F., Goldmann D., Schippers, A., (2020). Bioleaching of cobalt from Cu/Co-rich sulfidic mine tailings from the polymetallic Rammelsberg mine, Germany. Hydrometallurgy. https://doi.org/10.1016/j.hydromet.2020.105443

Tosun, YI, 2022, Cycled Pipe Leaching following Microwave Char Treatment of Copper Tailing Sludges for Cu and Zn Extraction, 10th İnternatıonal conference on applied sciences, İksad Yayınevi, SAMSUN

Tosun, YI, 2015, Piritli atıkların ve atık küllerinin mikrodalga kavurma ile degerlendirilmesi. 5. Madencilik ve Çevre Sempozyumu, TMMOB Maden Müh. Oda. Muğla

Acid Mine Drainage (AMD): Revisiting and Recent Insights

Hikmet Sis [1]*, Osman Dolmaz [2]

[1] İnönü University, Faculty of Engineering, Mining Engineering Department, 44280 Malatya, Türkiye

*Corresponding author: hikmet.sis@inonu.edu.tr (Hikmet Sis)

Abstract:

Acid Mine Drainage (AMD) is the most common environmental threat resulting from to mining activities. AMD can cause direct and indirect environmental problems and its adverse impact can be surprisingly large. The largest contribution of AMD into streams and lakes is from the numerous abandoned mined lands that were mined and left without reclamation. AMD issues can be handled in three different ways: prevention of AMD formation, prevention of migration of the AMD water, and treatment and remediation of the land and water. Prevention the formation from its source is very desirable as it eliminates the possibility of contamination of the environment. Isolation the surfaces of potential acid forming materials to avoid contact with air and water should be the most effective AMD prevention method. This study focused on pretreatments of the sulfide ore to prevent AMD generation or reduce the AMD generation potential of the ore. The effect of CO2 gas adsorption and hence isolation of particle surfaces on the AMD generation potential were investigated. CO2 adsorption was made in a steel reactor tank and AMD generation properties of the ore samples were tested in a humidity cell conformed to ASTM D5744 standard. For assessment, the pH, sulfate, iron and copper contents of the acidic water, both, from untreated and treated samples were determined. The comparison of the results showed that the CO2 gas adsorption at different temperature under pressures could affect the AMD generation of sulfide ore to some time. It was concluded that CO2 gas retarded the reaction of particles with air by covering their surfaces and pores. Thereby, the adsorption of CO2 gas on sulfide particles could slow or retard the AMD generation.

Keywords: AMD

Umrek And Mineral Processing

Halim Demirkan [1]*, Ahmet İbuk [1]

[1] Maden Mühendisleri Mesleki Gelişim Derneği

*Corresponding author: halim.demirkan@gmail.com (Halim Demirkan)

Abstract:

ABSTRACT In 1994, Australia (JORC), Canada (CIM), the USA (SME), Europe (PERC), and South Africa (SAMREC) came together to establish CRIRSCO to create an international common standard. Turkey has been accepted as the 13th official member of CRIRSCO. UMREK represents Turkey as a member of CRIRSCO.

The union was established to bring together professionals in the fields of geosciences, mining, and metallurgy (ore enrichment), to enhance cooperation among its members, and to collaborate with the "National Mineral Resource and Reserve Commission (UMREK). "The Code, which is most widely used for public reporting, i.e., in capital markets, is also commonly preferred in Bank Credit transactions.

Ore Processings are mentioned in the UMREK Code; in the sections on Terms Used in the Code (Appendix 1), Scope (Application), Competence and Responsibility, Modifying Factors, Reporting of Metal Equivalents, Resource, and Reserve Estimates.

Keywords: *CRISRSCO, UMREK, YERMAM, International code, Mineral Processing*

1. Introduction

In order to determine the resources, reserves, and quality of minerals, sufficient information about the mineral deposit must be obtained. In other words, resources and reserves are determined and classified to the extent that the quality and quantity of this information are sufficient. As a result of exploration studies conducted in a mining site and the subsequent evaluation efforts, not only the volume and tonnage of the deposit but also all physical, chemical, geological, mineralogical, technical, technological, economic, legal, environmental, and social characteristics must be revealed to determine the deposit's resources/reserves.

The mining sector is a high-risk industry. The main reason for this risk is the difficulty in predicting the quantity and quality of the asset that will be uncovered through exploration. Along with this high risk, the investment cost in mining is also significant. Reducing this risk depends on scientific and technological studies conducted at every stage of exploration and after exploration. The studies carried out during mineral exploration, research, and production, the data generated, analyzed and tested in accredited laboratories in accordance with international standards, and reported by competent technical personnel ensure that these efforts are transparent, reliable, and meet international standards. This creates a consensus among engineers, planners, miners, investors, and financial institutions in the globalized world and under free-market economic conditions. Due to the increase in international trade and mining investments, there has arisen a need to establish an internationally acceptable resource/reserve classification system.

2. CRIRSCO

Mining exploration and operation is one of the fields with the highest investment risk. Due to the high risk and susceptibility to manipulation in mining exploration, reports have been prepared inaccurately, causing significant financial losses to both mining investment companies and their shareholders. The most well-known manipulations include Poseidon (Australia 1969), Bre-X (Indonesia 1996), Cartaway (West Africa 1996), Timbuktu (West Africa 1996), and Delgratia (Mexico 1997).

The need for reporting standards arose due to the necessity for mining companies to present and manage their mineral resources and underground wealth in the best possible way, to access investment resources, and to use a common language and terminology. Additionally, reporting standards are essential to mitigate risks in exploration and mining, prevent manipulation, and protect and safeguard the rights of investors. The goal is to reduce risk as much as possible and prevent manipulations through conducting exploration and development activities within a discipline in an open, reliable, and transparent manner (Demirkan, H., 2017; Demirkan, H., 2018).

As a result, countries with developed mining sectors have created their own reporting standards and have empowered "competent persons" in specialized fields to prepare and take responsibility for these reports. Qualified members of non-governmental organizations (NGOs) to which mining and geoscience professionals belong are authorized as Competent Persons (QP, CP). Competent Persons are required to have practical experience in their areas of expertise, uphold ethical values, prioritize professional development, and provide references in these matters.

In 1994, Australia (JORC), Canada (CIM), the USA (SME), Europe (PERC), and South Africa (SAMREC) came together to form CRIRSCO (Committee for Mineral Reserves International Reporting Standards) to establish international common standards. CRIRSCO was organized as an umbrella organization to promote best practices in the global reporting of mineral exploration results, mineral resources, and mineral reserves. CRIRSCO currently has 15 members. In addition to the founding countries, these include Chile (Comisión Minera), Russia (NAEN), Indonesia (KOMBERS), Brazil (CBRR), Kazakhstan (KAZRC), Mongolia (MPIGM), Colombia, Turkey (UMREK), the Philippines, and India (IMIC). As of May 2018, Turkey was accepted as the 13th country to join CRIRSCO (CRIRSCO, 2024; Demirkan, H., 2018).

CRIRSCO Template

The CRIRSCO template has been presented to assist in the effective promotion and dissemination of best practices for reporting exploration targets, exploration results, mineral resources, and reserves, widely accepted in national or regional reporting codes and standards. It includes best practices from updates to the codes and standards published by National Reporting Organizations (NROs) over the past five years (Demirkan, H., 2017; CRIRSCO, 2024).

The template pertains to the reporting of minerals that are defined in reporting standards as being economic or potentially economic. It does not directly address the reporting of minerals that are non-economic or yet to be discovered. The CRIRSCO template covers all solid minerals, including base and precious metals, gemstones, construction and industrial minerals, natural stones, and energy materials such as uranium and coal. However, it does not include non-solid energy minerals such as petroleum, gas, water, or geothermal energy (Demirkan, H., 2017; CRIRSCO, 2024).

3. UMREK

The demand for CRIRSCO standards by capital markets and their recognition by banks has highlighted the need for similar practices in Turkey. In other countries, the Competent Person system and standards (Codes) are managed by non-governmental organizations (NGOs) through professionals directly recognized by CRIRSCO. However, this model faced challenges in Turkey due to the absence of such NGOs. Consequently, Turkey decided to establish a commission (UMREK) primarily led by the private sector, which would grant the title of "Competent Person" to qualified individuals from among its members and operate through an NGO. Naturally, it also became UMREK's responsibility to develop a National Code (UMREK Code) aligned with CRIRSCO standards.

The "National Mineral Resource and Reserve Reporting Commission (UMREK)" was established through the Law No. 6745, titled "Law on Supporting Investments on a Project Basis and Amending Certain Laws and Statutory Decrees," which was published in the Official Gazette on September 7, 2016 (Official Gazette, 2016). The UMREK Regulation was published in the Official Gazette on July 26, 2017, with issue number 30135. On October 3, 2017, the appointment of the UMREK Chairman and members was completed (Official Gazette, 2017a; Official Gazette, 2017b).

According to the regulation, the commission members are representatives from the General Directorate of Mining and Petroleum Affairs (MAPEG), the General Directorate of Mineral Research and Exploration (MTA), the Banking Regulation and Supervision Agency (BDDK) or the Banks Association of Turkey (TBB), the Capital Markets Board (SPK) or Borsa Istanbul (BIST), the Union of Chambers and Commodity Exchanges of Turkey (TOBB), and four experts from Turkey's mining sector who are registered with relevant NGOs. Together with the TOBB representative, the total number of members from the private sector is five.

4. YERMAM

YERMAM was established as a union on December 4, 2017, by a decision of the Council of Ministers, with the aim of bringing together domestic and international professionals in the fields of geosciences, mining, and ore processing, fostering cooperation among its members, and collaborating with UMREK (YERMAM, 2017a; YERMAM, 2024; and the Prime Ministry Directorate General of Laws and Decrees, 2017).

YERMAM was founded to enhance cooperation in economic and technical fields, to benefit from mutual knowledge, experience, and technologies. Its purpose is to bring together domestic and international professionals working in the fields of geosciences, mining, and metallurgy, to develop collaboration among its members, and to work in partnership with UMREK (YERMAM, 2017a; YERMAM, 2017b; YERMAM, 2017c; YERMAM, 2017d).

5. UMREK Competent Person

A Competent Person (QP, CP, YK), by general definition, is a professional with an engineering title working in the mining sector who is registered in the appropriate membership class (professional member) of Recognized Professional Organizations (RPOs) and is granted a certificate of competence (certificate) from among those recommended by the RPO (UMREK, 2018a).

Qualified and experienced professionals working in the fields of geosciences, mining, and mineral processing, who meet the specified membership criteria, commit in writing to adhere to the UMREK Code and the rules established by UMREK, and uphold ethical values, can apply to UMREK for Competent Person certification through YERMAM (UMREK, 2018c).

A Competent Person must maintain up-to-date and continuous professional development in the relevant field, in addition to possessing ethical values and practical experience, and must prioritize and ensure professional development. UMREK Competent Persons are required to submit an annual report to YERMAM, documenting their professional development with supporting evidence. Failure to do so will result in their membership being suspended for one year. If a professional's YERMAM membership ends for any reason, their Competent Person status will also be terminated (UMREK, 2018b; UMREK, 2018d).

A Competent Person is authorized to prepare exploration, resource, and reserve estimation reports in their area of expertise, in accordance with the UMREK Code, and to sign these reports along with a witness. However, it is important to remember that reports prepared under the UMREK Code are multidisciplinary efforts, and different professionals are responsible for various aspects of the report based on its content (UMREK, 2023).

In Turkey, of the 166 UMREK Competent Persons, 94 are geologists and 57 are mining engineers. The other Competent Persons include hydrogeologists, geophysicists, environmental engineers, and geodesy engineers (UMREK, 2024).

6. UMREK Code

6.1. Content

The purpose of the UMREK Code is to provide a minimum standard, in line with international terminology, for the public reporting of exploration targets, exploration results, mineral resources, or mineral reserves. Such reporting should include all the information that investors and professional advisors might reasonably expect to request or find in a public report in order to make a reasonable and balanced judgment regarding exploration targets, exploration results, mineral resources, or mineral reserves. The Code is advisory in nature.

According to the latest version of the CRIRSCO Template, updated in 2019, the UMREK Code, which complies with the CRIRSCO Template (2019), was accepted by CRIRSCO in February 2023 and was shared with mining sector stakeholders on the UMREK website on April 12, 2023. It is set to come into force in 2024 (UMREK, 2018; UMREK 2023).

UMREK 2024 Content:

1. Introduction
2. Scope
3. Competence And Responsibility
4. Reporting Terminology
5. Reporting Of Exploration Targets
6. Reporting Of Exploration Results
7. Reporting Of Mineral Resources
8. Reportıng Of Mineral Reserves
9. Technical Studies
10. Reporting Of Metal Equivalents
11. Commodity Pricing And Marketing
12. Permitting And Legal Requirements
13. Sustaınabılıty Considerations

Table 1 - Check List Of Assessment And Reporting Criteria

Table 2 – Guideline For Technical Studies

6.2. UMREK Code Applications

The Code is primarily used in public reporting globally, particularly in capital markets. It is also widely preferred by banks in credit assessments.

With the introduction of UMREK in Turkey, the Capital Markets Board (SPK), in its meeting held on September 21, 2017, decision number 34/1151, decided that reports prepared by Competent Persons proposed by YERMAM and determined by UMREK would be the basis for valuation services in the capital market, including mineral exploration and the valuation and reporting of mineral resources and reserves (UMREK 2024).

It has been stated that reports prepared by individuals authorized by UMREK would be beneficial in evaluating credit processes or other transactions of banks, participation banks, and companies that are members of the Banking Regulation and Supervision Agency (BDDK) and the Financial Institutions Association. In summary, the UMREK Code has gained broad support from the stock market, banks, and the mining sector (UMREK 2024).

In 2019, Turkey implemented a unique application by incorporating UMREK into its mining legislation. An amendment to Article 24 of the Mining Law No. 3213 added the following sentence: "Areas of probable reserves; if not converted into resources and/or reserves under the National Mineral Resource and Reserve Reporting Code within ten years in Group IV mining operation license areas and five years in other grup mining operation license areas, will be revoked" (Official Gazette, 1985; Official Gazette, 2019; Official Gazette, 2022).

Another instance of UMREK being incorporated into mining legislation is in the "Discovery Rights." The amendment to Article 15 of the law regarding Discovery Rights (Amended Clause: 14/2/2019-7164/15 art.) reads: "The license holder is considered the discoverer of the minerals reported as resources or reserves through technical reports prepared in accordance with the National Mineral Resource and Reserve Reporting Code during the exploration and/or operating license period. A discovery certificate is granted to the license holder who requests this right." This change, following the introduction of UMREK, has imposed significant technical and financial burdens compared to the previous state of Discovery Rights, requiring substantial investment for what is a small fee (1%). The General Directorate of Mineral Research and Exploration (MTA), which is subject to the same law, was relieved of this obligation with a 2024 amendment (Law No. 7501, 11/05/2024) (Official Gazette, 2024; Official Gazette, 1985).

6.3. Mineral Processing in the UMREK Code

In accordance with the purpose of the Code, general terms are listed in Annex 1, along with other terms that can be considered synonymous. Annex 2 contains the qualified person approval form and compliance declaration. The information provided in Annexes 3 through 12 offers further guidance and detailed information regarding the reporting of specific commodities or situations. Ore Enrichment Operations are directly addressed in the UMREK Code within the sections on terms used under the Code (Annex 1), Scope (Application), Competence and Responsibility, Modyfing Factors, Reporting of Equivalent Metals, and Resource and Reserve Estimates (UMREK, 2018; UMREK, 2023).

Items Related to the Code:

Appendix 1 – Glossary Of Generic Terms And Synonyms

Beneficiation (Processing, Preparation, Concentration, Smelting and Refining)

Physical and/or chemical separation of constituents of interest from a larger mass of material. Methods employed to prepare a final marketable product from material as mined. Examples include screening, flotation, magnetic separation, leaching, washing, roasting, smelting and refining etc.

Metallurgical Factor: One of a set of fundamental metallurgical or processing criteria taken into consideration when evaluating the recoveries or processing routes for a mine or project.

7. SCOPE

Application

The definition of Mineral is broad, and therefore the Code is applicable to a diverse range of commodities for which public reporting of Exploration Targets, Exploration Results, Mineral Resources and Mineral Reserves is required by a relevant regulatory authority, including but not limited to:

- Metalliferous minerals;
- Coal;
- Diamonds and other gemstones;
- Industrial Minerals;
- Cement feed materials and construction raw materials;
- Dimension Stone, Ornamental and Decorative Stone
- Other mineral raw materials; and

- Mineralised fill, remnants, pillars, low grade mineralisation, stockpiles, dumps and **tailings (remnant materials).**

8. Competence And Responsibility

The professional experience of the Competent Person in the related field must be up-to-date. Guidance

The Competent Person is generally expected to be a geoscientist (geologist, geophysicist or geological engineer, geophysical engineer) to be able to estimate and report Exploration Targets, Exploration Results or Mineral Resources, but for reporting Mineral Reserves, the Competent Person may be qualified in other fields such as mining engineering, **mineral processing engineering**, and may also be a minerals industry professional registered to an appropriate member grade of the RPO, who contributes to the modifying factors in the report.

9. Reporting Terminology

A Life of Mine Plan (LoMP) of at least Pre-Feasibility level can be used in an operating mine where there is no significant capital expenditure required.

Measured Mineral Resources may convert to either Proved Mineral Reserves or Probable Mineral Reserves. The Competent Person may convert Measured Mineral Resources to Probable Mineral Reserves because of uncertainties associated with some or all of the Modifying Factors, which are taken into account in the conversion from Mineral Resources to Mineral Reserves. This relationship is shown by the broken arrow in Figure 1. Definition

Modifying Factors are considerations used to convert Mineral Resources to Mineral Reserves. These include, but are not restricted to, mining, processing, metallurgical, infrastructure, economic, marketing, legal, environmental, social, governance (ESG) and regulatory factors.

10. Reporting Of Mineral Resources

Geological evidences and knowledge required for the estimation of the Mineral Resources must include sampling data supporting Inferred, Indicated and Measured Mineral Resource classifications. Sampling data must be present at suitable intervals indicating the geological, chemical, physical and mineralogical characteristics of the mineralization. A Mineral Resource can only be estimated when sampling data are available.

The term 'reasonable prospects for eventual economic extraction' implies an assessment (albeit preliminary) by the Competent Person in respect of all matters likely to influence the prospect of economic extraction including the approximate mining parameters. In other words, a Mineral Resource is not an inventory of all mineralisation drilled or sampled, regardless of ***cut-off grade***, likely mining dimensions, location, or continuity. It is a realistic inventory of mineralization which, under assumed and justifiable technical, economic and development conditions, might, in whole or in part, become economically extractable.

A Competent Person using the criteria listed in Table 1 of the public report with regards to estimation of Mineral Resources, must clearly explain and discuss these criteria. These explanations should also include the discussion of the technical and economic viability ***(Modifying Factors)*** for the applied cut-off assumptions.

11. Reporting Of Metal Equıivalents

The reporting of Exploration Results, Mineral Resources and/or Mineral Reserves for polymetallic deposits in terms of metal equivalents (a single equivalent grade of one major metal) must show details of all material factors contributing to the net value derived from each constituent.

Reporting on the basis of metal equivalents is not appropriate if metallurgical recovery information is not available or not able to be estimated with reasonable confidence.

Table 1 - Check List Of Assessment And Reporting Criteria

Section 2: Geological Setting, Deposit, Mineralisation

11.1. Geological Setting, Deposit, Mineralisation

(v)Significant minerals present in the deposit, their frequency, size and other characteristics, including a discussion of minor and gangue minerals where these will have an effect on the processing steps and the variability of each important mineral within the deposit.

Section 3: Exploration and Drilling, Sampling Techniques and Data

11.2. 3.3-Sample method, collection, capture and storage

(iii) A description of each data set (e.g., geology, grade, density, quality, geo-metallurgical characteristics etc.), sample type, sample-size selection and collection methods.

Section 5: Technical Studies

11.3. Metallurgical and Testwork

Mineral Resources

The possible processing methods and any processing factors that could have a material effect on the likelihood of eventual economic extraction. The appropriateness of the processing methods to the style of mineralisation.

Mineral Reserves

(i) The source of the samples, the representivity of the potential feed and the techniques used to obtain the samples, laboratory and metallurgical testing techniques.

(ii) The basis for assumptions or predictions regarding metallurgical amenability and any preliminary mineralogical test work should already be carried out.

(iii) The processing method(s), equipment, plant capacity, efficiencies, and personnel requirements.

(iv) The nature, amount and representativeness of metallurgical test work undertaken and the recovery factors used. A detailed flow sheet / diagram and a mass balance, especially for multi-product operations from which the saleable materials are priced for different chemical and physical characteristics.

(v) Assumptions or allowances made for deleterious elements and the existence of any bulk-sample or pilot-scale test work and the degree to which such samples are representative of the ore body as a whole.

(vi)Disclosure of whether metallurgical process is well-tested technology or novel in nature and if novel, justification of its use in Mineral Reserve estimation.

Appendix 3 – Reporting Of Mineralised Fill, Pıllars, Low Grade Mineralisation, Stockpiles, Dumps And Tailings

A3-1. The Code is applied when reporting all potentially economic materials. This can include mineralised fill, remnants, pillars, low grade mineralisation, stockpiles, dumps and tailings (remnant materials) where there are reasonable prospects for eventual economic extraction in the case of Mineral Resources, and where extraction is reasonably justifiable in the case of Mineral Reserves.

A3-2. Unless specified otherwise, Articles 1 to 13 of the Code (including Figure 1) apply.

A3-3. Table 1, as part of the Code, should be considered persuasive when reporting on mineralised fill, remnants, pillars, low grade mineralisation, stockpiles, dumps and tailings.

A3-4. Any mineral-bearing material defined in this Article, is thought to be similar to in situ mineralization in terms of Mineral Resource and Mineral Reserve reporting. Assessments related to the

extraction of such mineral-bearing materials must be carried out by experienced and professional people.

A3-5. If there are no reasonable prospects that the mineral-bearing materials defined in this Article can be operated wholly or partially in economic terms, such materials cannot be categorised as a Mineral Resource nor as a Mineral Reserve.

A3-6. If some parts of the mineral-bearing materials are currently sub-economic, and there is a reasonable expectation that these materials can become economic in the future, then these materials can be categorised as a Mineral Resource.

A3-7. If technical and economic studies indicate that the material can be mined in economic terms under the assumed realistic conditions, then the material can be classified as a Mineral Reserve. Guidance

The above Articles apply equally to low grade in situ mineralisation, sometimes referred to as 'mineralised waste' or 'marginal grade material', and often intended for stockpiling and treatment towards the end of mine life.

For clarity of understanding, it is recommended that tonnage and grade estimates of such material be itemised separately in Public Reports, although they may be aggregated with total Mineral Resource and Mineral Reserve figures.

Stockpiles are defined to include both surface and underground stockpiles, including broken ore in stopes, and can include ore currently in the ore storage system.

Mineralised material in the course of being processed (including leaching), if reported, should be reported separately.

12. CONCLUSION

Ore preparation and processing activities, which are part of mining, are among the most crucial factors in resource and reserve estimation. Since the technology and cost of ore preparation, known as the modifying factor, directly affect feasibility and reserves when estimating the conversion from resource to reserve, ore preparation and beneficiation activities must be thoroughly considered in reports prepared according to the UMREK Code.

REFERENCES

General Directorate of Laws and Decisions of the Prime Ministry, 2017. Cabinet Decision dated December 4, 2017, and numbered 11211.7.

CRIRSCO, 2024. "Committee for Mineral Reserves International Reporting Standards", https://www.crirsco.com/ (Haziran 2024)

DEMİRKAN, H. 2017. Ulusal Madenlerde Rezerv ve Kaynak Raporlama Komisyonu (UMREK) Çalıştay Notları, Halim DEMİRKAN, MAYEB Basın Yayın İnsan Kaynakları Ltd. Şti., Ankara,

DEMİRKAN, H. 2018. Process of Turkey (Dated June 2018) and Workshops Notes, National Resource and Reserves Reporting Committee of Turkey (UMREK), MAYEB Basın Yayın İnsan Kaynakları Ltd, Ankara,

Resmi Gazete, 1985. Maden Kanunu (04.06.1985 tarihli ve 3213 Sayılı), 15/6/1985 Sayı:18785, 15.06.1985, Ankara.

Resmi Gazete, 2016. Yatırımların Proje Bazında Desteklenmesi ile Bazı Kanun ve Kanun Hükmünde Kararnamelerde Değişiklik Yapılmasına Dair Kanun" (20.8.2016 tarih ve 6745 Sayılı), …Sayı:29824, 7.9.2016, Ankara.

Resmi Gazete, 2017a. UMREK (Ulusal Maden Rezerv ve Kaynak Raporlama Komisyonu) Yönetmeliği, Sayı:30135, 26.07.2017, Ankara.

Resmi Gazete, 2017b. Ulusal Maden Kaynak ve Rezerv Raporlama Komisyonu Hakkında Yönetmelikte Değişiklik Yapılmasına Dair Yönetmelik, Sayı:30285, 29.12.2017, Ankara.

Resmi Gazete, 2019. Maden Kanunu İle Bazı Kanunlarda Ve Kanun Hükmünde Kararnamede Değişiklik Yapılmasına Dair Kanun, Sayı:30700, 28.2.2019, Ankara

Resmi Gazete, 2022. Maden Yönetmeliği, Sayı: 32040, 11.12.2022, Ankara.

Resmi Gazete, 2024. Maden Kanunu ile Bazı Kanunlarda Değişiklik Yapılmasına Dair Kanun, Sayı: 32543, 11/05/2024, Ankara.

UMREK, 2018a, Ulusal Maden Kaynak ve Rezerv Raporlama Komisyonu, Ulusal Maden Kaynak ve Rezerv Raporlama Komisyonunun Çalışma Usul ve Esasları, Ankara.

UMREK, 2018b, Ulusal Maden Kaynak ve Rezerv Raporlama Komisyonu, Yetkin Kişiler İçin Sürekli Mesleki Gelişim (SMG) Rehberi, Ankara.

UMREK, 2018c, Ulusal Maden Kaynak ve Rezerv Raporlama Komisyonu, UMREK Yetkin Kişi Tebliği, Ankara.

UMREK, 2018d, Ulusal Maden Kaynak ve Rezerv Raporlama Komisyonu UMREK Yetkin Kişi Etik Kurallarına İlişkin Usul ve Esaslar Tebliği, Ankara.

UMREK Ulusal Kaynak ve Rezerv Raporlama Komisyonu, Ulusal Maden Kaynak ve Maden Rezerv Raporlama Kodu, 2018, Ankara.

UMREK Ulusal Kaynak ve Rezerv Raporlama Komisyonu, Ulusal Maden Kaynak ve Maden Rezerv Raporlama Kodu (2. Versiyon), Şubat 2023, Ankara.

UMREK -Ulusal Madenlerde Rezerv ve Kaynak Raporlama Komisyonu, https://www.umrek.com.tr (Haziran 2024)

YERMAM, 2017a. Yerbilimleri, Maden ve Metalürji Profesyonelleri Birliği Tüzüğü, 2017/11211 Sayılı Bakanlar Kurulu kararı, 04.12.2017, Ankara.

YERMAM, 2017b. Yerbilimleri Maden ve Metalurji Profesyonelleri Birliği, YERMAM Üyelik Şartları Yönergesi, YERMAM, Ankara.

YERMAM, 2017c. Yerbilimleri Maden ve Metalurji Profesyonelleri Birliği, YERMAM Kayıtlı Üye Mesleki Ahlak Kuralları, Ankara.

YERMAM, 2017d. Yerbilimleri Maden ve Metalurji Profesyonelleri Birliği, YERMAM Yetkin Kişiler İçin Sürekli Mesleki Gelişim (SMG) Rehberi, Ankara.

YERMAM, Yer Bilimleri, Maden ve Metalürji Profesyonelleri Birliği, https://www.yermam.org.tr (Haziran 2024).

Judicial Approach to the Planning and Environmental Impacts of the Ore Preparation and Enrichment Facilities: The Case of Türkiye

Kerem Canbazoğlu [1*]

[1] A member of Ankara Bar Association, Türkiye

*Corresponding author: kerem@cac.com.tr (Kerem Canbazoğlu)

Abstract:

In mining operations, ore preparation and enrichment processes are conducted within designated facilities. The Mining Law encompasses these ore preparation and enrichment facilities within its definition of facilities. The selection of both location and technology for such facilities is closely scrutinized during permitting processes and legal proceedings, significantly influencing the trajectory of mining projects.

During the 1990s, the Council of State took the stance that gold mining operations utilizing cyanide leaching were contrary to the public interest, resulting in the annulment of relevant permits. In contemporary administrative judicial practices, the focus has shifted towards an assessment of the legal status of the areas where such facilities are situated, along with a thorough technical examination of the location selection criteria and the adequacy of measures to prevent or mitigate potential environmental impacts.

Furthermore, recent rulings by the Constitutional Court, particularly in the context of individual applications, have addressed mining projects from the perspective of the right to respect for private life. These rulings have involved evaluating whether a fair balance has been struck between the applicant's interests and the public interest, with the Court issuing findings of violations in some cases.

Within this evolving judicial landscape, other significant legal concerns related to mining projects—such as the technologies employed in ore preparation and enrichment facilities, the chemicals used in these processes, and the disposal and management of mining-related wastes—have emerged. Following the Environmental Impact Assessment (EIA) process, it is imperative to provide the strongest possible justifications for site selection, unit positioning, and technical reasons, particularly with regard to land acquisition and expropriation issues in mining projects.

Keywords: *Constitutional Court, Council of State, Environmental Impact Assessment, Ore Preparation and Enrichment Facilities, Public Interest, Judicial Review*

1. Introduction

Access to raw materials and natural resources, as well as the ability to exploit them using the most efficient and value-added methods, is a critical factor in the development and prosperity of societies. Historically, a profound distinction has emerged between societies capable of achieving this and those that are not. Consequently, the extraction and utilization of natural resources, including mining, have played a pivotal role in shaping the trajectory of societies throughout history.

The utilization of natural resources, particularly coal, significantly accelerated development following the Industrial Revolution. Development is no longer approached as something to be achieved "at any cost but rather as a process that must be carried out while managing the socio-economic conditions of the local populations and ensuring the sustainable management of the natural environment affected by these activities". This shift in perspective has been addressed in numerous United Nations conferences, leading to the establishment of various principles. The 1972 Stockholm Conference led to the adoption of the Declaration on the Human Environment, marking an early recognition of environmental concerns. Subsequently, the concept of sustainable development was introduced in the 1987 Brundtland Report, where it was defined as "development that meets the needs of the present without

compromising the ability of future generations to meet their own needs". Building on this foundation, the 1992 Rio Conference adopted principles aimed at encouraging nations to adopt environmentally responsible governance models. Additionally, key international agreements such as the UN Framework Convention on Climate Change[4], the UN Convention on Biological Diversity[5], and the UN Convention to Combat Desertification[6] were opened for signature. In 2000, the UN Millennium Development Goals were established, and the Johannesburg World Summit on Sustainable Development took place in 2002, where significant evaluations related to mining were discussed.[7] In 2003, the Equator Principles were adopted by the International Finance Corporation to identify, assess, and manage the environmental and social risks that international financial institutions must consider in projects requiring financing[8]. In 2012, marking the 20th anniversary of the Rio Conference, the Rio+20 Summit was held. At this summit, the outcome document titled "The Future We Want" was announced, which also emphasized the importance of mining.[9] Later, at the UN Sustainable Development Summit held on 27 September

[4] The Framework Convention on Climate Change was approved by Law No. 4990 dated 16.10.2003 and ratified by the Council of Ministers with Decision No. 2003/6458 dated 11.11.2003. Later, the Paris Agreement, which was adopted during the 21st Conference of the Parties of the Framework Convention on Climate Change on 12.12.2015, was signed on behalf of the Republic of Türkiye on 22.04.2016.

[5] The ratification of the Convention on Biological Diversity was approved by Law No. 4177 dated 29.08.1996, and the Convention was ratified by the Council of Ministers with Decision No. 96/8857 dated 21.11.1996. It was then published in the Official Gazette No. 22860 on 27.12.1996.

[6] The Convention passed through the Turkish Grand National Assembly's (TBMM) Environment Commission on 21 November 1996 and was approved by the TBMM with Law No. 4340 on 11 February 1998. It was published in the Official Gazette No. 23258 on 14 February 1998. The ratification process was notified to the Secretariat, and Türkiye officially became a party to the Convention as of 31 August 1998.

[7] A/CONF.199/20 - Report of the World Summit on Sustainable Development "Mining, minerals and metals are important to the economic and social development of many countries. Minerals are essential for modern living. Enhancing the contribution of mining, minerals and metals to sustainable development includes actions at all levels to: 1.) Support efforts to address the environmental, economic, health and social impacts and benefits of mining, minerals and metals throughout their life cycle, including workers' health and safety, and use a range of partnerships, furthering existing activities at the national and international levels among interested Governments, intergovernmental organizations, mining companies and workers and other stakeholders to promote transparency and accountability for sustainable mining and minerals development; 2.) Enhance the participation of stakeholders, including local and indigenous communities and women, to play an active role in minerals, metals and mining development throughout the life cycles of mining operations, including after closure for rehabilitation purposes, in accordance with national regulations and taking into account significant transboundary impacts; 3.) Foster sustainable mining practices through the provision of financial, technical and capacity-building support to developing countries and countries with economies in transition for the mining and processing of minerals, including small-scale mining, and, where possible and appropriate, improve value-added processing, upgrade scientific and technological information and reclaim and rehabilitate degraded sites." [https://sustainabledevelopment.un.org/index.php?menu=1259], AD: 05.10.2024

[8] As of 2023, 131 financial institutions have adopted these principles and consider them in their projects. [https://equator-principles.com/signatories-epfis-reporting/]

[9] A/RES/66/288 - The Future We Want "We acknowledge that minerals and metals make a major contribution to the world economy and modern societies. We note that mining industries are important to all countries with mineral resources, in particular developing countries. We also note that mining offers the opportunity to catalyse broad-based economic development, reduce poverty and assist countries in meeting internationally agreed development goals, including the Millennium Development Goals, when managed effectively and properly. We acknowledge that countries have the sovereign right to develop their mineral resources according to their national priorities and responsibility regarding the exploitation of resources described in the Rio Principles. We further acknowledge that mining activities should maximize social and economic benefits, as well as effectively address negative environmental

2015, the 2030 Agenda for Sustainable Development was adopted with the signatures of 193 member states, consisting of 17 goals and 169 sub-goals. In 2015, the Paris Agreement was adopted at the 21st Conference of the Parties of the Framework Convention on Climate Change.[10] The Paris Agreement established the framework for the post-2020 climate change regime, with all countries, for the first time on a global scale, committing to reducing greenhouse gas emissions after 2020. Following this, the COVID-19 pandemic and border closures caused significant disruptions in international raw material supply chains. Countries once again recognized the importance of producing raw materials within their borders. With the addition of regional and global geopolitical developments and conflicts, the critical and strategic importance of raw materials increased further. As a result, the challenges of transitioning to carbon-neutral economic systems within the context of combating climate change, along with the dependency on raw materials for renewable resources, and the sustainable production of raw materials in global production chains, have once again brought mining to the forefront.

On the other hand, the concept of human rights has become increasingly significant in the 21st century as one of the key factors driving the need for access to raw materials, particularly in the aftermath of world wars. The adoption of the Universal Declaration of Human Rights by the United Nations General Assembly in 1948 and the enforcement of the European Convention for the Protection of Human Rights and Fundamental Freedoms in 1950[11] marked important milestones in this regard. Following these developments, numerous countries recognized fundamental rights and freedoms within their national constitutions, and many established constitutional courts to ensure that laws enacted by legislative bodies conform to fundamental constitutional principles[12]. In some cases, national constitutions have defined the relationship between international human rights treaties and domestic legal norms, thereby incorporating such treaties into domestic law[13]. Subsequently, certain countries enacted constitutional amendments granting constitutional courts—traditionally tasked with reviewing the conformity of legislative acts with the Constitution—the authority to examine whether violations of fundamental rights and freedoms, as enshrined in the Constitution, have occurred in processes carried out by public

---

and social impacts. In this regard, we recognize that Governments need strong capacities to develop, manage and regulate their mining industries, in the interest of sustainable development. 228. We recognize the importance of strong and effective legal and regulatory frameworks, policies and practices for the mining sector that deliver economic and social benefits and include effective safeguards that reduce social and environmental impacts, as well as conserve biodiversity and ecosystems, including during post-mining closure. We call on governments and businesses to promote the continuous improvement of accountability and transparency, as well as the effectiveness of the relevant existing mechanisms to prevent the illicit financial flows from mining activities." [https://sustainabledevelopment.un.org/index.php?menu=1259] Access date: 05.10.2024

[10] The law regarding the approval of the Paris Agreement, Law No. 7335 dated 06.10.2021, was accepted by the Turkish Grand National Assembly (TBMM) and published in the Official Gazette on 07.10.2021.

[11] The Republic of Türkiye signed the convention in 1950 and accepted individual applications to the European Court of Human Rights in 1987. In 1990, Türkiye also recognized the compulsory jurisdiction of the European Court of Human Rights.

[12] The Turkish Constitutional Court was established with the 1961 Constitution.

[13] The 5th paragraph of Article 90 of the 1982 Turkish Constitution states, "International agreements duly put into effect have the force of law. No appeal to the Constitutional Court shall be made with regard to these agreements, on the grounds that they are unconstitutional." With the amendment made in 2004, the following expression was added: "In the case of a conflict between international agreements, duly put into effect, concerning fundamental rights and freedoms and the laws due to differences in provisions on the same matter, the provisions of international agreements shall prevail." This clarified that the provisions of international treaties regarding fundamental rights and freedoms have superiority over the provisions of laws on the same subject.

authorities. These courts have also been empowered to determine appropriate remedies for such violations.[14]

As evidenced, the economic, social, and legal transformations of the 20th and 21st centuries, along with the pandemic, supply chain disruptions, rising regional and geopolitical risks, and the global response to climate change, have highlighted the need for a new mining model to ensure sustainable supply of raw materials. The importance of sustainable and responsible mining practices -those that adhere to environmental and social governance standards, address the needs of local communities in mining areas, and prioritize sustainability before, during, and after operations—has grown considerably[15].

The economic performance of mining projects is typically evaluated through three primary indicators: production value, added value, and employment levels[16]. The employment level is particularly tied to the social dimension in the regions where mining activities occur. A comprehensive assessment of mining's broader impact also involves the examination of additional factors such as water usage, emissions, productivity, profits, tax contributions, land use, communication, transparency, and community engagement. [17]

Moreover, public and stakeholder participation in the planning, operational, and post-mining phases of mining projects has gained increasing importance. Ensuring transparency towards relevant parties, fostering trust, establishing effective grievance mechanisms, and implementing robust oversight of activities are key measures that can be integrated into such projects. Thus, before making any significant decisions related to a mining project, mining companies should go beyond their own interests, incorporating the views of those most affected by the project into the mining activities. This approach would ensure that public input has been taken into account, even during the design phase of the project.[18]

The concept referred to as obtaining or granting a social license to operate, which emerged in the late 1990s when the mining sector failed to meet societal expectations, was first introduced by the Global Mining Initiative in 1998. This initiative, established by major metallic mining companies, aimed to develop the sector's role in ensuring sustainable development.[19]

This approach is not a legally binding contract or consent form but rather a process that eliminates the unknown and uncertain aspects of the activity for stakeholders involved in decision-making processes. In this way, potential reactions can be reduced, uncertainty in the raw material supply process will be minimized, and the public interest will be served.

---

[14] The Republic of Türkiye, through an amendment made in 2010 to Article 148 of the 1982 Constitution, granted the Constitutional Court the authority to review individual applications. "Everyone may apply to the Constitutional Court on the grounds that one of the fundamental rights and freedoms within the scope of the European Convention on Human Rights which are guaranteed by the Constitution has been violated by public authorities. In order to make an application, ordinary legal remedies must be exhausted. In the individual application, judicial review shall not be made on matters required to be taken into account during the process of legal remedies."

[16] Konstantinos Komnitsas, Social License to Operate in Mining: Present Views and Future Trends, Resources, Published: 25 June 2020, p.1

[17] Konstantinos Komnitsas, Social License to Operate in Mining: Present Views and Future Trends, Resources, Published: 25 June 2020, p.2

[18] Konstantinos Komnitsas, Social License to Operate in Mining: Present Views and Future Trends, Resources, Published: 25 June 2020, p.2

[19] Konstantinos Komnitsas, Social License to Operate in Mining: Present Views and Future Trends, Resources, Published: 25 June 2020, p.2

In cases where stakeholder participation is not secured prior to making significant decisions regarding a project—referred to as the acquisition of a social license—the balance between public interest and stakeholder interests can only be maintained through the enforcement of legal frameworks.

Therefore, it is essential that all technical aspects of mining activities be determined through comprehensive, scientifically substantiated studies that emphasize the advantages of alternative site selections. Based on these findings, the permitting processes for such activities should be conducted and finalized accordingly, followed by a judicial process in which claims are addressed during litigation.

2. Approach of the Turkish Judiciary to Mining

2.1. Authorities in General Addressing Mining-Related Disputes in the Turkish Judiciary

The Turkish judicial system is characterized by a division between judicial courts and administrative courts. Judicial courts handle disputes arising from labor issues within the mining sector and contractual disputes related to the operation of mining licenses. Additionally, conflicts may arise from shareholder agreements between partners of licensed companies or from contracts concerning the transfer of shares within these companies. Disputes concerning mining rights fall under the jurisdiction of civil courts located in the area where the mine is situated. However, for disputes arising from the partnership structures of mining rights holders or share transfer agreements, judicial courts in locations mutually designated by the parties may hold jurisdiction. Moreover, the parties may also opt to resolve such disputes through arbitration.

Disputes regarding public permits related to mining and other investments are handled by administrative courts. Administrative justice was originated in France, and its establishment was justified by the need to oversee administrative actions through specialized authorities that are more attuned to the principles of public service and the public interest, as opposed to courts that traditionally handle private disputes between individuals.

In current judicial practice, matters related to mining areas, such as licenses, permits, environmental impact assessments, administrative fines, and decisions regarding the jurisdiction of the administrative court for the province where the license is located, are reviewed by these administrative courts.[20] Additionally, administrative courts also examine the permits for non-agricultural use of agricultural land within the licensed area, changes in the allocation purpose of grazing lands, and decisions regarding forestry permits.

In the Turkish administrative judiciary system, there is a three-tiered structure. Actions regarding permits for mining licenses proceed from administrative courts to regional administrative courts and then to the Council of State (Danıştay). In contrast, lawsuits concerning environmental impact assessments related to mining undergo a two-stage judicial process; these cases are heard by administrative courts and then go directly to the Council of State for appeal review without passing through regional administrative courts.

Prior to the implementation of individual applications to the Constitutional Court in Turkey in 2010, cases related to mining were adjudicated by the European Court of Human Rights. Following 2010, the decisions rendered by the Constitutional Court concerning judicial proceedings related to mining activities—particularly those involving environmental impact assessment procedures—have garnered significant attention. The rulings of the Constitutional Court reflect an approach that is applicable not only to mining activities but also to various forms of investment. Furthermore, there have been instances where individual applications submitted by mining companies contesting decisions of the mining administration that impose restrictions on permitted activities have been upheld by the Constitutional Court, leading to findings of violations.

[20] Administrative courts operate as panels consisting of one president and two members to carry out their proceedings.

2.2. Legal Framework

In Article 56 of the Constitution of the Republic of Turkey provides that: "Everyone has the right to live in a healthy and balanced environment. It is the duty of the State and citizens to improve the natural environment, to protect the environmental health and to prevent environmental pollution". Additionally, Article 20, titled "Privacy of Private Life," includes the provision: "Everyone has the right to demand respect for his/her private and family life. Privacy of private or family life shall not be violated." This provision is recognized as the right to respect private life and is interpreted alongside the right to live in a healthy environment. Furthermore, Article 17, titled "Personal Inviolability, Corporeal and Spiritual Existence of the Individual" states: "Everyone has the right to life and the right to protect and improve his/her corporeal and spiritual existence." This provision is also considered another fundamental right and freedom taken into account in the evaluations regarding the right to a healthy environment.

Following the provisions in the 1982 Constitution, Environmental Law No. 2872 was published in 1983. The first regulation regarding the implementation of the EIA process was published in 1993.[21] The EIA Regulation has been amended multiple times, with the most recent version coming into force in 2022.

In addition to the EIA Regulation, there are several other regulations concerning the mining sector. These include the Environmental Permit and License Regulation, the Mining Waste Regulation, the Waste Management Regulation, and the Regulation on the Prevention of Major Industrial Accidents and Mitigation of Their Impacts, all of which govern mining activities and their environmental regulations.

Certain actions related to environmental protection are classified as intentional or negligent pollution under the Turkish Criminal Code, subject to criminal penalties. Additionally, administrative sanctions regulated by Environmental Law are also applicable. Moreover, within the framework of the general principles of environmental law, the "polluter pays" principle is outlined in Article 30 of the Environmental Law, which states, "Real and legal persons who are confronted with injury due to any activity causing environmental pollution or degradation or have any acknowledge on such activities can apply to the administrative bodies and demand cessation of that activity."

2.3. The Administrative Judiciary's Approach to the Mining-Environment Relationship Prior to the Acceptance of the Individual Application Procedure and the ECHR Decision

In Turkey, the mining sector, which went through nationalization laws in the 1970s, gained momentum after the enactment of the Mining Law No. 3213 in 1985. Within this momentum, exploration licenses were granted in 1989, followed by operating licenses and forest permits in 1991, and a ten-year operating license in 1992. Notably, in 1992, before the EIA Regulation came into force, a public meeting was held to inform the public about the project and subsequently, in 1994, the Ministry of Environment granted an operating permit for the gold mining project in Bergama as a result of environmental impact studies. This project became a significant topic in the public agenda.[22] Following the annulment of the activity permit by the İzmir Administrative Court and the subsequent decisions overturned by the Council of State, operations were continued as a result of the actions taken within the scope of implementing these

[21] The date of the initial Environmental Impact Assessment (EIA) Regulation, according to the provisions outlined in the supplementary article of the EIA Regulation, indicates a threshold related to being subject to Environmental Impact Assessment (EIA). Projects initiated after this date are not required to undergo the EIA process.

[22] In paragraphs 14 to 20 of the Taşkın and Others v. Türkiye case, the permit processes are summarized. https://hudoc.echr.coe.int/%E2%80%99/app/conversion/pdf/#{%22fulltext%22:[%22\%22Ta%C5%9Fk%C4%B1n%20and%20Others%20v.%20Türkiye%20(dec.)\%22%22]}

decisions.[23] [24] The extension of the operating license for the mining permit, forest permits, and approvals issued by the Ministry of Health have all been the subject of separate administrative lawsuits. While these administrative cases were ongoing, a decision by the Council of Ministers on March 29, 2022, approved the continuation of the activities.[25] The decision was annulled in 2004 on the grounds that it was not based on an environmental impact assessment, leading to the suspension of the mining activities in August 2004. Subsequently, on August 27, 2024, the Ministry of Environment and Forest provided a positive opinion following the final environmental impact review. [26]

While the legal and administrative processes were ongoing, the application made to the European Court of Human Rights ("ECHR") in 1998 was evaluated and concluded in 2004 as the Taşkın and Others v. Turkey case. ECHR found the application admissible under Article 6, which pertains to the right to a

[23] In its decision numbered 1996/5477 E, 1997/2312 K, the 6th Chamber of the Council of State stated: "...The case was filed against the decision of the Ministry of Environment permitting gold mining operations by ... Mining Inc. in the ... district of ... city, subject to the fulfillment of the conditions in the undertaking, monitoring during the pre-operation, operation, and after the cessation of operations, compliance with environmental regulations, and the implementation of other measures required by the relevant institutions and organizations under the applicable legislation. Considering the right to life of individuals and the state's duty to protect environmental health, prevent environmental pollution, and ensure that everyone can lead a life in physical and mental well-being, the decision to permit gold mining operations using the cyanide leaching method—which has been shown to pose potential risk factors in the Environmental Impact Assessment and expert reports, and which would undoubtedly affect human life directly or indirectly through environmental degradation—is not in compliance with the public interest."

[24] Following the Council of State's reversal decision, the İzmir Administrative Court annulled the permit issued by the Ministry of Environment. Subsequently, a consultative opinion was requested from the 1st Chamber of the Council of State regarding how to implement the annulment decision. A report prepared by a team of experts formed by TÜBİTAK was presented to the Ministry of Environment in 2000. Based on this report, and considering the conclusions reached by TÜBİTAK, the positive opinion of the Ministry of Environment, and the views of the General Secretariat of the Presidency, permission was granted for operations. In the case brought against the TÜBİTAK Report that served as the basis for the permit, the İzmir Administrative Court ruled for the annulment of the report. In 2021, the Council of State ruled that the report was a preparatory document, thus reversing the decision. The İzmir Administrative Court concluded that there was no executive action subject to the case, and the Council of State upheld this decision. See paragraphs 42 to 50 of the Taşkın and Others v. Türkiye case.

[25] The İzmir Administrative Court dismissed the case filed by the İzmir Bar Association regarding the principal decision of the Council of Ministers. However, the Council of State overturned the dismissal decision, noting that the decision had not been published in the Official Gazette and had not been disclosed to the public, thereby considering the impossibility faced by the plaintiff in obtaining a copy of the decision. See paragraphs 76 and 77 of the Taşkın and Others v. Türkiye case.

[26] See paragraphs 78 to 81 of the Taşkın and Others v. Türkiye case.

fair trial, and Article 8, which concerns the right to respect for private life, and issued violation decisions after examining the merits of the application in light of these rights. [27] [28]

In addition to this case, numerous environmental lawsuits have been filed concerning the EIA processes governed by the provisions of the EIA Regulation that took effect after 1993. A significant number of cases have also been initiated against energy investments, including hydroelectric power plants and thermal power plants, which were prominent during that period. These decisions have been examined by the 6th Chamber of the Council of State, which has developed specific approaches for similar disputes. The administrative judiciary's effective examination of EIA reports has raised the issue of how the Ministry will implement the annulment decisions based on the deficiencies identified in the expert assessments conducted by the courts. In this context, the Ministry of Environment and Forests issued Circular No. 2009/7 regarding the implementation of the suspension and annulment decisions made by administrative courts. This circular stated that if annulment decisions pertain to technical issues rather than procedural matters within the EIA process, it would allow for the continuation of the EIA process by revising the deficiencies noted in the EIA report, instead of restarting the entire process.

A lawsuit seeking to annul the regulation designed to enhance legal predictability for investors was dismissed[29]. Ongoing cases concerning the second EIA decisions, which were issued following the revision of the EIA Report under the Circular, are currently being heard in the administrative courts. The Council of State's approach to the judicial review of EIA decisions made subsequent to the revisions outlined in Circular No. 2009/7 focuses on whether the deficiencies identified in the initial court decision have been adequately addressed in the revised report.

2.4. The Administrative Judiciary's Approach to the Mining-Environment Relationship Post-2010 and the Constitutional Court's Individual Application Decisions

With the 2010 amendment to the Constitution, individuals can file applications before the Constitutional Court for violations of fundamental rights and freedoms guaranteed by the Constitution, including those encompassed by the European Convention on Human Rights, perpetrated by public authorities. Consequently, both EIA cases and applications pertaining to the 2009/7 General Directive have come to the forefront of the Constitutional Court's agenda. The Constitutional Court evaluates these applications within the framework of the right to respect for private life, as articulated in Article 20 of the Constitution.

In the summary of decisions published by the Constitutional Court in 2021, cases involving the right to respect for private life and the protection and development of material and spiritual existence included

---

[27] Under Article 8 of the European Convention on Human Rights (ECHR), the European Court of Human Rights (ECHR) concluded that there had been a violation of the right to respect for private life under articles through 115 to 126. The reasoning for the violation decisions emphasized that, in terms of content, the Council of State's public interest assessment had favored the applicants' rights to a healthy environment and life. Procedurally, it highlighted that informing the local community had started in 1992, prior to the first activity permit granted in 1994, allowing them access to evaluations regarding environmental impacts. Additionally, it determined that the 2000 Prime Ministry opinion and the 2022 Cabinet decision undermined the procedural safeguards established by Turkish law and administrative court decisions for the applicants, leading to violations. See Taşkın and Others v. Türkiye, paragraphs 115 to 126.

[28] The court also found a violation regarding the right to a fair trial under Article 6 of the European Convention on Human Rights. It assessed that, despite the annulment of the permit granted by the Ministry of Environment in 1997 by the İzmir Administrative Court and the subsequent approval of this decision by the Council of State in 1998, the national authorities failed to comply with this ruling within a reasonable time. This failure led to a violation of the applicants' right to a fair trial. See Taşkın and Others v. Türkiye, paragraphs 127 to 138.

[29] The decision of 14th Chamber of Council of State dated 10.01.2013

the following: a complaint by an applicant whose apartment faced the installation of a base station[30], a complaint regarding the establishment of a hydroelectric power plant near the applicant's residence[31], an application related to the rejection of a compensation lawsuit by a person whose water treatment facility was not completed by the municipality within the stipulated time[32], a complaint regarding the underground placement of electrical cables on the street where the applicant resides [33], a claim alleging a violation due to dust and noise from construction on a neighboring property[34] and an application made by an environmental association regarding the annulment against the 2018 Environmental Impact Assessment Regulation, which was rejected by the Court due to lack of standing.[35]

In a case concerning another hydroelectric power plant project, the Constitutional Court reviewed a lawsuit contesting the EIA decision on the grounds that the project would inundate the village, harm biodiversity, and disrupt ecological integrity. The local court, after conducting an on-site inspection and preparing an expert report, concluded that the plaintiffs' claims were unsubstantiated and that the project's adverse environmental impacts were deemed acceptable according to scientific standards.[36]

Prior to 2021, an application was made to the Constitutional Court concerning a lawsuit filed in the administrative court by an applicant who obtained a copy of a contract related to a mining site in Bartın, owned by the Turkish Hard Coal Enterprise, in accordance with a decision from the Information Access Assessment Board. The applicant's request for the termination of the contract—based on a clause stipulating that it would automatically terminate—was denied. The Constitutional Court concluded that the applicant's assertion of being a potential victim of the mining project was unfounded. Since the applicant did not possess a current, personal, and directly affected situation, the application was not examined on its merits, and a ruling of lack of jurisdiction was issued concerning the applicant.[37]

---

[30] Hüseyin Tunç Karlık and Zahide Şadan Karluk, App. No: 2013/6587, 24/3/2016, The Constitutional Court stated that the applicants brought their claims of negative impacts before the judicial authorities, and the court provided comprehensive explanations for its reasons for rejecting these claims. It concluded that there was no violation of Articles 17 and 20 of the Constitution.

[31] Mehmet Kurt [GK], App. No: 2013/2552, 25/2/2016, The Constitutional Court ruled that in the case where the applicant's lawsuit against the positive EIA decision for the hydroelectric power plant project was rejected, there was no need for a different assessment regarding the permission for the designated transformer station area and that no illegality was found. However, it concluded that the failure to examine the potential environmental disturbances caused by the transformer station violated the positive obligation under Article 17 of the Constitution concerning the protection of the individual's material and spiritual existence.

[32] Mehmet Kurt [GK], App. No: 2013/2552, 25/2/2016, The Constitutional Court ruled that the failure to reasonably justify the lack of compensation for moral damages in the case due to the incomplete water treatment facility within the stipulated time violated the right to respect for private life under Article 20 of the Constitution.

[33] Ahmet İsmail Onat, App. No: 2013/6714, 21/4/2016

[34] Gülcan Tutkun Berk, App. No: 2015/2334, 29/11/2018

[35] Egeçep Derneği, App. No: 2015/17415, 17/4/2019

[36] Ahmet Bilgin and others, App. No:2015/11709, In its decision, the Constitutional Court stated that the judicial authorities conducted a comprehensive and qualitative investigation into the risks and harmful effects of the activity, concluding that all necessary measures were included in the Environmental Impact Assessment (EIA) report based on expert reports. Therefore, the legality of the operating processes was sufficiently assessed by the courts in response to the claims. The Court found that there was no possibility of establishing a fair balance between the interests of the applicants and the public in this specific case, and that the limits of discretion had not been exceeded. Consequently, it ruled that it was not possible to conclude that the public authorities failed to fulfill their positive obligations regarding respect for private and family life in the context of the right to housing.

[37] Ayşe Sevtap Uzun, App. No: 2013/6260, 13/4/2016

2.5. Recent Decisions of the Constitutional Court Post-2020

On November 1, 2023, the First Chamber of the Constitutional Court deliberated on individual applications concerning two ongoing metal mining projects and issued two significant violation rulings regarding EIA decisions[38][39]. In these rulings, the Court emphasized that the lower courts had failed to adequately assess whether a fair balance had been struck between the applicants' rights and the public interest when the EIA decisions were made, particularly within the framework of the right to respect for private life. In the first case, the Court observed that the review of the agricultural and livestock impacts in the EIA report was carried out without the inclusion of an agricultural engineer in the expert panel appointed by the lower court, raising concerns regarding the sufficiency of the examination. In the second case, the Court underscored that for an EIA revision to be valid under Circular No. 2009/7, the deficiencies identified in the initial court ruling must not adversely affect other sections of the EIA report. The Court pointed out that both the ministry responsible for the EIA and the lower court failed to adequately explain why a deficiency identified in the expert report would not negatively impact the EIA decision, thereby resulting in a violation of the applicants' rights[40].

---

[38] In the case of Eşref Demir (App. No: 2020/12802), published in the Official Gazette on January 16, 2024, concerning the rejection of a lawsuit aimed at annulling the Environmental Impact Assessment (EIA) approval for the "Erzincan İliç Yakuplu Village Open Pit Mine Expansion and Capacity Increase Project," the Constitutional Court examined the claim of a violation of the right to respect for private life. The court found that the key allegations about the project's potential harm to agriculture and livestock were not adequately addressed. Specifically, the expert report did not sufficiently assess the impact of the project on livestock due to grazing areas being within the project zone, nor did it evaluate whether the necessary precautions were taken in the EIA report. Additionally, the court found that the reasoning provided by the lower courts based on the expert report was limited and did not directly address the applicant's specific claims. As a result, the court concluded that the applicant was not given a proper opportunity for these claims to be thoroughly considered by the judicial authorities. It held that public authorities failed to carefully evaluate the balance between public and individual interests in this case, and thus did not fulfill their positive obligations under the right to respect for private life. Consequently, the court ruled that Article 20 of the Constitution, which guarantees the right to respect for private life, had been violated.

[39] In the case of Yasemin Pelenk (App. No: 2017/33865), published in the Official Gazette on May 20, 2024, the Constitutional Court examined an individual application concerning the rejection of a lawsuit against the "EIA Positive Decision" based on a revised EIA report, which was issued under the 2009/7 General Notice. The court noted that the primary reasoning in the initial court decision—that the province where the project would take place would no longer be a living space—hindered the implementation of the 2009/7 General Notice. It emphasized that the EIA process should have been restarted rather than completed under this general notice, as the rationale for the initial annulment decision could adversely affect other sections of the report. Despite the applicant's claims that the capacity of the planned line for ore transportation did not align with the annual production capacity, the local court's assessment, which stated that this discrepancy would not negatively affect the EIA decision, prevented the establishment of a fair balance between the applicants' claims and public interests. The court concluded that public authorities did not approach the matter with the necessary diligence and failed to provide sufficient justification for maintaining a fair balance between public and individual interests. Consequently, it ruled that the public authorities did not fulfill their positive obligations regarding the right to respect for private life.

[40] In the mentioned application, to remedy the effects of the violation decision, the administrative court to which the case was referred stated that the report on which the EIA positive decision was based was insufficient due to the uncertainty regarding how the transportation of the portion of the annual production exceeding the capacity of the cableway line would be conducted and its potential environmental impacts. Consequently, it issued an annulment decision, leading to the initiation of a

The Constitutional Court's jurisprudence is not limited to mining; however, starting from 2023, it appears that the High Court has adopted a more sensitive approach in the judicial decisions regarding environmental impact assessments, particularly in lawsuits concerning EIA decisions based on the 2009/7 General Regulation. In one of these cases, following the annulment of the positive EIA decision for a project related to industrial and hazardous waste storage areas of a thermal power plant, the Constitutional Court identified a violation of rights during the judicial process concerning the second positive EIA decision obtained through a revision under the 2009/7 General Regulation.[41]

The principles established in the recent decisions of the Constitutional Court underscore the importance of EIA processes. It is essential that all potential impacts of a project are anticipated and that measures addressing these impacts are included in EIA Reports. Additionally, during the judicial phase, the claims of the plaintiffs must be examined by expert witnesses to determine whether these claims have been addressed in the EIA reports, allowing for a proper public interest assessment.

Lawsuits are not only filed against positive EIA decisions; sometimes, EIA processes may conclude due to negative institutional opinions, or as seen in a limited number of cases, projects may receive negative EIA decisions. Investors have the right to file lawsuits against these decisions. In such cases, if it is determined that the negative institutional opinions and their justifications are unfounded, the EIA process may continue from the point it left off. Following negative EIA decisions, new EIA reports can be prepared with project unit location changes to address the negative opinions, leading to the issuance of new EIA decisions. These decisions, similar to those under the 2009/7 General Regulation, are subject to judicial review. In such cases, the courts primarily examine whether the second project has any technical connection to the first project. If this is determined, they resolve the dispute in accordance with the review procedure in EIA lawsuits.

In addition to the Constitutional Court's decisions regarding the relationship between mining and the environment, it is also significant that the court issued rulings regarding the violation of property rights in cases rejected based on the provision that no compensation could be granted for damages incurred on properties within the Zonguldak coal basin under Law No. 3303. Furthermore, the systematic issue related to this matter was reported to the Grand National Assembly of Turkey (TBMM) in 2021.[42] Although these issues may arise as a result of coal mining, the prohibition of claiming damages in such cases, regardless of whether they stem from the operator or not, is not seen as compatible with property rights.[43][44] Due to the lack of legal regulation on this matter by the Turkish Grand National Assembly (TBMM), the Constitutional Court annulled the phrase "they cannot claim any rights or compensation

---

new EIA process that would also address this issue. (See EIA Announcements; [EEIA Announcements] [https://eced-duyuru.csb.gov.tr/eced-prod/duyurular.xhtml])

[41] In the case of Ahmet Kardam and others, App.No: 2019/29604, published on 27.03.2024, the Constitutional Court determined that the statements regarding the non-use of waste storage facilities and the assurance that existing waste would not be present on-site due to contracts made with third parties for sale or storage were not adequately addressed in the EIA report. The court concluded that the public authority did not approach the matter with the necessary diligence and failed to properly evaluate individual interests in relation to public interests.

[42] The third article of Law No. 3303, titled "Right to Compensation", stated the following: 1) "Owners of real estate identified and registered under this Law cannot assert any rights over the mines; they have no exploration or operation rights. 2) The exploration and operation rights of the institutions or allocation holders operating the mines shall continue unchanged, and all underground and above-ground facilities within the operation and safety areas, as well as their extensions, shall be preserved. Owners of real estate identified and registered under this Law cannot make any claims regarding rights and compensation based on property rights. 3) These matters shall be indicated in the declaration section of the land registry."

[43] Sabri Urhağ, App.No: 2017/34596, RG: 28.01.2021

[44] Hulusi Yılmaz, App.No: 2017/17428, RG:19.01.2023

for damages arising from mining operations" in its decision dated 13/07/2023, E: 2023/117, K: 2023/121.

The Constitutional Court has also adopted a protective approach towards mining in recent years, particularly regarding the frequent occurrences of investment conflicts related to the allocation of mining licenses to other investments. It is beneficial to mention this as well.[45] As is known, the ability to restrict mining activities in mining areas through various processes poses issues regarding license security and legal certainty. One of the practices that leads to such restrictions is investment conflicts. The current legal framework results in the victimization of mining license holders. The principles established by the Constitutional Court regarding restrictions on mining licenses are applicable to many administrative actions concerning licensed areas. The significance and necessity of addressing the right to peaceful enjoyment of property from the perspective of the license holder, both in legislative and judicial processes, has been expressed by the Constitutional Court.

According to the Court, a mining operation license represents economic value for the license holder, thus falling within the concept of "property". The inability to conduct mining in overlapping areas designated for other investments must be based on law, serve a legitimate purpose, and be proportionate concerning the right to peaceful enjoyment of property. The Court found no issues of legality or legitimate purpose (public interest) in prohibiting mining in part of a licensed area due to airport construction. However, it approached the dispute concerning the investment cost from the perspective of the principle of proportionality.

In this regard, it is suggested that the administrative processes and lawsuits related to the restriction decisions (such as special permission areas) may be examined in the future under the principles of suitability and necessity. The principle of proportionality (establishing a fair balance between public interest and individual interest) indicates that a suitable compensation mechanism must be provided for the damages incurred by the license holder due to restrictions. The ruling states that it should be assessed by administrative authorities and judicial bodies whether the investment expenses paid to the license holder by the administration are adequate in relation to the incurred damages.[46]

2.6. The Approach of Administrative Jurisdiction in Cases of Pasture Allocation Changes, Non-Agricultural Use and Expropriation

In mining activities, the selection of facility locations is significant not only during the EIA process but also for subsequent operational permits. Each institution involved in the permitting process can evaluate the site selection. Furthermore, if lawsuits related to these permits are filed, they are also examined by expert witnesses.

Especially concerning facilities that could coincide with pasture, agricultural land, and private property, this evaluation should be elaborated in the planning phase of the project. While it may not be possible to change the locations of the mining sites, it is evident that there can be various alternatives for the

[45] Kartal Madencilik, App.No: 2020/23443, RG: 13.06.2024

[46] The Constitutional Court has also pointed out a general issue experienced in administrative courts in its ruling: "It should be accepted that judicial authorities are not obliged to respond to every claim made by the parties. However, failing to respond with relevant and sufficient justification to claims that could affect the resolution of the dispute may render the recourse to judicial remedy meaningless, as the administration's arguments would be accepted as correct a priori. It is expected that the courts will take seriously and examine the issues that the applicant wishes to have assessed, and which form the essence of the dispute, discussing these matters adequately in their decisions. In this context, accepting the findings made by the administration as correct a priori in lawsuits filed against administrative actions significantly restricts the applicants' right to defense. Although administrative actions benefit from the presumption of legality, this presumption cannot be validly accepted from the perspective of the judicial authority examining the legality of the administrative action. Otherwise, a relatively superior status would be granted to administrative bodies, which would turn filing lawsuits against these actions into a futile effort." (See: Kartal Madencilik Decision, para. 53)

locations of ore processing and enrichment facilities, waste storage areas, and stockpiles. In these situations, the public benefit derived from mining must be balanced against other public interests. It is crucial to take precautions and measures for the other interest while pursuing one. For instance, if a mining facility is planned to coincide with pastureland, the process of reallocating the land according to the Pasture Law must be implemented. Similarly, if the site overlaps with private property, expropriation may be necessary for the acquisition of the property. If the site is agricultural land, and a decision is made regarding the public benefit of non-agricultural mining activities, permission may be granted for non-agricultural use in accordance with soil conservation projects.

In all these administrative processes, the village legal entity where the pasture is allocated, the owner of the agricultural land, or irrigation associations can file lawsuits. In these cases, expert examinations are conducted, primarily investigating the necessity of mining for the relevant area. During this process, the identification of the current site in comparison to other alternative locations is also scrutinized. Insufficient justification for all these issues may lead to annulment decisions, causing delays in the realization of projects for indefinite periods.

3. Material and Method

This study examines the development of the concept of environmental rights and its relation to mining. It outlines the fundamental rights associated with this issue and the judicial approach to their protection within the Turkish legal system. In this context, decisions from the Constitutional Court and Turkish Administrative Courts have been utilized as key sources.

4. 4. Conclusion

The significance of mining activities in meeting societal needs is undeniable. In projects that often span durations far exceeding a human lifetime, ensuring transparent stakeholder involvement from the planning stage serves to reduce uncertainty and enhance security. The principle of participation should be applied at every stage, including site selection and the permitting process for these projects. Nonetheless, judicial processes related to such projects may still arise. In these cases, the balance between objections to the project and the public benefit it generates can be effectively addressed through judicial procedures. In Turkish judicial practice, the Constitutional Court has issued significant rulings on environmental cases, particularly in its decisions on individual applications since 2010. Meanwhile, the Supreme Court has highlighted key protections for mining license holders. Concurrently, administrative courts continue to render decisions that aim to establish a balance between individual rights and the public interest, offering remedies in cases where this balance is disrupted. These developments emphasize the critical importance of thorough planning in mining projects. It is essential that the permitting processes conducted by various institutions and the statements made concerning the project remain consistent with one another.

Acknowledgements

I would like to thank Attorney Dr. A. Eren Altay and Intern Attorney Özge Balcıoğlu for their review and support.

References

https://sustainabledevelopment.un.org/index.php?menu=1259

https://equator-principles.com/signatories-epfis-reporting/]

https://sustainabledevelopment.un.org/index.php?menu=1259

Konstantinos Komnitsas, Social License to Operate in Mining: Present Views and Future Trends, Resources, Published: 25 June 2020

https://hudoc.echr.coe.int/%E2%80%99/app/conversion/pdf/#{%22fulltext%22:[%22\%22Ta%C5%9Fk%C4%B1n%20and%20Others%20v.%20Türkiye%20(dec.)\%22%22]}

https://eced-duyuru.csb.gov.tr/eced-prod/duyurular.xhtml

the 6th Chamber of the Council of State, 1996/5477 E, 1997/2312 K

Hüseyin Tunç Karlık and Zahide Şadan Karluk, App. No: 2013/6587, 24/3/2016,

Mehmet Kurt [GK], App. No: 2013/2552, 25/2/2016

Ahmet İsmail Onat, App. No: 2013/6714, 21/4/2016

Gülcan Tutkun Berk, App. No: 2015/2334, 29/11/2018

Egeçep Derneği, App. No: 2015/17415, 17/4/2019

Ahmet Bilgin and others, App. No:2015/11709

Ayşe Sevtap Uzun, App. No: 2013/6260, 13/4/2016

Eşref Demir, App. No: 2020/12802

Yasemin Pelenk, App. No: 2017/33865

Ahmet Kardam and others, App.No: 2019/29604, 27/03/2024

Constitutional Court's decision E: 2023/117, K: 2023/121.,13/07/2023

Sabri Urhağ, App.No: 2017/34596, 28/01/2021

Hulusi Yılmaz, App.No: 2017/17428, 19/01/2023

Kartal Madencilik, App.No: 2020/23443, 13/06/2024

Evaluation of a Complex Polymetallic Sulphide Ore

H. M. Toprak[1]*, H. Baştürkcü[1]

[1]Istanbul Technical University, Mineral Processing Engineering Department

*Corresponding author: toprakh17@itu.edu.tr (Havva Mine Toprak)

Abstract:

Copper and zinc are both metals with a wide range application through various industries. Copper, valued for its conductivity, ductility, and malleability, is crucial for electrical wiring, construction, and electronics. On the other hand, zinc, valued for its corrosion resistance and ability to form alloys, finds uses in batteries, and galvanizing steel. Both minerals, often found together in sulphide related mineral deposits. While copper primarily occurs in porphyry copper and volcanic massive sulphide (VMS) deposits, zinc is more commonly associated with hydrothermal vein deposits and Mississippi Valley-type (MVT) deposits, which are also sulphide-rich. However, both copper and zinc can be found in lesser quantities within oxide deposits. Copper can be present in sedimentary and skarn copper deposits, while zinc can occur in zinc carbonate deposits.

Enrichment of copper and zinc from sulphide ores primarily relies on flotation, a separation technique that utilizes the differing hydrophobicity of mineral surfaces. Flotation reagents selectively attach to valuable copper and zinc minerals, allowing them to be separated from gangue minerals and float to the top of a froth for collection. The ore that will be examined in this study have a sulphide-based mineralogy. Detailed mineralogical examinations identified primary sulphide minerals such as sphalerite and chalcopyrite. Additionally, the presence of secondary sulphide minerals like covellite and chalcocite was confirmed. Processing of complex sulphide ores, particularly those containing secondary copper minerals presents significant challenges. Thus, this study investigates the pre-enrichment opportunities for sulphide-based copper-zinc ores containing secondary copper minerals.

Keywords: *Copper, zinc, secondary copper minerals, sulphide deposits, pre-enrichment.*

1. Introduction

Copper and zinc, both metal plays irreplaceable role with their unique properties for a sustainable future. Archaeological evidence shows that copper was one of the first metals used at least 10,000 years ago for items such as coins and ornaments in Western Asia and it is used in electronic, construction, transportation, chemistry, jewellery, paint and notably in energy sector continuously. Copper has unique physical and chemical properties, including electrical conductivity, thermal conductivity, corrosion resistance, machinability and castability, and its high electrical conductivity and corrosion resistance features make it an ideal material for electrical wiring, transformers, and other components essential for the efficient transmission and distribution of electricity. In the context of wind power, copper is extensively used in the construction of wind turbines, from the generator windings to the electrical control systems. While annual growth of off-shore wind applications is expected to be 23.3% between 2021 and 2035; a single 10-megawatt offshore wind turbine requires approximately 80 tonnes of copper consumption, highlighting its criticality in this sector (ICA, 2023).

On the other hand, zinc is less prominent in the public consciousness, but it is equally vital for the green transition and a key component in various renewable energy technologies. It is employed in the manufacturing of batteries, including zinc-air batteries that offer promising potential for energy storage applications. Zinc thermal spray is used to protect offshore wind turbines and estimates shows that a 10-megawatt offshore wind turbine requires around 4 tonnes of zinc. In the realm of solar power, production of photovoltaic cells and galvanized steel support structures requires zinc to improve the efficiency and durability of these devices (International Zinc Association, n.d.). Besides of energy sector, it has a wide range usage in construction, healthcare, rubber, paint, and automative sectors, owing to

its unique properties which make it a fourth ranked metal in the global metal consumption (Ejtemaei et al., 2013). As the world accelerates its efforts to achieve net-zero emissions, the demand for key minerals, such as copper and zinc, is escalating at an unprecedented rate. According to the scenarios prepared to determine approximate metal needs in clean energy technologies, copper need is expected to reach 10 million tonnes for clean energy by 2030 and zinc need is expected to reach 472 thousand tonnes for only wind energy by 2030 through Stated Policies Scenarios (IEA, 2021; IEA, 2023.)

To be able to meet the increasing demand of copper and zinc, supply side of both minerals should be examined in detail. Copper and zinc are prevalent in nature, each occurring in distinct types of mineral deposits. Both minerals, often found together in sulphide related mineral deposits. While copper primarily occurs in porphyry copper and volcanic massive sulphide (VMS) deposits, zinc is more commonly associated with hydrothermal vein deposits and Mississippi Valley-type (MVT) deposits, which are also sulphide-rich (Sverdrup et al., 2019; Leach et al., 2010). However, both copper and zinc can be found in lesser quantities within oxide deposits. Copper can be present in sedimentary and skarn copper deposits, while zinc can occur in zinc carbonate deposits. World production and reserved for copper, zinc and mining properties in Türkiye with primary commodity of copper and zinc are showed in Table 1 and 2 accordingly.

Table 1. World Copper Mine and Refinery Production and Reserves, ktonnes (USGS, 2024)

Country	Mine production		Refinery production		Reserves
	2022	2023	2022	2023	
United States	1,230	1,100	952	890	50,000
Australia	819	810	401	450	100,000
Canada	520	480	278	310	7,600
Chile	5,330	5.000	2.150	2,000	190,000
China	1,940	1,700	11,100	12,000	41,000
Congo (Kinshasa)	2,350	2,500	1,770	1,900	80,000
Germany	–	–	609	610	–
Indonesia	941	840	310	200	24,000
Japan	–	–	1,550	1,500	–
Kazakhstan	593	600	494	440	20,000
Korea, Republic of	–	–	638	620	–
Mexico	754	750	486	480	53,000
Peru	2,450	2,600	391	400	120,000
Poland	393	400	586	590	34,000
Russia	936	910	1,010	1,000	80,000
Zambia	797	760	349	380	21,000
Other countries	2,850	3,100	2,830	2,900	180,000
World total (rounded)	21,900	22,000	25,900	27,000	1,000,000

Table 2. World Zinc Mine and Refinery Production and Reserves, ktonnes (USGS, 2024)

Country	Mine production		Reserves
	2022	2023	
United States	761	750	6,600
Australia	1,240	1,100	64,000
Bolivia	518	490	-
China	4,040	4,000	44,000
India	840	860	7,400
Kazakhstan	312	330	6,700
Mexico	744	690	14,000
Peru	1,370	1,400	21,000
Russia	300	310	25,000
South Africa	238	230	6,200
Sweden	234	220	4,100
Other countries	1,940	1,800	25,000
World total (rounded)	12,500	12,000	220,000

Copper is often found in sulphide ores, such as chalcopyrite ($CuFeS_2$), bornite (Cu_5FeS_4), and chalcocite (Cu_2S), which are typically associated with igneous and metamorphic rocks. These sulphide ores are extracted through mining and processed via flotation, roasting, and smelting to produce copper metal. Additionally, copper can be found in oxide forms like malachite ($Cu_2CO_3(OH)_2$) and azurite ($Cu_3(CO_3)_2(OH)_2$), which are processed differently through leaching and solvent extraction methods. Zinc, on the other hand, primarily occurs in sulphide minerals such as sphalerite (ZnS) and to a lesser extent in oxide forms like zincite (ZnO). Sphalerite is commonly processed through flotation to concentrate the zinc, followed by roasting and hydrometallurgical techniques to produce zinc metal (Sinclair, 2005). The mineralization type significantly influences the extraction and processing methods for each metal, with copper and zinc requiring tailored approaches to efficiently separate and refine the metals from their respective ores (Richards, 2019). Moreover, copper and zinc can be found together and mostly processed by flotation. Chalcopyrite, sphalerite and iron sulphides are present with this type of ore and various silicates, carbonates, and often talc, which presents flotation challenges, are typical gangue minerals. The enrichment approach is similar to the lead-zinc sulphide separation process. Zinc sulphate addition to the grind with sodium sulphide is used to depress sphalerite as an option for enhancing pyrite depression, copper is floated at a 10-11 pH with lime and xanthate, dithiophosphate and thionocarbamate collectors are used as additives (FMC, n.d.). In this study, the sample selected from Balikesir province of Türkiye, western region of country, will be tested with pre-enrichment methods to be able to examine for its further effects for flotation.

2. Material and methods

2.1. Material

Sample is selected from a complex polymetallic sulphide ore part of active mining site located in southeast of Balikesir provience, western part of Türkiye. Upper Paleozoic metamorphic rocks and Lower to Middle Miocene intrusive and volcanics are comprised in active mining site's regional geology. Upper Paleozoic metamorphics are the most common units from top to bottom; Dacite and Pyroclastic, Calcschist, Feldspar–Quartz Schist, Chlorite–Sericite Schist and Quartz Schist. The second-most common rocks are the Lower to Middle Miocene volcanics, comprised of altered dacite-rhyodacites characterized by lava flows and pyroclastics. The youngest units are mineralized gossan and ferricrete, along with talus, colluvium, and alluvium, all being weathering products of the host rock.

Area is a massive sulphide deposit hosted in schists. The sulphide zone is polymetallic with potentially economic values of zinc, copper, gold, and silver. Potentially economic gold–silver–copper–zinc mineralization is present to varying degrees, and is divided into five main types, as summarized in Table 3.

Table 3. Mineralization types in the mining area.

Horizon	Mineralization Type
Oxide	Gossan
Sulphide	Massive Pyrite
	Enriched
	Disseminated Sulphide

Production of gold and silver bearing dores continues in the oxide part of the active mining area and sulphide part is under the examination and construction for copper and zinc concentrates from the flotation process. Complex polymetallic sulphide zone (CPSZ) of the mineralization consists of mainly chalcocite–covellite within fine to medium-grained pyritic mass. Occurring near or along structural features, it is intensely fractured generally. Relative to other sulphide mineralisation zones in the area, CPSZ contains higher grade gold–silver–copper–zinc mineralisation.

CPSZ has elevated levels of copper, lead, and zinc and occurs near the contact of the mineralisation with the host; it is generally spotty in distribution, located at the base or up the sides of mineralised zones at contacts with the schist, and more typical in the southern part of the deposit. While it is enriched in chalcopyrite, covellite and chalcocite are also present in significant amounts. Sphalerite also tends to be high.

The raw ore sample used in the study contained 0.55% Cu, 0.38% Zn, and 0.49% Pb. Also, 2.88 ppm Au and 96 ppm Ag were determined in the sample, which carry additional economic value to the project. The metal distribution was traced through the particle size fractions. As is mentioned in the Method section, the cone crusher output material was subjected to sieve analysis and obtained size fractions were analysed. Regarding Table 4, it was understood that more than 75% of the metals were found above 0.5 mm.

Table 4. Particle size distribution of the cone crusher output

Particle Size Fraction (mm)	Cumulative Undersize (%)	Au		Ag		Cu		Pb		Zn	
		Content (ppm)	Distr. (%)	Content (ppm)	Distr. (%)	Content (%)	Distr. (%)	Content (%)	Distr. (%)	Content (%)	Distr. (%)
-12+6	100.0	3.27	28.60	117.00	30.90	0.63	28.80	0.49	25.20	0.52	34.20
-6+1	74.8	2.82	34.00	102.00	36.90	0.52	33.10	0.47	32.80	0.42	38.70
-1+0.5	39.9	2.60	12.20	82.00	11.50	0.45	11.00	0.54	14.70	0.30	10.70
-0.5+0.2	26.5	2.38	4.30	88.00	4.80	0.51	4.80	0.53	5.60	0.31	4.30
-0.2	21.2	2.84	20.90	72.00	15.90	0.58	22.30	0.51	21.80	0.22	12.20
Total		2.88	100.00	96.00	100.00	0.55	100.00	0.49	100.00	0.38	100.00

2.2. Method

In this study, ore is tested with pre-enrichment methods to be able to examine for its further effects for flotation. Pre-enrichment methods used for this study is showed as flowsheet in Figure 1.

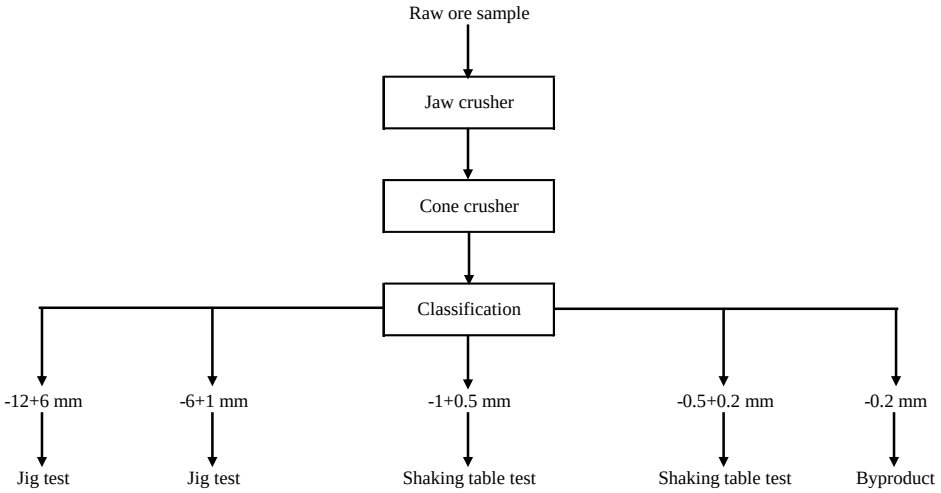


Figure 1. Experimental flowsheet

Prepared raw ore sample is treated to achieve necessary size reduction with jaw and cone crushers accordingly. After size reduction, classification is performed through 12 mm, 6 mm, 1 mm, 0.5 mm, 0.2 mm manual sieves. 2 classified samples, -12+6 mm and 16+1 mm are selected for the treatment with jig process. 2 classified samples, -1+0.5 mm and -0.5 mm are selected for shaking table tests and lastly particles below 0.2 mm is separated from the tests as byproduct. Tests are performed separately, and analysis performed on the obtained products to determine mineral content.

3. Results

3.1. Jig tests

Metal contents of the products, obtained from jig tests performed to -12+6 mm and -6+1 mm samples separately, are showed in the Table 5 and 6 accordingly. 3 products with different density as heavy, middling and light, are obtained from both jig tests performed. On the first jig test performed on -12+6 mm, 33.5% of the feed is obtained as heavy product with 3.8 ppm gold, 151 ppm silver, 1.3% copper, 0.6% lead and 1.0% zinc content. 38.9% of gold, 43.1% of silver, 69.1% of copper, 43.1% of lead and 65.8% of zinc in the total feed is obtained in the heavy product.

Table 5. Jig products -12+6mm distribution

Jig Products -12+6mm		Amount	Au		Ag		Cu		Pb		Zn	
		(%)	Content (ppm)	Distr. (%)	Content (%)	Distr. (%)	Content (%)	Distr. (%)	Content (%)	Distr. (%)	Content (%)	Distr. (%)
A1	**Heavy**	33.5	3.80	38.90	151.00	43.10	1.29	69.10	0.63	43.10	1.02	65.80
A2	**Middling**	31.6	4.04	38.90	152.00	40.80	0.38	19.30	0.56	36.00	0.35	21.20
A3	**Light**	34.9	2.08	22.20	54.00	16.10	0.21	11.60	0.30	20.90	0.19	13.00
	Feed	100.0	3.27	100.00	117.42	100.00	0.63	100.00	0.49	100.00	0.52	100.00

On the second jig test performed on -6+1 mm, 28.8% of the feed is obtained as heavy product with 4.56 ppm gold, 117 ppm silver, 1.2% copper, 0.6% lead and 0.8% zinc content. 46.6% of gold, 33.1% of silver, 63.5% of copper, 39.3% of lead and 54.3% of zinc in the total feed is obtained in the heavy product.

Table 6 . Jig Products -6+1mm Distribution

Jig Products -6+1mm		Amount	Au		Ag		Cu		Pb		Zn	
		(%)	Content (ppm)	Distr. (%)	Content (ppm)	Distr. (%)	Content (%)	Distr. (%)	Content (%)	Distr. (%)	Content (%)	Distr. (%)
B1	**Heavy**	28.8	4.56	46.60	117.00	33.10	1.15	63.50	0.64	39.30	0.80	54.30
B2	**Middling**	24.1	2.27	19.40	122.00	29.00	0.30	13.90	0.43	22.60	0.30	17.20
B3	**Light**	47.1	2.03	33.90	82.00	37.90	0.25	22.60	0.38	38.10	0.36	28.50
	Feed	100.0	2.82	100.00	101.74	100.00	0.52	100.00	0.47	100.00	0.42	100.00

3.2. Shaking table tests

Metal contents of the products, obtained from shaking table tests performed to -1+0.5 mm and -0.5+0.2 mm samples separately, are showed in the Table 7 and 8 accordingly. 4 products with different density as heavy, middling light 1 and light 2 , are obtained from both shaking table tests performed. On the first shaking table test performed on -1+0.5 mm, 3.1% of the feed is obtained as heavy product with 3.43 ppm gold, 55 ppm silver, 0.8% copper, 0.5% lead and 0.3% zinc content.

Table 7. Shaking table products -1+0.5mm distribution

Shaking Table Products -1+0.5mm		Amount	Au		Ag		Cu		Pb		Zn	
		(%)	Content (ppm)	Distr. (%)	Content (ppm)	Distr. (%)	Content (%)	Distr. (%)	Content (%)	Distr. (%)	Content (%)	Distr. (%)
C1	**Heavy**	3.1	3.43	4.10	55.00	2.10	0.79	5.40	0.54	3.10	0.26	2.60
C2	**Middling**	3.2	4.11	5.00	73.00	2.80	0.62	4.40	0.56	3.30	0.32	3.40
C3	**Light 1**	66.0	2.62	66.50	93.00	74.80	0.46	67.70	0.53	65.10	0.33	71.50
C4	**Light 2**	27.7	2.30	24.50	60.00	20.30	0.36	22.40	0.55	28.50	0.24	22.40
	Feed	100.0	2.60	100.00	82.04	100.00	0.45	100.00	0.54	100.00	0.30	100.00

On the second shaking table test performed on -0.5+0.2 mm, 7.7% of the feed is obtained as heavy product with 2.99 ppm gold, 52 ppm silver, 0.7% copper, 0.5% lead and 0.3% zinc content. 9.7% of gold, 4.6% of silver, 10.7% of copper, 7.3% of lead and 6.7% of zinc in the total feed is obtained in the heavy product.

Table 8. Shaking table products -0.5+0.2mm distribution

Shaking Table Products -0.5+0.2mm		Amount	Au		Ag		Cu		Pb		Zn	
		(%)	Content (ppm)	Distr. (%)	Content (ppm)	Distr. (%)	Content (%)	Distr. (%)	Content (%)	Distr. (%)	Content (%)	Distr. (%)
C1	**Heavy**	7.7	2.99	9.70	52.00	4.60	0.70	10.70	0.50	7.30	0.27	6.70
C2	**Middling**	11.8	2.365	11.70	80.00	10.70	0.73	17.00	0.54	12.00	0.33	12.50
C3	**Light 1**	62.6	2.525	66.30	104.00	73.80	0.52	63.10	0.58	67.60	0.34	67.20
C4	**Light 2**	17.9	1.63	12.20	54.00	10.90	0.26	9.20	0.39	13.10	0.24	13.70
	Feed	100.0	2.38	100.00	88.21	100.00	0.51	100.00	0.53	100.00	0.31	100.00

3.3. Flow-sheet design

After performed tests, as addition to existing processes, suggested flow sheet is showed in Figure 2. Raw ore crushed under 12 mm through the crushing unit of existing plant, should be classified through 6 mm vibrating screen to be able to obtain clear separation through jig processes. Particles above 6 mm and below 6 mm will be treated with separate jigs. Particles below 6 mm should be screened through 1 mm vibrating screen and below 1 mm particles should be separated to feed existing heap leach cycle. Heavy and light products of both jigs will be treated through dewatering screens separately. While screened heavy products of both jigs will be sent to stockpile for further enrichment steps, screened light products will be sent to existing heap leach cycle with particles below 1 mm.

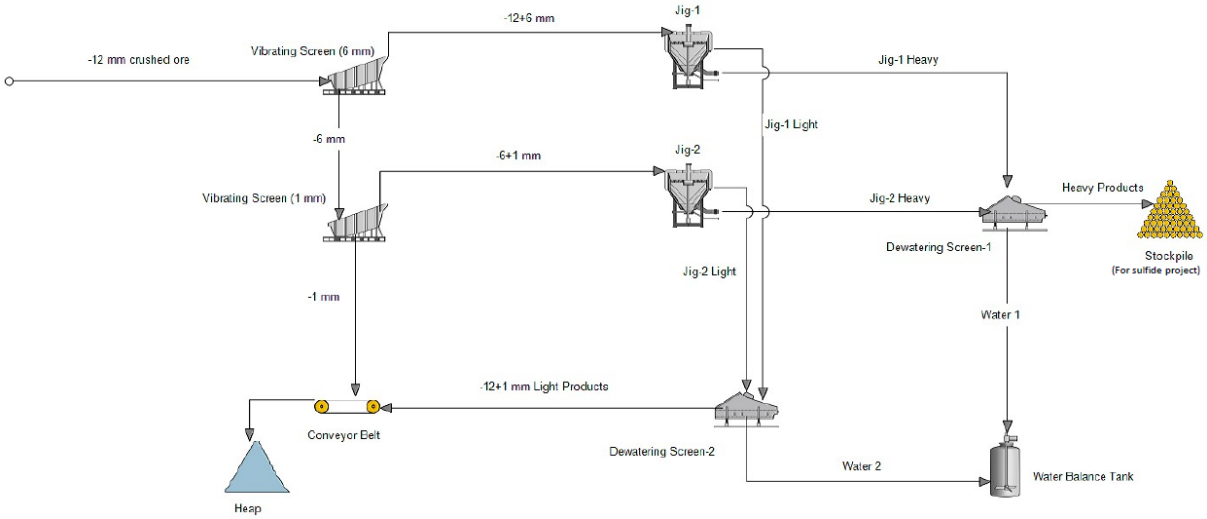


Figure 2. Flow sheet suggestion

4. Conclusion

With the proposed processes flow sheet;

- 2 combined products were formed: i) -12+6 mm and -6+1 mm heavy products are combined, ii) -12+6 mm, -6+1 mm, and -1 mm products are combined.
- As combined heavy product, 18.5% by mass of the feed can be separated with high copper content to feed further enrichment steps (Table 9),
- The heavy concentrate with high copper content will be consist of 27% of gold, 40.9% of copper, 43.5 of zinc contained in the total feed material successfully.
- The metal grades in the heavy product increased to 4.21 ppm Au, 133 ppm Ag, 1.22% Cu, 0.64% Pb, and 0.90% Zn.
- 82.5% by mass of the feed can be fed to the existing heap leach cycle in the mine site.
- Opex and capex details should be examined for further application in the existing plant.

Table 9. Combined results

Products	Amount	Au		Ag		Cu		Pb		Zn	
	(%)	Content (ppm)	Distr. (%)	Content (ppm)	Distr. (%)	Content (%)	Distr. (%)	Content (%)	Distr. (%)	Content (%)	Distr. (%)
Heavy product	18.5	4.21	27	132.56	25.5	1.22	40.9	0.64	23.7	0.9	43.5
Light product	81.5	2.58	73	87.74	74.5	0.4	59.1	0.46	76.2	0.26	56.5
Original feed	100	2.88	100	96.02	100	0.55	100	0.49	100	0.38	100

References

European Copper Institute. (2019). Electrical conductors.

Ejtemaei. M.. Gharabaghi. M.. Irannajad. M. (March 13. 2013). A review of zinc oxide mineral beneficiation using flotation method. Advances in Colloid and Interface Science 206 (2014) 68–78. ISSN 0001-8686. https://doi.org/10.1016/j.cis.2013.02.003.

FMC. (n.d.) Copper-Zinc ores. https://www.danafloat.com/uk/mining_ores/copper_zinc

International Copper Association (ICA). (March. 2023). Copper-The Pathway to Net Zero.

International Energy Agency (IEA). (2021). The Role of Critical Minerals in Clean Energy Transition. IEA. Paris https://www.iea.org/reports/the-role-of-critical-minerals-in-clean-energy-transitions

International Energy Agency (IEA). (2023). Critical Minerals Market Review 2023.

International Zinc Association. (n.d.). Renewable Energy. https://www.zinc.org/renewable-energy/

Leach. A.L.. Taylor. R.D.. Fey. D.L.. Diehl. S.F.. Saltus. R.W. (2010). A deposit model for Mississippi Valley-Type lead-zinc ores. Scientific Investigations Report 2010-5070-A. U.S. Geological Survey. https://doi.org/10.3133/sir20105070A

Sverdrup. H.U.. Olafsdottir. A.H.. Ragnarsdottir. K.V. (2019). On the long-term sustainability of copper. zinc and lead supply. using a system dynamics model. Resources. Conservation & Recycling: X. Volume 4. 2019. 100007. ISSN 2590-289X. https://doi.org/10.1016/j.rcrx.2019.100007.

Richards. A. W.. (April 12. 2019). Zinc processing. Encyclopedia Britannica. https://www.britannica.com/technology/zinc-processing/The-metal-and-its-alloys

Sinclair R.J. (2005). The Extractive Metallurgy of Zinc. The Australasian Institute of Mining and Metallurgy (AUSIMM) Spectrum Series. Volume Number 13. 2005. ISBN 9781920806347.

S&P Global IQ Pro. (September 5. 2024). Database screening for; Mining properties with primary commodity of copper/zinc.

United States Geological Survey (USGS). (2024). Copper 2024. Mineral Commodity Summaries. https://www.usgs.gov/centers/national-minerals-information-center/copper-statistics-and-information

United States Geological Survey (USGS). (2024). Zinc 2024. Mineral Commodity Summaries. https://www.usgs.gov/centers/national-minerals-information-center/zinc-statistics-and-information

Dizin

A

A. Ali Sirkeci · viii, 453
A. N. Ozturk · x, 581
A. Wu · x, 581
Abdou Azizi YOUPOUNGAM · v, 11
Abdulbagi Hassan Abdallah Mohamed · v, 11
Ádám Rácz · vi, 111
Adnan Ceylan · vi, 201
Ahmad Fathzadeh · v, 1
Akar H · vi, 135
Alaa ABBADI · vi, 111
Ali Ihsan Arol · vii, 299
Alim Gül · vii, ix, 209, 467
Alper ARUER · ix, 509
Alper Gönen · vii
Alperen KÖLE · ix, 477
Argun Çiper · x, 591
Arman Ehsani · vi, vii, 175, 283
Ataallah Bahrami · v, 1
Ayşe Gül Türe · x, 611

B

B. Aydın · vi, 193
B. E. Uğurlar · vi, 141
B. İbis · vi, 141
Barış Darcan · viii, 453
Basturkcu, E · vi, 135, 181
Begüm ÖZDUR · vii, ix, 235, 477
Behrouz Karimi Shahraki · v, 33
Behzad Mehrabi · v, 33
Beril Tanç Kaya · x, 591
Betül AYDOĞMUŞ · vi, 157
Beyzanur Keleş · v, 21
Bilge KÜÇÜKAYTAN · ix, 515
Birgül Benli · viii, ix, 433, 533
Brian Danyliw · ix, 551
Buğra ÖZDEMİR · x, 575
Burak KAYACIK · ix, 509
Buse Yılmaz · vii, 209

C

C. Dorfling · x, 581
C. Eyupoglu · x, 581
Ç. Ulusoy · vi, 141
Cankut Çendik · vii, 253
Ceyda Şavran · ix, 135, 467
Cugu S · vi, 135
Cugu S. · vi, 135
Cumhur Demirel · vii

D

D. T. Vooght · x, 581
D.O. Aksoy · vii, 277
Djamel Nettour · vi, 149
Doğukan Akardaş · x, 591

E

E. Cuhadar · x, 581
E. Eken Torunoglu · x, 581
E. Emilsson · x, 581
E. Esen · x, 581
E. Y. Yazici · x, 581
Ekrem Savaş · vi, 127
Elif Yilmaz · vi, 165
Emircan Uysal · x, 591
Emrah Durgut · vii, 269
Engin Can Çelik · vi, 127
Enrique Sanchez Vilches · ix, 459
Ersin Yener Yazici · vi, vii, 165, 581
Ezgi Akyildiz · vi, 183

F

F Heinicke · v, 65
F. Ahlatci · x, 581
F.Göktepe · vi, 193
Faik ALP · viii, 403
Faraz Soltani · vii, 335
Fatemeh Kazemi · v, 1
Fatih Çavuşlu · vii, 283
Fatih Özel · vii, 327
Fatma Arslan · x, 309, 567
Fehmi Can Süter · ix, 523
Feridun Boylu · vi, 83, 154
Fırat Burat · v, vii, x, 21, 215, 309, 591, 601
Furkan Enes ÖZEL · viii, 409

G

G. Akdogan · x, 581
Gizem Demirdağ Özel · vii, viii, 327, 372
Gökçe Çıkın · ix, 485
Gülay Bulut · vi, 201
Gülşah Güven · vii, 215
Gunaydın · vi
Gunaydın, N · 135
Gurkan, O.M. · vi, 135

H

H Lieberwirth · v, 65
H. Baştürkcü · vi, 141
Haci Deveci · vi, 165
Hacı Deveci · vii, 317
Haldun Kurama · x, 611
Halide Nur Dursun · v, x, 21, 591
Halil İPEK · vi, 157
Halim Demirkan · x, 642
Halim Recep Kayabaşı · vi, 175
Hande Burçin HARMANCI · ix, 477
Hasan Serkan GOKCEN · vi, 75
Hasret Demir · vii, 215
Hatice Turgut · viii, 453
Hikmet Sis · ix, x, 525, 641
Hüseyin Kömürcü · vii
Hüseyin SENDİR · vi, 103

I

İbrahim Alp · vii, 291
İbrahim ALP · v, 11
İbrahim GÖKTAŞ · vii, ix, 235, 477
Igor Volobaiev · x, 615
İhsan TOROĞLU · viii, 403
İlhan Ehsani · vii, 283
İlkay Bengü CAN · v, 41
Işıl Tokcan · v, 55

J

J. Ots · x, 581

K

K. Tahsin Perek · x, 567
Kemal Bilir · viii, 423
Kerem Canbazoğlu · x, 652
Kornel Tobiczyk · vi, 183
Kutay AYDINBURUN · ix, 477

L

L. Louw · x, 581
Ljudmilla Bokányi · vi, 111

M

M Pfeifer · v, 65
M. Petranikova · x, 581
M. Uğur Taşkıran · viii, 453
M. W. J. Kuhn · x, 581
M.Olgaç Kangal · ix, 467
M.Uğur Taşkıran · ix, 459
Mahmut Emre Çoban · viii, 443
Manuel Gonzalez · viii, 415
Marie-Veronique Durance · viii, 415
Mehdi Rahimi · vii, viii, 243, 335, 349
Mehmet BİLEN · viii, 359, 403
Mehmet Canbazoğlu · vii, viii, 327, 372
Melih Cingöz · vii
Melis N. ERDEM · viii, 387
Mert Kuzu · ix, 493
Mervenur Kirazoğlu · viii, 433
Mohamed Chettibi · vi, 149
Mohsen Mirzaei · viii, 349
Muhammad Zubair Rahim · vii, 299
Muhammed Esat Akça · ix, 525
Murat Erdemoğlu · ix, 525
Murat Mercimek · vii
Murat Olgaç KANGAL · viii, 443
Mustafa Özer · x, 567
Mustafa ÖZTÜRK · ix, 477

N

N. Elginoz · x, 581
Nassima Chebel · vi, 149
Nazlım İlkyaz Dinç · v, vii, x, 21, 309, 601
Nazmi ÜNAL · vi, 103

O

O. Celep · x, 581
Obaidullah ELCHI · vi, 75
Oğuzhan Mert Gürkan · vii, 209
Oktay Celep · vi, vii, 165
Oktay Şahbaz · viii, 391
Olena Tsyganovich · x, 615
Ömer Canıeren · viii, 343
Onur ATAŞ · viii, 359
Onur Güven · vi, 175
Orhan Ozdemir · vii, 269
Orhan Özdemir · vii, 261
Osman Dolmaz · x, 641
Osman Yavuz · vii, 269
Özgür ÖZCAN · ix, 541

P

Pshem Kowalczuk · vi, 183

Q

Qolamreza Parvareh · vii, 335

R

R. F. Maritz · x, 581
R.F. van Schalkwyk · x, 581

Reza Hassanpour Kashani · v, 1
Ruveyda Nur Aytop · ix, 485

S

S. Koca · vii, 277
Sadiye Kantarcı · vii, 283
Sahin, Y · vi, 135
Savran C · vi, 135
Savran C. · vi
Seda Özçelik · vii, 253
Sena Naz GÖKDEMİR · v, 41
Serhat Biçer · ix, 485
Serhat OZDOGAN · ix, 509
Serkan Çakmak · vii
Serkan CAYIRLI · vi, 75
Sevgi Karaca · viii, 391
Seyed Hossein Hashemi · vii, 335
Seyed Javad Mousavi · viii, 349
Seyed Ramin Banihashemi · vii, 243
Sezer Kabaoğlu · vii, 327
Stefanie Lode · vi, 183
Stephane Brochot · viii, 415
Şule Ilgın · vii, 309

T

Taha Boyraz · vii, 291
Taha BOYRAZ · v, 11
Tuğba Deniz Tombal Kara · vi, 175
Tuğba Türk · vii, 291
Tülay Türk · vii, ix, 225, 467
Tuncay Karaçay · vi, 127
Turan Uysal · ix, 525

U

Ugur Ulusoy · v, 21
Uğur Ulusoy · vii, 215
Utku Çağlar · viii, 423

V

Vedat DENİZ · vi, 91, 103
Vicente Sanz Solana · ix, 459
Vitaly Prokopenko · x, 615

Y

Y. Enes Pural · x, 567
Y. Hakan GÜRSOY · vi, 91, 103
Yahya K. UZUNER · ix, 509
Yakup UMUCU · vi, 91, 103, 157
Yasemin Ozturk · x, 559
Yıldırım İ. TOSUN · viii, x, 379, 633
Yıldız GÖKTAŞ · ix, 501
Yousef Ghorbani · v, 1
Yuce, A.E. · vi, 135
Yunus Emre Cavdar · vi, 165
Yunus Emre Çavdar · vii, 154, 261, 269
Yusuf Enes Pural · vi, 83
Yusuf Enes PURAL · viii, 443

Z

Zehra Bayın · vi, 127
Zeynep ÜÇERLER-ÇAMUR · viii, 443
Ziaeddin Pourkarimi · v, vii, viii, 33, 243, 335, 349

Altın Kadar Değerli Geleceğimizi

Bugünden Şekillendiriyoruz!



SÖĞÜT ALTIN MADENİ

Ülkemizin yeraltı zenginliklerini ülke ekonomisine kazandırıyor, çevre ve insan odaklı yaklaşımlarla **katma değer üretiyoruz.**

GÜBRETAŞ MADEN YATIRIMLARI A.Ş.

GENEL MÜDÜRLÜK
Mustafa Kemal Mah. Dumlupınar Bulvarı No: 266/95
Tepe Prime İş Merkezi -A Blok / Kat :17
Çankaya / ANKARA
TEL: +90 (312) 711 06 11

SÖĞÜT İLETİŞİM OFİSİ
Orta Mahalle Dellal Sok.
No: 1 /A Söğüt / BİLECİK
TEL: +90 (228) 214 31 00

SÖĞÜT ALTIN MADENİ
Söğüt - Eskişehir Yolu 6. Km.
Sırhoca Köyü Söğüt / BİLECİK
TEL: +90 (228) 214 30 00

Teknoloji neredeyse BİZ ORADAYIZ!

Dünyanın bakırdan beklentisini daha ileriye taşımak için madenden son ürüne kadar tüm üretim sürecini gerçekleştirmekle kalmıyor, üretim potansiyelimizi AR-GE çalışmalarımızla güçlendiriyoruz; sayısız sektöre yepyeni çözümler sunuyoruz.



ETİ BAKIR

GÜCÜMÜZÜ BİLGİ VE İNOVASYONDAN ALIYORUZ

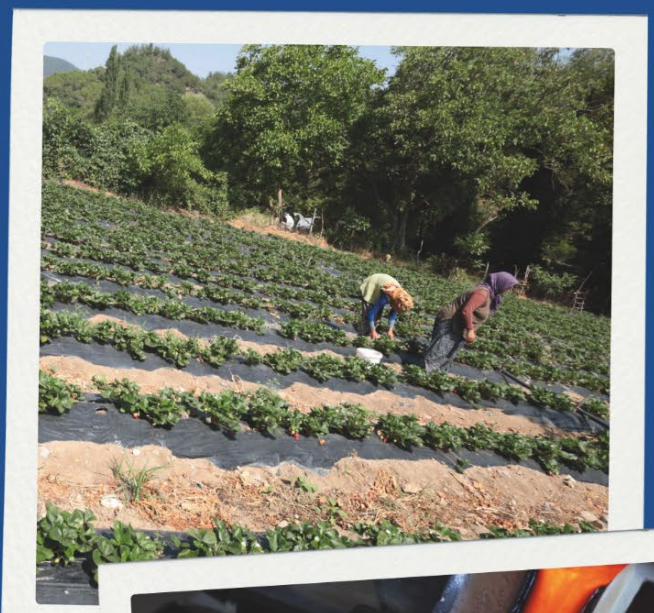
Türk sanayisinin öncü kuruluşlarından biri olmanın sorumluluğu ile kendi sektörlerimizde AR-GE faaliyetlerine liderlik ediyoruz. Bu ülke için çalışan 43 bin kişilik büyük ailemizle geleceğe değer katıyoruz.
Tam 43 yıldır!



Sosyal medya hesaplarımıza ulaşmak için QR kodu okutun.

CENGİZ HOLDİNG







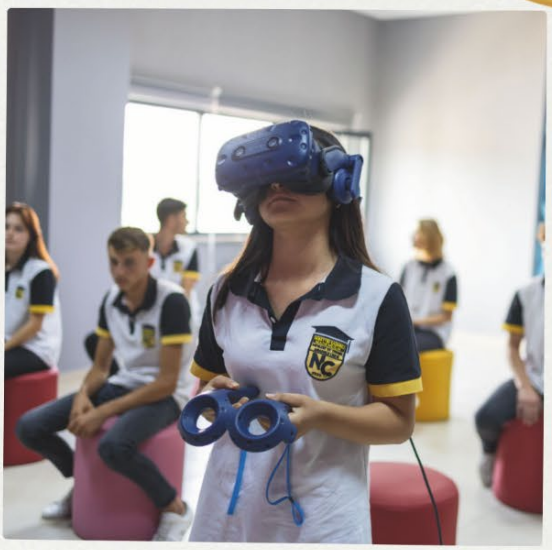


EBRD Sustainability Award

Gold Award

Environmental & Social Best Practice

Tümad Madencilik Sanayi
ve Ticaret A.Ş.





Avrupa İmar ve Kalkınma Bankası (EBRD) 2024
'ÇEVRE VE SÜRDÜRÜLEBİLİRLİK ALTIN ÖDÜLÜ' Çanakkale Lapseki ve Balıkesir
İvrindi'de uyguladığı başarılı çevresel ve sosyal projeleri nedeniyle
TÜMAD Madencilik Sanayi ve Ticaret A.Ş.'ye verildi.

TÜMAD
MADENCİLİK SANAYİ VE TİCARET A.Ş.

Geleceğe İyi Bakan **Kaleseramik Ar-Ge** İle Seramiğin Kalesiyiz.



Kale

Seramiğin lider markası olarak 51 yıl önce kurduğumuz Kaleseramik Ar-Ge Merkezi ile geleceği yakalayan ürünlere ve teknolojilere imza atıyoruz. Avrupa Seramik Topluluğu'na (ECerS) katılan ilk ve tek Türk laboratuvarı olmanın gururuyla çalışıyor, inovatif fikirlerimiz ve sürdürülebilir bakış açımızla dünyaya iyi bakıyoruz.

#İyiBakDünyana


Dimin
ÖNCELİĞİMİZ
İŞ GÜVENLİĞİ!
Çalışanlarımızın can güvenliği her zaman önceliğimizdir.
Mutlu ve sağlıklı çalışan politikamız sayesinde, geleceğe güvenle bakıyoruz.
www.dimin.com.tr
Ege Plaza İş Merkezi Konya Yolu Mevlana Bulvarı No:182 Kat:21/95 Çankaya/ANKARA
(+90) 312 909 11 21
info@dimin.com.tr
/dimin-madencilik



LİDYA MADENCİLİK

2010 yılında kurulan Lidya Madencilik, Çöpler Altın Madeni, Hod Maden Bakır & Altın Projesi ve Cevizlidere porfiri bakır yatağı gibi dünya çapında bir varlık portföyünü yönetmektedir. 2013'ten bu yana Türkiye'de üç maden yatağı keşfetmiştir. 2020 yılında PDAC tarafından Küresel Keşif Ödülü'ne layık görülmüştür. Altın ve bakır odaklı çalışmalarını sürdüren Lidya Madencilik, Gediktepe altın/gümüş madenini keşfederek sekiz yılda üretime geçirmiştir.

Sektöre bir yatırımcı olarak giren Lidya Madencilik, Türkiye ve yurt dışında madenlerin araştırılması, keşfi, geliştirilmesi, inşası ve işletilmesi süreçlerini kapsayan bir gelişim göstermiştir. Amerikan, Kanadalı ve İngiliz ortaklıkları ve küresel bir madencilik & finans ilişkileri ağına sahiptir. Gediktepe madenini işleten ve İngiltere borsasına kote olan ACG'nin %38'ine sahip olarak, yeni satın alımlarla İngiltere pazarında önde gelen bakır üreticilerinden biri olmayı hedeflemektedir. Son on yılda 5 birleşme ve satın alma anlaşması gerçekleştirmiş; son ikisi Türkiye'deki en büyük 10 M&A listesinde yer almıştır. Türkiye, Orta Asya ve Afrika'da çok ülkeli, çok emtialı ve çok aşamalı bir varlık portföyü oluşturmak amacıyla arama ve yatırım çalışmaları yürütmektedir.

LİDYA MINES EARTH TO PEOPLE

Lidya Mines was Established in 2010. Manages a world-class aset portolio including Çöpler gold mine, Hod Maden Copper&Gold Project and Cevizlidere porphyry Copper deposit. Discovered 3 deposits in Turkey since 2013. Awarded by PDAC with Global Exploration Award in 2020. Focused on gold&copper. Discovered and put Gediktepe gold/silver Mine in production in 8 years.

Evolved from starting as an investor through exploration, discovery, development, construction and operation of mines in Turkey and abroad. Enjoys/Leverages American & Canadian & British partnerships and a global network of mining&finance relationships. Owns 38% of UK-listed ACG, which operates Gediktepe mine and aspires to be one of the leading copper players in UK market through new acquisitions. Closed 5 M&A deals in the past decade; last 2 in the top 10 M&A list in Turkey. Explores in Turkey, C.Asia and Africa to build a robust multi-country, multi-commodity and multi-stage asset pipeline.

albacore

YENİLİKÇİ VE MODERN MADENCİLİK

Albacore, müşterilerine uzman danışmanlık ve temsilciliklerinin ürünlerine ilgi duyan işletme ve tesislere düzenli servis de dahil olmak üzere yenilikçi ve modern tarzda hizmet vermektedir. Konuya ilişkin sorunları kısa sürede çözebilmek ve müşterilerine evrensel düzeyde hizmet verebilmek için Albacore gerekli olan sistem bilgisine sahiptir. Bu çerçevede Albacore, gerektiğinde ortaya çıkan sorunlarda en seri ve en verimli şekilde yardım edebilecek, ilgili uzman firmaları da devreye sokar.

WWW.ALBACORE.COM.TR

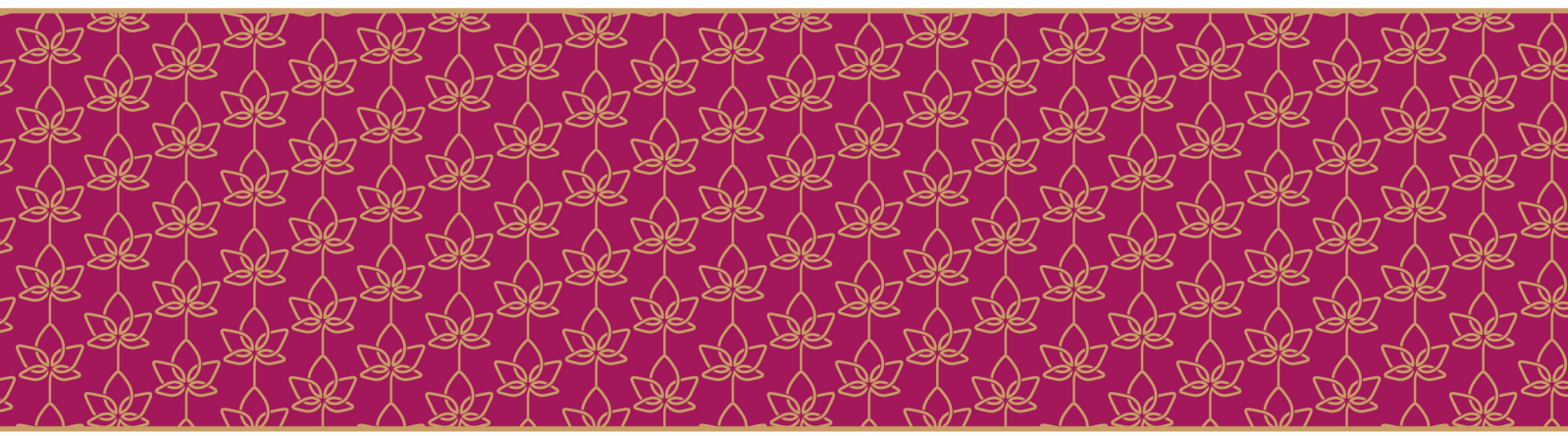

MUTAŞ
INNOVATIVE STEPS EFFICIENT RESULTS
EMAİL
bilgi@mutas.com
ADRES
Konak mah. Barış (120) sok.
No: 3/52-53 Nilüfer/BURSA
TELEFON
+90 224 441 22 78
KÜTAHYA
MANYEZİT
TAVŞANLI
KROM & MANYEZİT
KARABÜK
KUVARSİT
ANTALYA
POLİMETAL
TOKAT
BAKIR
REŞADİYE
BENTONİT

ESKİŞEHİR OSMANGAZİ UNIVERSITY
1970
+90 222 239 37 50 / 3414
maden@tm.ogu.edu.tr

Yurt Madenciliğini Geliştirme Vakfı

ARBER
arber@arber.com.tr
+90 312 441 07 00
www.arber.com.tr

www.imps2024.org



ESOGÜ BASIMEVİ

978-605-9975-87-2